This document was produced
by scanning the original publication.

Ce document est le produit d'une
numérisation par balayage
de la publication originale.

CYPRUS CRUSTAL STUDY PROJECT: INITIAL REPORT, HOLE CY-4

I.L. GIBSON, J. MALPAS, P.T. ROBINSON AND C. XENOPHONTOS

1989

Énergie, Mines et Ressources Canada
Energy, Mines and Resources Canada
Canada

GEOLOGICAL SURVEY OF CANADA
PAPER 88-9

Cyprus Crustal Study Project: Initial Report, Hole CY-4

edited by
I.L. Gibson, J. Malpas, P.T. Robinson and C. Xenophontos

1989

© Minister of Supply and Services Canada 1989

Available in Canada through

authorized bookstore agents and other bookstores

or by mail from

Canadian Government Publishing Centre
Supply and Services Canada
Ottawa, Canada K1A 0S9

and from

Geological Survey of Canada offices:

601 Booth Street
Ottawa, Canada K1A 0E8

3303-33rd Street N.W.,
Calgary, Alberta T2L 2A7

A deposit copy of this publication is also available for reference
in public libraries across Canada

Cat. No. M44-89/9E
ISBN 0-660-13279-6

Price subject to change without notice

This volume has been printed by the Geological Survey of Canada on behalf of the Cyprus Crustal Study Project from camera-ready copy prepared, under the direction of the volume editors, by Jocelyne Price and Louise Wallace in the Department of Earth Sciences, University of Waterloo. Most of the material is set in 10 pt. Times and was printed using the APS-Micro 5 Phototypesetter, and Waterloo SCRIPT computer software in the Department of Graphic Services, University of Waterloo.

Table of Contents

INTRODUCTION AND LITHOLOGIC DESCRIPTION PAGE

Hole CY-4 of the Cyprus Crustal Study Project: background and objectives
P.T. Robinson 1

Cyprus Crustal Study Project hole CY-4: lithologic unit summaries
P.T. Robinson 5

GEOLOGIC RELATIONS

The geology of the area immediately surrounding the CY-4 borehole of the Cyprus Crustal Project
J. Malpas, G. Case and P. Moore 31

Structural and petrologic relationships of the CY-4 drill hole of the Cyprus Crustal Study Project
J. Malpas, T. Brace and S.M. Dunsworth 39

Sheeted dykes from CY-4 and surface sections: Troodos ophiolite
W.R.A. Baragar, M.B. Lambert, N. Baglow and I.L. Gibson 69

Some dyke-gabbro relationships in the Troodos ophiolite, Cyprus
C.J. Stillman 107

MINERALOGY AND PETROLOGY

Petrological features of gabbroic and ultramafic rocks from deep drill CY-4, Cyprus
R. Laurent and R. Hebert 115

Igneous mineral stratigraphy and chemistry of the Cyprus Crustal Study Project drill core in the plutonic sequences of the Troodos ophiolite
P. Thy, P. Schiffman and E.M. Moores 147

Geochemical characteristics and petrogenesis of the ophiolite sequence rocks from drill hole CY-4, Troodos complex, Cyprus
H.M. Ali and M.O. Nassief 187

Fine scale modal layering and cyclic units in ultramafic cummulates from the CY-4 borehole, Troodos ophiolite: Evidence for an open system magma chamber
P.Browning, S.Roberts and T.Alabaster 193

GEOCHEMISTRY

Oxygen and carbon isotope studies of hydrothermal alteration in the Troodos ophiolite complex, Cyprus
N.J. Vibetti, R. Kerrich and W.S. Fyfe 221

Hypersaline fluids discovered in the Troodos ophiolite
N.J. Vibetti, R. Kerrich and W.S. Fyfe 229

PALAEOMAGNETIC AND ROCK MAGNETIC PROPERTIES

Magnetic properties, oxide petrography, and alteration in the Cyprus Crustal Study Project drill hole CY-4 section through the lower sheeted complex and upper plutonic complex of the Troodos, Cyprus, ophiolite
J.M. Hall, B. Fisher, C. Walls, T. Ward, L. Hall, H.P. Johnson and J. Pariso 235

Magnetic properties of an analog of the lower oceanic crust: magnetic logging and paleomagnetic measurements from drill hole CY-4 in the Troodos ophiolite
J. Pariso and H.P. Johnson 279

PHYSICAL PROPERTIES AND OTHER GEOPHYSICAL DATA

The physical properties of diabases, gabbros and ultramafic rocks from C.C.S.P. drill hole CY-4 at Palekori, Cyprus
G.C. Smith and F.J. Vine 295

In situ stress measurements and natural fracture logging in drill hole CY-4, the Troodos ophiolite, Cyprus
J. Baumgartner, F. Rummel, B.C. Haimson and M.Y. Lee 315

Geophysical structure of the Troodos ophiolite from dowhole logging
M.H. Salisbury, N.I. Christensen, F.J. Vine, G.C. Smith and S. Eleftheriou 331

Velocity structure of the Troodos Massif, an arc-derived ophiolite
N.I. Christensen and M.H. Salisbury 351

A gravity survey from Agrokipia to Papoutsa, Cyprus
S. Kramvis and K.L. Verosub 371

SUMMARY

Geology and geophysics of borehole CY-4 of the Cyprus Crustal Study Project: Summary
J. Malpas, P.T. Robinson and M. Salisbury 381

Back Pocket

Geologic map of the area surrounding the CY-4 borehole (Figure 1 of Malpas, Case and Moore, The geology of the area immediately surrounding the CY-4 borehole of the Cyprus Crustal Study Project)

Diagramatic stratigraphic column of the CY-4 borehole

Foreword

In 1978, an international consortium of scientists from Canada, Denmark, the United Kingdom, Iceland, the United States and West Germany successfully completed a research deep drilling project in Iceland. These scientists subsequently formed the International Crustal Research Drilling Group (ICRDG), to organize further deep drilling investigations and to compare the results with those from the Deep Sea Drilling Project and Ocean Drilling Program. It was hoped, in this way, to better understand the structure and composition of the ocean crust. The projects undertaken by the group are selected and organized by a Management Panel and each project is overseen by a Project Director. The members of the Management Panel during the period of 1980 to 1986 were: Dr. Abdul Razzak Bakor, King Abdul Aziz University, Saudi Arabia; Dr. Robert Baragar, Geological Survey of Canada, Canada; Dr. Tom Calon, Memorial University, Canada; Dr. George Constantinou, Geological Survey Department, Cyprus; Dr. Martin F.J. Flower, University of Illinois, U.S.A.; Dr. Ingvar Birgir Fridleifsson, Orkustofnun, Iceland; Dr. Ian G. Gass, The Open University, U.K.; Dr. Ian L. Gibson, University of Waterloo, Canada; Dr. James Hall, Dalhousie University, Canada; Dr. James Hawkins, Scripps Institution of Oceanography, U.S.A.; Dr. H.P. Johnson, University of Washington, U.S.A.; Dr. John Malpas, Memorial University, Canada; Dr. Eldridge Moores, University of California, U.S.A.; Dr. John Orcutt, Scripps Institution of Oceanography, U.S.A.; Dr. Andreas Panayiotou, Geological Survey Department, Cyprus; Dr. Paul T. Robinson, Chairman, Dalhousie University, Canada; Dr. Fritz Rummel, Ruhr-Universität Bochum, West Germany; Dr. Matthew Salisbury, Dalhousie University, Canada; Dr. Andrew Saunders, University of Leicester, U.K.; Dr. Hans-Ulrich Schminchke, Ruhr-Universität Bochum, West Germany; Dr. Gunther Schoenharting, University of Copenhagen, Denmark; Dr. M. Treuil, Université Pierre et Marie Curie, France; Dr. Fred Vine, University of East Anglia, U.K.

Ophiolites have long been recognized as portions of ancient oceanic lithosphere emplaced on to continental margins during periods of orogenesis. As such, complete ophiolites present a stratigraphy of the oceanic crust and the underlying upper mantle. P.T. Robinson proposed that ICRDG investigate the Troodos ophiolite in Cyprus. The Troodos ophiolite is one of the best studied and least deformed ophiolites available for investigation, and its unique domal structure permits sampling of the complete stratigraphy in a series of relatively shallow holes. An integrated petrological, structural and geophysical study of the ophiolite, involving both field mapping and diamond drilling was therefore planned. The proposal was formally approved by the Management Panel in May, 1980. P.T. Robinson was appointed Project Director with overall responsibility for the drilling operations and organization of the scientific investigations.

Avant-propos

En 1978, un groupe de scientifiques du Canada, du Danemark, du Royaume- Uni, de l'Islande, des États-Unis et de l'Allemagne de l'Ouest a complété avec succès, en Islande, un projet de forage à grande profondeur pour des fins de recherche. Ces chercheurs ont par la suite formé le Groupe international de forage pour la recherche sur la croûte (International Crustal Research Drilling Group, ICRDG) dans le but d'organiser d'autres projets de forage profond et de comparer les résultats de ces études à ceux obtenus dans le cadre du Projet de forage en mer profonde et du Programme de forage des fonds marins. Les scientifiques espéraient ainsi arriver à mieux comprendre la structure et la composition de la croûte océanique. Les projets entrepris par le Groupe sont sélectionnés et organisés par un comité de gestion, et chaque étude est supervisée par un directeur de projet. Les personnes suivantes ont été membres du Comité de gestion durant la période allant de 1980 à 1986: M. Abdul Razzak Bakor, université King Abdul Aziz, Arabie Saoudite; M. Robert Baragar, Commission géologique du Canada, Canada; M. Tom Calon, université Memorial, Canada, M. George Constantinou, Commission géologique de Chypre, Chypre; M. Martin F.J. Flower, University of Illinois, É.-U.; M. Ingvar Birgir Fridleifsson, Orkustofnun, Islande; M. Ian G. Gass, The Open University, R.-U.; M. Ian L. Gibson, université de Waterloo; M. James Hawkins, Scripps Institution of Oceanography, É.-U.; M. H.P. Johnson, University of Washington, É.-U.; M. John Malpas, université Memorial, Canada; M. Eldridge Moores, University of California, É.-U.; M. John Orcutt, Scripps Institution of Oceanography, É.-U.; M. Andreas Panayiotou, Commission géologique de Chypre, Chypre; M. Paul T. Robinson, président, université Dalhousie, Canada; M. Fritz Rummel, Ruhr-Universität Bochum, Allemagne de l'Ouest; M. Matthew Salisbury, université Dalhousie, Canada; M. Andrew Saunders, University of Leicester, R.-U.; M. Hans- Ulrich Schminchke, Ruhr-Universität Bochum, Allemagne de l'Ouest; M. Gunther Schoenharting, université de Copenhague, Danemark; M. M. Treuil, Université Pierre et Marie Curie, France, et M. Fred Vine, University of East Anglia, R.-U.

On admet depuis longtemps que les ophiolites sont des portions de l'ancienne lithosphère océanique qui ont été mises en place sur des marges continentales durant des périodes d'orogénèse. De ce fait, les complexes ophiolitiques complets représentent la stratigraphie de la croûte océanique et du manteau supérieur sous-jacent. Ainsi, M. P.T. Robinson a proposé que l'ICRDG étudie l'ophiolite de Troodos, à Chypre. Ce cortège ophiolitique est l'un des plus étudiés et des moins déformés que l'on puisse examiner; de plus, sa structure exceptionnelle en forme de dôme permet aux scientifiques d'échantillonner la colonne stratigraphique toute entière au moyen d'une série de sondages relativement peu profonds. On a donc proposé une étude intégrée, à la fois pétrologique, structurale et géophysique, de l'ophiolite de Troodos, comprenant des travaux de cartographie sur le terrain et des sondages au diamant. Ce projet a été officiellement approuvé

During the period 1980 to 1982, the Cyprus Government approved the project, supporting funds were obtained from a variety of sources, and field studies were started. A drilling contract with Bradley Bros., Noranda, Quebec, Canada was approved by the Management Panel in October 1981, and drilling began in April, 1982. The drilling continued intermittently until March, 1985, by which time five holes had been drilled at three sites. Total penetration was approximately 4563 metres with an average core recovery of over 95%.

Funding for the project came from a number of agencies: The Natural Sciences and Engineering Research Council, the International Development Research Centre, Dalhousie University, Memorial University and the University of Western Ontario (Canada); the Natural Science Research Council (Denmark); the Natural Environment Research Council and the Royal Society (United Kingdom); the National Science Foundation (United States); the Volkswagen Foundation (West Germany); King Abdul Aziz University (Saudi Arabia); and the Government of Cyprus. In all, a total of approximately Can. $1,575,000 was spent on drilling and related work and roughly equal amounts on field studies, geophysical logging and laboratory studies.

The core recovered from the drill holes is stored in a facility provided by the Government of Cyprus in Nicosia and can be accessed with the permission of the Management Panel of ICRDG through the Geological Survey Department of Cyprus. Lithological core logs were produced on site after recovery of the core and are available from ICRDG at the Centre for Marine Geology, Dalhousie University, Nova Scotia, Canada.

The ICRDG Management Panel acknowledges with thanks the support provided by the Geological Survey of Canada in publishing the Initial Report volumes as GSC Papers. Paper 85-29, Cyprus Crustal Study Project: Initial Report, Holes CY-2 and 2a, was published in 1987. The present volume describes the results from CY-4, a deep hole drilled through the sheeted dykes and gabbros and into the ultramafic unit. A final volume on Holes CY-1 and 1a, drilled through the pillow lavas, is planned. The volumes aim to present descriptions of the cores along with other geological, geophysical and geochemical data. No attempt has been made to reconcile differences in interpretation between authors of papers in the volume. The papers were reviewed by the editors who are grateful to colleagues who provided external reviews. The editors gratefully acknowledge the assistance of Louisa Horne, in supervising the editing and compilation of this volume.

par le Comité de gestion en mai 1980; M. Robinson a été nommé directeur du projet et a ainsi assumé la responsabilité globale des opérations de forage et de l'organisation des études scientifiques.

Entre 1980 et 1982, le gouvernement de Chypre a approuvé le projet, des fonds ont été obtenus de plusieurs sources diverses et les travaux ont commencé sur le terrain. Le Comité de gestion a approuvé, en octobre 1981, un contrat de forage conclu avec la société Bradley Bros., de Noranda (Québec), Canada, et les sondages ont débuté en avril 1982. Les forages se sont poursuivis de fa on intermittente jusqu'en mars 1985 et ainsi, cinq trous ont été forés à trois endroits. Au total, environ 4,563 m de forages ont été réalisés et on a récupéré, en moyenne, plus de 95% des carottes.

Un certain nombre d'organismes ont accordé une aide financière au projet, soit le Conseil de recherches en sciences naturelles et en géni, le Centre de recherches pour le développement international, l'université Dalhousie, l'université Memorial et l'université de Western Ontario (Canada), le Conseil de recherches en sciences naturelles (Danemark), le Natural Environment Research Council et la Royal Society (Royaume-Uni), la National Science Foundation (États- Unis), la fondation Volkswagen (Allemagne de l'Ouest), l'université King abdul Aziz (Arabie Saoudite) et le gouvernement de Chypre. En tout, un total d'environ 1,575,000 $ CAN a été consacré aux forages et aux travaux connexes; une somme comparable a été dépensée pour les études de terrain, les diagraphies géophysiques et les études en laboratoire.

Les carottes extraites des trous de forage sont entreposées à Nicossie, dans des installations fournies par le gouvernement de Chypre. Il est possible d'avoir accès à ces échantillons avec la permission du Comité de gestion de l'ICRDG, par l'entremise de la Commission géologique de Chypre. Des diagraphies de la lithologie des carottes ont été produites à l'emplacement du forage, immédiatement après l'extraction des carottes, et peuventtre obtenues de l'ICRDG en s'adressant au Centre de géologie marine (Centre for Marine Geology) de l'université Dalhousie (Nouvelle-Écosse), Canada.

Le Comité de gestion de l'ICRDG remercie la Commission géologique du Canada, qui a publié les volumes du rapport initial dans sa série d'études. L'étude 85-29 a été publiée en 1987 sous le titre *Cyprus Crustal Study Project: Initial Report, Holes CY-2 and 2a*. Le présent volume décrit les résultats obtenus au sondage CY-4, un forage profond qui a traversé les dykes et les gabbros stratifiés et a pénétré l'unité ultramafique. Enfin, on prévoit de publier un dernier volume qui portera sur les sondages CY-1 et 1a, forés à travers les laves en coussins. Ces volumes visent à donner des descriptions des carottes de me que d'autres données géologiques, géophysiques et géochimiques. On n'a pas cherché à accommoder les différences d'interprétation que l'on pourra noter entre les collaborateurs à ce volume. Les études ont été examinées par les rédacteurs, qui remercient les collègues qui leur ont soumis leurs critiques. Les rédacteurs savent également gré à Mme Louisa Horne pour l'aide qu'elle leur a apportée lors de la révision et de la compilation du présent volume.

ICRDG acknowledges with gratitude those agencies which have supported its research drilling programmes. A special thanks are due to Drs. G. Constantinou, A. Panayiotou and C. Xenophontos of the Geological Survey Department, Cyprus. This project is an example of the successful cooperation between a number of national governments, the industrial sector and the academic community.

ICRDG Management Panel
February, 1989

L'ICRDG exprime sa reconnaissance aux organismes qui ont appuyés ses programmes de forage à des fins de recherche. En particulier, les membres du Comité de gestion remercient M. M.G. Constantinou, A. Panayiotou et C. Xenophontos de la Commission géologique de Chypre. Ce projet est un bel exemple de coopération réussie entre un certain nombre de gouvernements nationaux, l'industrie et le milieu universitaire.

Comité de gestion de l'ICRDG
Février 1989

Hole CY-4 of the Cyprus Crustal Study Project: Background and Objectives

PAUL T. ROBINSON

Department of Geology, Dalhousie University,
Halifax, Nova Scotia, Canada B3H 3J5

Robinson, P.T., Introduction and Objectives; in *Cyprus Crustal Study Project: Initial Report, Hole CY-4, ed. I.L. Gibson, J. Malpas, P.T. Robinson and C. Xenophontos; Geological Survey of Canada, Paper 88-9, p. 1-4, 1989.*

Abstract

A 2 km drill hole (CY-4) was planned as part of the Cyrus Crustal Study Project to sample the lower part of the Troodos ophiolite. The hole was spudded in near the base of the sheeted dyke complex with the object of determining: (1) The intrusive and compositional relationships within the dyke complex. (2) The nature of the dyke gabbro transition. (3) The age relationships of the spatially associated dykes, gabbros, and plagiogranites. (4) The chemical and mineralogical variation within the plutonic section and hence whether the intrusives are a single magmatic sequence or a number of discrete plutons. (5) The nature and extent of hydrothermal alteration within the dykes and gabbros. It was anticipated that the drilling results, combined with field studies of the plutonic rocks and sheeted dykes, would provide a three-dimenmsional model for the lower part of the ophiolite. Drilling was successful with 2263 m of penetration into the dyke, gabbro, and ultramafic section. Studies of the core material and the field relationships are detailed in the accompanying nineteen papers.

Résumé

Un forage de 2 km. (CY-4) a été planifié dans le cadre du Projet d'Etudes de la Croute Cypriote pour échantillonner la partie inférieure de l'ophiolite de Troodos. Le forage a été effectué près de la base du complexe de dyke dans le but de déterminer: (1) Les corrélations intrusion-compostion dans le complexe de dyke. (2) La nature de la transition du gabbro dans le dyke. (3) Les ages relatifs des dykes, gabbros et plagiogranites rapprochés. (4) Les variations chimiques et minéralogiques dans la section plutonique pour déterminer si les intrusions sont en séquence ou un nombre de plutons indépendants. (5) La nature et l'importance des alterations hydrothermiques à l`intérieur des dykes et des des gabbros. L'objectif était que les résultats du forage, associés aux études de terrain des rocs plutoniques et des dykes procurent un modèle tri-dimensionnel de la partie inférieure de l'ophiolite. Le forage a réussi avec une pénétration de 2263 m dans le dyke, le gabbro, et la section ultramafique. Les études du matériel brut ainsi que des corrélations avec les observations sur le terrain sont offertes en détail dans les dix-neuf articles ci-inclus.

INTRODUCTION

The Cyprus Crustal Study Project was conceived as a joint field and research drilling investigation of the Troodos Massif, in order to develop a three dimensional model for the ophiolite. The main objective of the research drilling was to recover a complete section of the ophiolite from the top of the extrusive sequence to the base of the cumulate section. The domal structure of the Troodos Massif suggested that the entire crustal section could be sampled in two offset holes, each about 2.5 km deep. Hole CY-1, spudded in at the top of the lava pile, was intended to penetrate the entire extrusive sequence and most of the sheeted dykes. Unfortunately, this hole was lost after penetrating 485 m into the lavas but, the remainder of the extrusive sequence and the upper part of the sheeted dykes were sampled in hole CY-1a, spudded in about .5 km to the south, at a stratigraphic level roughly equivalent to the bottom of hole CY-1.

Holes CY-2 and 2a were drilled in the Agrokipia area to investigate the nature of hydrothermal circulation and ore formation in the oceanic crust (Robinson et al 1987).

Hole CY-4, located near the village of Palekhori, was spudded in near the base of the sheeted dykes and was intended to sample the dyke-gabbro contact, penetrate the entire plutonic sequence, and hopefully reach the Moho. The hole was terminated voluntarily at a depth of 2263 m, and bottomed in layered ultramafics. Subsequent geophysical investigations suggested that the petrologic Moho might lie about 500 m deeper in the section.

Drilling in the sheeted dykes and plutonic rocks was intended to answer a number of specific questions and help distinguish among competing structural models: 1) What are the intrusive and compositional relationships in the sheeted dyke complex? One early model for the sheeted dykes suggested that the dykes are compositionally uniform and that they contain a record of predominantly one way chilling. The chilling relationships were interpreted as indicating formation in a single, narrow spreading axis (Kidd and Cann, 1974). Desmet et al. (1980), on the other hand, postulated the existence of compositionally distinct dykes with specific age relationships. It was expected that these competing models could be resolved by the study of well preserved chilled margins in a continuously cored sequence.

2) What is the nature of the sheeted dyke-gabbro transition? Do the dykes decrease in abundance uniformly with depth or are there stepwise changes downward?

3) What are the age and compositional relationships among the plagiogranites, sheeted dykes and gabbros?

4) Does the plutonic section represent a single continuous sequence as postulated by Greenbaum (1972) or can intrusive contacts be recognized between separate plutons as suggested by Moores and Vine (1971), George (1978) and Allen (1975)?

5) What chemical and mineralogical variations can be recognized in the plutonic sequence and how can these be related to magma chamber processes?

6) What is the nature and extent of hydrothermal alteration in the dykes and gabbros?

It was anticipated that the drilling results, combined with field studies of the plutonic rocks and sheeted dykes, would provide a complete three-dimensional model for the lower part of the ophiolite. In fact, hole CY-4 was spectacularly successful, penetrating 2263 m with over 99% core recovery, thus providing a continuous sample of the lower sheeted dykes, the dyke-gabbro transition and most of the plutonic section. Study of the core material and adjacent field relationships, as outlined in this volume, provided answers to all of the questions posed and yielded a new model for the petrologic evolution of the Troodos ophiolite.

SITE SELECTION

Site selection for hole CY-4 was based on both geologic and operational criteria. Geologically, we hoped to find a site at which the entire section from the lower part of the sheeted dykes to the Moho could be penetrated in a single hole about 2000 m deep. Ideally, this site would lie in the same structural block as holes CY-1 and 1a, approximately along the trend of the sheeted dykes. Operational constraints included the need for a relatively flat area on which to place the drill rig, road access sufficient for heavy duty trucks and availability of water.

Based on the above criteria a site was selected about 1 km south of the village of Palekhori on the road to Agros (Figure 1). At this locality, sheeted dykes are exposed in road cuts adjacent to a large body of plagiogranite. Some of screens of plagiogranite are also present between the dykes, suggesting that the dyke-gabbro contact lay only a short distance be low the surface. A suitable platform was constructed on the shoulder of the road and water was obtained from a nearby stream.

The geologic relationships at this site turned out to be more complex than expected from the study of adjacent outcrops. Even though gabbros are exposed at a high level in the areas adjacent to the drill hole, mostly dykes were penetrated to a depth of about 600 m, and dykes persist to a depth of 1300 m. The drill hole apparently is located in a dyke swarm that extends to much greater depths than anticipated. This made it impossible to penetrate the complete plutonic section in a 2.0 to 2.5 km deep hole, which represented our financial and operational limit. On the other hand, the drilling results provided a much clearer picture of the dyke-gabbro transition and of the structural and petrological complexity of the gabbros. Ultimately, the hole was terminated for financial reasons at 2263 m.

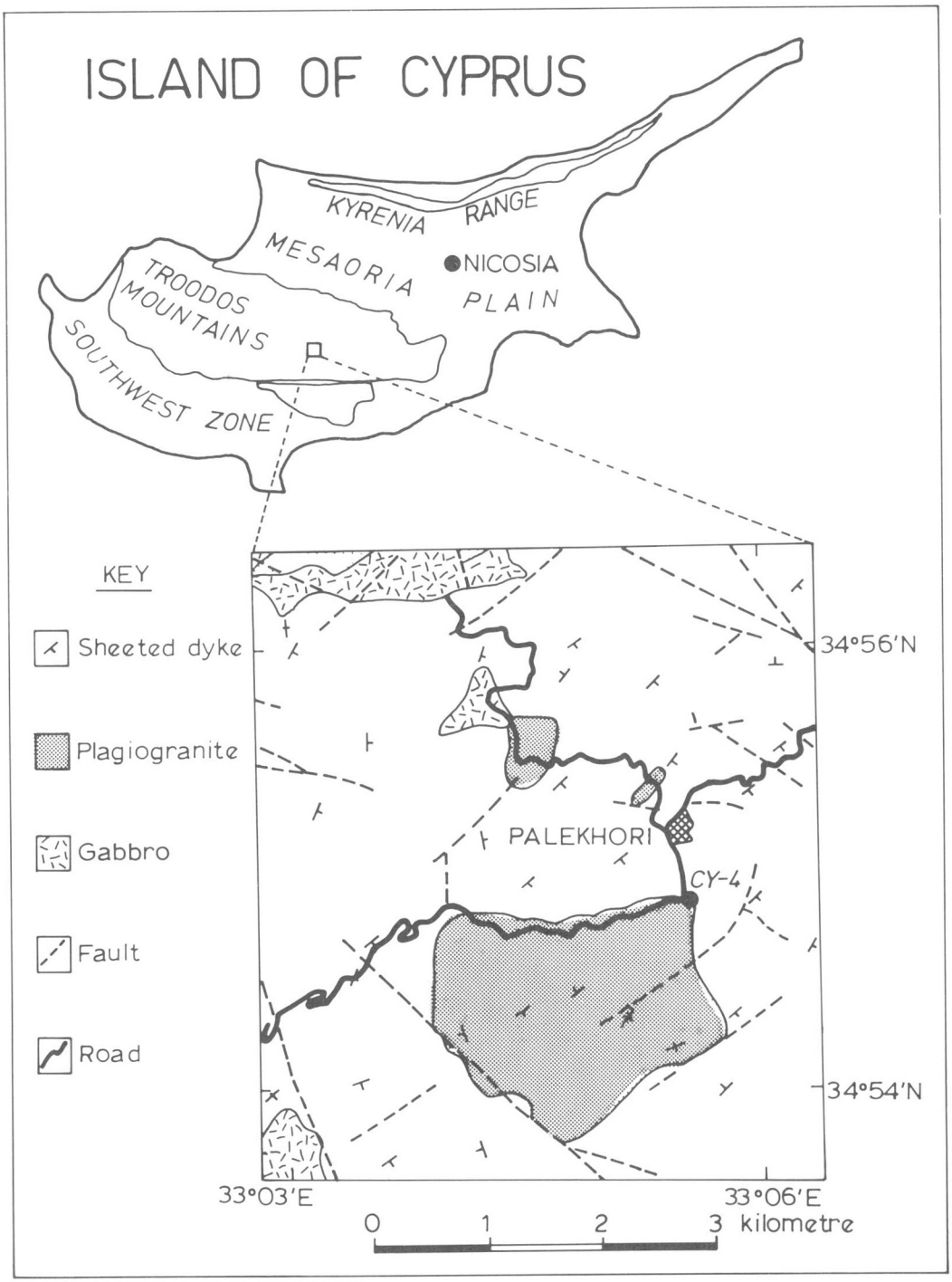

Figure 1: Location of CY-4 bore hole.

CORE DESCRIPTION

The core recovered from hole CY-4 was treated in much the same manner as that from holes CY-2 and 2a (Robinson et al 1987). The core was washed, reassembled and marked with an orientation line indicating the "up" direction. A continuous orientation line was used to indicate pieces that could be fitted together and aligned relative to one another. The depth was marked on the core in centimeters, extrapolated between drilling markers, which were usually placed in the core at 15 foot intervals.

A visual representation of each 1.5 m long core section was drawn on a core sheet and units identified and described. Individual units were recognized on the basis of cooling breaks, marked changes in grain size, lithology or mineralogy, or by changes in the degree or type of alteration. During description of the core, units were numbered sequentially down the hole. The unit numbers designate the core box in which the unit first appears.

After checking and editing, the core descriptions were bound and distributed to interested parties. Copies of these are available from the International Crustal Research Drilling Group, Centre for Marine Geology, Dalhousie University, Halifax, Nova Scotia, Canada. The individual units were recognized in the core were later grouped into 89 larger scale lithologic units (see Lithologic Description of CY-4).

REFERENCES

Allen, C. R.
1975: The petrology of a portion of the Troodos plutonic complex, Cyprus; unpublished Ph.D. thesis, University of Cambridge, p. 1-161.

Desmet, A., Gagny, Cl., Lapierre, H. and Rocci, G.
1980: Organisation spatio-temporelle du complexe filonien du Troodos: son enracinement dans la chambre magmatique; *in* Ophiolites, Proceeding of the International Ophiolite Symposium, Cyprus, 1979, ed. A. Panayiotou; Cyprus Geological Survey Department, Ministry of Agriculture and Natural Resources, p. 66-72.

George, R. P.
1978: Structure and petrology of the Olympus ultramafic complex *in* the Troodos ophiolite, Cyprus; Geological Society of America, Bulletin, v. 89, p. 845-865.

Greenbaum, D.
1977: The chromitiferous rocks of the Troodos ophiolite complex, Cyprus; Economic Geology, v. 72, p. 1175-1194.

Kidd, R. G. W. and Cann, J. R.
1974: Chilling statistics indicate an ocean-floor spreading origin for the Troodos complex, Cyprus; Earth and Planetary Science Letters, v. 24, no. 1, p. 151-155.

Moores, E.M. and Vine, F. J.
1971: The Troodos Massif, Cyprus and other ophiolites as oceanic crust; evaluation and implications; *in* A Discussion on the Petrology of Igneous and Metamorphic Rocks from the Ocean Floor; Philosophical Transactions of the Royal Society of London, Series A, v. 268, p. 433-466.

Robinson, P.T., Gibson, I.L. and Panayiotou, A. (ed.)
1987: Cyprus Crustal Study Project: Initial Report, Holes CY-2 and 2a, Geological Survey of Canada, Paper 85-29, 381 p.

Cyprus Crustal Study Project
Hole CY-4: Lithologic Unit Summaries

PAUL T. ROBINSON

Department of Geology, Dalhousie University,
Halifax, Nova Scotia, Canada, B3H 3J5

Robinson, P.T., Cyprus Crustal Study Project. Hole CY-4 lithologic unit summaries; in *Cyprus Crustal Study Project: Initial Report, Hole CY-4, ed. I.L. Gibson, J. Malpas, P.T. Robinson and C. Xenophontos; Geological Survey of Canada, Paper 88-9, p. 5-29, 1989.*

Abstract

Hole CY-4 is located at Lat. 34°54'06" N, Long. 33°05'380" E near the Agrokipia ore body on the north side of the Troodos ophiolite, Cyprus. The hole was drilled to a depth of 2263 m. Core recovery was 99%. More than two hundred cooling units were identified in the field and these have been grouped into seventy nine major lithologic units. For each of these major units, the following information is given: the position and nature of the upper and lower contact, the unit thickness, the dominant lithology, and the identification numbers of the cooling units grouped within the major lithologic unit. For each major lithologic unit, this heading is followed by a description detailing the lithology, texture, alteration mineralogy and major megascopic features.

Résumé

Le forage CY-4 est situé à Lat. 34°54'06"N, Long. 33°06'30"E près du dépôt de minerai d'Agrokipia sur le côté nord de l'ophiolite de Troodos, Cyprus. Le forage a atteint une profondeur de 2263 m. La récupération fut de 99%. Plus de deux cent unités de refroidissement furent identifiées sur le terrain et celles-ci ont été groupées en soixante-dix neuf unités lithologiques majeures. Pour chacune des ces unités majeurs, l'information suivante est donnée: la position et nature du contact supérieur et inférieur, l'épaisseur de l'unité, la lithologie dominante et les numéros d'identification des unités de refroidissement groupées à l'intérieur des unités lithologiques majeures. Pour chaque unité lithologique majeure, cette entête est suivie par une description détaillée de la lithologie, texture, minéralogie d'altération et charactéristiques mégascopiques majeures.

UNIT I

Upper Contact: 0.00 m, ambiguous
Lower Contact: 39.24 m, truncated
Thickness: 39.24 m
Lithology: Aphyric diabase dykes
Cooling Units: 1.01 - 11.03

Unit I consists of a series of grey, generally fine-grained, aphyric diabase dykes. Twenty one cooling units are present ranging from 0.03 to 8.33 m and averaging 1.91 m in vertical thickness. Four units are doubly chilled (3.01, 6.01, 10.03, and 11.02) and most other units have one chilled margin. The remainder are interpreted as dykes based on their similarity in lithology and texture to adjacent units with chilled margins. The rocks are massive with little brecciation. Veins and fractures average about 1% overall and range from hairline to 3 mm wide. Most are filled with white zeolite (laumontite?) but a few have early quartz, epidote, chlorite, and minor pyrite. Groundmass alteration averages about 20-25% and involves chloritization of mafic minerals and saussuritization of plagioclase. Some samples contain megascopic epidote in the groundmass.

UNIT II

Upper Contact: 39.24 m, intrusive
Lower Contact: 49.33 m, intrusive
Thickness: 10.09 m
Lithology: Olivine-phyric dyke
Cooling Units: 11.04 - 13.01

Unit II is a single dyke, 10.09 m thick, of light grey, fine- to medium-grained, sparsely phyric diabase. It is divided into three cooling units by a highly brecciated zone (cooling unit 12.01) near its centre. The contacts between massive and brecciated material are gradational and the rocks are lithologically similar. Phenocrysts of olivine, clinopyroxene and rare plagioclase make up 3-8% and range up to about 2 mm in size. Vesicles are sparse, 1% or less, small, and filled with quartz and epidote. In the massive portions, veins comprise 1-3% and are filled with early quartz and later carbonate and zeolite. Fractures make up about 50% of brecciated portions and are filled chiefly with zeolite and epidote. Groundmass alteration averages 5-10% but is higher in the coarse-grained and brecciated portions. It involves partial replacement of groundmass material by quartz, epidote, and zeolite, particularly adjacent to veins.

UNIT III

Upper Contact: 49.33 m, truncated
Lower Contact: 54.69 m, intrusive
Thickness: 5.36 m
Lithology: Aphyric diabase dykes
Cooling Units: 14.01 - 15.04

Six relatively thin dykes of aphyric diabase make up Unit III. Individual dykes range from .16 to 1.74 m and average .89 m in vertical thickness. Most have at least one chilled margin but two cooling units are truncated on both sides and are inferred to be dykes from their textures. The rocks are all light grey, fine- to medium-grained, non-vesicular diabase. Cooling unit 15.03 is cut by apophyses of dark, very fine-grained, chilled material, distinctly different from the host rock. Cooling unit 15.04 consists of 4-5 thin cooling units of diabase too small to log separately. Veins make up about 1-3% overall and range from hairline to 5 mm wide. They are filled chiefly with zeolite (laumontite?) and epidote. Groundmass alteration ranges up to 50% but averages about 15%. It involves chiefly replacement by chlorite and epidote.

UNIT IV

Upper Contact: 54.69 m, truncated
Lower Contact: 65.30 m, faulted(?)
Thickness: 10.61 m
Lithology: Sparsely phyric and aphyric diabase dykes
Cooling Units: 15.05 - 18.01

A 10.61-m-thick sequence of sparsely phyric to aphyric diabase dykes makes up Unit IV. The nine cooling units range from .08 to 2.77 m and average 1.18 m in vertical thickness. The intrusive relationships in this sequence are very complex but all units are believed to be dykes based on contact relationships and textures. Three of the cooling units (15.05, 16.02 and 17.02) are sparsely phyric with 1-5% phenocrysts. The crystals range up to 2 mm across and consist chiefly of clinopyroxene and minor olivine. The aphyric cooling units consist of grey, fine- to medium-grained diabase similar to the groundmass of the phyric units. Vesicles are absent in most dykes but range up to 2% in cooling unit 17.01. These vesicles are 1 mm across, spherical and filled with quartz and epidote. Veins and fractures average about 2-3% but range up to 10% in parts of cooling unit 17.03. Most veins are 1-2 mm wide and are filled with mixtures of epidote, quartz, chlorite, magnetite(?) and late zeolite (laumontite?). Groundmass alteration ranges up to about 30% and involves replacement of mafics by chlorite and minor

epidote. Some plagioclase appears to be saussuritized.

UNIT V

Upper Contact: 65.30 m, ambiguous
Lower Contact: 72.50 m, truncated
Thickness: 7.20 m
Lithology: Brecciated diabase dykes
Cooling Units: 18.02 - 20.03

Ten relatively thin cooling units of light grey, fine-grained, aphyric, highly fractured and brecciated diabase make up Unit V. Individual cooling units range from .46 to 1.59 m and average .88 m in vertical thickness. Most have chilled or truncated margins and the brecciation is most intense along the contacts. Cooling unit 19.01 contains trace amounts of plagioclase microphenocrysts; the other units are completely aphyric. Vesicles are absent but veins and fractures are very abundant, ranging up to 40% in some intervals. Most veins are from 1-5 mm wide and are filled with zeolite (laumontite?) accompanied by minor chlorite and Fe-oxides. Groundmass alteration averages 20-25% but ranges up to 60% in the most intensely brecciated zones. Highly altered zones are dark green in colour due to development of chlorite. Small amounts of zeolite are also present locally.

UNIT VI

Upper Contact: 72.50 m, intrusive
Lower Contact: 78.33 m, intrusive
Thickness: 5.83 m
Lithology: Aphyric diabase dykes
Cooling Units: 20.04 - 22.01

Unit VI is a 5.83-m-thick sequence of relatively narrow diabase dykes. The twelve cooling units present range from .08 to 1.89 m and average .49 m in vertical thickness. They all consist of light grey to greenish-grey, fine- to medium-grained, aphyric, non-vesicular diabase. Most cooling units have one or more chilled margins; the others are inferred to be dykes based on their textures and mineralogies. Most of the dykes are massive but considerable brecciation is apparent along the intrusive lower contact of cooling unit 22.01. Veins make up 10-15% of most units but are less abundant locally. Most are 2-3 mm wide and are filled with white zeolite (laumontite?) and chlorite. A few also have traces of epidote. Groundmass alteration ranges from 10-50% and averages about 20%. It chiefly involves replacement of mafic minerals by chlorite and of plagioclase by zeolite. Highly altered rocks are typically greenish-grey in colour whereas the fresher rocks are light grey.

UNIT VII

Upper Contact: 78.33 m, truncated
Lower Contact: 82.66 m, ambiguous
Thickness: 4.33 m
Lithology: Sparsely phyric diabase dykes
Cooling Units: 22.02 - 22.04

Unit VII consists of three cooling units of light grey, fine- to medium- grained diabase, one of which is highly brecciated. The upper and lower units are sparsely olivine- and clinopyroxene-phyric whereas the middle, brecciated unit is aphyric. The three cooling units range from 1.22 to 1.69 m and average 1.44 m in vertical thickness. Phenocrysts never exceed 1 modal percent and consist of about equal amounts of olivine and clinopyroxene, both of which are altered to clay minerals. Vesicles are absent except in cooling unit 22.02 where they make up less than 1% and average about 1 mm across. They are filled with quartz and epidote. Veins normally make up 1-5% but are somewhat more abundant in the brecciated zones. They range up to about 5 mm in width and are filled chiefly with zeolite, locally accompanied by chlorite. Groundmass alteration ranges from 15-30% and is highest in the brecciated zone. Chlorite replaces mafic minerals and zeolite replaces feldspar. In the highly brecciated rocks there are light coloured, bleached zones rich in epidote and chlorite.

UNIT VIII

Upper Contact: 82.66 m, ambiguous
Lower Contact: 98.88 m, truncated
Thickness: 16.22 m
Lithology: Diorite cut by diabase dykes
Cooling Units: 23.01 - 27.02

Unit VIII is a 16.22-m-thick interval of brecciated diorite cut by numerous thin diabase dykes. Six of the 12 cooling units are diorite and these range from .08 to 6.35 m in vertical thickness. The remaining units are thin dykes ranging from .13 to .90 m and averaging .44 m in vertical thickness. The diorite is a light grey, medium-grained rock composed of about 70% plagioclase, 20-25% amphibole and 5-10% pyroxene. Much of the diorite is intensely sheared, producing a breccia of diorite clasts in a comminuted, highly chloritized matrix. Distinct veins average <1% and range up to about 2 mm wide. They are filled entirely with white zeolite (laumontite?). Groundmass alteration ranges between about 10 and 60% and is highest in the brecciated zones. Alteration involves saussuritization of the plagioclase and chloritization of the mafic minerals. Minor epidote and pyrite are present locally. The diabase dykes are composed of dark grey, fine-grained, aphyric material

that is also commonly brecciated. The breccia consists of angular fragments, 1-2 cm across, in a comminuted, highly chloritized, matrix. The dyke contacts are presumably intrusive but many are ambiguous because of the brecciation. Veins range from 1-20%, are 1-5 mm wide and are filled with white zeolite. Groundmass alteration ranges from about 15-50% and is highest in the brecciated zones. Secondary minerals are chiefly chlorite with minor epidote.

UNIT IX

Upper Contact:	98.88 m, intrusive, sheared
Lower Contact:	110.50 m, intrusive
Thickness:	11.62 m
Lithology:	Sparsely phyric and aphyric diabase dykes
Cooling Units:	28.01 - 30.05

Ten dykes of light grey, fine- to medium-grained, aphyric to sparsely phyric diabase make up unit IX. Individual dykes range from .38 to 2.33 m and average 1.16 m in vertical thickness. Half of the dykes are aphyric, the other half contain sparse phenocrysts of clinopyroxene and olivine. Where present, the phenocrysts make up 2-3% and range up to about 3 mm across. They are completely replaced by chlorite. One of the dykes (cooling unit 30.04) is intensely brecciated and many others have sheared or brecciated margins. Brecciated areas contain clasts ranging from <1 mm to 2 cm across in a comminuted, highly altered matrix. There are no vesicles per se but several dykes have a few vug-like cavities, up to 1 cm across, lined with small zeolite crystals. Veins range from 2-5%, are up to 1 mm wide, and are filled with zeolite. Groundmass alteration averages about 10% but is significantly higher in the brecciated zones. It involves replacement of mafic minerals by chlorite and of feldspar by saussurite.

UNIT X

Upper Contact:	110.50 m, truncated
Lower Contact:	129.63 m, ambiguous
Thickness:	19.13 m
Lithology:	Microdiorite cut by diabase dykes
Cooling Units:	31.01 - 35.01

A 19.13-m-thick sequence of microdiorite cut by several diabase dykes makes up unit X. The four microdiorite screens range from .64 to 4.93 m and average 1.92 m in vertical thickness. They are light grey, fine- to medium-grained and composed of about 80% feldspar and 20% mafic minerals, chiefly hornblende. Cooling unit 31.01 is slightly phyric with about 3% of black, clinopyroxene crystals up to 2 mm across. Veins and fractures make up about 2-10%, range up to 5 mm wide and are filled with white zeolite, probably laumontite. Groundmass alteration averages about 10-15% but ranges up to 35% in a few slightly sheared zones. Secondary minerals are chiefly chlorite and epidote. Three dykes of fine- to medium-grained, generally aphyric diabase cut the microdiorite. These range from .16 to 8.07 m and average 3.82 m in vertical thickness. Cooling unit 32.02 is sparsely phyric with up to 3% of small, altered olivine crystals. Minor brecciation occurs along many of the dyke contacts and cooling unit 31.02 has zones and bands of brecciation. Breccia clasts range from 1 mm to 2 cm across and are angular to subangular. Veins average 2-3% but range up to 10% in some brecciated zones. They are filled chiefly with white zeolite (laumontite?), locally accompanied by chlorite and minor epidote. Chlorite also replaces mafic minerals in the groundmass. Groundmass alteration averages about 10% but is somewhat higher in the brecciated zones.

UNIT XI

Upper Contact:	129.63 m, ambiguous
Lower Contact:	145.31 m, intrusive
Thickness:	15.68 m
Lithology:	Aphyric to sparsely phyric diabase dykes
Cooling Units:	36.01 - 38.02

A 15.68-m-thick sequence of 8 diabase dykes makes up unit XI. The dykes range from .99 to 5.31 m and average 2.61 m in vertical thickness. Two cooling units, 37.02 and 37.03, are small dyke remnants without any recorded thicknesses. The dykes are light grey, fine-to medium-grained, very slightly phyric diabase. Most contain trace amounts of altered clinopyroxene phenocrysts; the others are completely aphyric. Contacts are intrusive or truncated and commonly show minor brecciation. Veins average 1-2% but are as much as 7-8% in a few thin zones. They range from 1-5 mm wide and are filled with chlorite and white zeolite, probably laumontite. Groundmass alteration ranges from 10-30% and involves replacement of mafic minerals by chlorite.

UNIT XII

Upper Contact:	145.31 m, truncated
Lower Contact:	153.40 m, truncated
Thickness:	8.09 m
Lithology:	Microdiorite cut by diabase dykes
Cooling Units:	40.01 - 42.03

Unit XII is a relatively thin sequence of microdiorite cut by two diabase dykes. The three microdiorite screens range from .10 to 2.10 m in vertical thickness. They consist of pale grey, medium-grained, plagioclase-rich material composed of about 55-65% plagioclase, 30-35% mafic minerals, chiefly amphibole, and 1-2% opaques. Sparse microphenocrysts of clinopyroxene range up to about 2 mm across. Narrow shear zones have produced minor brecciation at several levels. Veins range from about 1-5% and are up to 15 mm wide. An early generation of epidote and chlorite veins is cut by later zeolite veins. Groundmass alteration in the microdiorite chiefly involves replacement of mafic minerals by epidote and chlorite and averages 10-15%. The two dykes consist of light grey, fine-grained, massive, aphyric diabase locally cut by narrow shear zones. Veins average about 2%, range up to 2 mm wide, and are filled with zeolite. Groundmass alteration ranges from 15-30%, generally increasing with increasing grain size. It chiefly involves replacement of mafic minerals by chlorite.

UNIT XIII

Upper Contact:	153.40 m, intrusive
Lower Contact:	227.90 m, intrusive
Thickness:	74.50 m
Lithology:	Aphyric to sparsely phyric diabase dykes
Cooling Units:	42.04 - 61.01

A 74.50-m-thick sequence of generally aphyric or sparsely phyric diabase dykes makes up unit XIII. One dyke (cooling unit 43.03) is highly phyric with 30-35% clinopyroxene and olivine phenocrysts. In the other dykes, phenocrysts rarely exceed 3% and many dykes are entirely aphyric. The 35 dykes in this unit range from .05 to 21.98 m and average 2.16 m in vertical thickness. Most have one or more intrusive contacts; the others are identified as dykes on the basis of their textures. Both phyric and aphyric varieties are light-grey, fine- to medium-grained, massive rocks with little brecciation except along some contacts. Cooling unit 42.04 is highly brecciated with several narrow shear zones cutting the core. Where present, phenocrysts are generally small, subhedral crystals of clinopyroxene now altered to chlorite. Olivine is rare except in cooling unit 43.03. Vesicles are absent except in cooling unit 53.03 where they make up 1-2% of the rock. These are 1-2 mm across, irregular in shape, and filled with chlorite. Veins average 2-3% but range up 10% in some intervals. Most are hairline to 2 mm wide and are filled with zeolite, accompanied by minor epidote and chlorite. Groundmass alteration ranges from 5-60% and averages about 10%. It involves chloritization of the mafic minerals, particularly along fractures and veins.

UNIT XIV

Upper Contact:	227.90 m, truncated
Lower Contact:	228.89 m, truncated
Thickness:	.99 m
Lithology:	Microdiorite
Cooling Units:	62.01

A single screen of light grey, fine-grained, very slightly phyric microdiorite makes up unit XIV. Small phenocrysts, 1-2 mm across, of amphibole or pyroxene make up about 1%. Veins are small and sparse, generally less than 1 mm wide and never exceed 1%. They are filled with early epidote and later white zeolite. The groundmass is about 20% altered to chlorite and saussurite. Considerable bleaching of the groundmass is apparent along some fractures.

UNIT XV

Upper Contact:	228.89 m, intrusive
Lower Contact:	231.24 m, intrusive
Thickness:	2.35 m
Lithology:	Aphyric diabase dykes
Cooling Units:	62.02 - 62.06

A thin sequence of grey, fine- to medium-grained, generally massive, aphyric diabase dykes make up unit XV. Cooling unit 62.03 is a thin zone of highly sheared rock, probably fault gouge. Individual dykes range from .05 to 1.00 m and average .47 m in vertical thickness. Vesicles are absent but cooling unit 63.01 has a few zeolite-lined vugs up to 15 mm across. Veins average 2-3% overall and are up to 10 mm wide. They are filled chiefly with zeolite and minor chlorite. Groundmass alteration ranges from 10-40% and involves replacement of mafic minerals by chlorite.

UNIT XVI

Upper Contact: 231.70 m, faulted
Lower Contact: 244.90 m, faulted
Thickness: 13.20 m
Lithology: Massive and sheared microgabbro
Cooling Units: 63.01 - 65.01

Unit XVI consists of a highly sheared and brecciated sequence, 13.20 m thick, of microgabbro. Cooling units 63.10, 63.03 and 63.05 are relatively massive whereas units 63.02 and 64.01 are intensely sheared and fractured. All of the contacts within unit XVI are faulted or truncated, thus the origin of the sequence is not clear. The massive portions of the unit are relatively coarse-grained, suggesting that the material may be a microgabbro screen. Alternatively, the sequence may consist of one or more coarse-grained diabase dykes whose contacts have been obscured by faulting. Cooling unit 63.01 is slightly finer grained than the rest of the unit and has trace amounts of clinopyroxene microphenocrysts up to 2 mm across. The brecciated portions contain angular clasts, 2-20 mm across, in a comminuted matrix of the same material. There are no vesicles but cooling unit 63.01 contains a few zeolite-lined vugs up to 15 mm across. Veins range from 1-5% and average about 2% overall. They range up to 10 mm wide and are filled with zeolite and minor chlorite. Groundmass alteration varies from about 10% in the massive portions to 40% in the brecciated zones. Mafic minerals are partly to completely replaced by chlorite and the breccia matrix is altered to a mixture of chlorite, epidote and zeolite.

UNIT XVII

Upper Contact: 244.90 m, intrusive(?)
Lower Contact: 248.88 m, ambiguous
Thickness: 3.98 m
Lithology: Aphyric and slightly phyric diabase dykes
Cooling Units: 66.01 - 67.06

A thin sequence of light grey, fine- to medium-grained, aphyric to sparsely phyric, generally massive diabase dykes makes up unit XVII. Individual dykes range from .06 to 2.27 m and average .65 m in vertical thickness. Cooling unit 67.03 is a zone of fault breccia. Most of the rocks are aphyric but cooling units 66.01 and 67.02 contain small microphenocrysts of altered clinopyroxene. Vesicles are absent in all but cooling unit 67.05 where they make up about 1% and range up to 1 mm across. They are filled with zeolite. Veins average 1-2% overall but are up to 5% in some zones. Most are less than 3 mm wide and are lined with chlorite and filled with white zeolite. Groundmass alteration ranges from about 10-40% being highest in the coarser-grained portions. Mafic minerals are partly replaced by chlorite and plagioclase by saussurite.

UNIT XVIII

Upper Contact: 248.88 m, ambiguous
Lower Contact: 283.57 m, truncated
Thickness: 34.69 m
Lithology: Microdiorite cut by diabase dykes
Cooling Units: 67.07 - 75.02

A 34.69-m-thick sequence of microdiorite cut by numerous diabase dykes makes up unit XVIII. Thirteen cooling units of microdiorite are present as dyke screens. These range from .08 to 4.18 m and average 1.56 m in vertical thickness. With the possible exception of cooling unit 68.02, these all have truncated contacts. One contact on 68.02 appears to be intrusive but the evidence is ambiguous. The rocks are very light grey, fine- to medium-grained and aphyric. Some are logged as microdiorite, some as andesite based on a finer grain size. Several of the dykes are weakly brecciated, particularly along contacts, but most are massive. Cooling unit 68.03 has about 1% of small, subrounded clots of chlorite which could be altered crystals or possibly small vesicles. Veins are small and sparse, never exceeding 1% of the rock. Most are hairline stringers of zeolite. Groundmass alteration ranges from 10-20% and chiefly involves chloritization of the mafic minerals. Some of the feldspar is also saussuritized. Locally, the rock is bleached in narrow zones along fractures and veins. Thirteen diabase dykes cut this sequence. They are distinguished on the basis of colour, grain size and the presence of one or more intrusive contacts. Individual dykes range from .06 to 8.33 m and average 1.11 m in vertical thickness. Most of the dykes consist of grey, fine- to medium-grained, massive, aphyric diabase; a few (e.g. cooling units 74.01 and 75.01) contain 1-2% of clinopyroxene and olivine microphenocrysts up to 1 mm across. Veins make up about 1% of the unit, range up to 15 mm wide and are filled with early chlorite and epidote and later zeolite. Groundmass alteration to chlorite and epidote averages about 15-20%.

UNIT XIX

Upper Contact: 283.57 m, intrusive
Lower Contact: 307.35 m, intrusive
Thickness: 23.78 m
Lithology: Dykes
Cooling units: 76.01 - 82.03

A series of relatively uniform, grey, fine- to medium-grained, aphyric dykes makes up Unit XIX. The sequence is 23.78 m thick and consists of 15 distinct cooling units, most of which have sharp, steeply-dipping, chilled margins. Individual dykes range from .08 to 5.03 m and average 1.58 m in vertical thickness. Some of the dykes (e.g. cooling units 76.05 and 77.01) are brecciated, particularly along their contacts. Vesicles are non-existent but veins are fairly common. In most cooling units they make up less than 1% of the rock but they range up to 10% in cooling unit 76.02. They vary from hairline to about 3 mm wide and are filled largely with chlorite and zeolite, probably laumontite. Some fractures are also coated with chlorite. Groundmass alteration is difficult to estimate but is on the order of 20-25%, and involves replacement of plagioclase and pyroxene by chlorite and clay minerals. In some cases, the rocks are bleached adjacent to zeolite veins.

UNIT XX

Upper Contact:	307.35 m, truncated
Lower Contact:	361.00 m, truncated
Thickness:	51.20 m
Lithology:	Dykes with gabbro screens
Cooling units:	82.04 - 97.03

Unit XX is a 51.20-m-thick sequence of dykes with screens of plutonic rock. Of the 38 cooling units in this sequence 23 are dykes and 15 are plutonic rocks. The dykes are lithologically similar to those of Unit XIX and consist of grey, massive, fine-to medium-grained aphyric diabase. Most of the dykes have well defined chilled margins although some are truncated by intrusive contacts on adjacent cooling units. A few have minor breccia zones along their margins. The grain size within individual dykes normally increases systematically from the chilled margins to the centres but in a few cases irregular, coarse-grained patches are surrounded by finer-grained material. The dykes range from .07 to 6.72 m and average 1.05 m in vertical thickness. No vesicles are present. Veins average about 1% overall and range up to 2 mm in width. They are commonly lined with chlorite and filled with zeolite, probably laumontite. Minor hematite is also present and some veins have trace amounts of quartz and epidote. Groundmass alteration is variable and chiefly involves replacement of mafic minerals by chlorite. Weak staining occurs along some fractures. Cooling unit 97.02 is a .15-m-thick section of diabase containing about 10% veins filled with epidote, quartz and fine-grained siliceous material. It may be a small shear zone. The screens of plutonic rock range from .06 to 2.93 m and average .89 m in vertical thickness. They consist of light grey, medium-to coarse-grained, fairly uniform diorite or gabbro composed of about 70% plagioclase, 25% clinopyroxene and hornblende and 5% magnetite. Some rocks have a mottled texture produced by leucocratic patches composed entirely of plagioclase. A few units (e.g. cooling units 92.01 and 92.02) are very coarse-grained, essentially pegmatitic diorite. In unit 92.02 the pegmatitic material occurs in irregular patches. Veins are generally less than 1% of the rock but may be up to 3 or 4% in local concentrations. They are filled largely with zeolite, probably laumontite, and calcite but locally contain minor epidote. Groundmass alteration is quite extensive and involves replacement of most mafic minerals by chlorite. Many of the feldspars are cloudy, suggesting partial replacement by clay minerals and/or chlorite.

UNIT XXI

Upper Contact:	361.00 m, intrusive
Lower Contact:	418.42 m, intrusive
Thickness:	57.42 m
Lithology:	Dykes
Cooling units:	98.01 - 112.04

A 57.42-m-thick sequence of diabase dykes makes up Unit XXI. Twenty dykes are present in this sequence ranging from .15 to 6.41 m and averaging 2.87 m in vertical thickness. Most have sharp, steeply-dipping, chilled margins, although a few are truncated. Most of the dykes are dark grey, fine- to medium-grained, aphyric rocks composed of about equal amounts of plagioclase and mafic minerals. A few (e.g. cooling units 101.03 and 108.02) are coarse-grained, with almost microgabbroic textures. However, these are interpreted as dykes because they fine toward chilled margins. Small zones of brecciation occur along several dyke margins. A few dykes, such as cooling units 99.01, 101.01, 104.01 and 112.03, contain small, sparse (<5%) phenocrysts. These are probably clinopyroxene crystals completely replaced by chlorite. Cooling unit 98.02 has a patchy appearance due to the presence of elliptical features (ocelli?) up to 8 mm across, which contain plagioclase, black pyroxene(?) and a brown mineral which could be altered olivine. Veins make up 1-5% of the sequence and range up to about 10 mm wide. They are filled chiefly with laumontite(?), minor epidote, carbonate and chlorite. Groundmass alteration is variable. Most of the mafic minerals are replaced by chlorite and some of the plagioclase is cloudy, suggesting partial alteration to clay minerals. Narrow bleached zones occur along some veins.

UNIT XXII

Upper Contact: 418.42 m, truncated
Lower Contact: 439.50 m, truncated
Thickness: 21.08 m
Lithology: Dykes with gabbro screens
Cooling units: 113.01 - 118.04

Unit XXII is a sequence of 10 diabase dykes with minor screens of plutonic rock. The dykes range from .18 to 6.05 m and average 1.94 m in vertical thickness. Most have sharp, steeply-dipping chilled margins, but a few contacts are truncated or ambiguous. The dykes are grey, fine- to medium-grained, massive rocks. Most are aphyric but one thick dyke (cooling unit 114.01) has about 2% of small clinopyroxene crystals up to 2 mm across. This dyke also contains a few small xenoliths of gabbro and trondhjemite. Veins make up 2-5% of most dykes but are up to 10% in some brecciated ones. They range from hairline to 10 mm wide and are filled chiefly with laumontite(?), locally accompanied by small amounts of chlorite, calcite and epidote. Groundmass alteration is variable and involves replacement of mafic minerals by chlorite. The screens of plutonic rock are narrow (maximum 1 m) masses of diorite and gabbro. Contacts with the dykes are always truncated. The diorite (cooling unit 113.01) is a fine- to coarse-grained, leucocratic rock composed of about 65% plagioclase, 25% amphibole and 10% magnetite. Gabbroic material (cooling units 115.01 and 118.04) is similar to the diorite but is composed chiefly of plagioclase and clinopyroxene with lesser amphibole. Veins make up 2-3% of the plutonic rocks and consist chiefly of laumontite(?). Some fractures are coated with chlorite. Most of the mafic minerals are partly to completely replaced by chlorite and the plagioclase is cloudy. Pyrite is locally disseminated in the groundmass.

UNIT XXIII

Upper Contact: 439.50 m, intrusive
Lower Contact: 484.09 m, truncated
Thickness: 44.59 m
Lithology: Dykes
Cooling units: 118.05 - 128.01

Unit XXIII is a sequence of relatively thick, aphyric and sparsely phyric dykes. Individual dykes range from .15 to 7.50 m and average 2.79 m in vertical thickness. They typically have sharp, steeply-dipping chilled margins but some contacts are truncated or ambiguous. Most of the dykes are grey, fine- to medium-gained, massive, aphyric diabase. Four of the 20 cooling units (119.02, 120.01, 125.02 and 125.03) are slightly phyric and have <1% of altered clinopyroxene crystals up to about 1 mm across. Rare gabbro xenoliths, up to 10 cm across, are locally present and a few dykes have fine-grained inclusions. Veins make up 1-2% and range up to about 2 mm wide. They are filled largely with laumontite(?) with lesser amounts of epidote, chlorite and calcite. Groundmass alteration is variable from about 30 to 100% and involves nearly complete replacement of the mafic minerals by chlorite and locally epidote. The most intensely altered zones are adjacent to chlorite veins.

UNIT XXIV

Upper contact: 484.09 m, intrusive
Lower Contact: 521.15 m, ambiguous
Thickness: 37.06 m
Lithology: Thin dykes with diorite screens
Cooling units: 130.01 - 139.01

Unit XXIV is a 37.06-m-thick sequence of thin diabase dykes with two diorite screens. The dykes are lithologically similar to those of Unit XXIII and the distinction between the two sequences is simply on the average thickness of individual units. These cooling units range from .02 to 6.13 m but average only .71 m in vertical thickness. Of the 52 cooling units in this sequence only 10 are over 1 m in vertical thickness. Most are bounded by sharp, steeply-dipping chilled margins but a few contacts are truncated or ambiguous. Minor breccia occurs along some dyke contacts. The dykes consist of grey, fine- to medium-grained, massive aphyric diabase composed of about 60% plagioclase, 35% clinopyroxene and 5% iron oxides. Rare inclusions of coarser-grained material are locally present. Veins make up <1% to 5% of individual units and are mostly 1-2 mm wide. They are filled chiefly with white zeolite (laumontite?) and lesser amounts of epidote and calcite. A few zeolite veins also contain small amounts of chlorite and/or hematite. Monomineralic veins of epidote are also present. Groundmass alteration is variable from about 20-80% and involves replacement of mafic minerals by chlorite and plagioclase by clay minerals. Only two diorite screens are present (cooling units 130.08 and 133.02) and the largest is .54-m in vertical thickness. These are leucocratic, medium- to coarse-grained rocks composed of about 50-60% plagioclase, 35% clinopyroxene, 10-15% amphibole and minor iron oxides. The rocks commonly have a mottled texture due to irregular patches rich in plagioclase. Veins average about 3% and are mostly less than 1 mm wide. They are filled with laumontite(?) and epidote. Groundmass alteration is variable, between about 15 and 80%, and involves replacement of mafic minerals by chlorite and of plagioclase by clay minerals. Very extensive alteration occurs along some veins.

UNIT XXV

Upper Contact: 521.15 m, ambiguous
Lower Contact: 531.24 m, truncated
Thickness: 10.09 m
Lithology: Dykes with plutonic screens
Cooling units: 139.02 - 141.05

Unit XXV consists of 10 diabase dykes and 4 gabbroic or dioritic screens. It differs from Unit XXIV largely in the proportion of plutonic material. Most dykes have sharp, steeply-dipping, chilled margins but some have truncated or ambiguous contacts. They range from .12 to 3.48 m and average 1.28 m in vertical thickness. The dykes consist of light grey to greenish-grey, fine- to medium-grained, massive, aphyric diabase composed of plagioclase, clinopyroxene and iron oxides. The two thickest cooling units (139.04 and 140.02) are very slightly phyric and contain about 1% of small clinopyroxene crystals. Veins are highly variable from <1% to 80% of individual units. Cooling unit 141.02, which is .19 m thick, consists almost entirely of epidote and zeolite veins. Groundmass alteration is fairly extensive causing colour differences in the rock. Greenish-grey rocks are extensively replaced by epidote and chlorite whereas light grey varieties have more quartz. The plutonic screens consist of both gabbro and leucocratic diorite. The gabbros are light grey, coarse-grained rocks composed of about 60% plagioclase, 30% clinopyroxene and amphibole and 10% opaques. The dioritic material is similar to the gabbro but is lighter coloured, finer grained and somewhat more felsic. Veins average about 1-2% of these rocks and are filled chiefly with zeolite and minor epidote. Groundmass alteration is manifested in chloritization of the mafic minerals and saussuritization of the plagioclase.

UNIT XXVI

Upper Contact: 531.24 m, intrusive
Lower Contact: 546.54 m, intrusive
Thickness 15.30 m
Lithology: Dykes
Cooling units: 142.01 - 146.02

A 15.30-m-thick sequence of diabase dykes makes up Unit XXVI. The 21 dykes in this sequence range from .06 to 3.00 m and average .72 m in vertical thickness. Most dykes have sharp, steeply-dipping, chilled margins but some are truncated or have ambiguous contacts. They consist of light grey, fine- to medium-grained, massive, mostly aphyric diabase composed of about 60-65% plagioclase, 30-35% clinopyroxene and 5% iron oxides. A few mafic segregations are present in some of the dykes. Several of the cooling units are slightly clinopyroxene phyric and one (cooling unit 143.01) has about 30% phenocrysts. These are euhedral crystals of clinopyroxene, ranging up to 4 mm across, which are concentrated in the centre of a small dyke. Veins average 1-3% of most units and are mostly less than 1 mm wide. They are filled with zeolite and minor calcite. Small dark, shiny crystals occur in some veins and on fracture surfaces. Groundmass alteration is extensive and involves saussuritization of the plagioclase and chloritization of the mafic minerals. Cooling unit 145.04, a thin dyke, is almost completely altered to epidote and zeolite. It has a mottled grey to pinkish-grey colour.

UNIT XXVII

Upper Contact: 546.54 m, truncated
Lower Contact: 570.74 m, truncated
Thickness: 24.20 m
Lithology: Dykes with gabbro screens
Cooling units: 146.03 - 152.04

A sequence of relatively thin diabase dykes and gabbro screens makes up Unit XXVII. Fifteen of the 23 cooling units in this 24.20-m-thick sequence are dykes. These range from .06 to 5.57 m and average 1.32 m in vertical thickness. They are characterized by sharp, steeply-dipping, chilled margins but some contacts are truncated or ambiguous. There is no brecciation along contacts but some units are heavily fractured and veined. A number of dykes contain small xenoliths of coarser-grained gabbro similar to the screens. The dykes consist of grey, fine-to medium-grained, massive, aphyric diabase composed of about 60-65% plagioclase, 30-35% mafic minerals and 5% opaques. Coarser-grained lenses or patches of similar lithology are present locally. Veins make up less than 1% of most units but are more abundant in narrow zones of intense fracturing. They range up to about 2 mm wide and are filled with epidote, zeolite (laumontite?) and minor gypsum(?). Groundmass alteration is quite variable and commonly irregular. Mafic minerals are partly replaced by chlorite and epidote, and plagioclase is saussuritized. Light coloured zones of more intense alteration are present in a few units. The gabbro screens are somewhat thicker than those in the overlying units and range from .09 to 1.53 m in vertical thickness. They all have contacts truncated by the adjacent dykes. The rocks are varicoloured and mottled in various shades of white, green, grey and brown. They are medium- to coarse-grained and have a variable mineralogy averaging about 50% plagioclase and 50% mafic minerals. The lighter-coloured zones are typically richer in plagioclase. Sparse, thin veins are filled chiefly with zeolite, probably laumontite. The mottled appearance of these rocks reflects variations in the proportions of both primary and secondary minerals.

Groundmass alteration varies from about 40 to 80% and involves saussuritization of the plagioclase and replacement of the mafic minerals by chlorite and epidote.

UNIT XXVIII

Upper Contact:	570.74 m, intrusive
Lower Contact:	613.75 m, intrusive
Thickness:	43.01 m
Lithology:	Dykes with gabbro screens
Cooling units:	152.05 - 162.02

Unit XXVIII is a 43.01-m-thick sequence of dykes with some gabbro screens. This unit is distinguished from Unit XXVII by the sparsely phyric nature of many of the dykes. Twenty-two of the 30 cooling units in this sequence are dykes. They range from .11 to 7.01 m and average 1.66 m in vertical thickness. Contacts are sharp, typically intrusive or truncated. Minor brecciation is observed in several units. Most of the dykes consist of grey, fine- to medium-grained, massive, aphyric diabase composed of about 65% plagioclase, 30% mafic minerals and 5% opaques. Eight of the dykes are sparsely phyric and contain 1-4% of small, dark crystals, probably altered clinopyroxene. The phyric dykes are randomly scattered through the unit and are not correlated with thickness. They have both chilled and truncated contacts, thus no obvious age relations are present. Veins make up 1-3% and range up to about 5 mm wide. They are filled with zeolite, probably laumontite, locally accompanied by chlorite and epidote. The rocks appear to be completely altered but they still retain their primary igneous textures. The plagioclase is saussuritized and the mafic minerals are replaced by chlorite and epidote. The 8 gabbro screens in this sequence range from .23 to 2.05 m and average .86 m in vertical thickness. They all have contacts truncated by the adjacent dykes. Most are grey to dark grey, coarse-grained gabbro composed on average of 50% plagioclase and 50% mafic minerals. Some contain abundant green amphibole. Some also show significant variations in grain size and mineral proportions. Many are somewhat sheared and altered. Veins are up to 5% in some units and range from 1-5 mm in width. Zeolite (laumontite?) is the most common filling but minor carbonate is also present. The plagioclase is completely saussuritized and the mafic minerals are partly replaced by chlorite and amphibole(?).

UNIT XXIX

Upper Contact:	613.75 m, truncated
Lower Contact:	633.02 m, sheared
Thickness:	19.27 m
Lithology:	Gabbro
Cooling units:	163.01 - 164.06

Unit XXIX is a 19.27-m-thick sequence of gabbro between two series of diabase dykes. Nine cooling units, ranging from .18 to 12.17 m in vertical thickness, are recognized in this sequence. Most of the contacts between cooling units are gradational and reflect changes in grain size or mineralogy. A few are sheared and brecciated. The rocks consist chiefly of grey, medium- to coarse-grained, commonly homogeneous material composed of 50-60% plagioclase and 40-50% mafic minerals. Some leucocratic zones and layers are richer in plagioclase. Veins range from 1-5% and are up to 5 mm wide. They are filled chiefly by laumontite(?) with minor epidote and chlorite. Most of the mafic minerals are replaced by amphibole or chlorite and the plagioclase by saussurite.

UNIT XXX

Upper contact:	633.02 m, sheared
Lower contact:	653.30 m, truncated
Thickness:	20.28 m
Lithology:	Thin dykes
Cooling units:	167.01 - 172.07

A 16.06-m-thick sequence of relatively thin dykes makes up Unit XXX. Twenty-five cooling units are recognized, ranging from .07 to 6.72 m and averaging .82 m in vertical thickness. Most have sharp, steeply-dipping, chilled margins but a few have truncated or ambiguous contacts. The dykes consists of grey, fine- to medium-grained, massive, mostly aphyric diabase composed of about 50-60% plagioclase and 40-50% mafic and opaque minerals. Rare felsic layers are present locally and opaques make up as much as 15% of some samples. Six of the dykes are sparsely phyric with about 1-3% of altered clinopyroxene crystals about 1 mm across. Cooling units 172.01, 172.03 and 172.05, which are probably all parts of the same dyke, contain about 10% clinopyroxene phenocrysts up to 1 mm across. Veins make up about 1% of the dykes. They range from hairline to 1 mm in width, and are filled chiefly with white zeolite (laumontite?). Groundmass alteration is extensive but in most cases has not destroyed the original igneous textures. It involves replacement of the mafic minerals by chlorite and of the plagioclase by saussurite. Cooling unit 171.01 is highly altered and bleached diabase consisting largely of chlorite and saussurite. A few

grains of sulphide are also present in this unit.

UNIT XXXI

Upper contact:	653.30 m, truncated
Lower contact:	676.20 m, intrusive
Thickness:	22.90 m
Lithology:	Dykes and gabbro screens
Cooling units:	172.08 - 178.03

A 22.90-m-thick sequence of largely diabase dykes with some gabbro screens makes up Unit XXXI. Sixteen of the 24 cooling units in this sequence are dykes. They range from .04 to 3.13 m and average .91 m in vertical thickness. Most dykes have sharp, steeply-dipping chilled margins but a few have truncated contacts. The dykes consist chiefly of greenish-grey, fine- to medium-grained, massive, aphyric diabase composed of about 50-60% plagioclase and 40-50% mafic and opaque minerals. Irregular patches with gradational boundaries are found in some dykes. One dyke has traces of altered clinopyroxene crystals up to 1 mm across. One cooling unit (174.04) is a narrow dyke or vein of light grey, leucocratic material, probably plagiogranite. Veins make up 1% of most dykes and range up to about 3 mm wide. They are filled chiefly with zeolite and epidote. Groundmass alteration is fairly extensive and involves saussuritization of the feldspar and chloritization of mafic minerals. It is most extensive near felsic veins where the rock is commonly bleached. The 8 gabbro screens range from .10 to 4.09 m and average 1.08 m in vertical thickness. Individual screens are all truncated by dykes but cooling unit boundaries within the gabbros are gradational, reflecting changes in grain size or mineralogy. The screens consist of light grey, fine- to coarse-grained gabbro composed of about 50-60% plagioclase and 40-50% mafic minerals, largely clinopyroxene and hornblende. Some darker coloured layers have up to 70% mafic minerals and irregular leucocratic patches have high plagioclase contents. Cooling unit 173.01 shows some layering with alternating bands of finer- and coarser-grained material. Sparse (<1%), narrow veins are filled largely with white zeolite, probably laumontite. Groundmass alteration is variable, probably from about 30% to 80% and involves uralitization of the pyroxenes and saussuritization of the plagioclase. Epidote is abundant in most rocks. Cooling unit 176.01 is a bleached, fine-grained gabbro, rich in plagioclase.

UNIT XXXII

Upper contact:	676.20 m, truncated
Lower contact:	682.32 m, truncated
Thickness:	6.12 m
Lithology:	Gabbro and diorite
Cooling units:	178.04 - 179.05

A sequence of gabbro and diorite, 6.12 m thick, makes up Unit XXXII. Ten cooling units have been recognized, ranging from .08 to 1.60 m and averaging .61 m in vertical thickness. The sequence is truncated top and bottom by adjacent dykes but internal contacts are mostly gradational, reflecting changes in grain size, mineralogy and degree of alteration. Most of the rocks are grey to light grey, fine- to medium-grained, fairly uniform gabbro composed of 60-70% plagioclase, 30-40% mafic minerals and traces of opaques. Several cooling units have weak phase layering defined by alternating bands rich in plagioclase and mafic minerals. Some layers are dioritic in composition and one cooling unit (178.07) is a thin band of diorite composed of about 80% plagioclase and 20% amphibole. Veins average about 1% and range up to about 5 mm across. They are filled chiefly with white zeolite (laumontite?) and minor epidote. Cooling unit 179.03 has about 15% of vugs filled with gypsum(?), carbonate and an unidentified dark coloured mineral. Groundmass alteration is variable ranging from about 20% to 80%. Plagioclase is largely saussuritized and the primary mafic minerals are amphibolitized. Minor sulphide mineralization is present in a few units. Commonly, alteration is most intense adjacent to veins.

UNIT XXXIII

Upper contact:	682.32 m, intrusive
Lower contact:	710.73 m, ambiguous
Thickness:	28.41 m
Lithology:	Gabbro cut by thin dykes
Cooling units:	179.06 - 186.03

Unit XXXIII is a 28.41-m-thick sequence composed largely of gabbro cut by thin diabase dykes. Some of the cooling units identified as dykes have truncated contacts and relatively coarse grain sizes and may be microgabbros. However, they are lithologically most similar to known dykes and are classified as diabase. Cooling unit 184.01 is thin layer of fault breccia. Only 8 of the 22 cooling units in this sequence are gabbro but they account for the bulk of the unit. The gabbros range from .12 to 5.57 m and average 2.45 m in vertical thickness. They consist of grey, medium-grained, relatively uniform material with about equal amounts of plagioclase and mafic minerals. Some layers have a mottled appearance due to the presence

of coarser-grained magmatic segregations. Some layers are more felsic than the average. Veins make up 1-2% of the gabbros and range up to 5 mm in width. They are filled mostly with white zeolite, locally accompanied by epidote. Groundmass alteration is highest in the leucocratic zones and involves replacement of the plagioclase by epidote and sericite and of the mafic minerals by amphibole and chlorite. Epidote is locally abundant, particularly near veins. The dykes and probable dykes are grey, fine- to medium-grained, aphyric diabase. Definite dykes have sharp, steeply-dipping chilled margins but a number of probable dykes have truncated contacts. Modal compositions average about 50-60% plagioclase and 40-50% mafic minerals. Overall, veins are sparse but they range up to 10% in a few cooling units. They are 1-3 mm wide and filled chiefly with white zeolite and minor carbonate. Groundmass alteration involves nearly complete saussuritization of the plagioclase and amphibolitization of the mafic minerals. The fault breccia of cooling unit 184.01 marks a small shear zone in the gabbro. Intense fragmentation is accompanied by alteration to chlorite and epidote.

UNIT XXXIV

Upper contact:	710.73 m, ambiguous
Lower contact:	720.56 m, ambiguous
Thickness:	9.83 m
Lithology:	Gabbro
Cooling units:	186.04 - 188.05

A sequence of fine- to medium-grained, generally homogeneous gabbro, 9.83 m thick, makes up Unit XXXIV. The sequence is cut by dioritic veins (cooling units 188.03 and 188.05). Contacts between individual cooling units are transitional or sheared and three of the units (186.04, 187.02 and 188.01) are sheared and brecciated throughout. The ten cooling units of gabbro range from .12 to 2.59 m and average .97 m in vertical thickness. The dioritic veins are .05 and .11 m thick, respectively. The gabbros consist of about equal amounts of plagioclase and mafic minerals but leucocratic varieties are also present. Many units also have irregular patches of leucocratic material. The veins consist of fine-grained diorite or leucogabbro composed of about 60% plagioclase and 40% amphibole. Small, sparse zeolite veins are locally present. Many of the gabbros are extensively altered and recrystallized. The most intense recrystallization occurs in deformed zones. The plagioclase is saussuritized and the original mafic minerals have been completely amphibolitized.

UNIT XXXV

Upper contact:	720.56 m, transitional
Lower contact:	749.21 m, intrusive
Thickness:	28.65 m
Lithology:	Dykes and gabbro screens
Cooling units:	189.05 - 195.03

Unit XXXV is a mixed unit, 28.65 m thick, composed of approximately equal numbers of dykes and gabbro screens. Eleven dykes are present ranging from .69 to 2.81 m and averaging 1.57 m in vertical thickness. Contacts between the dykes are not as clear as in many other units. Some contacts are clearly intrusive but others are ambiguous or even gradational. Even definitely intrusive contacts lack well-developed chilled zones. The dykes consist of grey, fine-grained, generally uniform, aphyric diabase containing 55-60% plagioclase and 40-45% mafic minerals and opaques. A few rocks contain small patches or xenoliths of medium-grained gabbro. Veins are small (1-2 mm) and sparse, generally less than 2%. They are filled entirely with white zeolite (laumontite?). The host rock is extensively saussuritized and amphibolitized. The gabbroic rocks are grey, fine- to medium-grained and slightly layered. Modal mineralogy is about 40-50% plagioclase, 30-35% amphibole and 15-20% pyroxene. The faint layering is defined by small changes in grain size and slight variations in mineral proportions. Coarser-grained segregation patches are locally present and are typically more felsic than the host rock. Veins are $<1\%$, range up to 2 mm in width and are filled with white zeolite. Groundmass alteration involves variable saussuritization and amphibolitization.

UNIT XXXVI

Upper contact:	749.21 m, truncated
Lower contact:	762.71 m, truncated
Thickness:	13.50 m
Lithology:	Gabbro
Cooling units:	196.01 - 199.02

Unit XXXVI is a 13.50-m-thick sequence of gabbro with several veins and patches of leucocratic material, probably plagiogranite. The gabbroic units range from .50 to 3.19 m and average 1.67 m in vertical thickness. They consist of medium- to coarse-grained, rather variable gabbro composed of about 50-60% plagioclase and 40-50% mafic minerals, chiefly pyroxene, amphibole and opaques. Regular layering is not visible but some of the rocks have an irregular, mottled appearance due to the presence of leucocratic, presumably feldspathic, veins. The plagiogranite veins consist of white, mottled material containing quartz, plagioclase and minor K-feldspar(?). In the gabbros,

veins are small (1-2 mm), sparse (<1%) and filled almost entirely with white zeolite. In the plagiogranites, veins are larger (up to 5 mm) and more abundant (2-3%) but still filled with zeolite. Plagioclase in the rock is largely saussuritized and the pyroxene replaced by amphibole and chlorite.

UNIT XXXVII

Upper contact: 762.71 m, intrusive
Lower contact: 805.35 m, sheared
Thickness: 42.64 m
Lithology: Dykes and gabbro screens
Cooling units: 199.03 - 209.02

A 42.64-m-thick sequence of diabase dykes with gabbro screens makes up Unit XXXVII. Of the 22 cooling units in this sequence, half are dykes and half are gabbros. The dykes range from .07 to 7.07 m and average 2.40 m in vertical thickness. Most of them have sharp, steeply-dipping chilled margins but a few have truncated or ambiguous contacts. The dykes consist of light to dark grey, fine- to medium-grained, aphyric, generally massive, diabase composed of approximately equal amounts of plagioclase and mafic minerals. Veins are small and sparse and are filled entirely with white zeolite. Groundmass alteration is quite variable. Cooling unit 199.03 is dark grey and appears to be relatively fresh whereas the other dykes are lighter in colour, presumably reflecting more intense saussuritization. In some of the dykes there are small patches of more intense alteration composed of plagioclase, chlorite, amphibole and pyrite. The gabbros are light to medium-grey, medium- to coarse-grained rocks composed of 30-35% plagioclase, 20-25% clinopyroxene, 40-45% amphibole and 5% opaques. Thus, most of these rocks are more mafic than the gabbros in overlying units. There appears to be little grain size or phase layering. Veins are <1%, 1-2 mm wide and are filled with zeolite. Groundmass alteration is moderate with plagioclase being partly replaced by zeolite, clinopyroxene by amphibole and amphibole by chlorite.

UNIT XXXVIII

Upper contact: 805.35 m, sheared
Lower contact: 806.97 m, sheared
Thickness: 1.62 m
Lithology: Fault breccia
Cooling units: 209.03

Unit XXXVIII is a single cooling unit, 1.62 m thick, of white to light brown, sheared and altered gabbro. The original texture is largely obliterated and there are many slickensided surfaces. Hairline veins make up 2-3% of the unit and are filled with zeolite. The groundmass is nearly completely altered to chlorite, epidote, silica and zeolite.

UNIT XXXIX

Upper contact: 806.97 m, faulted
Lower contact: 859.35 m, faulted
Thickness: 52.38 m
Lithology: Dykes with gabbro screens
Cooling units: 210.01 - 222.02

Unit XXXIX is a 52.38-m-thick sequence of diabase dykes and gabbro screens lying between two faults. Ten cooling units are recognized; 5 dykes and 5 gabbros. The dykes range from .73 to 4.37 m and average 2.60 m in vertical thickness. Most have one or more steeply-dipping chilled margins attesting to their intrusive origin. They consist of grey, fine- to medium-grained, aphyric diabase composed of about 50% plagioclase and 50% mafic and opaque minerals. A few dykes have irregular leucocratic patches or layers. Veins make up <1% but range up to 20 mm wide. Early veins are filled with quartz and epidote whereas later ones contain chlorite and white zeolite. Groundmass alteration is limited and involves mostly partial replacement of the mafic minerals by chlorite. The gabbros form relatively thick masses, ranging up to 19.68 m in vertical thickness. Most of these cooling units have truncated contacts with the adjacent dykes. The rocks are chiefly grey, fine- to medium-grained and fairly uniform. An average mode is 50% plagioclase, 25% pyroxene, 22% amphibole and 3% opaques. No layering is apparent but some gabbros have thin segregation veins. Post-magmatic veins make up 1-2% and range up to about 2 mm in width. They are filled chiefly with white zeolite. Some early veins have epidote, quartz and minor chlorite. Groundmass alteration is rather patchy and involves bleaching of the rock accompanied by replacement of feldspar and mafic minerals by clay minerals, epidote and chlorite.

UNIT XL

Upper contact: 859.35 m, sheared
Lower contact: 860.80 m, sheared
Thickness: 1.45 m
Lithology: Fault breccia
Cooling units: 223.01

Unit XL consists of 1.45 m of brownish-grey, strongly sheared diabase. Shear planes are steep, nearly parallel to the core axis, and many surfaces are slickensided. One dioritic vein has brecciated fragments of unsheared gabbro. Sparse, narrow

veinlets are filled with zeolite. The rock appears to be completely altered to a mixture of about 90% chlorite and 10% zeolite.

UNIT XLI

Upper contact: 860.80 m, sheared
Lower contact: 891.15 m, truncated
Thickness: 30.35 m
Lithology: Gabbro
Cooling units: 223.02 - 228.02

A sequence of relatively fine-grained, homogeneous gabbro, 30.35 m thick, makes up Unit XLI. The gabbro is cut by several small veins of leucocratic diorite or plagiogranite and by one thin diabase dyke (cooling unit 225.01). Ten cooling units of gabbro are recognized and they have gradational contacts with one another. Individual units range from .11 to 12.00 m and average 2.91 m in vertical thickness. An average modal composition for the gabbro is about 55% clinopyroxene, 40% plagioclase and 5% amphibole. The amphibole occurs around the margins of the pyroxene grains. The dioritic veins and patches consist of about 80% plagioclase and 20% mafic minerals, mostly hornblende. Later stage veins are sparse, generally <1%, and are filled with chlorite, epidote and zeolite. Alteration in the gabbros is slight, probably no more than 5-10%. Chlorite replaces mafic minerals along fractures and epidote is present in some bleached zones adjacent to the dioritic patches. The one dyke is .50 m thick and consists of grey, fine-grained, aphyric diabase. A few narrow veins are filled with chlorite and epidote. Groundmass alteration is weak and involves partial replacement of mafic minerals by chlorite.

UNIT XLII

Upper contact: 891.15 m, intrusive
Lower contact: 930.70 m, gradational
Thickness: 39.55 m
Lithology: Gabbro cut by dykes
Cooling units: 228.03 - 235.01

A 39.55-m-thick sequence of gabbro and diorite cut by a few diabase dykes makes up Unit XLII. Of the 13 cooling units in this sequence, 6 are gabbro, 2 are diorite and 5 are diabase dykes. The gabbros and diorites range from .33 to 12.46 m and average 4.13 m in vertical thickness. They are light grey, fine- to medium-grained, rather heterogeneous rocks composed of about 50-55% plagioclase, 15-20% clinopyroxene, 10-15% orthopyroxene and 5-10% amphibole. Many of the gabbros are net veined with dioritic material which consists chiefly of plagioclase and hornblende. Late stage veins are sparse, small and filled with white zeolite. The gabbros show no alteration except for bleaching and discolouration along some hairline veins. The dykes consist of light grey, fine-grained, aphyric, homogeneous diabase, some of which is fractured and veined with dioritic material. Late stage veins make up about 1% and range up to 2 mm wide. They are filled chiefly with white zeolite. Groundmass alteration is weak, on the order of 10-15% and involves replacement of mafic minerals by chlorite.

UNIT XLIII

Upper contact: 930.70 m, transitional
Lower contact: 941.86 m, truncated
Thickness: 11.16 m
Lithology: Pyroxenite
Cooling units: 235.02 - 237.01

Unit XLIII consists of two cooling units of grey, melanocratic, medium-grained, gabbroic pyroxenite. An average mode is 70% clinopyroxene, 20% orthopyroxene and 10% plagioclase. Both the orthopyroxene and clinopyroxene are extensively replaced by green and brown hornblende. Veins make up about 2% and range up to 4 cm in width. They are filled with quartz, epidote and feldspar(?). Groundmass alteration, excluding amphibolitization, is on the order of 0-20%. It occurs mainly along networks of closely spaced fractures and results in zones in which the hornblende is partly replaced by epidote.

UNIT XLIV

Upper contact: 941.86 m, transitional
Lower contact: 976.59 m, transitional
Thickness: 34.37 m
Lithology: Gabbro
Cooling units: 237.02 - 242.03

Unit XLIV is a sequence of gabbro, 34.37 m thick, cut by several veins of diorite or plagiogranite. The 9 cooling units of gabbro range from .11 to 10.74 m and average 3.69 m in vertical thickness. Five leucocratic units (237.02, 240.01, 241.02, 241.04 and 242.02) are present and they average about .25 m in vertical thickness. One cooling unit (239.03) is a thin zone of sheared and altered gabbro. The gabbros are grey, medium-grained, fairly homogeneous rocks composed of about 40% plagioclase, 30% clinopyroxene and 30% orthopyroxene. One cooling unit (241.03) is darker coloured and somewhat richer in mafic minerals than the average. The leucocratic veins and patches consist of light grey, plagioclase-rich material with

sparse mafics, chiefly hornblende. The veins generally have sharp, albeit gradational, contacts with the host rocks whereas the irregular patches have much more diffuse boundaries. These irregular patches commonly have a mottled appearance produced by mixtures of felsic material and relict gabbro. The sheared gabbro of cooling unit 239.03 is highly veined and altered with little evidence of the original texture or mineralogy. Veins in the gabbro are quite abundant and range up to 8% of some units. Most are 1-3 mm wide and filled with light coloured felsitic material. A later generation of hairline veinlets, filled with white zeolite, is also present. Except in the sheared gabbro, groundmass alteration is slight - no more than a few percent. Rare, green, bleached zones around some veins are probably rich in epidote and chlorite. The highly sheared gabbro is almost entirely replaced by a mixture of chlorite and epidote.

UNIT XLV

Upper contact: 976.59 m, intrusive
Lower contact: 1017.24 m, intrusive
Thickness: 40.65 m
Lithology: Gabbro and dykes
Cooling units: 243.01 - 250.01

A 40.65-m-thick sequence of gabbro, cut by a few diabase dykes, makes up Unit XLV. Eight of the 15 cooling units in this sequence consist of gabbro or diorite and 7 are diabase dykes. They range from .32 to 8.41 m and average 3.91 m in vertical thickness. The gabbros consist of light grey, fine- to medium-grained, relatively uniform material composed of about 40% plagioclase, 30% clinopyroxene, 20% orthopyroxene, 5% amphibole and 5% opaques. Some more mafic layers have only 20-25% plagioclase and correspondingly higher proportions of pyroxene. Both brown and green amphibole is present. Veins are sparse, generally no more than 1%, and are less than 10 mm in width. An early set is filled with felsic material with minor amphibole and a later, cross-cutting set is filled with white zeolite. Groundmass alteration in the gabbros is almost nil and is restricted to discolouration along some veins, probably reflecting the development of chlorite. The dykes range from .12 to 7.92 m and average 1.87 m in vertical thickness. Except for cooling unit 243.01, they are relatively thin bodies. Most have sharp, steeply-dipping, chilled margins and are clearly intrusive. They consist of grey, fine-grained, uniform, aphyric diabase. Some units (e.g. 243.01) contain abundant (up to 20%) felsic veins. A few dykes also have narrow, later-stage veins filled with white zeolite. The rocks appear to be fresh except in narrow bands along some veins.

UNIT XLVI

Upper contact: 1017.24 m, truncated
Lower contact: 1044.91 m, truncated
Thickness: 27.67 m
Lithology: Gabbro
Cooling units: 250.02 - 255.02

A 27.67-m-thick sequence of gabbro cut by thin dioritic veins makes up Unit XLVI. Seven cooling units of gabbro are recognized, ranging from .35 to 14.33 m and averaging 3.75 m in vertical thickness. The gabbros are truncated above and below by dykes and internally by the dioritic veins. Other contacts are gradational, reflecting minor changes in grain size or composition. The gabbros are rather variable ranging from fine- to coarse-grained and from homogeneous to slightly layered. The thickest cooling units (251.05 and 252.01) are composed of grey, coarse-grained gabbro with a modal composition of about 50-60% plagioclase, 20-25% orthopyroxene, 10-15% clinopyroxene and 10% amphibole. Faint phase layering is present, reflecting variations in the proportions of plagioclase. The other gabbros are similar compositionally to these, but are fine- to medium-grained and homogeneous. The dioritic veins and patches are relatively thin and commonly have sharp, intrusive contacts. They are fine-grained, leucocratic rocks composed chiefly of feldspar, possibly quartz and 2-3% hornblende. Veins make up 1-2% of the gabbros and are chiefly filled with feldspathic material, actinolite(?) and epidote(?). Rare, late-stage veins are filled with white zeolite. All of the gabbros are basically fresh except for minor bleaching adjacent to some leucocratic veins and patches.

UNIT XLVII

Upper contact: 1044.91 m, intrusive
Lower contact: 1092.35 m, intrusive
Thickness: 47.44 m
Lithology: Dykes with gabbro screens
Cooling units: 255.03 - 263.01

Unit XLVII consists of numerous diabase dykes with sparse gabbro screens and numerous dioritic veins. The sequence is 47.44 m thick and contains 28 distinct cooling units. Fifteen of these are diabase dykes which range from .05 to 8.22 m and average 2.14 m in vertical thickness. Most of the dykes have sharp, steeply-dipping, chilled margins but a few are truncated by the dioritic veins. The dykes consist of light grey, fine-grained, homogeneous, aphyric diabase composed of 50-60% plagioclase and 40-50% mafic minerals, chiefly clinopyroxene, amphibole and opaques. Felsic veins, ranging up to 4 cm across,

make up 2-3% of the rock and consist chiefly of feldspathic material, accompanied by minor quartz(?) and magnetite. Later-stage zeolite veins are present in trace amounts. Most of the rocks are fresh and lack evidence of any groundmass alteration. A few specimens have a green cast suggesting growth of amphibole or epidote. The five cooling units of gabbro range from .37 to 5.68 m and average 2.63 m in vertical thickness. These consist of medium-grey, medium-grained, homogeneous microgabbro composed of about 50-60% plagioclase, 20-25% clinopyroxene, 15-20% orthopyroxene, 3% opaques and 2% amphibole. Locally, these rocks contain small, irregular, felsic patches. Felsic veins up to about 3 cm wide make up 1-4% of the gabbros. They consist chiefly of feldspar and quartz(?) accompanied by 10-15% amphibole and 5-10% magnetite. There is no significant groundmass alteration. The largest felsic veins, described as separate cooling units, range from about .10 to .52 m wide and consist of the same minerals the narrower veins.

UNIT XLVIII

Upper contact: 1092.35 m, truncated
Lower contact: 1104.01 m, truncated
Thickness: 11.66 m
Lithology: Gabbro
Cooling units: 263.02 - 265.04

Four cooling units of gabbro ranging from .35 to 8.33 m in vertical thickness make up Unit XLVIII. This 11.66-m-thick sequence is cut by several felsic or dioritic veins up to .46 m wide. The gabbros are greenish-grey, fine- to medium-grained and homogeneous. An average mode is 50-55% plagioclase, 20-25% clinopyroxene, 15-20% orthopyroxene, 2-3% amphibole and 1-2% opaques. Veins are small and sparse and filled chiefly with felsic material composed of plagioclase and minor amphibole. A few late-stage zeolite veins are also present. All of the primary minerals are fresh. The leucocratic veins consist of light grey, fine-grained, homogeneous diorite or plagiogranite composed of feldspar, quartz(?) and amphibole. The mafic minerals are commonly concentrated along the vein walls. The felsic veins show no signs of alteration.

UNIT XLIX

Upper contact: 1104.01 m, intrusive
Lower contact: 1116.25 m, sheared
Thickness: 12.24 m
Lithology: Dykes and gabbro
Cooling units: 265.05 - 267.01

Unit XLIX consists of approximately equal proportions of diabase dykes and gabbro. Gabbro screens make up 4 of the 7 cooling units and range from .29 to 3.07 m in vertical thickness. They consist of light grey, fine- to coarse-grained, relatively homogeneous material with a slight preferred orientation of the plagioclase grains. An average modal composition is 50% plagioclase, 25% clinopyroxene, 20% orthopyroxene and 5% amphibole. Felsic veins of plagioclase and minor amphibole average 1-2% of these rocks but range up to 12% in cooling unit 266.01. The rocks are completely fresh. Only three dykes are present and these range from .17 to 7.03 m in vertical thickness. They are bounded by sharp, intrusive contacts and consist of grey, fine-grained, aphyric, massive diabase. Veins consist entirely of felsic material accompanied by minor amphibole. The rocks are generally fresh but some contain minor pyrite in the groundmass.

UNIT L

Upper contact: 1116.25 m, sheared
Lower contact: 1116.55 m, sheared
Thickness: .30 m
Lithology: Fault breccia
Cooling units: 267.02

Unit L consists entirely of brownish- to greenish-grey, fine-grained, highly sheared and altered gabbro or diabase. The rock is highly fractured and net veined by zeolite. Groundmass alteration has completely obscured the original texture and mineralogy and the rock now consists of about 75% chlorite and 25% white zeolite.

UNIT LI

Upper contact: 1116.55 m, sheared
Lower contact: 1142.95 m, intrusive
Thickness: 26.40 m
Lithology: Dykes and gabbro
Cooling units: 267.03 - 272.01

A 26.40-m-thick sequence of diabase dykes and gabbro screens makes up Unit LI. Of the 13 cooling units in this sequence, 7 are dykes, 4 are gabbro screens and 2 are felsic veins. The dykes range from .56 to 4.33 m and average 2.24 m in vertical thickness. They consist of grey to greenish-grey, fine- to very fine-grained, massive, aphyric diabase composed of about 50% plagioclase and 50% mafic minerals, chiefly pyroxene. Rare pegmatitic patches, up to a few cm across, consist of about 70% amphibole, 20% plagioclase and 10% sulphides. Felsic or leucocratic veins, 1-3 mm wide, range up to about

2%. They are filled with feldspar, quartz(?), and minor amphibole. Most of the rocks are fresh but those with a greenish cast may have 5-10% epidote in the groundmass. The gabbro screens range from .26 to 7.99 m and average 2.50 m in vertical thickness. They consist chiefly of brownish-grey, medium- to coarse-grained, heterogeneous gabbro composed of about 40-50% plagioclase, 30-35% clinopyroxene, 10-15% orthopyroxene and 10% olivine(?). One cooling unit (269.01) has a distinctive mottled texture produced by the presence of brown patches, up to 10 mm across, which may be altered olivine. Coarse pegmatitic patches are also present and these consist chiefly of amphibole crystals up to 5 mm long. Veins make up 1-2% of the gabbros, range up to 4 mm wide and are filled with felsic material and minor amphibole. The rocks are generally fresh but some are slightly bleached adjacent to veins.

UNIT LII

Upper contact: 1142.95 m, truncated
Lower contact: 1163.30 m, sheared
Thickness: 20.40 m
Lithology: Gabbro
Cooling units: 272.02 - 274.03

Unit LII consists of 5 cooling units of gabbro and 1 felsic vein. The gabbros range from 1.00 to 8.70 m and average 4.04 m in vertical thickness. They are mostly light grey, medium- to coarse-grained and uniform. An average composition is 50% plagioclase, 30% clinopyroxene and 20% orthopyroxene. Cooling unit 273.01 contains a 20-cm-thick zone in which large phenocrysts (up to 2 cm) of pyroxene and possibly olivine(?) occur. Cooling unit 244.02 has a spotted appearance due to the presence of brown clots up to 1 cm across which are probably altered orthopyroxene. Both the plagioclase and pyroxene in these rocks show preferred orientations. Less common pegmatitic patches and felsic patches are rich in amphibole. Felsic veins composed of feldspar, quartz(?) and minor amphibole make up 1-2% of the rock. A few late stage veins are filled with white zeolite and rarely chlorite. Groundmass alteration is normally weak to non-existent but a 1.78-m-thick zone in cooling unit 272.02 shows extreme alteration in which the feldspars have been completely replaced by clay minerals and the mafic minerals by chlorite.

UNIT LIII

Upper contact: 1163.30 m, sheared
Lower contact: 1165.28 m, sheared
Thickness: 1.98 m
Lithology: Fault breccia
Cooling units: 276.01

A 1.98-m-thick section of highly sheared and altered gabbro makes up Unit LIII. The upper 47 cm are completely sheared and all traces of the original texture and mineralogy have been destroyed. In this zone, the rock is replaced by chlorite and net veined with white zeolite. Although also highly altered, the lower part of the unit is more coherent and the original character of the rock can be discerned. Feldspars are replaced by zeolite and perhaps clay minerals and the mafic minerals are replaced by chlorite. Net veining by zeolite is still prominent with veins up to 1 cm wide.

UNIT LIV

Upper contact: 1165.28 m, sheared
Lower contact: 1239.39 m, truncated
Thickness: 74.11 m
Lithology: Gabbro with rare dykes
Cooling units: 276.02 - 288.01

Units LIV consists of about 74 m of gabbro cut by 3 thin diabase dykes. The twenty cooling units of gabbro range from .09 to 16.61 m and average 3.65 m in vertical thickness. Boundaries between cooling units are typically gradational, reflecting changes in grain size or mineral proportions. The gabbros are chiefly light grey, medium- to coarse-grained, rather heterogeneous rocks with weakly developed foliation and phase layering. The mineralogy varies but an average composition is 50-60% plagioclase, 20-25% clinopyroxene, 10-15% orthopyroxene, 3% amphibole and 2% opaques. A few very coarse-grained layers have crystals up to 1 cm across. Veins are sparse but fairly wide, ranging up to 5 cm in some cases. A felsic vein or dykelet, 29 cm across, makes up cooling unit 285.03. A few smaller, later- stage veins contain quartz, chlorite and zeolite. Groundmass alteration is very weak in the gabbros. Narrow alteration halos occur around some veins and a few irregular felsic patches have minor amounts of epidote. The 3 dykes (cooling units 280.02, 281.02 and 282.02) range from .04 to 1.66 m in vertical thickness and consist of light grey, fine-grained, homogeneous, aphyric diabase. They are characterized by sharp, steeply-dipping chilled margins. An average modal composition is 50% plagioclase, 25% clinopyroxene, 15% orthopyroxene and 10% opaques. Veins make up 1-2% of the dykes, range up to 5 cm across, and

consist chiefly of felsic material and minor hornblende. Very rare, late-stage veins are filled with white zeolite. The groundmass is fresh except for minor bleaching along the larger veins.

UNIT LV

Upper contact: 1239.39 m, intrusive
Lower contact: 1283.06 m, truncated
Thickness: 43.67 m
Lithology: Gabbros with a few dykes
Cooling units: 289.01 - 294.05

A 43.67-m-thick sequence of gabbro, cut by a few diabase dykes, makes up Unit LV. Nine of the 14 cooling units in this sequence are gabbro. They range from .31 to 11.01 m and average 4.12 m in vertical thickness. Where in contact with dykes, these cooling units are truncated but internal contacts are gradational, reflecting changes in grain size and mineral proportions. The gabbros are mostly light grey, fine- to medium-grained, relatively homogeneous rocks composed of about 40-45% plagioclase, 15-20% clinopyroxene, 15-20% orthopyroxene, 10-15% amphibole and 5-10% opaques. Rare pegmatitic patches contain abundant coarse-grained amphibole and plagioclase. Cooling unit 294.04 is a coarse-grained, melanocratic gabbro with distinct layering. In this unit, plagioclase makes up only about 10-20% of the rock and the mafic minerals are correspondingly more abundant. Some of the layers contain round, pellet-shaped minerals which are probably olivine. Veins make up 1-3% of most units and are filled chiefly with felsic material composed of plagioclase, amphibole and some epidote. Very rare, later-stage veins are filled with white zeolite or chlorite. Alteration is weak, generally less than 5%, and involves mostly chloritization of the mafic minerals. This locally produces a mottled texture. One cooling unit (292.01) is composed of epidotized, saussuritized, chloritized and zeolitized material in which all evidence of the original texture and mineralogy has been destroyed. The rock is unsheared and now consists of about 40% epidote and 30% zeolite. This may be altered gabbro or it could have been a dyke. The latter possibility seem most likely because the alteration extends into the adjacent dyke of cooling unit 291.03. This zone is interpreted as a hydrothermal channelway. The five diabase dykes range from .11 to 3.33 m and average 1.37 m in vertical thickness. They are light grey, fine- to medium-grained and aphyric. An average mode is 45-55% plagioclase, 25-30% clinopyroxene, 10-15% orthopyroxene and 10% opaques. Veins make up 1-2%, range from hairline to 1 cm in width, and are filled chiefly with felsic material. Groundmass alteration is low except in cooling unit 291.03 where it is up to 30 or 40%. In this unit, the mafic minerals are replaced by amphibole and chlorite and the plagioclase by saussurite.

UNIT LVI

Upper contact: 1283.06 m, intrusive
Lower contact: 1288.41 m, intrusive
Thickness: 5.35 m
Lithology: Dykes
Cooling units: 296.01 - 297.02

Unit LVI consists of 3 diabase dykes ranging from .99 to 3.77 m in vertical thickness. Two of the dykes are fresh and have sharp, steeply-dipping, intrusive contacts; the third is completely altered. The fresh diabase is fine- to very fine-grained, uniform, aphyric material composed of about 45% plagioclase, 20% clinopyroxene, 20% orthopyroxene and 15% opaques. Felsic veins make up about 1% and range up to 1 cm in width. Small amounts of pyrite are present in some of the veins. Except in cooling unit 297.01, the rocks are quite fresh, exhibiting only minor bleaching along some veins. In the highly altered units, the rocks is green and is completely replaced by amphibole, epidote and plagioclase(?).

UNIT LVII

Upper contact: 1288.41 m, truncated
Lower contact: 1331.17 m, sharp
Thickness: 42.76 m
Lithology: Gabbro
Cooling units: 297.03 - 305.01

Unit LVII consists of 42.76 m of fine- to medium-grained gabbro and microgabbro with one pegmatitic dyke. Thirteen cooling units of gabbro are recognized, ranging from .17 to 8.24 m and averaging 3.21 m in vertical thickness. The pegmatitic dyke is .97 m thick. Contacts between cooling units are gradational, reflecting variations in grain size and mineral proportions. Most of the gabbro is uniform in texture and lacks significant layering, although some specimens have a weak mineral lamination. An average mode is 50-55% plagioclase, 20-25% clinopyroxene, 10-15% orthopyroxene, 10% magnetite and 5% amphibole. Cooling units 303.01 and 303.03 consist of very coarse-grained mafic gabbro with about 30-40% plagioclase and 60-70 % mafic minerals. The pegmatitic dyke consists of mottled white, yellow, brown and green, very coarse-grained material with about 40% plagioclase, 30% orthopyroxene, 25% clinopyroxene and 5% amphibole. The mafic minerals form large, subrounded crystals up to 6 cm across. Irregular felsic and pegmatitic patches are also

present in many of the gabbros. These range up to several centimetres across and have gradational boundaries with the host rock. The same material forms rare veins a few millimetres wide. A later generation of veins is filled with chlorite and white zeolite. Overall, the rocks are quite fresh but some are mottled suggesting variable growth of secondary amphibole and incipient alteration of the mafic minerals to chlorite. Some of the plagioclase, particularly adjacent to veins, is milky or cloudy suggesting some replacement by epidote.

UNIT LVIII

Upper contact:	1331.17 m, transitional
Lower contact:	1440.38 m, ambiguous
Thickness	109.21 m
Lithology:	Coarse-grained gabbro
Cooling units:	305.02 - 322.01

Unit LVIII is a 109.21-m-thick sequence of grey, generally coarse-grained, somewhat layered gabbro. One cooling unit (306.01) is a narrow, fine-grained felsic zone, possibly a small dyke. Cooling units 309.01 and 319.01 have sharp, possibly intrusive boundaries and are fine-grained. They may be narrow diabase dykes or layers of fine-grained microgabbro. Of the gabbros, about half are coarse grained and the remainder are medium- or fine-grained. The alternation of grain size indicates that Unit LVIII is layered on a large scale and a few of the thicker cooling units exhibit internal layering. An average composition for the gabbros is 40-50% plagioclase, 10-25% orthopyroxene, 10-25% clinopyroxene and 5-10% amphibole. Unlike higher level gabbros in Hole Cy-4, many of those in Unit LVIII have at least a few percent of olivine. The olivine is most abundant in the coarsest-grained units where it may be up to 10 or 15%. Pegmatitic zones, rich in plagioclase and hornblende, are common. Leucocratic or felsic zones are also present in some cooling units and these produce a mottled texture in the rock. Veins are rare in most units, much less than 1%. An early generation of veins consists largely of light coloured felsic material with some epidote, quartz and amphibole. These are mostly 1-2 mm wide but locally grade into irregular patches of groundmass alteration. A later generation of veins, most of which are also 1-2 mm wide, is filled chiefly with white zeolite or chlorite. Overall, groundmass alteration is weak and many of the gabbros are completely fresh. Where present, the olivine is typically replaced by dark chlorite or serpentine. Some pyroxenes and amphibole are also partly replaced by chlorite. Alteration is greatest in the immediate vicinity of felsic veins and patches where the rock is discoloured and primary minerals are partly replaced. Some sulphide grains are also present in the rock. Three cooling units (314.01, 319.02 and 321.07) show high degrees of alteration. In these units the original textures and mineralogies are almost completely obliterated and the rock consists of various mixtures of epidote, chlorite, quartz, feldspar and amphibole. Because there is no evidence of shearing, these units are considered to be zones of static hydrothermal alteration.

UNIT LIX

Upper contact:	1440.38 m, transitional
Lower contact:	1470.10 m, transitional
Thickness:	29.72 m
Lithology:	Fine-grained gabbro
Cooling units:	323.01 - 328.02

Unit LIX consists of 29.72 m of generally homogeneous gabbro. One of the 9 cooling units in this sequence (325.04) is relatively coarse grained; the remainder are fine- to medium-grained. Individual cooling units range from .17 to 9.14 m and average 3.30 m in vertical thickness. Contacts between the units are gradational, reflecting chiefly grain size changes. An average composition is 30-40% plagioclase, 30-40% clinopyroxene, 20-30% orthopyroxene, 5-10% amphibole and 5% opaques. A few of the cooling units have an almost porphyritic texture with very large orthopyroxene crystals up to 1 cm across. The more mafic gabbros also commonly have a few percent of large olivine crystals, particularly in the lower, coarser-grained part of individual cooling units. Veins are small and sparse. An early generation is filled with light-coloured felsic material. These commonly have diffuse margins and grade into bleached and altered zones, also felsic in character. A later set is filled with white zeolite and chlorite. Groundmass alteration is weak except in the vicinity of the felsic veins where the rock is bleached and probably altered to epidote. Olivine crystals are replaced by chlorite or serpentine and a few mafic minerals show marginal replacement by chlorite.

UNIT LX

Upper contact:	1470.10 m, ambiguous
Lower contact:	1503.39 m, transitional
Thickness:	33.29 m
Lithology:	Gabbro and altered gabbro
Cooling units:	329.01 - 333.02

Unit LX is a 25.88-m-thick sequence of fine- to coarse-grained gabbro, much of which is hydrothermally altered. Of the 10 cooling units in this sequence, 4 (329.01, 330.01, 330.03, and 333.01) are highly altered and 2 (330.04 and 333.02) are

partly altered. The cooling units range from .27 to 14.85 m and average 2.88 m in vertical thickness. The freshest gabbros are mostly fine- to medium-grained, non-laminated, homogeneous rocks composed of about 20-30% plagioclase, 35-40% clinopyroxene, 15-20% orthopyroxene, 5-10% amphibole and 5% opaques. Cooling units 329.04 and 320.02 are thin layers of mafic gabbro containing about 5-15% olivine and only 20% plagioclase. A few of the coarse-grained units have small irregular pegmatitic patches rich in feldspar and amphibole. Veins make up <1% of this sequence and are filled with felsic material or chlorite. Zeolite veins are extremely rare. The hydrothermally altered gabbros are extensively bleached and replaced by mixtures of epidote, chlorite, quartz, albite(?) and zeolite. In the most intensely altered zones, all traces of the original texture and mineralogy have been destroyed but the highly altered rocks grade into fresher units, suggesting that the protoliths were gabbro. In the freshest rocks, olivine is replaced by chlorite or serpentine and some disseminated sulphide grains are present. In transitional zones, the rock has a blotchy appearance due to incomplete or incipient alteration.

UNIT LXI

Upper contact:	1503.39 m, transitional
Lower contact:	1533.20 m, transitional
Thickness:	29.81 m
Lithology:	Layered gabbro
Cooling units:	335.01 - 339.02

Unit LXI is a sequence of light grey, fine- to coarse-grained, layered gabbro about 30 m thick. Eight cooling units are recognized, ranging from .37 to 10.13 m and averaging 3.73 m in vertical thickness. The thickest cooling unit (336.01) exhibits a regular alternation between fine- to medium-grained gabbro and coarse-grained gabbro and could be divided into thin units. Overall, the layering appears to be on about a metre scale. The fine- to medium-grained material consists of about 40-50% plagioclase, 35-45% clinopyroxene, 15% orthopyroxene and 1-2% olivine(?). The coarsest-grained layers tend to be more mafic in composition with about 30-35% plagioclase and correspondingly higher pyroxene. Some of the coarser-grained zones appear to be cumulate layers, others are vein-like with relatively sharp boundaries. Veins are sparse, <1%, hairline to 10 mm wide and filled with felsic material, chlorite and late stage zeolite. A few slickensided fractures are coated with chlorite. Alteration is low, generally <5% but up to 30% or 40% in a few zones. It is highest in and near fractures and veins. Olivine is completely replaced by chlorite or serpentine and orthopyroxene is commonly rimmed by the same material. In the highly altered zones, the mafics are extensively replaced and plagioclase is bleached and saussuritized. Some altered zones contain irregular patches of epidote, silica and zeolite.

UNIT LXII

Upper contact:	1533.20 m, transitional
Lower contact:	1545.45 m, transitional
Thickness:	12.25 m
Lithology:	Fine-grained gabbro
Cooling units:	340.01 - 341.04

A 12.25-m-thick sequence of mostly fine-grained, homogeneous gabbro makes up Unit LXII. Seven cooling units are present, ranging from .33 to 3.36 m and averaging 1.75 m in vertical thickness. Four of the fine-grained cooling units (340.01, 340.03, 341.01 and 341.04) have distinctive porphyritic textures. In these units large subhedral to anhedral mafic grains, up to 5 mm across, make up 10-15% of the rock. The grains are completely replaced by chlorite or serpentine and are altered olivine or pyroxene. Two thin cooling units (340.02 and 341.03) consist of coarse-grained gabbro. Several of the units have a well-developed, steeply-dipping foliation. An average mineralogy is 45% plagioclase, 50% pyroxene and 5% magnetite. Some orthopyroxene is present but clinopyroxene appears to be the dominant mafic phase. Irregular pegmatitic patches are scattered through these rocks. The coarse-grained gabbros are more feldspathic and have an average mode of 60-65% plagioclase, 30% clinopyroxene, and 15% orthopyroxene. Veins are small and sparse. They range from <1% to 3% and rarely exceed 3 mm in width. They are filled chiefly with chlorite, epidote, carbonate and white zeolite. Overall, these gabbros are relatively fresh. Some of the mafic minerals are marginally replaced by chlorite and some of the plagioclase is zeolitized.

UNIT LXIII

Upper contact:	1545.45 m, transitional
Lower contact:	1561.65 m, transitional
Thickness:	16.20 m
Lithology:	Homogeneous gabbro
Cooling units:	342.01 - 344.03

Unit LXIII is a sequence of light grey, fine- to medium-grained, homogeneous gabbro cut by a thin pegmatitic vein. Five cooling units of gabbro are present, ranging from .62 to 4.03 m and averaging 3.22 m in vertical thickness. The pegmatitic vein (cooling unit 344.01) is .12 m thick. An average modal composition of the gabbro is 55% plagioclase,

30% clinopyroxene and 15% orthopyroxene. A few specimens contain up to 5% amphibole. Some of the cooling units have irregular, relatively coarse-grained patches, 3-7 mm across. These tend to be a little richer in plagioclase than the finer-grained gabbros. In the pegmatitic vein crystals range up to 15 mm across and consist of 50-55% plagioclase, 35-40% clinopyroxene, 10% orthopyroxene and 5% amphibole. Veins are small and sparse (<1%), and are filled with about equal amounts of chlorite and white zeolite. Alteration is limited, and involves marginal replacement of pyroxene by chlorite, particularly adjacent to chlorite veins.

UNIT LXIV

Upper contact:	1561.65 m, transitional
Lower contact:	1568.51 m, transitional
Thickness:	6.86 m
Lithology:	Porphyritic gabbro
Cooling units:	345.01

Unit LXIV is a single cooling unit, 6.86 m thick, of light grey, fine- to medium-grained, porphyritic gabbro. A few non-porphyritic, coarse-grained patches, up to 10 cm wide, are present locally. The mineralogy is the same in both types and averages 50% plagioclase, 30% clinopyroxene, and 20% orthopyroxene. The porphyritic texture results from 10-15% of large (up to 4 mm) crystals of altered mafic material, either pyroxene or olivine. Veins make up <1% of this unit, range up to about 1 mm in width and are filled with chlorite and minor white zeolite. Alteration ranges from about 5-15% and is restricted to chloritization of the mafic minerals.

UNIT LXV

Upper contact:	1568.51 m, transitional
Lower contact:	1591.32 m, transitional
Thickness:	22.80 m
Lithology:	Fine-grained homogeneous gabbro
Cooling units:	346.01 - 348.02

A 22.80-m-thick sequence of generally fine- to medium-grained, homogeneous gabbro makes up Unit LXV. A single layer of coarser-grained gabbro, .94 m thick, is present near the centre of the unit. Two cooling units of fine-grained gabbro are present and these are 11.93 and 9.94 m thick, respectively. An average mode for these rocks is 50% plagioclase, 35% clinopyroxene and 15% orthopyroxene. The coarse-grained gabbro is somewhat more mafic and has about 30% plagioclase and 70% pyroxene. A few of the rocks show a faint foliation defined by elongate stringers of plagioclase and mafic minerals. Veins are <1%, hairline to 3 mm and filled with chlorite and zeolite. Most of the rocks are fresh and exhibit only very slight chloritization of the mafic minerals. In the coarse-grained layer many pyroxene crystals are partly replaced by amphibole. Sparse, disseminated pyrite is locally present.

UNIT LXVI

Upper contact:	1591.32 m, transitional
Lower contact:	1674.71 m, transitional
Thickness:	83.40 m
Lithology:	Layered gabbro
Cooling units:	350.01 - 364.03

Unit LXVI is a thick sequence of fine- to coarse-grained, generally layered gabbro. There are 24 cooling units in this 83.40-m-thick sequence ranging from .90 to 11.99 m and averaging 3.47 m in vertical thickness. Layering occurs on two scales; relatively fine, centimetre-scale layering within cooling units and coarser, metre-scale layering involving separate cooling units. Fine scale layering is well displayed in such cooling units as 350.01, 350.02, 352.01, 355.02, 358.01, 358.02, 360.01 and 362.01. The larger scale layering involves upward transitions from coarse-grained gabbro through medium-grained to fine-grained gabbro such as that defined by cooling units (from the base upward) 362.01, 361.03, 361.02 and 361.01. The lower coarser-grained units in these cycles typically display internal layering as well. Although there are some mineralogical variations associated with the grain size layering, the overall sequence is remarkably uniform. An average modal composition consists of 40-50% plagioclase, 40-50% clinopyroxene, 10-15% orthopyroxene and 1-2% amphibole. The coarsest-grained layers tend to have higher pyroxene and lower plagioclase contents. Some of the layers show well-developed cumulate textures with megacrysts of orthopyroxene. Veins are sparse, always <1%, and mostly less than 1-2 mm wide. They are filled chiefly with chlorite and zeolite although a few early veins have felsic material. Alteration is weak, typically on the order of 5-15%. It involves chloritization of the mafic minerals and is most intense adjacent to chlorite veins. Cooling unit 355.01 consists of highly altered gabbro in which the original rock has been converted to feldspathic material and epidote. Numerous later-stage zeolite and carbonate veins also cut this unit.

UNIT LXVII

Upper contact: 1674.71 m, transitional
Lower contact: 1700.40 m, transitional
Thickness: 25.69 m
Lithology: Coarse-grained gabbro
Cooling units: 364.04 - 366.01

Unit LXVII is a 25.69-m-thick sequence of mostly coarse-grained gabbro that becomes finer-grained at the top. Only two cooling units are present. Unit 366.01 consists of 18.29 m of light greenish-grey, coarse-grained gabbro which is overlain by 7.40 m of medium- to fine-grained, slightly porphyritic gabbro of unit 364.04. The coarse-grained gabbro has an average mode of 55% clinopyroxene, 30% plagioclase, 15% orthopyroxene and traces of interstitial amphibole. There are several narrow bands with 10-15% of large, chloritized mafic minerals, probably olivine. The upper finer-grained sequence also has large chloritized mafics, giving the rock a porphyritic appearance. It also has irregular zones of coarse-grained material at several levels. Hairline veins make up $<<1\%$ and are filled with chlorite and zeolite. Alteration is on the order of 15-20% and involves chiefly chloritization of the mafic minerals. A few small areas are more intensely bleached and altered. Traces of pyrite are disseminated throughout.

UNIT LXVIII

Upper contact: 1700.40 m, transitional
Lower contact: 1739.77 m, transitional
Thickness: 39.37 m
Lithology: Layered gabbro
Cooling units: 369.01 - 375.02

Unit LXVIII is a sequence, 39.37 m thick, of layered gabbro similar to that of Unit LXXI. There are 14 cooling units in this sequence, ranging from .47 to 5.67 m and averaging 2.75 m in vertical thickness. Layering is expressed by grain size variations both within and between cooling units. The grain size ranges from 1-2 mm up to a maximum of about 15 mm. Internal grain size layering is particularly well-developed in cooling units 370.01, 371.04 and 372.02. Upward fining of cooling units is repeated several times but one of the best developed is from cooling unit 371.04 at the base to 371.02 at the top. Although the mineralogy is somewhat variable, an average mode for the gabbros is about 50% plagioclase, 40% clinopyroxene, 10% orthopyroxene and traces of amphibole. Some of the coarser-grained layers have a few percent of large chloritized mafic minerals, either orthopyroxene or more likely olivine. These layers are usually more melanocratic than the other and have only 35-40% plagioclase. Veins make up from $<1\%$ to about 5% of individual cooling units. Most are 1-5 mm wide but a few range up to 8 cm across. The largest ones are filled with felsic material accompanied by minor amphibole. Smaller, later-stage veins are filled with chlorite and zeolite. Alteration is low (15%), and is typically restricted to chloritization of the mafic minerals, particularly olivine(?). In a few zones there is minor bleaching and zeolitization of the feldspars.

UNIT LXIX

Upper contact: 1739.77 m, transitional
Lower contact: 1753.95 m, transitional
Thickness: 14.18 m
Lithology: Layered olivine gabbro
Cooling units: 376.01 - 378.03

Unit LXIX consists chiefly of grey, fine- to medium-grained, somewhat layered, olivine gabbro. Eight cooling units are identified ranging from .77 to 2.62 m and averaging 1.77 m in vertical thickness. Several cooling units (e.g. 377.01, 378.02 and 378.03) show well-developed internal grain size layering. Cooling units 376.03, 376.02 and 376.01 define a graded sequence from coarse-grained gabbro at the base to fine-grained gabbro at the top. There are some irregular patches and vein-like masses of coarse-grained material scattered throughout the core. Mineralogically these gabbros differ from the overlying units in having 5-10% of large altered olivine crystals. Only 2 of the 8 cooling units (376.03 and 378.02) lack significant amounts of olivine. An average mode is 35-45% plagioclase, 35-45% clinopyroxene, 10-15% orthopyroxene, 5-10% olivine and 1-2% amphibole. Generally, the coarse-grained zones are the most feldspathic. Veins are small and sparse, generally $<1\%$, and filled largely with chlorite and zeolite. Alteration is variable from about 5-30% reflecting in part the proportion of olivine present. All of the olivine and some of the pyroxene is replaced by chlorite or serpentine and some of the plagioclase is bleached and zeolitized.

UNIT LXX

Upper contact: 1753.95 m, transitional
Lower contact: 1809.18 m, transitional
Thickness: 55.23 m
Lithology: Websterite
Cooling units: 378.04 - 388.01

Unit LXX is a 55.23-m-thick sequence of interlayered websterite and olivine websterite with a few thin layers of melanocratic gabbronorite. Eighteen cooling units are recognized ranging from .17 to 12.00 m and

averaging 3.07 m in vertical thickness. All but three of these (379.01, 382.02 and 384.03) are websterite or olivine websterite. Two of the cooling units (386.01 and 387.01) show well-developed internal layering defined largely on grain size changes. The websterites average about 75-80% clinopyroxene, 10-15% orthopyroxene, 5% olivine and 5% plagioclase. Trace amounts of interstitial amphibole are also present. The olivine websterites are similar in composition but have about 15-20% olivine and correspondingly smaller amounts of clinopyroxene. Conversely, the melanocratic gabbronorites have 20-25% plagioclase and little or no olivine. In a few cases there is an upward transition from olivine websterite to websterite to gabbronorite. Cooling units 384.05, 384.04 and 384.03 provide the best example of this but other sequences are present. Veins are small and sparse, rarely making up 1%. Some cooling units have no veins at all. Those that are present are hairline to 1 mm in width and are filled mostly with zeolite accompanied by minor chlorite or serpentine. Rare felsic veins are present in some cooling units. Alteration varies with the percent of olivine because this mineral is completely altered to chlorite or serpentine. Minor alteration of the pyroxene occurs in a few units.

UNIT LXXI

Upper contact:	1809.18 m, transitional
Lower contact:	1811.19 m, transitional
Thickness:	2.01 m
Lithology:	Coarse-grained gabbro
Cooling units:	388.02

A single cooling unit, 2.01 m thick, of light grey, coarse- to very coarse-grained, plagioclase-rich gabbro makes up Unit LXXI. Two small patches, about 10 cm across, of olivine-bearing websterite are present in the gabbro. Individual crystals are up to 5 cm across and the rock has a well-developed cumulate texture. An average mode is 50-60% plagioclase, 15-30% clinopyroxene, 20-25% orthopyroxene and 1-2% olivine. Veins make up $<<1\%$ and range up to 1 mm in width. They are filled with approximately equal amounts of chlorite and zeolite. Alteration is limited to slight replacement of the mafic minerals, particularly olivine, by chlorite or serpentine.

UNIT LXXII

Upper contact:	1811.19 m, transitional
Lower contact:	1855.79 m, transitional
Thickness:	44.60 m
Lithology:	Layered websterite
Cooling units:	389.01 - 397.05

Unit LXXII is a 44.60-m-thick sequence of layered websterite and olivine websterite. Twenty-five cooling units are recognized ranging from .31 to 7.93 m and averaging 1.78 m in vertical thickness. Layering is expressed by changes in both grain size and mineral proportions and occurs within and between cooling units. Internal layering primarily reflects alternations in grain size and is best developed in cooling units 389.03, 390.01, 393.01 and 395.04. Larger scale layering between cooling units reflects changes in both grain size and mineral proportions. A typical sequence begins at the bottom with coarse-grained olivine websterite and passes upward through medium-grained olivine-bearing websterite to medium- or fine-grained, olivine-poor websterite. There are many such cycles in this sequence but most of them are incomplete. Many of the coarser-grained units exhibit well-developed cumulate textures. The bulk of the unit consists of medium- to dark-grey, medium- to coarse-grained websterite with about 65-75% clinopyroxene, 15-20% orthopyroxene, 5-10% olivine and 5% plagioclase. Olivine is usually concentrated in the coarser-grained layers where it may make up 20-25% of the rock. Layers and patches of more feldspathic material are also common. The grain size varies from a few millimetres up to 15 or 20 cm. Typically, the orthopyroxene crystals are the largest, followed by olivine. The orthopyroxene crystals are euhedral to subhedral and the olivine is typically anhedral. Veins average $<1\%$ of the sequence and rarely exceed 3 mm in width. They are filled with zeolite and rare serpentine. Alteration is largely restricted to replacement of olivine by serpentine or chlorite. It varies from about 5-20% depending on the modal percent of olivine present.

UNIT LXXIII

Upper contact:	1855.79 m, transitional
Lower contact:	1866.72 m, transitional
Thickness:	10.93 m
Lithology:	Layered gabbro
Cooling units:	398.01

Unit LXXIII is a single cooling unit, 10.93 m thick, of coarse- to very coarse-grained, layered gabbro with some bands and zones of websterite and olivine websterite. Individual crystals in the gabbro range from about 3 to 30 mm and they display well-developed cumulate textures. The websterite and olivine websterite are finer-grained and form irregular patches and layers up to about 35 cm thick in the gabbro. An average mode for the gabbro is 60% plagioclase, 20% clinopyroxene, 20% orthopyroxene with traces of interstitial amphibole. Some more mafic gabbronorite layers have significantly higher percentages of clinopyroxene and lower percentages of

plagioclase. The websterite and olivine websterite consist of about 65-80% clinopyroxene, 10-15% orthopyroxene, 5-10% olivine and 5-10% plagioclase. Veins make up <<1% of the unit, range up to 2 mm in width and are filled chiefly with serpentine, zeolite and minor felsic material. Alteration is 5-10%, reflecting the proportion of olivine present. All of the olivine is replaced by serpentine or chlorite.

UNIT LXXIV

Upper contact:	1866.72 m, transitional
Lower contact:	1893.20 m, transitional
Thickness:	26.48 m
Lithology:	Websterite and olivine websterite
Cooling units:	400.01 - 404.01

Unit LXXIV is composed chiefly of medium- to coarse-grained websterite with well-defined phase layering resulting from olivine accumulation. Nine cooling units are identified, ranging from .86 to 4.70 m and averaging 2.20 m in vertical thickness. One of these (401.01) is a layer of pegmatitic gabbro, .86 m thick. The websterite consists of about 70-75% clinopyroxene, 15-20% orthopyroxene, 5% olivine and 5% plagioclase. Most of these rocks have well-developed cumulate textures and some show both size and phase layering. Zones of olivine accumulation are 10-15 cm thick and dip about 45o from the horizontal. In these zones, anhedral olivine crystals, 10-15 mm across, form 20-30% of the rock. There are also a few zones where olivine is abundant in the form of small anhedral interstitial grains. Veins average about 1% but are up to 3% in a few layers. They range from hairline to about 10 mm in width and are filled with felsic material, serpentine and minor zeolite. Alteration chiefly involves replacement of olivine by serpentine so it varies with the rock mode, between about 5 and 30%.

UNIT LXXV

Upper contact:	1893.20 m, transitional
Lower contact:	2097.80 m, transitional
Thickness:	204.60 m
Lithology:	Olivine websterite
Cooling units:	404.02 - 448.02

Unit LXXV is a thick unit composed chiefly of layered olivine websterite with lesser amounts of websterite, harzburgite and gabbronorite. Most of the rocks are medium- to coarse-grained with crystals up to 25 mm across. The rocks typically exhibit both grain size and phase layering on a centimetre to metre scale. Phase layering is defined primarily on variations in olivine content. Small amounts of olivine are present in most of the rocks but it is concentrated in layers or beds from about .1 to .4 m thick where it may form 30-40% of the rock. Some of these olivine-rich layers grade into harzburgite. Larger scale layering involving multiple cooling units usually is defined on changes in grain size and mineralogy. At the base of a cycle there may be coarse- to very coarse-grained olivine websterite or harzburgite which is succeeded upward by medium- to coarse-grained olivine-poor websterite and finally by medium-grained websterite. A few layers or patches of pegmatitic gabbronorite are locally present but these appear to be random intrusions rather than part of the layered sequences. An average mode for the olivine websterite is 60-70% clinopyroxene, 15-20% orthopyroxene, 5-15% olivine and 2-3% plagioclase. The clinopyroxene and orthopyroxene are subhedral to euhedral and the olivine occurs either as large euhedral crystals or as small anhedral grains interstitial to the pyroxene. The harzburgite layers consist of about 50% olivine, 30-35% orthopyroxene and 15-20% clinopyroxene. Minor amphibole sometimes rims the pyroxene. Pegmatitic gabbronorites consist largely of clinopyroxene (60%), orthopyroxene (20%) and plagioclase (15-20%). Most specimens also contain a few percent of olivine and amphibole. Many cooling units in this sequence are completely devoid of veins; others have up to 1%. Most veins are hairline to 1 mm and only a few are greater than 5 mm in width. Serpentine is the only common vein filling but felsic material is present locally. Alteration is essentially limited to replacement of olivine by serpentine and thus varies from about 5-50% depending of the modal composition of the rock.

UNIT LXXVI

Upper contact:	2097.80 m, transitional
Lower contact:	2126.45 m, transitional
Thickness:	28.65 m
Lithology:	Olivine websterite and gabbronorite
Cooling units:	448.03 - 455.03

Unit LXXVI is a mixed unit, 28.65 m thick, consisting of approximately equal amounts of olivine-bearing websterite and gabbronorite. Nineteen cooling units are recognized in this sequence ranging from .24 to 5.92 m and averaging 1.50 m in vertical thickness. Of these, 10 consist of relatively fine-grained gabbro and gabbronorite. Some of the units are so fine-grained (1-2 mm) that they are described as diabases but because they lack chilled margins they are probably microgabbro layers rather than dykes. The remaining cooling units consist chiefly of websterite and olivine websterite with a few thin

layers of harzburgitic peridotite. There is no obvious grain size or phase layering in this sequence. An average mode for the gabbronorite is 55% clinopyroxene, 25% plagioclase, 15% orthopyroxene, 3-5% olivine and 1% amphibole. The websterites and olivine websterites are composed chiefly of clinopyroxene and orthopyroxene with variable amounts of olivine and a few percent each of plagioclase and amphibole. Veins average about 1% but are somewhat more abundant in the lower part of the unit where they are up to 5%. Most are 2-3 mm wide and are filled with serpentine and minor zeolite. Alteration is weak to moderate and involves chiefly replacement of olivine and some orthopyroxene by serpentine. Plagioclase in the gabbros is partly saussuritized.

UNIT LXXVII

Upper contact:	2126.45 m, transitional
Lower contact:	2138.26 m, transitional
Thickness:	11.81 m
Lithology:	Gabbronorite
Cooling units:	455.04 - 457.02

Three cooling units of grey, fine- to medium-grained gabbronorite with minor websterite make up Unit LXXVII. The cooling units range from 2.72 to 6.19 m and average 2.94 m in vertical thickness. Slight grain size layering is present in cooling units 455.04 and 457.01 and phase layering is present in 457.01. The gabbronorites have an average mode of 50-60% plagioclase, 30-40% clinopyroxene and 5-10% orthopyroxene with trace amounts of olivine. The websterite and olivine websterite in cooling unit 457.01 are richer in pyroxene and olivine and correspondingly poorer in plagioclase. Veins make up <1% of this unit and range up to 2 mm in width. They are filled with serpentine and zeolite. Alteration is weak except in the olivine-bearing rocks of cooling unit 457.01. All of the olivine is replaced by serpentine.

UNIT LXXVIII

Upper contact:	2138.26 m, transitional
Lower contact:	2246.56 m, transitional
Thickness:	108.30 m
Lithology:	Olivine websterite
Cooling units:	458.01 - 484.04

Unit LXXVIII is a 108.30-m-thick sequence composed chiefly of olivine websterite with a few thin layers of pyroxene peridotite, websterite and gabbronorite. The rocks are mostly medium- to coarse-grained, with crystals ranging from about 1-15 mm and averaging 3-5 mm. A few pegmatitic patches have crystals up to 2-3 cm across. Faint igneous layering is defined by thin olivine and pyroxene-rich layers. There appears to be little or no pattern in the repetition of lithologic units in this sequence. An average composition for the olivine websterite is 65-75% clinopyroxene, 15-20% orthopyroxene, 5-10% olivine, 2-5% plagioclase and 1-2% amphibole. The peridotites contain 60-70% olivine, 20-30% clinopyroxene, 5-10% orthopyroxene and 1-3% plagioclase. Veins make up <1%, range up to about 3 mm in width and are filled chiefly with serpentine and minor amounts of zeolite and felsic material. Alteration averages about 10-15% but ranges up to about 50% in the peridotites. The olivine is partly to completely replaced by serpentine and some of the pyroxenes are rimmed by amphibole. Plagioclase is typically fresh but may be bleached to a milky colour in a few sections.

UNIT LXXIX

Upper contact:	2246.56 m, transitional
Lower contact:	2263.44 m, base of hole
Thickness:	16.88 m
Lithology:	Olivine websterite and peridotite
Cooling units:	484.05 - 487.03

Unit LXXIX consists of 16.88 m of alternating olivine websterite and peridotite. Eleven cooling units are recognized, ranging from .52 to 2.03 m and averaging 1.24 m in vertical thickness. Most of these consist of olivine websterite with a basal layer of pyroxene peridotite. Cooling units 484.05 and 487.02 are separate layers of peridotite. Faint igneous layering, defined by the relative abundance of olivine and pyroxene, dips about 50o from the horizontal. Larger scale alternations of lithologies is defined by the cooling units. Most of the rocks are medium- to coarse-grained with crystals ranging from about 2-20 mm across. The pyroxenes are euhedral to subhedral and the olivine is typically anhedral. The olivine occurs both as large oikocrysts and as smaller interstitial grains. An average mode for the olivine websterite is 70-75% clinopyroxene, 10-15% orthopyroxene and 15% olivine. In the peridotite it is 70-80% olivine, 15-25% clinopyroxene and 5% orthopyroxene. Veins make up about 1% on average and range up to about 5% in a few cooling units. They are hairline to 5 mm wide and are filled with serpentine and minor felsic material or zeolite. Alteration is variable but relatively high because of the higher percentages of olivine in these rocks. It averages 15-20% in the olivine websterite and 60-70% in the peridotites. Almost all of the olivine, and some of the orthopyroxene, is replaced by serpentine and some pyroxene grains are rimmed by amphibole.

The geology of the area immediately surrounding the CY-4 borehole of the Cyprus Crustal Study Project

J. MALPAS, G. CASE AND P. MOORE

Department of Earth Sciences,
Memorial University of Newfoundland, Canada, A1B3X5.

Malpas, J., Case, G. and Moore, P., The geology of the area immediately surrounding the CY-4 borehole of the Cyprus Crustal Study Project in *Cyprus Crustal Study Project: Initial Report, Hole CY-4, ed. I.L. Gibson, J. Malpas, P.T. Robinson and C. Xenophontos; Geological Survey of Canada, Paper 88-9, p. 31-37, 1989.*

Abstract

Hole CY-4 of the Cyprus Crustal Study Project sampled a variety of rock types characteristic of the upper plutonic sequence of a classic ophiolite. These include a range from ultramafic to plagiogranitic lithologies which show a variety of intrusive relationships with each other. These relationships suggest that the rocks were formed in a series of magma chambers in which differentiation processes were dominated by crystal fractionation and wall and roof rock assimilation. The action of seawater, both released into the magma by resorbtion of hydrated diabases and gabbros, and circulating through the cooling rocks, had a major effect on the crystallisation history, alteration and chemistry of the sequence.

Résumé

Le trou CY-4 de Projet d'Etude de la Croute Cypriote a échantillonné une variété de roches caractéristiques des séquences plutoniques supérieures d'un ophiolite classique. Celles-ci incluent une gamme des ultramafiques aux lithologies plagiogranitiques avec des intrusions les unes dans les autres. Ces corrélations suggèrent que ces rocs ont été formés dans une série de chambres magmatiques dans lesquelles les procédés de différentiation ont étés dominés par le fractionnement des cristaux et l'assimilation des rocs murs et plafonds. L'action de l'eau de mer, libérée dans le magma par le résorbement des diabases et gabbros hydratés, ainsi que par circulation dans la roche en refroidissement, a eu des effets importants sur la chimie et sur la transformation des cristaux de la séquence.

INTRODUCTION

Hole CY-4 of the Cyprus Crustal Study Project was designed to sample the transition from sheeted dykes to plutonic rocks and as much of the plutonic section as possible of the Troodos ophiolite, Cyprus. The Troodos Complex has always been taken as a type example of ophiolite stratigraphy and based upon this concept at the time drilling was planned, the hole was sited close to a plagiogranite body and spudded into sheeted diabase dykes. It was thought that with little penetration, the hole would pass from the sheeted dykes into plagiogranite and then down into gabbros, initially isotropic and subsequently layered, and eventually ultramafic cumulates. A program of detailed mapping was undertaken in concert with the drilling in order to facilitate the construction of a three dimensional model of the geological relationships.

A site approximately 1 km south of the village of Palekhori was considered to be the best location for drilling both logistically and geologically. In this area the geological relationships of the high level plutonic rocks involve four major rock types. In general these have distinctive petrological properties and compositions although hybrids or intermediates are observed in some places. These rock types are (1) ultramafic rocks, (2) gabbros, (3) plagiogranites and (4) diabase. Noteably, in this area there is no clear age progression among them and most types can be observed intruding each other in an almost random sequence.

ULTRAMAFIC ROCKS

The ultramafic rocks occur either as layered sequences 5 to 6 m thick or as solitary, sharply defined layers in foliated or layered gabbro. Rarely, thicker sequences are encountered as at Phterykoudhi village (Figure 1, in pocket). This particular occurrence shows many features attributable to crystal settling processes and varies in composition from wehrlitic at the base to orthopyroxenitic at the top. The layers range from 1 to 25 cms in thickness and commonly exhibit poikilitic texture. Solitary ultramafic layers elsewhere are really just olivine-rich gabbro and generally grade upwards over 10 to 30 cms into pyroxene gabbro. Both types of ultramafic occurrence appear to be cogenetic with the gabbro that immediately surrounds them and are therefore considered to represent cumulate layers produced during the early stages of fractionational crystallisation of the respective mafic magma chamber. Field relationships support this model since the ultramafic rocks appear to form suspended layers in the layered sequences at the bases of mafic plutons.

The order of mineral crystallisation in the best developed ultramafic sequences near Phterykoudhi appears to have been: olivine + spinel, clinopyroxene, and orthopyroxene and plagioclase. Mineral compositions are presented in Table 1. Olivine (av Fo_{79}) is nearly everywhere altered to serpentine. Clinopyroxene occurs as either a cumulus phase or interstitial together with plagioclase. Two mineral phases which are noted as occurring occasionally as oikocrysts are orthopyroxene (En_{80}) which is the most common and plagioclase (An_{90}). In some samples of lherzolites, plagioclase is observed as small twinned euhedral chadacrysts in orthopyroxene oikocrysts.

GABBROS

The field relationships exhibited by the gabbros in the area are ambiguous and variable. Gabbro is seen intruding and being intruded by a variety of rock types. These include diabase, diorite and plagiogranite. A variety of gabbro compositions is represented ranging between olivine gabbro, norite and quartz-bearing uralite gabbro. No particular composition appears to be indicative of a specific level in the stratigraphy although there is an overall trend that gabbros become less mafic higher in the plutonic sequence. Compositions of single intrusions also vary and a pluton may be more mafic at its base than near its roof. This kind of relationship is well developed in the Phterykoudhi village area where olivine and clinopyroxene are observed to gradually decrease in abundance moving upwards in a gabbro body. Typical gabbros in the area of CY-4 are grey, medium-grained rocks, hypidiomorphic in thin section, and although mineral banding is rarely detected, the crystals display no preferred orientation. The Cyprus Geological Survey has recognised most of these rock types as uralite-gabbro. They are composed of zoned plagioclase, green hornblende (uralite), chlorite and, in places, quartz. Plagioclase varies from euhedral cumulus to intercumulus crystals to quench-textured laths towards the roof of any one intrusive body. More mafic gabbros in the Phterykoudhi area typically contain plagioclase as an intercumulate component (in many places as oikocrysts with chadacrysts of olivine) while the less mafic gabbros contain plagioclase as elongate laths up to 1 cm in length. Small patches of myrmekitic exsolution are commonly observed in those gabbros which are transitional to more felsic dioritic and granophyric rocks. Clinopyroxene is observed as cumulus and intercumulus crystals which are in most places partly altered to green pleochroic amphibole. In the olivine-bearing gabbros, clinopyroxene is observed exsolving orthopyroxene as herring-bone lamellae in twinned crystals. Orthopyroxene is most common in the more mafic gabbros, particularly those that contain olivine. It is generally almost entirely altered to bastite or amphibole and opaques. Olivine, where present, is usually found as resorbed subhedral crystals, generally serpentinised especially along miriad fractures. Quartz is usually seen in small amounts and only in those gabbros in close proximity to hornblende-trondhjemite. It occurs in two forms, as exsolved blebs and patches of myrmekite and as anhedral crystals which fill spaces between altered laths of plagioclase. The quartz occurring as myrmekite is

considered both primary and secondary with respective proportions ambiguous in thin section. At Palekhori, gabbros outcrop as discontinuous zones along the perimeter of a large plagiogranite body and appear to become less mafic moving towards the plagiogranite contact. On the northeast margin of the body, xenoliths of gabbro are found in the plagiogranite, while on the southern margin, pegmatitic gabbro is found along the contact. This material is suspended in more normal, medium-grained material and contains primary bladed amphibole crystals up to three and four centimetres in length and often aggregated into greenish-black clots.

PLAGIOGRANITIC, DIORITIC AND OTHER GRANOPHYRIC ROCKS

The plagiogranites are considered to represent the end products of fractional crystallisation and show considerable petrologic diversity both in mineralogy and post-magmatic alteration. They are siliceous plutonic rocks containing widespread occurrences of albite, epidote, chlorite, actinolite and secondary quartz as the result of secondary hydrothermal metamorphism of greenschist facies grade (Gass and Smewing, 1973; Spooner et al., 1974). Wilson (1959) divided the plagiogranitic rocks into three major types, "hornblende-trondhjemite", "epidote-trondhjemite" and "quartz-granulite". In our reconsideration of the area only the "hornblende" and "epidote" varieties are recognised since the quartz-granulites are essentially quartz-rich diabasic rocks of the Sheeted Complex. The hornblende variety is more reasonably called a diorite and is transitional between the uralite gabbros and true plagiogranites. Modally, the essential minerals are quartz, zoned plagioclase, actinolite, minor amounts of diopside and epidote and accessory sphene and epidote. The distinctive features of this rock are the occurrence of abundant patches of myrmekitic intergrowth and the variable styles in which quartz occurs: 1. as radiating almost spherulitic intergrowths in feldspar, forming myrmekite; 2. as large, highly irregular crystals and; 3. as granular aggregates. In the Phterykoudhi area, the dioritic rocks have an alteration mineral assemblage of quartz, chlorite, carbonate and zeolite. At one locality just north of the village, the margins of a dioritic intrusion and adjacent sheeted diabase have been thoroughly obliterated and leached by hydrothermal activity. The resultant lithology is a chalky-white rock with green clots of epidote. Prehnite and zeolites fill vugs and partially open fractures. This rock may in part resemble the "epidote-trondhjemites" of Wilson (1959): "a medium-grained rock which, except for epidote, is remarkably free of ferromagnesian minerals.....almost a pure white rock in which green specks and irregular patches of granular epidote are conspicuous".

TABLE 1. Mineral analyses for samples from the Palekhori area

	1	2	3	4	5	6	7	8	9	10	11	12	13	14	15	16
	UM	UM	UM	UM	G	G	PL	PL	UM	UM	UM	UM	UM	UM	UM	UM
	PT185	PT285	PT385	PT585	A6684	A7484	A8684	52885	PT185	PT585	PT185R	PT185C	PT385	PT385C	PT385R	PT385
SiO_2	44.98	46.52	45.30	52.75	45.81	44.95	65.01	69.84	52.72	53.48	38.36	38.16	35.77	37.52	37.38	54.31
TiO_2	0.00	0.03	0.03	0.07	0.00	0.03	0.01	0.01	0.26	0.03	0.02	0.00	0.00	0.01	0.00	0.18
Al_2O_3	34.82	32.43	33.45	29.24	32.68	33.90	26.21	19.35	1.82	1.70	0.02	0.04	0.01	0.02	0.02	1.20
Cr_2O_3	0.02	0.00	0.02	0.00	0.02	0.02	0.05	0.00	0.33	0.26	0.00	0.04	0.01	0.00	0.00	0.09
FeO	0.45	0.57	0.52	0.46	0.58	0.67	0.09	0.13	5.58	5.08	20.50	19.93	24.14	24.25	24.34	13.62
MnO	0.00	0.01	0.02	0.00	0.02	0.00	0.00	0.00	0.07	0.13	0.24	0.27	0.09	0.08	0.09	0.23
MgO	0.04	0.09	0.02	0.09	0.04	0.09	0.00	0.02	17.53	18.55	40.07	40.04	38.97	38.33	38.05	28.42
CaO	18.73	17.38	19.16	12.60	19.69	18.53	0.43	0.79	20.93	20.77	0.12	0.10	0.06	0.05	0.04	1.71
Na_2O	0.84	1.05	0.96	4.46	0.51	0.83	7.56	10.64	0.21	0.07	0.00	0.00	0.00	0.00	0.00	0.00
K_2O	0.02	0.01	0.02	0.01	0.00	0.01	0.03	0.09	0.00	0.00	0.00	0.00	0.00	0.00	0.00	0.00
NiO	0.02	0.02	0.00	0.03	0.00	0.00	0.00	0.01	0.01	0.00	0.00	0.00	0.00	0.00	0.00	0.00
Total	99.92	98.11	99.50	99.71	99.35	99.70	99.39	100.88	99.46	100.07	99.43	98.79	99.17	100.30	99.97	99.84
Na	0.074	0.095	0.086	0.393	0.045	0.074	0.635	0.891	0.014	0.004	0.000	0.000	0.000	0.000	0.000	0.000
Mg	0.001	0.005	0.001	0.005	0.001	0.005	0.000	0.000	0.962	1.008	1.551	1.557	1.547	1.497	1.492	1.521
Al	1.898	1.792	1.835	1.569	1.795	1.866	1.340	0.984	0.079	0.073	0.000	0.000	0.000	0.000	0.000	0.050
Si	2.082	2.181	2.110	2.403	2.136	2.101	2.819	3.016	1.941	1.950	0.996	0.995	0.953	0.982	0.983	1.952
K	0.000	0.000	0.001	0.000	0.000	0.000	0.001	0.005	0.000	0.000	0.000	0.000	0.000	0.000	0.000	0.000
Ca	0.929	0.872	0.955	0.615	0.982	0.927	0.019	0.035	0.826	0.811	0.003	0.002	0.001	0.000	0.000	0.065
Ti	0.000	0.000	0.000	0.001	0.000	0.000	0.000	0.000	0.006	0.000	0.000	0.000	0.000	0.000	0.000	0.004
Cr	0.000	0.000	0.000	0.000	0.000	0.000	0.001	0.000	0.008	0.006	0.000	0.000	0.000	0.000	0.000	0.002
Mn	0.000	0.000	0.000	0.000	0.000	0.000	0.000	0.000	0.001	0.003	0.004	0.005	0.001	0.001	0.001	0.006
Fe	0.016	0.022	0.019	0.017	0.021	0.026	0.002	0.003	0.172	0.154	0.445	0.434	0.538	0.531	0.535	0.409
Ni	0.000	0.000	0.000	0.000	0.000	0.000	0.000	0.000	0.000	0.000	0.001	0.003	0.002	0.000	0.000	0.002
Total	5.000	4.966	5.008	5.002	4.981	4.999	4.817	4.934	4.009	4.009	3.000	2.996	3.042	3.013	3.012	4.012

UM = Ultramafic rock essentially plagioclase wehrlites, G = Gabbro, PL = Plagiogranite, C = Core, R = Rim
1–8 plagioclase; 9–10 clinopyroxene; 11-15 olivine; 16 orthopyroxene

The plagiogranite in the Palekhori area is generally more siliceous than the dioritic rocks found near Phterykoudhi. This is clearly evident in the field where the low modal abundance of amphibole and the dominance of feldspar laths and quartz as large equigranular crystals is obvious. The large plagiogranite stock in the Palekhori area alongside which hole CY-4 was sited, clearly intrudes sheeted diabase dykes and gabbroic rocks and contains many xenoliths of both. This is best observed in the northern and central portions of the pluton. The plagiogranite is also cut by numerous diabase dykes around its margin. In these areas the plagiogranite appears as wide screens and the number of cross cutting dykes decreases moving towards the center of the intrusion. On the western side of the plagiogranite, gabbro xenoliths are common in various stages of assimilation. The progressive assimilation of gabbro, or diabase, by the plagiogranite is clearly related to the local development of a dioritic lithology by resorbtion and mixing.

It appears, on the basis of the field evidence that the dioritic rocks of the upper parts of the Troodos plutonic series may therefore have two origins. Some are clearly a product of fractionation of a mafic and probably somewhat hydrous melt and lie on a differentiation trend that eventually produced the most silicic plagiogranitic rocks. However, others are a result of the assimilation of gabbroic and diabasic rocks by silicic plagiogranites and are especially common at the intrusive margins of plagiogranitic plutons.

THE SHEETED COMPLEX

The Sheeted Complex forms much of the outcrop in the area in question. Although most of the dykes exhibit a greenschist-grade metamorphism, original features are for the most part well preserved. The majority of the sheeted dykes are moderately to highly altered, fine- to medium-grained, aphyric diabases. Comparatively few unaltered, fine-grained clinopyroxene-and plagioclase-phyric dykes have also been recognised. Individual dykes range in width from less than 10 cm up to 4-5 m with the average being 1 m. Dyke trends vary from NNW-SSE and NNE-SSW. Variation is also apparent in the dip direction, with the majority of the dykes dipping to the east but a sizeable number to the west. The westerly dipping dykes are concentrated near or within the two plagiogranite bodies close to Askas village.

The sheeted appearance of the dykes, as well as their chilled margins are easily observed except where the alteration is particularly intense. This alteration generally is in the form of veins of zeolites with minor growth of epidote and chlorite, and varying degrees of silicification as a result of hydrothermal circulation.

The diabases consist of bytownite, uralite, not so rare quartz, minor opaques and secondary alteration minerals. Uralite replaces augitic pyroxene to various degrees everywhere. An important feature of the petrography is the occurrence of quartz which is inferred to be mostly primary on the basis of its abundance and appearance. The grains have dimensions commensurate with those of the surrounding minerals and commonly exhibit discreet crystal shapes. Since the diabase dykes collected close to plagiogranite bodies have generally similar quartz contents to those far away, there can be little metasomatic influence from plagiogranitic intrusions. It is likely that the widespread occurrence of these quartz-diabases is as feeders to the andesite-dacite-rhyodacite volcanic assemblage of Robinson et al (1983). This is consistent with the view of Malpas and Langdon (1984) that the feeders to these volcanics are predominant in this portion of the stratigraphy, with those to the more mafic and depleted volcanics occurring in dispersed fault-controlled swarms (Figure 2).

GABBRO AND PLAGIOGRANITE RELATIONSHIPS WITH THE DIABASE

Any discussion of plutonic rock-diabase intrusive relationships must consider the three observed alternatives (Figure 3): i) the gabbro or plagiogranite intrudes the diabase dykes, ii) the gabbro gives rise directly to diabase dykes, and iii) diabase dykes intrude the gabbro or plagiogranite. The third observation is of greatest importance in the development of a model for the origin of the dykes and the high level intrusives, since an abundance of diabase dykes intruding gabbro the plutonic rocks, especially ones of a higher degree of differentiation suggests the involvement of multiple magma chambers. A single magma chamber, such as that proposed by Greenbaum (1972), is unlikely in this case because the dykes are intruding and often chilled against the magmatic system which should have fed them. Thus a separate source for the dykes, such as one or more additional magma chambers, is required. Such chambers could be situated either below the dykes or along their strike (in which case dyke intrusion would be lateral rather than vertical). It is of course conceivable that both a gabbro and intruded diabase could have been generated in the same magma chamber system if the gabbro was present as a marginal wall rock or possibly sub-roof cumulate. This is not the case where plagiogranite is involved. Roof or wall rocks are also often identifiable by decrease in grain size towards a microgabbro at the margin of the pluton.

DIABASE DYKE CHILLING STATISTICS

Statistical analysis of chilled diabase dyke margins was first carried out in the Troodos Complex by Kidd and Cann (1974). They concluded from that study that the mechanism of formation of the Sheeted Complex involved ocean-floor spreading at a narrow locus to the present day west of the ophiolite's position. In their relatively uncomplicated model they did not consider the

involvement of multiple magma chambers and the possible shifting of injection centres (a form of ridge jumping) along the spreading ridge (Baragar et al., 1987). Furthermore, the results of dyke chilling statistics are by no means convincing. Kidd and Cann (1974) observed a predominance of margins chilled to the east in 19 of 23 dyke transects. These margins however, were in excess of those chilled to the opposite side by only a maximum of three with a range of one also common. A number of additional sections were measured during the course of field studies for the Cyprus Crustal Study Project and show quite different results from those of Kidd and Cann. More than half of those measured (12) exhibit either a bias of west-sided chills or no bias at all (See Figure 1). As Gass (1980) pointed out, there is no way of precluding the possibility that the diabase dykes situated between the areas used for statistical analysis might show a predominance of margins chilled in the opposite direction to that indicated in the measured sections. Another interesting point to note in the Askas dyke section of Figure 1, is that the predominance of dykes showing two-sided chilling suggests a much wider zone of injection than that estimated by Kidd and Cann. It is our impression that little reliance should be placed in the simplified model of seafloor spreading envisaged by the Kidd and Cann statistics, at least in terms of generation of the Troodos Complex.

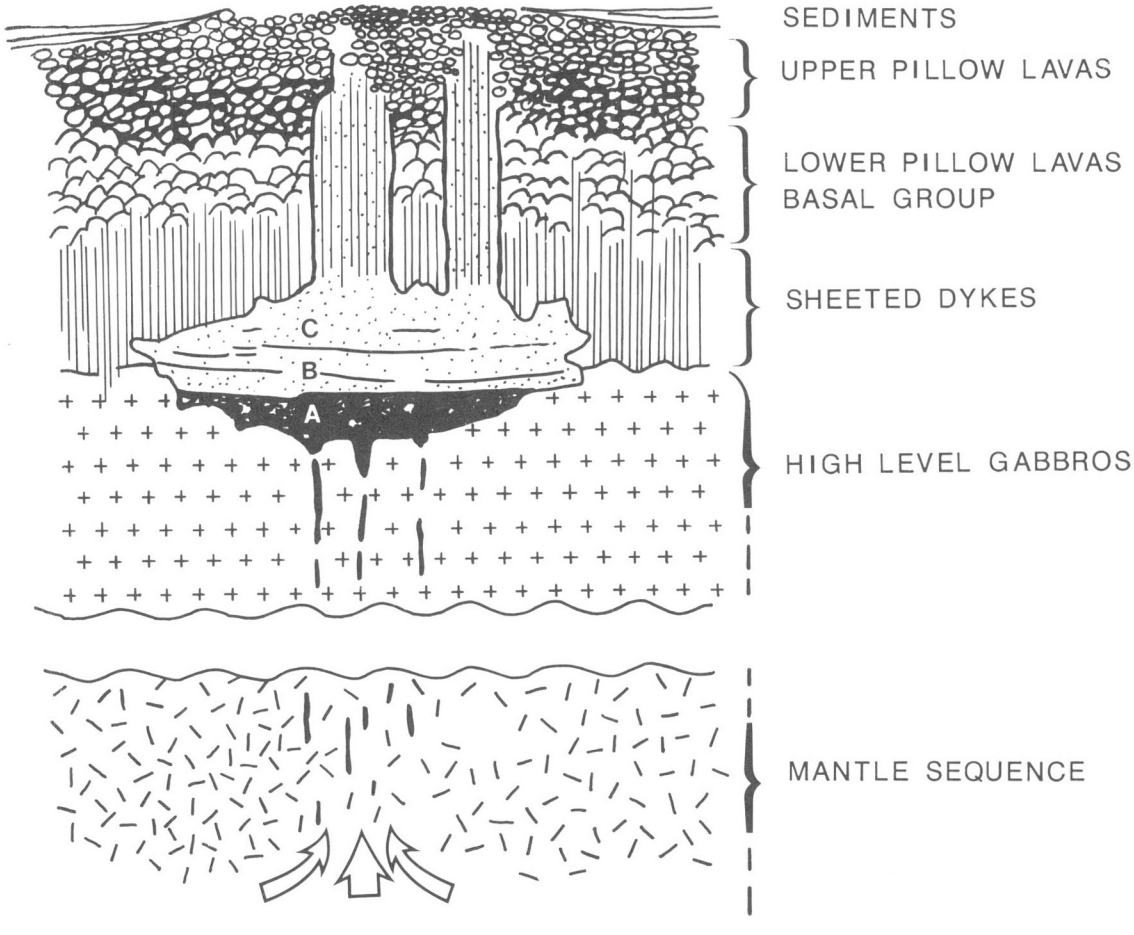

Figure 2: Late stage high level magma chambers feeding the Upper Pillow Lava sequence through a series of fault controlled dyke swarms. A, B, and C are progressive degrees of fractionation of the magma as a result of the cumulus crystallisation of olivine and/or pyroxene in the base of the chamber giving rise to the ultramafic horizons of the upper plutonic complex.

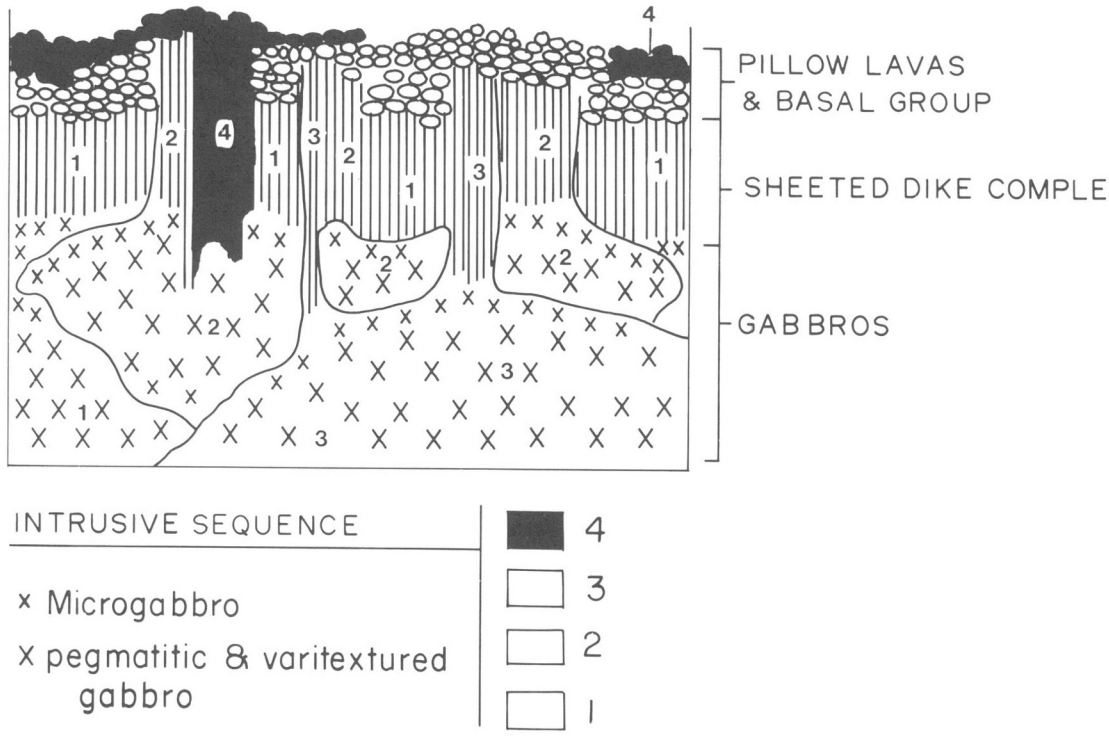

Figure 3: The complexity of the sheeted dyke horizon results from intrusion from multiple magma chambers such that the dyke swarm shows three possible relationships with the underlying plutonic rocks, i.e. intruded by plutonics, fed by plutonics or cutting plutonics.

ALTERATION AND METAMORPHISM

The high level plutonic rocks in the vicinity of the CY-4 borehole have essentially been modified in two distinct ways. The most common alteration is that of a pervasive greenschist to lower amphibolite facies metamorphism, while the second, more localised type of alteration is that of an intense hydrothermal leaching and epidotisation. The pervasive alteration is most likely the result of hydration and metamorphism involving seawater which percolated down through the rocks along numerous fractures during, or just after the formation of the ophiolite at a spreading centre (i.e. the recharge of hydrothermal circulation systems). The alteration zones characterised by intense leaching and epidotisation have been studied in some detail by Schiffman and Smith (1988) and Richardson et al. (1987), and are considered to be the result of activity within the upwelling limbs of the hydrothermal system which were apparently more focussed. These would have fed the discharge zones of hot fluids in the higher parts of the ophiolite, presumably in the form of black smoker-like activity which deposited the exhalative sulphide bodies. Noteably, the root zones of this upwelling are in many places (eg near Phterykoudhi village) associated with stocks of plagiogranite and diorite that appear to have intruded high into the basal section of the Sheeted Complex and which formed cupolas of cooling magma that acted as the heat engine for the hydrothermal circulation system.

SUMMARY

In general, the field relationships observed in the vicinity of CY-4 suggest:

a) for the most part, plagiogranite intrudes gabbro and the intrusive boundary is marked by assimilation of the more basic rock to produce dioritic lithologies. In a few areas, a case can be made for the progressive fractionation of a gabbroic magma to a plagiogranitic end product.

b) both gabbro and plagiogranite have intruded diabase dykes of the Sheeted Complex.

c) both gabbro and plagiogranite have been cut by numerous diabase dykes which in places give rise to a mappable unit consisting of approximately equal amounts of either gabbro and diabase or plagiogranite and diabase.

e) the dykes intruding the plagiogranites are generally younger than tho se which cut adjacent gabbro.

f) the high level plutonics and dyke complex of the ophiolite resulted from the intrusion of a number of magma chambers. These chambers appear to have been nestled both vertically and laterally and were probably of the order of 1 to 5 km in maximum dimension.

g) alteration of the high level plutonics is generally a result of the pervasive downflow of seawater as part of the recharge of the hydrothermal circulation systems which were driven by the heat from cooling magmatic bodies. Seawater may have entered the magma chamber by the assimilation of hydrated roof rocks and undoubtedly played a part in the generation of the plagiogranites by removing elements such as K and Rb (and metals ?) from the magmatic system. Localised silicified and epidotised zones, in many places associated with cupolas of plagiogranite and diorite, are a result of extensive leaching by the seawater at the roots of discharge zones.

REFERENCES

Baragar, W.R.A., Lambert, M.B., Baglow, N. and Gibson, I.L.
1987: Sheeted dykes of the Troodos ophiolite, Cyprus; *in* Mafic Dyke Swarms, ed. H.C. Halls and W.F. Fahrig; Geological Association of Canada, Special Paper 34, p. 257-272.

Gass, I.G.
1980: The Troodos Massif: its role in the unravelling of the ophiolite problem and its significance in the understanding of constructive margin processes; *in* Ophiolites: Proceedings of the International Ophiolite Symposium, Cyprus 1979, ed. A. Panayiotou, Cyprus Geological Survey Department, Ministry of Agriculture and Natural Resources, p. 23-35.

Gass, I.G. and Smewing, J.D.
1973: Intrusion, extrusion and metamorphism at constructive margins: evidence from the Troodos Massif, Cyprus; Nature, v. 242, p. 26-29.

Greenbaum, D.
1972: Magmatic processes at oceanic ridges: evidence from the Troodos Massif, Cyprus; Nature, Physical Sciences, v. 238, no. 80, p. 18-21.

Kidd, R.G.W. and Cann, J.R.
1974: Chilling statistics indicate an ocean floor spreading origin for the Troodos complex, Cyprus, Earth and Planetary Science Letters, v. 24, no. 1, p. 151-155.

Malpas, J. and Langdon, G.
1984: Petrology of the upper pillow lava suite, Troodos ophiolite, Cyprus; *in* Ophiolites and the Oceanic Lithosphere, ed. I.G. Gass, S.J. Lippard and A.W. Shelton; Geological Society of London Special Publication no. 3, Blackwell Scientific Publications, Oxford, p. 155-167.

Richardson, C.J., Cann, J.R., Richards, H.G. and Cowan, J.G.
1987: Metal depleted root zones of the Troodos ore-forming hydrothermal systems, Cyprus; Earth and Planetary Science Letters, v. 84, p. 243-253.

Robinson, P.T., Melson, W.G., O'Hearn, T. and Schmincke, -H.U.
1983: Volcanic glass compositions of the Troodos ophiolite, Cyprus; Geology, v. 11, no. 7, p. 400-404.

Schiffman, P. and Smith, B.M.
1988: Petrology and oxygen isotope geochemistry of a fossil seawater hydrothermal system within the Solea Graben, Northern Troodos ophiolite, Cyprus; Journal of Geophysical Research, v. 93, p. 4612-4624.

Spooner, E.T.C., Beckensdale, R.D., Fyfe, W.S. and Smewing, J.D.
1974: O^{18} enriched ophiolitic metabasic rocks from E. Liguria (Italy), Pindos (Greece) and Troodos (Cyprus); Contributions to Mineralogy and Petrology, v. 47, p. 41-62.

Wilson, R.A.M.
1959: The geology and mineral resources of the Xeros-Troodos area; Geological Survey of Cyprus Memoir #1, 135p.

Structural and Petrologic Relationships of the CY-4 Drill Hole of the Cyprus Crustal Study Project

J. MALPAS, T. BRACE AND S.M. DUNSWORTH

Department of Earth Sciences, Memorial University of Newfoundland,
St. John's, Newfoundland

Malpas, J., Brace, T. and Dunsworth, S.M. The regional geology and petrology of the CY-4 drillhole CYprus in *Cyprus Crustal Study Project: Initial Report, Hole CY-4, ed. I.L. Gibson, J. Malpas, P.T. Robinson and C. Xenophontos; Geological Survey of Canada, Paper 88-9, p. 39-67, 1989.*

Abstract

Hole CY-4 of the Cyprus Crustal Study Project was intended to sample the plutonic complex of the Troodos ophiolite from the base of the sheeted dykes down to mantle tectonites. Accompanying the drilling programme was an intensive field mapping project which together with the results from drilling was aimed at elucidating the complex magmatic and structural history of a fossil crustal accretion zone and the relationships between the plutonic series and the extrusive volcanic carapace of the ophiolite. The recognition of an older series of deformed plutonic rocks intruded by a series of undeformed cumulate rocks is the most significant evidence supporting the model of multiple magma chambers at the spreading axis. Geochemical evidence from from the CY-4 borehole supports the structural relationships and indicates that the borehole intersected two separate magma bodies which can be related to the major geochemical subdivisions of the pillow lava sequence.

Résumé

Le forage CY-4 du Projet d'étude de la croûte terrestre à Chypre avait pour objectif d'intersecter la séquence plutonique de l'ophiolite de Troodos depuis la base du complexe filonien jusqu'aux tectonites du manteau. Ce programme de forage était appuyé par un projet intensif de cartographie. Les résultats de ces deux activités devaient être combinés afin de mieux comprendre les histoires magmatiques et structurales complexes d'une zone d'accrétion fossile, et les relations existant entre les séries plutoniques et la carapace de roches volcaniques extrusives de l'ophiolite. L'identification de séries plutoniques anciennes déformées recoupées par des séries de cumulats non déformés est la preuve la plus éloquente supportant le modèle des chambres magmatiques multiples sous l'axe des dorsales en expansion. Les analyses géochimiques des carottes du trou CY-4 corroborent les relations structurales de terrain et indiquent que le forage a recoupé deux corps magmatiques distincts lesquels peuvent être corrélés avec les sous-groupes géochimiques majeurs identifiés dans la séquence de laves coussinées.

INTRODUCTION

Hole CY-4 is the fourth in a series of holes drilled in an effort to reassess the geology of the Troodos ophiolite, Cyprus. CY-4 penetrated 2263 m near the village of Palekhori, at 34°54'06" N and 33°05'38" E through the sheeted dyke complex and plutonic section of the ophiolite, but failed to reach ultramafic tectonites of the mantle section. The siting of CY-4 was controlled by both geological and logistical factors. Geologically, the hole was intended to sample as much of the plutonic sequence as possible. Logistics, on the other hand, required good access for vehicles, site stability and the availability of water. A site 1 km south of the village of Palekhori on the Palekhori-Agros road appeared to provide favourable conditions (Figure 1).

The area surrounding the drilling site consists of sheeted diabase dykes, gabbros, plagiogranites and ultramafic cumulate rocks in decreasing order of abundance. Mapping undertaken by the Geological Survey Department of Cyprus, indicated that the sheeted dyke complex is intruded by a high level plagiogranite body immediately adjacent to the drill site. Dykes of plagiogranite up to 3 metres wide, containing xenoliths of diabase cut the sheeted dykes in roadside outcrops. From our understanding of the ophiolite stratigraphy at the time of choosing the site, it was considered that the dykes would terminate some 70 to 100 metres below outcrop level in a plagiogranite stock. The plagiogranite was expected to grade into diorites and gabbros representing a major portion of the plutonic complex. The subsequent drilling and a further consideration of the regional geology carried out in an associated field programme described below, proved otherwise.

FIELD RELATIONSHIPS

The first indications of the complexity of magmato-tectonic relationships in the plutonic sequence came from detailed mapping north and west of Mount Olympus (Figure 2). This mapping revealed oblique, cross-cutting relationships between a number of lithological units. These relationships occur on all scales ranging from thin micro-gabbro dykes cross-cutting dunite and harzburgite to single ultramafic plutons of considerable size (>20 km^2 in plan view) cross-cutting harzburgite, dunite and layered gabbro. Oblique relationships between internal planar elements such as compositional layering or tectonite fabrics and the margins of individual plutons were also observed.

In this area two major plutonic suites can be distinguished on the basis of these cross-cutting relationships and on the relative ages of deformation and magmatism (Dunsworth and Calon, 1984; Malpas and Robinson, 1987).

The Early Suite

The early suite, distinguished by its penetratively deformed nature, consists of harzburgite tectonite, dunite with chromitite and layered olivine pyroxenite and gabbro. The entire suite shows evidence of high temperature deformation characterised by the development of penetrative L-S fabrics and small isoclinal folds (Figure 3). The enveloping surfaces of the major lithological boundaries within the suite are oriented at a high angle to the tectonite foliation. This fabric is generally parallel to compositional layering where present but, clearly cross-cuts layering in the hinges of isoclinal folds. Deformation of this early suite has led to the transposition of layering parallel to the tectonite fabric. L-fabrics and fold axes plunge eastward at moderately steep angles, and appear to lie on the enveloping surface of the main lithological boundaries. The geometry of the early suite structures reflects large scale, solid-state mantle upwelling which produced the domal form (Nicolas and Violette, 1982). Because this structure was intruded by a second suite of plutons, it is believed to have formed at the fossil spreading centre rather than by late stage serpentinite diapirism as suggested by Allen (1975). The structures imposed upon the plutonic rocks are considered to have formed during upward and lateral movement during seafloor spreading.

The internal geometry of these rocks poses severe restrictions on the interpretation of their petrological evolution. Igneous way-up criteria, if originally present, have for the most part been obliterated by the deformation. Also, it is difficult to ascertain unambiguous crystallisation sequences from textures because of extensive syn-tectonic recrystallisation (annealing) of all constituent minerals.

In the area of Pano Amiandos (Malpas and Brace, 1987), the deformation of early suite gabbros is clearly related to a major fault which emplaces deformed layered dunites, wehrlites and pyroxenites over the gabbros. The gabbros take on a mylonitic aspect close to the contact and the intensity of deformation gradually decreases away from the fault. The mylonite fabric and the fault strike are essentially parallel. The fact that these deformed gabbros are cut by veins and dykes of undeformed gabbros suggests that the deformation, and thus the faulting, were produced during the formation of the ocean crust.

Late Undeformed Plutons

Throughout the plutonic sequence, deformed rocks of the early suite are intruded by a series of essentially undeformed plutons which generally exhibit well preserved cumulate features and igneous textures (Figure 2). However, in a few areas e.g. near the Caledonian Falls and Prodhromos, these younger plutons are also modified by high temperature deformation along their margins. Indeed, the division into early and late suites is only applied locally since both deformation and magmatism were diachronous and lithologies of apparent late suite

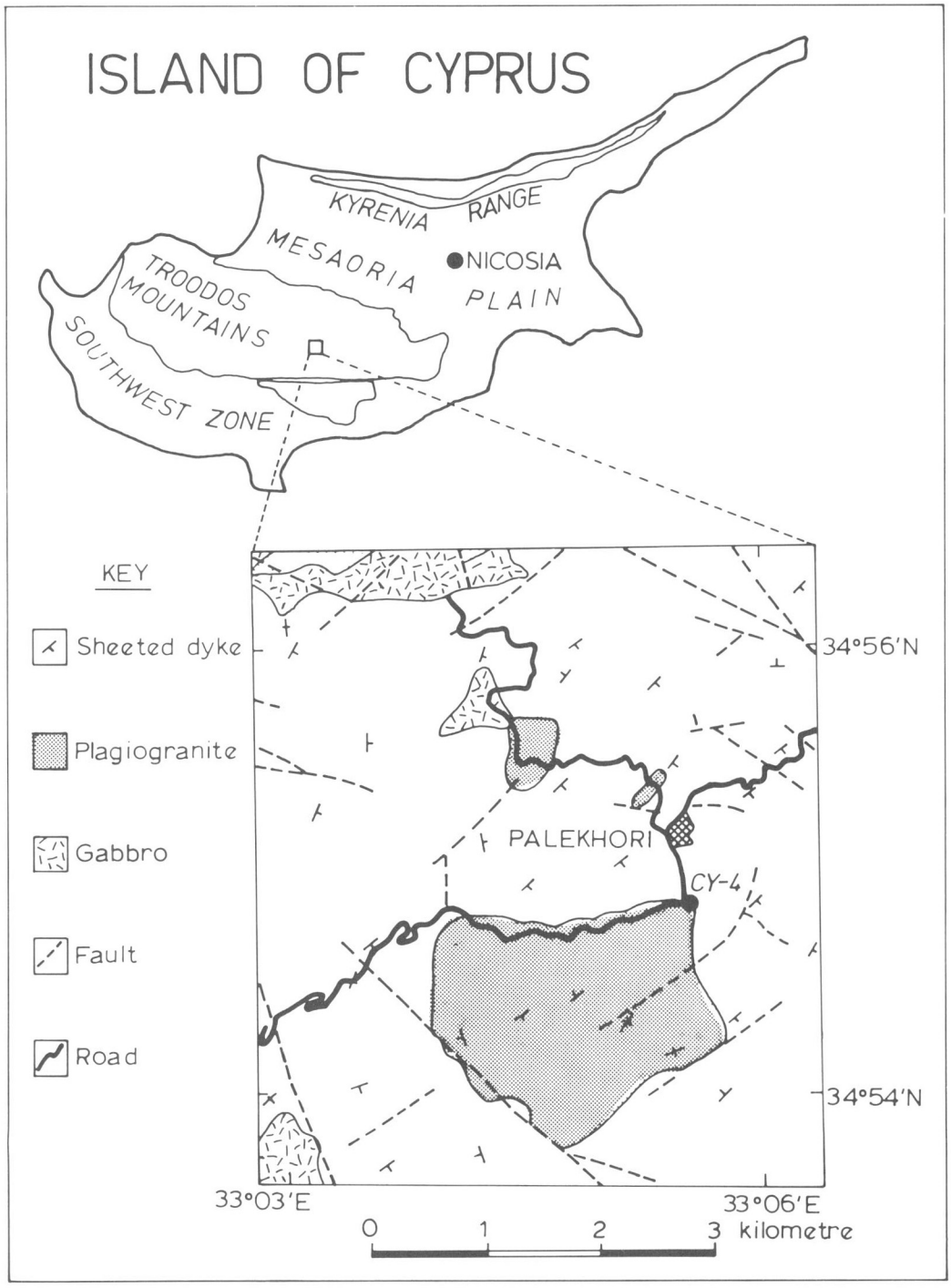

Figure 1: Location of the CY-4 borehole of the Cyprus Crustal Study Project on the margins of a major plagiogranite stock near Palekhori Village.

rocks in one area may be deformed elsewhere. Nevertheless, in the Mount Olympus region the later suite of rocks consists characteristically of plagioclase peridotites, pyroxenites, two-pyroxene gabbros, clinopyroxene-hornblende gabbros, plagiogranites and high-Mg microgabbro dykes. The most conclusive evidence of multiple intrusive relationships is the existence of xenoliths of early suite rocks in the margins of later intrusive bodies. These xenoliths are of various sizes, some being large enough to map at a 1:5000 scale. The xenoliths show various degrees of resorbtion and are often surrounded by accumulations of xenocrysts. The ultramafic components of the late suite are concentrated in a narrow, 1-2 km wide, north trending belt along the western flank of Mount Olympus, but, even here it is not unusual to find plagiogranites of this suite cutting ultramafic tectonites of the early suite, apparently very low in the stratigraphy.

The various ultramafic components of the late suite show mutually intrusive relationships. In the exposures in the lower part of the ophiolite section, these ultramafic components predominate over the more fractionated components in a volume ratio of 20:1. At this level, gabbroic and plagiogranitic phases are concentrated along the margins of plutons and they intrude rocks of the earlier suite as a series of veins or as swarms of vertical dykes which can be quite magnesium-rich (up to 16 wt. % MgO).

Higher in the stratigraphic sequence, for example in the immediate area of the CY-4 borehole, more fractionated rock types such as gabbro, diorite and plagiogranite become volumetrically more important than the ultramafic rocks (Figure 4). The intensity and penetration of deformation of older rocks are also considerably less and early and late suites are difficult to distinguish. At the top of the plutonic sequence microgabbros, magnetite-rich gabbros, diorites and plagiogranites form a roof assemblage with variable textures (varitextured gabbros).

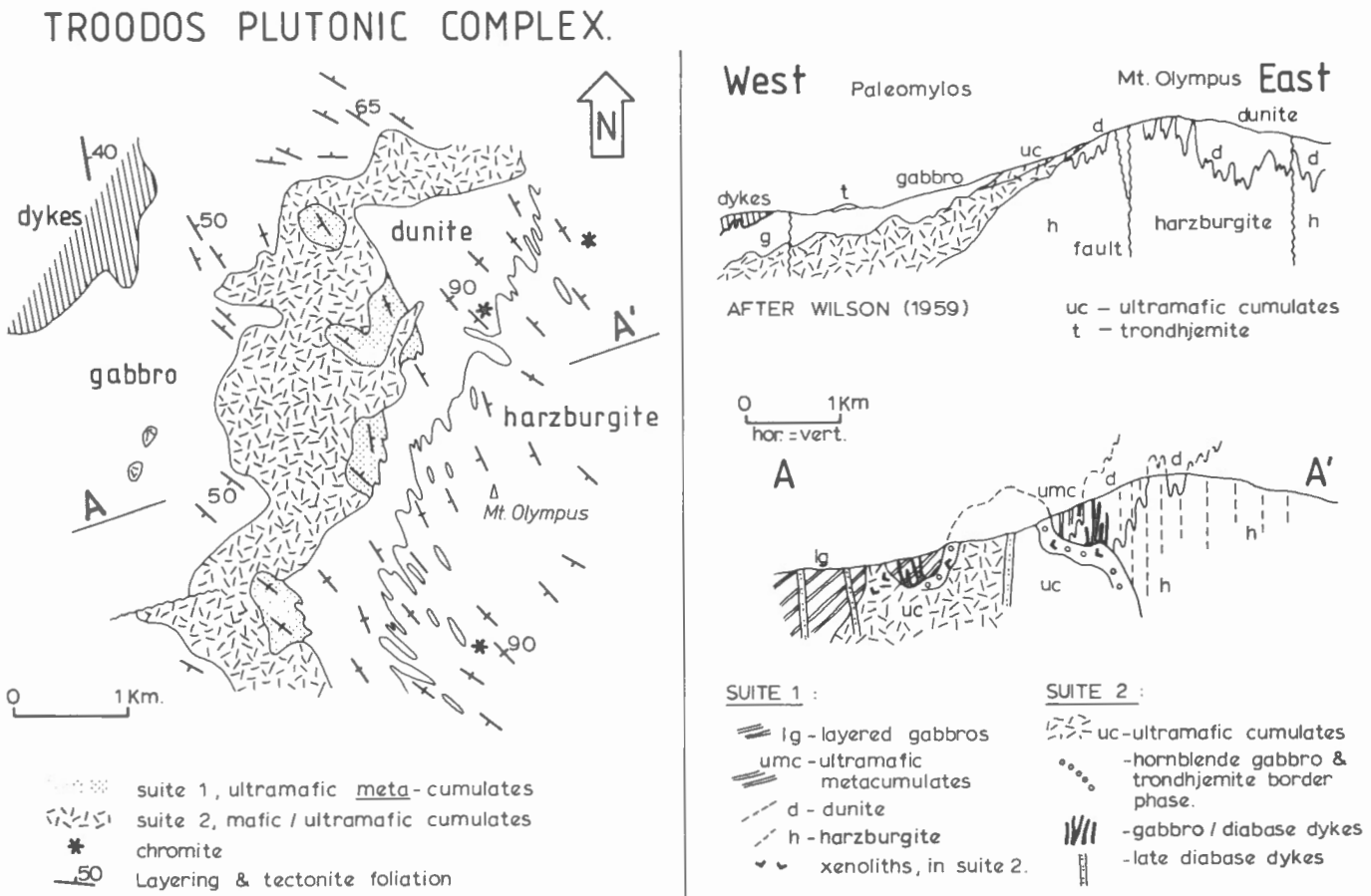

Figure 2: Reinterpretation of the field relationships in the lower part of the plutonic complex of the Troodos ophiolite to the west of Mt. Olympus a) in map form, b) as a cross section compared to the original cross section of Wilson (1959).

Figure 3a: Isoclinal folds in deformed pyroxenite/wehrlite complex at Pano Amiandos.

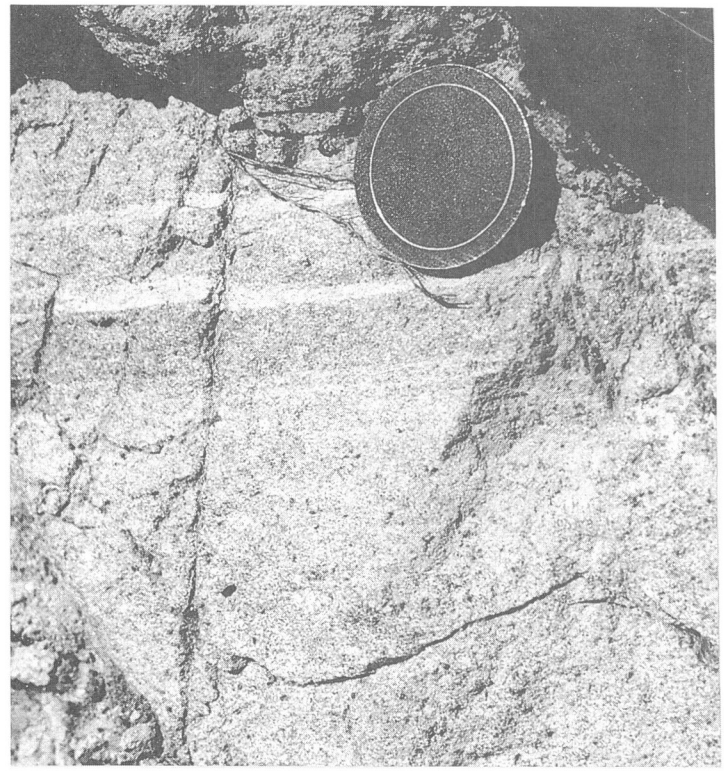

Figure 3b: Penetrative lineation fabric developed in early suite gabbros and cut by undeformed pegmatitic gabbros near Prodhromos.

At high levels in the plutonic sequence the multiple intrusive nature of the gabbros is best recognised on the basis of xenoliths of one gabbro lithology contained in a host gabbro of slightly different lithology. This is even more clear where the xenoliths are deformed gabbro and the host undeformed as is the case in a section of roadside outcrop just west of the village of Polystipos. Here, apparently cumulate gabbros display a marked horizontal banding. On closer examination this banding is seen to be the result of intrusive brecciation and polyphase deformation and not an igneous layering phenomenon. Thin, centimetre-wide bands are discontinuous and clearly flattened xenoliths of an early gabbro phase which now display very large aspect ratios (Figure 5). These xenoliths were completely recrystallised during deformation and in places preserve an internal relict deformation fabric with pyroxene porphyroblasts. The fabric is subparallel to the direction of maximum elongation of the xenoliths which itself is parallel to a distinct foliation in the host gabbro. In thin sections of the xenolith margins, the host gabbro contains polygonal pyroxene xenocrysts from the oldest gabbro phase.

The second gabbro also occurs as large rounded xenoliths in a third, undeformed gabbro phase 100 m to the east (Figure 6). The host to these inclusions is a gabbro which is varitextured with some pegmatitic patches and is associated in a layered sequence with poikilitic plagioclase lherzolite. Similar ultramafic lithologies are common in surrounding outcrops where they are clearly not the youngest phase since they are cut by pegmatitic gabbro dykes. The intrusion of the later undeformed gabbro stocks clearly post dates much of the sheeted dyke complex which is abruptly terminated against gabbros close by. At this intrusive contact a roof assemblage of varitextured hornblende gabbro and gabbro pegmatite is developed (Figure 7).

The multiple intrusive nature of the plutonic complex is thus consistent throughout the section from the mantle tectonites to the sheeted dykes.

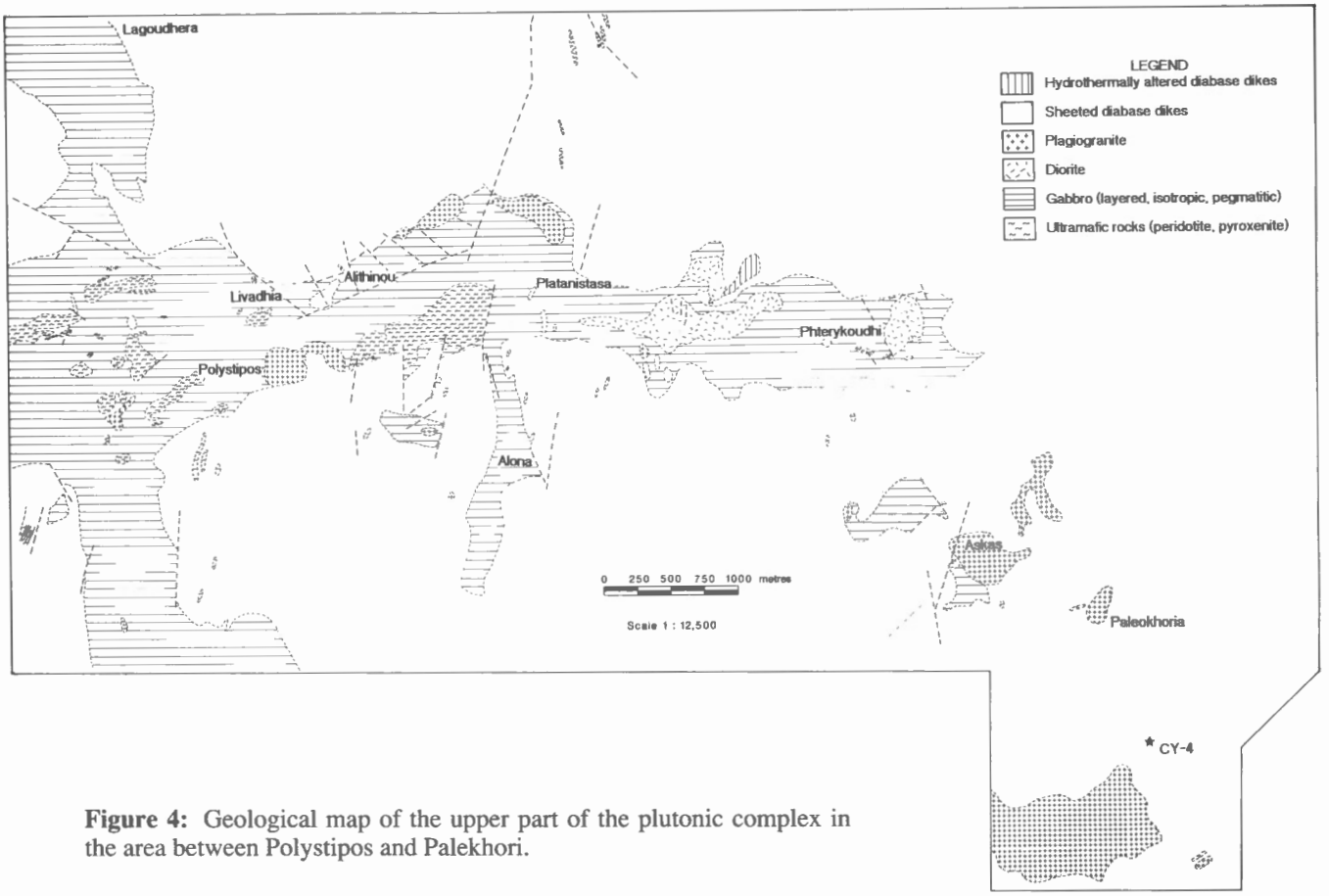

Figure 4: Geological map of the upper part of the plutonic complex in the area between Polystipos and Palekhori.

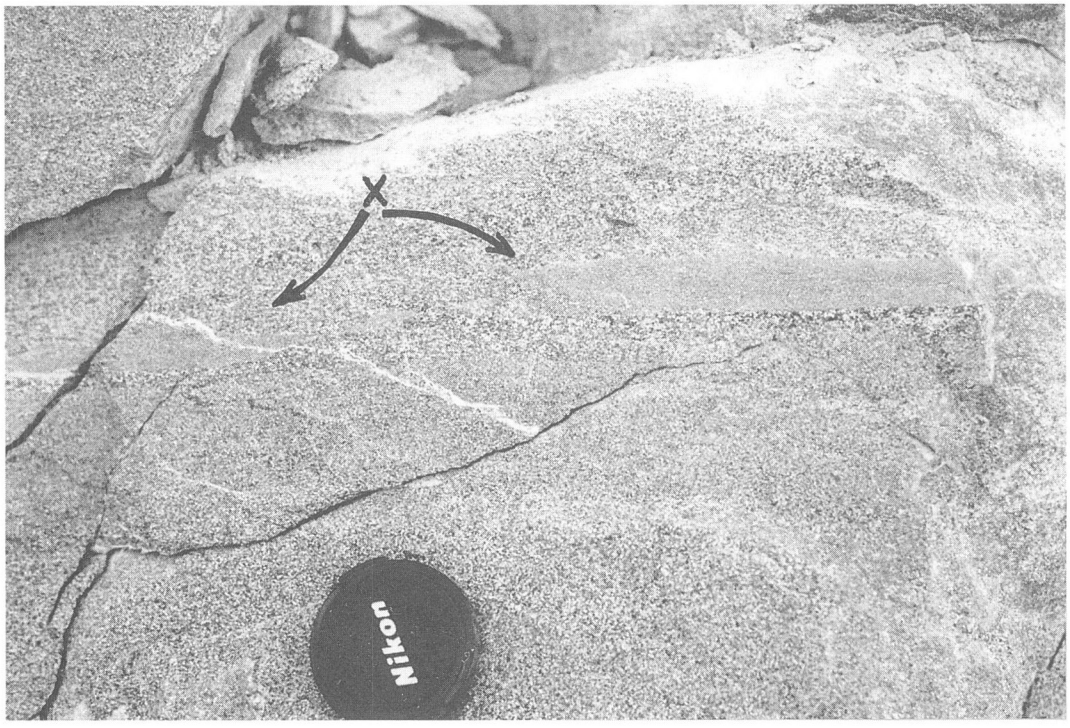

Figure 5: Deformed lensoid xenoliths of recrystallised gabbro in lineated gabbro host; see text for details. Outcrop is a few km west of Polystipos.

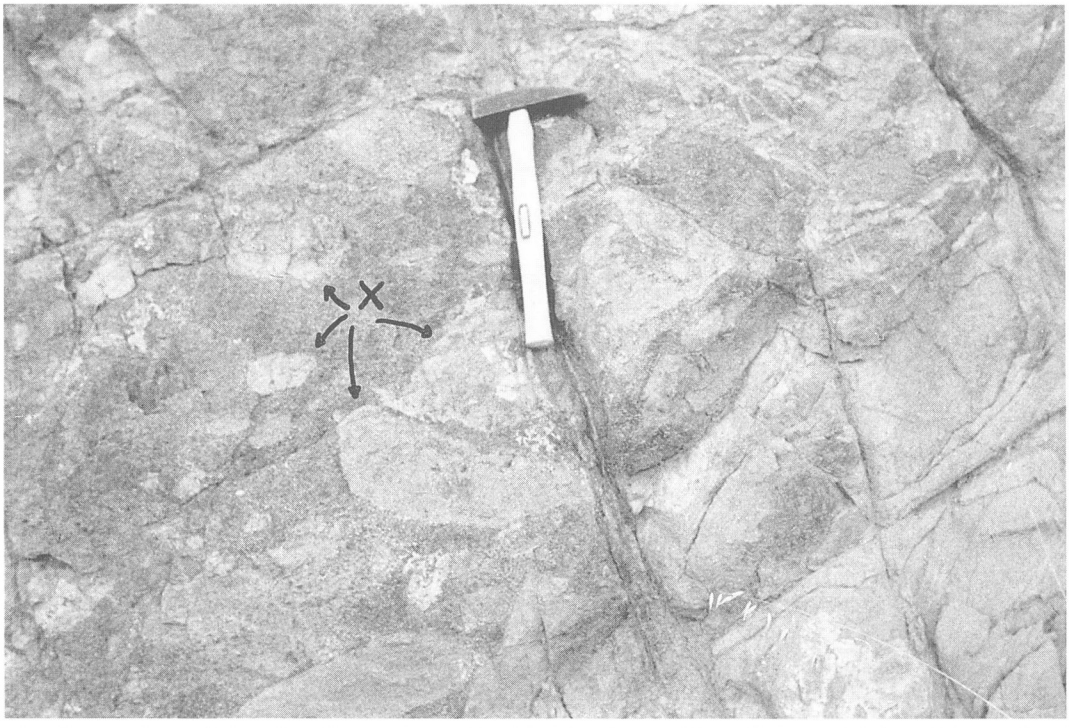

Figure 6: Rounded xenoliths of the host gabbro identified in Figure 5 included in a third, undeformed gabbro. Outcrop is 100 m east of Figure 5.

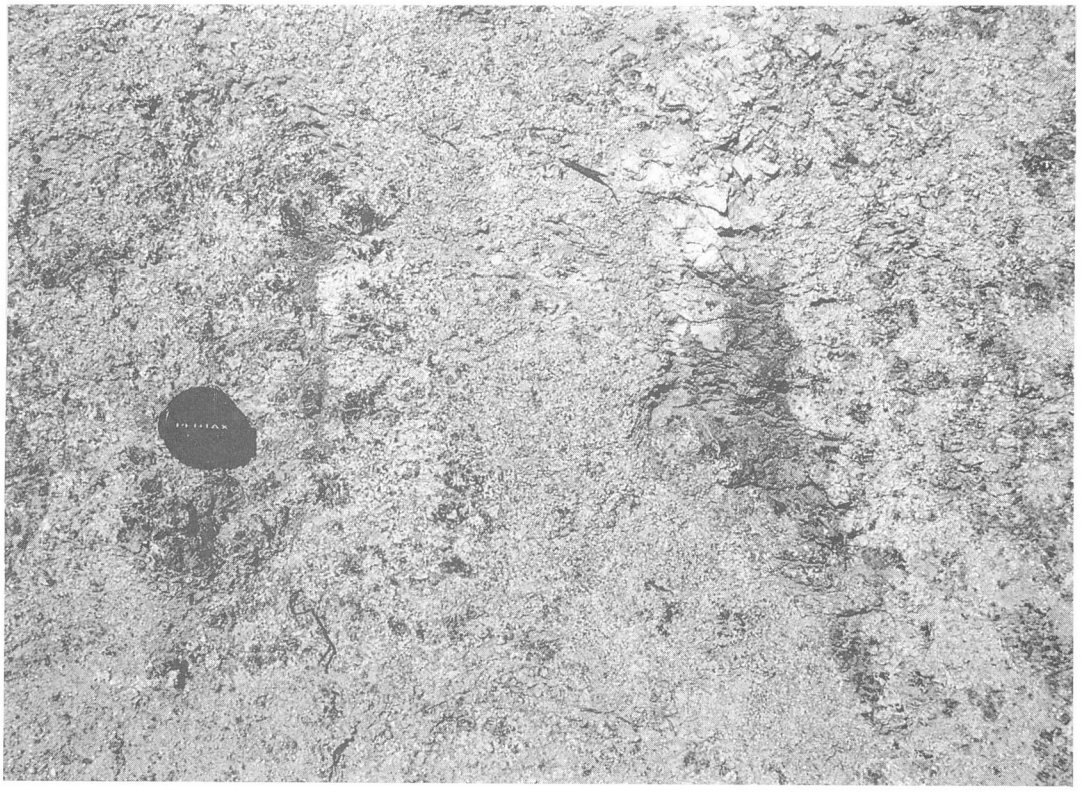

Figure 7: Varitextured gabbro from the roof complex of a small magma chamber near Livadhia.

Sheeted Dykes

Sheeted diabase dykes which separate the plutonic complex and the extrusive volcanic complex of the ophiolite make up the area immediately surrounding hole CY-4. The dykes trend NNW-SSE and are steeply dipping. In the field three contact relationships with surrounding plutonic rocks are observed, i) the sheeted complex is intruded by plutonic rocks (most common), ii) dykes intrude the plutonic rocks (less common) and iii) dykes arise directly from plutonic equivalents (least common). The relief on the sheeted dyke-plutonic contact is thus over 500 metres as swarms of dykes may cut through plutonics from depth and plutonics may punch high into the crustal section (Figure 8). It is through one of these deep dyke swarms that CY-4 apparently penetrated. Near the contact, dykes may in places be separated by screens of plagiogranite or gabbro, but, elsewhere dykes intrude other dykes. If the contact relationship is not exposed, a marked reduction of dykes from 100% sheeted complex to 5% dykes in plutonics over less than 10 metres along dyke strike, is generally a sign that the plutonics are intrusive, unless the contact is faulted.

Dykes range from a few centimetres to about 8 metres in width, but, most are generally less than two metres. Desmet et al (1980) have suggested a succession of dykes from oldest to youngest of diabasic, doleritic, ultrabasic and basaltic, but, recent results (Baragar et al, 1987) necessitate the reinterpretation of this sequence.

Varga and Moores (1985) have shown that the orientations of dykes within the sheeted complex reveal a primary spreading structure produced at a complex ridge-transform intersection. On the basis of listric and planar normal faults and rotated dykes that dip symmetrically towards graben axes, they have defined three fossil spreading centres. Faults become subhorizontal at depth and flatten into a detachment zone within the upper part of the plutonic complex. Such faults locally appear as subhorizontal to subvertical zones of highly sheared diabase and gabbro. CY-4 is located essentially along strike of the Ayios Epiphanios graben axis. Such a reinterpretation of the dyke complex in terms of structural and spreading related domains makes the chilling statistics of Kidd and Cann (1974) more difficult to interpret. These workers suggested an original spreading axis to the present day geographic east of the ophiolite complex and stated that ridge jumping had not occurred. Their data have not been duplicated by our studies nor by those of Baragar et al (this volume). Indeed no preferential chilling direction was identified.

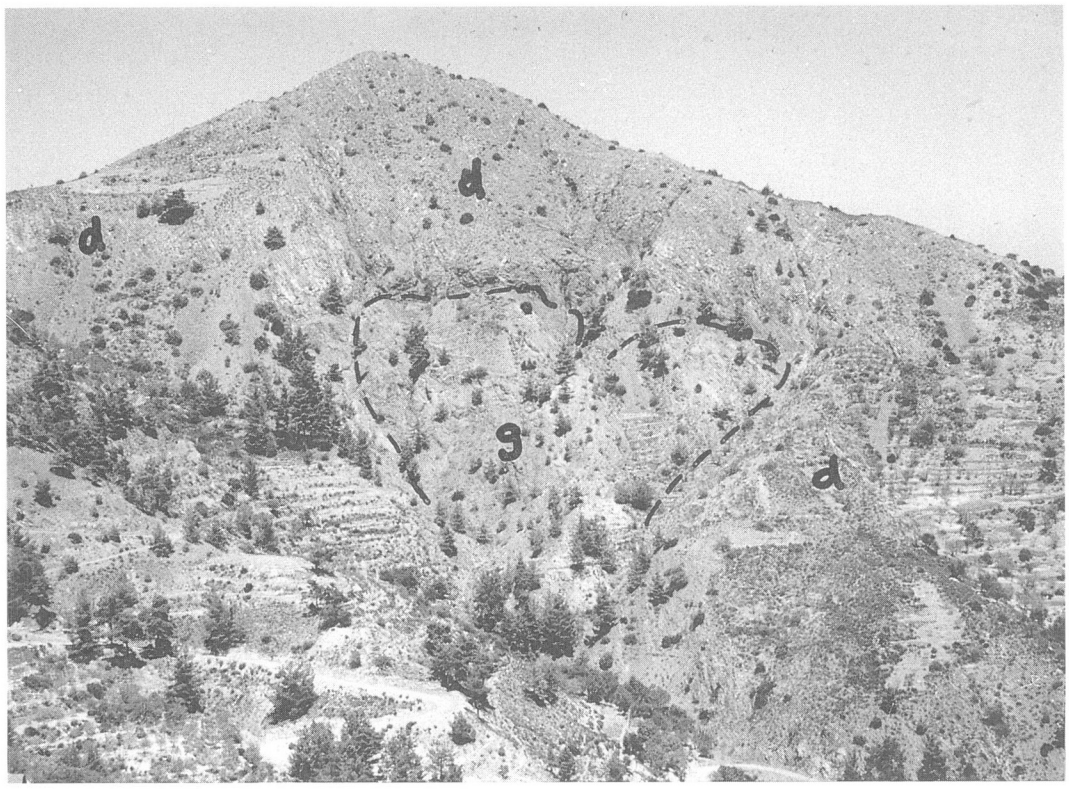

Figure 8: Cupola of dioritic gabbro (g) intruding the base of the sheeted dyke complex (d) near Phterykoudhi. Relief from bottom of valley to top of hill is approximately 250 m.

ROCK TYPES AND MINERALOGY

Ultramafic and Related Rocks

Where early and late cumulate suite rocks can be distinguished on the basis of deformation state and/or cross-cutting relationships, the early cumulates are olivine-pyroxenites, olivine gabbros and gabbro-norites. These are all adcumulate rocks with generally less than 10% intercumulus material. In olivine-pyroxenites and olivine-gabbro units the olivine occurs as both a cumulate and an intercumulate phase. Compositions range from Fo_{89} to Fo_{80} with no apparent systematic difference between textural types. On the other hand, the late cumulate suite comprises poikilitic wehrlites with pyroxene oikocrysts, poikilitic plagioclase wehrlites with intercumulus plagioclase and coarse-grained, massive amphibole gabbro-norites which are, in places, pegmatitic. The amphibole gabbro-norites are spatially associated with wehrlitic rocks of the late suite, occurring around pluton margins as segregations crystallised from more differentiated magma. Most rock types of the late suite display heteradcumulate textures and oikocrysts are common. Olivine occurs only as a cumulus phase with compositions averaging Fo_{84}. Benn and Laurent (1987) suggest that olivines from the late suite rocks are systematically enriched in Ni compared to olivines of the early suite rocks and that clinopyroxenes from the late suite rocks are likewise enriched in Cr. These features would suggest crystallisation of the late suite plutonics from a melt more refractory than the earlier suite magma. Data collected during this project is somewhat in disagreement with these findings. Figure 9 clearly indicates that, for the same forsterite content, olivines from the early suite cannot be distinguished in Ni content from those of the late suite. In addition, trace element data for the clinopyroxenes (Figure 10) show that although the majority of samples fall into two fields on the basis of Mg#, this simply reflects the degree of fractionation of the host rock and that those clinopyroxenes with similar Mg#'s have similar contents of Ti, no matter from which suite they come (Dunsworth, 1989). We have found no definitive way of separating on geochemical grounds, early and late suites as identified in the field (Dunsworth and Malpas, in prep.).

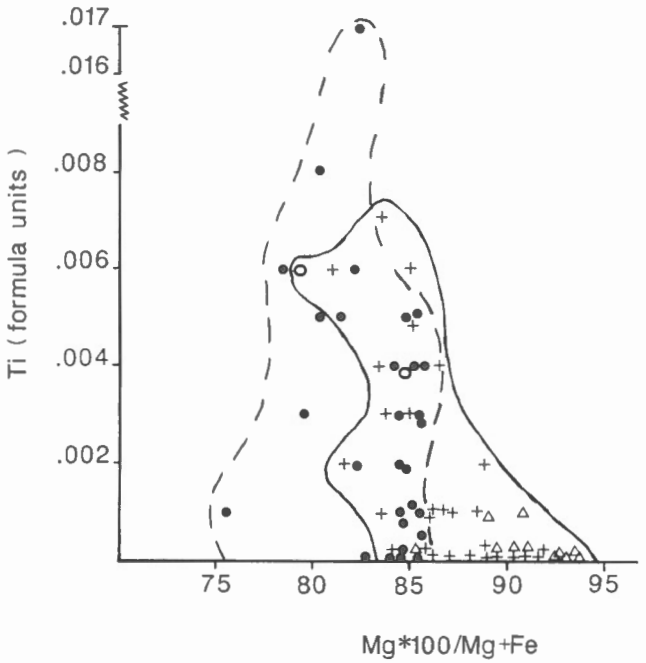

Figure 9: NiO wt. % contents of olivines from plutonic rocks. Closed circle enclosed by broken line: Early Suite, layered hypersthene and olivine gabbro; solid line encloses Late Suite, open circle - pyroxene-hornblende gabbro, open triangle - clinopyroxene-websterite, plus - ultramafic cumulates.

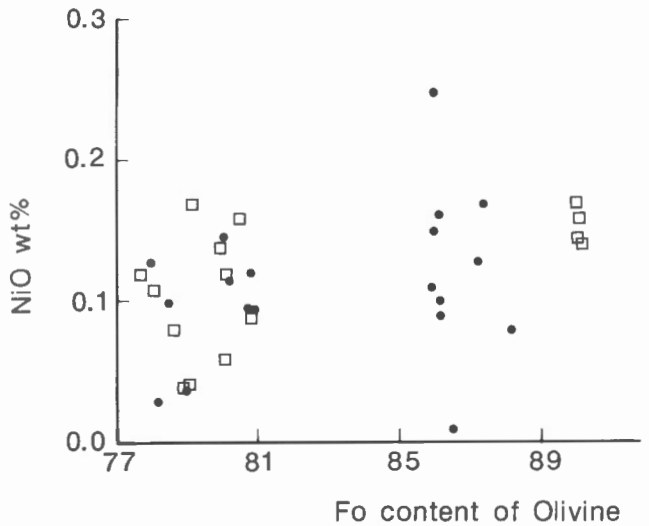

Figure 10: Ti vs Mg# for clinopyroxenes from early and late plutonic phases. Early Suite, open squares; Late Suite, solid circles.

The late suite differentiates commonly contain intercumulus amphibole in the plagioclase wehrlites and gabbro-norites. This amphibole occurs interstitially as anhedral crystals and does not appear to replace clinopyroxene. It is easily distinguished from fibrous metamorphic amphibole which in the same rocks replaces pyroxene along grain boundaries and in fractures.

Higher in the plutonic sequence, ultramafic cumulate rocks are not widespread and are mainly restricted to the Alithinou-Polystipos area. The most common rock types there are olivine norites and websterites, although wehrlites do occur. At this level these rocks occur as i) layered sequences and ii) thin bands within the layered gabbros. Generally, the latter occurrences are less basic than the former. Poikilitic and allotriomorphic textures are common. Exposures of the ultramafic-gabbro contacts are generally poor but, where visible, they appear gradational. Consequently, the ultramafic cumulates are cogenetic with at least part of the more extensive surrounding gabbro and they are considered to have formed during the early stages of fractional crystallisation of a picritic melt. The general lack of deformation features at this level make comparisons with the early and late suites of ultramafics recognised on Mount Olympus tenuous. However, their mineralogy, poikilitic textures and the rare occurrence of xenoliths of deformed rocks in related gabbros, all suggest that ultramafic rocks at this level are related to the younger series of intrusions lower in the stratigraphy.

Gabbros

The gabbros generally have a primary mineralogy of 40-75% plagioclase, 25-60% clinopyroxene, 0-25% orthopyroxene and 0-25% olivine. These minerals are partly or totally replaced by saussurite or sericite, actinolite and serpentine, respectively. Igneous amphibole is present in some rocks. Wilson (1959) divided the gabbros into melagabbro, olivine-gabbro, pyroxene-gabbro and uralite gabbro. Although these are satisfactory field descriptions, the stratigraphic significance that Wilson placed on them has not been substantiated by the present reinvestigation which rather recognises a distribution of all these types throughout the plutonic section (although admitting to a dominance of amphibole-gabbro towards the upper parts).

The melagabbros are medium- to coarse-grained rocks consisting of plagioclase, olivine, augite and hypersthene. Olivine-gabbros occur as either olivine-rich gabbros or less basic, poorly layered olivine-deficient gabbros. The pyroxene gabbros are typically massive to poorly layered, mesocratic rocks consisting of augite, hypersthene and plagioclase with some quartz in rocks transitional to diorites. These are the most widespread of the gabbro types. Massive, medium- to coarse-grained uralite-gabbros, sometimes referred to as the "high level gabbros", actually occur throughout the plutonic section. They consist of zoned plagioclase, augite-salite, hypersthene, uralitic hornblende, magnetite and quartz. Leucocratic, quartz-bearing pegmatitic veins, pods and

dykes associated with coarse acicular hornblende are very common near contacts with diorites and plagiogranites. Aldiss (1978) has referred to these gabbros as "segregation gabbros" and suggests that the felsic material forms from residual liquid separating from a crystal mush, rather than from two immiscible liquids. In this study, they are considered part of the varitextured gabbro assemblage (Pedersen and Malpas, 1984) which formed close to the roofs of magma chambers.

Diorites and Plagiogranites.

Diorites and plagiogranites intrude diabase and gabbro as veins, dykes and larger irregular bodies and are the most differentiated rocks in the sequence. In places these rocks are themselves cut by younger diabase and microgabbro dykes. Intrusive relationships are clear where the plagiogranites have stoped masses of hydrated diabasic material from the sheeted complex. The xenoliths show various stages of assimilation (Figure 11). Thus many dioritic rocks appear to result from assimilation of hydrated diabase and microgabbro by the plagiogranite and subsequent mixing. Others however, are part of the differentiation sequence from gabbro to plagiogranite and occur at transitional or non-intrusive boundaries between the two.

The most common rock type is hornblende-trondhjemite (Wilson, 1959), which consists of albite, quartz, hornblende, minor diopside and accessory ilmenite, sphene-and epidote. A variation of this lithology is epidote-trondhjemite which consists of albite, quartz and epidote with accessory sphene and ilmenite. Typically, quartz and plagioclase in these rocks show a variety of micrographic and granophyric intergrowth textures. The epidote-trondhjemites are more siliceous than the hornblende-trondhjemites and contain very few ferromagnesian minerals except for epidote which forms irregular green patches and specks in hand specimen. The widespread occurrence of secondary chlorite and actinolite results from hydrothermal metamorphism equivalent to greenschist facies (Gass and Smewing, 1973; Spooner 1980) although it can be argued that epidote and secondary quartz may form deuterically as water escaped by boiling during advanced fractionation of the magma. The first epidote group mineral to form is clinozoisite which replaces the more calcic cores of the plagioclases.

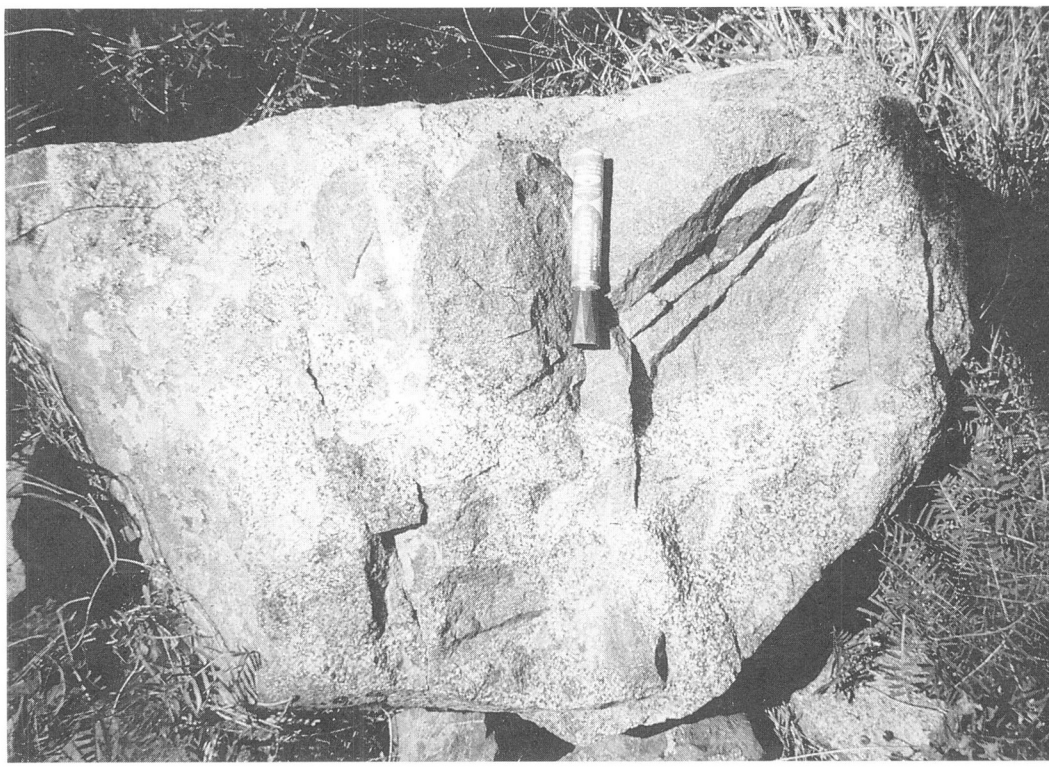

Figure 11: Variably resorbed, rounded xenoliths of diabase in plagiogranite host.

Diabase Dykes

Although hydrothermal alteration of the dykes to greenschist assemblages is common, and surface weathering is in places intense, primary igneous textures including chilled margins, are generally detectable. The dykes are black to grey-green, fine-grained aphyric basalts or basaltic andesites, with some minor olivine and pyroxene-phyric basalts which commonly occur together in swarms. Most, therefore, consist of the primary mineralogy plagioclase, clinopyroxene (augite), quartz, magnetite and ilmenite with secondary epidote, chlorite and uralite. Plagioclase is typically zoned with bytownite cores and labradorite rims. The augite is partly to totally replaced by uralite and secondary quartz is invariably present, constituting in some dykes up to 15% of the rock.

DRILLHOLE PETROLOGY

The section drilled in hole CY-4 can be divided into five distinct zones on the basis of lithology (Figure 12).

Zone 1: (0-675m) Sheeted diabase dykes
Zone 2: (675-900m) Fine- to medium-grained gabbros
Zone 3: (900-1330m) Fine- to medium-grained gabbro-norites and 2-pyroxene diabase dykes
Zone 4: (1330-1746m) Medium- to coarse-grained gabbro-norites
Zone 5: (1746-2263m) Medium- to coarse-grained websterites, olivine websterites and related rocks.

Contacts between these zones are either gradational (Zone 2-3), faulted (Zone 4-5) or intrusive (Zone 3-4). The uppermost zone consists of pervasively altered grey to greenish-grey, fine-grained, aphyric to marginally pyroxene- or plagioclase-phyric diabase dykes which dip steeply and reach vertical thicknesses of up to 7 metres. The primary mineralogy is essentially obscured by hydrothermal alteration although some fresh plagioclase phenocrysts (An_{58-65}) have been observed. Pyroxenes are invariably replaced by uralite beginning along crystal margins and proceeding to their cores. There is an abundance of secondary quartz and Fe-Ti oxides, the growth of which produces large grain size variations.

Zones 2 and 3 represent an amphibole gabbro-norite sequence cut by a series of plagiogranite, diabase and magnetite-gabbro dykes. The mineralogy of the dykes is typically fresh and they have granular textures suggestive of recrystallisation. The diabases contain plagioclase (An_{58-85}), clinopyroxene (Mg#, ie MgO/MgO+FeO = 65-76), orthopyroxene (En_{60-69}), Fe-Ti oxides and rare sulphides. The gabbro-norites are medium-grained rocks showing dominantly adcumulate textures. Plagioclase, both cumulus and intercumulus (An_{83-95}) is the dominant mineral and orthopyroxene (En_{66-80}) a common matrix component, crystallising before clinopyroxene. Magmatic hornblende is a late (deuteric?) phase often developed at the expense of both pyroxenes.

Some rocks in Zones 2 and 3 display a fine-scale planar igneous lamination but the majority are isotropic. Most contacts between rock types are gradational but others are defined by sharp changes in grain size. Dioritic and plagiogranitic rocks characteristically intrude the gabbros as veins and dykes and are themselves cut in places by diabase dykes. Several swarms of pyroxene-phyric diabase dykes occur in Zone 3 between 1100 and 1200 m. Between 1200 and 1220 m, cumulus Fe-Ti oxides occur in abundance and resemble the magnetite found in clots in the coarser-grained uralite gabbros in areas surrounding CY-4.

The top of Zone 4 is an intrusive boundary at which rocks lower in the drill core appear to intrude those higher up. The highest rocks of Zone 4 appear to be chilled against those of Zone 3 and there is a sharp grainsize change. Zone 4 comprises a well-layered section of interlayered medium-to coarse-grained gabbro-norites, with lesser amounts of gabbro, olivine gabbro-norite and plagioclase olivine websterite. The bottom of the zone is a sharp, inclined fault which marks the virtual disappearance of plagioclase as a cumulus phase. Cumulus olivine (Fo_{75-80}) first appears in small amounts at 1430 m and continues downward from that level. Green hornblende occurs as a late deuteric alteration phase.

Layering occurs on a 1 to 10 m scale and layers are generally homogeneous. However, grain size grading is observed in some, with more pegmatitic lithologies being common at the tops of the layers. Modal grading also occurs, with concentrations of pyroxene and olivine at the base, grading into plagioclase-rich tops. Textures vary from adcumulate in the gabbro-norites to mesocumulate in the websterites.

Zone 5 is formed of well-layered websterites, clinopyroxenites, wehrlites, lherzolites and gabbro-norites. Clinopyroxene (Mg# 80-92) is the dominant mineral and olivine (Fo_{75-88}) is especially abundant in the section below 2100 metres. Layers are of variable thickness from 5 cm to several metres. Contacts are usually marked by the appearance of one or more phases (phase layering) commonly accompanied by grain size changes. Although parallel laminations and modal laminations are well developed, parts of this section are affected by tectonic deformation which masks many original igneous features. Some olivine-rich layers are boudinaged and display porphyroclastic textures with granulation and kink-banding of individual olivine crystals. Recovery textures (annealing) take the form of polygonal neoblasts of olivine and subgrain development in the pyroxenes. The distribution of this deformation in isolated centimetre-thick sections of the core suggests that it is related to the development of a series of high temperature subhorizontal shear zones. The preferred mineral orientation in the rocks so produced was probably the cause of drilling difficulties that were encountered in the hole at this depth.

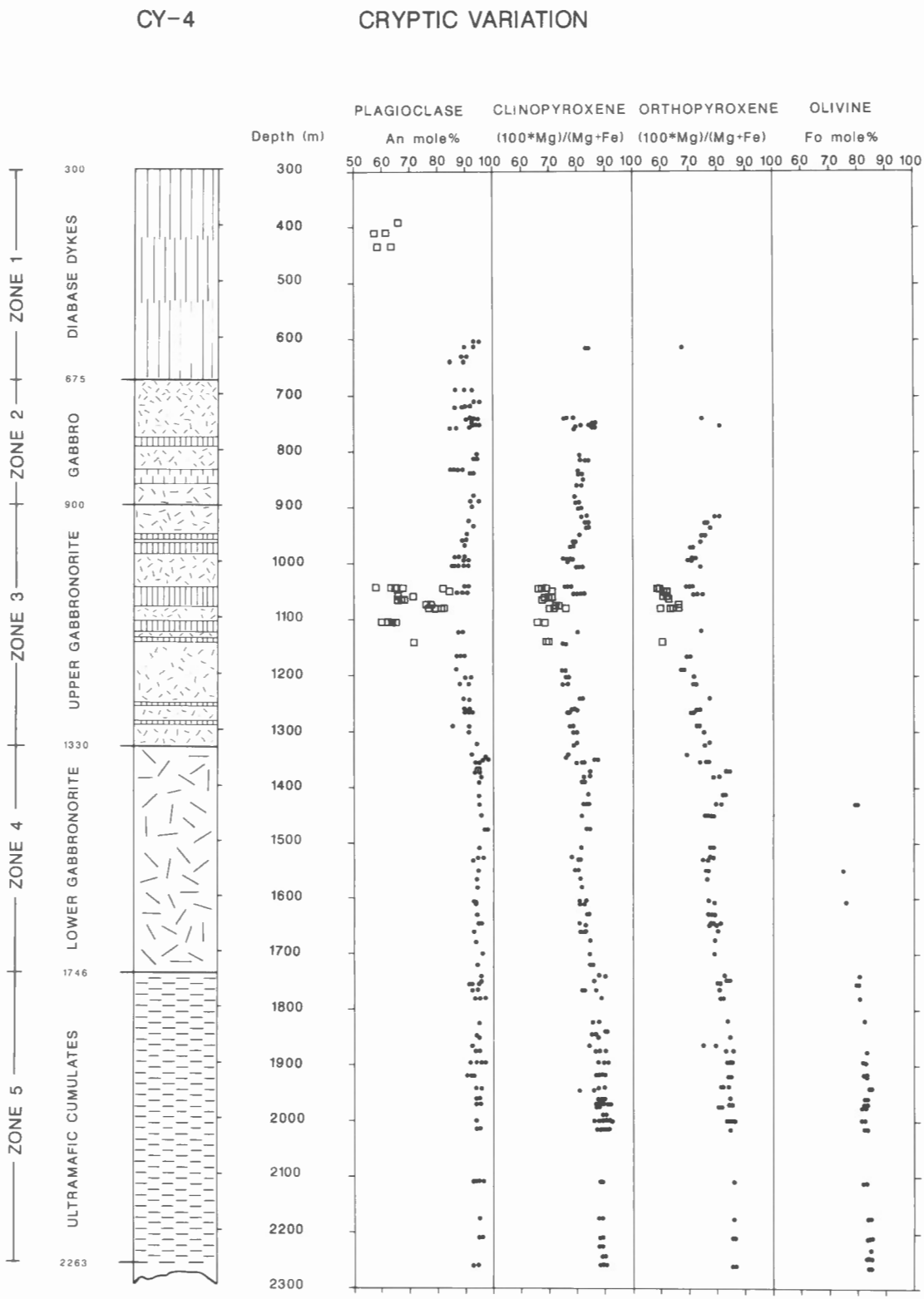

Figure 12: Zonal subdivision based on lithology and cryptic variation of mineral phases in the CY-4 borehole. (= diabase dykes)

Low temperature alteration throughout most of the plutonic section is limited to partial replacement of pyroxenes by actinolite. Plagioclase remains essentially unaltered. Olivine is partially serpentinised and veins of chrysotile occur in the sheared serpentinised lherzolites at the base of the section below 2000 m.

PHASE LAYERING AND CHEMISTRY

The upper part of the drill core, as explained above, shows the effects of alteration due to both ocean floor hydrothermal and recent groundwater circulation. Fresh plagioclase is therefore only sporadic and clino- and orthopyroxene are totally replaced by amphibole.

True phase layering is obvious in Zones 4 and 5. This phase layering is consistent with the crystallisation sequence described by previous workers (Greenbaum, 1972; Allen, 1975), olivine + chromite> clinopyroxene> orthopyroxene> plagioclase, although chromite does not itself exist in the drill core. Hence the cumulus assemblages ol + cpx + opx then ol + cpx + opx + pl, and finally cpx + opx + pl occur moving from the bottom of Zone 5 to the top of Zone 4 with plagioclase appearing as a cumulate phase at 1746 m (although a faulted contact) and olivine disappearing as a cumulate phase at 1430 m.

Clinopyroxene, orthopyroxene and plagioclase occur throughout zones 2 and 3 and are locally joined by cumulus Fe-Ti oxides.

Variation in phase chemistry with rock type is depicted in Figure 13. Except for the plagiogranites and samples which have been obviously silicified, plagioclases of the 2-pyroxene granular dykes have the lowest An contents (An_{54-85}). Comparisons with available analyses of plagioclases from the sheeted complex are tenuous as i) plagioclases in the sheeted complex are zoned and ii) the plagioclases in the 2-pyroxene dykes have probably reequilibrated chemically during recrystallisation.

The plagioclase in the upper gabbro-norite ranges in composition between An_{80} and An_{95} and averages An_{90}. Plagioclase in the lower gabbronorite and websterite is relatively uniform in composition (An_{90-97}) but is the most calcic. Although there is no systematic correlation between An content and FeO content, FeO decreases in the more ultrabasic rocks and plagioclase in the lower gabbro-norite and websterite generally contains FeO< 0.4 wt.%.

Orthopyroxene generally increases in MgO/MgO + FeO and decreases in Ti from the diabases through the gabbros to the websterites. Olivine, where analyses are available, decreases in Ni content and increases in Fo content from the lower gabbro-norite to the websterite. Such trends are not surprising.

The abundance of relatively high-Ca, high-Fe amphibole (CaO = 10-12 wt.%, FeO = 17-20 wt.%) in the diabase of the sheeted complex compared to high-Ca, low-Fe amphibole (CaO = 10-12 wt.%, FeO = 10-13 wt.%) which replaces clinopyroxene in the altered gabbro, suggests that the original pyroxene in the diabase was a clinopyroxene which was generally more Fe-rich than that in the gabbros. The 2-pyroxene granular dykes display the most evolved clinopyroxenes with Mg#'s of 65-76. The Mg #'s then increase with basicity of the host rocks. Cr plotted against Mg# (Figure 13d) shows an expected trend of increasing Cr with increasing Mg# although there is no marked difference between the upper and lower gabbro-norites.

Going up the drill core there is an overall trend towards less primitive compositions with increasing height (Figure 12). Plagioclase shows an overall decrease in An mole percent, clino- and orthopyroxenes show a decrease in MgO/MgO + FeO and olivine shows a decrease in Fo mole percent. However, there are perturbations of this general trend and a reversal to more primitive compositions at approximately 1500 m. This can be interpreted as a period of replenishment of the magma chamber and is perhaps the only major reversal of trends in the lower part of the sequence. More detailed studies of the lower ultramafic cumulates might suggest that lesser periods of replenishment also occurred, e.g. at 1940 m in olivine compositions (see also Alabaster et al, 1985). The junction between Zones 5 and 4 is clearly marked by a decrease in the Cr content of the clinopyroxenes (Figure 14).

The intrusive boundary recognised at 1330 m depth is marked by changes in the Mg# of the pyroxene and more particularly, by the Ti content of the clinopyroxene (Figure 13). A sharp discontinuity at 1330 m effectively separates the clinopyroxenes into an upper high-Ti series and a lower low-Ti series. This has been used by some workers to support the hypothesis that the two sequences formed in separate magma chambers (Thy, 1987), but in view of the evidence from the samples collected in the field, it is not clear that these relate directly to early and late suites.

The gabbro and gabbro-norite of Zones 2 and 3 show complex cryptic variations and there are indications of numerous trend reversals (1250, 1175, 1020 and 970 m for example). A number of these, especially the one at 970 m, occur over a broad zone of up to 50 metres. Although replenishment of the magma chambers is evident, the cryptic variation is not reflected by any phase layering except perhaps at 1746 m. This would suggest that thorough mixing occurred between magma already in the chambers and replenishing magmas that were already perhaps equally as evolved and saturated with the major mineralogical phases (Thy, 1987). Likewise the broad zones of trend reversals suggest replenishment by a small but steady magma stream over a period of time.

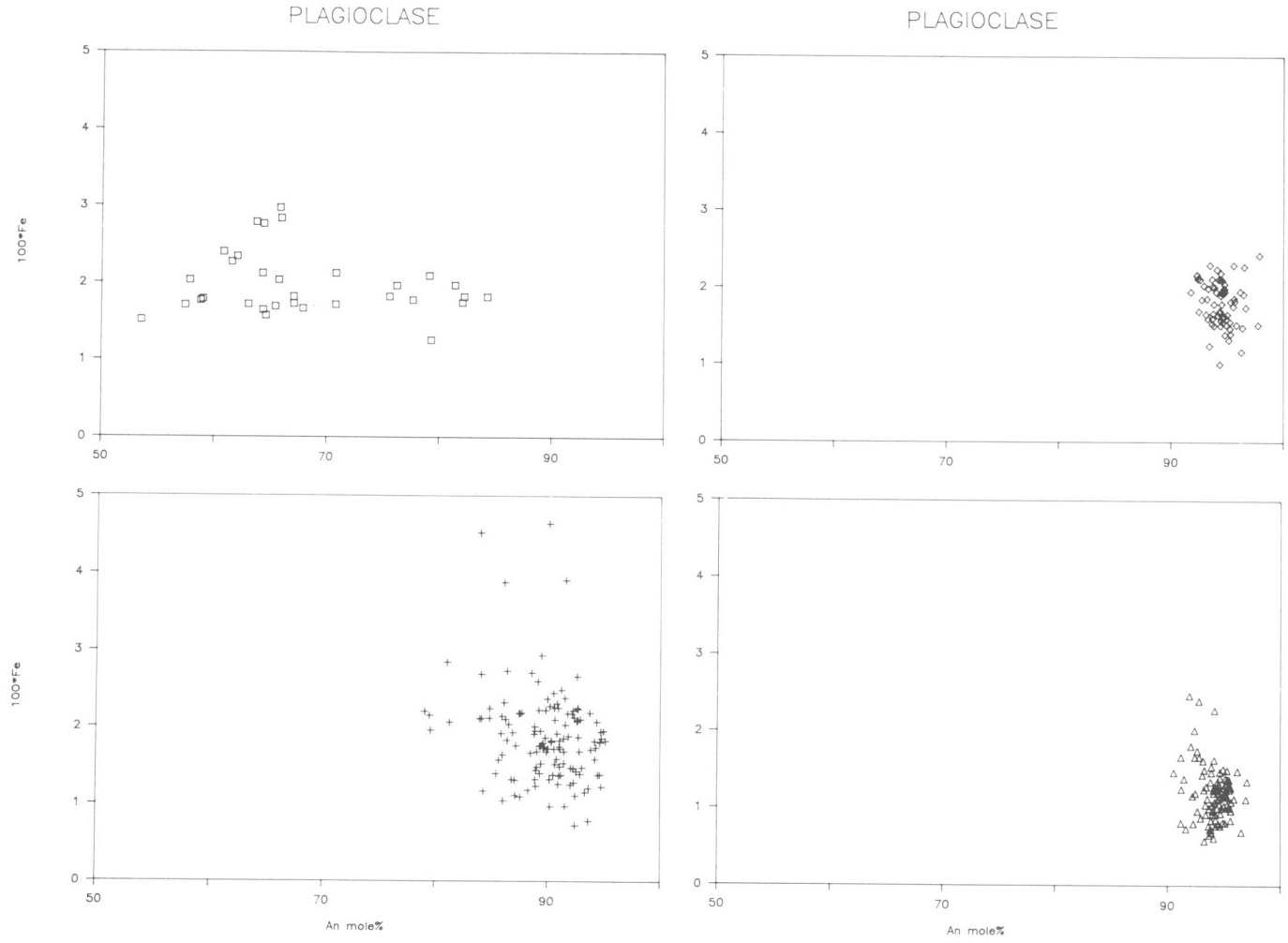

Figure 13a: Mineral chemistry of plagioclase in different lithologies of the CY-4 borehole. □ = diabase dykes, + = gabbros, ◇ = gabbro-norites and △ = ultramafic rocks.

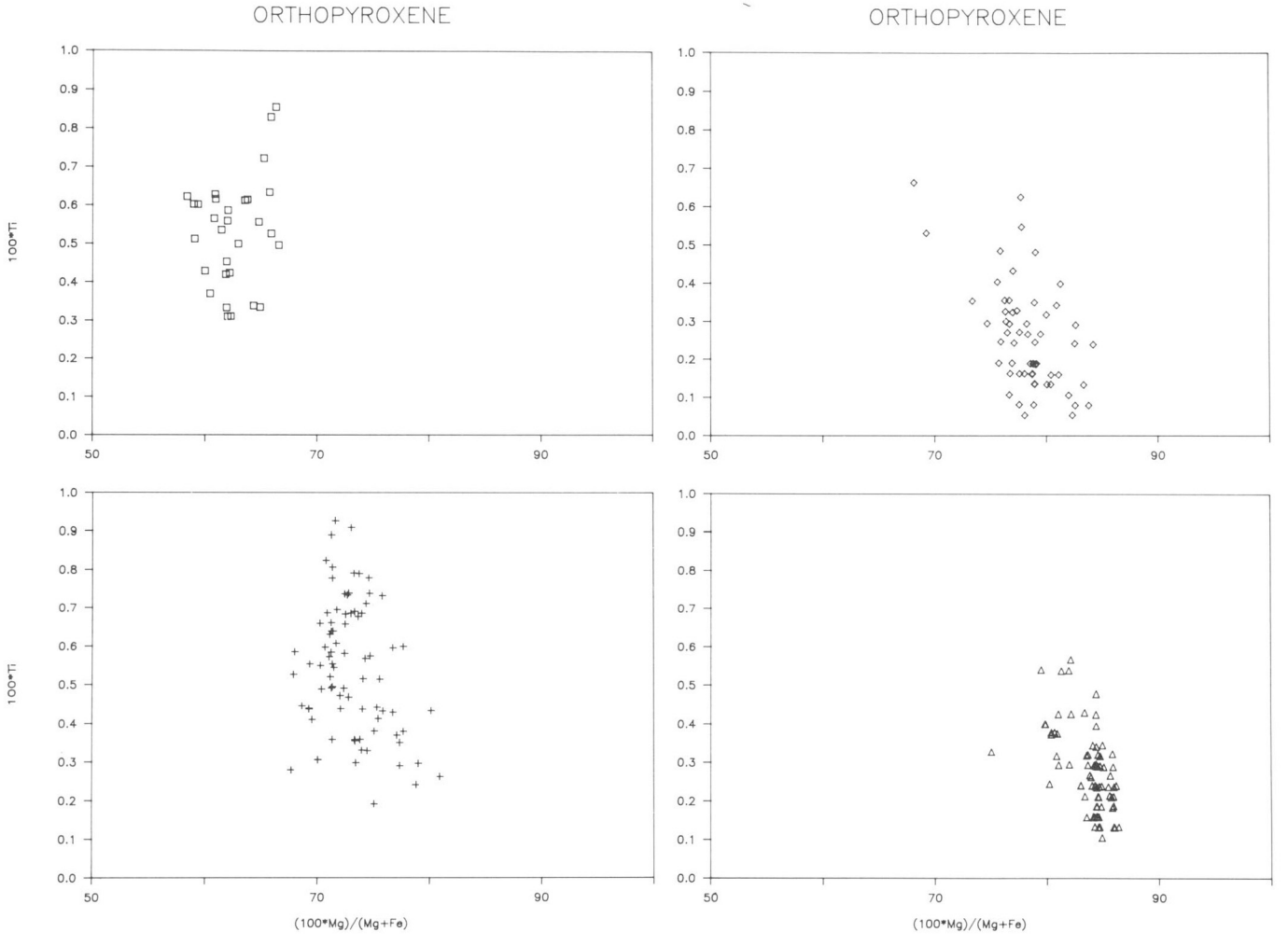

Figure 13b: Mineral chemistry of orthopyroxene in different lithologies of the CY-4 borehole. □ = diabase dykes, + = gabbros, ◊ = gabbro-norites and △ = ultramfic rocks.

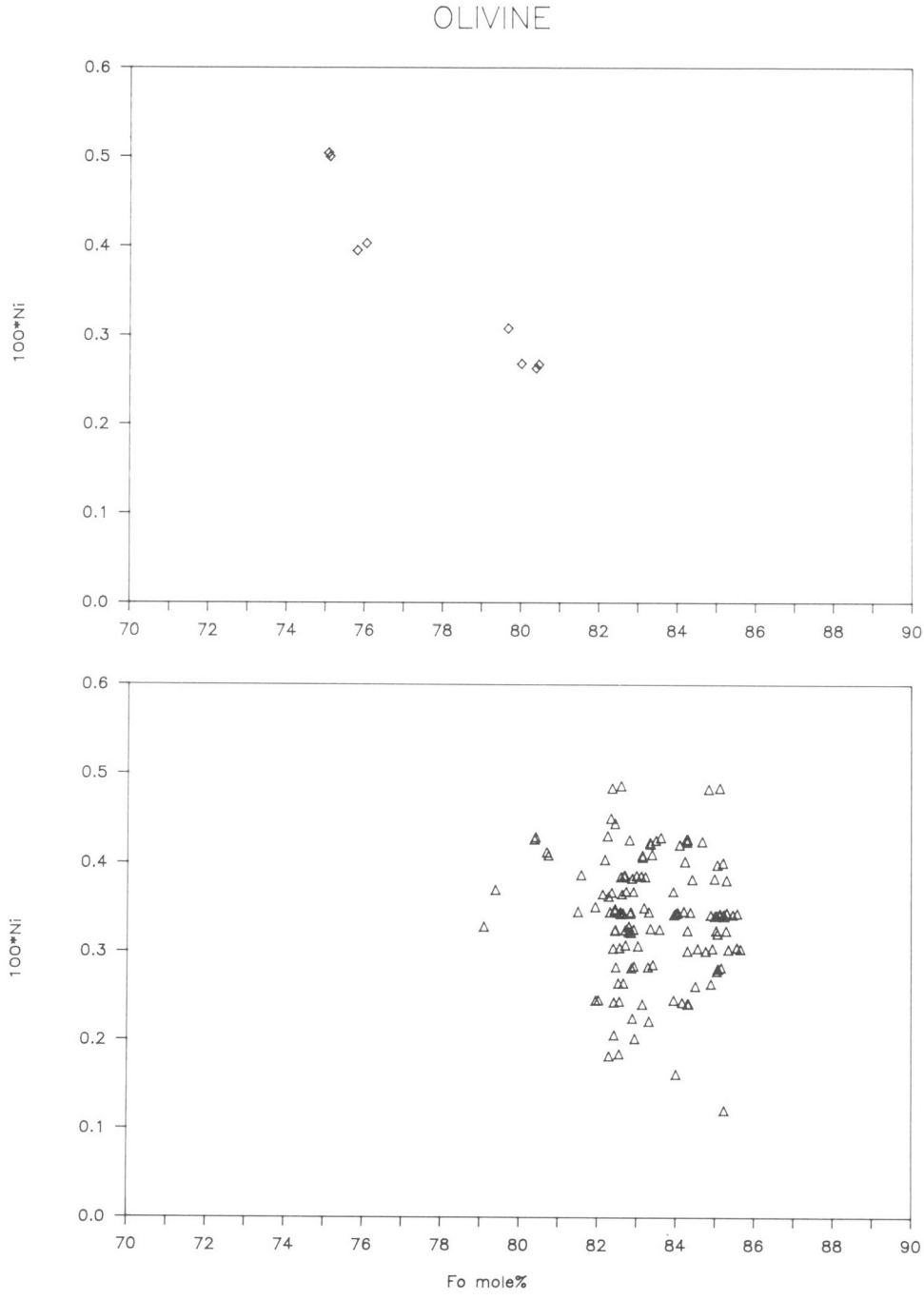

Figure 13c: Mineral chemistry of olivine in different lithologies of the CY-4 borehole. □ =diabase dykes, + = gabbros, ◇ =gabbro-norites and △ =ultramafic rocks.

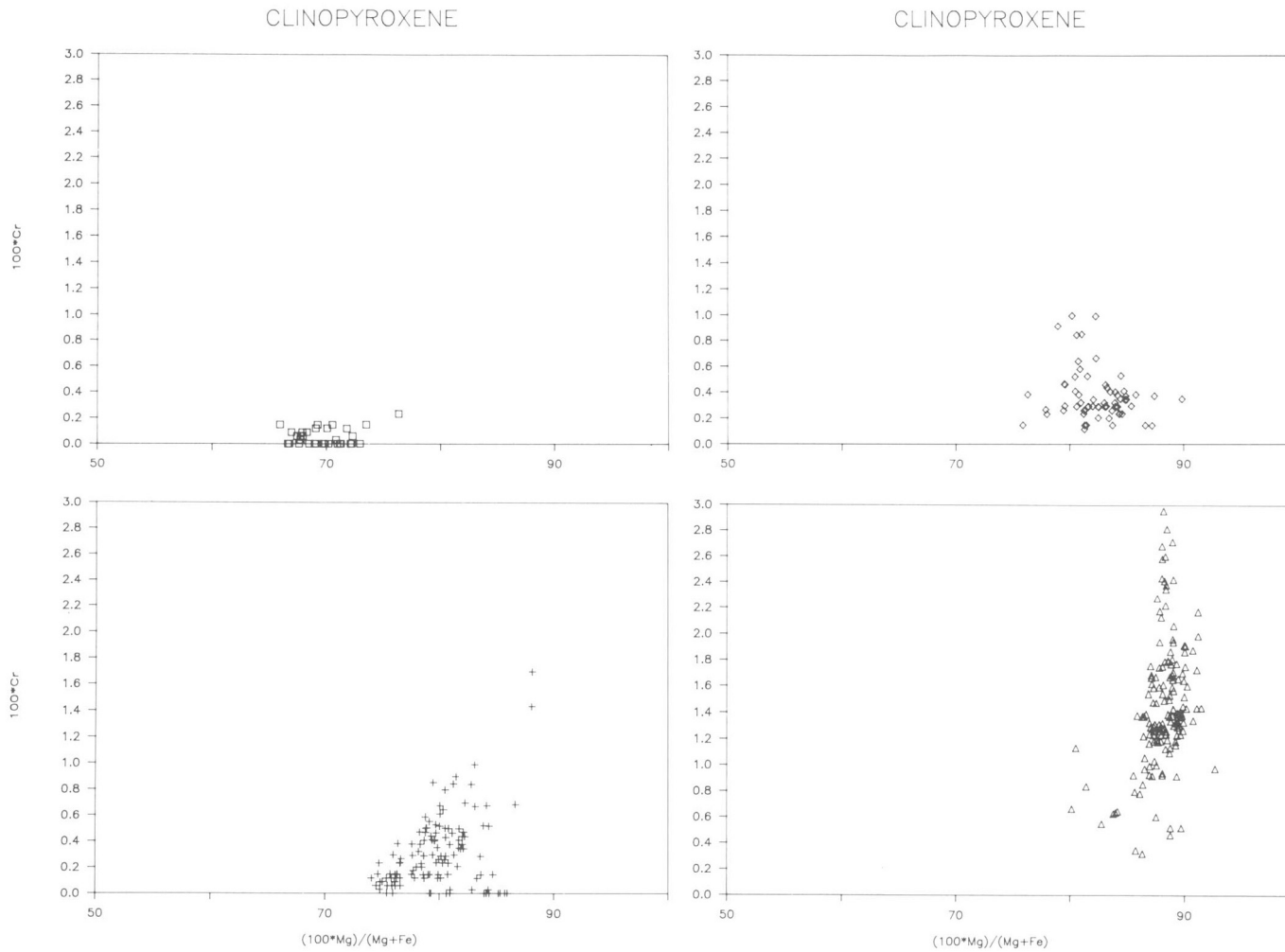

Figure 13d: Mineral chemistry of clinopyroxene in different lithologies of the CY-4 borehole. □ = diabase dykes, + = gabbros, ◊ = gabbro-norites and △= ultramfic rocks.

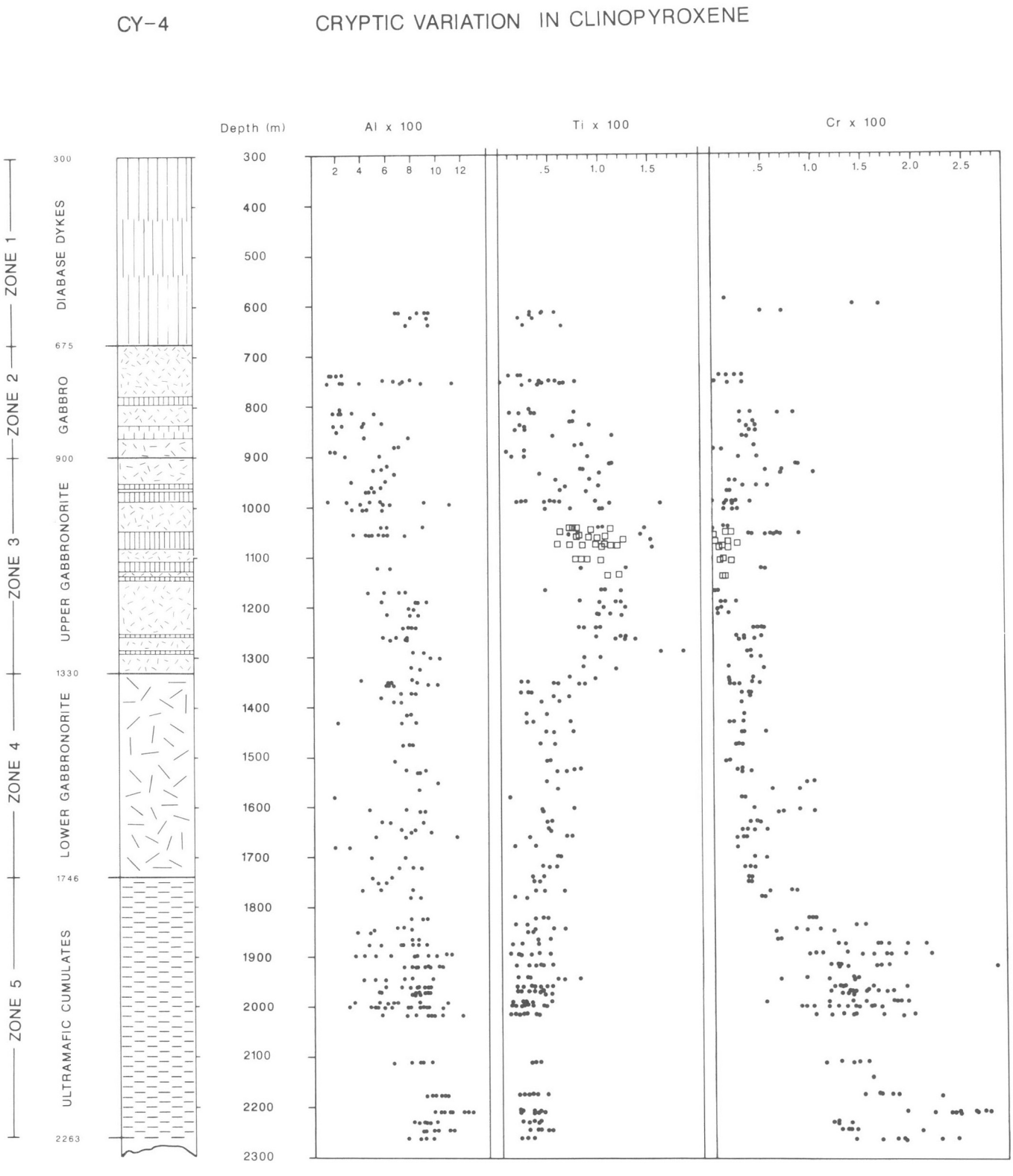

Figure 14: Variation in Al, Ti and Cr contents of clinopyroxenes with position in the CY-4 core (□ = diabase dyke).

TABLE 1: Microprobe analyses of plagioclases from CY-4

Depth (m)	Rock [# of analyses]	SiO_2	Al_2O_3	FeO	CaO	Na_2O	K_2O	Ab
321.19	Diorite [1]	54.95	27.54	0.40	11.58	5.53	0.04	46.25
327.93	Diorite [2]	49.57	31.32	0.72	15.71	1.83	0.01	17.40
396.67	Diabase [1]	51.97	28.38	0.77	13.29	3.79	0.04	33.96
412.44	Diabase [2]	55.40	27.47	0.57	12.09	4.50	0.03	40.16
435.84	Diabase [2]	54.66	28.54	0.61	12.22	4.25	0.03	38.60
525.07	Diorite [3]	49.68	30.72	0.55	15.30	2.42	0.03	22.19
547.15	Magnetite gabbro [2]	52.47	29.34	0.45	13.80	3.61	0.01	30.93
559.79	Diorite [3]	48.84	32.08	0.58	16.66	1.74	0.01	15.84
576.14	Diorite [2]	48.51	31.95	0.53	16.97	1.58	0.02	14.39
589.12	Magnetite gabbro [3]	49.97	30.78	0.53	15.31	2.09	0.02	19.79
605.50	Diabase [2]	46.50	33.07	0.54	18.30	0.70	0.01	6.43
614.12	Noritic gabbro [1]	44.49	32.60	0.67	18.88	0.82	0.02	7.28
616.49	Gabbro [2]	46.55	32.67	0.56	18.17	0.90	0.09	8.11
632.06	Diabase [3]	46.53	32.91	0.56	18.22	1.15	0.01	10.27
641.55	Diabase [2]	46.70	32.36	0.92	17.87	1.53	0.02	13.36
678.23	Trondhjemite [3]	54.50	27.67	0.39	12.54	4.79	0.04	40.78
691.25	Gabbro [3]	46.13	32.70	0.56	18.62	1.25	0.01	10.81
712.90	Gabbro [3]	45.83	33.24	0.52	19.44	0.76	0.00	6.63
718.78	Gabbro [3]	46.49	33.19	0.74	18.37	0.97	0.02	8.71
721.47	Gabbro [4]	47.09	32.56	0.53	18.17	1.33	0.01	11.63
739.40	Gabbro [1]	45.83	32.02	0.99	17.93	0.91	0.00	8.41
741.80	Noritic gabbro [1]	46.68	33.99	0.54	18.11	0.79	0.01	7.31
742.34	Gabbro [1]	46.63	33.16	0.43	16.87	1.04	0.01	10.03
746.55	Gabbro [1]	45.98	33.71	0.47	18.96	0.64	0.01	5.75
751.65	Gabbro [3]	45.79	33.46	0.56	18.31	0.69	0.00	6.37
753.24	Noritic gabbro [2]	46.35	33.20	0.54	18.61	0.90	0.04	7.97
755.43	Gabbro [2]	46.44	34.13	0.41	18.79	0.64	0.01	5.81
756.15	Gabbro [4]	46.30	33.85	0.47	18.90	0.64	0.01	5.79
756.95	Gabbro [2]	46.77	33.70	0.41	18.50	0.81	0.01	7.30
758.82	Gabbro [1]	45.85	33.36	0.35	17.58	0.96	0.00	8.99
761.04	Magnetite gabbro [2]	48.12	32.02	0.63	16.52	1.57	0.02	14.69
808.60	Gabbro [2]	45.71	34.07	0.34	18.96	0.65	0.01	5.80
816.35	Diabase [2]	45.88	34.18	0.43	18.74	0.63	0.00	5.74
816.60	Gabbro [2]	46.24	33.42	0.27	17.95	0.74	0.02	6.89
833.60	Gabbro [1]	47.99	32.04	0.30	15.91	1.62	0.03	15.53
834.50	Gabbro [3]	48.14	32.52	0.40	17.39	1.38	0.04	12.48
840.71	Gabbro [1]	46.13	33.12	0.25	18.48	0.93	0.02	8.34
842.93	Gabbro [1]	46.73	34.21	0.29	18.25	0.82	0.00	7.52
869.66	Gabbro [3]	57.24	27.03	0.26	9.53	6.57	0.08	55.21
880.12	Gabbro [2]	45.40	35.02	0.28	18.80	0.82	0.00	7.32
891.55	Gabbro [2]	45.77	34.66	0.36	19.18	0.78	0.01	6.82
902.74	Gabbro [2]	45.81	33.88	0.38	18.86	0.88	0.01	7.75
917.30	Pyroxenite [2]	49.81	31.51	0.37	15.40	2.49	0.01	22.60
927.30	Pyroxenite [2]	46.36	34.13	0.36	18.60	1.03	0.01	9.11
935.40	Pyroxenite [4]	47.53	32.57	0.37	16.76	2.08	0.01	18.28
949.60	Noritic gabbro [1]	44.64	33.42	0.46	18.96	1.12	0.00	9.66
961.30	Noritic gabbro [2]	46.26	33.06	0.33	18.82	1.21	0.01	10.37
969.60	Noritic gabbro [2]	46.11	33.80	0.50	17.97	1.18	0.01	10.62
991.60	Noritic gabbro [1]	46.45	32.94	0.45	18.16	1.14	0.01	10.19
993.91	Gabbro [2]	46.37	32.39	0.73	17.91	1.52	0.01	13.27
996.42	Noritic gabbro [2]	45.56	32.28	0.45	19.82	1.21	0.01	9.94
1006.20	Noritic gabbro [5]	46.72	32.97	0.47	17.85	1.41	0.00	12.48
1042.45	Noritic gabbro [3]	45.25	33.06	0.43	19.28	1.12	0.01	9.51
1047.50	Trondhjemite [7]	51.70	29.51	0.49	14.18	4.01	0.02	33.76
1047.50	Dyke [1]	45.02	33.46	0.30	19.38	0.89	0.03	7.66
1051.00	Dyke [1]	48.03	31.60	0.47	17.30	1.77	0.02	15.60
1054.60	Noritic gabbro [3]	45.14	33.24	0.29	18.89	1.18	0.00	10.18
1055.60	Noritic gabbro [1]	46.55	32.05	0.28	18.11	1.40	0.03	12.25
1056.85	Noritic gabbro [1]	47.83	32.13	0.34	16.72	1.14	0.02	10.97
1058.80	Dyke [2]	51.34	29.08	0.54	14.35	3.67	0.03	31.59
1065.70	Dyke [3]	52.32	28.63	0.54	13.27	3.69	0.02	33.45
1066.77	Dyke [1]	52.50	28.71	0.45	13.54	3.66	0.02	32.81
1074.50	Dyke [2]	49.90	30.23	0.47	15.44	2.60	0.01	23.30
1077.52	Dyke [5]	48.67	32.92	0.48	16.07	2.26	0.01	20.29
1106.37	Dyke [4]	52.67	28.53	0.57	13.06	4.51	0.01	38.42
1123.89	Noritic gabbro [2]	46.36	33.53	0.33	17.95	1.33	0.00	11.78
1138.19	Dyke [1]	49.60	31.66	0.45	15.28	3.48	0.01	29.17
1168.10	Noritic gabbro [4]	46.16	32.83	0.51	18.07	1.34	0.01	11.80

TABLE 1: Microprobe analyses of plagioclases from CY-4 (continued)

Depth (m)	Rock [# of analyses]	SiO_2	Al_2O_3	FeO	CaO	Na_2O	K_2O	Ab
1191.12	Noritic gabbro [2]	47.45	33.69	0.46	17.67	1.56	0.01	13.77
1203.68	Noritic gabbro [2]	46.61	34.19	0.54	18.14	1.01	0.01	9.17
1216.33	Noritic gabbro [5]	46.04	33.08	0.56	18.14	1.22	0.00	10.82
1242.74	Noritic gabbro [3]	45.85	33.21	0.41	18.60	1.08	0.01	9.53
1260.00	Noritic gabbro [4]	45.50	33.81	0.47	18.56	1.02	0.01	9.03
1266.70	Noritic gabbro [4]	45.52	33.09	0.49	18.65	1.07	0.01	9.43
1289.29	Noritic gabbro [2]	46.21	33.37	0.41	17.90	1.32	0.01	11.71
1302.54	Noritic gabbro [2]	45.92	33.96	0.54	18.56	1.05	0.00	9.25
1320.30	Noritic gabbro [1]	46.55	33.20	0.44	17.98	0.65	0.00	6.14
1342.70	Noritic gabbro [1]	45.75	32.76	0.50	19.63	0.97	0.00	8.21
1345.40	Gabbro [1]	46.47	33.43	0.56	18.29	0.84	0.00	7.67
1346.60	Gabbro [1]	45.46	34.11	0.45	19.49	0.37	0.00	3.32
1349.60	Gabbro [3]	44.68	34.24	0.53	19.31	0.37	0.00	3.33
1354.15	Gabbro [4]	44.54	34.14	0.50	19.06	0.71	0.00	6.36
1355.15	Gabbro [3]	44.93	34.04	0.47	19.25	0.67	0.00	5.90
1355.69	Noritic gabbro [3]	44.53	34.23	0.48	19.32	0.61	0.01	5.43
1368.50	Gabbro [3]	46.87	33.29	0.55	18.24	0.62	0.01	5.75
1373.10	Noritic gabbro [3]	45.92	33.90	0.38	18.89	0.61	0.01	5.56
1381.47	Noritic gabbro [2]	44.01	34.66	0.38	20.15	0.52	0.00	4.42
1391.69	Gabbro [2]	44.99	34.46	0.47	19.69	0.62	0.01	5.39
1414.74	Noritic gabbro [2]	44.09	34.42	0.41	19.39	0.61	0.01	5.34
1429.48	Olivine gabbro [2]	45.09	34.81	0.42	19.06	0.58	0.00	5.18
1450.09	Noritic gabbro [2]	44.45	34.22	0.42	19.62	0.54	0.00	4.75
1474.96	Gabbro [3]	44.80	34.16	0.41	19.96	0.38	0.01	3.35
1508.73	Noritic gabbro [2]	44.77	34.68	0.53	19.45	0.62	0.01	5.45
1525.32	Noritic gabbro [3]	46.07	33.42	0.56	18.49	0.49	0.00	4.59
1529.80	Noritic gabbro [2]	45.53	34.53	0.52	18.85	0.83	0.01	7.38
1549.62	Olivine gabbro [2]	44.74	34.36	0.52	19.68	0.63	0.01	5.43
1565.12	Noritic gabbro [2]	45.40	33.97	0.46	19.26	0.74	0.00	6.51
1581.15	Noritic gabbro [2]	45.34	34.17	0.49	18.58	0.64	0.00	5.87
1604.44	Noritic gabbro [2]	44.65	34.51	0.54	18.85	0.80	0.01	7.10
1610.10	Websterite [3]	44.29	34.30	0.54	19.51	0.69	0.01	6.01
1629.02	Noritic gabbro [2]	45.41	34.11	0.29	19.04	0.68	0.01	6.04
1646.27	Noritic gabbro [3]	45.06	34.50	0.42	19.16	0.57	0.00	5.07
1659.29	Noritic gabbro [2]	44.77	34.53	0.43	19.41	0.82	0.00	7.10
1678.13	Noritic gabbro [1]	45.21	33.77	0.41	18.86	0.70	0.00	6.29
1700.48	Noritic gabbro [2]	44.66	34.03	0.40	19.98	0.43	0.01	3.75
1720.69	Gabbro [2]	44.73	34.21	0.41	19.56	0.68	0.00	5.92
1740.93	Websterite [2]	44.98	34.33	0.39	19.72	0.54	0.01	4.68
1749.58	Noritic gabbro [2]	44.57	34.69	0.34	19.62	0.52	0.01	4.54
1753.89	Websterite [3]	45.27	34.07	0.43	18.41	0.80	0.01	7.30
1767.12	Pyroxenite [3]	46.86	33.02	0.53	17.97	0.76	0.01	7.07
1780.84	Websterite [3]	44.90	34.59	0.30	19.04	0.53	0.02	4.76
1823.87	Websterite [2]	44.79	34.44	0.28	19.26	0.58	0.01	5.17
1846.09	Pyroxenite [3]	46.28	33.27	0.26	18.80	0.71	0.01	6.36
1850.72	Pyroxenite [3]	44.99	34.39	0.36	18.94	0.63	0.00	5.64
1864.50	Noritic gabbro [3]	46.23	32.99	0.56	18.36	0.82	0.01	7.45
1874.40	Pyroxenite [3]	45.36	34.33	0.33	18.76	0.67	0.01	6.07
1875.56	Websterite [5]	45.08	34.77	0.37	19.13	0.56	0.01	5.02
1893.63	Websterite [3]	45.74	34.39	0.35	19.29	0.42	0.01	3.77
1896.35	Pyroxenite [3]	46.31	33.65	0.33	18.23	0.91	0.01	8.25
1897.15	Websterite [3]	45.23	34.53	0.35	18.56	0.56	0.01	5.17
1918.25	Websterite [3]	45.40	34.10	0.34	18.40	0.94	0.02	8.48
1918.85	Websterite [3]	45.37	34.24	0.34	18.40	0.68	0.02	6.29
1942.50	Websterite [2]	45.97	34.34	0.36	18.39	0.59	0.01	5.50
1960.55	Websterite [4]	45.19	34.89	0.20	18.79	0.64	0.03	5.77
1961.10	Websterite [5]	45.61	34.47	0.27	18.64	0.56	0.01	5.17
1969.00	Websterite [3]	44.84	34.53	0.26	18.75	0.56	0.02	5.12
1971.70	Websterite [2]	44.79	34.29	0.27	18.73	0.63	0.03	5.68
1999.17	Pyroxenite [4]	44.99	34.71	0.18	18.86	0.70	0.01	6.31
2000.15	Websterite [4]	44.76	34.77	0.22	19.02	0.65	0.01	5.83
2014.93	Websterite [4]	45.11	34.63	0.30	18.82	0.61	0.01	5.50
2016.50	Dunite [5]	44.73	34.37	0.31	18.92	0.59	0.01	5.34
2111.65	Websterite [5]	45.33	34.46	0.22	18.60	0.68	0.02	6.22
2174.10	Websterite [3]	44.88	34.29	0.28	18.98	0.50	0.02	4.55
2175.60	Websterite [3]	44.91	34.45	0.30	18.68	0.54	0.02	4.97
2208.00	Websterite [4]	44.39	34.68	0.27	18.92	0.52	0.01	4.73
2262.03	Websterite [4]	45.73	34.81	0.22	18.83	0.77	0.03	6.83

TABLE 2: Microprobe analyses of clinopyroxene from CY-4

Depth (m)	Rock [# of analyses]	SiO_2	Al_2O_3	TiO_2	Cr_2O_3	FeO	MnO	MgO	CaO	Na_2O	En	Fs	Wo
614.12	Noritic gabbro [3]	53.49	2.07	0.16	0.03	6.39	0.14	17.86	20.24	0.13	50.58	10.37	39.05
616.49	Gabbro [2]	53.50	1.54	0.14	0.03	5.83	0.15	17.81	19.89	0.08	51.05	9.61	39.34
625.30	Diabase [2]	53.71	1.98	0.10	0.55	4.31	0.14	17.91	21.47	0.10	51.25	7.13	41.62
640.40	Diabase [2]	53.87	1.95	0.16	0.21	5.53	0.14	18.28	20.50	0.09	51.62	8.97	39.41
739.40	Gabbro [4]	54.14	0.39	0.06	0.07	7.93	0.21	14.96	22.61	0.16	41.93	12.74	45.33
751.65	Gabbro [3]	54.37	1.56	0.18	0.00	5.39	0.14	17.48	22.22	0.10	48.57	8.62	42.81
753.24	Noritic gabbro [2]	54.06	1.70	0.20	0.01	6.74	0.16	17.77	20.89	0.14	49.26	10.73	40.01
755.43	Gabbro [2]	55.82	0.38	0.00	0.00	5.31	0.16	17.50	21.98	0.14	48.22	8.44	43.34
756.15	Gabbro [3]	54.62	1.51	0.17	0.00	6.43	0.17	17.02	21.17	0.17	48.00	10.45	41.55
756.95	Gabbro [1]	53.23	2.59	0.23	0.05	7.50	0.23	16.00	20.70	0.25	46.57	12.63	40.80
758.82	Gabbro [1]	54.38	0.53	0.08	0.10	7.37	0.22	15.25	22.62	0.13	42.81	11.96	45.23
808.60	Gabbro [1]	53.43	0.48	0.11	0.00	6.45	0.17	15.40	23.77	0.20	42.60	10.28	47.12
816.35	Diabase [1]	54.52	1.15	0.28	0.00	7.03	0.11	16.43	22.32	0.16	45.47	11.09	43.44
816.60	Gabbro [4]	54.29	0.52	0.09	0.18	6.16	0.18	15.81	22.84	0.20	44.34	9.99	45.67
833.60	Gabbro [2]	53.87	1.13	0.27	0.12	6.99	0.19	15.78	23.37	0.26	43.49	11.09	45.42
840.71	Gabbro [2]	54.19	0.73	0.20	0.14	6.62	0.19	15.98	22.74	0.20	44.47	10.62	44.91
842.93	Gabbro [1]	54.86	0.37	0.09	0.12	6.54	0.22	16.62	22.41	0.14	45.67	10.40	43.93
850.35	Pyroxenite [2]	54.36	0.33	0.08	0.14	6.03	0.19	15.56	23.23	0.34	43.79	9.29	46.92
862.90	Pyroxenite [2]	52.33	1.33	0.28	0.11	6.91	0.14	16.08	22.13	0.27	45.23	11.12	43.65
880.12	Gabbro [2]	52.37	1.54	0.29	0.15	7.42	0.16	15.66	22.73	0.32	43.75	11.87	44.38
891.55	Gabbro [2]	53.92	0.37	0.06	0.04	6.97	0.21	15.65	22.72	0.19	43.54	11.20	45.26
902.74	Gabbro [3]	54.53	0.83	0.15	0.12	6.76	0.12	15.77	22.39	0.24	44.40	10.87	44.73
917.30	Pyroxenite [2]	53.46	1.39	0.41	0.30	6.23	0.11	16.07	22.38	0.26	45.63	10.07	44.30
927.30	Pyroxenite [2]	53.63	1.20	0.30	0.21	5.90	0.16	16.26	22.40	0.20	45.99	9.63	44.38
935.40	Pyroxenite [2]	53.20	1.01	0.25	0.29	5.76	0.12	16.52	22.04	0.26	46.76	9.34	43.90
949.60	Noritic gabbro [2]	52.96	1.02	0.26	0.07	6.75	0.16	15.69	22.43	0.54	44.07	10.87	45.06
961.30	Noritic gabbro [3]	52.97	1.20	0.31	0.15	7.22	0.16	15.36	22.19	0.17	43.88	11.80	44.32
969.60	Noritic gabbro [3]	54.15	1.04	0.25	0.05	7.68	0.07	15.71	21.51	0.31	44.54	12.31	43.15
991.06	Gabbro [2]	56.00	0.29	0.07	0.01	8.14	0.13	14.29	21.78	1.24	43.06	9.81	47.13
991.60	Noritic gabbro [4]	53.29	1.24	0.21	0.08	7.68	0.18	15.06	22.50	0.18	44.43	13.04	42.53
993.91	Gabbro [2]	53.22	1.20	0.18	0.06	7.46	0.13	15.18	23.64	0.27	42.05	11.79	46.16
996.42	Noritic gabbro [2]	51.56	1.93	0.48	0.06	8.24	0.20	15.02	21.61	0.26	43.35	13.65	43.00
1006.20	Noritic gabbro [4]	52.96	0.96	0.29	0.06	6.80	0.17	15.67	22.71	0.24	43.96	10.97	45.07
1042.45	Noritic gabbro [4]	51.91	1.48	0.39	0.04	8.13	0.17	14.78	22.70	0.25	41.86	13.18	44.96
1047.50	Dyke [6]	51.85	1.17	0.29	0.01	11.68	0.35	13.48	21.15	0.20	38.43	19.24	42.33
1051.00	Dyke [1]	53.68	1.04	0.22	0.00	10.65	0.27	14.61	20.65	0.24	41.39	17.33	41.28
1054.60	Noritic gabbro [5]	52.99	1.26	0.38	0.21	6.78	0.15	15.74	22.99	0.24	44.03	10.89	45.08
1055.60	Noritic gabbro [5]	52.99	1.07	0.29	0.20	7.03	0.17	15.46	22.14	0.25	44.07	11.51	44.42
1058.80	Dyke [5]	52.18	1.01	0.32	0.00	10.91	0.30	13.96	20.73	0.18	40.03	18.04	41.93
1065.70	Dyke [2]	53.11	1.26	0.39	0.00	11.05	0.30	14.35	19.72	0.22	41.59	18.42	39.99
1066.77	Dyke [2]	53.22	1.19	0.34	0.02	11.75	0.34	13.91	18.84	0.20	41.07	20.00	38.93
1074.50	Dyke [2]	52.67	1.08	0.32	0.03	9.77	0.25	15.01	21.18	0.23	42.20	15.80	42.00
1077.52	Dyke [9]	53.06	1.19	0.33	0.02	10.14	0.32	14.71	20.04	0.22	42.46	16.94	40.60
1106.37	Dyke [5]	51.69	1.20	0.29	0.03	11.78	0.27	13.72	20.70	0.27	39.13	19.30	41.57
1123.89	Noritic gabbro [2]	53.33	1.30	0.37	0.18	7.10	0.18	16.23	21.15	0.25	46.24	11.62	42.14
1138.19	Dyke [2]	51.89	1.18	0.40	0.05	11.16	0.29	14.37	21.03	0.16	40.45	18.08	41.47
1168.10	Noritic gabbro [4]	52.22	1.38	0.32	0.01	8.69	0.18	14.76	21.73	0.30	42.19	14.20	43.61
1191.12	Noritic gabbro [4]	52.46	1.78	0.37	0.05	8.88	0.20	14.85	21.27	0.22	42.86	14.70	42.44
1203.68	Noritic gabbro [2]	52.81	1.80	0.41	0.03	8.64	0.19	15.35	20.77	0.26	44.25	14.29	41.46
1216.33	Noritic gabbro [4]	52.01	1.69	0.38	0.04	8.44	0.16	14.99	21.80	0.24	42.87	13.81	43.32
1242.74	Noritic gabbro [5]	52.47	1.76	0.33	0.16	6.44	0.14	16.13	21.68	0.26	46.31	10.60	43.09
1260.00	Noritic gabbro [3]	52.69	1.50	0.41	0.11	7.53	0.17	15.48	21.09	0.24	44.89	12.53	42.58
1266.70	Noritic gabbro [3]	52.07	1.59	0.45	0.11	8.51	0.21	15.43	20.99	0.16	44.29	14.04	41.67
1289.29	Gabbro [2]	52.25	1.94	0.62	0.12	8.09	0.18	16.02	20.86	0.20	45.81	13.27	40.92
1302.54	Noritic gabbro [2]	52.33	2.25	0.33	0.17	7.50	0.16	16.11	20.87	0.13	46.66	12.44	40.90
1320.30	Noritic gabbro [1]	53.33	1.81	0.30	0.05	7.54	0.14	16.87	19.62	0.13	48.71	12.44	38.85
1326.01	Noritic gabbro [1]	50.93	1.93	0.41	0.17	7.48	0.20	15.71	22.41	0.24	44.31	12.14	43.55
1342.70	Noritic gabbro [1]	52.09	0.86	0.24	0.13	8.25	0.25	14.95	23.16	0.08	41.46	13.23	45.31
1345.40	Gabbro [1]	52.93	1.80	0.34	0.05	9.06	0.19	16.02	19.33	0.11	46.49	15.06	38.45
1349.60	Gabbro [3]	53.22	1.58	0.08	0.08	4.82	0.17	17.46	22.28	0.06	48.96	7.86	43.18
1354.15	Gabbro [2]	52.80	2.20	0.20	0.06	6.24	0.21	15.88	21.48	0.10	46.55	10.60	42.85
1355.15	Gabbro [3]	53.54	1.40	0.27	0.14	7.26	0.18	15.86	21.83	0.08	45.08	11.86	43.06
1373.10	Noritic gabbro [3]	53.53	1.78	0.09	0.12	5.69	0.17	17.63	21.63	0.11	49.28	9.16	41.56

TABLE 2: Microprobe analyses of clinopyroxene from CY-4 (continued)

Depth (m)	Rock [# of analyses]	SiO_2	Al_2O_3	TiO_2	Cr_2O_3	FeO	MnO	MgO	CaO	Na_2O	En	Fs	Wo
1381.47	Noritic gabbro [2]	53.19	1.26	0.22	0.13	6.14	0.10	17.01	22.26	0.14	47.19	9.70	43.11
1391.69	Gabbro [2]	53.53	1.57	0.19	0.10	6.71	0.16	17.28	20.99	0.08	48.51	10.82	40.67
1414.74	Noritic gabbro [2]	52.92	1.76	0.13	0.11	5.81	0.15	16.64	21.88	0.16	47.44	9.53	43.03
1429.48	Olivine gabbro [3]	53.77	1.33	0.16	0.07	5.95	0.18	16.26	22.77	0.18	45.66	9.67	44.67
1450.09	Noritic gabbro [3]	52.80	1.53	0.21	0.13	6.66	0.15	16.40	21.56	0.15	46.65	10.86	42.49
1474.96	Gabbro [3]	52.64	1.74	0.18	0.09	5.58	0.13	16.49	23.35	0.14	46.02	8.94	45.04
1508.73	Noritic gabbro [2]	53.23	1.51	0.17	0.05	6.88	0.13	16.89	20.84	0.11	47.93	11.15	40.92
1525.32	Noritic gabbro [2]	51.76	1.88	0.27	0.09	7.72	0.19	15.34	22.72	0.09	43.35	12.53	44.12
1529.80	Noritic gabbro [2]	52.63	1.93	0.22	0.11	6.71	0.14	16.14	21.87	0.14	46.11	10.98	42.91
1549.62	Olivine gabbro [2]	51.90	2.27	0.16	0.33	7.30	0.17	16.01	20.90	0.12	46.67	12.21	41.12
1565.12	Noritic gabbro [2]	52.55	1.94	0.21	0.25	6.94	0.15	16.63	21.08	0.16	47.49	11.35	41.16
1581.15	Noritic gabbro [2]	54.05	0.38	0.03	0.10	6.36	0.18	15.16	24.26	0.12	41.96	10.14	47.90
1604.44	Noritic gabbro [2]	53.49	1.37	0.21	0.22	6.30	0.19	16.23	22.29	0.12	45.92	10.30	43.78
1610.10	Websterite [3]	52.77	2.03	0.15	0.26	6.79	0.13	17.09	20.45	0.09	49.01	11.12	39.87
1629.02	Noritic gabbro [3]	53.08	1.57	0.17	0.14	5.58	0.18	16.01	23.32	0.09	45.26	9.12	45.62
1646.27	Noritic gabbro [2]	53.17	1.74	0.17	0.16	7.13	0.21	16.53	20.62	0.11	47.50	11.83	40.67
1649.10	Noritic gabbro [2]	52.96	1.99	0.18	0.11	6.31	0.17	17.03	20.98	0.08	48.69	10.38	40.93
1659.29	Noritic gabbro [3]	52.42	1.81	0.19	0.10	6.56	0.12	16.12	22.16	0.12	45.89	10.66	43.45
1678.13	Noritic gabbro [2]	53.94	0.52	0.09	0.08	5.21	0.16	15.94	23.00	0.10	45.15	8.52	46.33
1700.48	Noritic gabbro [2]	52.00	1.36	0.21	0.16	5.37	0.14	16.63	23.22	0.09	46.35	8.61	45.04
1720.69	Gabbro [3]	53.04	1.80	0.17	0.12	5.31	0.15	16.64	22.63	0.12	47.16	8.68	44.16
1740.93	Websterite [2]	53.72	1.27	0.14	0.13	3.87	0.09	16.99	24.08	0.04	47.21	6.19	46.60
1749.58	Noritic gabbro [2]	53.82	1.26	0.13	0.12	4.81	0.15	16.66	23.01	0.03	47.02	7.84	45.14
1767.12	Pyroxenite [3]	53.72	1.32	0.17	0.25	6.02	0.13	17.00	21.45	0.11	48.08	9.78	42.14
1780.84	Websterite [2]	53.81	1.88	0.07	0.17	4.03	0.16	17.95	21.08	0.12	51.68	6.76	41.56
1823.87	Websterite [3]	53.41	1.99	0.15	0.34	4.67	0.13	17.51	22.16	0.11	49.58	7.63	42.79
1838.24	Wehrlite [2]	53.75	1.63	0.07	0.52	3.47	0.11	17.86	22.67	0.08	50.41	5.67	43.92
1846.09	Pyroxenite [3]	54.16	1.36	0.18	0.32	5.19	0.14	17.84	21.48	0.13	49.95	8.37	41.68
1850.72	Pyroxenite [2]	54.28	0.93	0.10	0.31	4.25	0.12	16.66	23.38	0.18	46.84	6.88	46.28
1864.50	Noritic gabbro [3]	53.22	1.87	0.16	0.22	6.09	0.15	17.94	20.36	0.08	50.83	9.90	39.27
1874.40	Pyroxenite [3]	54.44	1.62	0.07	0.59	4.43	0.11	18.60	21.26	0.11	52.10	7.15	40.75
1875.56	Websterite [4]	53.68	1.66	0.10	0.58	4.38	0.12	18.29	21.59	0.15	51.37	7.09	41.54
1893.63	Websterite [3]	52.23	2.93	0.14	0.41	4.42	0.13	17.52	22.39	0.08	50.13	7.30	42.57
1896.35	Pyroxenite [4]	54.61	1.19	0.08	0.51	3.74	0.11	18.35	21.81	0.09	51.52	6.06	42.42
1897.15	Websterite [4]	53.94	1.95	0.08	0.60	4.18	0.11	18.36	21.24	0.10	52.19	6.92	40.89
1918.25	Websterite [3]	53.04	2.28	0.15	0.58	4.41	0.11	17.04	22.34	0.21	49.08	7.31	43.61
1918.85	Websterite [4]	53.87	1.90	0.10	0.45	3.99	0.13	17.63	22.27	0.11	50.18	6.56	43.26
1919.00	Wehrlite [4]	53.91	2.05	0.12	0.73	4.54	0.12	18.66	19.85	0.13	53.89	7.55	38.56
1942.50	Websterite [3]	54.09	1.93	0.09	0.44	3.87	0.12	17.48	22.53	0.18	49.76	6.36	43.88
1944.64	Pyroxenite [3]	53.69	1.14	0.24	0.37	6.40	0.16	16.64	21.82	0.26	46.75	10.32	42.93
1960.55	Websterite [4]	53.75	2.00	0.15	0.45	4.37	0.10	17.75	21.90	0.16	50.44	7.13	42.43
1961.10	Websterite [5]	54.39	1.74	0.09	0.53	3.86	0.11	18.33	21.46	0.11	52.06	6.32	41.62
1969.00	Websterite [5]	53.74	1.72	0.08	0.54	4.00	0.11	18.69	21.13	0.13	52.76	6.51	40.73
1971.70	Websterite [4]	54.07	2.06	0.11	0.50	4.60	0.12	18.38	20.72	0.09	52.49	7.56	39.95
1974.20	Websterite [3]	53.48	1.89	0.16	0.46	4.82	0.10	18.06	21.40	0.16	50.96	7.79	41.25
1989.60	Pyroxenite [4]	53.92	1.53	0.07	0.61	3.63	0.10	17.71	22.93	0.13	49.76	5.87	44.37
1990.25	Pyroxenite [4]	53.51	1.60	0.12	0.43	3.84	0.09	17.29	22.93	0.13	48.98	6.26	44.76
1999.17	Pyroxenite [4]	54.16	1.06	0.08	0.43	3.23	0.12	17.69	23.82	0.07	48.87	5.19	45.94
2000.15	Websterite [5]	53.85	2.13	0.11	0.49	4.10	0.10	17.98	21.59	0.11	51.45	6.74	41.81
2000.75	Websterite [4]	54.71	1.55	0.06	0.45	4.96	0.11	19.27	19.41	0.22	54.34	8.01	37.65
2014.93	Websterite [4]	53.80	2.17	0.12	0.44	4.37	0.11	18.71	20.65	0.16	53.17	7.13	39.70
2016.50	Dunite [4]	53.42	2.01	0.08	0.59	3.77	0.11	19.08	20.72	0.09	54.08	6.16	39.76
2111.65	Websterite [5]	53.62	1.90	0.12	0.47	3.88	0.10	17.18	22.72	0.12	49.17	6.38	44.45
2174.10	Websterite [4]	53.14	2.30	0.12	0.59	3.97	0.11	17.74	21.92	0.09	51.02	6.59	42.39
2175.60	Websterite [4]	53.86	2.34	0.09	0.64	4.50	0.13	18.26	20.64	0.12	52.69	7.49	39.82
2208.00	Websterite [5]	52.92	2.42	0.10	0.86	4.06	0.11	17.57	21.79	0.16	50.97	6.78	42.25
2209.55	Wehrlite [5]	52.71	2.63	0.12	0.83	4.21	0.11	18.19	20.71	0.08	53.03	7.06	39.91
2227.05	Pyroxenite [4]	53.25	2.13	0.08	0.42	4.22	0.13	17.48	22.41	0.11	49.76	6.95	43.29
2229.06	Wehrlite [3]	53.52	2.07	0.12	0.45	3.77	0.10	17.95	21.97	0.04	51.30	6.21	42.49
2244.75	Wehrlite [4]	53.24	2.40	0.13	0.53	3.77	0.11	17.41	21.96	0.18	50.62	6.33	43.05
2245.63	Websterite [4]	53.45	2.09	0.16	0.45	3.59	0.11	17.51	22.50	0.09	50.26	5.94	43.80
2262.03	Websterite [3]	53.46	2.09	0.08	0.62	4.29	0.12	19.03	20.83	0.11	53.12	6.79	40.09
2263.22	Websterite [4]	54.00	2.08	0.09	0.69	3.77	0.11	17.45	22.39	0.12	50.18	6.26	43.56

TABLE 3: Microprobe analyses of orthopyroxene from CY-4

Depth (m)	Rock [# of analyses]	SiO_2	Al_2O_3	TiO_2	Cr_2O_3	FeO	MnO	MgO	CaO	NiO	En	Fs	Wo
614.12	Noritic gabbro [1]	54.97	1.00	0.10	0.00	17.98	0.38	21.12	2.36	0.03	64.24	31.32	4.44
741.80	Noritic gabbro [1]	52.29	1.81	0.12	0.02	16.15	0.29	26.44	2.84	0.05	71.45	24.91	3.64
753.24	Noritic gabbro [1]	55.75	1.06	0.10	0.05	12.92	0.31	30.78	1.61	0.06	79.01	19.04	1.95
917.30	Pyroxenite [3]	54.61	1.04	0.12	0.42	13.06	0.25	28.08	2.63	0.06	76.08	20.20	3.72
927.30	Pyroxenite [3]	54.88	0.58	0.18	0.17	15.44	0.30	28.16	0.90	0.06	75.37	23.63	1.00
935.40	Pyroxenite [1]	53.69	1.24	0.22	0.36	14.10	0.22	27.57	2.03	0.09	75.61	22.00	2.39
949.60	Noritic gabbro [3]	53.54	0.73	0.17	0.04	15.94	0.30	27.09	1.24	0.06	73.65	24.74	1.61
961.30	Noritic gabbro [3]	54.45	0.66	0.28	0.11	17.02	0.31	26.60	1.06	0.02	72.29	26.43	1.28
969.60	Noritic gabbro [3]	53.89	0.59	0.28	0.04	18.75	0.40	25.66	1.05	0.02	69.51	29.11	1.38
991.60	Noritic gabbro [5]	54.18	0.85	0.20	0.03	18.22	0.32	25.67	1.11	0.04	70.24	28.46	1.30
993.91	Noritic gabbro [1]	54.75	0.56	0.15	0.04	19.21	0.22	24.63	1.00	0.05	68.36	30.24	1.40
996.42	Noritic gabbro [2]	53.95	0.79	0.19	0.04	18.37	0.40	25.01	1.16	0.02	69.32	29.18	1.50
1006.20	Noritic gabbro [6]	54.25	0.70	0.14	0.03	16.86	0.30	26.14	1.17	0.03	71.93	26.47	1.60
1042.45	Noritic gabbro [5]	53.57	0.93	0.17	0.02	18.88	0.35	24.66	1.14	0.02	68.68	30.05	1.27
1047.50	Dyke [4]	52.09	0.68	0.21	0.02	24.65	0.63	19.87	1.48	0.04	57.01	40.66	2.33
1051.00	Dyke [5]	53.30	0.55	0.16	0.02	23.26	0.58	21.19	1.38	0.02	59.95	37.85	2.20
1054.60	Noritic gabbro [5]	54.39	0.63	0.25	0.05	16.49	0.28	26.83	1.09	0.05	73.01	25.60	1.39
1055.60	Noritic gabbro [4]	54.24	0.63	0.22	0.08	17.36	0.33	25.51	1.01	0.04	71.05	27.63	1.32
1058.80	Dyke [5]	52.96	0.48	0.16	0.02	23.36	0.59	21.25	1.32	0.02	59.92	37.89	2.19
1065.70	Dyke [1]	54.01	0.52	0.18	0.00	22.75	0.60	21.70	1.41	0.04	60.94	36.77	2.29
1074.50	Dyke [2]	53.97	0.80	0.19	0.00	20.95	0.52	23.07	1.25	0.01	64.60	33.75	1.65
1077.52	Dyke [9]	53.52	0.80	0.22	0.03	21.57	0.55	22.44	1.30	0.02	63.22	34.98	1.80
1106.37	Dyke [2]	52.12	0.63	0.14	0.00	23.95	0.61	20.35	1.51	0.00	58.20	39.40	2.40
1123.89	Noritic gabbro [2]	54.64	0.98	0.20	0.11	16.60	0.32	26.81	1.03	0.05	73.21	25.90	0.89
1138.19	Dyke [2]	52.22	0.60	0.21	0.00	23.79	0.56	20.75	1.52	0.03	58.86	38.73	2.41
1168.10	Noritic gabbro [3]	54.10	0.81	0.14	0.01	19.03	0.33	24.40	1.24	0.05	68.11	30.30	1.59
1191.12	Noritic gabbro [2]	53.35	0.76	0.20	0.01	19.99	0.43	23.80	1.38	0.04	66.20	31.87	1.93
1203.63	Noritic gabbro [3]	53.94	0.95	0.19	0.02	18.36	0.32	25.72	1.24	0.01	70.06	28.56	1.38
1216.33	Noritic gabbro [5]	53.51	1.03	0.21	0.02	17.91	0.30	25.15	1.13	0.03	70.32	28.55	1.13
1242.74	Noritic gabbro [2]	54.92	1.06	0.14	0.09	14.34	0.27	27.77	1.26	0.06	76.24	22.48	1.28
1260.00	Noritic gabbro [4]	53.99	1.04	0.26	0.08	16.98	0.30	25.69	1.33	0.05	71.56	26.98	1.46
1266.70	Noritic gabbro [6]	53.45	1.00	0.27	0.05	17.81	0.35	24.88	1.31	0.05	69.89	28.61	1.50
1289.29	Noritic gabbro [2]	54.02	1.07	0.30	0.07	17.11	0.25	25.80	1.43	0.04	71.43	26.95	1.62
1302.54	Noritic gabbro [2]	54.10	1.27	0.11	0.07	15.78	0.31	26.72	1.40	0.06	73.75	24.90	1.35
1320.30	Noritic gabbro [2]	56.36	1.07	0.13	0.01	14.81	0.30	28.22	1.47	0.03	75.55	22.70	1.75
1326.01	Noritic gabbro [2]	54.53	1.20	0.23	0.08	15.50	0.32	27.10	1.30	0.02	74.38	24.36	1.26
1342.70	Noritic gabbro [2]	53.20	1.09	0.22	0.03	19.24	0.38	23.76	1.49	0.04	67.09	31.05	1.86
1355.15	Noritic gabbro [3]	54.73	1.00	0.15	0.09	14.90	0.29	26.67	2.13	0.06	73.48	23.46	3.06
1355.69	Noritic gabbro [2]	54.13	0.98	0.12	0.08	15.58	0.33	26.15	2.29	0.04	72.02	24.57	3.41
1373.10	Noritic gabbro [3]	55.20	1.62	0.06	0.16	10.36	0.27	30.08	2.45	0.05	81.03	16.06	2.91
1381.47	Noritic gabbro [2]	55.44	1.16	0.05	0.06	12.98	0.28	28.55	1.70	0.02	77.72	20.26	2.02
1414.74	Noritic gabbro [3]	56.60	1.20	0.03	0.04	11.17	0.23	29.18	1.61	0.03	80.49	17.65	1.86
1429.48	Olivine gabbro [2]	55.72	1.32	0.08	0.04	12.52	0.31	28.71	1.11	0.04	77.63	20.45	1.92
1450.09	Noritic gabbro [6]	54.69	1.21	0.05	0.06	13.96	0.27	27.33	1.81	0.04	75.66	22.10	2.24
1508.73	Noritic gabbro [2]	54.94	1.23	0.12	0.03	14.23	0.27	27.80	1.23	0.05	76.54	22.38	1.08
1525.32	Noritic gabbro [3]	53.94	1.08	0.20	0.06	13.96	0.31	28.21	1.97	0.05	75.86	21.52	2.62
1529.80	Noritic gabbro [3]	54.84	1.08	0.09	0.05	15.41	0.28	27.57	1.14	0.01	74.99	23.97	1.04
1549.62	Olivine gabbro [3]	54.02	1.30	0.11	0.09	14.95	0.31	26.83	1.73	0.07	74.34	23.70	1.96
1565.12	Noritic gabbro [2]	54.90	1.19	0.07	0.08	14.71	0.27	27.08	1.76	0.04	74.71	23.17	2.12
1604.44	Noritic gabbro [2]	53.67	1.26	0.08	0.13	14.80	0.29	27.91	1.96	0.04	74.94	22.70	2.36
1610.10	Websterite [2]	54.70	1.33	0.09	0.12	13.33	0.30	28.13	1.71	0.08	77.20	20.95	1.85
1629.02	Noritic gabbro [3]	54.55	1.17	0.10	0.13	13.82	0.28	27.94	2.14	0.03	75.74	21.45	2.81
1646.27	Noritic gabbro [4]	54.74	1.18	0.13	0.09	13.12	0.30	28.63	2.35	0.02	76.65	20.15	3.20
1649.10	Noritic gabbro [4]	54.50	1.17	0.10	0.12	13.26	0.24	27.96	2.40	0.06	76.07	20.59	3.34
1659.29	Noritic gabbro [2]	55.53	1.25	0.05	0.06	12.54	0.23	28.59	1.30	0.08	79.06	19.78	1.16
1678.13	Noritic gabbro [2]	54.81	1.37	0.07	0.05	13.48	0.22	28.23	1.16	0.03	78.01	21.23	0.76
1700.48	Noritic gabbro [2]	54.40	1.25	0.06	0.07	13.60	0.26	28.33	1.57	0.07	77.18	21.16	1.66
1740.93	Websterite [2]	55.20	1.28	0.10	0.10	11.28	0.25	30.12	1.38	0.04	81.32	17.45	1.23
1749.58	Noritic gabbro [3]	55.15	1.21	0.14	0.19	10.33	0.17	30.04	2.36	0.06	80.98	15.87	3.15
1753.89	Websterite [3]	54.56	1.03	0.13	0.19	12.73	0.26	28.86	1.75	0.03	78.10	19.74	2.16
1767.12	Pyroxenite [3]	55.23	1.26	0.14	0.25	12.25	0.22	29.22	1.98	0.06	78.83	18.87	2.30
1780.84	Websterite [3]	54.71	0.94	0.19	0.10	11.72	0.24	29.70	2.00	0.06	79.31	17.90	2.79
1823.87	Websterite [3]	55.86	1.02	0.09	0.29	10.49	0.24	31.11	1.35	0.06	82.70	16.00	1.30
1850.72	Pyroxenite [4]	55.04	1.42	0.13	0.24	10.04	0.22	30.71	2.05	0.08	82.32	15.41	2.27

TABLE 3: Microprobe analyses of orthopyroxene from CY-4 (Continued)

Depth (m)	Rock [# of analyses]	SiO_2	Al_2O_3	TiO_2	Cr_2O_3	FeO	MnO	MgO	CaO	NiO	En	Fs	Wo
1864.50	Noritic gabbro [3]	54.86	1.04	0.16	0.17	13.75	0.30	27.61	1.90	0.03	75.82	21.69	2.49
1874.40	Pyroxenite [2]	54.60	1.55	0.09	0.22	11.10	0.19	30.48	0.98	0.05	82.65	17.17	0.18
1875.56	Websterite [1]	54.12	2.30	0.08	0.14	9.38	0.10	31.32	0.70	0.06	—	—	—
1893.63	Websterite [2]	54.96	1.27	0.08	0.27	10.20	0.20	30.84	0.82	0.05	83.81	15.76	0.43
1896.35	Pyroxenite [3]	55.32	1.39	0.11	0.26	10.41	0.20	30.13	1.48	0.05	82.49	16.29	1.22
1897.15	Websterite [3]	55.77	1.48	0.06	0.25	10.12	0.20	31.38	0.72	0.05	84.12	15.79	0.09
1918.25	Websterite [3]	55.25	1.70	0.08	0.27	10.12	0.23	30.52	1.03	0.05	83.32	15.92	0.76
1918.85	Websterite [3]	55.61	1.64	0.08	0.26	9.93	0.18	30.85	1.05	0.03	84.36	15.46	0.18
1942.50	Websterite [3]	55.18	1.35	0.10	0.21	11.58	0.21	29.91	0.92	0.03	81.98	17.47	0.55
1960.55	Websterite [2]	55.07	1.64	0.08	0.24	10.08	0.21	30.57	1.04	0.03	84.04	15.85	0.11
1961.10	Websterite [3]	55.35	1.55	0.08	0.24	9.91	0.21	30.49	1.54	0.09	83.32	15.49	1.19
1969.00	Websterite [3]	55.43	1.43	0.14	0.27	10.09	0.19	30.52	1.30	0.07	83.43	15.75	0.82
1971.70	Websterite [3]	55.64	1.50	0.12	0.25	9.95	0.19	30.79	1.29	0.05	83.79	15.48	0.73
1974.20	Websterite [3]	54.69	0.64	0.16	0.20	12.62	0.23	30.24	0.87	0.04	80.06	19.07	0.87
1999.17	Pyroxenite [3]	55.67	1.56	0.09	0.20	9.65	0.18	31.05	1.58	0.06	83.86	14.88	1.26
2000.15	Websterite [2]	55.05	1.57	0.06	0.25	8.76	0.18	30.68	1.71	0.06	84.67	13.83	1.50
2014.93	Websterite [3]	55.45	1.52	0.06	0.25	9.91	0.19	30.37	1.63	0.04	83.12	15.50	1.38
2111.65	Websterite [3]	55.64	1.58	0.07	0.30	9.08	0.18	31.31	1.48	0.03	84.93	14.09	0.98
2174.10	Websterite [1]	56.23	1.61	0.07	0.30	9.27	0.24	31.61	0.97	0.00	—	—	—
2208.00	Websterite [3]	54.40	1.70	0.08	0.37	9.27	0.17	31.62	1.77	0.07	84.51	14.14	1.35
2262.03	Websterite [3]	54.52	1.59	0.10	0.32	9.31	0.13	31.90	1.97	0.05	84.15	13.96	1.89

TABLE 4: Microprobe analyses of olivine from CY-4

Depth (m)	Rock [# of analyses]	SiO_2	Al_2O_3	TiO_2	Cr_2O_3	FeO	MnO	MgO	CaO	NiO	Fo
1429.48	Olivine gabbro [2]	38.86	0.02	0.03	0.01	18.66	0.23	41.93	0.08	0.14	79.85
1549.62	Olivine gabbro [2]	37.99	0.00	0.00	0.02	22.88	0.26	39.01	0.07	0.24	75.09
1610.10	Websterite [2]	37.88	0.01	0.00	0.01	21.98	0.27	39.29	0.07	0.19	75.93
1740.93	Websterite [2]	39.10	0.00	0.00	0.01	18.37	0.21	42.80	0.06	0.13	80.44
1753.89	Websterite [3]	38.96	0.03	0.01	0.00	18.95	0.25	42.06	0.07	0.18	79.64
1780.84	Websterite [3]	38.71	0.01	0.00	0.04	18.22	0.19	42.88	0.12	0.20	80.62
1823.87	Websterite [2]	39.10	0.02	0.02	0.00	16.43	0.22	43.82	0.08	0.16	82.46
1875.56	Websterite [3]	38.86	0.02	0.01	0.00	15.60	0.10	44.42	0.03	0.18	83.48
1893.63	Websterite [4]	39.14	0.00	0.01	0.01	16.97	0.19	43.42	0.05	0.18	81.88
1897.15	Websterite [4]	39.49	0.00	0.01	0.01	16.44	0.20	44.26	0.03	0.21	82.61
1918.25	Websterite [5]	39.36	0.00	0.01	0.02	16.27	0.18	43.73	0.04	0.19	82.59
1918.85	Websterite [5]	39.36	0.01	0.00	0.02	15.95	0.21	44.21	0.04	0.16	83.00
1919.00	Wehrlite [5]	39.39	0.00	0.01	0.01	16.01	0.19	44.54	0.05	0.20	83.08
1942.50	Websterite [5]	39.85	0.01	0.01	0.01	14.26	0.17	45.90	0.04	0.16	85.03
1960.55	Websterite [5]	39.28	0.14	0.01	0.02	16.09	0.18	44.11	0.04	0.17	82.87
1961.10	Websterite [5]	39.10	0.01	0.01	0.01	16.18	0.18	43.72	0.05	0.13	82.66
1969.00	Websterite [5]	39.37	0.01	0.00	0.02	16.45	0.20	44.13	0.03	0.16	82.56
1971.70	Websterite [6]	39.20	0.01	0.00	0.02	16.26	0.21	44.28	0.04	0.19	82.77
1974.20	Websterite [5]	39.11	0.02	0.02	0.01	16.43	0.20	44.20	0.06	0.13	82.59
2000.15	Websterite [3]	39.05	0.00	0.02	0.01	16.50	0.21	43.73	0.03	0.19	82.38
2000.75	Websterite [6]	39.32	0.02	0.00	0.02	16.65	0.19	44.03	0.04	0.15	82.36
2014.93	Websterite [5]	39.46	0.01	0.01	0.02	16.06	0.16	44.75	0.04	0.13	83.12
2016.50	Dunite [3]	39.19	0.01	0.00	0.01	15.07	0.17	44.98	0.07	0.11	84.04
2111.65	Websterite [5]	39.10	0.02	0.00	0.01	15.87	0.19	44.28	0.03	0.17	83.12
2174.10	Websterite [3]	39.72	0.00	0.02	0.00	14.48	0.11	45.19	0.02	0.20	84.69
2175.60	Websterite [6]	39.53	0.00	0.01	0.01	14.62	0.19	45.51	0.02	0.17	84.59
2208.00	Websterite [4]	39.60	0.02	0.01	0.03	14.82	0.18	44.89	0.02	0.18	84.24
2209.55	Wehrlite [5]	39.63	0.00	0.01	0.02	14.18	0.18	46.14	0.05	0.18	85.15
2229.06	Wehrlite [5]	39.43	0.00	0.00	0.02	13.98	0.18	46.21	0.05	0.17	85.35
2244.75	Wehrlite [5]	39.68	0.01	0.01	0.07	14.98	0.19	44.92	0.04	0.16	84.13
2245.63	Websterite [6]	39.40	0.08	0.01	0.03	13.89	0.16	45.80	0.05	0.15	85.32
2262.03	Websterite [4]	39.60	0.00	0.00	0.02	14.95	0.19	45.21	0.05	0.20	84.21
2263.22	Websterite [5]	39.47	0.01	0.00	0.02	14.16	0.18	45.69	0.04	0.16	85.05

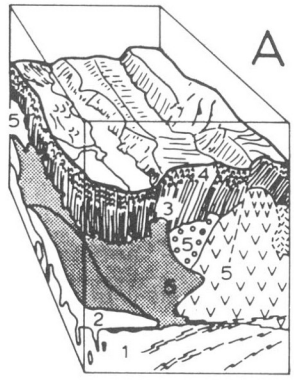

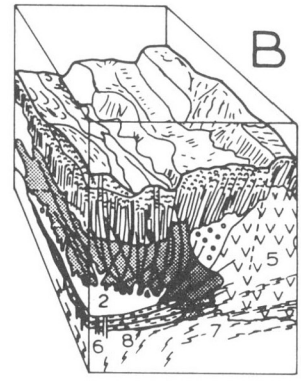

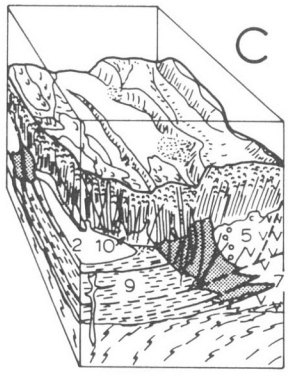

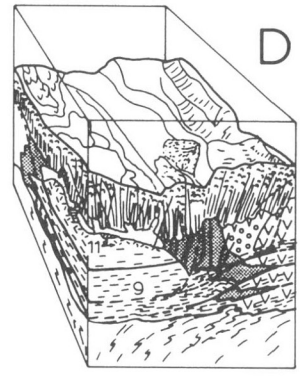

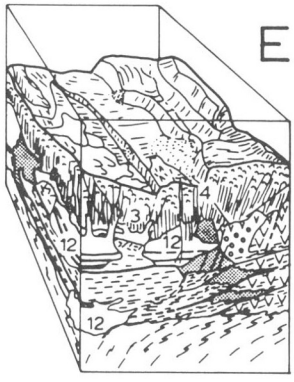

Figure 15: Sequential development of the Troodos plutonic complex by the intrusion of multiple magma bodies and penecontemporaneous deformation associated with spreading. a. Accumulation of magma at the base of the crust is controlled by lithological and density contrasts between crustal and mantle rocks. The shape of the chamber is controlled in part by the regional stress field. b. Upward progression of the magma chamber through existing gabbroic rocks is accomplished by stoping and assimilation. At this stage heat is supplied by the latent heat of crystallisation of ultramafic rocks at the base of the advancing chamber. The magma is still buffered somewhat in composition by the steady input from below and by the assimilation of dominantly gabbroic rocks. c. Cut off from a source supply and cooled by hydrothermal circulation from above, the magma chamber shrinks in size and undergoes more advanced fractionation. Note that the older parts of the crust undergo high temperature deformation during lateral spreading. d. Final consolidation of the magma chamber produces the most fractionated rock types, plagiogranites, which are trapped between the isotropic gabbros and the varitextured gabbros of the roof assemblage. e. The repetition of this sequence with magma chambers of different sizes and composition results in the complex plutonic arrangement observed in Cyprus. These magma chambers are intruded in a zone of spreading rather than along a single 'axis'. Key. 1 mantle tectonites, 2 magma chamber, 3 sheeted dykes, 4 pillow lavas, 5 older plutonic bodies, 6 input of primitive magma from mantle source, 7 high temperature deformation during lateral spreading, 8 ultramafic layers, 9 layered gabbros, 10 roof assemblage of varitextured gabbros, 11 plagiogranite and diorite bodies, 12 later plutonic bodies.

MAGMA CHAMBER MODELS

The field relationships of the plutonic rocks of the Troodos ophiolite are complex and variable. Although a sequence of synchronous magmatism and high temperature deformation allows the recognition of distinct magma bodies in the lower plutonics, no such clear cut distinction is possible in the higher parts of the sequence. In general, local magma compositions appear to be independent of the time of emplacement as plagiogranites are observed intruding mafic rocks and vice versa. Diabase dykes of various compositions also display complex field and petrologic relationships with the plutonic rocks. All of these relationships do however, support the existence of multiple magma chambers since it is unlikely that a single fractionating magma chamber (Greenbaum, 1972) would produce the large number of cross-cutting features observed.

The proposed model for the petrogenesis of the plutonic rocks of Troodos is depicted in Figure 15 and the relationship of CY-4 to the stratigraphy so derived in Figure 16. The upper plutonic suite is constructed from relatively small multiple magma chambers, each produced from melts which were derived by fractional crystallisation from larger, more mafic chambers, the remains of which are seen lower in the crust. These deeper plutons are dominated by ultramafic rocks with lesser gabbros and few plagiogranitic differentiates. It is perceived in this model that magmas at varying stages of fractionation intruded into the higher levels of the plutonic sequence during formation of the crust and individual chambers were able to generate segments of the sheeted diabase complex in small spreading centres possibly all within a wider 'spreading zone'. Fractional crystallisation is considered to have been a dominant process operating as the melts cooled, locally producing layered sequences either by crystal settling or double diffusive convection across liquid/liquid boundary layers. Periodic replenishment of the magma chambers allowed the accumulation of mafic phases at the lower levels of the nested plutons. High temperature deformation, in some places involving reverse faulting, produced penetrative fabrics in some of the earlier formed plutonic rocks during the spreading mechanism, and the fact that some but not all plutonic rocks are deformed further suggests that the ophiolite is actually a sample of the spreading zone.

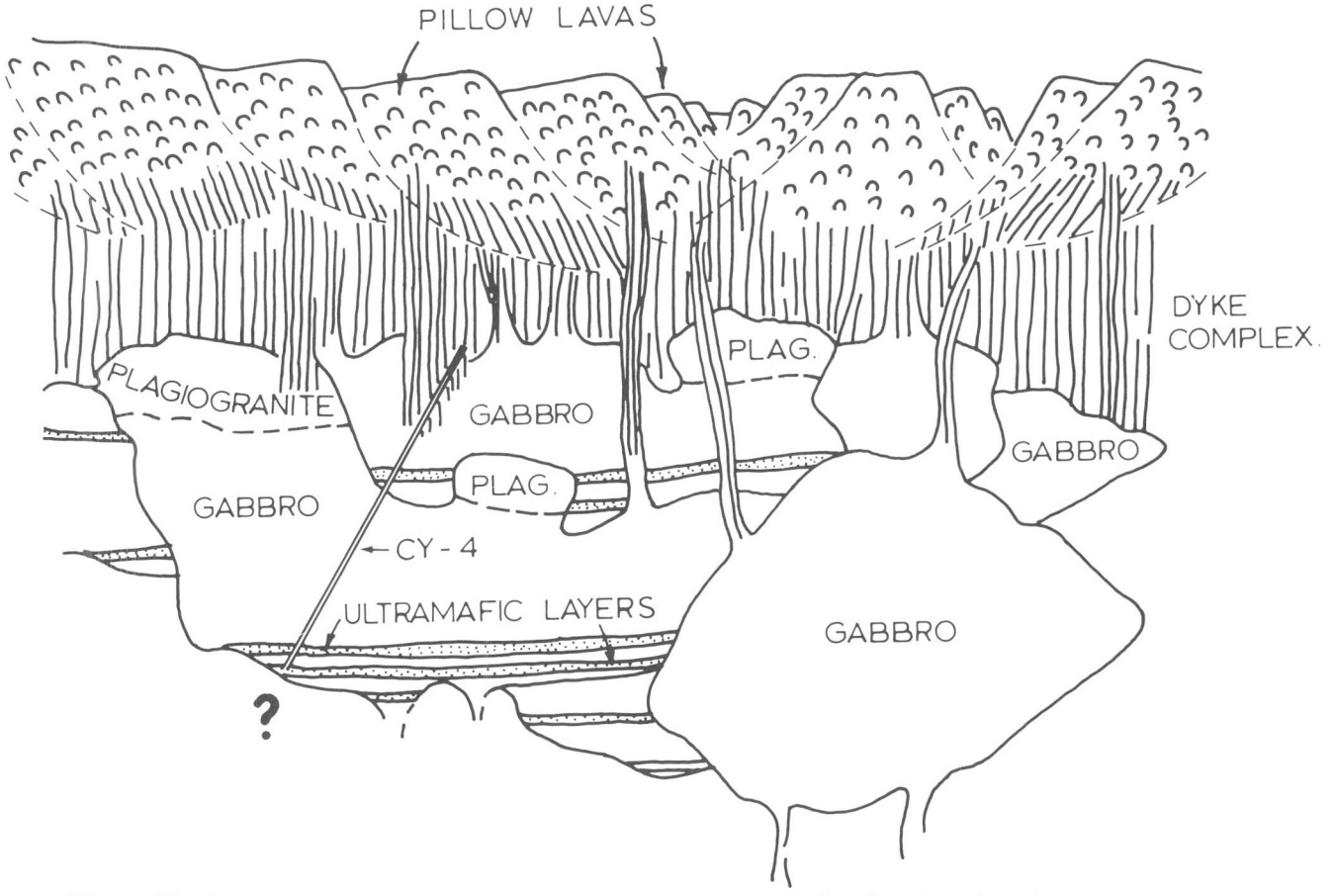

Figure 16: The position of CY-4 with respect to a multiple magma chamber plutonic series. With continued drilling, CY-4 would probably enter the gabbros of another chamber. CY-4 is shown with schematic section restored to "horizontal" position as formed in the ocean crust.

Above the high level plutonics, hydrothermal circulation of seawater actively cooled the crust. This circulation appears to have been driven by the heat of the crystallising magma chambers and upwelling zones are apparently focussed above high level intrusions or cupolas in the crustal section. Seawater came close to the magma bodies via a system of fractures and faults in the sheeted dyke complex related to the brittle failure of the extending crust and the development of listric and planar normal faults. This circulation induced a pervasive greenschist-facies alteration in the recharge zones and localised zones of extreme hydrothermal alteration and metal leaching at the base of the discharge zones. Water actually entered the magmas by assimilation of hydrated, metamorphosed roof rocks and led to volatile transport of hygromagmatophile elements from the magma and the formation of plagiogranites. It remains to be seen how much of the base metal content of the hydrothermal system, which eventually fed the exhalative sulphide deposits, was actually derived from this 'magmatic' water.

The CY-4 drill core records the intrusive relationship of two of these high level magma chambers. The upper part of the core sampled the older of the two in which the crystallisation sequence was cpx, opx, pl ± oxides. This sequence also shows a number of periods of magma replenishment by a relatively evolved magma in a relatively steady state open system showing limited crystal fractionation. The lower part of the drill core exhibits only one major replenishment period and the phase layering suggests a relatively closed fractionation system. The interpretation of the drill core petrology supports the model of multiple magma chambers predicted from the field work.

The fact that ultramafic rocks were recovered at depths of 1746 m and deeper does not mean that layer three of the ocean crust is particularly thin as represented in Troodos. These ultramafic rocks are not necessarily from horizons close to the Moho but more likely from the basal part of a high level pluton. From the field evidence it can be predicted that with further drilling, gabbros of another magma chamber would be intersected (Figure 16).

It is also tempting to correlate the transition from low to higher titanium content of the pyroxenes at 1330 m with two independent magma suites, and the relative time of intrusion of these two suites with the two suites of volcanic rocks identified by Robinson et al (1983). These workers identified a younger suite of low-Ti, high-Mg (boninitic) lavas which overlie an older, high-Ti suite of arc tholeiitic lavas. If such a correlation is made then the lower and younger plutonic rocks (Zones 4 and 5) of the drill core might be related to the upper and younger volcanic suite. Caution must be applied here, however, since evidence is available from only the one drill hole. In addition, field evidence from the plutonic section (Dunsworth, 1989) and the sheeted complex (Baragar et al, 1987) suggest that both magma types were available at the same time when viewed on the larger scale of the whole ophiolite. Indeed, recent interpretation of the volcanic sequence (Gibson, pers. com.) suggests the same.

ACKNOWLEDGEMENTS

Thanks are due to a number of students who formed part of the Memorial team remapping the Troodos plutonic section, namely Jim Scott, Chris Ash, Paul Moore, Glenn Case and David Butler. Also to Tom Calon of Memorial University and Costas Xenophontos and the Geological Survey Department, Nicosia for both scientific and logistical support. The field programme is summarised in map sheets (Malpas and Brace, 1987) published by the Geological Survey Department of Cyprus and was funded by the NSERC of Canada through Operating and Collaborative Special Project grants.

REFERENCES

Alabaster, T., Gass, I.G., Roberts, S. and Tindle, A.
1985: Phase and cryptic variations within the cumulate ultramafic sequence of CY-4: Troodos Ophiolite Deep Sea Drilling Project; Transactions of the American Geophysical Union, v. 66, p. 1123.

Aldiss, D.R.
1978: Granitic rocks of ophiolites; unpublished PhD thesis, Open University, p. 198.

Allen, C.R.
1975: The petrology of a portion of the Troodos plutonic complex, Cyprus; unpublished Ph.D. thesis, University of Cambridge, p. 1-161.

Benn, K. and Laurent, R.
1987: Intrusive suite documented in the Troodos ophiolite plutonic complex, Cyprus; Geology, v. 15, p. 821-824.

Baragar, W.R.A., Lambert, M.B., Baglow, N. and Gibson, I.L.
1987: Sheeted dykes of the Troodos ophiolite, Cyprus; *in* Mafic dyke swarms, ed. H.C. Halls and W.F. Fahrig; Geological Association of Canada, Special Paper 34.

Desmet A., Lapierre H., Rocci G., Gagny C.L., Parrot J.F. and Delaloye M.
1978: Constitution and significance of the Troodos sheeted complex; Nature, v. 272, p. 527-530.

Dunsworth S.M. and Calon T.
1984: Relationships between deformation and magmatism in the plutonic complex, Troodos ophiolite, Cyprus. Geological Association of Canada - Mineralogical Association of Canada, Annual Meeting, London, Ontario, Programme with Abstracts, v. 9, p. 59.

Dunsworth S.M. and Malpas J.
In prep.: Geochemistry of the plutonic series of the Troodos ophiolite, Cyprus and relationships to models of crustal accretion.

Gass, I.G. and Smewing, J.D.

1973: Intrusion, extrusion and metamorphism at The Plutonic Complex, Troodos Ophiolite, Cyprus; Geological Association of Canada Annual Meeting, Programme with Abstracts, v. 9 p. 59.

Gass, I.G. and Smewing, J.D.
1973: Intrusion, extrusion and metamorphism at constructive margins: evidence from the Troodos Massif, Cyprus; Nature, v. 242, p. 26-29.

Greenbaum, D.
1972: Magmatic processes at ocean ridges: evidence from the Troodos Massif, Cyprus; Nature, Physical Science,v. 238, no. 80 p. 18-21.

Kidd, R.G.W. and Cann, J.R.
1974: Chilling statistics indicate an ocean floor spreading origin for the Troodos complex, Cyprus; Earth and Planetary Science Letters, v. 24, no. 1, p. 151-155.

Malpas, J. and Brace, T.
1987: The geology of the Pano Amiandos-Palekhori area, Cyprus, 1:12500 map with marginal notes; Geological Survey of Cyprus.

Malpas, J. and Robinson, P.T.
1987: Chromite mineralisation in the Troodos ophiolite, Cyprus; *in* Evolution of Chromium Orefields, ed. C.W. Stowe; van Nostrand-Rheinghold, p. 220-237.

Nicolas, A. and Violette, J.P.
1982: Mantle flow at oceanic spreading centres: models derived from ophiolites; Tectonophysics, v. 81, p. 319-339.

Pedersen, R.B. and Malpas, J.
1984: The origin of oceanic plagiogranites from the Karmoy ophiolite, western Norway; Contributions to Mineralogy and Petrology, v. 88, p. 36-52.

Robinson P.T., Melson, W.G., O'Hearn, T. and Schmincke, H-U.
1983: Volcanic glass compositions of the Troodos ophiolite, Cyprus; Geology, v. 11, no. 7, p. 400-404.

Spooner, E.T.C.
1980: Cu-mineralisation and seawater convection in ocean crust: the ophiolite ore deposits of Cyprus; Geological Society of America Special Paper 20, p. 665-704.

Thy, P.
1987: Petrogenetic implications of mineral crystallisation trends of Troodos cumulates; Geological Magazine, v. 124, p. 1-11.

Varga, R.J. and Moores, E.M.
1985: Spreading structure of the Troodos ophiolite; Geology, v. 13, p. 846-850.

Wilson, R.A.M.
1959: The geology of the Xeros-Troodos area; Cyprus Geological Survey Department Memoir #1, p. 136.

Sheeted Dykes from CY-4 and Surface Sections: Troodos Ophiolite

W.R.A. BARAGAR[1], M.B. LAMBERT[1], N. BAGLOW[2] AND I.L. GIBSON[3]

[1]Geological Survey of Canada, 588 Booth St., Ottawa, Ont., Canada, K1A 0E4
[2]Geological Survey of Zimbabwe, P.O. Box 8039, Harare, Zimbabwe
[3]Department of Earth Sciences, University of Waterloo, Waterloo, Ont., Canada, N2L 3G1

Baragar, W.R.A., Lambert, M.B., Baglow, N. and Gibson, I.L., Sheeted dykes from CY-4 and surface sections: Troodos Ophiolite; in *Cyprus Crustal Study Project: Initial Report, Hole CY-4, ed. I.L. Gibson, J. Malpas, P.T. Robinson and C. Xenophontos; Geological Survey of Canada, Paper 88-9, p. 69-106, 1989.*

Abstract

The uppermost 600 m of the CY-4 drillhole and 10 road-cut sections provide vital data pertaining to genesis of the Troodos ophiolite. The dyke zone is prime evidence of spreading. Chilling statistics on dyke margins show little systematic bias, suggesting dyke emplacement in a spreading zone exceeding 50 - 100 m in width. Range and distribution of dyke compositions parallel that of the lavas but lack the break in continuity, between 4-5.5% MgO, shown in glasses from pillows; a break that divides the lavas into distinctive upper and lower suites. Equivalent suites in the dykes, identified by discriminators indicative of the upper lava suite (MgO >5.5%, TiO_2 <0.85%, Cr >40 ppm) are termed the depleted and non-depleted suites respectively. Unlike their lava equivalents, dykes show no age preference as determined by cutting relations. Much of their compositional variation can be modelled by crystal fractionation but some must be attributed to distinctive mantle sources. Accordingly, the dykes are thought to have originated at discrete, fractionating centres along the spreading axis. From each centre they extend both vertically and longitudinally, and mutually interleave at the level of the sheeted dyke zone. Metamorphism of the dyke zone to the actinolite facies is attributed to the combined effects of heat from the underlying plutonic complex and the residual influence of marine waters percolating from above.

Résumé

Les 600 premiers mètrés du forage CY-4 ainsi que 10 coupes routières fournissent des données vitales sur la gènèse de l'ophiolite de Troodos. La zone de dykes est une bonne évidence d'expansion. Une étude sur la zone de trempe des dykes suggère l'emplacement de ceux-ci dans un milieu à expansion excédant une largeur de 50 à 100 m. L'étendue et la distribution de la composition des dykes sont semblables à celle des laves mais ne montrent pas la discontinuité, entre 4-5.5% MgO, observable dans les verres des coussins. Cette discontinuité divise distinctement les laves en une suite supérieure et une inférieure. Des suites équivalentes pour les dykes, définies en utilisant des discriminants caractéristiques des laves de las suite supérieure (MgO > 5.5%, TiO_2 < 0.85%, Cr > 40 ppm), sont appelées respectivement suite appauvrie et suite non-appauvrie. Contrairement à leur équivalents effusifs, les dykes ne montrent aucune préférences temporelles comme il fut déterminé à partir de relations entre échantillons. La majorité des variations compositionelles peuvent être expliquées par la cristallisation fractionnée. Cependant, certaines variations ne peuvent s'expliquer qu'en considérant une source distincte dans le manteau. Par conséquent, on pense que les dykes se sont formés dans des centres de fractionnement distincts, distribués le long de l'axe de la zone d'expansion. A partir de chaque centre, ils s'étendent verticalement et horizontalement et deviennent alternatifs au niveau des dykes groupés. Le métamorphisme de la zone de dykes au faciès de l'actinolite est attribué à l'action combinée de l'eau de mer et de la chaleur provenant du complexe plutonique sous-jacent.

INTRODUCTION

The presence of a sheeted dyke zone is compelling evidence for the origin of an ophiolite complex at a spreading zone, irrespective of whether that zone is a mid-ocean ridge, a back-arc spreading centre, or even a distending island arc. The dykes in turn are the essential link between rocks of the underlying plutonic complex and overlying volcanic pile and presumably constitute the most complete record available of magma compositions generated at the spreading zone. A major objective of this study is to present a representative compositional spectrum of the Troodos sheeted dykes and to relate it as far as possible to that of the lavas and the plutonic rocks.

The study is based on the part of the sheeted dyke zone (about 630 m) exposed in the core of CY-4 drill hole and on 10 mapped road-cut sections, aggregating about 1 km in length, distributed through the sheeted dyke zone. The locations of the drill hole and the road-cut sections are shown in the map of Figure 1. Progressively deeper levels within the sheeted dyke zone are represented by the following road-cut sections respectively: Ayia Koroni, (with screens of pillow lava), Nikitari 2, Nikitari 1, Ayios Theodhoros, and Kakopetria (adjoining screens of gabbro). Sections at Makheras Monastery, Kionia 3, and Prophitis Elias are at uncertain intermediate levels. The drill hole is collared in sheeted dykes and transects the lower-most 630 m of the dyke zone before passing into the plutonic complex.

Data from the road-cut sections were used in an earlier publication (Baragar et al., 1987) but are presented in detail in this report, together with those from CY-4, with a view to bringing together here a complete data set for the sheeted dykes.

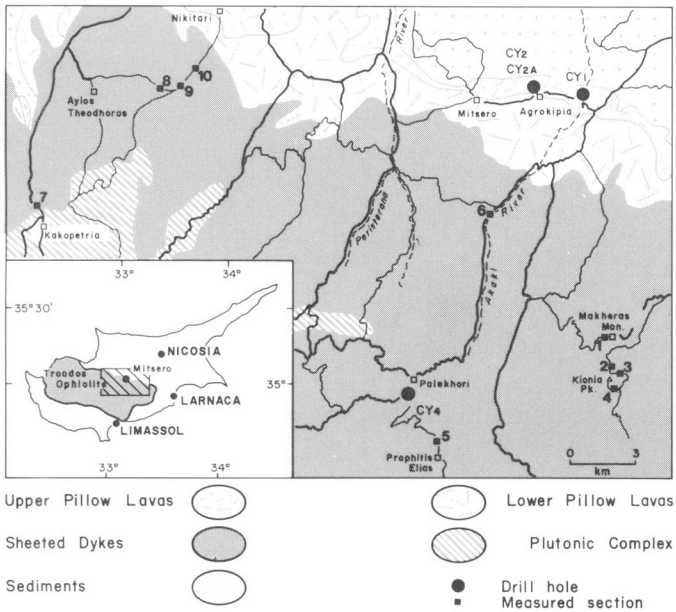

Figure 1: Index map of part of Troodos Complex showing location of Cyprus Crustal Study Project drill holes and road-cut sections. Identity of the road-cut sections as follows: (1) Makheras, (2) Kionia 1, (3) Kionia 2, (4) Kionia 3, (5) Prophitis Elias, (6) Ayia Koroni, (7) Kakopetria, (8) Ayios Theodhoros, (9) Nikitari 1, (10) Nikitari 2. Inset map shows location of index map within the Troodos ophiolite (grey).

METHODS

A total of 622 'dykes' (dykes and partial dykes) were mapped in the road-cut sections and a further 400 logged in the drill core of CY-4 to a depth of 630 m, approximately the base of the sheeted dyke zone. Virtually all the road-cut dykes and more than one third of those in CY-4 were sampled and a total of 590 samples analyzed for major and a variety of trace elements. In three of the best exposed road-cut sections (Kionia 3, Ayios Theodhoros, and Kakopetria) samples from all 'dykes' were analyzed. In the remaining sections about half the dykes were analyzed. We believe that this is a representative sample of the sheeted dyke zone.

All major and trace element analyses except for those of the REE were done in Geological Survey of Canada laboratories; the major elements by XRF supplemented by rapid chemical methods and trace elements by XRF energy dispersive (Rb, Sr, Nb, Y, Zr) and optical emission spectroscopy techniques (Ba, Sr, La, Yb, V, Cu, Co, Cr, Ni). The estimated probable errors in relative per cent concentration are: major elements; SiO_2: 1%, TiO_2: 1%, Al_2O_3: 1%, Fe_2O_3: 1%, FeO: 2%, MgO: 1%, CaO: 1%, Na_2O: 1%, K_2O: 1%; trace elements by XRF: 10%; and trace elements by optical emission: 15%. Electron microprobe analyses of minerals were performed by M. Bonardi using a Cameca Camebax probe equipped with four automated wavelength dispersive spectrometers standardized on natural minerals. Operating conditions were as follows: 15 KV accelerating voltage, 30 nanoamperes beam current, 5 micron beam size, and 10 seconds counting time. The estimated probable error for major elements is 1-2% of the measured value. Rare earth elements and Th, Ta, and Hf were analyzed at University of Waterloo by I.L. Gibson using instrumental neutron activation procedures (Gibson and Jagam, 1980).

FIELD RELATIONS

General

Interdyke relationships can be interpreted from the core log of CY-4 (Figure 2) and seen particularly well in the excellent exposures of the road-cut sections (Figure 3). The dykes have a strong preferred orientation, generally trending from northwesterly in the Nikitari-Kakopetria region, through northerly near CY-4, to northeasterly in the Kionia-Makheras area. Most dip at high angles but notable exceptions are the shallow-dipping dykes in Ayia Koroni section near the top of the sheeted dyke zone, and in Kakopetria near its base. In Kionia 3 a distinctly later set of low-dipping dykes transects the moderately to steeply dipping dykes which form the bulk of the section. Dips in the drill core are not reliable but are commonly at a low angle to the core, which would indicate steep dips; at the surface where the hole was collared the dip is at 75 degrees west.

The interior of the sheeted dyke zone is an intricate plexis of subparallel dykes intrusive only into one another. At the top of the dyke zone the sheeted dykes pass into pillow lavas through a transitional zone of dykes and lava screens a few 10's of metres thick. Gass (1980) reports that the abundance of dykes can change from 70% to 20% within a stratigraphic distance of 25 to 50 m. At the base of the dyke zone the transition may be more complex. Gabbro and plagiogranite of the plutonic substratum cut and are cut by dykes (Moores and Vine, 1971) and Allan (1975; noted in Gass, 1980) describes gradational relationships of dykes into gabbro. Desmet et al. (1980) describes a zone of dyke 'enrootment' at the top of the plutonic complex where the dyke population rises rapidly upward, finally displacing entirely the encasing gabbros. In CY-4 the base of the dyke zone might be placed at about 630 m depth where the proportion of gabbro screens increases abruptly to become the dominant rock type (Figure 2). Nevertheless, dykes and swarms of dykes persist in declining numbers to a depth of about 1300 m.

Dykes range in thickness from about 10 m to less than 1 cm, but commonly the full thickness of a dyke is obscured by successive intrusion of dykes by dykes, so that only partial thicknesses are locally apparent. These are distinguished in this report by inverted commas as - 'dykes'. Dyke relationships in Kionia 3, the longest and best exposed of the road-cut sections, have been analyzed in some detail. The section exposes a true sheeted dyke thickness of 163 m comprising 105 discrete intrusions. The average thickness is 1.3 m and 80% of the dykes are between 0.5 and 2 m thick. Only 6% of the dykes are greater than 4 m thick. The emplacement of dykes in the Kionia section can be shown to take place in concentrations around local spreading centres (determined by distances that a single dyke has split apart) with separations of commonly 6 to 10 m. One segmented dyke for which only one chilled margin has been identified has been split into ten parts by nine younger dykes with an aggregate thickness of at least 10 m.

Relative ages of dykes can be determined locally by their cutting or chilling relationships to one another. Within the sheeted dyke zone the younger dykes invariably have sharply chilled contacts against older dykes indicating the existence of a marked temperature difference between the dyke and walls at the time of intrusion. This contrasts with relationships observed below the dyke zone in CY-4 where the margins of many dykes show barely perceptible fining in contact with gabbroic wall rocks where the temperature difference appears to have been much less. However, even within the sheeted dyke zone the age relationships between dykes are not always clear. Commonly dykes are emplaced side by side so that chilled margins adjoin and then relative ages are indeterminate. In places, such mutual boundaries can be traced along strike to a point where the boundary of one overlaps the other and the intrusive relationship becomes clear. Although most dykes have fairly regular contacts, some are complicated by apophyses a centimetre or so thick that undulate through parts of adjoining dykes and in some cases find other dyke contacts along which to intrude. This commonly obscures contact relationships.

Chilling Relations

Following Cann (1974), Kidd and Cann (1974), and Kidd (1977) the chilling characteristics of dykes in a sheeted dyke zone should be indicative of their position relative to the spreading ridge at which they were formed. This stems from Cann's view (1974) in which ocean crust is postulated to form by repeated dyke injection within a narrow zone (in terms of dyke width) at a spreading ridge. Thus, there is a high probability that dykes will intrude and split earlier-formed dykes so that on each side of the spreading ridge a preponderance of partial dykes will have their chilled margin on the side farthest from the ridge. Hence, in ophiolites the direction of the spreading ridge from the locality observed should be on the side opposite to that having the majority of one-way chills. In Troodos a statistical tally of one-way chills by Kidd and Cann (1974) and Kidd (1977) showed a slight but persistent bias of east-side chills, which led them to conclude that the spreading ridge relative to the present orientation of the dykes was to the west.

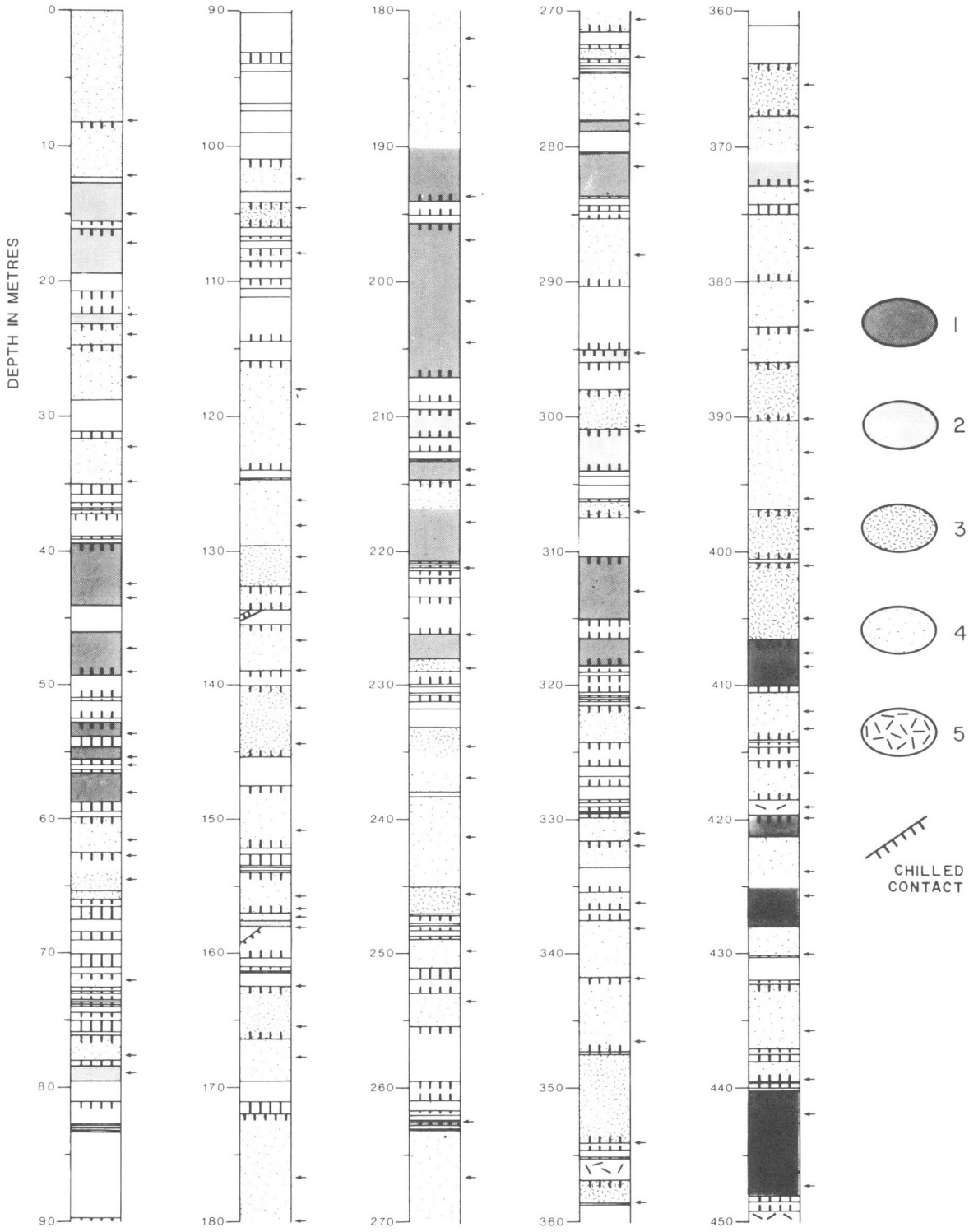

Figure 2: Drill log of CY-4 core to 900 m depth showing individual dykes patterned in accordance with compositional classification (see text). Patterns (1) to (4) represent the number of the critical depleted suite characteristics (dsc) the dyke possesses: (1) = 3 dsc, (2) = 2 dsc, (3) = 1 dsc, (4) = 0 dsc; (5) = gabbro screens of the plutonic complex. Unanalyzed dykes are unpatterned. Chilled margins are marked by hachures abutting the contact and directed inward. Locations of analyzed samples are marked by arrows.

CY-4 DRILL LOG

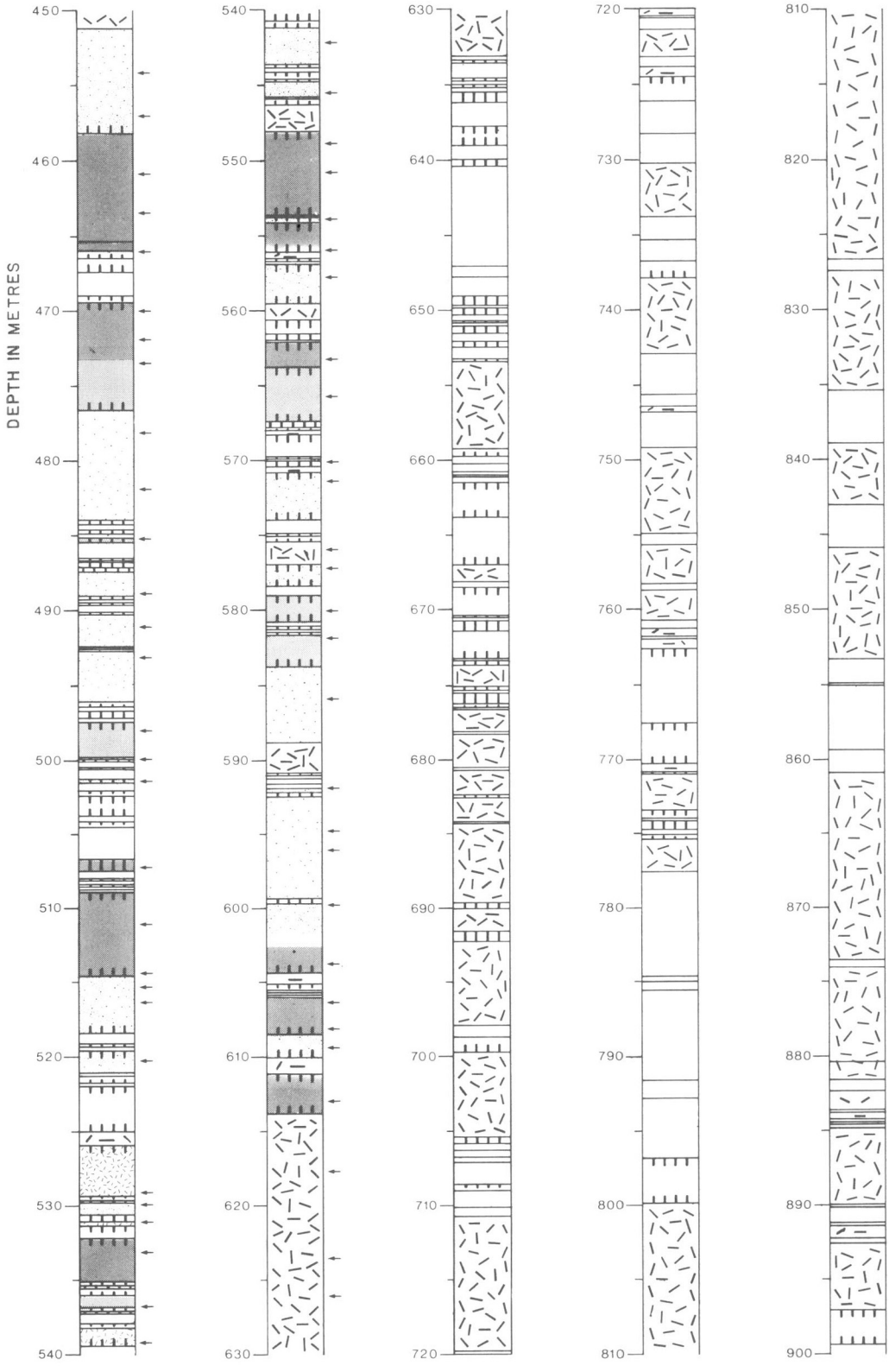

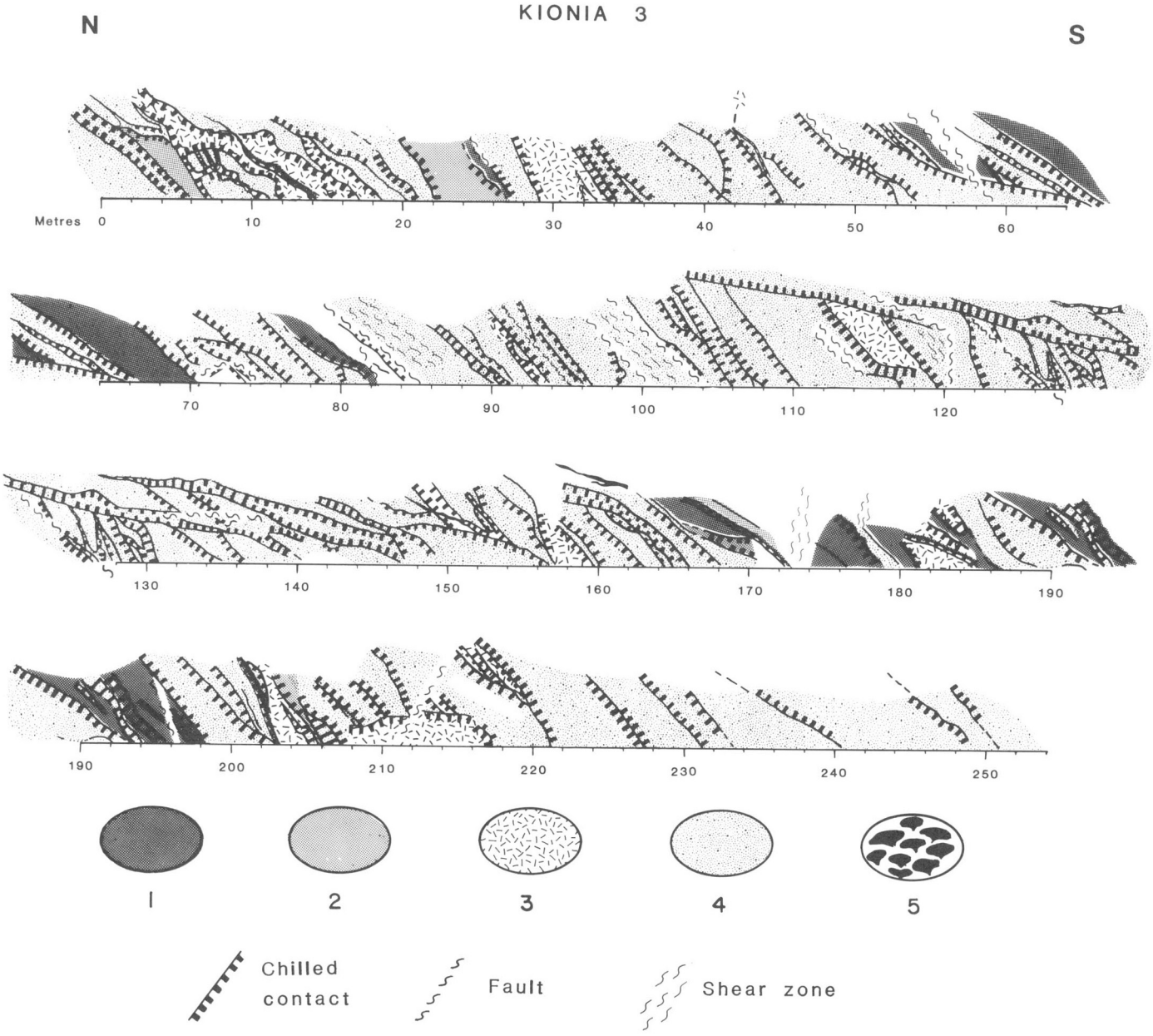

Figure 3: Mapped sections along road-cuts through the Troodos sheeted dykes. Typical strike azimuths for dykes in each section as follows: Nikitari 1 - 280°, Nikitari 2 - 330°, Ayios Theodhoros - 315°, Kakopetria - 315°, Makheras Monastery - 045°, Kionia 1 - 080°, Kionia 2 - 065°, Kionia 3 - 065°, Prophitis Elias - 040°, Ayia Korani - 330°. Patterns (1) to (4) same as for Figure 2; (5) pillow lava screens.

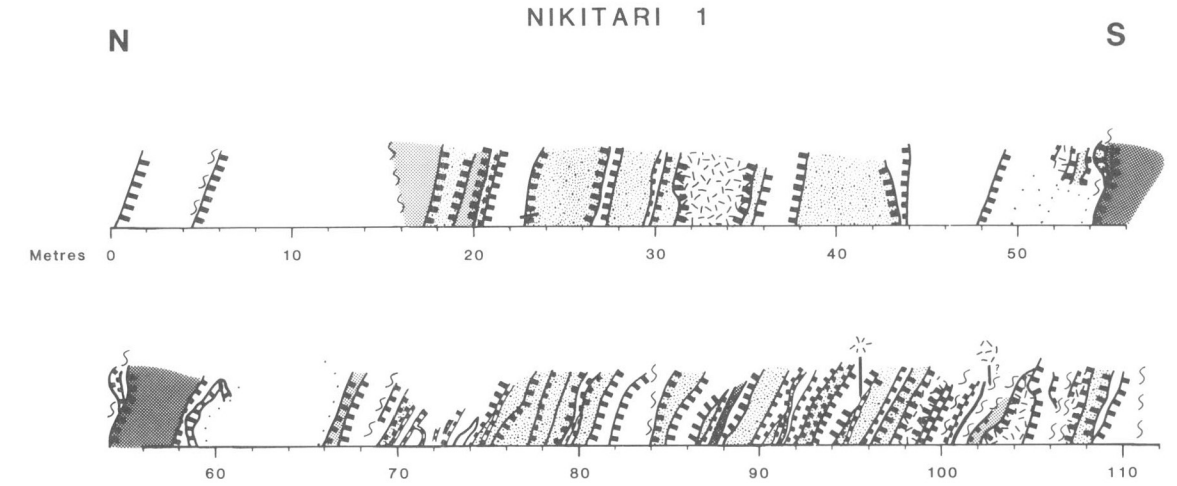
NIKITARI 1
N
S
Metres 0
10
20
30
40
50
60
70
80
90
100
110

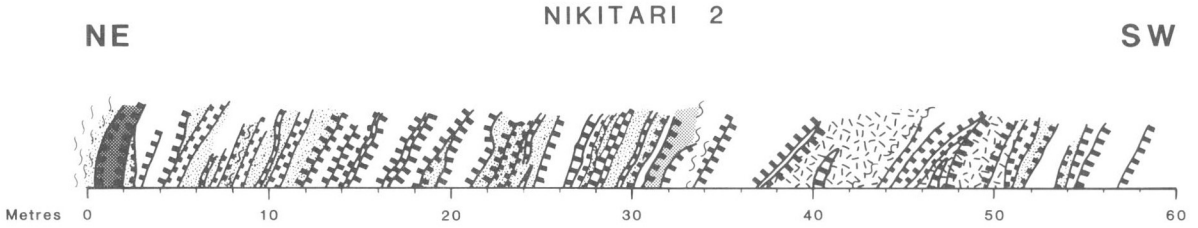
NIKITARI 2
NE
SW
Metres 0
10
20
30
40
50
60

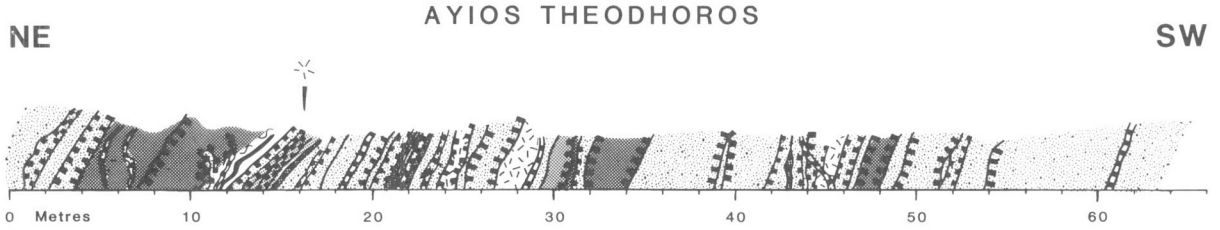
AYIOS THEODHOROS
NE
SW
0 Metres
10
20
30
40
50
60

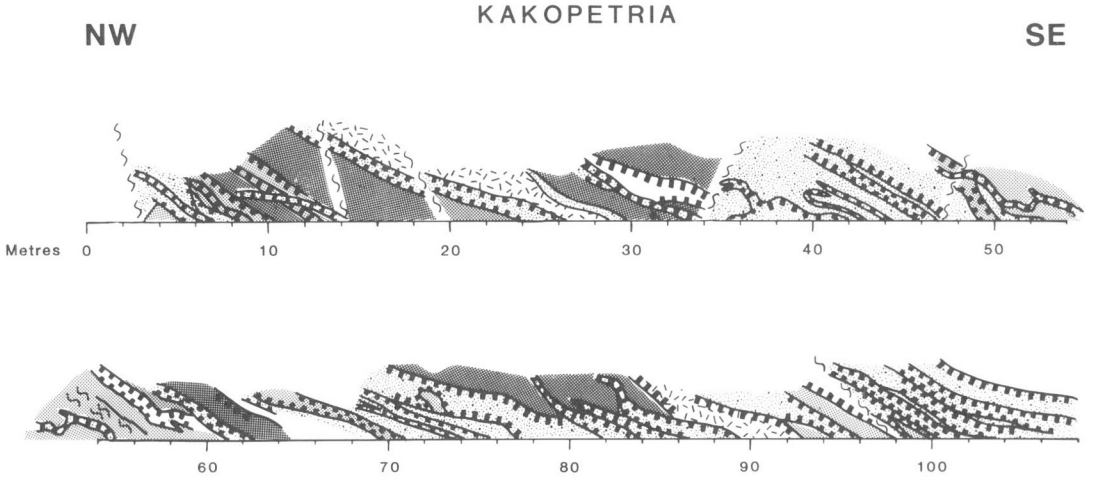
KAKOPETRIA
NW
SE
Metres 0
10
20
30
40
50
60
70
80
90
100

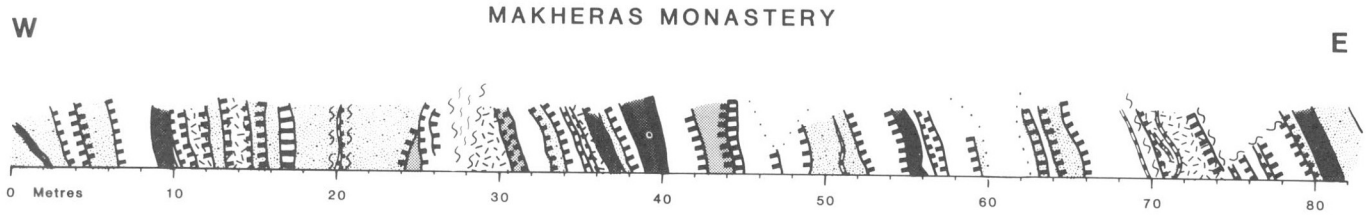
W
MAKHERAS MONASTERY
E
0 Metres
10
20
30
40
50
60
70
80

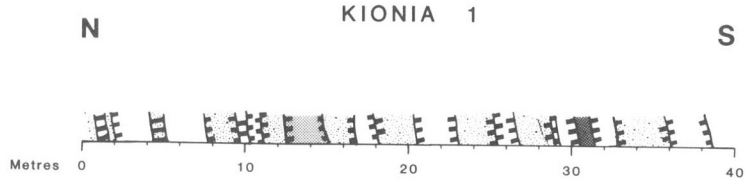
N
KIONIA 1
S
Metres 0
10
20
30
40

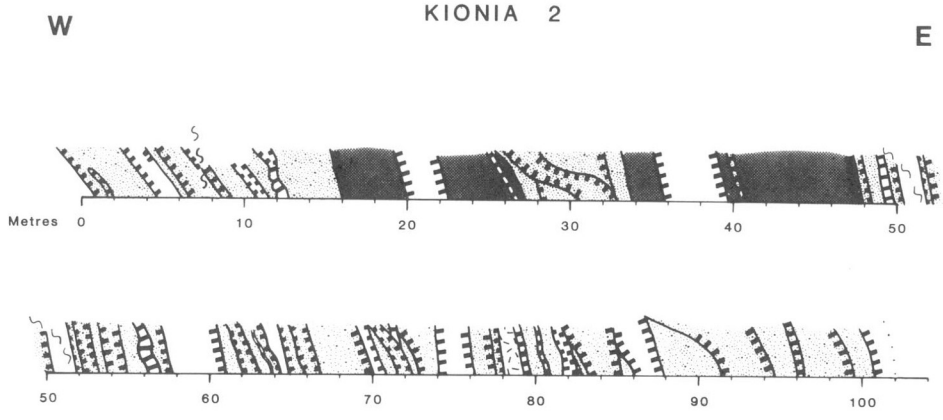
W
KIONIA 2
E
Metres 0
10
20
30
40
50
50
60
70
80
90
100

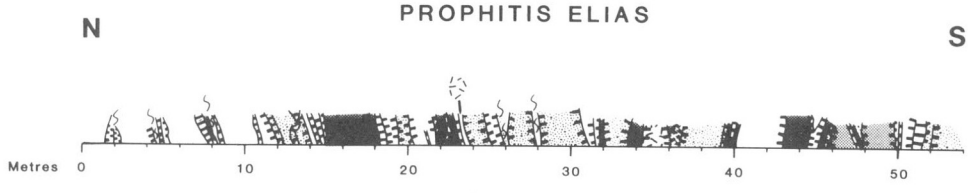
N
PROPHITIS ELIAS
S
Metres 0
10
20
30
40
50

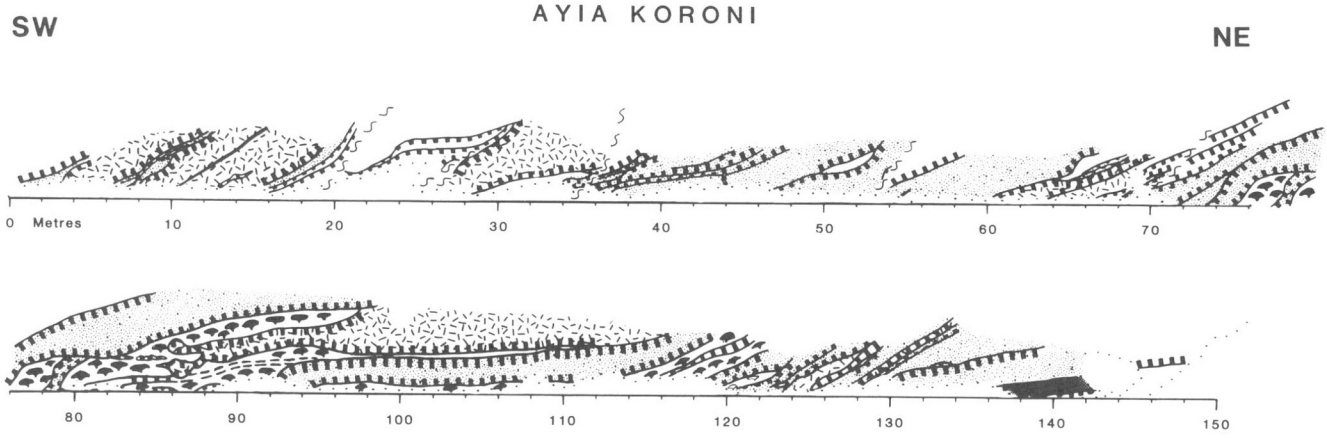
SW
AYIA KORONI
NE
0 Metres
10
20
30
40
50
60
70
80
90
100
110
120
130
140
150

Our chilling characteristics of 'dykes' in the road-cut sections and CY-4 drill core are illustrated in the histograms of Figure 4 where they are divided into four categories; west-side chilled, east-side chilled, both margins chilled, and no chills. The latter are screens of earlier dykes which actually belong to one of the other categories, but since relationships are not always clear they have been recorded separately. This does not, of course, alter the chilling statistics. The interpretation of west and east sides for each of the road-cut sections, despite the variation in strike of the dykes, follows from the observation that the trend is consistently northerly. For the CY-4 drill core we have assumed that the westerly dip of dykes at the surface persists to the base of the sheeted dyke zone, and the upper contact in each case is, therefore, the westerly contact. The results give little support to the conclusions of Kidd and Cann (ibid.). Five sections have an east-chilling bias, three, a west-chilling bias, and two, no bias and the drill intersection shows a strong west-chilling bias. Little overall bias is evident. Assuming an average dyke width of 1.5 m, calculations show that for a zone of intrusion at the spreading ridge of little more than about 10-20 m, a very large sample would be required to detect any chilling bias (Baragar et al., 1987). With the uncertainty of interpretation in at least 5% of the determinations we have no confidence that a chilling bias is detectable.

PETROGRAPHY

General

The dykes in outcrop and in drill core are mostly aphyric, or very sparsely phyric, fine-grained, grey rocks with surprisingly little variation in colour given their wide range in composition. Rarely, dykes are sparsely amygdaloidal or weakly layered parallel to their boundaries, but display few other internal structures. Their petrography is predominantly metamorphic, but some primary minerals survive and the textures generally owe more to the igneous than to the metamorphic phase of their crystallization history. A summary of the petrography is given in Figure 5 where the columns represent modal estimates of the principal constituent minerals averaged for all thin sections for which the corresponding analyses fall within the appropriate 0.5 or 0.25% MgO range. The diagram, therefore, illustrates the change in petrography across the spectrum of compositions present. It is based on 223 thin sections from CY-4 and all road-cut sections. Phenocrysts are noted below a column if present in any of the thin sections which compose the average for that range, but they rarely exceed 1 or 2% of the rock.

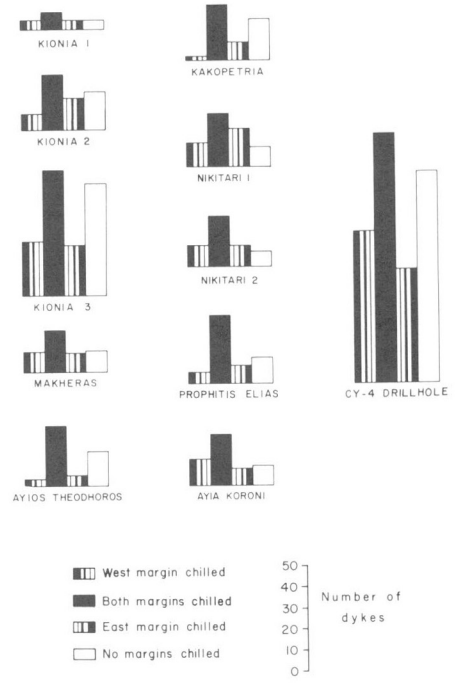

Figure 4: Histogram showing frequencies of dykes with chilling characteristics as indicated. 'No margins chilled' refers to screens which are parts of dykes belonging to one of the other categories but not identified here.

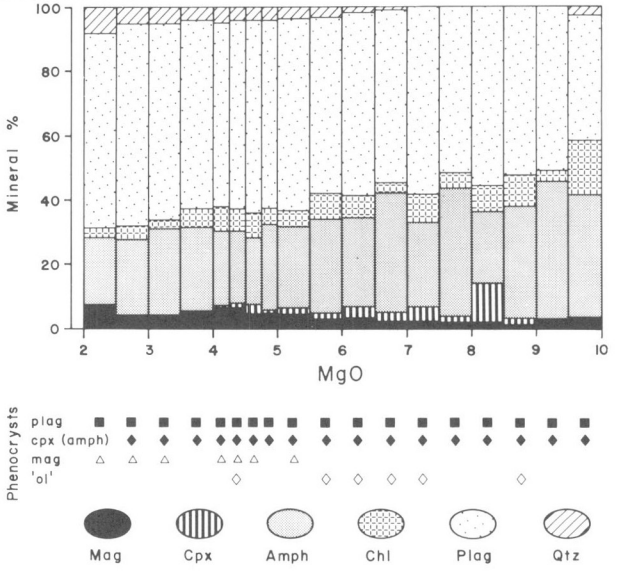

Figure 5: Summary of modal composition of dykes from sections and CY-4. Shown are the average estimated modes from samples for which the corresponding analyses fall within the appropriate 0.5 or 0.25% MgO range. Phenocryst species are indicated as present below a column if found in any of the thin sections within that MgO range. They rarely form more than 1-2% of the rock. 'Ol' represents olivine and olivine pseudomorphs.

Primary Petrography

The dyke rocks appear to have been originally composed of essentially plagioclase, clinopyroxene (± orthopyroxene), and magnetite with varying, but uncertain, quantities of olivine at the high-magnesian end and minor interstitial quartz at the low-magnesian end of the spectrum. Plagioclase dominates and persists at a fairly constant level throughout (about 60%). Magnetite is at a maximum at about 4 or 5% MgO and declines both ways, but most markedly with increasing MgO content. This mimics the variation of the total iron content with MgO in the chemical plots (Figure 7). Plagioclase and clinopyroxene appear to have been phenocrysts throughout the compositional range accompanied by olivine at the high-magnesian end and magnetite at the low-magnesian end. Olivine is represented by pseudomorphs only, and can be identified with variable certainty. Hence, the lack of recognizable olivine phenocrysts corresponding to some of the higher MgO levels in Figure 5 is probably due to lack of preservation. Most likely olivine is a liquidus phase above about 5.5% MgO and magnetite below it. As will be seen subsequently, 5.5% MgO is one of the discriminating values we have used to separate the Upper Pillow Lava type (depleted suite) with greater MgO content from Lower Pillow Lava type (non-depleted suite) with less. A petrographic distinction between the two lava suites, noted by Robinson et al. (1983), is the presence of olivine phenocrysts in the depleted, and magnetite in the non-depleted suites. In addition, chromite, which is confined to the depleted suite among the lavas, is present in some of the higher magnesian dyke samples. Thus, the petrography of the dykes tends to divide them into suites which correspond to the major divisions of the lava sequence.

A few of the dykes contain irregular xenocrysts of plagioclase and, more rarely, clinopyroxene. At least one of the dykes is highly charged with coarse (1.5-2 mm), angular fragments of plagioclase and augite crystals, obviously formed in a slowly cooled environment. Hence, it seems likely that the xenocrysts are cumulate crystals from a deeper level reservoir remobilized by the activity of dyke intrusion.

Metamorphic Petrography

The dykes are now composed predominantly of metamorphic minerals; actinolite, plagioclase, chlorite, and trace amounts of epidote. However, relict clinopyroxene is not uncommon and plagioclase in many of the dykes appears fresh (i.e., calcic and normally zoned). The grade of metamorphism probably corresponds to greenschist facies but the mineral proportions are very different than those in a normal regionally metamorphosed assemblage. Chlorite is generally a minor component (3-15%, most 5-10%) and epidote is minor to rare. Magnetite is intact (in the sense of being solid and uncorroded) or only marginally altered to sphene. Plagioclase commonly appears to be primary or is clouded by a finely divided mixture of mostly indeterminate minerals but not typically saussurized. The assemblage would be consistent with metamorphism under conditions of very low water/rock ratios (Mottl, 1983). It closely resembles the actinolite facies defined by Elthon and Stern (1978) for the Sarmiento ophiolite of Chile, and later (Elthon, 1981) for ocean crust in general.

In the Sarmiento ophiolite, Elthon and Stern define four facies which can be broadly related to the pseudostratigraphy of the complex and generally increase in intensity downward: zeolite facies (pillow lavas), greenschist facies (pillow lavas - sheeted dykes), lower actinolite facies (sheeted dykes - upper gabbros), and upper actinolite facies (upper gabbros). The petrography of the Troodos sheeted dykes corresponds mainly to Elthon and Stern's lower actinolite facies (predominantly calcic plagioclase and green fibrous actinolitic amphibole with an Al_2O_3 content of 2-5%) but has at least one of the characteristics of their upper actinolite facies in that titanomagnetite is little altered to sphene. Both paucity of epidote and lack of magnetite alteration are consistent with very limited water circulation and low water/rock ratios as we noted above.

The effect of metamorphism varies to some degree between sections. The Makheras section, for example, has the highest proportion of primary clinopyroxene and appears to be the least metamorphosed, but it is not so well-defined that this difference can be related to depth within the sheeted dyke zone. However, in CY-4 some systematic downward variations in chemistry and mineralogy can be attributed to a waning influence of water in the effectiveness of the metamorphism. These changes are illustrated in Figure 6. The alteration index is based upon the observation that the principal systematic differences in major element compositions between sheeted dykes and glasses of the pillow lavas is that the sheeted dykes show an apparent loss in CaO and gain in K_2O (Figure 7). These are thought to be changes that may be attributable to reaction between deeply penetrating sea water and wall rock. Hence, an index which utilizes the differences in CaO and K_2O contents, at equivalent MgO levels, between dyke samples and 'unaltered' samples (assumed to be the same as the lava glasses), should be a measure of the degree of alteration (details of the calculation are given in the caption to Figure 6).

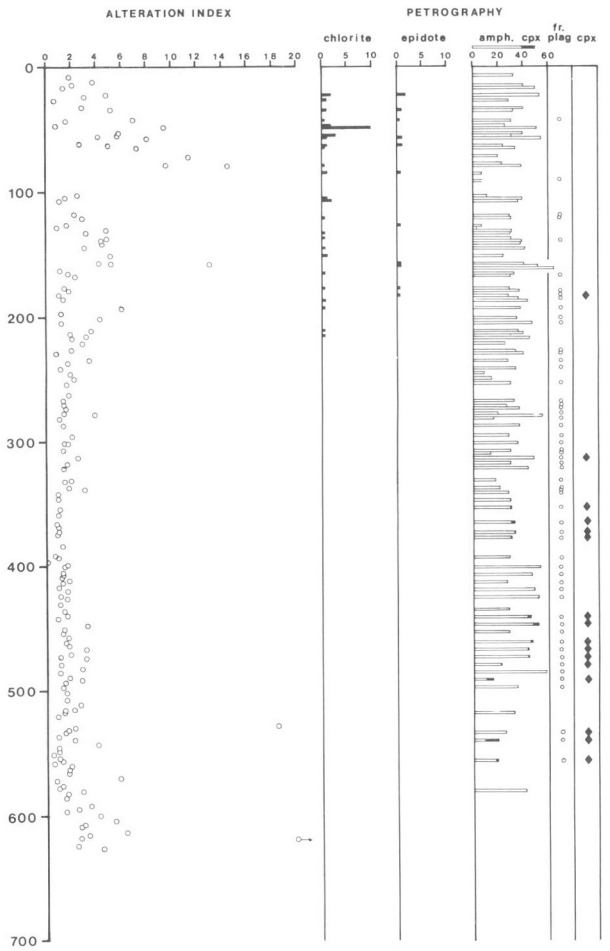

Figure 6: Downhole variation in chemical and petrographic indicators of metamorphic conditions. Vertical scale is metres depth in CY-4. Chlorite, epidote, and amphibole-clinopyroxene bar lengths correspond to modal per cent. Alteration index is based on the apparent depletion of CaO and enrichment of K_2O in the sheeted dykes compared to the lava glasses at the same differentiation (MgO) level (Figure 7). Assuming the lava glasses reflect the original composition of the dyke magmas the ratio $\Delta K_2O/\Delta CaO$ (Δ = average differences in oxide between glass and dyke) in a given MgO interval should be a measure of the degree of alteration of the dyke rock. Alteration index used = $\Delta K_2O/\Delta CaO \times 10^2$ for appropriate 0.5% MgO interval. Amph = amphibole, cpx = clinopyroxene, fr. plag = fresh plagioclase.

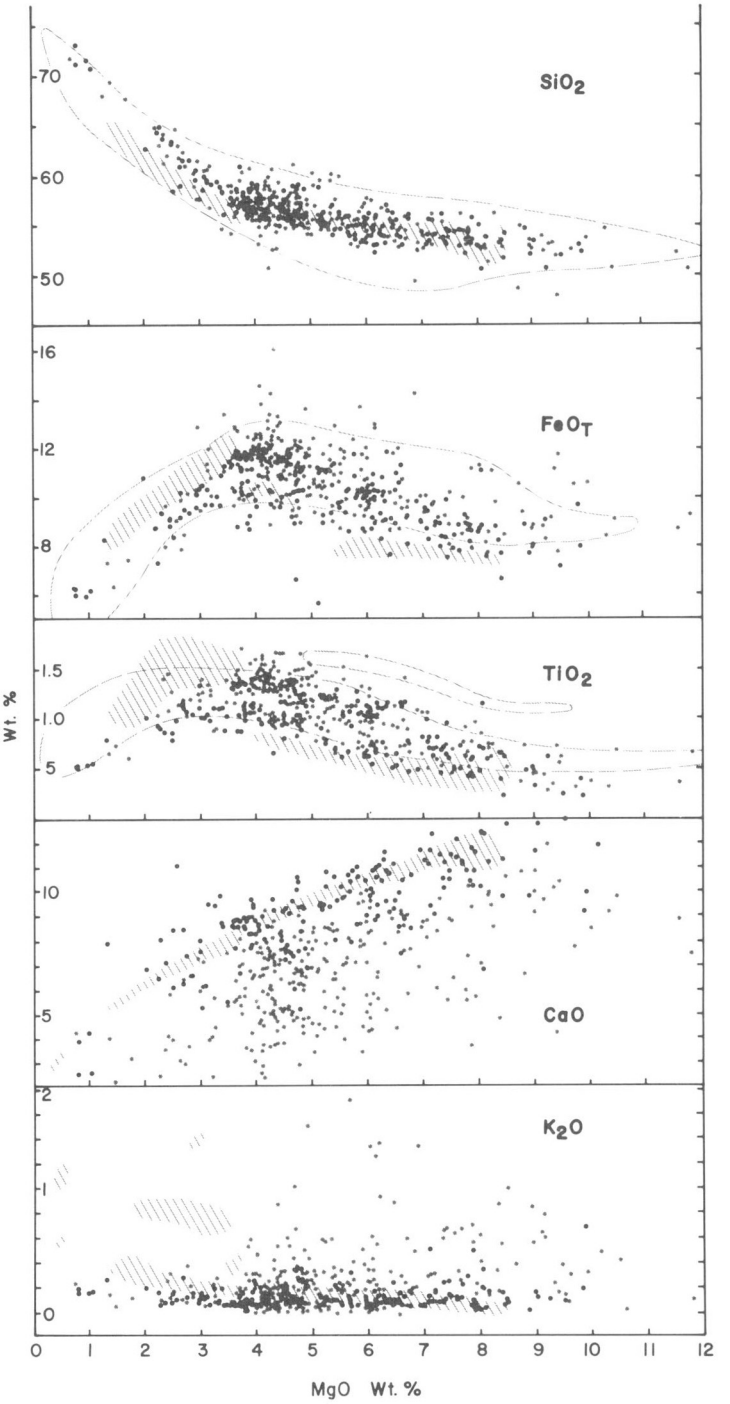

Figure 7: Variation diagrams of major elements vs. MgO. Analyses of core from CY-4 in black, from road-cut sections in grey. Cross hatching marks the field of lava glasses (Robinson et al., 1983) and dashed outlines (for SiO_2, FeO_T, and TiO_2) that of crystalline lavas (P.T. Robinson, pers. comm., 1985).

Note that the alteration index is variable but generally high in the upper part of CY-4 but declines to a consistently low average level at about 225 m which it retains to the bottom of the sheeted dyke zone at about 630 m. Within roughly the same zone of high alteration index in the upper part of the drill hole chlorite and epidote are commonly present in minor amounts but are virtually absent below it. On the other hand the incidence of fresh plagioclase and clinopyroxene increases dramatically downward. Clearly, alteration of the dykes decreases towards the base of the sheeted dyke zone. Thy et al. (1988) report that the alteration persists within the plutonic complex to about 850 m depth below the collar of CY-4. Below this depth the rocks are generally fresh. The energy source for the metamorphism was undoubtedly the magma chamber that produced the plutonic complex but, as previously argued (Baragar et al., 1987), the burden of energy transfer to higher levels was probably borne by the dykes themselves. Above the sheeted dyke zone, metamorphic effects attributable to the heat source below diminish abruptly, as the proportion of dykes drops within the lava sequence (Gillis, 1983; Gillis and Robinson, 1985). Thus, metamorphism is largely confined to the sheeted dyke zone and could be largely self-induced. The water required is probably marine, which attained limited access to the dyke zone through the intrusion of dykes into the water-laden pillow lava sequence and locally through fault and fissure zones (Baragar et al., 1987).

CHEMISTRY

General

The petrochemistry of the pillow lava sequence which has been extensively studied in a stratigraphic context (e.g. Gass and Smewing, 1973; Smewing et al., 1975; Robinson et al., 1983; Schmincke et al., 1983; Malpas and Langdon, 1984; Thy et al., 1985) is the obvious standard to which the sheeted dykes should be related. The lavas have been divided traditionally into Upper and Lower Pillow units primarily on the basis of field and petrographic criteria. Robinson et al. (1983) and Schmincke et al. (1983), on the basis of petrographic and chemical data from glass and whole rock samples, redefined the boundaries of the two divisions but reaffirmed their stratigraphic relationships. The upper division was classed as basalt and basaltic andesite with boninitic affinities and the lower division as andesite-dacite-rhyolite of an evolved arc tholeiite type. We have designated them as the depleted and non-depleted suites respectively (Baragar et al., 1987), in recognition of the generally lower level of incompatible elements in the basalt-basaltic andesite than in the andesite-dacite-rhyolite suites, although for the latter 'non-depleted' is not strictly true in all respects. To subdivide the dykes into chemically equivalent suites we have chosen three chemical parameters which appear to be the most significant discriminators of the upper or depleted suite. The choice is based on chemical data from the lava glasses of Robinson et al. (1983) and from the systematic sampling of CY-1 drill core which transects the uppermost 475 m of the lava sequence and is probably the most representative collection available of the depleted suite. The discriminators are: MgO $>5.5\%$, TiO_2 $<0.85\%$, and Cr >40ppm (Baragar et al., 1987). Other elements are generally consistent with the division effected by these elements; incompatible elements are poorer and compatible elements richer in the depleted than in the non-depleted suites. Transitional analyses with mixed criteria may represent truly transitional compositions or analytical error in one or two of the critical elements. In classifying analyses, therefore, either the presence of both two and three of the criteria are assumed to mark the depleted suite or the level of confidence of the division is given by noting the number of the criteria present; 0, 1, 2, 3.

The Upper Pillow Lavas or depleted suite was itself divided (Cameron, 1985; McCulloch and Cameron, 1983) on the basis of distinctive chemical and isotopic characteristics into three discrete groups designated I, II, and III. These represent magmas that were successively depleted in both high- and low-field strength incompatible elements. Group III rocks are a close approach to boninites in composition and are typically present in the Arakapas fault zone. The depleted suite of this study spans the compositional range of Cameron's Groups I and II.

Chemical Variation

The chemical characteristics of the sheeted dykes are summarized in the variation diagrams of Figure 7 (major elements), Figure 8 (trace elements), and Figure 9 (REE) and the analyses are recorded in Tables 1 and 2 (see Appendix). Plots of analyses from CY-4 are in black and from the road-cut sections in grey. Also shown in Figure 7 are the fields of glass analyses (cross hatched; from Robinson et al., 1983) and of crystalline whole rock analyses (dashed outlines; from P.T. Robinson, pers. comm., 1985) from the pillow lava sequence.

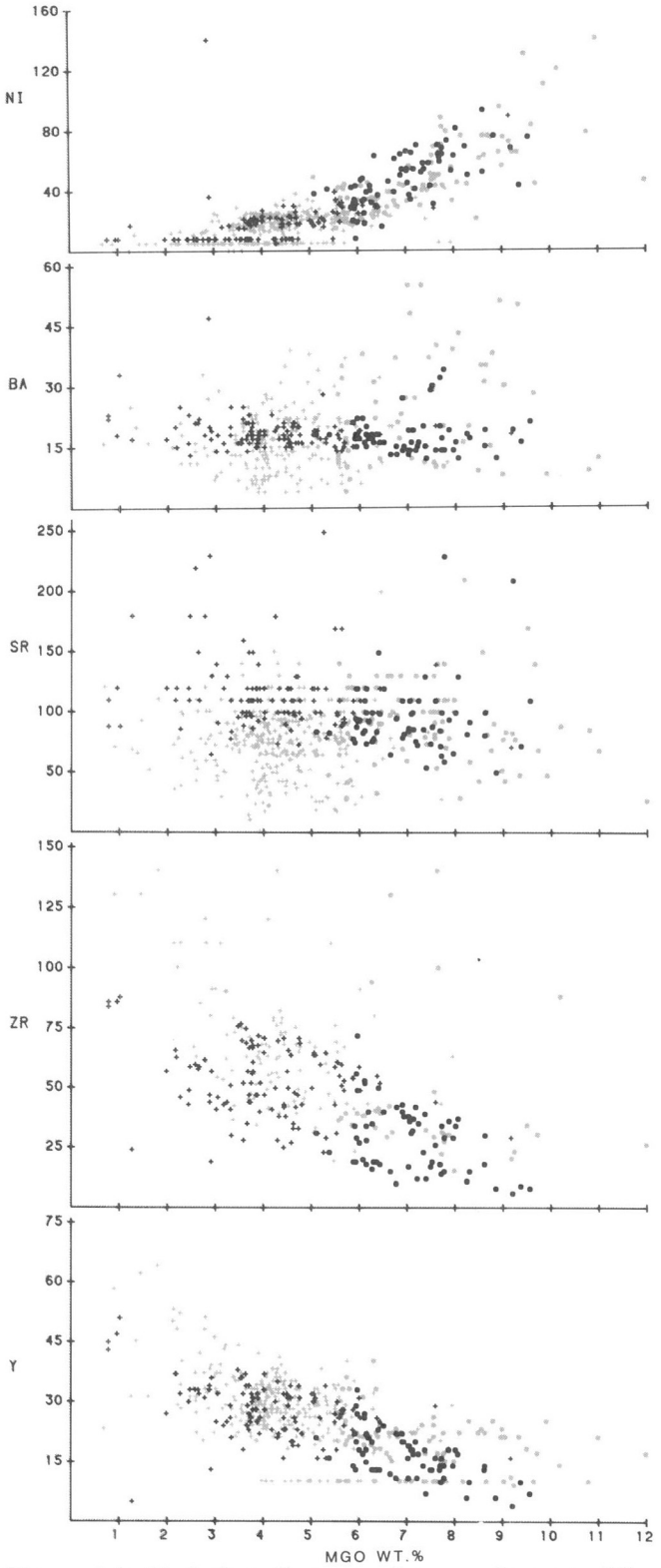

Figure 8A: Variation diagram of trace elements, Ni, Ba, Sr, Zr, Y vs. MgO. CY-4 analyses: black; road-cut sections: grey; circles: depleted suite; crosses: non depleted suites.

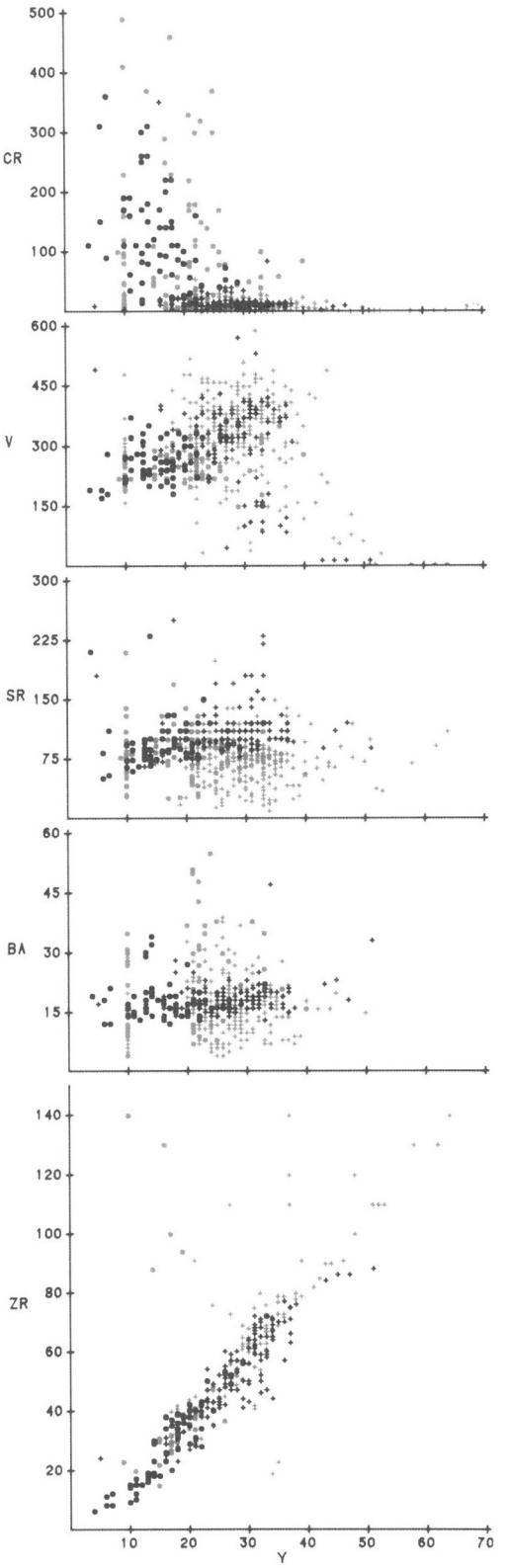

Figure 8B: Variation diagram of trace elements Cr, V, Sr, Ba, Zr vs. Y. For explanations see Figure 8A.

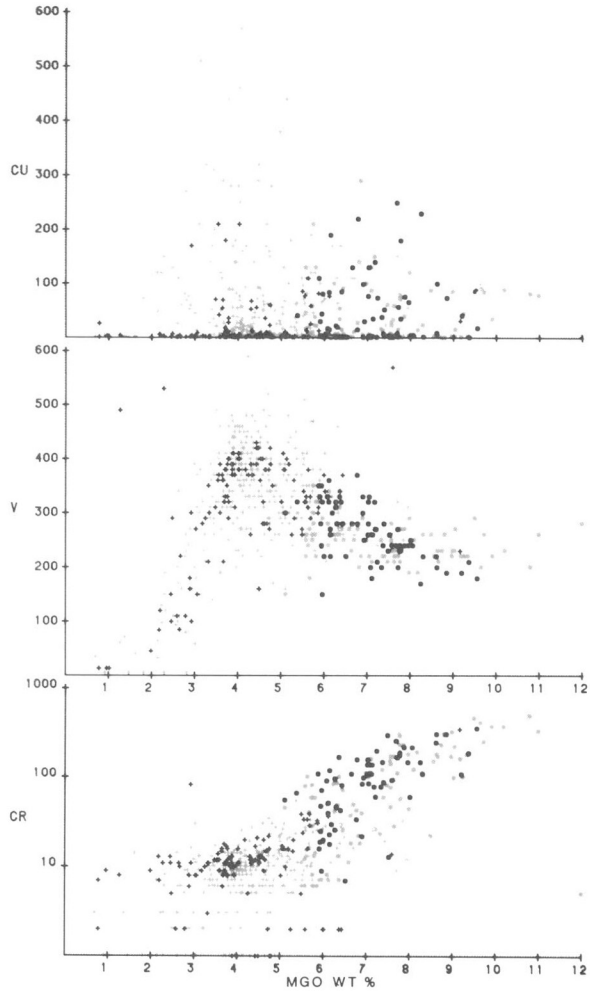

Figure 8C: Variation diagrams of trace elements Cu, V, Cr vs. MgO. For explanations see Figure 8A.

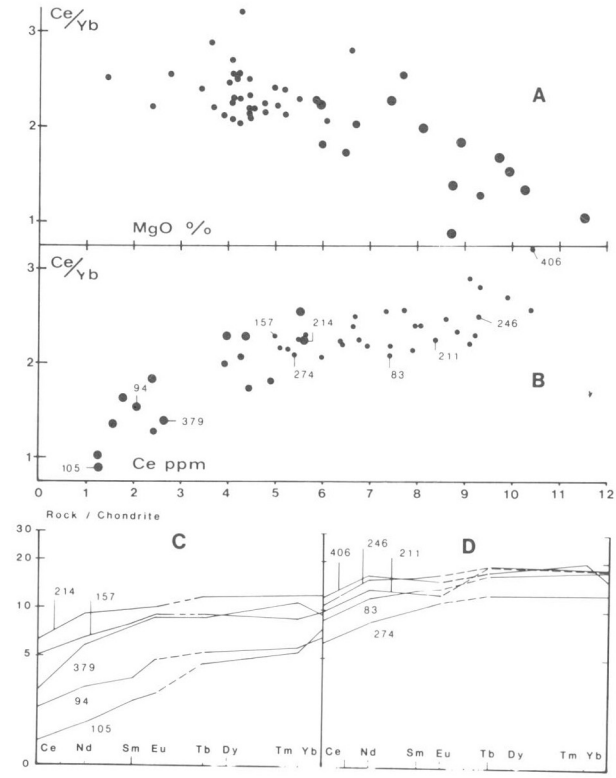

Figure 9: (A) Variation diagram: Ce/Yb vs. MgO Largest circles mark analyses with three depleted suite characteristics (dsc), middle-size circles, with two dsc, and small circles with one and zero dsc. Numbers refer to sample numbers which are all prefaced with BL-82 (see tables). (B) Variation diagram: Ce/Yb vs. Ce (C) Chondrite-normalized rare earth element patterns for depleted-suite samples. (D) Chondrite-normalized rare earth element patterns for non-depleted suite samples.

The major element variations (Figure 7) illustrate some principal characteristics of the chemistry of the sheeted dykes. The range and general distribution of dyke compositions are similar to that of the lavas as might be expected from their assumed co-magmatic relationship. However, the continuity of compositions of the lava glasses, particularly for TiO_2 and FeO, is disrupted between about 4% and 5.5% MgO, whereas no equivalent break is observed in the distribution of dyke compositions. In the lavas the discontinuity marks the division between upper (depleted) and lower (non-depleted) suites. Since the gap cannot be bridged by normal fractionation processes, Robinson et al. (1983) concluded that the two suites are genetically independent. The fact that both sheeted dykes and crystalline lavas (dashed outline in Figure 7) show similar scatter and distribution of analyses, might suggest that the break is simply obscured in the case of the whole rock analyses by limited remobilization of elements during alteration. This is not borne out, however, by some of the more immobile trace elements. Zr-Y (Figure 8B) and Ce/Yb-Ce (Figure 9) variation plots, for example, show a continuous and fairly even distribution of analyses throughout the compositional range. For descriptive purposes at least, we will assume that the chemistry of the sheeted dykes forms a simple evolutionary sequence. Its principal characteristic, apart from an exponential rise in silica, is its moderate iron-enrichment trend which peaks for both FeO_T and TiO_2 at about 4% MgO.

Secondary mobilization of elements is distinctly evident in the distributions of CaO and K_2O as previously noted. The analyses of both oxides tend to concentrate along the narrow fields of the lava glass analyses and from there to spread to lower and higher values respectively. Obviously relative to the lava glasses and presumably to the original compositions of the dykes, CaO has been lost and K_2O gained. This is not entirely the result to be expected from reaction of

heated sea water and basalt. Although CaO is normally lost, according to Mottl (1983), MgO is invariably gained in almost direct proportion and K_2O is more commonly leached than gained. For the sheeted dykes the covariance of MgO and such normally immobile elements as Zr, Y, (Figure 8A and B) or Ce/Yb (Figure 9) indicates that in these rocks MgO is probably little mobile. The environment of the sheeted dykes is not the same as that studied by Mottl (1983). Minor quantities of sea water which reach the depths of the sheeted dykes may well be impoverished in MgO while still unsaturated in CaO, and as part of the reaction leading to the actinolite facies, exchanges potash for lime. It is interesting that the CY-4 analyses (Figure 7) show much less alteration of K_2O and CaO than do those from the road-cut sections, most of which are probably at higher levels within the sheeted dyke zone. This would support the previously discussed evidence of the declining influence of water downward in CY-4 drill hole. The variations of SiO_2, FeO_T and TiO_2 analyses, although more scattered than those of the lava glasses, do have reasonably good coherence and distinct trends, thus, are probably reliable measures of primary compositions.

Trace element variations against MgO and Y, as measures of differentiation, are plotted in the diagrams of Figure 8A to C. Separate symbols are used for samples classed as depleted and non-depleted types. As in the case of the major elements the distributions of trace elements of CY-4 are generally more coherent and define better trends than those of the road-cut sections. This can also be attributed to a lesser degree of alteration in the CY-4 samples. For the Y-based plots it may also be partly due to a slightly less sensitive analytical method that was used for some road-cut samples. In any event, the CY-4 analyses are to be preferred for interpretation.

Both Zr and Y show a distinct negative correlation with MgO and marked covariance with one another. No distinction in trends and no discontinuity is evident between the two suites. Ba and Sr also increase with differentiation but to a much lesser degree and show little tendency for a precipitous rise at the felsic end of the compositional spectrum. The trends are consistent with the petrography in which plagioclase is observed to remain at a nearly constant level throughout the series and no K-feldspar is recognized, even at the high silica end. As expected, Cr and Ni decline sharply with increasing differentiation. The rapid early decline in Cr may be related more to the extraction of chromite than of pyroxene. The decline in both elements levels off near the transition from depleted to non-depleted types where, presumably, olivine and chromite cease crystallizing. The V content rises gradually to a maximum at about 4-5% MgO (30 ppm Y) then declines abruptly towards the felsic end of the plot in conformity with the variation in iron.

REE behavior in the sheeted dykes is shown in the various plots of Figure 9. Samples assigned to depleted and non-depleted suites are designated separately and their respective REE patterns shown in different plots. The principal points of interest are: 1) samples across the entire range of compositions are LREE depleted; 2) the degree of LREE depletion is negatively correlated with the Ce/Yb ratio and declines steadily with the measure of increasing differentiation (Ce and 1/MgO); 3) the overall abundance of REE increases steadily with differentiation; and 4) there is no marked Eu anomaly. The general similarity of REE patterns throughout the compositional range and their gradual systematic change with degree of differentiation (as measured by MgO and Y) suggests a common origin for all the dyke magmas. This presents difficulties which will be discussed later, but there is little reason to believe that the depleted and non-depleted suites are of independent origin.

The REE patterns reported by McCulloch and Cameron (1983) and Cameron (1985) for Groups I and II of the Troodos lavas closely match some of the intermediate members of the depleted suite (e.g. 94 and 379, Figure 9) among the dyke rocks. The most depleted of the dykes (e.g. 105), however, shows no evidence of the 'U' pattern which records a superimposed LREE enrichment and is characteristic of Cameron's Group III lavas. This is attributed, by Cameron (1985), to a late enrichment of the source region in incompatible elements. Thus, as noted previously, Group III magmas do not seem to be represented among the dykes of our sample.

Compositions of Mineral Phases

A few of the primary minerals found in dykes from the road-cut sections were analyzed by electron microprobe. The results are given in Table 3 (see Appendix) and plotted in the various diagrams of Figure 10. The latter are the same diagrams as used by Thy et al. (1988) for mineral analyses of the plutonic rocks in CY-4. These workers found that compositions of mineral phases analyzed systematically through the plutonic complex and in dykes intrusive into its upper part were suggestive of a three-fold division of these rocks into: lower cumulates (below 1330 m in CY-4), upper gabbros (1330-640 m), and dykes (intrusive into the upper gabbros). The lower cumulates comprise ultramafic rocks (mainly websterites) below 1750 m and coarse-grained gabbroic cumulates above. The upper gabbros are medium to fine-grained, contain patches of trondhjemite, and are host to the dykes which are presumed to be extensions from the sheeted dyke zone above. Mineral compositions from each of these divisions group into distinctive but overlapping fields.

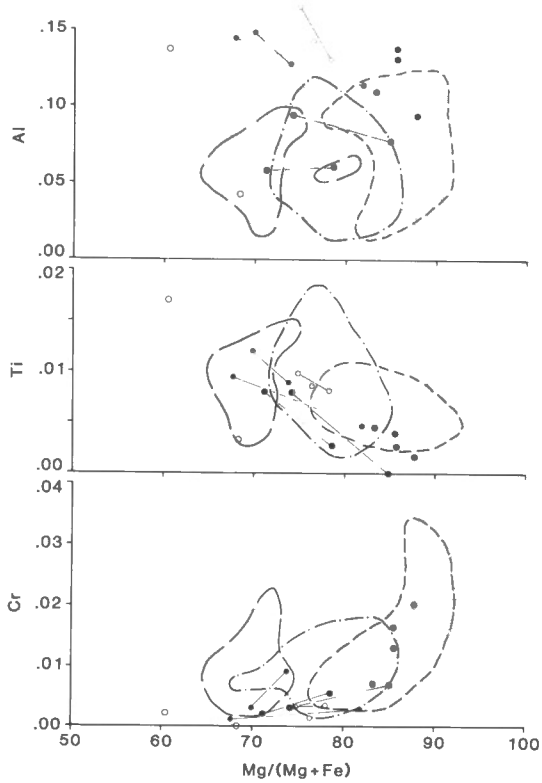

Figure 10A: Minor element variation vs. Mg/(Mg + Fe) for clinopyroxene analyses of selected dyke samples from the road-cuts. Shown for comparison are the fields of clinopyroxene analyses from the plutonic complex (after Thy et al., 1988): lower cumulates (short dashes), upper gabbros (dash-dot), dykes intrusive into the upper gabbros (long dashes). Large filled circles: three dsc; small filled circles: two dsc; small open circle: one dsc; large open circle: zero dsc. Tie lines join phenocrysts (rare xenocrysts) and groundmass pyroxenes of the same sample. Minor elements are in mole fractions based on clinopyroxene formula of six oxygens.

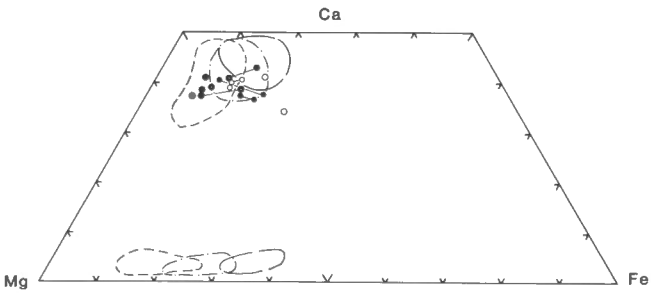

Figure 10B: Clinopyroxene analyses from the sheeted dykes shown in the pyroxene quadralateral with the fields of analyses from the plutonic complex. Symbols the same as in Figure 10A.

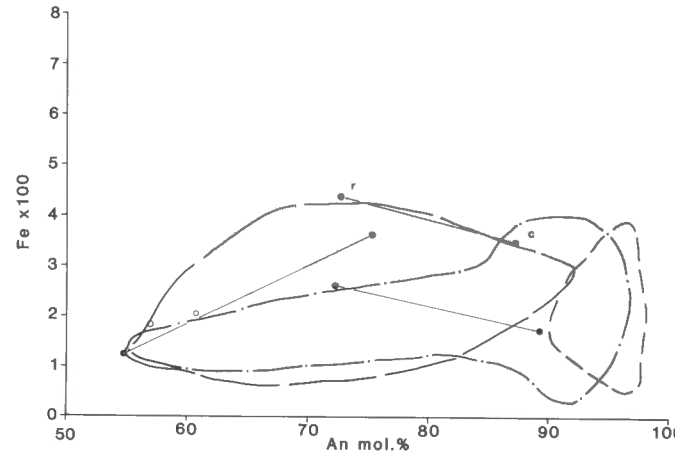

Figure 10C: Iron vs. Anorthite content in analyses of plagioclase from selected samples of the sheeted dykes. The fields of plagioclase analyses from the plutonic complex (Thy et al., 1988) are shown for comparison. Symbols the same as in Figure 10A. Iron is total iron in mole fractions based on plagioclase formula of eight oxygens.

Thy et al. (1988) interpret the lower cumulate body as being intrusive into the upper gabbros and distinctly later. Further, the lower cumulates on one hand, and the upper gabbros and associated dykes on the other, are considered to be discrete magmatic systems related to the Upper Pillow Lavas (depleted suite) and Lower Pillow Lavas (non-depleted suite) respectively.

In Figures 10A and B our analyses of clinopyroxenes from dykes of the sheeted dyke zone are compared with the fields of clinopyroxene analyses of Thy et al. (1988) from the plutonic complex. Clearly, our analyses, although few in number, embrace all three fields. Those representing depleted samples generally coincide with the lower cumulate field of Thy et al. (1988) and those from non-depleted samples, with the upper gabbro or dyke fields. We have few plagioclase analyses (Figure 10C) and they cover only the fields of upper gabbros and dykes. However, the sample is too small to be representative and the absence of analyses in the lower cumulate field is hardly significant.

The mineral analyses, as few as they are, are consistent with the chemical data in supporting the view that the major part of the range of Troodos magmas is represented in the sheeted dyke zone. It remains to be determined if the two parts of the compositional spectrum, the depleted and non-depleted suites, which seem to be better defined in the lava sequence (Upper and Lower Pillow Lavas) and in the plutonic complex (lower cumulates - upper gabbros), can be separated in the sheeted dykes into distinctive age groups.

FIELD RELATIONSHIPS BETWEEN DEPLETED AND NON-DEPLETED SUITE DYKES

In Figures 2 and 3, showing the road-cut sections and CY-4 drill core log respectively, the analyzed dykes are patterned in conformity with the level of their depleted suite characteristics. Combining dykes with both two and three of the depleted suite characteristics as depleted suite dykes, 23% of analyzed dykes in the road-cut sections and 37% in CY-4 belong to the depleted suite. Although widely distributed (all road-cut sections have at least one), they have a tendency to concentrate in swarms. Note, for example, the concentration of depleted suite dykes in the western part of Kionia 2 section or between 190 and 230 m depth in CY-4 drill log.

Paradoxically, in view of the generally higher stratigraphic position of the depleted suite in the lava sequence, depleted suite dykes are not consistently younger than non-depleted suite dykes, as casual inspection of Figures 2 and 3 will show. In fact, very commonly, as can be seen in the Kakopetria and Kionia sections, they are screens. Local anomalies in such relationships could be explained by assuming some overlap in the times of emplacement of the two suites as, in fact, can be observed in the interfingering of depleted and non-depleted suite flows at their transition in the lava sequence (Initial Report, CY-1a, in prep.). However, their contemporaneity at the level of the sheeted dykes appears to be more general than would be suggested by the volcanic stratigraphy. To examine the relationships quantitatively we have divided the dykes into relative age categories on the basis of their chilling characteristics. At each locality the youngest dykes are those with both margins chilled; older dykes have one margin chilled, and the oldest are screens. If the depleted-suite dykes were consistently, or even mainly, younger one would expect them to have a preponderance of two-sided chilling. The histograms of Figure 11 show the distribution of chilling characteristics for dykes of three, and two and three combined, depleted-suite criteria, respectively, compared with those for the dyke population as a whole. The road-cut sections and CY-4 are represented separately. Although in the road-cut sections the depleted suite dykes do have a majority of doubly-chilled margins, it is not more so than the dyke population as a whole, and in CY-4 the double-chilling of depleted suite dykes is distinctly less than that of the other categories. Hence, the age relationship between depleted and non-depleted suites which seems evident in the lavas and possibly the plutonic rocks can not be recognized in the sheeted dykes. In fact, we conclude that the full range of compositions was available during dyke emplacement.

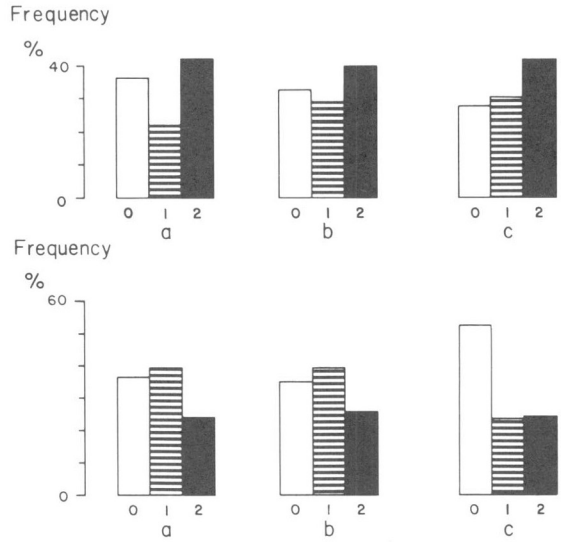

Figure 11: Distribution of chilling characteristics (zero, one, and two chilled margins) among dykes with: (a) three dsc, (b) three and two dsc, and (c) all dykes in the population. Upper histograms are for dykes in road-cut sections; lower histograms for those in CY-4 drill hole.

DISCUSSION

One of the most striking features of the chemistry of the sheeted dykes is the evident continuity of the compositional trends. Division into suites based on the two-part division of the pillow lava sequence yields no chemically discrete fields in compositional space but only arbitrary divisions of what appears to be continuous variation spectrums. An obvious interpretation is that the entire magma series represented by the sheeted dykes is interrelated by a common set of processes from the same or similar primary magmas. We have previously shown (Baragar et al., 1987) that much of the compositional variation in the sheeted dykes can be explained by closed-system fractional crystallization but that changes in TiO_2 and the REE contents, at least, can not be accommodated by the same mechanism. Accordingly, it is necessary to also consider the derivation of the magma from multiple sources of varied primary compositions, and possibly, open-system fractionation. The lack of a preferred order of emplacement between depleted and non-depleted suite dykes supports the view that magma was delivered from more than one contemporary source. These various points can be integrated in a model which envisages the presence of multiple magma chambers distributed along a spreading ridge and fed from mantle sources of slightly different composition. Fractionation proceeds independently in each of the magma chambers; by closed or almost closed-system

fractionation in some, by open-system fractionation in others. Obviously, from such a system, magmas at any stage of fractionation could coexist. Dykes fed from the individual magma chambers would both rise to the surface to produce flows and would spread longitudinally in the plane of least principal stress, parallel to the spreading axis (Baragar et al., 1987). Thus, at depth, dykes from the different intrusive centres would interleave to form a zone of continuous dyking which, in any one section, would comprise a mosaic of compositions.

CONCLUSIONS

The principle conclusions resulting from our work on the Troodos sheeted dykes are as follows:

1. No one-way chilling bias could be determined with confidence in the sheeted dykes. This probably means that the zone of intrusion at the spreading axis exceeded approximately 50-100 m.
2. The dykes are metamorphosed to the actinolite facies (Elthon and Stern, 1978; Elthon, 1981), indicative of conditions of low water/rock ratios. The effect of water declines downward in the dyke zone, as evident by increasing proportions of primary minerals, and disappears about 200 m below the base of the sheeted dyke zone.
3. The compositional range and trends of the sheeted dykes generally match those of the pillow lava sequence, but lack the discontinuity between Upper and Lower Pillow Lava types (depleted and non-depleted, respectively) that is evident in analyses of the lava glasses. Continuity over the range of compositions in the dykes is common to both major and trace elements and is believed to be primary.
4. Most of the compositional variation can be attributed to fractionation in high-level, closed-system magma chambers. Variation in TiO_2 and REE is probably also controlled by some initial differences in magma sources.
5. Clinopyroxene compositions of the sheeted dykes span much of the range of clinopyroxene compositions found by Thy et al. (1988) to be present in the plutonic complex transected by CY-4. Thus the entire compositional spectrum of the ophiolite is probably represented within the sheeted dykes.
6. When the dykes are divided into depleted and non-depleted suites, on the basis of chemical criteria characteristic of Upper and Lower Pillow Lava types, they show no preferred age relationship to one another, unlike their surface counterparts. This indicates that both ends of the compositional spectrum co-existed and suggests the presence of more than one source.
7. Individual dykes in any given cross-section are postulated as originating at discrete, fractionating centres distributed along a spreading zone and interleaved by longitudinal intrusion from their various sources. Thus, contemporaneous magmas at different fractionation stages may be juxtaposed at a common site some distance from their sources.

ACKNOWLEDGEMENTS

We are indebted to the International Crustal Research Drilling Group and particularly its Cyprus Project Director, P.T. Robinson, and Chairman, J.M. Hall for the organizational framework under which this study was carried out. Its presence greatly reduced our own logistic burdens and it placed us in the stimulating company of researchers of like interests. We would also like to acknowledge our debt to members of the Cyprus Geological Survey Department who were a constant source of information on the geology and geography of Troodos. Special thanks are owed to Dr. C. Milligan and Mr. C. Kalotaris for generously providing us with their map and samples of the Prophitis Elias section. Richard Ernst kindly read a draft of the manuscript and offered useful suggestions for its improvement. Finally, we are indebted to the anonymous reviewers of this paper, obtained by the editors of the volume, for a number of very useful suggestions.

REFERENCES

Allen, C.R.
1975: The petrology of a portion of the Troodos plutonic complex, Cyprus; unpublished Ph.D. thesis, Cambridge University, England, p. 1-161.

Baragar, W.R.A., Lambert, M.B., Baglow, N. and Gibson, I.L.
1987: Sheeted dykes of the Troodos ophiolite, Cyprus; *in* Mafic Dyke Swarms, ed. H.C. Halls and W.F. Fahrig; Geological Association of Canada, Special Paper, no. 34, p. 257-272.

Cameron, W.E.
1985: Petrology and origin of primitive lavas from the Troodos ophiolite, Cyprus; Contributions to Mineralogy and Petrology, v. 89, p. 239-255.

Cann, J.R.
1974: A model for ocean crustal structure developed; Geophysical Journal of the Royal Astronomical Society, v. 39, p. 169-187.

Desmet, A., Gagny, C., Lapierre, H. and Rocci, G.
1980: Organisation spatio-temporelle du complexe

filonien du Troodos: son enracinement dans la chambre magmatique; *in* Ophiolites, Proceedings of the International Ophiolite Symposium, Cyprus, 1979, ed. A. Panayiotou; Cyprus Geological Survey Department, Ministry of Agriculture and Natural Resources, p. 66-72.

Elthon, D.
1981: Metamorphism in oceanic spreading centers; *in* The Sea; Ideas and Observations on Progress in the Study of the Seas, Volume 7, The Oceanic Lithosphere, ed. C. Emiliani; John Wiley and Sons, New York, p. 285-303.

Elthon, D. and Stern, C.
1978: Metamorphic petrology of the Sarmiento ophiolite complex, Chile; Geology, v. 6, p. 464-468.

Gass, I.G.
1980: The Troodos Massif: its role in the unravelling of the ophiolite problem and its significance in the understanding of constructive margin processes; *in* Ophiolites: Proceedings of the International Ophiolite Symposium, Cyprus, 1979, ed. A. Panayiotou, Cyprus Geological Survey Department, Ministry of Agriculture and Natural Resources, p. 23-35.

Gass, I.G. and Smewing, J.D.
1973: Intrusion, extrusion and metamorphism at constructive margins: evidence from the Troodos Massif, Cyprus; Nature, v. 242, p. 26-29.

Gibson, I.L. and Jagam, P.
1980: Instrumental neutron activation analysis of rocks and minerals; *in* Short Course in Neutron Activation Analysis in the Geosciences, Halifax, May 1980, ed. G.K. Muecke; Mineralogical Association of Canada, Short Course Handbook, v. 5.

Gillis, K.M.
1983: Low temperature alteration of the extrusive sequence, Troodos ophiolite, Cyprus; Geological Association of Canada - Mineralogical Association of Canada, Annual Meeting, Victoria, Canada, 1983, Program with Abstracts, v. 8, p. A27.

Gillis, K.M. and Robinson, P.T.
1985: Low-temperature alteration of the extrusive sequence, Troodos ophiolite, Cyprus; Canadian Mineralogist, v. 23, p. 431-441.

Kidd, R.G.W.
1977: A model for the process of formation of the upper oceanic crust; Geophysical Journal of the Royal Astronomical Society, v. 50, p. 149-183.

Kidd, R.G.W. and Cann, J.R.
1974: Chilling statistics indicate an ocean-floor spreading origin for the Troodos complex, Cyprus; Earth and Planetary Science Letters, v. 24, no. 1, p. 151-155.

Malpas, J. and Langdon, G.
1984: Petrology of the upper pillow lava suite, Troodos ophiolite, Cyprus; *in* Ophiolites and Oceanic Lithosphere, ed. I.G. Gass, S.J. Lippard and A.W. Shelton; Geological Society of London, Special Publication, no. 13, Blackwell Scientific Publications, Oxford, p. 155-167.

McCulloch, M.T. and Cameron, W.E.
1983: Nd-Sr isotopic study of primitive lavas from the Troodos ophiolite, Cyprus: evidence for a subduction-related setting; Geology, v. 11, p. 727-731.

Moores, E.M. and Vine, F.J.
1971: The Troodos Massif, Cyprus, and other ophiolites as oceanic crust: evaluation and implications; *in* A Discussion on the Petrology of Igneous and Metamorphic Rocks from the Ocean Floor; Philosophical Transactions of the Royal Society of London, Series A, v. 268, p. 443-466.

Mottl, M.J.
1983: Metabasalts, axial hot springs and the structure of hydrothermal systems at mid-ocean ridges; Geological Society of America, Bulletin, v. 94, no. 2, p. 161-180.

Robinson, P.T., Melson, W.G., O'Hearn, T. and Schmincke, H.-U.
1983: Volcanic glass compositions of the Troodos ophiolite, Cyprus; Geology, v. 11, no. 7, p. 400-404.

Schmincke, H.-U., Rautenschlein, M., Robinson, P.T. and Mehegan, J.M.
1983: Troodos extrusive series of Cyprus: a comparison with oceanic crust; Geology, v. 11, no. 7, p. 405-409.

Smewing, J.D., Kapo, S.O. and Gass, I.G.
1975: Metabasalts from the Troodos massif, Cyprus: genetic implications deduced from petrography and trace element geochemistry; Contributions to Mineralogy and Petrology, v. 54, p. 49-64.

Thy, P., Brooks, C.K. and Walsh, J.N.
1985: Tectonic and petrogenetic implications of major and rare earth element chemistry of Troodos glasses, Cyprus; Lithos, v. 18, no. 3, p. 165-178.

Thy, P., Schiffman, P. and Moores, E.M.
1988: Igneous mineral stratigraphy and chemistry of the Cyprus Crustal Study Project drill core in the plutonic sequences of the Troodos ophiolite; *in* Cyprus Crustal Study Project: Initial Report, Hole CY-4, ed. I.L. Gibson, J. Malpas, P.T. Robinson and C. Xenophontos; Geological Survey of Canada, Paper 88-9.

APPENDIX

TABLE 1A. Major Element Analyses, Road-Cut Sections

Id	S.G.	Ch	SiO_2	Al_2O_3	Fe_2O_3	FeO	MgO	CaO	Na_2O	K_2O	TiO_2	P_2O_5	MnO	S	Cr_2O_3	CO_2	H_2O	Total
BL83								AYIA KORONI SECTION										
3	2.64		52.20	14.90	4.10	6.80	7.96	3.13	4.50	0.18	1.20	0.13	0.16	0.02	0.01	0.10	5.00	100.40
4	2.70	1	53.80	15.00	7.50	4.90	4.08	2.88	6.80	0.00	1.38	0.11	0.14	0.02	0.00	0.00	2.70	99.40
5	2.64	1	62.80	13.80	5.00	3.70	2.81	2.63	5.40	0.12	1.17	0.19	0.13	0.01	0.00	0.00	2.30	100.10
6	2.70	2	52.40	14.60	4.30	7.90	6.33	2.92	4.40	0.06	1.49	0.11	0.19	0.00	0.01	0.70	4.50	99.90
7	2.66	0	65.50	13.00	4.40	3.60	3.02	2.47	4.70	0.17	0.90	0.17	0.13	0.03	0.00	0.00	2.50	100.60
8	2.59	2	43.80	17.50	3.70	8.80	12.00	1.11	3.90	0.00	0.78	0.08	0.28	0.02	0.01	0.00	8.50	100.60
18	2.72	2	54.70	14.30	4.10	7.10	5.93	2.60	4.80	0.00	1.39	0.14	0.20	0.00	0.00	1.10	4.10	100.50
21A	2.72	2	54.70	14.10	4.30	6.80	5.50	2.87	4.90	0.00	1.36	0.12	0.21	0.00	0.00	1.20	4.10	100.30
22	2.73	1	54.60	15.00	4.60	6.00	5.39	2.73	5.00	0.08	1.29	0.10	0.15	0.01	0.01	0.20	3.50	98.80
24	2.65	1	62.20	14.00	3.30	5.30	2.83	2.38	4.90	0.06	1.05	0.19	0.21	0.24	0.00	0.70	2.70	100.10
25	2.67	1	56.50	14.10	4.70	5.80	4.41	2.73	4.90	0.00	1.20	0.14	0.24	0.15	0.00	0.80	3.30	99.10
28	2.63	0	62.90	14.10	4.20	4.50	2.30	2.64	5.50	0.05	1.01	0.20	0.14	0.12	0.00	0.70	2.00	100.40
29	2.70	2	52.40	14.00	4.50	7.40	5.71	3.18	4.90	0.00	1.38	0.12	0.19	0.00	0.00	0.60	4.40	98.80
30	2.72	2	52.80	14.50	4.70	7.10	5.54	4.16	4.50	0.05	1.36	0.10	0.19	0.00	0.00	1.60	3.80	100.40
31A	2.67	2	52.20	14.20	3.60	7.10	4.71	4.33	4.90	0.03	1.26	0.10	0.17	0.07	0.00	2.60	3.90	99.10
32	2.73	2	53.00	14.70	3.50	7.70	5.10	3.76	4.80	0.02	1.32	0.12	0.23	0.07	0.00	2.00	4.00	100.40
33	2.70	0	54.60	13.90	3.80	7.50	5.35	3.48	4.00	0.01	1.41	0.11	0.25	0.00	0.00	1.70	4.00	100.10
34	2.67	2	53.90	14.60	3.90	7.80	5.56	3.61	4.60	0.00	1.45	0.11	0.24	0.00	0.01	1.30	3.80	100.90
35	2.67	2	55.40	13.80	3.80	7.40	4.48	3.34	4.40	0.01	1.31	0.13	0.24	0.32	0.00	1.90	3.90	100.50
38	2.70	2	53.70	14.70	3.90	7.50	5.76	4.09	3.60	0.35	1.20	0.11	0.30	0.27	0.00	0.70	4.20	100.40
39	2.74	2	54.40	15.00	2.80	8.60	4.69	3.40	3.90	0.18	1.40	0.13	0.22	0.61	0.00	0.90	4.30	100.50
41	2.73	2	52.80	13.70	4.60	7.70	4.38	3.90	3.50	0.16	1.32	0.13	0.23	0.35	0.00	1.80	4.00	98.60
42	2.70	2	54.70	14.30	4.10	7.00	5.32	3.18	4.60	0.00	1.37	0.12	0.24	0.00	0.00	1.60	4.10	100.70
43	2.68	1	52.80	13.90	4.80	6.70	4.79	4.17	4.50	0.04	1.30	0.11	0.27	0.00	0.00	2.40	3.90	99.60
44	2.62	0	51.10	15.60	2.60	7.60	7.72	2.62	4.40	0.00	0.87	0.09	0.39	0.00	0.00	1.60	5.00	99.70
47	2.69	2	54.10	13.90	4.20	7.10	5.54	2.63	3.70	0.00	1.33	0.14	0.36	0.00	0.00	1.40	4.60	99.00
48	2.63	1	62.80	13.50	6.10	3.10	2.24	1.66	5.80	0.02	0.91	0.15	0.17	0.00	0.00	0.00	2.90	99.40
49	2.67	0	59.50	14.10	5.50	5.20	3.25	1.97	5.50	0.06	1.05	0.16	0.20	0.00	0.00	0.60	3.20	100.40
50	2.63	1	58.50	13.90	5.40	4.50	2.16	4.07	2.30	0.15	1.22	0.19	0.19	0.15	0.00	0.00	6.40	99.20
51	2.68	1	50.40	14.20	2.30	6.10	9.73	6.00	1.70	1.03	0.69	0.06	0.18	0.00	0.04	1.90	5.10	99.50
BL82								PALEKHORI ROAD										
P3B	2.88		50.70	14.39	3.59	7.90	5.62	9.55	1.29	0.04	1.52	0.10	0.20	0.17	0.01	0.10	2.90	98.19
P3D	2.72		70.19	12.80	4.00	2.59	0.71	4.15	2.70	0.24	0.49	0.13	0.04	0.03	0.00	0.00	1.00	99.19
P3H	2.90		49.79	15.60	1.79	5.80	9.00	12.39	0.69	0.12	0.51	0.04	0.15	0.06	0.05	0.00	2.90	99.00
P3F	2.74		60.79	14.80	1.60	6.30	2.62	6.33	4.19	0.38	1.07	0.10	0.12	0.01	0.01	0.10	1.39	100.00
P110	2.70		53.20	13.69	3.50	7.69	4.61	4.31	4.30	0.06	1.42	0.10	0.21	0.02	0.01	2.90	3.29	99.40
P117	2.60		62.70	13.80	3.79	5.09	2.15	2.34	5.40	0.10	1.00	0.19	0.20	0.10	0.01	1.20	1.70	99.80
P120	2.58		52.70	14.00	4.19	7.40	5.18	3.73	4.80	0.03	1.42	0.10	0.20	0.00	0.01	2.00	3.09	99.00
BL82								NIKITARI 2										
406	2.49	1	53.50	14.00	6.50	7.69	4.05	3.53	4.19	0.06	1.47	0.10	0.23	0.00	0.01	0.00	2.70	98.09
410	2.71	0	53.40	15.10	4.69	6.80	5.74	4.63	4.00	0.23	1.17	0.08	0.16	0.00	0.01	0.40	2.90	99.30
411	2.77	2	52.00	14.60	3.79	6.80	6.31	7.27	2.79	0.17	1.34	0.12	0.23	0.08	0.01	0.20	2.70	98.40
417	2.58		50.09	15.50	3.70	7.19	7.44	5.37	4.00	0.21	0.89	0.06	0.17	0.01	0.01	1.20	3.00	99.00
421	2.63	1	51.90	14.89	3.20	6.59	7.34	5.27	4.59	0.57	0.85	0.06	0.16	0.04	0.01	0.30	2.59	98.50
423	2.67	1	55.20	14.19	5.40	6.30	4.21	4.91	3.79	0.19	1.17	0.10	0.20	0.00	0.01	0.10	2.20	98.00
426	2.60	1	55.00	14.10	5.09	6.59	3.87	4.59	5.09	0.16	1.32	0.10	0.23	0.00	0.01	0.00	1.89	98.09
432	2.65	2	55.59	14.00	6.30	6.30	3.90	3.56	4.30	0.15	1.54	0.12	0.20	0.00	0.01	0.00	2.70	98.80
435	2.56	1	52.70	14.39	7.59	5.90	4.21	4.96	4.50	0.19	1.57	0.12	0.20	0.00	0.01	0.00	2.40	98.80
442	2.66	1	55.09	14.00	7.00	5.50	3.89	4.81	3.50	0.13	1.25	0.08	0.19	0.00	0.01	0.00	2.40	98.00
444	2.60	0	56.00	14.50	7.00	6.00	4.19	3.68	4.19	0.15	1.22	0.10	0.19	0.00	0.01	0.00	2.90	100.30
446	2.63	1	56.29	14.50	4.69	7.19	4.49	4.62	3.70	0.19	1.25	0.08	0.21	0.00	0.01	0.00	2.20	99.50
448	2.66	2	53.50	14.50	5.40	8.19	4.71	4.71	3.40	0.24	1.50	0.12	0.16	0.00	0.01	0.00	2.90	99.40
451	2.53	2	61.90	13.50	4.09	6.09	2.62	2.90	5.90	0.08	1.15	0.12	0.17	0.00	0.01	0.00	1.79	100.40
452	2.57	0	62.79	13.69	3.70	5.50	2.51	3.00	4.69	0.12	1.09	0.13	0.17	0.00	0.01	0.00	1.89	99.40
456	2.60	1	52.29	14.19	5.09	6.90	4.49	4.46	4.59	0.08	1.54	0.10	0.20	0.00	0.02	2.20	2.59	98.69
457	2.53	2	52.29	16.60	3.00	5.69	7.49	3.54	5.69	0.62	0.71	0.06	0.16	0.01	0.02	0.60	3.09	99.80
BL82								NIKITARI 1										
330	2.70	1	56.00	13.80	5.69	5.80	3.37	5.25	3.50	0.16	1.28	0.12	0.20	0.00	0.01	1.79	1.79	98.90
331	2.66	2	53.70	14.69	4.19	6.30	5.61	4.78	3.70	0.34	0.94	0.06	0.23	0.00	0.02	1.20	2.79	98.69
335	2.64	1	56.29	14.60	3.09	6.19	4.83	6.53	2.70	0.33	0.73	0.08	0.19	0.00	0.01	1.00	1.89	98.59

Id	S.G.	Ch	SiO_2	Al_2O_3	Fe_2O_3	FeO	MgO	CaO	Na_2O	K_2O	TiO_2	P_2O_5	MnO	S	Cr_2O_3	CO_2	H_2O	Total
BL82								NIKITARI 1 (cont.)										
336	2.57	1	57.29	14.80	3.29	6.19	5.12	4.25	3.29	0.34	0.62	0.08	0.16	0.00	0.01	0.50	2.50	98.50
338	2.64		56.70	14.69	3.59	5.30	5.11	6.31	2.70	0.21	0.64	0.06	0.13	0.00	0.01	0.80	2.00	98.30
343	2.61	2	51.40	14.30	5.69	5.80	5.96	4.12	4.09	0.30	1.03	0.06	0.16	0.01	0.01	1.29	3.70	98.00
344	2.56	1	65.09	13.10	3.79	3.79	1.64	3.04	4.90	0.12	0.57	0.10	0.08	0.01	0.01	1.39	0.80	98.50
346	2.64	1	55.09	14.10	6.50	6.59	3.51	5.50	3.70	0.16	1.43	0.12	0.21	0.01	0.01	0.40	1.20	98.50
347	2.39	2	53.79	14.80	6.40	4.50	3.04	5.43	6.00	0.08	0.82	0.10	0.17	0.00	0.01	3.29	1.60	100.09
349	2.50	2	59.09	13.69	5.30	4.00	2.32	3.79	5.69	0.17	1.20	0.12	0.12	0.02	0.01	1.29	1.70	98.69
352	2.64	2	50.09	12.39	5.80	7.09	3.14	6.87	4.59	0.06	1.25	0.10	0.16	0.40	0.01	5.00	1.79	98.80
354	2.61	0	53.00	14.30	6.00	6.40	4.50	6.49	3.40	0.25	1.42	0.08	0.21	0.00	0.01	0.89	1.39	98.30
356	2.63	2	47.50	15.10	3.20	7.30	7.58	7.87	2.50	0.55	0.67	0.06	0.21	0.00	0.03	2.79	3.50	98.80
358	2.66	0	54.00	14.10	5.69	6.40	4.62	5.78	4.00	0.25	1.42	0.10	0.20	0.00	0.01	0.69	1.39	98.69
362	2.56	1	58.50	14.10	5.69	5.90	3.01	3.85	4.09	0.23	1.28	0.10	0.12	0.00	0.01	0.00	1.39	98.30
365	2.64	1	56.20	15.19	3.20	6.00	4.56	6.55	3.20	0.32	0.89	0.08	0.16	0.00	0.01	0.69	1.60	98.69
366	2.58	2	55.70	15.50	3.59	6.09	4.63	6.03	4.09	0.51	0.96	0.08	0.15	0.00	0.01	0.60	1.70	99.80
368	2.60	0	61.50	14.00	4.30	5.30	2.25	3.43	5.00	0.25	1.36	0.17	0.12	0.00	0.01	0.10	1.00	98.90
373	2.54	2	54.50	15.39	3.90	6.50	4.87	4.43	4.69	0.57	0.96	0.08	0.15	0.00	0.01	0.50	2.00	98.59
376	2.62	1	48.40	14.89	3.79	6.69	8.50	3.90	4.00	0.16	0.64	0.04	0.16	0.00	0.01	2.29	4.59	98.09
379	2.67	1	52.09	15.10	3.70	5.59	8.31	6.30	2.50	0.57	0.67	0.06	0.16	0.00	0.03	0.10	3.20	98.50
381	2.56	2	58.70	13.50	7.59	4.80	3.06	2.34	5.90	0.10	1.20	0.10	0.10	0.00	0.01	0.00	1.79	99.19
385	2.58	0	54.00	14.80	3.09	6.00	5.63	5.53	4.40	0.44	0.92	0.08	0.16	0.00	0.01	0.80	2.50	98.50
390	2.62	2	57.90	14.60	5.59	4.09	4.12	4.12	4.00	0.32	0.85	0.08	0.12	0.00	0.01	0.40	3.09	99.40
391	2.62	1	55.79	14.80	4.09	5.40	4.47	4.65	5.40	0.26	0.92	0.08	0.17	0.00	0.01	0.20	2.40	98.90
393	2.66	0	53.50	15.30	4.00	6.30	4.97	5.06	4.80	0.57	1.00	0.10	0.19	0.01	0.01	0.20	3.09	99.09
395	2.56	2	54.59	14.89	6.40	5.59	3.76	4.11	5.80	0.47	1.35	0.10	0.16	0.00	0.01	0.89	2.20	100.50
398	2.60	1	55.29	15.10	4.50	5.40	4.31	5.03	5.50	0.53	1.00	0.10	0.17	0.00	0.01	0.40	1.89	99.19
400	2.68	2	55.20	15.00	4.90	5.80	5.24	4.81	3.70	0.25	0.94	0.06	0.20	0.01	0.01	0.30	2.79	99.30
401	2.63	0	53.29	14.60	2.90	5.80	6.83	5.80	4.30	0.66	0.66	0.06	0.21	0.00	0.01	0.10	3.20	98.50
BL82								AYIOS THEODHOROS										
210	2.53		55.70	15.20	5.10	4.30	4.75	4.72	5.20	0.32	0.94	0.11	0.18	0.00	0.01	0.00	3.90	100.40
211	2.49	2	51.29	16.29	7.40	7.40	3.93	2.39	6.40	0.06	1.53	0.10	0.17	0.01	0.01	0.20	2.90	100.19
212	2.67	0	56.20	14.60	4.80	5.19	4.21	6.22	3.79	0.34	0.94	0.08	0.16	0.02	0.01	0.20	1.70	98.50
213	2.54	2	53.80	14.30	5.50	6.10	4.30	4.63	5.40	0.10	1.39	0.14	0.18	0.00	0.00	0.90	3.50	100.30
214	2.52	0	54.59	15.19	3.09	5.40	5.68	6.81	3.59	0.60	0.64	0.06	0.17	0.02	0.02	0.80	2.59	99.50
215	2.54	2	51.59	16.29	5.00	6.90	4.74	3.20	6.09	0.06	1.35	0.12	0.21	0.02	0.01	0.50	3.00	99.09
216	2.63	2	50.20	15.90	3.60	6.30	4.33	6.02	6.10	0.05	1.22	0.12	0.20	0.00	0.00	2.60	3.70	100.50
217	2.61		50.70	14.00	5.70	5.60	4.37	8.47	5.00	0.17	1.38	0.13	0.27	0.00	0.01	2.50	2.40	100.80
218	2.59	2	52.50	15.30	4.69	4.50	7.00	5.31	4.40	0.64	0.69	0.05	0.19	0.00	0.03	0.30	3.79	99.40
219	2.57	0	54.10	15.30	5.90	5.90	4.24	5.85	4.20	0.21	1.51	0.14	0.17	0.00	0.00	0.00	3.10	100.70
220	2.74	0	54.40	13.50	6.00	5.50	4.15	6.65	3.50	0.12	1.39	0.12	0.17	0.00	0.01	1.50	1.79	98.90
221	2.57	2	53.00	16.00	3.40	5.20	6.65	4.48	6.00	0.18	0.75	0.08	0.18	0.00	0.01	0.80	4.20	100.90
222	2.55	2	52.90	15.40	5.10	5.10	6.28	5.30	4.90	0.38	0.81	0.09	0.18	0.00	0.01	0.00	4.00	100.50
224	2.54		60.40	14.69	5.00	3.70	2.65	3.56	5.80	0.20	0.98	0.10	0.12	0.00	0.01	0.00	1.89	99.09
225	2.47	2	51.50	16.00	6.80	7.09	3.93	2.26	6.50	0.04	1.46	0.10	0.15	0.00	0.01	0.10	2.70	98.69
226	2.56	1	53.30	15.50	4.70	5.50	5.42	5.54	4.90	0.31	0.97	0.11	0.16	0.00	0.00	0.40	3.70	100.60
229	2.66	2	47.80	15.00	4.20	3.40	10.20	9.75	1.90	0.63	0.56	0.08	0.14	0.02	0.06	0.00	6.60	100.40
230	2.68	0	52.90	15.10	3.40	5.70	6.67	6.19	3.50	1.24	0.68	0.06	0.18	0.01	0.00	0.50	4.10	100.30
231	2.61	0	55.50	13.80	6.40	6.00	3.95	5.72	3.79	0.20	1.42	0.12	0.20	0.00	0.01	0.20	1.79	99.19
232	2.50	1	62.29	13.80	5.09	3.20	2.31	3.98	5.00	0.31	1.04	0.12	0.12	0.00	0.01	0.20	1.00	98.69
233	2.50	2	51.79	15.10	6.00	5.69	4.33	4.77	5.50	0.06	1.36	0.10	0.19	0.00	0.01	1.29	2.50	98.80
234	2.48	1	62.00	14.00	5.10	3.50	3.13	4.10	5.20	0.29	0.98	0.11	0.13	0.00	0.00	0.10	1.90	100.60
235	2.62	2	50.60	15.20	3.60	6.00	7.66	7.31	1.90	0.87	0.85	0.07	0.20	0.00	0.01	0.00	4.20	98.50
236	2.64	0	55.90	13.30	6.80	5.40	4.31	5.30	4.30	0.19	1.41	0.14	0.18	0.00	0.00	0.00	2.60	99.90
237	2.53	2	54.70	14.40	6.00	5.90	4.45	3.80	4.90	0.10	1.51	0.12	0.15	0.00	0.00	0.60	3.60	100.30
238	2.53	0	55.20	14.89	4.09	5.09	6.11	5.03	5.40	0.87	0.66	0.06	0.17	0.00	0.01	0.50	2.09	100.30
239	2.44	2	48.40	15.19	8.39	5.00	5.36	3.10	5.19	0.02	1.20	0.06	0.23	0.00	0.01	1.79	4.90	99.00
240	2.43	2	54.00	14.00	6.30	4.19	3.78	5.25	6.09	0.08	1.50	0.12	0.17	0.00	0.01	1.60	1.39	98.69
241	2.70	2	52.10	15.20	2.10	6.10	7.64	6.87	2.50	1.79	0.53	0.06	0.20	0.00	0.03	0.90	4.00	100.00
242	2.64	0	53.40	14.50	6.80	5.80	4.12	4.69	5.30	0.21	1.45	0.12	0.20	0.00	0.01	0.00	1.70	98.30
243	2.43	2	52.00	14.69	8.60	6.09	3.87	2.71	5.59	0.05	1.46	0.10	0.20	0.00	0.01	0.10	2.50	98.09
244	2.61	0	57.20	14.70	4.90	5.10	4.12	5.75	4.20	0.19	1.25	0.14	0.25	0.00	0.00	0.00	2.70	100.60
245	2.61	2	51.70	14.30	7.00	5.60	6.03	3.53	4.70	0.36	1.08	0.08	0.18	0.00	0.01	0.10	5.90	100.60
246	2.57	0	52.40	14.30	8.30	4.80	4.16	3.59	4.59	0.16	1.54	0.10	0.24	0.00	0.02	0.10	3.70	98.09
247	2.54	2	55.50	14.80	6.80	5.30	3.90	3.34	5.09	0.21	1.42	0.12	0.17	0.00	0.01	0.10	2.79	99.59
248	2.60	0	52.00	14.80	6.10	6.00	5.52	3.16	4.10	0.23	1.12	0.09	0.17	0.03	0.00	0.30	6.20	99.80
249	2.58	0	52.80	15.30	2.60	6.70	7.73	6.30	3.60	0.50	0.56	0.09	0.21	0.00	0.01	0.00	4.10	100.50
250	2.67	1	52.20	15.40	3.20	5.90	7.58	7.56	2.60	0.70	0.94	0.10	0.20	0.01	0.02	0.20	3.90	100.50
251	2.49	1	54.60	15.00	6.20	5.50	4.79	4.11	5.00	0.14	1.09	0.10	0.17	0.00	0.00	0.00	3.50	100.20

Id	S.G.	Ch	SiO_2	Al_2O_3	Fe_2O_3	FeO	MgO	CaO	Na_2O	K_2O	TiO_2	P_2O_5	MnO	S	Cr_2O_3	CO_2	H_2O	Total
BL82								AYIOS THEODHOROS (cont.)										
252	2.60	2	50.20	15.10	3.90	7.19	7.58	6.71	3.09	0.16	0.80	0.05	0.23	0.00	0.02	0.10	3.50	98.59
253	2.46	1	67.40	13.19	4.80	1.89	1.39	2.12	5.50	0.06	0.71	0.16	0.08	0.01	0.00	0.10	1.10	98.69
254	2.50	0	56.70	14.60	6.30	4.00	3.59	4.87	4.90	0.31	1.64	0.16	0.19	0.01	0.01	0.10	2.09	99.59
255	2.57	1	54.90	14.70	8.20	3.90	3.57	4.70	4.10	0.29	1.39	0.13	0.13	0.00	0.00	0.00	3.60	99.70
256	2.48	2	63.70	13.40	6.40	3.20	1.48	2.78	5.80	0.15	0.95	0.31	0.12	0.01	0.00	0.00	2.10	100.40
257	2.49	2	51.60	15.30	8.50	4.10	5.64	3.41	4.60	0.22	0.80	0.07	0.17	0.00	0.01	0.00	5.20	99.70
258	2.50	2	53.10	15.30	7.20	4.20	5.37	4.75	4.30	0.93	1.09	0.08	0.17	0.00	0.00	0.00	4.00	100.50
259	2.54	2	48.70	15.60	12.40	5.00	3.99	1.79	4.80	0.03	1.29	0.14	0.19	0.00	0.01	0.00	6.20	100.10
260	2.58		72.50	12.50	2.90	2.00	0.92	2.05	5.40	0.13	0.60	0.15	0.10	0.01	0.01	0.00	1.20	100.40
261	2.42		57.70	15.10	7.30	2.70	2.63	3.86	5.00	0.31	1.14	0.13	0.13	0.01	0.00	0.00	3.70	99.80
262	2.49	2	49.50	15.50	8.00	1.90	8.00	4.15	3.70	0.76	0.54	0.07	0.17	0.00	0.00	0.00	8.20	100.50
263	2.60	0	54.70	14.50	7.70	3.90	4.39	3.94	6.00	0.46	1.25	0.12	0.16	0.02	0.00	0.00	3.20	100.40
264	2.57	2	54.59	14.60	7.00	5.59	3.68	3.31	4.80	0.19	1.46	0.12	0.12	0.01	0.02	0.40	2.90	98.80
265	2.45	2	55.10	15.00	8.00	4.90	3.40	2.60	5.90	0.08	1.47	0.14	0.15	0.00	0.00	0.00	3.60	100.40
266	2.51	0	56.59	14.30	5.19	3.79	4.03	4.81	4.69	0.51	0.87	0.08	0.13	0.01	0.01	0.60	2.29	98.00
267	2.49	0	58.50	14.40	6.20	4.30	2.95	3.69	5.50	0.24	1.20	0.16	0.16	0.00	0.00	0.00	3.10	100.40
268	2.54		56.79	14.30	6.19	5.09	3.01	3.87	5.19	0.13	1.21	0.12	0.13	0.01	0.01	0.00	2.50	98.80
270	2.63		54.90	15.20	3.40	6.50	6.13	4.44	3.20	0.63	0.80	0.08	0.13	0.00	0.00	0.00	5.00	100.40
BL82								MAKHERAS MONASTERY										
155	2.88		53.29	15.89	3.40	6.90	5.72	9.75	2.20	0.12	0.94	0.08	0.23	0.01	0.01	0.00	1.79	100.40
157	2.74	2	51.00	16.00	2.50	5.40	7.12	8.50	3.90	0.35	0.64	0.05	0.16	0.04	0.03	0.20	3.20	99.09
158	2.71	1	51.50	14.39	4.59	6.30	5.02	7.94	3.59	0.02	1.04	0.08	0.17	0.01	0.01	0.10	3.79	98.69
160	2.73	2	52.40	15.30	4.00	6.00	6.00	7.58	3.40	0.34	0.89	0.06	0.19	0.00	0.01	0.10	3.00	99.30
162	2.73	1	53.59	14.69	4.19	6.90	5.00	6.96	3.29	0.19	1.14	0.08	0.20	0.00	0.01	0.10	2.90	99.40
164	2.73	2	50.00	15.10	7.69	8.39	4.11	4.53	3.90	0.10	1.57	0.10	0.17	0.00	0.01	0.10	3.79	99.69
166	2.68		50.90	15.10	4.00	6.00	6.06	8.39	3.29	0.01	0.87	0.06	0.19	0.00	0.01	0.10	4.40	99.50
170	2.78	1	51.29	13.39	2.00	6.00	9.66	8.68	2.09	0.44	0.28	0.02	0.19	0.00	0.06	0.20	4.40	98.80
171	2.74	2	53.70	15.30	3.90	6.59	5.06	6.93	3.70	0.30	1.04	0.10	0.19	0.00	0.01	0.20	2.90	99.90
172	2.72	0	51.00	14.19	6.59	5.80	4.75	7.56	3.20	0.04	1.39	0.08	0.17	0.00	0.02	0.10	3.70	98.59
176	2.73	1	52.90	15.39	3.79	6.40	5.59	7.65	3.20	0.20	0.82	0.08	0.17	0.00	0.01	0.10	3.00	99.40
178	2.84	2	50.59	15.69	2.00	5.90	7.78	9.48	3.09	0.20	0.69	0.06	0.16	0.03	0.04	0.10	3.29	99.19
181	2.81	2	50.40	15.60	2.20	5.40	7.78	9.56	3.50	0.35	0.66	0.06	0.16	0.02	0.05	0.10	2.90	98.69
182	2.79	0	51.29	15.80	3.50	6.50	5.69	8.43	3.29	0.27	1.00	0.08	0.19	0.02	0.01	0.10	2.59	98.80
187	2.66	2	54.79	14.69	2.79	6.80	5.83	5.40	4.00	0.06	0.71	0.06	0.19	0.02	0.01	0.10	4.09	99.69
188	2.71		55.40	14.19	4.00	6.09	4.06	6.68	3.20	0.06	0.91	0.08	0.16	0.02	0.01	0.00	4.00	98.80
191	2.76	1	53.00	14.80	3.29	6.40	6.25	8.00	3.20	0.25	0.87	0.06	0.16	0.00	0.03	0.20	2.70	99.30
192	2.68	2	53.29	15.19	4.69	6.50	4.66	6.33	4.40	0.27	1.14	0.10	0.21	0.01	0.01	0.10	2.09	99.09
195	2.72	0	55.79	14.10	5.69	6.40	3.56	6.81	2.79	0.19	1.22	0.08	0.17	0.01	0.01	0.10	1.70	98.59
197	2.70	2	50.20	15.19	4.00	6.19	5.65	7.90	3.79	0.10	1.03	0.08	0.17	0.01	0.01	0.10	3.50	98.00
199	2.80	1	51.70	15.30	3.20	6.59	5.80	9.54	2.59	0.19	0.92	0.06	0.17	0.01	0.02	0.10	2.00	98.30
201	2.68	2	52.50	15.69	2.00	7.40	6.46	7.41	3.90	0.23	0.62	0.06	0.16	0.01	0.02	0.10	3.00	99.69
203	2.78	1	52.70	14.80	6.90	6.30	4.25	7.44	3.09	0.24	1.25	0.08	0.19	0.02	0.01	0.10	1.89	99.40
205	2.72		54.90	14.50	6.19	5.90	3.81	6.37	3.59	0.30	1.36	0.10	0.16	0.02	0.01	0.10	1.89	99.30
206	2.73	2	48.79	13.89	2.09	6.19	10.80	8.32	2.79	0.15	0.32	0.02	0.20	0.01	0.08	0.10	4.69	98.50
BL82								KIONIA 1										
55	2.69		53.79	14.80	4.19	7.50	4.12	7.15	3.40	0.20	1.36	0.12	0.16	0.00	0.02	0.10	3.29	100.30
57	2.70	0	54.00	14.50	4.40	7.19	4.00	7.40	3.00	0.16	1.34	0.10	0.16	0.01	0.00	0.30	2.09	98.69
59	2.69	2	53.90	14.60	3.70	8.00	4.21	6.93	3.29	0.23	1.25	0.10	0.13	0.01	0.01	0.30	2.40	99.09
61	2.65	2	53.40	15.00	3.40	7.90	3.95	6.62	4.00	0.25	1.35	0.10	0.19	0.02	0.01	0.30	2.50	99.00
65	2.70	2	53.00	15.39	1.89	7.40	5.75	8.01	3.40	0.08	0.91	0.06	0.16	0.03	0.02	0.30	4.30	100.69
66	2.74	1	54.90	14.19	3.79	7.90	3.70	6.18	2.70	0.30	1.18	0.08	0.16	0.02	0.01	0.20	2.09	97.50
68	2.73	1	54.29	14.80	1.60	8.89	4.38	6.86	3.59	0.44	1.18	0.08	0.16	0.03	0.01	0.20	2.09	98.69
75	2.80	0	52.79	15.80	1.39	7.09	6.34	8.83	3.20	0.60	0.55	0.03	0.17	0.04	0.02	0.40	2.40	99.69
77	2.73	2	54.50	14.60	3.59	8.19	3.90	7.31	3.00	0.17	1.38	0.12	0.17	0.03	0.01	0.10	2.00	99.30
BL82								KIONIA 2										
83	2.74	1	54.29	14.19	3.40	8.39	3.92	6.99	2.90	0.10	1.21	0.10	0.19	0.03	0.01	0.10	3.09	99.00
84	2.94	2	46.09	16.79	2.40	9.10	9.06	9.99	1.60	0.34	0.58	0.05	0.21	0.04	0.04	0.10	3.20	99.69
87	2.72	1	53.59	14.50	4.00	7.80	4.02	7.13	3.20	0.08	1.22	0.10	0.17	0.00	0.01	0.50	3.29	99.69
89	2.70	2	54.00	14.39	2.90	7.30	4.75	7.37	3.70	0.10	1.11	0.10	0.19	0.00	0.01	0.10	2.70	98.90
92	2.86	0	55.70	15.10	4.80	7.69	4.36	7.53	1.60	0.02	1.00	0.06	0.19	0.01	0.01	0.10	1.70	100.00
94	2.79	1	50.50	12.80	1.10	8.89	9.35	8.00	2.29	0.50	0.33	0.03	0.24	0.00	0.03	0.20	4.40	98.59
96	2.84	1	51.40	14.00	0.69	8.19	8.98	9.86	2.70	0.42	0.31	0.03	0.21	0.02	0.06	0.10	2.79	99.90
98	2.85	0	55.50	14.60	4.69	6.69	3.45	8.27	2.29	0.08	1.25	0.10	0.19	0.02	0.01	0.30	1.29	98.90

Id	S.G.	Ch	SiO_2	Al_2O_3	Fe_2O_3	FeO	MgO	CaO	Na_2O	K_2O	TiO_2	P_2O_5	MnO	S	Cr_2O_3	CO_2	H_2O	Total
BL82								KIONIA 2 (cont.)										
99	2.75	1	52.29	14.60	4.00	7.90	4.05	8.35	2.29	0.02	1.21	0.12	0.17	0.02	0.01	0.10	4.90	100.19
100	2.75	2	53.90	14.19	3.70	7.59	4.25	7.15	2.70	0.10	1.25	0.10	0.20	0.02	0.01	0.20	3.50	98.90
105	2.49	1	45.20	15.80	1.70	8.19	8.11	10.10	2.50	0.82	0.33	0.02	0.25	0.02	0.02	2.00	4.90	99.90
106	2.72	2	53.20	14.39	3.59	7.90	3.73	7.44	2.29	0.16	1.32	0.08	0.20	0.00	0.02	0.20	3.29	98.00
107	2.73	1	54.09	14.50	2.50	8.39	4.61	6.59	2.79	0.27	1.17	0.10	0.19	0.00	0.01	0.30	3.09	98.69
110	2.73	1	52.20	14.39	2.90	8.60	4.68	7.55	3.20	0.20	1.28	0.10	0.20	0.00	0.01	0.20	2.90	98.50
114	2.73	2	52.90	14.50	3.79	7.69	3.68	8.55	2.29	0.01	1.28	0.12	0.17	0.01	0.01	0.10	4.30	99.50
116	2.71	2	53.20	13.89	4.40	7.40	3.81	7.27	2.90	0.13	1.22	0.08	0.19	0.01	0.01	0.10	3.79	98.50
117	2.71	0	54.70	14.30	3.09	8.00	4.09	6.43	2.90	0.15	1.24	0.10	0.21	0.02	0.01	0.10	3.09	98.50
122	2.66	0	57.40	14.00	3.20	6.80	2.79	6.96	2.50	0.16	1.17	0.12	0.12	0.06	0.01	0.00	3.79	99.19
123	2.72	2	59.09	14.00	3.40	6.09	2.89	6.87	2.40	0.13	1.20	0.10	0.13	0.02	0.00	0.00	2.79	99.19
127	2.69	2	54.50	14.19	3.20	8.10	4.09	7.06	3.09	0.25	1.22	0.08	0.17	0.01	0.01	0.20	3.00	99.30
128	2.73	1	51.29	14.39	3.50	7.30	4.40	8.48	2.59	0.31	1.04	0.08	0.19	0.03	0.02	0.40	4.50	98.59
131	2.60	2	56.20	14.00	3.09	7.69	4.00	5.84	2.59	0.05	1.35	0.12	0.16	0.03	0.01	0.10	4.69	100.00
132	2.76	1	54.90	14.50	3.70	8.00	3.59	7.36	2.79	0.13	1.31	0.08	0.19	0.03	0.01	0.00	1.89	98.59
134	2.73	1	52.90	14.30	3.09	8.30	3.89	8.83	1.79	0.16	1.35	0.10	0.15	0.03	0.02	0.10	3.40	98.50
135	2.68	1	52.09	14.89	3.09	8.39	4.96	7.53	3.00	0.10	1.11	0.10	0.19	0.03	0.01	0.10	3.00	98.59
136	2.80	0	54.29	13.89	4.69	7.50	4.09	8.30	2.00	0.28	1.36	0.08	0.17	0.00	0.01	0.00	2.59	99.30
140	2.86	1	55.59	15.19	2.70	7.30	5.50	9.75	2.00	0.12	1.00	0.08	0.20	0.00	0.01	0.10	1.20	100.80
141	2.82	0	55.50	14.89	5.09	7.40	4.12	5.25	2.50	0.02	0.98	0.06	0.10	0.53	0.01	0.80	2.90	100.09
142	2.70	2	58.09	14.10	4.19	5.90	2.64	6.28	2.90	0.12	1.14	0.10	0.13	0.00	0.01	0.00	2.40	98.09
145	2.82	0	56.70	14.69	3.40	6.50	4.91	4.19	2.79	0.06	0.89	0.06	0.06	0.96	0.02	0.00	3.20	98.50
146	2.74	2	53.40	14.69	2.09	8.89	4.50	7.69	1.89	0.21	1.13	0.08	0.16	0.06	0.01	0.10	3.90	99.00
148	2.62	2	52.70	15.00	3.50	7.59	5.21	6.59	2.59	0.24	1.00	0.08	0.19	0.03	0.02	0.40	4.50	99.69
150	2.76	0	53.59	14.39	3.20	7.59	5.19	8.16	2.59	0.23	1.14	0.08	0.20	0.04	0.01	0.00	2.29	98.80
153	2.74	1	49.09	14.10	1.79	8.19	9.04	7.22	3.20	0.33	0.28	0.02	0.24	0.00	0.02	0.60	6.40	100.59
82CLQ								KIONIA 3										
IV	2.54	0	52.30	16.00	3.10	7.60	4.71	5.83	4.60	0.06	1.17	0.10	0.20	0.00	0.01	0.50	4.00	100.20
V	2.76		53.79	15.10	2.70	7.90	5.05	8.30	2.59	0.19	1.14	0.12	0.19	0.00	0.01	0.00	1.89	99.00
III	2.68	2	54.29	14.60	4.09	7.90	4.59	6.50	2.90	0.25	1.17	0.08	0.20	0.00	0.01	0.00	2.29	98.90
I	2.64	0	56.00	14.39	3.40	8.00	3.96	6.38	2.70	0.12	1.24	0.10	0.20	0.10	0.01	0.10	1.70	98.50
1	2.67	2	53.00	14.20	3.80	8.30	3.98	6.25	2.70	0.12	1.37	0.12	0.19	0.33	0.00	0.00	4.60	99.00
2	2.68	1	54.10	14.20	3.70	7.90	3.90	5.74	2.90	0.25	1.33	0.12	0.22	0.11	0.01	0.00	4.10	98.70
3	2.71	2	53.40	14.80	2.90	8.00	5.08	8.18	2.40	0.31	1.14	0.10	0.20	0.00	0.01	0.00	2.70	99.30
4	2.72	2	51.40	15.10	3.09	6.80	6.72	8.37	2.59	0.33	0.98	0.06	0.19	0.00	0.01	0.10	2.90	98.69
4A	2.77	1	54.50	14.80	2.10	6.70	5.50	7.89	2.50	0.35	0.91	0.08	0.19	0.00	0.01	0.00	3.30	98.90
4B	2.67	2	51.40	15.50	1.90	8.80	6.20	6.41	3.70	0.20	0.93	0.07	0.24	0.01	0.01	0.00	4.60	100.00
4C	2.70	1	54.30	14.40	2.30	6.40	5.21	8.57	2.60	0.42	0.83	0.08	0.18	0.00	0.00	0.00	4.30	99.70
4D	2.80	2	51.70	16.00	3.09	9.39	4.33	8.12	3.90	0.10	1.35	0.08	0.25	0.00	0.01	0.00	1.20	99.50
5	2.73	1	51.20	15.50	2.90	7.00	6.66	8.20	3.09	0.32	1.00	0.06	0.17	0.00	0.02	0.00	2.70	99.00
5B	2.62	1	53.60	15.30	4.30	6.70	3.94	5.59	4.90	0.06	1.33	0.11	0.17	0.00	0.01	0.00	3.90	99.90
6	2.60	2	59.10	15.10	3.70	5.40	2.71	4.70	4.70	0.08	1.06	0.13	0.13	0.00	0.01	0.00	3.50	100.40
7	2.66	1	53.90	14.30	5.40	7.10	4.35	5.88	4.20	0.19	1.33	0.10	0.19	0.00	0.00	0.00	3.50	100.50
8	2.65	2	53.29	14.69	4.40	7.69	4.53	5.97	4.00	0.17	1.32	0.10	0.20	0.00	0.01	0.00	2.00	98.50
9	2.82	1	52.70	14.70	1.90	7.10	6.42	9.60	2.80	0.41	0.77	0.09	0.19	0.00	0.02	0.00	3.60	100.40
10	2.71	2	53.40	14.70	3.50	8.80	4.34	6.53	2.90	0.17	1.23	0.12	0.21	0.00	0.00	0.00	4.70	100.70
11	2.55	2	58.70	14.60	3.70	6.10	2.82	4.76	4.80	0.01	1.14	0.12	0.16	0.00	0.01	0.00	3.30	100.30
12	2.82	1	52.40	15.30	1.50	6.90	6.47	9.64	2.20	0.51	0.83	0.09	0.19	0.00	0.01	0.00	3.70	99.80
13	2.57	0	56.80	14.70	2.40	5.70	4.10	6.89	3.20	0.31	0.79	0.08	0.16	0.01	0.00	0.10	4.20	99.50
14	2.60	2	53.80	14.80	4.50	6.50	3.88	7.03	3.70	0.11	1.14	0.07	0.15	0.01	0.01	0.40	3.00	99.10
15	2.63	1	66.59	13.50	4.69	3.00	1.28	3.95	4.30	0.15	0.64	0.13	0.05	0.00	0.00	0.00	0.50	98.80
15I	2.76	1	53.90	15.10	2.50	7.09	5.68	9.33	2.09	0.36	0.69	0.06	0.20	0.00	0.01	0.00	2.20	99.19
16	2.77	2	53.20	15.50	4.19	5.09	5.59	9.23	2.79	0.40	0.67	0.05	0.20	0.00	0.01	0.00	1.89	98.90
17	2.70	2	55.00	14.50	5.10	6.50	4.12	6.40	3.10	0.38	1.02	0.07	0.14	0.00	0.01	0.00	3.40	99.70
18	2.70	2	52.60	14.80	5.20	6.70	5.07	6.11	4.10	0.14	0.95	0.10	0.17	0.00	0.00	0.00	4.00	100.00
19	2.77	1	56.70	14.60	5.40	6.09	3.78	6.66	3.70	0.32	1.03	0.08	0.17	0.00	0.01	0.00	1.10	99.69
20	2.71	2	53.90	14.39	3.79	7.90	4.00	5.77	3.90	0.12	1.38	0.10	0.17	0.01	0.01	0.10	3.00	98.69
21	2.85	1	52.70	15.19	0.89	8.10	7.06	9.45	2.59	0.69	0.50	0.04	0.25	0.00	0.03	0.10	1.79	99.40
22I	2.80	0	52.70	14.69	2.00	6.80	7.65	9.18	3.70	0.44	0.41	0.04	0.19	0.00	0.04	0.10	2.70	100.69
23	2.59	2	49.90	16.30	1.10	6.40	5.74	7.69	5.20	0.05	0.79	0.06	0.13	0.09	0.01	0.10	5.10	98.80
25	2.70	2	49.00	15.30	1.90	6.50	9.51	8.55	3.40	0.04	0.68	0.05	0.16	0.00	0.06	0.20	5.10	100.50
26	2.50	2	50.40	15.50	4.80	7.90	4.23	5.84	4.40	0.11	1.37	0.13	0.20	0.00	0.01	0.00	4.20	99.00
27	2.63	2	45.50	16.40	6.20	6.10	4.15	11.70	0.70	0.19	1.08	0.08	0.17	0.00	0.00	0.00	8.80	100.90
28	2.73	2	54.90	14.89	4.59	7.50	3.89	7.36	3.09	0.15	1.27	0.10	0.16	0.23	0.02	0.10	2.09	100.40
29	2.72	0	58.00	13.70	6.30	5.50	3.42	5.96	4.20	0.09	0.90	0.07	0.17	0.00	0.01	0.00	2.20	100.50
30	2.58	2	52.20	14.20	3.00	6.70	5.87	7.82	3.80	0.00	1.01	0.09	0.16	0.00	0.01	1.30	4.30	100.50
31	2.75	0	53.50	14.70	1.90	6.50	6.71	9.17	2.60	0.70	0.74	0.07	0.19	0.01	0.02	0.00	3.30	100.20

Id	S.G.	Ch	SiO_2	Al_2O_3	Fe_2O_3	FeO	MgO	CaO	Na_2O	K_2O	TiO_2	P_2O_5	MnO	S	Cr_2O_3	CO_2	H_2O	Total
82CLQ									KIONIA 3 (cont.)									
32	2.65	2	51.29	15.80	2.50	7.40	6.40	8.37	3.90	0.19	0.94	0.10	0.19	0.00	0.01	0.20	3.70	100.90
33	2.73	2	48.29	15.19	2.00	6.80	9.92	9.31	2.79	0.08	0.64	0.06	0.16	0.00	0.08	0.60	3.70	99.69
34	2.83	0	52.79	14.80	1.39	7.09	7.99	9.26	2.79	0.89	0.60	0.05	0.20	0.00	0.04	0.00	2.29	100.30
35	2.54	0	54.60	15.00	6.20	6.30	3.67	4.78	4.60	0.11	1.19	0.13	0.13	0.00	0.00	0.00	3.60	100.20
36	2.69		51.40	15.50	2.40	5.90	7.88	7.99	3.40	0.08	0.66	0.05	0.13	0.00	0.04	0.20	4.40	100.10
37	2.75		52.10	14.90	2.00	5.90	7.79	8.54	2.30	0.24	0.59	0.05	0.14	0.02	0.05	0.10	4.60	99.40
39	2.68		51.70	14.30	4.19	8.39	5.83	6.36	2.79	0.19	0.96	0.08	0.16	0.25	0.02	0.10	5.00	100.50
40	2.67	2	47.20	15.30	1.79	7.00	11.00	6.96	3.09	0.16	0.60	0.03	0.15	0.16	0.06	0.60	4.69	98.90
41	2.83		53.90	15.00	3.00	6.09	6.80	8.56	3.50	0.33	0.62	0.05	0.21	0.01	0.02	0.10	1.70	100.00
42	2.70	2	51.50	14.00	3.50	9.00	5.77	6.12	2.50	0.16	0.96	0.08	0.17	0.42	0.02	0.10	5.09	99.50
44	2.65	1	57.59	14.89	3.79	6.69	2.87	5.81	4.40	0.15	1.14	0.10	0.16	0.13	0.01	0.10	2.20	100.09
45	2.73	2	52.29	14.80	3.50	7.40	5.05	8.30	2.40	0.21	1.04	0.08	0.17	0.16	0.01	0.10	4.19	99.80
48	2.62	2	56.79	14.69	4.69	6.59	3.35	5.24	4.80	0.08	1.13	0.08	0.16	0.01	0.01	0.10	2.40	100.19
050	2.74	2	53.79	14.89	4.09	5.80	5.00	8.10	2.50	0.36	0.82	0.08	0.19	0.00	0.01	0.10	3.29	99.19
51	2.65	2	53.50	14.10	2.20	7.50	5.38	7.80	4.19	0.15	0.92	0.06	0.21	0.01	0.02	0.10	2.79	99.09
54	2.77	1	55.79	15.60	3.79	6.59	4.56	8.08	2.90	0.30	0.94	0.08	0.17	0.01	0.01	0.10	1.89	100.90
58	2.74	1	54.90	14.10	6.19	6.40	3.93	6.58	2.29	0.19	1.28	0.12	0.13	0.01	0.01	0.30	3.09	99.59
58L	2.74	1	56.20	14.39	5.40	6.69	4.06	6.75	3.00	0.08	1.25	0.10	0.13	0.01	0.01	0.00	2.20	100.40
59	2.70	2	55.20	14.60	3.20	7.50	4.40	6.25	3.00	0.05	1.32	0.16	0.17	0.00	0.01	0.10	4.50	100.60
060	2.59	2	54.70	14.60	3.79	7.19	4.50	3.96	3.90	0.04	1.31	0.10	0.17	0.00	0.01	0.50	4.00	98.80
061	2.64	0	57.70	14.30	5.30	5.50	3.96	4.46	5.59	0.12	0.94	0.06	0.16	0.00	0.01	0.10	1.50	99.90
62	2.77	1	51.90	15.30	2.59	6.50	6.46	8.76	3.79	0.50	0.85	0.06	0.17	0.00	0.02	0.10	2.90	100.00
63	2.65	2	54.09	14.30	4.19	6.80	4.30	7.19	3.00	0.06	1.32	0.12	0.16	0.01	0.01	0.10	4.00	99.69
64	2.72	1	57.50	14.39	3.90	6.50	3.62	5.86	3.29	0.26	1.11	0.08	0.16	0.01	0.01	0.20	2.50	99.50
65	2.72	2	52.50	14.69	5.09	6.59	5.27	6.68	2.20	0.40	1.04	0.06	0.16	0.01	0.02	0.00	4.90	99.69
066	2.69	2	52.29	14.60	4.69	7.09	4.53	6.83	3.40	0.32	1.25	0.06	0.16	0.00	0.02	0.10	3.70	99.00
67	2.70	0	58.40	14.80	3.80	6.10	3.27	5.23	3.40	0.12	1.16	0.11	0.19	0.00	0.01	0.00	3.30	99.90
68	2.76	0	52.60	15.10	1.50	7.40	6.33	8.60	1.90	0.51	0.87	0.08	0.21	0.04	0.01	0.00	4.40	99.50
69	2.73	2	54.59	15.30	3.40	7.50	4.75	7.31	3.00	0.35	1.02	0.08	0.17	0.04	0.02	0.00	3.00	100.69
70	2.69		53.29	15.60	4.00	7.50	5.15	6.21	3.29	0.20	1.15	0.10	0.19	0.01	0.01	0.20	3.59	100.50
71	2.66	1	56.00	14.90	3.70	6.40	3.97	4.73	4.00	0.21	1.15	0.11	0.16	0.00	0.00	0.00	4.10	99.40
72	2.68	1	56.40	14.50	4.80	6.90	3.46	5.40	3.59	0.20	1.20	0.10	0.12	0.01	0.01	0.00	2.70	99.50
72A	2.63	1	51.50	15.30	3.59	6.19	5.75	8.04	3.90	0.55	0.96	0.06	0.17	0.01	0.01	0.10	2.79	99.00
72B	2.84	1	50.29	16.79	7.90	6.19	4.21	8.04	4.80	0.10	1.04	0.08	0.20	0.01	0.01	0.10	0.89	100.69
73	2.76	0	51.00	15.19	4.40	7.90	5.52	6.83	3.59	0.51	1.07	0.08	0.19	0.01	0.01	0.50	3.20	100.00
74	2.65	2	53.50	14.60	5.50	6.59	4.12	6.88	3.50	0.30	1.24	0.08	0.15	0.01	0.01	0.40	2.79	99.80
76	2.65	2	55.40	14.89	4.30	6.90	3.62	5.53	4.09	0.53	1.31	0.10	0.16	0.01	0.01	0.10	2.79	99.80
80	2.76	1	55.29	14.60	4.40	7.00	4.59	6.38	2.79	0.26	1.14	0.10	0.17	0.02	0.01	0.10	2.79	99.80
81	2.70	2	57.10	14.40	3.40	6.50	4.76	3.65	4.10	0.07	1.23	0.12	0.13	0.00	0.00	0.00	4.90	100.40
82	2.71	1	54.80	14.10	4.60	6.70	4.29	5.95	2.90	0.21	1.35	0.11	0.18	0.00	0.01	0.20	4.90	100.20
84	2.65	1	51.70	14.50	6.19	6.80	5.18	5.43	4.69	0.20	1.10	0.08	0.20	0.02	0.01	0.10	2.70	99.00
85	2.61	1	62.70	13.30	5.00	4.30	2.58	3.57	5.00	0.05	0.98	0.15	0.11	0.00	0.00	0.00	2.40	100.20
86	2.61	1	55.60	14.50	5.50	6.30	3.82	5.40	3.80	0.37	1.12	0.12	0.15	0.00	0.00	0.10	3.40	100.20
88	2.54	1	53.10	14.50	6.50	6.50	4.20	5.69	4.10	0.03	1.36	0.11	0.17	0.00	0.01	0.00	4.10	100.40
90	2.73	2	52.59	14.89	3.79	7.19	5.62	7.50	2.40	0.26	0.98	0.10	0.21	0.00	0.01	0.10	3.29	99.00
91	2.69	0	57.20	14.30	4.80	6.10	3.39	5.59	4.30	0.16	0.93	0.08	0.15	0.00	0.01	0.30	2.50	99.90
92	2.57	1	55.90	14.30	3.80	7.60	3.73	4.89	4.50	0.02	1.27	0.10	0.15	0.00	0.00	0.00	3.70	100.00
93	2.64	2	53.20	15.00	3.60	6.90	4.98	6.18	3.40	0.03	1.28	0.12	0.15	0.00	0.01	0.60	4.80	100.30
94	2.65	2	52.50	15.00	3.40	6.90	4.77	6.38	3.90	0.08	1.24	0.12	0.15	0.00	0.02	0.20	4.09	98.90
95	2.73		54.70	15.10	4.09	7.50	4.08	7.12	3.20	0.20	1.27	0.10	0.16	0.00	0.01	0.10	2.70	100.30
97	2.78	1	51.90	14.10	2.50	6.19	8.81	9.31	2.79	0.26	0.41	0.03	0.21	0.00	0.05	0.10	2.29	99.09
99	2.65	0	53.70	14.10	4.90	7.40	3.94	5.86	2.90	0.03	1.26	0.10	0.15	0.00	0.01	0.00	4.70	99.20
100	2.68	1	57.70	14.30	4.00	7.20	2.92	5.94	3.20	0.08	1.31	0.13	0.18	0.00	0.00	0.00	3.40	100.40
101	2.70	2	52.70	14.80	3.20	7.80	4.74	8.17	2.40	0.16	1.10	0.10	0.19	0.00	0.01	0.10	4.30	99.90
103	2.71	2	54.29	14.50	4.80	7.69	3.87	6.28	3.40	0.17	1.09	0.08	0.16	0.00	0.01	0.10	3.20	99.69
104	2.73	1	53.70	14.80	5.10	6.60	3.87	6.60	3.10	0.19	1.13	0.09	0.16	0.01	0.01	0.00	3.80	99.30
105	2.83	0	51.90	15.10	2.00	7.00	7.56	9.92	2.79	0.25	0.42	0.03	0.21	0.00	0.03	0.10	2.40	99.69
106	2.71	2	55.00	14.80	4.00	7.00	4.46	6.40	3.50	0.19	1.10	0.08	0.20	0.01	0.01	0.00	2.70	99.50
107	2.67	2	55.00	15.40	2.60	7.80	4.11	5.81	4.30	0.09	1.20	0.11	0.20	0.07	0.01	0.00	4.20	100.90
108	2.61	2	53.20	14.69	3.90	6.90	5.24	5.71	3.79	0.03	1.32	0.10	0.17	0.00	0.01	0.30	4.40	99.80
109	2.68	2	53.79	14.39	5.30	6.80	4.49	6.65	3.20	0.13	1.42	0.10	0.15	0.01	0.02	0.10	4.09	100.59
110	2.70	0	54.50	14.50	4.00	7.19	5.15	6.18	3.00	0.17	1.17	0.08	0.16	0.01	0.01	0.10	3.40	99.69
111	2.62	2	52.00	14.89	4.59	7.19	5.66	5.09	3.90	0.08	1.21	0.10	0.19	0.01	0.01	0.10	5.40	100.50
112	2.54	1	55.90	16.00	3.10	7.00	3.22	4.98	5.60	0.01	1.44	0.14	0.18	0.01	0.00	0.00	3.20	100.90
113	2.72	2	56.90	14.89	4.00	6.40	3.46	6.18	3.40	0.13	1.11	0.08	0.19	0.01	0.01	0.10	2.29	99.19
114	2.68	0	56.40	14.50	5.20	5.80	3.37	5.81	3.80	0.14	1.15	0.12	0.17	0.04	0.01	0.00	3.80	100.40
115	2.76	2	53.50	16.10	3.40	6.80	4.87	8.24	3.50	0.17	1.10	0.08	0.20	0.01	0.01	0.10	2.50	100.59
116	2.74	0	58.60	14.50	4.00	6.50	3.25	6.40	3.20	0.13	1.14	0.11	0.21	0.00	0.00	0.10	2.70	100.90
117	2.71	2	53.70	14.60	2.90	7.60	4.30	6.47	2.90	0.18	1.13	0.09	0.21	0.00	0.01	0.00	4.50	98.70

Id	S.G.	Ch	SiO_2	Al_2O_3	Fe_2O_3	FeO	MgO	CaO	Na_2O	K_2O	TiO_2	P_2O_5	MnO	S	Cr_2O_3	CO_2	H_2O	Total
82CLQ								KIONIA 3 (cont.)										
118	2.60	2	53.70	15.40	3.80	7.10	4.15	6.16	3.90	0.05	1.26	0.12	0.14	0.01	0.00	0.00	4.80	100.70
119	2.70	1	52.59	14.69	3.50	6.59	5.59	8.27	3.00	0.27	1.00	0.08	0.16	0.01	0.01	0.10	3.79	99.69
120	2.68	1	54.70	15.00	3.50	6.80	4.62	8.11	3.20	0.20	0.98	0.08	0.16	0.02	0.01	0.10	3.09	100.59
121	2.86	0	47.40	11.30	2.50	8.10	12.80	10.00	1.89	0.25	0.26	0.03	0.25	0.02	0.15	0.10	5.30	100.40
122	2.72	2	52.70	14.50	2.59	7.59	5.75	8.93	2.70	0.10	0.69	0.04	0.20	0.02	0.01	0.10	4.00	100.09
123	2.76	0	54.59	14.00	4.19	6.69	4.24	8.08	2.90	0.12	1.21	0.08	0.15	0.02	0.01	0.00	2.29	98.69
123B		2	51.70	14.19	3.20	8.69	6.33	8.93	2.79	0.08	0.69	0.06	0.21	0.02	0.02	0.10	2.50	99.59
124	2.68	2	54.50	14.50	5.90	6.90	2.81	5.77	2.70	0.06	1.31	0.10	0.10	0.16	0.01	0.00	5.19	100.09
125	2.65	2	59.70	14.70	1.80	5.10	3.42	7.19	3.00	0.07	0.82	0.11	0.13	0.00	0.01	0.10	4.10	100.40
126	2.79	2	51.79	15.39	2.79	7.80	5.77	9.26	2.29	0.05	1.00	0.08	0.16	0.02	0.01	0.10	2.70	99.30
126	2.69	2	46.70	16.60	2.70	11.00	6.50	6.55	3.20	0.08	1.00	0.08	0.17	0.01	0.01	0.00	5.69	100.40
127	2.80	2	49.90	15.19	1.39	6.59	8.75	11.39	1.39	0.20	0.24	0.02	0.20	0.00	0.04	0.20	4.90	100.40
128	2.74	0	53.20	14.69	4.80	7.59	3.81	8.27	1.89	0.06	1.39	0.10	0.16	0.00	0.01	0.00	4.40	100.40
131	2.73	1	52.70	15.50	1.40	6.60	6.10	9.52	2.20	0.14	0.79	0.09	0.17	0.01	0.00	0.00	4.80	100.00
132	2.72	2	53.00	14.69	4.30	8.30	3.45	6.62	3.00	0.06	1.32	0.08	0.16	0.00	0.02	0.00	4.59	99.69
133	2.76	2	53.59	14.39	4.69	7.90	3.51	7.72	2.09	0.05	1.27	0.10	0.16	0.00	0.01	0.00	3.90	99.50
134	2.78		53.50	15.10	4.30	6.80	4.56	9.06	2.29	0.05	1.18	0.08	0.16	0.00	0.01	0.10	3.20	100.50
135	2.67	2	53.40	14.69	2.29	7.69	5.59	7.50	4.00	0.06	0.71	0.05	0.16	0.00	0.03	0.10	2.40	98.69
M82								PROPHITAS ELIAS										
8	2.60	0	51.79	15.19	3.79	5.09	7.38	6.97	4.09	0.16	0.62	0.05	0.20	0.00	0.03	0.00	2.70	98.19
13	2.69	2	53.29	15.60	5.30	6.40	5.38	7.03	2.20	0.28	0.91	0.06	0.20	0.00	0.01	0.00	2.09	98.90
14	2.68	1	55.70	14.80	5.00	6.50	4.50	6.16	3.20	0.38	0.94	0.06	0.16	0.00	0.01	0.10	1.70	99.19
15	2.80	0	53.59	16.10	5.09	5.09	3.56	8.80	4.90	0.08	1.42	0.17	0.20	0.00	0.01	0.00	0.50	99.59
18	2.76	1	51.09	15.80	2.79	6.90	6.91	8.05	3.50	0.60	0.55	0.04	0.20	0.00	0.02	0.00	2.50	99.19
19	2.71	0	52.79	15.19	2.09	7.30	6.38	8.67	2.90	0.20	0.69	0.04	0.23	0.00	0.02	0.00	1.70	98.30
22	2.68	2	54.59	14.60	5.09	6.59	4.09	5.30	4.00	0.08	1.28	0.12	0.16	0.00	0.01	0.10	2.40	98.59
24A	2.60	2	54.59	13.89	8.19	4.40	5.19	4.94	5.09	0.25	0.96	0.06	0.15	0.00	0.01	0.10	2.00	100.00
28	2.76	0	54.40	15.39	2.70	7.69	5.00	5.75	5.19	0.05	0.76	0.06	0.16	0.00	0.01	0.00	1.70	99.00
29		2	55.29	14.39	4.00	6.00	4.75	6.65	3.59	0.31	0.96	0.08	0.16	0.03	0.02	0.10	2.50	98.90
31	2.69	2	54.50	15.10	6.19	5.30	4.37	5.13	4.50	0.21	1.22	0.08	0.13	0.00	0.01	0.00	2.70	99.50
32	2.78	2	54.59	15.00	6.69	6.00	4.12	5.53	4.69	0.06	1.31	0.08	0.19	0.00	0.01	0.00	2.59	100.90
35		2	55.90	13.69	5.40	6.00	3.51	5.06	4.40	0.04	1.28	0.10	0.17	0.03	0.01	0.10	2.59	98.40
37	2.69	2	59.20	14.00	5.80	4.59	3.12	4.37	4.90	0.28	0.85	0.08	0.12	0.00	0.01	0.00	1.20	98.59
38		1	50.79	14.60	1.60	6.90	8.57	9.62	2.40	0.80	0.41	0.01	0.23	0.03	0.03	0.10	3.50	99.59
39		2	53.90	15.10	6.80	5.50	4.02	5.68	4.30	0.19	1.38	0.12	0.19	0.03	0.01	0.00	3.00	100.30
40		1	53.59	15.00	6.69	6.30	4.06	5.80	3.09	0.20	1.42	0.12	0.17	0.03	0.01	0.00	3.29	99.69
41		2	54.29	15.00	7.40	5.09	3.85	5.06	4.69	0.12	1.35	0.10	0.15	0.03	0.01	0.00	3.40	100.59
42		0	51.00	15.00	1.60	7.09	8.67	10.50	1.50	0.62	0.43	0.03	0.27	0.05	0.03	0.10	2.59	99.59
46	2.67	0	51.70	15.19	3.90	6.19	7.11	6.15	3.70	0.66	0.49	0.04	0.17	0.00	0.02	0.00	2.50	98.00
49	2.60	2	52.40	15.30	9.10	4.40	4.03	3.51	5.80	0.06	1.35	0.10	0.16	0.00	0.02	0.00	2.79	99.09
50	2.75	1	51.79	15.80	3.50	5.40	7.19	8.47	3.40	0.28	0.42	0.02	0.17	0.00	0.01	0.00	2.29	98.90
53	2.56	0	55.70	14.69	4.00	5.00	4.62	5.90	4.90	0.44	0.94	0.08	0.13	0.00	0.02	0.00	1.50	98.00
54	2.76	2	51.50	16.39	4.09	5.50	6.87	7.96	4.90	0.12	0.48	0.03	0.16	0.02	0.01	0.10	2.09	100.30
59	2.64	1	53.70	14.80	6.00	5.69	4.38	6.03	4.19	0.36	1.28	0.08	0.20	0.00	0.01	0.00	1.70	98.59
60			52.59	15.10	7.59	5.09	3.81	4.41	4.80	0.03	1.39	0.10	0.23	0.04	0.01	0.00	4.00	99.19
BL82								KAKOPETRIA										
271	2.63	1	57.40	14.10	5.00	6.10	3.97	3.56	3.70	0.59	1.15	0.10	0.13	0.02	0.00	0.00	4.40	100.30
272	2.53	2	56.80	15.10	4.10	5.60	4.90	2.75	4.30	1.28	0.98	0.11	0.14	0.00	0.00	0.00	4.30	100.40
273	2.65	2	57.50	15.20	4.10	4.70	4.18	4.08	5.90	0.18	1.00	0.10	0.12	0.01	0.00	0.20	2.90	100.20
274	2.66	2	57.00	14.50	4.59	6.19	4.28	4.34	3.70	0.60	0.94	0.08	0.12	0.01	0.01	0.10	3.59	100.00
275	2.63	0	52.90	15.30	1.50	6.59	7.25	5.55	3.50	0.69	0.71	0.06	0.17	0.02	0.01	0.00	4.00	98.30
276	2.59	2	57.40	15.90	3.80	5.50	3.06	4.41	6.70	0.00	1.02	0.12	0.11	0.01	0.00	0.00	2.50	100.50
277	2.59	0	53.20	14.69	1.89	7.50	7.86	4.56	3.20	0.98	0.62	0.05	0.20	0.02	0.01	0.10	4.80	99.69
278	2.61	2	57.40	13.69	4.30	6.30	4.80	3.90	3.50	0.57	0.89	0.06	0.12	0.00	0.01	0.69	3.20	99.50
280	2.61	2	54.60	15.10	3.10	6.90	5.91	4.43	3.30	0.53	0.87	0.07	0.13	0.00	0.00	0.00	5.00	100.00
281	2.75	0	51.70	15.69	1.60	6.19	8.64	8.86	2.70	0.66	0.44	0.04	0.17	0.00	0.03	0.10	3.59	100.40
283	2.67	2	56.50	14.10	4.19	6.50	4.00	4.75	3.79	0.35	0.91	0.06	0.13	0.00	0.00	0.10	3.50	99.00
284	2.61	2	56.70	13.90	3.50	5.50	3.76	5.60	5.30	0.20	0.94	0.10	0.15	0.01	0.00	1.70	3.00	100.40
285	2.72	0	52.20	14.90	1.60	5.80	9.19	8.73	2.30	0.63	0.42	0.05	0.15	0.03	0.02	0.00	4.70	100.60
286	2.73	2	58.20	14.00	4.00	6.40	4.49	2.79	4.19	0.02	1.09	0.06	0.16	0.00	0.01	0.00	3.59	99.00
287	2.62	0	55.29	14.89	2.79	6.80	5.77	4.18	4.09	0.91	0.85	0.06	0.17	0.00	0.01	0.20	4.30	100.40
288	2.48	0	53.90	16.30	2.90	7.80	4.67	3.22	5.70	0.01	1.02	0.09	0.15	0.05	0.00	0.20	3.70	99.70
289	2.70	1	56.30	15.20	3.20	7.20	4.87	3.93	3.80	0.85	0.90	0.09	0.17	0.04	0.00	0.10	3.80	100.50
290	2.66	2	53.09	15.60	2.09	7.40	6.37	5.58	2.70	1.29	0.69	0.06	0.16	0.01	0.01	0.00	4.30	99.40
291	2.59	1	57.00	13.80	4.20	5.90	4.13	5.25	3.80	0.33	1.01	0.10	0.14	0.03	0.00	0.20	4.30	100.20

Id	S.G.	Ch	SiO_2	Al_2O_3	Fe_2O_3	FeO	MgO	CaO	Na_2O	K_2O	TiO_2	P_2O_5	MnO	S	Cr_2O_3	CO_2	H_2O	Total
BL82								KAKOPETRIA (cont.)										
292	2.66	1	52.80	16.10	1.90	7.00	7.41	6.24	2.80	0.63	0.67	0.07	0.16	0.02	0.01	0.00	4.90	100.70
293	2.66	0	51.90	16.10	1.80	7.30	7.81	6.01	2.90	0.73	0.69	0.08	0.16	0.05	0.01	0.00	4.90	100.50
294	2.62	2	54.40	13.80	3.40	7.30	3.89	6.97	1.29	0.42	0.94	0.08	0.15	0.01	0.01	0.00	5.40	98.09
295	2.58	0	53.59	15.39	2.50	7.50	5.59	4.28	4.00	1.28	0.78	0.06	0.16	0.01	0.01	0.10	3.29	98.69
296	2.62	0	54.40	15.50	2.10	7.40	5.87	5.03	3.70	1.23	0.81	0.06	0.16	0.07	0.00	0.00	4.20	100.60
297	2.62	2	61.20	13.20	3.60	6.60	3.19	3.90	5.10	0.05	1.03	0.10	0.14	0.07	0.00	0.20	2.20	100.60
298	2.69	1	56.59	14.89	3.79	6.50	4.08	4.81	3.59	0.85	0.89	0.06	0.16	0.01	0.01	0.00	2.29	98.50
299	2.60	2	53.59	15.69	2.70	6.80	5.80	5.66	3.79	1.34	0.71	0.05	0.16	0.01	0.01	0.20	3.29	99.80
300	2.67	0	55.29	15.00	3.59	6.50	4.34	4.97	4.19	1.00	0.89	0.08	0.16	0.01	0.01	0.20	2.50	98.90
301	2.66	2	56.30	15.40	3.30	6.70	4.85	4.37	3.50	1.15	0.96	0.10	0.16	0.00	0.00	0.00	3.60	100.40
302	2.78	0	55.90	15.00	5.30	6.40	4.54	5.70	3.30	0.38	1.08	0.10	0.18	0.01	0.00	0.00	2.40	100.30
303	2.49	2	52.90	14.50	3.70	5.90	3.71	9.18	0.00	0.36	1.02	0.10	0.13	0.07	0.00	0.20	8.20	99.90
304	2.86	2	55.70	15.10	4.69	6.30	4.03	7.69	2.50	0.16	1.00	0.08	0.20	0.01	0.02	0.00	1.00	98.50
305	2.81	0	56.29	14.89	5.09	6.00	4.08	7.08	2.90	0.20	1.00	0.08	0.20	0.00	0.01	0.00	1.29	99.19
306	2.62	2	54.80	14.20	4.20	7.10	4.35	5.24	3.20	0.36	1.12	0.08	0.17	0.06	0.00	0.00	4.40	99.30
307	2.63	2	58.50	14.60	4.00	6.19	3.79	2.92	5.19	0.06	1.00	0.08	0.15	0.00	0.01	0.10	2.40	99.09
308	2.74	1	53.10	15.30	1.40	6.50	7.74	7.71	1.80	0.52	0.66	0.07	0.18	0.07	0.01	0.00	3.40	98.50
309	2.77	0	51.80	16.70	2.50	6.30	7.58	8.34	2.40	0.21	0.64	0.09	0.20	0.08	0.02	0.00	3.70	100.60
310	2.57	2	58.70	13.60	3.30	6.90	3.85	4.75	3.00	0.05	1.14	0.11	0.14	0.03	0.00	0.00	3.50	99.10
311	2.75		63.50	14.20	4.70	4.60	1.83	4.68	3.50	0.24	1.10	0.33	0.08	0.03	0.00	0.00	0.90	99.70
312	2.80	0	51.09	15.60	1.50	6.80	8.19	10.30	2.29	0.42	0.47	0.04	0.16	0.00	0.03	0.10	2.90	100.19
313	2.82	2	60.29	14.50	3.70	6.19	2.34	5.75	3.40	0.13	1.43	0.20	0.12	0.43	0.01	0.00	1.00	99.59
314	2.55	0	50.40	14.90	2.40	7.00	5.11	10.20	0.40	0.28	0.73	0.06	0.13	0.04	0.01	0.20	8.50	100.30
315	2.59	2	58.29	14.60	4.30	5.69	3.65	3.48	4.90	0.57	0.98	0.08	0.15	0.00	0.01	0.10	2.00	99.00
316	2.55	0	53.20	16.20	2.20	6.60	6.60	4.55	3.80	1.36	0.73	0.06	0.18	0.06	0.01	0.00	4.50	100.10
317	2.86	0	50.80	15.70	1.80	6.30	9.25	11.30	1.20	0.23	0.55	0.05	0.17	0.07	0.02	0.00	2.90	100.40
318	2.62	1	52.90	15.70	3.70	6.10	6.36	5.05	3.20	0.96	0.81	0.09	0.15	0.05	0.00	0.00	5.30	100.50
319	2.61	2	55.20	15.19	4.09	6.19	5.77	4.18	3.90	1.25	0.78	0.05	0.16	0.00	0.01	0.00	3.20	99.90
320	2.92	0	51.79	15.69	2.09	6.50	7.62	12.50	0.80	0.06	0.46	0.03	0.19	0.00	0.04	0.00	0.60	98.40
321	2.62	2	56.20	14.00	6.20	5.40	4.72	4.28	4.70	0.50	1.09	0.10	0.14	0.00	0.00	0.00	3.60	100.90
322	2.67	1	55.30	15.20	3.10	6.50	5.98	5.15	3.30	0.77	0.79	0.08	0.19	0.00	0.00	0.00	2.50	98.90
323	2.55	2	52.70	14.90	4.10	5.60	6.38	5.06	3.20	0.46	0.83	0.09	0.14	0.09	0.00	0.00	5.00	98.60
324	2.65	1	57.40	13.80	2.09	6.40	5.28	5.15	3.09	1.67	0.71	0.06	0.16	0.00	0.01	0.00	2.09	98.00
325	2.63	2	55.29	14.89	5.40	5.40	4.56	4.31	3.50	1.45	0.92	0.06	0.16	0.00	0.01	0.00	2.70	98.69
326	2.60	1	54.90	14.60	4.00	5.90	5.59	3.99	3.40	1.61	0.80	0.08	0.18	0.00	0.00	0.00	4.50	99.60
327	2.63	2	55.50	13.60	6.90	5.30	4.41	4.78	4.19	0.66	1.10	0.06	0.15	0.00	0.01	0.00	2.59	99.40

Id: Identification, S.G.: Specific Gravity, Ch: chill

TABLE 1B. Trace Element Analyses, Road Cut Section

Id	Rb	Ba	Nb	La	Sr	Zr	Y	V	Cu	Co	Cr	Ni
***BL83**					AYIA KORONI SECTION							
3	2	0	0		100	63	29	310	55	29	12	5
4	3	0	0		37	68	30	410	18	29	8	5
5	3	0	1		120	120	48	80	1	5011	0	5
6	3	0	2		80	64	32	460	64	6035	0	16
7	3	0	0		91	93	46	58	45	15	1	5
8	0	0	0		26	34	17	280	1	29	5	46
18	2	0	1		23	76	35	380	100	6033	0	16
21A	2	0	1		19	68	34	370	110	9031	0	18
22	1	0	0		47	45	23	400	5	26	0	5
24	1	0	2		100	110	51	5	69	14	1	5
25	2	0	0		42	79	39	310	9	27	6	5
28	3	0	4		38	110	52	5	150	15	1	5
29	1	0	0		40	67	33	470	120	40	10	25
30	1	0	0		78	61	29	400	72	31	8	15
31A	0	0	0		36	68	33	370	63	30	7	5
32	0	0	0		25	67	33	390	68	34	10	16
33	1	0	0		47	64	30	420	37	37	9	20
34	2	0	1		40	65	30	510	63	48	9	19
35	1	0	0		38	73	35	380	91	42	5	5
38	3	0	0		110	43	24	470	46	41	7	5
39	2	0	0		96	75	31	340	210	28	6	5
41	3	0	0		100	72	36	360	140	31	6	5
42	0	0	0		29	60	31	340	19	37	5	5
43	0	0	0		74	67	33	400	280	42	5	5
44	0	0	0		27	43	20	320	150	46	9	5
47	0	0	0		17	69	33	390	40	40	7	5
48	2	0	1		77	100	48	130	120	5029	0	5
49	0	0	1		71	90	44	210	1	24	5	5
50	3	0	2		35	110	53	32	48	23	1	5
51	5	0	2		68	30	17	260	84	47	250	44
BL82					PALEKHORI ROAD							
P3B		10		36	83		30	410	82	33	25	33
P3D		16		38	120		23	35	2	4	3	5
P3H		8		33	77		23	230	85	38	320	95
P3F		16		44	110		30	100	26	15	3	11
P110A		8		15	65		10	310	51	20	6	16
P117		15		58	72		50	64	120	25	7	12
P120		34		32	25		26	430	100	29	11	23
BL82					NIKITARI 2							
406		8		15	47		29	450	460	27	17	20
410		17		41	65		29	340	60	29	10	13
411		17		36	78		28	320	110	30	25	24
417		15		15	83		10	220	23	19	19	21
421		55		45	100		24	250	16	31	23	30
423		14		42	69		27	360	2	22	10	13
426		10		41	58		29	370	2	19	10	13
432		15		42	70		33	280	170	28	13	13
435		14		44	74		32	480	2	28	15	19
442		17		43	73		28	370	56	27	9	18
444		15		50	65		33	390	93	28	13	13
446		17		53	64		33	390	2	27	14	18
448		19		54	63		35	430	2	39	15	20
451		14		62	42		37	200	2	34	14	10
452		11		15	66		31	110	130	19	2	5
456		9		15	42		28	400	94	29	10	11
457		37		15	100		20	210	61	26	81	40
BL82					NIKITARI 1							
330		13		15	69		24	290	6	22	7	14
331		19		36	69		31	350	110	34	13	30
335		16		15	68		22	170	3	23	30	30
336		22		34	64		29	150	2	29	45	49
338		13		15	68		26	160	2	21	30	33
BL82					NIKITARI 1 (cont.)							
343		20		15	59		22	350	66	29	9	21
344		16		15	51		31	40	2	3	14	5
346		16		78	66		44	490	20	32	17	29
347		8		50	55		33	180	2	20	30	25
349		11		15	61		28	190	2	12	6	5
352		9		56	29		39	380	510	36	13	20
354		14		32	64		23	420	2	19	11	18
356		30		51	91		26	240	4	40	170	63
358		14		57	73		35	490	2	26	14	25
362		14		48	72		36	390	2	26	12	20
365		15		38	60		24	220	6	22	17	20
366		19		34	65		20	260	2	26	15	18
368		15		15	78		29	97	2	11	3	5
373		24		30	64		22	260	2	25	10	20
376		9		40	42		22	260	87	30	22	21
379		20		58	58		25	260	23	36	110	44
381		8		46	42		37	310	2	26	11	11
385		21		44	79		27	260	2	27	10	20
390		19		41	73		27	220	57	22	7	5
391		12		36	91		24	230	2	20	15	13
393		31		37	97		23	260	4	23	15	21
395		23		15	83		22	350	13	24	10	5
398		13		43	93		28	270	10	22	19	21
400		12		47	64		25	310	180	30	12	18
401		21		34	110		21	200	140	28	22	30
***BL82**					AYIOS THEODHOROS							
210	2	0	0		140	49	27	290	1	29	10	23
211	1	4	2	15	39	85	41	380	2	36	9	17
212	3	24	5	15	120	59	36	270	5	25	11	25
213	1	0	1		63	76	33	390	1	36	5	15
214	3	35	1	55	120	47	26	180	7	32	40	35
215	1	6	1	15	63	75	38	320	11	29	3	15
216	1	0	0		70	69	35	360	4	28	1	5
217	1	0	1		120	82	41	430	1	26	6	19
218	3	27	0	15	68	33	20	250	100	23	110	43
219	4	0	0		150	79	35	410	1	29	8	18
220	0	10	0	15	100	81	39	350	2	19	8	22
221	2	0	1		97	42	22	230	1	29	37	29
222	3	0	0		94	40	19	250	6	34	41	34
224	1	11	3	15	100	83	41	110	2	9	6	5
225	1	5	1	15	43	70	39	440	5	42	9	25
226	1	0	0		110	50	27	300	1	32	11	24
229	1	0	1		88	30	14	230	88	43	370	120
230	7	0	0		130	32	16	280	1	40	18	39
231	3	16	1	15	110	77	36	370	2	22	8	22
232	2	21	0	15	99	83	43	150	2	12	3	5
233	1	9	0	55	51	75	35	440	4	40	9	25
234	4	0	3		110	79	37	150	1	14	9	5
235	5	0	0		100	34	17	240	1	33	28	43
236	2	0	1		140	84	37	380	1	21	6	5
237	2	0	1		68	76	34	400	1	32	5	5
238	5	38	3	56	130	37	23	240	9	29	50	43
239	0	6	0	39	29	36	28	450	62	31	9	20
240	1	7	5	15	79	81	39	290	2	17	3	17
241	9	0	0		140	21	10	210	59	34	93	48
242	1	12	0	15	100	80	41	380	12	18	9	22
243	1	6	0	15	41	76	39	370	10	34	9	25
244	1	0	0		120	84	37	300	3	18	5	5
245	4	0	2		91	36	21	410	72	40	18	18
246	1	8	0	43	29	77	34	360	20	32	9	24
247	3	12	3	36	92	79	41	320	3	24	10	24
248	3	0	1		76	37	24	410	97	34	6	5
249	2	0	0		84	22	15	230	4	43	110	50
250	0	0	0		100	48	24	250	29	35	140	58
251	0	0	0		94	57	29	340	9	38	6	16
252	0	11	2	15	88	38	23	230	6	46	46	50

Id	Rb	Ba	Nb	La	Sr	Zr	Y	V	Cu	Co	Cr	Ni
***BL82**					AYIOS THEODHOROS (cont.)							
253	4	20	5	38	81	120	61	71	3	11	3	11
254	1	16	1	15	120	100	39	190	8	19	3	17
255	3	0	0		130	75	37	410	1	35	6	5
256	2	0	4		92	130	62	5	1	17	1	5
257	1	0	0		88	37	26	240	8	56	100	42
258	7	0	3		110	56	27	370	13	34	7	23
259	3	0	0		44	68	34	400	28	77	10	16
260	2	0	2		70	130	58	5	4	1	1	5
261	3	0	1		52	63	31	340	1	22	1	5
262	5	0	1		99	15	15	290	120	42	44	33
263	4	0	1		93	73	27	330	9	28	12	19
264	1	10	2	15	90	75	38	340	3	33	8	17
265	2	0	1		73	79	36	360	1	33	7	5
266	2	26	0	15	130	63	28	230	3	15	3	17
267	3	0	3		130	91	39	160	1	18	16	5
268	1	7	3	15	70	77	42	200	3	21	3	5
270	3	0	3		93	38	19	340	1	40	7	21
BL82					MAKHERAS MONASTERY							
155		11		42	69		27	290	190	31	33	43
157		12		15	110		10	210	87	22	160	55
158		5		15	29		10	320	2	25	19	24
160		9		15	110		10	220	68	20	26	24
162		12		15	95		10	290	25	25	21	21
164		11		33	77		23	390	2	24	10	21
166		6		15	29		10	210	10	23	28	34
170		28		32	140		10	200	90	32	410	83
171		13		53	100		30	280	44	30	13	23
172		4		15	51		10	480	2	27	15	29
176		12		15	99		10	260	46	30	12	23
178		10		15	140		10	210	79	28	230	70
181		20		15	110		22	240	73	33	300	88
182		15		37	100		28	320	18	35	18	30
187		7		15	43		21	220	22	30	14	25
188		7		15	42		24	270	69	28	9	23
191		10		15	90		21	260	100	27	83	45
192		14		41	100		28	400	4	33	12	25
195		16		33	95		25	400	2	27	7	18
197		6		15	54		10	270	20	26	10	23
199		14		15	92		10	230	120	20	29	25
201		12		37	100		24	280	91	34	71	35
203		17		37	98		32	590	3	39	10	25
205		16		15	100		28	400	6	28	7	25
206		9		15	85		10	200	81	31	490	78
BL82					KIONIA 1							
55		19		41	89		33	410	2	28	11	22
57		17		46	81		35	460	2	29	8	24
59		17		15	77		10	370	170	25	9	22
61		17		15	96		26	460	2	26	9	17
65		4		15	28		10	260	6	19	81	25
66		21		36	79		29	360	12	27	10	24
68		24		33	110		21	370	2	27	10	25
75		31		34	75		10	260	6	28	48	35
77		19		51	79		34	440	2	32	11	24
BL82					KIONIA 2							
83		21		44	92		30	410	2	26	11	25
84		30		38	83		21	270	15	48	220	75
87		10		40	81		34	410	2	31	14	24
89		20		34	120		29	390	6	30	14	24
92		18		46	93		33	380	6	21	27	30
94		50		39	47		21	220	2	41	180	65
96		51		46	51		21	220	2	44	170	65
98		17		15	80		21	280	35	21	6	18
99		4		15	17		26	350	77	25	9	17

Id	Rb	Ba	Nb	La	Sr	Zr	Y	V	Cu	Co	Cr	Ni
BL82					KIONIA 2 (cont.)							
100		19		15	84		21	330	22	21	8	17
105		43		48	28		22	250	2	29	120	45
106		25		31	87		26	380	20	28	14	25
107		39		15	92		26	320	68	27	9	25
110		26		15	92		26	400	10	27	8	25
114		5		15	30		27	360	27	26	8	22
116		22		41	86		31	430	88	31	14	25
117		19		31	87		27	350	10	26	11	24
122		33		15	120		20	220	81	12	5	12
123		27		45	100		28	270	53	18	8	14
127		28		47	65		36	370	32	28	12	24
128		31		35	66		27	370	37	27	11	25
131		7		45	24		34	360	55	32	9	22
132		21		15	84		27	460	3	26	9	22
134		23		15	110		20	420	14	23	7	5
135		15		30	87		10	300	6	26	12	25
136		28		15	100		23	430	2	18	10	13
140		15		15	78		20	260	2	24	11	21
141		18		44	84		27	340	160	32	25	24
142		21		15	100		27	170	110	14	3	5
145		22		38	93		27	350	25	32	27	26
146		25		15	100		27	340	320	22	14	24
148		29		15	96		10	280	2	22	15	22
150		23		15	100		24	370	6	27	8	25
153		30		49	42		10	230	2	42	98	56
***82CLQ**					KIONIA 3							
IV	2		0	10	97	68	33	290	1	33	9	5
V	1	18	1		92	66	33	300	56	31	17	23
III	2	16	0		87	58	26	370	51	29	14	23
I	1	15	0		89	66	33	390	180	31	10	21
1	2		0	10	97	71	34	400	140	39	8	5
2	3		0	10	91	63	32	470	39	40	8	20
3	2	21	1		100	60	29	370	130	35	26	28
4	3	20	0		93	49	22	260	110	31	16	23
4A	3		0	10	100	44	20	290	6	35	6	5
4B	2		0	10	110	43	22	330	170	40	11	19
4C	3		0	10	110	41	20	300	1	36	5	5
4D	1	20	1		100	69	34	410	10	38	10	15
5	1	20	0		92	46	21	280	110	31	18	23
5B	0		0	10	88	65	29	440	140	29	6	5
6	1		1	10	97	85	42	160	60	25	6	5
7	1		1	10	100	63	30	480	18	37	8	5
8	2	18	0		92	56	29	420	90	34	12	16
9	2		0	10	110	41	21	270	15	44	29	34
10	1		0	10	97	54	28	410	36	27	9	5
11	1		2	10	79	61	33	230	1	23	2	5
12	1		0	10	110	39	18	250	4	36	25	26
13	3		1	10	140	49	28	270	7	33	5	5
14	0		0	10	100	34	20	480	1	32	2	5
15	3	25	5		96	82	46	60	4	11		
15I	3	32	3		92	31	23	270	3	38	16	21
16	3	28	0		89	38	27	220	17	38	79	40
17	4		0	10	97	41	24	460	1	30	7	5
18	2		1	10	120	31	22	410	7	28	6	5
19	3	23	2		110	40	25	370	5	21	8	14
20	0	16	0		93	61	31	400	38	29	9	16
21	3	55	0		110	15	11	220	6	33	100	33
22I	4	40	1		130	13	8	220	4	39	170	50
23	1		2	10	47	39	19	250	59	36	58	41
25	2		1	10	190	34	18	290	85	48	460	130
26	2		0	10	84	78	38	410	1	38	9	24
27	1		0	10	52	41	31	450	22	30	5	5
28	2	15	0		94	71	35	370	89	39	14	22
29	2		3	10	100	42	31	330	52	34	8	17
30	0		0	10	58	54	26	330	4	39	25	29
31	3		0	10	120	31	15	250	11	37	49	39
32	2	15	0		120	51	24	260	170	32	18	23

Id	Rb	Ba	Nb	La	Sr	Zr	Y	V	Cu	Co	Cr	Ni
***82CLQ**					KIONIA 3 (cont.)							
33	0	8	0		69	32	32	220	34	34	370	110
34	6	39	0		140	26	12	190	3	33	180	55
35	1		2	10	100	63	33	330	290	37	6	5
36	1		1	10	98	30	18	270	39	37	230	79
37	2		1	10	130	27	17	270	71	40	290	82
39	3	21	1		110	53	24	320	130	47	58	35
40	2	12	1		78	30	16	260	78	38	330	140
41	3	37	0		140	18	13	270	27	32	42	33
42	4	21	2		98	51	25	350	210	53	59	44
44	3	13	2		110	60	35	240	76	26	9	13
45	3	26	1		120	58	31	310	17	23	23	23
48	1	11	1		110	55	31	300	28	22	10	
50	4	38	0	30	110	32	20	330	7	33	14	26
51	?	12	0		89	49	25	300	64	29	54	23
54	3	21	1		87	44	25	330	7	31	13	16
58	3	16	1	32	91	68	35	420	1100	50	14	22
58L	2	12	1		85	72	37	360	26	29	11	20
59	0		0	10	76	77	35	360	46	31	10	16
60	2	10	2		81	68	33	330	36	33	10	16
61	1	14	0	44	95	37	23	400	20	35	15	24
62	2	32	0		220	41	22	260	8	40	27	23
63	2	8	0		64	71	32	400	22	32	13	23
64	2	20	1		110	66	33	190	120	23	9	
65	3	28	1		110	46	22	330		32	9	14
66	3	22	0	33	110	56	29	430		35	14	16
67	2		0	10	110	72	34	210	320	31	7	5
68	3		0	10	130	40	17	300	970	48	16	24
69	2	22	0	30	110	46	24	280		8	11	18
70	1	15	0	36	96	52	24	360	440	38	9	16
71	1		0	10	95	60	30	230	82	30	7	5
72	1	18	0	35	110	59	30	290	6	30	10	11
72A	2	37	0	42	150	43	24	380		35	11	19
72B	3	27	6	31	120	42	19	440	14	28	10	24
73	1	30	0		120	44	23	350		43	11	14
74	0	27	0	35	130	54	28	420	25	37	14	24
76	2	19	0	33	93	71	33	270	51	32	9	
80	0	22	0	35	84	59	30	370	78	34	14	24
81	2		0	10	85	65	30	280	10	28	2	5
82	1		0	10	69	62	31	330	20	30	6	5
84	2	15	2	38	94	46	30	390	5	32	20	24
85	2		3	10	79	67	33	93	1	19	2	5
86	2		1	10	90	45	26	430	1	30	6	5
88	0		0	51	69	56	29	430	1	25	9	5
90	1	22	0	32	110	46	23	310		33	15	24
91	1		1	10	110	36	24	390	1	36	9	16
92	1		1	10	17	71	34	410	6	37	8	15
93	0		0	10	71	69	29	390	31	35	15	26
94	3	10	1	32	76	71	31	400	57	35	23	23
95	2	19	1		97	68	35	390	10	37	11	21
97	3	38	0	50	110	7	7	260		41	300	75
99	2		1	10	110	62	30	450	13	38	8	18
100	3		1	10	100	80	38	270	60	30	2	5
101	1	22	0	35	110	51	26	360	160	34	13	23
103	3	22	1	42	120	48	28	410	14	31	12	16
104	3		3	10	130	51	29	440	1	34	5	5
105	4	29	0	38	130	22	19	260	8	40	150	51
106	2	17	0	30	110	48	26	380	72	32	9	21
107	1		0	10	94	63	31	410	570	65	2	19
108	1	7	0	53	40	67	31	440	20	42	21	28
109	2	22	0	51	110	70	32	450	290	43	13	23
110	2	17	0	50	100	56	28	360	8	36	15	23
111	0	8	0		70	61	28	350		33	13	21
112	0		0	10	69	90	43	230	3	24	2	5
113	1	16	1		94	55	30	260	200	29	7	
114	1		0	10	130	57	28	310	140	31	6	5
115	0	15	0		99	58	27	320	50	32	13	23
116	1		0	10	110	62	29	260	1	29	2	5
117	1		0	10	120	56	27	350	12	29	6	5
118	0		0	10	73	67	34	420	16	34	6	5
***82CLQ**					KIONIA 3 (cont.)							
119	1	22	0	52	120	55	26	330	13	35	27	28
120	0	18	0		120	50	25	310	6	30	7	14
121	3	11	1		62	8	10	200	5	44	1200	200
122	0	17	0	32	110	28	20	300	10	33	28	29
123	1	17	3		110	54	30	450	11	32	13	16
123	3	16	2	32	76	35	37	280	7	38	85	34
124	1	15	0	31	89	80	42	260	270	30	9	13
125	2		3	10	120	73	36	140	170	17	13	5
126	1	16	1	68	87	58	26	350	23	45	24	43
126	0	11	0		72	54	26	280	6	30	21	29
127	1	15	1		73	6		230	6	43	230	76
128	2	14	2	32	100	65	33	460	440	33	13	16
131	2		0	10	120	38	21	280	3	35	8	22
132	0	13	0		89	67	31	370	310	43	11	14
133	1	16	0	35	98	66	30	370		26	10	16
134	2	13	2		99	61	29	330	5	33	12	21
135	1	13	0	33	84	34	19	250	130	40	78	33
***M82**					PROPHITAS ELIAS							
8	1	11	0	40	110	22	17	220	13	28	120	40
13	3	20	2	15	110	38	23	290	28	23	23	24
14	3	35	1	44	110	36	23	420	8	37	21	34
15	0	13	0	15	190	120	40	320	2	19	11	16
18	5	23	2	15	84	18	11	290	5	31	39	44
19	1	26	2	34	140	31	21	310	54	42	100	34
22	2	13	1	15	78	70	35	400	58	34	14	24
24A	2	20	2	38	96	35	23	480	3	22	13	24
28	0	12	0	15	77	30	22	390	380	46	22	34
29	1	21	0	38	120	40	33	340	150	29	34	38
31	2	15	0	15	100	58	29	390	26	27	10	5
32	1	7	0	15	31	61	31	340	35	29	9	21
35	0	7	0	15	66	75	41	320	22	26	6	16
37	2	29	0	31	110	42	29	300	210	30	13	24
38	2	35	0	54	160	12	10	220	2	38	150	61
39	1	13	0	15	94	60	38	380	2	22	9	11
40	1	14	0	39	98	67	30	460	250	32	8	16
41	1	8	0	43	84	66	38	400	280	27	10	21
42	4	35	0	41	94	14	15	210	2	32	170	63
46	2	48	0	33	130	16	11	260	130	40	110	56
49	2	7	2	15	61	67	35	380	280	49	10	21
50	1	27	0	31	160	11	9	270	150	34	26	41
53	0	20	0	15	120	37	27	320	61	25	30	26
54	0	17	0	15	160	16	10	220	290	31	18	29
59	1	17	1	15	110	61	30	420	2	28	12	14
60	1	6	0	15	51	66	39	340	91	23	8	14
***BL82**					KAKOPETRIA							
271	3	0	1		34	52	27	200	1	28	1	5
272	6	0	3		38	48	26	340	1	27	1	5
273	2	0	4		120	52	28	330	1	21	1	5
274	1	8	4	15	67	47	30	310	3	24	5	18
275	2	16	1	15	130	36	23	240	3	28	26	35
276	0	0	3		46	54	32	370	13	23	1	5
277	5	11	4	15	100	28	21	250	3	34	32	41
278	2	7	2	15	56	44	31	250	3	22	3	12
280	4	0	2		98	41	18	360	1	38	7	19
281	6	31	5	33	100	23	17	230	3	35	180	76
283	0	6	4	15	61	46	31	290	3	23	5	14
284	2	0	1		82	47	24	310	4	23	1	5
285	3	0	1		82	20	11	220	1	39	160	72
286	0	4	1	15	23	56	30	160	6	17	3	5
287	3	10	1	15	46	42	26	280	3	27	6	19
288	1	0	2		40	44	23	460	170	31	1	5
289	5	0	3		110	45	21	350	7	38	7	21
290	5	22	2	15	130	33	22	270	3	28	13	22
291	4	0	3		22	55	31	300	1	26	1	5
292	4	0	2		73	32	17	220	1	37	59	43

Id	Rb	Ba	Nb	La	Sr	Zr	Y	V	Cu	Co	Cr	Ni
***BL82**					KAKOPETRIA (cont.)							
293	3	0	2		70	30	15	230	1	39	57	43
294	2	7	2	15	35	44	29	340	16	27	8	21
295	6	11	3	15	110	40	27	260	3	28	6	21
296	5	0	1		120	34	21	320	1	36	6	18
297	1	0	2		50	53	28	320	1	30	1	5
298	2	16	0	15	120	50	28	270	2	23	6	14
299	5	14	4	15	130	37	23	260	38	28	13	21
300	2	22	4	46	140	46	30	380	2	36	13	31
301	5	0	2		120	43	24	330	1	33	6	5
302	3	0	2		92	42	18	440	12	30	6	5
303	3	0	2		14	45	25	360	3	30	1	5
304	1	17	1	15	100	47	22	390	17	27	11	21
305	2	16	1	15	100	46	28	350	56	27	9	21
306	2	0	2		63	39	21	480	1	30	5	5
307	1	7	0	33	61	60	34	250	2	27	8	18
308	4	0	3		92	31	15	220	15	35	110	65
309	2	0	1		78	29	21	280	23	40	76	47
310	0	0	1		23	56	30	310	3	25	1	5
311	3	0	1		110	140	64	5	72	20	1	5
312	3	16	1	15	220	25	15	190	14	34	190	76
313	3	18	0	15	110	120	50	120	1000	28	8	13
314	1	0	0		18	33	19	290	1	33	6	21
315	2	11	1	15	100	49	27	310	110	23	8	17
316	7	0	3		130	29	17	270	1	36	11	25
317	3	0	0		77	23	9	220	44	39	100	65
318	4	0	1		120	33	18	310	1	34	13	23
319	5	16	0	15	140	33	18	300	2	28	8	21
320	0	10	0	15	59	14	9	230	33	35	170	69
321	3	0	0		110	39	21	520	1	35	7	5
322	3	0	2		110	39	22	290	1	34	7	18
323	4	0	0		32	40	22	340	34	39	7	26
324	7	16	2	15	130	36	20	240	2	26	5	21
325	5	16	0	34	130	41	25	350	6	32	11	21
326	7	0	1		140	36	20	320	1	32	6	15
327	3	13	0	15	100	42	24	470	2	31	10	21

*denotes Sr, Y, Zr analyses by xrf

TABLE 1C. Major Element Analyses, CY-4 Drill Hole

Depth	SiO_2	Al_2O_3	Fe_2O_3	FeO	MgO	CaO	Na_2O	K_2O	TiO_2	P_2O_5	MnO	S	Cr_2O_3	CO_2	H_2O	Total
8.08	56.50	14.00	5.09	5.69	3.76	7.40	3.00	0.10	1.04	0.10	0.10	0.01	0.01	0.00	3.00	99.69
12.20	57.00	14.30	4.19	5.50	3.93	8.12	2.40	0.19	1.07	0.08	0.12	0.00	0.01	0.00	2.90	99.90
15.00	53.40	15.60	3.50	5.40	5.94	10.60	0.69	0.12	0.67	0.04	0.15	0.00	0.01	0.00	2.50	98.50
17.20	53.59	16.00	3.70	5.59	6.00	10.69	1.29	0.10	0.73	0.04	0.13	0.00	0.01	0.00	2.29	100.19
22.50	51.90	16.00	2.79	5.69	6.15	8.80	2.59	0.23	0.71	0.04	0.15	0.00	0.01	0.00	3.40	98.50
23.90	55.40	15.39	4.50	5.69	3.79	7.53	3.09	0.15	1.09	0.08	0.13	0.00	0.01	0.00	3.09	100.09
27.10	56.59	14.80	4.80	5.59	3.68	8.22	2.40	0.04	1.07	0.10	0.12	0.00	0.01	0.00	2.09	99.59
32.25	54.40	15.19	5.80	6.09	4.52	7.19	2.59	0.13	1.36	0.06	0.23	0.00	0.01	0.00	2.09	99.80
34.75	55.00	14.89	4.30	6.50	4.65	8.18	2.29	0.25	1.20	0.10	0.15	0.00	0.01	0.00	2.50	100.00
42.40	52.40	14.89	3.09	5.50	7.68	9.66	1.39	0.19	0.47	0.02	0.20	0.00	0.05	0.10	2.90	98.59
43.55	54.79	15.00	5.00	5.00	6.15	8.83	1.20	0.08	0.62	0.03	0.16	0.00	0.03	0.10	2.20	99.30
47.20	52.79	14.89	4.19	4.80	8.61	9.43	1.50	0.02	0.48	0.05	0.15	0.00	0.05	0.10	3.29	100.40
49.05	50.29	15.00	4.00	5.59	9.37	8.69	1.39	0.19	0.39	0.03	0.13	0.00	0.04	0.10	4.30	99.50
53.65	52.00	15.30	2.29	5.90	7.12	10.00	1.89	0.24	0.62	0.05	0.16	0.00	0.03	0.10	3.09	99.00
55.40	53.90	14.80	2.40	5.50	7.09	9.74	1.79	0.23	0.67	0.05	0.13	0.00	0.03	0.10	2.70	99.19
55.90	53.90	15.10	3.29	4.80	6.52	8.20	3.50	0.16	0.76	0.06	0.12	0.00	0.01	0.00	2.90	99.40
57.95	50.70	15.80	3.09	6.19	7.59	10.50	2.40	0.28	0.62	0.05	0.15	0.00	0.02	0.10	2.70	100.19
61.65	60.20	14.39	5.09	4.59	2.79	6.41	3.50	0.16	1.04	0.12	0.08	0.00	0.01	0.00	1.79	100.30
62.70	59.09	14.80	4.69	4.69	2.59	6.02	4.00	0.27	1.10	0.08	0.08	0.00	0.01	0.00	2.40	99.90
64.55	53.70	15.60	3.20	5.40	5.49	7.62	3.90	0.31	0.89	0.06	0.12	0.00	0.01	0.10	3.50	100.09
72.00	56.40	14.19	4.90	5.00	4.58	4.96	4.30	0.33	1.00	0.10	0.10	0.00	0.01	0.10	3.00	99.00
77.35	56.40	14.39	4.90	4.40	4.50	5.75	4.00	0.33	1.25	0.10	0.08	0.00	0.01	0.10	2.79	99.09
78.80	50.70	15.50	3.29	5.19	7.52	9.69	2.20	0.47	0.57	0.04	0.12	0.00	0.04	0.30	3.20	98.90
102.30	68.80	13.30	4.00	2.40	1.02	2.42	4.90	0.17	0.55	0.12	0.05	0.00	0.01	0.00	1.20	99.00
104.55	51.20	14.80	3.50	7.09	6.02	9.13	2.00	0.08	1.10	0.05	0.21	0.03	0.01	0.10	3.20	98.69
107.90	54.70	15.50	4.00	7.00	4.63	7.37	2.79	0.05	1.02	0.06	0.17	0.25	0.00	0.00	2.40	100.00
118.05	54.09	14.80	3.20	8.19	4.31	8.07	2.59	0.12	1.32	0.10	0.23	0.33	0.01	0.00	2.00	99.50
120.55	53.70	14.69	4.09	7.69	4.43	7.16	2.40	0.12	1.35	0.08	0.21	0.16	0.01	0.10	2.20	98.50
126.20	72.59	12.19	4.09	2.29	0.78	2.45	4.50	0.19	0.51	0.10	0.04	0.02	0.00	0.00	1.00	100.80
128.15	70.50	13.30	4.09	2.50	0.78	3.78	3.70	0.16	0.53	0.08	0.03	0.04	0.01	0.10	0.80	100.50
130.30	52.29	16.39	5.19	5.50	5.25	7.75	3.79	0.21	0.69	0.03	0.15	0.02	0.01	0.20	2.90	100.40
133.05	55.50	15.60	5.59	5.69	4.43	7.59	3.00	0.15	1.03	0.06	0.15	0.00	0.01	0.00	2.00	100.90
136.60	56.00	14.60	5.19	6.69	4.43	7.08	2.59	0.21	1.17	0.08	0.16	0.00	0.02	0.00	2.00	100.40
138.80	57.50	14.00	3.90	6.59	4.80	7.53	2.50	0.20	1.11	0.06	0.16	0.00	0.01	0.00	2.00	100.40
141.70	52.00	15.30	4.19	6.80	6.37	7.21	3.40	0.15	1.14	0.08	0.20	0.00	0.01	0.00	3.50	100.40
144.30	51.09	15.39	4.00	7.30	6.43	8.56	2.40	0.13	1.15	0.06	0.20	0.00	0.02	0.00	3.20	100.00
150.80	54.00	14.89	4.69	7.00	4.77	6.62	3.09	0.20	1.38	0.08	0.17	0.00	0.01	0.00	2.79	99.80
156.70	55.40	14.80	4.59	6.80	3.90	8.12	3.09	0.23	1.32	0.10	0.10	0.00	0.01	0.00	1.70	100.30
157.25	54.50	14.60	3.59	7.50	4.72	8.55	2.59	0.26	1.13	0.06	0.15	0.01	0.01	0.00	2.40	100.19
157.90	53.70	13.60	1.79	7.50	6.90	9.04	2.79	0.48	0.80	0.06	0.16	0.01	0.04	0.00	2.70	99.69
162.40	50.79	15.89	3.00	7.90	6.00	9.18	3.09	0.06	1.15	0.08	0.19	0.02	0.02	0.00	2.20	99.69
165.30	53.29	15.69	3.20	7.19	5.59	9.80	2.29	0.10	1.07	0.06	0.19	0.00	0.02	0.00	1.89	100.50
167.65	54.79	14.60	4.69	7.09	4.02	7.81	2.50	0.12	1.31	0.08	0.16	0.00	0.02	0.00	1.79	99.09
176.65	53.09	15.10	3.90	7.19	5.05	9.07	1.89	0.08	1.21	0.08	0.16	0.01	0.00	0.00	1.60	98.59
178.85	53.50	15.10	3.79	7.40	5.19	9.14	2.00	0.10	1.22	0.06	0.16	0.00	0.01	0.00	1.70	99.50
182.00	53.90	15.10	4.09	7.00	5.06	9.01	1.89	0.06	1.20	0.08	0.16	0.01	0.01	0.00	1.70	99.30
185.50	53.79	15.10	3.50	7.69	4.75	9.10	2.29	0.08	1.24	0.06	0.20	0.19	0.02	0.00	1.39	99.50
193.60	50.59	16.20	1.60	6.00	7.37	10.60	2.29	0.21	0.71	0.05	0.13	0.00	0.04	0.00	2.79	98.69
196.90	54.79	15.19	3.29	6.80	5.88	8.87	2.70	0.06	0.64	0.04	0.17	0.02	0.02	0.00	1.79	100.40
201.35	54.00	15.00	3.59	6.19	7.03	8.80	2.09	0.16	0.62	0.04	0.13	0.00	0.03	0.00	2.29	100.09
204.55	54.90	15.00	3.59	6.59	6.08	8.85	2.50	0.06	0.67	0.06	0.17	0.01	0.03	0.00	1.70	100.19
210.35	52.90	16.60	2.59	6.09	5.93	8.56	3.29	0.16	0.53	0.04	0.16	0.00	0.01	0.00	3.00	99.90
213.90	54.50	15.39	2.59	6.50	6.30	9.33	1.79	0.10	0.51	0.02	0.17	0.01	0.01	0.00	2.09	99.30
214.95	57.20	15.10	4.69	5.59	4.43	7.62	2.50	0.15	0.80	0.04	0.12	0.01	0.01	0.00	2.00	100.30
217.85	54.29	15.60	2.79	6.19	6.43	9.67	2.29	0.10	0.53	0.04	0.16	0.01	0.02	0.00	2.29	100.40
221.25	56.90	14.19	5.30	6.80	3.59	6.46	2.90	0.13	1.03	0.10	0.16	0.01	0.01	0.00	2.00	99.80
226.20	53.79	14.89	2.50	7.69	6.36	8.32	2.59	0.08	0.64	0.04	0.19	0.02	0.03	0.00	2.40	99.59
228.70	70.59	12.89	4.09	2.20	0.96	4.12	3.40	0.16	0.53	0.08	0.04	0.01	0.01	0.00	1.00	100.19
234.50	52.20	15.10	4.40	7.40	5.63	8.37	2.29	0.16	1.25	0.06	0.15	0.01	0.02	0.00	3.20	100.30
236.82	53.00	15.00	4.40	7.09	5.30	9.35	1.70	0.10	1.27	0.10	0.16	0.01	0.01	0.00	2.00	99.50
241.26	54.70	15.00	4.19	7.30	5.09	9.31	1.89	0.06	1.24	0.08	0.20	0.01	0.01	0.00	1.50	100.69
245.50	62.70	14.39	5.19	4.30	2.46	5.97	3.29	0.15	0.78	0.06	0.06	0.00	0.01	0.00	1.20	100.69
249.73	61.90	13.69	6.19	5.09	1.99	6.71	2.29	0.20	1.00	0.16	0.08	0.01	0.00	0.00	1.00	100.40
253.66	57.09	14.60	5.59	6.00	3.73	8.83	1.79	0.10	1.10	0.08	0.13	0.01	0.01	0.00	1.29	100.50
262.42	52.59	16.39	1.70	7.19	7.21	10.30	1.89	0.08	0.46	0.02	0.19	0.01	0.02	0.00	2.29	100.40
266.61	54.20	15.19	5.40	6.30	4.58	9.45	2.00	0.08	1.35	0.08	0.15	0.01	0.01	0.00	1.60	100.50
270.63	54.70	15.00	4.69	7.09	4.53	8.95	2.20	0.08	1.34	0.08	0.16	0.01	0.01	0.00	1.70	100.69
273.44	56.00	15.39	2.59	6.80	5.31	10.39	0.89	0.10	0.67	0.04	0.16	0.02	0.01	0.00	1.60	100.00
277.58	55.29	15.19	6.09	5.80	3.79	8.06	2.29	0.08	1.28	0.12	0.12	0.01	0.01	0.00	1.29	99.50
278.10	49.90	15.80	2.00	7.09	9.16	12.89	0.69	0.12	0.62	0.05	0.20	0.00	0.06	0.00	1.79	100.50

Depth	SiO_2	Al_2O_3	Fe_2O_3	FeO	MgO	CaO	Na_2O	K_2O	TiO_2	P_2O_5	MnO	S	Cr_2O_3	CO_2	H_2O	Total
281.32	55.20	15.19	5.69	4.80	5.97	9.93	1.20	0.06	0.62	0.03	0.19	0.00	0.03	0.00	0.69	99.69
287.92	56.09	15.19	5.09	5.50	4.74	9.18	1.60	0.08	0.89	0.04	0.20	0.01	0.02	0.00	1.20	99.80
295.50	55.09	16.50	1.79	7.00	5.91	10.30	1.50	0.12	0.62	0.03	0.15	0.03	0.01	0.00	1.50	100.59
300.62	58.59	15.00	2.90	7.30	2.92	7.40	2.59	0.10	1.32	0.20	0.10	0.03	0.01	0.00	1.70	100.19
301.00	51.00	15.30	3.00	7.40	5.94	10.19	2.09	0.10	1.14	0.08	0.20	0.00	0.02	0.00	1.89	98.50
307.00	57.50	15.60	3.59	6.40	4.30	9.18	2.00	0.08	0.67	0.04	0.17	0.05	0.01	0.00	1.10	100.69
313.01	52.79	15.60	1.79	6.30	7.69	11.39	1.10	0.10	0.46	0.02	0.17	0.00	0.05	0.00	1.60	99.19
317.52	55.29	14.89	3.00	6.19	6.27	10.50	1.20	0.10	0.64	0.03	0.17	0.00	0.05	0.00	1.50	100.00
321.66	52.79	15.30	3.40	6.90	6.12	10.19	1.70	0.08	1.09	0.06	0.19	0.02	0.01	0.00	1.70	99.59
331.02	63.00	14.00	4.50	4.50	2.18	6.28	2.70	0.16	0.91	0.10	0.10	0.00	0.01	0.00	0.89	99.40
331.86	56.50	14.89	5.09	5.69	3.70	8.27	2.00	0.08	1.03	0.08	0.13	0.00	0.01	0.00	1.00	98.59
336.25	60.20	14.69	4.30	5.40	2.67	7.18	2.29	0.12	1.06	0.08	0.15	0.00	0.01	0.00	0.89	99.00
338.10	57.59	15.39	4.19	5.69	3.32	8.51	2.09	0.19	1.10	0.08	0.12	0.00	0.01	0.00	1.00	99.40
341.81	55.70	14.89	4.50	5.90	4.18	9.38	2.00	0.06	0.98	0.06	0.10	0.01	0.01	0.00	0.89	98.69
346.42	53.50	15.10	2.79	7.19	5.68	10.30	1.60	0.06	1.04	0.06	0.19	0.01	0.02	0.00	1.50	99.19
353.95	54.00	16.00	2.50	7.19	5.49	9.62	2.79	0.06	1.03	0.08	0.16	0.05	0.01	0.00	1.60	100.59
358.64	53.00	15.80	2.79	7.59	5.63	10.60	1.50	0.06	1.13	0.06	0.20	0.02	0.02	0.00	1.20	99.69
365.44	52.20	15.10	3.29	7.59	5.68	10.69	1.60	0.05	1.17	0.06	0.20	0.00	0.02	0.00	1.20	98.80
368.50	57.20	14.89	4.09	6.30	3.59	8.60	2.00	0.06	0.87	0.06	0.16	0.00	0.01	0.00	1.20	99.19
372.62	52.59	15.19	2.59	7.59	5.96	10.60	1.79	0.06	1.03	0.06	0.20	0.01	0.02	0.00	1.50	99.40
373.30	57.20	14.89	4.59	6.50	3.34	8.39	2.09	0.06	0.87	0.06	0.19	0.00	0.01	0.00	1.10	99.30
377.36	55.70	15.10	3.59	8.39	3.64	8.43	2.50	0.00	1.34	0.13	0.19	0.03	0.01	0.00	1.10	100.09
381.50	58.29	15.10	5.19	5.40	2.65	8.32	3.00	0.01	1.15	0.19	0.06	0.00	0.01	0.00	1.20	100.69
383.65	54.50	15.89	3.09	5.90	4.62	10.30	2.00	0.08	1.03	0.06	0.10	0.00	0.02	0.00	1.70	99.30
390.10	52.70	15.39	2.50	7.50	5.86	9.50	2.20	0.04	1.10	0.08	0.17	0.01	0.02	0.00	1.89	99.09
392.60	55.40	14.60	4.30	7.40	3.89	8.62	2.00	0.06	1.39	0.08	0.20	0.00	0.01	0.00	1.60	99.69
396.00	55.70	14.89	4.40	7.50	3.76	8.62	2.00	0.01	1.35	0.10	0.20	0.00	0.01	0.00	1.10	99.80
398.30	52.40	15.69	3.09	7.30	5.87	10.30	2.29	0.10	1.13	0.08	0.20	0.00	0.02	0.00	1.60	100.19
400.90	53.29	14.89	2.79	7.50	5.55	10.10	1.79	0.08	1.10	0.08	0.19	0.00	0.02	0.00	1.60	99.00
404.90	54.70	15.00	4.30	7.69	3.78	8.73	2.09	0.08	1.38	0.08	0.19	0.01	0.02	0.00	1.39	99.50
407.40	52.20	15.69	2.79	7.59	6.11	10.89	1.89	0.08	1.11	0.08	0.20	0.03	0.02	0.00	1.60	100.40
408.60	51.90	14.69	3.09	7.40	6.40	10.10	1.70	0.06	1.11	0.06	0.20	0.04	0.02	0.00	2.70	99.59
411.85	53.20	14.80	6.50	5.59	4.03	8.20	2.20	0.10	1.40	0.10	0.17	0.01	0.01	0.00	2.90	99.19
413.25	56.40	15.00	4.90	6.80	3.56	8.68	2.00	0.08	1.34	0.10	0.17	0.08	0.01	0.00	1.20	100.30
416.50	57.20	14.50	5.50	5.00	3.75	8.75	2.70	0.06	0.98	0.06	0.06	0.10	0.01	0.00	1.70	100.50
419.80	52.50	15.69	2.70	6.00	6.93	11.30	1.20	0.08	0.76	0.06	0.16	0.00	0.03	0.00	2.00	99.59
423.80	56.00	14.69	4.09	7.40	3.54	7.50	2.50	0.06	1.31	0.08	0.15	0.50	0.01	0.00	1.79	99.69
425.60	52.09	15.30	2.59	6.30	7.03	11.10	1.10	0.08	0.80	0.03	0.17	0.01	0.03	0.00	2.59	99.40
429.95	59.70	14.50	5.40	4.59	2.93	7.87	2.79	0.08	1.11	0.16	0.06	0.00	0.01	0.00	1.39	100.69
435.70	55.09	14.39	4.40	7.40	3.78	8.00	2.20	0.08	1.36	0.10	0.19	0.00	0.01	0.00	1.89	99.00
439.20	55.40	14.60	4.90	6.40	3.70	8.64	2.70	0.10	1.11	0.08	0.12	0.00	0.01	0.00	1.79	99.69
441.75	51.70	15.60	2.20	6.40	7.87	12.10	1.10	0.03	0.71	0.06	0.16	0.00	0.04	0.10	1.70	99.80
447.20	53.00	15.10	1.89	6.90	7.49	10.89	1.29	0.12	0.50	0.02	0.20	0.00	0.06	0.00	2.29	99.80
450.60	56.29	14.50	4.59	7.00	3.48	8.33	1.79	0.08	1.29	0.08	0.20	0.00	0.01	0.00	1.10	98.80
453.90	55.79	14.89	4.69	7.19	3.65	8.62	2.00	0.08	1.35	0.08	0.20	0.00	0.01	0.00	1.00	99.69
456.90	56.09	14.60	4.59	7.19	3.71	8.36	1.89	0.10	1.32	0.10	0.19	0.00	0.01	0.00	1.29	99.59
460.70	52.00	15.89	2.29	5.59	7.72	11.30	1.70	0.06	0.60	0.04	0.16	0.00	0.03	0.00	1.89	99.40
463.40	52.40	15.89	2.09	6.19	8.30	11.10	1.60	0.06	0.41	0.04	0.17	0.00	0.03	0.00	2.20	100.59
466.05	52.50	15.89	1.60	6.19	7.34	11.00	1.39	0.12	0.48	0.03	0.16	0.00	0.02	0.00	2.20	98.90
470.00	53.40	15.89	2.40	5.90	6.15	11.30	1.39	0.12	0.76	0.06	0.10	0.00	0.02	0.00	1.60	99.30
472.05	51.70	15.69	2.40	6.50	7.96	12.10	1.00	0.04	0.71	0.05	0.17	0.00	0.03	0.00	1.70	100.00
473.45	51.00	14.89	3.00	6.80	7.18	10.39	1.79	0.13	0.92	0.04	0.19	0.01	0.02	0.00	2.50	98.90
478.10	57.09	14.60	4.90	5.19	3.93	8.37	2.09	0.06	0.98	0.08	0.10	0.03	0.01	0.00	1.50	99.09
481.85	55.00	15.10	4.50	5.19	4.33	8.85	2.59	0.15	0.92	0.08	0.10	0.02	0.01	0.00	1.70	98.59
485.00	53.59	15.60	2.00	5.59	6.27	10.80	2.00	0.06	0.73	0.06	0.10	0.32	0.01	0.00	1.60	98.69
488.70	58.20	14.19	5.69	4.30	3.03	9.20	1.89	0.12	1.03	0.08	0.06	0.00	0.01	0.10	1.20	99.09
491.05	58.09	14.80	5.69	4.40	3.18	9.25	2.00	0.19	1.10	0.06	0.06	0.00	0.08	0.10	1.20	100.30
493.10	58.00	14.30	6.00	4.40	3.25	9.57	1.39	0.10	1.09	0.06	0.06	0.00	0.01	0.00	1.00	99.19
497.90	53.00	16.10	4.19	5.40	6.19	11.10	1.60	0.08	0.80	0.06	0.12	0.00	0.01	0.00	1.29	100.00
501.35	57.59	15.50	2.59	4.19	4.68	10.19	2.40	0.10	0.94	0.08	0.06	0.00	0.02	0.00	1.39	99.80
507.15	52.40	16.00	2.79	5.59	7.02	12.10	1.39	0.08	0.71	0.06	0.16	0.01	0.03	0.00	1.50	99.90
510.95	52.70	15.30	0.89	4.19	7.05	14.80	1.89	0.17	0.69	0.04	0.08	0.00	0.02	0.10	1.29	99.30
514.35	51.79	15.60	2.20	6.09	7.13	10.80	1.89	0.10	0.69	0.05	0.16	0.00	0.03	0.00	2.29	98.80
515.30	56.50	14.80	5.09	6.09	4.03	8.82	1.89	0.08	0.94	0.06	0.16	0.00	0.01	0.00	1.29	99.90
516.20	55.00	15.60	5.09	6.09	4.47	9.18	2.40	0.08	0.96	0.06	0.15	0.00	0.01	0.00	1.10	100.30
520.15	61.79	13.80	4.19	5.30	2.28	6.86	2.09	0.08	0.85	0.08	0.15	0.00	0.01	0.00	1.00	98.50
529.05	47.40	16.50	5.80	5.19	7.59	6.34	3.70	0.33	1.10	0.10	0.12	0.00	0.01	0.30	5.19	99.69
529.80	57.00	15.00	2.20	3.50	5.02	9.12	4.19	0.12	0.89	0.08	0.06	0.00	0.01	0.20	2.59	100.19
530.78	54.59	15.30	5.09	5.30	4.59	9.73	1.60	0.10	0.82	0.05	0.08	0.00	0.01	0.00	1.70	99.00
533.18	54.59	15.30	4.19	5.69	5.38	9.91	1.50	0.08	0.62	0.03	0.16	0.00	0.01	0.00	1.39	99.00
536.75	51.09	15.60	3.20	6.69	6.77	11.39	2.20	0.05	0.49	0.04	0.12	0.00	0.02	0.00	2.00	99.69

Depth	SiO_2	Al_2O_3	Fe_2O_3	FeO	MgO	CaO	Na_2O	K_2O	TiO_2	P_2O_5	MnO	S	Cr_2O_3	CO_2	H_2O	Total
539.10	54.59	15.69	4.19	5.40	5.53	10.39	1.20	0.13	0.67	0.06	0.10	0.00	0.01	0.00	1.29	99.40
542.15	57.70	14.69	4.19	4.69	3.85	9.10	2.00	0.24	1.14	0.10	0.06	0.00	0.01	0.00	1.60	99.50
545.30	57.70	15.10	3.90	5.30	3.87	9.57	2.29	0.06	1.14	0.10	0.08	0.00	0.01	0.10	1.39	100.69
548.80	54.50	15.50	2.70	6.59	6.65	10.50	1.10	0.05	0.47	0.03	0.16	0.01	0.03	0.00	1.50	99.80
550.80	54.59	15.00	1.79	6.80	7.77	10.60	0.89	0.02	0.42	0.03	0.17	0.02	0.04	0.00	1.70	100.00
553.80	56.79	16.29	4.69	3.90	2.48	10.69	1.29	0.10	0.96	0.12	0.08	0.00	0.01	0.00	1.20	98.59
555.90	52.40	15.10	3.00	6.00	6.78	10.89	1.50	0.06	0.80	0.06	0.17	0.00	0.04	0.00	2.09	99.00
557.70	63.20	14.10	3.90	3.59	2.20	7.81	1.79	0.06	0.89	0.10	0.06	0.02	0.01	0.00	1.10	98.90
559.70	53.50	16.60	4.69	4.80	5.13	10.50	1.50	0.12	0.78	0.04	0.12	0.02	0.01	0.00	1.50	99.50
563.20	53.20	15.69	2.09	6.80	7.71	10.19	1.79	0.06	0.43	0.04	0.20	0.00	0.03	0.00	2.29	100.69
565.75	51.20	15.19	4.59	5.69	6.12	10.39	1.89	0.10	1.14	0.06	0.16	0.00	0.02	0.00	2.79	99.40
570.00	50.59	15.19	3.20	5.50	8.01	9.31	2.59	0.15	0.64	0.05	0.15	0.00	0.02	0.10	3.40	99.00
571.40	62.20	14.19	4.80	4.40	2.45	8.29	1.60	0.08	0.85	0.08	0.06	0.00	0.01	0.00	0.89	100.09
575.90	60.50	16.79	5.30	3.29	1.27	7.69	2.09	0.25	0.78	0.00	0.04	0.00	0.01	0.00	1.10	99.30
577.30	57.40	14.80	4.40	5.09	3.87	9.23	2.09	0.06	1.11	0.10	0.06	0.00	0.01	0.00	1.20	99.50
580.10	51.59	15.80	2.70	6.80	6.90	10.80	1.39	0.13	0.98	0.05	0.16	0.05	0.02	0.00	2.29	99.80
581.80	54.70	15.89	3.20	5.80	5.11	9.92	1.70	0.10	0.75	0.06	0.20	0.00	0.01	0.00	1.50	99.00
585.70	57.59	14.89	5.30	5.19	3.06	5.49	4.40	0.06	0.96	0.10	0.15	0.01	0.02	0.00	2.20	99.59
591.85	55.20	15.89	6.00	4.50	2.89	4.99	5.50	0.12	0.98	0.08	0.12	0.00	0.01	0.00	3.09	99.40
594.70	55.20	15.00	5.90	4.59	2.89	5.80	4.30	0.10	0.96	0.08	0.08	0.00	0.00	0.00	3.79	99.00
596.05	53.90	15.69	6.30	5.19	3.32	5.25	5.69	0.06	1.00	0.10	0.10	0.00	0.01	0.00	3.40	100.19
599.70	52.40	15.10	6.09	5.59	4.25	7.61	3.29	0.20	1.14	0.06	0.10	0.00	0.01	0.00	3.50	99.40
603.70	50.90	15.60	2.29	5.09	7.77	10.60	1.89	0.16	0.58	0.03	0.13	0.00	0.04	0.00	3.50	98.69
606.30	49.00	15.60	2.20	5.30	8.06	12.30	1.60	0.10	0.60	0.05	0.12	0.00	0.04	0.00	3.59	98.59
608.10	52.50	15.60	2.29	5.19	7.24	11.10	1.79	0.13	0.60	0.04	0.13	0.04	0.04	0.00	2.40	99.19
609.30	59.70	14.30	4.59	4.50	3.67	8.69	1.79	0.16	0.87	0.06	0.12	0.00	0.01	0.10	1.70	100.30
612.94	49.79	15.39	1.60	5.90	8.62	11.10	2.29	0.16	0.51	0.04	0.13	0.06	0.06	0.00	3.50	99.09
615.10	50.00	16.60	1.60	5.40	9.20	12.39	0.60	0.10	0.25	0.00	0.13	0.00	0.02	0.00	3.09	99.50
617.65	52.40	16.29	1.60	5.00	8.25	12.30	0.60	0.08	0.24	0.02	0.15	0.00	0.03	0.00	2.29	99.30
618.85	50.29	15.80	1.70	6.09	9.56	9.55	2.20	0.66	0.23	0.00	0.16	0.00	0.06	0.00	4.50	100.90
623.50	52.79	15.80	3.00	5.50	7.40	11.80	0.40	0.10	0.50	0.03	0.16	0.00	0.02	0.00	1.60	99.19
625.95	52.09	15.19	1.10	6.80	8.85	12.39	0.50	0.13	0.33	0.01	0.16	0.00	0.05	0.00	2.09	99.90

TABLE 1D. Trace Element Analyses, CY-4 Drill Hole

Depth	Rb	Th	U	Ba	Nb	Sr	Zr	Y	Yb	V	Cu	Co	Cr	Ni
8.08	1	2	0	20	0	120	56	30	1	330	33	26	8	8
12.20	2	1	2	19	0	110	52	26	1	310	15	26	8	8
15.00	1	3	5	15	2	120	29	20	2	240	20	31	25	28
17.20	0	2	2	17	0	94	27	18	1	220	15	27	20	19
22.50	2	6	0	20	1	120	28	22	2	220	15	26	18	18
23.90	2	3	1	21	0	110	57	28	1	320	35	26	8	8
27.10	1	3	2	18	1	110	57	29	1	320	15	24	8	8
32.25	3	3	4	17	2	100	50	29	1	360	86	27	11	8
34.75	2	3	3	21	0	98	48	26	2	380	100	33	12	8
42.40	3	3	1	20	2	85	18	13	1	240	2500	34	260	70
43.55	0	0	1	18	0	74	18	15	1	270	1900	33	120	34
47.20	1	1	1	15	0	81	18	13	1	220	92	28	250	52
49.05	0	2	2	16	0	72	9	10	1	210	15	30	190	43
53.65	0	1	2	19	1	100	32	18	1	180	30	25	110	34
55.40	1	4	4	16	1	99	31	18	1	200	15	26	140	37
55.90	3	6	4	16	3	120	40	24	1	220	15	22	7	16
57.95	2	1	1	14	0	110	26	16	1	240	15	31	94	31
61.65	2	7	2	18	2	180	62	31	1	110	15	12	2	8
62.70	2	2	5	21	2	220	60	33	1	110	15	8	2	8
64.55	2	6	5	20	1	170	43	25	1	260	15	22	5	8
72.00	3	4	4	18	1	85	64	31	1	280	15	5025	0	8
77.35	3	3	5	19	2	120	57	32	2	160	15	22	1	8
78.80	1	1	1	30	0	88	19	13	1	260	15	32	13	43
102.30	2	5	4	33	2	88	88	51	4	13	15	5011	0	8
104.55	1	4	2	19	1	110	49	26	1	340	61	39	2	25
107.90	0	0	3	21	0	110	35	20	1	380	360	32	9	8
118.05	1	5	3	20	1	100	70	35	1	390	680	37	12	5
120.55	1	5	3	20	2	110	71	32	1	390	560	36	12	8
126.20	2	5	6	22	1	88	84	43	4	13	15	4	2	8
128.15	0	4	3	23	2	110	86	45	4	13	260	10	7	8
130.30	1	4	0	28	0	250	23	18	1	260	15	30	2	22
133.05	2	4	1	21	0	110	42	26	1	430	15	39	1	21
136.60	1	2	0	17	0	100	43	23	1	420	15	39	1	18
138.80	1	1	1	16	1	95	43	22	1	350	15	38	1	18
141.70	1	3	2	18	0	100	55	26	2	340	15	44	2	29
144.30	1	3	0	18	0	120	52	25	1	370	15	43	2	29
150.80	2	0	3	18	0	110	69	31	1	390	15	35	1	8
156.70	2	5	0	18	0	140	72	31	2	410	15	36	1	20
157.25	1	1	0	20	0	130	47	23	1	380	78	35	2	26
157.90	2	2	0	27	0	110	40	20	2	300	15	47	22	64
162.40	2	4	7	19	2	93	59	31	1	370	78	49	2	31
165.30	1	5	3	17	0	110	55	26	2	330	130	41	2	25
167.65	1	2	0	19	1	120	65	33	2	410	69	39	1	20
176.65	1	2	3	18	1	110	64	30	1	410	49	42	16	19
178.85	1	0	0	17	0	100	60	26	1	390	33	40	16	19
182.00	1	6	4	19	1	120	65	32	1	380	76	41	17	18
185.50	2	4	5	20	1	100	71	34	1	420	610	42	16	18
193.60	1	2	1	15	0	130	39	18	2	240	77	37	150	58
196.90	0	0	0	21	0	78	19	14	1	350	1100	39	110	42
201.35	0	2	0	19	0	86	17	11	1	320	15	41	160	53
204.55	1	2	4	22	2	83	20	17	1	330	170	40	92	47
210.35	0	0	2	18	0	95	19	13	2	280	48	39	19	32
213.90	1	4	2	16	1	78	19	13	1	280	200	36	47	32
214.95	0	3	0	18	0	110	25	16	1	390	42	33	17	16
217.85	2	5	0	16	0	99	18	13	1	280	15	32	82	37
221.25	2	3	3	22	0	160	52	32	1	390	15	31	9	8
226.20	1	3	1	18	0	84	19	13	1	330	15	42	170	63
228.70	3	7	5	18	3	120	86	47	4	13	33	12	9	8
234.50	0	3	0	19	0	170	60	28	1	380	15	42	16	19
236.82	2	5	7	17	2	120	65	34	1	360	15	36	15	16
241.26	1	3	4	19	1	100	64	31	1	380	110	40	16	17
245.50	2	2	0	23	0	110	49	30	1	100	15	21	11	8
249.73	3	5	3	17	3	120	57	27	1	45	15	20	9	8
253.66	0	2	3	19	1	97	44	25	1	380	15	37	9	8
262.42	1	0	0	15	1	73	12	11	1	270	15	39	61	41
266.61	1	3	5	16	1	120	64	34	1	400	15	40	13	18
270.63	1	1	1	16	1	120	66	31	1	400	36	38	13	8
273.44	1	2	1	16	1	79	29	16	1	290	31	33	20	20
277.58	3	7	2	18	2	110	61	31	1	290	30	25	11	8
278.10	2	7	1	18	1	71	29	16	1	230	310	48	350	89

Depth	Rb	Th	U	Ba	Nb	Sr	Zr	Y	Yb	V	Cu	Co	Cr	Ni
281.32	0	4	0	22	0	120	72	33	1	150	35	22	9	8
287.92	1	2	3	16	3	73	33	19	1	270	230	39	22	22
295.50	1	5	2	17	2	75	34	22	1	330	300	35	16	20
300.62	0	0	0	17	0	65	19	13	1	300	1700	39	83	36
301.00	1	9	1	17	1	88	56	29	1	350	440	41	48	34
307.00	2	0	2	20	2	74	28	21	1	260	530	33	13	8
313.01	2	4	3	32	3	72	18	14	1	240	86	38	260	64
317.52	1	4	0	18	0	76	16	13	1	310	15	35	97	43
321.66	1	2	1	16	1	84	52	26	1	330	770	42	37	30
331.02	2	3	1	20	2	110	66	37	3	84	65	22	13	8
331.86	2	4	4	23	2	100	47	27	2	320	180	37	18	19
336.25	1	3	2	22	1	110	59	32	2	220	15	28	10	8
338.10	0	1	1	20	0	110	51	26	2	350	15	30	11	17
341.81	0	3	0	23	0	110	41	23	2	380	15	34	20	22
346.42	0	7	5	16	0	92	53	28	2	290	590	36	39	29
353.95	1	7	1	15	1	90	59	27	2	270	860	35	39	26
358.64	0	2	2	14	0	89	51	27	1	310	1100	41	34	31
365.44	0	1	2	15	0	95	49	24	2	330	260	41	29	32
368.50	1	1	0	25	0	89	28	18	1	300	15	32	12	8
372.62	1	4	5	18	0	93	49	27	1	320	810	45	72	43
373.30	3	2	1	25	0	84	30	21	1	300	15	36	11	8
377.36	2	1	0	21	0	97	75	37	2	370	550	38	15	21
381.50	0	4	0	21	0	150	58	33	2	85	44	23	11	8
383.65	0	0	0	20	0	100	33	19	2	280	40	25	20	22
390.10	1	1	0	15	0	100	54	23	1	300	820	35	33	28
392.60	3	6	2	17	0	93	68	32	2	390	37	35	13	18
396.00	2	3	1	19	0	97	70	32	2	390	120	40	17	20
398.30	1	3	6	15	0	110	54	28	2	310	130	41	31	30
400.90	1	4	2	18	0	98	61	30	3	320	780	44	34	34
404.90	1	0	2	17	0	87	67	31	2	400	280	42	16	21
407.40	0	4	7	16	0	85	53	26	2	320	840	40	40	33
408.60	0	0	2	18	0	150	50	23	1	320	850	33	43	30
411.85	2	4	2	15	1	100	71	37	3	400	2100	35	11	23
413.25	1	3	2	17	1	100	70	36	2	370	420	34	14	8
416.50	0	0	0	18	0	110	52	26	2	350	110	21	11	8
419.80	0	3	1	15	0	82	38	20	2	250	300	38	100	54
423.80	2	6	4	16	2	110	77	36	2	360	2100	33	12	15
425.60	0	0	2	14	0	87	38	19	2	280	1300	39	110	54
429.95	3	9	6	19	4	130	57	36	2	100	45	21	11	8
435.70	0	3	0	21	1	150	68	31	2	400	360	37	12	17
439.20	1	0	0	21	0	150	44	23	1	380	15	28	9	8
441.75	2	7	5	19	2	94	36	18	2	240	760	39	220	73
447.20	0	0	2	29	0	74	17	13	1	230	40	37	300	58
450.60	2	4	3	16	2	96	76	38	1	310	710	25	12	8
453.90	1	3	2	17	1	100	69	34	2	360	700	32	16	15
456.90	0	3	0	16	0	110	67	34	1	330	1800	26	11	8
460.70	2	1	2	17	1	100	34	16	2	200	570	32	170	59
463.40	1	2	1	17	2	92	15	10	2	220	20	35	110	50
466.05	1	2	0	20	0	86	23	14	2	200	380	34	79	52
470.00	0	4	2	15	0	100	34	18	2	260	31	32	23	25
472.05	0	0	0	14	0	66	29	14	1	240	660	33	150	53
473.45	1	2	3	14	0	76	42	20	1	320	1400	43	79	54
478.10	0	3	0	18	0	120	40	22	1	370	46	34	10	20
481.85	0	2	0	17	0	120	38	22	1	370	130	40	11	22
485.00	2	5	2	17	0	100	35	20	1	320	220	44	26	40
488.70	0	4	2	14	0	140	41	25	1	270	33	25	8	8
491.05	1	2	0	16	0	120	43	24	1	280	33	32	9	16
493.10	1	1	5	14	1	130	44	25	1	290	20	32	10	8
497.90	2	2	4	17	0	93	40	21	1	300	20	41	30	39
501.35	2	2	1	16	2	130	42	25	3	280	37	31	15	30
507.15	3	3	0	13	0	85	38	16	2	260	770	41	140	66
510.95	1	1	7	14	2	110	36	19	2	330	38	27	86	45
514.35	2	2	3	19	0	86	37	17	1	260	350	40	140	65
515.30	2	6	2	18	2	95	47	28	1	380	20	39	16	27
516.20	3	5	4	15	3	90	38	23	1	420	20	39	21	30
520.15	0	2	1	25	0	86	46	32	1	530	33	25	11	8
529.05	4	6	3	20	0	140	44	29	1	570	20	28	14	28
529.80	3	8	7	16	4	120	50	32	3	320	38	25	8	20
530.78	1	6	1	15	0	110	27	20	1	320	20	31	13	23
533.18	1	1	3	18	2	83	23	16	1	320	410	39	67	41
536.75	2	2	6	15	1	95	10	11	1	370	150	49	34	39

Depth	Rb	Th	U	Ba	Nb	Sr	Zr	Y	Yb	V	Cu	Co	Cr	Ni
539.10	1	4	2	14	1	100	31	18	1	340	20	39	24	39
542.15	1	3	2	15	1	120	47	28	1	390	20	33	10	22
545.30	1	7	3	15	3	120	47	28	1	380	20	29	13	19
548.80	1	2	3	13	1	65	15	12	1	280	1300	37	110	46
550.80	1	1	2	14	2	59	15	11	1	240	1800	38	190	64
553.80	0	5	1	13	0	180	59	33	2	290	76	18	5	8
555.90	1	0	0	13	0	95	42	22	1	280	2200	41	160	61
557.70	1	4	4	15	2	120	63	37	2	120	54	21	7	8
559.70	3	4	0	19	1	120	31	16	1	400	47	38	10	26
563.20	0	0	1	14	0	64	14	10	1	270	20	41	170	62
565.75	3	7	4	16	0	110	52	27	1	360	150	41	52	48
570.00	2	4	3	16	1	100	34	18	1	250	57	41	61	63
571.40	1	1	3	16	1	120	43	30	2	150	20	26	13	8
575.90	2	3	2	17	1	180	24	5	1	490	40	17	8	17
577.30	0	1	0	16	0	110	47	25	1	370	20	31	11	21
580.10	1	3	3	14	1	79	43	22	1	330	990	48	85	50
581.80	0	7	5	18	1	84	31	21	1	300	20	35	56	38
585.70	2	4	1	18	1	91	46	32	1	150	98	25	8	8
591.85	1	6	2	20	2	230	47	33	1	160	20	22	6	8
594.70	0	11	2	47	1	700	44	34	1	180	20	28	8	8
596.05	0	0	2	18	1	78	41	29	2	210	20	22	3	8
599.70	3	1	2	19	3	180	50	30	2	370	33	27	5	8
603.70	1	5	1	34	0	230	29	14	2	230	350	34	180	68
606.30	2	1	1	12	0	130	37	17	2	240	54	38	220	81
608.10	1	2	1	16	1	110	35	17	2	210	740	32	200	70
609.30	3	1	0	14	1	120	35	24	2	210	72	25	6	8
612.94	4	4	3	19	0	100	30	14	2	200	1000	37	310	93
615.10	0	5	3	19	0	210	6	4	2	190	410	36	110	68
617.65	2	4	1	18	2	82	11	6	2	170	2300	31	150	69
618.85	4	4	5	21	1	110	8	7	1	180	180	38	360	75
623.50	0	0	0	12	0	54	12	7	2	280	520	33	89	54
625.95	0	0	1	12	0	50	8	6	2	190	740	33	310	76

TABLE 2. Instrumental Neutron Activation Analyses

Field No.	Ce	Nd	Sm	Eu	Gd	Tb	Tm	Yb	Th	Ta	Hf	Ce/Yb
BL82-57	9.21	8.89	3.05	1.19		.87		4.03	.23			2.29
BL82-65	4.89	4.88	1.90	.77		.57		2.68	.21	.06		1.82
BL82-66	7.89	8.05	2.71	1.04	3.72	.82		3.69	.32	.10		2.14
BL82-68	6.95	6.31	2.11	.93	3.29	.66	.40	3.17	.30			2.19
BL82-83	7.42	7.17	2.56	1.01	3.76	.77		3.57	.29			2.08
BL82-92	7.44	6.76	2.40	.99		.73		3.41	.30	.15		2.18
BL82-94	2.03	1.90	.65	.33	.72	.25	.17	1.33		.08	.42	1.53
Bl82-100	8.84	8.79	2.93	1.13	4.53	.86	.50	3.80	.31			2.33
BL82-105	1.29	1.11	.47	.20	.99	.21	.16	1.46	.15	.04		.88
BL82-136	7.73	7.27	2.39	1.04	3.35	.73		3.00				2.57
BL82-142	10.39	9.92	3.24	1.30	4.96	.94		4.05	.34	.09		2.57
BL82-153	1.80	1.23	.64	.28		.19		1.07	.17	.06		1.68
BL82-157	4.39	3.95	1.43	.63	2.33	.43	.26	1.92	.22	.05		2.29
BL82-162	6.77	6.73	2.20	.95	3.64	.68	.42	2.99	.27			2.26
BL82-170	1.56	.94		.23	.73	.21	.16	1.16		.04		1.35
BL82-172	6.40	6.32	2.15	.92	3.35	.69	.41	2.87	.29			2.23
BL82-176			2.02	.74	2.70	.56		2.42	.27		1.27	
BL82-178	3.94	4.07		.63	3.31	.44		1.98	.19			1.99
BL82-191	4.46	4.56		.77	3.54	.55		2.57	.16			1.73
BL82-195	6.41	6.01		.84	3.94	.66		2.91	.27			2.20
BL82-206	1.25	1.17		.22	1.14	.19		1.19	.18	.03		1.05
BL82-211	8.38	8.63		.96	5.56	.90		3.73	.30	.09		2.25
BL82-214	5.62	5.53		.71	3.11	.56		2.51	.26	.07		2.24
BL82-215	8.08	8.45		1.00	4.48	.83		3.35	.28			2.41
BL82-232	9.10	8.59		1.02	4.75	.95		4.13	.37	.13		2.21
BL82-246	9.30	9.29		1.17	4.68	.89		3.72	.38	.13		2.50
BL82-253	12.83	12.96		1.19	6.32	1.21		5.09	.43			2.52
BL82-264		8.51		1.16	4.70	.87		3.54	.30	.10		
BL82-274	5.40	4.96		.77	2.73	.59		2.59	.26			2.08
BL82-281	2.39	2.14		.41	1.45	.30		1.31		.02		1.83
BL82-290	4.28	4.01		.59	2.08	.46		2.07	.19			2.07
BL82-295	3.98	3.56		.49	1.86	.40		1.75	.21			2.27
BL82-298	5.96	6.05		.84	3.26	.66		2.88	.33	.10		2.07
BL82-304	5.65	5.15		.78	3.15	.58		2.45	.27	.09		2.31
BL82-305	6.70	5.64	.18	.89	2.98	.60	.43	2.68	.27	.08	1.73	2.50
BL82-324	5.00	3.91	.13	.70	2.01	.45	.38	2.20	.25	.06	1.29	2.27
BL82-325	5.48	3.96	6.66	.70	2.40	.52	.41	2.44	.30	.05	1.22	2.25
BL82-346	9.12	7.94	.23	1.05	3.52	.73	.54	3.16	.33	.08	2.29	2.89
BL82-352	7.95	8.16	.27	1.08	4.37	.81	.58	3.31	.31	.07	1.74	2.40
BL82-366	5.25	5.29	.20	.75	2.94	.58	.42	2.45	.25	.07	1.50	2.15
BL82-376	2.43	3.09	.14	.54	1.90	.38	.33	1.92	.13		.79	1.27
BL82-379	2.65	3.53	.11	.59	2.14	.41	.33	1.91	.22	.04	.90	1.39
BL82-393	6.64	6.20	.13	.91	3.91	.67	.49	2.78	.34	.06	1.76	2.39
BL82-398	5.08	5.57	.39	.71	2.97	.56	.41	2.34	.23	.05	1.44	2.17
BL82-406	10.45	10.07	.51	1.06	4.56	.84	.62	3.24	.30		1.95	3.22
BL82-411	9.32	9.36	1.05	1.25	4.10	.85	.59	3.32	.25	.08	2.23	2.81
BL82-421	5.54	4.88	.61	.74	2.61	.54	.41	2.17	.25		1.28	2.55
BL82-426	8.59	8.11	.48	.98	4.66	.84	.61	3.47	.33	.11	2.06	2.47
BL82-432	9.93	9.43	.42	1.24	4.99	.92	.64	3.68	.38	.11	2.40	2.70
BL82-442	7.35	6.99	1.45	.97	3.49	.68	.52	2.87	.34	.07	1.81	2.56

TABLE 3. Representative Mineral Analyses

(A) Pyroxenes

Field No. BL82	105[1]	105	157	170	206	229	320[2]	320	65[1]	65	176[1]	176	199[1]	199	417	128	304
Average of n	3	3	3	3	3	3	3	6	3	3	3	3	3	3	3	3	3
SiO_2	53.38	51.70	53.29	53.29	54.09	52.46	53.40	51.90	51.20	49.84	53.09	51.31	52.15	51.53	52.01	49.07	53.30
Al_2O_3	1.78	2.16	2.57	3.07	2.20	3.20	1.58	1.30	2.88	3.34	2.64	3.30	3.01	3.80	3.29	3.04	.97
FeO	5.99	10.03	6.34	5.54	4.86	5.27	7.95	10.08	10.16	12.00	6.67	12.27	8.05	9.09	8.25	16.06	11.26
MgO	19.15	16.41	18.10	18.69	19.89	17.87	16.54	14.32	16.37	15.58	17.22	14.77	16.60	15.55	16.57	14.11	14.10
CaO	18.73	19.34	19.43	18.93	18.57	20.19	20.31	21.08	18.52	17.79	19.91	18.22	19.71	19.67	19.03	16.66	20.07
Na_2O	.09	.03	.15	.08	.09	.16	.18	.33	.24	.24	.17	.20	.22	.23	.19	.00	.24
K_2O	.05	.05	.00	.00	.02	.00	.01	.05	.04	.02	.01	.01	.01	.01	.02	.05	.01
TiO_2	.01	.28	.17	.10	.06	.15	.10	.28	.31	.43	.17	.34	.29	.36	.31	.60	.19
MnO	.12	.23	.18	.19	.16	.16	.19	.31	.25	.30	.18	.31	.24	.26	.23	.39	.52
Cr_2O_3	.24	.11	.25	.57	.72	.45	.19	.07	.32	.10	.12	.04	.12	.10	.05	.08	.00
Si	1.952	1.920	1.936	1.928	1.945	1.914	1.960	1.952	1.901	1.879	1.940	1.906	1.914	1.897	1.916	1.873	1.985
Al	.077	.094	.110	.131	.093	.138	.068	.058	.126	.148	.114	.145	.130	.165	.143	.137	.043
Fe	.183	.311	.193	.168	.146	.161	.244	.317	.316	.378	.204	.381	.247	.280	.254	.513	.351
Mg	1.044	.909	.980	1.008	1.066	.972	.905	.803	.906	.875	.938	.818	.908	.853	.910	.803	.783
Ca	.734	.769	.756	.734	.716	.789	.799	.849	.737	.719	.779	.725	.775	.776	.751	.681	.801
Na	.006	.002	.011	.005	.006	.012	.013	.024	.017	.018	.012	.14	.015	.016	.014	.000	.017
K	.002	.002	.000	.000	.001	.000	.000	.002	.002	.001	.000	.000	.000	.000	.001	.002	.000
Ti	.000	.008	.005	.003	.002	.004	.003	.008	.009	.012	.005	.010	.008	.010	.009	.017	.003
Mn	.004	.007	.006	.006	.005	.005	.006	.010	.008	.010	.006	.010	.008	.008	.007	.013	.017
Cr	.007	.003	.007	.016	.020	.013	.006	.002	.009	.003	.003	.001	.004	.003	.001	.002	.000
Sum	4.010	4.026	4.003	3.999	4.000	4.002	4.003	4.025	4.032	4.043	4.001	4.009	4.010	4.009	4.005	4.041	3.999
Fe	9.34	15.65	10.28	9.08	7.81	8.61	12.79	16.02	16.11	19.18	10.90	20.22	13.16	15.02	13.58	25.67	18.85
Mg	53.24	45.67	50.65	52.61	55.15	50.44	46.32	40.58	46.27	44.39	48.64	42.30	46.85	44.50	47.35	40.20	40.11
Ca	37.42	38.68	39.07	38.31	37.04	40.94	40.89	42.90	37.62	36.43	40.43	37.49	39.99	40.48	39.07	34.13	41.03
No. depleted suite criteria	3	3	3	3	3	3	3	3	2	2	2	2	1	1	1	0	0

[1]Phenocrysts, [2]Xenocrysts

(B) Plagioclase

Field No. BL82	96 Core	96 Rim	229[2]	229	320[2]	320	199	304
Average of n	3	3	3	3	3	3	3	3
SiO_2	46.55	49.61	55.33	52.11	46.33	50.35	53.29	54.43
Al_2O_3	33.67	31.48	27.84	28.78	33.64	31.27	29.24	28.88
FeO	.56	.60	.43	1.24	.54	.89	.70	.64
MgO	—	—	.18	.47	.19	.10	.08	.08
CaO	17.58	14.72	10.52	13.38	17.73	14.60	12.47	11.70
Na_2O	1.72	3.07	3.71	3.67	1.19	3.06	4.45	4.85
K_2O	.11	.07	1.69	.05	.02	.07	.03	.04
Total	100.19	99.54	99.72	99.77	99.87	100.38	100.36	100.68
Formula on basis of 8 oxygens								
Si	2.150	2.285	2.510	2.384	2.139	2.294	2.412	2.447
Al	1.833	1.709	1.487	1.553	1.831	1.679	1.559	1.531
Fe	—	—	.016	.048	.021	.034	.027	.024
Mg	—	—	.010	.032	.013	.001	.006	.005
Ca	.858	.726	.510	.656	.887	.713	.605	.564
Na	.154	.274	.326	.325	.107	.027	.391	.423
K	.006	.004	.010	.003	.000	.000	.002	.002
Sum.	5.001	4.998	4.869	5.030	4.988	4.748	5.003	4.998
An	84.4	72.3	54.67	76.34	89.17	72.22	60.66	56.99
Ab	14.9	27.3	34.88	23.31	10.73	27.36	39.18	42.78
Or	.6	.4	10.45	.35	.10	.43	.16	.23
No. depleted suite criteria	3	3	3	3	3	3	1	0

(C) Chromite

	206
MgO	13.74
FeO	12.86
Cr_2O_3	57.78
Fe_2O_3	4.30
Al_2O_3	10.93
TiO_2	.16
V_2O_5	.21
Total	99.98
Mg	1.317
Fe++	.692
Cr	2.937
Fe+++	.208
Al	.828
Ti	.008
V	.010
Sum	6.000
	3

[2]Xenocrysts

Some Dyke-Gabbro Relationships in the Troodos Ophiolite, Cyprus

C.J. STILLMAN

Department of Geology, Trinity College, Dublin, Ireland

Stillman, C.J., Some dyke-gabbro relationships in the Troodos Ophiolite, Cyprus; in *Cyprus Crustal Study Project: Initial Report, Hole CY-4, ed. I.L. Gibson, J. Malpas, P.T. Robinson and C. Xenophontos*; *Geological Survey of Canada, Paper 88-9, p. 107-113, 1989.*

Abstract

This study derives from a brief field-mapping survey made in 1983 to support the petrographic and geochemical logging of core from drill hole CY-4. Two areas were examined: the first south and east of Agros, about 6.5 km west of CCSP Hole CY-4, where the passage from sheeted dykes to underlying gabbros is well exposed, the second, east of Kato and Pano Amiandos, and 8.5 km west of Agros, where deeper layered gabbros are seen. The form and nature of the dyke-gabbro interface and the geometric relationship of the dykes to the gabbro layering were shown to be consistent with a model of magma emplacement in a cluster of small discrete plutons, which fed dykes through dilational fissures related to the roofs of the plutons. The sheeted dyke complex does not appear to be emplaced from a single narrow fissure, but from a large number of such fissures each of limited length and related to specific small magma chambers. Whole-rock chemical analysis of a limited number of samples indicates that the magma parental to the dykes and probably the gabbros is of a supra-subduction zone origin, mostly of early island arc tholeiite affinity, though some may be of a boninitic character.

Résumé

Cette réflexion découle d'un levé cartographique rapide effectué en 1983 dans le but d'appuyer les descriptions pétrographiques de carottes et les études géochimiques du forage CY-4. Deux régions ont été revisées: la première, au sud et à l'est d'Agros, à quelques 6.5 km à l'ouest du trou CY-4, est localisée là où la zone de transition entre les dykes du complexe filonien et les gabbros sous-jacents est bien exposée, et la seconde, à l'est de Kato et Pano Amiandos, à quelques 8.5 km à l'ouest d'Agros, couvre la zone des gabbros lités du niveau stratigraphique sous-jacent. La forme et la nature de l'interface dykes-gabbros ainsi que la relation géométrique entre les dykes et les gabbros lités s'accordent avec un modèle d'emplacement magmatique. de petits plutons alimentés par des dykes injectés dans des fractures de tension localisées au toit des plutons. Le complexe filonien ne semble pas s'être formé à partir d'une simple fissure étroite mais plutôt à partir d'un grand nombre d'ouvertures, chacune d'extension longitudinale limitée et rattachée à plusieurs chambres magmatiques propres. Les analyses chimiques sur roches totales d'un nombre limité d'échantillons, indiquent que le magma parent des dykes et probablement des gabbros s'est probablement formé dans un environnement au-dessus d'une zone de subduction ce qui explique l'affinité tholéiitique d'arc prédominante et même le caractère boninitique plus rare des échantillons.

INTRODUCTION

This study derives from a brief field mapping survey made in 1983 to support the petrographic and geochemical logging of core from drill hole CY-4, which is sited in the dyke swarm approximately 0.5 km south of Palekhori. The survey was based on the detailed 2 inches to 1 mile maps published by the Geological Survey of Cyprus to accompany Memoir 1 (Wilson and Ingham, 1959) and Memoir 7 (Bear, 1960).

The core from hole CY-4 demonstrates a down-hole passage from sheeted dykes to gabbros and continues down through the gabbro body. This apparently crystallized with an isotropic gabbro at the top, the upper parts of which are fine grained and doleritic in texture and are cut by abundant thin veins of granitoid material. Below this level, mineralogical layering is associated with cumulates which become progressively more mafic towards the base.

A noteworthy feature is the relationship between the dykes and the gabbros which they cut and chill against, especially the geometric relationship between the attitude of the layering and the azimuth of the dykes. The angle between these is acute, seldom more than 45°. This type of relationship is not unknown in ophiolite gabbros, and is well described by Rothery (1983), who believes that in the Oman ophiolite the near parallelism of dykes and layering reflects originally steep or vertical layering in the plutonic rocks. The implications of Rothery's model have a bearing on the size, shape and sequential formation of gabbro magma chambers at spreading ridge axes and their relationships with an overlying sheeted dyke swarm.

To test the applicability of Rothery's model to the Troodos complex, mapping was carried out by the author in two areas adjacent to the site of hole CY-4. These were selected to investigate the gabbros at two different levels, one at the dyke-gabbro interface and another at a level at which layering was more continuously developed. The passage from sheeted dykes, forming the upper levels of CY-4, to underlying gabbros is well exposed in the valleys around Agros and the neighboring village, Ayios Ioannis (see Figure 1b). Here, as in CY-4, the upper gabbros, show relatively little layering and grade downward from microgabbro to medium-grained, isotropic gabbro. The layering is best seen beneath this zone, in gabbros extending down to the cumulus-rich ultramafic rocks. This can be seen in the region west of CY-4 in the vicinity of Kato and Pano Amiandos (see Figure 1a).

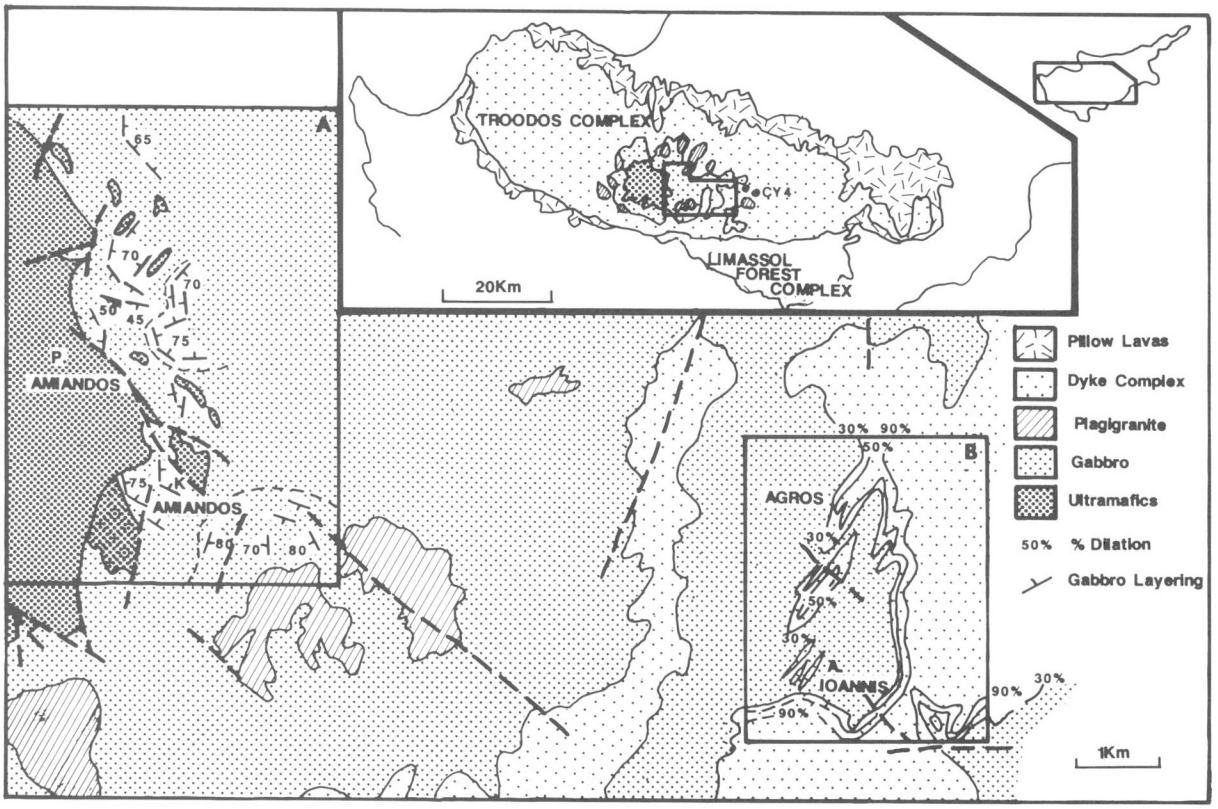

Figure 1: Outline geological map of Amiandos-Agros area of the Troodos Massif (after the 2 inches to 1 mile geological maps published with Memoirs Nos. 1 and 7 of the Geological Survey of Cyprus) modified with added detail by the author in two areas: A - an area around Pano and Kato Amiandos; B - an area around Agros. Inset geological sketch map of the Troodos Complex generalized after Gass (1980).

GEOMETRY OF THE DYKE-GABBRO JUNCTION

The junction between gabbro and dykes in the region east and south of Agros (Figure 1b) is far from planar. Defined by mapping the relative proportions of dykes and gabbro host rocks, and determining the percent dilation from the formula of Speight et al's (1982) formula:

%dilation = (total thickness of dykes in measured section divided by component length of the section) x 100

the sheeted dyke swarm in general passes downward with reduced number of dykes and percent dilation from 100% to less than 30% over a vertical distance of from 250 to 500 m. However, in a number of narrow zones which extend in a NE-SW direction, dyke swarms penetrate the gabbros to a much greater depth. Dyke distribution in these zones shows a Gaussian intensity profile, a distribution which suggests growth by the addition of dykes randomly about the swarm axis (Walker, 1986). The swarms achieve a dilation of 100% in the axial region and are commonly sheeted with one-sided chills. Each zone clearly demonstrates multiple emplacement from a single injection zone, a mechanism which is supposedly characteristic for the entire growth of ophiolitic sheeted dyke swarms (Cann, 1974; Kidd, 1977). However, the dyke distribution in the Agros pluton clearly indicates a number of such injection zones. Such a pattern of repeated multiple injection building up a major sheeted dyke complex is very reminiscent of that recently described by the author from the Fuerteventura (Canary Islands) basal complex (Stillman, 1987). Here the dykes were emplaced by multiple injection into a large number of parallel fissures, none of which are more than a few kilometers long. Each fissure seems to have acted as a conduit for several successive phases of intrusion. This whole process continued for at least 36 M.a. although most of the dykes were emplaced over a shorter interval of around 10 M.a. The implication here is that the dykes were emplaced in a large number of fissures developed within a linear extensional stress zone in the crust; not from a single fissure.

Observations at the deeper levels of these narrow swarms seem to suggest that some, possibly most, are rooted in the subjacent gabbro magma chamber in a manner first described by Allen (1975). They may thus represent the fissure systems operative above the gabbro magma chamber, when active on or near the ridge crest. Significantly a number of these injection zones can be recognised, and each can be traced along strike for only a few kilometers.

Within the 90-100% swarm, dykes of different emplacement ages can be defined from the chilling statistics; a distinction somewhat dubiously supported by the chemistry of the rocks. In the basal regions, dykes can be seen which continue downward through the gabbro and show no recognisable root zone at this level of exposure. These probably relate to newer magma chambers at other levels and have penetrated upwards or laterally through layered gabbros formed in a pre-existing overlying magma chamber. As Rothery (1983) points out, such a disposition requires sequentially-developed magma chambers of finite length, width and depth, presumably distributed along the ridge axis. If the dykes belonging to the narrow swarms were rooted in the gabbro were emplaced in fissures produced by the dilation of the gabbro roof zone overlying ocean crust, then possibly the dimensions of the swarms relate to the size and orientation of the gabbro chambers.

If the steep layering seen in CY-4 gabbros is to be explained by the Rothery (1983) model, then its geometry should relate to the walls of the magma chambers. In the area 9 km west of Agros, around the villages of Kato and Pano Amiandos, cumulus layering is extremely well developed in the gabbros. Mapping of the gabbro texture, mineralogy and layering (see Figure 1a) suggests the possible existence of a number of small plutons. Conclusive proof of their identity must await a more extensive petrological and chemical study, but a prima facie case exists for the recognition of a cluster of discrete plutons which, in the Amiandos area, may well be nested. The pluton dimensions appear to be appropriate to the scale suggested by the Agros dyke zones.

GEOCHEMISTRY AND PETROGENESIS

Modern studies on the petrogenesis of the Troodos complex (Robinson et al., 1983; Schmincke et al., 1983) have shown that the early views of a simple island arc setting (Miyashiro, 1973), ocean floor spreading (Smewing et al., 1975), or early spreading followed by arc volcanism (Pearce, 1975) do not explain the volcanic stratigraphy which appears more complex than the simple 2-fold (Lower-Upper Pillow Lava) subdivision hitherto envisaged. They also demonstrate a geochemical discontinuity within the lava section which, they suggest, could mark the change from an initial arc to a later spreading event.

As Pearce et al. (1984) point out, to make sense of the conflicting interpretations it is necessary to use both petrological-geochemical and geological evidence. All the Troodos basalt geochemistry indicates a supra-subduction zone (SSZ) origin (Pearce et al., 1984), but does not distinguish between a spreading axis above a subduction zone and an arc edifice. It is necessary to examine the dyke swarm to look for evidence of the spreading axis.

Despite extensive study of the lavas, comparatively little discrimination of the intrusives has yet been published. Baragar et al. (1987), working with the dyke swarm, have distinguished two suites, a high-Mg 'depleted' suite with some boninitic characteristics, typical of upper levels of the lava sequence, and a normal 'non-depleted' suite of arc tholeiite to intermediate composition apparently equivalent to the lower parts of the lava sequence. They classify samples with high MgO, Cr, and

low TiO_2, LIL elements as 'depleted', whilst those with lower MgO, Cr, and higher TiO_2, LIL elements as 'non-depleted'. They show that about 25% of the dykes may be identified as belonging to the high-Mg suite and these tend to cluster in swarms indicative of temporal association. However, unlike the distribution of the suites in the lavas, equivalent suites in the dykes show no age preference as determined by cutting relationships. This, they believe, must indicate that the various suites coexisted at the time of emplacement, favouring a view of multiple chamber sourcing for the magmas.

The limited amount of chemical data available to the present study (see Table 1) would tend to support both this view and the conclusion of Pearce et al. (1984) that the magmas were all from a supra-subduction zones (SSZ). The dykes would be classified as 'depleted' on the basis of the criteria of Baragar et al. (1987). Conclusions from this preliminary study must, of course, be tentative, not only because the data set is so small, but because of the problems inherent in the use of whole rock analyses of gabbros which have commonly crystallised with some degree of cumulus segregation. To minimise this problem the gabbros chosen from the Agros and Ayios Ioannis areas are isotropic microgabbros with doleritic texture, found in close association with the roots of dykes with near identical texture and mineralogies. Comparison of their chemistry with that of the dykes seems reasonable, a view supported by the consistency of their analyses, and the regularity of the differences between them and the dykes intruding them. The gabbros from the Amiandos area are a different matter. Here the cumulate layering is well developed and proximity to the ultramafic cumulates indicate that the gabbro samples are taken from a deep level in the pluton. Yet the nature of the chemical difference may not all be attributable to post-emplacement processes.

Figure 2 shows the geochemical patterns normalised to N-type MORB. Pearce et al. (1984) present such patterns for E-type MORB, for ocean island basalts and for basalts affected by subduction (i.e. basalts from island arcs). The most distinctive feature common to the SSZ basalts is the selective enrichment in certain elements relative to MORB (Sr, K, Rb, Ba, Th, ±Ce, ±Sm, ±P) and a relative lack of enrichment in others (Ta, Nb, Hf, Zr, Ti, Y, Yb).

The data available for the present paper (Table 1 and Figure 2a) indicate that the sampled dykes broadly reflect these SSZ basalt features of enrichment and lack of enrichment, with the notable exception of Sr, K, and Rb, the low values for which possibly result from hydrothermal alteration. It would also indicate some differences between dykes; viz sample 1, compared with samples 16 and 51. The Agros/Ayios Ioannis gabbros show a less-enriched pattern; differences in the Ti/Zr and Ti/Y ratios suggest the influence of cumulate crystallisation; the reversal of the Th/Nb ratio may have a more fundamental cause. The nature of the Amiandos magma cannot confidently be ascribed from this data.

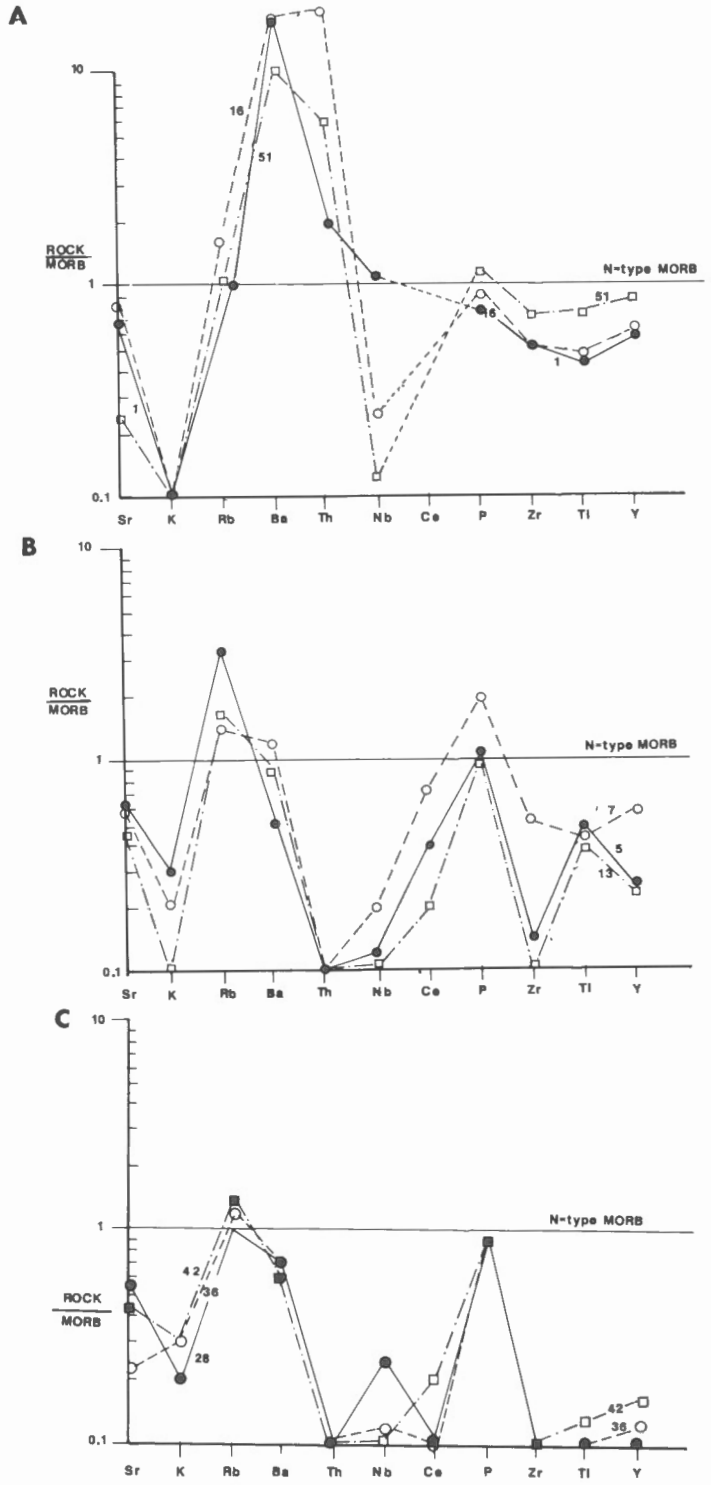

Figure 2: Geochemical patterns, (normalized to an average N-Type MORB (Pearce et al., 1984) for dykes and gabbros listed in Table 1. A: dykes 1, 16, 51; B: gabbros 5, 7, 13, from Agros area; C: gabros 28, 36, 42, from Amiandos area.

Figure 3 plots the analyses on the Cr/Y diagram as used by Pearce et al. (1984, Figure 8). The diagram illustrates a number of features relevant to this discussion. As explained by Pearce et al. (1984) the Y/Cr diagram may be used as a tool in petrogenetic investigation because neither element appears to be significantly affected by the processes causing heterogeneity in the convecting upper mantle. Hence a Cr/Y composition for the mantle can be predicted from various independent lines of evidence. The composition of melts derived from this mantle can be presented as partial melt trends modelled according to the degree of partial melting, and fractional crystallisation can be represented by crystallisation vectors. The combination of trends required to reach a given basalt composition can be termed the 'petrogenetic pathway' for that basalt. Pathway 'C' represents the pathway for a typical basalt from a MORB ophiolite, and 'B' the pathway for a typical SSZ ophiolite. Projection of the compositions back to the primary melting trends indicates that the SSZ basalt primary magma was derived by a greater degree of melting than the MORB ophiolite basalts. Pathway 'A' represents the pathway for basalt from a typical boninitic suite from an ophiolite. As Pearce points out, projection of this composition back to the partial melting trend would appear to indicate 80% melting, clearly an impossible value. Thus, it is necessary to propose that the source of these magmas was not the convecting upper mantle but an already depleted sub-oceanic lithosphere, melting of which would produce the low Y boninites and perhaps some of the island arc tholeiites with a geologically reasonable degree of melting.

The analysed dykes are clearly not MORB ophiolite basalts. Their analyses plot on a fractional crystallisation vector parallel to and between pathways 'B' and 'C' and suggest a source magma transitional to an early island arc tholeiite. This may be derived by a somewhat higher degree of melting than MORB, possibly connected with higher H_2O content. The Y values are marginally higher than most of those recorded from the Troodos ophiolite basalt lavas (Pearce et al., 1984, Figure 6). This might suggest some difference in source, with the bulk of erupted basalts being derived from a still higher degree of melting of the mantle. The gabbros from Agros (and Ayios Ioannis) fall within the typical Troodos composition envelope, and appear to be from a Troodos basalt magma, but it is interesting that both 5 and 13 are close to the boninitic trend.

The gabbros from Amiandos show similar Cr values but their Y values are so low that their compositions must be modified by the accumulation of early-formed ferromagnesian minerals.

The significance of water in affecting the compositions of these basaltic rocks must not be overlooked. A point to be borne in mind when comparing the conclusions from the Cr/Y plot and the multielement diagrams is that the SSZ compositions are modified by enrichment in H_2O from the down-going slab, which is partly responsible for the increased melting and for the enhancement in LIL elements. However, study of Figure 2 suggests that the subsequent movements of water, involved in the ubiquitous hydrothermal metamorphism observed throughout the lavas, dykes and upper parts of the gabbro, might be more significant. Compared with typical SSZ basalts, the dykes are deficient in Sr, Rb, and in particular, K. These elements are particularly mobile in water. Ba and Th retain typical SSZ values and the Th/Nb ratio remains >1, again typical of SSZ basalts. The somewhat smaller K-deficiency in gabbros 5, 7 and 13, may be a function of the lower degree of hydrothermal alteration in the gabbros as compared with the dykes.

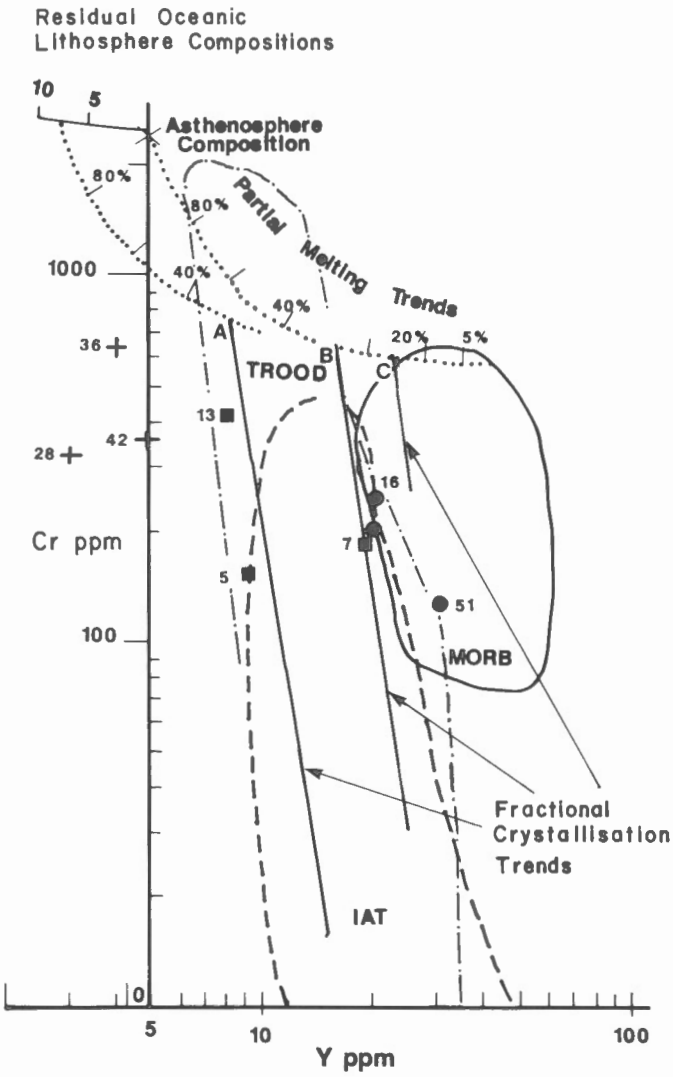

Figure 3: Cr/Y values for dykes and gabbros, plotted on diagram after Pearce et al. (1984, Figure 8) (sample numbers as above). MORB = field of MORB ophiolite basalts, IAT = field of island arc tholeiites, TROOD = field of Troodos basalts (from Pearce et al., 1984, Figure 6)

CONCLUSIONS

The geometric relationship of dykes and gabbro layering, and the form of the dyke-gabbro interface are consistent with a model such as that of Rothery (1983), in which the steep gabbro layering is a primary feature. The plutonic rocks form a cluster of discrete plutons, each of which is associated with its own dyke swarm. Accordingly, the sheeted dyke complex is not produced by emplacement within a single dilational fissure but from a large number of such fissures, each related to its own magma chamber. The chemical data indicate that the basaltic magma parental to both gabbros and dykes is of a supra-subduction zone origin, mostly of an early island arc tholeiite affinity though some may be of boninitic character. None of the analyses indicate an evolved arc composition. There is some suggestion that the magma chambers may have somewhat different compositions but there are insufficient data in the present set to confirm this.

As to whether the whole assemblage represents magmatism at a spreading axis above a subduction zone, or whether there is evidence of the construction of an arc edifice, none of the analyses indicate an evolved arc composition. Furthermore within the areas mapped there is no indication of a central eruptive centre, rather continued uprise of magmas in an extensional crustal tectonic regime.

From the dimensions of the plutons estimated in this study which appear to be consistent with those postulated by Rothery (1983) for the Oman ophiolite, it seems possible that the gabbro penetrated by hole CY-4, which is situated some 7 kms east of Agros, may have crystallised from a magma chamber distinct and separate from any of the gabbros which are exposed extensively at the surface to the west and south of the drill site. No conclusions may be drawn concerning the relative time of emplacement of this chamber, and the chemistry of the gabbros should not be taken as representative of the entire Troodos plutonic suite, for it is clearly composite.

ACKNOWLEDGEMENTS

This study was carried out under the auspices of the Cyprus Crustal Study Project of the International Crustal Research Drilling Group, and thanks are due to Paul Robinson, Director of the Project. Especial thanks go to John Malpas for providing financial assistance for this particular study, to many colleagues, especially Bob Baragar and Julian Pearce for helpful discussion.

REFERENCES

Allen, C.R.
1975: The petrology of a portion of the Troodos plutonic complex, Cyprus; unpublished Ph.D. thesis, University of Cambridge, England, p. 1-161.

Baragar, W.R.A., Lambert, M.B., Baglow, N. and Gibson, I.
1987: Sheeted dykes of the Troodos ophiolite, Cyprus; *in* Mafic Dyke Swarms, ed. H.C. Halls and W.F. Fahrig; Geological Association of Canada Special Paper, no. 34, p. 257-272.

Bear, L.M.
1960: The geology and mineral resources of the Agros-Apsiou area; *in* The Geology and Mineral Resources of the Agros-Skrotiri area, ed. L.M. Bear and S.W. Morel; Geological Survey of Cyprus, Memoir, no. 1.

Cann, J.R.
1974: A model for ocean crustal structure developed; Geophysical Journal of the Royal Astronomical Society, v. 39, p. 169-187.

Gass, I.G.
1980: The Troodos Massif: its role in the unravelling of the ophiolite problem and its significance in the understanding of constructive margin processes; *in* Ophiolites: Proceedings of the International Ophiolite Symposium, Cyprus, 1979, ed. A. Panayiotou, Cyprus Geological Survey Department, Ministry of Agriculture and Natural Resources, p. 23-35.

Kidd, R.G.W.
1977: A model for the process of formation of the upper oceanic crust; Geophysical Journal of the Royal Astronomical Society, v. 50, p. 149-183.

Miyashiro, A.
1973: The Troodos ophiolitic complex was probably formed in an island arc; Earth and Planetary Science Letters, v. 19, no. 2, p. 218-224.

Pearce, J.A.
1975: Basalt geochemistry used to investigate past tectonic environments on Cyprus; Tectonophysics, v. 25, no. 1-2, p. 41-67.

Pearce, J.A., Lippard, S.J. and Roberts, S.
1984: Characteristics and tectonic significance of supra-subduction zone ophiolites; *in* Marginal Basins Geology, ed. B.P. Kokelaar and M.F. Howells; Geological Society of London, Special Publication, v. 16, p. 77-94.

Robinson, P.T., Melson, W.G., O'Hearn, T. and Schmincke, H.-U.
1983: Volcanic glass compositions of the Troodos ophiolite, Cyprus; Geology, v. 11, no. 7, p. 400-404.

Rothery, D.A.
1983: The base of the sheeted dyke complex. Oman Ophiolite: implications for magma chambers at oceanic spreading centres; Journal of the Geological Society of London, v. 140, p. 287-296.

Schmincke, H.-U., Rautenschlein, M., Robinson, P.T. and Mehegan, J.M.
1983:

Troodos extrusive series of Cyprus: a comparison with oceanic crust; Geology, v. 11, no. 7, p. 405-409.

Smewing, J.D., Simonian, K.O. and Gass, I.G.
1975: Metabasalts from the Troodos Massif, Cyprus: genetic implications deduced from petrography and trace element geochemistry; Contributions to Mineralogy and Petrology, v. 51, p.49-64.

Speight, J.M., Skelhorn, R.R., Sloan, T. and Knaap, R.J.
1982: The dyke swarms of Scotland; *in* Igneous Rocks of the British Isles, ed. D.S. Sutherland; Wiley, New York, p. 449-460.

Stillman, C.J.
1987: A Canary Island dyke swarm: implications for the formation of oceanic islands by extensional fissural volcanism; *in* Mafic Dyke Swarms, ed. H.C. Halls and W.F. Fahrig; Geological Association of Canada Special Paper, no. 34, p. 243-255.

Walker, G.P.L.
1986: Koolau dike complex, Oahu: intensity and origin of a sheeted dyke complex high in a Hawaiian volcanic edifice; Geology, v. 14, p. 310-313.

Wilson, R.A.M. and Ingham, F.T.
1959: The geology and mineral resources of the Xeros-Troodos area; Cyprus Geological Survey Department, Ministry of Agriculture and Natural Resources, Memoir, no. 1, p. 1-184.

Petrological Features of Gabbroic and Ultramafic Rocks from Deep Drill CY-4, Cyprus

ROGER LAURENT AND REJEAN HEBERT

Geology Department, Laval University, Quebec, P.Q., Canada, GIK 7P4

Laurent, R. and Hébert, R., Petrological features of gabbroic and ultramafic rocks from deep drill CY-4, Cyprus; in *Cyprus Crustal Study Project: Initial Report, Hole CY-4, ed. I.L. Gibson, J. Malpas, P.T. Robinson and C. Xenophontos; Geological Survey of Canada, Paper 88-9, p. 115-145, 1989.*

Abstract

The CY-4 plutonic sequence, below 1000 meters, consists of: (1) a lower ultramafic unit (2263-1746 m); (2) a median layered gabbronorite unit (1746-1533 m); (3) an upper massive gabbronorite unit (1533-1000 m). Unit 1 is a well layered suite of isomodal websterite mesocumulates interbedded with lherzolitic and gabbronoritic layers. Below 1900 m, these rocks show evidence of high temperature ductile deformation. Low chromium and aluminum Cpx is the dominant phase (Wo_{43-45} - En_{51-48} - Fs_{6-7}). Unit 2 is layered and mainly consists of two-pyroxene gabbro adcumulates. An-rich Pl is the predominant mineral. Unit 3 is a relatively uniform noritic gabbro. Ranges of mineral compositions in the gabbroic units are limited: Pl (An_{89-94}), Opx (En_{66-75}) and Cpx (Wo_{47-44} - En_{44-41} - Fs_{9-15}). Bulk chemistry and cryptic mineral variations show that the sequence forms a single differentiation suite recording distinct fractionation stages of the same magma. Thus, the plutonic sequence appears to have evolved in a relatively confined system, where increasing water pressure was a significant factor, rather than under conditions of a magma chamber periodically replenished by fresh influxes of parental magma. The differentiation trend is dominated by the effect of the co-crystallization and fractionation of Cpx and Opx. The calculated 'liquid line of descent' of the cumulates is in line with the trend defined by UPL glass suggesting that the CY-4 plutonic rocks and Troodos upper volcanic rocks are comagmatic.

Résumé

Au-dessous de 1000 mètres, le sondage profond CY-4 se subdivise en: (1) une unité inférieure ultramafique (2263-1746 m); (2) une unité médiane de gabbronorite litée (1746-1533 m); (3) une unité supérieure de gabbronorite structuralement homogène (1533-1000 m). L'unité 1 est composée d'une série bien litée de mésocumulats isomodaux de composition websteritique interstratifiés avec des lits de lherzolite et de gabbronorite. Ces roches, au-dessous de 1900 m, ont été déformées plastiquement à haute température. Un Cpx pauvre en aluminium et chrome constitue la phase minéralogique principale (Wo_{43-45} - En_{51-48} - Fs_{6-7}). L'unité 2 est litée et consiste surtout en adcumulats gabbroïques à deux pyroxènes. C'est un plagioclase calcique qui constitue le composant minéralogique principal. L'unité 3 est composée d'un gabbro noritique structuralement et minéralogiquement homogène. Les variations de composition des minéraux des unités gabbroïques sont limitées: Pl (An_{89-94}), Opx (En_{66-75}) and Cpx (Wo_{47-44} - En_{44-41} - Fs_{9-15}). Les variations chimiques des roches totales et des minéraux indiquent que la séquence plutonique constitue une seule suite de différenciation. Elle résulte d'une évolution en milieu relativement confiné, où une pression d'eau croissante représente un facteur caractéristique, plutôt que d'une évolution dans les conditions d'une chambre magmatique remplie périodiquement par des apports de magma primitif. La tendance de différenciation est contrôlée par l'effet de la cristallisation et du fractionnement simultanés de Cpx et Opx. La courbe calculée de la composition des liquides ayant produit les cumulats s'aligne avec la courbe définie par la composition des verres UPL, ce qui suggère fortement que les roches plutoniques de CY-4 sont comagmatiques avec les roches volcaniques supérieures du Troodos.

INTRODUCTION

The main objective of the deep drill hole CY-4 was to provide a vertical view of the plutonic complex and, by combining the information from surface geology with the core section, to produce a three-dimensional model of the ophiolite. This structural information is considered to be fundamental in order to better understand the geometrical relationships between the various plutonic rock units as well as their relations with the dyke complex. A second and important objective for CY-4 was to provide a detailed description of a continuous section of plutonic rocks for making possible precise comparisons between ophiolites and drilled ocean crust sequences. This report is a contribution towards these two goals; discussions are kept to a minimum and more complete interpretations will be given in forthcoming publications.

CY-4 provides a continuous record of 2263 m through the sheeted dyke complex and plutonic section of the Troodos ophiolite. On the basis of observations of the core, we have divided the CY-4 section into the following five main units (Figure 1): (1) 0-700 m basal part of the sheeted dyke complex; (2) 700-1000 m chilled roof of the plutonic section, which consists of fine-grained gabbro and gabbro breccias intruded by suites of diabase dykes, felsic veins and plagiogranite bodies showing complex cross-cutting relationships. This section of the sheeted dykes and the chilled gabbro roof is pervasively metamorphosed. Below 1000 m, the metamorphic overprint decreases rapidly so that most of the plutonic section is unmetamorphosed. It is divided into: (3) an upper gabbronorite unit between 1000 and 1533 m, later described as plutonic unit 3; (4) a weakly layered gabbronorite unit between 1533 and 1746 m, later described as plutonic unit 2; and (5) a lower ultramafic unit between 1746 and 2263 m, the bottom of the drill hole, which is later described as plutonic unit 1. Numbering of the plutonic units follows normal stratigraphic rules, and we have assumed that the plutonic sequence 'youngs' upwards. For financial reasons, the drilling was stopped at 2263 m in July 1984 before reaching the dunitic unit thought to form the base of the ultramafic sequence. Petrological evidence discussed in this report suggests that basal dunite may occur at a depth around 2550 m, that is about 300 m deeper than the bottom of CY-4.

Sampling

One hundred and twenty-two representative samples were selected during the hand specimen core description on the basis of their petrographic interest. Each sample is about 10 cm long, and half of the core section thick with a diameter of 4.5 cm. Thin sections of all samples were prepared and studied. Four samples of hornblende metagabbro and metadiabase were taken from the chilled gabbro roof above 1000 m but were not studied in detail because of their greenschist facies metamorphism. One hundred and eighteen samples are from below 1000 m. After petrographic study, 74 homogeneous and, when possible, unaltered samples were chemically analyzed for major elements and some compatible trace elements such as Ni, Cr, Co and V. The chemistry of the mineral phases in 16 selected samples was determined with the microprobe. All samples were analyzed at Laval University, but half of the samples were also analyzed by R. Hébert at the Centre Océanographique de Bretagne. Duplication of the microprobe analyses shows our results are reproducible. The number of samples taken in the plutonic units varies according to the nature of the rocks. Only a small number of samples have been selected from the third plutonic unit which is very uniform in structure and mineralogy. On the other hand, many samples have been taken from the compositionally layered units 1 and 2. The positions of the 74 samples studied in detail are given in Table 1 and Figure 2.

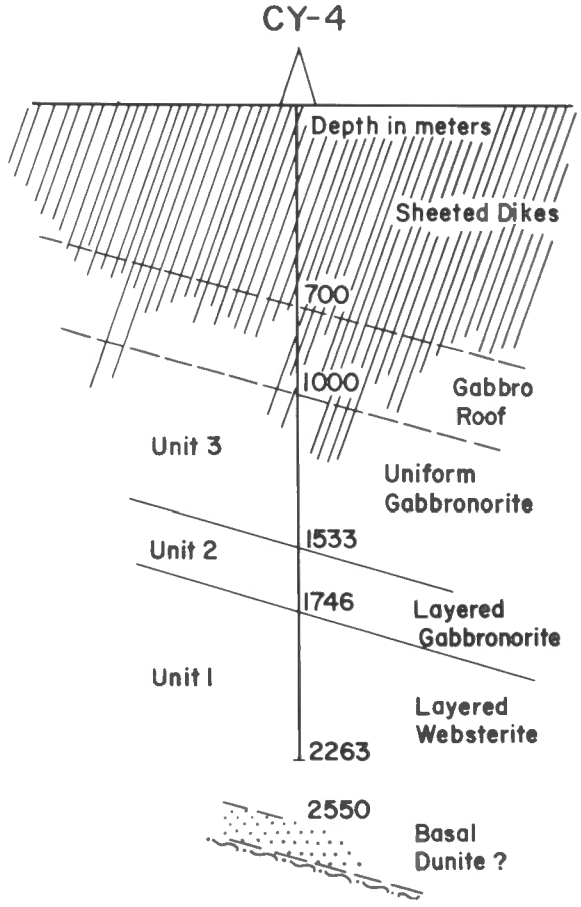

Figure 1: Schematic section of deep drill CY-4.

TABLE 1. Modal Composition of CY-4 Plutonic Rocks

Depth	Unit (note 1)	Rock-type	Grain size (mm)	Ol	Opx	Cpx	Pl	Am	Ox	SM
			Gabbro Zone							
1012.10	249.04	Gbn	0.6	–	24	14	60	1	1	x
1169.50	276.02	Gbn	0.7	–	22	16	60	–	2	x
1282.70	294.05	Gbn	0.1/1.5	–	30	15	55	–	<	–
1362.80	309.02	Ho-Gbn	2.1	–	20	5	50	25	<	x
1449.60	325.01	Ho-Gbn	2.0	–	8	10	65	12	<	5
1529.05	338.04	Ho-Gbn	2.5	–	15	5	50	30	<	xS
1529.70	338.04	Gbn	1.5	–	22	13	50	13	<	x
1538.95	341.02	Pl-Web	2.0	–	15	30	15	35	<	x
1540.02	341.02	Pl-Web	2.0	–	10	50	15	25	<	xS
1545.53	342.01	Gbn	2.5	–	33	12	45	8	<	x
1545.73	342.01	Gbn	0.9	–	38	15	46	1	<	x
1548.90	342.01	Gbn	0.7	–	37	14	45	3	1	x
1549.62	343.01	Ol-Gbn	1.2	10	50	14	22	1	<	3
1550.32	343.02	Gbn	1.2	–	20	28	50	1	1	x
1551.60	343.02	Gbn	2.5	–	25	25	48	2	<	x
1554.10	344.01	Ho-Gbn	6.0	–	2	–	65	10	3	20
1574.80	346.01	Gb	1.5	2	5	30	63	–	<	x
1580.12	346.01	Gbn	3.0	–	15	15	55	14	<	1
1590.20	348.02	Gbn	1.5	–	25	29	45	–	<	1S
1599.65	350.02	Gbn	1.5	–	9	40	50	–	<	1
1616.15	353.01	Ol-Gb	1.5	16	3	36	45	–	<	x
1619.85	355.02	Gbn	1.5	–	29	15	55	–	<	1
1659.30	361.03	Gbn	2.5	–	20	18	45	15	<	2
1710.80	371.01	Gbn	1.5	3	18	16	60	3	<	x
1711.20	371.01	Ho-Gb	2.5	–	–	40	40	20	<	x
1714.72	371.03	Gbn	2.8	–	24	36	32	5	<	3
1719.15	371.04	Gbn	1.1	–	18	28	44	5	<	5
1727.95	373.01	Gb	3.0	–	3	30	55	11	<	1
1731.18	374.02	Ho-Gbn	1.0	–	10	30	48	10	<	2
1733.15	374.03	Gbn	2.2	–	12	25	53	5	<	5
1745.14	377.01	Ol-Gbn	1.5	8	7	40	25	15	<	5
1745.75	377.01	Pl-Ol-Web	2.5	5	25	50	20	–	<	x
			Pyroxenitic Zone							
1748.10	377.02	Clinopx	1.5	–	5	90	–	–	1	4
1750.10	378.01	Ol-Gbn	2.0	14	18	33	33	1	<	1
1794.60	385.03	Clinopx	10.0	–	5	60	3	25	1	6
1798.85	386.01	Pl-Web	3.0	2	20	45	25	8	<	x
1801.30	387.01	Web	6.0	1	13	65	10	7	<	4
1809.90	388.02	Gbn	10.0	–	21	21	50	2	<	6
1813.40	389.03	Web	2.0	3	11	75	8	–	<	3
1835.60	393.01	Ol-Web	2.5	13	12	70	1	–	<	4
1837.86	393.02	Ol-Web	6.0	30	5	55	3	2	<	5
1849.66	395.04	Ol-Web	7.0	5	30	40	2	2	<	21

TABLE 1 (cont.) Modal Composition of CY-4 Plutonic Rocks

Depth	Unit (note 1)	Rock-type	Grain size (mm)	Ol	Opx	Cpx	Pl	Am	Ox	SM
1855.20	397.05	Ol-Web	1.5	30	15	50	–	–	<	5
1859.30	398.01	Gbn	4.0	–	10	55	25	5	<	5
1869.15	400.01	Ol-Pl-Web	3.0	5	20	60	10	–	<	5
1871.86	400.03	Ol-Pl-Web	1.8	8	6	50	10	16	1	9
1875.30	401.02	Ho-Web	2.5	1	8	48	5	22	1	15
1877.87	401.03	Ho-Web	2.0	2	18	37	4	19	<	20
1879.92	402.01	Ol-Web	1.1	15	25	33	1	4	2	20
1907.10	406.03	Ol-Web	2.8	10	25	52	10	–	<	3
1952.55	414.04	Pl-Ol-Web	2.5	5	15	63	15	–	<	2
1995.95	423.04	Ol-Web	10.0	10	5	80	2	–	<	3
2048.60	436.01	Ol-Pl-Web	2.3	4	15	70	6	–	<	5
2059.35	439.03	Lherz	1.5	50	–	23	2	–	<	25
2063.05	440.01	Ol-Pl-Web	5.0	10	19	50	8	–	<	13
2101.30	449.03	Gbn	2.0	–	20	59	20	–	<	1
2113.83	452.02	Ol-Web	2.0	8	22	58	–	1	1	10
2115.80	452.02	Ol-Clinopx	3.0	8	6	80	3	–	<	3
2117.83	452.02	Ol-Web	2.4	5	13	72	1	–	<	9
2119.10	453.02	Ol-Web	2.2	7	10	75	1	–	<	7
2122.15	453.02	Ol-Web	2.9	15	16	64	2	–	1	2
2130.10	455.04	Gbn	0.7	–	20	30	45	3	<	2
2151.85	460.01	Ol-Pl-Web	0.7	10	10	60	15	–	<	5
2163.15	464.01	Ol-Web	2.5	15	8	60	5	–	<	12
2190.25	470.03	Ol-Pl-Web	3.0	7	15	70	3	–	<	5
2204.10	472.04	Pl-Lherz	1.6	35	6	40	4	–	<	15
2210.35	475.02	Pl-Ol-Web	3.0	15	7	50	13	–	<	15
2243.10	483.01	Wehr	1.4	55	–	25	–	–	<	20
2253.85	485.03	Ol-Cpx	2.3	8	4	78	2	–	<	8
2254.30	485.03	Lherz	2.5	60	5	18	–	–	1	16
2254.72	485.03	Ol-Cpx	3.1	5	5	74	3	–	1	12
2262.05	487.02	Wehr	2.0	45	–	20	–	–	2	33
2262.90	487.03	Ol-Web	3.0	15	10	60	–	–	<	15
2263.08	487.03	Ol-Cpx	2.5	8	4	82	1	–	<	5

Gb: gabbro, Ol: olivine, Gbn: gabbronorite, Opx: orthopyroxene, Clinopx: clinopyroxenite, Cpx: clinopyroxene, Web: websterite, Pl: plagioclase, Lherz: lherzolite, Ho: hornblende, Wehr: wehrlite, Am: amphibole, Chr: chromite, Ox: oxide, S: sulfide, <: less than 1%, SM: secondary minerals (note 2), x: disseminated

(1) Unit numbers designate the core box in which the lithologic unit first appears. Most of lithologic units recognized in the plutonic section by core describers are simple or complex layers. Ref. Louisa Horne and Paul T. Robinson (editors), 1985: Hole Cy-4 Core Descriptions, Cyprus Crustal Study Project, 4 volumes.

(2) Actinolite is the most common secondary mineral, together with smaller amounts of magnetite and chlorites. Carbonates, epidote, albite, quartz, etc. are rare. Olivine is partly serpentinized in the ultramafic rocks of the pyroxenitic zone (lizardite, chrysotile, brucite, talc and magnetite).

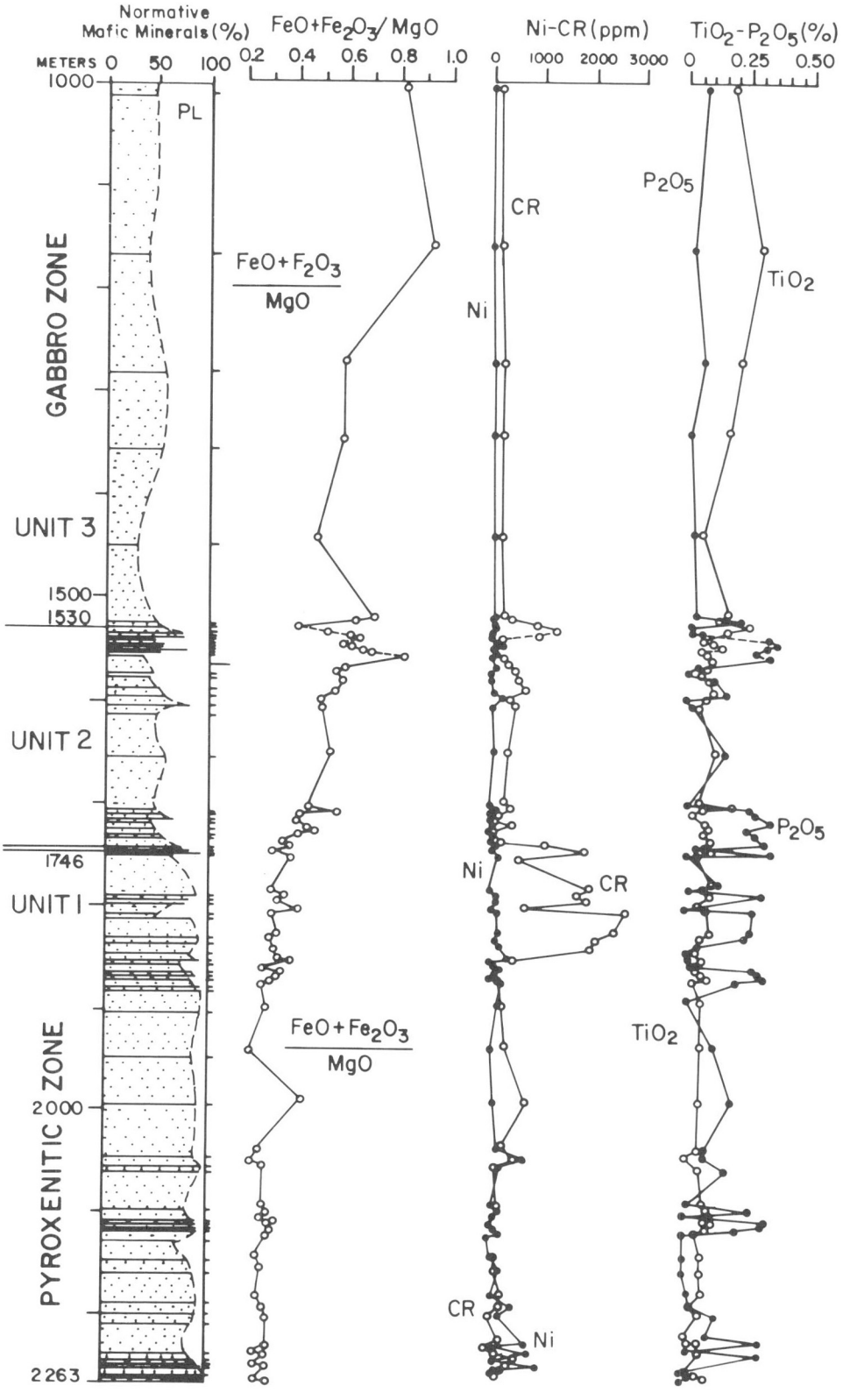

Figure 2: Modal variations in the CY-4 section between 1000 and 2263 m.

Analytical Methods

Petrographic work used standard thin sections. Modal compositions were determined by averaging modal data obtained from point counting of thin sections with visual estimates made directly on core samples under a binocular microscope. Because of the layered structure of many rocks and their coarse grain size, this method better reflects the whole mineral composition of the sample than 'precise' data on only one or two thin sections. Some minerals were identified independently by X-ray powder-diffraction using a Gandolfi 114.6 mm diameter camera with nickel-filtered CuKα radiation.

Microprobe analyses were done at Laval University with an ARL electron microprobe at 20 kV and 0.1 mA using natural olivine, diopside, chromite and plagioclase standards. Integration time was 10 seconds for each measurement which was repeated five times. A minimum of three and a maximum of ten different points were analyzed in each mineral grain. Beam diameter was 3 microns. The data were corrected using a ZAF program. Replicate analyses of standards indicate that the determinations have a relative accuracy of ± 1 to 2% for major elements. The microprobe was operated by J.P. Tremblay, a professional technician. Between two and fifteen grains of each mineral phase were separately analyzed and compared for the same sample, and the average composition was calculated. No systematic differences in composition between the core and the margin of analyzed minerals were noted, and microprobe traverses across olivine and plagioclase grains revealed no detectable zoning.

Bulk chemistry was determined at Chimitec, a professional laboratory specializing in rock analyses in Quebec City. Major elements were analyzed by Plasma Emission Spectrometry, with separate titration for FeO-Fe_2O_3. The trace elements were analyzed by atomic absorption with detection limits of 2 ppm for Ni and Cr, and of 1 ppm for Co and V.

RESULTS

Structures and Petrography

The plutonic section is divided, on the basis of structure, composition and a distinct order of mineral crystallization, into three major units. The petrographic results are summarized in Table 1 and illustrated in Figures 2 and 3. Plutonic rock names are based on the IUGS system (Streckeisen, 1976). Terminology used to describe the cumulate rocks is from Wager et al. (1960), Jackson (1971) and Irvine (1982).

Unit 1 is ultramafic and well layered; it consists mainly of websterite with layers of gabbronorite, clinopyroxenite, wehrlite and lherzolite. Clinopyroxene is the predominant mineral. In the basal part of this unit, below 2100 m, olivine is more abundant than orthopyroxene. Except in gabbronoritic layers, plagioclase occurs only as a postcumulus phase interstitial to the mafic minerals. The layers are variable in thickness from medium-thick (5 cm-1 m) to several meters thick. Their contacts are usually defined by a sharp change in mode (phase contact) often associated with a parallel change in grain size. Planar lamination and mineral ratio layering are well developed at the centimeter scale within the layers. Thick layers show grain size layering but tend to be more uniform in structure and composition than medium-thick layers, the latter being modally and texturally graded. Medium-thick layers vary in composition and texture from lherzolite or olivine-rich websterite, with orthocumulus and mesocumulus textures, to clinopyroxenite with adcumulus texture. The majority of the layers, however, are isomodal mesocumulates, their intercumulus phases forming between 7 and 25% of the rock (Irvine, 1982, p. 137).

Unit 2 is a well layered gabbroic cumulate composed of interlayered two-pyroxene gabbro, olivine-bearing gabbro and plagioclase-rich websterite. Plagioclase is the predominant mineral, and clinopyroxene crystallizes before orthopyroxene. Cumulus olivine occurs sporadically within this unit and only in small amounts. A prismatic green hornblende, as a late magmatic phase, is ubiquitous and its content varies from 1% to less than 20%. The layers are predominantly thick, from 1 to more than 10 meters, and homogeneous in composition. They usually grade at their top into a felsic and pegmatitic zone of leuco-gabbronorite or hornblende gabbro. A smaller number of layers display modal grading with concentrations of pyroxene and some olivine at the base, grading up into plagioclase-rich tops. Textures vary from mesocumulus to adcumulus. The majority of the gabbronorites are adcumulates, their intercumulus phases forming less than 7% of the rock (Irvine, 1982, p. 137). They show planar and modal lamination at the centimeter scale, and grain-size layering at the meter scale.

Unit 3 is a relatively uniform noritic gabbro and amphibole gabbronorite. Plagioclase is the predominant mineral and, in contrast with the underlying units, orthopyroxene becomes the most important mafic component. In this unit orthopyroxene crystallizes before clinopyroxene. Magmatic hornblende is often a major late phase which developed at the expense of both pyroxenes. Layering in this unit is not megascopically visible. Grain sizes vary from coarse to fine with an average of 1 to 2 mm. Some intervals display fine planar lamination with perfect adcumulus texture, while others are structurally isotropic with a small percentage of intercumulus phases. Many contacts

between the rocks are gradational; other contacts are defined at sharp grain size changes. Several swarms of diabase dykes occur near the top of unit 3, particularly between 1100 and 1200 m.

One of the most significant features of the plutonic section is the apparently continuous co-crystallization of clinopyroxene and orthopyroxene. Another feature of interest is the occurrence of magmatic amphibole, as a postcumulus and reaction replacement phase, even in the ultramafic unit 1, but more abundantly up section in plutonic units 2 and 3. Development of this amphibole indicates the presence of water in the magma and that the water activity increased progressively with increasing percentage of crystallization of the magma column.

Veins a few centimeters thick and irregular bodies (of unknown size) of leuco-gabbro are injected into the sequence at various depths. These veins are parallel to the layering or cut across it. In the Semail ophiolite of Oman, they are considered by Pallister and Hopson (1981) to represent filter-pressed interstitial melt from the neighbouring cumulates. Between 1000 and 1900 m, deformation is restricted to narrow shear zones and faults. In contrast, olivine-rich layers from 1900 to 2263 m show boudinage structures and porphyroclastic textures defining a tectonite fabric. Deformation textures of minerals in these rocks include granulation of olivine with formation of kink bands and wavy substructure, and with generation of twins in pyroxenes. Development of polygonal neoblasts of olivine and partial recrystallization of pyroxenes tend to anneal the rocks. These textural features indicate that the ultramafic cumulates at the base of the plutonic section have been ductilely deformed at high temperatures. Deformation of the same type has been observed in the gabbroic rocks of the Troodos by George (1978) and, more recently, studied in detail by Dunsworth and Calon (1984), Benn (1986), and Benn and Laurent (1986). Low temperature alteration in most of the plutonic section is limited to the partial replacement of pyroxenes by an acicular actinolite, while the calcic plagioclase remains unaltered. Olivine is partly serpentinized and the extent of its alteration increases with depth. Veinlets of chrysotile occur in the serpentinized and deformed lherzolitic cumulates at the base of the plutonic section below 2000 m.

Whole Rock Chemistry

Major and trace element compositions of the gabbroic and ultramafic rocks from CY-4 are given in Tables 2a and 2b, and normative compositions are given in Table 2c. The rocks have been produced by fractional crystallization of magma. Ideally they represent solidus compositions of the evolving system and their chemistry reflects the accumulation of cumulus mineral grains. However, complications due to imperfect separation of crystals and liquid are frequently encountered (Irvine, 1979, p. 257). Intercumulus phases, which may react and equilibrate with the cumulus minerals, result from crystallization of interstitial trapped liquid. Thus, whole rock chemistry reflects cumulus compositions and variable proportions of pore liquid, as well as subsequent reaction relationships.

The average compositions of the pyroxenite zone (unit 1) and the gabbro zone (units 2 and 3), given in Table 3, show that the main differences are in the respective MgO and Al_2O_3 contents. MgO and Al_2O_3 are negatively correlated (Figure 4a) reflecting the crystallization sequence characterized by the strong fractionation of MgO in early formed olivine and pyroxene. The high normative orthopyroxene content of most rocks reflects the SiO_2 oversaturated character of the magma, which was also characterized by an initial $CaO:Al_2O_3$ ratio close to 1. Enrichment of Al_2O_3 in the residual melt was necessary to reach saturation (in cotectic conditions) which initiated late stage crystallization of calcic plagioclase.

FeO(total) and TiO_2 are plotted against FeO(total):MgO ratios, an index of fractionation in Figures 4b and 4c. Iron contents in pyroxenites and gabbros are similar, while the FeO:MgO ratio varies from an average value of 0.30 in pyroxenites to 0.55 in gabbros. Significant increases in TiO_2 are also observed with increasing fractionation.

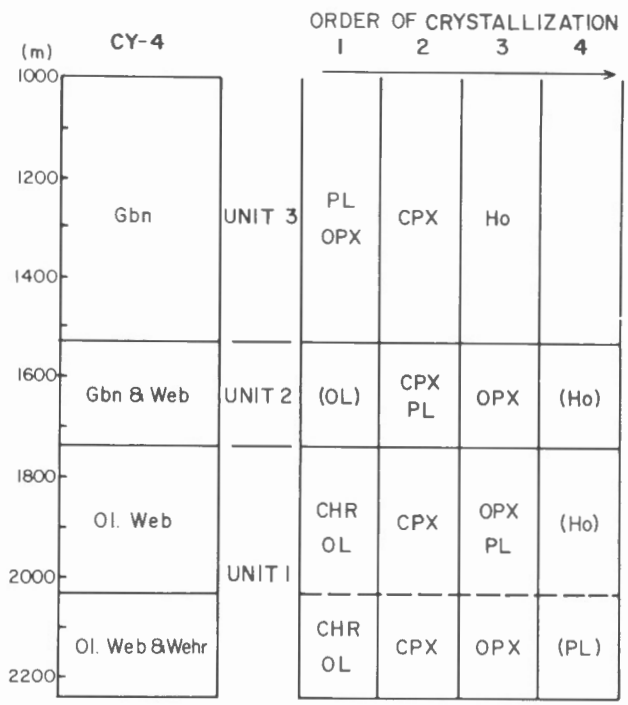

Figure 3: Order of mineral crystallization in the CY-4 plutonic units.

TABLE 2A: Whole Rock Chemistry - Major Elements

(m)	SiO_2	TiO_2	Al_2O_3	Fe_2O_3	FeO	MgO	MnO	CaO	Na_2O	K_2O	P_2O_5	LOI	SUM
						Gabbro Zone							
1012.10	49.00	0.19	18.20	1.69	6.32	9.79	0.15	13.40	0.85	<.01	0.08	0.20	99.87
1169.50	48.30	0.29	20.40	1.79	5.39	7.60	0.12	14.50	1.05	<.01	<.01	0.30	99.74
1282.70	48.60	0.20	15.00	1.70	5.07	11.30	0.13	14.50	0.65	<.01	0.06	1.30	98.51
1362.80	48.80	0.16	16.30	1.66	4.49	10.20	0.13	15.50	0.58	<.01	<.01	0.90	98.72
1449.60	46.40	0.06	25.40	1.56	1.49	6.10	0.06	18.48	0.44	<.01	0.04	0.40	100.43
1529.05	48.80	0.16	17.85	1.74	5.18	9.70	0.13	13.50	0.57	0.12	0.05	1.25	99.05
1529.70	51.40	0.14	15.10	1.70	5.52	11.30	0.15	13.20	0.64	0.10	0.28	1.10	100.63
1538.95	54.00	0.23	4.16	1.40	4.82	15.50	0.12	16.60	0.68	0.09	0.04	1.95	99.59
1540.02	52.10	0.20	5.48	2.02	6.48	15.60	0.18	16.20	0.23	0.10	0.04	0.85	99.48
1545.53	51.40	0.09	14.70	1.47	6.28	12.50	0.16	11.90	0.53	0.08	0.09	0.95	100.15
1545.73	47.60	0.09	14.50	1.99	5.66	11.80	0.15	13.80	0.58	0.02	0.40	1.15	97.74
1548.90	47.10	0.12	14.60	1.91	5.78	12.90	0.15	11.90	0.76	0.03	0.42	1.35	97.02
1549.62	47.80	0.14	6.49	2.90	8.66	18.80	0.21	8.59	0.40	0.03	0.38	3.40	97.80
1550.32	47.70	0.08	16.60	1.85	5.12	10.50	0.13	13.80	0.73	0.02	0.34	1.05	97.92
1551.60	48.30	0.09	16.70	0.95	5.61	9.54	0.12	15.00	0.58	0.03	0.41	0.25	97.58
1554.10	49.80	0.11	20.50	1.27	4.37	6.59	0.11	12.20	0.66	0.11	0.06	3.20	98.98
1574.80	49.50	0.10	16.60	1.19	4.81	10.20	0.12	14.40	0.16	0.01	0.08	2.40	99.57
1580.12	50.70	0.09	19.20	0.99	4.34	9.14	0.11	14.70	0.64	0.05	0.01	0.65	100.62
1590.20	52.00	0.11	15.60	1.56	5.00	11.00	0.15	14.90	0.59	0.06	0.12	0.44	101.53
1599.65	50.10	0.13	16.20	1.79	4.26	10.60	0.13	16.70	0.54	0.10	0.21	0.90	101.66
1616.15	50.40	0.10	5.74	1.94	9.05	21.60	0.21	9.44	0.01	0.01	0.01	1.10	99.61
1619.85	48.50	0.08	17.15	1.22	4.74	11.60	0.12	12.80	0.45	0.10	0.05	2.25	99.06
1659.30	51.70	0.15	13.50	1.85	5.29	12.80	0.15	13.20	0.52	0.09	0.19	0.65	100.09
1710.80	50.20	0.07	16.40	1.05	4.16	11.20	0.11	14.50	0.01	0.01	0.07	1.25	99.03
1711.20	48.20	0.22	15.40	2.20	4.00	10.40	0.12	14.00	0.73	0.12	0.02	3.90	99.31
1714.72	50.00	0.12	10.20	2.26	4.11	14.40	0.14	14.80	0.51	0.03	0.31	0.65	97.53
1719.15	47.20	0.06	18.10	1.05	3.14	9.88	0.09	16.30	0.57	0.04	0.33	0.65	97.41
1727.95	52.10	0.11	16.20	0.56	4.69	11.40	0.12	13.10	0.54	0.09	0.42	1.25	100.58
1731.18	48.30	0.11	15.70	1.40	4.10	11.30	0.11	15.10	0.63	0.04	0.30	0.75	97.84
1733.15	46.00	0.09	17.60	1.71	2.98	10.60	0.10	16.70	0.62	0.03	0.33	1.90	98.66
1745.14	50.30	0.12	7.47	1.94	4.33	17.40	0.14	18.00	0.38	0.05	0.39	0.60	101.12
1745.75	50.80	0.10	6.87	3.20	3.55	17.20	0.13	14.90	0.06	0.07	0.06	2.45	99.39

TABLE 2A (cont.) Whole Rock Chemistry - Major Elements

(m)	SiO_2	TiO_2	Al_2O_3	Fe_2O_3	FeO	MgO	MnO	CaO	Na_2O	K_2O	P_2O_5	LOI	SUM
						Pyroxenite Zone							
1748.10	52.40	0.13	2.09	1.52	4.15	17.50	0.14	18.60	0.26	0.06	0.42	1.85	99.12
1750.10	47.70	0.06	13.00	1.73	4.47	15.80	0.11	14.60	0.24	0.07	0.02	2.35	100.15
1794.60	53.80	0.13	2.70	1.04	4.78	18.10	0.15	16.80	0.33	0.07	0.15	1.00	99.05
1798.85	51.30	0.11	6.85	1.48	4.78	17.10	0.13	15.80	0.24	0.07	0.02	1.25	99.13
1801.30	52.00	0.12	6.81	1.18	4.57	17.10	0.14	15.50	0.29	0.06	0.38	1.25	99.40
1809.90	49.00	0.07	17.20	0.44	4.46	11.60	0.10	13.80	0.51	0.07	0.01	2.55	99.81
1813.40	52.00	0.09	4.60	2.15	4.13	19.30	0.15	16.50	0.23	0.12	0.35	0.85	100.47
1835.60	50.70	0.11	1.99	2.02	5.24	21.00	0.16	15.10	0.22	0.11	0.32	2.05	99.02
1837.86	51.70	0.09	4.26	2.31	4.21	19.90	0.14	15.20	0.25	0.11	0.31	1.76	100.24
1849.66	49.70	0.07	7.00	1.77	4.80	19.80	0.13	13.90	0.11	0.06	0.07	1.85	99.26
1855.20	49.30	0.07	2.34	1.57	6.79	24.70	0.17	13.40	0.08	<.01	0.02	2.55	100.99
1859.30	50.30	0.12	10.20	1.62	3.98	14.40	0.13	16.30	0.27	<.01	0.03	1.70	99.05
1869.15	51.60	0.08	4.49	1.58	3.74	18.60	0.13	17.10	0.16	<.01	0.06	1.60	99.14
1871.86	48.60	0.08	3.75	2.57	4.78	20.70	0.14	14.90	0.29	0.04	0.33	1.80	97.98
1875.30	51.60	0.09	4.69	2.57	4.64	21.10	0.15	15.00	0.35	0.06	0.36	1.00	101.61
1877.87	51.40	0.10	3.88	1.44	4.38	18.30	0.14	17.90	0.37	0.07	0.38	1.10	99.46
1879.92	47.50	0.06	1.61	2.82	4.36	24.30	0.13	14.00	0.25	0.07	0.24	2.73	98.07
1907.10	51.20	0.09	2.30	1.59	4.93	21.70	0.14	16.00	0.08	<.01	<.01	0.70	98.73
1952.55	51.70	0.08	4.41	1.58	2.84	18.30	0.12	18.90	0.17	<.01	0.15	1.20	99.45
1995.95	49.60	0.08	3.42	1.58	7.04	18.96	0.11	17.50	<.01	<.01	0.24	1.10	99.63
2048.60	49.60	0.07	4.37	1.57	4.26	21.60	0.13	15.50	0.10	<.01	0.08	1.45	98.73
2059.35	41.00	0.02	0.92	1.52	7.20	34.60	0.13	3.76	<.01	<.01	0.07	9.80	99.02
2063.05	49.40	0.08	2.89	1.58	5.32	24.10	0.14	13.90	0.07	<.01	0.21	1.80	99.49
2101.30	52.20	0.09	7.27	1.59	3.31	16.80	0.13	18.10	0.18	<.01	0.02	0.40	100.09
2113.83	48.90	0.10	2.36	1.24	4.95	19.70	0.14	17.30	0.31	0.05	0.31	2.60	97.96
2115.80	51.90	0.10	3.12	1.60	4.40	20.20	0.15	17.60	0.11	<.01	<.01	0.60	99.78
2117.83	48.70	0.09	2.37	2.86	4.68	22.60	0.15	14.60	0.29	0.05	0.40	1.00	97.79
2119.10	50.60	0.12	2.67	1.96	4.68	20.20	0.15	17.20	0.32	0.05	0.39	1.10	99.44
2122.15	49.10	0.10	2.43	2.45	5.06	22.60	0.15	16.20	0.28	0.04	0.27	1.25	99.93
2130.10	49.00	0.06	14.80	1.56	2.66	13.40	0.11	15.80	0.28	<.01	<.01	0.35	98.02
2151.85	48.80	0.07	5.62	1.57	3.82	19.50	0.13	16.80	0.13	<.01	<.01	2.80	99.24
2163.15	49.70	0.08	5.05	1.58	4.48	20.50	0.14	16.70	0.14	<.01	<.01	1.00	99.37
2190.25	51.90	0.11	2.77	1.61	3.74	19.00	0.14	18.80	0.10	<.01	0.04	0.45	98.66
2204.10	45.80	0.05	2.98	1.55	6.41	26.50	0.15	11.70	0.04	<.01	0.05	3.80	99.03
2210.35	48.60	0.08	5.92	1.58	4.87	21.30	0.14	15.30	0.22	<.01	0.14	1.85	100.00
2243.10	39.70	0.02	0.65	1.52	9.52	35.60	0.14	3.47	<.01	<.01	0.09	8.95	99.66
2253.85	48.80	0.09	4.25	1.86	4.64	20.90	0.14	16.80	0.33	0.03	0.30	1.85	99.99
2254.30	40.60	0.03	1.12	1.53	8.43	35.90	0.16	4.73	<.01	<.01	0.04	8.35	100.89
2254.72	49.00	0.09	2.06	3.23	3.78	22.10	0.16	16.20	0.30	0.05	0.30	4.40	101.67
2262.05	34.60	0.02	0.69	7.29	4.47	41.70	0.16	2.04	0.01	0.02	0.01	11.60	102.61
2262.90	49.80	0.09	2.49	1.59	4.30	21.40	0.14	17.40	0.08	<.01	0.04	1.75	99.08
2263.08	51.00	0.11	3.42	2.34	4.36	21.30	0.15	18.00	0.04	0.03	0.01	1.25	102.01

TABLE 2B Whole Rock Chemistry - Trace Elements (ppm)

	Trace Elements (ppm)								
(m)	Ni	Cr	Co	V	(m)	Ni	Cr	Co	V
	Gabbro Zone					Pyroxenite Zone			
1012.10	8	139		56	1748.10	58	1750	14	
1169.50	19	115		81	1750.10	146	511	30	
1282.70	8	156		21	1794.60	33	1955	4	
1362.80	13	87		23	1798.85	62	1732	12	
1449.60	10	108		21	1801.30	62	1885	12	
1529.05	29	232	7		1809.90	44	653	10	
1529.70	16	258	6		1813.40	80	2650	15	
1538.95	23	851	6		1835.60	168	2425	31	
1540.02	23	1133	4		1837.86	153	2075	30	
1545.53	18	870	4		1849.66	172	2031	27	
1545.73	22	91	8	28	1855.20	312	420		19
1548.90	42	68	10	22	1859.30	18	215		20
1549.62	160	76	30	28	1869.15	69	236		16
1550.32	21	36	4	23	1871.86	155	141	32	10
1551.60	33	40	8	23	1875.30	135	130	26	8
1554.10	16	127	3		1877.87	30	148	4	12
1574.80	28	180	8		1879.92	240	215	42	12
1580.12	14	297	2		1907.10	187	247		15
1590.20	12	463	2		1952.55	46	270		16
1599.65	31	668	4		1995.95	69	700		19
1616.15	230	237	46		2048.60	188	208		15
1619.85	18	306	4		2059.35	680	500		24
1659.30	23	331	6		2063.05	236	202		14
1710.80	18	214	6		2101.30	34	202		18
1711.20	38	315	10		2113.83	232	148	36	10
1714.72	15	64	6	20	2115.80	134	198		14
1719.15	9	40	4	20	2117.83	110	165	20	8
1727.95	10	360	2		2119.10	120	165	16	12
1731.18	9	28	4	20	2122.15	220	202	35	21
1733.15	27	68	12	20	2130.10	19	132		15
1745.14	44	100	12	20	2151.85	143	160		15
1745.75	107	1055	18		2163.15	195	182		16
					2190.25	86	213		18
					2204.10	500	204		13
					2210.35	224	134		12
					2243.10	780	276		16
					2253.85	170	130	22	16
					2254.30	800	144		8
					2254.72	200	324	34	20
					2262.05	1000	245	98	16
					2262.90	193	212		14
					2263.08	130	148	22	14

TABLE 2C Normative Composition (weight percent)

(m)	Q	Or	Ab	An	He	Di	Fs	En	Fa	Fo	Mt	Ch	Il	Ap
						Gabbro Zone								
1012.10	0.66	0.06	7.19	45.81	4.32	11.90	7.86	18.86			2.45	0.03	0.36	0.19
1169.50	0.60	0.06	8.88	50.91	4.61	12.28	5.70	13.23			2.59	0.03	0.55	0.02
1282.70	0.74	0.06	5.50	37.98	5.21	21.57	5.03	18.14			2.46	0.03	0.38	0.14
1362.80	1.44	0.06	4.91	41.84	5.31	22.60	4.02	14.92			2.41	0.02	0.30	0.02
1449.60		0.06	3.72	67.29	1.45	17.50	0.61	6.38	0.05	0.49	2.26	0.02	0.11	0.09
1529.05	2.69	0.72	4.93	46.81	3.84	13.24	6.17	18.56			2.58	0.05	0.31	0.12
1529.70	4.53	0.59	5.44	38.21	4.39	16.21	6.46	20.76			2.48	0.06	0.27	0.65
1538.95	3.84	0.54	5.89	8.22	8.65	51.47	3.02	15.66			2.08	0.18	0.45	0.09
1540.02	2.32	0.60	1.97	13.81	9.92	43.78	4.96	19.07			2.97	0.24	0.38	0.09
1545.53	3.97	0.48	4.52	37.78	3.81	13.12	8.42	25.29			2.15	0.19	0.17	0.21
1545.73	0.33	0.12	4.91	36.90	4.82	18.32	6.31	20.89			2.88	0.02	0.17	0.93
1548.90		0.18	6.43	36.33	3.16	12.77	6.80	23.96	0.49	1.57	2.77	0.02	0.23	0.97
1549.62		0.18	3.38	15.82	3.95	15.47	10.81	36.95	0.61	1.88	4.20	0.02	0.27	0.88
1550.32	0.73	0.12	6.18	41.96	4.08	15.34	5.81	19.04			2.68	0.01	0.15	0.79
1551.60	1.47	0.18	4.91	42.87	6.05	17.18	6.38	15.79			1.38	0.01	0.17	0.95
1554.10	8.54	0.68	5.83	54.96	1.70	4.59	6.39	15.01			1.92	0.03	0.22	0.15
1574.80	4.94	0.06	1.39	45.84	4.63	17.08	5.66	18.22			1.78	0.04	0.20	0.19
1580.12	3.50	0.30	5.42	49.37	4.06	14.76	5.02	15.92			1.44	0.06	0.17	0.02
1590.20	3.91	0.35	4.94	39.30	5.32	21.07	5.02	17.33			2.24	0.10	0.21	0.27
1599.65	1.35	0.59	4.53	41.16	5.43	26.15	3.35	14.07			2.57	0.14	0.24	0.48
1616.15		0.06	0.09	15.82	5.01	20.26	11.00	38.76	1.41	4.52	2.85	0.05	0.19	0.02
1619.85	1.48	0.61	3.93	45.94	2.92	12.48	6.46	24.05			1.83	0.07	0.16	0.12
1659.30	4.28	0.53	4.42	34.42	4.40	19.65	5.89	22.94			2.70	0.07	0.29	0.44
1710.80	5.33	0.06	0.09	45.68	3.84	17.98	4.95	20.19			1.56	0.05	0.14	0.17
1711.20	2.40	0.74	6.47	40.23	3.93	21.80	3.53	17.04			3.34	0.07	0.44	0.05
1714.72	1.93	0.18	4.31	25.45	4.45	31.88	3.37	21.08			3.28	0.01	0.23	0.72
1719.15		0.24	4.82	46.71	3.80	21.59	2.75	13.62	0.15	0.69	1.52	0.01	0.11	0.76
1727.95	5.54	0.54	4.60	41.78	3.34	13.34	6.43	22.39			0.82	0.08	0.21	0.98
1731.18	0.36	0.24	5.33	39.89	4.34	21.94	4.08	17.97			2.03	0.01	0.21	0.70
1733.15		0.18	5.25	45.15	3.35	24.74	1.13	7.27	0.92	5.36	2.48	0.02	0.17	0.76
1745.14		0.30	3.21	18.53	6.15	47.73	1.50	10.13	1.27	7.76	2.81	0.02	0.23	0.90
1745.75	3.06	0.43	0.52	18.83	3.25	41.51	2.24	24.92			4.78	0.23	0.20	0.14

TABLE 2C (cont.) Normative Composition(weight percent)

(m)	Q	Or	Ab	An	He	Di	Fs	En	Fa	Fo	Mt	Ch	Il	Ap
						Pyroxenite Zone								
1748.10	1.51	0.36	2.26	4.48	7.63	61.44	2.32	16.29			2.26	0.38	0.25	1.00
1750.10		0.42	2.08	34.94	4.07	26.77	2.94	16.86	1.47	7.68	2.56	0.11	0.12	0.05
1794.60	2.13	0.42	2.85	5.79	8.06	53.79	3.61	21.00			1.54	0.42	0.25	0.35
1798.85	0.12	0.42	2.07	17.77	6.48	42.69	4.12	23.68			2.19	0.37	0.21	0.05
1801.30	1.55	0.36	2.50	17.41	5.97	40.20	4.21	24.72			1.74	0.41	0.23	0.90
1809.90	0.56	0.43	4.44	45.67	3.75	15.89	6.05	22.33			0.66	0.14	0.14	0.02
1813.40		0.71	1.95	11.19	5.00	49.02	2.72	23.25	0.20	1.55	3.13	0.57	0.17	0.81
1835.60		0.67	1.92	4.24	6.44	49.46	3.48	23.30	0.88	5.36	3.02	0.52	0.22	0.76
1837.86		0.66	2.15	10.32	4.61	45.88	3.17	27.50	0.13	1.05	3.40	0.45	0.17	0.73
1849.66		0.36	0.95	18.90	4.62	35.94	3.74	25.40	0.97	5.97	2.63	0.44	0.14	0.17
1855.20		0.06	0.68	5.99	6.64	41.16	3.07	16.57	3.70	18.11	2.28	0.09	0.13	0.05
1859.30	1.34	0.06	2.28	26.59	5.44	37.34	3.10	18.55			2.35	0.05	0.23	0.07
1869.15		0.06	1.35	11.50	5.53	51.94	2.57	21.06	0.11	0.83	2.29	0.05	0.15	0.14
1871.86		0.24	2.45	8.81	5.12	44.52	2.24	16.97	1.42	9.77	3.73	0.03	0.15	0.76
1875.30		0.35	2.96	11.05	4.71	43.38	2.88	23.15	0.89	6.51	3.73	0.03	0.17	0.83
1877.87		0.41	3.13	8.72	7.18	54.13	2.22	14.56	0.70	4.15	2.09	0.03	0.19	0.88
1879.92		0.41	2.11	3.06	3.96	46.99	1.21	12.50	1.96	18.38	4.09	0.05	0.11	0.56
1907.10		0.06	0.68	5.89	6.52	51.45	2.80	19.28	1.23	7.64	2.30	0.05	0.17	0.02
1952.55		0.06	1.44	11.24	4.55	59.49	1.34	15.21	0.19	1.95	2.29		0.15	0.35
1995.95		0.06	0.08	9.25	10.68	49.80	2.85	11.58	2.38	8.79	2.29	0.15	0.15	0.56
2048.60		0.06	0.85	11.44	4.99	46.17	2.04	16.46	1.52	11.16	2.28	0.05	0.13	0.19
2059.35		0.06	0.08	2.43	1.37	11.06	2.65	18.60	6.86	43.73	2.20	0.11	0.04	0.16
2063.05		0.06	0.59	7.54	5.27	42.12	2.74	19.05	2.38	15.02	2.29	0.04	0.15	0.49
2101.30	0.41	0.06	1.52	19.00	5.10	50.55	2.13	18.40			2.30	0.04	0.17	0.05
2113.83		0.30	2.62	4.90	7.94	54.47	1.33	7.95	2.05	11.10	1.80	0.03	0.19	0.72
2115.80		0.06	0.93	7.99	6.66	55.87	2.27	16.58	0.83	5.48	2.32	0.04	0.19	0.02
2117.83		0.30	2.45	5.02	4.58	46.43	1.87	16.53	1.59	12.77	4.15	0.03	0.17	0.93
2119.10		0.30	2.71	5.70	6.63	54.20	1.89	13.45	1.27	8.22	2.84	0.03	0.23	0.90
2122.15		0.24	2.37	5.25	5.96	51.88	1.10	8.38	2.42	16.71	3.55	0.04	0.19	0.63
2130.10	0.33	0.06	2.37	39.09	2.71	28.16	2.25	20.32			2.26	0.03	0.11	0.02
2151.85		0.06	1.10	14.72	5.14	48.87	1.32	10.94	1.39	10.48	2.28	0.03	0.13	0.02
2163.15		0.06	1.18	13.12	5.92	49.05	1.56	11.27	1.82	11.94	2.29	0.04	0.15	0.02
2190.25		0.06	0.85	7.08	6.34	61.34	1.80	15.18	0.34	2.59	2.33	0.05	0.21	0.09
2204.10		0.06	0.34	7.92	4.90	34.47	1.83	11.22	4.89	27.18	2.25	0.04	0.09	0.12
2210.35		0.06	1.86	15.13	5.37	41.89	1.64	11.14	2.55	15.75	2.29	0.03	0.15	0.32
2243.10		0.06	0.08	1.70	1.66	10.17	2.04	10.90	10.55	51.17	2.20	0.06	0.04	0.21
2253.85		0.18	2.79	10.02	6.00	50.30	0.88	6.43	2.36	15.63	2.70	0.03	0.17	0.69
2254.30		0.06	0.08	2.98	2.00	13.99	1.25	7.67	9.50	52.71	2.22	0.03	0.06	0.09
2254.72		0.30	2.54	4.13	3.82	54.47	0.95	11.78	1.12	12.61	4.68	0.07	0.17	0.69
2262.05	*		1.79	0.05	2.07			2.05	72.56	10.64	0.05	0.04	0.02	
2262.90		0.06	0.68	6.40	6.21	56.57	1.25	9.92	1.67	12.01	2.30	0.05	0.17	0.09
2263.08		0.18	0.34	9.06	5.82	57.31	1.25	10.70	1.42	11.05	3.39	0.03	0.21	0.21

*NOTE: Depth 2262.05 - Le 0.09, Ne 0.05, La 1.74

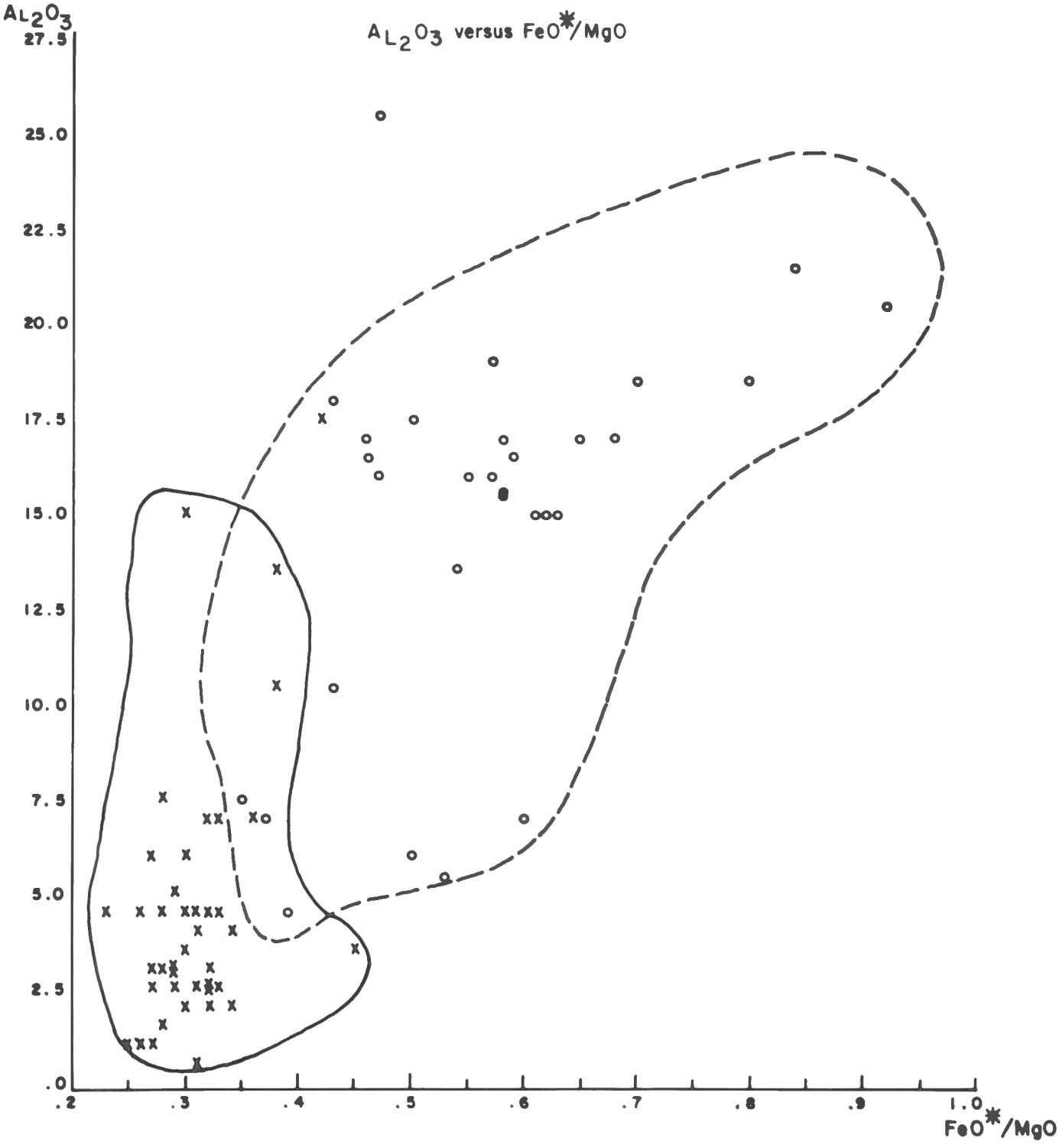

Figure 4a: Al_2O_3 plotted against the FeO (total):MgO ratio as a fractionation index. cross = pyroxenite, circle = gabbronorite.

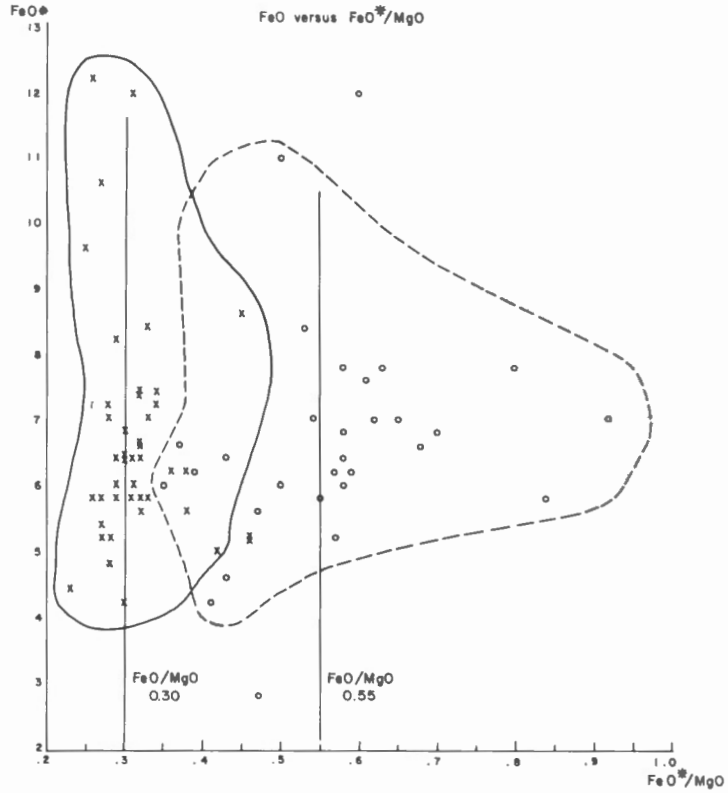

Figure 4b: FeO (total) plotted against the FeO (total):MgO ratio as a fractionation index. cross = pyroxenite, circle = gabbronorite.

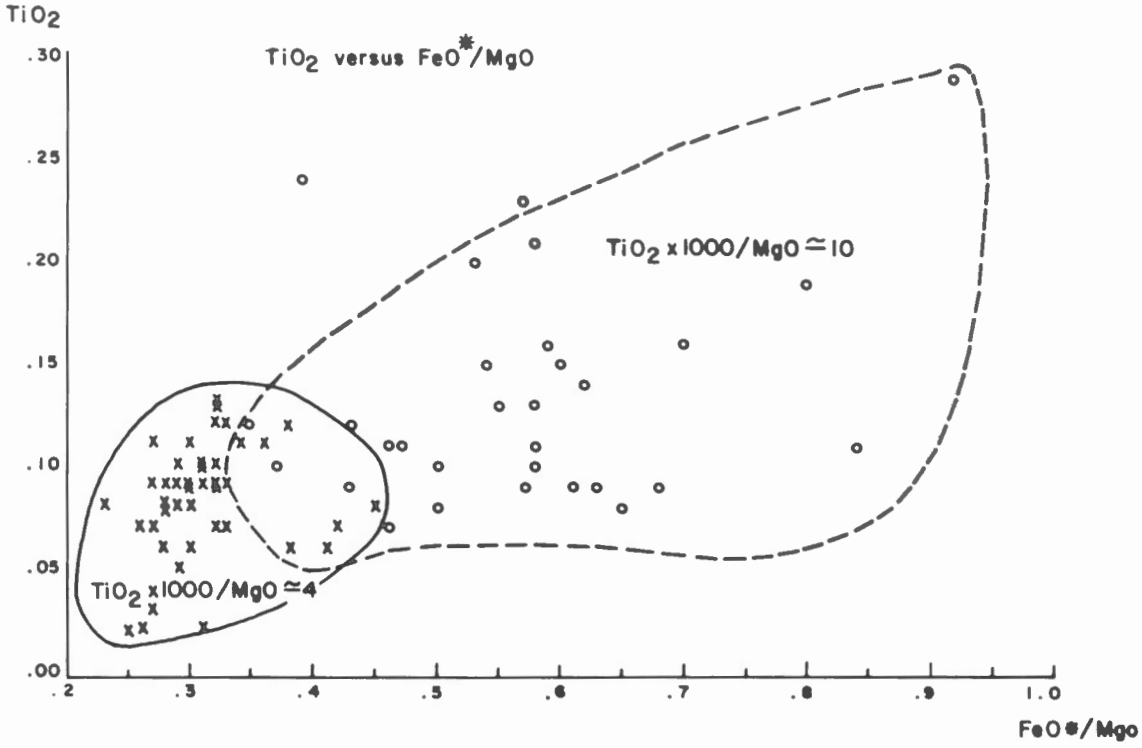

Figure 4c: TiO_2 plotted against the FeO (total):MgO ratio as a fractionation index. cross = pyroxenite, circle = gabbronorite.

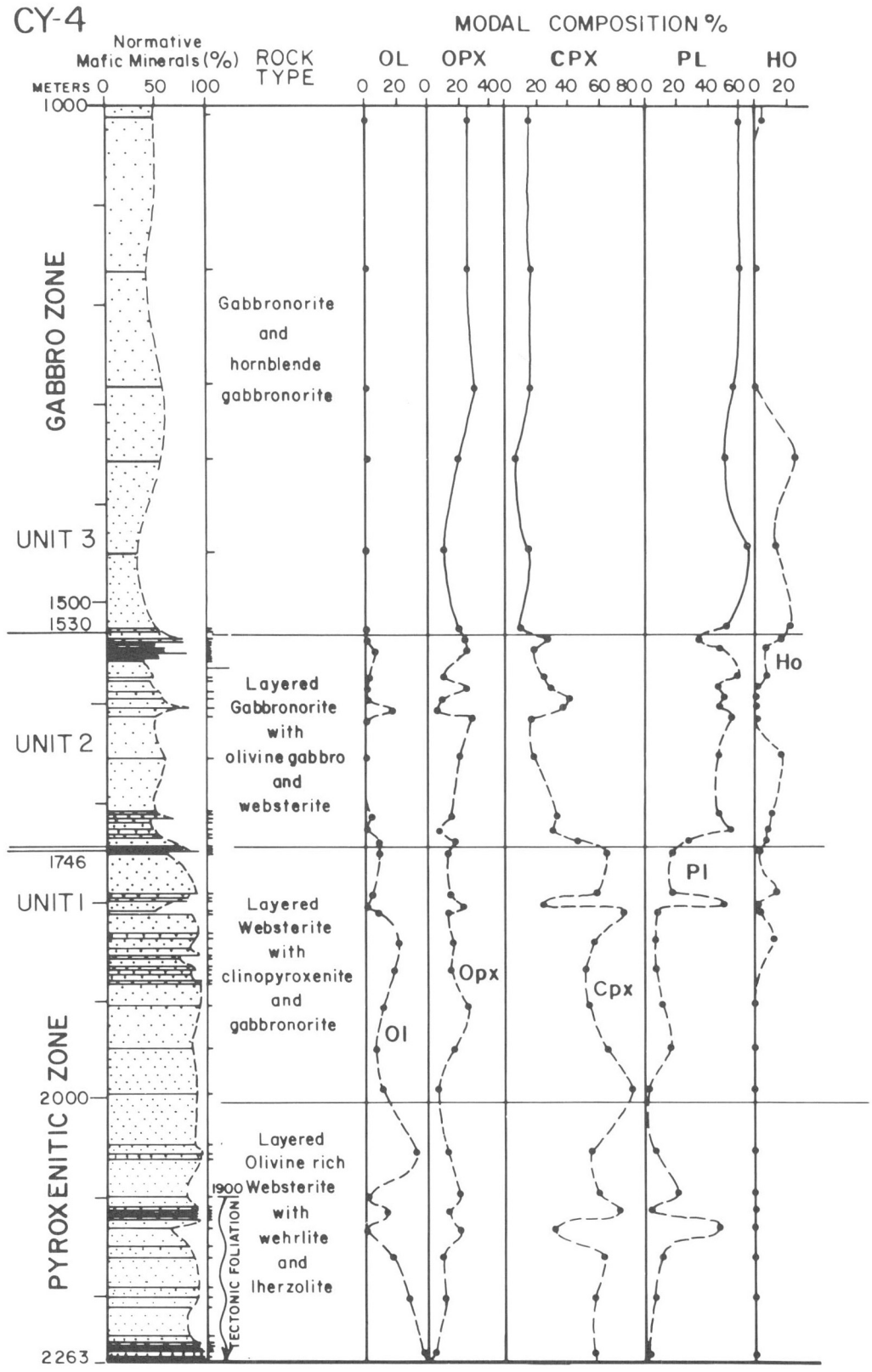

Figure 5: Chemical variations in the CY-4 section between 1000 and 2263 m.

The extent of chemical variation throughout the plutonic section is illustrated by plotting the differentiation index $(FeO+Fe_2O_3):MgO$, and the elements Ni, Cr, TiO_2 and P_2O_5 versus depth (Figure 5). The iron-magnesium ratio varies from around 0.2 at the base to a little less than 1 at the top. This trend, with the exception of a disturbed zone marking a significant change of regime at the interface between units 2 and 3 (1530 m deep), indicates a regular evolution of a single magmatic suite. The same information is indicated by the variation of Ni, a compatible trace element strongly fractionated by olivine. Chromium, partitioned into spinels and pyroxenes, changes at the boundaries between the units. Chromium reaches maximum values near the tops of units 1 and 2 where spinel is absent. Unit 3 is depleted in Cr compared to the underlying units. The incompatible elements titanium and phosphorus show slight enrichment up-section. TiO_2 follows closely the iron-magnesium ratio. P_2O_5 shows wide variations in units 1 and 2 because phosphorus is concentrated in layers with high proportions of intercumulus phases, a relation also observed in the Skaergaard intrusion (Wager, 1960). Unit 3, which is depleted in Cr_2O_3, is also poor in P_2O_5.

At a smaller scale, distinct chemical variation occurs within the compositionally layered pyroxenite and gabbro zones. Chemical features in a 10-m-thick section of olivine websterite from unit 1 versus a 35-m-thick section of gabbronorite from unit 2 are illustrated in Figure 6. The iron-magnesium ratio in websterite varies from 0.20 to 0.30, and in gabbronorite from 0.30 to 0.60. The Cr:Ni ratio, which is mainly controlled by the modal pyroxene:olivine ratio, is about 1 or less than 1 in websterite, while it varies in gabbronorite from higher than 1 to higher than 10. The $CaO:Al_2O_3$ ratio reflects the modal proportions of clinopyroxene and plagioclase; it is variable in websterite around an average value of about 5. In contrast, this ratio has a value of about 1 in gabbronorite, remaining relatively constant. SiO_2 varies greatly in websterite from less than 40% to more than 50% but is more uniform in gabbronorite, remaining close to 50%. In summary, the greatest chemical variations are observed in unit 1 of the basal plutonic section. Unit 2 still displays significant chemical variations but on a narrower range than unit 1. The chemical homogeneity of unit 3 is likely to reflect the conditions of crystallization of the more viscous residual melt evolved after fractionation of the underlying units 1 and 2. Some chemical changes do occur in unit 3 though they are not documented here due to the small number of samples studied in this unit.

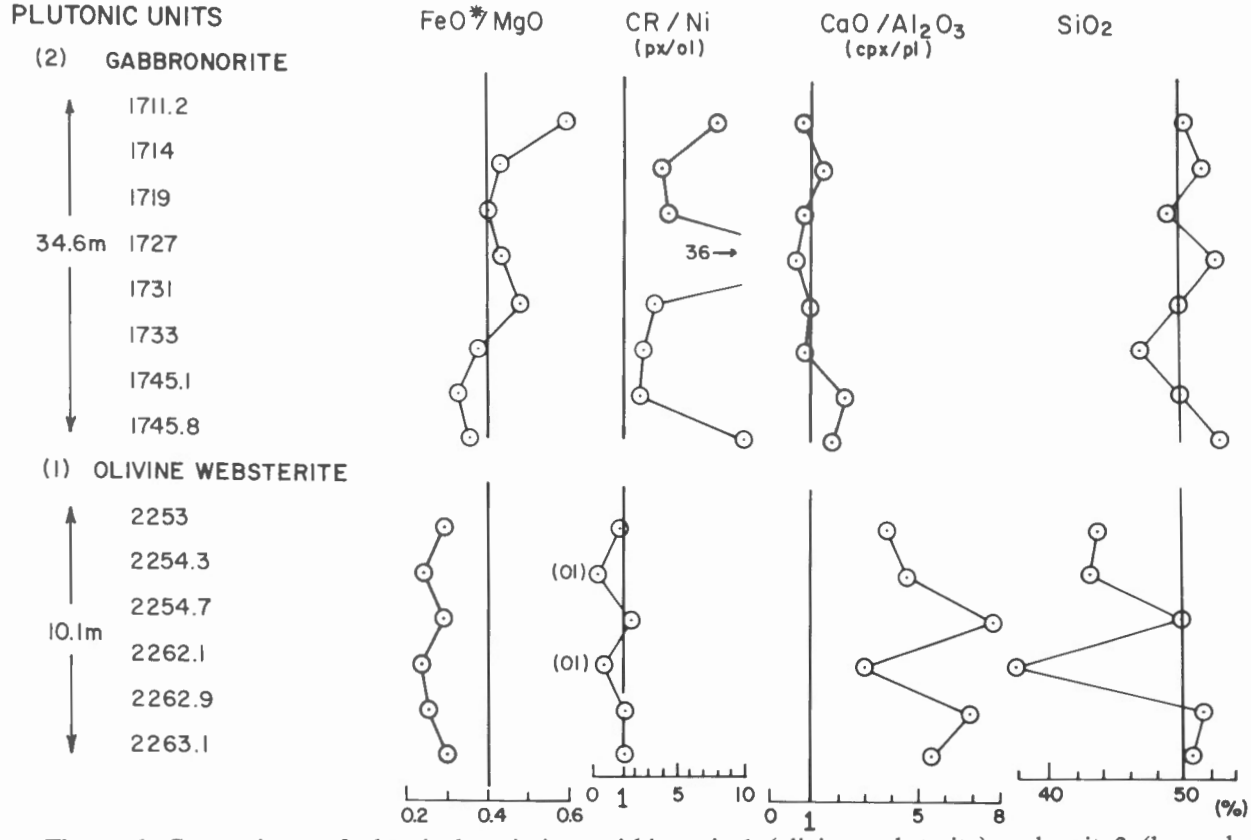

Figure 6: Comparisons of chemical variations within unit 1 (olivine websterite) and unit 2 (layered gabbronorite).

TABLE 3. Average Composition of CY-4 Plutonic Rocks

	Gabbro Zone		Pyroxenite Zone	
Number of samples	32		42	
wt. %				
SiO_2	50.50	46.38-55.31	50.46	38.02-54.87
TiO_2	0.13	0.06- 0.29	0.09	0.02- 0.13
Al_2O_3	14.98	4.26-25.39	4.57	0.72-17.68
Fe_2O_3	1.71	0.56- 3.30	1.96	0.45- 8.01
FeO	5.07	1.49- 9.19	4.98	2.72-10.49
MgO	12.15	6.10-21.93	22.18	11.93-45.82
MnO	0.14	0.06- 0.22	0.14	0.10- 0.18
CaO	14.56	9.10-18.47	15.22	2.24-19.23
Na_2O	0.54	0.01- 1.06	0.20	0.01- 0.52
K_2O	0.05	0.01- 0.13	0.04	0.01- 0.12
P_2O_5	0.18	0.01- 0.44	0.16	0.01- 0.43
ppm				
Ni	34	8 - 230	206	18 - 1000
Cr	285	28 - 1133	592	130 - 2650
Co	9	2 - 46	26	4 - 98
V	28	20 - 81	15	8 - 24

Average composition from analyses recalculated to 100% on a volatile-free basis.

TABLE 4A. Microprobe Analyses of Olivine

	Web 1801.30		Web 1813.40		Ol-Web 1835.60		Ol-Web 1837.86	
SiO_2	39.16	0.9850	40.23	1.0212	39.89	0.9963	40.21	0.9964
Al_2O_3	–	–	–	–	–	–	0.01	0.0004
FeO	17.55	0.3691	16.57	0.3517	18.00	0.3759	17.05	0.3534
MgO	44.20	1.6570	42.25	1.5982	43.57	1.6215	44.56	1.6458
MnO	0.13	0.0029	0.22	0.0047	0.30	0.0063	0.24	0.0051
CaO	0.02	0.0005	–	–	–	–	0.04	0.0011
Cr_2O_3	0.00	0.0001	–	–	–	–	0.03	0.0006
NiO	nd	–	0.15	0.0031	0.19	0.0038	nd	–
Sum	101.06	3.0146	99.42	2.9789	101.95	3.0038	102.15	3.0028
%Fo	81.67		81.96		81.18		82.11	

	Ol-Web 1855.20		Ol-Pl-Web 2048.60		Ol-Pl-Web 2151.85		Lherz 2254.30	
SiO_2	37.70	0.9805	40.58	0.9958	40.74	1.0035	39.24	0.9837
FeO	16.15	0.3512	14.95	0.3068	13.97	0.2877	12.57	0.2636
MgO	43.32	1.6797	46.29	1.6932	46.23	1.6968	47.15	1.7619
MnO	0.18	0.0124	0.19	0.0040	0.22	0.0045	0.15	0.0033
CaO	–	–	0.05	0.0012	0.01	0.0003	–	–
Cr_2O_3	0.06	0.0011	–	–	–	–	–	–
NiO	0.12	0.0024	0.17	0.0034	0.19	0.0038	0.20	0.0039
Sum	97.27	3.0162	102.22	3.0043	101.36	2.9966	99.31	3.0163
%Fo	82.70		84.66		85.50		86.65	

NOTE: Analyses recalculated on the basis of O=4.0

TABLE 4B. Microprobe Analyses of Orthopyroxene

	Gbn	1012.15	Gbn	1529.70	Gbn	1590.20	Gbn	1659.30	Web	1801.30
SiO_2	52.12	1.9213	54.49	1.9496	53.96	1.9507	55.22	1.9611	55.20	1.9389
TiO_2	0.20	0.0056	0.08	0.0021	0.08	0.0022	0.07	0.0017	0.06	0.0015
Al_2O_3	1.02	0.0447	1.24	0.0521	1.31	0.0559	0.89	0.0374	1.49	0.0618
FeO	20.21	0.6321	15.79	0.4725	15.02	0.4541	15.29	0.4542	10.48	0.3081
MgO	24.57	1.3693	27.62	1.4732	27.56	1.4849	28.75	1.5216	31.56	1.6522
MnO	0.37	0.0117	0.31	0.0094	0.27	0.0084	0.33	0.0099	0.22	0.0065
CaO	1.52	0.0609	1.54	0.0589	1.55	0.0600	0.79	0.0301	1.45	0.0545
Na_2O	0.13	0.0096	0.03	0.0018	0.01	0.0006	0.01	0.0008	0.00	0.0002
K_2O	0.02	0.0011	–	–	–	–	–	–	–	–
Cr_2O_3	0.00	0.0001	0.07	0.0020	0.05	0.0015	0.03	0.0009	0.11	0.0030
Sum	100.16	4.0562	101.16	4.0217	99.82	4.0183	101.38	4.0177	100.57	4.0268
%Wo		2.95		2.93		2.99		1.49		2.70
%En		66.01		73.15		73.98		75.47		81.74
%Fs		31.07		23.93		23.04		23.04		15.56

	Web	1813.40	Web	1835.60	Web	1837.86	Web	1855.20
SiO_2	56.90	1.9701	56.42	1.9732	56.56	1.9584	55.01	1.9087
TiO_2	0.06	0.0015	0.09	0.0092	0.06	0.0014	0.56	0.0146
Al_2O_3	1.44	0.0593	1.26	0.0521	1.65	0.0672	1.50	0.0614
FeO	11.18	0.3275	11.90	0.3479	10.11	0.2928	11.60	0.3367
MgO	29.34	1.5318	29.06	1.5143	31.53	1.6269	31.89	1.6490
MnO	0.18	0.0053	0.41	0.0122	0.30	0.0087	0.24	0.0069
CaO	2.40	0.0901	1.79	0.0670	1.16	0.0431	1.59	0.0589
Na_2O	0.04	0.0026	0.06	0.0021	0.01	0.0007	0.01	0.0007
Cr_2O_3	0.26	0.0071	0.62	0.0172	0.18	0.0049	0.21	0.0056
NiO	–	–	–	–	–	–	0.04	0.0011
Sum	101.80	3.9953	101.61	3.9952	101.54	4.0041	102.63	4.0436
%Wo		4.61		3.45		2.19		2.88
%En		78.37		78.00		82.52		80.38
%Fs		17.03		18.55		15.29		16.75

	Web	1952.55	Web	2048.60	Web	2151.85	Lherz	2254.30
SiO_2	56.02	1.9442	55.90	1.9362	55.25	1.9359	53.99	1.8879
TiO_2	0.09	0.0025	0.06	0.0016	0.07	0.0019	0.56	0.0147
Al_2O_3	1.53	0.0634	1.33	0.0549	1.41	0.0581	2.08	0.0857
FeO	10.67	0.3144	10.46	0.3072	8.65	0.2534	9.35	0.2734
MgO	31.32	1.6433	31.74	1.6619	32.59	1.7017	33.13	1.7265
MnO	0.25	0.0075	0.25	0.0073	0.23	0.0069	0.21	0.0062
CaO	1.04	0.0393	1.59	0.0599	1.85	0.0695	1.18	0.0042
Na_2O	0.01	0.0004	0.01	0.0007	–	–	0.02	0.0014
Cr_2O_3	0.16	0.0046	0.13	0.0035	0.1 4	0.0039	0.33	0.0091
NiO	–	–	0.02	0.0005	0.02	0.00 04	0.05	0.0014
Sum	101.09	4.0195	101.46	4.0335	100. 20	4.0315	100.90	4.0105
%Wo		1.96		2.95		3.43		2.16
%En		81.98		81.77		83.77		84.21
%Fs		16.06		15.44		12.81		13.64

NOTE: Analyses recalculated on the basis of O=6.

TABLE 4C. Microprobe Analyses of Clinopyroxene

	Gbn	1012.15	Gbn	1529.70	Pl-Web	1538.95	Gbn	1590.20
	ox wt%	O=6.0	ox wt%	O=6.0	ox wt%	O=6.0	ox wt%	O=6.0
SiO_2	50.03	1.9142	52.79	1.9576	52.53	1.9481	52.09	1.9425
TiO_2	0.31	0.0089	0.20	0.0057	0.22	0.0060	0.26	0.0074
Al_2O_3	1.24	0.0568	1.77	0.0776	1.62	0.0711	1.45	0.0637
FeO	8.85	0.2872	7.09	0.2200	6.15	0.1909	7.13	0.2224
MgO	14.78	0.8550	16.71	0.9234	15.76	0.8710	16.29	0.9056
MnO	0.23	0.0076	0.18	0.0057	0.15	0.0046	0.14	0.0045
CaO	21.87	0.9096	20.13	0.7999	22.81	0.9063	21.60	0.8631
Na_2O	0.25	0.0188	0.13	0.0091	0.15	0.0107	0.11	0.0082
K_2O	–	–	0.01	0.0003	0.01	0.0003	0.01	0.0006
Cr_2O_3	–	–	0.07	0.0021	0.15	0.0043	0.09	0.0028
Sum	97.55	4.0579	99.09	4.0012	99.54	4.0133	99.19	4.0209
%Wo	44.18		41.05		45.93		43.25	
%En	41.52		47.38		44.15		45.39	
%Fs	14.31		11.58		9.92		11.36	

	Gbn	1659.30	Gb	1728.05	Clinopx	1748.10	Web	1801.30
	ox wt%	O=6.0	ox wt%	O=6.0	ox wt%	O=6.0	ox wt%	O=6.0
SiO_2	54.07	1.9663	53.57	1.9784	52.69	1.9385	53.37	1.9643
TiO_2	0.13	0.0035	0.05	0.0013	0.14	0.0038	0.06	0.0016
Al_2O_3	1.64	0.0703	0.37	0.0162	1.75	0.0760	1.34	0.0581
FeO	7.58	0.2305	5.44	0.1680	4.63	0.1423	3.95	0.1217
MgO	15.53	0.8416	16.18	0.8907	17.26	0.9466	17.53	0.9617
MnO	0.19	0.0057	0.18	0.0058	0.12	0.0039	0.13	0.0041
CaO	22.29	0.8687	23.89	0.9455	22.74	0.8963	22.35	0.8815
Na_2O	0.15	0.0100	0.09	0.0067	0.10	0.0074	0.07	0.0049
K_2O	–	–	–	–	0.01	0.0003	0.01	0.0004
Cr_2O_3	0.05	0.0017	0.06	0.0018	0.19	0.0055	0.21	0.0061
NiO	–	–	–	–	–	–	–	
Sum	101.65	3.9998	99.83	4.0142	99.63	4.0205	99.03	4.0043
%Wo	44.60		47.04		45.06		44.77	
%En	43.20		44.31		47.59		48.84	
%Fs	12.10		8.64		7.35		6.39	

NOTE: Analyses recalculated on the basis of O=6

TABLE 4C (cont.) Microprobe Analyses of Clinopyroxes

	Web	1813.40	Ol-Web	1835.60	Ol-Web	1837.86	Ol-Web	1855.20
SiO_2	54.95	1.9869	54.99	1.9946	53.72	1.9569	52.65	1.9242
TiO_2	0.07	0.0020	–	–	0.14	0.0037	0.40	0.0110
Al_2O_3	1.54	0.0656	1.33	0.0567	2.02	0.0869	1.33	0.0571
FeO	4.91	0.1484	3.83	0.1160	4.33	0.1319	4.37	0.1332
MgO	17.01	0.9166	17.09	0.9238	17.20	0.9341	18.85	1.0238
MnO	0.13	0.0039	0.11	0.0035	0.15	0.0047	0.16	0.0048
CaO	21.38	0.8282	21.92	0.8516	22.08	0.8617	22.27	0.8698
Na_2O	–	–	0.19	0.0136	0.09	0.0062	0.08	0.0056
K_2O	0.47	0.0135	–	–	–	–	–	–
Cr_2O_3	0.47	0.0135	0.566	0.0161	0.29	0.0082	0.42	0.0122
NiO	–	–	–	–	–	–	0.05	0.0014
Sum	100.66	3.9768	100.02	3.9759	100.02	3.9946	100.57	4.0432
%Wo	43.66		44.94		44.59		42.83	
%En	48.32		48.75		48.34		50.38	
%Fs	8.03		6.31		7.07		6.79	

	Web	1952.55	Ol-Pl-Web	2048.60	Ol-Pl-Web	2151.85	Lherz	2254.30
SiO_2	53.21	1.9516	53.56	1.9480	52.53	1.9370	50.97	1.8802
TiO_2	0.08	0.0022	0.06	0.0017	0.11	0.0031	0.89	0.0247
Al_2O_3	1.31	0.0571	1.67	0.0723	2.13	0.0928	2.24	0.0974
FeO	4.02	0.1251	4.30	0.1321	3.95	0.1218	4.05	0.1250
MgO	16.84	0.9333	17.54	0.9600	17.97	0.9987	17.74	0.9753
MnO	0.17	0.0052	0.16	0.0049	0.19	0.0059	0.17	0.0052
CaO	23.18	0.9246	22.33	0.8786	21.48	0.8488	22.89	0.9049
Na_2O	0.14	0.0098	0.10	0.0069	0.10	0.0068	0.09	0.0067
Cr_2O_3	0.31	0.0090	0.29	0.0182	0.27	0.0077	0.64	0.0187
NiO	–	–	0.03	0.0008	0.06	0.0017	0.07	0.0022
Sum	99.25	4.0180	100.03	4.0233	98.77	4.0131	99.76	4.0404
%Wo	46.51		44.48		43.20		45.01	
%En	46.93		48.58		50.29		48.51	
%Fs	6.56		6.95		6.50		6.47	

NOTE: Analyses recalculated on the basis of O=6

TABLE 4D. Microprobe Analyses of Plagioclase

	Gbn	1012.15	Gbn	1529.70	Web	1538.95	Gbn	1590.20	Gbn	1659.30
SiO_2	44.78	2.083	44.58	2.0810	44.43	2.0612	44.30	2.0746	44.5 8	2.0763
Al_2O_3	34.66	1.901	35.00	1.9254	35.15	1.9222	34.54	1.9066	35.10	1.9266
FeO	0.50	0.020	0.46	0.0182	0.49	0.0191	0.53	0.0208	0.38	0.0146
MgO	0.04	0.003	0.01	0.0008	0.06	0.0041	0.08	0.0053	0.01	0.0007
MnO	0.07	0.003	–	–	0.01	0.0004	–	–	0.01	0.0005
CaO	18.13	0.904	17.85	0.8926	18.84	0.9365	18.44	0.9252	18.11	0. 9036
Na_2O	1.18	0.107	0.80	0.0722	0.70	0.0632	0.84	0.0763	0.81	0. 0734
K_2O	–	–	0.01	0.0004	0.01	0.0004	0.01	0.0006	0.01	0.0007
Sum	99.36	5.020	98.70	4.9905	99.69	5.0071	98.73	5.0095	99.00	4. 9965
%Ab	10.50		7.47		6.32		7.62		7.50	
%Or	–		0.05		0.04		0.05		0.07	
%An	89.50		92.48		93.63		92.32		92.43	

	Gb	1728.05	Web	1801.30	Web	1813.40	Web	1835.60	Web	1837.86
SiO_2	44.23	2.0608	43.96	2.0650	45.73	2.0109	47.44	2.1468	45. 56	2.0851
Al_2O_3	35.19	1.9323	35.00	1.9378	36.20	1.9313	34.53	1.8410	35.66	1.9238
FeO	0.37	0.0146	0.27	0.0105	–	–	–	–	0.27	0.0102
MgO	0.02	0.0014	0.00	0.0002	–	–	–	–	0.06	0.0042
MnO	–	–	0.02	0.0008	–	–	–	–	0.00	0.0001
CaO	18.72	0.9345	18.24	0.9181	19.26	0.9345	18.14	0.8798	18.25	0.8949
Na_2O	0.61	0.0548	0.71	0.0642	0.60	0.0528	1.44	0.1262	0.72	0 .0643
K_2O	0.00	0.0002	0.02	0.0009	–	–	–	–	0.02	0.0011
Sum	99.16	4.9987	98.21	4.9976	101.79	4.9895	101.62	4.9976	100.55	4.9838
%Ab	5.53		6.55		5.50		12.54		6.70	
%Or	0.02		0.09		–		–		0.12	
%An	94.42		93.36		94.50		87.46		93.19	

	Web	1952.55	Web	2048.60	Web	2151.85
SiO_2	42.82	2.000	44.95	2.060	45.02	2.069
Al_2O_3	36.08	1.987	35.78	1.933	35.45	1.920
FeO	0.34	0.013	0.30	0.012	0.29	0.012
MgO	0.06	0.004	0.05	0.004	0.06	0.004
MnO	0.06	0.003	0.08	0.003	0.05	0.002
CaO	19.47	0.974	19.04	0.935	19.22	0.946
Na_2O	0.62	0.056	0.64	0.056	0.43	0.038
K_2O	–	–	–	–	–	–
Sum	99.39	5.035	100.87	5.003	100.55	4.992
%Ab	5.45		6.40		3.88	
%Or	–		–		–	
%An	94.55		93.60		96.12	

NOTE: Analyses recalculated on the basis of O=8.

TABLE 4E. Microprobe Analyses of Amphiboles

	Gbn	1529.70	Pl-Web	1538.95	Gbn	1659.30	Gb	1728.05
SiO_2	51.87	7.3733	53.47	7.5395	52.68	7.5256	53.64	7.7434
TiO_2	0.62	0.0663	0.64	0.0679	0.28	0.0302	0.05	0.0049
Al_2O_3	5.17	0.8685	2.84	0.4726	3.77	0.6369	2.04	0.3477
FeO	8.74	1.0405	8.96	1.0571	8.43	1.0089	11.92	1.4396
MgO	18.75	3.9726	19.52	4.1019	19.45	4.1401	16.58	3.5659
MnO	0.12	0.0139	0.14	0.0162	0.13	0.0164	0.30	0.0372
CaO	11.02	1.6794	11.99	1.8109	11.01	1.6858	12.34	1.9084
Na_2O	0.71	0.1951	0.28	0.0767	0.54	0.1513	0.10	0.0281
K_2O	0.02	0.0044	0.03	0.0046	0.02	0.0040	0.00	0.0002
Cr_2O_3	0.06	0.0070	0.29	0.0321	0.02	0.0020	0.09	0.0102
OH	2.11	1.0000	2.12	1.0000	2.10	1.0000	2.08	1.0000
Sum	99.19	16.2210	100.28	16.1794	98.43	16.2011	99.14	16.0855
FM Ratio	0.210		0.207		0.200		0.293	

	Clinopx	1748.10	Web	1801.30	Ol-Web	1837.86
SiO_2	49.41	6.9932	52.67	7.3820	54.81	7.5796
TiO_2	0.48	0.0511	0.34	0.0355	0.20	0.0205
Al_2O_3	7.64	1.2739	5.32	0.8772	3.74	0.6090
FeO	7.20	0.8526	5.49	0.6432	6.72	0.7780
MgO	18.97	4.0021	20.20	4.2207	20.44	4.2121
MnO	0.04	0.0049	0.07	0.0081	0.26	0.0308
CaO	12.39	1.8784	12.04	1.8071	11.46	1.6980
Na_2O	0.90	0.2465	0.55	0.1499	0.42	0.1135
K_2O	0.01	0.0011	0.02	0.0040	0.04	0.0072
Cr_2O_3	0.82	0.0916	0.55	0.0612	0.64	0.0703
OH	2.12	1.0000	2.14	1.0000	2.17	1.0000
Sum	99.97	16.3953	99.38	16.1888	100.91	16.1191
FM Ratio	0.176		0.134		0.160	

NOTE: Analyses recalculated on the basis of 0=24

TABLE 4F. Microprobe Analyses of Spinels (chromite)

	Web	1801.30	Web	1813.40	Ol-Web	1835.60
SiO_2	–	–	0.81	0.2450	1.13	0.3346
TiO_2	1.26	0.2775	1.17	0.2660	2.16	0.4841
Al_2O_3	7.52	2.5358	9.10	2.8740	9.24	2.4190
Fe_2O_3	32.14	7.0300	–	–	–	–
FeO	30.79	7.4398	57.30	14.4570	55.98	13.8670
MgO	1.70	0.7255	3.33	1.4980	3.23	1.4240
MnO	0.44	0.1062	0.65	0.1670	0.79	0.1960
CaO	0.03	0.0103	0.53	0.1720	1.02	0.3257
Cr_2O_3	25.91	5.8672	27.43	6.5450	27.61	6.4640
NiO	–	–	0.06	0.0160	0.06	0.0160
Sum	99.80	23.9924	100.38	26.2400	101.22	25.5260
Cr/Cr+Al	0.70		0.69		0.73	
Mg/Mg+Fe	0.09		0.09		0.05	

	Ol-Web	1837.86	Ol-Web	1855.20	Lerz	2254.30
TiO_2	1.50	0.3214	0.31	0.0620	0.24	0.0044
Al_2O_3	7.33	2.4683	20.72	6.4860	23.74	6.8841
Fe_2O_3	39.46	8.4851	15.32	2.9203	6.65	1.2299
FeO	28.88	6.9037	39.33	8.7330	19.02	3.9137
MgO	3.16	1.3480	6.68	2.6430	19.98	4.0237
MnO	0.28	0.0686	0.49	0.1100	0.45	0.0924
Cr_2O_3	19.48	4.4016	33.80	7.0950	40.10	7.7977
NiO	–	–	0.09	0.0190	0.07	0.0141
Sum	100.11	23.9967	101.42	25.1480	101.25	24.0000
Cr/Cr+Al	0.64		0.52		0.53	
Mg/Mg+Fe	0.16		0.32		0.51	

NOTE: Analyses calculated on the basis of 0=32

TABLE 4G. Microprobe Analyses of Magnetite and Ilmenite

	Gbn	1529.70	Pl-Web	1538.95	Gbn	1590.20
SiO_2	0.10	0.0298	0.04	0.0136	0.47	0.1433
TiO_2	2.00	0.4718	0.17	0.0403	1.95	0.4476
Al_2O_3	0.59	0.2166	0.24	0.0904	1.68	0.6046
Fe_2O_3	61.44	14.4583	61.40	14.7483	56.84	13.1220
FeO	31.95	8.3589	29.68	7.9238	31.64	8.1133
MgO	0.11	0.0528	0.07	0.0310	0.27	0.1221
MnO	0.14	0.0362	0.25	0.0669	0.47	0.1219
CaO	0.10	0.0350	0.13	0.0448	0.22	0.0709
Cr_2O_3	1.35	0.3335	4.14	1.0434	4.94	1.1975
Sum	97.77	23.9929	96.12	24.0024	98.46	23.9431

	Gbn	1659.30	Gbn	1659.30	Gb	1728.05
SiO_2	–	–	0.05	0.0024	–	–
TiO_2	0.91	0.2112	48.05	1.8339	51.55	1.9593
Al_2O_3	0.57	0.2080	–	–	–	–
Fe_2O_3	65.83	15.2810	8.23	0.3160	1.74	0.0661
FeO	31.56	8.1419	38.48	1.6333	42.73	1.8061
MgO	0.11	0.0518	0.14	0.0105	0.46	0.0348
MnO	0.05	0.0136	4.52	0.1943	2.83	0.1213
CaO	0.03	0.0098	0.04	0.0022	0.20	0.0109
Cr_2O_3	0.33	0.0805	0.21	0.0084	0.15	0.0058
Sum	99.40	23.9979	99.77	4.0010	99.67	4.0044

Note: Analyses recalculated on the basis of O=32 (Magnetite) and O=6 (Ilmenite).

Mineral Chemistry and Cryptic Variations

Samples were selected for microprobe analysis to ascertain the composition of the main fractionating minerals and to test for significant changes at the unit boundaries. Olivine, orthopyroxene, clinopyroxene, plagioclase, amphiboles, Cr-spinel and Fe-Ti oxides were analyzed (Tables 4a-4g).

Pyroxene compositions are plotted in Figure 7. Coexisting olivine compositions are shown along the base of the quadrilateral, and tie lines connect coexisting assemblages. There is a distinct iron enrichment trend in olivine and pyroxenes from the basal pyroxenites to the upper gabbronorites. However, the fractionation of mineral compositions between 2263 and 1000 m is limited. Olivine compositions within the pyroxenitic zone vary from Fo_{87} to Fo_{81}; some chromite is associated with olivine. In the gabbronorites, olivine is rare and the primary oxide is chromiferous magnetite; exsolution lamellae of ilmenite occur in hornblende. Compositions of clinopyroxene vary from $Wo_{43}En_{51}Fs_6$ in the basal olivine websterite to $Wo_{44}En_{41.5}Fs_{14.5}$ in the upper gabbronorites. The clinopyroxenes are low in chromium and aluminum ($<0.70\%$ Cr_2O_3, $<2.25\%$ Al_2O_3) and they are poor in titanium (average values vary from 0.10 to 0.30% TiO_2). Orthopyroxene varies from En_{85} at the base to En_{66} at the top of the plutonic sequence. The composition of postcumulus plagioclase varies only from An_{95} to An_{92} in the pyroxenite; in the gabbronorites, pseudo-cumulus plagioclase has a composition close to An_{90}.

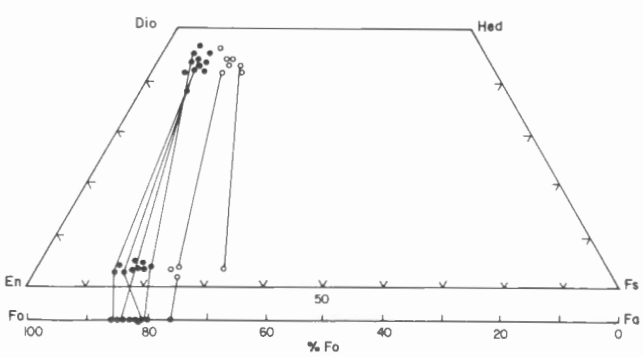

Figure 7: Pyroxene compositions from the CY-4 plutonic rocks, plotted in En-Wo-Fs quadrilateral, and compared to coexisting olivine. Solid circle = pyroxenites, open circles = gabbronorites.

Compositions of mineral phases are shown in Figure 8. These data suggest that there is a significant change between the top of unit 1 and the base of unit 2, which is shown by a break in the compositional trend of orthopyroxene and clinopyroxene. On the other hand, the break at top of unit 2 does not seem to be a major one, being documented here only by a change in the clinopyroxene composition. Figure 9 shows the cation Fe:(Fe+Mg) ratios of olivine, orthopyroxene, clinopyroxene and hornblende versus the sample depth. The compositional break at the top of unit 1, the pyroxenitic zone, is evident. More analyses of this critical zone are needed in order to understand the origin of this feature (depositional gap or tectonic break ?). All phases, with the possible exception of amphibole, are in apparent equilibrium. Differences in Fe:(Fe+Mg) ratios between coexisting olivine-orthopyroxene pair on one side and clinopyroxene on the other are due to their distinct Fe:Mg partition coefficients (Roeder and Emslie, 1970; Stern, 1979). Most pyroxenes have abundant exsolution lamellae and their original compositions must be evaluated by combining the composition of the host and exsolution lamellae in their respective proportions (Lindsley, 1983). In this work, pyroxene compositions were obtained by averaging up to 10 different points within one analyzed grain, thus hopefully covering the composition of both host and exsolution lamellae. In any case, mass balance rules indicate that subsolidus re-equilibration has probably not significantly altered the cryptic chemical variations observed, because pyroxenes and olivine are the most abundant phases.

Evolution of the iron-magnesium ratio is well defined. Extrapolation of this trend in Figure 9 from the base of unit 1 downward suggests that the dunitic zone may be situated 280 m below the present bottom of CY-4 at the approximate depth of 2540 m, assuming that the dunite has a Fe:(Fe+Mg) value of 0.10 (Fo_{90}) and that there is no tectonic complication. From variations of the iron-magnesium ratio and nickel contents of olivines, between 1800 and 2260 m, (Figure 10a), it is possible to predict that the basal dunite is likely to consist of olivine Fo_{90} with a maximum Ni content of 2600 ppm (0.33% NiO)(Figure 10b). This is consistent with results obtained by Hébert (1985) and Benn (1986) on the composition of dunites directly overlying the mantle harzburgite southwest of the CY-4 site, as well as with former petrological studies of Troodos dunites (Wilson, 1959; Allen, 1975; Greenbaum, 1972; 1977).

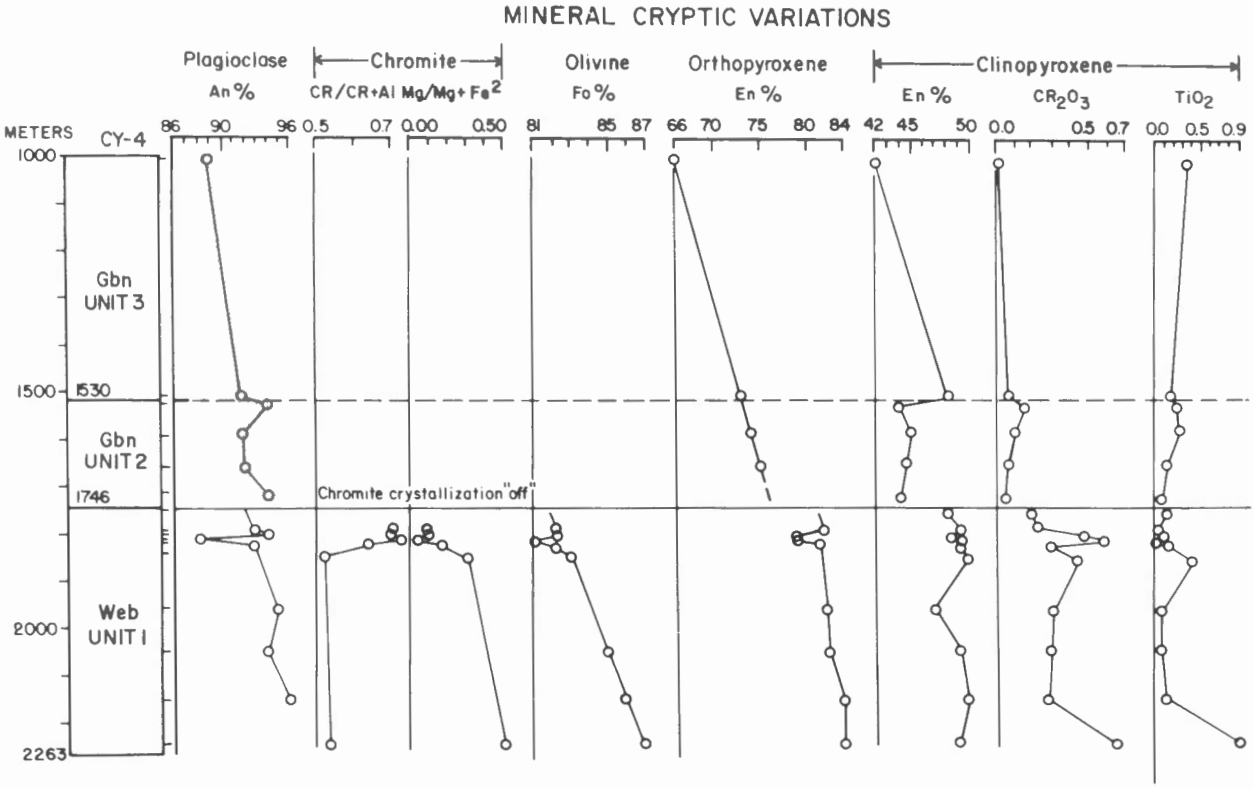

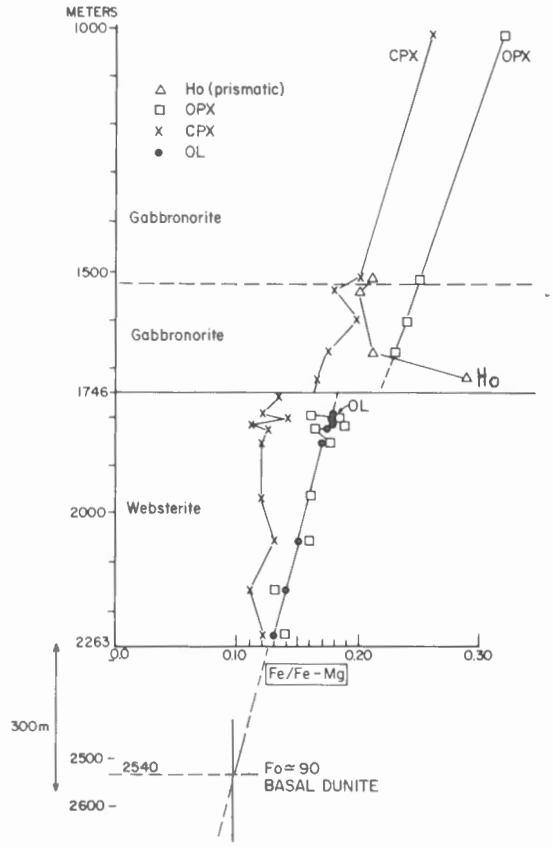

Figure 8: Variations of mineral chemistry in the CY-4 section between 1000 and 2263 m.

Figure 9: Cation Fe:(Fe+Mg) ratio of olivine (Ol), orthopyroxene (Opx), clinopyroxene (Cpx) and amphibole (Ho) plotted according to position in the CY-4 section.

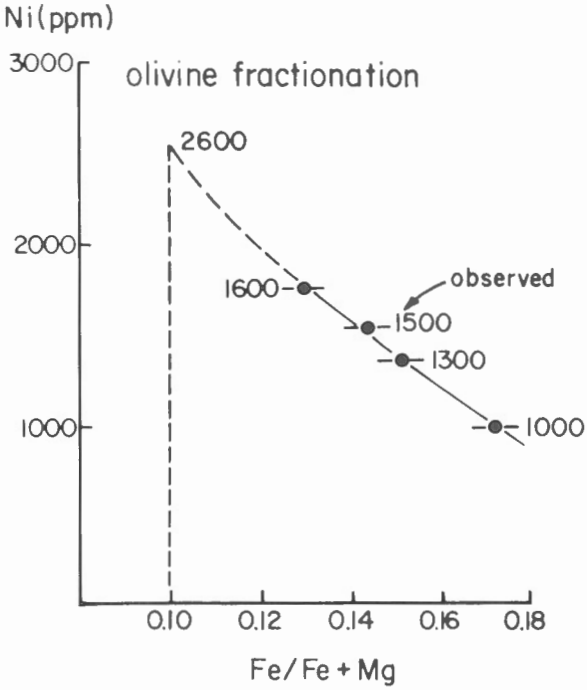

Figure 10a: Nickel content of olivine plotted against its cation Fe:(Fe+Mg) ratio.

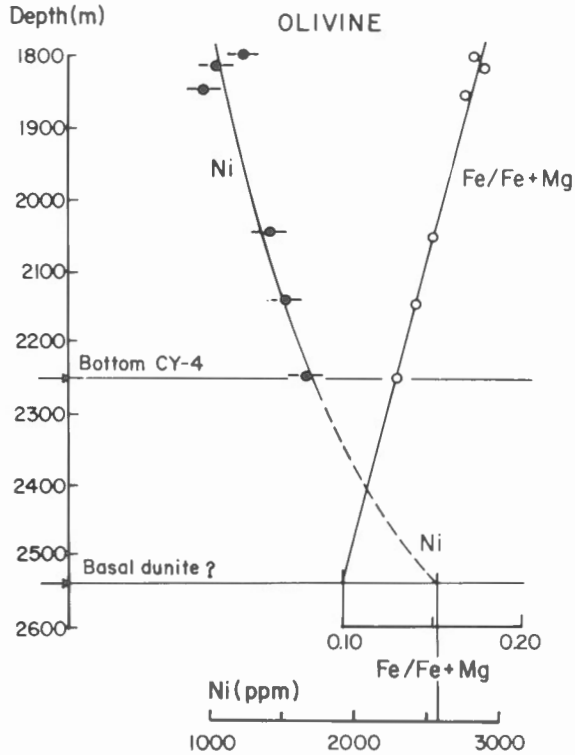

Figure 10b: Nickel content and Fe:(Fe+Mg) ratio of olivine plotted according to position in the CY-4 section.

DISCUSSION AND PRELIMINARY CONCLUSIONS

The plutonic section has been divided into three major units characterized by distinct mineral and chemical compositions, as well as by different orders of mineral crystallization. The sequence appears to form a single differentiation suite derived from the same parental magma. The three plutonic units correspond to an early, median and late fractionation stage of the magma, respectively. The only significant break (documented here) within the sequence is at the top of unit 1.

Some of the pertinent phase relations are exhibited by the simple system Olivine (Fo) - Clinopyroxene (Di) - Silica (SiO_2). The liquidus boundaries at 1 atm (Kushiro, 1972) and 10 kbar (Presnall et al., 1979) are shown in Figure 11. The parental magma may have formed at high pressure (about 10 kbar or more) through cotectic partial melting of aluminous lherzolite with olivine, orthopyroxene and clinopyroxene as the main mineral components. All phases take part in the initial melting at high pressure and the composition of the melt is determined by the phase relations. At lower pressures, the field of Fo is enlarged and the parental magma precipitated olivine to form the basal dunite. This unit, though not reached by drilling, is known from field observations. Iron:magnesium ratios of olivine and pyroxene also indicate that olivine is the first mafic mineral to crystallize from the magma. Fractionation of olivine drove the liquid composition to the Fo-Di join, and then to the reaction point Fo-Di-low calcium pyroxene. The path X to R in Figure 11 is documented by unit 1, the olivine websterites and websterites, with cumulus olivine, clinopyroxene, orthopyroxene and postcumulus orthopyroxene and plagioclase. The assemblage olivine and orthopyroxene is incongruent because the peritectic field boundary in the system at low pressure does not allow concomitant crystallization of olivine and orthopyroxene. However, most websterites contain only small amounts of olivine and their olivine:orthopyroxene ratio decreases rapidly up section. They may represent physically mixed cumulates grading between pure olivine cumulates (dunites) and pure pyroxene cumulates (websterites). It is also possible that this early stage of crystal fractionation occurred at relatively high pressure. Such conditions may have promoted cotectic crystallization of olivine and orthopyroxene followed later by lowering of pressure and further differentiation with a peritectic relationship (Irvine, 1970).

Early crystallization at high pressure and temperature is also suggested by the metamorphic overprint documented in the basal cumulates. The late appearance of plagioclase in the crystallization order seems to be characteristic of the magmatic evolution

and not to be controlled by the physical properties of the plagioclase (e.g. its low density preventing its accumulation on the floor of the magma chamber). If plagioclase had crystallized before clinopyroxene, we would have observed inclusions of plagioclase in clinopyroxene. We do not see this relation in the basal ultramafic cumulates below 2000 m. Some inclusions of plagioclase, however, occur in clinopyroxene above 2000 m. The anorthitic composition of plagioclase reflects high initial $CaO:Na_2O$ ratios (>10) in the parental magma. High water pressures may also have increased the anorthite content of plagioclase (Moores and Thy, 1985), as suggested by experimental studies of the system Ab-An-H_2O (Johannes, 1978). The liquid composition moved later from R to T. T represents the cotectic at low pressure where the system becomes silica oversaturated and the upper noritic gabbros of unit 3 with orthopyroxene, clinopyroxene, plagioclase and quartz are precipitated. Hornblende also occurs as a late magmatic phase in both pyroxenites and gabbros, demonstrating the growing importance of water in the system during successive stages of fractional crystallization. After the initial crystallization of chromite with olivine, oxides did not fractionate in significant amounts within unit 1. The vanadium content of the melt increased with differentiation, the average gabbronorite being clearly richer in V than the pyroxenites (Tables 2a and 3).

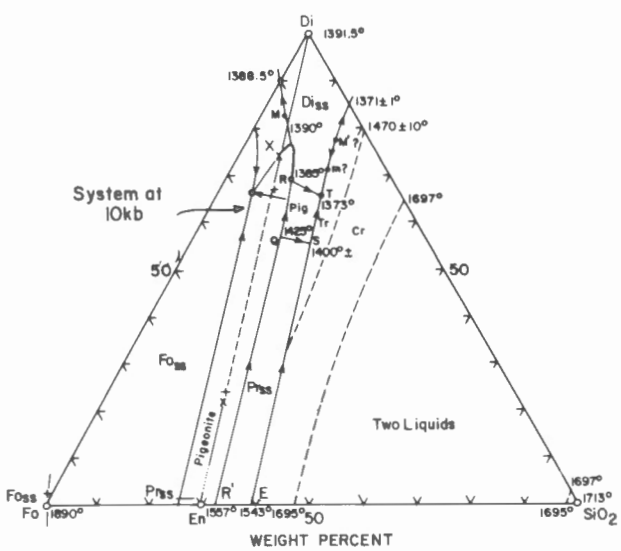

Figure 11: Phase equilibrium diagram of the system Fo-Di-SiO_2 at atmospheric and at 10 Kbars pressure (Kushiro, 1972; Presnall et al., 1979). The fractionation path X to R is represented by the CY-4 plutonic units.

In order to define quantitatively the differentiation trend, we have calculated the magnesium-iron ratio of the various liquid fractions from the Mg:Fe ratios of their analyzed cumulate minerals (Figure 12). The Mg:Fe liquid-crystal partition coefficients used were 0.30 for olivine (Roeder and Emslie, 1970) and 0.24 for coexisting clinopyroxene (Stern, 1979). During the fractional crystallization of this sequence, liquids varied in their Mg:Fe ratio from 2.07 to 0.71. The most primitive liquid documented at the base of the sequence had a Mg:Fe ratio of 2.01, while in the most evolved liquid at the top of unit 3 this ratio is only 0.71. These data also show that olivine crystallized first, but that its crystallization range is narrower than that of clinopyroxene. Clinopyroxene is the most important phase controlling the differentiation trend of the sequence. In Figure 13, the calculated liquid compositions are plotted with depth and define a 'liquid line of descent' of the magma. The graphs show the evolution of the Mg:Fe ratio of liquids calculated both from olivine and clinopyroxene, as well as the TiO_2 content of clinopyroxene, using a clinopyroxene-liquid partition coefficient of 0.3 (Pearce and Norry, 1979). This calculation shows that the initial TiO_2 content of the parental magma was at most 0.50%.

It is interesting to compare the 'liquid line of descent' calculated from the composition of the cumulus minerals with the differentiation trend of the volcanic rocks. We have selected the glass compositions reported by Robinson et al. (1983) and Thy et al. (1985) to define a true 'liquid line of descent'. These data are plotted in the MFA diagram of Figure 14 together, with the composition of the CY-4 cumulates and their calculated 'liquid line of descent'. The lines characterize a tholeiitic trend of differentiation and the main glass trend (shown by a heavy line in Figure 14) matches the calculated line of cumulates. A second line defined by glass compositions is apparent and calculation shows it could be derived from the main liquid line through fractionation of 3 to 4% of magnetite. The inferred position (and composition) of the parental magma is shown in the same diagram. The Mg:Fe ratio is well defined in this diagram but the A (alkalis) parameter is not as certain. In spite of this lack of precision, the general relations suggest that the plutonic and volcanic rocks are comagmatic.

Unit 1 consists mainly of layered isomodal mesocumulates. The layering reflects large variations in mineralogy and chemistry at the meter scale. However, from the base to the top of this unit, from layer to layer, there is a gradual progression of chemical composition. The FeO:MgO ratio increases regularly following the distinct iron enrichment trend of olivine and pyroxenes, while contents of compatible trace elements Ni, Cr and Co decrease. Progressive

crystallization caused the irreversible fractionation trend of the bulk magma. Ranges of chemical variation diminish through unit 2; unit 3 is relatively uniform in composition. Phase and cryptic variations observed by Alabaster et al. (1985) in three groups of layers within unit 1 at 1891-1897 m, 2087-2095 m and 2209-2225 m respectively, were interpreted to result from periodic replenishment of the magma chamber. We suggest that these cycles were caused by periodic convective overturn of magma during the early stages of cooling and fractionation that lasted as long as the melt behaved as a newtonian fluid. The chemical variations observed in our study are not similar to the cyclic units described in the Semail ophiolite of Oman (e.g. Pallister and Hopson, 1981; Smewing, 1981). The cyclic units of the Semail were caused by fresh influxes of parental magma which mixed with the evolved magma. This replenishment process leads to production of distinct cycles of crystal fractionation. Also, this type of system repeatedly generates lavas of uniform composition. Clearly, magma supply and conditions of fractionation were different for the Troodos lavas and CY-4 rocks. The plutonic sequence appears to have evolved in a confined system rather than in a compositionally steady-state magma chamber. A magma chamber of the 'CY-4 type', isolated from major supplies of unfractionated magma, would not yield lavas of uniform composition, but a spectrum of flows of variable composition as seen in the Troodos volcanic suites.

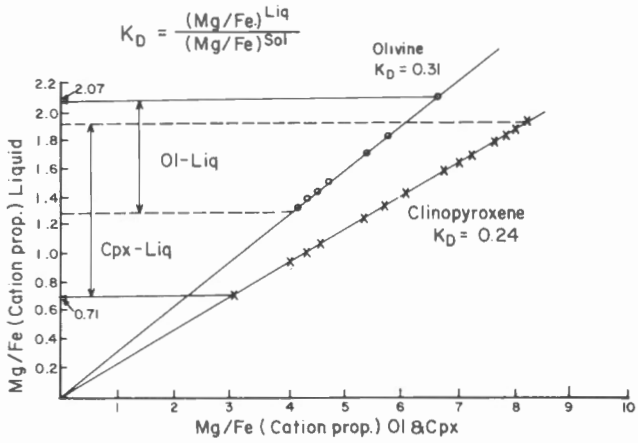

Figure 12: Calculated cation Mg:Fe ratio of melt from olivine and clinopyroxene equilibria. Solid circle = olivine; cross = clinopyroxene.

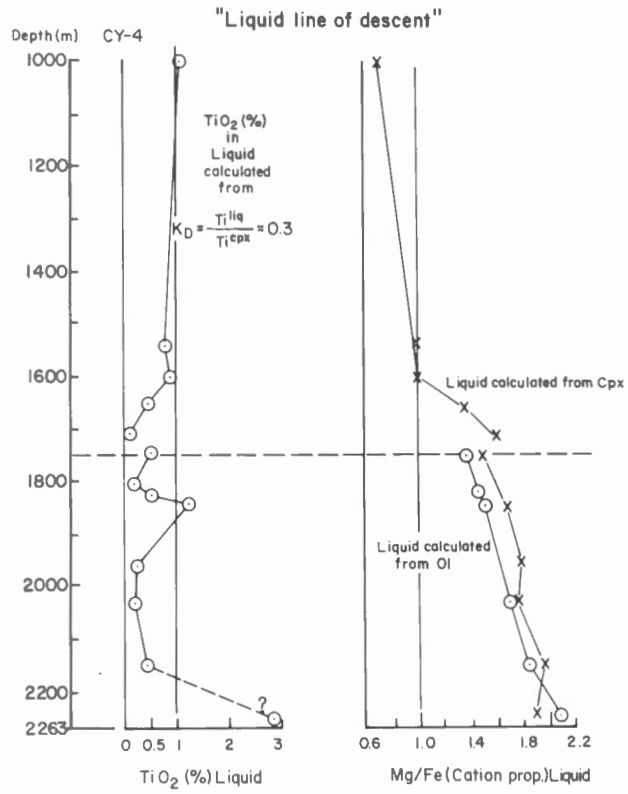

Figure 13: Calculated TiO_2 content and cation Mg:Fe ratio of the parental melt of the plutonic rocks according to position in the CY-4 section.

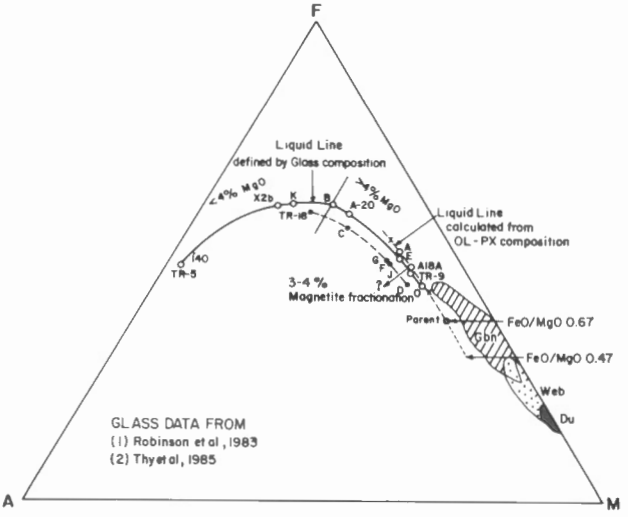

Figure 14: MFA diagram showing compositional relations between the volcanic and plutonic rocks. Fields of plutonic rocks (Du = dunite, Web = websterite, Gbn = gabbronorite) and calculated melt composition are plotted and compared to the true 'liquid line of descent' defined by volcanic glass.

ACKNOWLEDGEMENTS

We are grateful to John Malpas, Tom Calon, Sherry Dunsworth and Costas Xenophontos for sharing their field knowledge of the Troodos, and for lively discussions with them as well as with Eldridge Moores, Robert Baragar, Paul Robinson and Jim Hall. The Cyprus Geological Survey and, in particular, Costas Xenophontos are thanked for help while in Cyprus. We thank also Keith Benn, Claude Dion and Yves Thibault for assistance in the petrographic work and Jacques Belanger for computer assistance. Funding for this project was provided by a NSERC (Canada) operating grant to R. Laurent and by the NSERC 'Collaborative Special Project, Cyprus'.

REFERENCES

Alabaster, T., Gass, I.G., Roberts, S. and Tindle, A.
1985: Phase and cryptic variations within the cumulate ultramafic sequence of CY-4-Troodos ophiolite deep drill project; EOS, American Geophysical Union, Transactions, v. 66, no. 46, p. 1123.

Allen, C.R.
1975: The petrology of a portion of the Troodos plutonic complex, Cyprus; unpublished Ph.D. thesis, Cambridge University, England, p. 1-161.

Benn, K.
1986: Petrology of the Troodos plutonic complex in the Caledonian Falls area, Cyprus; unpublished M.Sc. thesis, Laval University, Quebec, p. 1-223.

Benn, K. and Laurent, R.
1986: Two plutonic suites of distinct age documented in the Troodos ophiolite, Cyprus; Geological Association of Canada-Mineralogical Association of Canada, Joint Annual Meeting, Ottawa, Ontario, Program with Abstracts, p. 45.

Dunsworth, S.M. and Calon, T.
1984: Relationships between deformation and magmatism in the plutonic complex, Troodos ophiolite, Cyprus; Geological Association of Canada-Mineralogical Association of Canada, Joint Annual Meeting, London, Ontario, Program with Abstracts, p. 59.

George, R.P., Jr.
1978: Structural petrology of the Olympus ultramafic complex in the Troodos ophiolite, Cyprus; Geological Society of America, Bulletin, v. 89, p. 845-865.

Greenbaum, D.
1972: Magmatic processes at ocean ridges: evidence from the Troodos massif, Cyprus; Nature, Physical Science, v. 238, no. 80, p. 18-21.
1977: The chromitiferous rocks of the Troodos ophiolite complex, Cyprus; Economic Geology, v. 72, p. 1175-1194.

Hébert, R.
1985: Pétrologie des roches ignées océaniques et comparaisons avec les complexes ophiolitiques du Québec, de Chypre et de l'Appenin; unpublished Ph.D. thesis, Université de Bretagne Occidentale, Brest, p. 1-542.

Irvine, T.N.
1970: Crystallization sequences in the Muskox Intrusion and other layered intrusions: I. Olivine-pyroxene-plagioclase relations; South Africa Special Publication I, p. 441-476.
1979: Rocks whose composition is determined by crystal accumulation and sorting; *in* The Evolution of the Igneous Rocks, Fiftieth Anniversary Perspectives, ed. H.S. Yoder, Jr.; Princeton University Press, Princeton, New Jersey, p. 245-306.
1982: Terminology for layered intrusions; Journal of Petrology, v. 23, p. 127-162.

Jackson, E.D.
1971: Origin of ultramafic rocks by cumulus processes; Fortschritte Mineralogy, v. 48, p. 128-174.

Johannes, W.
1978: Melting of plagioclase in the system Ab-An-H_2O and Qz-Ab-An-H_2O at PH_2O = 5 kbars, an equilibrium problem; Contributions to Mineralogy and Petrology, v. 66, p. 295-303.

Kushiro, I.
1972: Determination of liquidus relations in synthetic silicate systems with electron probe analysis: the system forsterite-diopside-silica at 1 atmosphere; American Mineralogist, v. 57, p. 1260-1271.

Lindsley, D.H.
1983: Pyroxene thermometry; American Mineralogist, v. 68, p. 477-493.

Moores, E.M. and Thy, P.
1985: Mineral crystallization trends of the Troodos ophiolite: evidence for genesis and formation; EOS, American Geophysical Union, Transactions, v. 66, no. 46, p. 1123.

Pallister, J.S. and Hopson, C.A.
1981: Samail ophiolite plutonic suite: field relations, phase variation, cryptic variation and layering, and a model of a spreading ridge magma chamber; Journal of Geophysical Research, v. 86, no. B4, p. 2593-2644.

Pearce, J.A. and Norry, M.J.
1979: Petrogenetic implications of Ti, Zr, Y and Nb variations in volcanic rocks; Contributions to Mineralogy and Petrology, v. 69, no. 1, p. 33-47.

Presnall, D.C., Dixon, J.R., O'Donnell, T.H. and

Dixon, S.A.
1979: Generation of mid-ocean ridge tholeiites; Journal of Petrology, v. 20, p. 3-36.

Robinson, P.T., Melson, W.G., O'Hearn, T. and Schmincke, H.-V.,
1983: Volcanic glass compositions of the Troodos ophiolite, Cyprus; Geology, v. 11, no. 7, p. 400-404.

Roeder, P.L. and Emslie, R.F.
1970: Olivine-liquid equilibrium; Contributions to Mineralogy and Petrology, v. 29, p. 275-289.

Smewing, J.D.
1981: Mixing characteristics and compositional differences in mantle-derived melts beneath spreading axes: evidence from cyclically layered rocks in the ophiolite of north Oman; Journal of Geophysical Research, v. 86, no. B4, p. 2645-2659.

Stern, C.
1979: Open and closed system igneous fractionation within two Chilean ophiolites and the tectonic implication; Contributions to Mineralogy and Petrology, v. 68, p. 243-258.

Streckeisen, A.L.
1976: To each plutonic rock it's proper name: Earth-Science Reviews, v. 12, p. 1-33.

Thy, P., Brooks, C.K. and Walsh, J.N.
1985: Tectonic and petrogenetic implications of major and rare earth element chemistry of Troodos glasses, Cyprus; Lithos, v. 18, no. 3, p. 165-178.

Wager, L.R.
1960: The major element variation of the layered series of the Skaergaard intrusion and a re-estimation of the average composition of the hidden layered series and of the successive residual magmas; Journal of Petrology, v. 1, p. 364-398.

Wager, L.R., Brown, G.M. and Wadsworth, W.J.
1960: Types of igneous cumulates; Journal of Petrology, v. 1, p. 73-85.

Wilson, R.A.M.
1959: The geology of the Xeros-Troodos area; Cyprus Geological Survey Department, Ministry of Agriculture and Natural Resources, Memoir, no. 1, p. 1-184.

Igneous Mineral Stratigraphy and Chemistry of the Cyprus Crustal Study Project Drill Core in the Plutonic Sequences of the Troodos Ophiolite

P. THY*[1,2], P. SCHIFFMAN[1] AND E.M. MOORES[1]

*Present address: NASA, Johnson Space Centre, SN4, Houston, TX, U.S.A., 77058
[1]Department of Geology, University of California, Davis, CA, 95616, U.S.A.
[2]Geologisk Institut, Arhus Universitet, DK-8000 Arhus C, Denmark

Thy, P., Schiffman, P. and Moores, E.M., Igneous mineral stratigraphy and chemistry of the Cyprus Crustal Study Project drill core in the plutonic sequences of the Troodos ophiolite; in *Cyprus Crustal Study Project: Initial Report, Hole CY-4, ed. I.L. Gibson, J. Malpas, P.T. Robinson and C. Xenophontos; Geological Survey of Canada, Paper 88-9, p. 147-185, 1989.*

Abstract

The CY-4 drillhole of the Cyprus Crustal Study Project penetrated dykes, gabbros, and ultramafic cumulates of the Troodos ophiolite near Palekhori. Above 640 m, the borehole section consists mainly of fine-grained, granular, two-pyroxene dykes. From 640 to 1330 m, dykes become progressively less common and medium-grained, olivine-free, two-pyroxene gabbros gradually dominate. The contact at 1330 m is intrusive. The younger sequence from 1330 to 1754 m, consists of gabbroic cumulates containing plagioclase (An_{90-86}) and pyroxenes with Ti contents comparable to those of the dyke, but with higher Mg-numbers. The section from 1754 to 2263 m comprises relatively coarse-grained websteritic cumulates with plagioclase ($An_{>95}$) and the pyroxenes characterized by very low-Ti and high-Cr contents. The Fo mol.%, An mol.%, and Mg-numbers of cumulus phases generally decreases upward in the core. The lower cumulate complex probably formed in a slow- or non-spreading environment. In contrast the upper cumulate complex reflects a relatively faster spreading environment. The results of the present investigation suggest that the central ultramafic cumulates of the Troodos ophiolite did not form in a large, steady-state, frequently replenished, axial magma chamber (Abstract abbreviated by the editors without the authors'consent).

Résumé

Le forage CY-4 du projet d'étude de la croute cypriote a pénétré des dykes, gabbros et cumulats ultramafiques appartenant à l'ophiolite de Troodos près de Palekhori. Les 640 premiers mètres ont montré principalement des dykes à deux pyroxènes, à grains fins et à texture granulaire. De 640 à 1330 mètres, ces dykes deviennent progressivement plus rares étant graduellement remplacés par des gabbros à deux pyroxènes, sans olivine et à grains moyens. Le contact à 1330 mètres est intrusif. La séquence plus récente, entre 1330 et 1754 m, est formée de cumulats gabbroïques constitués de plagioclases An_{90-86} et de pyroxènes ayant un contenu en titane semblable à celui des dykes, mais plus riche en Mg. Entre 1754 et 2263 m on retrouve des cumulats webstéritiques à grains relativement grossiers formés de plagioclases $An_{>95}$ et de pyroxènes caractérisés par leur contenu réduit en titane et élevé en Cr. Le %mol Fo, le %mol An et les concentrations en Mg des cumulats décroissent généralement vers le haut du forage. Le complexe inférieur de cumulats s'est probablement formé dans un milieu à expansion lente ou nulle alors que le complexe supérieur réflète un milieu à expansion relativement plus rapide. Les résultats de la présente étude suggèrent que les cumulats ultramafiques centraux de l'ophiolite de Troodos ne se sont pas formés dans une grande chambre magmatique axiale fréquemment regénérée et à comportement régulier. (Résumé condensé par les êditeurs sans le consentement des auteurs.)

INTRODUCTION

The Troodos plutonic complex, Cyprus, forms part of one of the most extensively studied ophiolitic complexes in the world (cf., Gass and Masson-Smith, 1963; Gass, 1967, 1980; Gass and Smewing, 1973; Moores and Vine, 1971). The plutonic complex is exposed in a central uplifted core as tectonized peridotite and serpentinite, stratigraphically overlain successively by ultramafic and gabbroic cumulates, a sheeted dyke complex, extrusive pillowed lavas, and pelagic sediments. Early field mapping and petrographic work by members of the Geological Survey Department of Cyprus established the field relations and major subdivisions of the central plutonic complex (e.g., Wilson, 1959; Bear, 1960; Pantazis, 1967). A refractory and tectonized harzburgite forms the main part of the mantle sequence and has been studied extensively (Menzies and Allen, 1974; Allen, 1975; George, 1978). Subordinate members are plagioclase lherzolite and chromitite-dunite lenses (Menzies and Allen, 1974; Allen, 1975; Greenbaum, 1977).

The cumulate sequences range from chromite-bearing dunites, to wehrlites and pyroxenites, and gabbros (Allen, 1975; Greenbaum, 1977; Johan et al., 1982). The ultramafic and gabbroic cumulates are believed to have crystallized from magmas derived by partial melting of a mantle represented by the depleted harzburgites (Menzies and Allen, 1974; Smewing et al., 1975; Wood, 1979). Greenbaum (1972a), Allen (1975), and Thy (1987) defined the general crystallization sequence in the cumulates as ch, ch + ol, ol + di, ol + di + en, ol + di + en + pl, di + en + pl and di + en + pl + oxides. Thy (1984, 1987) and Dunsworth and Calon (1984), however, pointed to the possibility for several parental liquid series. Although there is a gross upward cryptic variation towards more evolved iron- and sodium-rich compositions, evidence for periodic magma replenishment to more primitive compositions can be seen in the ultramafic (Allen, 1975) and the gabbroic cumulates. The cumulate sequences of the Troodos plutonic complex have traditionally been explained as having accumulated in a large magma-chamber underlying a spreading ridge crest (Greenbaum, 1972a). Evidence presented by Allen (1975) and Thy (1987), however, points to a multiple chamber model.

Hole CY-4 of the International Crustal Research Drilling Group was drilled in the sheeted dyke complex near Palekhori at 34°54′06″N and 33°05′38″E, and sampled the lower sheeted dyke complex, gabbros, and websteritic cumulates. It was terminated before reaching the lower cumulates and tectonized harzburgites. A total of 2263 metres of core, representing a recovery of above 99%, was collected and a complete sequence of gabbroic and ultramafic cumulates was obtained. The present study was intended as a preliminary investigation of phase layering and cryptic variation in the cumulates in order to model magma chamber processes and crustal construction forming the Troodos ophiolite. Preliminary results of this study have been presented by Thy (1987), Thy and Moores (1986), Moores and Thy (1985), and Thy et al. (1986).

RESULTS

Stratigraphy and Structures

A summary of the CY-4 drill core is given in Figure 1, showing the distribution of the three major rock types (i.e., dykes, upper gabbros, and lower gabbroic and websteritic cumulates), based on information given in the original core descriptions (C.C.S.P., 1985) and petrographic observations made during the course of this study.

Only core below 489 m was examined in this study. The upper part of the core is composed of greyish, fine-grained, aphyric to slightly pyroxene-plagioclase phyric, doleritic, sheeted dykes (Figure 1). The thickness of individual dykes ranges from 0.2 to 7 metres, and the dykes are mostly steeply inclined. The contacts are truncated or chilled, but glass is not preserved. Medium- to coarse-grained gabbroic screens or small, high-level intrusions are present in the core below 230 m, but gabbroic rocks become abundant only below 630 m (Figure 1). Gabbroic rocks total only 16 metres in the first 650 metres of the core. The amount of dykes decreases downwards, and the last dyke in the core is at 1290 m. Dykes below 650 m have an aggregate thickness of 136 metres. There appears to be a small subsidiary peak in dyke intensity between 1040 and 1140 m.

The gabbros are generally greenish-grey, medium- to coarse-grained, and include feldspathic, gabbroic, and pyroxenitic varieties, apparently related to igneous layering. Igneous layering and lamination occur below 680 m, but are most common below 800 m. Patches and layers, sometimes amphibole-bearing, have coarse-grained pegmatitic textures. There are no convincing indications of chilled contacts within the upper gabbroic sequence. The first gabbro analyzed in this study came from 605 m.

An intrusive contact at approximately 1330 m separates upper level, medium-grained gabbroic cumulates from lower level, coarser grained gabbroic cumulates. The upper few metres of the lower gabbros appear to be chilled. The contact at approximately 1750 m between gabbroic and lower websteritic cumulates is not intrusive, although a rather sharp modal transition is observed. The gabbros of the lower cumulate sequence are greyish-green, medium- to coarse-grained, equigranular, and leucocratic to mesocratic. Grain-size and modal layering are rare.

The lower websteritic cumulates are light grey, medium- to coarse-grained rocks showing grain-size and modal layering dominantly due to variations in plagioclase and olivine contents. Medium- to fine-grained gabbroic rocks are locally intercalated with the websterites. The contacts between these gabbros and 'host' websterite are sometimes, but not always, visibly intrusive. Pegmatitic gabbroic rocks are also present in the ultramafic sequence.

The rocks above 850 m have been pervasively altered (Figure 1). Those below 850 m exhibit variable degrees of alteration ranging from minor development of hornblende to metre(s)-thick zones of amphibolite. Zeolite veins are ubiquitous throughout much of the core. The dykes below 850 m are very fresh and exhibit a characteristic granular texture. Trondhjemitic veins and intrusive masses are often found in the upper gabbroic rocks, apparently related to hydrothermal metamorphism. A major shear zone occurs between 714 to 718 m.

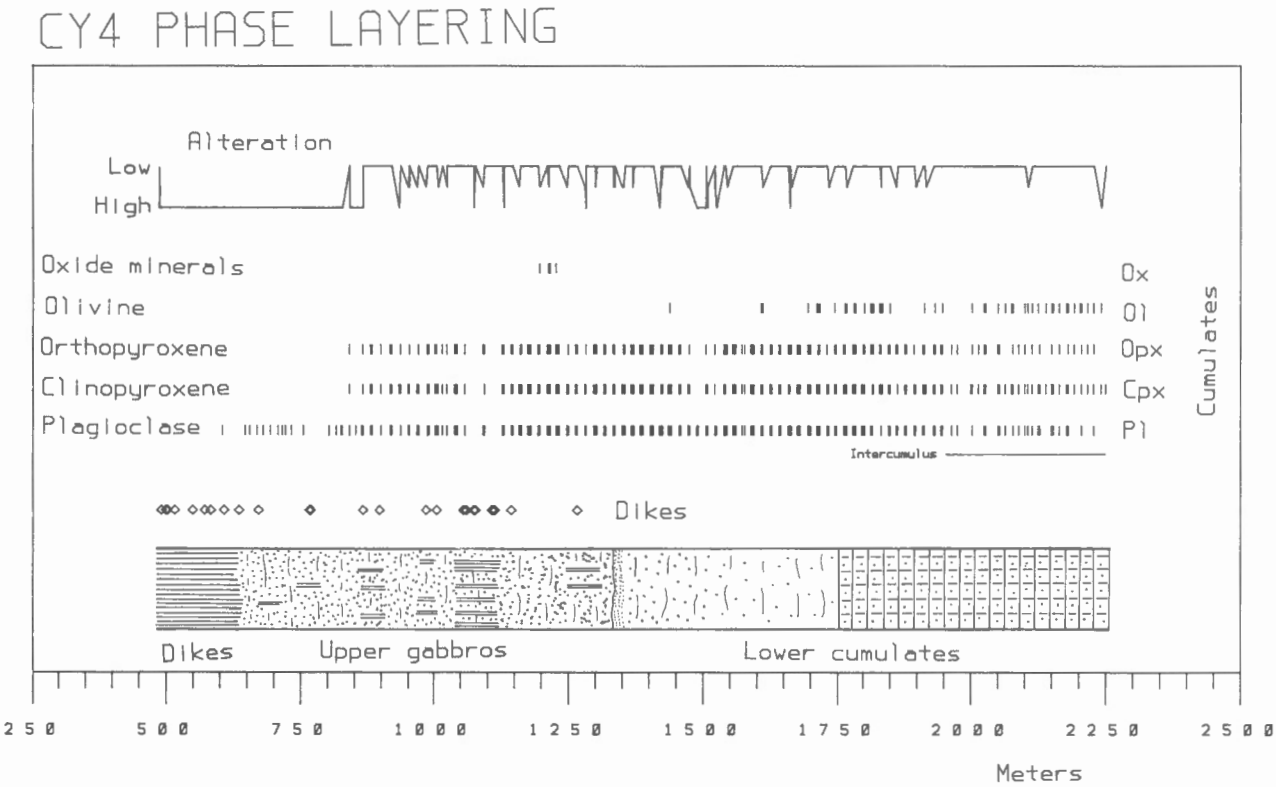

Figure 1: Graphic representation and phase layering of the CY-4 drill core. Only the occurrences of the following three major rock types are shown: (1) fine-grained dykes, (2) medium-grained upper level gabbros, (3) medium- to coarse-grained lower level gabbros and ultramafic cumulates. The range in the appearance of the cumulus phases plagioclase, clinopyroxene, orthopyroxene, olivine, and Fe-Ti oxides is shown for the gabbroic to ultramafic cumulates. Below 1754 m plagioclase ceases to occur as an early precipitating phase and is mainly found in an interstitial (or intercumulus) texture (see Figure 6 for details for the lower part of the core). Fe-Ti oxides occur locally as minor phases in, particularly, the upper gabbros. Fe-Cr spinels rarely occur as an accessory phase in the ultramafics. Interstitial brown hornblende occurs in the upper part of the gabbros, sometimes associated with interstitial Fe-Ti oxides. The intensity of the shading reflects the sampling density. The dykes contain plagioclase, clinopyroxene, orthopyroxene, Fe-Ti oxides, and sulphides. The intensity of secondary alteration and metamorphism is shown on an arbitrary scale based on the 'preservation' of the four main mineral phases (pl, cpx, opx, ol). Above approximately 850 m the hydrothermal alteration and neocrystallization have often obliterated the primary igneous mineralogy (both gabbros and dykes), and only plagioclase can be analyzed.

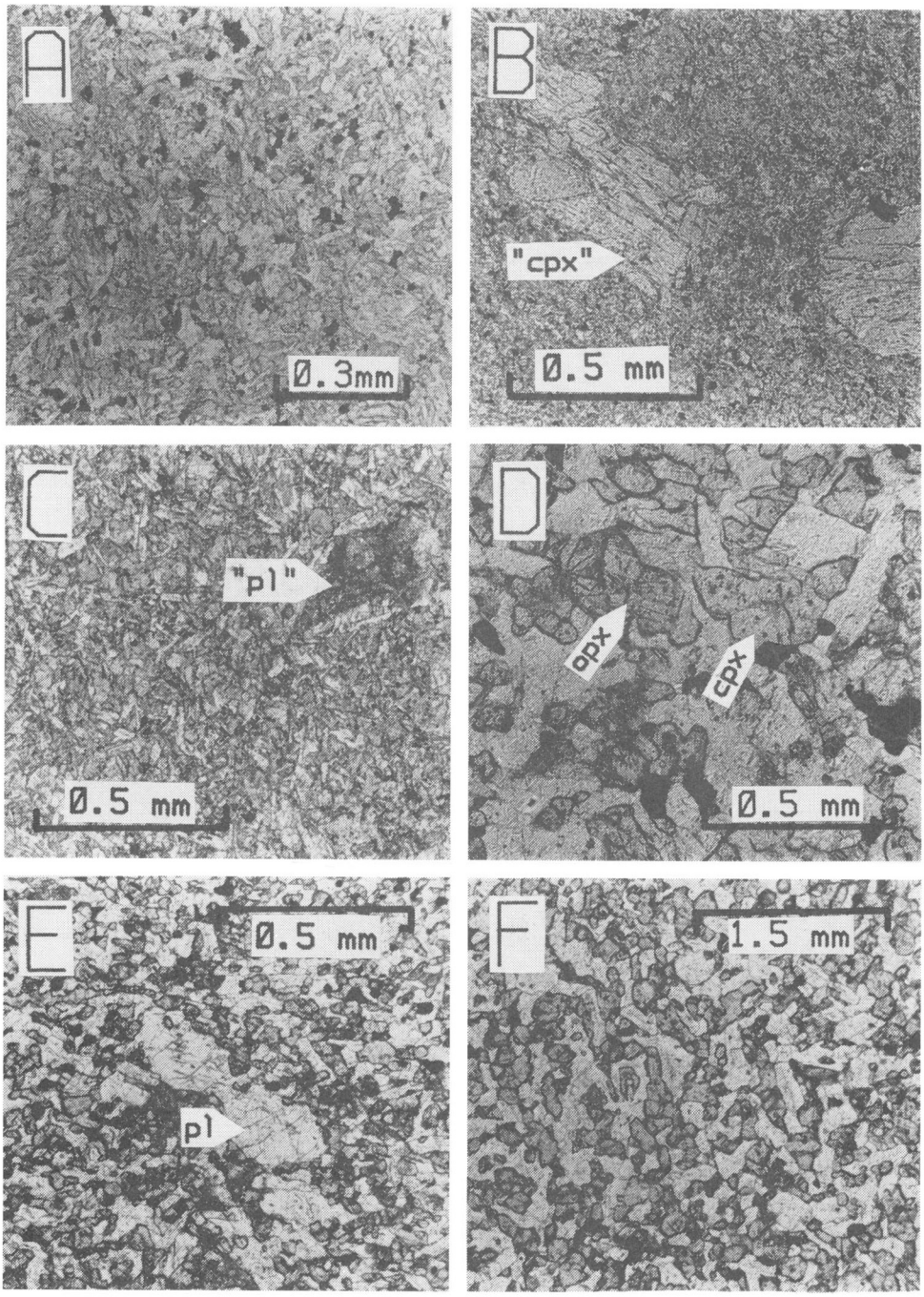

Figure 2: Photomicrographs of typical textures of dyke rocks. (A) Fine-grained, doleritic textured dyke rock. Mafic minerals in groundmass are recrystallized into amphiboles, but plagioclase is relatively unaffected by metamorphism (CY4-489.37). (B) Doleritic textured dyke with amphibolitized clinopyroxene phenocrysts ('cpx'). Groundmass mafic minerals are also recrystallized into amphiboles (CY4-570.88). (C) Doleritic textured dyke with altered, probably xenocrystic plagioclase ('pl'). Mafic groundmass phases are completely recrystallized into amphiboles, however, plagioclases still appear fresh and the original texture is partly preserved (CY4-608.06). (D) Groundmass of granular, annealed dyke rock showing orthopyroxene (opx) with high relief and clinopyroxene (cpx) with medium relief. Other phases are plagioclase, magnetite, ilmenite, and sulphides (CY4-1075.49). (E) Granular, annealed dyke groundmass with 'relict' plagioclase (pl) phenocrysts (CY4-1054.23). (F) Typical, fine-grained, granular groundmass of dyke rock (CY4-1071.68).

Petrography

Dykes

The sheeted dykes above 850 m are aphanitic to fine-grained, aphyric to slightly phyric, and doleritic in texture (Figure 2A-C). Former clinopyroxene phenocrysts have been uralitized by green amphibole (Figure 2B), but plagioclase phenocrysts are commonly preserved (Figure 2C). The abundance of calcic amphiboles in the groundmass points to high-Ca pyroxene as the most important primary mafic mineral. The groundmass plagioclases vary in composition from anorthite to andesine.

The dykes below approximately 850 m are typically fresh and unmetamorphosed. Their fine- to medium-grained, granular textures (Figure 2D-F) are strikingly different from the doleritic textures of the sheeted dykes. Phenocrystic calcic plagioclase is sometimes found in relatively coarse grained patches in the granular dykes (Figure 2E). Chemically, the groundmass plagioclases are similar to the most calcic ones found in the groundmasses of the doleritic dykes. These plagioclases are accompanied by clinopyroxene, orthopyroxene, Fe-Ti oxides, and sulphides (Figure 2D). The oxides are lamellar to granular intergrowths of ilmenite and magnetite, only locally exhibiting an interstitial texture to the silicates (Figure 2D). Brown amphibole is rarely present. The relatively fine-grained, granular fabric (Figure 2D) and the compositionally homogeneous nature of the minerals (Figure 3, CY4-1071.68) suggest solid state re-equilibration and homogenization during cooling (annealing). The present data do not indicate any substantial chemical differences between the upper, doleritic and lower, granular dykes.

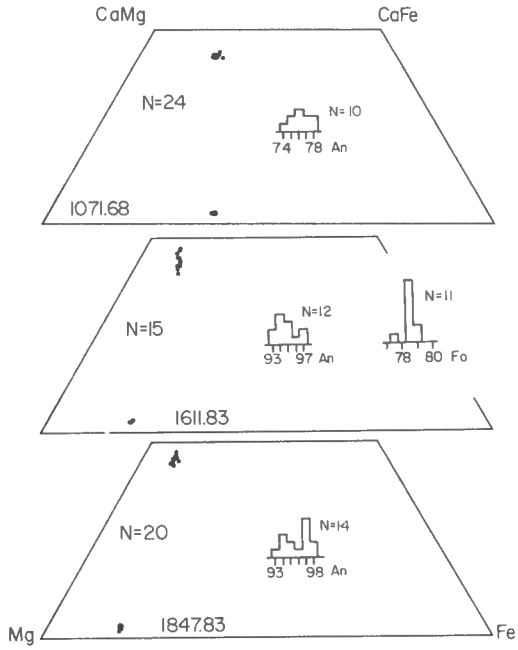

Upper Gabbros

The gabbros above 1330 m are fine- to medium-grained and equigranular to subequigranular in texture (Figure 4A-D). Adcumulate to mesocumulate textures (Wager et al., 1960) are common with pyroxene typically interstitial to plagioclase (Figure 4B,D). A cumulate origin is also suggested by occasional layering and mineral lamination (Figure 4A), the rather restricted range in mineral compositions (e.g., An_{95-89}) and the general lack of zoning and late interstitial crystallizing phases (e.g., Fe-Ti oxides, amphibole, and apatite).

Plagioclase, clinopyroxene, and orthopyroxene, in order of decreasing abundance, occur throughout the core (Figure 1). Plagioclase compositions range from anorthite to labradorite. Minor phases include Fe-Ti oxides and brown amphibole, the latter being partly of metamorphic origin. Characteristically, brown amphibole and minor Fe-Ti oxides only occur in significant amounts in the upper part of the sequence (above approximately 1025 m). Cumulus, or near cumulus, and intercumulus Fe-Ti oxides also occur locally between 1200 to 1220 m (Figures 1 and 4F).

Cumulus processes have strongly affected the occurrence of the primary phases in the upper gabbros. Fe-Ti oxide minerals exhibit, within a narrow zone, a wide range in modal abundance and texture from cumulus to interstitial (Figure 4F). This may be related to accumulative processes forming the cumulates and the layering. Pyroxenitic layers or patches may also have formed by crystal accumulation (Figure 4C,E).

Although primary phases in most samples show restricted zoning, some samples have plagioclase, which is normally zoned from anorthite in cores to andesine in rims or late crystallizing grains. The occurrence of quartz in the groundmass of strongly amphibolitized samples imply that metamorphic processes may have produced some of the observed zoning in plagioclase. There may also be a correlation between strong normal plagioclase zoning (An_{95-56}) and appearance of high amounts of brown amphibole. However, normal plagioclase zoning (An_{95-45}) can also be found in amphibole-free samples, suggesting that intercumulus crystallization alone can produce the observed zoning.

Figure 3: Major element compositional ranges in pyroxenes, plagioclase, and olivine. Based on a large amount (34-38) of analyses on each of three representative samples to show the maximum variation from rim to cores of granular and interstitial grains. Sample CY4-1071.68 is a fine-grained, granular dyke; CY4-1611.83 is a medium-grained gabbro with large interstitial orthopyroxene; CY4-1847.83 is a medium-grained pyroxenite with interstitial plagioclase, large interstitial orthopyroxene and only a few olivine grains (Fo_{85}).

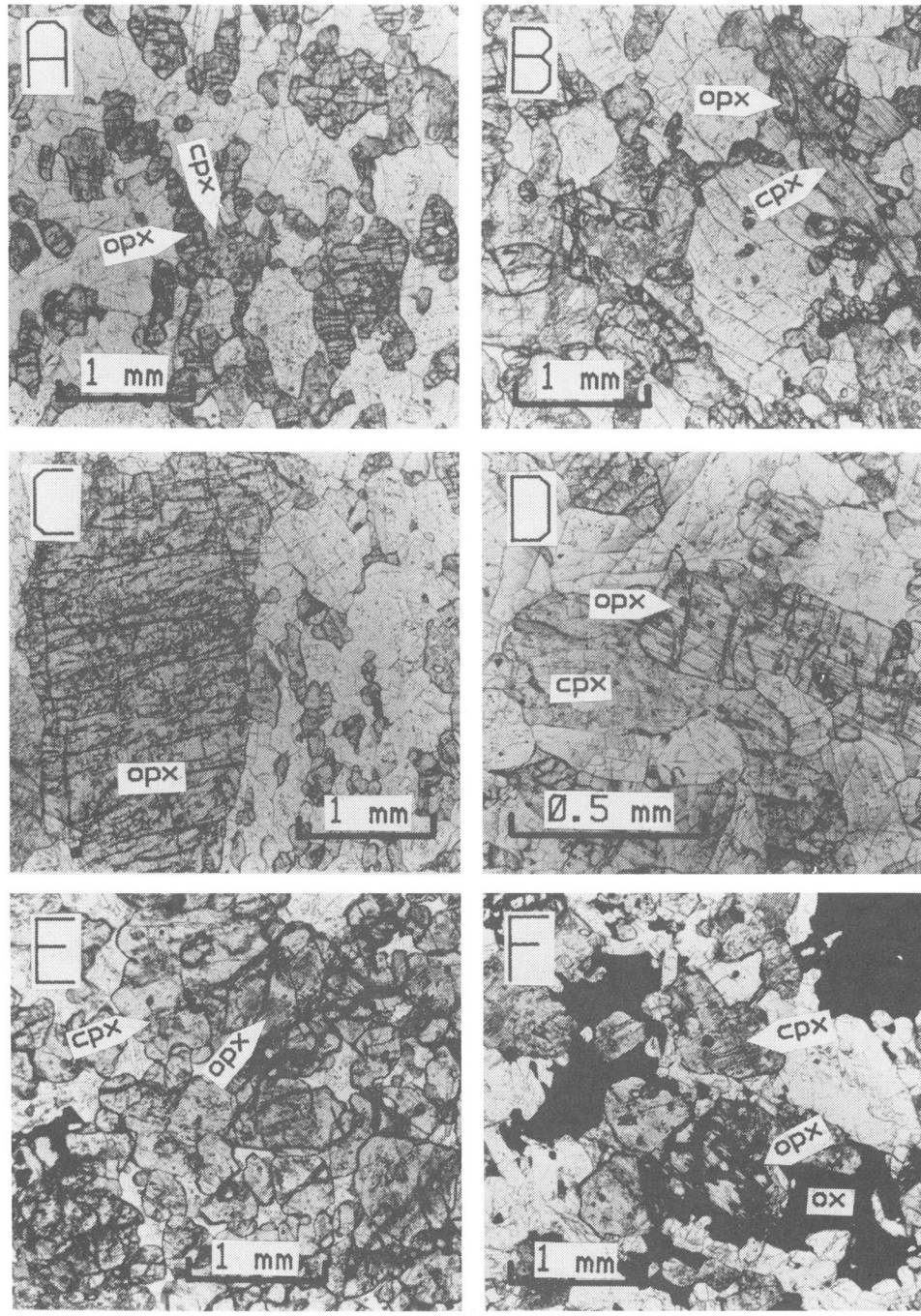

Figure 4: Photomicrographs of typical rock textures of the upper gabbro sequence. (A) Ad- to mesocumulate, two-pyroxene gabbro. Orthopyroxenes (opx) tend to appear in granular (or cumulus) textures, whereas the texture of clinopyroxene (cpx) may be either granular or interstitial (CY4-1317.62). (B) Meso- to orthocumulate, two-pyroxene gabbro. Clinopyroxenes appear dominantly as interstitial phases (CY4-1124.34). (C) Large orthopyroxene grain in fine-grained, two-pyroxene gabbro (CY4-1317.62). (D) Medium-grained, two-pyroxene gabbro. Orthopyroxenes appear as elongated grains, whereas clinopyroxenes appear as either granular or interstitial grains (CY4-1145.85). (E) Melanocratic layer in two-pyroxene gabbro. The layer is composed of cumulus orthopyroxene and clinopyroxene and interstitial plagioclases (CY4-1140.88). (F) Mesocratic, Fe-Ti oxide-rich (ox) layer from the pl + cpx + opx + oxide cumulus zone. The orthopyroxenes are partially altered and the oxides occur dominantly as interstitial grains (CY4-1196.03).

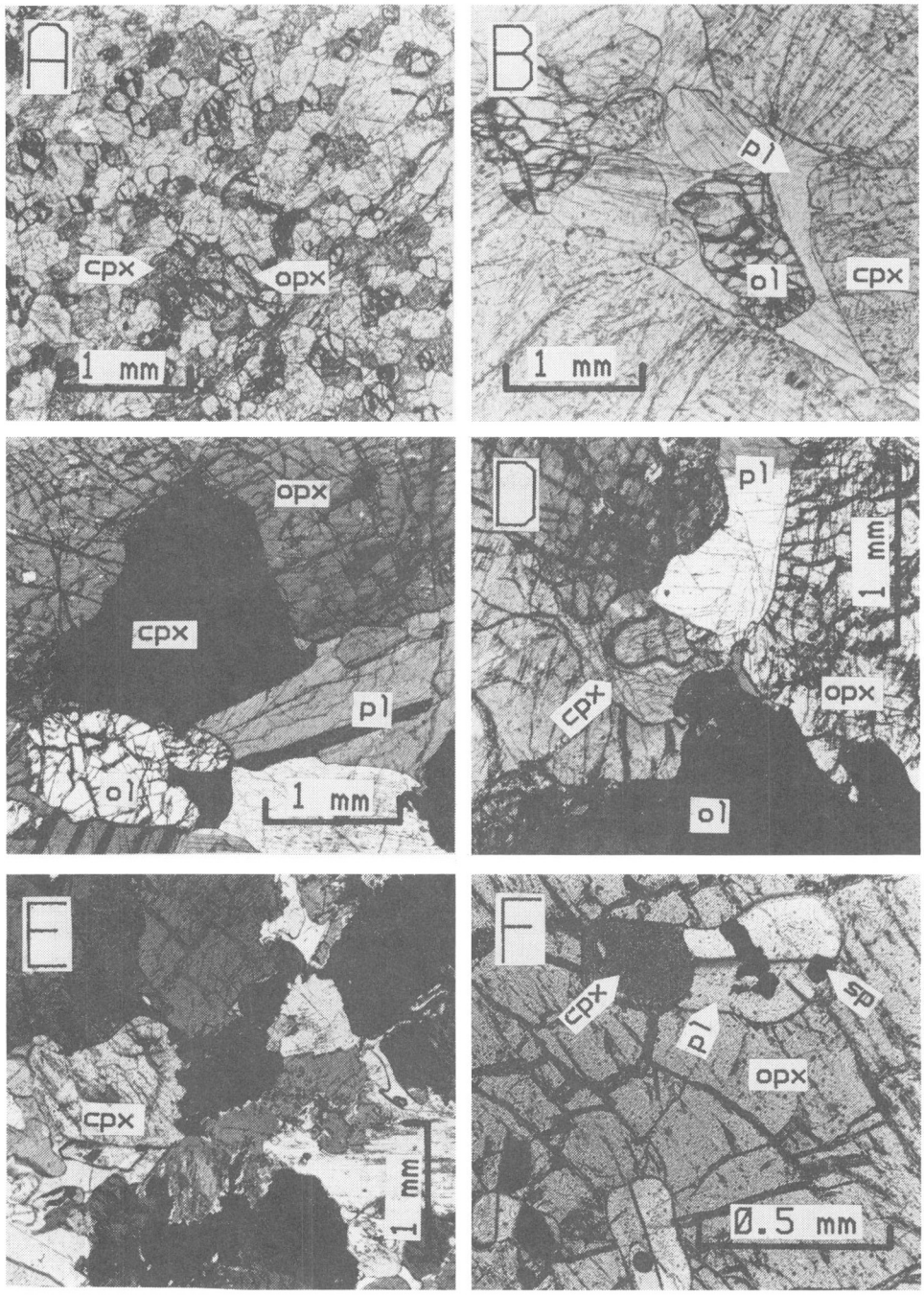

Figure 5: Photomicrographs of typical rock textures of the lower gabbroic and websteritic sequence. (A) Fine-grained, granular, two-pyroxene gabbro. This sample comes from the top of the lower gabbroic and websteritic cumulus sequence and may be a chilled facies (CY4-1330.82). (B) Medium- to coarse-grained, olivine (ol) and pyroxene websteritic cumulate with interstitial plagioclase (pl) (CY4-1763.15). (C) Medium-grained, olivine, plagioclase, and two-pyroxene gabbroic cumulate (crossed nicols). Orthopyroxenes tend to develop coarse interstitial textures with only limited included grains (CY4-1745.00). (D) Coarse- to medium-grained, olivine and two-pyroxene websteritic cumulate (CY4-1799.06; crossed nicols). Clinopyroxene and plagioclase appear in an interstitial fabric. (E) Medium-grained clinopyroxenite cumulate with minor interstitial plagioclase (CY4-1847.83). (F) Large interstitial orthopyroxene with inclusions of plagioclase and clinopyroxene in a mesocratic, gabbroic cumulate. The cpx-pl-sp composite grain may represent a trapped liquid inclusion (CY4-1693.82).

The majority of the analyzed samples (Appendix 1) can be characterized as uralitized or amphibolitized gabbros. Orthopyroxene sometimes shows incipient recrystallization and development of a fine-grained granulation texture (Figure 7A). Clinopyroxene frequently shows recrystallization to a homogeneous, chemically identical clinopyroxene phase containing irregular orthopyroxene lamellae (Figure 7B-C).

Lower Gabbros and Websteritic Cumulates

Except for a general increase in grain-size, there are few textural differences between the upper and the lower gabbroic cumulates (Figure 5). The boundary between the two gabbro series is mainly based on chemical criteria such as plagioclase and pyroxene compositions (see section on mineral chemistry). The uppermost sample analyzed (CY4-1330.82), chemically belonging to the lower gabbroic sequence, has a granoblastic, relatively fine-grained texture (Figure 5A) and probably represents a chilled facies. Most of the lower gabbroic and websteritic cumulates are medium-grained, but coarse-grained textures are also common. The samples typically exhibit adcumulate to mesocumulate textures (Figure 5B-E) with locally large interstitial orthopyroxene (Figure 5C,F). The transition from gabbroic to websteritic cumulates is defined by a modal decrease in plagioclase (e.g., Figure 5B) with no clear petrographic or chemical indications for an intrusive relationship. Grain-size and modal layering are developed throughout the entire sequence.

The general phase layering of the lower cumulate sequence is shown in Figure 1, and in more detail in Figure 6. Clinopyroxene occurs throughout the sequence and has a dominantly granular (cumulus) texture (Figure 5E). However, orthopyroxene ranges from granular and often elongated to, in the lower part of the section, large interstitial (intercumulus) grains (below 1754 m, Figure 6). Sometimes, but not always, microcrysts of clinopyroxene, olivine, and plagioclase occur as inclusions in the interstitial orthopyroxenes (Figure 5C,F). Plagioclase, in general, ceases to occur as a cumulus phase below 1754 m, and in the websteritic series, if present, occurs dominantly as small interstitial grains (Figure 5B). Olivine is an important, but rarely abundant, phase below 1600 m (Figure 6). Below this depth, and as olivine becomes more abundant, orthopyroxene occurs either interstitially or is absent (Figure 6). The highest position in the core where olivine is found is 1435.37 m. Gabbroic layers occur as part of the websterite sequence (Figure 6) and appear, mineralogically and chemically, to be a conformable part of the cumulates.

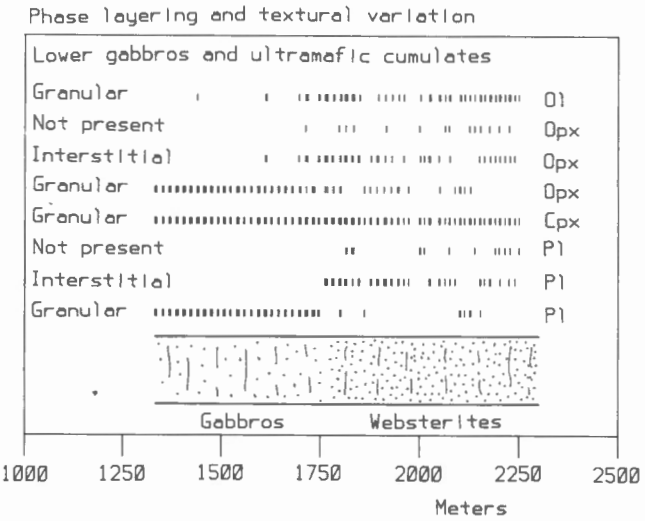

Figure 6: Phase layering and textural variation of the lower gabbros and ultramafic cumulates. The range in the dominating textural varieties of plagioclase (Pl), clinopyroxene (Cpx), orthopyroxene (Opx), and olivine (Ol). Clinopyroxene and olivine occur in a granular (or adcumulus) texture throughout the core. Plagioclase and orthopyroxene range from granular (cumulus) to interstitial (intercumulus), or are not present in some samples. See discussion in text of the textural variation. The schematic representation of the core shows the modal boundary between the upper gabbroic cumulates and the lower websteritic cumulates. However, conformable gabbroic cumulates occur intercalated within the ultramafic section as revealed by the occurrence of granular plagioclase between 2080 and 2160 m.

The cumulus plagioclases in the lower gabbros and websterites are highly calcic and show limited compositional variation (Figure 3). Interstitial plagioclase grains in the websteritic cumulates are compositionally similar to cumulus plagioclase in gabbroic rocks found at the same stratigraphical levels (compare CY4-1611.83 and CY4-1847.83, Figure 3). This suggests that the rocks are mainly adcumulative in origin with little interstitial crystallization of trapped liquids. The development of large interstitial orthopyroxene crystals may reflect variable growth rates and does not necessarily imply intercumulus crystallization (see discussion of phase layering). Interstitial brown amphibole and Fe-Ti oxides are rare. Some relatively rare Fe-Cr spinels included in pyroxenes may be secondary. Chromian spinels have not been observed in the websterite cumulates.

Exsolution lamellae in the pyroxenes of the lower cumulates are more common than those in the upper gabbros, but are still not as significant as observed in slowly cooled cratonic plutons. Recrystallization of primary clinopyroxene to a homogeneous

clinopyroxene with vermicular exsolutions (Figure 7B,C) is also more commonly observed than in the upper gabbros. The fine-grained granular texture of orthopyroxene, as observed in the upper gabbros, is also more common (Figure 7A). Cataclastic granulation and recrystallization of plagioclase occur locally, but are never observed in the samples with recrystallized pyroxenes.

Metamorphism and Hydrothermal Alteration

Alteration under amphibolite, greenschist, and zeolite facies conditions is recorded throughout the drill core. Amphibolite facies metamorphism, characterized by the development of both green and brown hornblenditic amphiboles, was the earliest and most pervasively developed subsolidus recrystallization event. Amphibolite zones, which occur discontinuously within the CY-4 core, apparently developed under largely static, hydrothermal conditions. Although the intrusive rocks exhibit the effects of some cataclastic deformation (as outlined above), they do not record evidence of ubiquitous cataclastic or mylonitic subsolidus deformation, such as has been documented from oceanic fracture zones (e.g., Honnorez et al., 1984) and some other ophiolite complexes (e.g., Karson et al., 1984).

Amphiboles in a wide variety of habits are found throughout the entire length of the core, although their occurrence is most widespread in the upper, plagioclase-bearing doleritic and gabbroic rocks (Figure 7D-F). Brown amphiboles occur as subhedral to anhedral replacements to, and overgrowths on, both clino- and orthopyroxenes. Locally, these amphiboles poikilitically enclose pyroxenes and plagioclase. In gabbros between approximately 880 and 1020 m, rare brown amphibole has a distinctive 'intercumulus' habit (Figure 7D) suggesting that it may be a late magmatic phase. Green amphiboles have more distinctly metamorphic habits (Figure 7E) and are the principal constituents of extensively amphibolitized zones in which euhedral to subhedral green hornblenditic amphiboles have pervasively replaced all other mafic gabbroic or doleritic phases (Figure 7E,F). The amphibolites apparently developed adjacent to fractures which were active hydrothermal fluid conduits at greenschist and low pressure amphibolite facies conditions. Veins filled with prismatic to granular, euhedral to subhedral green amphibole are characteristic of the incipient development of amphibolite zones.

Green and brown hornblenditic amphiboles are locally replaced by pale to green, acicular to fibrous actinolitic amphiboles. These occur both as 'uralitic-like' overgrowths on, and patchy intergrowths within, the earlier-formed amphiboles and, more rarely, pyroxenes. The fibrous amphiboles are locally intergrown with brown, Mg-rich chlorite, colourless prehnite, or, more rarely, clinozoisite. Sodic plagioclase, quartz and sphene occur in some altered samples. These associations are suggestive of localized recrystallization under low temperature greenschist or prehnite-actinolite facies metamorphic conditions (Liou et al., 1985).

Subgreenschist alteration includes localized: (1) serpentinization of olivine and orthopyroxene, (2) rodingitization of plagioclase, and (3) the ubiquitous development of cross-cutting zeolite veins (at all depths in the core). Rodingite includes a wide variety of phases, partly including fine-grained hydrogrossular, prehnite, pectolite, and chlorite. Zeolite veining (laumontite and analcime) is the most pervasive form of subgreenschist facies alteration in the core.

Trondhjemitic Veins and Intrusions

Felsic veins appear to be intrusive mainly into the upper gabbros and sheeted dykes. Thick felsic intrusive bodies typically exhibit sharp intrusive contacts; however, veins occur with more transitional or diffusive relations to their hosts. The felsic veins are mineralogically trondhjemites and composed of fine-grained, inequigranular andesine to oligoclase (An_{50-25}) and quartz with minor mafic phases typically replaced by chlorite. Granophyric textures are locally present. Some mafic phases in these felsic dykes may have chemical compositions comparable with those in their hosts (e.g., plagioclase with the composition An_{28} and clinopyroxene with the composition $En_{38}Fs_{13}Wo_{49}$ coexist in a mafic trondhjemite sample, CY4-882.15).

Sampling and Analytical Techniques

Samples between 489 m and the base of the hole at 2263 m were obtained for analysis. A complete list of analyzed samples in this study and their designated petrographic units, according to the original core descriptions, are given in Appendix 1. Individual samples are identified by depth in metre (prefixed by 'CY4'). Polished sections were prepared from a total of 295 samples, each sample containing at least one (generally plagioclase) or more primary igneous minerals. The samples analyzed represent a total of 815 metres, or 46 per cent, of the petrographic units of the examined core. The sampling density is on an average 0.17 samples per metre, but ranges from 0.10 in the dykes, to 0.20 in the gabbroic rocks, and 0.14 samples in the ultramafic cumulates (Figure 1). Only a few trondhjemitic intrusive rocks were analyzed.

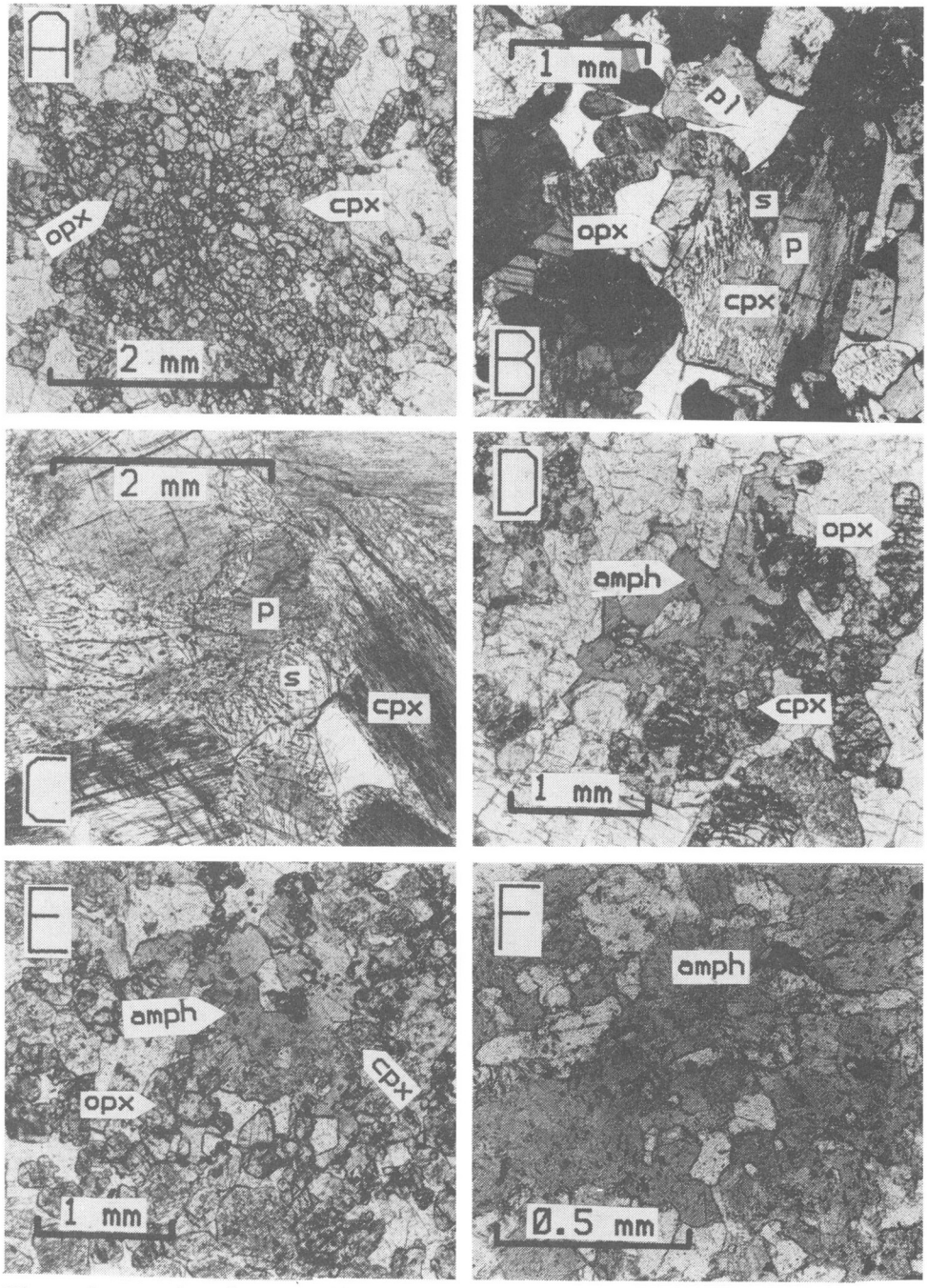

Figure 7: Photomicrographs of recrystallization, alteration and metamorphic textures. (A) Granulation of orthopyroxene into a fine-grained mosaic in a medium-grained, two-pyroxene gabbro. Clinopyroxenes appear to retain their primary texture (CY4-1124.34). (B) Marginal recrystallization of clinopyroxene into a homogeneous clinopyroxene with vermicular exsolutions. This sample is from the medium-grained, websteritic cumulates (CY4-1847.83, crossed nicols). s = secondary clinopyroxene, p = primary clinopyroxene. (C) Marginal recrystallization of clinopyroxene to a homogeneous clinopyroxene with vermicular exsolutions, enlarged compared to Figure 7B (CY4-1895.25). (D) Interstitial, brown-greenish hornblende in medium-grained, two-pyroxene gabbro (CY4-1014.32). This amphibole may be of late magmatic origin. (E) Metamorphic green hornblende in fine- to medium-grained, two-pyroxene gabbro (CY4-900.34). (F) Amphibolized, fine-grained, granular dyke rock (CY4-1071.68).

Approximately 2000 point analyses were made with the microprobe. Minerals analyzed were plagioclase, diopside, enstatite, olivine, spinels, ilmenite, and amphiboles. Only assumed primary igneous minerals were systematically analyzed, and no attempt was made to analyze the secondary minerals in detail. Routinely, two spot analyses were obtained from the cores of each of the major silicate minerals in each section, but amphiboles and Fe-Ti oxides were analyzed only for selected samples. The analyses were made with the energy-dispersive microprobe systems at University of Copenhagen (LINK system) and University of California at Davis (KEVEX), using standard ZAF reduction procedures (Colby, 1968) and natural and synthetic minerals and glasses as standards. The accelerating voltage was 15 kV, specimen currents were 100-300 nA, and counting times were up to 200 seconds. The lower limit of detection is between 0.10 and 0.20 wt.% oxides for all elements. For the present study, no significant and systematic differences were detected between the two microprobe laboratories.

All mineral structural formulae, aside from Fe-Ti oxides, were calculated to fixed amounts of oxygen. Pyroxenes were normalized to 6 oxygens, olivine to 4, plagioclase to 8, all assuming total iron as Fe^{2+}. Amphiboles were calculated to 23 oxygens assuming 2(OH)-groups and all iron as Fe^{2+}. Spinels were normalized to 3 cations, and ilmenite to 2, calculating Fe^{2+} and Fe^{3+} assuming stoichiometry. Representative analyses are given in Tables 1-7 and the results are summarized in Appendix 1. The mineral compositions given in Appendix 1 are in general the highest Mg/(Mg + Fe) or Ca/(Ca + Na) ratios obtained for the mafic phases and plagioclase, respectively. A full listing of analyses can be obtained from the first author on request.

Mineral Chemistry

All analyses are shown on Figures 8-11 as a function of depth in the drill core and in subsequent figures (Figures 12-18) as a function of petrographic characterization as either dykes, upper gabbros or lower cumulates. The latter group includes gabbroic and websteritic cumulates (Figures 1 and 6). The main emphasis in this section is on the definition and chemical characterization of the three major petrographic rock types. Late trondhjemitic intrusions will not be discussed. A subsequent section will discuss cryptic variation and phase layering. Finally, the data from the CY-4 drill core are compared to information from the extrusive sequences (Malpas and Langdon, 1984; Cameron, 1985; Thy et al., 1985; and work in progress) and the cumulate and mantle sequences (Allen, 1975; Johan et al., 1982).

Plagioclase

The compositional variations of plagioclase, given as mol.% An, are shown on Figures 8 and 9 as a function of stratigraphy. Representative analyses are given in Table 1. The compositions of plagioclase, more calcic than An_{50}, are projected on the Fe versus An diagram in Figure 12. There is little variation in Fe within and between the three petrographic groups (Figure 12). Potassium contents are mostly close to or below detection limit and were not systematically analyzed. Ti and Mg occur in small amounts (<0.20 wt.% oxides) but also were not systematically analyzed.

(a) Dykes. The An content of groundmass plagioclase shows extensive variation between An_{89} and An_{40}, but clusters between An_{70} and An_{60} (Figure 12). These variations may either be primary (i.e., attributable to groundmass crystallization) or secondary (i.e., attributable to amphibolite facies metamorphism). There is no clear difference in plagioclase compositions between the upper doleritic dykes and the lower granular textured dykes (Figure 9). Analyzed phenocrysts in doleritic dykes (not given on diagrams) have An contents of about 75. The range observed in plagioclase phenocrysts/ microphenocrysts from the lower pillow lava glasses (Thy et al., 1985) conforms with the main variation seen in the dyke rocks. A few dykes low in the stratigraphy (Figure 8) contain plagioclase more calcic that An_{85}, which suggests a compositional transition to more primitive magmas similar to those represented by the upper gabbros (see discussion on pyroxene chemistry). Rare plagioclase crystals with a composition of An_{93} are probably xenocrystic and derived from the gabbros.

(b) Upper Gabbros. The cumulus plagioclases show a narrow compositional variation between An_{95} to An_{85} with a mean value of An_{90} (Figure 12). A trend towards An_{50}, or below, is probably due to the inclusion of metamorphic grains. The restricted compositional variation can be attributed to limited crystallization of interstitial liquids.

(c) Lower Gabbros and Websteritic Cumulates. The cumulus plagioclases show a narrow variation between An_{98} to An_{92} with a mean value around An_{96} (Figure 12). Despite the fact that plagioclases in the websterites occur in an interstitial or intercumulus texture, these do not, as would be expected, show significantly lower An contents. Also, gabbroic layers and intrusions in the websteritic sequence contain plagioclases whose composition is indistinguishable from those of interstitial plagioclase in the websterites. The plagioclases analyzed in this study are similar to those analyzed by Allen (1975) from Troodos cumulates (Figures 8-9) and suggest that little evolution occurs in the plagioclases not sampled by the CY-4 drilling.

TABLE 1. Composition and Structural Formula of Representative Plagioclase Analyses

	Doleritic Dykes			Granular Dykes			
	498.64	581.90	766.34	866.37	1002.65	1075.49	1142.57
SiO_2	53.73	44.94	51.12	52.38	50.40	50.86	47.91
Al_2O_3	29.22	33.56	30.41	31.25	30.84	31.29	33.05
FeO	0.57	0.77	0.73	0.28	0.74	0.72	0.60
CaO	11.93	18.57	14.61	13.66	14.35	14.97	16.43
Na_2O	4.49	0.83	3.30	4.00	3.36	3.04	1.92
Total	99.94	98.67	100.17	101.57	99.69	100.88	99.91
Cations calculated to 8 oxygens							
Si	2.432	2.108	2.331	2.344	2.309	2.303	2.200
Al	1.559	1.856	1.634	1.649	1.666	1.671	1.789
Fe	0.022	0.030	0.028	0.010	0.028	0.027	0.023
Ca	0.579	0.933	0.714	0.655	0.705	0.726	0.808
Na	0.394	0.075	0.292	0.347	0.299	0.267	0.171
Sum	4.985	5.002	4.998	5.005	5.007	4.995	4.991
An mol.%	59.5	92.5	71.0	65.4	70.2	73.1	82.5

	Granular Dykes	Upper Gabbros					
	1265.29	839.78	866.36	1128.34	1213.34	1281.69	1317.62
SiO_2	47.83	44.26	45.19	46.66	47.52	45.17	45.57
Al_2O_3	33.78	34.83	36.07	33.86	33.72	34.23	34.19
FeO	0.84	0.14	0.27	0.67	0.60	0.62	0.77
CaO	17.51	18.91	19.28	18.06	17.79	18.68	18.05
Na_2O	1.52	0.33	0.66	1.24	1.25	0.53	1.02
Total	101.48	98.47	101.47	100.49	100.88	99.23	99.60
Cations calculated to 8 oxygens							
Si	2.170	2.073	2.058	2.141	2.167	2.102	2.112
Al	1.807	1.923	1.936	1.832	1.813	1.878	1.869
Fe	0.032	0.005	0.010	0.026	0.023	0.024	0.030
Ca	0.851	0.949	0.941	0.888	0.869	0.931	0.897
Na	0.134	0.030	0.058	0.110	0.111	0.048	0.092
Sum	4.994	4.980	5.003	4.998	4.982	4.983	4.999
An mol.%	86.4	96.9	94.2	89.0	88.7	95.1	90.7

	Lower Gabbros			Lower Ultramafic Cumulates			
	1330.82	1437.35	1745.00	1761.54	1912.75	2099.66	2203.50
SiO_2	44.38	44.12	44.75	43.75	44.58	43.97	44.82
Al_2O_3	34.78	35.32	35.25	35.61	34.80	35.37	35.37
FeO	0.70	0.26	0.51	0.46	0.37	0.52	0.42
CaO	18.76	19.23	19.09	18.96	18.56	18.30	19.05
Na_2O	0.43	0.67	0.22	0.32	0.67	0.43	0.23
Total	99.05	99.60	99.82	99.10	98.98	98.59	99.89
Cations calculated to 8 oxygens							
Si	2.072	2.050	2.070	2.041	2.079	2.058	2.071
Al	1.914	1.935	1.922	1.959	1.913	1.951	1.926
Fe	0.027	0.010	0.020	0.018	0.014	0.020	0.016
Ca	0.938	0.957	0.946	0.948	0.927	0.918	0.943
Na	0.039	0.060	0.020	0.029	0.061	0.039	0.021
Sum	4.991	5.013	4.978	4.994	4.995	4.986	4.977
An mol.%	96.0	94.1	98.0	97.0	93.9	95.9	97.9

SAMPLE DESCRIPTIONS FOR TABLES 1-7:

Dykes:

498.64 Fine-grained, aphyric dolerite.
581.90 Fine-grained, pl-px porphyric dolerite, plagioclase phenocryst.
681.02 Fine-grained, amphibolized dolerite.
766.34 Fine-grained, aphyric dolerite.
866.37 Fine-grained, granular dyke in contact with gabbro 866.36.
898.06 Fine-grained, granular dyke.
1002.65 Fine-grained, granular dyke.
1058.72 Fine-grained, granular dyke.
1075.49 Fine-grained, granular dyke.
1142.57 Fine-grained, granular dyke.
1265.29 Fine-grained, granular dyke.

Upper Gabbros:

839.78 Medium-grained gabbro.
866.36 Medium-grained gabbro in contact with dyke 866.37.
884.01 Medium-grained gabbro with interstitial brown amphibole.
1000.87 Medium-grained gabbro.
1127.01 Medium-grained, amphibolized gabbro.
1128.34 Medium-grained gabbro.
1196.03 Medium-grained, mesocratic gabbro with large interstitial Fe-Ti oxides.
1212.25 Fine- to medium-grained gabbro.
1213.34 Fine- to medium-grained gabbro.
1278.96 Medium-grained gabbro.
1281.69 Fine- to medium-grained gabbro.
1317.62 Fine- to medium-grained, laminated and layered gabbro.

Lower Gabbros and Websterites:

1330.82 Fine- to medium-grained, granular gabbro. Probably a chilled facies to the lower gabbroic complex.
1437.35 Medium- to coarse-grained, leucocratic gabbro.
1608.72 Medium-grained, mesocratic gabbro.
1745.00 Medium-grained gabbro.
1761.54 Coarse-grained pyroxenite, interstitial plagioclase.
1764.98 Medium-grained pyroxenite.
1798.02 Medium-grained, amphibolized gabbro to pyroxenite.
1859.50 Coarse-grained, amphibolized gabbro.
1912.75 Medium- to coarse-grained pyroxenite, interstitial plagioclase.
2012.00 Coarse-grained pyroxenite.
2099.66 Fine- to medium-grained gabbro.
2203.50 Medium-grained wehrlite, interstitial plagioclase.

TABLE 2. Composition and Structural Formula of Representative Clinopyroxene Analyses

	Granular Dykes						U. Gabbros
	866.37	1002.65	1058.72	1075.49	1142.57	1265.29	839.78
SiO_2	51.43	52.38	52.15	52.45	51.75	51.42	53.56
TiO_2	0.44	0.10	0.43	0.42	0.52	0.41	—
Al_2O_3	1.61	0.73	1.15	1.34	1.91	2.11	0.58
FeO	10.21	10.59	11.42	10.24	9.34	10.11	6.94
MnO	0.42	0.35	—	0.37	0.29	—	0.18
MgO	13.00	13.98	14.04	14.28	14.66	14.46	15.56
CaO	21.36	21.09	20.44	20.92	20.90	20.66	22.80
Cr_2O_3	—	—	0.21	0.35	0.18	0.41	0.17
Total	98.47	99.22	99.84	100.37	99.55	99.58	99.79
Cations calculated to 6 oxygens							
Si	1.959	1.979	1.960	1.956	1.939	1.930	1.984
Ti	0.013	0.003	0.012	0.012	0.015	0.012	—
Al	0.072	0.033	0.051	0.059	0.084	0.093	0.025
Fe	0.325	0.335	0.359	0.319	0.293	0.317	0.215
Mn	0.014	0.011	—	0.012	0.009	—	0.006
Mg	0.738	0.787	0.787	0.794	0.818	0.809	0.859
Ca	0.872	0.854	0.823	0.836	0.839	0.831	0.905
Cr	—	—	0.006	0.010	0.005	0.012	0.005
Sum	3.992	4.002	3.999	3.998	4.002	4.005	3.999
En mol.%	38.1	39.9	40.0	40.7	42.0	41.3	43.4
Fs mol.%	16.8	16.9	18.2	16.4	15.0	16.2	10.9
Wo mol.%	45.1	43.2	41.8	42.9	43.0	42.5	45.7
Mg#	69.4	70.2	68.7	71.3	73.7	71.8	80.0
Ti/Al	0.181	0.091	0.235	0.203	0.179	0.129	—

	Upper Gabbros						L. Gabbros
	866.36	1000.87	1128.34	1213.34	1281.69	1317.62	1330.82
SiO_2	53.53	53.33	52.65	51.69	51.97	50.91	52.64
TiO_2	0.10	0.25	0.52	0.56	0.50	0.43	0.15
Al_2O_3	0.65	1.07	1.56	1.94	1.97	2.27	1.34
FeO	6.39	8.51	7.25	8.57	7.50	8.44	4.95
MnO	0.24	—	0.24	0.32	—	0.37	0.25
MgO	15.79	15.39	15.87	15.45	15.47	14.98	16.31
CaO	23.10	21.78	21.63	21.11	21.55	20.55	23.22
Cr_2O_3	—	0.18	0.28	0.22	0.21	—	0.41
Total	99.80	100.51	100.00	99.86	99.17	97.95	99.27
Cations calculated to 6 oxygens							
Si	1.980	1.969	1.947	1.926	1.939	1.931	1.951
Ti	0.003	0.007	0.014	0.016	0.014	0.012	0.004
Al	0.028	0.047	0.068	0.085	0.087	0.101	0.059
Fe	0.198	0.263	0.224	0.267	0.234	0.268	0.153
Mn	0.008	—	0.008	0.010	—	0.012	0.008
Mg	0.871	0.847	0.875	0.858	0.860	0.847	0.901
Ca	0.916	0.862	0.857	0.843	0.861	0.835	0.922
Cr	—	0.005	0.008	0.006	0.006	—	0.012
Sum	4.003	3.998	4.001	4.012	4.001	4.006	4.010
En mol.%	43.9	43.0	44.7	43.6	44.0	43.4	45.6
Fs mol.%	10.0	13.3	11.5	13.6	12.0	13.7	7.8
Wo mol.%	46.1	43.7	43.8	42.8	44.0	42.9	46.6
Mg#	81.5	76.3	79.6	76.3	78.6	76.0	85.5
Ti/Al	0.107	0.149	0.206	0.188	0.161	0.119	0.068

	Lower Gabbros			Lower Ultramafic Cumulates			
	1437.35	1608.72	1745.00	1761.54	1912.75	2099.66	2203.50
SiO_2	53.60	51.76	53.50	52.47	53.13	52.01	53.43
TiO_2	0.11	0.34	0.12	0.18	—	—	—
Al_2O_3	1.24	2.73	2.20	2.28	2.04	1.95	2.34
FeO	3.55	5.68	4.88	4.79	3.90	3.85	4.09
MnO	—	0.26	0.22	0.28	0.26	0.29	0.27
MgO	16.90	16.30	17.84	17.87	18.04	17.22	18.02
CaO	23.33	22.61	21.26	20.95	21.70	23.06	19.94
Cr_2O_3	0.69	0.48	0.40	0.50	1.14	0.41	0.78
Total	99.42	100.16	100.42	99.32	100.21	98.79	98.87
Cations calculated to 6 oxygens							
Si	1.967	1.906	1.943	1.930	1.934	1.929	1.957
Ti	0.003	0.009	0.003	0.005	—	—	—
Al	0.054	0.119	0.094	0.099	0.088	0.085	0.101
Fe	0.109	0.175	0.148	0.147	0.119	0.119	0.125
Mn	—	0.008	0.007	0.009	0.008	0.009	0.008
Mg	0.924	0.895	0.966	0.979	0.979	0.952	0.984
Ca	0.917	0.892	0.827	0.826	0.846	0.916	0.783
Cr	0.020	0.014	0.011	0.015	0.033	0.012	0.023
Sum	3.994	4.018	4.001	4.009	4.006	4.023	3.981
En mol.%	47.4	45.6	49.7	50.2	50.4	47.9	52.0
Fs mol.%	5.6	8.9	7.6	7.6	6.1	6.0	6.6
Wo mol.%	47.0	45.5	42.7	42.2	43.5	46.1	41.4
Mg#	89.5	83.6	86.7	86.9	89.2	88.9	88.7
Ti/Al	0.056	0.076	0.032	0.051	—	—	—

TABLE 3. Composition and Structural Formula of Representative Orthopyroxene Analyses

	Granular Dykes						U. Gabbros
	898.06	1002.65	1058.72	1075.49	1142.57	1265.29	839.78
SiO_2	52.77	52.53	52.06	53.06	53.46	52.80	53.97
TiO_2	0.13	0.21	0.27	0.32	0.35	0.37	—
Al_2O_3	0.23	0.42	0.81	0.82	0.99	1.14	0.39
FeO	22.43	22.60	23.67	22.14	20.00	20.21	17.30
MnO	0.49	0.63	0.55	0.62	0.49	—	0.50
MgO	21.55	21.56	20.79	22.04	23.95	23.96	25.80
CaO	1.26	1.33	1.49	1.42	1.47	1.61	0.80
Cr_2O_3	0.17	—	0.36	0.18	—	0.14	0.16
Total	99.03	99.28	100.00	100.60	100.71	100.23	98.92
Cations calculated to 6 oxygens							
Si	1.992	1.981	1.962	1.969	1.961	1.947	1.986
Ti	0.004	0.006	0.008	0.009	0.010	0.010	—
Al	0.010	0.019	0.036	0.036	0.043	0.050	0.017
Fe	0.708	0.713	0.746	0.687	0.613	0.623	0.533
Mn	0.016	0.020	0.018	0.019	0.015	—	0.016
Mg	1.212	1.212	1.168	1.219	1.309	1.317	1.415
Ca	0.051	0.054	0.060	0.056	0.058	0.064	0.032
Cr	0.005	—	0.011	0.005	—	0.004	0.005
Sum	3.997	4.004	4.007	4.001	4.008	4.015	4.003
En mol.%	61.5	61.3	59.2	62.1	66.1	65.7	71.5
Fs mol.%	35.9	36.0	37.8	35.0	31.0	31.1	26.9
Wo mol.%	2.6	2.7	3.0	2.9	2.9	3.2	1.6
Mg#	63.1	63.0	61.0	64.0	68.1	67.9	72.7
Ti/Al	0.400	0.316	0.222	0.250	0.233	0.200	—

	Upper Gabbros						L. Gabbros
	866.36	1000.87	1128.34	1213.34	1281.69	1317.62	1330.82
SiO_2	55.13	53.70	53.66	53.53	53.48	52.52	54.26
TiO_2	0.21	0.24	0.31	0.36	0.32	0.28	0.17
Al_2O_3	0.51	0.80	0.95	1.27	1.18	1.39	1.18
FeO	17.44	20.01	16.33	17.11	16.46	16.97	12.99
MnO	0.42	—	0.30	0.37	0.39	0.41	0.46
MgO	26.53	24.07	26.78	25.89	26.10	25.46	28.42
CaO	0.99	1.23	1.13	1.39	1.35	1.29	1.70
Cr_2O_3	—	0.21	0.18	0.26	—	0.20	0.15
Total	101.23	100.26	99.64	100.18	99.28	98.52	99.33
Cations calculated to 6 oxygens							
Si	1.981	1.972	1.955	1.948	1.957	1.945	1.956
Ti	0.006	0.007	0.008	0.010	0.009	0.008	0.005
Al	0.022	0.035	0.041	0.054	0.051	0.061	0.050
Fe	0.524	0.615	0.497	0.521	0.504	0.526	0.392
Mn	0.013	—	0.009	0.011	0.012	0.013	0.014
Mg	1.420	1.318	1.454	1.404	1.423	1.405	1.527
Ca	0.038	0.048	0.044	0.054	0.053	0.051	0.066
Cr	—	0.006	0.005	0.007	—	0.006	0.004
Sum	4.003	4.001	4.014	4.011	4.009	4.014	4.013
En mol.%	71.7	66.5	72.9	71.0	71.9	70.9	77.0
Fs mol.%	26.4	31.0	24.9	26.3	25.4	26.5	19.7
Wo mol.%	1.9	2.5	2.2	2.7	2.7	2.6	3.3
Mg#	73.1	68.2	74.5	73.0	73.9	72.8	79.6
Ti/Al	0.273	0.200	0.195	0.185	0.176	0.131	0.100

	Lower Gabbros			Lower Ultramafic Cumulates			
	1437.35	1608.72	1745.00	1761.54	1912.75	2099.66	2203.50
SiO_2	56.87	53.20	55.91	54.93	55.86	54.41	55.42
TiO_2	—	0.21	0.15	0.24	—	0.23	0.19
Al_2O_3	1.23	1.67	1.57	1.48	1.37	1.50	1.78
FeO	9.50	12.68	9.76	10.49	10.21	9.45	8.57
MnO	0.47	0.22	—	0.21	0.34	0.23	0.23
MgO	31.52	28.42	31.36	30.45	31.07	31.51	31.41
CaO	1.56	1.61	1.82	1.71	1.20	1.59	1.36
Cr_2O_3	0.17	0.35	0.21	0.29	0.33	0.40	0.45
Total	101.32	98.36	100.78	99.80	100.38	99.32	99.41
Cations calculated to 6 oxygens							
Si	1.971	1.935	1.951	1.946	1.961	1.931	1.951
Ti	—	0.006	0.004	0.006	—	0.006	0.005
Al	0.050	0.072	0.065	0.062	0.057	0.063	0.074
Fe	0.275	0.386	0.285	0.311	0.300	0.280	0.252
Mn	0.014	0.007	—	0.006	0.010	0.007	0.007
Mg	1.628	1.541	1.631	1.608	1.625	1.667	1.648
Ca	0.058	0.063	0.068	0.065	0.045	0.060	0.051
Cr	0.005	0.010	0.006	0.008	0.009	0.011	0.013
Sum	4.001	4.018	4.010	4.012	4.007	4.026	4.001
En mol.%	83.0	77.5	82.2	81.0	82.5	83.0	84.5
Fs mol.%	14.0	19.4	14.4	15.7	15.2	14.0	12.9
Wo mol.%	3.0	3.1	3.4	3.3	2.3	3.0	2.6
Mg#	85.5	80.0	85.1	83.8	84.4	85.6	86.7
Ti/Al	—	0.083	0.062	0.097	—	0.095	0.068

TABLE 4. Composition and Structural Formula of Representative Olivine Analyses

	Lower Gabbros			Lower Ultramafic Cumulates			
	1437.35	1608.72	1745.00	1764.98	1912.75	2099.66	2203.50
SiO_2	40.07	38.24	39.11	39.33	39.40	39.51	39.47
FeO	15.54	20.58	16.51	16.84	16.15	13.95	13.11
MnO	0.19	0.28	0.21	0.20	0.33	0.29	0.27
MgO	46.01	41.45	43.79	44.32	45.20	46.84	45.46
CaO	—	0.13	—	0.18	0.14	0.11	0.14
NiO	0.17	0.54	0.29	0.26	0.37		
Total	101.98	101.22	99.91	101.13	101.59	100.70	98.45
Cations calculated to 4 oxygens							
Si	0.989	0.979	0.992	0.987	0.983	0.982	0.999
Fe	0.321	0.441	0.350	0.353	0.337	0.290	0.278
Mn	0.004	0.006	0.005	0.004	0.007	0.006	0.006
Mg	1.693	1.581	1.655	1.658	1.680	1.736	1.715
Ca	—	0.004	—	0.005	0.004	0.003	0.004
Ni	0.003	0.011	0.006	0.005	0.007		
Sum	3.011	3.021	3.008	3.013	3.017	3.018	3.001
Fo mol.%	84.1	78.2	82.5	82.4	83.3	85.7	86.1

TABLE 5. Composition and Structural Formula of Representative Spinel Analyses

	Granular Dykes			Upper Gabbros		
	898.06	1002.65	1142.57	1196.03	1212.25	1213.34
SiO_2	0.33	0.32				
TiO_2	3.43	2.00	1.50	0.90	4.47	1.37
Al_2O_3	1.70	1.47	0.78	0.99	2.78	1.55
FeO	85.61	86.70	88.59	89.44	83.69	85.99
MnO	0.23	0.19	0.86	0.65	0.25	0.48
MgO	0.28	0.19				
Cr_2O_3	0.16	0.26	—	—	1.20	0.85
V_2O_5	1.00	1.38	2.04	2.17	2.81	2.96
Fe_2O_3	57.27	59.71	62.66	63.75	52.70	59.39
FeO	34.06	32.95	32.19	32.06	36.25	32.54
Total	98.46	98.48	100.03	100.52	100.47	99.13

TABLE 6. Composition and Structural Formula of Representative Ilmenite Analyses

	Granular Dykes		Upper Gabbros	
	898.06	1142.57	1196.03	1213.34
SiO_2	0.20	0.19		
TiO_2	48.25	47.82	47.11	47.95
Al_2O_3	—	—	0.18	0.26
FeO	48.62	50.00	48.61	47.49
MnO	1.41	1.46	2.07	2.49
Cr_2O_3	—	—	0.60	0.30
V_2O_5		1.32	1.01	1.15
Fe_2O_3	7.13	8.78	8.97	7.32
FeO	42.20	42.10	40.53	40.90
Total	99.19	101.67	100.48	100.37

TABLE 7. Composition and Structural Formula of Representative Amphibole Analyses

	Brown Amphiboles			Green Amphiboles			Fibrous
	884.01	1798.02	2012.00	681.02	1278.96	1859.50	1127.01
SiO_2	50.43	50.70	52.30	50.96	51.44	54.32	53.48
TiO_2	1.49	0.93	0.91	0.48	0.29	—	0.14
Al_2O_3	6.31	5.73	5.26	5.51	5.42	4.49	3.70
FeO	9.09	10.09	6.72	13.76	9.52	6.64	12.91
MnO	0.18	0.23	0.15	0.37	0.21	0.28	0.38
MgO	17.70	17.86	19.54	15.17	20.09	21.91	17.00
CaO	11.66	11.63	11.98	11.58	10.71	10.71	10.37
Na_2O	1.64	0.92	0.93	0.67	0.54	0.83	0.54
K_2O	0.30	0.33	0.29	0.26	0.25	0.26	0.26
Cr_2O_3	—	—	1.11	—	—	0.38	—
Total	98.80	98.42	99.19	98.76	98.47	99.82	98.78
Cations calculated to 23 oxygens							
Si	7.130	7.209	7.274	7.324	7.252	7.440	7.594
Ti	0.158	0.099	0.095	0.052	0.031	—	0.015
Al	1.052	0.961	0.862	0.934	0.901	0.725	0.619
Fe	1.075	1.200	0.782	1.654	1.122	0.761	1.533
Mn	0.022	0.028	0.018	0.045	0.025	0.032	0.046
Mg	3.730	3.785	4.050	3.249	4.221	4.472	3.598
Ca	1.767	1.772	1.785	1.783	1.618	1.572	1.578
Na	0.450	0.254	0.251	0.187	0.148	0.220	0.149
K	0.054	0.060	0.051	0.048	0.045	0.045	0.047
Cr	—	—	0.122	—	—	0.041	—
Total	15.437	15.368	15.290	15.275	15.363	15.310	15.179

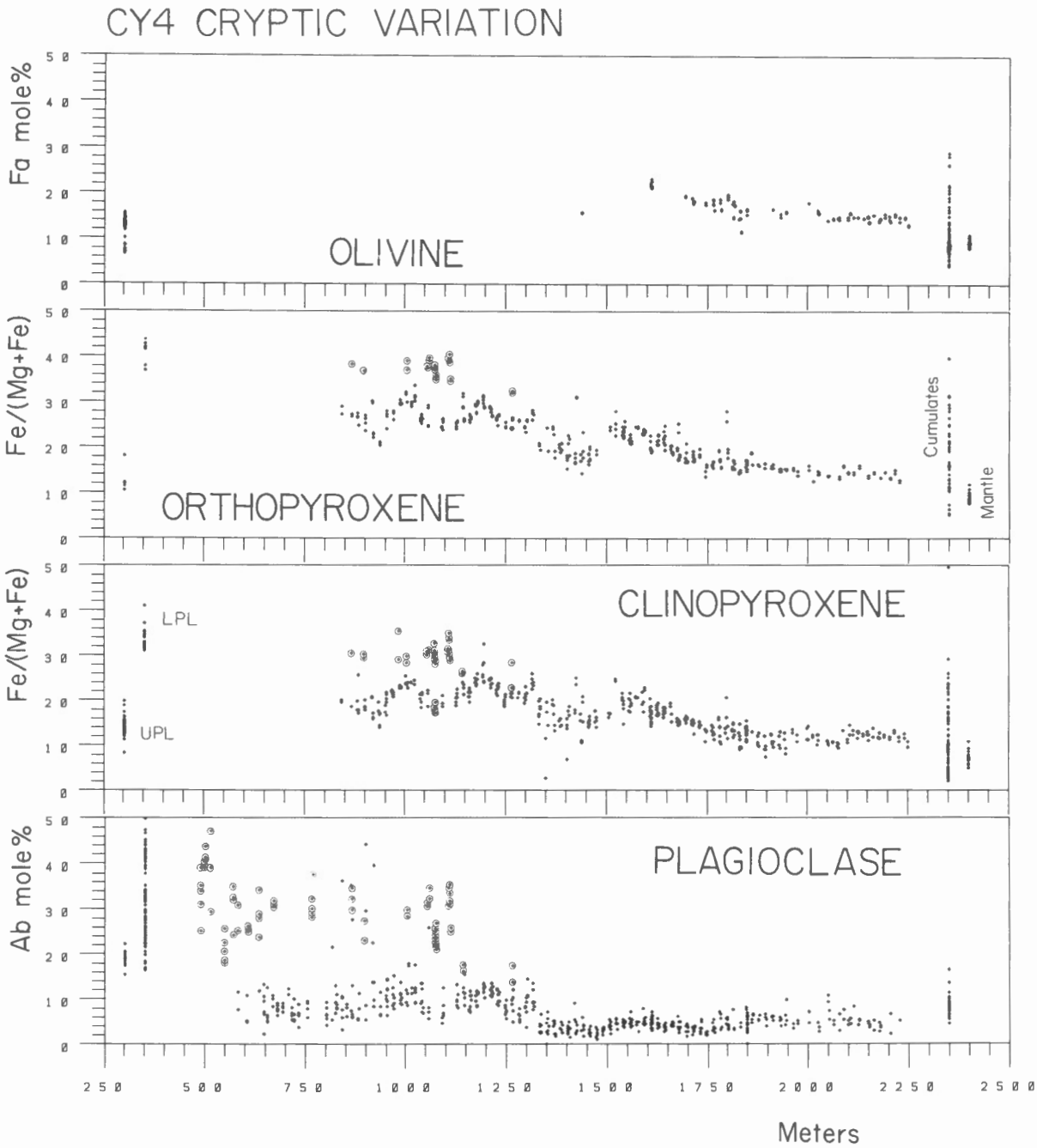

Figure 8: Major element cryptic variation of plagioclase, clinopyroxene, orthopyroxene, and olivine in the CY-4 drill core from 489.37 to 2250.05 m. Dots are cumulus compositions of gabbroic and ultramafic rocks and circled dots are mineral compositions of dyke rocks. Below 1754 m the cumulus status of plagioclase changes to mainly interstitial precipitated. The ranges shown at 300 and 350 m depth are phenocrysts of UPL and LPL, respectively (Malpas and Langdon, 1984; Cameron, 1985; Thy and Xenophontos, unpub. rep.). The data at 2350 m are for cumulus phases from Allen (1975) and Johan et al. (1982) and at 2400 m for mantle minerals from the same sources.

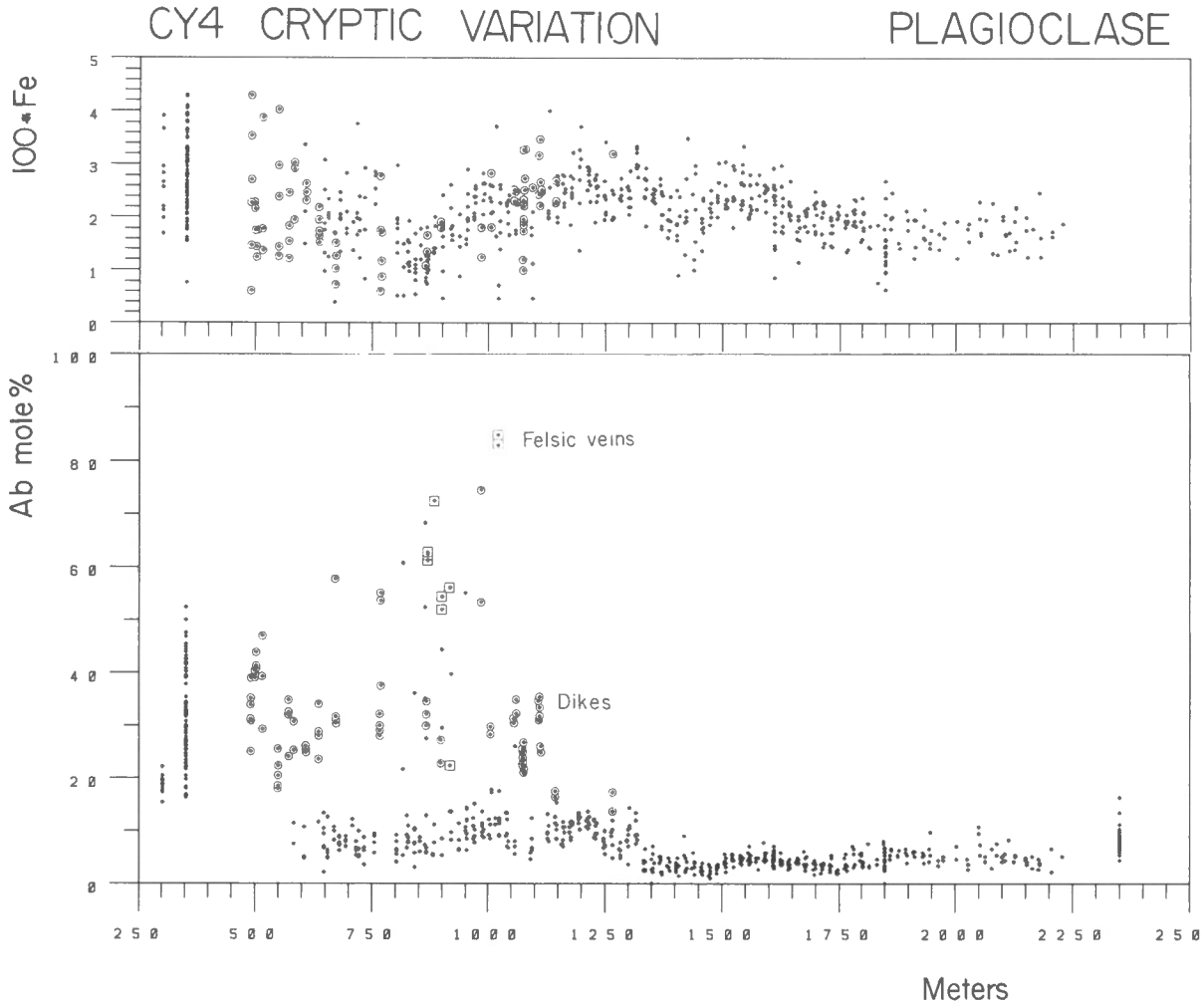

Figure 9: Cryptic variation of plagioclase in the CY-4 drill core. Same data as shown in Figure 8 but An mol.% extended to 100. Circled dots are dyke rocks and squared dots are trondhjemitic veins. The iron content of plagioclase is given as 100 times Fe calculated to 8 oxygen. Plagioclase phenocrysts/xenocrysts of the dykes are not shown.

Ca-rich Pyroxenes

The major element variation of the Ca-rich pyroxenes is shown in terms of the magnesium number (Mg# = Mg/(Mg + Fe), all iron as Fe^{2+}) in Figure 8, and the variations in the minor elements are given in Figure 10. The chemical variations are also illustrated in Figures 13-17 according to petrography, and representative analyses are given in Table 2. Sodium was not systematically analyzed, but is in general below 0.20 wt.% Na_2O which is close to the detection limit. Potassium is always below the detection limit.

(a) Dykes. The high-Ca groundmass pyroxenes in the granular textured dykes are salites and augites (Figure 13), but the majority plot in the augite field of Poldervaart and Hess (1951). These pyroxenes are relatively iron-rich (Mg#s between 74 and 64) compared to the gabbroic pyroxenes (Figure 14). The few analyses of salites with relatively high Mg#s (near 81) come from highly altered samples. Deleting these would create a nearly complete compositional separation of the dyke augites from those found in the gabbros. The concentration of the minor elements Al, Ti, and Cr in the dyke clinopyroxenes are indistinguishable from those found in clinopyroxenes from the host gabbros (Figures 14-16). The Ti/Al ratios (Figure 17) range between 0.07 and 0.22 with a mean value of 0.17, and the Cr contents are often below the limit of detection. Augite phenocrysts are ubiquitously uralitized in the examined dyke samples.

The Fe-Mg contents of augites analyzed from the CY-4 dyke rocks are similar to those reported from the andesitic glasses of the lower pillow lavas (Thy et al., 1985). However, the latter have lower Ca and higher Ti and Al.

(b) Upper Gabbros. Compositionally, the cumulus Ca-rich pyroxenes range from diopside and salite to augite, but are mainly augites (Figure 10). The Mg#s (84-74) are higher than those observed for the dyke clinopyroxenes. However, the gabbroic augites have minor element contents generally comparable to those of the dyke augites (Figures 14-17). The Ti/Al ratios range between 0.06 and 0.24 with a mean value of 0.16, which is slightly lower than that in dyke augites (mean of 0.17). There appears to be a systematic decline in the absolute contents of Al and Ti with decreasing depth in the core from the intrusive contact at 1330 m (Figure 10). The Ti-Al content of augites of the upper gabbros are intermediate between the Ca-rich pyroxene phenocrysts found in the lower and upper pillow lava sequences (Thy et al., 1985; and work in progress). The absolute values of Ti and Al show a wide variation (Figure 10), but the Ti/Al ratios correspond relatively well to those observed for phenocrysts of the lower pillow lavas. Only a few of the cumulus augites analyzed by Allen (1975) and Johan et al. (1982) are compositionally comparable to those in the upper gabbros from the CY-4 core.

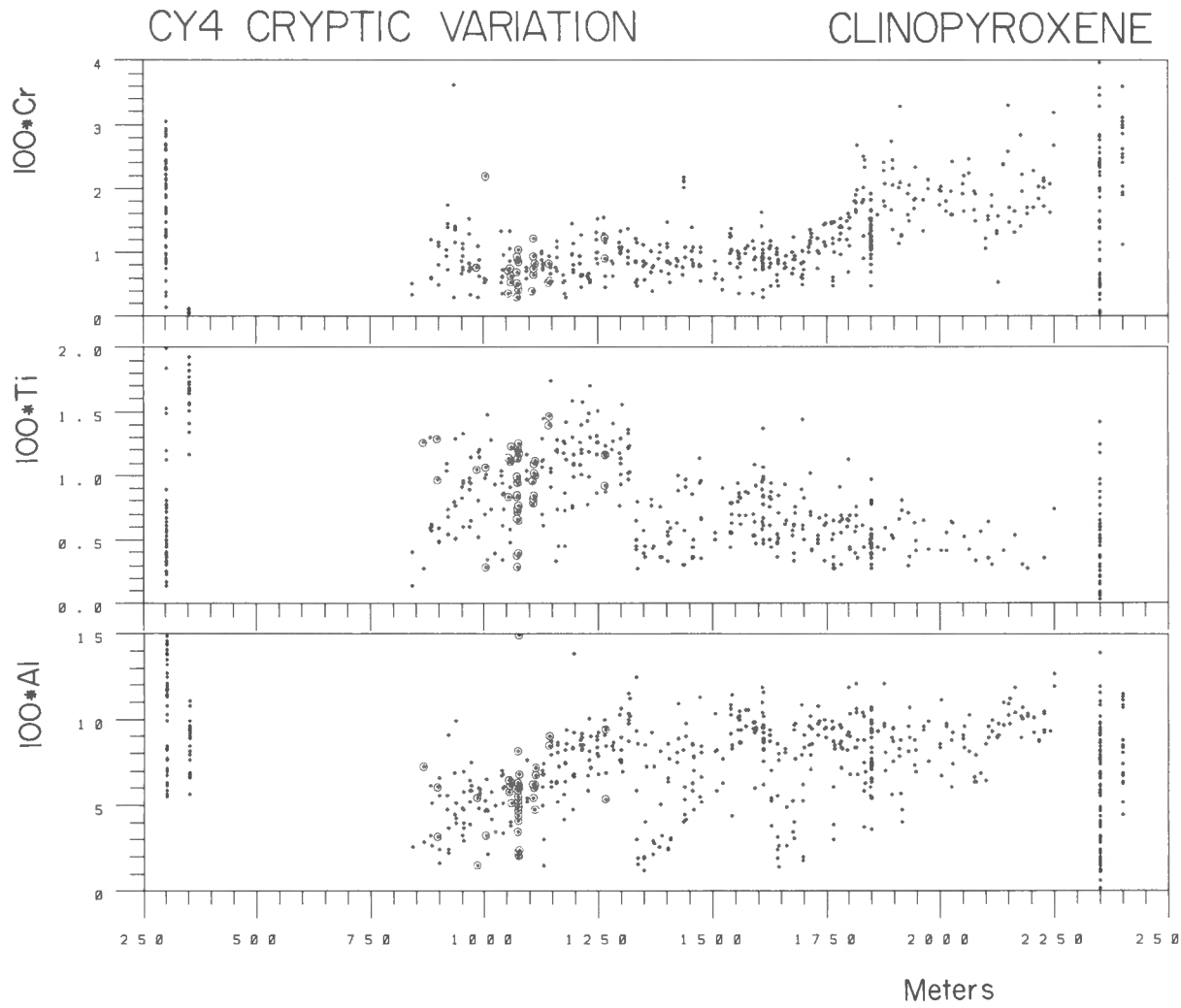

Figure 10: Minor element cryptic variation of clinopyroxene in the CY-4 drill core. Same data as shown in Figure 8. Al, Ti, and Cr are calculated as 100 times cations normalized to 6 oxygens. Circled dots are dyke rocks.

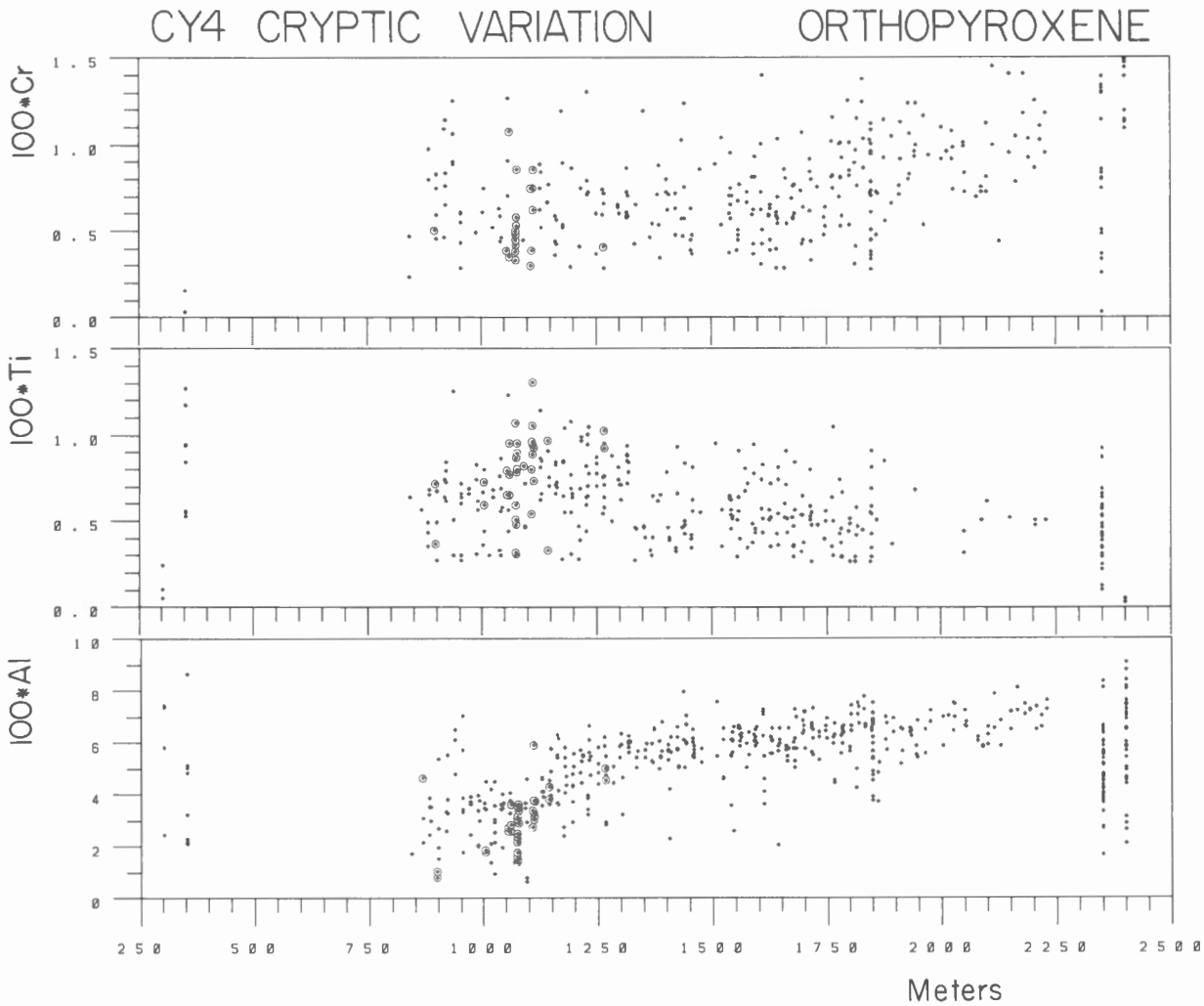

Figure 11: Minor element cryptic variation of orthopyroxene in the CY-4 drill core. Same data as shown in Figure 8. Al, Ti, and Cr are calculated as 100 times cations normalized to 6 oxygens. Circled dots are dyke rocks.

(c) Lower Gabbros and Websteritic Cumulates. Cumulus Ca-rich pyroxenes include endiopside, diopside, and augite (Figure 13), but mainly cluster in the diopside and endiopside fields of Poldervaart and Hess (1951). The Mg#s (90-80) are relatively higher than those observed for the augites of the upper gabbros (Figure 14). The Al and Ti contents appear to extend towards higher and lower values, respectively, than those observed for the upper gabbros and the dyke rocks (Figures 14-15). Corresponding Ti/Al ratios, between 0.03 and 0.21 with a mean value of 0.07, are thus far lower than those observed (mean of 0.16) for the augites of the upper gabbro sequence (Figure 17). Cr contents are significantly higher and exhibit a strong positive correlation with Mg#s not seen for the upper gabbro clinopyroxenes (Figure 16). The Ca-rich pyroxenes of the lower gabbros and websteritic cumulates have diagnostically high Cr contents, high Mg#s, and low Ti/Al ratios. The diopsides of the lower cumulates compare reasonable well with phenocryst phases found in the upper pillow lava sequence (Thy et al., 1985; and work in progress). In general, the findings of Allen (1975) and Johan et al. (1982) agree with the present results. The presence of Mg-rich diopsidic cumulus pyroxenes (i.e., Mg#s >90) reported by Allen (1975) and Johan et al. (1982) suggest the existence of cumulates more primitive than those sampled by the CY-4 drill core.

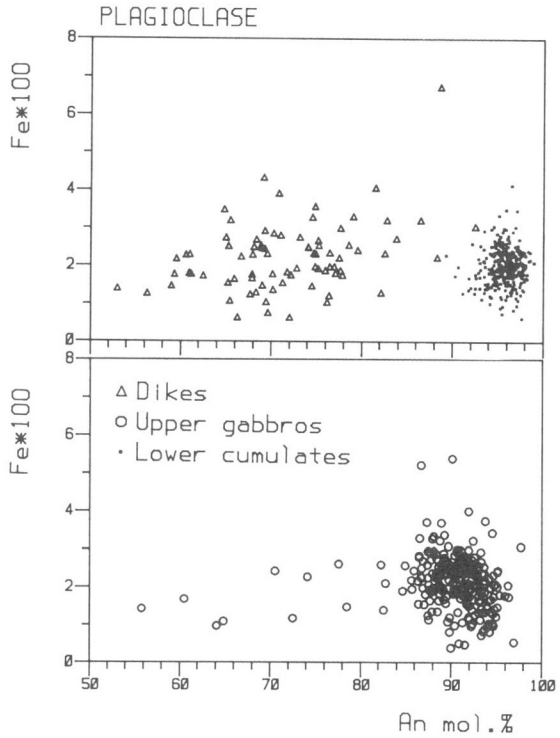

Figure 12: Fe versus An mol.% for analyzed plagioclases. Triangles are dyke rocks, circles are upper level gabbros and dots are lower level gabbros and ultramafics. Iron is calculated as 100 times Fe normalized to 8 oxygens. Analyses with below 50 mol.% An are not shown.

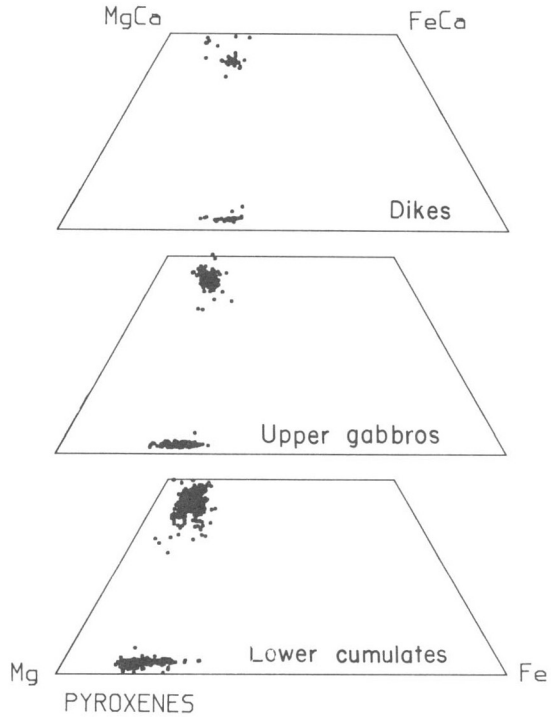

Figure 13: Pyroxene compositions in the Mg-Ca-Fe triangular diagram. Same data as shown in preceding and subsequent figures.

Ca-poor Pyroxenes

The minor element variations of the Ca-poor pyroxenes are given in Figure 11, and representative analyses are given in Table 3. Elsewhere, the compositional variations of the Ca-poor pyroxenes are shown in the same figures as for the Ca-rich pyroxenes. Potassium and sodium are generally below the detection limit and were not systematically analyzed. In all the samples examined optically, the Ca-poor pyroxenes are orthopyroxenes, and no indications of structural inversion are preserved.

(a) Dykes. The compositional variations of the groundmass orthopyroxenes closely parallel those of the augites (Figure 8). The Mg#s are between 66 and 59 (Figure 13), and the minor elements Al, Ti, and Cr show the same general systematics as seen for the augites (Figures 14-17). The orthopyroxenes have Mg#s and Al and Ti contents nearly identical to those of phenocrysts in lower pillow lava glasses (Figures 8 and 11).

(b) Upper Gabbros. The cumulus orthopyroxenes have Mg#s between 78 and 68 (Figures 13-14), clearly higher than the range for the dyke orthopyroxenes. As was the case for the augites, Al and Ti contents of upper gabbro orthopyroxenes are intermediate between the dykes and the lower cumulates (Figures 14 and 15). The Al content decreases upward in the stratigraphy from the intrusive contact at 1330 m; however, contrary to what was observed for the augites (Figure 10), Ti shows no systematic variation as a function of stratigraphy (Figure 11).

(c) Lower Gabbros and Websterites. The cumulus orthopyroxenes show compositional variations closely paralleling the pattern observed for diopsides. The Mg#s range from 88 to 74. The analyses given by Allen (1975) and Johan et al. (1982) for cumulates, not sampled by the drill core, extend the Mg#s (91-90) to the same range as observed for mantle orthopyroxenes (92-90). Orthopyroxene phenocrysts of the upper pillow lavas, analyzed by Cameron (1985) and Malpas and Langdon (1984), have Mg#s of 90-88.

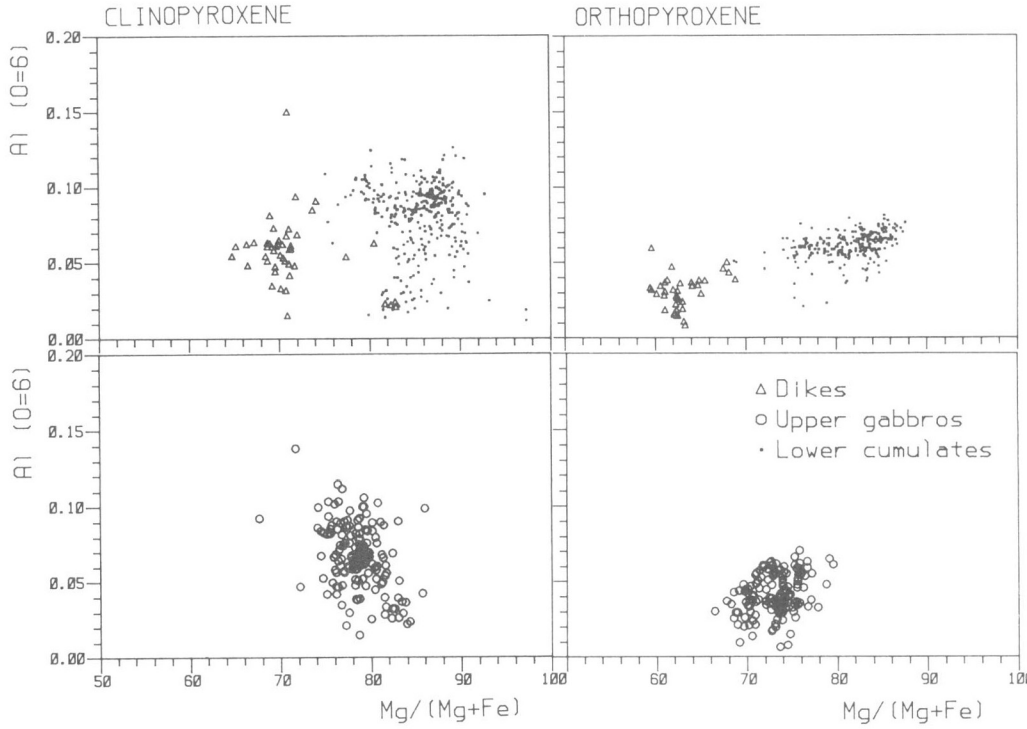

Figure 14: Al (O = 6) versus Mg# (Mg/(Mg + Fe)) for CY-4 pyroxenes. A few clinopyroxenes from dyke rocks plotting in the same field as the lower level gabbros and cumulates are due to one metamorphosed and questionable sample. Deleting this sample would give a complete separation of the two groups.

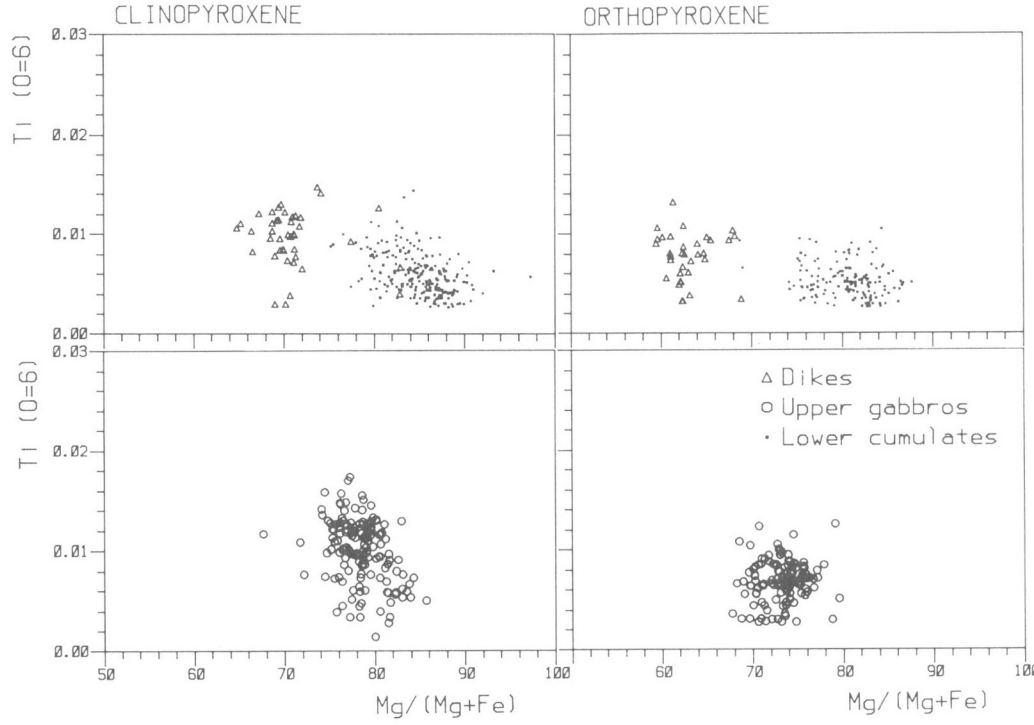

Figure 15: Ti (O = 6) versus Mg# for CY-4 pyroxenes.

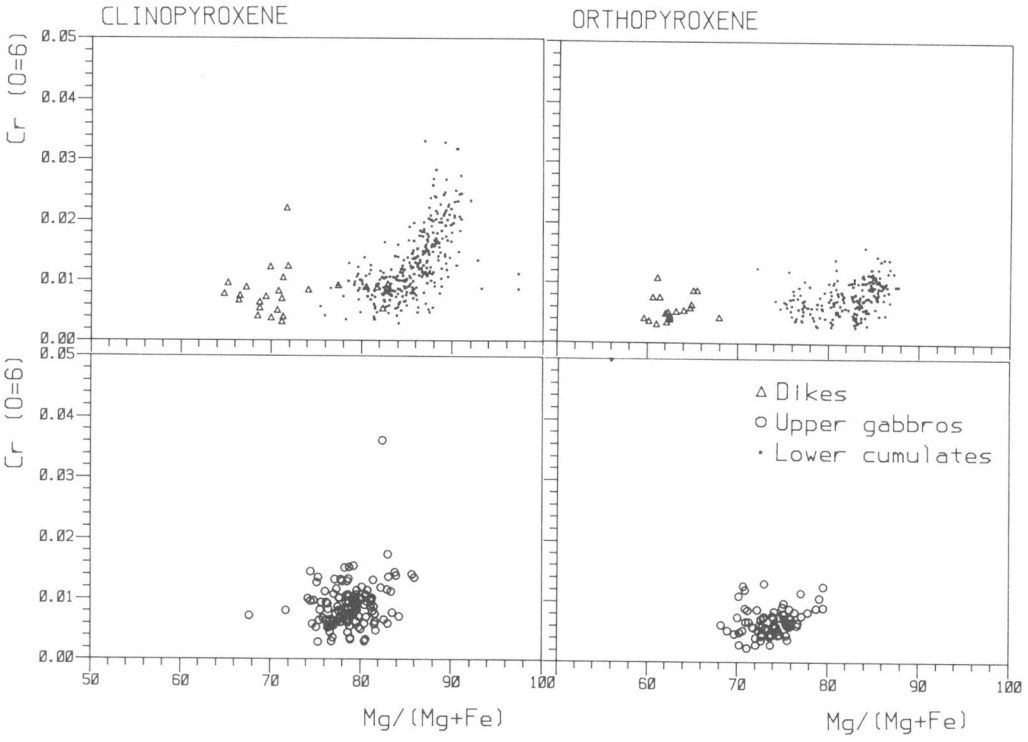

Figure 16: Cr (O = 6) versus Mg# for CY-4 pyroxenes.

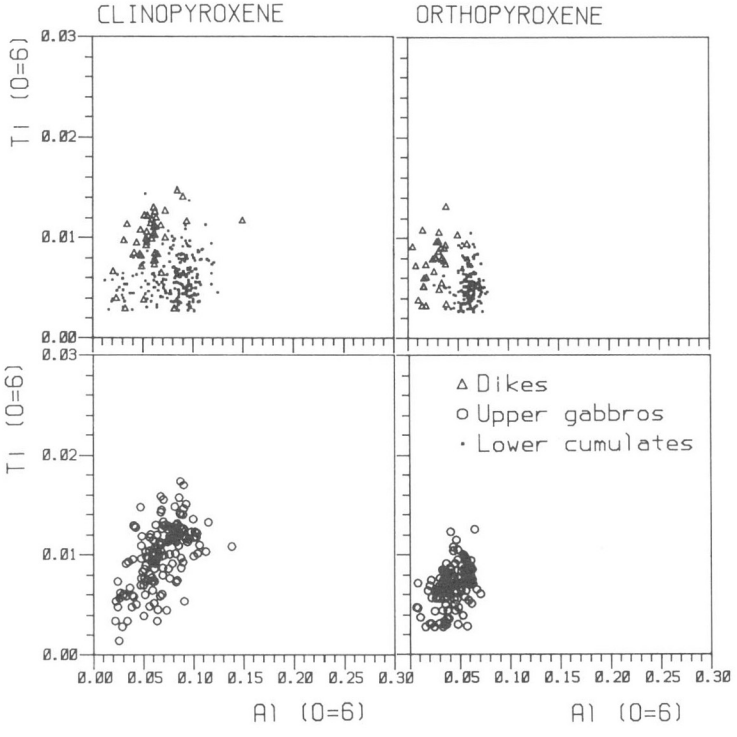

Figure 17: Ti versus Al (O = 6) for CY-4 pyroxenes.

Olivine

Olivine is only present in the lower gabbroic and websteritic sequences. Representative analyses are given in Table 4. Mol.% Fo ranges between 88 and 77 (Figures 8 and 18). There is little, if any, clear correlation between Fo and the minor elements Ca and Mn (Figure 18). Ni however, shows a weak positive correlation with Fo (Figure 18). The maximum Fo content for cumulus olivine analyzed in this study compares well with that of phenocrysts of the upper pillow lavas (Fo_{88-84}). Cumulus olivine compositions reported by Allen (1975) and Johan et al. (1982) range, in general, between Fo_{93} and Fo_{78}. These values agree with those observed for mantle olivines (Fo_{92-89}) and olivine phenocrysts in picrites (Fo_{93-89}).

Fe-Ti Oxides

Fe-Ti oxides occur throughout the core as minor primary or secondary phases. Only locally in the upper gabbros do ilmenite and titanomagnetite become volumetrically important phases. Representative analyses are given in Tables 5 and 6. Compositionally, the ilmenites have a low hematite component, and the magnetites show limited solid solution with ulvöspinel (Figure 19). The gabbroic magnetites are notably less Ti and Fe^{2+} rich than phenocrysts found in the lower pillow lavas (Figure 19). The Fe-Ti oxide minerals presumably have undergone subsolidus re-equilibration and oxidation.

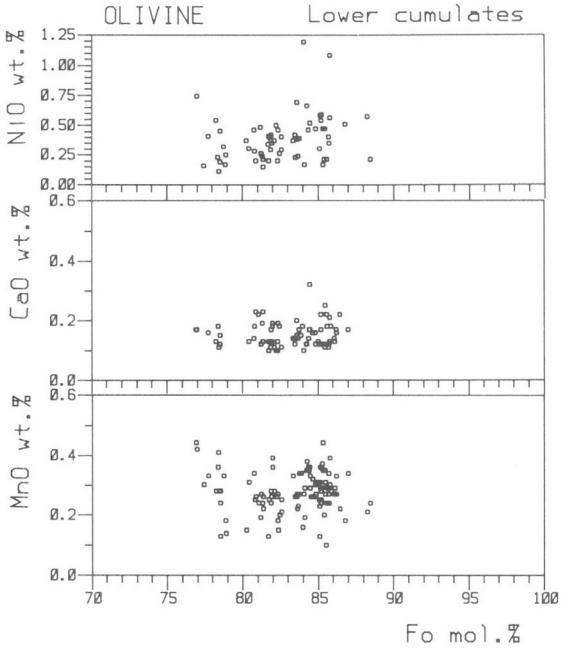

Figure 18: Minor element contents (wt.% oxides) of olivine from the lower gabbros and ultramafic cumulates of CY-4.

The spinels show, in terms of trivalent cations, limited alumina substitution (Figure 20). An observed trend towards Cr-spinels is apparent in a few analyses of probably secondary spinels included in the high-Cr pyroxenes of the lower cumulate sequence. These Cr-bearing spinels differ from the chromites of the chromitites not sampled by the drilling (Figure 20; Greenbaum, 1972b).

Amphiboles

Compositionally, the amphiboles include magnesio-hornblende, actinolitic hornblende, and actinolite (Figure 21; classification after Leake (1978)). Representative analyses are presented in Table 7. Pleochroic brown amphiboles are dominantly magnesio-hornblende, pleochroic green amphiboles are dominantly actinolitic hornblende (but also include actinolite), and paragenetically later fibrous amphiboles are dominantly actinolite (Figure 21). The Al and Ti contents of the amphiboles decrease in the same order (Figure 22). Total alkalis do not exceed 0.5 cations/23 oxygens (Figure 21A). Fe/(Fe + Mg) contents vary between 0.18 and 0.42 and show no systematic relationship with inferred metamorphic grade (Figure 21). Rather, they exhibit a notable correlation with Fe/(Fe + Mg) of coexisting pyroxenes. Brown pleochroic hornblendes whose textures imply a late magmatic origin are compositionally indistinct from other brown hornblendes of pronounced subsolidus origin. Both brown and green amphiboles of the websteritic sequence contain appreciable Cr_2O_3 between 0.18 and 1.44 wt.%. These chromium amphiboles have Fe/(Fe + Mg) contents generally not exceeding 0.20. Chlorine, although not reported, occurs in detectable quantities in some green amphiboles, but rarely or never in brown or fibrous amphiboles.

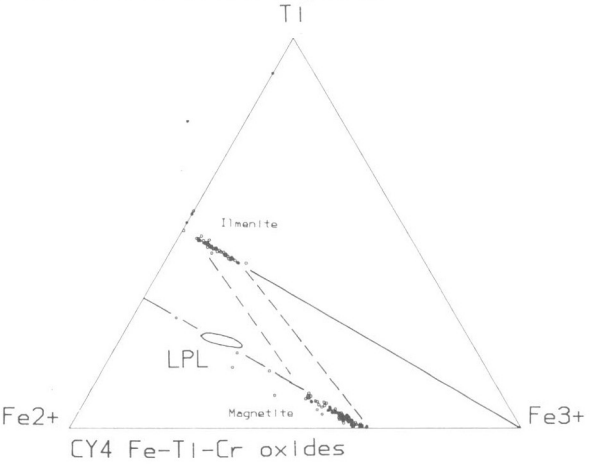

Figure 19: Fe-Ti-Cr oxides from the CY-4 drill core. Calculations of Fe^{2+} and Fe^{3+} assume stoichiometry. LPL outlines lower pillow lava phenocryst titanomagnetites.

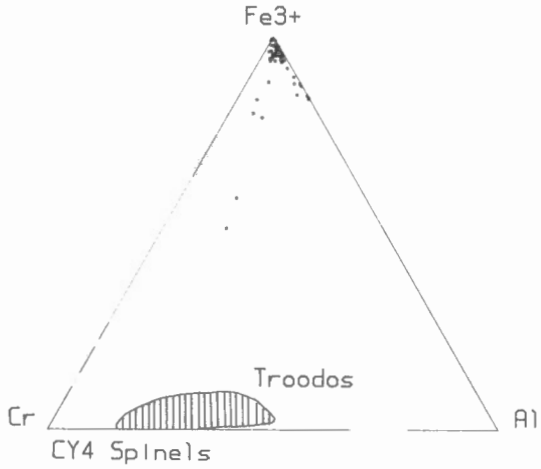

Figure 20: Cr-Fe^{3+}-Al relations of CY-4 spinels. Calculations assume spinel stoichiometry. The general field for Troodos chromites are based on Greenbaum (1972b, 1977), Johan et al. (1982), Cameron et al. (1980), Cameron (1985), and Thy and Xenophontos (work in progress).

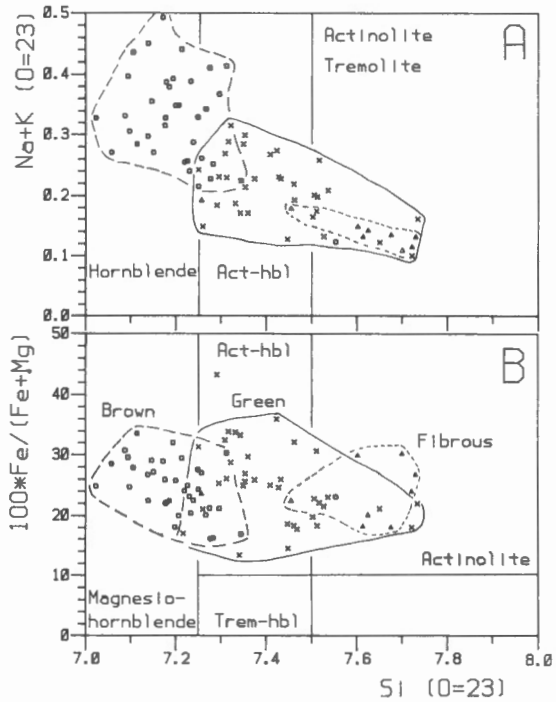

Figure 21: Composition of amphiboles in the CY-4 drill core. (A) Fe/(Fe + Mg) versus Si (O = 23, and all iron as Fe^{2+}). (B) Na + K versus Si (O = 23). Symbols differentiate brown, green, and fibrous amphiboles as described in the text. All amphiboles were recalculated on the basis of an anionic charge of 46.

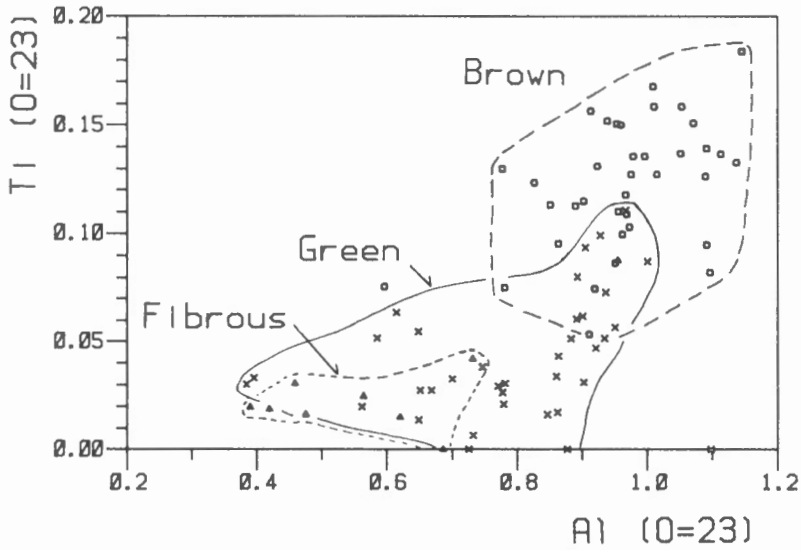

Figure 22: Ti versus Al (O = 23) for CY-4 amphiboles. Same analyses and symbols as used in Figure 21.

DISCUSSION

The Dykes

Texturally, the granular dykes show extensive solid state, grain boundary adjustments (e.g., Vernon, 1970). Compositionally, minerals in the granular dykes are clearly more iron- and sodium-rich than stratigraphically corresponding cumulus phases of the host. Moreover, the presence of Fe-Ti oxides and sulphides distinguishes the dykes from the host gabbros. As expected, constituent minerals of the annealed dyke rocks show less chemical variation than would be expected for simply chilled rocks and cluster around mean values. These mean compositions probably result from chemical annealing and therefore approach subsolidus equilibrium compositions. This suggests that a given phenocryst phase might be expected to be compositionally more primitive than the corresponding, but annealed, groundmass phase: for example, the relict plagioclase phenocrysts in annealed dykes are more calcic (An_{74}) than groundmass plagioclase (An_{67}). For these reasons, the observed compositions most likely represent only estimates of liquidus values. On the other hand, the three-phase assemblages seen in both the dyke groundmasses and the host cumulates suggest that, with caution, valid comparisons can be made.

Despite the fact that the cumulates record crystal fractionation, as revealed by the composition of the major cumulus phases, these compositions do not extend to values as low as those observed for the annealed groundmass phases of the dykes. In fact, a clear compositional separation between dykes and gabbros is apparent for both plagioclase and pyroxenes. These compositional data suggest that the parental magmas to the dykes were of a more evolved nature than those which formed the host gabbroic cumulates. However, these magmas may represent a cogenetic suite, inasmuch as the minor element ratios (Ti/Al) for pyroxenes in both dykes and upper cumulates are nearly identical.

There are compositional similarities between the groundmass phases of the dyke rocks and phenocryst/microphenocrysts observed in the andesite glasses of the lower pillow lavas (Thy et al., 1985; and work in progress). However, the existence of silicic members in the lower pillow lavas has been documented by Robinson et al. (1983) and Mehegan and Robinson (1985), and suggests that these extrusives, in part, were more extensively evolved than the dyke complex. Furthermore, a few dykes low in the stratigraphy (1270-1140 m) contain relatively calcic plagioclase (An_{86-84}), augite (Mg# 77-74), and orthopyroxene (Mg# 69-68), which points to the existence of a suite of more basaltic dykes, poorly represented in the drill core samples.

Data on the mineralogy and mineral chemistries of the sheeted dyke complex are at present very limited (e.g., Schiffman et al., 1985). Geochemical studies suggest the existence of a wide range in dyke compositions, from basaltic andesites to andesites (Moores and Vine, 1971; Desmet et al., 1980), consistent with the findings of this study. Baragar et al. (1985) reported preliminary results of an extensive geochemical study of the sheeted dyke complex and suggested a compositional bimodality of 'depleted' versus 'undepleted' dykes; however, unlike their extrusive equivalents, these two suites overlap both compositionally and temporally. Clearly, a detailed documentation of the lateral, as well as vertical, variation in the dyke chemistry and phenocryst compositions is needed. There are, however, indications from the available data (Schiffman et al., 1985) that the upper gabbros, sheeted dyke complex and lower pillow lavas represent a cogenetic suite compositionally ranging from basalts (or basaltic andesites), to andesites, dacites, and rhyodacites.

The Cumulates

Cumulus Phase Layering

Phase layering, as defined by the appearance or disappearance of cumulus phases (Hess, 1960, p. 51), provides important constraints on the nature and evolution of the parental magmas. (The term, phase layering, is used synonymously with phase contact (Jackson, 1967) and cumulus appearance/termination (Irvine, 1982).) However, phase layering in the CY-4 drill core is pronounced only in the lower gabbros and websterites.

Clinopyroxene occurs as a cumulus phase throughout the entire sampled sequence. Plagioclase appears systematically as a cumulus phase only in the gabbroic cumulates above 1754 m (Figure 6). Except in less important gabbroic members below 1754 m, plagioclase is present only as a minor interstitial phase. Olivine first occurs at 1437.35 m in a sample whose phase assemblage and compositions record a reversal in magma composition (see discussion on cryptic layering). Aside from this occurrence, olivine appears systematically as a cumulus phase at 1600 m and then is consistently present to the bottom of the drill core (Figure 6).

The systematics of orthopyroxene crystallization behavior are ambiguous. Above 1700 m, orthopyroxene occurs dominantly as a granular (or cumulus) phase, but below 1700 m its frequency as an interstitial phase increases (Figure 6). Despite this, the overall modal abundance of orthopyroxene below 1754 m does not decrease in a manner similar to that observed for plagioclase. Furthermore, there appears to be a significant correlation between the presence of cumulus olivine and the appearance of interstitial orthopyroxene. In many samples below 1700 m, the disappearance of orthopyroxene may be ascribed to

accumulative processes (and/or to its characteristically large grain-size) and need not necessarily reflect a peritectic relationship amongst olivine, orthopyroxene, and liquid. Furthermore, the absence of orthopyroxene corona textures and the apparent coexistence of orthopyroxene and olivine in many samples argues against such a peritectic relationship. An alternative possibility to crystallization from an intercumulus liquid, should therefore be looked for in order to explain the development of the interstitial textures observed for orthopyroxene in the Troodos cumulates. It is tentatively suggested that precipitation and growth of olivine may increase the growth rate of orthopyroxene in the melt, and thus enhance development of interstitial textures.

Based on the above arguments, it appears that cumulus orthopyroxene and clinopyroxene co-precipitated throughout the sequence. The critical cumulus phase layering observed, going upward in in the CY-4 drill core, is therefore restricted to (1) the appearance of plagioclase at approximately 1750 m and (2) the disappearance of olivine at approximately 1600 m. This implies the sequence of cumulate zones: ol + cpx + opx, ol + cpx + opx + pl, and cpx + opx + pl. Information given by Greenbaum (1972a) and Allen (1975) suggest, aside from the consideration of chromite stability, that ol and ol + cpx cumulate zones were not sampled by the drilling.

The petrogenetic significance of gabbroic members which occur within the websterite sequence (e.g., samples collected between CY4-2099.66 and CY4-2127.30) is not clear from the available data; however, they may be a genetically related and conformable part of the websterite sequence. More detailed studies of their field relationships to the ultramafic cumulates are, however, clearly warranted (e.g., Alabaster et al., 1985).

The upper gabbroic cumulates exhibit less evidence for crystal fractionation than do the lower cumulates (Figure 1). Orthopyroxene, clinopyroxene, and plagioclase occur as cumulus phases throughout the sequence. However, cumulus Fe-Ti oxides occur only at depths between 1196 to 1213 m, and their crystallization is terminated by a compositional reversal exhibited by other cumulus phases. Thus, the cumulate zones in the upper cumulate sequence are restricted to pl + cpx + opx and pl + cpx + opx + oxide. The available data also suggest that the upper cumulates constitute a sequence which is not genetically related to the lower cumulate sequence.

The observed phase layering (ol, cpx, opx, pl) of the Troodos cumulates differs from the sequence normally observed in oceanic basalts (ol, pl, cpx, opx) by the relatively late appearance of plagioclase and the lack of a reaction-relationship between olivine and orthopyroxene. This produces a unique cumulate sequence which cannot be accounted for by low pressure, phase equilibria in tholeiitic basalt systems (cf., Irvine, 1979). The Troodos crystallization sequence shows similarities to that observed in Mariana trench cumulates (Bloomer and Hawkins, 1983), the Betts Cove ophiolite (Church and Riccio, 1977), and the Papuan Ultramafic Belt (Davies, 1969), all of which display the sequence: ol, opx, cpx, pl. To date, the best known analogy for the Troodos crystallization sequence, however, comes from the Marum ophiolite, Papua New Guinea (Jaques, 1981). The Marum ophiolite, which does not contain a sheeted dyke complex, has been suggested to be of either back-arc or ocean basin origin (Jaques, 1981). This unique crystallization sequence, suggests that both the Marum and Troodos ophiolites were derived from a similar parental magma, whose composition is substantially different from those of oceanic basalts (Jaques, 1981; Thy, 1984). However, this conclusion does not apply to the upper gabbro sequence of the Troodos plutonics, which shows less extensive crystal fractionation, ambiguous phase layering, and close compositional correlation to the sheeted dyke complex (i.e., both the upper gabbro sequence and the dyke complex are spreading related). Because the present information indicates that the sheeted dyke complex of the Troodos is compositionally unrelated to the central ultramafic cumulate complex, the similarities between the lower Troodos and the Marum ultramafic cumulate sequences also include the absence of associated sheeted dyke complexes.

Cryptic Variation and Magma Evolution

Going upward in the core, the solid solution series of pyroxenes and olivine in the lower gabbroic and websteritic cumulates show steady evolutions toward more iron-rich compositions (Figure 8). A reversal to more magnesium-rich compositions occurs at about 1500 m, although this is not clearly recorded in the minor elements (Figures 10-11). Only minor variation in plagioclase composition is observed for the lower cumulates, and the reversal at 1500 m is manifested only as a few mole per cent rise in anorthite content and a slight decrease in Fe content (Figure 9). As there is no clear evidence for an intrusive contact associated with the phase discontinuity at 1500 m, the whole sequence below 1330 m is most simply interpreted as recording just one major reversal which reflects replenishment of the crystallizing magma chamber. This model is supported by the similarities in phase assemblages and in minor element contents of the pyroxenes below and above 1500 m.

As discussed in an earlier section, the intrusive contact at 1330 m is mainly manifested by a sharp increase in grain-size. However, major and most minor element phase compositions do not indicate a strong discontinuity at this depth (Figures 8-12). The best indication is revealed by the Ti contents of

clinopyroxene, which show a sharp break at 1330 m (Figure 10), separating the clinopyroxene compositions into a stratigraphically lower, low-Ti sequence and an upper, high-Ti sequence. The major element contents of plagioclase and pyroxenes are less effective in distinguishing between the lower and upper sequences (Figure 8). From a chemical point of view, the intrusive contact at 1330 m is therefore mainly based on the Ti content of the clinopyroxenes.

The upper gabbros show a complex cryptic variation particularly in the pyroxenes (Figure 8). At least two reversals are apparent from the compositional data shown in Figure 8. The first, above the intrusive contact at 1330 m, occurs at approximately 1175 m and the second at approximately 1000 m. These transitions clearly occur over a broad zone: between 1175 and 1075 m for the first reversal, and between 1000 and 930 m for the second. A similar, approximately 50 metre wide zone is also apparent at the reversal in the lower cumulate sequence at 1500 m. Unfortunately, the pyroxenes above 850 m have been amphibolitized and are not preserved, but available plagioclase data for gabbroic rocks seem to indicate that major reversals are not present above 850 m (Figure 8).

Little variation is actually observed in the minor element phase compositions in upper cumulates, probably due in part to low concentrations and relatively high analytical uncertainty. Iron in plagioclase appears to decrease upward from 1100 to 750 m, but the large scatter above 750 m (Figure 9) may be due to increased hydrothermal alteration and recrystallization. There also appears to be a systematic decrease in Al in clinopyroxenes above 1330 m (Figure 10); the Ti contents of clinopyroxene may exhibit a similar pattern but with a greater variation due to analytical uncertainty. Although Al content of the orthopyroxenes appears to change stratigraphically upward, corresponding Ti content remains nearly constant (Figure 11). Thus, the reversals recorded by the major elements are apparently not reflected in the minor elements.

It is significant to note that, although reversals in the compositions of the cumulus phases are revealed, the replenishing primitive magmas did not cause cyclic repetition of primitive phase assemblages. This suggests that the replenished magma was relatively evolved and saturated with plagioclase, clinopyroxene, and orthopyroxene for the upper gabbros and clinopyroxene, orthopyroxene, plagioclase, and olivine for the lowermost cumulates. However, Alabaster et al. (1985) have described phase and cryptic repetition on a much smaller scale between wehrlites, websterites, and gabbros in the lower part of the CY-4 drill core.

Magma Chamber Models

The chemical reversals recorded in the cumulate sequences are best interpreted as reflecting compositional replenishments of a relatively evolved magma chamber. Such replenishments are well documented from ophiolitic cumulate complexes such as the Oman ophiolite (Pallister and Hopson, 1981; Smewing, 1981; Browning, 1984) and the Bay of Islands ophiolite complex (Elthon et al., 1984; Komor et al., 1985). Data from the Oman cumulate sequences indicate relatively abrupt transitions between primitive and fractionated cumulates. This has been attributed to rapid mixing in a partially open magma chamber, which resulted in abrupt changes in fractionation trends (e.g., Browning, 1984). However, such abrupt changes are not present in the Troodos CY-4 cumulates which display progressive reversals in their fractionation trends (Figure 8). Progressive filling and mixing between residual and primitive magmas would cause steady reversals in the fractionation trends. This model would, however, still require nearly instantaneous mixing and thus not allow for the development of zoning in the magma chamber.

It has been suggested that primitive magmas injected into a relatively evolved magma chamber would most likely be denser and hotter than the residual liquid, and therefore spread along the floor of the chamber with only a limited tendency to mix with the main body of the magma (Huppert and Sparks, 1980). Such a density contrast is required in order to initiate a double-diffusive interface and lateral accretion which along an inclined floor may produce progressive reversals (Irvine et al., 1983; Wilson and Larsen, 1985). Injection of a dense primitive magma and crystallization in the basal zone has been suggested for the Oman magma chamber by Smewing (1981). A dense bottom layer would, as a consequence of the cotectic crystallization of plagioclase and pyroxenes observed in the Troodos cumulates, increase in density and consequently inhibit overturn and mixing of the bottom layer with the main magma body (Huppert and Sparks, 1984). The model of Huppert and Sparks (1980) only works if the replenishing magma is 'picritic' and initially crystallizes olivine lowering the magma density. The replenishing magmas for the Troodos cumulates, however, were not picritic but most likely basaltic and relatively evolved in composition. This is mainly deduced from the retained cotectic crystallization of plagioclase, orthopyroxene, and clinopyroxene from the replenished magma after each compositional reversal. An increase in density during crystallization is supported by the observations that (1) the Troodos glasses exhibit iron-enrichment, (2) the CY-4 cumulates exhibit cryptic iron-enrichment trends, and (3) magnetite only rarely occurs as an early cumulus phase in the CY-4 samples. It is therefore suggested that the replenishing magma for the Troodos

cumulates was not significantly different in density from the residual magma. This situation would tend to favour rapid mixing and not the development of a zoned chamber (e.g., Huppert and Sparks, 1984).

The gradational reversals recorded in the Troodos cumulates may, therefore, be caused by the steady-state filling of the magma chamber with the resultant continuous mixing between a residual liquid and a relatively primitive basaltic liquid. This situation would allow for a fairly magnesian-rich replenishing magma (picritic), as only small amounts of mixed primitive liquid would be required to shift the fractionation trends as observed. However, this possibility is not supported, as it would tend to developed a zoned magma chamber, and consequently strongly 'picritic' reversals in the fractionation trends and phase assemblages. Progressive reversals in fractionation trends have been found in the non-ophiolitic, Fongen-Hyllingen intrusion (Wilson and Larsen, 1985). However, progressive reversals in this intrusion have been attributed to the gradual introduction of hot, dense and primitive liquid along the inclined floor of a relatively evolved, stratified and lateral accreting magma chamber (Wilson and Larsen, 1985). The injection of a dense magma along the floor is required for the initiation of double-diffusive convection and the development of a laterally accreting magma chamber model as suggested by Huppert and Sparks (1980), Irvine et al. (1983), and Wilson and Larsen (1985). The detailed, two-dimensional investigations on which Wilson and Larsen (1985) based their model suggest that caution is needed when interpreting cumulus variation trends collected from one-dimensional profiles or drill cores, such as in this study.

Despite uncertainties in the detailed models, it is clear that magma replenishment is necessary for producing the observed cryptic variation in the Troodos cumulates. The frequency of magma replenishments can be related to tectonic environment. A low frequency reflects a slow- or non-spreading environment, whereas a high frequency reflects a fast-spreading environment. This is clearly consistent with the assumed fast-spreading environments as inferred for the Oman and Bay of Islands ophiolites (Pallister and Hopson, 1981; Browning, 1984; Elthon et al., 1984) and non-spreading plutons such as the Fongen-Hyllingen intrusion (Wilson et al., 1981; Wilson and Larsen, 1985), the Rhum intrusion (Faithfull, 1985; Dunham and Wadsworth, 1978), and the Skaergaard intrusion (Wager and Brown, 1968; Maaløe, 1976). Fast-spreading environments are characterized by steady-state, open-system evolution, resulting in extensive magma replenishments and limited crystal fractionation such as has been observed in the Oman cumulates (Pallister and Hopson, 1981). In slow- or non-spreading environments, magma chambers are characterized by closed-system evolution with infrequent magma replenishments, resulting in extensive crystal fractionation (e.g., Wager and Brown, 1968; Wilson and Larsen, 1985).

The phase chemistry and layering of lower gabbroic and websteritic cumulates of the Troodos complex clearly suggest crystallization in a relatively closed magma chamber within a slow- or non-spreading tectonic environment. On the other hand, the upper gabbros appear to reflect crystallization in a relatively open magma chamber and consequently a higher spreading rate. This observation contrasts to the conclusions of Greenbaum (1972a), and subsequent workers, who have argued that the ultramafic cumulates of the Troodos complex were formed in an axial magma chamber within an oceanic spreading center. The discrepancy in interpretations may in part reflect the difference in the scales of the investigations. For example, data presented for the Bay of Islands ophiolite by Komor et al. (1985) suggest that compositional reversals occur on a scale of less than a few metres. Similar trends of detailed cryptic layering and replenishment within the lower part of the Troodos CY-4 core have been noted by Alabaster et al. (1985). The sampling intervals used by Komor et al. (1985) and Alabaster et al. (1985) are far below that used in the present study. Clearly, further data and evaluation are needed in order to understand the relationship between these observations and small scale versus large scale cryptic zonations.

CONCLUSIONS

The CY-4 drill core contains at least two compositionally distinct sequences. The lower part of the drill core is a coarse-grained websteritic to gabbroic cumulate complex which exhibits the cumulate sequence ol + cpx + opx, ol + cpx + opx + pl, and cpx + opx + pl. Going upward in the core, this cumulate sequence shows systematic and steady fractionation trends towards lower temperature compositions in all cumulus phases, and contains evidence for only one major magma chamber replenishment. This reflects crystallization in a relatively closed magma chamber within a slow- or non-spreading environment. Presumably, this same magma chamber also crystallized the cumulates exposed in the central plutonic complex of the Troodos ophiolite, which rest unconformably on tectonized harzburgites. This hypothesis strongly conflicts with traditional beliefs that the central cumulate complex represents a steady-state, replenished, axial magma chamber (e.g., Greenbaum, 1972a). Cumulus phases in the lower gabbroic and ultramafic complex are compositionally correlative with those of phenocrysts found in the upper pillow lavas of the extrusives, and probably both crystallized from a low-Ti, relatively magnesian, basaltic andesite

parental magma. The cumulus phase layering (ol, cpx, opx, pl) shows a strong similarity to that found for the Marum ophiolite, Papua New Guinea (Jaques, 1981).

The lower cumulate complex is intrusive into the upper gabbroic complex. This upper, and older, complex exhibits the cumulate sequence: cpx + opx + pl and cpx + opx + pl + oxides. The upper cumulates have phase chemistries which reflect extensive magma replenishments. At least two replenishments are recorded. Considering the relative stratigraphic thickness of the two cumulate sequences, this represents a four-fold increase in the frequency of replenishments with respect to the lower cumulate sequence. The reversals seen in the Troodos cumulates appear to reflect progressive filling and mixing with more primitive magmas. These progressive reversals contrast with the more abrupt reversals observed in other ophiolitic cumulates such as at Oman and the Bay of Islands. The magmas which replenished the Troodos magma chamber were basaltic and of a relatively evolved nature. The high rate of magma replenishments inferred for the upper gabbro sequence is interpreted to reflect processes in a relatively steady state, open-system characterized by limited crystal fractionation, analogous to the models developed for the Oman and Bay of Islands ophiolites. This would suggest a relatively faster spreading regime than inferred for the lower cumulate sequence. The mineral chemistries suggest that the parental magmas to the Troodos upper cumulates, were relatively more Fe- and Ti-rich than those which formed the lower cumulates. The upper cumulus phases are compositionally similar to those of the sheeted dykes and the lower pillow lavas, and hence further support their spreading related origin.

The upper gabbro complex is intruded by relatively evolved dykes, whose abundance increases upwards towards the sheeted dyke complex. Although the compositions of annealed groundmass phases in the majority of these dykes reflect their crystallization from relatively evolved magmas, the similarities in phase assemblages and the minor element contents of pyroxenes suggest that both dykes and host gabbros belong to the same magmatic suite, which may have also formed the lower pillow lavas. This observation is consistent with a spreading related origin for the cryptic variation observed in the upper cumulates. Dykes genetically related to the lower cumulate sequence were not sampled in the CY-4 drill core.

The present investigation does not reaffirm the traditional view that the central plutonic complex of the Troodos ophiolite represents a steady-state, multiply replenished magma chamber. Rather, it suggests that spreading related magmatic activity in the Troodos ophiolite was confined to the upper gabbroic and dyke sequences.

ACKNOWLEDGEMENTS

The authors are grateful for permission to work on samples from the CY-4 core of the International Crustal Research Group's Cyprus Crustal Study Project. G. Schönharting (Copenhagen) supplied the samples. Microprobe analyses were in part collected with the JEOL 733/superprobe at Geologisk Centralinstitut, Københavns Universitet. The first author is in debt to J. Rønsbo for access to the Copenhagen microprobe. L. Nielsen, I. Aaes, J. Villesen (all Århus) and N. Winter (Davis) made the 300 polished thin sections. Comments on the manuscript from R.G. Coleman and P.T. Robinson were very helpful. PT acknowledges grants from the Danish Natural Science Research Council, the NATO Science Fellowship Programme, and the Carlsberg Foundation; PS acknowledges NSF grant EAR83-16544; EMM acknowledges NSF grants EAR83-06959, EAR84-11854 and EAR86-10503.

REFERENCES

Alabaster, T., Gass, I.G., Roberts, S. and Tindle, A.
1985: Phase and cryptic variations within the cumulate ultramafic sequence of CY-4-Troodos ophiolite deep drill project; EOS, American Geophysical Union, Transactions, v. 66, no. 46, p. 1123.

Allen, C.R.
1975: The petrology of a portion of the Troodos plutonic complex, Cyprus; unpublished Ph.D. thesis, University of Cambridge, England, p. 1-161.

Baragar, W.R., Lambert, M.B., Baglow, N. and Gibson, I.
1985: Sheeted dykes of the Troodos ophiolite; EOS, American Geophysical Union, Transactions, v. 66, p. 1124.

Bear, L.M.
1960: The geology and mineral resources of the Akaki-Lythrodondha Area; Cyprus Geological Survey Department, Ministry of Agriculture and Natural Resources, Memoir, no. 3, p. 1-122.

Bloomer, S.H. and Hawkins, J.W.
1983: Gabbroic and ultramafic rocks from the Mariana trench: an island arc ophiolite; *in* The Tectonic and Geologic Evolution of Southeast Asian Seas and Islands: Part 2, ed. D.E. Hayes; Geophysical Monograph, no. 27, American Geophysical Union, Washington D.C., p. 294-317.

Browning, P.
1984: Cryptic variation within the cumulate sequence of the Oman ophiolite: magma chamber depth and petrological implications;

in Ophiolites and Oceanic Lithosphere, ed. I.G. Gass, S.J. Lippard and A.W. Shelton; Geological Society of London, Special Publication, no. 13, Blackwell Scientific Publications, Oxford, p. 71-82.

Cameron, W.E.
1985: Petrology and origin of primitive lavas from the Troodos ophiolite, Cyprus; Contributions to Mineralogy and Petrology, v. 89, p. 239-255.

Cameron, W.E., Nisbet, E.G. and Dietrich, V.J.
1980: Petrographic dissimilarities between ophiolitic and ocean-floor basalts; *in* Ophiolites, Proceedings of the International Ophiolite Symposium, Cyprus, 1979, ed. A. Panayiotou; Cyprus Geological Survey Department, Ministry of Agriculture and Natural Resources, p. 182-192.

C.C.S.P. (Cyprus Crustal Study Project)
1985: Hole CY-4 core descriptions. Compiled by Horne, L. and Robinson, P.T., 4 volumes.

Church, W.R. and Riccio, L.
1977: Fractionation trends in the Bay of Islands ophiolite of Newfoundland: polycyclic cumulate sequences in ophiolites and their classification; Canadian Journal of Earth Sciences, v. 14, p. 1156-1165.

Colby, J.W.
1968: Quantitative microprobe analysis of thin insulating films; Advances in X-ray Analysis, v. 11, p. 287-305.

Davies, H.L.
1969: Peridotite-gabbro-basalt complex in eastern Papua; Australian Bureau of Mineral Resources, Geology and Geophysics Bulletin, v. 128, p. 1-48.

Desmet, A., Gagny, C., Lapierre, H. and Rocci, G.
1980: Organisation spatio-temporelle du complexe filonien du Troodos: son enracinement dans la chambre magmatique; *in* Ophiolites, Proceedings of the International Ophiolite Symposium, Cyprus, 1979, ed. A. Panayiotou; Cyprus Geological Survey Department, Ministry of Agriculture and Natural Resources, p. 66-72.

Dunham, A.C. and Wadsworth, W.J.
1978: Cryptic variation in the Rhum layered intrusion; Mineralogical Magazine, v. 42, p. 347-356.

Dunsworth, S.M. and Calon, T.
1984: Relationships between deformation and magmatism in the plutonic complex, Troodos ophiolite, Cyprus; Geological Association of Canada Annual Meeting, London, May 1984, Programs with Abstracts, v. 9, p. 59.

Elthon, D., Casey, J.F. and Komor, S.C.
1984: Cryptic mineral chemistry variations in a detailed traverse through the cumulate ultramafic rocks of the North Arm mountain massif of the Bay of Islands ophiolite, Newfoundland; *in* Ophiolites and Oceanic Lithosphere, ed. I.G. Gass, S.J. Lippard and A.W. Shelton; Geological Society of London, Special Publication, no. 13, Blackwell Scientific Publications, Oxford, p. 83-100.

Faithfull, J.W.
1985: The lower eastern layered series of Rhum; Geological Magazine, v. 122, p. 459-468.

Gass, I.G.
1967: The ultramafic volcanic assemblage of the Troodos massif, Cyprus; *in* Ultramafic and Related Rocks, ed. P.J. Wyllie; John Wiley, New York, p. 121-134.
1980: The Troodos Massif: its role in the unravelling of the ophiolite problem and its significance in the understanding of constructive margin processes; *in* Ophiolites: Proceedings of the International Ophiolite Symposium, Cyprus, 1979, ed. A. Panayiotou, Cyprus Geological Survey Department, Ministry of Agriculture and Natural Resources, p. 23-35.

Gass, I.G. and Masson-Smith, D.
1963: The geology and gravity anomalies of the Troodos massif, Cyprus; Philosophical Transactions of the Royal Society of London, Series A, v. 255, no. 1060, p. 417-467.

Gass, I.G. and Smewing, J.D.
1973: Intrusion, extrusion and metamorphism at constructive margins: evidence from the Troodos massif, Cyprus; Nature, v. 242, p. 26-29.

George, Jr., R.P.
1978: Structural petrology of the Olympus ultramafic complex in the Troodos ophiolite, Cyprus; Geological Society of America, Bulletin, v. 89, p. 845-865.

Greenbaum, D.
1972a: Magmatic processes at ocean ridges: evidence from the Troodos massif, Cyprus; Nature, Physical Science v. 238, no. 80, pp. 18-21.
1972b: The geology and evolution of the Troodos plutonic complex and associated chromite deposits, Cyprus. Ph.D. thesis, University of Leeds, p. 1-142.
1977: The chromitiferous rocks of Troodos ophiolite complex, Cyprus; Economic Geology, v. 72, p. 1175-1194.

Hess, H.H.
1960: Stillwater igneous complex, Montana, a quantitative mineralogical study; Geological Society of America, Memoir, v. 80, p. 1-230.

Honnorez, J., Mevel, C. and Montigny, R.
1984: Geotectonic significance of gneissic amphibolites from the Vema fracture zone, equatorial Mid-Atlantic ridge; Journal of Geophysical Research, v. 89, p. 11379-11400.

Huppert, H.E. and Sparks, R.S.J.
1980: The fluid dynamics of a basaltic magma chamber replenished by influx of hot, dense ultrabasic magma; Contributions to Mineralogy and Petrology, v. 75, p. 279-289.
1984: Double-diffusive convection due to crystallization in magmas; Annual Review of Earth and Planetary Sciences, v. 12, p. 11-27.
Irvine, T.N.
1979: Rocks whose composition is determined by crystal accumulation and sorting; *in* The Evolution of the Igneous Rocks, Fiftieth Anniversary Perspectives, ed. H.S. Yoder, Jr.; Princeton University Press, Princeton, New Jersey, p. 245-306.
1982: Terminology for layered intrusions; Journal of Petrology, v. 23, p. 127-162.
Irvine, T.N., Keith, D.W. and Todd, S.G.
1983: The J-M platinum-palladium reef of the Stillwater complex, Montana: II. Origin of double-diffusive convective magma mixing and implications for the Bushveld complex; Economic Geology, v. 78, p. 1287-1334.
Jackson, E.D.
1967: Ultramafic cumulates in the Stillwater, Great Dyke, and Bushveld intrusions; *in* Ultramafic and Related Rocks, ed. P.J. Wyllie; John Wiley, New York, pp. 20-38.
Jaques, A.L.
1981: Petrology and petrogenesis of cumulate peridotites and gabbros from the Marum ophiolite complex, northern Papua New Guinea; Journal of Petrology, v. 22, p. 1-40.
Johan, Z., Le Bel, L. and Georgiou, E.
1982: Environnement petrologique des gisements de chromite du complexe ophiolitique du Troodos (Chypre); Bureau de Recherches Geologiques et Minieres, Orleans, p. 1-65.
Karson, J.A., Casey, J.F., Elthon, D.L. and Titus, M.
1984: Deformed and metamorphosed rock assemblages recognized in the Bay of Islands ophiolite complex; Ofioliti, v. 9, p. 463-486.
Komor, S.C., Elthon, D. and Casey, J.F.
1985: Mineralogic variation in a layered ultramafic cumulate sequence at the North Arm mountain massif, Bay of Islands ophiolite, Newfoundland; Journal of Geophysical Research, v. 90, p. 7705-7736.
Leake, B.E.
1978: Nomenclature of amphiboles; Mineralogical Magazine, v. 42, p. 533-563.
Liou, J.G., Maruyama, S. and Cho, M.
1985: Phase equilibria and mineral parageneses of metabasites in low-grade metamorphism; Mineralogical Magazine, v. 49, p. 321-333.
Maaløe, S.
1976: The zoned plagioclase of the Skaergaard intrusion, East Greenland; Journal of Petrology, v. 17, p. 398-419.
Malpas, J. and Langdon, G.
1984: Petrology of the upper pillow lava suite, Troodos ophiolite, Cyprus; *in* Ophiolites and Oceanic Lithosphere, ed. I.G. Gass, S.J. Lippard and A.W. Shelton; Geological Society of London, Special Publication, no. 13, Blackwell Scientific Publications, Oxford, p. 155-167.
Mehegan, J.M. and Robinson, P.T.
1985: Lava compositions of the Troodos ophiolite, Cyprus; EOS, American Geophysical Union, Transactions, v. 66, no. 46, p. 1123.
Menzies, M.A. and Allen, C.R.
1974: Plagioclase lherzolite-residual mantle relationships within two eastern Mediterranean ophiolites; Contributions to Mineralogy and Petrology, v. 45, p. 197-213.
Moores, E.M. and Thy, P.
1985: Mineral crystallization trends of the Troodos ophiolite: evidence for genesis and formation; EOS, American Geophysical Union, Transactions, v. 66, no. 46, p. 1123.
Moores, E.M. and Vine, F.J.
1971: The Troodos Massif, Cyprus, and other ophiolites as oceanic crust: evaluation and implications; *in* A Discussion on the Petrology of Igneous and Metamorphic Rocks from the Ocean Floor; Philosophical Transactions of the Royal Society of London, Series A, v. 268, p. 443-466.
Pallister, J.S. and Hopson, C.A.
1981: Samail ophiolite plutonic suite: field relations, phase variation, cryptic variation and layering, and a model of a spreading ridge magma chamber; Journal of Geophysical Research, v. 86, no. B4, p. 2593-2644.
Pantazis, T.M.
1967: The geology and mineral resources of the Pharmakas-Kalavasos area; Cyprus Geological Survey Department, Ministry of Agriculture and Natural Resources, Memoir, no. 8, p. 1-190.
Poldervaart, A. and Hess, H.H.
1951: Pyroxenes in the crystallization of basaltic magma; Journal of Geology, v. 59, p. 472-489.
Robinson, P.T., Melson, W.G., O'Hearn, T. and Schmincke, H.-U.
1983: Volcanic glass compositions of the Troodos ophiolite, Cyprus; Geology, v. 11, no. 7, p. 400-404.
Schiffman, P., Moores, E., Thy, P., Smith, B. and Varga, R.
1985: Petrological and hydrothermal evolution of the Solea graben, northern Troodos ophiolite, Cyprus; EOS, American Geophysical Union, Transactions, v. 66, p. 1128.
Smewing, J.D.

1981: Mixing characteristics and compositional differences in mantle-derived melts beneath spreading axes: evidence from cyclically layered rocks in the ophiolite of North Oman; Journal of Geophysical Research, v. 86, no. B4, p. 2645-2659.

Smewing, J.D., Simonian, K.O. and Gass, I.G.
1975: Metabasalts from the Troodos massif, Cyprus: Genetic implications deduced from petrography and trace element geochemistry; Contributions to Mineralogy and Petrology, v. 51, p. 49-64.

Thy, P.
1984: On the nature of the Troodos boninites, Cyprus; Ofioliti, v. 9, p. 555-568.
1987: Petrogenetic implications of mineral crystallization trends of Troodos cumulates, Cyprus; Geological Magazine, v. 124, p. 1-11.

Thy, P., Brooks, C.K. and Walsh, J.N.
1985: Tectonic and petrogenetic implications of major and rare earth element chemistry of Troodos glasses, Cyprus; Lithos, v. 18, no. 3, p. 165-178.

Thy, P. and Moores, E.M.
1986: Genesis and formation of oceanic crust: evidence from the Cyprus Crustal Study Project drilling in the plutonic sequences of the Troodos ophiolite; 14th General Meeting of the International Mineralogical Association, Stanford, July 1986.

Thy, P., Schiffman, P. and Moores, E.M.
1986: Primary igneous mineral stratigraphy and chemistry of the plutonic sequences of the Troodos ophiolite, Cyprus; Geological Association of Canada Annual Meeting, Ottawa, May 1986, Programs with Abstracts, v. 11, p. 137.

Vernon, R.H.
1970: Comparative grain-boundary studies of some basic and ultrabasic granulites, nodules and cumulates; Scottish Journal of Geology, v. 6, p. 377-351.

Wager, L.R. and Brown, G.M.
1968: Layered Igneous Rocks; Oliver and Boyd, Edinburgh.

Wager, L.R., Brown, G.M. and Wadsworth, W.J.
1960: Types of igneous cumulates; Journal of Petrology, v. 1, p. 73-85.

Wilson, J.R., Esbensen, K.H. and Thy, P.
1981: Igneous petrology of the synorogenetic Fongen-Hyllingen layered basic complex, south-central Scandinavian Caledonides; Journal of Petrology, v. 22, p. 584-627.

Wilson, J.R. and Larsen, S.B.
1985: Two-dimensional study of a layered intrusion - the Hyllingen series, Norway; Geological Magazine, v. 122, p. 97-124.

Wilson, R.A.M.
1959: The geology of the Xeros-Troodos area; Cyprus Geological Survey Department, Ministry of Agriculture and Natural Resources, Memoir, no. 1, p. 1-184.

Wood, D.A.
1979: Dynamic partial melting: its application to the petrogeneses of basalts erupted in Iceland, the Faeroe Islands, the Isle of Skye (Scotland) and the Troodos massif (Cyprus); Geochimica et Cosmochimica Acta, v. 43, p. 1031-1046.

APPENDIX 1. Petrographic and Chemical Summary of Primary Phases in Analyzed Samples from the CY-4 Drill Core

Meter	Unit	Type	Petrology							Phase compositions			
			Texture			Phases				An	Mg#	Mg#	Fo
			1	2	3					pl	cpx	opx	ol
489.37	131.05	dyke	f	p	a	ox	pl			74.82			
489.86	131.06	dyke	f	a	a	ox	pl			69.09			
498.64	133.05	dyke	f	a	a	ox	pl			61.06			
499.68	133.05	dyke	f	a	a	ox	pl			59.26			
515.03	137.01	dyke	f	a	a	ox	pl			70.77			
548.78	146.04	dyke	f	a	a	ox	pl			82.11			
570.69	152.04	dyke	f	p	a	ox	pl			67.61			
570.88	152.05	dyke	f	p	a	ox	pl			75.93			
581.90	155.03	dyke	f	p	a	ox	pl			92.52			
604.63	160.01	gabbro	m	g	a		pl			95.11			
608.06	161.01	dyke	f	p	a	ox	pl			75.13			
635.66	168.04	dyke	f	p	a	ox	pl			88.30			
645.10	169.03	gabbro	m	g	a		pl			97.71			
655.44	172.08	gabbro	m	g	a		pl			95.09			
667.10	175.02	gabbro	m	g	a		pl			91.78			
670.05	176.03	dyke	f	a	a	ox	pl			69.58			
679.53	179.02	gabbro	m	g	a		pl			93.69			
693.97	182.01	gabbro	m	g	a		pl			93.02			
707.78	185.05	gabbro	m	g	a		pl			89.01			
716.86	187.05	gabbro	m	g	a		pl			94.73			
720.23	188.04	gabbro	m	g	a		pl			94.97			
731.98	191.03	gabbro	m	g	a		pl			96.34			
753.81	196.02	gabbro	m	g	a		pl			94.19			
766.34	199.03	dyke	f	a	a	ox	pl			71.96			
768.00	200.01	dyke	f	a	a	ox	pl			62.45			
802.36	208.01	gabbro	m	g	a		pl			93.70			
802.94	208.01	gabbro	m	g	a		pl			95.90			
814.68	210.01	gabbro	m	g	a		pl			94.54			
824.48	210.01	gabbro	m	g	a		pl			93.20			
828.32	215.02	gabbro	m	g	a		pl			92.18			
839.78	218.01	gabbro	m	g	a		pl	cp	op	96.94	80.53	72.66	
840.87	218.01	gabbro	m	g	a		pl			94.24			
852.68	219.02	gabbro	m	g	a		pl			93.96			
863.42	223.02	gabbro	m	g	a		pl			92.66			
864.93	223.02	gabbro	m	g	a		pl			93.30			
866.36	223.02	gabbro	m	g	a		pl	cp	op	94.17	81.49	73.05	
866.37	223.02	dyke	f	a	f	ox	pl	cp	op	70.19	69.41	61.82	
867.75	223.02	vein	m	g	a					38.86			
881.08	227.02	gabbro	m	g	a		pl	cp	op	94.73	82.31	73.43	
882.15	227.03	vein	m	g	f					27.81	74.29		
884.01	227.06	gabbro	m	g	f		pl	cp	op	92.28	83.02	75.15	
898.06	229.03	dyke	f	g	f	ox	pl	cp	op	77.07	70.68	63.29	
899.56	230.01	vein?	m	g	a		pl	cp	op	48.22	82.19	73.76	
900.35	230.01	gabbro	m	g	f		pl	cp	op	94.69	81.66	76.36	
915.02	232.02	gabbro	m	g	a		pl	cp	op	86.28	79.61	70.14	
915.03	232.02	vein	m	g	a					44.07			
917.84	232.02	gabbro	m	g	a		pl	cp	op	91.73	83.79	77.11	
920.08	232.02	gabbro	m	g	f		pl	cp	op	91.61	84.26	77.82	
934.03	235.02	gabbro	m	g	a		??	cp	??		82.35		
935.05	235.02	gabbro	m	g	a		pl	cp	op	93.66	83.94	79.50	
936.86	235.02	gabbro	m	g	a		pl	cp	op	93.31	85.98	79.47	
949.55	237.03	gabbro	m	g	f		pl	cp	op	90.07	82.58		
951.76	239.02	gabbro	m	g	f		pl	cp	op	93.65	83.51	75.88	
952.10	239.02	gabbro	m	g	f		pl	cp	op	91.59	78.74		
953.68	239.04	gabbro	m	g	f		pl	cp	op	88.07	83.36	73.13	
966.50	242.03	gabbro	m	g	a		pl	cp	op	91.44	77.95		
967.88	242.03	gabbro	m	g	a		pl	cp	op	91.51	78.30		
968.96	242.03	gabbro	m	g	f		pl	cp	op	92.17	78.23	72.43	
970.10	242.03	gabbro	m	g	f		pl	cp	op	90.92	79.22	73.94	
984.22	243.01	dyke	f	g	a	ox	pl	cp	??	46.79	70.88		
985.76	245.01	gabbro	m	g	f		pl	cp	op	91.06	76.72	70.17	
986.85	245.01	gabbro	m	g	f		pl	cp	op	89.02	77.41	70.52	
988.88	245.01	gabbro	m	g	f		pl	cp	op	91.25	77.42	70.51	
1000.87	247.05	gabbro	m	g	f		pl	cp	op	90.74	76.32	68.19	
1002.65	248.01	dyke	f	g	f	ox	pl	cp	op	71.68	71.70	62.96	
1003.97	248.02	gabbro	m	g	f		pl	cp	op	91.57	76.67	70.02	
1005.24	248.02	gabbro	m	g	a		pl	cp	op	82.74	77.20		
1014.32	249.04	gabbro	m	g	a		pl	cp	op	88.87	76.14	70.47	

Meter	Unit	Type	Petrology							Phase compositions			
			Texture				Phases			An	Mg#	Mg#	Fo
			1	2	3					pl	cpx	opx	ol
1020.68	251.01	vein	m	g	a					17.34			
1022.02	251.04	gabbro	m	g	a		pl	cp	op	90.84		69.72	
1023.52	251.05	gabbro	m	g	a		pl	cp	op	90.99	76.69	69.78	
1036.33	252.01	gabbro	m	g	a		pl	cp	op	91.02	79.81	74.05	
1037.92	252.01	gabbro	m	g	a		pl	cp	op	90.58	78.87	73.11	
1039.47	252.01	gabbro	m	g	f		pl	cp	op	92.87	81.62	74.54	
1040.75	252.01	gabbro	m	g	f		pl	cp	op	93.07	78.87	73.66	
1054.23	256.04	dyke	f	g	f	ox	pl	cp	op	69.53	69.94	62.38	
1055.45	257.01	gabbro	m	g	f		pl	cp	op	94.38	78.42	71.18	
1056.95	257.04	gabbro	m	g	f		pl	cp	op	92.94	81.57	75.26	
1058.72	257.05	dyke	f	g	f	ox	pl	cp	op	67.91	68.67	61.02	
1071.68	258.02	dyke	f	g	f	ox	pl	cp	op	77.78	71.14	62.97	
1073.43	260.02	dyke?	f	g	a	??	??	cp	??		82.85		
1074.62	260.02	dyke	f	g	f	ox	pl	cp	op	78.99	72.01	65.03	
1075.49	260.02	dyke	f	g	f	ox	pl	cp	op	73.13	71.31	64.04	
1089.50	262.02	gabbro	m	g	f		pl	cp	op	95.37		75.59	
1090.84	262.02	gabbro	m	g	f		pl	cp	op	93.58	81.54	76.16	
1091.47	262.02	gabbro	m	g	f		pl	cp	op	91.47	79.02	74.44	
1106.31	266.02	dyke	f	g	f	ox	pl	cp	op	69.21	68.99	60.97	
1107.82	266.02	dyke	f	g	f	ox	pl	cp	op	68.35	66.51	59.58	
1109.33	266.02	dyke	f	g	f	ox	pl	cp	op	68.99	69.84	61.34	
1110.75	266.02	dyke	f	g	f	ox	pl	cp	op	75.20	71.10	65.47	
1124.34	269.01	gabbro	m	g	f		pl	cp	op	90.58	81.23	75.76	
1125.90	269.01	gabbro	m	g	f		pl	cp	op	91.41	80.59	74.69	
1127.01	269.01	gabbro	m	g	a		pl	cp	op		78.64		
1128.34	269.01	gabbro	m	g	f		pl	cp	op	91.94	79.59	74.07	
1140.88	271.03	gabbro	m	c	f		pl	cp	op	88.53	76.21	71.25	
1142.57	272.01	dyke	f	g	f	ox	pl	cp	op	83.81	74.09	68.83	
1144.51	272.02	gabbro	m	g	a		pl	cp	op	88.69	78.70	74.19	
1145.85	272.02	gabbro	m	g	f		pl	cp	op	91.38	78.79	73.89	
1156.83	274.03	gabbro	m	g	f		pl	cp	op	92.67	79.15		
1158.05	274.03	gabbro	m	g	f		pl	cp	op	92.97	80.54	74.30	
1160.08	274.03	gabbro	m	g	f		pl	cp	op	91.74	77.71	73.05	
1160.98	274.03	gabbro	m	g	f		pl	cp	op	90.16	78.21	73.63	
1174.08	277.01	gabbro	m	g	f		pl	cp	op	90.37	76.14	70.85	
1175.68	277.01	gabbro	m	g	f		pl	cp	op	91.64	76.89	72.35	
1176.98	277.01	gabbro	m	g	f		pl	cp	op	88.63	76.37	70.84	
1177.85	278.01	gabbro	m	g	f		pl	cp	op	88.77	75.49	70.31	
1191.43	281.04	gabbro	m	g	f		pl	cp	op	88.52	74.76	70.22	
1192.82	281.04	gabbro	m	g	f		pl	cp	op	87.46	74.43	69.03	
1194.32	281.04	gabbro	m	g	f		pl	cp	op		76.06	71.12	
1196.03	281.05	gabbro	m	g	f	ox	pl	cp	op	89.68	71.72		
1209.38	282.04	gabbro	m	g	a		pl	cp	op	89.21	75.62	71.32	
1210.94	282.04	gabbro	m	g	f		pl	cp	op	89.56	76.61		
1212.25	282.04	gabbro	m	g	f	ox	pl	cp	op	88.35	77.41	72.08	
1213.34	282.04	gabbro	m	g	f	ox	pl	cp	op	88.72	76.26	73.20	
1226.27	286.01	gabbro	m	g	f		pl	cp	op	91.26	78.47	73.99	
1227.96	286.01	gabbro	m	g	f		pl	cp	op	91.40	79.06	75.23	
1229.52	287.01	gabbro	m	g	f		pl	cp	op	90.54	77.59	72.94	
1230.28	287.01	gabbro	m	g	f		pl	cp	op	90.59	77.05	72.86	
1244.30	289.03	gabbro	m	g	a		pl	cp	op	93.30	81.37		
1245.78	289.03	gabbro	m	g	a		pl	cp	op	91.98	80.49		
1246.84	289.03	gabbro	m	g	f		pl	cp	op	92.80	79.26	75.58	
1248.70	289.03	gabbro	m	g	f		pl	cp	op	94.50	78.67	75.48	
1262.63	292.02	gabbro	m	g	f		pl	cp	op	91.11	79.21	75.80	
1264.13	292.02	gabbro	m	g	f		pl	cp	op	95.12	79.53	75.91	
1265.29	293.01	dyke	f	g	f	ox	pl	cp	op	86.42	77.40	67.87	
1278.96	294.05	gabbro	m	g	a		pl	cp	op	93.45	79.60		
1280.55	294.05	gabbro	m	g	a		pl	cp	op	93.61			
1281.69	294.05	gabbro	m	g	f		pl	cp	op	95.12	78.61	74.04	
1296.42	298.01	gabbro	m	g	f		pl	cp	op	92.06	80.78	75.65	
1297.93	298.01	gabbro	m	g	f		pl	cp	op	92.93	80.12	76.61	
1299.61	298.01	gabbro	m	g	a		pl	cp	??	96.25	78.69		
1300.82	299.01	gabbro	m	g	a		pl	cp	op	89.53	78.59	74.23	
1313.68	301.02	gabbro	m	g	f		pl	cp	op	88.03	75.31	71.76	
1314.27	302.01	gabbro	m	g	f		pl	cp	op	92.44	77.63	74.02	
1316.25	302.01	gabbro	m	g	f		pl	cp	op	91.05	76.41	72.48	
1317.62	302.01	gabbro	m	g	f		pl	cp	op	91.72	76.81	72.78	
1330.82	305.01	gabbro	f	g	f		pl	cp	op	96.02	85.45	79.59	

Meter	Unit	Type	Petrology							Phase compositions			
			Texture			Phases				An	Mg#	Mg#	Fo
			1	2	3					pl	cpx	opx	ol
1332.34	305.02	gabbro	c	g	a	pl	cp	??		97.58	83.13		
1333.43	305.02	gabbro	c	g	a	pl	cp	??		97.35	81.46		
1335.69	305.02	gabbro	c	c	f	pl	cp	op		97.67	82.04	80.55	
1348.63	307.02	gabbro	c	g	a	pl	cp	op		97.38	97.28		
1349.94	307.02	gabbro	c	g	a	pl	cp	op		94.45	82.74		
1351.50	308.01	gabbro	c	g	a	pl	cp	op		97.86		75.56	
1353.25	308.01	gabbro	c	g	a	pl	cp	op		96.10	85.61	80.66	
1365.77	309.02	gabbro	m	g	f	pl	cp	op		96.09	80.96	75.89	
1367.48	309.02	gabbro	c	g	a	pl	cp	op		97.85	83.21	76.99	
1369.07	311.01	gabbro	c	g	a	pl	cp	??		97.77	81.31		
1369.68	311.01	gabbro	m	g	a	pl	cp	op		98.30	86.78	82.29	
1383.35	313.01	gabbro	m	g	f	pl	cp	op		96.70	84.66	79.98	
1384.88	313.01	gabbro	m	g	a	pl	cp	op		96.95	85.78	80.96	
1388.49	314.02	gabbro	m	g	a	pl	cp	op		97.68	85.68	80.40	
1401.53	315.02	gabbro	m	g	a	pl	cp	op		96.58	85.71	82.71	
1402.78	315.02	gabbro	m	g	a	pl	cp	op		97.89	86.34	84.68	
1403.94	315.02	gabbro	m	g	a	pl	cp	op		95.24	82.43	78.96	
1405.75	315.02	gabbro	m	g	a	pl	cp	op		98.51	83.40	81.71	
1418.52	319.03	gabbro	c	g	a	pl	cp	op		94.63			
1419.93	319.03	gabbro	c	g	a	pl	cp	op		97.78	82.82	83.47	
1421.22	319.03	gabbro	m	g	a	pl	cp	op		97.51		82.14	
1422.73	319.03	gabbro	m	g	a	pl	cp	op		97.07	76.56	68.94	
1436.02	322.01	gabbro	m	g	a	pl	cp	op		97.17	84.69	82.82	
1437.35	322.01	gabbro	m	g	a	pl	cp	op	ol	94.23	89.46	85.53	84.49
1439.44	322.01	gabbro	m	g	a	pl	cp	op		98.39	84.85	82.17	
1441.02	323.01	gabbro	f	g	f	pl	cp	op		96.17	80.38	76.54	
1453.07	325.04	gabbro	m	g	f	pl	cp	op		97.85	86.01	83.60	
1454.30	325.04	gabbro	m	g	a	pl	cp	op		97.63	85.03	81.22	
1455.90	325.04	gabbro	m	g	a	pl	cp	op		96.19	85.41	80.16	
1457.58	325.04	gabbro	m	g	a	pl	cp	op		97.65	84.53	82.65	
1471.23	329.02	gabbro	m	g	a	pl	cp	op		98.53	84.99		
1473.68	329.02	gabbro	m	g	a	pl	cp	op		98.06	84.58	81.37	
1474.86	329.03	gabbro	m	g	a	pl	cp	??		98.96	86.21		
1487.53	330.04	gabbro	m	g	a	pl	cp	op		98.03			
1488.02	330.04	gabbro	m	g	a	pl	cp	??		97.33			
1491.25	330.04	gabbro	m	g	a	pl	cp	??		96.89			
1504.02	335.01	gabbro	c	g	a	pl	cp	op		96.29			
1505.55	335.01	gabbro	c	g	a	pl	cp	op		95.83	84.01	76.08	
1506.88	335.01	gabbro	c	g	a	pl	cp	??		96.17			
1507.60	335.01	gabbro	c	g	a	pl	cp	??		97.78	83.09		
1520.53	338.01	gabbro	c	g	f	pl	cp	op		94.63	75.89	75.81	
1522.23	338.03	gabbro	c	g	a	pl	cp	op		95.71		77.30	
1524.04	338.03	gabbro	c	g	a	pl	cp	??		96.77			
1538.48	341.02	gabbro	f	g	f	pl	cp	op		96.17	79.96	77.36	
1539.06	341.02	gabbro	f	g	f	pl	cp	op		95.06	79.56	76.29	
1539.65	341.02	gabbro	f	g	a	pl	cp	op		95.67	81.93	77.88	
1541.05	341.02	gabbro	f	g	f	pl	cp	op		96.29	85.43	76.63	
1542.48	341.04	gabbro	m	g	a	pl	cp	op		95.10		75.38	
1554.74	344.02	gabbro	m	g	f	pl	cp	op		95.64	82.38	78.35	
1556.32	344.02	gabbro	m	g	f	pl	cp	op		95.31	80.04	77.92	
1558.02	344.03	gabbro	f	g	f	pl	cp	op		96.25	82.78	79.03	
1559.06	344.03	gabbro	f	g	f	pl	cp	op		95.98	81.33	79.02	
1572.03	346.01	gabbro	m	g	f	pl	cp	op		95.78	79.39	75.46	
1576.43	346.01	gabbro	m	g	f	pl	cp	op		97.32	79.58	75.71	
1589.34	348.02	gabbro	m	g	f	pl	cp	op		95.60	80.99	77.01	
1590.92	348.02	gabbro	m	g	f	pl	cp	op		95.14	82.64	77.04	
1592.12	350.01	gabbro	c	g	a	pl	cp	op		95.87	80.45	76.43	
1594.99	350.02	gabbro	m	g	f	pl	cp	op		95.53	77.92	76.67	
1607.17	352.01	gabbro	m	g	f	pl	cp	op		96.61	81.59	78.59	
1608.72	352.01	gabbro	m	g	f	pl	cp	op	ol	95.83	83.64	80.21	78.21
1610.35	353.01	gabbro	m	g	f	pl	cp	op	ol	96.55	82.38		76.95
1611.83	353.01	gabbro	m	g	f	pl	cp	op	ol	97.16	85.83	81.02	78.90
1623.75	355.02	gabbro	m	g	f	pl	cp	op		96.47	83.49	79.20	
1625.08	356.01	gabbro	m	g	f	pl	cp	op		95.87	81.60	78.66	
1626.49	356.02	gabbro	m	g	f	pl	cp	op		96.43	82.91	78.24	
1627.84	356.03	gabbro	m	g	f	pl	cp	op		96.32	83.42	79.23	
1641.57	358.02	gabbro	m	g	f	pl	cp	op		97.21	83.88	78.74	
1642.13	358.02	gabbro	m	g	a	pl	cp	op		96.12	83.96	78.10	
1644.27	359.01	gabbro	m	g	a	pl	cp	op		97.05	81.96	80.55	

Meter	Unit	Type	Petrology							Phase compositions			
			Texture			Phases				An	Mg#	Mg#	Fo
			1	2	3					pl	cpx	opx	ol
1645.18	359.01	gabbro	m	g	a	pl	cp	op		96.24	82.86	77.21	
1658.57	361.03	gabbro	m	g	a	pl	cp	op		96.13	81.42	80.24	
1660.15	361.03	gabbro	m	g	a	pl	cp	op		95.86			
1661.34	361.03	gabbro	c	g	a	pl	cp	op		96.13	84.88	81.06	
1663.14	362.01	gabbro	c	g	a	pl	cp	op		96.07		81.44	
1675.94	364.04	gabbro	m	g	a	pl	cp	op		96.37	84.81	80.46	
1677.32	364.04	gabbro	m	g	a	pl	cp	op		97.67	84.50	76.62	
1678.88	364.04	gabbro	m	g	a	pl	cp	op		97.63	85.62	82.60	
1680.32	364.04	gabbro	m	g	a	pl	cp	op		96.33	85.38	81.84	
1693.82	366.01	gabbro	c	g	a	pl	cp	op	ol	97.33	84.39	83.14	80.78
1695.68	366.01	gabbro	c	g	a	pl	cp	op		95.85	84.36	80.87	
1697.45	366.01	gabbro	m	g	a	pl	cp	op		98.20	85.01	83.03	
1698.44	366.01	gabbro	c	g	a	pl	cp	op		97.20	84.23	83.11	
1710.73	371.01	gabbro	m	g	a	pl	cp		ol	98.06	85.25		81.06
1712.38	371.02	gabbro	m	g	f	pl	cp	op	ol	97.36	85.63	82.92	82.24
1714.10	371.03	gabbro	m	g	a	pl	cp	op		96.72	84.67	81.46	
1715.54	371.04	gabbro	f	g	f	pl	cp	op	ol	96.41	87.57	83.00	81.72
1729.45	374.02	gabbro	m	g	a	pl	cp	op		97.77	86.04	80.18	
1731.15	374.02	gabbro	m	g	f	pl	cp	op		96.66	85.65	82.01	
1732.68	374.03	gabbro	m	g	a	pl	cp	op		96.61	85.71		
1745.00	377.01	gabbro	m	g	f	pl	cp	op	ol	97.68	89.18	86.26	82.54
1746.46	377.01	gabbro	m	g	a	pl	cp	op	ol	98.05	87.12	84.13	
1761.54	379.02	webst	c	g	f	pl	cp	op	ol	97.04	86.92	83.80	
1763.15	379.02	webst	m	g	f	pl	cp	op	ol	96.47	87.85	83.26	81.35
1764.98	379.02	webst	m	g	f	pl	cp	op	ol	96.58	87.18	84.31	82.43
1765.98	379.02	webst	m	g	f	pl	cp	op	ol	97.68	88.72		83.63
1778.47	382.03	webst	m	g	a	pl	cp	op		92.99	84.35	80.61	
1780.27	382.03	webst	m	g	f	pl	cp	op	ol	96.85	86.08	82.81	81.86
1781.23	382.03	webst	c	g	f	pl	cp	op	ol	94.30	89.19	82.97	81.32
1782.69	382.03	webst	c	g	f	pl	cp	op	ol	96.43	89.76	84.41	83.56
1795.69	385.03	webst	c	g	f	pl	cp			95.61	87.38		
1798.02	386.01	webst	m	g	f	pl	cp	op	ol	94.59	84.02	74.13	
1799.06	386.01	webst	c	g	f	pl	cp	op	ol	96.93	85.82	82.15	80.73
1800.23	386.01	webst	m	g	f	pl	cp	op	ol	96.49	88.57	81.00	81.20
1811.35	389.01	webst	m	g	f	pl	cp	op	ol	92.47	86.89	84.75	82.31
1812.79	389.02	webst	m	g	f		cp		ol		88.34		85.40
1815.08	389.03	webst	m	g	f	pl	cp	op	ol	96.92	88.34	82.92	82.10
1816.25	389.03	webst	m	g	f		cp	op	ol		87.91	84.69	82.56
1828.14	391.03	webst	m	g	f		cp	op	ol		87.24	85.72	85.70
1829.70	392.01	webst	c	g	f	pl	cp	op	ol	96.36	90.97		85.30
1831.80	392.02	webst	c	g	a		cp	op	ol		88.85	85.39	83.93
1833.12	392.03	webst	m	g	f		cp		ol		90.73		88.47
1844.76	395.01	webst	m	g	f	pl	cp	op		92.46	86.16	84.07	
1846.23	395.03	webst	m	g	f	pl	cp	op		95.32	88.83	85.14	
1847.83	395.04	webst	m	g	f	pl	cp	op	ol	97.64	87.51	83.54	84.72
1848.67	395.04	webst	m	g	f	pl	cp	op	ol	96.63	89.24	84.68	83.74
1859.50	398.01	webst	c	g	a	pl	cp	op		95.44		81.17	
1860.95	398.01	webst	c	g	a	pl	cp	op		93.57	87.04	83.76	
1874.75	401.02	webst	c	g	f	pl	cp	op		94.81	89.93	83.78	
1877.86	401.03	webst	m	g	f	pl	cp	op		93.78	90.23	84.00	
1892.20	404.01	webst	m	g	f	pl	cp	op		98.14	90.87	84.44	
1895.25	404.02	webst	m	g	f	pl	cp	op	ol	96.11	92.73		
1910.00	407.02	webst	c	g	f	pl	cp	op		94.11	87.90	84.80	
1912.75	407.03	webst	m	g	f	pl	cp	op	ol	94.94	89.71	84.43	83.30
1915.35	408.01	webst	c	g	f	pl	cp				90.46		
1927.75	410.02	webst	m	g	f	pl	cp	op		94.78	89.90	85.20	
1930.40	410.03	webst	c	g	f	pl	cp	op	ol	95.99	90.71	85.01	85.02
1943.77	413.01	webst	m	g	a	pl	cp	op		95.87	88.85	84.70	
1946.50	413.03	webst	c	g	a	pl	cp	op	ol	94.76	91.98	84.76	84.04
1960.65	416.02	webst	m	g	f	pl	cp	op	ol	96.59	87.21	84.82	
1972.45	418.02	webst	m	g	f	pl	cp	op		95.71	89.19	85.99	
1998.37	424.03	webst	m	g	f		cp				88.84		
2001.20	425.03	webst	m	g	f	pl	cp	op	ol	98.96	88.74	84.82	81.99
2012.00	428.02	webst	c	g	f		cp	op			88.35	87.33	
2023.10	430.02	webst	c	g	f	pl	cp	op	ol	95.42	90.08	85.82	84.08
2026.40	431.03	webst	m	g	f	pl	cp	op	ol	97.30	89.06	85.86	84.47
2049.00	436.01	webst	m	g	f	pl	cp	op	ol	90.61	89.27	86.30	85.77
2052.20	437.03	webst	m	g	f	pl	cp	op	ol	94.68	89.88	86.07	
2062.95	440.01	webst	c	g	f	pl	cp		ol	95.76	89.52		85.69

Meter	Unit	Type	Petrology								Phase compositions			
			Texture			Phases					An	Mg#	Mg#	Fo
			1	2	3						pl	cpx	opx	ol
2074.45	443.01	webst	c	g	a		cp		ol			90.19		85.42
2077.10	443.02	webst	m	g	f	pl	cp	op	ol	96.96		90.64	86.74	85.49
2088.50	445.08	webst	m	g	f	pl	cp	op		94.61		86.86	84.15	
2099.66	449.02	webst	f	g	f	pl	cp	op	ol	95.92		89.57	85.59	85.68
2103.00	449.03	webst	m	g	f	pl	cp	op	ol	95.56		87.73		84.38
2113.35	452.02	webst	m	g	f	pl	cp	op	ol	91.80		87.74	85.73	85.16
2124.60	455.01	webst	m	g	f	pl	cp		ol	95.79		88.51		85.12
2127.30	455.04	webst	f	g	f	pl	cp	op		94.93		87.33	84.28	
2138.37	458.01	webst	c	g	a		cp		ol			88.17		85.30
2149.70	460.01	webst	m	g	f	pl	cp	op	ol	95.60		87.87	86.48	85.19
2152.75	461.01	webst	m	g	f	pl	cp		ol	96.46		88.91		86.43
2163.60	464.01	webst	m	g	f	pl	cp	op	ol	97.05		88.22	85.56	84.61
2175.45	466.02	webst	m	g	f	pl	cp		ol	97.23		88.45		86.18
2178.25	467.01	webst	m	g	f	pl	cp	op	ol	96.39		88.57	86.67	85.60
2189.55	470.03	webst	m	g	f		cp	op	ol			88.19	85.43	85.18
2201.20	472.04	webst	m	g	a		cp		ol					85.69
2203.50	472.04	webst	m	g	f	pl	cp	op	ol	97.86		88.19	86.72	86.21
2215.25	476.01	webst	m	g	f		cp	op	ol			87.34	85.53	84.79
2225.65	479.01	webst	m	g	f	pl	cp		ol	94.93		88.24		85.21
2228.00	479.03	webst	m	g	a		cp	op	ol			89.33	87.62	86.17
2239.55	482.01	webst	m	g	a	pl	cp	op	ol			88.52		85.27
2250.05	484.05	webst	c	g	a		cp		ol			90.50		

Meter is depth in the core. *Unit* is petrographic or cooling units as used in the original core descriptions. *Type* is the petrographic type (vein = trondhjemitic intrusive material; gabbro = cumulate gabbroic sequence; webst = cumulate pyroxenitic sequence). *Texture* summarizes: (1) grain-size (f = fine; m = medium; c = coarse); (2) texture (p = porphyritic; a = aphyric; g = granular); (3) metamorphism (a = altered, f = fresh). *Phases* are the primary igneous assemblages (ox = Fe-Ti oxides; pl = plagioclase; cp = clinopyroxene; op = orthopyroxene; ol = olivine). The primary phases are in part based on interpretation of the secondary assemblages, except for above 500 meters depth where metamorphism is intensive and only relict phases are listed. The *phase compositions* are given for plagioclase as An mol.%, clinopyroxene as Mg/(Mg+Fe*) (Mg#), orthopyroxene as Mg# and for olivine as Fo mol.%. The compositions listed are the most calcium- or magnesium-rich phases analyzed for individual samples.

Geochemical Characteristics and Petrogenesis of the Ophiolite Sequence Rocks from Drill Hole CY-4, Troodos Complex, Cyprus

H.M. ALI AND M.O. NASSIEF

Faculty of Earth Sciences, King Abdulaziz University, Jeddah, Saudi Arabia

Ali, H.M. and Nassief, M.O., Geochemical characteristics and petrogenesis of the ophiolite sequence rocks from drill hole CY-4, Troodos Complex, Cyprus; in *Cyprus Crustal Study Project: Initial Report, Hole CY-4, ed. I.L. Gibson, J. Malpas, P.T. Robinson and C. Xenophontos; Geological Survey of Canada, Paper 88-9, p. 187-191, 1989.*

Abstract

Borehole CY-4 drilled in the southeastern part of the Troodos ophiolite sampled a sequence of diabasic, gabbroic, and mafic and ultramafic cumulate rocks. Thirteen representative samples were analyzed for major and trace elements. High Mg, Ni, and Cr contents and low contents of Fe, Ti, alkali, and incompatible elements are characteristic features of the cumulate rocks. The first group of elements is depleted in the upper part of the section and the later group is enriched. Olivine-rich ultramafic cumulates were derived from magma in equilibrium with mantle peridotite whereas the clinopyroxene-rich cumulates were derived from fractionated magma. Plagioclase-clinopyroxene (mafic) cumulates were probably formed from late, derivative magmas. The overall effect was a progressive lowering of Mg/Mg+Fe ratio during crystallization. The resulting magma is represented by the gabbroic and diabasic rocks. The diabases are characterized by their low K-tholeiitic affinity and MORB/IAT setting.

Résumé

Le trou de forage CY-4 exécuté dans la partie sud-est de l'ophiolite de Troodos a pénétré une séquence de cumulats diabasiques, gabbroïques, mafiques et ultramafiques. Treize échantillons représentatifs ont été analysés afin de déterminer leur contenu en éléments majeurs et en trace. Ces cumulats sont caracterisés par des contenus élevés en Mg, Ni et Cr et réduits en Fe et Ti. Dans la partie supérieure de la section, le premier groupe d'éléments est appauvri alors que le deuxième est enrichi. Les cumulats ultramafiques, riches en olivines, furent dérivés d'un magma fractionné. Les cumulats mafiques à plagioclases et pyroxènes furent probablement formés à partir d'un magma secondaire tardif. L'effet d'ensemble fut un abaissement progressif de la proportion Mg/Mg+Fe durant la cristallisation. Le magma résiduel est représenté par les roches gabbroïques et diabasiques. Les diabases sont caractérisées par leur basse affinité K-tholeiitique et leur contexte MORB/IAT.

INTRODUCTION

The Cretaceous ophiolite sequence of the Troodos Complex (Gass, 1980) is composed mainly of mafic and ultramafic volcanic and plutonic rocks (Gass, 1960) forming a well developed complete ophiolite sequence as defined in the Penrose conference on ophiolites (1972). Bore hole CY-4, drilled in the southeastern part of the complex (Figure 1), penetrated four major zones (Nassief and Ali, 1987); a diabasic/gabbroic zone, a massive gabbro zone, a cumulate gabbro zone, and an ultramafic cumulate zone. Petrographic study of 45 samples indicated that: (1) the sheeted dyke zone consists of an upper altered diabase, composed mainly of plagioclase (An_{52-68}), tremolite and opaques; and a lower diabase composed of plagioclase (An_{60-68}), altered pyroxene and opaques; (2) in the diabasic/gabbroic zone the gabbros consist mainly of plagioclase (An_{65-68}), clinopyroxene, tremolite and opaques; (3) the massive gabbro zone consists of plagioclase, diopsidic augite, tremolite and opaques; (4) the cumulate gabbro zone consists of calcic plagioclase (An_{70}), orthopyroxene, clinopyroxene, tremolite and opaques and (5) the ultramafic zone consists of different proportions of clinopyroxene, orthopyroxene, and olivine representing cumulate minerals and plagioclase occurring as an intercumulate phase.

GEOCHEMISTRY

A total of 45 samples from drill core CY-4 were analyzed for major oxides and trace elements in the laboratories of the Faculty of Earth Sciences, King Abdulaziz University, Jeddah, Saudi Arabia (Table 1, Nassief and Ali, 1987). XRF was used for the determination of major oxides, whereas atomic absorption and plasma spectroscopy (DCP) were used for the trace elements. Thirteen representative samples were selected for further trace element analysis (Table 1). These analyses were carried out by neutron activation at the Atomic Energy of Canada laboratories.

The chemical characteristics of different zones show a large degree of variability (Table 1) probably reflecting variations in proportions and/or types of the mineral constituents especially in the cumulate rocks. The MgO content is relatively low in the diabasic zone and increases generally to a maximum in the ultramafic cumulates. The CaO content shows the same trend but with a certain degree of irregularity. The Al_2O_3 content increases generally from the sheeted dykes to the gabbroic rocks then decreases sharply in the ultramafic cumulates. FeO, TiO_2, and alkali contents are generally highest in the diabasic rocks.

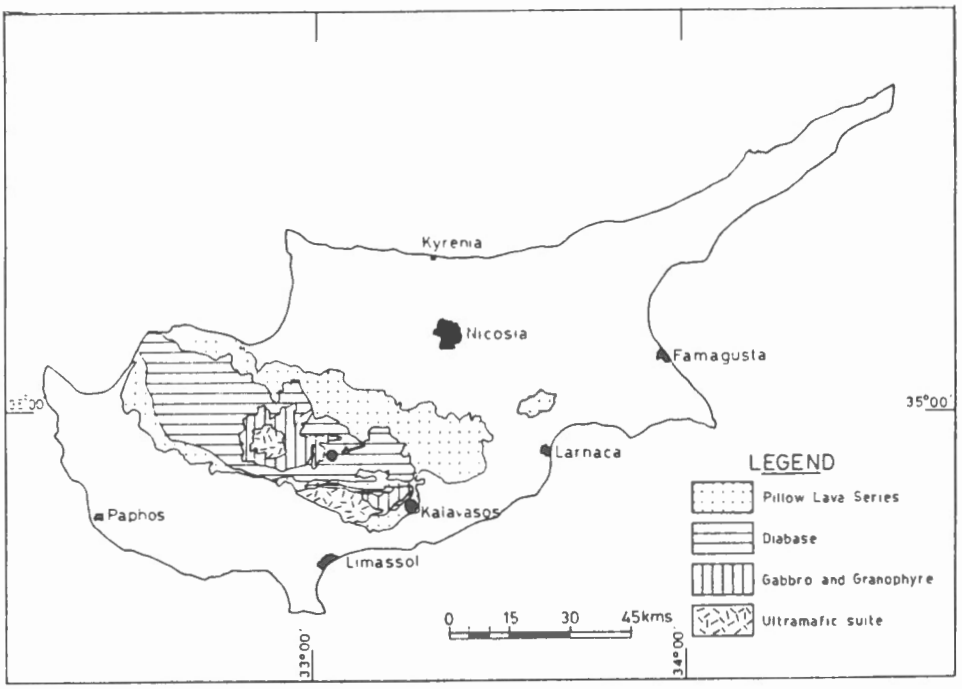

Figure 1: Generalized geological map of the Troodos complex, Cyprus (Bear, 1963) showing the location of drill hole CY-4.

TABLE 1: Major Element (wt.%) and Trace Element (ppm) Analysis of Selected Rocks from CY-4 Drill Hole, Cyprus

Sample No.	N4	N8	N10	N17	N19	N21	N26	N27	N28	N30	N38	N39	N45
SiO_2	54.64	56.18	56.32	51.74	47.31	46.74	48.61	49.17	48.03	52.91	42.86	48.57	38.00
TiO_2	1.32	0.89	1.85	0.20	1.22	0.28	0.14	0.12	0.12	0.17	0.06	0.10	0.04
Al_2O_3	16.04	14.88	14.23	15.60	16.20	18.33	18.08	18.49	18.48	3.88	1.82	5.24	1.30
FeO	6.21	6.25	5.24	3.91	7.97	5.35	4.11	3.95	4.81	4.88	3.30	3.95	2.80
Fe_2O_3	4.35	3.92	4.52	1.21	4.09	1.26	0.76	0.82	0.78	1.00	5.69	1.75	10.50
MnO	0.08	0.17	0.09	0.1	0.21	0.14	0.11	0.11	0.12	0.15	0.12	0.10	0.10
MgO	3.65	3.65	3.98	8.08	7.46	8.78	8.50	9.12	9.53	16.79	28.69	20.99	36.29
CaO	8.42	8.35	7.71	13.53	11.90	14.41	16.84	16.82	14.33	18.15	8.74	14.70	0.68
Na_2O	3.24	2.90	3.10	1.49	1.82	1.08	0.54	0.47	0.60	0.14	0.11	0.23	0.06
K_2O	0.34	0.21	0.23	0.11	0.13	0.08	0.10	0.13	0.90	0.11	0.07	0.10	0.09
P_2O_5	0.38	0.37	0.25	0.55	0.50	0.58	0.69	0.60	0.58	0.72	0.12	0.18	0.57
Total*	98.67	97.77	96.82	98.79	98.81	97.04	98.56	99.90	98.32	99.01	91.58	95.91	90.61
Zn	22	39	29	34	63	45	26	28	73	49	37	39	39
Nb	23	47	21	22	24	17	17	27	32	27	40	36	39
Ni	44	33	38	116	75	120	126	138	144	271	324	226	414
Zr	103	184	84	98	72	66	66	99	99	ND	ND	ND	ND
Pb	3	9	13	24	17	8	5	17	32	5	ND	ND	ND
Y	11	12	9	8	8	6	8	9	99	ND	ND	ND	ND
Cr	14	13	8	269	56	96	539	786	292	1092	1225	1300	1925
Sr	136	87	102	77	104	81	44	46	46	18	22	47	12
Rb	ND	ND	ND	14	6	ND	ND	11	12	ND	ND	ND	ND
Th	8	ND	ND	14	9	9	ND	14	15	9	ND	ND	ND
Co	82	54	58	43	56	43	29	30	33	33	125	79	150
La	0.10	ND	1.71	ND	ND	ND	ND	ND	ND	ND	ND	ND	ND
Sm	1.4	0.73	ND	0.59	1.1	0.19	0.13	0.09	0.11	0.12	0.05	0.07	0.02
Eu	0.6	0.4	0.3	0.2	0.6	0.1	0.2	0.1	ND	ND	ND	ND	ND
Yb	5.7	ND	ND	ND	ND	ND	ND	ND	ND	ND	ND	ND	ND
Lu	0.35	0.15	0.4	0.4	ND	ND	0.26	ND	ND	ND	ND	ND	ND
FeO**/MgO	2.77	2.68	2.34	0.62	1.56	2.44	0.56	0.51	0.58	0.34	0.30	0.26	0.34
Mg/Mg+Fe	0.21	0.25	0.28	0.59	0.37	0.54	0.62	0.64	0.61	0.72	0.75	0.77	0.73
Zr/Y	9.36	15.33	9.33	12.25	9.00	11.00	8.25	11.00	1.00	—	—	—	—

*Low totals are for rocks with high H_2O (analyzed) and/or CO_2, N4,8,10: diabase, N17,19,21: massive gabbro, N26,27,28: cumulate gabbro, N30,38,39: Cpx-rich ultramafics, N45: Dunite rocks, ND: Not detected, FeO**: total iron oxide calculated as FeO.

The diabasic and gabbroic rocks have higher contents of P_2O_5, Sr, Zr, Y, and REEs and lower contents of Ni and Cr than the mafic and ultramafic cumulates. The trace element patterns for different zones were normalized to average MORB (Figure 2). This plot shows the relatively lower Sr, K, Y and Yb contents of the cumulate rocks and the higher contents of Rb, Nb, Zr and Cr. The gabbroic and diabasic rocks are characterized by their relatively lower K, Zr, Sm, Ti, Y, Yb and Cr contents and higher Rb, Nb and P contents.

PETROGENESIS

The ultramafic zone consists essentially of dunite, harzburgite, and clinopyroxenite. The forsteritic nature of olivine, the high Mg/Mg+Fe ratio (0.72), the distinctive depletion in incompatible elements Ti, P, Zr, and REE and enrichment in Ni and Cr of the dunitic rocks (Figure 2) suggest their derivation from a highly magnesian magma. Such magma is likely to be formed in equilibrium with mantle peridotite with an Mg/Mg+Fe ratio of 0.90 at relatively low pressures (Laurent et al., 1980)

The clinopyroxene-rich ultramafic cumulates (e.g. Sample N30) have lower Mg and Ni than the olivine-rich rocks. The forsterite content (Fo_{81-83}) is also lower (R. Laurent, pers. comm., 1985). Such rocks are not expected to be derived from a magma in equilibrium with mantle peridotite but probably are the products of further fractionation, after the removal of olivine cumulates.

The mafic cumulates, consisting mainly of cumulate gabbro and gabbronorite, are generally characterized by their more evolved nature compared to the ultramafic cumulates. This is indicated by their lower Mg/Mg+Fe ratios, higher incompatible element contents, and their position on the Al_2O_3-CaO-MgO diagram (Figure 3). The

progressive lowering of the Mg/Mg+Fe ratio during crystallization of the ultramafic cumulates, by olivine and Mg-rich clinopyroxene fractionation, probably resulted in a magma with the observed geochemical characteristics of the mafic cumulates.

Mafic cumulates grade upsection, with increasing amounts of plagioclase, into massive gabbroic rocks. The latter are generally characterized by even lower Mg/Mg+Fe ratios and enrichment in total iron, Ti, alkalies, Sr, Zr, and REE. Sample N18 (Table 1, Nassief and Ali, 1987) represents a plagiogranite unit with the distinct chemical characteristics of extremely evolved magma. This sample, as well as the dioritic rocks of the gabbroic zone, may represent the end products of magmatic differentiation.

The CIPW norm calculations (Table 2, Nassief and Ali, 1987) show the sheeted dykes to be hypersthene normative (tholeiitic). The tholeiitic affinity of these rocks is clearly seen on the AFM diagram (Figure 4) which also shows FeO enrichment. The low K_2O (0.3%) content is comparable to that of the low-K tholeiites of Peccetillo and Taylor (1976). The Troodos diabasic rocks are comparable to both MORB and IAT. Such an affinity is well defined on a Zr-TiO_2 diagram (Figure 5). These geochemical characteristics suggest a tholeiitic parent magma and a MORB/IAT setting for the sheeted dykes. Low Mg, Ni, and Cr contents and relative enrichment in Ti, Fe_{tot}, P, Zr, Y and REE indicate that the parental magma of these dykes had evolved by fractional crystallization of olivine from the mantle melt. The remaining magma probably evolved through fractionation of clinopyroxene and plagioclase.

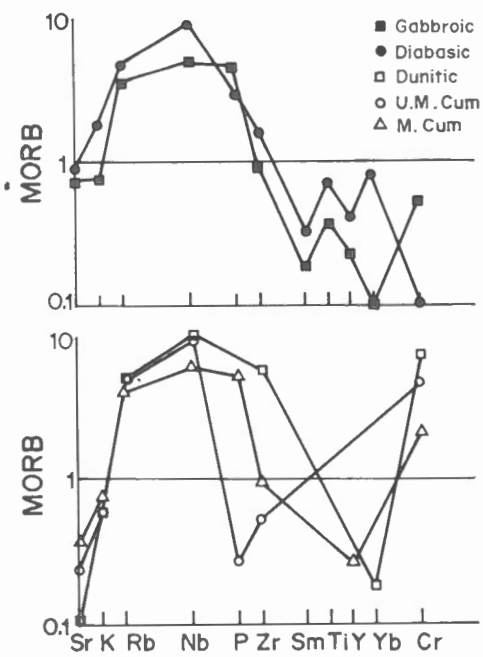

Figure 2: Geochemical patterns (after Pearce, 1980) for the CY-4 ophiolite sequence.

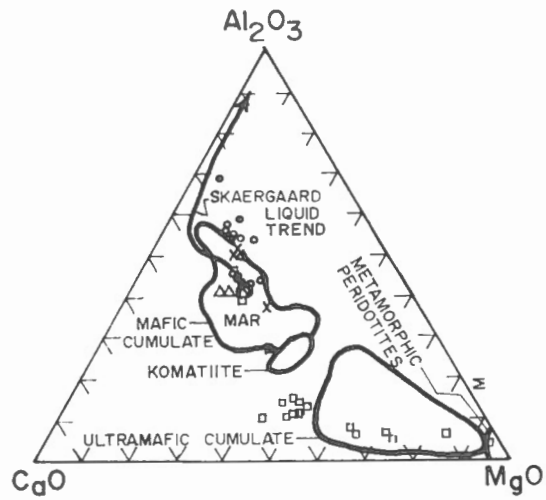

Figure 3: MgO-Al_2O_3-CaO diagram (Coleman, 1977) for rock sequence of drill hole CY-4, Troodos ophiolite (after Nassief and Ali, 1987).

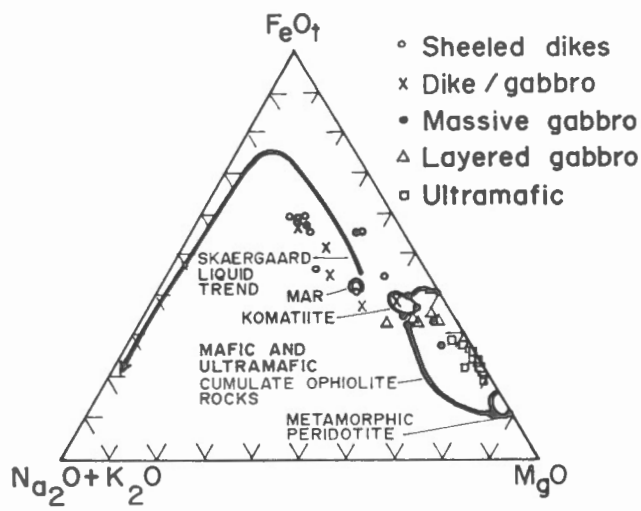

Figure 4: AFM diagram of mafic and ultramafic rocks of drill hole CY-4, Troodos Massif, (after Nassief and Ali, 1987).

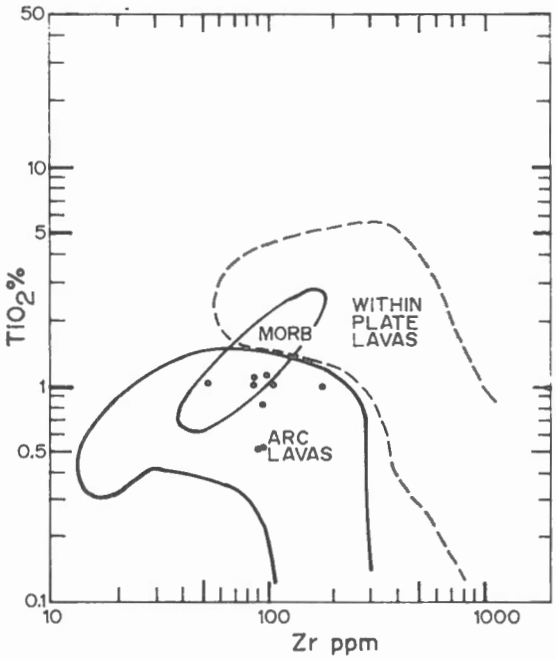

Figure 5: TiO_2-Zr diagram (after Pearce, 1980) for sheeted dykes from CY-4 drill hole, Troodos complex. AFM diagram of mafic and ultramafic rocks of drill hole CY-4, Troodos Massif, (after Nassief and Ali, 1987).

CONCLUSIONS

The variability in geochemical characteristics of different zones of the ophiolite reflects the variations in proportion and/or type of mineral constituents. The ultramafic dunitic cumulates were derived from a highly magnesian magma in equilibrium with mantle peridotite. Such magma may represent the initial magma for the whole sequence which gave rise to different rock types through progressive lowering of the Mg/Mg+Fe ratio, depletion in compatible elements, and enrichment in incompatible elements. The sheeted dykes are characterized by their low-K tholeiitic affinity and MORB/IAT setting. Mineral chemistry and the study of different zones in other bore holes is expected to add more information, especially concerning the lateral variation in the gross structure of the ophiolite.

ACKNOWLEDGEMENTS

This research, which is a part of the Cyprus Crustal Study Project (CCSP), was financially supported by the Faculty of Earth Sciences, King Abdulaziz University, Jeddah, Saudi Arabia. The authors are grateful to Prof. J. Roobol for his discussion and critical review of the paper.

REFERENCES

Anonymous
1972: Penrose field conference on ophiolites; Geotimes, v. 17, p. 24-25.

Bear, L.M.
1963: Geologic Map of Cyprus (1:250,000); Cyprus Geological Survey Department, Ministry of Agriculture and Natural Resources.

Coleman, R.G.
1977: Ophiolites: Ancient Oceanic Lithosphere?; Springer-Verlag, Berlin; Heidelberg; New York, p. 1-229.

Gass, I.G.
1960: The geology and mineral resources of the Dhali area; Cyprus Geological Survey Department, Ministry of Agriculture and Natural Resources, Memoir, no. 4, p. 1-116.
1980: The Troodos Massif: its role in the unravelling of the ophiolite problem and its significance in the understanding of constructive margin processes; *in* Ophiolites: Proceedings of the International Ophiolite Symposium, Cyprus, 1979, ed. A. Panayiotou, Cyprus Geological Survey Department, Ministry of Agriculture and Natural Resources, p. 23-35.

Laurent, R., Delaloye, M., Vuagnat, M., and Wagner, J.J.
1980: Composition of parental basaltic magma in ophiolites; *in* Ophiolites: Proceedings of the International Ophiolite Symposium, Cyprus, 1979, ed. A. Panayiotou, Cyprus Geological Survey Department, Ministry of Agriculture and Natural Resources, p. 172-181.

Nassief, M.O., and Ali, H.M.
1987: Petrochemistry of the sheeted dykes, mafic and ultramafic rocks of CY-4 drill hole, Cyprus crustal study project; Researches in Earth Science, Scientific Publishing Center Publications, King Abdulaziz University, Saudi Arabia.

Pearce, J.A.
1980: Geochemical evidence for the genesis and eruptive setting of lavas from Tethyan ophiolite; *in* Ophiolites, Proceedings of the International Ophiolite Symposium, Cyprus, 1979, ed. A. Panayiotou; Cyprus Geological Survey Department, Ministry of Agriculture and Natural Resources, p. 261-272.

Peccetillo, A., and Taylor, S.R.
1976: Geochemistry of Eocene calc-alkaline volcanic rocks from the Kostamonu area, N. Turkey; Contributions to Mineralogy and Petrology, v. 53. p. 63-81.

Fine-scale Modal Layering and Cyclic Units in Ultramafic Cumulates from the CY-4 Borehole, Troodos Ophiolite: Evidence for an Open System Magma Chamber

PAUL BROWNING[1], STEPHEN ROBERTS[2] AND TONY ALABASTER[3]

[1]Department of Earth Sciences, University of Cambridge,
Cambridge, CB2 3EQ, UK.
[2]Department of Geology, The University,
Southampton, SO9 5NH, UK.
[3]British Antarctic Survey, High Cross, Madingley Road,
Cambridge, CB3 0ET, UK.

Browning, P., Roberts, S. and Alabaster, T., Fine-scale modal layering and cyclic units in ultramific cumulates from the CY-4 borehole, Troodos ophiolite: evidence for an open system magma chamber, in drillhole CY-4, the Troodos Ophiolite, Cyprus; in *Cyprus Crustal Study Project: Initial Report, Hole CY-4, ed. I.L. Gibson, J. Malpas, P.T. Robinson and C. Xenophontos; Geological Survey of Canada, Paper 88-9, p. 193-220, 1989.*

Abstract

The ultramafic cumulates intersected in the lower third of the CY-4 borehole are characterised by a series of cyclic units which are defined by modal layering on about a three metre scale. Wavelength dispersive electron microprobe data on mineral phases for selected intervals of core sampled at about a one metre spacing reveal cryptic variation at this scale. Particularly striking is the rapid variation in mineral composition with height and the overall coherence in mineral chemistry between coexisting phases within the cyclic units. The cyclic units suggest a process involving fractional crystallisation in an open system magma chamber. Rapid variation in Cr_2O_3 content indicates that a cyclic unit 1.65 m thick formed by crystallisation of a magma body of 1.80 m vertical dimension. This thickness is orders of magnitude less than the total thickness of the Troodos cumulate pile; models involving large and well-mixed magma chambers are precluded. The unexpected overall coherence in vertical profiles of compatible and incompatible elements suggests that, in this cumulate pile, the geochemical consequences of compaction and the concomitant expulsion of an intercumulus melt were limited in extent.

Résumé

Les cumulats ultramafiques intersectés dans le tiers inférieur du forage CY-4 consistent en plusieurs séries cycliques définies par un litage modal répété environ à tous les trois mètres. Les analyses de minéraux (à la microsonde électronique dotée de spectromètres à dispersion de longueurs d'onde) provenant d'intervalles choisis des carottes de forage et espacés d'environ un mètre, révèlent une variation cryptique à cette échelle. La variation rapide de la composition minérale avec la stratigraphie est particulièrement frappante. De plus la variation de la chimie des minéraux est cohérente pour toutes les phases coexistantes et ce, à l'intérieur de chacune des unités cycliques. La cyclicité minéralogique suggère un processus de formation par cristallisation fractionnée dans une chambre magmatique en système ouvert. La variation rapide de la teneur en Cr_2O_3 indique qu'une unité cyclique de 1.65 m d'épaisseur s'est formée par la cristallisation d'un volume magmatique de 1.80 m d'épaisseur. Cette épaisseur est de plusieurs ordres de grandeur inférieure à la puissance totale de la séquence de cumulats de l'ophiolite de Troodos de telle sorte que les modèles magmatiques impliquant des grandes chambres bien homogènes sont invalides. La cohérence globale inattendue des éléments compatibles et incompatibles dans les profils de variation verticaux suggère que pour cette séquence particulière de cumulats, les conséquences géochimiques de la compaction et de l'expulsion simultanée du liquide intercumulus furent peu importantes.

INTRODUCTION

Despite the opportunity in recent years to directly sample the upper third of the oceanic crust and thus investigate the nature of the geological processes that operate in its generation and modification at constructive plate margins, the lower two-thirds remains beyond our technological reach. Consequently our understanding of the processes that occur at these deeper levels remains correspondingly meagre. Therefore studies of the deeper levels of land-bound ophiolite complexes remain our only opportunity to directly examine rocks that are probably very similar to those occurring at lower crustal depths in modern oceanic environments.

Investigations of many ophiolite complexes have established that those structural levels equated with the lower half of modern oceanic crust are characterised by medium-to-coarse-grained gabbroic and ultramafic igneous rocks which frequently show well developed cumulate textures and layering (e.g. Allen, 1975; Browning, 1984; Elthon et al., 1984). Although there is a consensus that such cumulate rocks are the crystallisation products of slowly cooled basaltic magma chambers, debate continues over the size, shape, thermal and compositional structure of the magma body; the open or closed nature of the system; the mechanisms by which cumulate textures and layering develop; the role of post-cumulus processes in modifying the primary magmatic physical and chemical signature.

The CY-4 borehole has provided a continuous sample through a series of layered gabbroic and ultramafic rocks that formed in a slowly cooled basaltic magma chamber (or chambers) in the oceanic crust, probably at or near a constructive plate margin. In this paper we present electron microprobe data for material collected at about one metre intervals from selected ultramafic sections. Sampling at such a scale provides valuable insights into the nature of the processes operating in oceanic magma chambers and indeed in layered intrusions in general.

GEOLOGICAL SETTING

The Troodos Massif is a late Cretaceous ophiolite which even prior to the recent investigations of the International Crustal Research Drilling Group (ICRDG), represented one of the world's most extensively studied ophiolite complexes (see Gass, 1980 for review). The ophiolite has a roughly annular outcrop pattern, in which tectonized harzburgite crops out centrally and gives way to progressively higher structural units, so that the uppermost extrusives occupy the periphery.

Previous studies on the Troodos cumulate sequence include those of Greenbaum (1972a,b), Allen (1975), George (1978) and more recently Thy (1987), Thy et al. (1988). Greenbaum (1972a,b) established that the cumulate sequence shows a gross upward succession of dunite-wehrlite-pyroxenite-gabbro, produced by the crystallisation order (ol+sp) → cpx → opx → plag.

He considered the cumulates to have crystallised within a periodically replenished steady state magma chamber. In contrast, Allen (1975), whilst confirming the gross upward stratigraphy and crystallisation order of the cumulate pile, interpreted the cumulates as the crystallisation products of a series of discrete magma chambers.

The deep borehole CY-4 of the ICRDG commenced in the Sheeted Dyke Complex near Palekhori at 34°54'06"N and 33°05'38"E, and penetrated the base of the Sheeted Dyke Complex and underlying gabbroic and ultramafic cumulates (Figure 1). A total of 2263 m of core was recovered, the hole terminating within the ultramafic cumulates at some unknown distance above tectonized harzburgites.

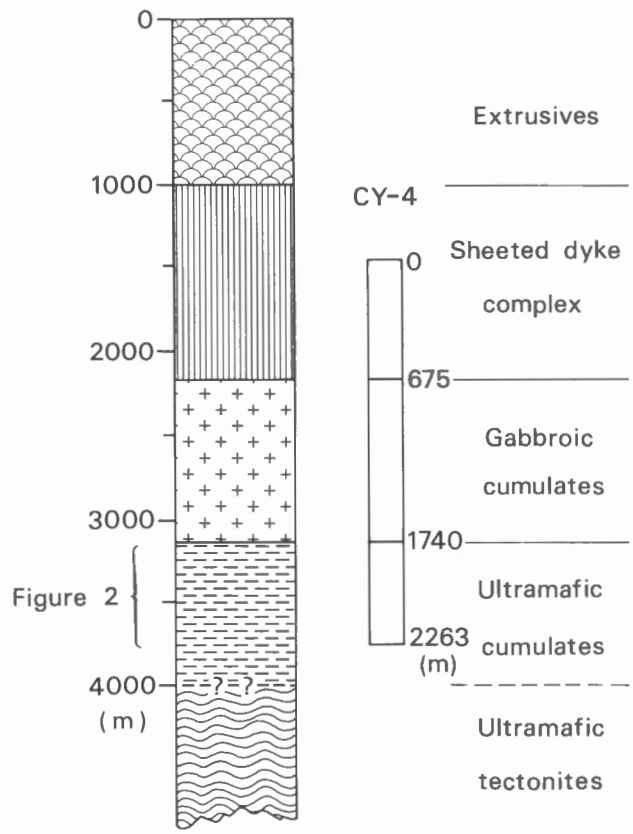

Figure 1: Simplified cross section of the Troodos ophiolite. The vertical interval sampled by the CY-4 borehole is shown as are downhole depths to major stratigraphic divisions within the ophiolite. The interval covered by Figure 2 is indicated. The true depth to the contact with the underlying ultramafic tectonites is uncertain.

Initial studies of the CY-4 core by Thy et al. (1989) recognized three major petrographic and compositional breaks at 1330, 1500 and 1750 m depth; the boundary at 1330 m is considered to be intrusive, where upper medium grained gabbros are intruded by coarse grained gabbroic cumulates. Furthermore, from a consideration of phase chemistry they proposed that the upper gabbros crystallised within an open system magma chamber whereas the lowermost ultramafic cumulates fractionated within a closed system. That the lowermost cumulates crystallised in a closed system environment has found further support in recent work by Brace et al. (1987) and Laurent (1987). This paper presents data which cast doubt on this interpretation.

ANALYTICAL METHODS

All mineral composition data presented were collected on a fully automated, wavelength dispersive, Cambridge Instruments Microscan 9 microprobe at the Open University. Analyses were performed at an accelerating potential of 20 kV, a specimen current of 30.5 nA and a typical spot size of 10-15 microns, with a ZAF correction being provided on-line. Where possible up to six analyses were completed per mineral phase per rock sample, checking for zoning on the core and rim of at least one grain.

RESULTS

Six detailed profiles, between 8 and 16 m thick, were sampled at a density of around one sample per metre, within the ultramafic cumulates of the CY-4 borehole between 1740 and 2263 m (Figures 1 and 2). Each of the profiles sampled well developed modal layering. In the lower profiles the layers invariably display olivine-rich bases grading to olivine-poor tops, with the crystallisation order (Ol+Sp) → Cpx → Opx producing a typical rock succession of wehrlite → clinopyroxenite → websterite. Up section, the layers become less mafic; for example, at 1893 m a typical layer comprises an olivine-clinopyroxenite base followed by websterite and gabbro (Figure 5).

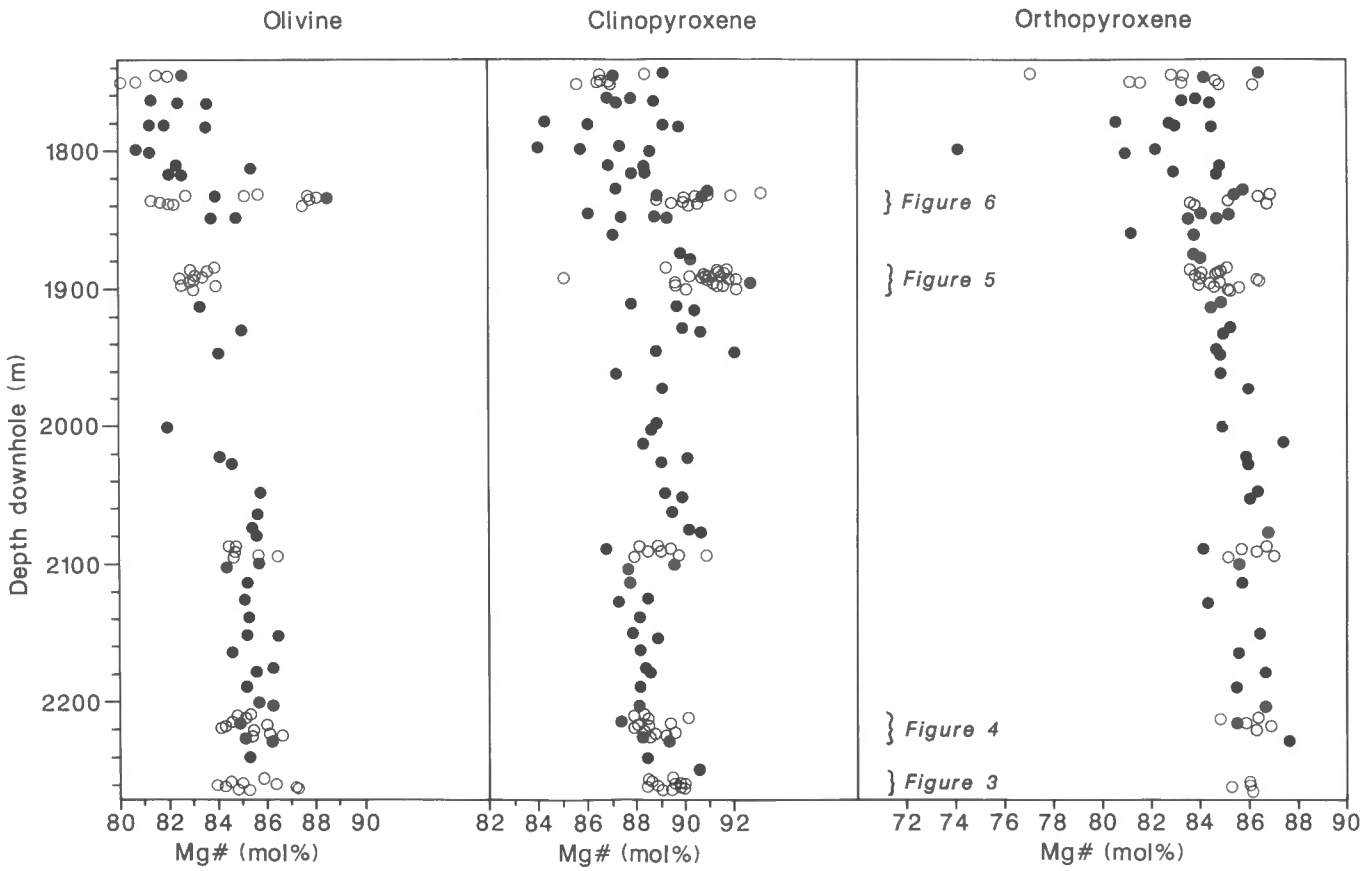

Figure 2: Vertical profiles for Mg number in olivine, clinopyroxene and orthopyroxene from lower ultramafic cumulates intersected by CY-4 borehole. Open circles: this study; filled circles: Thy et al. (1989). Only the most magnesian compositions analysed at any one depth are shown. Error bars indicate the 2σ uncertainty on an individual analysis. The vertical intervals covered by Figures 3-6 are shown.

TABLE 1. Microprobe data for olivines in lower ultramafic cumulates from CY-4

Depth (m)	ID	SiO_2	TiO_2	FeO*	MnO	MgO	CaO	NiO	Total
1745.10	XG	39.30	0.02	17.51	0.26	42.80	0.06	0.14	100.09
1745.10	XH	39.34	0.02	17.31	0.26	42.91	0.07	0.11	100.02
1745.10	XI	39.41	0.02	17.51	0.23	42.94	0.09	0.14	100.34
1745.10	XJ	39.46	0.02	17.45	0.25	42.87	0.09	0.15	100.29
1745.10	XK	39.47	0.02	17.48	0.25	42.77	0.07	0.14	100.20
1745.10	XL	39.58	0.02	17.55	0.25	43.04	0.07	0.14	100.65
1745.70	YH	39.48	0.02	17.66	0.25	43.15	0.07	0.14	100.77
1745.70	YJ	39.46	0.02	17.62	0.25	43.06	0.06	0.11	100.58
1745.70	YL	39.25	0.02	17.60	0.28	43.19	0.07	0.14	100.55
1745.70	YM	39.37	0.02	17.48	0.26	43.24	0.09	0.12	100.58
1745.70	YO	39.52	0.02	17.23	0.25	43.20	0.07	0.11	100.40
1745.70	YQ	39.80	0.04	17.16	0.26	43.41	0.04	0.11	100.82
1745.70	YR	39.62	0.02	17.09	0.26	43.65	0.06	0.11	100.81
1750.05	XA	39.35	0.04	18.35	0.26	42.74	0.04	0.11	100.89
1750.05	XX	39.24	0.02	18.68	0.26	41.98	0.07	0.14	100.39
1750.05	XZ	39.26	0.02	18.48	0.28	41.89	0.04	0.11	100.08
1750.05	XY	39.46	0.02	18.48	0.26	41.88	0.04	0.14	100.28
1750.05	YM	39.00	0.02	18.12	0.25	42.53	0.06	0.11	100.09
1750.50	XV	39.11	0.02	19.05	0.25	41.58	0.07	0.12	100.20
1750.50	XY	39.31	0.02	18.64	0.28	41.96	0.06	0.15	100.42
1750.50	XZ	38.95	0.02	18.84	0.29	41.96	0.06	0.15	100.27
1750.50	YA	39.08	0.02	18.98	0.26	41.59	0.06	0.12	100.11
1750.50	YB	39.14	0.02	18.98	0.26	41.89	0.06	0.11	100.46
1830.90	XQ	40.37	0.02	13.78	0.19	46.28	0.06	0.15	100.85
1830.90	XR	40.30	0.02	13.95	0.22	46.24	0.06	0.14	100.93
1830.90	XT	40.46	0.02	13.84	0.19	46.14	0.07	0.14	100.86
1830.90	XU	40.15	0.02	14.03	0.20	46.21	0.06	0.11	100.78
1830.90	XV	40.44	0.02	14.00	0.20	46.02	0.06	0.18	100.92
1830.90	YA	39.69	0.02	13.96	0.22	45.99	0.04	0.12	100.04
1831.80	XB	39.68	0.02	16.48	0.23	43.71	0.09	0.14	100.35
1831.80	XF	39.98	0.02	16.29	0.23	43.79	0.07	0.17	100.55
1831.80	XG	39.69	0.02	16.51	0.23	43.57	0.09	0.14	100.25
1831.80	XH	39.81	0.02	16.53	0.22	43.46	0.06	0.14	100.24
1831.80	XI	39.93	0.02	16.42	0.23	43.49	0.07	0.14	100.30
1831.80	XK	39.56	0.02	16.57	0.25	43.65	0.09	0.12	100.26
1831.80	XJ	39.58	0.02	16.55	0.25	44.07	0.04	0.12	100.63
1832.20	YK	39.87	0.02	14.26	0.20	45.60	0.06	0.12	100.13
1832.20	YL	40.15	0.02	14.25	0.22	45.40	0.06	0.15	100.25
1832.20	YM	40.31	0.02	14.21	0.22	45.30	0.06	0.12	100.24
1832.20	YN	40.09	0.02	14.16	0.22	45.40	0.07	0.09	100.05
1832.20	YO	40.12	0.02	14.44	0.23	45.41	0.04	0.15	100.41
1832.20	YP	40.20	0.02	14.39	0.23	45.11	0.06	0.11	100.12
1832.30	YB	40.05	0.02	13.52	0.19	46.49	0.07	0.17	100.51
1832.30	YF	40.18	0.02	13.37	0.20	46.42	0.07	0.18	100.44
1832.30	YH	40.31	0.02	12.46	0.19	47.21	0.04	0.15	100.38
1832.30	YI	40.85	0.02	12.13	0.19	47.09	0.06	0.15	100.49
1832.30	YL	40.73	0.02	11.83	0.19	47.36	0.04	0.11	100.28
1832.30	YM	40.22	0.02	12.02	0.20	47.38	0.04	0.17	100.35
1833.40	YL	40.43	0.02	11.74	0.19	47.42	0.07	0.15	100.02
1833.40	YM	40.53	0.02	11.62	0.19	47.49	0.06	0.14	100.05

TABLE 1. (cont.)

Depth (m)	ID	SiO_2	TiO_2	FeO*	MnO	MgO	CaO	NiO	Total
1833.40	YN	40.58	0.02	11.48	0.31	47.56	0.06	0.12	100.13
1833.40	YO	40.56	0.02	11.72	0.17	47.47	0.06	0.15	100.15
1833.40	YP	40.58	0.04	11.58	0.20	47.47	0.06	0.15	100.08
1833.40	WR	40.65	0.02	11.63	0.17	47.63	0.06	0.17	100.33
1834.40	XO	40.50	0.02	11.92	0.16	47.26	0.06	0.15	100.07
1834.40	XP	40.68	0.00	11.92	0.20	47.23	0.06	0.15	100.24
1834.40	XQ	40.52	0.02	12.07	0.20	47.13	0.07	0.12	100.13
1834.40	XR	40.44	0.02	11.85	0.17	47.41	0.04	0.15	100.08
1834.40	XS	40.29	0.04	11.77	0.19	47.48	0.07	0.17	100.01
1835.60	XJ	39.23	0.02	17.79	0.26	43.30	0.09	0.20	100.89
1835.60	XS	39.76	0.02	17.65	0.26	43.19	0.07	0.18	101.13
1835.60	XU	39.67	0.02	17.75	0.28	42.77	0.06	0.18	100.73
1835.60	XV	39.39	0.04	17.71	0.25	43.23	0.03	0.17	100.82
1837.05	XA	39.58	0.02	17.55	0.26	42.97	0.07	0.17	100.62
1837.05	XB	39.77	0.02	17.67	0.26	43.01	0.06	0.18	100.97
1837.05	XC	39.57	0.02	17.44	0.23	43.00	0.07	0.17	100.50
1837.05	XD	39.56	0.02	17.72	0.23	43.20	0.06	0.18	100.97
1837.05	XE	39.48	0.02	17.37	0.25	42.93	0.07	0.17	100.29
1837.05	XF	39.64	0.02	17.29	0.23	43.34	0.06	0.12	100.70
1838.00	XT	39.35	0.02	17.56	0.25	42.96	0.04	0.18	100.36
1838.00	YB	39.28	0.02	17.15	0.25	43.06	0.09	0.17	100.02
1838.00	XM	39.76	0.02	17.07	0.25	42.85	0.09	0.18	100.22
1838.00	XN	39.72	0.02	17.02	0.23	42.81	0.07	0.18	100.05
1838.00	XD	39.78	0.02	17.04	0.25	42.87	0.07	0.18	100.21
1838.00	XZ	39.66	0.02	16.87	0.25	43.22	0.07	0.14	100.23
1838.40	YC	39.60	0.02	17.00	0.23	43.02	0.04	0.20	100.11
1838.40	YD	39.52	0.02	16.83	0.23	43.42	0.07	0.14	100.23
1838.40	YE	39.45	0.02	16.75	0.23	43.45	0.09	0.17	100.16
1838.40	YF	39.84	0.02	16.99	0.25	43.22	0.07	0.14	100.53
1838.40	YG	39.64	0.02	17.23	0.23	42.90	0.06	0.12	100.23
1839.50	XT	40.62	0.02	12.03	0.17	47.16	0.06	0.14	100.20
1839.50	XU	40.73	0.02	12.11	0.20	46.96	0.06	0.15	100.23
1839.50	XV	40.40	0.02	12.23	0.17	47.11	0.06	0.12	100.11
1839.50	XW	40.61	0.02	12.17	0.19	46.99	0.07	0.14	100.19
1884.25	XA	40.24	0.02	15.49	0.20	45.22	0.07	0.15	101.39
1884.25	XB	39.97	0.02	15.64	0.22	44.99	0.07	0.14	101.07
1884.25	XC	40.06	0.02	15.54	0.23	44.91	0.06	0.17	100.99
1886.45	XX	39.83	0.02	16.37	0.23	43.71	0.06	0.18	100.42
1886.45	XX	40.18	0.02	16.48	0.22	43.78	0.07	0.18	100.95
1886.45	XX	40.11	0.04	16.37	0.22	43.93	0.04	0.17	100.90
1886.45	XX	40.10	0.02	16.16	0.23	43.99	0.04	0.18	100.76
1886.55	XI	39.93	0.02	15.76	0.25	45.02	0.04	0.11	101.13
1886.55	XJ	39.95	0.02	16.17	0.23	44.82	0.06	0.18	101.43
1886.55	XL	40.08	0.02	16.09	0.25	44.77	0.06	0.15	101.42
1886.55	XM	39.88	0.02	15.92	0.25	44.85	0.07	0.15	101.14
1889.30	XD	39.93	0.02	16.00	0.20	43.91	0.06	0.17	100.29
1889.30	XI	39.99	0.02	16.04	0.25	44.17	0.04	0.18	100.69
1889.30	XJ	39.69	0.02	16.04	0.23	43.94	0.06	0.20	100.18
1889.30	XK	39.57	0.02	16.04	0.22	44.07	0.06	0.20	100.18
1890.70	ZZ	39.52	0.02	16.30	0.22	43.86	0.06	0.20	100.18

TABLE 1. (cont.)

Depth (m)	ID	SiO_2	TiO_2	FeO*	MnO	MgO	CaO	NiO	Total
1890.70	ZZ	39.48	0.02	16.26	0.23	43.97	0.07	0.21	100.24
1890.70	ZZ	40.17	0.02	16.17	0.23	44.15	0.04	0.17	100.97
1890.70	ZZ	39.88	0.02	16.28	0.23	43.96	0.06	0.21	100.64
1891.05	XI	39.48	0.02	15.96	0.25	44.24	0.06	0.15	100.16
1891.05	XN	40.30	0.02	15.84	0.23	44.61	0.06	0.15	101.21
1891.05	XO	40.19	0.02	15.76	0.23	44.42	0.06	0.14	100.82
1891.05	XQ	39.51	0.02	15.99	0.25	44.47	0.06	0.17	100.47
1892.20	XA	40.08	0.02	16.83	0.25	43.60	0.06	0.20	101.04
1892.20	XB	39.99	0.02	16.94	0.25	43.44	0.06	0.20	100.90
1892.20	XC	39.80	0.02	16.84	0.22	43.37	0.04	0.21	100.50
1892.20	XD	39.85	0.02	16.99	0.22	43.27	0.06	0.18	100.59
1892.20	XJ	39.87	0.02	16.57	0.25	43.73	0.06	0.17	100.67
1893.40	XE	39.96	0.02	16.34	0.20	43.77	0.06	0.18	100.53
1893.40	XF	39.89	0.02	16.33	0.26	43.97	0.07	0.18	100.72
1893.40	XG	40.01	0.02	16.27	0.23	43.80	0.06	0.17	100.56
1893.40	XH	39.62	0.02	16.35	0.23	43.64	0.06	0.17	100.09
1893.40	XI	39.67	0.02	16.19	0.26	44.19	0.07	0.18	100.58
1894.10	XF	39.36	0.02	16.32	0.25	44.46	0.06	0.23	100.70
1894.10	XG	39.45	0.02	16.35	0.23	44.39	0.04	0.18	100.66
1894.10	XH	39.71	0.02	16.44	0.22	44.19	0.06	0.18	100.82
1894.10	XJ	39.46	0.02	16.23	0.23	44.53	0.06	0.18	100.71
1895.40	YA	39.53	0.04	16.54	0.23	44.26	0.09	0.18	100.87
1895.40	YB	39.71	0.02	16.38	0.25	44.24	0.04	0.14	100.78
1895.40	YE	39.78	0.04	16.38	0.26	43.86	0.06	0.18	100.56
1895.40	YF	39.79	0.02	16.50	0.23	43.91	0.09	0.18	100.72
1895.40	YS	39.65	0.02	16.46	0.23	43.85	0.09	0.17	100.47
1895.40	YP	39.58	0.02	16.40	0.26	44.18	0.06	0.15	100.65
1896.90	YC	39.70	0.02	16.45	0.22	43.64	0.07	0.18	100.28
1896.90	XU	39.54	0.02	16.49	0.23	43.71	0.07	0.17	100.23
1896.90	XV	39.52	0.02	16.57	0.20	43.53	0.06	0.17	100.07
1896.90	YB	39.34	0.02	16.56	0.25	43.69	0.07	0.18	100.11
1896.90	YD	39.54	0.02	16.56	0.25	43.49	0.07	0.17	100.10
1896.90	YE	39.43	0.02	16.50	0.23	43.64	0.06	0.18	100.06
1896.90	YF	39.27	0.02	16.54	0.25	43.77	0.06	0.17	100.08
1897.40	XR	40.02	0.02	15.41	0.23	45.14	0.03	0.14	100.99
1897.40	XS	40.08	0.02	15.62	0.22	44.82	0.06	0.15	100.97
1897.40	XT	39.81	0.02	15.69	0.23	44.62	0.09	0.17	100.63
1897.40	XU	39.69	0.02	15.64	0.23	44.93	0.09	0.15	100.75
1900.30	YA	40.02	0.02	16.27	0.23	43.68	0.06	0.18	100.46
1900.30	YB	39.77	0.02	16.40	0.22	43.61	0.06	0.17	100.25
1900.30	YC	40.22	0.02	16.26	0.25	43.88	0.06	0.17	100.86
1900.30	YD	40.05	0.02	16.06	0.23	44.06	0.07	0.17	100.66
2087.20	XE	39.97	0.02	15.12	0.23	44.85	0.04	0.15	100.38
2087.20	XF	39.98	0.02	14.86	0.25	44.88	0.06	0.14	100.19
2087.20	XG	40.03	0.02	14.89	0.23	45.06	0.06	0.17	100.46
2087.20	XH	40.13	0.02	14.75	0.22	44.89	0.04	0.17	100.22
2087.40	YA	39.63	0.02	15.65	0.23	44.42	0.04	0.17	100.16
2087.40	XY	39.63	0.02	14.68	0.22	45.67	0.04	0.18	100.44
2087.40	XL	39.86	0.02	14.93	0.22	45.50	0.04	0.18	100.75
2087.40	XM	40.05	0.02	15.04	0.25	45.34	0.04	0.17	100.91

TABLE 1. (cont.)

Depth (m)	ID	SiO_2	TiO_2	FeO*	MnO	MgO	CaO	NiO	Total
2087.40	XN	39.83	0.02	14.81	0.22	45.15	0.04	0.15	100.22
2091.10	YK	40.05	0.02	14.82	0.19	45.48	0.06	0.15	100.77
2091.10	XL	40.08	0.02	14.68	0.23	45.38	0.06	0.18	100.63
2091.10	XM	40.16	0.02	14.60	0.22	45.24	0.04	0.20	100.48
2093.65	XE	40.63	0.02	13.88	0.22	46.20	0.06	0.20	101.21
2093.65	XF	40.24	0.02	13.82	0.20	46.24	0.04	0.17	100.73
2093.65	XG	40.10	0.02	13.90	0.22	46.24	0.04	0.18	100.70
2093.65	XH	39.91	0.02	13.97	0.23	46.28	0.06	0.17	100.64
2094.00	XB	40.44	0.02	13.45	0.23	46.19	0.04	0.18	100.55
2094.00	XH	40.16	0.02	13.29	0.22	46.29	0.06	0.14	100.18
2094.00	XI	40.53	0.02	13.15	0.22	46.48	0.06	0.18	100.64
2094.00	XC	40.25	0.02	13.09	0.20	46.35	0.06	0.15	100.12
2094.00	XE	40.18	0.02	13.10	0.20	46.33	0.07	0.15	100.05
2094.00	XF	40.31	0.02	13.06	0.20	46.64	0.06	0.15	100.44
2094.00	XG	40.16	0.02	13.40	0.22	46.46	0.06	0.17	100.49
2095.20	YF	39.73	0.02	14.83	0.20	45.53	0.06	0.15	100.52
2095.20	YG	39.71	0.02	14.64	0.23	45.22	0.06	0.17	100.05
2095.20	YH	39.65	0.02	14.75	0.20	45.55	0.04	0.17	100.38
2095.20	YI	39.81	0.02	14.87	0.20	45.13	0.04	0.18	100.25
2095.20	YJ	39.73	0.02	14.71	0.22	45.34	0.04	0.18	100.24
2208.90	XA	40.20	0.02	14.32	0.22	45.96	0.04	0.17	100.93
2208.90	XB	40.16	0.02	14.18	0.20	45.95	0.04	0.20	100.75
2208.90	XC	40.21	0.00	14.19	0.20	45.91	0.04	0.18	100.73
2208.90	XD	39.89	0.02	14.32	0.23	45.97	0.06	0.14	100.63
2208.90	XE	40.02	0.02	14.17	0.20	46.09	0.04	0.14	100.68
2210.20	YA	40.44	0.02	14.83	0.20	45.73	0.04	0.18	101.44
2210.20	YB	40.42	0.02	14.71	0.22	45.84	0.06	0.18	101.45
2210.20	YC	40.45	0.02	14.78	0.23	45.69	0.04	0.18	101.39
2210.20	YD	39.91	0.02	14.79	0.25	45.40	0.06	0.15	100.58
2210.20	YE	39.82	0.02	14.68	0.22	45.33	0.06	0.15	100.28
2211.35	YD	39.69	0.02	16.19	0.22	43.75	0.06	0.15	100.08
2211.35	YE	40.01	0.02	15.75	0.22	44.13	0.06	0.15	100.34
2211.35	YF	40.25	0.02	14.21	0.23	45.18	0.04	0.14	100.07
2211.35	YG	40.11	0.02	14.33	0.20	45.27	0.06	0.12	100.11
2211.35	YI	40.12	0.02	14.18	0.22	45.39	0.04	0.17	100.14
2211.35	YJ	40.02	0.02	14.48	0.23	45.22	0.07	0.17	100.21
2211.35	YO	40.13	0.02	14.86	0.22	44.84	0.06	0.15	100.28
2215.20	YQ	39.92	0.02	15.53	0.25	44.37	0.04	0.15	100.28
2215.20	YR	39.89	0.02	15.31	0.22	44.44	0.04	0.18	100.10
2215.20	YU	40.18	0.02	15.32	0.25	44.52	0.04	0.17	100.50
2215.20	YV	40.13	0.02	14.89	0.23	44.64	0.06	0.15	100.12
2215.20	YX	40.13	0.02	14.98	0.25	44.69	0.06	0.18	100.31
2215.20	XE	39.78	0.02	15.67	0.25	44.12	0.07	0.18	100.09
2215.20	XH	40.18	0.02	14.68	0.20	44.95	0.04	0.18	100.25
2216.50	XE	40.45	0.04	13.78	0.22	46.11	0.07	0.15	100.82
2216.50	XF	40.34	0.02	13.74	0.20	46.26	0.04	0.15	100.78
2216.50	XI	40.44	0.02	13.70	0.20	46.07	0.04	0.14	100.63
2216.50	XK	40.39	0.02	13.79	0.23	46.37	0.06	0.20	101.06
2216.50	XL	40.37	0.02	13.50	0.23	46.41	0.04	0.15	100.76
2217.60	XR	40.18	0.02	15.11	0.23	45.16	0.07	0.15	100.92

TABLE 1. (cont.)

Depth (m)	ID	SiO_2	TiO_2	FeO*	MnO	MgO	CaO	NiO	Total
2217.60	XS	39.80	0.02	15.03	0.22	44.97	0.06	0.14	100.24
2217.60	XT	39.71	0.02	15.10	0.23	44.76	0.07	0.17	100.06
2217.60	XU	39.86	0.02	14.98	0.22	44.84	0.09	0.14	100.15
2217.60	XV	39.96	0.02	15.00	0.22	45.04	0.06	0.15	100.45
2217.60	XW	39.86	0.02	15.05	0.23	44.75	0.06	0.17	100.14
2217.60	XX	40.15	0.02	14.98	0.20	44.92	0.06	0.17	100.50
2218.40	YB	39.65	0.02	15.15	0.25	45.07	0.06	0.17	100.37
2218.40	YC	40.44	0.02	15.46	0.22	45.11	0.04	0.20	101.49
2218.40	YD	40.50	0.02	15.23	0.25	44.93	0.04	0.17	101.14
2218.40	YE	40.02	0.02	15.64	0.23	44.68	0.06	0.17	100.82
2218.40	YF	39.62	0.02	15.28	0.20	45.18	0.11	0.17	100.51
2220.45	XY	40.38	0.02	14.30	0.20	45.79	0.06	0.15	100.90
2220.45	XZ	40.70	0.02	14.02	0.20	46.14	0.04	0.14	101.26
2220.45	XA	40.72	0.02	14.40	0.22	45.85	0.04	0.15	101.40
2222.90	XC	40.35	0.02	13.58	0.22	46.42	0.07	0.18	100.84
2222.90	XL	40.12	0.02	13.46	0.19	46.07	0.06	0.15	100.07
2222.90	XN	40.15	0.02	13.41	0.22	46.35	0.06	0.17	100.38
2222.90	XO	40.19	0.02	13.46	0.19	46.49	0.06	0.12	100.53
2222.90	XP	40.30	0.02	13.30	0.19	46.18	0.04	0.17	100.20
2222.90	XQ	40.47	0.02	13.65	0.19	46.14	0.06	0.15	100.68
2222.90	XG	40.00	0.02	13.39	0.22	46.17	0.06	0.14	100.00
2224.20	YG	39.98	0.02	13.03	0.20	46.90	0.06	0.15	100.34
2224.20	YH	39.96	0.02	13.92	0.22	46.53	0.06	0.15	99.86
2224.20	YI	39.59	0.02	12.99	0.19	46.61	0.04	0.14	99.58
2224.20	YJ	40.34	0.02	13.05	0.22	46.73	0.07	0.14	100.57
2224.20	YK	40.27	0.02	12.95	0.20	46.98	0.04	0.17	100.63
2225.00	WD	40.85	0.02	14.17	0.22	46.43	0.03	0.15	101.87
2225.00	WE	40.62	0.02	14.13	0.22	46.31	0.06	0.11	101.47
2225.00	WG	40.87	0.02	14.24	0.22	46.43	0.04	0.12	101.94
2254.55	XM	40.22	0.02	13.62	0.22	45.74	0.06	0.17	100.05
2254.55	XN	40.01	0.02	13.81	0.22	45.79	0.07	0.17	100.09
2254.55	XO	40.18	0.02	13.73	0.19	45.73	0.06	0.15	100.06
2254.55	XP	40.32	0.02	13.62	0.20	45.71	0.06	0.15	100.08
2254.55	XQ	40.22	0.02	13.63	0.22	45.69	0.06	0.15	99.99
2254.55	XT	40.68	0.02	13.65	0.20	46.42	0.07	0.14	101.18
2254.55	XV	40.78	0.02	13.74	0.20	46.52	0.06	0.18	101.50
2256.90	YQ	40.01	0.02	15.16	0.23	44.71	0.06	0.18	100.37
2256.90	YR	39.60	0.02	15.12	0.23	44.90	0.06	0.20	100.13
2256.90	YS	39.80	0.02	14.74	0.20	45.11	0.04	0.18	100.09
2256.90	YT	40.12	0.02	14.78	0.22	44.79	0.04	0.20	100.17
2256.90	YU	40.10	0.02	14.78	0.23	44.87	0.04	0.14	100.18
2256.90	WL	40.05	0.02	14.86	0.22	44.77	0.06	0.18	100.16
2258.00	YN	40.17	0.02	14.63	0.22	45.97	0.04	0.14	101.19
2258.00	YT	40.22	0.02	14.64	0.22	46.02	0.06	0.15	101.33
2258.00	YV	40.01	0.02	14.53	0.22	45.98	0.06	0.15	100.97
2258.00	YW	39.87	0.02	14.51	0.20	46.10	0.06	0.17	100.93
2258.00	YZ	39.98	0.02	14.53	0.22	45.94	0.06	0.15	100.90
2258.00	XA	40.12	0.02	14.45	0.23	45.82	0.00	0.17	100.81
2258.00	XC	40.12	0.02	14.44	0.22	45.86	0.04	0.15	100.85
2258.00	XB	40.21	0.02	14.56	0.23	45.94	0.04	0.15	101.15

TABLE 1. (cont.)

Depth (m)	ID	SiO_2	TiO_2	FeO*	MnO	MgO	CaO	NiO	Total
2259.00	XC	40.08	0.02	13.40	0.20	46.81	0.07	0.17	100.75
2259.00	XE	40.57	0.02	13.25	0.20	46.81	0.06	0.14	101.05
2259.00	XF	40.32	0.02	13.21	0.20	46.66	0.06	0.14	100.61
2259.00	XG	40.31	0.02	13.17	0.22	46.81	0.04	0.17	100.74
2259.00	XH	40.53	0.02	13.35	0.19	46.63	0.06	0.17	100.95
2259.70	XA	39.76	0.02	15.73	0.20	44.95	0.04	0.24	100.94
2259.70	XB	39.84	0.02	15.81	0.23	44.98	0.04	0.18	101.10
2259.70	XC	39.67	0.02	15.88	0.23	44.95	0.06	0.21	101.02
2259.70	XD	39.71	0.02	15.42	0.20	45.24	0.04	0.18	100.81
2259.70	XE	39.55	0.02	15.58	0.25	44.85	0.06	0.18	100.49
2259.70	XF	39.73	0.02	15.43	0.22	44.66	0.04	0.20	100.30
2260.70	YA	39.91	0.00	15.21	0.22	45.05	0.04	0.18	100.61
2260.70	YB	39.96	0.02	14.92	0.22	44.81	0.06	0.21	100.20
2260.70	YC	40.06	0.02	15.28	0.20	44.83	0.03	0.18	100.60
2260.70	YD	39.81	0.02	15.20	0.20	44.67	0.04	0.21	100.15
2260.70	YE	39.73	0.02	15.01	0.20	45.01	0.06	0.18	100.21
2260.70	YF	39.83	0.02	15.17	0.22	44.66	0.04	0.18	100.12
2261.30	XA	40.20	0.02	12.36	0.22	46.96	0.06	0.20	100.02
2261.30	XB	40.27	0.02	12.47	0.20	46.86	0.07	0.18	100.07
2261.30	XC	40.34	0.02	12.35	0.19	46.91	0.06	0.15	100.02
2261.30	XD	40.51	0.02	12.40	0.20	46.77	0.06	0.18	100.14
2261.30	XE	40.33	0.04	12.41	0.22	46.78	0.06	0.17	100.01
2262.00	YB	40.92	0.02	12.54	0.20	47.65	0.07	0.17	101.57
2262.00	YD	40.88	0.02	12.63	0.22	47.40	0.06	0.18	101.39
2262.00	YE	40.73	0.02	12.50	0.20	47.58	0.09	0.15	101.27
2262.00	YJ	40.35	0.02	12.51	0.19	47.37	0.07	0.14	100.65
2262.00	YK	40.44	0.02	12.55	0.20	47.40	0.07	0.15	100.83
2262.00	YL	40.60	0.02	12.51	0.20	47.74	0.09	0.17	101.33
2262.00	XR	40.68	0.02	12.47	0.22	47.71	0.06	0.20	101.36
2262.90	XO	40.38	0.02	14.59	0.23	45.67	0.06	0.15	101.10
2262.90	XP	40.39	0.02	14.63	0.22	45.50	0.04	0.14	100.94
2262.90	XQ	40.02	0.02	14.63	0.20	45.31	0.03	0.17	100.38
2262.90	XR	39.78	0.02	14.79	0.22	45.13	0.04	0.18	100.16
2262.90	XS	39.48	0.02	14.79	0.23	45.15	0.04	0.17	99.88
2262.90	XT	39.71	0.02	14.50	0.22	45.06	0.04	0.20	99.75
2263.30	VA	40.30	0.02	14.21	0.22	46.01	0.06	0.17	100.99
2263.30	VD	40.39	0.02	14.26	0.23	45.73	0.07	0.15	100.85
2263.30	VE	40.28	0.02	14.32	0.22	45.83	0.09	0.15	100.91
2263.30	VF	40.31	0.02	14.27	0.23	45.84	0.09	0.15	100.91
2263.30	VG	40.08	0.02	14.20	0.23	46.09	0.06	0.18	100.86

TABLE 2. Electron microprobe data for clinopyroxene in lower ultramafic cumulates from CY-4

Depth (m)	ID	SiO_2	TiO_2	Al_2O_3	FeO*	MnO	MgO	CaO	Na_2O	Cr_2O_3	Total
1745.10	XM	53.03	0.17	1.86	4.96	0.14	16.96	22.10	0.08	0.19	99.49
1745.10	XN	53.04	0.09	2.06	4.36	0.13	17.28	22.16	0.13	0.31	99.56
1745.10	XO	53.38	0.09	2.05	5.14	0.16	18.15	20.69	0.05	0.24	99.95
1745.10	XP	53.73	0.08	2.04	4.04	0.14	17.31	22.13	0.08	0.28	99.83
1745.10	XQ	53.31	0.09	1.93	5.07	0.17	17.83	20.99	0.06	0.28	99.73
1745.10	XR	53.28	0.08	1.98	4.22	0.16	17.71	21.98	0.06	0.30	99.77
1745.70	YK	53.19	0.17	1.93	5.02	0.16	17.79	21.22	0.11	0.21	99.80
1745.70	YN	53.09	0.09	1.97	5.04	0.14	17.82	20.87	0.08	0.23	99.33
1745.70	YP	52.74	0.21	2.02	4.85	0.16	16.56	22.47	0.10	0.19	99.30
1745.70	YS	52.96	0.17	1.94	4.97	0.14	17.00	21.81	0.13	0.28	99.40
1745.70	YT	53.11	0.11	2.01	5.00	0.14	17.61	21.20	0.11	0.26	99.55
1745.70	YU	53.39	0.19	1.98	5.25	0.16	17.25	21.31	0.16	0.21	99.90
1745.70	YW	53.20	0.09	2.02	4.82	0.19	17.40	21.38	0.08	0.19	99.34
1745.70	YY	53.00	0.23	2.01	5.24	0.16	17.23	21.42	0.13	0.23	99.65
1749.70	YW	53.28	0.25	1.92	5.41	0.14	16.48	22.01	0.11	0.16	99.76
1749.70	YY	53.40	0.09	2.01	4.89	0.16	17.90	21.20	0.08	0.23	99.96
1749.70	XA	53.59	0.06	1.96	5.04	0.16	17.53	21.48	0.06	0.21	100.09
1750.05	XC	53.21	0.09	2.05	4.77	0.14	17.83	21.39	0.09	0.21	99.77
1750.05	XQ	53.63	0.09	0.45	5.34	0.19	15.33	24.36	0.14	0.14	99.67
1750.05	XR	53.75	0.08	0.35	5.63	0.16	15.04	24.45	0.13	0.12	99.71
1750.05	XS	53.34	0.25	0.93	5.45	0.16	16.07	22.82	0.16	0.17	99.35
1750.05	YP	53.26	0.25	0.93	5.60	0.17	16.30	22.65	0.14	0.17	99.47
1750.50	XA	53.18	0.17	2.00	4.99	0.16	16.59	22.14	0.11	0.19	99.53
1750.50	XC	52.92	0.21	1.90	5.88	0.16	16.84	21.23	0.11	0.19	99.44
1750.50	XD	53.05	0.13	1.98	5.24	0.16	16.94	21.84	0.11	0.23	99.68
1750.50	XK	52.96	0.11	2.06	4.60	0.14	16.68	22.44	0.11	0.17	99.27
1750.50	XW	53.32	0.19	1.94	5.41	0.16	16.69	22.10	0.10	0.17	100.08
1750.80	ZQ	53.39	0.21	1.87	5.35	0.17	15.91	22.74	0.13	0.16	99.93
1750.80	ZS	53.64	0.13	0.97	5.64	0.19	15.70	23.25	0.22	0.14	99.88
1750.80	ZV	53.36	0.09	1.98	4.86	0.16	17.40	21.90	0.05	0.19	99.99
1750.80	ZY	53.16	0.26	1.73	5.48	0.16	15.87	22.83	0.19	0.24	99.92
1750.80	ZZ	53.87	0.11	0.43	5.39	0.19	15.37	23.83	0.13	0.09	99.41
1750.80	XF	53.70	0.30	0.97	5.83	0.17	15.90	22.70	0.21	0.17	99.95
1751.75	XI	53.45	0.23	1.34	5.42	0.16	16.67	22.11	0.13	0.19	99.70
1751.75	XJ	53.44	0.08	1.99	4.85	0.13	18.18	21.09	0.05	0.24	100.05
1751.75	XK	53.08	0.23	1.69	5.32	0.14	16.96	21.90	0.13	0.23	99.68
1751.75	XO	53.04	0.09	1.99	5.31	0.16	18.21	20.51	0.06	0.23	99.60
1751.75	XR	53.24	0.21	1.92	5.87	0.19	17.03	21.24	0.10	0.17	99.97
1752.50	XA	53.58	0.26	1.19	5.27	0.17	16.01	23.13	0.18	0.21	100.00
1752.50	ZK	53.35	0.23	1.74	5.14	0.14	15.84	22.96	0.16	0.17	99.73
1752.50	XD	53.90	0.21	1.48	4.95	0.16	16.55	22.21	0.17	0.16	99.79
1752.50	ZF	54.09	0.15	0.49	4.95	0.16	15.86	23.92	0.18	0.12	99.92
1752.50	ZG	53.77	0.13	1.82	6.77	0.17	18.66	18.35	0.10	0.16	99.93
1830.90	XP	53.44	0.09	2.17	3.52	0.13	16.94	23.12	0.11	0.47	99.99
1830.90	XS	54.28	0.06	1.28	2.42	0.11	18.40	21.87	0.06	0.49	99.97
1830.90	XY	54.00	0.06	1.18	3.98	0.13	18.82	21.14	0.14	0.52	99.97
1830.90	YS	53.59	0.04	1.20	3.94	0.14	18.03	22.02	0.13	0.45	99.54
1830.90	YT	53.05	0.17	2.08	4.09	0.14	16.96	22.97	0.13	0.47	100.06
1830.90	YU	53.10	0.15	2.05	3.80	0.14	16.94	22.43	0.13	0.40	99.14
1830.90	YV	53.96	0.06	1.24	3.39	0.13	18.00	22.55	0.09	0.54	99.96

TABLE 2. (cont.)

Depth (m)	ID	SiO_2	TiO_2	Al_2O_3	FeO*	MnO	MgO	CaO	Na_2O	Cr_2O_3	Total
1830.90	YW	53.89	0.04	1.18	4.08	0.13	18.90	21.12	0.09	0.54	99.97
1831.80	XE	54.28	0.06	1.24	3.42	0.13	18.94	20.88	0.08	0.65	99.68
1831.80	XC	52.91	0.17	2.06	4.26	0.13	17.58	21.72	0.13	0.37	99.33
1831.80	XE	53.85	0.04	1.20	3.35	0.13	18.93	21.01	0.11	0.65	99.27
1831.80	XL	53.91	0.06	1.04	3.62	0.14	19.21	20.66	0.06	0.56	99.26
1831.80	XD	53.37	0.15	2.12	4.47	0.14	17.03	21.94	0.14	0.45	99.81
1832.20	WG	54.71	0.06	0.96	4.05	0.14	24.51	11.92	0.00	0.50	96.85
1832.20	WF	54.09	0.04	1.10	3.17	0.14	19.17	20.05	0.05	0.59	98.40
1832.20	WE	53.92	0.06	1.04	3.55	0.13	18.88	21.38	0.05	0.63	99.64
1832.20	WC	53.98	0.06	1.13	3.25	0.13	18.18	22.28	0.08	0.70	99.79
1832.20	WD	54.69	0.06	1.23	4.56	0.13	19.98	19.33	0.05	0.61	100.64
1832.20	WA	55.91	0.06	0.90	5.90	0.16	25.75	11.45	0.02	0.46	100.61
1832.20	YS	53.37	0.15	2.06	3.93	0.13	17.22	22.35	0.06	0.35	99.62
1832.20	YU	54.01	0.06	1.07	3.35	0.09	18.62	21.61	0.03	0.54	99.38
1832.20	YY	53.74	0.06	1.07	3.21	0.11	18.39	22.00	0.06	0.66	99.30
1832.20	XA	53.29	0.13	1.91	3.83	0.14	16.77	23.03	0.13	0.49	99.72
1832.20	XB	53.67	0.09	1.89	3.53	0.13	17.65	22.31	0.06	0.52	99.85
1832.20	XC	54.44	0.08	0.63	2.64	0.11	16.86	24.81	0.05	0.11	99.73
1832.20	XD	53.91	0.06	1.32	3.55	0.13	18.51	21.59	0.05	0.61	99.73
1832.20	XE	53.76	0.08	1.32	3.20	0.11	18.05	22.40	0.05	0.66	99.63
1832.20	XF	53.68	0.09	1.66	4.49	0.13	19.11	20.14	0.08	0.54	99.92
1832.30	YC	53.81	0.06	1.49	3.91	0.13	18.18	21.57	0.14	0.65	99.94
1832.30	YD	53.78	0.06	1.57	3.80	0.14	18.12	21.86	0.11	0.63	100.07
1832.30	YE	53.12	0.13	2.16	3.80	0.11	16.94	22.68	0.13	0.56	99.63
1832.30	YG	53.82	0.06	1.41	3.84	0.13	18.49	21.50	0.11	0.68	100.04
1832.30	YJ	52.86	0.13	2.44	3.73	0.13	16.98	22.43	0.17	0.63	99.50
1832.30	YK	53.03	0.09	1.91	3.55	0.14	17.43	22.63	0.14	0.61	99.53
1832.30	YR	53.44	0.08	1.83	3.56	0.11	17.49	22.57	0.12	0.61	99.81
1832.30	YO	53.75	0.06	1.42	3.69	0.14	17.99	22.32	0.09	0.63	100.09
1832.30	YP	53.37	0.06	1.46	3.34	0.11	17.79	22.77	0.09	0.66	99.65
1833.40	YV	53.93	0.04	1.41	3.76	0.13	18.39	21.27	0.06	0.78	99.77
1833.40	YW	53.79	0.06	1.47	3.59	0.11	18.38	21.05	0.06	0.77	99.28
1833.40	YX	54.01	0.06	1.29	4.09	0.14	19.84	19.36	0.06	0.71	99.56
1833.40	YY	53.80	0.06	1.32	4.84	0.13	19.77	19.39	0.06	0.71	100.08
1833.40	YZ	53.69	0.04	1.16	3.67	0.13	18.50	21.15	0.06	0.72	99.12
1833.40	WA	53.27	0.04	1.59	3.46	0.13	17.81	21.96	0.09	0.79	99.14
1833.40	WB	54.00	0.06	1.34	3.44	0.13	18.28	21.62	0.05	0.79	99.71
1834.40	XI	53.48	0.06	1.89	3.90	0.14	18.85	20.31	0.11	0.70	99.44
1834.40	XJ	53.70	0.06	1.62	3.95	0.14	18.99	20.61	0.06	0.73	99.86
1834.40	XK	53.29	0.06	1.63	3.58	0.14	18.07	21.78	0.09	0.72	99.36
1834.40	XL	53.59	0.06	1.55	3.59	0.14	17.82	21.97	0.09	0.73	99.54
1834.40	XM	53.87	0.06	1.30	3.69	0.13	18.41	21.47	0.06	0.73	99.72
1834.40	XN	54.00	0.06	1.39	4.04	0.13	18.85	20.57	0.05	0.82	99.91
1835.60	XL	53.18	0.19	2.10	4.78	0.14	16.36	22.25	0.19	0.42	99.61
1835.60	XO	53.82	0.04	1.10	4.16	0.14	18.20	21.62	0.13	0.42	99.63
1835.60	XQ	53.98	0.10	0.76	3.65	0.13	16.38	24.75	0.05	0.09	99.89
1835.60	XM	53.45	0.08	1.72	4.67	0.13	18.04	21.34	0.11	0.50	100.04
1835.60	VO	53.35	0.13	2.20	3.94	0.13	17.20	22.26	0.16	0.47	99.84
1835.60	VP	53.28	0.17	2.05	4.39	0.14	16.24	22.99	0.22	0.37	99.85
1835.60	VQ	53.35	0.19	1.87	4.69	0.14	16.48	22.36	0.21	0.42	99.71

TABLE 2. (cont.)

Depth (m)	ID	SiO_2	TiO_2	Al_2O_3	FeO*	MnO	MgO	CaO	Na_2O	Cr_2O_3	Total
1835.60	VS	53.61	0.11	1.11	3.87	0.13	16.52	24.12	0.06	0.23	99.76
1837.05	XU	53.95	0.10	0.70	3.38	0.11	16.98	24.48	0.02	0.12	99.84
1837.05	XV	54.21	0.06	1.32	3.69	0.13	18.36	21.65	0.08	0.45	99.95
1837.05	XW	54.19	0.06	1.16	4.21	0.13	18.75	20.91	0.09	0.45	99.95
1837.05	YB	52.77	0.17	2.11	5.10	0.14	17.27	21.41	0.11	0.40	99.48
1837.05	YC	53.44	0.11	0.82	3.62	0.14	16.40	24.85	0.03	0.10	99.51
1837.05	YE	53.26	0.19	2.17	5.11	0.16	17.54	21.08	0.11	0.38	100.00
1838.00	YE	53.56	0.08	1.19	3.52	0.14	16.80	23.28	0.20	0.38	99.15
1838.00	XY	53.40	0.11	0.94	3.86	0.14	16.38	24.14	0.09	0.14	99.20
1838.00	XW	52.61	0.19	2.18	4.58	0.14	16.57	22.56	0.09	0.37	99.29
1838.00	XX	53.31	0.11	2.06	3.86	0.11	17.37	22.42	0.09	0.47	99.80
1838.00	UN	53.00	0.17	1.54	4.42	0.14	16.17	23.78	0.10	0.28	99.60
1838.40	XM	53.31	0.17	2.13	4.61	0.14	16.37	22.38	0.13	0.35	99.59
1838.40	XN	54.30	0.06	1.16	3.88	0.14	19.05	20.81	0.05	0.37	99.82
1838.40	XO	54.00	0.06	1.20	3.42	0.11	18.37	21.75	0.08	0.49	99.48
1838.40	XR	53.41	0.21	1.77	4.97	0.14	16.59	22.32	0.14	0.38	99.93
1838.40	XT	53.41	0.09	1.31	3.66	0.13	16.53	23.82	0.13	0.49	99.57
1839.50	X	53.93	0.08	1.54	4.18	0.14	19.00	20.20	0.06	0.52	99.65
1839.50	XB	53.44	0.08	1.64	3.39	0.11	17.25	22.94	0.08	0.51	99.44
1839.50	XC	53.80	0.06	1.64	3.42	0.14	17.63	22.46	0.09	0.47	99.73
1839.50	XE	53.60	0.09	1.61	3.55	0.13	17.95	22.12	0.06	0.52	99.63
1839.50	XF	53.59	0.08	1.61	3.79	0.16	17.61	22.38	0.09	0.51	99.82
1839.50	XG	53.51	0.08	1.57	3.60	0.13	18.10	22.02	0.06	0.52	99.59
1839.50	XH	53.62	0.06	1.62	3.59	0.16	17.48	22.57	0.09	0.52	99.71
1884.25	VF	53.50	0.13	2.10	4.42	0.13	17.19	21.86	0.14	0.00	99.47
1884.25	VG	54.11	0.08	1.29	4.11	0.13	18.79	20.19	0.09	0.61	99.40
1884.25	VH	53.09	0.11	2.15	4.69	0.13	17.48	21.36	0.11	0.57	99.69
1884.25	VI	53.39	0.13	2.16	4.55	0.16	17.15	21.85	0.13	0.57	100.09
1884.25	VL	53.29	0.09	1.56	4.00	0.13	18.68	21.44	0.09	0.64	99.92
1885.50	ZC	53.61	0.11	1.84	4.64	0.16	17.84	20.76	0.14	0.57	99.67
1885.50	ZF	54.84	0.06	1.07	3.00	0.11	18.64	21.29	0.06	0.65	99.72
1885.50	ZG	54.98	0.04	1.11	3.77	0.13	21.03	17.83	0.09	0.42	99.40
1885.50	ZL	53.26	0.15	1.99	4.36	0.14	16.40	22.79	0.13	0.38	99.60
1886.45	XX	53.45	0.17	1.95	4.16	0.13	16.61	22.70	0.14	0.56	99.87
1886.45	XA	53.96	0.04	1.16	3.77	0.13	18.59	21.23	0.09	0.66	99.63
1886.45	XX	53.98	0.08	1.26	3.20	0.13	18.99	21.56	0.03	0.56	99.79
1886.55	XA	53.62	0.08	1.58	3.18	0.13	17.80	22.83	0.09	0.65	99.96
1886.55	XB	53.39	0.19	2.22	4.71	0.16	18.38	20.44	0.11	0.38	99.98
1886.55	XH	54.22	0.04	1.11	2.97	0.09	18.38	22.04	0.06	0.63	99.53
1886.55	XK	54.02	0.04	0.97	3.09	0.13	18.38	22.59	0.08	0.61	99.91
1886.55	XN	53.95	0.09	1.66	3.60	0.14	19.39	20.53	0.05	0.65	100.06
1886.55	XO	54.40	0.04	1.05	3.11	0.11	18.86	21.69	0.06	0.70	100.02
1886.55	XP	53.76	0.06	1.09	3.07	0.11	18.48	22.37	0.05	0.70	99.69
1886.55	XT	53.38	0.08	1.82	3.88	0.14	18.24	21.83	0.08	0.54	99.99
1886.55	XU	53.96	0.04	1.04	3.59	0.13	20.29	19.58	0.70	0.70	99.38
1887.60	VD	53.57	0.15	1.92	4.01	0.13	17.53	21.75	0.13	0.59	99.78
1887.60	VA	53.11	0.13	1.76	4.00	0.13	17.93	22.09	0.13	0.61	99.89
1887.60	VC	53.60	0.06	1.10	3.42	0.09	19.46	21.33	0.09	0.65	99.80
1887.60	VE	54.14	0.06	1.20	3.09	0.13	18.76	21.96	0.05	0.56	99.95
1887.60	VG	53.33	0.21	1.28	4.39	0.13	16.70	23.22	0.16	0.54	99.96

TABLE 2. (cont.)

Depth (m)	ID	SiO_2	TiO_2	Al_2O_3	FeO*	MnO	MgO	CaO	Na_2O	Cr_2O_3	Total
1887.60	VH	52.52	0.09	2.42	3.83	0.14	16.54	23.81	0.13	0.44	99.92
1888.30	VA	53.69	0.06	1.87	3.04	0.09	17.61	22.47	0.09	0.68	99.60
1888.30	VD	53.36	0.08	1.71	3.31	0.13	17.76	22.03	0.11	0.89	99.38
1888.30	VF	53.83	0.08	1.65	3.10	0.11	18.04	22.13	0.09	0.73	99.76
1888.30	VG	53.92	0.08	1.26	3.18	0.13	18.92	20.99	0.06	0.65	99.19
1888.30	VI	54.79	0.04	1.28	3.66	0.13	21.30	17.86	0.06	0.82	99.94
1888.30	VJ	53.44	0.06	1.39	4.40	0.13	18.57	21.17	0.13	0.73	100.20
1889.30	XI	53.91	0.06	1.59	3.32	0.13	18.43	21.85	0.08	0.68	100.05
1889.30	XJ	54.09	0.06	1.14	3.88	0.13	18.43	21.18	0.09	0.61	99.61
1889.30	XL	54.13	0.08	1.45	4.54	0.16	18.13	20.61	0.09	0.68	99.87
1889.30	XM	53.67	0.09	1.78	3.51	0.13	18.37	21.46	0.08	0.70	99.79
1890.35	YG	54.16	0.08	0.74	3.03	0.11	17.31	24.34	0.06	0.18	100.01
1890.35	YH	53.27	0.15	1.68	3.90	0.13	16.70	23.32	0.16	0.63	99.94
1890.35	YI	53.70	0.11	0.86	3.63	0.13	17.03	23.73	0.08	0.31	99.58
1890.35	YK	53.96	0.09	0.72	3.65	0.14	17.05	23.95	0.09	0.23	99.88
1890.35	YL	53.45	0.09	1.94	3.29	0.11	18.05	22.22	0.11	0.84	100.10
1890.35	YN	53.95	0.13	0.64	3.56	0.11	16.80	24.23	0.09	0.21	99.72
1890.35	YO	53.92	0.08	0.62	3.32	0.13	17.24	24.34	0.05	0.16	99.86
1890.35	YR	54.12	0.10	0.51	3.51	0.13	17.16	24.21	0.05	0.14	99.93
1890.70	ZZ	52.87	0.19	2.02	4.54	0.14	16.68	22.46	0.14	0.47	99.51
1890.70	ZZ	53.78	0.06	1.38	3.32	0.11	18.68	21.30	0.05	0.63	99.31
1890.70	ZZ	54.45	0.04	1.01	3.49	0.11	18.64	21.51	0.09	0.65	99.99
1890.70	ZZ	53.52	0.11	1.89	3.60	0.13	16.93	23.05	0.13	0.79	100.15
1891.05	XG	53.79	0.09	1.77	3.38	0.14	17.53	22.58	0.09	0.68	100.07
1891.05	XH	52.87	0.09	1.87	3.55	0.13	17.20	22.65	0.11	0.77	99.24
1891.05	XJ	53.78	0.09	1.86	3.98	0.14	18.33	20.45	0.11	0.78	99.52
1891.05	XK	53.27	0.13	2.15	3.87	0.14	16.70	22.91	0.14	0.68	99.99
1891.75	XX	53.25	0.28	1.30	5.16	0.16	16.49	22.57	0.21	0.42	99.84
1891.75	XY	53.41	0.26	1.20	5.25	0.16	16.48	22.61	0.21	0.36	99.94
1892.20	XL	53.51	0.09	1.90	3.77	0.11	18.24	21.38	0.08	0.71	99.79
1892.20	XM	54.13	0.06	1.10	4.08	0.14	19.37	19.54	0.08	0.64	99.15
1892.20	XR	53.71	0.11	1.82	4.65	0.14	17.60	21.24	0.13	0.59	99.99
1892.20	XT	54.31	0.06	1.10	3.79	0.13	18.74	21.00	0.11	0.58	99.82
1892.20	XV	54.53	0.06	1.04	3.58	0.13	19.43	20.49	0.08	0.65	99.99
1892.20	XF	53.79	0.06	1.44	3.24	0.11	17.78	22.49	0.09	0.66	99.66
1892.20	XM	53.60	0.08	1.80	4.02	0.13	18.35	21.17	0.08	0.70	99.93
1892.20	VO	52.58	0.28	2.00	5.63	0.16	16.00	22.30	0.19	0.42	99.56
1893.00	VO	53.68	0.08	1.77	3.44	0.14	17.96	21.94	0.08	0.79	99.88
1893.00	VQ	55.02	0.06	1.13	4.96	0.14	24.58	12.58	0.03	0.55	99.05
1893.00	VS	53.77	0.08	1.39	3.07	0.11	17.20	23.18	0.11	0.68	99.59
1893.00	VT	53.63	0.09	1.79	3.41	0.11	18.01	22.17	0.08	0.65	99.94
1893.40	XW	54.35	0.04	1.22	2.96	0.11	18.60	21.64	0.09	0.94	99.95
1893.40	XX	53.08	0.15	2.19	5.04	0.16	17.61	20.74	0.11	0.52	99.60
1893.40	XY	54.07	0.06	1.22	3.30	0.13	18.69	21.28	0.09	0.87	99.71
1893.40	XZ	54.32	0.04	0.93	2.86	0.08	18.70	21.71	0.08	0.77	99.49
1893.40	YA	54.04	0.08	1.34	3.17	0.13	18.77	21.30	0.08	0.72	99.63
1893.40	YB	53.71	0.04	1.24	3.34	0.09	18.50	21.40	0.09	0.87	99.28
1893.40	YC	54.23	0.08	1.44	3.37	0.11	18.11	21.89	0.09	0.68	100.00
1893.40	YD	54.16	0.06	1.49	4.05	0.11	19.03	20.24	0.09	0.61	99.83
1894.10	XN	54.37	0.04	1.12	3.25	0.09	19.60	20.87	0.03	0.75	100.12

TABLE 2. (cont.)

Depth (m)	ID	SiO_2	TiO_2	Al_2O_3	FeO*	MnO	MgO	CaO	Na_2O	Cr_2O_3	Total
1894.10	XP	54.79	0.04	1.14	3.90	0.13	22.08	17.17	0.03	0.73	100.01
1894.10	XQ	54.39	0.06	1.08	3.18	0.11	18.91	21.12	0.05	0.73	99.63
1894.10	XR	54.56	0.06	1.07	2.86	0.11	17.96	23.01	0.08	0.74	100.45
1895.40	YD	53.14	0.17	2.12	4.82	0.14	17.04	21.69	0.19	0.56	99.87
1895.40	YG	53.48	0.11	2.00	3.84	0.13	17.65	21.87	0.13	0.71	99.92
1895.40	YJ	53.37	0.19	1.95	4.51	0.13	16.67	22.27	0.16	0.52	99.77
1895.40	YQ	53.22	0.17	2.00	4.46	0.11	16.99	22.32	0.14	0.50	99.91
1895.40	YR	53.68	0.06	1.51	3.79	0.13	18.38	21.63	0.11	0.66	99.95
1896.30	ZM	53.60	0.17	1.32	4.72	0.14	17.12	21.93	0.19	0.54	99.73
1896.30	ZP	54.11	0.19	0.94	4.05	0.14	16.36	23.31	0.14	0.40	99.64
1896.30	ZQ	53.90	0.06	1.11	2.90	0.16	17.05	23.56	0.12	0.82	99.68
1896.30	ZT	54.68	0.06	0.35	3.03	0.13	16.55	25.00	0.05	0.11	99.96
1896.90	XX	53.30	0.11	1.92	3.67	0.13	18.00	21.97	0.08	0.75	99.93
1896.90	XS	53.49	0.09	1.81	3.48	0.13	17.56	22.61	0.14	0.66	99.97
1896.90	XT	53.45	0.11	2.31	3.90	0.11	17.48	21.82	0.14	0.63	99.95
1896.90	XW	54.20	0.06	1.08	3.38	0.13	18.96	21.37	0.09	0.65	99.92
1896.90	XZ	53.20	0.08	1.91	4.14	0.13	8.46	21.04	0.13	0.66	99.75
1896.90	YA	53.92	0.06	1.04	3.18	0.12	19.16	21.42	0.09	0.75	99.75
1896.90	YJ	53.98	0.04	1.14	3.14	0.11	19.04	21.63	0.09	0.73	99.90
1897.40	XA	54.00	0.06	0.91	3.37	0.13	19.23	20.49	0.08	0.73	99.00
1897.40	XE	53.68	0.06	1.20	4.15	0.13	17.95	21.30	0.11	0.71	99.29
1897.40	XC	54.98	0.06	0.89	3.80	0.13	22.64	16.31	0.03	0.75	99.61
1897.40	XD	53.62	0.08	1.69	3.42	0.11	18.19	21.91	0.06	0.80	99.91
1897.80	XK	53.71	0.08	1.43	3.80	0.16	18.50	21.47	0.08	0.66	99.89
1897.80	XM	53.62	0.06	1.38	4.21	0.14	17.84	21.84	0.08	0.61	99.78
1897.80	XO	53.09	0.19	1.85	4.62	0.13	16.78	22.40	0.14	0.52	99.72
1897.80	XP	54.17	0.06	1.18	4.05	0.13	18.91	20.64	0.09	0.63	99.86
1897.80	XR	53.29	0.19	1.59	4.90	0.16	17.18	21.82	0.16	0.52	99.81
1897.80	XU	53.11	0.19	1.88	4.97	0.14	17.08	21.85	0.11	0.56	99.89
1899.80	XB	54.24	0.06	1.06	4.08	0.13	19.44	20.18	0.09	0.66	99.94
1899.80	XF	54.33	0.06	1.22	4.05	0.09	18.94	20.81	0.09	0.63	100.22
1899.80	XG	53.49	0.11	2.07	3.44	0.13	17.30	22.63	0.05	0.58	99.80
1899.80	XH	53.90	0.06	1.20	3.35	0.09	18.50	22.22	0.05	0.56	99.93
1899.80	XE	53.65	0.04	1.03	2.86	0.11	18.77	22.50	0.08	0.86	99.90
1900.30	YH	54.36	0.06	1.18	3.90	0.14	18.18	20.88	0.09	0.68	99.47
1900.30	YI	53.98	0.06	1.21	4.61	0.13	19.13	19.85	0.13	0.73	99.83
1900.30	YJ	54.18	0.06	1.38	3.60	0.14	18.39	21.51	0.09	0.37	99.72
1900.30	YK	53.50	0.06	1.26	3.73	0.13	17.83	22.31	0.09	0.72	99.63
2087.20	XO	53.33	0.15	1.96	4.35	0.14	17.34	21.83	0.14	0.42	99.66
2087.20	XP	53.10	0.11	2.18	4.01	0.13	16.90	22.50	0.14	0.40	99.47
2087.20	XQ	53.11	0.11	2.16	3.86	0.14	17.34	22.20	0.13	0.35	99.40
2087.20	XR	53.35	0.13	2.03	4.64	0.14	18.35	20.13	0.11	0.33	99.21
2087.40	WC	53.02	0.13	2.15	4.65	0.13	17.79	21.17	0.13	0.31	99.48
2087.40	XO	53.16	0.11	2.28	4.35	0.14	18.15	21.14	0.11	0.38	99.82
2087.40	XP	53.25	0.13	2.32	4.64	0.14	17.78	20.98	0.09	0.50	99.83
2087.40	XS	53.05	0.11	2.29	4.32	0.13	17.80	21.74	0.13	0.42	99.99
2089.00	ZN	52.77	0.13	2.93	3.63	0.13	17.00	22.41	0.12	0.36	99.53
2089.00	ZV	52.99	0.09	2.26	3.60	0.13	17.07	23.10	0.13	0.31	99.68
2089.00	ZP	52.72	0.11	3.27	4.23	0.13	17.14	21.27	0.09	0.49	99.45
2089.00	ZR	53.12	0.13	2.06	4.60	0.16	17.50	21.91	0.16	0.35	99.99

TABLE 2. (cont.)

Depth (m)	ID	SiO_2	TiO_2	Al_2O_3	FeO*	MnO	MgO	CaO	Na_2O	Cr_2O_3	Total
2089.00	ZX	53.41	0.15	1.50	4.01	0.14	17.15	23.16	0.06	0.38	99.96
2089.00	ZW	53.63	0.17	1.27	3.80	0.14	17.03	23.25	0.09	0.35	99.73
2090.90	ZZ	53.40	0.13	2.19	3.70	0.11	16.53	23.22	0.08	0.37	99.83
2090.90	ZZ	53.59	0.11	1.76	3.72	0.13	16.49	23.82	0.06	0.26	99.94
2090.90	ZZ	53.60	0.17	1.50	3.72	0.14	16.91	23.32	0.05	0.33	99.74
2090.90	ZZ	53.45	0.15	1.72	3.91	0.13	16.78	23.18	0.08	0.33	99.73
2091.10	XA	53.61	0.09	2.20	4.82	0.14	18.84	19.22	0.11	0.40	99.43
2091.10	XC	53.63	0.15	2.26	4.33	0.14	18.41	20.21	0.09	0.38	99.60
2091.10	XR	53.44	0.13	2.20	4.00	0.13	17.23	21.86	0.11	0.28	99.38
2091.10	XQ	53.36	0.09	2.34	4.02	0.14	17.16	22.19	0.13	0.51	99.94
2093.65	XJ	53.07	0.11	1.92	3.81	0.14	18.19	21.41	0.06	0.05	99.16
2093.65	XK	53.24	0.09	2.06	3.72	0.11	17.56	21.93	0.06	0.40	99.17
2093.65	XL	53.31	0.09	1.99	3.51	0.13	17.27	22.58	0.09	0.47	99.44
2094.00	XA	53.75	0.15	1.21	3.03	0.13	16.96	23.89	0.11	0.30	99.53
2094.00	XD	53.22	0.13	2.49	3.67	0.11	17.51	22.28	0.11	0.37	99.89
2094.00	XJ	53.76	0.17	1.58	3.18	0.11	17.03	23.50	0.12	0.51	99.96
2094.00	YA	53.45	0.13	2.22	3.32	0.11	17.21	22.66	0.26	0.37	99.73
2094.00	YB	53.53	0.09	2.12	3.56	0.11	17.74	22.20	0.12	0.47	99.94
2095.20	YQ	52.59	0.13	2.26	4.14	0.13	16.94	22.17	0.13	0.54	99.03
2095.20	YR	53.00	0.17	2.18	4.29	0.11	16.87	22.22	0.60	0.37	99.37
2095.20	YT	53.37	0.11	2.31	4.08	0.16	16.20	22.60	0.14	0.42	99.39
2095.20	YU	53.13	0.15	2.25	4.60	0.14	17.57	21.35	0.13	0.37	99.69
2208.90	XV	52.74	0.11	2.46	3.95	0.13	16.77	22.46	0.08	0.94	99.64
2208.90	XX	52.70	0.09	2.12	4.15	0.14	17.37	22.00	0.08	1.01	99.66
2208.90	XY	52.47	0.09	2.26	3.99	0.14	16.74	22.34	0.11	1.03	99.17
2208.90	XZ	53.89	0.08	1.83	4.81	0.16	19.37	18.67	0.05	0.78	99.64
2210.20	YV	53.28	0.13	2.25	4.60	0.16	17.79	21.28	0.11	0.40	100.00
2210.20	YW	52.45	0.17	2.38	4.09	0.13	16.62	22.63	0.17	0.56	99.20
2210.20	YX	52.59	0.11	2.15	4.32	0.16	17.47	21.70	0.11	0.44	99.05
2210.20	YY	52.59	0.19	2.16	4.27	0.14	17.09	22.09	0.13	0.45	99.11
2210.20	YZ	53.17	0.13	2.07	4.50	0.14	17.74	21.56	0.09	0.40	99.80
2210.20	XA	53.75	0.11	2.05	5.98	0.17	20.90	16.54	0.08	0.38	99.96
2211.35	YL	53.93	0.13	1.00	3.25	0.13	16.64	23.78	0.14	0.21	99.21
2211.35	YA	53.46	0.11	2.03	4.01	0.14	17.10	22.53	0.13	0.42	99.93
2211.35	YB	53.35	0.08	2.27	3.95	0.16	17.61	21.86	0.11	0.40	99.79
2211.35	YH	53.34	0.09	2.29	4.21	0.14	17.84	21.36	0.14	0.47	99.88
2211.35	YK	53.27	0.11	2.44	4.41	0.14	17.61	21.27	0.14	0.54	99.93
2212.40	XB	53.48	0.11	2.03	3.97	0.13	17.14	23.08	0.14	0.14	100.22
2212.40	XI	52.71	0.15	2.58	4.37	0.16	17.21	21.98	0.17	0.49	99.82
2212.40	XJ	52.90	0.15	2.18	4.04	0.14	16.68	23.23	0.14	0.47	99.93
2212.40	XK	52.33	0.13	2.62	3.94	0.13	16.29	23.41	0.09	0.47	99.41
2215.20	YS	53.49	0.13	1.68	3.48	0.14	16.51	23.89	0.13	0.30	99.75
2215.20	YT	53.51	0.11	2.48	5.20	0.16	19.43	18.35	0.13	0.47	99.83
2215.20	YU	53.35	0.19	2.16	4.55	0.14	17.31	21.62	0.13	0.43	99.88
2215.20	YY	53.21	0.17	2.07	3.91	0.13	16.40	23.42	0.14	0.42	99.87
2215.20	YZ	53.35	0.08	1.88	4.39	0.13	17.72	21.52	0.13	0.50	99.70
2215.20	XK	53.42	0.15	1.76	3.84	0.13	16.28	23.72	0.09	0.40	99.79
2215.20	XL	53.98	0.15	1.23	3.48	0.13	16.43	23.85	0.14	0.28	99.67
2216.50	XG	53.45	0.09	1.88	4.23	0.16	18.12	20.76	0.06	0.45	99.20
2216.50	XH	53.20	0.13	1.98	3.99	0.14	17.19	22.33	0.11	0.37	99.44

TABLE 2. (cont.)

Depth (m)	ID	SiO_2	TiO_2	Al_2O_3	FeO*	MnO	MgO	CaO	Na_2O	Cr_2O_3	Total
2216.50	XJ	53.07	0.08	2.16	4.48	0.16	18.29	20.99	0.09	0.56	99.88
2216.50	XN	53.20	0.09	2.11	4.51	0.16	17.82	21.41	0.11	0.40	99.81
2216.50	XP	53.26	0.08	2.16	4.74	0.14	18.80	19.68	0.08	0.43	99.37
2216.50	XR	53.23	0.09	2.03	4.32	0.16	18.71	20.16	0.11	0.54	99.35
2216.50	XS	53.57	0.08	1.83	4.78	0.14	19.13	19.20	0.09	0.47	99.29
2217.60	XN	53.68	0.08	2.13	4.61	0.13	17.95	20.67	0.17	0.47	99.89
2217.60	XO	53.54	0.11	2.13	4.54	0.14	17.62	21.06	0.14	0.45	99.73
2217.60	XP	53.30	0.11	2.28	4.18	0.11	16.89	21.90	0.16	0.44	99.37
2217.60	XK	53.12	0.19	2.05	4.02	0.14	16.38	23.30	0.17	0.44	99.81
2217.60	XL	53.45	0.11	2.13	4.32	0.14	17.76	21.25	0.16	0.44	99.76
2217.60	XQ	53.32	0.15	2.02	4.30	0.14	16.88	22.53	0.16	0.44	99.94
2218.40	YQ	52.76	0.17	2.18	4.21	0.13	17.20	22.01	0.13	0.44	99.23
2218.40	YV	52.77	0.13	2.15	4.58	0.14	17.70	21.44	0.09	0.43	99.43
2218.40	XW	52.94	0.15	2.17	4.46	0.16	17.57	21.53	0.14	0.45	99.57
2218.40	XY	53.18	0.15	2.20	4.28	0.14	17.12	21.86	0.14	0.44	99.51
2220.45	XV	53.00	0.11	2.27	4.16	0.14	17.47	21.46	0.09	0.54	99.24
2220.45	XX	53.80	0.11	2.20	4.71	0.16	18.55	19.95	0.08	0.50	100.06
2220.45	XC	53.41	0.09	2.09	4.58	0.16	18.27	20.58	0.13	0.56	99.87
2220.45	XA	53.24	0.15	2.02	4.19	0.16	17.43	22.16	0.06	0.51	99.92
2220.45	XB	53.86	0.06	1.53	4.35	0.14	18.49	20.79	0.09	0.64	99.95
2220.45	XC	53.11	0.11	2.25	4.42	0.13	17.96	21.17	0.09	0.54	99.78
2222.00	ZZ	52.88	0.17	2.40	3.94	0.14	16.99	22.80	0.09	0.51	99.92
2222.00	ZZ	52.71	0.11	2.50	3.84	0.13	16.74	23.21	0.13	0.44	99.81
2222.00	ZZ	53.02	0.19	2.40	3.81	0.13	16.99	22.80	0.14	0.45	99.93
2222.00	ZZ	53.50	0.13	1.77	3.55	0.14	17.16	22.90	0.09	0.65	99.89
2222.90	XA	53.04	0.13	2.39	4.08	0.14	17.10	22.25	0.17	0.56	99.86
2222.90	XB	53.57	0.11	2.27	4.18	0.13	17.93	20.97	0.09	0.54	99.79
2222.90	XD	53.21	0.11	2.25	4.07	0.13	17.88	21.66	0.13	0.52	99.96
2222.90	XF	53.81	0.09	2.00	4.08	0.14	17.87	21.27	0.09	0.54	99.89
2222.90	XH	53.37	0.09	1.88	4.09	0.14	18.07	21.62	0.13	0.45	99.84
2222.90	XI	53.31	0.11	2.31	4.05	0.14	17.74	21.39	0.11	0.56	99.72
2222.90	XJ	53.22	0.13	2.23	4.16	0.14	18.01	21.36	0.09	0.59	99.93
2222.90	XK	53.15	0.11	2.40	4.30	0.16	18.12	21.18	0.09	0.54	100.05
2222.90	XM	53.27	0.11	2.33	4.57	0.14	19.03	19.85	0.06	0.59	99.95
2224.20	-	53.27	0.11	2.47	3.90	0.13	17.18	22.56	0.06	0.61	100.29
2224.20	YL	52.27	0.13	2.69	4.09	0.14	16.61	22.71	0.11	0.52	99.27
2224.20	YM	53.18	0.09	1.83	3.69	0.13	17.14	22.34	0.09	0.66	99.15
2224.20	YN	52.63	0.13	2.47	4.02	0.13	17.29	22.18	0.08	0.58	99.51
2225.00	XC	52.64	0.13	2.34	4.28	0.11	18.09	21.44	0.08	0.56	99.67
2225.00	XE	53.48	0.09	2.22	4.71	0.14	18.90	19.58	0.09	0.68	99.89
2225.00	XF	53.56	0.08	1.95	4.44	0.13	18.13	20.88	0.08	0.64	99.89
2225.00	XG	53.41	0.11	2.25	4.44	0.17	18.01	20.95	0.08	0.49	99.91
2225.00	XH	53.22	0.08	2.08	4.05	0.13	17.62	21.91	0.09	0.68	99.86
2254.55	XR	52.69	0.09	2.32	3.85	0.13	17.06	22.05	0.11	0.89	99.19
2254.55	XT	52.56	0.15	2.70	3.42	0.13	16.36	23.64	0.09	0.42	99.47
2254.55	XU	53.31	0.09	2.48	4.64	0.16	19.47	18.84	0.08	0.68	99.75
2254.55	XZ	52.79	0.11	2.58	3.78	0.13	16.55	22.92	0.11	0.85	99.82
2254.55	XY	52.69	0.13	2.91	3.77	0.13	16.85	22.72	0.09	0.66	99.95
2255.70	XA	52.57	0.13	2.22	4.00	0.14	16.99	22.57	0.11	0.58	99.31
2255.70	XB	53.06	0.13	2.18	3.98	0.13	16.69	22.86	0.13	0.56	99.72

TABLE 2. (cont.)

Depth (m)	ID	SiO_2	TiO_2	Al_2O_3	FeO*	MnO	MgO	CaO	Na_2O	Cr_2O_3	Total
2255.70	XC	52.76	0.15	2.38	4.02	0.16	16.71	22.67	0.13	0.51	99.49
2255.70	XD	53.09	0.13	2.30	4.02	0.11	16.69	22.75	0.16	0.54	99.79
2255.70	XE	53.03	0.13	2.17	3.83	0.09	16.56	23.31	0.11	0.54	99.77
2255.70	XF	53.18	0.13	2.28	3.91	0.13	16.90	22.62	0.16	0.52	99.83
2255.70	XG	53.05	0.15	2.42	3.94	0.13	16.77	22.79	0.14	0.54	99.93
2255.70	XH	52.94	0.15	2.32	3.93	0.13	16.77	22.79	0.14	0.54	99.71
2256.90	WG	53.16	0.11	1.96	3.74	0.13	16.35	23.58	0.09	0.47	99.59
2256.90	WI	53.43	0.09	1.97	5.34	0.16	19.48	18.71	0.11	0.62	99.91
2256.90	WJ	53.09	0.11	2.35	4.04	0.14	17.23	22.02	0.13	0.58	99.69
2256.90	WK	53.32	0.15	2.36	4.01	0.14	16.86	22.13	0.16	0.56	99.69
2256.90	WM	53.00	0.13	2.33	4.50	0.13	17.46	21.80	0.11	0.54	100.00
2256.90	WQ	53.33	0.11	2.16	4.53	0.14	18.39	20.35	0.11	0.73	99.85
2258.00	YO	53.51	0.08	2.06	3.65	0.11	17.74	22.07	0.11	0.51	99.84
2258.00	YP	53.27	0.11	2.13	4.43	0.11	18.12	21.20	0.11	0.44	99.92
2258.00	YS	53.15	0.09	2.52	3.43	0.14	16.77	23.01	0.13	0.56	99.80
2258.00	YU	53.46	0.09	2.05	4.33	0.14	18.42	20.72	0.16	0.50	99.87
2258.00	YX	53.44	0.09	2.00	3.90	0.13	17.71	22.06	0.09	0.58	100.00
2258.00	YY	53.39	0.09	1.99	3.46	0.14	17.10	23.02	0.13	0.59	99.91
2258.80	XI	53.47	0.13	1.54	3.46	0.13	16.77	23.79	0.09	0.49	99.87
2258.80	XJ	53.27	0.11	2.03	3.94	0.16	16.95	22.82	0.11	0.49	99.88
2258.80	XK	53.57	0.11	1.95	3.93	0.13	17.00	22.49	0.09	0.51	99.78
2258.80	XL	53.32	0.13	2.16	4.01	0.14	17.07	22.63	0.13	0.45	100.04
2258.80	XM	53.33	0.11	2.14	3.87	0.14	17.12	22.61	0.09	0.54	99.95
2258.80	XN	52.91	0.15	2.12	4.11	0.14	16.96	22.49	0.09	0.51	99.48
2259.00	XA	53.33	0.15	2.48	3.69	0.13	16.93	22.48	0.13	0.59	99.91
2259.00	XB	53.36	0.09	2.14	3.59	0.14	17.90	21.60	0.08	0.65	99.55
2259.00	XD	53.43	0.11	2.25	3.60	0.13	18.17	21.50	0.09	0.66	99.94
2259.00	XI	53.38	0.09	2.07	4.16	0.14	18.33	21.07	0.08	0.66	99.98
2259.70	XG	53.34	0.13	1.90	3.72	0.14	16.37	23.66	0.19	0.49	99.94
2259.70	XH	53.00	0.19	2.19	4.32	0.13	16.25	23.21	0.17	0.49	99.95
2259.70	XI	53.33	0.09	1.72	3.86	0.13	16.38	23.80	0.14	0.45	99.90
2259.70	XK	53.62	0.09	2.13	4.01	0.14	18.02	21.13	0.16	0.59	99.89
2260.70	YG	53.10	0.15	1.99	4.29	0.14	17.98	21.49	0.13	0.59	99.86
2260.70	YH	53.20	0.15	2.01	4.02	0.14	16.62	22.98	0.14	0.56	99.82
2260.70	YQ	52.50	0.21	2.28	3.97	0.13	16.40	23.04	0.14	0.51	99.18
2260.70	YR	52.69	0.15	2.39	3.86	0.13	16.14	23.13	0.16	0.54	99.19
2260.70	XJ	53.23	0.15	2.13	4.51	0.14	17.58	21.64	0.13	0.52	100.03
2260.70	XK	53.11	0.15	2.06	4.08	0.13	16.96	22.21	0.19	0.52	99.41
2260.70	XL	53.10	0.27	1.50	4.08	0.13	16.45	22.79	0.27	0.56	99.15
2260.70	XM	52.75	0.17	1.99	4.26	0.14	16.67	22.51	0.16	0.49	99.14
2260.70	XO	53.25	0.13	1.99	3.87	0.11	16.62	22.79	0.16	0.56	99.48
2261.30	XH	52.96	0.17	2.65	3.83	0.13	16.67	22.52	0.09	0.84	99.86
2261.30	XI	52.87	0.13	2.62	3.88	0.14	17.52	21.93	0.09	0.87	100.05
2261.30	XJ	52.80	0.13	2.66	3.63	0.13	16.57	22.97	0.13	0.87	99.89
2261.30	XK	53.43	0.13	2.15	4.06	0.14	17.86	21.22	0.11	0.77	99.90
2261.30	XL	53.26	0.09	2.48	3.84	0.13	17.98	21.22	0.09	0.85	99.96
2261.30	XN	52.93	0.13	3.03	3.67	0.13	16.89	22.12	0.11	0.77	99.78
2261.30	XO	53.04	0.08	2.45	4.05	0.14	17.20	21.97	0.13	0.92	99.98
2261.30	XP	53.10	0.09	2.35	3.59	0.13	17.76	21.52	0.11	0.94	99.59
2262.00	YA	53.25	0.08	2.21	3.87	0.11	17.88	21.67	0.09	0.75	99.91

TABLE 2. (cont.)

Depth (m)	ID	SiO_2	TiO_2	Al_2O_3	FeO*	MnO	MgO	CaO	Na_2O	Cr_2O_3	Total
2262.00	YC	53.48	0.09	2.04	3.91	0.14	18.08	21.35	0.11	0.66	99.86
2262.00	YH	53.10	0.13	2.32	3.66	0.14	17.40	22.22	0.13	0.85	99.95
2262.00	YI	53.49	0.06	2.05	4.01	0.13	18.77	20.65	0.09	0.68	99.93
2262.00	XN	53.13	0.08	2.25	3.55	0.13	17.97	21.38	0.11	0.80	99.40
2262.00	XO	52.36	0.13	3.29	3.43	0.13	16.53	23.29	0.11	0.66	99.93
2262.00	XQ	53.32	0.13	2.25	3.78	0.16	18.07	21.29	0.11	0.80	99.91
2262.90	YA	53.43	0.17	2.30	4.02	0.14	16.94	22.18	0.13	0.63	99.94
2262.90	YC	53.39	0.09	2.18	3.79	0.13	16.89	22.78	0.13	0.70	100.08
2262.90	YE	53.03	0.15	2.55	4.33	0.14	17.18	21.84	0.14	0.59	99.95
2262.90	YD	53.18	0.13	2.25	3.88	0.14	16.26	22.92	0.14	0.68	99.58
2262.90	YF	53.47	0.11	2.19	4.34	0.14	17.46	21.20	0.17	0.64	99.72
2262.90	XN	53.46	0.11	1.51	3.49	0.13	16.61	24.27	0.06	0.28	99.92
2262.90	XO	52.95	0.17	2.42	3.98	0.14	16.54	23.01	0.11	0.66	99.98
2263.30	VB	53.33	0.11	2.24	3.86	0.14	16.93	22.65	0.13	0.68	100.07
2263.30	VC	53.37	0.08	2.10	3.88	0.13	17.72	21.33	0.13	0.78	99.52
2263.30	VI	53.33	0.09	2.22	3.81	0.13	17.33	22.15	0.11	0.73	99.90
2263.30	VJ	53.18	0.08	2.23	4.23	0.16	18.09	20.70	0.11	0.84	99.62
2263.30	VL	53.45	0.08	2.27	5.56	0.16	20.50	17.10	0.09	0.83	100.04
2263.30	VM	53.32	0.09	2.15	3.73	0.14	16.69	22.73	0.14	0.80	99.84
2263.30	VT	53.02	0.11	2.37	4.01	0.14	17.19	21.99	0.16	0.91	99.90

TABLE 3. Electron microprobe data for orthopyroxene in lower ultramafic cumulates from CY-4

Depth (m)	ID	SiO_2	TiO_2	Al_2O_3	FeO*	MnO	MgO	CaO	Na_2O	Cr_2O_3	Total
1744.80	XB	54.11	0.13	1.21	17.32	0.32	25.35	1.53	0.02	0.03	100.02
1744.80	XD	54.14	0.13	0.85	18.05	0.37	24.89	1.59	0.02	0.02	100.06
1744.80	XG	54.05	0.13	0.94	17.36	0.37	25.53	1.52	0.03	0.03	99.96
1744.80	XH	53.62	0.14	1.33	17.73	0.34	25.13	1.56	0.00	0.03	99.88
1744.80	XK	54.05	0.14	1.10	17.12	0.32	25.69	1.54	0.00	0.05	100.01
1744.80	XE	54.53	0.16	1.41	14.55	0.31	27.37	1.51	0.02	0.08	99.94
1744.80	XF	54.33	0.18	1.46	14.58	0.31	27.50	1.56	0.00	0.07	99.99
1744.80	XJ	54.37	0.13	1.24	14.92	0.28	27.38	1.53	0.00	0.07	99.92
1745.10	XS	55.35	0.09	1.34	11.15	0.26	29.79	1.55	0.02	0.12	99.67
1745.10	XT	55.51	0.11	1.32	11.02	0.25	29.79	1.66	0.02	0.12	99.80
1745.10	UN	55.40	0.11	1.33	11.29	0.23	30.52	0.76	0.00	0.12	99.76
1745.70	YV	55.65	0.13	1.34	10.80	0.25	30.01	1.59	0.03	0.12	99.92
1745.70	YX	55.63	0.13	1.36	10.76	0.26	30.03	1.62	0.02	0.12	99.93
1749.70	YX	55.43	0.07	1.34	9.92	0.23	30.61	1.82	0.02	0.08	99.52
1749.70	XB	55.07	0.11	1.21	11.64	0.26	30.11	0.80	0.02	0.07	99.29
1749.70	XF	55.33	0.13	1.35	11.76	0.25	29.97	1.10	0.00	0.08	99.97
1749.70	YT	55.28	0.15	1.30	12.10	0.26	29.27	1.55	0.00	0.07	99.98

TABLE 3. (cont.)

Depth (m)	ID	SiO_2	TiO_2	Al_2O_3	FeO*	MnO	MgO	CaO	Na_2O	Cr_2O_3	Total
1749.70	YU	55.56	0.07	1.30	10.45	0.27	30.35	1.87	0.02	0.10	99.99
1749.70	YV	55.79	0.07	1.32	10.14	0.23	30.55	1.78	0.00	0.10	99.98
1749.70	XH	55.78	0.07	1.21	11.40	0.25	30.45	0.72	0.00	0.07	99.96
1750.05	XB	54.96	0.13	1.28	12.09	0.23	29.20	1.63	0.00	0.08	99.60
1750.05	XF	55.11	0.11	1.32	12.61	0.25	28.74	1.72	0.03	0.10	99.99
1750.05	XG	55.14	0.11	1.30	12.79	0.30	28.54	1.67	0.02	0.10	99.97
1750.50	XG	55.25	0.11	1.24	12.81	0.30	29.43	0.73	0.00	0.08	99.95
1750.50	XH	54.97	0.13	1.36	13.17	0.28	27.91	1.70	0.00	0.10	99.62
1750.50	XJ	54.48	0.11	1.28	13.31	0.26	28.05	1.67	0.00	0.08	99.24
1750.50	XX	55.48	0.15	1.21	11.98	0.28	29.50	1.28	0.00	0.07	99.95
1750.80	ZO	55.12	0.11	1.37	11.68	0.23	29.34	1.69	0.00	0.12	99.66
1750.80	ZR	55.27	0.09	1.32	11.15	0.25	29.83	1.69	0.00	0.07	99.67
1750.80	ZT	55.37	0.09	1.28	11.83	0.23	29.42	1.61	0.00	0.10	99.93
1750.80	ZU	55.81	0.07	1.30	10.74	0.23	29.87	1.77	0.00	0.08	99.87
1751.75	XL	55.90	0.09	1.30	9.87	0.23	30.68	1.67	0.02	0.10	99.84
1751.75	XM	55.51	0.11	1.32	11.24	0.25	29.52	1.71	0.02	0.10	99.78
1751.75	XN	55.92	0.07	1.30	10.23	0.22	30.42	1.75	0.02	0.12	100.05
1752.50	XC	55.61	0.09	1.36	11.20	0.23	29.52	1.76	0.00	0.08	99.85
1752.50	ZH	55.66	0.07	1.27	10.31	0.25	29.79	1.75	0.00	0.10	99.20
1752.50	ZI	55.81	0.07	1.29	8.88	0.22	30.83	1.94	0.00	0.12	99.16
1752.50	ZM	55.83	0.07	1.30	10.33	0.23	30.10	1.74	0.00	0.10	99.70
1830.90	XW	56.12	0.09	1.43	8.92	0.20	31.19	1.74	0.03	0.20	99.92
1830.90	XZ	56.18	0.09	1.36	8.53	0.22	31.55	1.73	0.03	0.25	99.94
1830.90	YY	55.76	0.09	1.41	9.20	0.22	31.27	1.71	0.02	0.22	99.90
1832.20	YT	56.15	0.09	1.36	8.75	0.20	30.99	1.71	0.02	0.20	99.47
1832.20	WB	56.56	0.13	1.41	8.85	0.20	31.10	1.58	0.02	0.20	100.05
1835.60	XK	55.52	0.09	1.47	10.82	0.23	29.66	1.74	0.02	0.20	99.75
1835.60	XN	55.46	0.05	1.50	9.85	0.22	31.35	0.85	0.02	0.25	99.55
1835.60	XP	55.34	0.09	1.64	10.93	0.25	30.33	0.95	0.02	0.17	99.72
1835.60	XT	55.45	0.07	1.65	9.53	0.22	30.61	1.97	0.02	0.24	99.76
1835.60	VR	55.66	0.11	1.34	10.95	0.22	30.21	1.19	0.02	0.17	99.87
1837.05	XX	55.52	0.09	1.57	10.63	0.23	30.04	1.65	0.03	0.22	99.98
1837.05	XZ	55.62	0.09	1.50	10.71	0.23	30.63	1.06	0.03	0.20	100.07
1837.05	YA	55.33	0.09	1.46	10.74	0.23	30.32	1.18	0.02	0.20	99.57
1837.05	YD	55.10	0.09	1.26	11.74	0.30	30.11	0.62	0.03	0.15	99.40
1838.00	XQ	55.79	0.09	1.26	10.92	0.23	30.75	0.63	0.02	0.17	99.86
1838.00	XR	55.59	0.11	1.34	10.77	0.23	30.21	1.62	0.02	0.18	100.07
1838.00	XU	55.65	0.09	1.48	9.78	0.23	30.54	1.72	0.02	0.22	99.73
1838.00	XV	55.70	0.07	1.43	8.62	0.22	31.42	1.80	0.02	0.20	99.48
1838.00	XP	55.49	0.09	1.32	10.85	0.25	30.63	1.06	0.03	0.22	99.94
1838.40	XL	55.70	0.09	1.23	10.58	0.25	30.53	0.98	0.02	0.18	99.56
1838.40	XP	55.67	0.07	1.64	11.07	0.25	30.50	0.59	0.02	0.17	99.98
1838.40	XQ	55.59	0.09	1.45	11.14	0.26	29.79	1.23	0.02	0.18	99.75
1838.40	XS	55.50	0.11	1.43	11.36	0.25	29.38	1.62	0.02	0.12	99.79
1884.25	VE	55.91	0.09	1.57	9.78	0.20	31.19	0.91	0.00	0.30	99.95
1884.25	VJ	55.28	0.07	1.60	10.22	0.22	31.38	0.69	0.05	0.32	99.83
1884.25	VK	55.82	0.09	1.59	9.94	0.22	30.69	1.32	0.02	0.32	100.01
1884.25	VM	55.61	0.09	1.57	9.71	0.20	30.80	1.67	0.02	0.29	99.96
1884.25	XD	55.47	0.07	1.57	9.75	0.22	30.89	1.75	0.02	0.29	100.03
1885.50	ZB	55.21	0.07	1.48	11.73	0.23	29.48	1.38	0.03	0.27	99.88

TABLE 3. (cont.)

Depth (m)	ID	SiO_2	TiO_2	Al_2O_3	FeO*	MnO	MgO	CaO	Na_2O	Cr_2O_3	Total
1885.50	ZH	55.65	0.05	1.45	10.51	0.22	29.97	1.92	0.02	0.28	100.07
1885.50	ZI	55.23	0.11	1.46	10.88	0.23	30.12	1.55	0.02	0.17	99.77
1885.50	ZK	55.34	0.09	1.45	11.26	0.20	29.19	2.16	0.03	0.22	99.94
1886.45	XX	56.04	0.09	1.50	10.19	0.25	30.28	1.31	0.03	0.27	99.96
1886.45	XX	55.69	0.11	1.45	10.74	0.25	29.80	1.45	0.03	0.33	99.85
1886.45	XX	55.78	0.07	1.63	9.97	0.20	30.92	0.95	0.00	0.27	99.79
1886.45	XX	56.14	0.07	1.39	10.30	0.23	30.71	0.86	0.02	0.28	100.00
1886.55	XS	55.49	0.09	1.52	9.87	0.23	30.84	1.70	0.00	0.22	99.96
1886.55	XY	55.53	0.09	1.84	9.93	0.22	30.83	1.28	0.00	0.25	99.97
1886.55	XW	55.46	0.09	1.50	9.96	0.22	30.79	1.72	0.02	0.22	99.98
1887.60	VB	55.06	0.11	1.55	10.23	0.25	30.81	1.57	0.02	0.23	99.83
1887.60	VF	55.61	0.07	1.47	9.79	0.22	30.24	2.17	0.02	0.24	99.93
1887.60	VW	55.74	0.09	1.53	10.51	0.23	30.85	0.98	0.02	0.27	100.22
1888.30	VK	55.53	0.09	1.55	10.38	0.23	30.69	1.12	0.02	0.23	99.84
1888.30	VL	55.12	0.09	1.55	10.52	0.23	30.95	1.25	0.00	0.20	99.91
1889.30	XK	55.87	0.13	1.45	10.36	0.25	29.96	1.75	0.00	0.23	100.00
1890.70	ZZ	55.60	0.11	1.52	10.22	0.23	30.16	1.80	0.03	0.18	99.85
1890.70	ZZ	55.69	0.09	1.64	10.42	0.23	30.79	0.73	0.02	0.20	99.81
1891.75	XZ	55.73	0.07	1.45	10.37	0.19	30.26	1.72	0.02	0.17	99.98
1891.75	XC	55.46	0.09	1.54	10.22	0.23	30.43	1.74	0.02	0.25	99.98
1891.75	XG	55.05	0.16	0.88	12.91	0.28	29.43	1.09	0.02	0.18	100.00
1892.20	XK	55.46	0.13	1.61	10.19	0.23	29.95	1.87	0.02	0.23	99.69
1892.20	XO	55.87	0.11	1.47	10.33	0.23	29.82	1.68	0.00	0.23	99.74
1892.20	XS	56.44	0.09	1.54	8.74	0.19	30.84	1.77	0.02	0.30	99.93
1892.20	YH	54.99	0.11	2.04	10.55	0.25	30.13	1.22	0.02	0.23	99.54
1892.20	XE	55.55	0.13	1.61	10.04	0.23	30.31	1.80	0.02	0.25	99.94
1892.20	XG	54.98	0.11	1.52	10.96	0.26	29.92	1.82	0.02	0.20	99.79
1892.20	XI	54.78	0.09	1.48	10.87	0.25	30.21	1.75	0.00	0.22	99.65
1892.20	XP	54.88	0.07	1.50	11.50	0.26	29.93	0.07	0.03	0.22	99.88
1892.20	XQ	55.33	0.11	1.54	10.51	0.23	30.34	1.64	0.00	0.18	99.88
1893.00	VU	55.49	0.07	1.59	8.85	0.22	31.46	1.73	0.02	0.34	99.77
1893.00	VV	55.57	0.07	1.52	9.74	0.23	30.73	1.70	0.02	0.30	99.88
1893.00	VW	55.52	0.07	1.50	10.12	0.20	30.48	1.72	0.02	0.30	99.93
1893.00	VX	55.31	0.07	1.48	10.59	0.25	30.21	1.62	0.00	0.27	99.80
1894.10	XS	56.15	0.09	1.50	10.11	0.23	30.52	1.77	0.00	0.20	100.57
1894.10	XT	56.21	0.07	1.17	10.43	0.25	31.29	0.70	0.00	0.18	100.20
1894.10	XU	55.91	0.05	1.43	9.78	0.20	30.62	1.68	0.00	0.25	99.92
1895.40	YH	55.44	0.11	1.59	10.30	0.22	30.44	1.51	0.05	0.28	99.94
1895.40	YT	55.36	0.11	2.25	9.97	0.22	30.12	1.52	0.05	0.25	99.85
1895.40	YM	55.06	0.15	1.52	10.30	0.25	30.48	1.48	0.02	0.27	99.53
1895.40	YO	55.67	0.07	1.08	10.05	0.23	30.50	0.68	0.02	0.23	99.53
1896.30	ZI	55.69	0.09	1.54	10.33	0.22	30.23	1.41	0.02	0.25	99.78
1896.30	ZJ	55.30	0.11	2.15	10.60	0.25	30.11	1.23	0.02	0.22	99.99
1896.30	ZK	55.15	0.07	1.48	10.39	0.25	30.25	1.18	0.02	0.22	99.01
1896.30	ZL	55.30	0.07	1.46	10.78	0.25	30.26	1.48	0.03	0.25	99.88
1896.90	XR	55.95	0.11	1.15	10.18	0.22	31.20	0.85	0.03	0.25	99.94
1896.90	XY	55.71	0.09	1.48	10.33	0.25	30.65	1.39	0.02	0.23	100.10
1896.90	YL	55.69	0.09	1.50	10.08	0.23	30.02	1.82	0.00	0.22	99.65
1897.80	XJ	55.66	0.09	1.41	10.51	0.25	30.81	1.03	0.02	0.17	99.95
1897.80	XL	55.39	0.07	1.61	9.21	0.20	30.61	1.77	0.02	0.35	99.23

TABLE 3. (cont.)

Depth (m)	ID	SiO_2	TiO_2	Al_2O_3	FeO*	MnO	MgO	CaO	Na_2O	Cr_2O_3	Total
1897.80	XT	55.64	0.11	1.19	10.95	0.25	30.26	1.32	0.00	0.30	100.02
1899.80	XA	56.06	0.07	1.52	9.47	0.22	30.38	1.90	0.02	0.30	99.94
1899.80	XD	55.68	0.07	1.48	10.33	0.22	30.27	1.26	0.02	0.28	99.61
1899.80	XP	55.66	0.09	1.47	10.20	0.23	29.92	1.88	0.03	0.23	99.71
1900.30	YE	56.04	0.07	1.43	9.51	0.22	30.66	1.68	0.02	0.29	99.92
1900.30	YF	55.34	0.11	1.59	10.12	0.20	30.45	1.75	0.02	0.29	99.87
1900.30	YG	55.66	0.11	1.52	10.27	0.23	29.82	2.01	0.02	0.23	99.87
1900.30	YL	55.40	0.07	1.50	10.08	0.23	30.53	1.74	0.00	0.22	99.77
2087.40	YS	55.99	0.07	1.54	8.62	0.19	31.49	1.84	0.02	0.22	99.98
2087.40	YT	55.52	0.06	1.50	8.78	0.22	31.08	1.66	0.00	0.22	99.04
2087.40	XT	55.69	0.05	1.43	9.93	0.25	30.77	1.84	0.02	0.18	100.16
2087.40	XU	55.37	0.07	1.37	10.70	0.23	30.12	1.81	0.00	0.17	99.84
2089.00	ZU	56.26	0.07	0.99	9.61	0.22	32.21	0.62	0.00	0.18	100.16
2089.00	ZM	55.76	0.09	1.35	9.87	0.22	31.27	1.32	0.02	0.15	100.05
2091.10	XD	55.67	0.06	1.50	9.02	0.20	31.83	1.34	0.02	0.20	99.84
2091.10	XF	56.00	0.05	1.43	9.45	0.23	30.69	1.78	0.00	0.19	99.82
2091.10	XG	55.93	0.07	1.46	9.45	0.22	31.28	1.29	0.02	0.20	99.92
2091.10	XH	56.43	0.09	0.63	10.29	0.22	31.55	0.56	0.00	0.17	99.94
2091.10	XI	55.85	0.07	1.52	9.21	0.20	30.80	2.07	0.00	0.20	100.00
2091.10	XJ	56.08	0.06	1.47	8.95	0.19	30.88	1.76	0.02	0.19	99.60
2094.00	YC	56.34	0.09	1.41	8.48	0.19	31.84	1.61	0.02	0.17	100.15
2095.20	YP	55.44	0.07	1.46	9.65	0.23	30.93	1.34	0.00	0.20	99.32
2095.20	YS	55.28	0.09	1.39	9.71	0.27	30.82	1.65	0.02	0.24	99.47
2211.35	YM	56.05	0.06	1.52	9.06	0.22	31.01	1.76	0.02	0.27	99.97
2211.35	YN	55.99	0.07	1.48	9.25	0.22	31.09	1.61	0.02	0.25	99.98
2211.35	YP	56.02	0.09	1.54	8.91	0.22	31.25	1.65	0.05	0.24	99.97
2211.35	XJ	55.98	0.07	1.58	8.75	0.22	31.12	1.81	0.02	0.27	99.82
2212.40	XA	55.84	0.07	1.50	9.75	0.22	30.55	1.77	0.00	0.24	99.94
2215.20	XA	55.94	0.11	1.50	9.35	0.22	31.11	1.27	0.02	0.25	99.77
2215.20	XB	55.92	0.09	1.54	9.31	0.23	30.94	1.54	0.02	0.25	99.84
2215.20	XC	55.79	0.09	1.52	9.29	0.20	31.17	1.47	0.02	0.25	99.80
2215.20	XD	56.08	0.09	1.52	9.20	0.22	31.34	1.48	0.00	0.24	100.17
2215.20	XF	55.67	0.07	1.57	9.90	0.25	31.23	0.92	0.02	0.27	99.90
2215.20	XG	55.91	0.09	1.48	9.47	0.23	31.01	1.45	0.03	0.25	99.92
2217.60	XM	56.24	0.09	1.56	8.44	0.20	31.37	1.63	0.03	0.27	99.83
2220.45	XW	55.13	0.05	2.31	9.54	0.25	31.14	0.75	0.00	0.34	99.51
2220.45	XD	55.64	0.09	1.61	9.17	0.20	31.40	1.60	0.02	0.25	99.98
2220.45	XE	55.93	0.07	1.65	8.93	0.22	31.20	1.65	0.02	0.25	99.88
2220.45	XH	55.72	0.09	1.54	9.03	0.23	31.38	1.64	0.00	0.29	99.92
2220.45	XI	55.99	0.07	1.50	8.87	0.20	31.32	1.71	0.02	0.29	99.97
2256.90	WH	55.87	0.09	1.56	9.04	0.23	31.22	1.28	0.00	0.25	99.54
2256.90	WS	55.54	0.09	1.54	9.22	0.19	31.13	1.29	0.00	0.27	99.27
2256.90	WP	55.98	0.09	1.61	9.07	0.22	30.99	1.68	0.00	0.25	99.89
2259.70	XJ	55.72	0.09	1.54	9.49	0.22	31.03	1.48	0.03	0.27	99.87
2259.70	XL	55.90	0.09	1.54	9.34	0.22	31.19	1.50	0.06	0.22	100.06
2259.70	XM	55.84	0.07	1.58	8.93	0.20	30.86	2.29	0.05	0.25	100.07
2260.70	YJ	55.59	0.09	1.61	9.46	0.20	30.73	1.39	0.02	0.32	99.41
2260.70	XN	55.66	0.07	1.54	9.56	0.25	30.46	1.35	0.02	0.29	99.20
2260.70	XO	55.50	0.09	1.59	9.64	0.22	30.69	1.21	0.00	0.29	99.23
2263.30	VH	55.83	0.07	1.57	8.99	0.23	31.28	1.57	0.02	0.27	99.83

Texturally the ultramafic lithologies are medium to coarse grained rocks showing adcumulus or mesocumulate textures, with rapid variations in grain size developed within an individual layer. Olivine occurs almost exclusively as a cumulus phase. In the lowermost profiles, below 2254 m, the olivine grains are variably serpentinised (10-100%), contain trails of melt/fluid inclusions, and show evidence of plastic deformation. Modally the most significant phase is clinopyroxene, which shows both cumulus and intercumulus habit, is often twinned and occasionally displays an intergrowth with orthopyroxene. It is notable that as deep as 2000 m the clinopyroxene shows the effects of hydrothermal alteration being replaced by brown amphibole/actinolite, with sulphides, typically pyrrhotite and pentlandite, present around the grain boundaries. Orthopyroxene is predominantly an intercumulus phase, becoming a cumulus phase around 2095 m. The intercumulus orthopyroxene occur as poikilitic laths, up to 12 mm in long dimension, enclosing olivine and clinopyroxene grains. Relict plagioclase is present throughout the core, occurring as a rodingitised intercumulus phase in the lowermost core, becoming a cumulus phase towards the top of rhythmic units around 1884 m. Small subhedral chrome-spinel grains which show a close spatial association with clinopyroxene grains, are a ubiquitous accessory phase throughout the lowermost part of the core.

Mineral chemistry data for olivine, clinopyroxene and orthopyroxene from these intervals are presented in Tables 1-3. The entire lower ultramafic unit has been analysed by Thy et .al. (1989) at a sampling density of about one specimen every six metres. Vertical profiles for the most primitive Mg number measured at any one depth for olivine, clinopyroxene and orthopyroxene are shown in Figure 2 using data from this study and Thy et al. (1989). As has been noted by other workers (e.g. Brace et al., 1987; Laurent, 1987; Thy et al., 1987) an overall trend to lower Mg numbers is discernible with decreasing depth. For example, over the 520 m thickness of the lower ultramafic cumulates the ambient olivine composition could be said to decrease from Fo87 to Fo81. What has been ignored however, and is clear from both the data presented in this study and by Thy et al. (1989), is that rapid compositional gradients are superimposed on this gradual trend. To illustrate, at about 1830 m and over less than one metre the olivine composition changes from Fo88 to Fo82, a change that is as great as the contrast seen over the entire lower ultramafic cumulates. Clearly, if such rapid compositional variation characterises the cumulate rocks of the Troodos ophiolite, then sampling on the scale of a metre or less is essential.

Rationale for erecting cyclic units

Profiles for four of the six closely sampled intervals are presented in Figures 3-6. Only profiles for olivine and clinopyroxene are given as orthopyroxene, plagioclase and spinel occur too infrequently to yield a continuous profile and only those elements or element ratios that display significant variation with height are shown.

Although the scale of sampling adopted in this study might be considered small compared to similar studies conducted on cumulates from other layered intrusions, it is evident that the rapidity of compositional variation with height requires a still finer scale study before unambiguous chemical trends could be confidently identified. Inevitably, then, the trends and resulting cyclic units identified on Figures 3-6 are to some extent interpretative. To maintain a consistency of interpretation from one interval to the next, the following rationale has been adopted:

1. Abrupt increases in the olivine mode were considered the best petrographic indicator of the onset of a new cyclic unit. In one case (see below) a sudden decrease in the orthopyroxene and plagioclase mode was used to define the start of a cyclic unit.

2. Following provisional division of an interval on the basis of modal variations in olivine, confirmatory evidence was sought in terms of phase chemistry. Because the Mg numbers and particularly the incompatible element contents of ferromagnesian silicates are likely to suffer re-equilibration by percolating intercumulus liquid during solidification of the cumulate pile, most weight was placed on compatible element abundances that possess the lowest transport velocities (McKenzie, 1984) and are therefore the least likely to suffer redistribution. In general a good correspondence was found between high olivine modes and high Cr_2O_3 contents in coexisting clinopyroxene. No significant variation could be detected in the NiO content of olivine; the average abundance (ca. 0.15 wt %) is less than half that usually found in olivines of similar Fo content from other ophiolite complexes.

3. Having strengthened the case for a cyclic unit by identifying strong correlations between olivine mode and compatible element abundance, trends were then drawn through the profiles to explore the degree of coherence to the cryptic variation overall. Because of the zoning shown by phases in any one sample for some elements or element ratios, trends have been drawn connecting points with the highest Mg number or compatible element abundance or the lowest incompatible element content. Given that orthocumulate processes are most likely to decrease Mg numbers or compatible element contents or increase incompatible element abundances, it is considered that this procedure yields trends closest to original primocryst compositions. Where an element or element ratio has behaved within a cyclic unit as would be expected during fractional crystallisation, a solid line has been drawn (a "normal" gradient); where the opposite has occurred a broken line is shown (a "reverse" gradient).

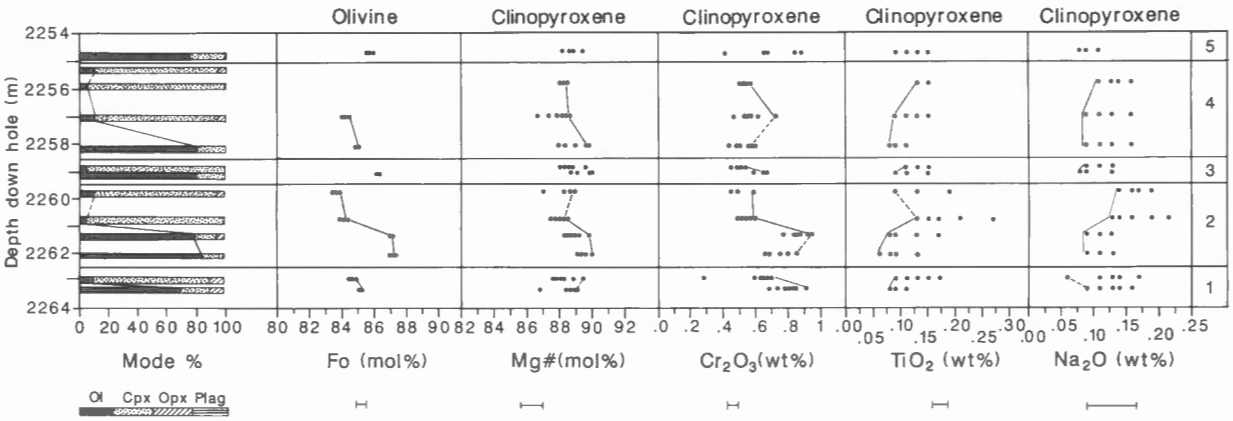

Figure 3: Vertical profiles for modal percentages and various chemical parameters for olivine and clinopyroxene in samples from Interval 1 (2254-2264 m). This interval has been subdivided into cycles based on criteria discussed in the main text; solid horizontal lines reflect confidence in subdivisions; broken horizontal lines reflect uncertainty. Solid lines connecting data points reflect trends expected during fractional crystallisation ("normal" gradients) whereas broken lines indicate the opposite ("reverse" gradients). Error bars indicating the 2σ uncertainty on an individual analysis are based on counting statistics and follow Browning (1982).

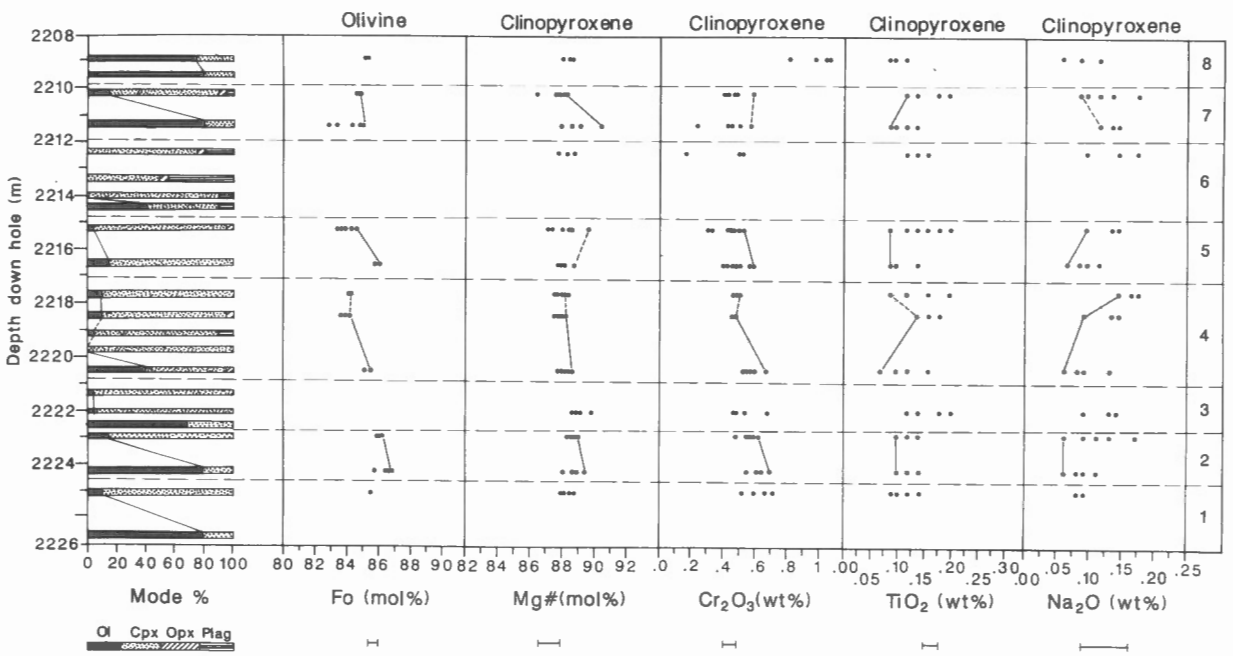

Figure 4: Vertical profiles for modal percentages and various chemical parameters for olivine and clinopyroxene in samples from Interval 2 (2208-2226 m). See caption to Figure 3 for detailed explanation.

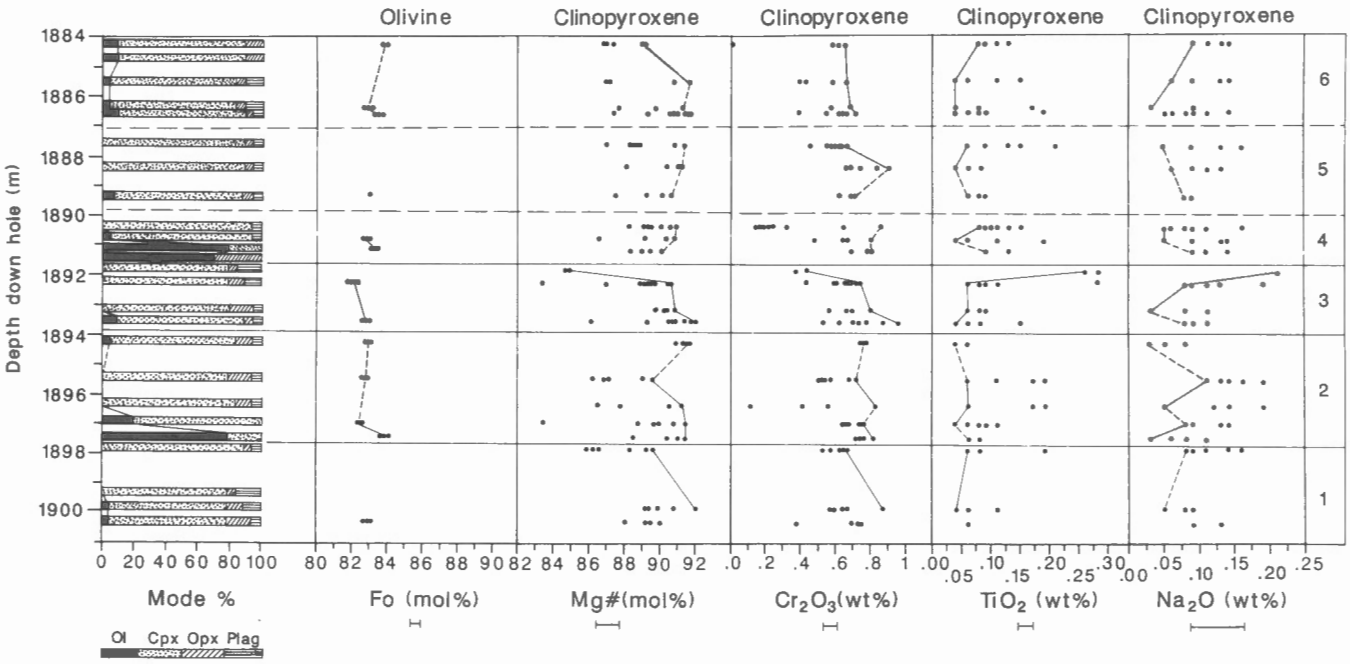

Figure 5: Vertical profiles for modal percentages and various chemical parameters for olivine and clinopyroxene in samples from Interval 4 (1884-1901 m). See caption to Figure 3 for detailed explanation.

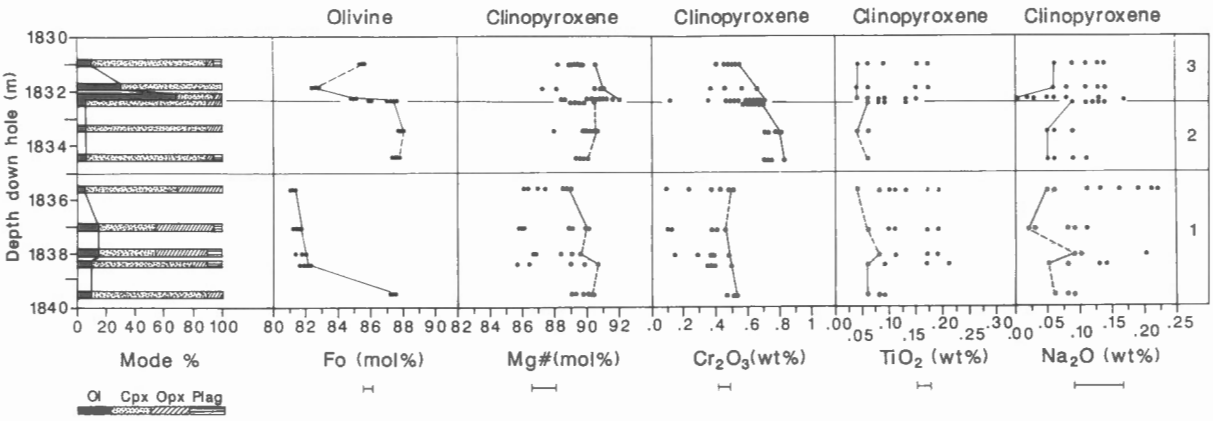

Figure 6: Vertical profiles for modal percentages and various chemical parameters for olivine and clinopyroxene in samples from Interval 5 (1830-1840 m). See caption to Figure 3 for detailed explanation.

Interval 1 (2254-2264 m)

Five cyclic units have been inferred for this interval (Figure 3). Cycles 2 and 4, the best defined, are about three metres in thickness. Although the Cr_2O_3 content of clinopyroxene is seen to increase concomitantly with olivine mode, the highest values occur at the middle rather than the base of the units. Rapid changes in composition are evident; for example, in Cycle 2 the olivine decreases in Fo content from 87 to 84 in just over two metres.

Interval 2 (2208-2227 m)

Eight cyclic units have been erected for this interval (Figure 4). As the sample density is low and mineral chemistry data is lacking, the units are based more on petrography than cryptic variation. Cycle 6 is characterised by the mode of plagioclase increasing to 30% at the top of the unit.

Interval 4 (1884-1901 m)

Five cycles have been identified in this interval (Figure 5) and the sampling density (about every 0.75 m) is sufficient for considerable confidence to be placed on the proposed interpretation. Again, cycle of the order of three metres in thickness are developed. Cycle 3 displays rapid normal compositional gradients; in less than two metres the Mg number of clinopyroxene decreases from 92 to 85. The top of Cycle 2 is noteworthy in that it displays a "cryptic regression" (Irvine pers. comm. in Komor et al., 1985); Mg numbers, compatible and incompatible elements all show a coherent reverse gradient prior to the onset of Cycle 3. Reverse gradients also characterise the entire thickness of Cycle 4; indeed, it might be argued that two successive reverse gradients succeed each other within this cyclic unit.

Interval 5 (1830-1840 m)

This interval (Figure 6), containing three cycles, contrasts with the other sections investigated in that the bases of cycles are not all marked by an increase in the olivine mode. The top of Cycle 1 is marked by a decrease in the mode of orthopyroxene and plagioclase, an increase in the Mg number of olivine and clinopyroxene, and an increase in the Cr_2O_3 content of clinopyroxene. Cycle 2 displays reverse gradients for Mg number in olivine and clinopyroxene. The division between cycles 2 and 3 has been made on the basis of the abrupt increase in olivine mode. This coincides with a rapid decrease in the Fo content of olivine and to a lesser extent in the Mg number of clinopyroxene. This trend in olivine composition is not sustained; the reversal higher in cycle 3 is not matched by changes in Mg number and Cr_2O_3 content of clinopyroxene. Little coherent behaviour can be discerned for incompatible elements in clinopyroxene within this interval.

DISCUSSION

It has been demonstrated that the lower ultramafic unit is characterised by well developed modal layering that defines ol + sp → ol + cpx → ol + opx → ol + cpx + opx + plag cyclic units on about a three metre scale. This small scale petrographic variation is accompanied by systematic and rapid changes in phase chemistry with height. The cryptic variation is perhaps surprising in its overall coherence; Mg numbers of ferromagnesian silicates and compatible element abundances decrease with height as incompatible element contents increase. What are the implications of these results for models of the magmatic evolution of the Troodos ophiolite and to basaltic magma chambers in general?

An open or closed system?

Recent work on cumulates from the CY-4 borehole by Thy et al. (1989), Brace et al. (1987) and Laurent (1987) have recognised the role of periodic replenishment by primitive magma to account for the cryptic variation shown by the gabbroic cumulates that dominate the upper portions of the borehole (Figure 1), but the magmatic evolution of the lower predominantly ultramafic unit is generally considered to be rather more mundane. Thy et al. (1989) summarise the currently accepted position: "The phase chemistry and layering of lower gabbroic and websteritic cumulates of the Troodos complex clearly suggest crystallisation in a relatively closed magma chamber within a slow- or non-spreading tectonic environment. On the other hand, the upper gabbros appear to reflect crystallisation in a relatively open magma chamber and consequently a higher spreading rate".

We contend that such conclusions regarding the magmatic evolution of the lower ultramafic cumulates are artifacts of an inappropriate scale of sampling. If resetting of Mg numbers and compatible element contents of ferromagnesian cumulus phases can be used to infer replenishment of a magma chamber by primitive parental magma (rather than being generated by some other process), then the data presented here demonstrate that the cumulates of the lower ultramafic unit in the CY-4 borehole crystallized in a thoroughly open system.

Magma chamber size?

If it can be assumed that over the period a particular cyclic unit crystallizes the melt is temporarily in a closed system, then it is instructive to calculate the volume of magma which fractionated to form the layers of cumulates of that cyclic unit. Browning (1984) has shown that the well known Rayleigh equation for fractional crystallisation can be rearranged to express the height of liquid column l that fractionated to produce a cyclic unit of thickness c

$$l = \frac{c}{[1-Cxl/Cxo]^{1/(D-1)}}$$

where Cxo and Cxl are the elemental concentrations of the first and last formed cumulates in the cycle and D is the bulk distribution coefficient for the element of interest. The ratio c/l is equal to the mass fraction of the original volume of liquid that has crystallized.

Of the sections studied, Cycle 3 of Interval 4 (Figure 5) is the best defined cyclic unit investigated. Over 1.65 metres the clinopyroxene mode remains uniform at 80%, and the Cr_2O_3 content of this phase decreases from 0.94 to 0.42 wt % (maximum values at any particular height). Given that clinopyroxene dominates the mineralogy of the fractionating assemblage and has a mineral-liquid distribution coefficient for Cr of 10 (Cox et al., 1979) we can make the simplifying assumption that the olivine, orthopyroxene and plagioclase contain negligible Cr which yields a bulk distribution coefficient of about 8. Substituting these values into the above expression yields

$$l = \frac{1.65}{[1-0.42/0.94]^{1/(8-1)}} = 1.80\ m.$$

If a less extreme case is taken like Cycle 5 of Interval 2 (Figure 4) a similar magma column height of 1.78 m for a cyclic unit 1.3 m thick is derived.

These results are impossible to reconcile with a well-mixed magma chamber of a vertical dimension comparable to the overall thickness of the Troodos cumulates (i.e. several kilometers). Using a similar approach on data from gabbroic cumulates from the Oman ophiolite Browning (1984) inferred magma column heights of about 100 m for a 30 m thick olivine gabbro cyclic unit, again orders of magnitude smaller than the total thickness of cumulates. Similar conclusions may be drawn from the work of Komor et al. (1985) on ultramafic cumulates from the Bay of Islands ophiolite.

Which magma chamber model?

It appears that the rate of change of compatible element chemistry with height in ophiolitic cumulates is too rapid to permit their formation from large (in comparison to the thickness of the cyclic units) bodies of magma. A number of magma chamber models could satisfy the paradoxical relationship between small calculated magma column heights and large overall thicknesses of ophiolitic cumulate sequences:

1. A large magma chamber that was in some way stratified so that a discrete volume of the magma body could behave temporarily as a smaller closed system for the period of crystallisation required to form the cumulate cyclic unit. This stratification may have been brought about by ponding of dense primitive replenishments at the base of the magma chamber (Huppert and Sparks, 1980) or by in situ development of double diffusive convection in response to thermal and chemical gradients established within the magma body (McBirney and Noyes, 1979; Turner and Chen, 1974).

2. A magma chamber with a rapidly subsiding floor might allow a large thickness of cumulate to form from a magma body with an otherwise limited vertical dimension (Dewey and Kidd, 1977).

3. Elthon et al. (1984) have suggested a model for the formation of ultramafic cumulates in the Bay of Islands ophiolite involving crystallisation within the mantle in a vertical feeder zone at depths exceeding 30 km. These ultramafic cumulates are then "conveyor-belted" up to form the lower portion of the oceanic crust. This model, which interestingly has much in common with that proposed by Reinhardt (1969) for Oman ophiolite, may fly in the face of conventional wisdom, but does offer a narrow conduit which might satisfy the requirement for a small fictive magma volume.

The nature of the replenishment process?

The sustained reverse gradients at the top of cycle 2 and forming the whole of Cycle 4 in Interval 4 (Figure 5) have also been documented from Oman (Browning, 1984) and Bay of Islands (Komor et al., 1985). It would appear that the bases of most cyclic units are marked by an abrupt shift in the phase chemistry of the cumulates. These rapid "resets" are interpreted in terms of an open system magma chamber model to reflect more-or-less instantaneous mixing of a primitive replenishing magma pulse. Sustained reverse gradients (or "cryptic regressions") are, on the other hand, interpreted to record a more gradual resetting of the magma chamber chemistry by a prolonged input of primitive magma without catastrophic mixing.

The role of compaction

McKenzie (1984) has argued that compaction of partially molten cumulate piles that are thicker than a kilometre should occur with accompanying upward migration of intercumulus liquid. If this process occurs it would be expected that the cumulate pile should behave in the manner of a chromatographic column; elements with a particular affinity to the matrix mineralogy should be strongly held whereas those which are highly incompatible should partition and move with the migrating intercumulus liquid. Such a mechanism should lead to dispersion of the original profiles of cryptic variation that were imposed on the cumulate profile during the fractional crystallisation and mixing processes that led to the formation of the cumulate cyclic units. The "decoupling" that sometimes occurs between incompatible elements (e.g. Ti and Na in clinopyroxene) and compatible elements (e.g. Cr in clinopyroxene, Ni in olivine) in gabbroic cumulates from the Oman ophiolite (Browning, 1984) might be attributed

to this process. However as far as the data presented here are concerned, the overall coherence in cryptic variation for all elements, compatible and incompatible, suggests such a process has not been extensive in effect. Why this should be so is presently unclear; however contrasts in residual porosity, cooling rates and the mechanical properties of the cumulate pile are likely to be important controlling factors.

CONCLUSIONS

The lower ultramafic cumulates of the CY-4 borehole show cyclic units defined by modal layering on about a three metre scale. The correspondence of these cyclic units with cryptic variation in mineral chemistry, the extreme rapidity of changes in cryptic variation, and the general coherence of all chemical parameters as a function of height, lead us to conclude that:

1. The ultramafic cumulates developed by fractional crystallisation is an open system magma chamber.

2. The calculated volume of the magma body contributing to the formation of any one cyclic unit was very small, being of similar magnitude to the scale of the cyclic layering itself; this imposes severe constraints on the magma chamber model adopted for the Troodos ophiolite.

3. The role of intercumulus melt migration has not been significant in substantially perturbing the primary magmatic chemical profile developed in the cumulate pile.

It should be stressed that no study of ophiolitic cumulates has yet addressed the problem of looking outside the vertical dimension; the results of Wilson et al. (1987) on the Fongen-Hyllingen Complex suggest that much is still to be learnt about cryptic variation in layered igneous rocks. More generally it is appropriate to emphasise the value of small scale (more than one sample per metre) investigations of layered intrusions by the highest precision analytical methods available. Energy dispersive (rather than wavelength dispersive) microprobe studies at a sampling density of one sample per six or ten metres on cumulates from the CY-4 borehole have led other workers (cf. Thy et al., 1988; Brace et al., 1987; Laurent, 1987) to some different, and in our view fallacious, conclusions.

ACKNOWLEDGEMENTS

The help and encouragement of Ian Gass were instrumental in ensuring the completion of this work. The following are thanked for their help in ensuring the rapid preparation of this paper: Paul Holbrook for data preparation; Jacqueline Hodkinson for typing; John Taylor, Andrew Lloyd and Sheila Ripper for diagrams; Andy Tindle for assistance with the microprobe.

REFERENCES

Allen, C.R.
1975: The petrology of a portion of the Troodos plutonic complex, Cyprus; unpublished Ph.D. thesis, University of Cambridge, England p. 1-161.

Brace, T., Moore, P., Case, G., Saunders, J., Xenophontos, C. and Malpas, J.
1987: Geology and petrochemistry of rocks from CY-4 borehole of the Cyprus crustal study project and the surrounding area; Ophiolites and Oceanic Lithosphere: Troodos 87 (abstract), Cyprus Geological Survey Department, Ministry of Agriculture and Natural Resources, p. 10.

Browning, P.
1982: The petrology, geochemistry and structure of the plutonic rocks of the Oman ophiolite; unpublished Ph.D. thesis, Open University, England, p. 1- 404.

Browning, P.
1984: Cryptic variation within the cumulate sequence of the Oman ophiolite: Magma chamber depth and petrological implications; *in* Ophiolites and Oceanic Lithosphere, ed. I. G. Gass, S. J. Lippard and A. W. Shelton; Blackwells, London, p. 72-82.

Cox, K., Bell, J.D. and Pankhurst, R.J.
1979: The Interpretation of Igneous Rocks; Allen and Unwin, London, p. 1-450.

Dewey, J.F. and Kidd, W.S.F.
1977: Geometry of plate accretion; Bulletin of the Geological Society of America, v. 88, p. 960-968.

Elthon, D., Casey, J.F. and Komor S.C.
1984: Cryptic mineral chemistry variations in a detailed traverse through the cumulate ultramafic rocks of the North Arm mountain massif of the Bay of Islands ophiolite, Newfoundland; *in* Ophiolites and Oceanic lithosphere, ed. I. G. Gass, S. J. Lippard and A.W. Shelton; Blackwells, London, p. 83-100.

Gass, I.G.
1980: The Troodos massif: Its role in the unravelling of the ophiolite problem and its significance in the understanding of plate margin processes; *in* Ophiolites, Proceedings of the International Ophiolite: Symposium, Cyprus, 1979, ed. A. Panayiotou; Cyprus Geological Survey Department, Ministry of Agriculture and Natural Resources, p. 23-25.

George, R.P.J.
1978: Structural petrology of the Olympus ultramafic complex in the Troodos ophiolite, Cyprus; Bulletin of the Geological Society of America, v. 89, p. 18-21.

Greenbaum, D.

1972a: Magmatic processes at ocean ridges: Evidence from the Troodos Massif, Cyprus; Nature, Physical Science, no. 80. v. 238, p. 18-21.

1972b: The geology and evolution of the Troodos plutonic complex and associated chromite deposits, Cyprus; unpublished Ph.D. thesis, University of Leeds, England, p. 1-142.

Huppert, H.E. and Sparks, R.S.J.

1980: The fluid dynamics of a basaltic magma chamber replenished by influx of hot, dense ultrabasic magma; Contributions to Mineralogy and Petrology, v. 75, p. 279-289.

Komor, S.C., Elthon, D. and Casey, J.F.

1985: Mineralogic variation in a layered ultramafic cumulate sequence at the North Arm mountain massif, Bay of Islands ophiolite, Newfoundland; Journal of Geophysical Research, v. 90, p. 7705-7736.

Laurent, R.

1987: Petrology and formation of the Troodos CY-4 plutonic suites, Cyprus; Ophiolites and Oceanic Lithosphere: Troodos 87 (abstract), Cyprus Geological Survey Department, Ministry of Agriculture and Natural Resources, p. 22.

McBirney, A.R. and Noyes R.M.

1979: Crystallisation and layering of the Skaergaard Intrusion; Journal of Petrology, v. 20, p. 487-544.

McKenzie, D.P.

1984: The generation and compaction of partially molten rock; Journal of Petrology, v. 25, p. 713-765.

Reinhardt, B.M.

1969: On the genesis and emplacement of ophiolites in the Oman mountains geosyncline; Schweizenische Mineralogische und Petrographische Mitteilungen, v. 49, p. 1-30.

Thy, P.

1987: Petrogenetic implications of mineral crystallisation trends of Troodos cumulates, Cyprus; Geological Magazine, v. 124, p. 1-11.

Thy, P., Schiffman, P. and Moores, E.M.

1989: Igneous mineral stratigraphy and chemistry of the Cyprus Crustal Study Project drill core in the plutonic sequences of the Troodos ophiolite; *in* Cyprus Crustal Study Project Initial Report Hole CY-4, ed. I.L. Gibson, J. Malpas, P.T. Robinson and C. Xenophontos; Geological Survey of Canada, Paper 88-9.

Turner, J.S. and Chen, C.F.

1974: Two-dimensional effects in double-diffusive convection; Journal of Fluid Mechanics, v. 63, p. 577-592.

Wilson, J.R., Menuge, J.F., Pedersen, S. and Engell-Sorensen, O.

1987: The southern part of the Fongen-Hyllingen layered mafic complex, Norway: Emplacement and crystallisation of compositionally stratified magma; *in* Origins of Igneous Layering, ed. I. Parsons; Reidel, Dordrecht, p. 145-184.

Oxygen and Carbon Isotope Studies of Hydrothermal Alteration in the Troodos Ophiolite Complex, Cyprus

N.J. VIBETTI[1], R. KERRICH[2] AND W.S. FYFE[1]

[1]The Department of Geology, The University of Western Ontario,
London, Ontario, Canada N6A 5B7
[2]Department of Geological Sciences, University of Saskatchewan,
Saskatoon, Saskatchewan, Canada, S7N 0W0

Vibetti, N.J., Kerrich, R. and Fyfe, W.S., Oxygen and carbon isotope studies of hydrothermal alteration in the Troodos ophiolite complex, Cyprus; in *Cyprus Crustal Study Project: Initial Report, Hole CY-4, ed. I.L. Gibson, J. Malpas, P.T. Robinson and C. Xenophontos*; *Geological Survey of Canada, Paper 88-9, p. 221-228, 1989.*

Abstract

Oxygen isotopic analyses of samples from the sheeted complex and gabbroic sequence of the Troodos ophiolite complex show that subsolidus hydrothermal oxygen isotope exchange with seawater occurred throughout the sheeted complex, high level gabbros and locally even penetrated down into the layered gabbros and ultramafic rocks. Sheeted dykes and high level gabbros show variable depletions ($\delta^{18}O$ = 2.2 to 4.6) whereas deeper level altered gabbros are variably depleted or enriched ($\delta^{18}O$ = 1.1 to 10.4) relative to fresh oceanic basalts. The enrichments at depth in the gabbros are in part due to exchange at much lower temperatures with isotopically evolved seawater than has occurred with the overlying rocks. Late stage calcite bearing vein assemblages show a variable depletion ($\delta^{13}C$ = −9.7 to −15.7) indicative of the presence of some dissolved biogenic carbon during the waning stage of fluid circulation through the uppermost parts of the ophiolite.

Résumé

Les analyses des isotopes de l'oxygène ont été effectuées sur des échantillons du complexe filonien et de la séquence gabbroïque du complexe ophiolitique de Troodos. Les résultats indiquent que le rééquilibrage isotopique au subsolidus, en conditions hydrothermales avec l'eau de mer, s'est produit partout dans le complexe filonien, les gabbros supérieurs et voire même au niveau des gabbros lités et des roches ultramafiques. Les dykes du complexe filonien et les gabbros supérieurs montrent un allégement variable ($\delta^{18}O$ = 2.2 à 4.6) alors que les gabbros métamorphisés plus profonds ont à la fois des rapports allégés ou alourdis ($\delta^{18}O$ = 1.1 à 10.4) comparativement aux basaltes océaniques frais. Les alourdissements en profondeur dans les gabbros résultent en partie de l'échange, à beaucoup plus basses températures, avec de l'eau de mer isotopiquement plus évoluée que celle ayant interagit avec les roches stratigraphiquement superposées. Des veines tardives comprenant entre autre de la calcite ont des rapports allégés ($\delta^{13}C$ = −9.7 à −15.7) indicateurs de la présence de carbone biogénique dissous durant le stade terminal de la circulation des fluides au travers les niveaux stratigraphiques supérieurs de l'ophiolite.

INTRODUCTION

Studies of ophiolite suites have revealed the generally pervasive nature of hydrothermal alteration which is considered to be the direct result of seawater convecting through oceanic crust in response to cooling (Spooner and Fyfe, 1973; Heaton and Sheppard, 1977; Gregory and Taylor, 1981; Stakes and Vanke, 1986). The oxygen isotope composition of fresh and altered oceanic rocks, specifically of ophiolites, has been employed to deduce the magnitude and conditions of basalt-seawater interaction and to constrain the isotopic budget of the hydrosphere (Muehlenbachs and Clayton, 1972a; Gregory and Taylor, 1981; Holland, 1984). This paper reports a detailed isotopic study of representative samples of fresh and altered diabase dykes, gabbros and ultramafic rocks as well as mineral separates in order to establish the oxygen isotope profile of the Troodos ophiolite as encountered in drill hole CY-4. Carbon isotope analyses have also been performed on calcite containing rocks mostly from the upper region of diabase dykes encountered by the drill hole. The present study reveals broad hydrothermal alteration in CY-4 of the same basic nature as shown by previous studies, but with significant later retrograde activity.

ALTERATION ASSEMBLAGES

The predominant type of alteration encountered in the diabase dykes in CY-4 to a depth of about 1 km is of greenschist facies grade. Mineralogically, the rocks are characterized by the transformation of igneous plagioclase to albite (Ab_{95-100}) and of augite to chlorite and actinolite. Fe-Ti oxides have been replaced by secondary sulphides. The alteration is not totally pervasive and appears to have been influenced to a high degree by fractures and shear zones over a scale ranging from millimetres to metres, which were presumably pathways for fluid infiltration. Late retrograde activity is evidenced by the presence of zeolite facies assemblages predominantly in veins and shear zones characterized by the presence of laumontite-stilbite-analcite-calcite and minor gypsum. It should be noted that gypsum is extremely common in pillow interstices in many parts of the Cyprus ophiolite. Spectacular examples occur at the old Kokkinoyia mine.

In the high level and layered gabbros at depths extending from 1 to 2 km, three distinct alteration patterns exist, which in order of increasing depth are low grade amphibole-bearing gabbros, high grade amphibole-bearing gabbros, and serpentinized mafic and ultramafic rocks extending to the deepest levels (ICRDG, 1985). The high level gabbros have been subjected to local low grade alteration characterized by Ca-plagioclase (An_{95-100}) and hornblende, locally comprising up to 95% of the rock, and variable but minor amounts of sphene, clinozoisite, epidote and quartz. Igneous textures are generally well preserved and the rocks show little sign of alteration megascopically. Alteration zones within these gabbros can be classified into a low temperature type and high temperature type (Vibetti, 1986) with the dividing temperature in the range 180-230°C based on the stability field of laumontite as defined by Liou (1971) and the geothermal gradients postulated during ocean floor metamorphism (Spooner and Fyfe, 1973; Gass and Smewing, 1973; Coleman, 1977).

Typical high temperature alteration assemblages in the amphibole-bearing gabbros include: quartz-actinolite-chlorite; quartz-chlorite; quartz-epidote-chlorite; quartz-epidote-anorthite; quartz-andradite-prehnite; anorthite-prehnite-pumpellyite ± quartz. The low temperature alteration is retrograde and evident mainly in vuggy veins and shear zones. The dominant mineralogy is late-stage laumontite-stilbite with interstitial calcite and minor amounts of other Ca-zeolites (chabasite, analcime, thomsonite) identified mainly by XRD analysis.

The layered amphibole-bearing gabbros have been subjected to local higher grade hydrothermal alteration accompanied by calcium metasomatism. Characteristic minerals are anorthite (An_{97-100}) hornblende, diopside replacing metamorphic hornblende, and minor sphene, epidote, clinozoisite and andradite garnet which is commonly observed being replaced by prehnite. Late stage retrograde prehnite, pumpellyite and clinozoisite replace anorthite. Diopside, in many instances with relict hornblende still discernible, has reacted to tremolite-actinolite at grain boundaries. The presence of these secondary minerals throughout the gabbroic sequence strongly suggests low-grade retrograde metamorphism.

Stratigraphically below the layered gabbros, olivine bearing ultramafic rocks, chiefly websterites, peridotites and lenses of dunite show partial to complete alteration to serpentine. Coarse grained calc-silicate rocks, containing the critical assemblage (quartz)-anorthite-prehnite-diopside-tremolite, occur frequently in close proximity to serpentinized ultramafic rocks, and appear to be byproducts of the reactions between fluids derived from serpentinization and the country rocks. Though hydrogrossular has not been identified in these rocks, the processes responsible for them can best be termed as rodingitisation (See Rice, 1983). Note that hydrogrossular is present at lower levels (see Barriga et al., 1985).

ANALYTICAL METHODS

Conventional procedures were employed for the extraction of oxygen from silicate minerals with bromine pentafluoride, followed by quantitative conversion to CO_2 (Clayton and Mayeda, 1963). Carbonate minerals were reacted with 100 percent H_3PO_4 at 25°C (McCrea, 1950). Isotopic data are reported in the conventional notation as – values in per mil relative to SMOW for oxygen, and relative to PDB for carbon. The oxygen standard is NBS-28 quartz, which gave a value of 9.6 per mil (cf.

Coplen et al., 1983). Reproducibility of $\delta^{18}0$ values has averaged ±0.18 per mil (2 σ.)

Fractionations, or differences in δ among minerals are quoted as Δ, defined as:

$$\Delta A-B = 10^3 \ln A-B \approx \delta A-\delta B$$

where δ is the fractionation factor for the coexisting minerals A and B, an approximation which holds for ≤ 10.

RESULTS

Oxygen isotope data for 34 whole rocks are reported in Table 1, together with sample descriptions. The feldspar-water oxygen isotope fractionation curves of O'Neil and Taylor (1967) were used to calculate $\delta^{18}O$ H_2O in equilibrium with the rocks using the plagioclase thermometer and assuming a range of temperatures consistent with the hydrothermal alteration mineral assemblages present. Water/rock ratios in oxygen units were calculated from the isotopic data according to the W/R equation of Taylor (1974) using the lower temperature limits.

Diabase dykes are characterized by a range of $\delta^{18}O$ values spanning 2.2 to 6.4. The freshest sample among them (Table 1; CY-227 $\delta^{18}O$=5.4; CY-145 $\delta^{18}O$=4.2) gave the highest $\delta^{18}O$ values, although such values are at the low end, or below, $\delta^{18}O$ values of fresh oceanic basalts at 5.7±0.3 per mil (Gregory and Taylor, 1981). The other samples, though fresh in appearance megascopically, have minor degrees of augite alteration to actinolite, with fresh unaltered plagioclase grains in thin section.

High level and layered gabbros with fresh textures in thin section, have a range of $\delta^{18}O$ values from 4.6 to 6.4 per mil (Table 1; samples CY-117, CY-017, CY-023, CY-036, CY-064, CY-A2,) indicating that oxygen isotope exchange had occurred despite their petrographic appearance of being unaltered. Various hydrothermally altered gabbros (Table 1) gave a much wider range of 1.1 to 10.4 per mil $\delta^{18}O$. The sample with the lowest value, CY-073, is a metagabbro bearing hydrothermal diopside and anorthite (An_{100}) from a bleached zone in CY-4 at 1618.40 m which has been left porous on the cm scale by heated hydrothermal fluids (see ICRDG, 1985) and yields the highest water/rock ratio. Sample CY-012 from 1115.80 m has a $\delta^{18}O$ value of 10.4 per mil, the highest recorded whole rock result in this study. The sample is derived from a medium grained gabbro which exhibits a slight preferred orientation of the plagioclase feldspar, and where the only evidence of alteration is the presence of minor chlorite replacing clinopyroxene, visible only in thin section.

Serpentinized ultramafic rocks composed mainly of relict olivine, enstatite, clinopyroxene and the serpentine minerals lizardite (major), chrysotile and minor antigorite yielded $\delta_{18}O$ values in the range 3.6 to 5.5, whereas, serpentinites of 2.0 to 9.3 per mil (Magaritz and Taylor, 1974).

VEINS

Diopside, separated from two domains of essentially diopsidic rocks developed as an alteration product of gabbro, both have $\delta^{18}O$ values of +0.2 (Table 2), representing a shift of −5.5 per mil relative to fresh gabbros. The high inferred temperatures for stabilization of hydrothermal diopside, combined with low $\delta^{18}O$ values, are consistent with the pattern of ^{18}O depletion recorded in the high-temperature alteration of the Samail ophiolite (Gregory and Taylor, 1981).

Arrays of quartz-actinolite veins are sporadically present in the section, and are characteristic of the greenschist facies hydrothermal alteration. For three samples analyzed, the $\delta^{18}O$ of quartz is in the relatively restricted interval of 5.9 to 7.0 per mil, whereas actinolite ranges from 1.2 to 6.8 per mil. Consequently, quartz-actinolite fractionations are dispersed (Δ=0.9 to 4.7), reflecting disequilibrium conditions. Temperatures of quartz-actinolite vein formation are not well constrained. Primary fluid inclusions in quartz yield filling temperatures of 190 to 260°C (Vibetti et al. 1988a). Based on these temperature estimates, the $\delta^{18}O$ of fluids involved in this generation of veins would have been −1.5 (290°C) to −3.5 (220°C) per mil (quartz-water equation of Matsuhisha et al. 1979).

Veins mineralogically composed of quartz, andradite, and actinolite occur in fresh gabbro at 1,200 m. Quartz ($\delta^{18}O$ = 3.4) in this vein type is depleted relative to the generation of quartz-antinolite veins (Table 2). Assuming hydrothermal temperatures of 450±50°C, quartz would have been in equilibrium with water of 0.2 per mil (500°C) to −17 pr mil (400°C).

Anorthite-bearing veins, containing variable quantities of quartz, actinolite and epidote are characterized by systematically depleted $\delta^{18}O$ values of 0.8 to 2.4. Those values are in keeping with the variably ^{18}O depleted plagioclase form deeper level and higher temperature alteration zones of the Samoul ophiolite (Gregory and Taylor, 1981). Relict hypersthenes also have lower $\delta^{18}O$ values than isotopically undisturbed pyroxenes in fresh gabbros. The plagioclase and hypersthene exchanged with an external fluid reservoir at temperatures of 400-500°C. In two samples the anorthite is ^{18}O-enriched ($\delta^{18}O$ = 8.9-12.6); this is interpreted in terms of isotopic exchange at lower temperatures, and/or with relatively ^{18}O-enriched fluids.

INTERPRETATION

The $\delta^{18}O$ value of hydrothermal fluids and the temperature of interaction of the fluids with rock are the major controls of the oxygen isotopic ratios of silicates in equilibrium with fluids. Both theoretical and experimental work show that silicate-water fractionations are large and positive at low temperatures and diminish rapidly with increase in temperature.

TABLE 1: $\delta^{18}O$ compositions of whole rocks at specific depths in CY-4.

Sample	CY-4 Depth(m)	Description	$\delta^{18}O$ Whole Rock	$\delta^{18}O$ of H_2O eqn.**	W/R+
CY-253	266.45	Sheeted diabase (200–400°C)	2.2	−7.0 to −0.6	n.d
CY-239	356.75	Sheeted diabase (200–400°C)	3.4	−6.0 to 0.5	n.d
CY-227	443.85	Sheeted diabase (200–400°C)	5.4	−4.0 to 2.5	n.d
CY-212	515.70	Sheeted diabase (200–400°C)	2.8	−6.4 to 0.0	n.d
CY-145	836.15	Sheeted diabase (200–400°C)	4.2	−5.2 to 1.4	n.d
CY-119	979.95	High level gabbro (400–600°C)	3.4	2.2 to 4.2	0.9
CY-117	994.10	High level gabbro (400–600°C)	4.6	3.4 to 5.4	0.3
CY-006	1073.15	Quartz-epidote-albite-anorthite alteration zone in diabase (268–354°C)	3.8	1.2 to 3.0*	1.1
CY-012	1115.50	Chlorite bearing alteration zone in gabbro	10.4	9.0 to 11.07	n.d.
CY-017	1147.70	Fresh gabbro	4.6	3.3 to 5.3*	0.3
CY-021	1175.35	Andradite + quartz + prehnite + epidote vein in gabbro	4.0	−1.2 to 0.8	n.d.
CY-023	1186.30	High level gabbro	5.4	4.0 to 6.0	0.1
CY-B81	1236.70	Andradite bearing leached zone in gabbro	8.0	6.6 to 8.6	n.d.
CY-030	1245.30	Laumontite + actinolite + epidote alteration in gabbro	3.0	1.8 to 3.8	1.2
CY-036	1283.00	High level gabbro	5.4	4.0 to 6.0	0.1
CY-B80	1310.20	Leached zone in pegmatite gabbro	5.0	3.8 to 5.8	0.2
CY-039	1318.20	Chlorite + epidote + quartz + laumontite alteration in gabbro	3.5	2.2 to 4.2	0.8
CY-R4	1322.95	Epidote + prehnite + carbonate alteration zone in gabbro	2.8	1.4 to 3.4	1.5
CY-040	1329.70	Laumontite + quartz + epidote vein in gabbro	8.0	6.8 to 7.6	n.d.
CY-059	1478.45	Serpentine intrusion in gabbro	5.5	4.2 to 6.2	n.d.
CY-063	1496.00	Zeolite bearing alteration zone in gabbro	6.6	5.3 to 7.4	n.d.
CY-064	1503.10	Fresh gabbro	5.5	4.2 to 6.2	0.1
CY-066	1536.65	Fresh gabbro	6.4	5.0 to 7.0	n.d.
CY-073	1618.40	Diopside bearing leached zone in gabbro	1.1	−0.2 to 1.8	15.3
CY-084	1708.30	Serpentinite vein in gabbro	3.6	—	—
CY-087	1730.55	Quartz-plag. vein in gabbro	4.6	3.4 to 5.4	0.3
CY-089	1742.70	Serpentine intrusion in gabbro	5.4	—	—
CY-WX	1977.00	Serpentinized olivine websterite	4.6	—	—
CY-A1	1850.44	Serpentinized olivine websterite	5.0	—	—
CY-A2	1860.30	Very coarse grained gabbro.	5.2	3.9 to 5.9	0.1
CY-B2	1996.30	Epidotized websterite	−0.5	−1.8 to 0.2	1.4
CY-WXO	1981.00	serpentinized olivine websterite	−0.9	—	—
CY-B15	2228.20	Serpentinite in olivine websterite	1.2	—	—
CY-B17	2235.30	Serpentinized pyroxene peridotite	2.2	—	—

** $\delta^{18}O$ of H_2O calculated as being in equilibrium with the rocks using feldspar geothermometry as defined by O'Neil and Taylor, 1967 based on temperature ranges and plagioclase composition consistent with prevailing metamorphic mineral assemblages in rock type.

* Temperature range used for $\delta^{18}O$ of H_2O equation derived from fluid inclusion thermometry (Th).

+ W/R = water rock ratio calculated according to Taylor's (1974) equation based on the assumption that $\delta^{18}O$ initial = −0.5% for Cretaceous seawater; $\delta^{18}O$ rock initial = 5.7 ± 0.3.

TABLE 2: Oxygen isotope composition of mineral separates from specified vein types.

Sample description	Sample number	$\delta^{18}O$ quartz	$\delta^{18}O$ act	$\delta^{18}O$ di	$\delta^{18}O$ a	$\delta^{18}O$ an	$\delta^{18}O$ hyp	$\delta^{18}O$ ep
Quartz-actinolite veins	121	5.9	1.2					
	004	7.5	5.3					
	024	7.7	6.8					
Diopsidic alteration	A1			0.2				
	B1			0.2				
Quartz-andradite-actinolite	021v	3.4	1.3					
Plagiclase ± quartz	017					0.8	3.1	
± epidote veins	025					1.8		
	113					1.3	1.6	
	227		1.2			2.3		
	006	3.9	2.0			2.4		−1.1
	147		6.2			2.6		0.6
	B77	6.4				8.9		
	152v				26.2			

act = actinolite; di = diopside; a = analcime; an = anorthite; hyp = hypersthene; epidote.

TABLE 3: Isotopic compositions of calcite-bearing rocks.

Sample	CY-4 Depth (m)	Description	$\delta^{13}C$ calcite	$\delta^{13}C$ dolomite	$\delta^{18}O$ calcite	$\delta^{18}O$ dolomite
CY-225	462.10	Calcite + laumontite bearing shear zone in diabase	−14.7	−14.6	+21.2	+24.0
CY-218	493.95	Calcite crystals in vugs of shear zone in diabase	−14.0	−13.4	+20.8	+21.3
CY-207	535.80	Calcite + laumontite + stilbite on fracture plane in diabase	−12.8	−3.3	+21.1	+19.0
CY-175	705.40	Laumontite + calcite crystals in shear zone in diabase	−12.4		+20.4	
CY-155	794.50	Calcite + laumontite crystals in vugs of diabase shear zone.	−9.7		+19.7	
CY-126	941.10	Pyrite + calcite crystals on fracture plane in gabbro	−14.5	−15.3	+21.8	+21.3
CY-125	948.85	Laumontite + calcite crystals in vugs in gabbro shear zone	−15.1	−15.2	+20.5	+19.6
CY-019	1165.20	Calcite + laumontite in shear zone in gabbro	−15.7		+20.4	
CY-B72	1642.70	Calcite + laumontite in vein in gabbro	+1.2	+0.7	+11.5	+11.2

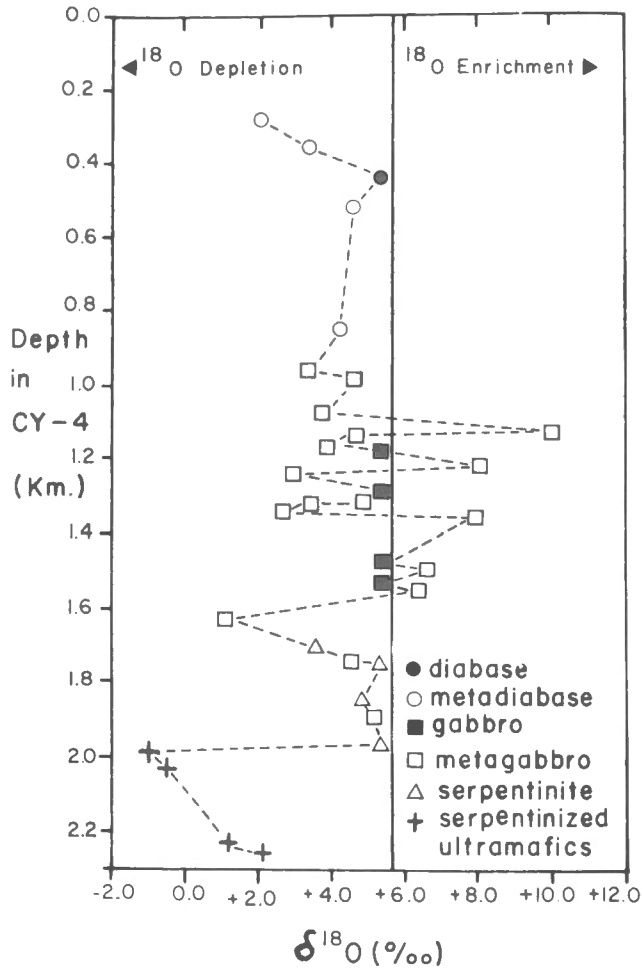

Figure 1: The relationship between depth in the CY-4 borehole and the $\delta^{18}O$ concentration.

The $\delta^{18}O$ values of the analyzed samples from Troodos in this study (Table 1, Figure 1) with few exceptions show negative shifts in $\delta^{18}O$, or depletions, relative to a $\delta^{18}O$ value for fresh tholeiitic basalts of +5.7 ±0.3 per mil (Gregory and Taylor, 1981). The maximum observed negative isotopic shift is 6.6 per mil, whereas the maximum positive shift is by 4.7 per mil to whole rock values of –0.9 and +10.4 per mil, respectively (samples CY-WXO and CY-012, respectively). The overall trend is that the $\delta^{18}O$ whole rock values decrease downwards producing larger depletions in the cumulate gabbros and ultramafics.

The ^{18}O depletions are the result of water/rock interactions at temperatures greater than the particular temperature range above which the whole rock-water fractionations become less than the isotopic difference between fresh basalt and seawater, thus correlating the $\delta^{18}O$ decrease downwards with the original direction of increasing temperature. A temperature for hydrothermal metamorphism of 300°C to approximately 350°C is suggested by the secondary mineral paragenesis albite-chlorite-actinolite in the diabase dykes and greater than 400°C in the high level gabbros by the critical assemblage anorthite-andradite-diopside. Accordingly, the data are interpreted as primarily indicative of high temperature (>400°C) hydrothermal alteration of the ophiolite by hydrothermal fluids.

The samples whose $\delta^{18}O$ values are enriched (>5.7 ±0.3 per mil) are interpreted as being the products of low temperature hydrothermal fluid/rock interaction. Previous studies (e.g. Spooner et al., 1974; Heaton and Sheppard, 1977; Gregory and Taylor, 1981) of isotopic variation in ophiolites have shown both ^{18}O depletion at deeper levels, with the enriched rocks primarily confined to the top level pillow lavas and flows. The present study reveals numerous fluctuations from ^{18}O depleted to ^{18}O enriched values deep within the gabbroic sequence imlying a complex history of hydrothermal alteration, with varying temperatures, $\delta^{18}O$ fluid, and degree of retrograde alteration.

CARBON ISOTOPE SYSTEMATICS OF CARBONATES

Isotope analyses were conducted on secondary calcite bearing assemblages from late laumontite-stilbite-calcite veins, vugs and shear zones in CY-4 (Table 3). Most of the samples occurred in the depth range 450 - 1200 m in the sheeted diabase dykes and high level gabbros (Fig. 2). The $\delta^{13}C$ values obtained span –15.7 to +1.2 per mil, and the $\delta^{18}O$ values range from +11.2 to +24.0 per mil. The $\delta^{13}C$ values are clustered between –9 and –16 per mil with an isolated sample, which is the deepest occurring one, having a value of +1.2 per mil. The first 5 calcite bearing samples, which occur in the sheeted diabase dykes, show a constant increase in $\delta^{13}C$ from –15 to –10 per mil with

increasing depth. The samples occurring in the high level gabbros have negative $\delta^{13}C$ values clustered at −15 per mil.

DISCUSSION OF CARBON ISOTOPE DATA

The average value of $\delta^{13}C$ for sedimentary marine carbonates is close to 0 per mil, while that for igneous carbon is close to −5 per mil. Carbon derived from biogenic processes is isotopically more negative than igneous carbon, as low as −35 per mil (Ohmoto and Rye, 1979). The oxygen isotopic compositions of the carbonates is variable and depends on the extent to which exchange has occurred with hydrothermal fluids. Secondary carbonates formed by low temperature (<300°C) seawater alteration of fresh basalts have carbon and oxygen isotope compositions ranging from −5 to +2 per mil (PDB) and from 25 to 30 per mil (SMOW), respectively (Muehlenbachs and Clayton, 1972a; Muehlenbachs, 1977). High temperature (>300°C) seawater/rock interaction produces carbonates with oxygen and carbon isotopic compositions ranging from −1 to +23 per mil (SMOW) and from −7 to −4 per mil (PDB), respectively (Muehlenbachs and Clayton, 1972b). However, while these possible carbon reservoirs appear to be distinctive, large ranges of $\delta^{13}C$, up to 50 per mil in a single deposit are known to result from fluctuations in temperature, Eh and pH during carbonate precipitation from solution, and mixing of carbon from different carbon reservoirs (Ohmoto, 1972). The carbonates from Troodos reported in this study may appear to be too depleted in terms of $\delta^{13}C$ to be consistent with an origin from marine HCO_3^- alone, and the negative $\delta^{13}C$ values may reflect a contribution from low ^{13}C organic rich sediments.

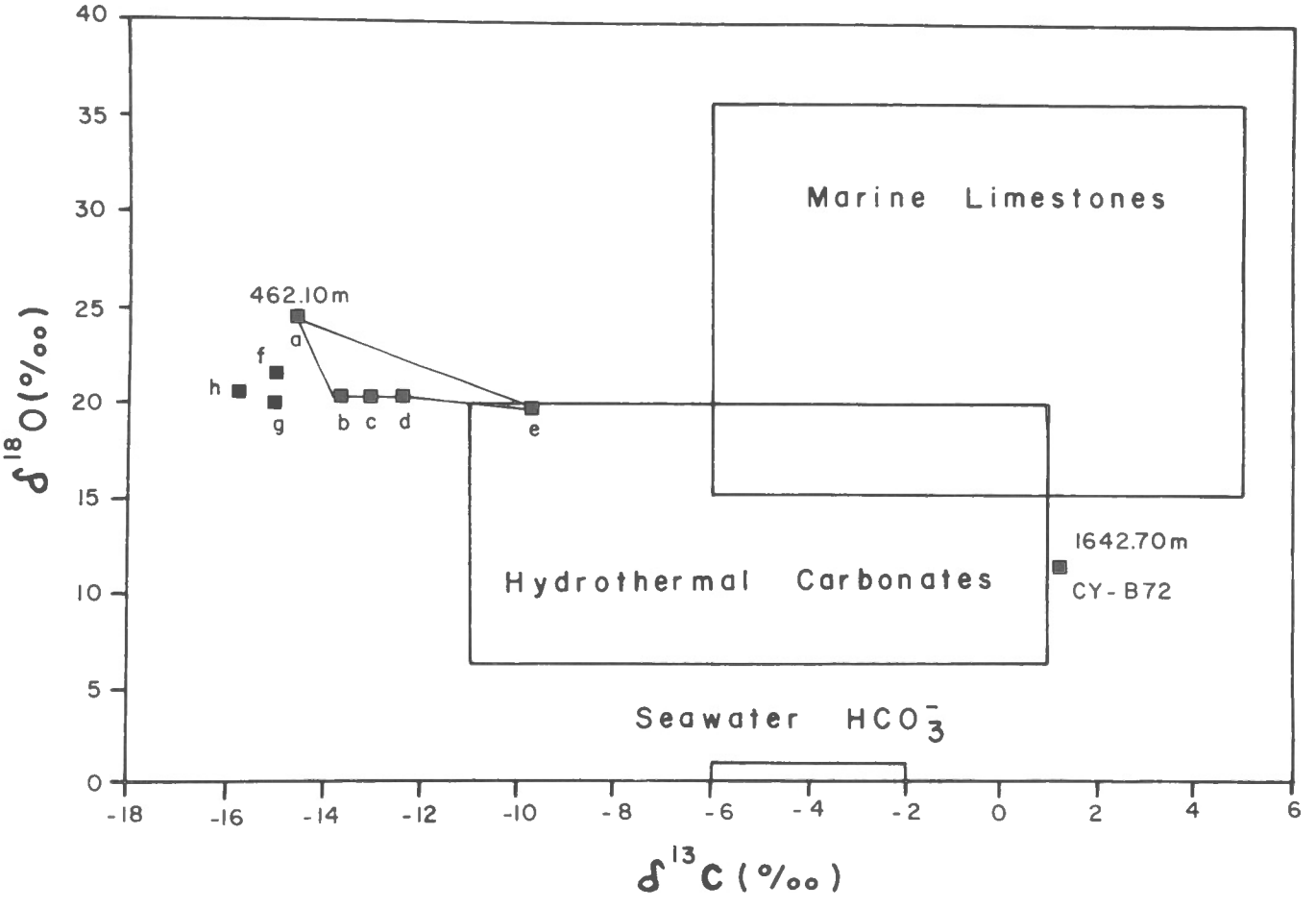

Figure 2: The $\delta^{18}O$ and $\delta^{13}C$ concentrations of calcuim carbonate samples from CY-4.

SUMMARY

Oxygen isotope analyses of samples from the sheeted complex and gabbroic sequence of the Troodos ophiolite show a complex pattern of ^{18}O enrichments or depletions over a 2.2 km vertical interval, signifying pervasive oxygen isotope exchange with seawater. ^{18}O enrichments and depletions are due to low and high temperature alteration respectively, with maximum temperatures of 400-500°C (anorthite-hypersthene), and minimum temperatures of <50°C (analcime). Calculated fluid-rock ratios range from minimum values of 0.1 to 15.3. The complexity in the oxygen isotope distribution arises not only from varying temperature of exchange and water/rock ratio, but also from variable degrees of retrograde exchange during waning temperatures. Calcite in late laumontite-calcite alteration zones is variably ^{13}C-depleted, likely due to the oxidation of low ^{13}C organic material in sediments. Most of the observed stages of alteration are considered to be the consequence of seawater convection through the ophiolite sequence. However, some of the alteration may have been in response to fluid advection during abduction, particularly where calculated $\delta^{18}O$ values of water are negative.

REFERENCES

Barriga, F., Munha, J., Fyfe, W.S. and Vibetti, N.J.
1985: Extreme hydrothermal alteration in the intrusive layers of the Troodos ophiolite (Cyprus); EOS, American Geophysical Union, Transactions, v. 66, no. 46, p. 1128.

Clayton, R.N. and Mayeda, R.K.
1963: The use of bromine pentafluoride in the extraction of oxygen from oxides and silicates for isotopic analysis; Geochimica et Cosmochimica Acta, v. 27, p. 43-52.

Coleman, R.G.
1977: Ophiolites: Ancient Oceanic Lithosphere?; Springer-Verlag, Berlin; Heidelberg; New York.

Coplen, T.B., Kendall, C. and Hopple, J.
1983: Comparison of stable isotope reference samples; Nature, London, v. 360, p. 236-238.

Gass, I.G. and Smewing, J.D.
1973: Intrusion, extrusion and metamorphism at constructive margins: evidence from the Troodos Massif, Cyprus; Nature, v. 242, p. 26-29.

Gregory, R.T. and Taylor, H.P.
1981: An oxygen isotope profile in a section of Cretaceous oceanic crust, Samail Ophiolite, Oman: evidence for ^{18}O buffering of the oceans by deep (>5 km) seawater hydrothermal circulation at mid-ocean ridges; Journal of Geophysical Research, v. 86, no. B4, p. 2737-2755.

Heaton, T.H.E. and Sheppard, S.M.F.
1977: Hydrogen and oxygen isotope evidence for seawater-hydrothermal alteration and ore deposition, Troodos complex, Cyprus; *in* Volcanic Processes in Ore Genesis, Geological Society of London, Special Publication, no. 7, p. 42-57.

Holland, H.D.
1984: The chemical evolution of the atmosphere and oceans; Princeton University Press, Princeton, N.J., p. 1-582.

ICRDG
1985: CY-4 core descriptions; Dalhousie University, Halifax, Nova Scotia, v. 2, 3, 4,

Liou, J.G.
1971: P-T stabilities of laumontite, wairakite, lawsonite and related minerals in the system $CaAl_2Si_2O_3$-SiO_2-H_2O; Journal of Petrology, v. 12, p. 370-411.

Matsushisha, Y., Goldsmith, J.R. and Clayton, R.N.
1979: Oxygen isotope fractionation in the system quartz-albite-anorthite-water; Geochimica et Cosmochimica Acta, v. 43, p. 1131-1140.

McCrea, J.M.
1950: The isotope chemistry of carbonates and a paleotemperature scale; Journal of Chemical Physics, v. 18, p. 849.

Muehlenbachs, K. and Clayton, R.N.
1972a: Oxygen isotope studies of fresh and weathered submarine basalts; Canadian Journal of Earth Sciences, v. 9, p. 172-184.
1972b: Oxygen isotope geochemistry of submarine greenstones; Canadian Journal of Earth Sciences, v. 9, p. 471-478.

Ohmoto, H.
1972: Systematics of sulphur and carbon isotopes in hydrothermal ore deposits; Economic Geology, v. 67, p. 551-578.

O'Neil, J.R. and Taylor, H.P.
1967: The oxygen isotope and cation exchange chemistry of feldspars; American Mineralogist, v. 52, p. 1414-1437.

Rice, J.M.
1983: Metamorphism of rodingites: Part 1. Phase relations in a portion of the system CaO-MgO-Al_2O_3-SiO_2-CO_2-H_2O; American Journal of Science, v. 283(A), p. 121-150.

Spooner, E.T.C. and Fyfe, W.S.
1973: Sub-sea-floor metamorphism, heat and mass transfer; Contributions to Mineralogy and Petrology, v. 42, p. 287-304.

Taylor, H.P.
1974: The application of oxygen and hydrogen isotope studies to problems of hydrothermal alteration and ore deposition; Economic Geology, v. 69, p. 843-883.

Vibetti, N.J.
1986: Hydrothermal metamorphism at Troodos, Cyprus; unpublished Ph.D. thesis, University of Western Ontario, London, Ontario,

Hypersaline Fluids Discovered In The Troodos Ophiiolite

N.J. VIBETTI[1], R. KERRICH*[1,2], AND W.S. FYFE[1]

[1]The Department of Geology, The University of Western Ontario, London, Ontario, Canada N6A 5B7
[2]Present address: Department of Geological Sciences, University of Saskatchewan, Saskatoon, Saskatchewan, Canada, S7N 0W0

Vibetti, N.J., Kerrich, R., Fyfe, W.S., Hypersaline fluids discovered in the Troodos ophiolite; in *Cyprus Crustal Study Project: Initial Report, Hole CY-4, ed. I.L. Gibson, J. Malpas, P.T. Robinson and C. Xenophontos; Geological Survey of Canada, Paper 88-9, p. 229-234, 1989.*

Abstract

Two distinct hydrothermal fluids have been identified in the Troodos ophiolite from fluid inclusion studies of alteration minerals encountered in drillhole CY-4. Alteration mineral assemblages signify zeolite (laumontite-stilbite-analcite-calcite±gypsum) to greenschist (albite-actinolite-epidote-anorthite-quartz-diopside) facies conditions of hydrothermal alteration. The first population of primary fluid inclusions are two phase liquid + vapour, with Te = –31 to –19°C, Tm = –5 to –0.1°C, and Th = 140 to 354°C, corresponding to NaCl thermal waters of 8 to 0.7 wt.% NaCl equivalent salinity, plausibly evolved seawater. A second population of primary fluid inclusions contain liquid, vapour ± NaCl daughter crystals, where Te = –55 to –43°C, Tm = –34 to –0.3°C, and Th = 130 to 300°C. Such fluids are dominantly hypersaline $CaCl_2$-NaCl brines, involved in local Ca-metasomatism of the ophiolite. Enhanced salinities may have resulted from the reaction of seawater with peridotite to produce serpentine + brine. Sporadic low salinity fluids may represent either condensate from a boiling hydrothermal fluid, or a third, late-stage aqueous reservoir.

Résumé

Deux types distincts de fluides hydrothermaux ont été identifiés dans les inclusions fluides étudiées dans les minéraux métamorphiques de forage CY-4 recoupant l'ophiolite de Troodos. Les assemblages de minéraux métamorphiques, produits dans des conditions hydrothermales, varient du faciès zéolites (laumontite-stilbite-analcime-calcite±gypsum), au facies schists verts (albite-actinolite-epidote-anorthite-quartz-diopside). Le premier groupe d'inclusions fluides primaires sont à phases mixtes (liquide + vapeur) avec Te = –31 à –19°C, Tm = –5 à –0.1°C et Th = 140 à 354°C. Ces valeurs correspondent à une eau saline chaude à salinité équivalente variant de 8 à 0.7% en poids de NaCl, c'est-à-dire une eau marine évoluée. Le deuxième groupe d'inclusions fluides primaires contient des phases liquide et vapeur et des cristaux de NaCl dérivés génétiquement de ces phases. Ce groupe est caractérisé par: Te = –55 à –43°C, Tm = –34 à –0.3°C et Th = 130 à 300°C. Ces fluides sont essentiellement des saumures à composants $CaCl_2$ et NaCl dérivant du métasomatisme calcique local de l'ophiolite. Ces salinités extrêmes peuvent s'être formées par la réaction de l'eau de mer avec une péridotite produisant un assemblage serpentine + saumure. Des fluides à faible salinité disséminés peuvent représenter soit la condensation d'un fluide hydrothermal près du point d'ébullition ou bien des réservoirs aqueux tardifs.

INTRODUCTION

One of the main characteristics of the Troodos ophiolite as exposed in drill hole CY-4 is the extensive hydrothermal alteration over almost the entire sequence as recorded to a depth of over 2200 m (ICRDG, 1984, 1985). Alteration zones and veins reveal a definite mineralogic sequence with increasing depth indicative of increasing temperature of fluids, but with some later retrograde events. The major mineralogic trend in the altered zones and veins is as follows: laumontite-stilbite-analcite-calcite-gypsum in the upper diabasic rocks; laumontite-calcite-albite-chlorite-epidote-quartz in the lower diabasic rocks; albite-actinolite-epidote-anorthite-quartz-diopside-prehnite-andradite-anhydrite-pumpellyite-chlorite-hornblende(hydrothermal)-late laumontite in upper gabbroic rocks, and serpentine-chlorite-quartz-plagioclase (hydrothermal)-late zeolite in the layered gabbros and ultramafics (Vibetti, 1986). This range of mineral assemblages represents zeolite to greenschist facies conditions of hydrothermal alteration. Individual veins and alteration zones range in width from less than 1 mm to over 1.5 mm. Most veins are 1 mm to 2 cm in width. Vein infill ranges from monomineralic to complex polymineralic and shear zones are common. Many fractures appear to have been used as fluid pathways more than once (See ICRDG, 1984, 1985).

Fluids responsible for this alteration are of particular interest because of the unique environment of formation of ophiolites and their subsequent mechanism of cooling which is thought to be dominated by the convective circulation of seawater through hot basalt, now well documented and experimentally verified to be responsible for the formation of massive sulphide metal deposits on the ocean floor (see Emiliani, 1981; Rona et al., 1983).

Drill hole CY-4 at Palekhori is situated at least 15 km from the nearest known massive sulphide metal deposit and its core can be assumed to be largely representative of oceanic crust peripheral to a focussed discharge zone of a convective hydrothermal system that has led to the formation of metallic deposits. A study of fluid inclusions in a part of this core was undertaken with the objective of determining a portion of the P-T-X evolution of seawater from a cold dilute solution to a chemically evolved counterpart involved in the alteration of the basalts.

ANALYTICAL METHODS

The study was performed by thermometric determinations of fluid present as small (5 μm to 30 μm) inclusions in vein quartz from CY-4. The eutectic temperature (T_e) provides an indication of the solute chemical composition; the last melting temperature (T_m) is a measure of the salinity of the fluid, and the homogenization temperatures (T_h) signifies the minimum temperature of the fluids at the time of trapping (see Roedder, 1979; Crawford, 1981).

Inclusions were examined in doubly polished thin sections of 60-70 μm thickness. Microthermometric measurements were carried out on a Linkam TH600 heating and freezing stage operational across the temperature range −180.0°C to +600°C (Shepard, 1981) mounted on the stage of a Leitz Periplan microscope (Table 1). Liquid nitrogen was used to cool pure nitrogen gas which acted as a coolant for the sample and stage down to approximately −100°C to ensure freezing of the inclusions since super cooling is commonly necessary as a result of metastable persistence of the liquid phase. The sample was allowed to warm up slowly and phase changes (T_e, T_m) were observed and recorded. Measurements were repeated, and used only where the fluid inclusion under observation gave consistent readings, to circumvent the possibility of stretching and (or) leakage. The precision of melting temperatures obtained is ±0.2°C for the range under which measurements were made. Homogenization and melting measurements were carried out on the same inclusion. Controlled heating of the fluid inclusion to the temperature at which the gas bubble homogenized with the fluid (T_h) gave the homogenization temperature. The reproducibility for this value is considered to be ±1°C above 199.9°C and ±0.2°C below this for the Linkam TH600 apparatus.

RESULTS

Two populations (Fig. 1) of primary fluid inclusions were identified mainly by size, shape and distribution with respect to other observed inclusions in the sample sections (see Roedder, 1979). Several secondary populations also occur, commonly as smaller inclusions of irregular sizes (5 μm - 20 μm), greater numbers, and often located on fracture planes. Primary inclusions are generally larger (15 μm - 30 μm) fewer in number, isolated or occur in small clusters. Gas bubble to fluid volume ratios are generally consistent and suggest that boiling has not occurred in these fluids (see Roedder, 1984).

The first population of primary fluid inclusions are two-phase liquid + vapour inclusions (Fig. 1) characterized by eutectic melting temperatures (T_e) in the range −31°C to −19°C, final melting temperatures (T_m) −5°C to −0.1°C and minimum homogenization temperatures (T_h) 140°C to 354°C. The second population of primary inclusions occurs in the lower part of the observed depth range and consists of two, three and four-phase liquid + vapour + daughter crystal(s) inclusions whose daughter crystals appear to be composed of NaCl and $CaCl_2$ according to their crystal morphology (NaCl), eutectic temperatures of liquid phase (NaCl, $CaCl_2$), and phase transition behaviour (See Hollister and Crawford, 1981; Roedder, 1984). This second population of primary inclusions is characterized by very low eutectic temperatures of −55°C to −43°C (liquid + vapour), final melting temperatures −34°C to −0.3°C (liquid + vapour) and minimum homogenization temperatures of 130°C to 300°C.

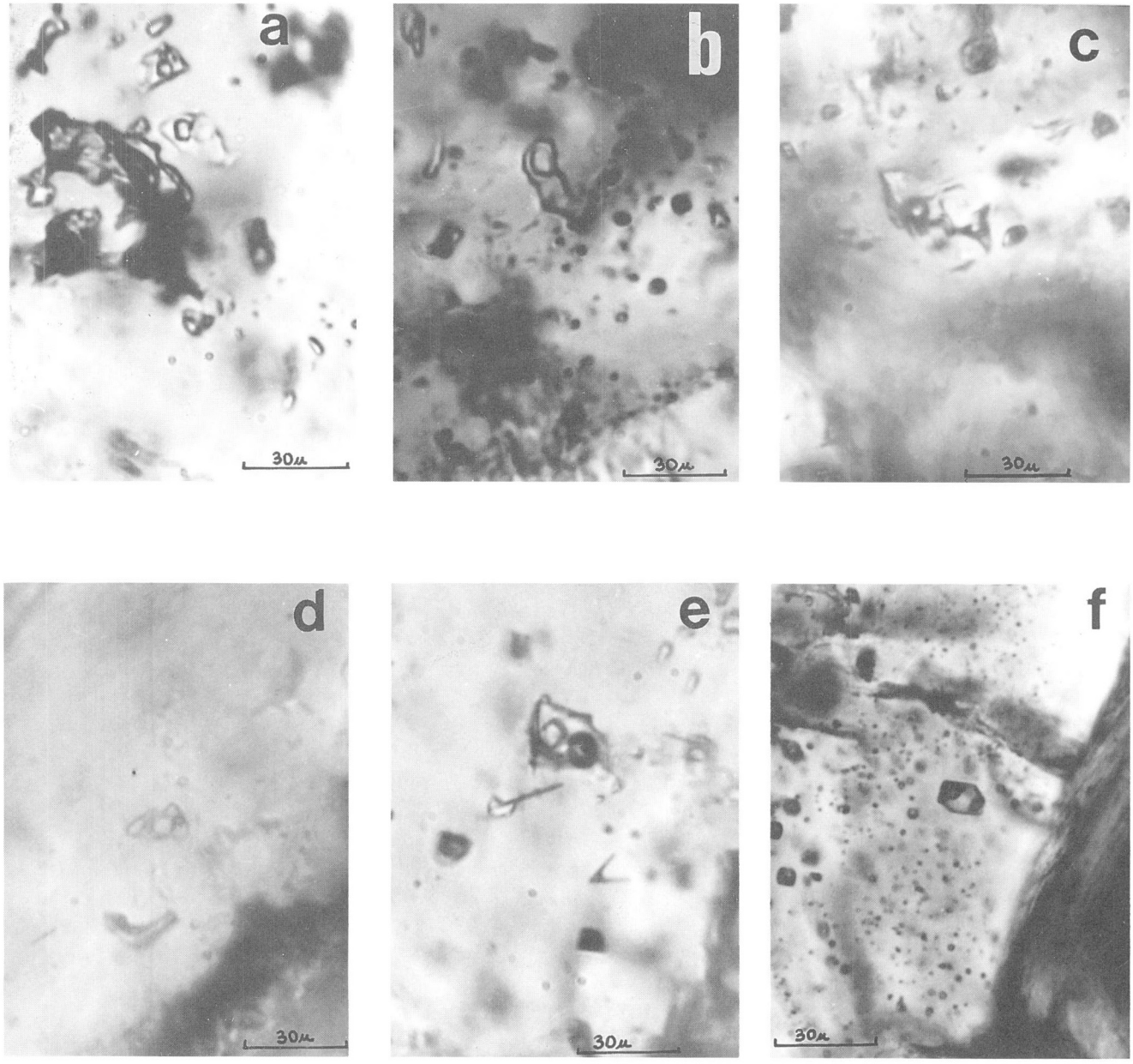

Figure 1: Fluid inclusions in vein quartz from CY-4 containing halite (c,d,e) other daughter crystals (a,b,d) and vapour bubbles (c,d,e,f). Absence of vapour bubbles (a,b) is indicative of low (100°C) homogenization temperatures.

DISCUSSION

The overall high homogenization temperatures of the fluids (Table 1) and varied freezing point depressions indicate that these are plausible hydrothermal fluids which have evolved from seawater. This conclusion is in keeping with independent evidence from stable isotopes (Heaton and Sheppard, 1977). Conversion of final melting temperatures of the first primary population to salinity expressed in weight percent NaCl equivalent according to the data of Potter et al. (1978), yields salinities in the range 8.0 to 0.7 weight percent NaCl equivalent. The salinity of seawater ranges from 3.2 weight percent to 3.75 weight percent NaCl equivalent, and may rise to 4.1 weight percent NaCl equivalent in small ocean basins such as the Red Sea and Mediterranean (Riley and Chester, 1971). Taking into account an accuracy of ±0.2°C, the majority of freezing points obtained are slightly above that of seawater, and indicate that the fluids involved in alteration and fracture infilling have undergone extensive modification of chemical composition and become generally more saline. Increases in salinity of the magnitude observed may be generated by oceanic crust hydration by seawater via processes such as seawater + basalt → spilite + brine (Hutchinson et al., 1980). This is in accord with the alteration mineralogy of the diabasic rocks in which quartz veins occur which show low temperature hydration metamorphism of the zeolite and greenschist facies. The last melting temperatures (–0.1°C, Table 1) could either reflect metastable persistence of the ice phase, or fluids of less than seawater salinity. If the latter explanation has validity, such low salinity fluids could be generated by condensation of a steam phase after boiling, though no evidence for boiling was observed in the samples examined, or represent low salinity, non-marine fluids present during obduction. The low eutectic temperatures and the presence of daughter crystals encountered in fluid inclusions of the second population of primaries suggest that the brines in the inclusions are saturated with respect to NaCl and enriched in $CaCl_2$. This conclusion is based on the phase diagrams of Roedder (1971) for the NaCl-KCl-H_2O system, and Crawford et al. (1979) for the $CaCl_2$-NaCl-H_2O and NaCl-$MgCl_2$-$CaCl_2$-H_2O systems. The addition of KCl to an NaCl-H_2O brine lowers the eutectic point from –20.8°C to –22.9°C, while the addition of $CaCl_2$ or $MgCl_2$ results in a much greater depression of T_e. Eutectic temperatures below –35°C occur mainly in $CaCl_2$ bearing systems (Crawford et al., 1979).

TABLE 1: Thermometric determinations.

No. of phases present	No. of measured inclusions	Range T_e °C	Median T_e °C	Range T_m °C	Median T_m °C	Range Th °C	Median Th °C
		CY-121, 970.0 m, Quartz vein in gabbro					
2	8	−22.3 to −19.5	−20.5	−4.5 to −2.6	−3.5	220 to 250	230
3	5	−25.1 to −20.3	−21.7	−6.7 to −4.4	−4.8	261 to 268	264
		CY-120, 973.0 m, Quartz + chlorite vein in gabbro					
2	17	−26.0 to −19.1	−20.4	−4.8 to −0.1	−3.8	160.6 to 185.9	180.0
3	10	−26.4 to −20.8	−22.1	−6.0 to −3.5	−4.7	187.8 to 216	211
		CY-118 983.6 m, Quartz-albite-epidote vein in micro-gabbro					
2	21	−55.0 to −51.0	−52.4	−23.1 to −18.5	−19.6	257 to 289	280
2	10	−21.6 to −19.2	−20.6	−6.8 to −3.1	−4.5	347 to 364	361
		CY-004, 1058.0 m, quartz vein in diabase					
2	15	−24.0 to −11.8	−19.7	−6.7 to −3.0	−4.7	253 to 315	300
3	7	−22.1 to −16.3	−20.1	−3.8 to −2.7	−3.0	220 to 239	361
3†	6	−48.0 to −43.0	−45.8	−34.0 to −31.2	−31.8	128 to 137	135
		CY-006, 1073.1 m, quartz-anorthite-albite-epidote alteration zone in diabase					
2	20	−26.3 to −18.4	−21.8	−6.2 to −4.0	−4.7	268 to 354	275
		CY-024, 1195.9 m, quartz-anorthite-actinolite vein in gabbro					
2	15	−25.1 to −14.2	−19.8	−6.3 to −1.5	−5.3	198 to 323	295
3	8	−53.0 to −48.5	−49.7	−35.0 to −30.2	−31.4	170.5 to 189.1	172.1
4‡	3	−30.7 to −29.7	−30.0	−23.2 to −21.0	−21.9	300 to 306	301

Measurement errors: −100 to +199.9°C ± 0.2°C; 200 to 600°C ± 1.0°C.

† 2 daughter crystals + liquid phase. ‡ gas bubble + 2 daughter crystals + liquid phase.

TABLE 2: Ca-metasomatism history

Igneous spilitization		multistage Ca-metasomatism	
Early	Late	Early	Late
Calcic-Plagioclase →	albite→	anorthite→	prehnite + andradite
	calcite	quartz	quartz
	ca-zeolites	epidote	pumpellyite
		sphene	
Augitic Pyroxene→	chlorite	actinolite→	diopside
		hornblende	
		Al-amphibole	
Stage of normal to slightly above normal seawater salinity fluid inclusions		Stage of high salinity fluid inclusions	

The system $NaCl$-$CaCl_2$-H_2O has a eutectic temperature of −52.0°C while the systems $FeCl_3$-H_2O and $AlCl_3$-H_2O both have eutectic temperatures of −55.0°C (Crawford et al., 1979; Roedder, 1984). Crawford (1979) notes that the presence of $MgCl_2$, $FeCl_2$, or $FeCl_3$ is difficult to determine from freezing and heating measurements alone, and hence the possibility of the presence of K+, Ca^{2+}, Mg^{2+}, Fe^{2+} and Fe^{3+} ions in solution cannot be precluded. A major constraint however to the actual fluid composition(s) is afforded by the alteration mineralogy, of which the quartz is a part, and is presumably the product of the interaction of the hydrothermal fluids and the host rock. In general, the assemblages are calc-silicate and are products of massive Ca-metasomatism which may be characterized as shown in Table 2.

Hence the fluid inclusions appear to be related to late Ca-Fe metasomatism and as a result, the high salinities encountered may partially be due to the 'salting-out' effect of Ca^{2+}, Mg^{2+} and Fe^{2+}, addition of which is known to drastically decrease NaCl solubility. Linke (1958) showed that at 25°C in the system $CaCl_2$-$NaCl$-H_2O, NaCl has a solubility of only 1.02%. At higher temperatures the solubility is even less (Harris, 1979).

An important mechanism capable of producing high salinity fluids in the oceanic environment is the process of serpentinization which proceeds exothermally via reactions such as:

$$\underset{\text{olivine}}{2Mg_2SiO4} + 3H_2O \rightarrow \underset{\text{serpentine}}{Mg_3Si_2O_5(OH)_4} + \underset{\text{brucite}}{Mg(OH)_2}$$

$$\Delta H^\circ = -19.5 \text{ kcal mol}^{-1}$$

$$\underset{\text{pyroxene}}{MgSiO_3} + \underset{\text{olivine}}{Mg_2SiO_4} + 2H_2O \rightarrow \underset{\text{serpentine}}{Mg_3Si_2O_5(OH)_4}$$

$$\Delta H^\circ = -16 \text{ kcal mol}^{-1}$$

i.e. Peridotite + seawater → serpentine + more saline fluid. Continued reactions of this kind have been shown by Macdonald and Fyfe (1985) to depend on the rate of penetration of water through serpentine minerals to the peridotites as the reaction itself is quite rapid geologically. Their experiments indicate that serpentine layers act as semipermeable membranes which allow H_2O to diffuse through to the unreacted anhydrous assemblages up to 300 times faster than the influx of NaCl and other dissolved salts, thus increasing salinity by membrane separation. Such processes may be important in situations as observed at Troodos where the scale of serpentinization is extensive (Wilson, 1959; Bear, 1963; Gass, 1968; Moores and Vine, 1971) and Ca-metasomatism and rodingitization (Barriga et al., 1985) widespread, with the residual fluids probably injected into overlying rocks as a result of the large bulk expansion and fracturing accompanying serpenitization. These high salinity fluids may also explain the Cl-rich amphiboles present in some oceanic rocks as reported by Vanko (1986). Precipitation of quartz is most simply explained if the veins represent local discharge (cooling) pathways. If highly evolved brines, rich in $CaCl_2$, cause replacement of albite by anorthite and other calcic phases, silica will be produced in such reactions leading to supersaturation with respect to quartz in the hydrothermal fluids. Some features of the alteration might be best explained by rising fluids derived from rodingitisation in the ultramafic portions of the section (see Barriga et al., 1985). In any event, there is clear evidence for two fluids (seawater shallow - hypersaline brines deep), and in the overall convective system there must be potential for mixing, which would explain much of the variability in the fluid inclusion data. Fluids of low salinity may indicate either that boiling occurred sporadically, with separation and condensation of the vapour phase, or alternatively that a third fluid reservoir was present at some stage.

REFERENCES

Barriga, F., Munha, J., Fyfe, W.S. and Vibetti, N.J.
1985: Extreme hydrothermal alteration in the intrusive layers of the Troodos ophiolite (Cyprus); EOS Transactions American Geophysical Union, v. 65, no. 46, p. 1128.

Bear, L.M.
1963: The mineral resources and mining industry of Cyprus; Cyprus Geological Survey Bulletin, no.1, p. 1-208.

Crawford, M.L., Kraus, D.W., and Hollister, L.S.
1979: Petrologic and fluid inclusion study of calc-silicate rocks, Prince Rupert, British Columbia; American Journal of Science, v. 279, p. 1135-1159.

Crawford, M.L.
1981: Phase equilibria in aqueous fluid inclusions; ed. L.S. Hollister and M.L. Crawford; Mineral Association of Canada, Short Course Handbook, no. 6.

Emiliani, C. (ed.)
1981: The Sea; Wiley-Interscience, New York, v. 7, p. 1738

Gass, I.G.
1968: Is the Troodos Massif of Cyprus a fragment of Mesozoic ocean floor?; Nature, London, v. 220, p. 39-42.

Harris, D.M.
1979: Preeruption variations of H_2O, S and Cl in a subduction zone basalt; EOS, Transactions American Geophysical Union, v. 60, p. 968.

Heaton, T.H.E. and Sheppard, S.M.F.
1977: Hydrogen and oxygen isotope evidence for seawater-hydrothermal alteration and ore deposition, Troodos complex, Cyprus; *in* Volcanic Processes in Ore Genesis, Institution of Mining and Metallurgy and Geological Society, London, p. 42-57.

Hollister, L.S. and Crawford, M.L.
1981: Phase equilibria in aqueous fluid inclusions; Mineral Association of Canada, Short Course Handbook no. 6, p. 304.

Hutchinson, R.W., Fyfe, W.S. and Kerrich, R.
1980: Deep fluid penetration and ore deposition; Minerals Science and Engineering, v. 12, no. 3.

ICRDG
1984: CY-4 Core descriptions; Unpublished report, Dalhousie University, Halifax, Nova Scotia, Canada, v. 1.

ICRDG
1985: CY-4 Core descriptions; Unpublished reports. Dalhousie University, Halifax, Nova Scotia, Canada, v. 2, v. 3, v. 4.

Linke, N.F.
1958: Solubilities of inorganic and metal-organic compounds (4th Ed.) 1, Van Nostrand, Princeton, New Jersey, p. 1407

Macdonald, A.H. and Fyfe, W.S.
1985: Rate of serpenitization in seafloor environments; *in* Oceanic Lithosphere, e.d. F.G. Sharman and J. Francheteau; Tectonophysics, v. 116, p. 123-135.

Moores, E.M. and Vine, F.J.
1971: The Troodos Massif, Cyprus and other ophiolites as oceanic crust: evaluation and implications; Philosophical Transactions of the Royal Society of London, v. 268, p. 443-466.

Potter, R.W. II, Clynne, M.A. and Brown, D.L.
1978: Freezing point depressions of aqueous sodium chloride solutions; Economic Geology, v. 73, p. 284-285.

Riley, J.P. and Chester, R.
1971: Introduction to marine chemistry; Academic Press, London-New York,

Roedder, E.
1971: Fluid inclusion studies on the porphyry-type ore deposits at Bingham, Utah, Butte, Montana and Climax, Colorado; Economic Geology, v. 66, p. 98-120.

Roedder, E.
1979: Fluid inclusions as samples of ore fluids; *in* Geochemistry of Hydrothermal Ore Deposits, 2nd Ed., ed. H.L. Barnes, Wiley, New York, p. 684-737.

Roedder, E.
1984: Fluid inclusions; Reviews in Mineralogy, Mineralogical Society of America, v. 12.

Rona, P.A., Bostrom, K., Laubier, L., Smith, K.L. Jnr. (eds.)
1983: Hydrothermal Processes at Seafloor Spreading Centres; Plenum Press, New York-London, p. 796.

Shepard, T.J.
1981: Temperature-programmable, heating-freezing stage for microthermometric analysis of fluid inclusions; Economic Geology, v. 76 p. 1421-1247.

Vanko, D.A.
1986: High-chlorine amphiboles from oceanic rocks: Product of highly-saline hydrothermal fluids?; American Mineralogist, v. 71 p. 51-59.

Vibetti, N.J.
1986: Hydrothermal metamorphism at Troodos, Cyprus; Ph.D. thesis, University of Western Ontario, London, Ontario, Canada.

Wilson, R.A.M.
1959: The geology of the Xeros-Troodos area; Memoir Geological Survey of Cyprus, no. 1, p. 135.

Magnetic Properties, Oxide Petrography, and Alteration in the Cyprus Crustal Study Project Drill Hole CY-4 Section through the Lower Sheeted Complex and Upper Plutonic Complex of the Troodos, Cyprus, Ophiolite

J.M. HALL[1], B. FISHER[1], C. WALLS[1], T. WARD[1], L. HALL[1], H.P. JOHNSON[2] AND J. PARISO[2]

[1]Department of Marine Geology, Dalhousie University, Halifax, Nova Scotia, Canada B3H 3J5
[2]Department of Oceanography, University of Washington, Seattle, Washington, U.S.A. 98195

Hall, J.M., Fisher, B., Walls, C., Ward, T., Hall, L., Johnson, H.P. and Pariso, J., Magnetic properties, oxide petrography, and alteration in the Cyprus Crustal Study Project drillhole CY-4 section through the lower sheeted complex and upper plutonic complex of the Troodos ophiolite, Cyprus; in *Cyprus Crustal Study Project: Initial Report, Hole CY-4, ed. I.L. Gibson, J. Malpas, P.T. Robinson and C. Xenophontos; Geological Survey of Canada, Paper 88-9, p. 235-278, 1989.*

Abstract

This report describes the distribution of five magnetic and nine oxide petrographic properties for the 2263 m vertical section through the Troodos Cyprus ophiolite, sampled in the Cyprus Crustal Study Project drillhole CY-4. The magnetic properties reported are intensity of natural remanence, Jo, initial susceptibility, K, mean demagnetization field, MDF, saturation magnetization, Js, and Curie Temperature, Tc. The Fe-Ti oxide parameters reported are deuteric oxidation state, hydrothermal oxidation state, low temperature oxidation state, titanomagnetite secondary reconstruction, chains of secondary magnetite, overgrowths of secondary magnetite, martite, secondary hematite replacement of magnetite, and a measure of the ratio of primary to secondary magnetite. The principal general results are the close correspondence between the main lithologic, magnetic and oxide alteration zones, and the intense polyphase alteration in the dike zone, with clearly decreased intensity of alteration in the dikes of the Sheeted Complex-Plutonic Complex transition zone.

Résumé

Cet article décrit la distribution des propriétés magnétiques (5) et des caractères pétrographiques (9) des oxydes présents dans les 2263 m de section verticale dans l'ophiolite de Troodos obtenue lors du forage CY-4 du Projet d'étude de la chroûte terrestre à Chypre. Les propriétés magnétiques concernées sont: rémanence naturelle, Jo; susceptiblilité primaire, K; champ démagnétisant moyen, MDF; saturation magnétique, Js; et le point Curie, Tc. Les observations sur les oxydes ferro-titanés comprennent: état d'oxydation météorique, état d'oxydation météorique, état d'oxydation hydrothermale, état d'oxydation à basse température, cristallisation de titanomagnétite secondaire, trains de magnétite secondaire, croissance épitaxique de magnétite secondaire, martite, remplacement de la magnétite par de l'hématite secondaire, et une évaluation de la proportion magnétite primaire versus magnétite secondaire. Les résultats généraux principaux sont facilement corrélables aux horizons lithologiques, magnétiques et oxydés de même qu'à l'intense transformation polyphasée dans les dykes. Ceci s'accompagne d'une transformation décroissante avec la profondeur dans les dykes du complexe filonien vers la zone de transition.

INTRODUCTION

The Cyprus Crustal Study Project (CCSP) is a multi-disciplinary international re-examination of the Troodos, ophiolite with two major objectives: to determine features of oceanic crust to depths that cannot be reached in the present oceans and to determine the origin of ophiolites. The project used research drilling as a major tool. This report describes initial results from the magnetic and oxide petrographic examination of material from CCSP Drill hole CY-4. A complementary report (Pariso and Johnson, 1989) will describe the paleomagnetism of the CY-4 section. The Troodos ophiolite (Coleman, 1977; Gass, 1980) is an uplifted segment of Tethyan crust produced in a spreading environment. The Troodos ophiolite is notable in apparently having experienced little alteration and tectonic disruption other than acquired as in-situ oceanic crust. The ophiolite sequence consists of a pseudo-stratigraphic succession in which an Extrusive Series, consisting of pillowed and sheeted submarine extrusives, overlies a transition to a dike complex, termed the Basal Group. An underlying zone consisting largely of thin, parallel, subvertical basic dikes, the Sheeted Complex, is succeeded at depth by a transition to the Plutonic Complex of higher level gabbros with minor plagiogranites and lower level ultramafics.

CCSP Drill hole CY-4, at 2263 m depth, the deepest research hole of the project, with a recovery of 99.9%, is located at 34°54′06″N, 33°05′38″E near the village of Palekhori. The top of the hole is located in the lower part of the Sheeted Complex. The transition to the underlying Plutonic Complex extends from 300 to 1300 m depth, but the change in dike density from 75% to 25% occurs over a 190 m interval from 630 to 820 m. The dominant plutonic lithology in this transition zone is isotropic gabbro, of one or more varieties, of which a small number of occurrences of magnetite gabbro are of particular interest. The gabbro occurs as screens between dikes that clearly predate the dikes. In contrast, the plagiogranites and related lithologies occur as thin dikes, or as the matrix in intrusive breccias, and clearly postdate both basic dikes and gabbro screens. The plagiogranites and allied lithologies occur most commonly in the 700 to 1100 m interval, and comprise a maximum close to 20% of the section in the 900-1000 m interval. The interval from 1300 m to 1750 m comprises a substantial number of units of a variety of types of isotropic or faintly layered gabbros, below which begins a transition to a series of ultramafic rocks, with the abundance of ultramafics increasing towards the bottom of the hole at 2263 m. The ultramafic lithologies are all cumulate in nature, indicating that while the Plutonic Complex has been sampled over a depth interval of almost a kilometer, the petrologic crust-mantle boundary, marked by a change from cumulate to tectonite textures, was not reached. The olivine bearing gabbros and ultramafics at below 1750 m depth are variably serpentinized, with serpentinization increasing sharply over the last 50 to 100 m of the section.

The question of the relevance of properties of the Troodos ophiolite to in-situ oceanic crust will be discussed in detail elsewhere. For the properties considered in this report, magnetization and alteration, it is likely that the Troodos results from the Sheeted Complex are particularly relevant, as a similar complex has been identified in the in-situ oceanic crust at DSDP site 504B (Anderson et al., 1985). Gabbros and ultramafics are also well known from fault scarps in the in-situ ocean basins, e.g. Bonatti et al. (1979), but their relationship to each other, and other constructional units, and their alteration characteristics, are not yet well known.

A number of other investigations of the magnetization and alteration of ophiolitic rocks are available for comparison with the Troodos results. Banerjee (1980) reviews a number of ophiolites and finds that several, including Troodos, have probably only experienced sea-floor processes. Banerjee reviews a number of properties, such as intensity of remanent magnetization and thermomagnetic behaviour, that are dealt with in this report. His results are similar to some of the results reported here, but are based on only small sets of samples that are not related exactly in depth. Luyendyk et al. (1982) and Luyendyk and Day (1982) report on some magnetic and oxide properties of the Sheeted Complex and gabbroic components of the Samail ophiolite of Oman. Their studies are extensive, but are restricted to samples from discrete sites, and they are faced with the difficulty of resolving sea-floor effects from the effects of prolonged subaerial weathering.

Study of the CY-4 drill core section offers several advantages over these previous studies. Firstly, subaerial weathering is not a concern except over the uppermost few meters of the section. Secondly, continuous core recovery allows uniformly spaced sampling, based on full knowledge of the relationship of all lithologic units present. This combination of circumstances should allow representative properties of different constructional units, and any broad trends with depth, to be ascertained with confidence, and the history of sea-floor alteration to be followed without interference from other effects.

MAGNETIC PROPERTIES (TABLE 1)

Five magnetic properties are reported here: the intensity of natural remanence (Jo), initial susceptibility (K), mean demagnetization field (MDF), saturation magnetization (Js), and Curie temperature (Tc). Measurements of Jo, K and MDF were shared

between Dalhousie University and the University of Washington. Jo and MDF measurements at Dalhousie University were made using a Schonstedt DSM-2 magnetometer and a GSD-5 alternating field demagnetization unit, while those made at the University of Washington involved use of a cryogenic magnetometer and Schonstedt demagnetization unit. Js and Tc measurements were made as described in Hall and Ryall (1977), at Dalhousie University.

Close to 1000 measurements are available for Jo, K and MDF, or about one measurement every two meters on average. The comparable figures for Js and Tc are 460 and 185, or about one measurement for every five and twelve meters on average, respectively.

(i) Intensity of Natural Remanence, Jo

The distribution with depth of Jo (Figure 1) shows most values to be $\leq 20 \times 10^4$ cgs with a number of narrow or broader areas of notably higher values, i.e.: (a) A sharp peak between 500 and 600 m with values extending up to 100×10^4 cgs.; (b) A number of zones extending over most of the interval between 700 and 1500 m depth in which a significant number of values of up to 50×10^{-4} cgs, and a few values of up to 100×10^{-4} cgs, occur.; (c) Two zones, from 1830 to 1970 m, and from 2200 to the bottom of the hole at 2263 m, in which Jo extends up to 200×10^{-4} cgs.

Petrologically, the dike component of the section can be subdivided into aphyric and phyric categories. Figure 2 shows that these have similar Jo depth distributions with, for example, high values from both categories occurring in the 500-600 m depth interval. Two lithologies within the plutonic group show distinctive Jo values (Figure 3). Some of the high level gabbros, listed in the Core Description volumes as magnetite gabbros, occurring as screens within the dikes, show high Jo values, while others show only average values. This scatter could be due to the strong heterogeneity of some of these magnetite gabbros, in which clusters of millimeter sized opaques occur at spacings of the order of centimeters. Again, many of the more highly serpentinized ultramafics below 1900 m depth show strong Jo. Degree of serpentinization has been assessed semi-quantitatively by assigning a colour to each mini-core sample (see caption to Table 1 for details), darkness being taken as a measure of intensity of serpentinization. Samples with a darkness equivalent to a colour code of $S<4$ are distinguished on Figure 3 by a filled triangular symbol. It will be noted that all nine most strongly magnetized ultramafic samples ($94<Jo<184 \times 10^{-4}$ cgs) are in the strongly serpentinized category as are a number of moderately strongly magnetized samples ($20<J<60 \times 10^{-4}$ cgs). Several strongly serpentinized samples show quite weak Jo, e.g., at 2059.50 m (16.6×10^{-4} cgs) and at 2113.35 m (7.01×10^{-4} cgs). A possible explanation for these low values lies in the very soft nature of part of the magnetization of many highly serpentinized ultramafics. It would be easy for these samples to acquire significant soft components in the laboratory in opposition to a more stable primary component.

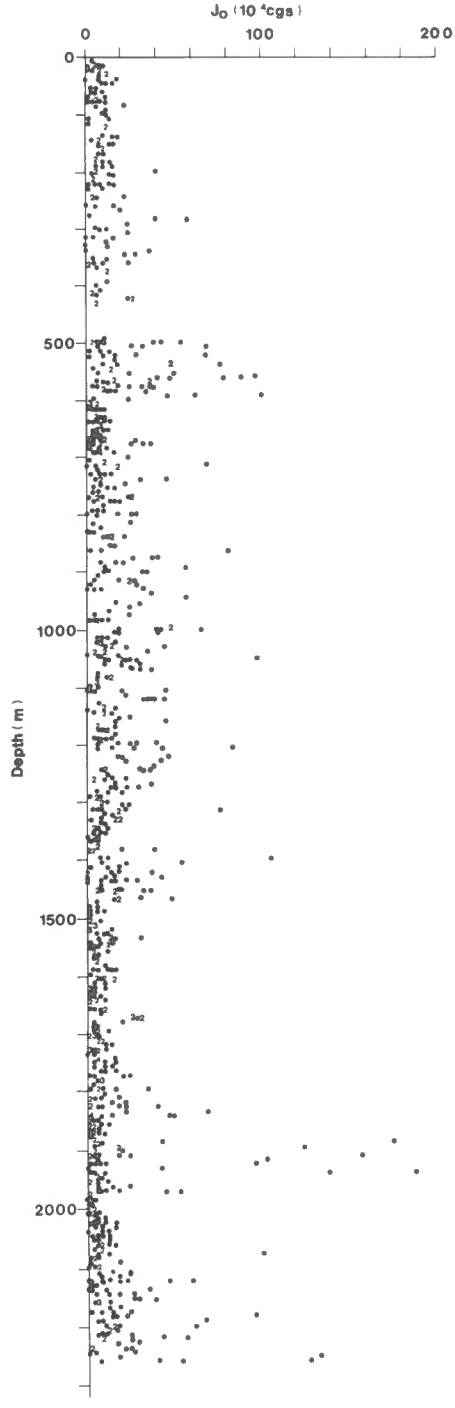

Figure 1: Drill hole CY-4. Distribution with depth of intensity of natural remanence, Jo, for all lithologies.

TABLE 1. Magnetic and Oxide Petrographic Properties of Samples from CCSP Drill Hole CY-4

Depth	Unit	Lith	Sent to	Jo $\times 10^{-4}$	K $\times 10^{-4}$	MDF	Js	Tc	Oxide Classifications or Comments
11.35	2.01	A	J.H.	3.05	7.6	180	0.73	535	Sr6m4 P:S=-1.0
12.00	@	A	A.W.	6.23	24.08	90			
12.65	3.02	A	J.H.	9.20	27.5	130			
13.99	@	A	J.H.	7.42	28.4	80	2.15		
15.65	4.01	A	A.W.	5.53	11.01	380			
18.13	4.02	A	A.W.	1.88	8.03	350			
21.41	6.01	A	A.W.	3.97	20.43	310			
22.45	6.02	A	J.H.	1.49	5.8	245	0.16	540	Sr6m1ah1 P:S=-1.0
23.45	6.03	A	J.H.	8.55	39.5	140			
23.86	@	A	A.W.	8.95	38.23	120			
28.05	7.01	A	A.W.	7.19	25.38	165			
31.00	8.01	A	J.H.	12.3	89.9	105	5.07		
32.48	9.02	A	J.H.	11.5	76.7	145			sm int incr in J
36.48	10.2	A	A.W.	0.51	108.44	325	2.11		
39.17	11.3	A	A.W.	7.59	19.12	130			
39.86	11.4	P	A.W.	18.8	42.30	120			
42.25	@	P	J.H.	9.91	49.0	220	2.77		C3 H3 L1 Sr5-6m3-4o1-3 P:S=-0.99
43.48	@	P	A.W.	15.6	54.46	195			
48.15	13.1	P	A.W.	12.2	40.97	135	1.56		
52.23	15.1	A	J.H.		11.3				
53.07	15.3	A	A.W.	3.67	4.6	>500	2.20		sm int incr in J
54.30	15.4	A	J.H.		1.5				
55.84	16.1	A	A.W.	6.97	1.3	>500			sm int incr in J
58.85	17.1	A	A.W.	6.01	38.23	140	2.36		
61.82	17.3	A	A.W.	9.13	58.18	180			
62.64	18.1	A	J.H.	3.13	78.8	335	4.82	560	int incr in J C1 H1-2 L1 Sr6 P:S=-1.0
64.81	@	A	J.H.		27.1				
67.61	19.3	A	A.W.	12.6	58.09	50	3.26		
72.59	20.4	A	A.W.	2.79	28.33	95			
72.90	20.5	A	A.W.	7.92	98.32	90			
73.65	20.8	A	A.W.	12.4	92.65	40	5.15		
73.78	20.9	A	A.W.	5.81	58.45	90			
74.53	21.2	A	A.W.	6.52	26.77	60			
75.35	21.3	A	J.H.		13.6				
76.41	21.5	A	A.W.	2.31	30.56	90			
76.51	@	A	J.H.		15.0				
78.02	22.1	A	A.W.	4.52	55.00	95	3.25		
84.49	23.5	A?	A.W.	22.6	50.21	70	2.38		
85.15	@	A?	J.H.		55.0				
86.22	23.5	A?	J.H.	6.41	40.4	135	2.60		int incr in J C3 H2-3 L1 Sr0-6m1 P:S=+0.50
88.30	@	A?	J.H.		47.9				
91.65	25.2	D	A.W.	11.1	33.97	55	2.11		
96.25	26.3	D	J.H.		69.8				unoriented
97.40	27.2	D	J.H.		47.8				unoriented
98.30	@	D	J.H.	11.3	40.8	55	2.66	535	unoriented C2-3 H2-3 L1 Sr0-2(3-6)ah1 P:S=+0.50
102.67	28.2	A	A.W.	9.65	61.74	55	5.16		
105.82	29.2	A	A.W.	2.98	18.01	125			
107.28	30.2	A	J.H.		4.2				
107.61	30.3	SLP	A.W.	13.5	56.00	65	4.11		
107.82	@	SLP	J.H.		57.5				
109.40	30.4	SLP	J.H.		101.0				unoriented
114.26	31.2	A	A.W.	1.38	46.36	70	2.18		
118.25	32.2	P	J.H.		55.0				
119.21	@	P	J.H.		61.8				
120.55	@	P	J.H.	12.7	59.5	165	3.17	535	sm int incr in J C2-3 H1-3 L1 Sr5-6 P:S=-0.99
123.53	@	P	A.W.	11.4	63.35	65	3.24		
129.05	35.1	SPP	J.H.		68.4				unoriented
130.50	36.1	A	J.H.		73.8				
131.63	@	A	J.H.		43.9				
134.17	37.1	SPP	A.W.	17.6	91.75	55	0.53		
136.83	37.5	SPP	A.W.	9.98	63.00	30			sm incr in J at dn=100
139.13	38.1	A	A.W.	16.9	70.72	35	1.90		
141.50	38.2	A	J.H.		54.1				
141.90	@	A	J.H.	4.44	48.0	135	2.58	540	C2-3 H2-3(4) L1 Sr6ah1 P:S=-1.0
143.95	@	A	J.H.		42.6				
144.00	@	A	A.W.	8.10	42.15	80			
147.05	40.1	PP	A.W.	8.30	64.36	70	6.55		
151.18	40.2	A	A.W.	15.1	50.04	70			
152.88	42.2	A	J.H.		67.8				

Depth	Unit	Lith	Sent to	Jo $\times 10^{-4}$	K $\times 10^{-4}$	MDF	Js	Tc	Oxide Classifications or Comments
153.09	@	A	A.W.	13.8	92.28	45	4.97		
154.12	42.5	A	J.H.		25				
154.90	42.6	A	J.H.		111.4				
156.85	@	A	A.W.	8.12	51.43	65	2.54		
160.35	43.4	SLP	A.W.	9.32	34.77	85			
163.38	44.5	P	J.H.	10.3	49.5	105	2.62	540	C2-3 H2-3(4) L1 Sr6(5) P:S=-1.0
164.62	@	P	J.H.		50.3				
165.49	@	P	J.H.		36.1				
166.00	@	P	A.W.	9.48	41.18	105	2.55		
171.13	47.1	A	A.W.	8.78	47.64	245			
173.64	47.2	A	J.H.		55.4				
175.46	@	A	J.H.	6.78	56.1	240	0.61		int incr in J
176.58	@	A	J.H.	5.44	58.4	295			
185.18	@	A	J.H.	14.2	56.8	115	3.17	525	C2-3 H2(3) L1 Sr6 P:S=-1.0
186.42	@	A	J.H.	9.22	64.6	190			sm int incr in J
187.90	@	A	J.H.	10.1	64.1	100	3.89		
192.85	@	A	A.W.	5.74	14.50	250			
194.22	53.1	SLP	A.W.	15.9	67.95	60			
196.84	53.3	SLP	J.H.	40.6	37.4	110	2.34		
197.80	@	SLP	J.H.	5.82	40.2	65			
198.78	@	SLP	J.H.	5.31	47.7	70	3.00	550	C2-3 H3-4 L1 Sr2-6ah1 P:S=-.75
208.24	56.1	SLP	J.H.	15.2	65.4	95	5.60		
209.20	57.1	SLP	J.H.		53.9				
209.24	@	SLP	A.W.	13.9	55.67	45			
210.66	57.2	A	A.W.	3.53	22.39	40			
210.88	@	A	J.H.		25.7				
212.82?	58.1	A	A.W.	4.72	27.93	155			
213.43	58.3	A	A.W.	3.27	30.24	100	2.02		
219.43	58.4	SPP	J.H.		82.9				
219.58	@	SPP	A.W.	5.91	31.62	45	2.01		
221.06	60.3	A	A.W.	1.48	13.25	145			
221.38	60.4	A	J.H.		34.2				
221.83	60.5	A	A.W.	13.1	52.26	30			
222.32	60.6	SLP	J.H.		38.2				
222.45	@	SLP	A.W.	7.40	40.25	40			
224.75	60.7	A	A.W.	16.8	72.88	30	5.17		
227.78	61.1	P	A.W.	1.36	12.86	30			
230.26	62.4	A	A.W.	10.5	76.55	35	3.35		
231.48	63.1	SPP	J.H.		0.5				
233.62	63.2	A?	J.H.		60.3				
234.49	63.3	A	J.H.		63.7				
245.12	66.1	SPP	J.H.		43.4				
245.35	@	SPP	A.W.	21.0	85.82	35			
245.89	@	SPP	J.H.	4.73	84.5	115	4.19	525	C2-3 H2-3 L1 Sr5-6 P:S=-0.95
247.68	67.2	A?	A.W.	6.39	41.69	40			
248.85	67.6	A	A.W.	4.72	59.89	40	4.16		
255.00	68.3	A	J.H.		89.0				
255.84	69.1	A	J.H.		60.9				
257.32	@	A	J.H.		48.5				
258.15	@	A	A.W.	16.6	78.93	30	4.01		
260.72	70.1	A	A.W.	6.31	24.74	45			
262.41	70.5	A	A.W.	0.35	0.70	350	0.23		sm int incr in J
267.39	71.1	A	J.H.		69.3				
269.20	@	A	J.H.		67.5				
270.58	@	A	J.H.		62.6				
270.96	@	A	A.W.	19.5	67.15	40	4.03		
272.50	73.2	A	A.W.	2.40	15.92	80			
279.45	74.2	A	J.H.		115.1				
280.50	75.2	G	J.H.	39.9	97.5	15	4.22	540	C2-3 H3(4) L1-2 Sr2-6 P:S=-0.95
282.09	@	G	J.H.		103.0				
283.43	@	G	A.W.	58.1	122.56	35	4.51		
289.50	76.5	A	A.W.	24.4	61.24	45	4.06		
291.35	77.1	A?	J.H.		33.0				
292.30	@	A?	J.H.		79.0				
292.95	@	A?	J.H.		76.6				unoriented
296.40	79.2	A	A.W.	8.93	50.4	40	2.75		
300.96	80.2	A	A.W.	5.04	34.78	115	2.15		C2-3 H2(3-4) L1 Sr0-6 P:S=0.0
301.19	@	A	J.H.	11.01	35.6	210	1.96	565	int incr in J
302.86	@	A	J.H.		48.9				
303.88	81.1	A	J.H.		12.2				

Depth	Unit	Lith	Sent to	Jo $\times 10^{-4}$	K $\times 10^{-4}$	MDF	Js	Tc	Oxide Classifications or Comments
306.96	82.3	A	A.W.	23.4	76.27	35			
311.65	83.1	A	A.W.	4.20	11.16	75	1.32		
313.12	@	A	J.H.		9.8				
314.28	@	A	J.H.		1.0				
315.34	86.1	A	A.W.	10.1	55.0	35			int incr in J
315.48	@	A	J.H.		45.0				
317.38	86.2	P	A.W.	15.0	41.34	30	1.44		
324.78	89.1	A	J.H.		43.5				
325.02	@	A	A.W.	11.2	49.88	30	3.46		
326.15	89.2	A	J.H.		61.8				
328.05	89.4	G	J.H.		89.1		6.36	530	5% mt
329.35	90.3	D	A.W.	12.3	76.5	45			
332.00	90.7	A	A.W.	28.0	101.01	30			
336.10	91.2	D	J.H.		72.6				
336.63	@	D	A.W.	37.5	82.02	125	6.68		
337.17	92.1	D	J.H.		65.6		0.16	560	0.5-2.0mm mt rept C2-3 H3 L1 Sr1-6 P:S=-0.25
337.25	@	D	A.W.	35.4	67.97	40	7.57		
339.05	92.2	A/P	J.H.		77.5				
341.78	93.1	A	A.W.	21.1	102.10	40	4.78		
347.53	94.2	A	A.W.	27.1	79.88	30	4.36		
347.85	@	A	J.H.		83.5				
348.10	@	A	J.H.		77.5				
351.05	@	A	J.H.		39.9				
354.04	@	A	A.W.	4.81	26.52	145	1.52		
354.34	96.1	A	A.W.	11.3	40.78	40			
357.70?	97.1	P	A.W.	23.3	103.20	30			
360.27	97.3	A	J.H.	2.73	35.6	495	1.72		int incr in J C2-3 H2(3) L1 Sr0-6 P:S=0.0
360.82	@	A	A.W.	1.68	26.99	460			int incr in J
361.12	98.1	A	A.W.	10.2	73.23	40			
361.64	@	A	J.H.		88.8				
362.77	@	A	J.H.		71.6				
363.86	98.2	SPP	A.W.	3.64	45.02	300			
367.53	98.2	SPP	A.W.	6.73	37.79	110			
372.73	99.1	P	A.W.	11.3	30.30	65			
373.12	101.1	SLP	J.H.		83.4				
374.45	101.2	A	A.W.	11.5	74.83	35	3.33		
374.85	101.3	A	J.H.		39.9				unoriented
390.27	104.2	A	A.W.	12.2	41.51	60	2.06		
394.05	106.1	A	J.H.		67.0				
395.58	@	A	J.H.		71.8				
396.12	@	A	J.H.		72.9				
396.90	107.1	A	A.W.	5.05	23.65	115	1.27		
405.73	108.2	A	J.H.		62.4				
407.37	110.1	A	J.H.		38.1				
408.36	@	A	J.H.		42.3				
409.97	111.1	A	A.W.	8.38	29.81	60	2.42		
413.83	111.2	G	A.W.	4.18	57.24	215	2.50		
414.22	112.2	A	A.W.	4.95	61.81	325			
414.30	112.3	SLA	A.W.	5.16	57.24	95			
417.42	112.4	A	J.H.		70.9				
418.32	@	A	A.W.	26.3	63.39	35			
418.82	113.1	D	J.H.		120.2		2.58	565	10% mt rept
419.69	113.2	G	J.H.	25.8	94.2	55	4.03	540	Sr6 P:S=-1.0
419.78	@	G	A.W.	23.8	95.18	35			
427.84	115.2	A	A.W.	5.33	15.63	145			
428.72	@	A	J.H.		60.2				
430.08	@	A	J.H.		99.4				
430.19	116.1	A	A.W.	5.33	17.66	105	0.98		
431.61	116.2	A	J.H.		83.3				
439.42	118.3	A	A.W.	1.34	2.68	185			
439.92	118.5	A	A.W.	4.62	31.72	90			
440.26	119.2	SLP	A.W.	7.63	33.63	90			
440.33	@	SLP	J.H.	9.49	75.2	35	3.96	555	Sr6ah1 P:S=-1.0
441.67	@	SLP	J.H.		23.5				
443.24	@	SLP	J.H.		19.3				
448.50	121.1	A	A.W.	4.90	29.56	200	1.77		
451.99	121.4	A	J.H.		75.7				
453.91	@	A	J.H.		76.1				
455.12	@	A	J.H.		88.6				
464.04	123.1	A	J.H.	5.04	14.8	380	0.52	530	Sr6(ah1) P:S=-1.0

Depth	Unit	Lith	Sent to	Jo $\times 10^{-4}$	K $\times 10^{-4}$	MDF	Js	Tc	Oxide Classifications or Comments
465.00	@	A	A.W.	5.92	15.53	235			
466.02	125.2	SLP	A.W.	6.45	3.34	350			
466.04	@	SLP	J.H.		2.5				
466.28	@	SLP	A.W.	3.32	10.00	245	0.29		
466.54	125.3	SLP	J.H.		53.6				
467.48	@	SLP	A.W.	1.40	32.5				large soft component, no reliable MDF
470.55	126.3	A	A.W.	5.73	18.60	80	0.63		
475.36	@	A	J.H.		37.3				
476.26	@	A	A.W.	15.5	30.00	90			
476.89	128.1	A	J.H.		150.5				
478.42	@	A	J.H.	33.9	92.1	45	5.41	555	C(2-3) H3 L1 Sr5-6m1ah3 P:S=-1.0
484.40	130.2	A	A.W.	34.4	120.19	40			
484.73	130.3	A	A.W.	18.7	104.03	40			
485.33	130.5	A	A.W.	9.49	38.24	45			
485.62	130.6	A	H.P.	85.3	141	69	6.96		
486.19	@	A	A.W.	9.41	122.10	270			int incr in J
486.25	@	A	H.P.	25.4	143	116			
486.87	130.9	A	A.W.	12.6	99.40	40			
489.38?	131.5	A	A.W.	9.75	49.48	55	3.46		
495.40	132.4	A	H.P.	37.6	179	36			
496.56	133.2	A	H.P.	53.5	185	37	6.79		
497.10	133.3	A	A.W.	41.7	140.87	30			
497.53	133.5	A	H.P.	10.6	68.0	107			
499.89	134.2	A	A.W.	3.74	135.24	15			
500.47	134.4	A	A.W.	6.95	114.52	30	6.58		
501.26	134.6	A	A.W.	7.53	104.80	45			
501.70	134.7	A	A.W.	4.19	13.49	230			
507.29	135.5	A	A.W.	5.75	19.71	190	1.12		
507.76	135.6	A	A.W.	25.8	73.64	40			
508.56	136.4	A	A.W.	31.6	70.94	40			
509.20	@	A	H.P.	68.5	169	78			
509.89	@	A	H.P.	13.1	14.4	255			
511.10	@	A	H.P.	7.95	4.37	295	0.16		
514.45	136.4	A	A.W.	1.66	4.83	375			
518.45	138.1	P	A.W.	27.0	53.22	50			
519.40	138.3	P	A.W.	68.0	84.04	35			
519.87	138.4	A	J.H.	2.85	40.1	500	4.16	545	int incr in J Sr6ah2 P:S=-1.0
519.87	@	A	H.P.	16.4	65.0	136			
521.63	139.4	SLP	H.P.	9.45		64	0.37		
525.68	140.1	G	G.S.				12.67		
529.75	141.3	A	U.B.				8.82	475	unoriented
530.88	141.4	A	J.H.	16.0	73.8	60			
533.02	142.2	A	H.P.	48.2	77.9	45			
533.04	@	A	J.H.	75.7	87.1	40	3.16	530	C1-3 H1-2 L1 Sr5-6 P:S=-1.0
534.15	@	A	H.P.	48.9	94.1	50			
535.28	143.2	SLP	J.H.	9.94	94.7	60	3.50	540	Sr6ah1 P:S=-1.0
539.22	143.9	SLP	J.H.	17.8	78.9	195			sm int incr in J
540.30	144.1	A	U.B.				1.05		unoriented Sr6 P:S=-1.0
542.14	144.3	SLP	H.P.	14.8	113	39			
543.70	145.1	A	H.P.	4.17	27.8	59			
545.54	145.5	A	H.P.	14.1	104	58			
547.92	146.3	G	G.S.				15.86 /0.30	510	
548.68	146.4	A	J.H.	6.56	44.1	490			sm incr in J at dn=75
553.52	146.4	A	H.P.	50.0	180	42	4.98		
555.25	148.3	A	H.P.	23.9	83.2	85			
556.32	148.4	G	J.H.	87.7	191.9	40	5.04		
557.33	148.7	A	J.H.	39.4	107.4	40	4.60		H3-4 Sr6ah1 P:S=-1.0
577.33	@	A	H.P.	31.4	165	50			
559.37	@	A	J.H.	96.7	192.6	45			
559.65	149.1	A	J.H.	47.9	109.4	165	6.85	560	
560.95	149.2	A	J.H.	77.3	190.2	40			
563.97	150.4	A	J.H.	10.3	65.0	155	3.12	530	C1(2) H(3) L(1) Sr6 P:S=-1.0
565.09	@	A	H.P.	35.2	91.5	65			
566.38	@	A	H.P.	35.4		53			
567.08	@	A	J.H.	16.3	46.0	175			
568.78	@	A	J.H.	12.5	79.6	55	6.54		
568.78	@	A	H.P.	16.6	142	82			
570.88	152.5	SLP	J.H.	5.84	25.4	100			
573.90	@	SLP	J.H.	6.65	40.6	115			incr in J at dn=100

Depth	Unit	Lith	Sent to	Jo $\times 10^{-4}$	K $\times 10^{-4}$	MDF	Js	Tc	Oxide Classifications or Comments
574.90	153.2	A	J.H.	4.26	56.4	35			
575.18	153.3	A	J.H.	23.2	111.8	75			
576.22	153.4	G	U.B.				16.71 /0.72	530	
577.02	154.1	SLP	J.H.	36.4	91.5	40			
577.02	@	SLP	H.P.	18.8	107	50			
577.98	@	SLP	J.H.	37.6	66.4	40			
579.51	154.3	A	J.H.	14.1	60.2	130			
579.51	@	A	H.P.	10.6	69.4	162			
580.24	@	A	J.H.	12.5	107.4	65	3.08	540	Sr6(ah1) P:S=-1.0
580.24	@	A	H.P.	10.7	64.3	134			
581.90	155.3	SLP	J.H.	15.5	64.3	40			
583.64	155.3	SLP	J.H.	34.7	72.6	55	3.80		
589.72	156.1	G	H.P.	78.7	126	50	9.43	525	
590.30	@	G	H.P.	39.0	105	43	0.90		
591.26	157.3	A	J.H.	23.4	105.9	50			
599.38	159.1	SLP	J.H.	23.2	123.2	45	3.18	545	C1(2) H(3) L(2) Sr6m1ah2 P:S=-1.0
601.12	159.2	A	H.P.	4.14	9.20	400			
602.45	@	A	H.P.	6.83	19.4	200			
603.95	@	A	J.H.	2.30	12.3	>500	0.30& 0.54	520	incr in J at dn=50 C1(2) H(3) L(1) Sr6ah1 P:S=-1.0
603.95	@	A	H.P.	2.27	10.6	550			
604.63	160.1	G	G.S.				0.67	535	
605.36	161.1	A/SLP	J.H.	1.11	9.5	225			
608.06	@	A/SLP	J.H.	5.84	11.3	455			int incr in J
609.41	161.3	A	J.H.	0.27	1.8	40			
610.85	162.1	G	U.B.				0.15	540	
611.45	162.2	A/SLP	J.H.	2.10	37.2	500			incr in J at dn=100
612.62	@	A/SLP	J.H.	3.12	3.0	410	0.37	520	mt rare
614.03	163.1	G	J.H.	6.53	3.0	230	0.17	540	
614.03	@	G	H.P.	9.31	6.96	191			
615.22	@	G	H.P.	3.64	3.43				
616.94	163.3	G	G.S.	7.68	0.99	500	12.77	530	
617.55	163.3	G	G.S.				0.35		
619.80	164.2	G	G.S.				0.53	505	
623.19	164.6	G	U.B.				0.24	540	
625.87	@	G	H.P.	5.09	6.08	435			
626.08	@	G	J.H.	6.70	8.9	350			
628.16	@	G	H.P.	7.68	8.58	450	0.56		
629.48	@	G	H.P.	9.29	35.3	44			
633.74	167.3	A	J.H.	3.98	2.3	440	0.16		
634.50	168.1	A	J.H.	1.62	16.7	195			
636.30	168.5	A	J.H.	5.92	4.5	365			sm int incr in J
638.66	168.6	A	J.H.	14.0	75.5	70	1.55	550	C1-2 H1(2)L1 Sr0(6)? P:S=+1.0 (or-0.50)
638.66	@	A	H.P.	9.16	51.1	100			
640.36	169.3	A	J.H.	8.92	2.2	400	0.12	510	mt rare
640.36	@	A	H.P.	8.76	2.12	20			
641.52	@	A	H.P.	8.10	6.5	470			
649.80	171.5	P	J.H.	5.68	29.5	45	0.92		
651.13	172.3	P	H.P.	3.06	25.2				
652.20	172.5	P	J.H.	5.89	40.3	65			
652.20	@	P	H.P.	6.80	56.4	147			
652.53	172.6	A	J.H.	11.9	40.3	295			
653.59	172.8	SLP	H.P.	9.70	14.4	280	0.31		
659.37	174.1	A/P?	J.H.	3.43	51.2	80	2.51	540	C1(2) H1 L1 Sr(5)6(ah1) P:S=-0.99
660.73	174.2	A/P?	J.H.	5.29	14.9	195	0.14	525	int incr in J pol-thin missing
660.96	174.5	A?/P?	J.H.	7.55	7.97	185			
663.57	174.6	A	J.H.	9.80	54.7	95			
663.57	@	A	H.P.	7.37	65.2	115			
665.02	175.1	A	H.P.	10.8	53.8	82	2.90		
666.45	@	A	J.H.	3.84	23.9	165			
666.45	@	A	H.P.	2.49	17.5	265			
668.00	176.1	PLG	J.H.				0.04	615	unoriented
668.62	176.3	A	J.H.	2.60	35.4	80			
670.05	@	A	J.H.	28.5	80.3	35			
671.29	176.6	A	J.H.	8.14	43.3	60			
673.43	177.3	A	J.H.	25.8	105.3	50	3.54	525	
675.77	178.3	A	J.H.	3.42	3.1	325			
675.77	@	A	H.P.	2.49	4.21	460			
677.25	178.6	G	H.P.	7.49	3.78	261	0.08		

Depth	Unit	Lith	Sent to	Jo $\times 10^{-4}$	K $\times 10^{-4}$	MDF	Js	Tc	Oxide Classifications or Comments
678.12	@	G	J.H.	32.3	4.5	250			sm int incr in J
678.12	@	G	H.P.	36.3	14.0	200			
681.02	179.4	A	J.H.	2.96	3.3	325	0.06	540	Sr6ah3 P:S=-1.0
684.03	180.1	A/P?	J.H.	12.1	38.2	140			
685.35	180.3	G	J.H.	8.76	3.1	430	0.18	520/565	int incr in J minor mt rept
686.42	@	G	U.B.				0.65	565	minor mt rept
687.95	@	G	H.P.	8.80	9.15	325	0.17	555	minor mt rept
689.45	@	G	J.H.	8.64	3.5	385	0.84		
689.94	181.1	A	J.H.	6.98	77.2	45			
689.94	@	A	H.P.	16.2	107	70			
691.02	181.2	A	J.H.	7.03	1.2	445	0.05& 0.17	550	sm incr in J at dn=50 oxides rare
691.02	@	A	H.P.	8.14	2.82	530			mt rare
693.05	182.1	A	J.H.	4.40	4.4	385	0.24	525	
700.93	183.3	G	H.P.	24.3	80.3		7.04	530	
702.02	@	G	J.H.				0.33		unoriented
702.17	@	G	H.P.	10.8	44.1	45	1.00		int incr in J at dn=100
702.17	@	G	J.H.	0.99	29.7	30			
702.17	@	G	H.P.	10.8	44.1	37			
703.47	184.2	G	H.P.	2.98	1.16	430	0.12	555	
705.15	@	G	G.S.				6.64		unoriented
707.78	185.5	A/P?	G.S.				1.10	530	
710.28	186.3	A	J.H.	0.90	13.7	>500			sm incr in J at dn=150
712.28	186.5	G	U.B.				0.42	560	
712.79	187.1	G	H.P.	5.99	1.62	425			
713.90	@	G	J.H.	17.9	3.6	295			
713.90	@	G	H.P.	18.0	6.73	290			
716.20	187.4	G	H.P.	68.0	17.8	181	2.15	560	
716.86	187.5	G	G.S.				0.56	560	
718.30	188.2	G	G.S.				0.12	515	
720.23	188.4	G	J.H.	6.45	1.4	405	0.17	515	sm int incr in J mt rare
722.82	189.2	G	U.B.				0.10	525	
726.08	190.1	A	J.H.	9.51	30.8	330			
726.08	@	A	H.P.	14.2	39.7	305			
726.46	@	A	H.P.	7.41	30.3	427			
728.88	190.2	UNK	H.P.	1.38	0.55	470			
730.26	191.1	G	G.S.				0.20	520	
731.98	191.3	G	G.S.				0.13	535	
733.94	192.2	A	J.H.	30.9	48.4	140			
734.90	@	A	J.H.	7.93	27.9	375	1.46	530	
735.62	@	A	J.H.	5.51	1.4	430	0.09	525	
737.02	192.4	A	H.P.	45.5	25.9	243			
738.88	193.1	G	H.P.	7.01	1.6	440	0.07	545	
740.45	193.2	G	H.P.	7.68	1.96	365	0.10	525	
744.07	194.1	A?	J.H.	22.2	59.5	170	2.65	555	C2 H2-3 L1 Sr6(5) P:S=-0.99
746.50	195.2	G	U.B.				0.10	525	
748.28	195.3	A	U.B.				1.24	525	
751.59	196.1	G	H.P.	3.47	4.25	367			
752.63	196.2	G	H.P.	12.0	3.28	240			
753.75	@	G	J.H.	16.7	1.4	205			
756.74	197.3	G	G.S.				0.18	530	
758.55	198.1	PLG	U.B.				3.72	530	
762.48	199.2	G	J.H.	5.32	3.8	380	0.07	530	
762.48	@	G	H.P.	4.94	1.08	400			
763.74	199.3	A?	J.H.	2.61	33.9	475	0.14	535	int incr in J C1-2 H1-2 L1 Sr0-6 P:S=0.0
763.74	@	A?	H.P.	7.28	52.8	151			
764.38	@	A?	J.H.	6.07	32.2	190			
764.38	@	A?	H.P.	5.67	31.7	400			
766.34	@	A?	J.H.	26.9	61.6	70			
767.64	200.1	A?	J.H.	23.7	56.4	195	2.32	540	C1-2 H1,3 L1 Sr(0-6)? P:S=? Pol-thin lost
769.98	@	A?	J.H.	26.7	80.7	215	3.32/ 0.23	540	sm int incr in J C1(2) H1(2-3) L1 Sr0-6 P:S=-0.70
771.10	201.3	G	U.B.				1.57	525	unoriented
774.42	202.3	A	H.P.	13.6	79.0	240			
775.04	202.4	A	J.H.	16.2	9.0	150			
775.04	@	A	H.P.	17.2	16.0	195			
775.28	202.5	A	H.P.	4.57	3.46	300			
778.42	203.1	A	G.S.				1.69	555	
779.28	@	A	J.H.	9.79	4.4	245	0.51		Sr6ah4 P:S=-1.0
782.32	@	A	U.B.				2.88	540	

Depth	Unit	Lith	Sent to	Jo $\times 10^{-4}$	K $\times 10^{-4}$	MDF	Js	Tc	Oxide Classifications or Comments
786.08	205.1	A	H.P.	4.26	0.76	243	0.08	530	
786.97	@	A	H.P.	9.34	1.03	510			
787.87	@	A	H.P.	6.90	0.93	540			
794.08	206.2	Db/G	U.B.				0.23		
795.67	@	Db/G	U.B.				0.12	560	
797.08	207.1	A	J.H.	28.3	69.5	340			int incr in J
798.38	@	A	H.P.	0.14	0.31	325			
799.68	@	A	H.P.	5.88	9.70	460			
801.08	208.1	G	J.H.	25.5	11.6	190	1.32		
801.08	@	G	H.P.	18.0	5.94	325			
804.55	209.2	G	G.S.				0.27	535	
808.04	210.1	G	U.B.				0.23		mt rare Sr6 P:S=-1.0
810.86	@	G	H.P.	24.6	6.02	193			
812.30	@	G	H.P.	3.84	3.01				
815.98	@	G	G.S.				0.06	535	
823.22	@	G	H.P.	8.36	1.98	375			
825.96	@	G	H.P.	0.90	0.43	385	0.24	540	
826.85	215.1	A	J.H.	4.07	63.2	135	8.12	540	C1-2 H2-3 L1 Sr0-1,6 P:S=+0.75
827.72	215.2	A	J.H.	2.34	0	>500			int incr in J
834.05	@	A	U.B.				0.005	330/530	
836.20	217.1	A	J.H.	9.40	57.5	195	3.92/ 1.65& 3.11	545	C1-2 H1-2 L1-2 P:S=+1.0
836.20	@	A	H.P.	12.7	46.8	148			
837.07	@	A	J.H.	22.6	61.2	155	0.11	515	C1-2 H1-2 L1 Sr1 P:S=+0.95
837.07	@	A	H.P.	14.1	68.8	178			
839.37	218.1	G	H.P.	13.7	64.9	96			
848.52	219.2	G	H.P.	15.5	5.05	252	0.32		
849.85	@	G	H.P.	14.2	4.73	231			
855.55	222.2	A	J.H.	79.0	81.3	125	4.26& 6.30	550	Sr6 P:S=-1.0
859.40	223.1	G	H.P.				0.08	530	unoriented
861.18	223.2	G	H.P.	8.40	1.55	351			
861.62	@	G	H.P.	2.32	0.73	288			
864.93	@	G	G.S.				0.16	530	
873.16	225.1	A	J.H.	37.6	40.7	130	1.55	525	C1-2 H1 L1 P:S=+1.0
875.03	225.2	PLG/G	H.P.	39.7	8.73	171	0.09	540	
877.03	@	PLG/G	H.P.	25.1	4.33	285			
878.36	@	PLG/G	H.P.	19.0	4.31	194			
879.75	@	PLG/G	H.P.	7.58	2.69	440			
884.01	227.6	G	J.H.	15.8	1.9	260			
885.29	227.10	PLG	G.S.				0.28	460/540	
889.54	@	PLG	J.H.	9.14	2.8	245			
891.15	228.3	A	J.H.	55.7	42.3	195	3.06/ 0.74	525	C1-2 H1-3 L1 P:S=+1.0
892.24	229.1	PLG/G	H.P.		0.13	29			
893.40	229.2	PLG	H.P.	32.3	4.90	200			
896.18	@	PLG	H.P.	9.89	1.81	423			
897.01	229.3	A?	J.H.	33.3	69.7	70	4.14	520	C1-3 H1-3 L1 P:S=+1.0
898.06	@	A?	J.H.	12.6	85.1	85	3.77	530	C1-2 H1-3 L1-2 P:S=+1.0
902.58	230.1	PLG/G	J.H.	5.88	2.3	285	1.01		
909.40	232.1	A?	J.H.	28.8	10.1	185	2.80	525	Sr6 P:S=-1.0
909.40	@	A?	H.P.	23.7	7.07	156			
911.49	@	A?	H.P.	23.1	89.0	156			
912.02	@	A?	H.P.	18.1	59.7	179			
913.52	232.2	PLG/G	H.P.	4.75	6.62	330	0.61		
921.12	@	PLG/G	J.H.	28.3	5.4	315	0.25		
923.42	@	PLG/G	J.H.	2.77	0.6	185			
926.90	234.2	G	H.P.	7.44	2.69	230	0.07		
928.32	@	G	H.P.	3.34	0.83	235			
929.58	235.1	U/G	H.P.	0.15	0.19	520			
931.40	235.2	PLG	H.P.	31.0	9.20	177	0.42		
937.45	237.1	G/PLG/U	J.H.	36.1	7.0	225	0.53		int incr in J
943.64	237.3	PLG/G	H.P.	55.0	15.1	230	0.31		
944.78	@	PLG/G	H.P.		50.9	136			
947.17	@	PLG/G	H.P.	16.3	4.56	141			
947.80	@	PLG/G	H.P.	29.9	11.7	170	0.33		
953.68	239.4	G	G.S.				0.25		
955.43	@	G	U.B.				0.36		
956.76	@	G	U.B.				0.22		

Depth	Unit	Lith	Sent to	Jo $\times 10^{-4}$	K $\times 10^{-4}$	MDF	Js	Tc	Oxide Classifications or Comments
957.12	@	G	U.B.				0.20		
960.98	241.1	PLG/G	J.H.	23.7	3.1	195	0.28	535	C1 H1 L1 Sc1r0(6)? P:S=+0.80
965.69	242.1	G	H.P.	12.9	12.6	173	0.54		
975.78	242.3	PLG/G	J.H.	23.0	4.4	135			
976.76	243.1	A	J.H.	3.01	57.5	295	2.94& 3.73	520	int incr in J C1-2 H1-3 L1 P:S=+1.0
977.87	@	A	H.P.	7.94	57.5	300			
979.42	@	A	H.P.	4.56	75.8	195			
981.02	@	A	H.P.	12.5	47.6	93			
982.35	@	A	J.H.	6.63	51.0	95	0.77	550	C1-2 H2-3(1,4)L1-2 P:S=+1.0
982.35	@	A	H.P.	5.89	65.3	93			
984.22	@	A	J.H.	2.94	102.0	340	4.03	540	C1-2 H1(2)L1 Sr1-0 P:S=-0.80
995.60	246.1	A?P?	J.H.	39.1	21.4	180			
995.60	@	A?P?	H.P.	47.3	34.6	140			
997.47	247.3	PLG/G	H.P.	17.8	11.5	178	0.40	555	mt rept C1-2 H1-2 L1-2 P:S=+1.0
999.08	247.5	PLG/G	J.H.	42.9	19.1	165			int incr in J
999.08	@	PLG/G	H.P.	64.8	25.1	156			
1000.17	@	PLG/G	H.P.	48.0	22.2	175			
1001.25	248.1	A	J.H.	16.1	70.1	70	2.97	530	C1-2 H1-3 L1 P:S=+1.0
1002.65	@	A	J.H.	40.1	73.9	60	4.07	540	C1-2 H1-3 L1 P:S=+1.0
1007.44	@	PLG	J.H.	18.2	14.6	140	3.61		sm int incr in J
1008.40	249.3	A?	J.H.	7.29	32.4	185			int incr in J
1008.75	249.4	PLG/G	U.B.				4.03		
1009.65	@	PLG/G	U.B.				0.51		
1012.00	@	PLG/G	U.B.				0.47		
1013.63	@	PLG/G	H.P.	11.0	15.5	224			
1014.98	@	PLG/G	H.P.	6.93	5.28	224	0.40		
1016.48	@	PLG/G	H.P.	8.03	4.29	275	0.22		
1017.90	250	A	J.H.	8.27	12.3	160			sm int incr in J
1017.90	@	A	H.P.	7.99	15.0	200			
1020.68	251.1	PLG/G	J.H.	6.63	23.2	35	1.13		
1022.02	251.4	PLG/G	J.H.	15.1	14.3	200			sm int incr in J
1023.52	251.5	G	J.H.	14.4	26.3	145			
1024.73	@	G	J.H.	21.2	19.5	145	4.29		
1026.33	@	G	J.H.	10.5	14.4	235			
1027.54	@	G	J.H.	14.1	11.4	290			
1030.78	252.1	PLG/G	H.P.	43.3	18.7	187	2.14		
1032.23	@	PLG/G	J.H.	4.54	8.3	190			
1032.23	@	PLG/G	H.P.	3.56	21.9	146			
1033.44	@	PLG/G	H.P.	34.3	7.48				
1034.92	@	PLG/G	J.H.	10.6	7.3	150	0.45		sm incr in J at dn=100
1034.92	@	PLG/G	H.P.	9.98	8.66	179			
1039.47	@	PLG/G	J.H.	7.69	3.0	175	0.46		
1042.19	255.2	PLG	J.H.	17.3	4.2	165			
1043.88	@	PLG	J.H.	5.03	4.8	400			int incr in J
1045.17	255.3	A?P?	J.H.	0.15	0.0	610	2.15		sm int in J and at dn=75/no mt
1048.02	255.5	A	J.H.	28.1	68.6	105			
1048.02	@	A	H.P.	20.4	80.5	200			
1049.55	@	A	J.H.	20.2	38.2	55			
1049.55	@	A	H.P.	22.2	53.3	113			
1050.28	256.1	A?P?	J.H.	95.9	132.8	85			
1050.80	256.3	A?P?	J.H.	23.0	57.7	225	0.84	530	C1-2 H1-3 L2 Sr4-5(1-3,6) P:S=-0.50
1050.80	@	A?P?	H.P.	11.2	38.1	242			
1053.09	256.4	A	H.P.	10.8	64.6	100			
1054.23	@	A	J.H.	10.6	54.6	80	2.71 3.19	515	C1-2 H2-3 L1 P:S=+1.0
1056.15	257.2	A	J.H.	19.6	75.4	60			
1058.72	257.5	A	J.H.	30.1	68.4	55	3.66		
1064.65	258.2	V	J.H.	36.5	57.5	90	3.65		
1066.01	@	V	H.P.	25.6	96.7	78			
1067.68	@	V	H.P.	29.8	77.0	70			
1068.42	@	V	H.P.	23.1	64.2	80			
1070.04	@	V	H.P.	6.62	20.5	139	0.18		
1078.50	261.6	A	J.H.	12.8	10.4	75			
1080.02	@	A	J.H.	13.9	17.5	80	1.21	310/505	C1-2 H1(2) L1 P:S=+1.0
1082.72	261.7	PLG/G	H.P.	6.64	2.18	352			
1084.05	@	PLG/G	H.P.	13.7	12.3	156			
1086.00	@	PLG/G	H.P.	5.36	2.25	197	0.42		
1087.35	262.1	A	J.H.	5.68	23.7	365			int incr in J
1087.35	@	A	H.P.	6.56	31.0	278			

Depth	Unit	Lith	Sent to	Jo $\times 10^{-4}$	K $\times 10^{-4}$	MDF	Js	Tc	Oxide Classifications or Comments
1093.60	263.3	PLG	J.H.	2.22	15.6	50	1.45		
1095.28	263.4	PLG/G	J.H.	6.87	2.5	235			
1100.92	263.4	PLG/G	H.P.	1.84	0.77	400	0.19		
1102.33	265.1	PLG	H.P.	0.06	0.24	505			
1103.85	265.4	A?P?	H.P.	4.38	1.91	230			
1105.33	265.7	A?	J.H.	20.3	44.1	50	1.39	500	C1-2 H2-3 L1-2 P:S=+1.0
1105.33	@	A?	H.P.	44.4	49.0	32			
1112.23	266.2	A	J.H.	22.2	63.7	55	2.38	505	C1-2 H2-4 L1-2 P:S=+1.0
1118.36	267.3	A?	H.P.	10.9	63.6	166			
1119.47	268.2	A?	J.H.	21.1	55.4	40	2.49	515	C1-2 H2-3 L1-2 Sr0-2 P:S=+0.90
1119.90	@	A?	H.P.	13.7	63.4	66			
1121.30	@	A?	H.P.	12.9	61.9	50			
1121.92	@	A?	H.P.	16.9	99.4	47			
1123.22	268.4	A?	J.H.	6.93	71.1	90	3.90		
1132.02	270.1	A	J.H.		56.7				unoriented
1135.37	270.3	A	H.P.	10.8	45.5	169			
1136.58	@	A	J.H.	10.1	25.2	125	1.11	315/530	sm int incr in J
1136.58	@	A	H.P.	0.28	0.26	425			C1-2 H1-3 L1 P:S=+1.0
1137.79	271.1	PLG	J.H.	0.36	0.2	400	0.02		sm int incr in J no mt
1137.79	@	PLG	H.P.	16.0	32.5	89			
1139.99	271.2	A	J.H.	10.9	41.0	45	2.05	515	C1-2 H3-4 L1 P:S=+1.0
1139.99	@	A	H.P.	10.8	36.0	87			
1142.57	272.1	A	J.H.	13.9	43.7	90			
1143.95	272.2	G	J.H.	3.05	25.6	195	0.14		
1151.31	273.2	PLG/G	H.P.	18.6	15.9	155			
1153.78	274.2	G	H.P.	23.1	25.0	150	0.52& 0.37	520/555	ol pseudo. by mt
1155.02	274.3	G	H.P.	44.8	26.7	108			
1160.98	@	G	J.H.	16.2	14.6	100	0.50		
1162.62	@	G	J.H.	16.1	11.7	145			
1168.16	276.2	G	J.H.	6.98	10.9	155	0.26		
1168.16	@	G	H.P.	6.05	10.3	186			
1169.96	@	G	J.H.	12.2	14.6	135			
1169.96	@	G	H.P.	10.2	14.4	178			
1171.07	277.1	G	H.P.	7.76	53.7	140	4.41		
1172.38	@	G	J.H.	12.7	8.8	155	0.82		
1172.38	@	G	H.P.	5.79	14.2	298			
1174.08	@	G	G.S.				0.91		
1175.68	@	G	G.S.				0.44	550	5% mt rept C1-3 H1-3 L1 Sr0-1 P:S=+0.90
1176.98	@	G	G.S.				0.61		
1177.85	278.1	G	J.H.	16.2	17.3	145			
1183.59	279.1	G	U.B.				0.28		
1185.37	280.1	G	H.P.	7.17	24.8	188	1.10		
1187.32	@	G	H.P.	6.54	24.6	242			
1188.57	@	G	H.P.	7.88	22.6	241			
1189.89	280.2	A?	J.H.	10.8	39.0	80	1.37	535	C1-3 H1-3 L1-2 Sr0(1)? P:S=+1.0
1189.89	@	A?	H.P.	3.03	38.1	208			
1191.43	281.4	G	J.H.	14.1	38.4	176			sm int incr in J
1192.82	@	G	J.H.	27.6	29.1	195			sm incr in J at dn=100
1195.78	281.5	G	J.H.	17.9	80.1	40	4.06		
1196.03	@	G	J.H.	24.7	10.2	180			
1197.67	@	G	J.H.	5.04	3.3	205			int incr in J
1198.73	282.4	G	J.H.	39.1	19.0	140			int incr in J
1200.55	@	G	J.H.	42.6	14.3	195	0.70		int incr in J
1203.32	@	G	H.P.	13.2	22.6	158			
1204.98	@	G	H.P.	5.31	5.19	236			
1205.96	@	G	H.P.	26.9	20.2	152	0.41		
1207.32	@	G	H.P.	82.0	27.6	135			
1220.47	285.4	G	H.P.	45.1	35.8	118	0.68		
1221.65	286.1	G	J.H.	20.1	19.5	155			sm int incr in J
1221.65	@	G	H.P.	18.8	19.2	183			
1222.95	@	G	H.P.	42.2	19.7	135			
1225.15	@	G	H.P.	21.5	4.68	178	0.41		
1236.67	287.1	G	J.H.	37.2	9.9	135	0.55		
1238.50	288.1	G	H.P.	32.4	4.73	160			
1239.96	289.1	A	J.H.	7.72	13.7	120			
1239.96	@	A	H.P.	9.03	18.0	125			
1241.35	289.2	G	J.H.	36.3	13.2	145			
1241.35	@	G	H.P.	30.1	8.11	90			
1242.87	289.3	G	H.P.	9.40	3.30	295	0.18		

Depth	Unit	Lith	Sent to	Jo $\times 10^{-4}$	K $\times 10^{-4}$	MDF	Js	Tc	Oxide Classifications or Comments
1251.56	291.2	G	J.H.	11.4	21.3	225	0.11	550	mt rare C1 H1 L1 P:S=+1.0
1253.66	291.3	A	J.H.	3.75	17.4	140	3.46	540	int incr in J C1-3 H3-4 L1 Sr0-6o1 P:S=0.0
1256.63	292.2	G	J.H.	22.2	10.5	160			
1256.63	@	G	H.P.	10.4	2.95	50			
1258.09	@	G	H.P.	13.7	4.55	200	0.19		
1260.13	@	G	H.P.	4.33	4.23	400			
1265.29	293.1	A?	J.H.	35.0	108.8	75	4.67		
1266.87	294.2	A	J.H.	16.0	88.4	110			
1272.75	294.5	G	H.P.	29.1	5.78	221	1.01		
1274.17	@	G	J.H.	21.3	2.0	200			
1274.17	@	G	H.P.	16.1	4.03	261			
1275.45	@	G	H.P.	13.3	5.55	281			
1276.59	@	G	H.P.	11.8	2.76	278	0.16		
1280.55	@	G	J.H.	20.5	79.4	140			
1283.16	296.1	A?	J.H.	6.51	50.6	90	2.36	540	C1-2 H1-3 L1 P:S=+1.0
1284.86	@	A?	J.H.	6.64	62.8	220	2.43	520	int incr in J C2(1) H2(1) L2(1) P:S=+1.0
1286.27	@	A?	J.H.		20.5		0.27		(C1 H1)6 (L1) P:S=+1.0 rare mt.
1287.62	297.2	A?	J.H.	2.42	50.4	175			sm incr in J at dn=100
1289.33	297.3	G	J.H.	6.64	1.7	250			
1290.27	@	G	H.P.	7.96	1.72	258	0.13		
1292.08	@	G	H.P.	7.95	2.71	287			
1295.09	298.1	G	J.H.	7.66	0.6	175	0.17		
1295.09	@	G	H.P.		2.68	240			
1297.93	@	G	J.H.	11.5	2.8	205			
1302.08	300.1	G	J.H.	20.1	4.6	200	0.19		int incr in J
1306.63	@	G	J.H.	23.8	39.7	120			
1307.75	@	G	H.P.	6.59	28.9	180	1.13		
1309.72	@	G	J.H.	22.0	7.3	220			
1309.72	@	G	H.P.	18.6	8.32	235			
1310.43	301.1	G	J.H.	8.59	2.6	220	0.06	575	(C1 H1,6 L1) P:S=+1.0 rare mt.
1310.43	@	G	H.P.	3.15	1.22	280			
1311.97	301.2	G	H.P.	17.3	4.26	260			
1313.68	@	G	J.H.	75.7	47.1	140			
1317.62	302.1	G	J.H.	9.81	4.3	205	0.39		
1321.18	303.1	G	J.H.	14.0	5.8	220			
1323.82	303.3	G	J.H.	16.9	1.9	185	0.30		
1325.15	@	G	H.P.	15.1	3.04	253			
1326.79	@	G	H.P.	8.22	0.99	335			
1328.19	@	G	H.P.	18.7	4.93	200	0.50		
1329.64	304.1	G	J.H.	17.4	5.4	145			
1329.64	@	G	H.P.	2.43	1.10	357			
1330.82	305.1	G	J.H.	9.98	2.8	200	0.28		
1337.24	306.2	G	J.H.	8.72	1.5	240	0.28		
1338.93	@	G	J.H.	3.73	0.9	230			sm int incr in J
1340.49	@	G	J.H.	4.24	1.3	250	0.07	550	C1 H1-2 L1 P:S=+1.0
1343.36	@	G	H.P.	6.32	3.51	260			
1344.76	@	G	H.P.	12.9	4.73	236			
1345.65	307.1	G	J.H.	8.39	2.2	210	0.08		
1345.65	@	G	H.P.	9.44	2.93	225			
1347.10	307.2	G	H.P.	3.24	1.15	275			
1353.25	308.1	G	J.H.	0.10	0.3	445	0.06		
1359.60	309.2	G	H.P.	5.05	2.04	209			
1360.97	@	G	H.P.	3.22	1.34	247	0.05		
1362.62	@	G	H.P.	2.46	1.02	98			
1364.12	@	G	H.P.	5.73	2.89	445	0.15		
1369.68	311.1	G	J.H.	5.01	0.9	220	0.07		
1374.07	@	G	U.B.				0.14	550	C1 H1 L1 P:S=+1.0
1375.88	@	G	J.H.	6.09	2.2	235	0.32		
1377.28	@	G	H.P.	1.04	0.82	264			
1378.65	@	G	H.P.	38.0	7.75				
1380.92	@	G	J.H.	3.10	1.9	195	0.41		
1380.92	@	G	H.P.	2.82	1.88				
1381.65	@	G	J.H.	19.8	4.5	190			
1381.65	@	G	H.P.	3.94	1.07	330			
1386.43	314.1	G	J.H.	0.59	0.6	420	0.05		int incr in J
1395.03	315.2	G	J.H.	11.3	2.9	290			int incr in J
1395.03	@	G	H.P.	8.46	1.08	46	0.22		
1396.95	@	G	H.P.	103	18.2				
1398.48	@	G	H.P.	0.15	0.29	380			
1399.68	@	G	H.P.	22.8	6.97	180			

Depth	Unit	Lith	Sent to	Jo $\times 10^{-4}$	K $\times 10^{-4}$	MDF	Js	Tc	Oxide Classifications or Comments
1401.53	@	G	J.H.	53.5	8.9	140	1.02	575	sm int incr in J C1 H1-2 L1 P:S=+1.0
1402.78	@	G	J.H.	8.08	2.2	185			
1407.38	318.1	G	J.H.	2.58	0.0	365	0.04		
1411.48	318.4	G	J.H.	18.8	4.3	155	0.95		
1412.58	@	G	H.P.	12.5	4.45	194			
1415.83	@	G	J.H.	17.1	2.2	165			
1415.83	@	G	H.P.	36.1	6.33	178			
1416.78	319.2	G	J.H.	0.26	0.6	395	0.01		int incr in J
1416.78	@	G	H.P.	0.04	0.17	315			
1418.52	319.3	G	J.H.	13.4	2.2	215	0.53		
1424.72	321.2	G	J.H.	16.1	5.5	140			
1425.93	321.4	G	J.H.	9.57	1.2	225	0.26		
1426.53	321.5	G	J.H.	42.7	7.8	135			
1428.54	321.7	G	J.H.	0.41	0.6	>500			int incr in J
1430.25	321.8	G	J.H.	0.61	2.5	200	0.08		
1430.25	@	G	H.P.	8.67	3.58	245			
1431.65	@	G	J.H.	27.2	10.8	125			
1431.65	@	G	H.P.	21.9	9.67	146			
1433.67	322.1	G	H.P.	15.3	4.15	173			
1434.57	@	G	H.P.	13.6	5.02	152	0.10	575	C1 H1 L1 (Sc3) P:S=+0.99
1442.05	323.1	G	J.H.	8.39	2.4	215			
1444.50	@	G	J.H.		7.0				
1447.50	@	G	J.H.	15.9	7.5	200			
1447.50	@	G	H.P.	20.5	10.0	198			
1448.47	@	G	J.H.	17.8	2.4	200			
1448.47	@	G	H.P.	8.76	1.15	226			
1450.22	325.2	G	J.H.	36.4	9.1	165			
1450.22	@	G	H.P.	31.7	10.2	176			
1450.50	325.3	G	J.H.	15.9	2.7	280			int incr in J
1451.73	325.4	G	J.H.	6.41	4.7	245			
1451.73	@	G	H.P.	6.46	2.47	146			
1460.82	327.2	G	J.H.	18.8	8.1	180			
1463.47	@	G	U.B.				0.02	550	C1 H1 L1 P:S=+1.0
1465.46	@	G	H.P.	48.8	27.2	150			
1466.82	328.1	G	H.P.	29.4	11.9	162			
1468.15	@	G	J.H.	17.1	4.6	185			
1468.15	@	G	H.P.	15.0	7.97	194			
1469.73	328.2	G	H.P.	6.41	2.75	267	0.27		
1481.55	330.4	G/S6.5	H.P.	2.57	1.07	300	0.26		
1482.98	@	G/S7	H.P.	5.95	2.04	348			
1484.12	@	G/S6	J.H.	10.0	4.4	245			
1484.12	@	G/S6	H.P.	5.62	5.95	364			
1486.37	@	G/S6.5	H.P.	2.06	0.87	350	0.11		
1491.25	@	G/S6	G.S.				0.06	555	C1 H1 L1 P:S=+1.0
1498.56	333.2	G	H.P.	2.64	0.62	400	0.09		
1500.98	@	G	H.P.	1.68	0.81	388			
1502.70	@	G	H.P.	1.03	0.64	300	0.11		
1505.55	335.1	G	J.H.	7.55	3.3	370			int incr in J
1506.88	@	G	J.H.	4.52	2.0	340	0.25		sm int incr in J
1512.50	336.1	G	J.H.	3.45	1.1	245	0.06		
1513.04	@	G	J.H.	3.19	1.7	225			sm int incr in J
1515.72	@	G	H.P.	2.62	1.92	266			
1516.85	@	G	H.P.	2.88	1.10	39			
1517.77	@	G	J.H.	1.18	1.4	355	0.11		
1519.10	@	G	H.P.		2.69				
1520.53	338.1	G	J.H.	14.6	5.5	285			
1524.76	338.4	G	J.H.	6.98	7.5	150	0.26		
1525.96	@	G	J.H.	9.55	5.5	180			
1528.39	@	G	J.H.	12.9	3.0	320	0.11	545	C1 H1-2 L1 P:S=+1.0
1529.85	339.1	G	J.H.	29.4	2.7	205			
1531.95	339.2	G	H.P.	5.56	2.42	286			
1534.68	340.1	G	H.P.	15.5	2.33	400	0.06		
1536.15	@	G	J.H.	14.8	8.48	210			
1536.15	@	G	H.P.	14.3	5.30	252			
1537.23	340.2	G	J.H.	8.24	2.79	265			
1539.65	341.2	G	J.H.	11.0	4.6	235	0.23		
1541.05	@	G	J.H.	13.4	4.0	280			sm int incr in J
1542.48	341.4	G	J.H.	1.69	1.8	320			sm int incr in J
1544.45	@	G	J.H.	11.7	3.7	210			
1545.65	342.1	G	J.H.	5.01	6.6	180	0.11		

Depth	Unit	Lith	Sent to	Jo $\times 10^{-4}$	K $\times 10^{-4}$	MDF	Js	Tc	Oxide Classifications or Comments
1549.08	@	G	H.P.	4.38	1.84	262			
1550.43	343.2	G	H.P.	2.36	1.39	244			
1551.75	@	G	H.P.	3.04	2.12	267	0.11	540	C1(2) H1(2-3) L1 Sr(0-1,6)? P:S=+0.90 or -1.0
1554.74	344.2	G	J.H.	12.6	4.4	260	0.17		
1557.93	344.3	G	J.H.	4.46	3.1	175			
1559.06	@	G	J.H.	3.08	3.8	180			
1562.45	345.1	G	J.H.	5.53	1.8	220	0.06		
1566.43	@	G	J.H.	3.12	2.7	170	0.11		
1567.85	@	G	H.P.	6.55	3.10	250			
1569.47	346.1	G	H.P.	5.14	2.93	225	0.13		
1581.22	348.1	G	J.H.	9.18	4.1	225	0.34		
1583.70	348.2	G	J.H.	16.5	6.0	180			
1583.70	@	G	H.P.	13.1	6.11	204			
1585.16	@	G	H.P.	3.53	2.50	269	0.13	540	C1 H1 L1 (Sr6)? P:S=+1.0
1586.73	@	G	H.P.	11.8	4.75	264			
1588.27	@	G	H.P.	6.09	3.66	211	0.14		
1598.15	350.2	G	J.H.	2.40	2.6	200	0.11		sm int inc in J
1600.90	@	G	H.P.	7.98	4.52	274			
1602.44	@	G	J.H.	9.42	5.0	200			
1602.44	@	G	H.P.	9.48	5.55	245			
1603.55	@	G	J.H.	16.5	5.5	240	0.33		sm int incr in J
1603.55	@	G	H.P.	16.9	4.66	300			
1605.23	@	G	J.H.	6.73	1.9	185			
1605.23	@	G	H.P.	5.25	2.91	254			
1610.35	353.1	G	J.H.	9.98	3.7	150	0.10	545	Sc6c3 P:S=-1.0
1613.13	@	G	J.H.	3.81	1.0	190			
1617.98	@	G	H.P.	9.24	3.94	282	0.35		
1619.27	355.2	G	J.H.	2.34	0.7	410			
1619.27	@	G	H.P.	3.08	0.84	475			
1620.75	@	G	J.H.	2.94	1.6	205	0.13		
1620.75	@	G	H.P.	2.73	1.93	253			
1622.03	@	G	H.P.	2.78	0.71	465			
1625.08	356.1	G	J.H.	3.81	2.6	145	0.21		
1633.57	357.1	G	J.H.	7.38	3.6	140	0.06		
1635.62	358.1	G	J.H.	2.84	2.5	245			
1635.62	@	G	H.P.	3.90	2.02	213			
1637.22	@	G	J.H.	6.58	2.6	175	0.21		
1638.58	@	G	H.P9.16		3.4	110			
1640.04	@	G	H.P.	5.73	2.76	176			
1641.57	@	G	J.H.	1.41	2.9	130	0.12	525	C1 H1(2-4) L1 P:S=+1.0
1652.68	361.1	G	H.P.	7.07	1.27	385	0.09		
1654.12	@	G	H.P.	9.98	3.85	166			
1655.33	361.2	G	J.H.	3.17	3.4	170			
1655.33	@	G	H.P.	2.93	2.77	194			
1656.02	361.3	G	H.P.	9.11	2.36	188	0.31		
1666.05	363.1	G	J.H.	7.17	6.8	35			int incr in J at dn=150
1669.64	363.2	G	H.P.	4.77	3.20	214	0.13	555	C1 H1(2) L1 P:S=+1.0
1672.28	364.2	G	J.H.	7.30	5.3	135			
1672.28	@	G	H.P.	8.45	6.41				
1672.86	@	G	H.P.	4.40	2.28	168			
1673.98	364.3	G	H.P.	6.13	4.85	300	0.37		
1678.88	364.4	G	J.H.	3.10	2.6	155	0.17		int incr in J
1682.66	366.1	G	J.H.	20.4	9.2	115	0.84		
1687.38	@	G	H.P.	6.12	4.85	158	0.25		
1688.77	@	G	H.P.	4.82	3.64	180			
1691.62	@	G	H.P.	5.18	4.10	168			
1692.43	@	G	H.P.	6.05	2.96	143	0.08		
1695.68	@	G	J.H.	12.6	2.9	225			
1697.45	@	G	J.H.	4.48	1.9	190	0.21		
1702.84	@	G	J.H.	1.97	2.8	135	0.11	530	C1 H1 L1 P:S=+1.0
1704.03	369.2	G	J.H.	2.19	5.7	185			
1705.24	370.1	G	J.H.	3.23	3.0	135			
1705.24	@	G	H.P.	3.29	1.61				
1705.53	@	G	J.H.	3.37	2.5	185			
1705.53	@	G	H.P.	5.49	2.26	201			
1708.16	@	G	J.H.	8.03	5.5	185	0.10		
1708.16	@	G	H.P.	5.76	3.19	266			
1709.23	@	G	H.P.	6.76	1.62	190			
1710.73	371.1	G	J.H.	7.49	6.7	135			

Depth	Unit	Lith	Sent to	Jo $\times 10^{-4}$	K $\times 10^{-4}$	MDF	Js	Tc	Oxide Classifications or Comments
1715.54	371.4	G	J.H.	10.8	6.5	135	0.34		
1716.88	@	G	J.H.	13.3	5.4	135			
1721.45	372.2	G	J.H.	5.11	5.0	140	0.15		
1722.73	@	G	H.P.	3.71	1.31	202			
1723.88	@	G	H.P.	1.86	1.76	185			
1725.58	373.1	G	J.H.	2.34	0.7	200	0.15		
1725.58	@	G	H.P.	2.70	0.40	235			
1727.36	@	G	J.H.	9.92	2.7	185			
1727.36	@	G	H.P.	5.03	1.46	197			
1731.15	374.2	G	G.S.				0.11	545	
1734.16	375.1	G	J.H.	3.02	1.0	235	0.07		
1735.82	375.2	G	J.H.	0.80	0.9	335			
1739.47	@	G	H.P.	6.05	0.63	218	0.06		
1740.92	376.1	G	J.H.	16.3	8.6	175			
1740.92	@	G	H.P.	6.58	2.49	655			
1742.52	376.2	G	J.H.	6.47	3.9	130			
1742.52	@	G	H.P.	6.50	3.14	160			
1744.79	376.2	G	H.P.	4.55	0.75	730	0.05		
1750.53	378.1	G/S5	J.H.	15.1	8.1	130	0.11	525/565	C1.0 H1.0 L1.0 Sc4 P:S=-0.60
1751.65	378.2	G/S4.5	J.H.	10.1	5.2	135			
1755.66	378.4	U/G/S5.5	H.P.	3.97	1.26	251	0.03		
1757.52	379.1	G/S5.5	H.P.	9.35	8.03	134			
1759.00	@	G/S5	H.P.	13.4	6.44	135			
1759.68	379.2	U/G/S4.5	J.H.	9.54	5.9	160	0.15		
1759.68	@	U/G/S4.5	H.P.	7.10	2.82	200			
1761.54	@	U/G/S6	G.S.				0.08	530	
1763.15	@	U/G/S5	J.H.	15.1	11.0	110	0.76		
1770.38	@	U/G/S5	U.B.				0.16	575	
1771.80	381.1	U/G/S4	J.H.	2.36	4.0	220	0.06		
1772.93	382.1	U/G/S5.5	H.P.	3.59	1.20	217			
1774.48	@	U/G/S5	J.H.	23.8	10.7	125			
1774.48	@	U/G/S5	H.P.	20.7	9.78	136			
1775.77	382.3	U/G/S5	J.H.	7.37	32.1	175	0.09		
1775.77	@	U/G/S5	H.P.	8.11	4.41	186			
1777.52	@	U/G/S5.5	H.P.	6.29	4.80	138			
1778.37	@	U/G/S6	J.H.	8.09	5.0	130	0.50		
1780.27	@	U/G/S5.5	G.S.				0.13	530	C1.0 H1.0(6) L1.0 Sr0(6)? P:S=+1.0
1787.09	@	U/G/S5.5	J.H.	3.95	2.4	185			
1790.96	385.2	U/G/S6	H.P.	7.64	4.28	130	0.23		
1791.96	@	U/G	H.P.	33.8	13.2	118			
1793.54	@	U/G/S6	H.P.	6.73	3.08	200			
1794.83	385.3	U/G/S6.5	H.P.	1.77	1.29	202			
1795.69	@	U/G/S6.5	J.H.	5.63	1.8	130	0.16		
1797.25	386.1	U/G/S7	J.H.	16.9	6.3	180			sm int incr in J
1798.02	@	U/G/S6.5	G.S.				0.04	555	
1801.03	387.1	U/G/S5.5	J.H.	9.62	5.7	135			
1806.61	@	U/G/S7.5	H.P.	3.83	4.49	237	0.06		
1807.92	388.1	U/G/S5.5	H.P.	8.18	4.24	149			
1809.25	388.2	G/S8&6	H.P.	1.09	0.29				
1810.41	@	G/S7	H.P.	1.78	0.33	600	0.04	790	C1.0 H1.0 L1.0 P:S=+1.0
1812.79	389.2	U/G/S6	J.H.	17.8	15.5	145			
1815.08	389.3	U/G/S6	J.H.	14.0	11.8	150	0.29		
1820.16	@	U/G/S5.5	J.H.	21.9	11.4	115	0.44	555	
1822.55	390.1	U/G/S5.5	J.H.	17.9	14.3	125			
1823.59	@	U/G/S6.5	J.H.	2.79	1.0	210			
1823.59	@	U/G/S6.5	H.P.	2.39	1.26	220			
1824.02	@	U/G/S6	H.P.	6.57	4.69	160			
1826.09	@	U/G/S6	H.P.	22.8	15.9	85	0.58		
1827.36	391.2	U/G/S6	H.P.	40.5	9.74	158			
1828.14	391.3	U/G/S6	J.H.	7.03	5.7	110			
1829.70	392.1	U/G/S6.5	J.H.	21.0	17.2	125			
1831.80	392.2	U/G/S7&4	J.H.	67.0	41.0	185	1.49	565	int incr in J
1836.22	393.1	U/G/S5&8	J.H.	1.86	2.8	210	0.13		sm int incr in J
1836.22	@	U/G/S5&8	H.P.	1.59	1.40	195			
1838.57	394.1	U/G/S6&4	J.H.	45.9	10.9	90			
1838.57	@	U/G/S6&4	H.P.	13.0	22.4	111			
1838.68	@	U/G/S4	J.H.	1.22	13.9	>500			incr in J at dn=100
1839.85	@	U/G/S6&4	J.H.	0.25	14.7	100			
1839.85	@	U/G/S&4	H.P.	47.8	15.0	75			
1841.10	@	U/G/S6	H.P.	8.40	4.30	120	0.10	520	C1.0 H1.0 L1.0 Sc5 P:S=-0.90

Depth	Unit	Lith	Sent to	Jo $\times 10^{-4}$	K $\times 10^{-4}$	MDF	Js	Tc	Oxide Classifications or Comments
1843.33	394.3	U/G/S7	H.P.	2.01	2.19	181			
1844.76	395.1	U/G/S7	J.H.	5.24	4.0	130	0.20		
1846.23	395.3	U/G/S6	J.H.	3.39	5.1	185			
1849.83	396.1	U/G/S7	H.P.				0.32	505/555	C1.0 H1.003(6)L1.0 Sc1 P:S=+1.0
1851.08	397.1	U/S7	J.H.	2.24	1.1	215			
1851.08	@	U/S7	H.P.	2.80	1.68	249			
1852.30	397.3	G/S7	J.H.	3.86	2.3	240			int incr in J
1852.30	@	G/S7	H.P.	7.92	3.98	202			
1853.75	397.5	U/S6.5	J.H.		2.0				
1853.75	@	U/S6.5	H.P.	2.23	10.6	125			
1855.20	@	U/S7	H.P.	3.25	1.71	240	0.19		
1856.50	398.1	G/U/S7	J.H.	2.61	3.30	120			
1857.95	@	G/U/S6.5	J.H.	11.8	13.0	115			
1859.50	@	G/U/S6.5	J.H.	6.95	18.1	165			
1860.95	@	G/U/S7	J.H.	2.51	3.3	220	0.05	515	no oxides
1867.70	400.1	U/S6	H.P.	1.76	1.25	354	0.04		
1869.32	@	U/S6	H.P.	4.38	2.79	193			
1870.95	400.2	U/S6	H.P.	3.67	5.38		0.14	520	C1.0 H2.5 L1.0 So(sp)2c3 P:S=+0.96
1872.10	400.3	U/S5.5	H.P.	5.88	5.40	158			
1873.25	401.1	G/S6	J.H.	10.4	0.0	595			incr & decr in J to dn=500
1874.75	401.2	U/S6.5	J.H.	4.68	1.9	240	0.07		int incr in J
1876.80	401.3	U/S6.5	J.H.	3.18	1.7	260			sm int incr in J
1877.85	@	U/S6.5	J.H.	2.09	1.4	290			int incr in J
1880.90	402.1	U/S6.5	U.B.				0.23	555	C1.0 H1.3 L1.0 So(sp)3c2 P:S=+0.49
1883.80	@	U/S5.5	J.H.	41.9	14.4	130	2.44	580	int incr in J
1885.65	403.1	U/S6.5	H.P.	8.82	7.92	155			
1886.75	403.2	U/S3	H.P.	171	96.3	100	5.94		
1888.40	@	U/S6	H.P.	5.28	1.17	169			
1889.50	@	U/S6	H.P.	5.11	3.77	165			
1890.80	@	U/S6	J.H.	17.8	8.0	160	0.27	555	sm int incr in J C1.0 H1.0 L1.0 Sc4o(sp)1 P:S=-0.93
1892.20	404.1	U/G/S6	J.H.	3.02	2.3	265			int incr in J
1893.60	404.2	U/S5.5	J.H.	121.0	51.0	185	3.62	585	int incr in J
1895.25	@	U/S6	J.H.	17.4	8.3	150			
1901.70	405.2	U/S6.5	U.B.				0.09	555	C1.0 H1.04(6) L1.0 So(sp)4 P:S=+0.20
1903.15	406.1	U/S6.5	H.P.	3.88	2.44	318			
1904.25	406.1	U/S6	A.W.	19.9	13.47	50			
1904.65	406.2	U/S6.5	H.P.	4.37	2.55	262			
1905.80	@	U/S6.5	H.P.	3.77	3.22	208	0.49		
1906.82	406.3	U/S6.5	H.P.	2.95	2.79	249			
1908.70	407.1	U/S5	J.H.	24.7	8.8	145			
1909.55	@	U/S7.5&3	A.W.	153.0	64.09	45			
1910.00	407.2	U/S6.5	J.H.	2.62	2.1	250	0.04	515	C1.0 H1.0 L1.0 So(sp)1 P:S=+0.99
1911.50	@	U/S6	J.H.	17.0	8.6	115			
1912.75	407.3	U/S6	J.H.	6.52	2.9	225	0.48		sm incr in J at dn=50
1914.01	407.3	U/S7.5&3	A.W.	99.9	55.49	135			
1920.25	408.4	U/S6	H.P.	5.70	3.14	192	0.24	535	C1.0 H1.0 L1.0 Sc(1)o(sp)3 P:S=+0.80
1921.55	409.1	U/S5.5	H.P.	4.04	44.7	237			
1923.20	409.2	U/S6	H.P.	7.36	2.22	173			
1924.75	@	U/S4.5	H.P.	93.5	43.1	124			
1925.90	410.1	U/S5	J.H.	9.65	3.8	150	0.24		
1927.75	410.2	U/S6	J.H.	1.32	1.7	235			
1929.20	410.3	U/S6	J.H.	0.87	1.1	145			
1930.40	@	U/S6	J.H.	41.8	17.0	90	2.87	570	
1937.80	411.2	U/S6.5	H.P.	1.92	0.89	275	0.03		
1938.25	@	U/S2	A.W.	184.0	167.06	75			
1938.59	@	U/S6&3	H.P.	136	94.4	98			
1941.20	412.2	U/S6	H.P.	9.68	8.69	181	0.20	540	C1.0 H1.0(6) L1.0 Sc4o(sp)(1) P:S=-0.36
1942.45	413.1	U/S5.5	J.H.	4.38	2.78	230			incr in J at dn=75
1943.77	@	U/S6	J.H.	6.51	3.5	240			
1945.20	413.2	U/S6	J.H.	8.56	5.7	145	5.45		incr in J at dn=50
1946.50	413.3	U/S6.5	J.H.	6.27	1.6	275			int incr in J
1950.80	414.2	U/S6	U.B.				0.05	430/510	C1.0 H1.08 L1.0 So(sp)1-5 P:S=+0.86
1953.95	414.4	U/S6.5	H.P.	2.63	1.47	292			
1955.20	@	U/S6	H.P.	11.8	6.98	158	0.09		
1956.70	415.2	U/S6	H.P.	2.41	2.48	183			
1958.00	415.3	U/S6	H.P.	5.38	3.52	216			
1959.20	416.1	U/S6	J.H.	14.2	4.4	165			
1960.65	416.2	U/S6	J.H.	5.21	4.6	175	0.09	525	C1.0 H1.0 L1.0 Sc6o(sp)3 P:S=-0.99
1962.40	416.3	U/S5.5	J.H.	23.6	11.0	130			
1968.10	418.1	U/S6.5	H.P.	6.03	2.87	228	0.06		

Depth	Unit	Lith	Sent to	Jo $\times 10^{-4}$	K $\times 10^{-4}$	MDF	Js	Tc	Oxide Classifications or Comments
1969.75	418.2	U/S6.5	H.P.	8.31	5.10	190			
1971.30	@	U/S6	J.H.	17.3	11.4	140	1.76	580	int incr in J
1971.30	@	U/S6	H.P.	51.9	22.5	150			
1972.45	@	U/S6	J.H.	44.9	31.0	80			
1973.90	@	U/S6.5	J.H.	9.95	6.1	130			
1975.35	419.1	U/S6.5	J.H.	2.42	4.0	335	0.08		
1980.70	420.2	U/S7	H.P.	1.06	1.26		0.06	530	C1.0 H1.1 L1.0 So(sp)1 P:S=+0.85
1982.10	421.3	U/S6	H.P.	3.42	2.26	290			
1984.00	421.4	U/S6	H.P.	2.71	2.95	233			
1984.70	@	U/S7	J.H.	1.88	2.5	305	0.09		
1988.80	422.2	U/S7	J.H.	1.37	4.1	300			incr in J at dn=50 poorly oriented
1989.40	@	U/S6.5	A.W.	0.13	1.92	425			
1991.60	423.2	U/S7.5	U.B.				0.05	715	C1.0 H1.2 L1.0 So(sp)(1) P:S=+1.0
1994.47	@	U/S7.5	H.P.	2.08	0.75	390			
1996.55	424.1	U/S7	H.P.	0.02	0.46		0.03		
1997.07	424.3	U/S7	H.P.	0.90	0.81	320			
1998.37	@	U/S5.5	J.H.	4.67	2.5	220			
1999.65	425.2	U/S6	J.H.	3.97	2.8	270			
2001.20	425.3	U/S6	J.H.	4.50	2.7	260	0.08	565	C1.0 H1.98(6) L1.0 Sr0(6)? P:S=+0.98
2006.90	427.1	U/S5.5	H.P.	3.61	1.67	295	0.08		
2008.15	@	U/S6.5	H.P.	2.20	0.90	370			
2008.75	427.3	U/S6	H.P.	0.75	0.00				
2010.60	428.1	U/G/S6	J.H.	5.87	3.2	330	0.02	weak	C1.0 H1.001(6)L1.0 So(sp)2 P:S=+0.98
2012.00	428.2	U/S6.5	J.H.	1.51	3.4	265			
2013.50	@	U/S6.5	J.H.	5.98	4.5	275	0.14		sm int incr in J
2019.18	430.1	U/S6	H.P.	9.13	5.69	208			
2020.50	@	U/S6.5	H.P.	5.08	1.34	282	0.03	495/555	C1.0 H1.1 L1.0 So(sp)1 P:S=+0.98
2021.95	430.2	U/S5.5	H.P.	16.3	6.65	197			
2023.10	@	U/S5.5	J.H.	10.3	7.4	275			
2024.60	431.1	U/S6	J.H.	2.32	1.3	>500	0.07		sm int incr in J
2026.40	431.3	U/S6	J.H.	3.46	5.0	80			
2030.25	@	U/S6	U.B.				0.16	575	C1.0 H1.0(6) L1.0 Sc5o(sp)2 P:S=+0.45
2032.00	433.2	U/S6	H.P.	3.08	0.91	432			
2033.50	@	U/S6.5	H.P.	7.49	1.70	275			
2034.75	@	U/S6	H.P.	16.7	6.52	215	0.17		
2036.10	@	u/S5	J.H.	15.5	9.4	205			
2037.70	@	U/S5	J.H.	12.8	8.2	175			
2039.30	@	U/S6&4	J.H.	0.66	4.9	230			
2041.70	@	U/S5.5	J.H.	8.42	4.9	220	0.26	580	sm int incr in J at dn=50 C1.0 H1.0(6) L1.0 Sc6o(sp)1 P:S=-0.82
2044.75	435.3	U/S5	H.P.	7.24	4.17	242	0.11		
2046.10	436.1	U/S6	H.P.	1.12	1.57	433			
2047.60	@	U/S5	H.P.	12.9	5.00	201			
2049.00	@	U/S6	J.H.	6.04	5.3	175			
2051.00	437.1	U/S6	J.H.	5.66	3.6	235	0.05	575	C1.0 H1.6 L1.0 So(sp)2 P:S=+0.50
2052.20	437.3	U/S6.5	J.H.	12.0	4.4	265			
2058.10	439.1	U/S6.5	H.P.	3.07	1.58	207	0.15		
2059.50	439.3	U/S2.5	H.P.	16.6	183	45			
2060.65	439.6	U/S5	H.P.	6.26	8.88	260	0.09	525	C1.0 H1.2 L1.0 Sc4o(sp)3 P:S=+0.16
2062.10	440.1	U/S5	J.H.	8.54	5.0	190			sm int incr in J
2062.95	@	U/S4.5	J.H.	11.7	6.4	205			sm int incr in J
2064.85	@	U/S5.5	J.H.	8.44	2.9	270	0.05		sm int incr in J
2070.20	442.1	U/S6	H.P.	3.45	1.31	323	0.11	560	
2071.50	@	U/S6	H.P.	8.99	5.29	200			
2073.15	@	U/S6	H.P.	7.48	4.59	232			
2074.45	443.1	U/S3	J.H.	98.7	46.0	135			int incr in J at dn=50
2075.85	443.2	U/S6	J.H.	5.77	8.8	285	0.12		int incr in J and sm incr at dn=75
2077.10	@	U/S6	J.H.	11.1	8.2	180			sm int incr in J
2081.50	444.1	U/S6	U.B.				0.21	585	
2082.75	445.1	U/S5.5	H.P.		34.0				
2084.35	445.4	U/S6.5	H.P.	4.55	1.29	271			
2085.63	445.6	U/S6	H.P.	5.51	6.32	218	0.22		
2087.30	445.8	U/S6	J.H.	2.23	1.5	305			sm int incr in J
2088.50	@	U/S6	J.H.	4.92	2.7	280			
2089.60	446.1	U/S5.5	J.H.	1.33	2.8	275			
2091.25	447.1	U/S6	U.B.				0.11	555	
2096.80	448.2	U/S5	H.P.	17.6	14.4	145	0.35		
2098.20	448.4	U/S5.5	H.P.	3.88	2.40	289			
2099.65	449.2	Db/S6	J.H.	0.18	2.9	325			int incr in J
2101.50	449.3	U/S6	J.H.	5.12	3.8	190	0.07	570	sm int incr in J

Depth	Unit	Lith	Sent to	Jo $\times 10^{-4}$	K $\times 10^{-4}$	MDF	Js	Tc	Oxide Classifications or Comments
2103.00	@	U/S6	J.H.	6.56	3.3	230			int incr in J
2107.80	451.1	U/S5.5	H.P.	13.8	3.72	260	0.13		
2109.30	@	U/S5.5	H.P.	5.50	1.82	206			
2110.80	@	U/S6	H.P.	23.5	6.00	175	0.35	575	
2112.00	@	U/S6	J.H.	23.3	6.1	180			
2113.35	452.2	U/S3.5	J.H.	7.01	6.9	235			incr in J at dn=75
2114.90	@	U/S6	J.H.	17.5	6.1	180	0.31		
2120.40	453.2	U/S6	J.H.	21.0	4.0	180	0.29	560	incr in J at dn=75
2120.40	@	U/S6	H.P.	12.0	2.27	228			
2121.50	@	U/S5	H.P.	8.73	2.85	270			
2122.60	@	U/S4.5	H.P.	17.7	6.84	237			
2123.85	454.2	U/S6.5&4	A.W.	58.5	53.82	150			sm int incr in J
2124.60	455.1	G/S6	J.H.	1.83	3.1	295			int incr in J
2125.45	455.3	U/S5.5	J.H.	8.76	7.5	295	0.05		int incr in J
2126.05	455.3	U/S5&3	A.W.	45.4	43.82	120			
2127.30	455.4	G/S6	J.H.	0.37	4.8	345			int incr in J and sm incr at dn=100
2130.35	@	G/S6	U.B.				0.03	weak	
2132.95	457.1	U/G/S6.5	H.P.	1.16	0.43	306			
2134.40	457.2	G/S7	H.P.	4.38	0.92	340			
2136.00	@	G/S6	H.P.	0.49	0.31	453	0.04		
2137.20	@	G/S5.5	J.H.	1.11	6.1	330			sm int incr in J and at dn=100
2138.37	458.1	U/S3.5	J.H.	34.7	18.0	105			
2139.90	@	U/S6	J.H.	10.3	4.7	240			
2142.65	@	U/S6	U.B.				0.24	500/565	C1.0 H1.0 L1.0 Sc5o(sp)4 P:S=+0.70
2145.45	@	U/S5.5	H.P.	25.1	17.4	157			
2147.40	460.1	U/S4.5	H.P.	3.31	0.88	241	0.08		
2147.96	@	U/S7	H.P.	18.6	0.73	27			
2149.70	@	U/S5.5	J.H.	11.2	5.2	235			sm int incr in J
2151.30	@	U/S4.5	J.H.	4.11	4.8	220	0.13	470/555	sm int incr in J C1.0 H1.0 L1.0 Sc4o(sp)3 P:S=+0.68
2152.75	461.1	U/S5	J.H.	6.58	4.7	210			sm int incr in J
2158.10	463.2	U/S5.5	H.P.	15.7	8.71	155	0.06		
2159.40	@	U/S6	H.P.	4.27	0.84	248			
2160.45	@	U/S6	H.P.	6.24	2.25	232	0.08	600	C1.0 H1.1(6) L1.0 Sr5(0,6)?o(sp)2 P:S=+0.74
2162.35	@	U/S5.5	J.H.	12.1	6.9	250			int incr in J
2163.60	464.1	U/S5.5	J.H.	5.54	5.3	245			int incr in J
2164.90	@	U/S5	J.H.	5.50	5.0	235	0.06	560	sm int incr in J
2171.15	@	U/S4.5	H.P.	17.9	10.9	158	0.17	550	C1.0 H1.0 L1.0 Sc4o(sp)3 P:S=+0.79
2172.40	@	U/S5	H.P.	12.6	4.56	219			
2174.00	466.2	U/S4.5	H.P.	23.2	9.68	214			
2175.45	@	U/S5	J.H.	14.2	6.4	225	0.15		
2177.00	467.1	U/S6	J.H.	1.60	1.6	350			
2178.25	@	U/S5.5	J.H.	7.43	6.1	200			
2181.50	468.1	U/S5	U.B.				0.10	525	C1.0 H1.1 L1.0 So(sp)2 P:S=+0.72
2184.25	469.1	U/S4.5	H.P.	16.7	5.64	193			
2185.50	@	U/S4.5	H.P.	22.2	9.10	193	0.21		
2187.10	469.2	U/S3.5	H.P.	94.2	53.9				
2188.35	470.1	U/S4.5	J.H.	14.7	7.1	195			sm int incr in J
2189.55	470.3	U/S5	J.H.	8.44	6.1	185			int incr in J
2190.75	@	U/S4.5	J.H.	6.32	5.9	215	0.26	570	
2196.45	471.1	U/S4.5	H.P.	66.3	31.7	182	0.38	575	
2198.00	472.2	U/S4.5	H.P.	18.7	8.03				
2199.87	472.4	U/S5.5	H.P.	13.0	8.36	184			
2201.20	@	U/S4.5	J.H.	59.7	25.0	115	2.28	575	C1.0 H1.0 L1.0 Sc5 P:S=+0.20
2202.00	@	U/S4.5	J.H.	13.1	7.2	240			
2203.50	@	U/S5.5	J.H.	10.1	8.0	190	1.12		
2210.10	475.2	U/G/S4.5	J.H.	16.2	8.2	220	0.48	565	
2210.10	@	U/G/S4.5	H.P.	11.8	4.31	210			
2211.30	@	U/G/S5	H.P.	12.2	4.36	220			
2212.40	@	U/G/S6	H.P.	8.14	2.06	220			
2213.95	@	U/G/S6	J.H.	6.13	5.1	285			
2215.25	476.1	U/G/S5	J.H.	23.9	13.0	210	0.65		
2216.50	@	U/G/S5.5	J.H.	10.1	8.9	195			
2220.20	477.2	U/S4.5	U.B.				0.48	490/570	
2222.00	477.4	G/S6	H.P.	7.39	1.21	298	0.08		
2222.90	478.2	U/S6	H.P.	7.66	3.48	232			
2224.40	@	U/S6&3.5	H.P.	56.2	98.0	118			
2225.65	479.1	U/S4.5	J.H.	24.0	11.0	165			
2227.10	479.2	G/S6.5	J.H.	0.64	2.7	390	0.04		int incr in J
2228.00	479.3	U/S4.5	J.H.	28.8	15.0	140			

Depth	Unit	Lith	Sent to	Jo $\times 10^{-4}$	K $\times 10^{-4}$	MDF	Js	Tc	Oxide Classifications or Comments
2230.25	480.2	U/S5	U.B.				0.16	540	
2234.10	481.1	U/S5.5	H.P.	15.1	5.34	271	0.07		
2237.30	481.3	U/S4.5	H.P.	20.1	30.7	173			
2238.60	482.1	U/S5.5	J.H.	1.00	5.3	440			int incr in J
2239.55	@	U/S5	J.H.	23.2	11.0	200			
2241.10	482.4	U/S6.5	J.H.	1.82	4.3	335	0.04	weak	sm int incr in J
2246.75	484.1	U/S7	H.P.	3.89	0.80	353	0.03		
2248.55	484.3	U/S7	H.P.	0.99	0.41	400			
2249.90	484.5	U/S4	H.P.	25.5	11.5	203			
2250.65	@	U/S4	J.H.	130.0	60.0	100	1.40	570	
2253.75	485.3	U/S5	J.H.	17.8	7.5	335	0.14		sm int incr in J
2259.05	486.4	U/S4&2	H.P.	123	85.6	105			
2261.25	487.2	U/S4.5	J.H.	52.8	23.4	195	1.39	575	
2261.25	@	U/S4.5	H.P.	40.5	26.1	167			
2263.10	487.3	U/S5	H.P.	7.79	2.63	300	0.23		

EXPLANATION OF ABBREVIATIONS USED IN TABLE 1 AND FIGURES 20-23:

Unit: xxx.x is short form for Unit xxx.0x, e.g. U.118.3 = U.118.03; '@' means 'same number as above'; J. Hall also has all the bottom pieces of samples starting from depth 500.00 m; '?' means there is doubt about a depth or a value.

Sent to: J.H. - J.M. Hall, Dalhousie University; A.W. - AiSu Wu, Dalhousie University; G.S - Gunter Schoenharting, Denmark; H.P. - H. Paul Johnson, University of Washington; U.B. - U. Bleil, Germany; F.V. - Fred Vine, England.

Lithology: A - aphyric dike, P - pyric dike, G - gabbro, U - ultramafic, D - diorite, Db - diabase, PLG - plagiogranite, V - vein, SM - sheared material, UNK - unknown, M - moderately, SL - slightly, P - partially, SP - sparsely, / - and/or, S - serpentinization has been recognized and noted either in the core description for the unit or in the oxide petrology description. A colour code number has been given to each mini-core based on the Munsel soil colour chart with a Hue 2.5Y and 0 chroma, 8 - white, 7 - light gray, 6 - gray, 5 - gray, 4 - dark gray, 3 - very dark gray, 2 - black (if two numbers are found this means that there are two distinctly different coloured areas in the mini-core).

Js: Where there is a large difference between the two Js values and there is no justification for averaging them they are tabulated in the following format: the Curie Js (if measured) is listed first, separated from the second measurement by a slash (/); multiple Js values not derived from Curie measurements are separated by ampersands (&).

Comments: sm - small, int - initial, incr - increase, decr - decrease, dn - demag. step, mt - magnetite, rept - reported, ol - olivine, pseudo - pseudomorphed, pol-thin - polished thin section, C 1-6 - deuteric oxidation, H 1-6 - hydrothermal oxidation, (6) - presence of ghosts after probable magnetite, L 1-6 - low temperature oxidation, S - secondary magnetite, r 0-6 - reorganized, c 0-6 - chains, o 0-4 - overgrowths on magnetite, o(sp)0-4 - overgrowths on spinel, m 0-4 - martite, ah 0-4 - secondary alteration by hematite, P:S = the ratio of primary to secondary magnetite based on the following formula: Pmag - Smag / Pmag + Smag, (x) - means this component is very rare, (x)? - means that this component may or may not occur and in unknown quantities, i.e. there are suggestions of its existence but the evidence is very poor.

Values for the numerical system: C,H,L: 1 - unoxidized, 2-6 - increasing degree of oxidation;
Sr: 0 - no reorganization, 1-5 - increasing reorganization, 6 - completely reorganized;
Sc,So,So(sp): (% volume by weight) 0 - none, 1 - $X*10^{-4}$, 2 - $X*10^{-3}$, 3 - $X*10^{-2}$, 4 - $X*10^{-1}$, 5 - $X*10^{+0}$, 6 - $X*10^{+1}$;
Sm,Sah: (1) - very rare, 1 - rare, 2 - uncommon, 3 - common, 4 - abundant.

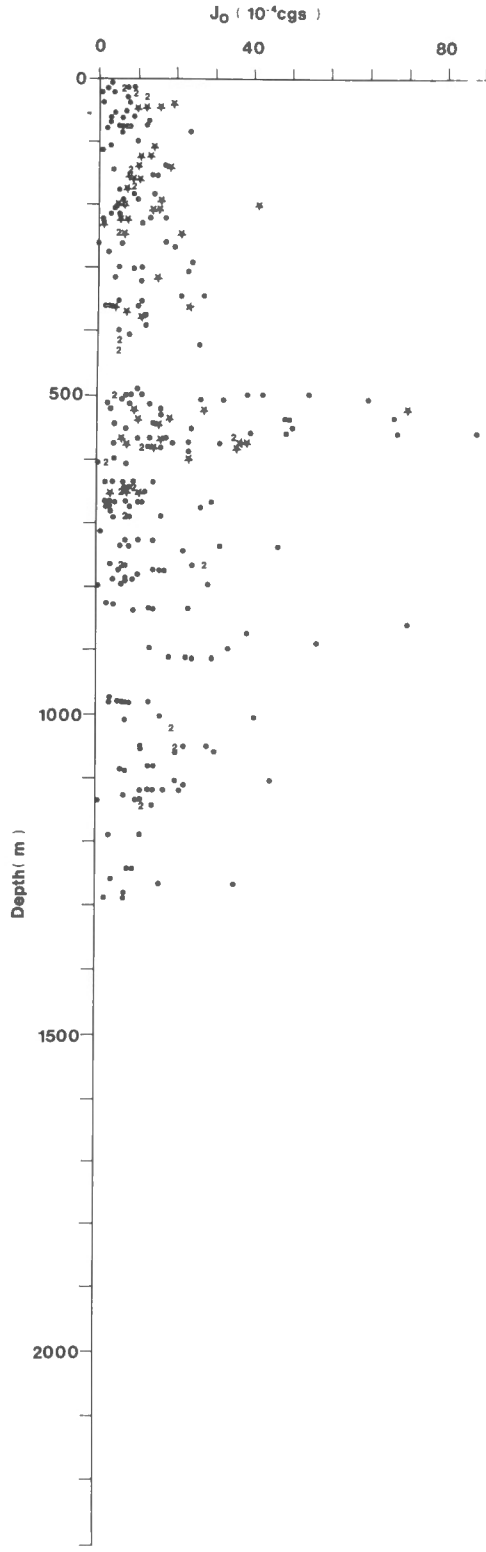

Figure 2: Drill hole CY-4. Distribution with depth of Jo for dikes. Filled circles: aphyric dikes. Stars: phyric dikes.

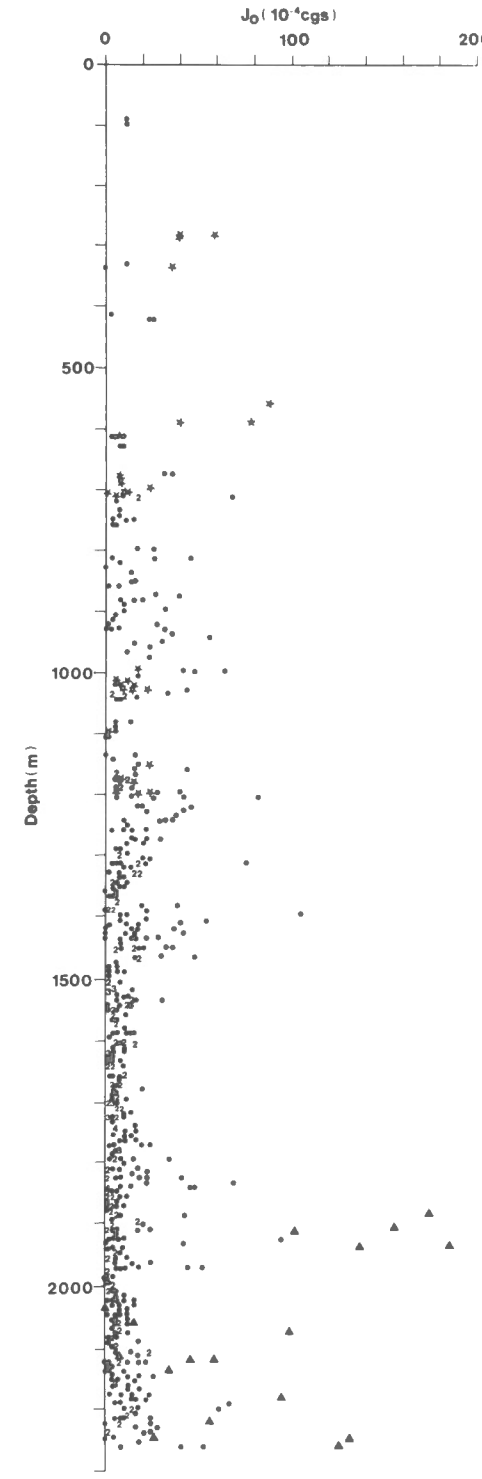

Figure 3: Drill hole CY-4. Distribution with depth of Jo for plutonic lithologies. Filled circles: plagiogranites, gabbros and ultra-mafics showing minor serpentinization ($S \geq 4$ in Table 1). Stars: magnetite gabbros. Filled triangles: markedly serpentinized ultramafics ($S < 4$ in Table 1).

Figure 4 illustrates one of several smoothed forms of the depth distribution of Jo, in this case a five point running average. Comparison of Figure 4 with Figure 1 shows that smoothing has enhanced the three prominent peaks of Figure 1, between 500 and 600 m, 1900 and 2000 m and 2200 m and the bottom of the section at 2263 m. Differences in the width of the belt of smoothed values (Figure 4), for example, between the 0-400 m and 700 and 1500 m intervals, reflect the lesser or greater number of values of Jo>20 evident in Figure 1.

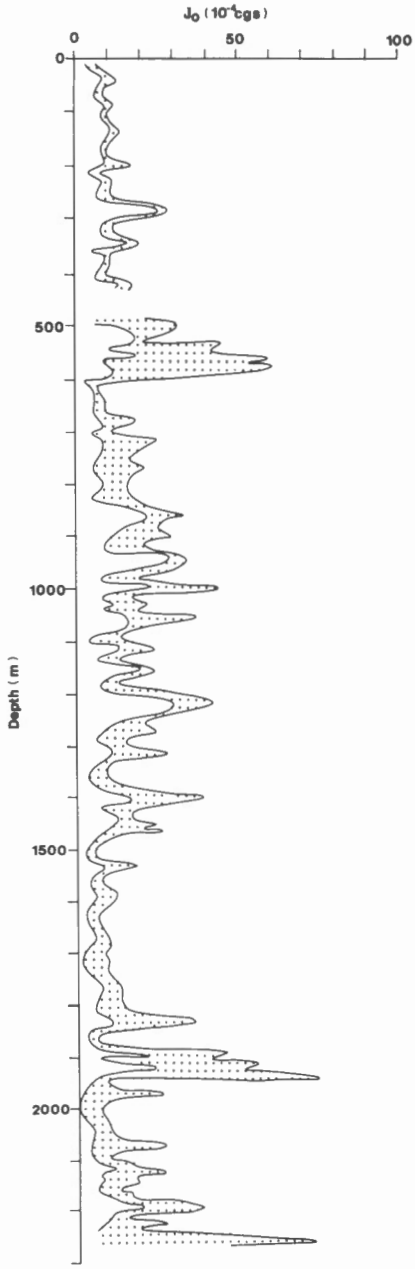

Figure 4: Drill hole CY-4. Smoothed distribution of Jo with depth.

Figure 5 and Table 2 show the distributions and average values of Jo for the main lithological groups occurring in the CY-4 section. It is notable that all groups have very similar average values, the range being only from 12 to 19 $\times$ 10^{-4} cgs. This is consistent with the confinement of most Jo values to the 0-20 $\times$ 10^{-4} cgs interval as evident in Figure 1. All lithologies show skewed distributions of Jo as presented on a linear Jo scale. Some lithologies show tails extending to values of the order of 100 $\times$ 10^{-4} cgs, in particular, the aphyric dikes (Figure 5c) and the ultramafics (Figure 5i). We have no explanation for the high values for a small number of aphyric dikes. The higher values of Jo for the ultramafics are closely related to serpentinization.

(ii) Initial Susceptibility, K

The distribution of K with depth shows four broad zones (Figure 6). From 0 to 600 m depth, K is broadly distributed in the range 20 to 120 $\times$ 10^{-4} cgs, with occasional values of up to 200 $\times$ 10^{-4} cgs in the lowest 100 m of this interval. From 600 to 1300 m depth, values of up to 100 $\times$ 10^{-4} cgs remain commonplace but a concentration of values of $K \leq 10$ $\times$ 10^{-4} cgs distinguishes this zone from the 0-600 m zone. From 1300 to 1750 m values of $K \leq 10$ $\times$ 10^{-4} cgs are almost ubiquitous. From 1750 m to the bottom of the hole at 2263 m values of $K \leq 10$ $\times$ 10^{-4} cgs continue to dominate but a significant number of higher values, extending up to 200 $\times$ 10^{-4} cgs, are present.

It is evident that the four susceptibility zones are closely related to the main lithologic divisions of the section (Figures 7 and 8). Thus, the relatively high susceptibility of the 0-600 m zone, and most of the values in excess of 10 $\times$ 10^{-4} cgs in the 600 to 1300 m are for dike samples. Figure 7 shows that there is little difference between the aphyric and phyric dikes, except that the very highest values in the 500-600 m interval are all from aphyric dike samples. Figure 8 shows that the highest level gabbro screens at depths of less than 600 m have generally as high K values as the enclosing dikes. Among these high K screens are a substantial number described in the Core Description volumes as magnetite-gabbros. The concentration of lower values in the 600-1300 m interval, and the similar low values that dominate the 1300-1750 m interval, are associated with the late plagiogranites and the isotropic gabbro, occurring as screens at about 1300 m, and then continuously in the 1300 to 1750 m interval. The concentration of lower values in the 1750-2263 m interval corresponds to little altered gabbros and ultramafic samples, while the higher values correspond to the most highly serpentinized samples.

TABLE 2. CCSP Drill Hole CY-4: Average Values of Magnetic Properties for Lithological Groupings of Samples*

Lithological Grouping/Property	J_o (number of samples)(10^{-4}cgs)	K (10^{-4}cgs)	MDF (oe)	J_s (cgs)
All Samples	15 ± 19(937)	27 ± 35(1013)	198 ± 116(923)	1.44 ± 2.18(446)
All Dikes	14 ± 14(301)	53 ± 36(366)	155 ± 133(300)	2.70 ± 1.84(139)
Aphyric Dikes	14 ± 14(252)	53 ± 38(305)	167 ± 138(252)	2.73 ± 1.87(114)
Phyric Dikes	15 ± 12(48)	58 ± 26(60)	88 ± 64(47)	2.70 ± 1.65(23)
All Plutonics	15 ± 21(615)	12 ± 22(626)	219 ± 98(602)	0.85 ± 2.09(300)
Plagiogranites	18 ± 16(47)	10 ± 10(49)	217 ± 104(48)	0.88 ± 1.14(27)
Gabbros	13 ± 14(325)	10 ± 22(328)	229 ± 105(317)	1.00 ± 2.56(165)
Gabbro-Ultramafics	12 ± 13(60)	8 ± 8(60)	183 ± 82(60)	0.29 ± 0.33(25)
Ultramafics	19 ± 32(178)	13 ± 25(179)	217 ± 80(172)	0.50 ± 1.08(77)

*the scatter parameter given is one standard deviation

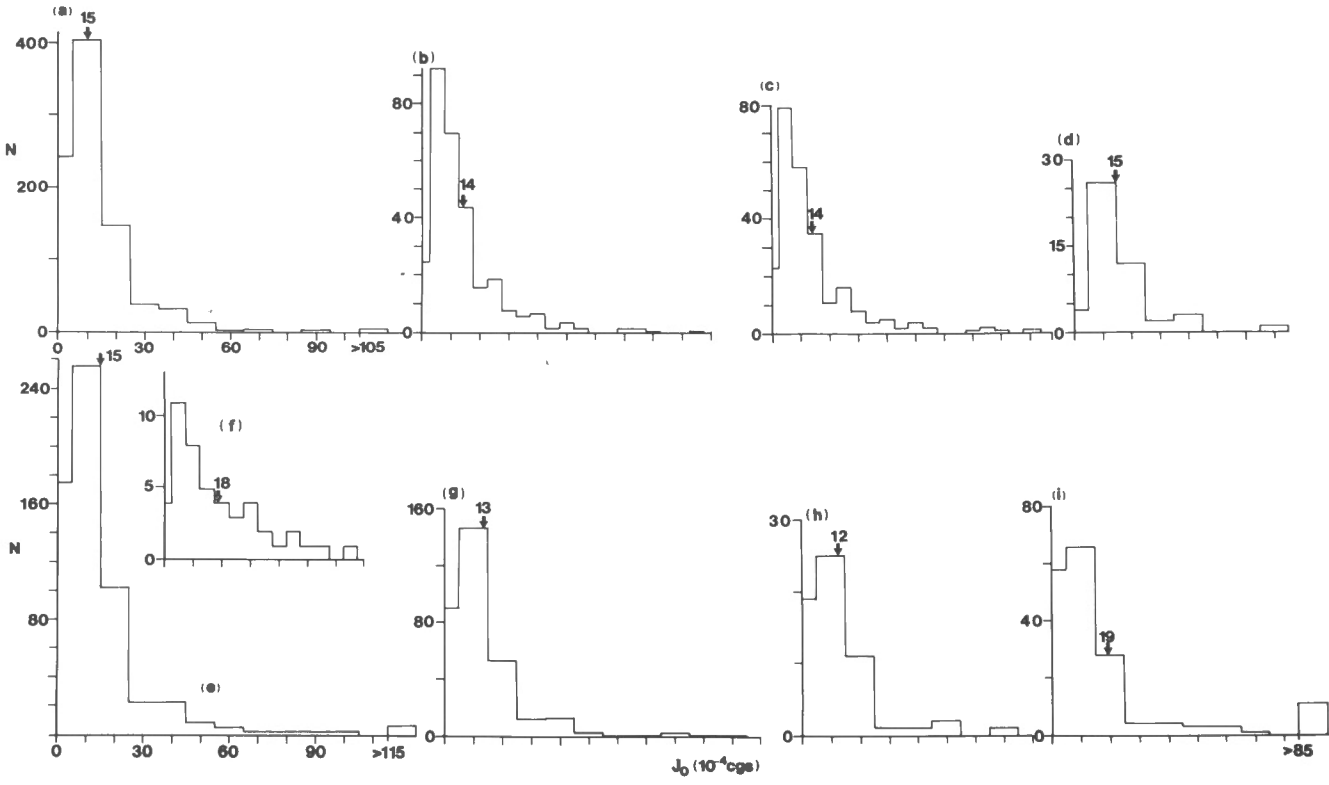

Figure 5: Drill hole CY-4. Distribution of Jo for the different lithologies present. (a) All samples; (b) all dikes; (c) aphyric dikes; (d) phyric dikes; (e) all plutonics; (f) plagiogranites; (g) gabbros; (h) gabbro-ultramafics; (i) ultramafics. Figures on histograms are average values of Jo for each grouping (see also Table 2).

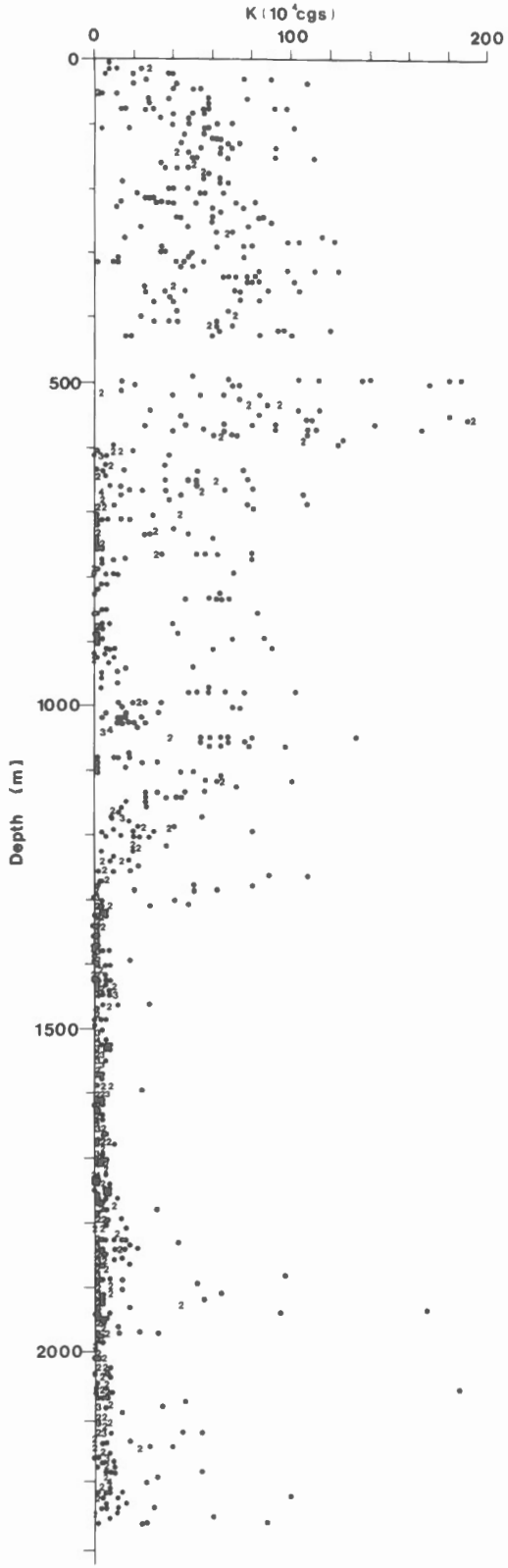

Figure 6: Drill hole CY-4. Distribution with depth of initial susceptibility, K, for all lithologies.

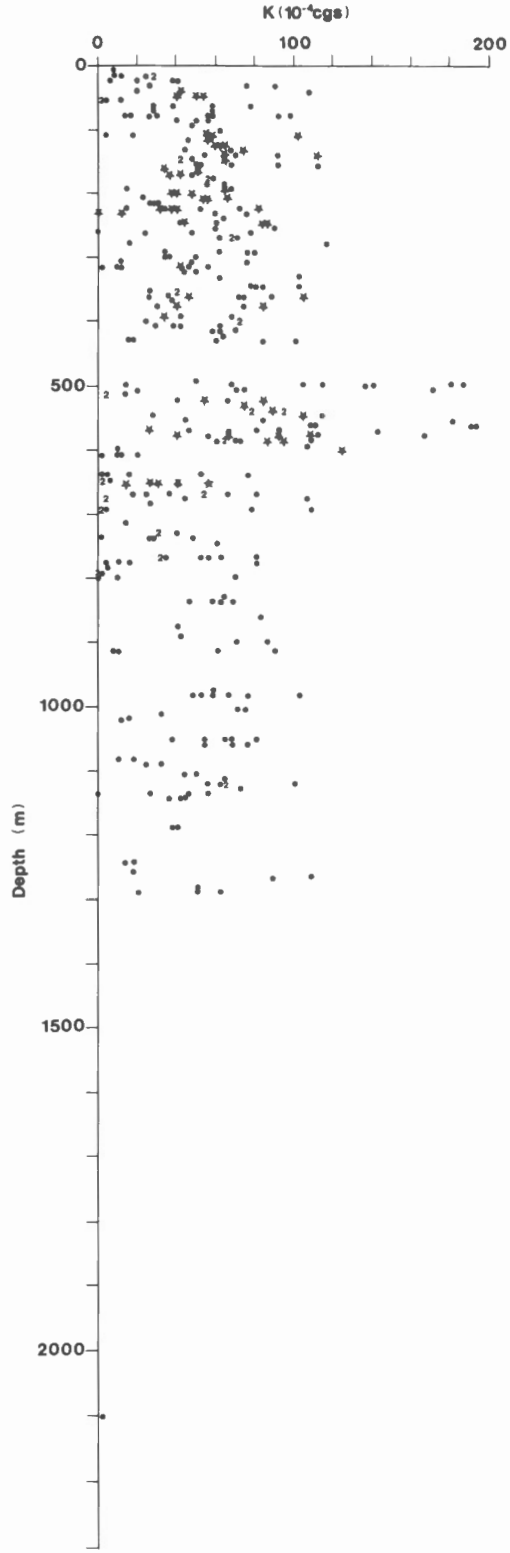

Figure 7: Drill hole CY-4. Distribution with depth of K for dikes. Filled circles: aphyric dikes. Stars: phyric dikes.

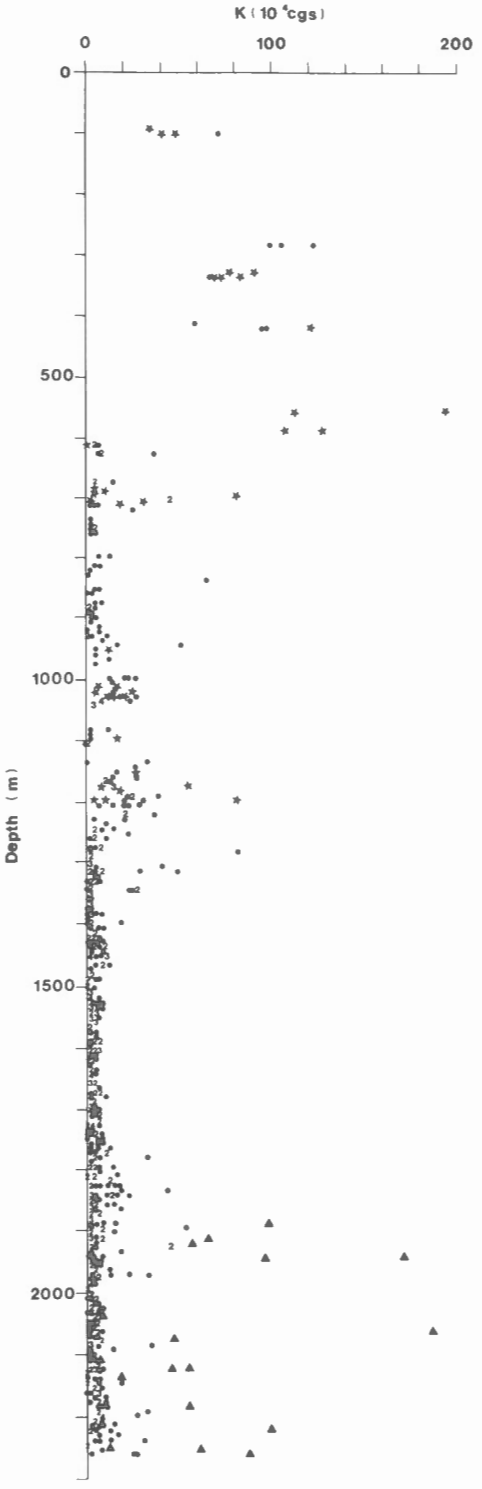

Figure 8: Drill hole CY-4. Distribution with depth of K for plutonic lithologies. Filled circles: plagiogranites, gabbros and ultramafics showing minor serpentinization (S≥ 4 in Table 1). Stars: magnetite gabbros. Filled triangles: markedly serpentinized ultramafics (S<4 in Table 1).

Figure 9 and Table 2 show the distributions and average values for K for the mean lithologic groupings of the CY-4 section. The histograms of Figure 9 show clearly the strong differences between the ranges and average values of K for the different lithologies. Thus, the dike values peak in the 40-80 $\times$ 10^{-4} cgs interval, with average values of between 50 and 60 $\times$ 10^{-4} cgs. The smaller numbers of atypically high values in the aphyric dikes, gabbro and ultramafic groups are evident as extended tails to 200 $\times$ 10^{-4} cgs in the respective histograms.

(iii) Mean Demagnetization Field, MDF

The distribution with depth of MDF shows three broad zones (Figure 10). From 0 to 700 m values occur over a broad range from about 50 to 500 oe, but are concentrated from 50 to 150 oe, with many values towards the lower end of this range. From 700 to 1000 or 1100 m, most values are between 150 and 500 oe, that is to say, the lower values that form the most important part of the 0-700 m interval are largely absent in this second depth zone. From 1000-1100 m, to the bottom of the section at 2263 m, values are generally between 150 and 300 oe, and show a suggestion of an irregular rise and fall with depth.

Figure 11 and Table 2 show the distributions and average values of MDF for the main lithologic groupings occurring in the CY-4 section. The relative abundance of low MDF values for dike samples is evident from the peaks in the 25-75 oe interval, while the plutonics show rather symmetrical distributions with average MDF values of about 200 oe located within the peak interval of distributions.

MDF is related to a number of oxide parameters, notably effective grain size. The results for the CY-4 section suggest that the effective grain size is generally at a minimum in the 0-700 m interval, at a maximum in the 700 to 1000-1100 m interval, and has intermediate values over the remainder of the section.

(iv) Saturation Magnetization, Js

The distribution with depth of Js shows four broad zones (Figure 12). In the 0-600 m interval, Js is broadly distributed over the range from 0.1 to 12 cgs, with most values in the 2-6 cgs range. From 600 to 1300 m depth, values range up to 4 cgs but cluster in the 0-1 cgs range. From 1300 m to 1800 m values are almost all less than 1 cgs; a few higher values are in the 1-2 cgs range. From 1800 m depth to the bottom of the section at 2263 m, values are again concentrated in the 0-1 cgs range but occasional higher values range up to 6 cgs. Figure 13 shows that most dike values are in excess of 1 cgs, except in the 450 m to 800 m interval where a significant number of values of less than 1 cgs occur. There is no obvious

distinction between the range of Js values for the aphyric and phyric lithological groups except that the small group of values in excess of 5 cgs in the 500-600 m interval are all for samples from aphyric dikes. From Figure 14, it is evident that among the plutonics the magnetite gabbros are frequently distinguished by high Js values. It is also noteworthy that the single highly serpentinized ultramafic in the Js data set shows the high value of Js in the 1800-2263 m interval. The broad zones in the depth distribution of Js correspond closely with the major lithologic groups present in the section. Thus, the relatively high values of Js in the 0-600 m interval are, with very few exceptions, for dike samples. In the 600-1300 m interval the higher values are mainly for dike samples while the values of less than 1 cgs are mainly for samples from gabbro screen or plagiogranites. The low values from 1300-1800 m are for isotropic gabbros, and from 1800-2263 m are for little serpentinized ultramafics.

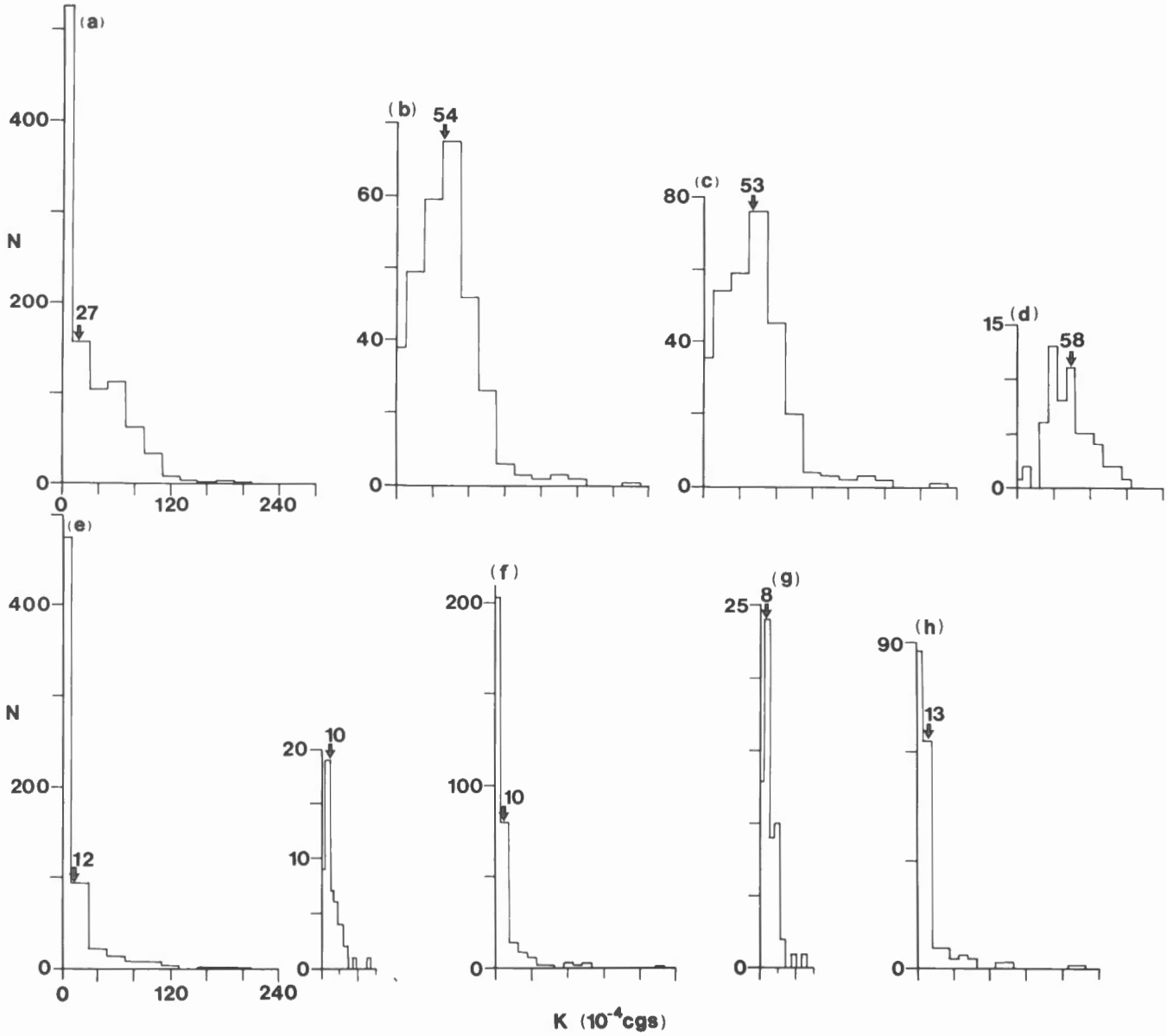

Figure 9: Drill hole CY-4. Distribution of K for the different lithologies present. (a) All samples; (b) all dikes; (c) aphyric dikes; (d) phyric dikes; (e) all plutonics; (f) plagiogranites; (g) gabbros; (h) gabbro-ultramafics; (i) ultramafics. Figures on histograms are average values of K for each group.

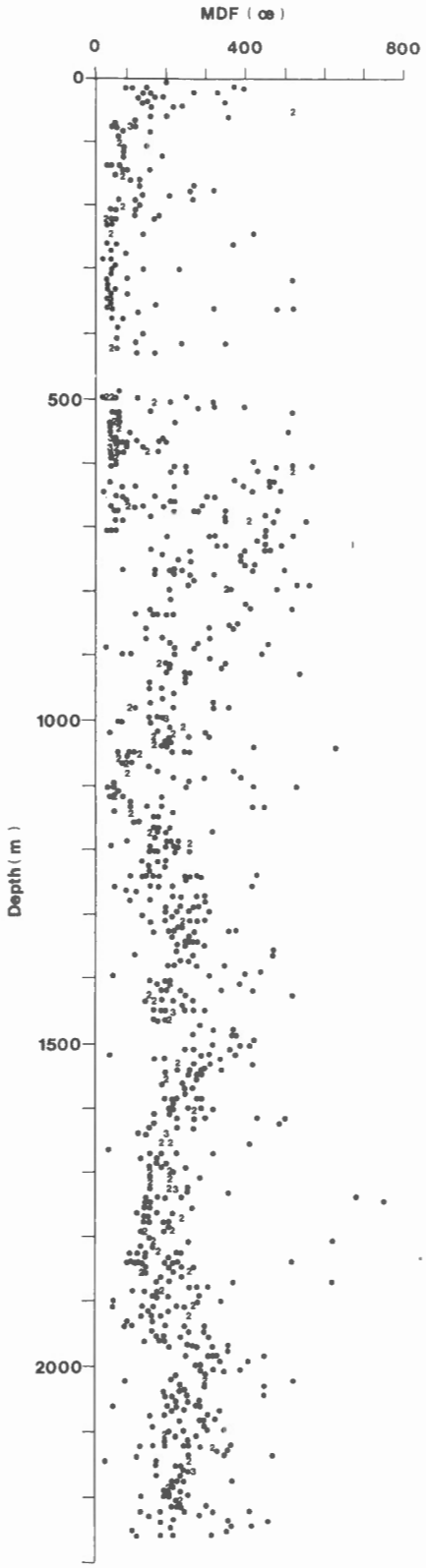

Figure 10: Drill hole CY-4. Distribution with depth of mean demagnetizing field, MDF.

Figure 14 and Table 2 show the distributions and average values of Js for the main lithologic groupings occurring in the CY-4 section. The distributions for the dikes are only moderately skewed, with average values of close to 2.7 cgs within the principal peaks of distributions. The dike average values are between a factor of three and nine greater than the average values for the plutonic groups. Most plutonic distributions are strongly skewed towards the lowest interval, 0-1 cgs, and have average values of 0.3 to 0.9 cgs within this lowest interval. Among the plutonic lithologies, the long tail of high values associated with magnetite gabbros is noteworthy in the gabbro group, as is the restricted range of low values (0-2 cgs) and low average value (0.29 cgs) for the plagiogranites.

(v) Curie Temperature, Tc

The distribution with depth of Tc (Figure 16) shows that generally Tc is strongly confined to the 500-600°C interval throughout the CY-4 section. There are a small number of samples that differ significantly from this simple distribution pattern. Three aphyric dike samples in the 830 to 1140 m interval show well developed double Curie points during heating, with the lower Curie points in the 310-330°C interval and the higher Curie points in the commonplace 500-600°C interval. Two other samples in the 830-1150 m depth interval, and seven samples in the 1750-2263 m interval also show a variety of double Curie points. The difference between Curie points in each sample is $\leq$100 °C. At least one and frequently both Curie points for these samples are within the 500-600°C temperature interval. Two samples in the ultramafic interval, below 1750 m, show single high Curie points, a gabbro at 1810.41 m with a Tc of 790°C and an ultramafic at 1991.60 with a Tc of 715°C.

Figure 17 and Table 2 show the distribution and average values of Tc for the main lithologic groupings occurring in the CY-4 section. These histograms emphasize the very restricted distribution of Tc which is independent of lithology.

OXIDE PETROGRAPHY

Nine properties were measured quantitatively or semi-quantitatively for each of 100 polished surfaces representing all the lithologies present in the section. Sample depths, lithologies and oxide petrographic properties are listed in Table 1 and are shown as depth profiles in Figures 18 and 19. All oxide identifications and measurements were made using a Reichert Zeto Pan Pol microscope at a magnification of $\times$1375.

The properties measured were: (i) titanomagnetite deuteric oxidation state (symbolized

by C), (ii) titanomagnetite hydrothermal oxidation state (H), (iii) titanomagnetite low temperature oxidation state (L), (iv) titanomagnetite secondary reconstruction (Sr), (v) secondary magnetite chains (Sc), (vi) secondary magnetite overgrowths (So), (vii) the development of martitic alteration in magnetite (Sm), (viii) the development of hematitic alteration in magnetite (Sah), (xi) the relative abundance of primary and secondary magnetite (Ratio R).

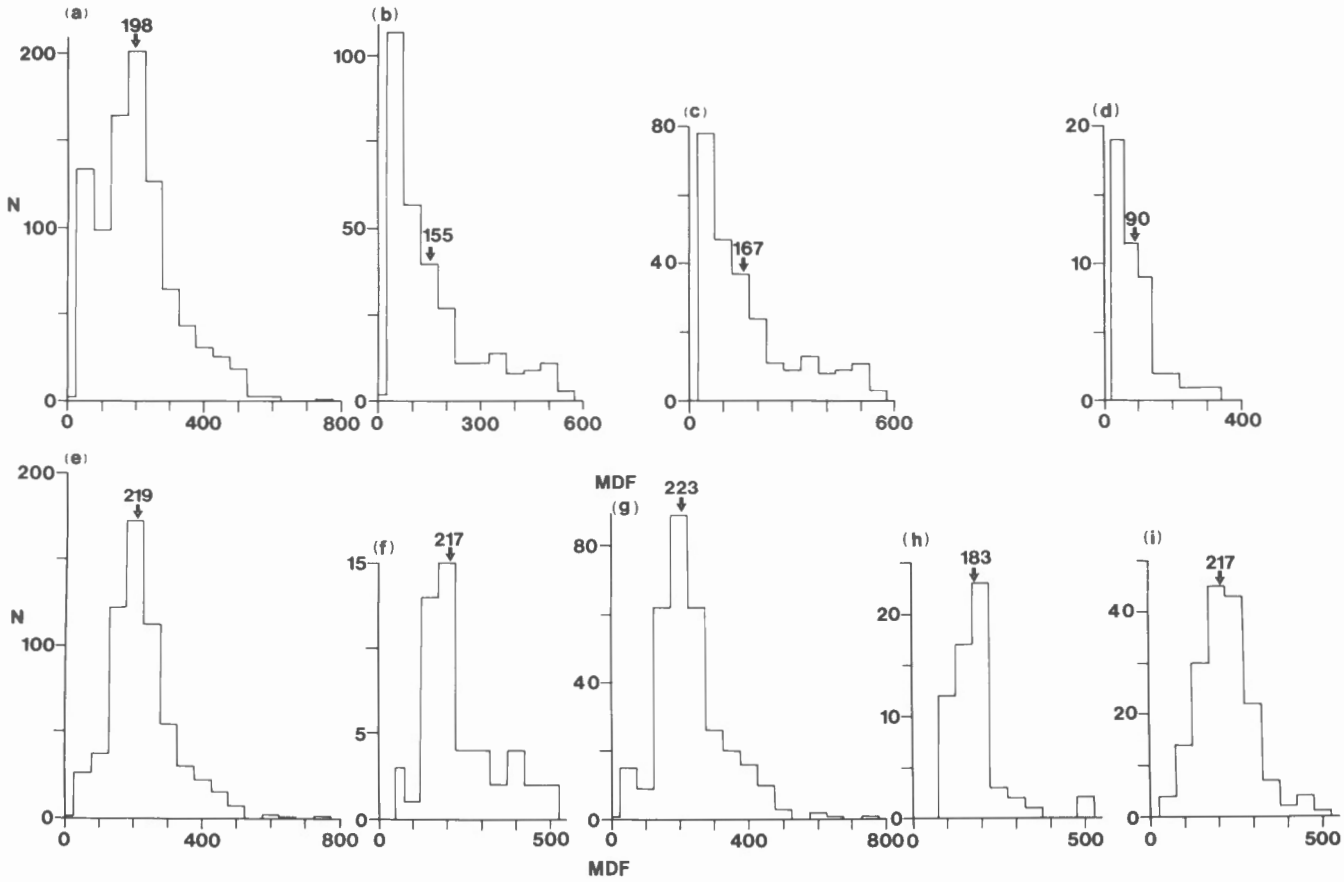

Figure 11: Drill hole CY-4. Distribution of MDF in the different lithologies present. (a) All samples; (b) all dikes; (c) aphyric dikes; (d) phyric dikes; (e) all plutonics; (f) plagiogranites; (g) gabbros; (h) gabbro-ultramafics; (i) ultramafics. Figures on histograms are average values of MDF for each group.

The nature of each property measured and the results of each set of measurements are given below.

(i) Titanomagnetite Deuteric Oxidation State, C

This is a high temperature form of oxidation, occuring during the initial cooling of a rock unit. Several stages of increasing intensity of oxidation are recognized. Before oxidation commences rock units contain uniform grey brown titanomagnetite grains. Oxidation first results in the subsolidus exsolution of ilmenite lamellae. When all the titanium present has been partitioned into ilmenite, oxidation continues with the alteration of the ilmenite lamellae. Eventually the residual, near-pure magnetite alters to phases such as titaniferous hematite, rutile and pseudobrookite. Characteristically, this and other forms of alteration vary rapidly spatially within a rock unit on scales from micrometres to metres (e.g. Watkins and Haggerty, 1968). Another characteristic of many of the samples examined is that the results of several types of alteration are superimposed. Care is needed to identify a complete paragenetic sequence. The range of alteration stages observed are conveniently classified for within-sample averaging purposes on a 1 (unaltered) to 6 (completely oxidized) scale (Ade-Hall et al., 1971).

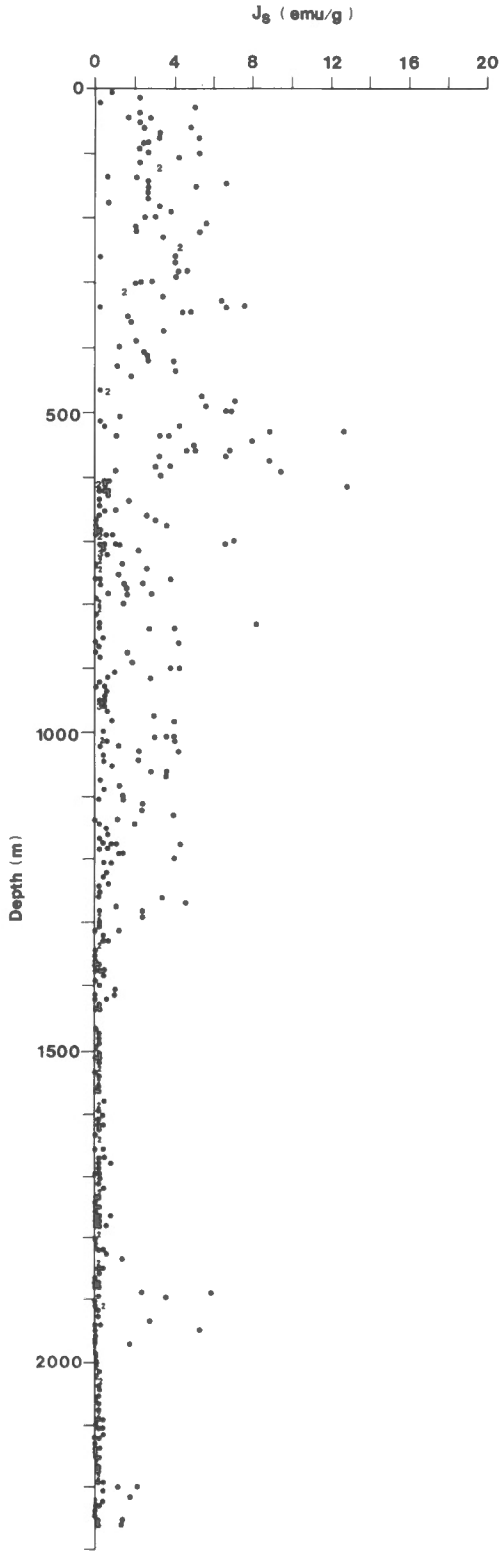

Figure 12: Drill hole CY-4. Distribution with depth of saturation magnetization, Js.

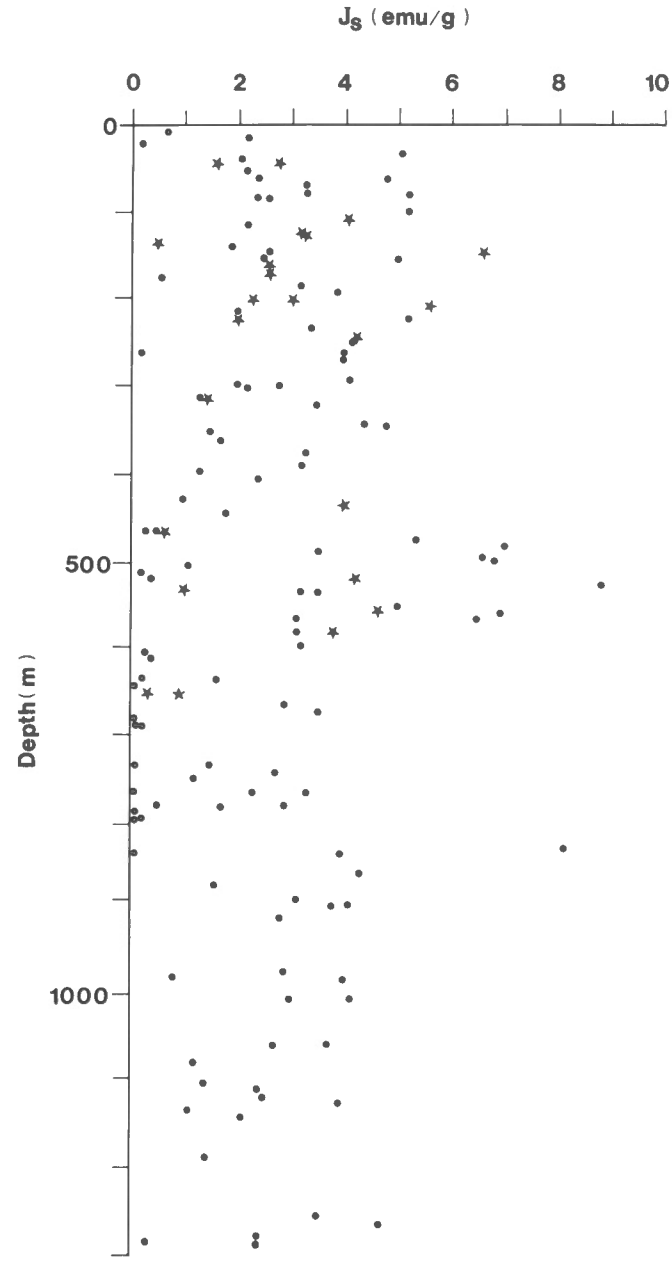

Figure 13: Drill hole CY-4. Distribution with depth of Js for dikes. Filled circles: aphyric dikes. Stars: phyric dikes.

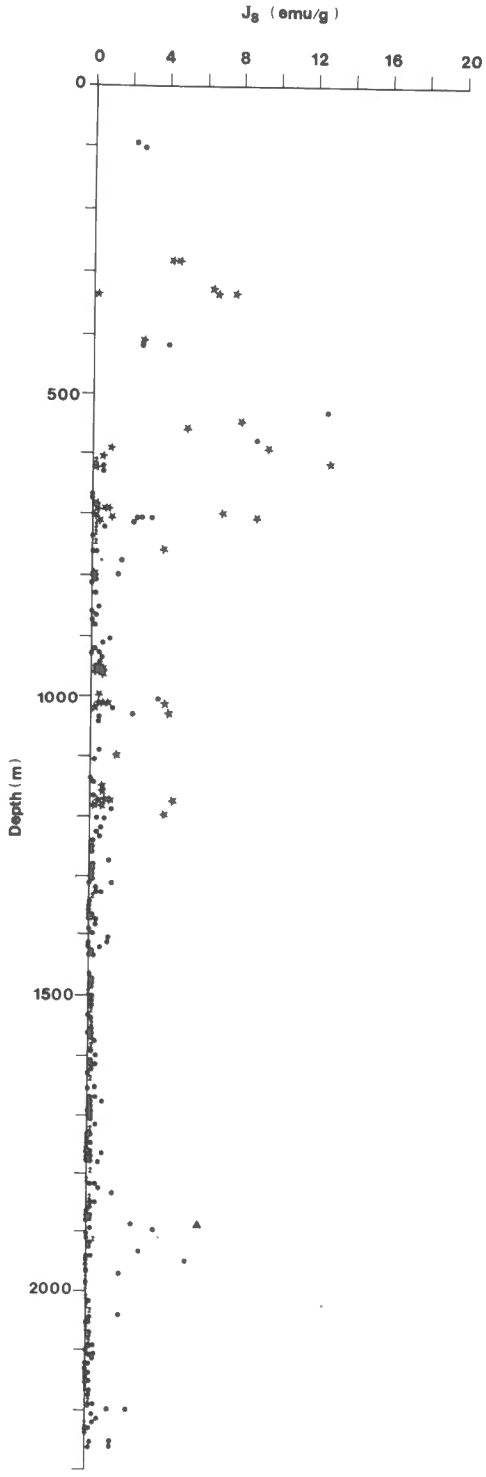

Figure 14: Drill hole CY-4. Distribution with depth of Js for plutonic lithologies. Filled circles: plagiogranites, gabbros and ultramafics showing minor serpentinization (S≥4 in Table 1). Stars: magnetite gabbros. Filled triangles: markedly serpentinized ultramafics (S<4 in Table 1).

Within the CY-4 section, titanomagnetite deuteric oxidation is largely found within the dike component, where it occurs almost ubiquitously at moderate levels of development. This is evident from Figure 18 where samples with C>1 only occur at depths of less than 1289 m: there are no thin basic dikes below this point. There is a significant decrease in the degree of deuteric oxidation with depth within this upper part of the section. Thus, from the drill collar to a depth of close to 500 m, C typically has values of from 2 to 3. The only gabbro screen sample examined in this interval, at 290 m depth, also shows this level of deuteric alteration. Mineralogically, this level of deuteric alteration indicates the presence in individual samples of titanomagnetites with a range of ilmenite lamellae density from one to a few lamellae (C=2)(Figures 20b and 21c), to complete partitioning of titanium into lamellae, where lamellae account for about half the area of a grain (C=3)(Figure 20c). As in minor basaltic intrusives from other locations, the higher degrees of deuteric oxidation are not seen in the CY-4 dikes (Ade-Hall and Lawley, 1970). A single sample at 515 m depth provides a transition from the 0-500 m interval for which 2<C<3 to the 500-1289 m interval for which 1<C<2 for almost every sample. Exceptions to this general restriction are for dike samples at 897, 1176 and 1253 m and a gabbro screen at 1275 m for which 1<C<3. As in the 0-500 m interval a number of gabbro screens, for example, at 960 m, show the same range in C as the basic dikes in the interval. Mineralogically, 1<C<2 indicates the presence in individual samples of titanomagnetites either with no ilmenite lamellae or at the most with a few lamellae.

With the doubtful exception of a gabbro sample at 1552 m depth, no sample below 1289 m has experienced deuteric oxidation.

(ii) Titanomagnetite Hydrothermal Alteration State, H

This category includes a series of hydrothermal alteration states produced through the interaction of titanomagnetite, in a range of deuteric alteration states, with hot fluids (Ade-Hall et al., 1971). Using results from Iceland (Robinson et al., 1982), where the occurrence of different titanomagnetite alteration states can be correlated with the occurrence of secondary silicate minerals of known stability fields, it is possible to estimate the fluid temperatures needed to produce the different alteration states. As in the case of deuteric oxidation, the hydrothermal alteration state often varies from grain to grain within a sample, suggesting that fluid access to grains, as well as fluid temperature, is important in determining the resulting alteration state. The temperatures equated below with successive alteration states are based on the first occurrence with depth of the state. For a sample characterized by grains showing a range of alteration

states, it is suggested that the most altered grains were most likely to have reached or approached equilibrium with the hydrothermal fluid, and thus should be used as a guide to the temperature of the altering fluid.

The first indication of hydrothermal alteration (H=2 on a 1 to 6 scale), is the presence of either or both small areas of ≤1 μm anatase granules in titanomagnetite ('granulation', Figures 20a and 21c) or the incipient replacement of ilmenite lamellae, produced during deuteric oxidation, by sphene (Figure 20d). The fluids responsible for this stage were probably at temperatures of between 50 and 150°C, with the presence of incipient sphene probably indicating temperatures near the higher end of the interval.

Grains with H=3 are largely or completely granulated or show complete replacement of ilmenite lamellae by sphene (Figures 20d, 22a,b, and c). Fluid temperatures of 150°C to 250°C are estimated for this state of alteration.

Grains with H=4 show, in addition to the features characteristic of H=3, variable erosion of grains (Figure 21a). Fluid temperatures of about 260°C are estimated for this state of alteration.

Grains with H=5 or 6 are characterized by the partial or complete, respectively, leaching of iron from grains, leaving translucent pseudomorphs, probably largely consisting of titanium oxides (Figure 21b). Fluid temperatures of 290°C and higher are estimated for these states of alteration.

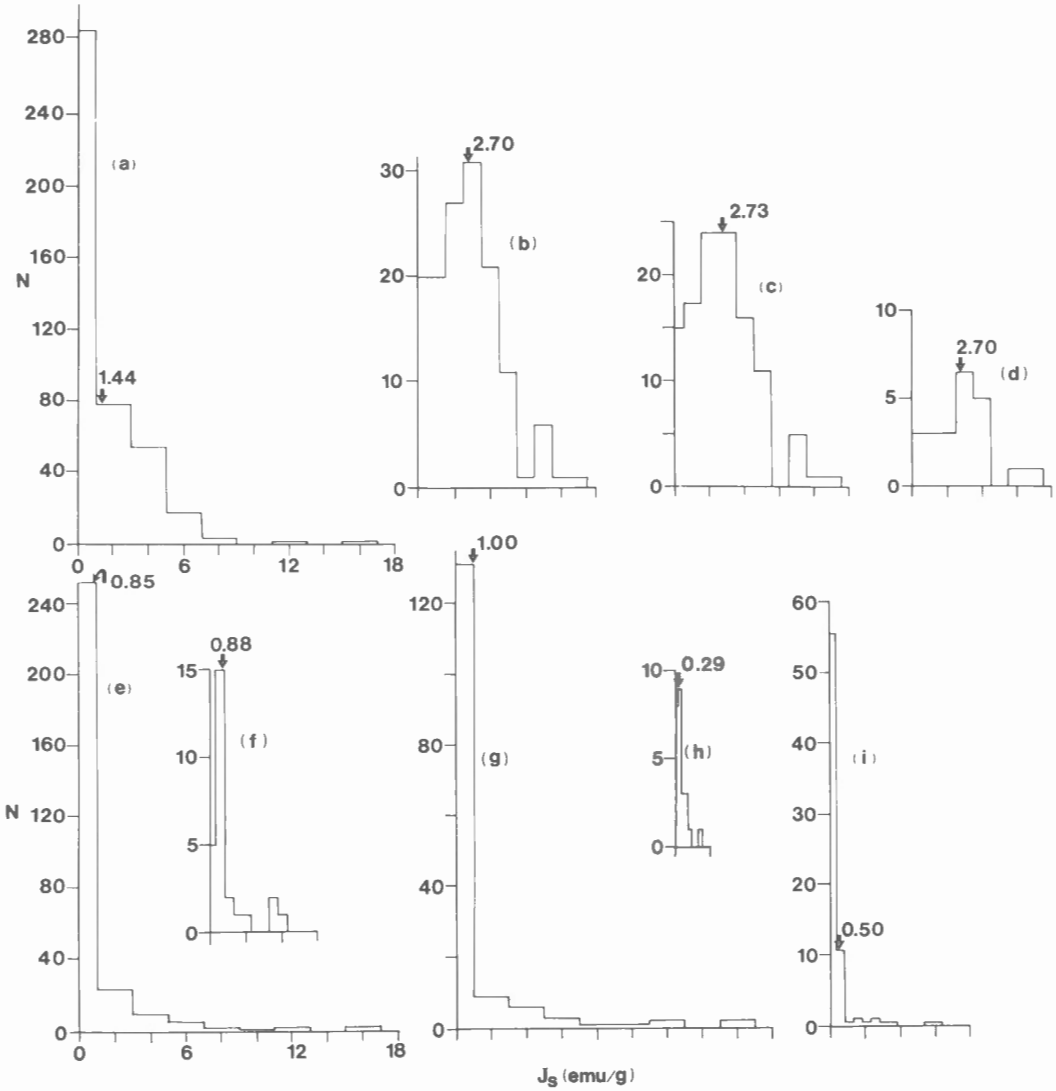

Figure 15: Drill hole CY-4. Distribution of Js in the different lithologies present. (a) All samples; (b) all dikes; (c) aphyric dikes; (d) phyric dikes; (e) all plutonics; (f) plagiogranites; (g) gabbros; (h) gabbro-ultramafics; (i) ultramafics.

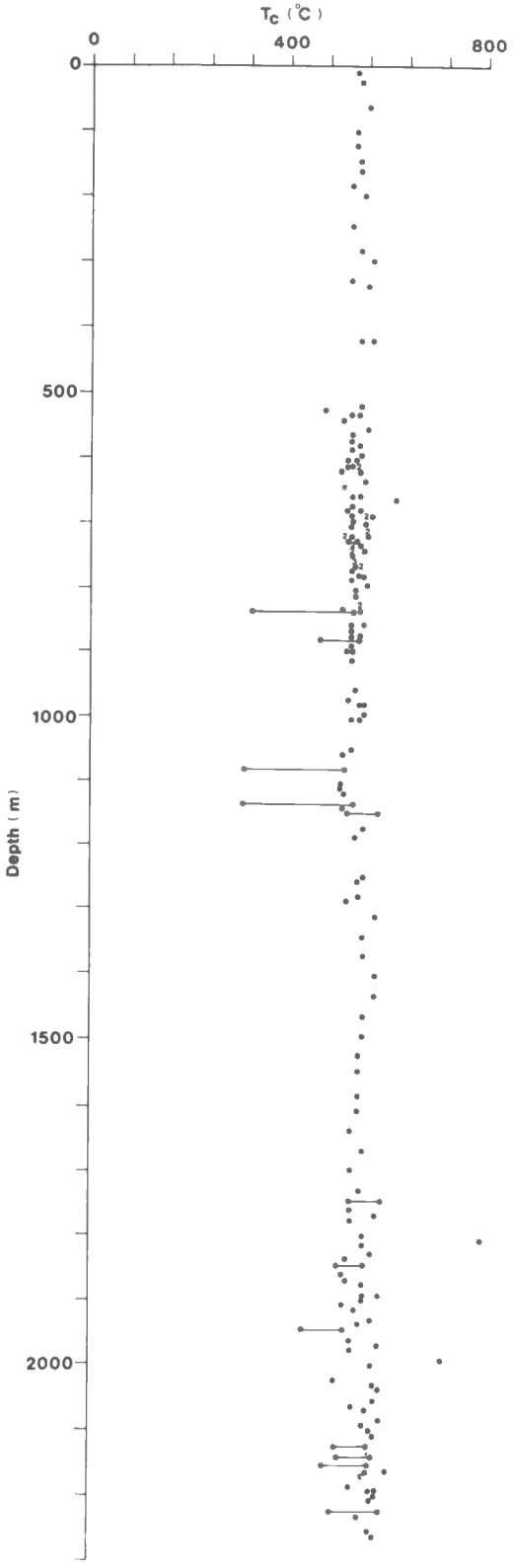

Figure 16: Drill hole CY-4. Distribution with depth of Curie temperature, Tc.

A number of subsequent alteration processes often makes the direct determination of the hydrothermal alteration state difficult. Thus, reconstruction, or recrystallization, two processes described in detail below, result in the partial or complete loss of the characteristic textures of the different hydrothermal alteration states. However, particularly in the instance of sphene, the characteristic products of hydrothermal alteration are not lost, but are just locally redistributed, allowing the hydrothermal alteration component of the history of a sample to be estimated.

In the CY-4 section hydrothermal alteration is very widespread in the dikes of the 0-1290 m interval. Sample average values (Figure 18) are typically in the $2<H<3$ range, with a small number of lower or higher values, in the 0-600 m interval. While similar values are common at below 600 m depth, a substantial number of samples contain a significant number of grains that have not experienced hydrothermal alteration. This two-stage, downwards decrease in hydrothermal alteration matches closely the steps in the downwards decrease in deuteric oxidation. The gabbroic samples in the 1290-1750 m interval only rarely show a history of hydrothermal alteration. This is also the case for many of the ultramafics and gabbros at below 1750 m depth. However, as is indicated in Figure 1, a significant number of the samples below 1750 m are characterized by the presence of unaltered magnetite either as chains after the decomposition of olivine, or as elongate grains along the cleavage planes of silicates, together with occasional small, sharply defined translucent grains that resemble the $H=6$ hydrothermal alteration state of magnetite. For this reason, bracketed $H=6$ points have been shown in addition to $H=1$ points in Figure 18. It is noted, however, that the absence and grains in intermediate hydrothermal alteration states in these samples would be surprising if the identification of these grains as pseudomorphs after iron-titanium oxides is correct. The possibility exists that the small white translucent grains are quite unrelated to Fe-Ti oxides and their alteration. It is planned to test this possibility shortly by electron probe microanalysis.

(iii) Titanomagnetite Low Temperature Oxidation State, L

This type of oxidation results from the interaction of water at probably no more than a few tens of degrees centigrade with titanomagnetite. It is particularly well developed in the uppermost part of in-situ oceanic crust where cold sea water saturation or continued drawdown has occurred. A five stage scale of increasing alteration has been recognised by Johnson and Hall (1978). Only the first and second stages are preserved in CY-4 Fe-Ti oxides, although

higher stages may have been present in samples that subsequently experienced other alteration processes. The first stage is marked by the absence of any low temperature oxidation effects and the second by the presence of curved cracking in Ti-magnetite grains. This cracking is apparently the result of volume change associated with increasing cation deficiency in the single phase Fe-Ti oxide, there being insufficient thermal energy to produce the phase splitting into magnetite and ilmenite as seen in stage 2 of the deuteric oxidation sequence. Well developed L2 alteration (Figure 21c) is present in a significant number of dikes in the 850 to 1200 m depth interval and in two gabbroic screens within the dike component of the section, at 280 m and 1000 m depth.

(iv) Titanomagnetite Secondary Reconstruction, Sr

Secondary magnetite is widespread in the CY-4 section. We follow Hall (1985) in differentiating between the formation of magnetite (s.s.) through deuteric oxidation during initial cooling and other, later processes generating secondary magnetite. Three general occurrences of secondary magnetite are recognized in the CY-4 section: in reconstructed or recrystallized grains in dike or screen samples, and as overgrowths and chains of small grains largely in ultramafic and occasionally in deeper gabbroic samples.

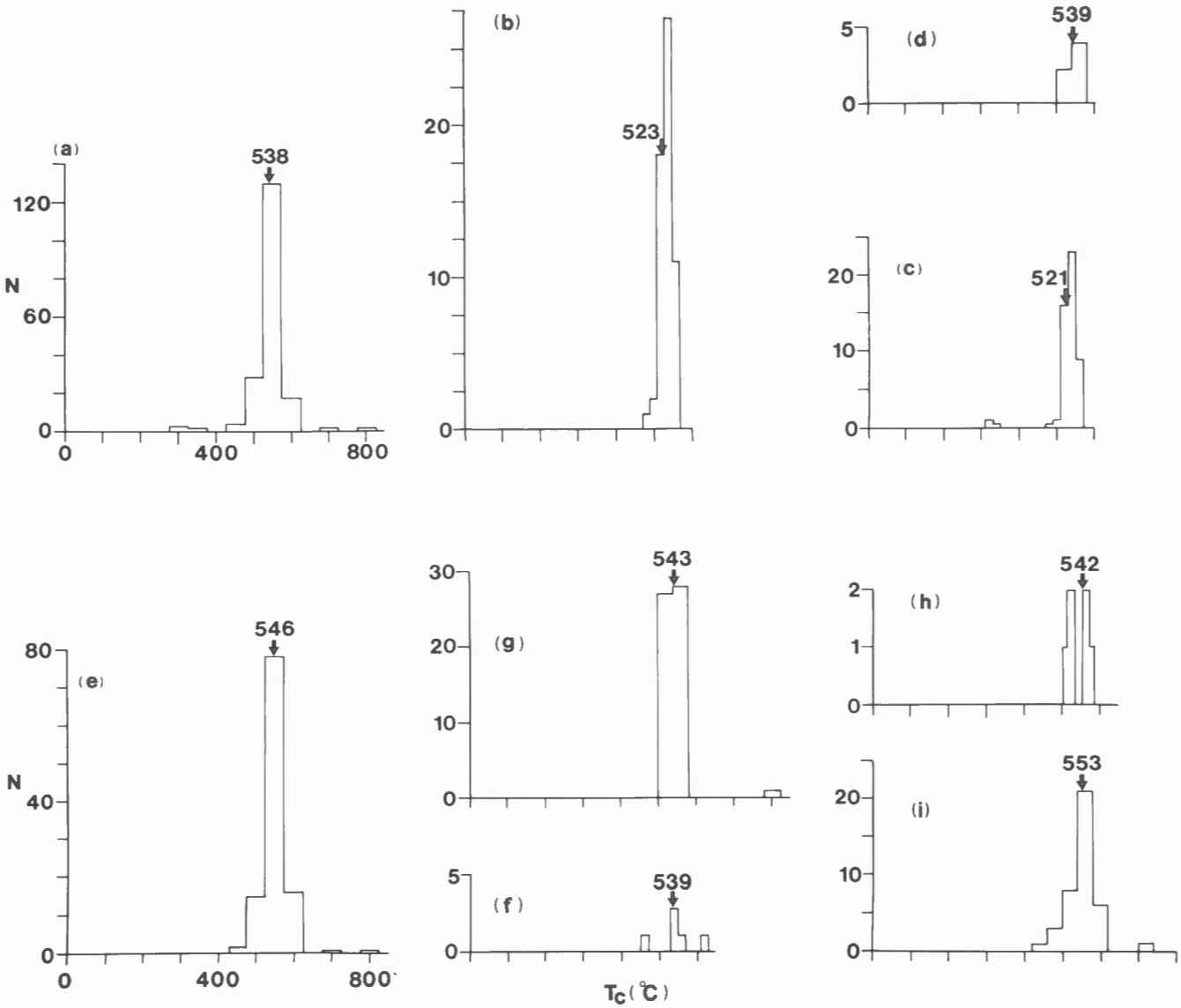

Figure 17: Drill hole CY-4. Distribution of Tc in the different lithologies present. (a) All samples; (b) all dikes; (c) aphyric dikes; (d) phyric dikes; (e) all plutonics; (f) plagiogranites; (g) gabbros; (h) gabbro-ultramafics.

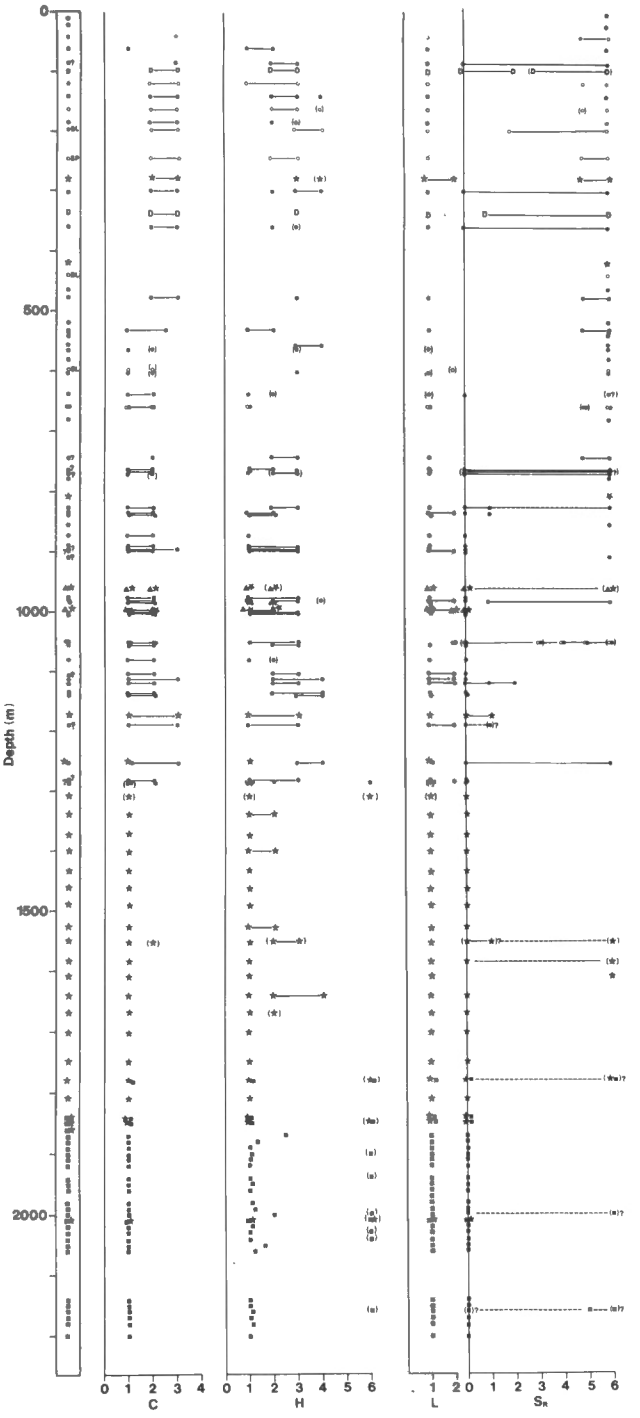

Figure 18: Drill hole CY-4. Distribution of Fe-Ti oxide parameters with depth, I. Explanation of profiles from left to right. Lithological classification of samples: filled circles: aphyric dikes; open circles: phyric dikes (SP: sparsely phyric, SL: slightly phyric); star: gabbro; star and filled triangle together: plagiogranite; star and filled square together: gabbro-ultramafic; filled square: ultramafic; C: titanomagnetite deuteric oxidation state (as defined in text); H: titanomagnetite hydrothermal alteration state (as defined in text); Sr: degree of secondary reconstruction or recrystallization of magnetite (as defined in text).

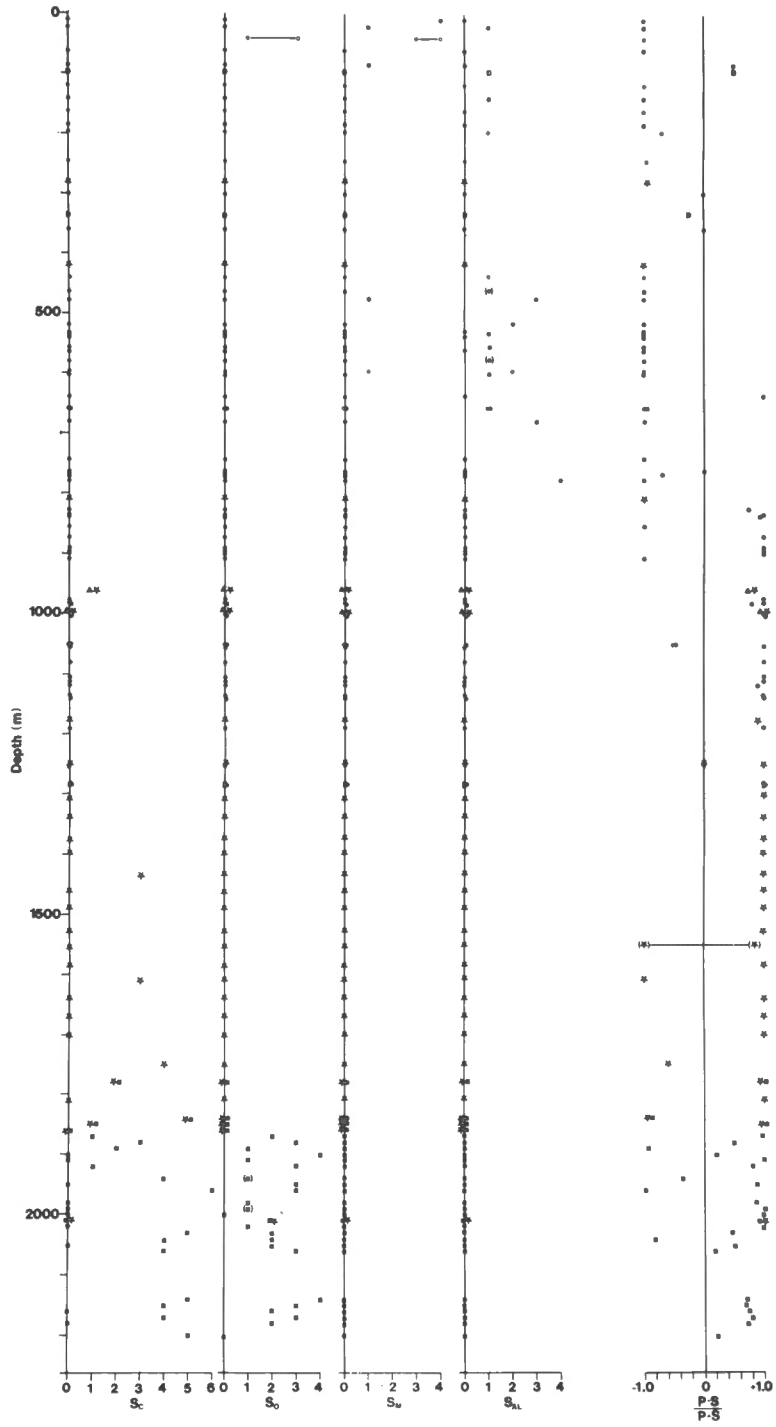

Figure 19: Drill hole CY-4. Distribution of Fe-Ti oxide parameters with depth, II. Lithological symbols as in Figure 18. Explanation of profiles from left to right. Sc: degree of development of chains of secondary magnetite; So: degree of development of overgrowths of secondary magnetite (as defined in text); Sm: degree of development of martite exsolution in magnetite (as defined in text); Sah: degree of development of secondary hematite in magnetite (as defined in text). Ratio of primary to secondary magnetite in samples. P: volume of primary magnetite; S: volume of secondary magnetite.

Reconstructed magnetites were first recognized at depth in the Icelandic crust where they occur in deeply buried flows which had previously experienced substantial hydrothermal alteration and later a high density of dike injection (Hall, 1985). Among various indicators of reconstruction noted in the Iceland section, the expulsion of hydrothermal sphene replacements of lamellar ilmenite, produced during deuteric oxidation, provides clear evidence of the marked internal reorganization of grains, presumably with opportunity for remagnetization (Hall, 1985, Fig. 6). Similar, frequently more extreme, reconstruction of magnetite grains is widespread in the dike component of the CY-4 section (Figures 21d, 22a,b and c). A more drastic kind of reconstruction, perhaps more properly termed recrystallization, also occurs in some dike samples. The Fe-Ti oxides in these samples occur as aggregates of many grains of magnetite, which is often rather porous, ilmenite and sphene (Figure 22d). A scale from 0 to 6, indicating the degree of reconstructions has been devised. Figure 1 shows the range of reconstruction states present in individual samples. Many dike samples contain only completely reconstructed or recrystallized magnetites (Sr=6) while others show a range of states. Sr=6 grains are usually recognizable by the peripheral association of sphene with otherwise apparently quite fresh and unaltered magnetite. Since sphene does not occur as a primary mineral in diabasic rocks, its presence and association with magnetite must indicate a history of the hydrothermal alteration of deuterically oxidized titanomagnetite. In a number of samples, particularly at below 1500 m depth, small, fresh well defined magnetites occur occasionally as minor components of the Fe-Ti oxides present. These may represent reconstructed primary grains, but in the absence of associated sphene, this cannot be ascertained definitely. These samples are indicated in Figure 1 by a bracketed Sr=6 point joined by a broken line to the Sr=0 state of the dominant Fe-Ti oxides.

As indicated above, reconstruction is a very important process in the dike component of CY-4, in which almost all samples are affected to a depth of about 800 m. From 800 m to 1290 m, the last occurrence of a basic dike, reconstruction is present in only about one-third of the samples, the remainder showing only primary, deuteric or hydrothermal alteration features.

(v) Secondary Magnetite Chains, Sc

Secondary magnetite resulting from the breakdown of olivine during serpentinization is a common feature of the olivine bearing gabbros and ultramafics. One characteristic form of this magnetite is as chains of small equidimensional or rounded grains, with the location of chains clearly controlled by the cracks in the olivine pseudomorphs. The small magnetite grains are frequently quite fresh and unaltered in appearance, but also occur with apparently porous cores, as is illustrated in Figure 23c. Based on quantitative observations of the net area of chain-type secondary magnetite, a logarithmic scale of secondary chain abundance has been devised where 0 indicates absence of chains, 1 indicates an abundance of between 10^{-4} and 10^{-3} weight percent, and so on up to 6 for an abundance in excess of 10 weight percent. Below 1750 m depth, where chains are common, average values of chain occurrence increase with depth, $0 \leq Sc \leq 3$ being typical for the 1750-2050 m interval, and $4 \leq Sc \leq 5$ from 2050 m to 2200 m.

(vi) Secondary Magnetite Overgrowths, So

This is the second typical occurrence of secondary magnetite in the gabbro-ultramafic section below 1850 m depth. Overgrowths characteristically form on primary spinel grains, often with an intermediate zone between the spinel core and magnetite overgrowth (Figure 23d). A scale of overgrowth abundance, from So=1 (10^{-4} to 10^{-3} weight percent) to So=4 (10^{-2} or greater weight percent) has been devised, with values shown in Figure 1. As in the case of secondary chains, average overgrowth abundance increases with depth, with $1 \leq So \leq 3$ typically from 1850 to 2000 m, and $2 \leq So \leq 3$ from 2000 to 2200 m.

(vii) Martitic Alteration in Magnetite, Sm

The widespread martitic alteration of magnetite consists of lamellar exsolution of hematite in magnetite. The lamellae are controlled by the octahedral planes of the magnetite, and often differ morphologically from ilmenite lamellae resulting from high temperature, deuteric oxidation, by being more ragged, or distinctly tapered (Figure 23a). The physical conditions for the formation of martite are not well known. Ramdohr (1980) indicates that while high temperature oxidation is required in the laboratory, occurrences in mineral deposits probably formed at much lower temperatures. Ramdohr (1980) also identifies a mechanism called 'martitization due to heating' which is effective when magnetite is heated in an oxidizing atmosphere. Elmore and Van der Voo (1982) suggest, from a study of the Keeweenawan Copper Harbor Conglomerate, that martitization occurs both in detrital and authigenic grains. Since hematite also occurs as irregular, peripheral alteration zones in magnetites in CY-4 samples, it is reasonable to suggest the aggregation of hematite into lamellae requires significant thermal energy, and thus may fall into Ramdohr's 'martitization due to heating' class.

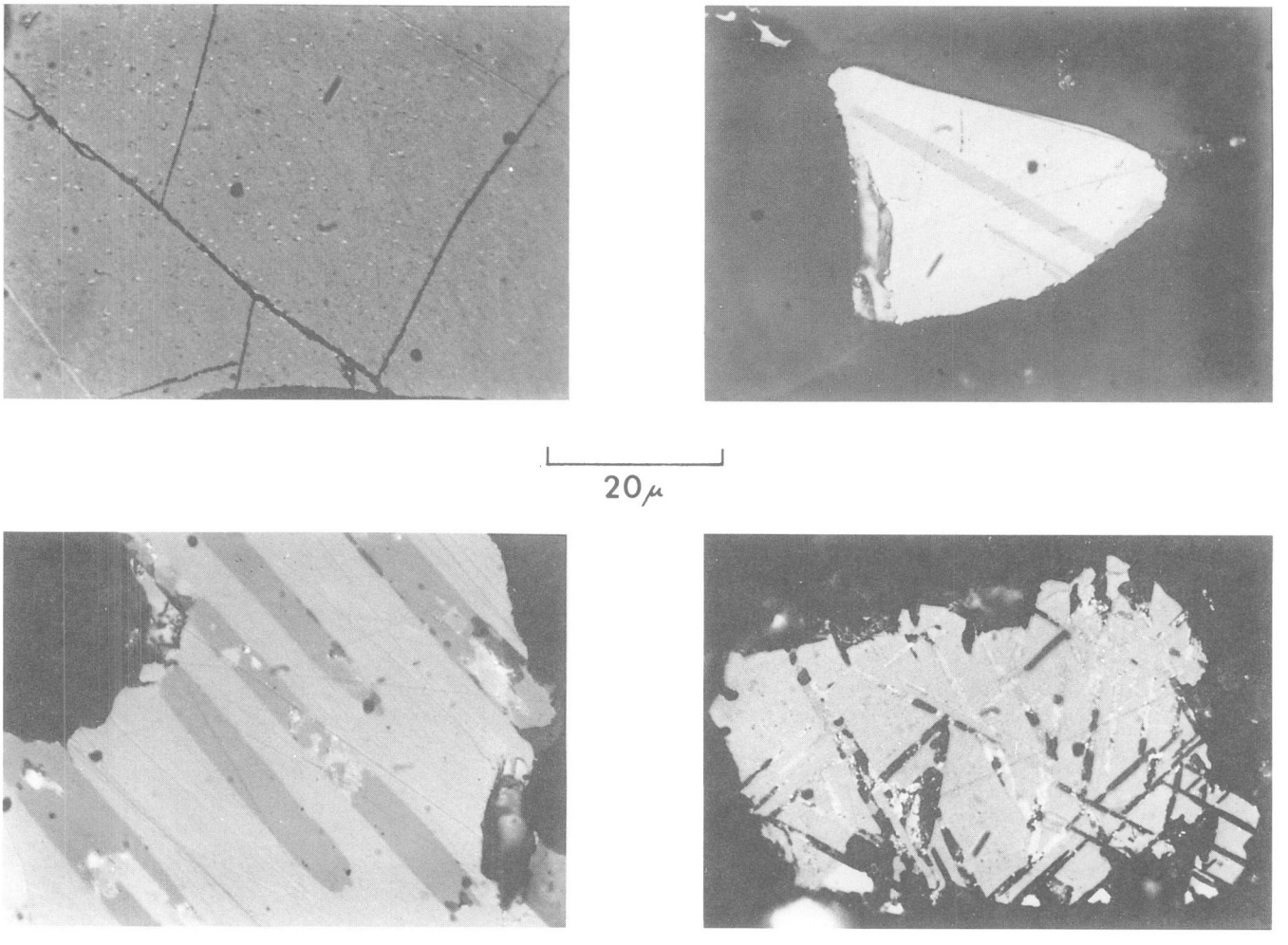

Figure 20: (a) Drill hole CY-4, 898.06 m depth. Unit 229.03 (described as a dark gray, very fine grained massive aphyric diabase dike). Primary titanomagnetite showing occasional cracking and widespread small exsolved granules (white spots). Alteration classification (see text) C1 H2 L2 Sr0. (b) Drill hole CY-4, 873.16 m depth. Unit 223.02 (described as a fine grained, homogeneous, amphibolitized gabbro). Titanomagnetite (very light grey) containing several lamellar exsolution bodies of ilmenite (medium gray) C2 H1 L1 Sr0. (c) Drill hole CY-4, 280.50 m depth. Unit 75.02 (described as a very light grey, fine to medium grained, aphyric felsic diabase or andesite dike). Titanomagnetite (light grey) containing fairly abundant lamellar exsolution bodies of ilmenite (medium grey) showing incipient replacement by sphene (black) and a combination of white and light grey phase ('woven' texture) C3 H2 L1 Sr0. (d) Drill hole CY-4, 98.30 m depth. Unit 27.02 (described as millimeter size dioritic fragments in a chloritic matrix). Primary titanomagnetite (medium grey) that experienced moderate deuteric oxidation is shown. The ilmenite lamellae (light grey) produced by this oxidation are replaced in a peripheral zone by sphene (dark grey) while in the core of the grain they are partly replaced by a fine mixture of white and grey phases. Small aggregations of sphene also occur within the lower part of the grain. C3 H3 L1 Sr0-1.

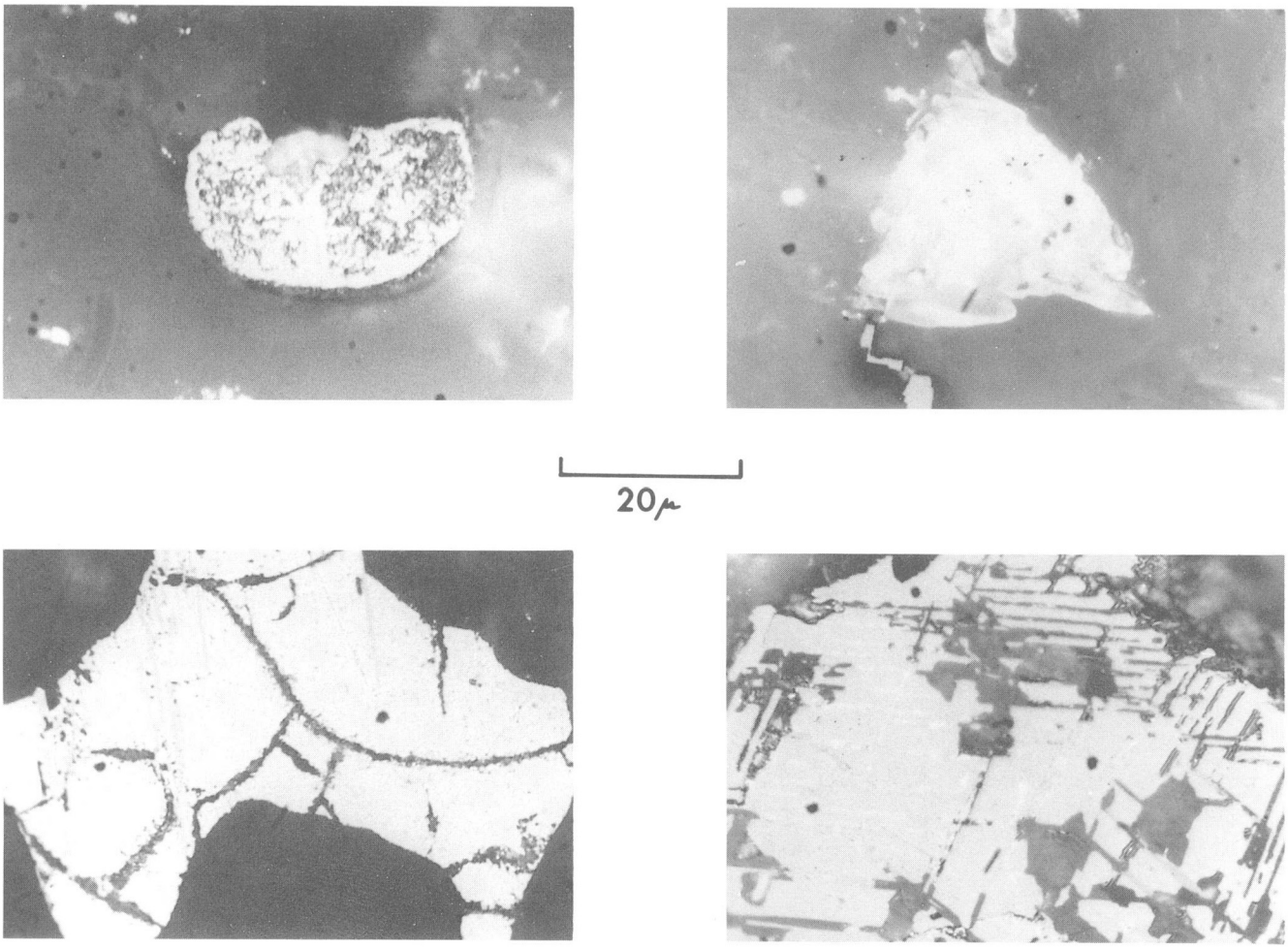

Figure 21: (a) Drill hole CY-4, 763.75 m depth. Unit 199.03 (described as dark grey, fine grained, holocrystalline, relatively fresh diabase dike). Titanomagnetite containing a high density of small anatase granules. The darker area is characterized by substantial corrosion of the remaining magnetite. C1 H4 L1 Sr0. (b) Drill hole CY-4, 1253.66 m depth. Unit 291.03 (described as a very fine grained aphyric diabase dike). The triangular white area is a pseudomorph, probably consisting of anatase, after an Fe-Ti oxide which from its morphology was likely to have been titanomagnetite. C(?) H6 L(?) Sr0. (c) Drill hole CY-4, 1284.86 m depth. Unit 296.01 (described as a medium grey, fine grained equigranular diabase dike). Titanomagnetite (light grey) that has experienced mild deuteric oxidation, indicated by the presence of light grey ilmenite lamellae, and later low temperature oxidation, resulting in the curved cracks along which black, non opaque material is replacing the magnetite, is shown. C2 H1-2 L2 Sr0. (d) Drill hole CY-4, 98.30 m depth. Unit 27.02 (described as millimeter size dioritic fragments in a chloritic matrix). Primary titanomagnetite (medium grey) that experienced moderate deuteric oxidation is shown. The ilmenite lamellae (light grey) produced by this oxidation are replaced in a peripheral zone by sphene (dark grey) while in the core of the grain they are partly replaced by a fine mixture of white and grey phases. Large aggregations of sphene occur. C3 H3 L1 Sr2.

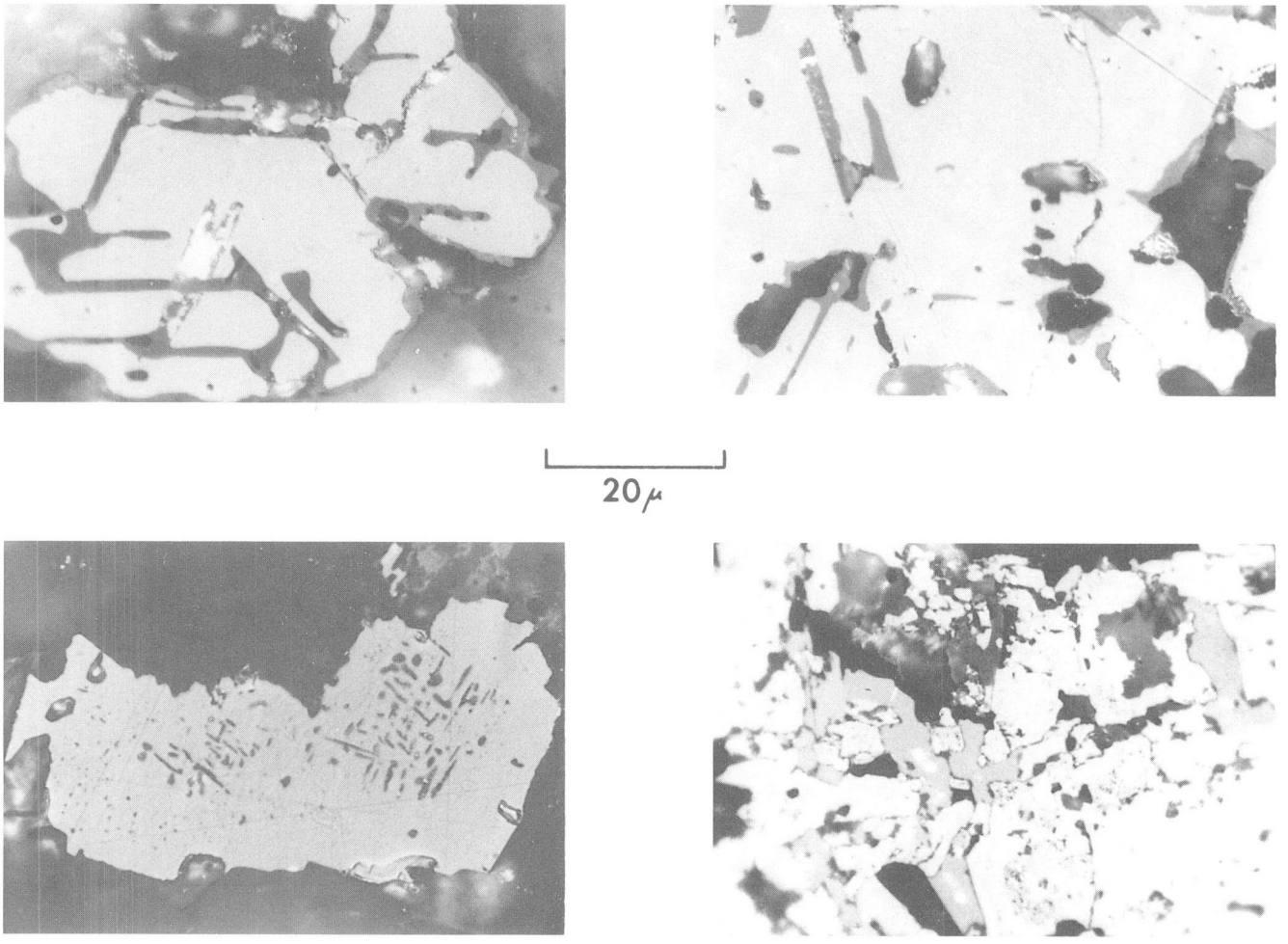

Figure 22: (a) Drill hole CY-4, 478.42 m depth. Unit 128.01 (described as a medium grey, fine to medium grained massive aphyric diabase dike). The light coloured grain was originally a primary titanomagnetite. Deuteric oxidation during initial cooling led to the sub solidus exsolution of ilmenite lamellae. These lamellae were later entirely replaced by sphene (dark grey), which, during recrystallization of the magnetite was partly aggregated within the grain and partly expelled from the grain to form a continuous peripheral rim. C?3 H3 L1 Sr3-4. (b) Drill hole CY-4, 478.42 m depth. Unit 128.01. A deuteric oxidation class 2-3 grain is shown. The ilmenite lamellae were completely replaced by sphene (dark grey) as the result of later hydrothermal alteration. Much of the sphene is now found along grain boundaries or as linings of several of the larger holes in the grain. The remaining sphene occurs in isolated lamellae like bodies within the grain. Both textural features indicate that incomplete expulsion and aggregation of sphene accompanied recrystallization of the magnetite. C2-3 H3 L1 Sr5. (c) Drill hole CY-4, 245.89 m depth. Unit 66.01 (described as a light grey, fine grained, massive aphyric diabase). Largely recrystallized, titanium free magnetite (uniform medium grey). The few sphene lamellae (after ilmenite) are mostly restricted to two areas within the core of the grain. C3 H3 L1 Sr5. (d) Drill hole CY-4, 120.55 m depth. Unit 32.02 (described as a light grey to greenish, medium to coarse grained massive sub-ophitic diabase dike). Locally porous recrystallized magnetite (medium grey) contains aggregates of sphene (grey black) and many largely peripherally located ilmenite grains (light or dark grey). It is suggested that this texture has resulted from the recrystallization of magnetite containing ilmenite lamellae or included ilmenite that was partly replaced by sphene. C?2-3 H2 L1 Sr=6.

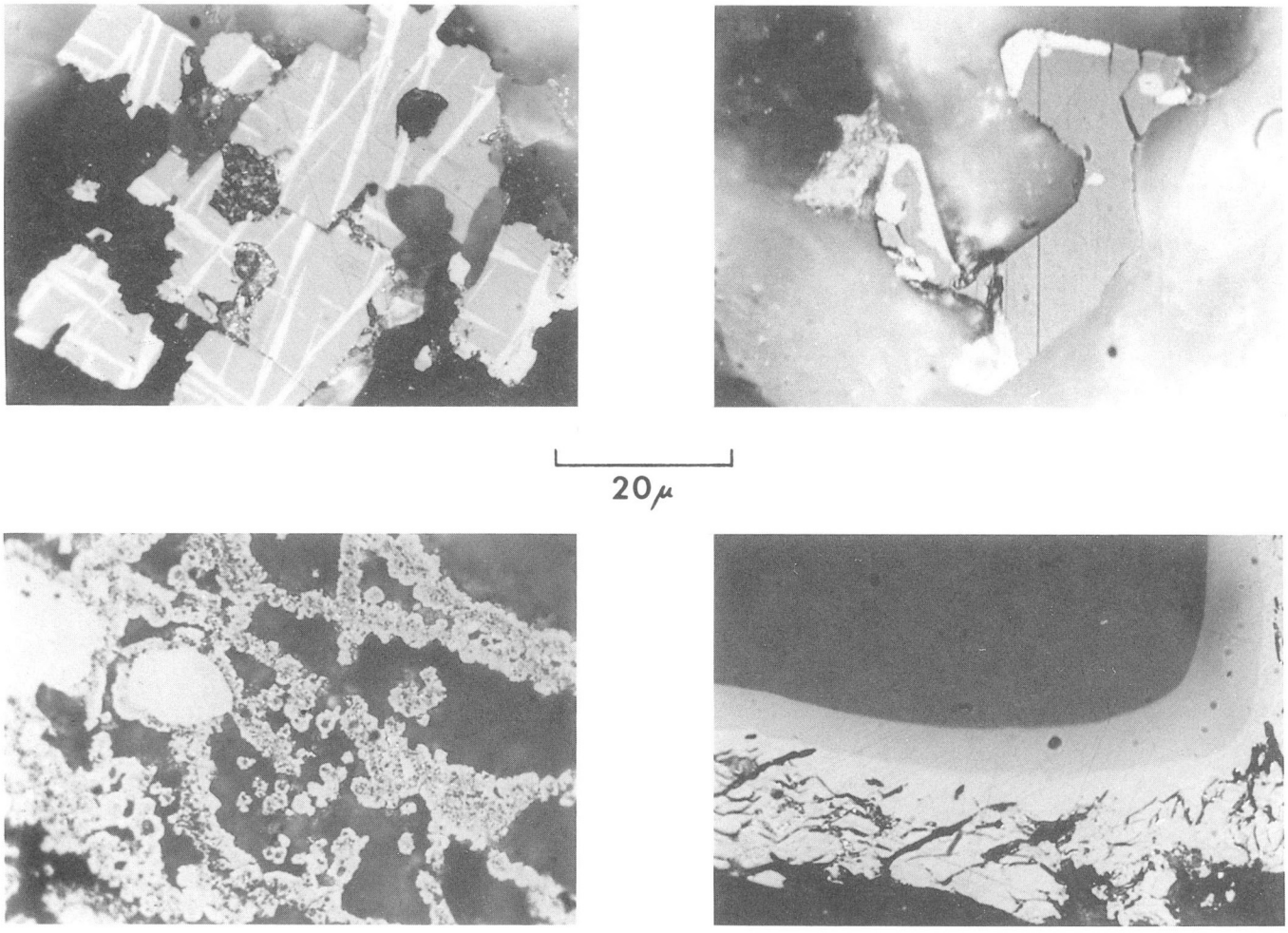

Figure 23: (a) Drill hole CY-4, 11.35 m depth. Unit 2.01 (described as a light grey, medium to coarse grained massive aphyric diabase dike). Violet-brown, titanium-free magnetite (medium grey) probably of secondary origin shows well developed martitization (M4). Peripheral sphene bodies probably represent sphene produced by the hydrothermal alteration of lamellar or included ilmenite and later expelled during recrystallization. C?>1 H?3 L1 Sr=6. (b) Drill hole CY-4, 603.95 m depth. Unit 159.02 (described as a medium grey fine grained holocrystalline equigranular aphyric diabase dike). Probably wholly secondary magnetite (medium grey) with substantial largely peripheral secondary hematite (white)(Sah3). C? H? L1 Sr=6. (c) Drill hole CY-4, 2201.20 m depth. Unit 472.04 (described as a greenish-grey/dark greenish-grey coarse grained olivine websterite). Chains of rounded grains of secondary magnetite after olivine (Sc6). Typically porous or granulated. C1 H?1-2 L1 Sr0. (d) Drill hole CY-4, 2261.25 m depth. Unit 487.02 (described as a dark, medium-coarse grained cumulate pyroxene peridotite). A core of spinel (dark grey) rimmed by a greenish continuous zone and further by an outer zone of discontinuous secondary magnetite (So(sp)4). C1 H1 L1 Sr0.

In the CY-4 section martitized magnetite only occurs in a small number of dike samples within the 0-600 m depth interval and is only common in two samples at shallower than 100 m depth (Table 1, Figure 1). In all of these samples, the martitized grains are completely reconstructed magnetites, i.e., Sr=6.

(viii) The Development of Hematitic Alteration in Magnetite, Sah

As noted above, irregular, largely peripheral hematization of magnetite also occurs in CY-4 samples (Figure 23b). As in the case of martitization, hematitic alteration is restricted to dike samples, in this case within the 0-800 m depth interval. Hematitic alteration is only common or abundant in the 500 to 800 m interval, and occurs only in completely reconstructed grains.

(ix) The Relative Abundance of Primary and Secondary Magnetite, Ratio R

This ratio describes the relative abundance of magnetite of the types that are defined here as being primary, and those defined as secondary. Primary magnetite includes magnetite derived from titanomagnetite through deuteric oxidation and titanomaghemite derived from titanomagnetite through low temperature, single-phase oxidation. Magnetite resulting from deuteric oxidation is included in the primary category since deuteric oxidation is only known to occur during the initial cooling of thin volcanic units, and therefore, in the absence of later alteration, will carry a remanence with the direction of the ambient field during the initial cooling of the unit. Titanomaghemite resulting from low temperature oxidation has also been shown generally to retain initial cooling ambient field directions (Hall, 1977). Thus, primary phases are defined as those likely to retain initial cooling ambient field directions. Secondary magnetite, in contrast, includes forms that may have been acquired magnetizations in directions different from the initial cooling ambient field direction. For the CY-4 samples, this category includes reconstructed and recrystallized magnetites in dike samples, and chain and overgrowth secondary magnetite in gabbros and ultramafics. From quantitative and semi-quantitative measurements, the ratio

$$R = \frac{P-S}{P+S}$$

where P and S are the volumes of primary and secondary oxide, respectively, has been calculated. This ratio has a value of +1 where all magnetite is primary, and -1 where all magnetite is secondary. From Table 1 and Figure 1 it is apparent that secondary magnetite is the only form of magnetite in most dike and screen samples in the 0-800 m depth interval. Of 38 samples examined in this interval, 29 (27 dike, 2 screen) contain only secondary magnetite, three contain dominant secondary magnetite, three equal volumes of primary and secondary magnetite, two some secondary magnetite and one only primary magnetite. The lower part of the dike component, from 800 to 1290 m depth, is dominated by primary magnetite, as are the gabbroic screens in this interval. Samples dominated by, or containing some secondary magnetite, occur in the upper 100 m of this interval, and again occasionally, in the remainder of this interval. Secondary magnetite is absent in the 1290 to 1550 m depth interval, and then reappears in the chain and overgrowth forms characteristic of the serpentinization of olivine in gabbros and ultramafic.

SUMMARY AND DISCUSSION

The magnetic and oxide petrographic properties of the CY-4 samples generally relate closely to the major lithologic divisions of the section. The important lithologic divisions from the aspect of the depth distribution of the magnetic and oxide properties are as follows:

(i) 0 to 500-700 m. Lithologically this interval consists largely of dikes. The dikes are characterized by generally low ($\leq 20 \times 10^{-4}$ cgs) Jo, except in the 500-600 m interval, broadly distributed K generally in the 20-120 $\times 10^{-4}$ cgs range, relatively low MDF, concentrated in the 50-150 oe range, and relatively high Js, with most values in the 2-6 cgs range. All samples have Curie points in the 500-600°C range. In terms of oxide parameters, this interval is characterized by the highest degrees of deuteric oxidation, hydrothermal alteration and martitization found in the CY-4 section. The magnetite of almost all samples is completely reconstructed, and recrystallized magnetites only occur in this interval.

(ii) 500-700 to 1300 m. Lithologically this interval contains the major part of the transition from the Sheeted Complex to the Plutonic Complex. Dike density decreases from 75% to 25% over the 190 m interval from 630 to 820 m. The plutonic lithologies present consist of screens of various types of gabbros, of which the magnetite gabbros are most relevant here, and dikes and intrusive breccia matrices of plagiogranites and diorites that postdate the basic dikes. The interval is characterized by moderate Jo with occasional values extending up to 100 $\times 10^{-4}$ cgs, by both high and low K and Js distributions, corresponding generally to the dike and plutonic lithologies, respectively, a broad range of MDF containing a significant number of high (>500 oe) values. The magnetite gabbros are exceptional in the plutonic group in frequently showing Jo, K and Js

values as high as those for the dikes in the interval. Curie temperatures are again almost all in the 500-600°C range, but three double Curie point samples, with the lower Tc in the 300-350°C interval, are of interest. In terms of oxide petrographic parameters, this is an interval of intermediate levels of deuteric and hydrothermal alteration. As in the 0 to 500-700 m interval, screens tend to show similar alteration intensities to enclosing dikes. Reconstruction, and therefore secondary oxide abundance, is important to about 900 m depth, below which most oxide is primary. A number of dikes in this interval show very limited oxide alteration, which is largely restricted to the low temperature type of alteration well known from shallow (<0.5 km) depths in in-situ oceanic crust. The double Curie point type of thermomagnetic behaviour noted above occurs in dikes in this category.

(iii) 1300 to about 1750 m. Lithologically this interval consists of various types of gabbro. Jo shows moderate values to about 1460 m depth, below which low values ($\leq 20 \times 10^{-4}$ cgs) predominate. K and Js are, with rare exceptions, very low in this interval while MDF shows predominantly moderate to high values of 200-400 oe. Curie temperatures are without exception, confined to the narrow range between 525°C and 575°C. Oxide parameters indicate that this is the zone of least overall alteration in the CY-4 section. Deuteric oxidation, low temperature oxidation, secondary overgrowths, martitization and secondary hematite are all absent in the samples examined from this interval. Hydrothermal alteration and secondary magnetite chains are present in only a small number of samples. A small number of samples contain ambiguous secondary oxide. These oxides are homogeneous and unaltered and often have sharply defined outlines. However, these oxide grains are not associated with sphene, and no grains in an intermediate state of reconstruction occur in these samples. For this reason these samples have been assigned the alternate classifications S0 or S6, with these values linked by a broken line in Figures 18 and 19.

(iv) 1750 m to the bottom of the recovered section at 2263 m. Lithologically this interval consists of a variety of ultramafic and gabbroic rocks. In terms of magnetic properties, it closely resembles the 1300 to 1750 m interval except that where serpentinization of olivine is strongly developed, very different properties are encountered. Highly serpentinized samples show the strongest Jo values in the section, of up to 180×10^{-4} cgs, high K values in the 30 to 180×10^{-4} cgs range, low MDF and high Js. In Tc they are indistinguishable from the less altered olivine bearing rocks in this interval. Two samples in the 1750-2263 m interval have Curie temperatures in excess of 700°C. Both are very little serpentinized. In terms of oxide parameters, this section shows no deuteric oxidation, martitization or secondary hematite. A number of samples contain white translucent grains that could either be titanium oxide pseudomorphs after titanomagnetite, or phases quite unrelated to oxides. The presence of these grains has, in samples otherwise showing no other evidence of hydrothermal alteration, been indicated by bracketed symbols in Figure 18. The more serpentinized samples in the 1750-2263 m interval frequently show chains or overgrowth of secondary magnetite, and this is reflected in the many samples with primary to secondary ratios of less than +1.00.

Some preliminary comments can be made on the evolution of the rocks and thus the magnetic properties in the CY-4 section.

The dikes of the 0 to 500-700 m interval, and in part, those in the 500-700 m to 1300 m interval, have experienced a complex polyphase alteration history. This history would not be evident from the magnetic properties alone. Thermomagnetic analyses and measurement of Js show the ubiquitous presence of fairly abundant near pure magnetite in samples from this interval. Comparison of Jo, K and MDF would suggest a fairly coarse effective grain size. Before an understanding was gained of the evolution of oxide minerals in basic igneous rocks, these combinations of properties would have been thought to be evidence of the suitability of the material for the determination of paleomagnetic poles for the time of initial cooling of the dikes. In fact, the magnetite of almost all of the dikes studied in this interval is entirely secondary, and the times of origin of each contribution to the remanence needs careful consideration. The exact paragenesis of these rocks will be discussed in detail elsewhere. However, it can be stated with confidence that the Fe-Ti oxides of these dikes have a more complex history than any other Fe-Ti oxides known to the authors. In the most extreme cases, original homogeneous titanomagnetites experienced in succession at least mild deuteric oxidation, intense hydrothermal alteration, reconstruction or recrystallization, and either or both martitization and replacement of secondary magnetite by secondary hematite. It is possible that these oxides also experienced low temperature oxidation at an early stage in their evolution. However, all traces of this process, if indeed it was active, have been obliterated by the intense action of later processes.

The serpentinized gabbros and ultramafics of the 1750-2263 m interval often contain substantial secondary magnetite, and the question again arises as to the time of origin and magnetization of this material.

ACKNOWLEDGEMENTS

We should like to acknowledge the efforts of many individuals and groups without which this report could not have been prepared. In particular, we wish to thank Dr. George Constantinou, Director, Geological Survey Department, Cyprus, and his colleagues, for permission to work in Cyprus and for much generous support in the field, the drilling operatives and staff of Bradley Bros. Ltd., of Noranda, P.Q., for the excellent core recovered from the deep hole, CY-4, and Mr. Ferenc Stefani and Ms. Jane Barrett for high quality photography and manuscript preparation.

Finally, we should like to thank the people of Cyprus, and particularly of the village of Palekhori, for their unfailing hospitality and willing help.

The drilling work at Site CY-4 and the subsequent work on samples from the drill core was supported by NSERC (Canada) Grants A4652, A9917, G1563 and A7812, and by NSF grants EAR 82-18096 and EAR 83-11776.

REFERENCES

Ade-Hall, J.M. and Lawley, A.E.
1970: An unsolved problem - opaque petrological differences between Tertiary basaltic dykes and lavas; *in* Mechanism of Igneous Intrusion, ed. G. Newall and N. Rast; Geol. J. Special Issue, Gallery Press, Liverpool, v. 2, p. 217-230.

Ade-Hall, J.M., Palmer, H.C. and Hubbard, T.P.
1971: The magnetic and opaque petrological response of basalts to regional hydrothermal alteration; Geophysical Journal of the Royal Astronomical Society, v. 24, p. 137-174.

Anderson, R.N., Honnorez, J. and Becker, K.
1985: Initial Reports of the Deep Sea Drilling Project, Volume 83; U.S. Government Printing Office, Washington, D.C., v. 83.

Banerjee, S.K.
1980: Magnetism of the oceanic crust: evidence from ophiolite complexes; Journal of Geophysical Research, v. 85, p. 3557-3566.

Bonatti, E., Chermak, A. and Honnorez, J.
1979: Tectonic emplacement of crust in oceanic transform zones; *in* Deep Drilling Results in the Atlantic Ocean: Ocean Crust, ed. M. Talwani, C.G. Harrison, and D.E. Hayes; Maurice Ewing Series 2, American Geophysical Union, Washington, D.C., p. 239-248.

Coleman, R.G.
1977: Ophiolites: Ancient Oceanic Lithosphere?; Springer-Verlag, Berlin; Heidelberg; New York, p. 1-229.

Elmore, R.D. and Van der Voo, R.
1982: Origin of hematite and its associated remanence in the Copper Harbor Conglomerate (Keeweenawan), Upper Michigan; Journal of Geophysical Research, v. 87, p. 10918-10928.

Gass, I.G.
1980: The Troodos Massif: its role in the unravelling of the ophiolite problem and its significance in the understanding of constructive margin processes; *in* Ophiolites: Proceedings of the International Ophiolite Symposium, Cyprus, 1979, ed. A. Panayiotou, Cyprus Geological Survey Department, Ministry of Agriculture and Natural Resources, p. 23-35.

Hall, J.M.
1977: Does TRM occur in oceanic Layer 2 basalts? Journal of Geomagnetism & Geoelectricity, v. 29, p. 411-419.
1985: The Iceland Research Drilling Project crustal section: variation of magnetic properties with depth in Icelandic-type oceanic crust; Canadian Journal of Earth Sciences, v. 22, no. 1, p. 85-101.

Hall, J.M. and Ryall, P.J.C.
1977: Rock magnetism of basement rocks, Leg 37; *in* Initial Reports of the Deep Sea Drilling Project, Volume 37, ed. F. Aumento, W.G. Melson et al.; U.S. Government Printing Office, Washington, D.C., v. 37, p. 489-501.

Johnson, H.P. and Hall, J.M.
1978: A detailed rock magnetic and opaque mineralogical study of the basalts of the Nazca Plate; Geophysical Journal of the Royal Astronomical Society, v. 52, p. 45-64.

Luyendyk, B.P. and Day, R.
1982: Paleomagnetism of the Samail ophiolite, Oman: 2. The Wadi Kadir gabbro section; Journal of Geophysical Research, v. 87, p. 10903-10917.

Luyendyk, B.P., Laws, B.R., Day, R. and Collinson, T.B.
1982: Paleomagnetism of the Samail ophiolite, Oman: 1. The Sheeted Dike complex at Ibra; Journal of Geophysical Research, v. 87, p. 10883-10902.

Pariso, J.E. and Johnson, H.P.
1989: Magnetic properties of an analog of the lower oceanic crust: magnetic logging, and paleomagnetic measurements from drill hole CY-4 in the Troodos Ophiolite; *in* Cyprus Crustal Study Project: Initial Report, Hole CY-4, ed. I.L. Gibson, J. Malpas, P.T. Robinson and C. Xenophontos; Geological Survey of Canada, Paper 88-9.

Ramdohr, P.
1980: The Ore Minerals and Their Intergrowths, 2nd Edition; Pergamon Press, p. 1-1207.

Robinson, P.T., Hall, J.M., Christensen, N.I., Gibson, I.L., Fridliefsson, I.B., Schmincke, H.-U. and Schoenharting, G.
1982: The Iceland Research Drilling Project: synthesis of results and implications for the nature of Icelandic and oceanic crust; Journal of Geophysical Research, v. 87, p. 6657-6667.

Watkins, N.D. and Haggerty, S.E.
1968: Oxidation and magnetic polarity in single Icelandic lavas and dikes; Geophysical Journal of the Royal Astronomical Society, v. 15, p. 305-315.

Magnetic Properties of an Analog of the Lower Oceanic Crust: Magnetic Logging and Paleomagnetic Measurements from Drill Hole CY-4 in the Troodos Ophiolite

JANET E. PARISO AND H. PAUL JOHNSON

School of Oceanography, University of Washington, Seattle, Washington, 98195, U.S.A.

Pariso, J.E. and Johnson, H.P., Magnetic properties of an analog of the lower oceanic crust: magnetic logging and paleomagnetic measurements from Drill Hole CY-4 in the Troodos Ophiolite; in *Cyprus Crustal Study Project: Initial Report, Hole CY-4, ed. I.L. Gibson, J. Malpas, P.T. Robinson and C. Xenophontos; Geological Survey of Canada, Paper 88-9, p. 279-293, 1989.*

Abstract

Analysis of magnetic logging and paleomagnetic results show that there are five distinct magnetic zones within the lower crustal intrusive rocks drilled at site CY-4. These zones are defined by both the lithology and alteration of the drilled section. The upper zone, A, is composed of altered diabase dikes which exhibit a relatively high natural remanent magnetization (J_o) and magnetic susceptibility (k). Zone B dikes are characterized by the highest J_o and k within CY-4, a large amount of scatter in I_o and I_s, and the least stable magnetization within the section. Lithologically, zone C is the transition between sheeted dikes and gabbros. The dikes within this zone have magnetic properties similar to those of zone A dikes, while the gabbros are characterized by low k and moderate J_o. Additionally, the dikes bear components of secondary magnetization which cause a great deal of scatter in NRM directions. Zone D is composed solely of gabbro which have the lowest observed J_o and k within CY-4. Finally, zone E is composed of interlayered gabbro and ultramafic units. The higher J_o and k observed within this zone is caused by formation of secondary magnetite during serpentinization.

Résumé

Les analyses des données magnétiques mesurées et des résultats paléomagnétiques montrent 5 zones magnétiques distinctes dans les roches intrusives de la croûte inférieure traversée au site CY-4. Ces zones se définissent par leur lithologie et altération observables le long de la section percée. La zone supérieure, A, est composée de dykes de diabase altérés offrant un magnétisme naturel rémanent (J_o) et une susceptibilité magnétique (k) relativement élevés. Les dykes de la zone B sont caractérisés par les valeurs les plus éléres de J_o et de k obtenus le long de CY-4, une grande variation des valeurs de I_o, I_s, et enfin le magnétisme le moins stable du forage. Lithologiquement, la zone C est la transition entre les dykes groupés et les gabbros. Les dykes de cette zone ont des propriétés magnétiques semblables à celles des dykes de la zone A, alors que les gabbros sont caractérisés par une basse valeur de k et modérée de Jo. De plus, les dykes portent les composantes d'un magnétisme secondaire qui cause une importante fluctuation des directions MNR. La zone D est composée uniquement de gabbros ayant les valeurs les plus basse de J_o et de k obtenues le long du forage CY-4. Finallement, la zone E est composée d'unités gabbroïques et ultramafiques interlitées. Les valeurs plus élevées de J_o et de k obtenues dans cette zone sont dûes à la formation de magnétite secondaire durant le processus de serpentinisation.

INTRODUCTION

Marine magnetic anomalies are widely used in the study of oceanic geological and geophysical processes and have been central to our current understanding of plate tectonic processes. The interpretation of these anomalies and the degree to which they can be resolved, however, depends upon our knowledge of the vertical magnetic structure of oceanic crust. Inversion of marine magnetic anomalies, ophiolite studies, and DSDP studies of the upper layers of oceanic crust, indicate that the upper extrusive layer can, in many instances, account for the magnetic anomalies observed at the sea surface (Atwater and Mudie, 1973; Klitgord et al., 1975; Macdonald, 1977; Johnson, 1979; Johnson and Pariso, 1985). Other studies, however, suggest that the magnetic anomaly source layer is much more complex than the 500 m thick block model originally hypothesized by Talwani and others (1971) and may include the sheeted dike complex and possibly even the gabbroic layer (Kent et al., 1978; Banerjee, 1980). With the exception of DSDP hole 504B, which penetrated the sheeted dike complex, magnetic studies of the lower layers of oceanic type crust have been restricted to unoriented dredge samples from fracture zones (Fox and Opdyke, 1973; Kent et al., 1978) and ophiolite studies (Vine and Moores, 1972; Levi and Banerjee, 1977; Swift and Johnson, 1984) and thus our understanding of the magnetic properties of the intrusive section of oceanic crust is as yet incomplete.

In the following study, we use both downhole magnetic logging data and discrete sample magnetic data to characterize the magnetic structure of the intrusive complex of the Troodos ophiolite. Our samples were taken from drill hole CY-4 of the International Crustal Research Drilling Group which extends from the sheeted dike complex, through the isotropic and layered gabbros and into the layered ultramafics (see Figure 1 for the depth relationship of CY-4 to a model ophiolite section). The near-perfect core recovery (99.9%) and deep penetration (2263 m) obtained in CY-4 make it an excellent section with which to study the magnetic properties of lower oceanic crust and their relationship to lithology, alteration, and morphology of the intrusive complex. In addition, the detailed sampling of the CY-4 drillcore make it an ideal suite of samples with which to correlate magnetic logging data. While downhole magnetic logging techniques have commonly been used to acquire directional data within boreholes, we hope to show that this technique is also an excellent means of examining lithology and alteration within a borehole.

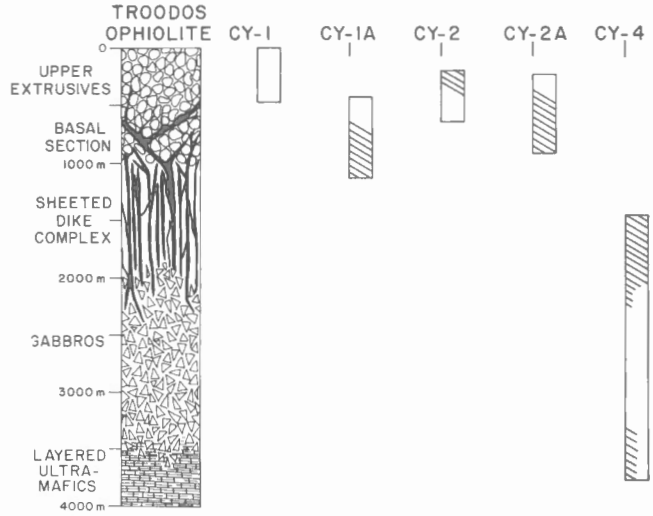

Figure 1: Schematic drawing of the depth relationship between holes drilled by the Cyprus Drilling Project and a model ophiolite section. Shading within the columns represents alteration within the section.

MEASUREMENT TECHNIQUES

Logging Techniques

Downhole magnetic measurements were made in July of 1984 using a three-axis fluxgate magnetometer and a susceptibility tool. Sampling density during logging was one measurement per 10 cm in a borehole whose diameter changed from 10.2 cm to 5.72 cm at approximately 860 m. Due to a limited cable length, the maximum sampling depth of the three-axis fluxgate was 2080 m and additionally, pressure limitations of the susceptibility probe constrained its measurement depth to above 1580 m. Steel casing remained in the drill hole from 640 m to 860 m and prevented logging of this section.

The total magnetic field anomaly was calculated by taking the horizontal and vertical magnetic field components measured by the downhole magnetometer, and vectorally subtracting the earth's field as measured at the drillsite. The resulting horizontal and vertical components were then added vectorally to determine the total magnetic field anomaly, which thus represents the anomaly due to the remanent magnetization together with the magnetization which is induced in the rock surrounding the borehole by the earth's field.

Discrete Sample Measurements

We used 400 minicore samples from the drillcore (interval 400-2263 m) to study the magnetic

properties. Magnetic susceptiblity (k) was measured with a single-axis Schonstedt viscous remanent magnetometer and, as a test for anisotropy, three orthogonal susceptibility measurements were made on each sample. Since there did not appear to be any systematic anisotropy, we averaged these components to determine whole rock susceptibility.

Remanent magnetization was measured using a three-axis SCT cryogenic magnetometer and a Schonstedt spinner magnetometer. Stepwise demagnetization was performed with a Schonstedt single-axis AF demagnetizer at 5, 10, 20, 30 nT (where 1 nT = 10 oe) on all samples and at higher levels if necessary to bring the sample below the mean demagnetizing field. The mean demagnetizing field (MDF) was determined by finding the field at which the magnetization fell below one-half of the original natural remanent magnetization (J_o). This quantity is used to judge the stability of the magnetization; that is, the ease with which magnetization is removed. The stable inclination (I_s) was determined by plotting the horizontal magnetic component against the vertical magnetic component at each demagnetizing step and finding the angle at which they form a straight line to the origin. This method assumes that the primary component (that which passes through the origin) is the hardest component, and further, allows us to determine whether the NRM directions (I_o) are equivalent to the stable directions.

RESULTS AND DISCUSSION

Magnetics data from CY-4 are presented in Figures 2, 3, and 4 (magnetic logging measurements) and Figures 5 and 6 (discrete sample measurements). In our discussion of these results, we will first present a brief summary of the salient characteristics of magnetic logging data, and follow with a detailed analysis of the magnetic zones using the discrete sample paleomagnetic data.

Logging Results

Examination of the logging data presented in Figures 2, 3, and 4 has led us to divide CY-4 into five different magnetic zones which we have identified with the letters A through E. The uppermost zone, A, extends from 0 m to 477 m and is composed almost entirely of diabase dikes. It is characterized by a consistently strong magnetic field anomaly (typically about 2500 γ, where 1 γ = 1 nT)) and susceptibility signal (averaging 0.025 SI or 0.002 cgs). Both the total magnetic field anomaly and susceptibility show a slight, but distinct increase in mean value with depth throughout this zone. A sharp increase in both the magnetic field anomaly (to 6000 γ) and susceptibility (to 0.037 SI or 0.0029 cgs) occurs at 477 m and is maintained to 600 m to define zone B. This relatively short zone is again composed primarily of diabase dikes, but does contain a few gabbro screens.

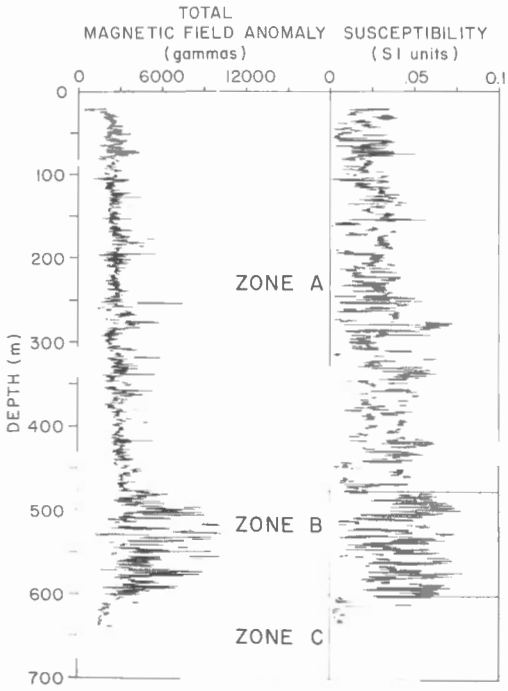

Figure 2: Magnetic logging data plotted versus depth in drill hole CY-4. Zones A and B are composed primarily of diabase dikes. The increase in mean value and amplitude of signal between the two zones is thought to be due to a change in the style of alteration. Zone C represents the beginning of seismic layer 3 and the transition between sheeted dikes and gabbro. The region between 640 m and 860 m was not logged because of the presence of steel casing in the hole. Note that for total magnetic field 1 gamma = 1 nT and for susceptibility 1 cgs unit = 4π(SI).

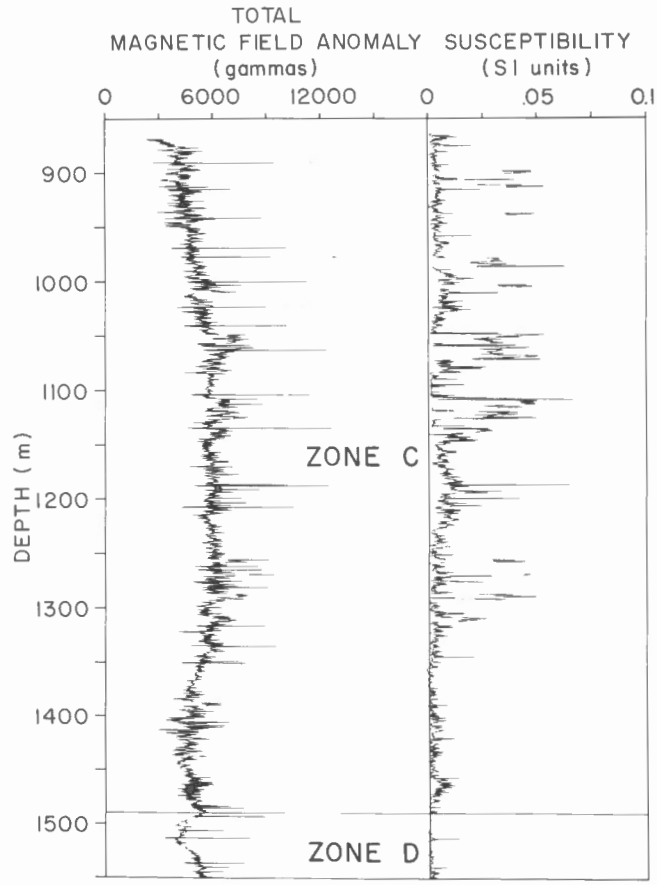

Figure 3: Magnetic logging data plotted versus depth in drill hole CY-4. Peaks in the susceptibility record identify individual diabase dikes which were intruded within gabbro. The abrupt drop in signal amplitude at 1485 m defines the beginning of magnetic zone D. Note that for total magnetic field 1 gamma = 1 nT and for susceptibility 1 cgs unit = 4π(SI).

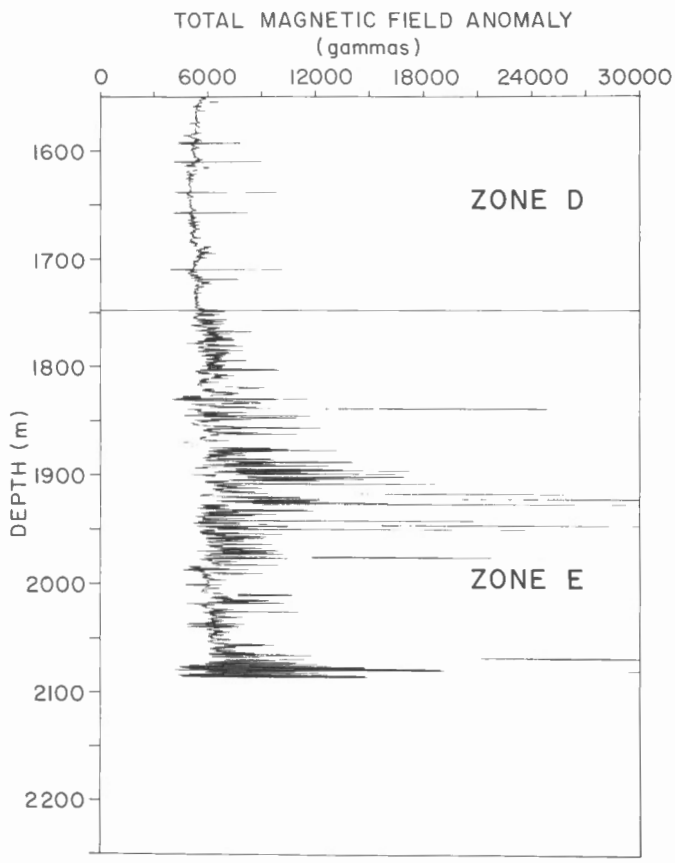

Figure 4: Magnetic logging data is plotted versus depth in drill hole CY-4. The abrupt increase in signal amplitude at 1745 m marks the appearance of the first ultramafic units. Large positive anomalies which increase with depth are a result of serpentinization and the formation of secondary magnetite. Note that for total magnetic field 1 gamma = 1 nT and for susceptibility 1 cgs unit = 4π(SI).

A dramatic decrease in amplitude and mean value of both the total magnetic field anomaly and susceptibility mark the beginning of zone C at 600 m. This change in magnetic properties is coincident with a change in seismic velocities from those of layer 2C to layer 3 (Salisbury, 1985) and marks the beginning of the rapid transition between sheeted dikes and gabbros. The character of the magnetic logs remains essentially the same throughout layer C which extends to a depth of 1488 m. Although there is a change in mean value between 640 m and 860 m, it is most likely due to a decrease in hole diameter at 860 m which results in a higher field reading. It should also be noted that this data is unfiltered and that intermittent spikes in the data (up to 14000 γ) which occur in zones C and D may be due to bad data points resulting from problems with the downhole magnetometer. Since the spikes commonly consist of four or less data points (implying a 40 cm sample area) and do not correlate with any features in the very detailed drillcore descriptions, we feel this to be the most likely explanation.

Zone D begins below 1488 m, extends through 1745 m and is magnetically the quietest within CY-4. Lithologically this zone is composed entirely of gabbro. The appearance of the first ultramafic units below 1745 m is coincident with an increase in both susceptibility and magnetic field anomaly and is the upper boundary of the last magnetic unit, zone E. The magnetic anomaly within this zone increases with depth as the abundance of ultramafic units rises and becomes extremely large in the lowest units where serpentinization is at a maximum.

Paleomagnetic Results

Paleomagnetic data is presented in Table 1, and displayed in Figures 5 and 6. It should be noted that zone A is represented in our data set by logging results only. For paleomagnetic data from this zone, the reader is referred to Hall et al. (1988).

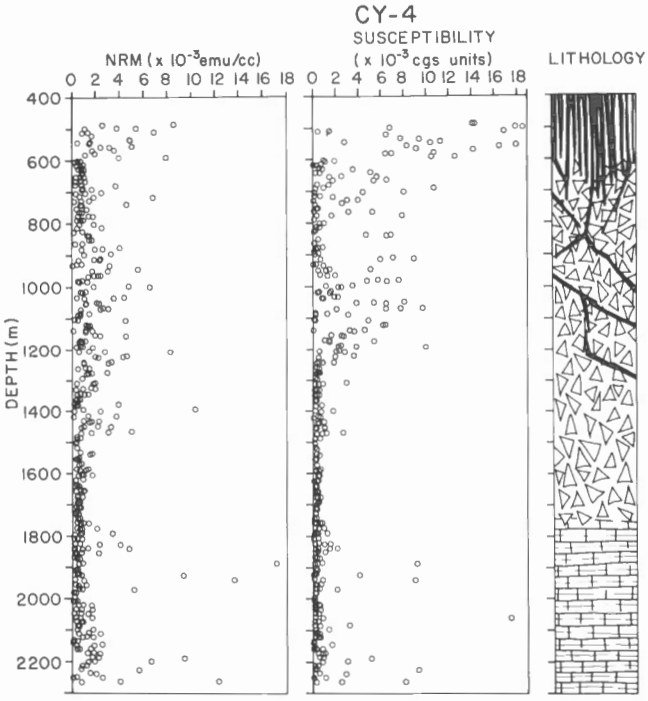

Figure 5: Results of natural remanent magnetization (J_o) and susceptibility (k) measurements made on minicore samples from CY-4 are plotted versus depth. Note that 1 Amp/m = 10^{-3} emu/cc and 1 cgs susceptibility unit = 4π(SI).

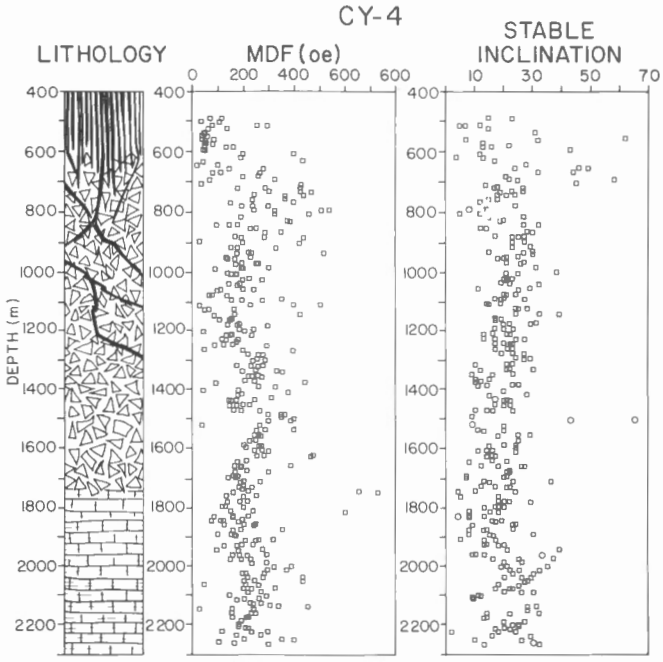

Figure 6: Mean demagnetizing field (MDF) and stable inclination (I_s) are plotted versus depth for drill hole CY-4. Circular symbols denote negative inclinations. Note that 10 oersted = 1 nT.

TABLE 1. Results of Magnetic Properties Measurements on CY-4 Minicore Samples

Depth (m)	Lithology	J_0 (emu/cc)	k (cgs)	Q	I_0	MDF (oe)	I_s
485.62	Diabase	8.53E-03	1.41E-02	0.39	30.8	69	15
486.25	Diabase	2.54E-03	1.43E-02	0.36	82.8	116	23
495.40	Diabase	3.76E-03	1.79E-02	0.42	69.8	36	
496.56	Diorite	5.35E-03	1.85E-02	0.58	51.0	37	
497.53	Diabase	1.06E-03	6.80E-03	0.31	23.2	107	
509.20	Diabase	6.85E-03	1.69E-02	0.81	29.5	78	12
509.89	Diabase	1.31E-03	1.44E-03	1.82	7.2	255	5
511.10	Diabase	7.95E-04	4.37E-04	3.64	8.0	295	7
519.87	Diabase	1.64E-03	6.50E-03	0.50	27.1	136	15
521.63	Diabase	9.45E-04			40.4	64	
533.02	Diabase	4.82E-03	7.79E-03	1.24	75.3	45	31
534.15	Diabase	4.89E-03	9.41E-03	1.04	77.7	50	
542.14	Diabase	1.48E-03	1.13E-02	0.26	46.9	39	
543.70	Diabase	4.17E-04	2.78E-03	0.30	67.1	59	
545.54	Diabase	1.41E-03	1.04E-02	0.27	64.7	58	
553.52	Diabase	5.00E-03	1.80E-02	0.56	53.8	42	62
555.25	Diabase	2.39E-03	8.33E-03	0.57	38.5	85	7
557.33	Diabase	3.14E-03	1.65E-02	0.38	31.6	50	32
565.09	Diabase	3.52E-03	9.15E-03	0.77	45.1	65	
566.38	Diabase	3.54E-03			58.7	53	13
568.78	Diabase	1.66E-03	1.42E-02	0.23	43.2	82	
577.02	Diabase	1.88E-03	1.07E-02	0.35	51.2	50	22
579.51	Diabase	1.06E-03	6.94E-03	0.30	35.1	162	13
580.28	Diabase	1.07E-03	6.43E-03	0.33	-43.0	134	16
589.72	Gabbro	7.87E-03	1.26E-02	1.25	40.8	50	
590.30	Gabbro	3.90E-03	1.05E-02	0.74	64.0	43	43
601.12	Diabase	4.14E-04	9.20E-04	0.90	8.2	400	
602.45	Diabase	6.83E-04	1.94E-03	0.70	23.6	200	
603.95	Diabase	2.27E-04	1.06E-03	0.43	28.8	550	12
614.03	Gabbro	9.31E-04	6.96E-04	2.68	3.9	191	4
615.22	Gabbro	3.64E-04	3.43E-04	2.12	15.9		
616.94	Gabbro	7.68E-04	9.88E-05	15.55	13.8	500	13
625.87	Microgabbro	5.09E-04	6.08E-04	1.67	29.2	435	17
628.16	Microgabbro	7.68E-04	8.58E-04	1.79	35.1	450	
629.48	Microgabbro	9.29E-04	3.53E-03	0.53	49.6	44	
638.68	Diabase	9.16E-04	5.11E-03	0.36	29.7	100	28
640.36	Diabase	8.76E-04	2.12E-04	8.26	22.4	20	
641.52	Diabase	8.10E-04	6.47E-04	2.50	26.6	470	
651.13	Diabase	3.06E-04	2.52E-03	0.24	58.7		46
652.20	Diabase	6.80E-04	5.64E-03	0.24	56.0	147	49
653.59	Gabbro	9.70E-04	1.44E-03	1.34	33.6	280	24
663.57	Diabase	7.37E-04	6.52E-03	0.23	45.6	115	32
665.02	Diabase	1.08E-03	5.38E-03	0.40	-43.9	82	44
665.15	Diabase	2.49E-04	1.75E-03	0.28	34.0	265	
675.15	Diabase	2.49E-04	4.21E-04	1.18	20.8	460	
677.25	Metagabbro	7.94E-04	3.78E-04	4.20	21.4	261	
678.12	Metagabbro	3.63E-03	1.40E-03	5.19	24.4	200	21
687.95	Microgabbro	8.80E-04	9.15E-04	1.92	28.0	325	22
689.94	Diabase	1.62E-03	1.07E-02	0.30	47.4	70	58
691.02	Microgabbro	8.14E-04	2.28E-04	7.14	20.0	530	25
700.93	Microgabbro	2.43E-03	8.03E-03	0.60	65.9		
702.17	Gabbro	1.08E-03	4.41E-03	0.49	45.5	37	45
703.47	Microgabbro(?)	2.98E-04	1.16E-04	5.12	17.1	430	14
712.79	Gabbro	5.99E-04	1.62E-04	7.38	23.4	425	18
713.90	Gabbro	1.80E-03	6.73E-04	5.34	21.8	290	17
716.02	Gabbro	6.80E-03	1.78E-03	7.66	23.3	181	27
726.08	Diabase	1.42E-03	3.97E-03	0.71	34.7	305	27
726.46	Diabase	7.41E-04	3.03E-03	0.49	47.4	427	23
728.88	Diabase	1.38E-04	5.54E-05	4.99	18.7	470	19
737.02	Diabase	4.55E-03	2.59E-03	3.51	31.5	243	24
738.88	Gabbro	7.01E-04	1.55E-04	9.04	23.3	440	18
740.45	Gabbro	7.68E-04	1.96E-04	7.85	20.1	365	21
751.59	Gabbro	3.47E-04	4.25E-04	1.63	64.7	367	18
752.63	Gabbro	1.20E-03	3.28E-04	7.32	18.5	240	15
762.48	Gabbro	4.94E-04	1.08E-04	9.13	14.9	400	12
763.74	Diabase	7.28E-04	5.28E-03	0.28	25.2	151	
764.38	Diabase	5.67E-04	3.17E-03	0.36	38.4	400	
774.42	Diabase	1.36E-03	7.90E-03	0.35	30.0	240	24
775.04	Gabbro	1.72E-03	1.60E-03	2.14	20.7	195	15

Depth (m)	Lithology	J_0 (emu/cc)	k (cgs)	Q	I_0	MDF (oe)	I_s
775.28	Diabase	4.57E-04	3.46E-04	2.64	13.5	300	13
786.08	Diabase	4.26E-04	7.63E-05	11.17	14.6	243	13
786.97	Diabase	9.34E-04	1.03E-04	18.21	8.6	510	
787.87	Diabase	6.90E-04	9.34E-05	14.77	3.9	540	
789.38	Diabase	1.44E-05	3.05E-05	0.94	-2.1	325	-8
799.68	Diabase	5.88E-04	9.70E-04	1.21	12.6	460	12
801.08	Gabbro	1.80E-03	5.94E-04	6.07	5.2	325	5
810.86	Gabbro	2.46E-03	6.02E-04	8.16	32.4	193	27
812.30	Gabbro	3.84E-04	3.01E-04	2.55	67.1		15
823.22	Gabbro	8.36E-04	1.98E-04	8.46	23.9	375	20
825.96	Gabbro	9.03E-05	4.30E-05	4.20	21.8	385	19
836.20	Diabase	1.27E-03	4.68E-03	0.54	-38.0	148	
837.07	Diabase	1.41E-03	6.88E-03	0.41	44.9	178	27
839.37	Microgabbro	1.37E-03	6.49E-03	0.42	80.3	96	32
848.52	Gabbro	1.55E-03	5.05E-04	6.12	16.5	252	12
849.85	Microgabbro	1.42E-03	4.73E-04	6.01	17.7	231	14
861.18	Gabbro	8.40E-04	1.55E-04	10.87	33.3	351	28
861.62	Gabbro	2.32E-04	7.30E-05	6.37	32.3	288	30
875.03	Gabbro	3.97E-03	8.73E-04	9.11	21.4	171	17
877.03	Gabbro	2.51E-03	4.33E-04	11.59	25.8	285	27
878.36	Gabbro	1.90E-03	4.31E-04	8.83	26.1	194	25
879.75	Gabbro	7.58E-04	2.69E-04	5.63	41.0	440	23
892.24	Diorite		1.34E-05	0.00		29	
893.04	Gabbro	3.23E-03	4.90E-04	13.17	24.7	200	27
896.18	Gabbro	9.89E-04	1.81E-04	10.90	24.9	423	23
909.40	Diabase	2.37E-03	7.07E-03	0.67	34.8	156	29
911.49	Diabase	2.31E-03	8.90E-03	0.52	31.9	156	23
912.02	Diabase	1.81E-03	5.97E-03	0.61	33.1	179	
913.52	Metagabbro	4.75E-04	6.62E-04	1.44	20.0	330	
926.90	Gabbro	7.44E-04	2.69E-04	5.52	26.6	230	30
928.32	Gabbro	3.34E-04	8.29E-05	8.06	14.1	235	15
929.58	Plag-Granite	1.49E-05	1.91E-05	1.56	23.9	520	27
931.40	Gabbroic Pyroxenite	3.10E-03	9.20E-04	6.74	30.2	177	30
943.64	Gabbro	5.50E-03	1.51E-03	7.28	25.1	230	25
944.78	Metagabbro		5.09E-03	0.00		136	21
947.17	Gabbro	1.63E-03	4.56E-04	7.16	18.2	141	18
947.80	Gabbro	2.99E-03	1.17E-03	5.11	21.6	170	20
960.98	Gabbro	2.35E-03	6.44E-04	7.31	25.0	196	27
962.18	Gabbro	2.12E-03	1.97E-03	2.16	22.1	258	21
963.35	Gabbro	1.80E-03	1.28E-03	2.81	23.3	254	27
965.69	Gabbro	1.29E-03	1.26E-03	2.04	21.3	173	26
977.87	Diabase	7.94E-04	5.75E-03	0.28	67.6	300	
979.42	Diabase	4.56E-04	7.58E-03	0.12	65.2	195	
981.02	Diabase	1.25E-03	4.76E-03	0.52	58.6	93	
982.35	Diabase	5.89E-04	6.53E-03	0.18	25.0	93	
995.06	Diabase	4.73E-03	3.46E-03	2.74	41.0	140	38
997.40	Gabbro	1.78E-03	1.15E-03	3.10	19.6	178	21
999.08	Gabbro	6.48E-03	2.51E-03	5.16	22.8	156	21
1000.17	Gabbro	4.80E-03	2.22E-03	4.31	21.0	175	25
1013.63	Gabbro	1.10E-03	1.55E-03	1.42	15.7	224	21
1014.98	Gabbro	6.93E-04	5.28E-04	2.62	24.3	224	23
1016.48	Gabbro	8.03E-04	4.29E-04	3.74	23.9	275	21
1017.90	Gabbro	7.99E-04	1.50E-03	1.07	35.2	200	20
1030.78	Gabbro	4.33E-03	1.87E-03	4.64	25.8	187	19
1032.23	Gabbro	3.56E-04	2.19E-03	0.32	33.7	146	22
1033.44	Gabbro	3.43E-03	7.48E-04	9.17	39.7		
1034.92	Gabbro	9.98E-04	8.66E-04	2.31	28.4	179	32
1048.02	Diabase	2.04E-03	8.05E-03	0.51	28.4	200	29
1049.55	Diabase	2.22E-03	5.33E-03	0.83	21.8	113	11
1050.80	Diabase	1.12E-03	3.81E-03	0.59	-3.5	242	
1053.09	Diabase	1.08E-03	6.46E-03	0.34	29.1	100	25
1066.01	Diabase	2.56E-03	9.67E-03	0.53	24.9	78	
1067.68	Diabase	2.98E-03	7.70E-03	0.77	22.1	70	20
1068.42	Diabase	2.31E-03	6.42E-03	0.72	22.6	80	24
1070.04	Diabase	6.62E-04	2.05E-03	0.65	19.3	139	21
1082.72	Gabbro	6.64E-04	2.18E-04	6.08	19.7	352	20
1084.05	Gabbro	1.37E-03	1.23E-03	2.24	20.5	156	17
1086.00	Gabbro	5.36E-04	2.25E-04	4.75	18.7	197	19
1087.35	Diabase	6.56E-04	3.10E-03	0.42	40.2	278	27
1100.92	Gabbro	1.84E-04	7.69E-05	4.79	17.1	400	19

Depth (m)	Lithology	J_0 (emu/cc)	k (cgs)	Q	I_0	MDF (oe)	I_s
1102.33	Gabbro	6.75E-06	2.39E-05	0.56	6.4	505	14
1103.85	Gabbro	4.38E-04	1.91E-04	4.58	20.5	230	19
1105.33	Diabase	4.44E-03	4.90E-03	1.81	9.0	32	15
1118.36	Diabase	1.09E-03	6.36E-03	0.34	36.9	166	24
1119.90	Diabase	1.37E-03	6.34E-03	0.43	59.2	66	28
1121.30	Diabase	1.29E-03	6.19E-03	0.42	45.6	50	25
1135.37	Diabase	1.08E-03	4.55E-03	0.47	52.7	169	
1136.58	Diabase	2.84E-05	2.58E-05	2.20	26.3	425	24
1137.79	Plag-Granite	1.60E-03	3.25E-03	0.99	47.3	89	32
1139.99	Diabase	1.08E-03	3.60E-03	0.60	61.4	87	39
1151.31	Gabbro	1.86E-03	1.59E-03	2.34	14.1	155	17
1153.78	Gabbro	2.31E-03	2.50E-03	1.85	20.5	150	17
1155.02	Gabbro	4.48E-03	2.67E-03	3.36	22.5	108	19
1168.16	Gabbro	6.05E-04	1.03E-03	1.18	22.2	186	31
1169.96	Gabbro	1.02E-03	1.44E-03	1.42	25.8	178	29
1171.07	Gabbro	7.76E-04	5.37E-03	0.29	14.9	140	22
1172.38	Gabbro	5.79E-04	1.42E-03	0.81	41.3	298	20
1185.37	Gabbro	7.17E-04	2.48E-03	0.58	36.7	188	17
1187.32	Gabbro	6.54E-04	2.46E-03	0.53	33.3	242	20
1188.57	Gabbro	7.88E-04	2.26E-03	0.70	28.6	241	23
1189.89	Diabase	3.03E-04	3.81E-03	0.16	59.1	208	
1191.92	Gabbro	1.69E-03	9.94E-03	0.34	55.0	47	
1203.32	Gabbro	1.32E-03	2.26E-03	1.16	20.0	158	16
1204.98	Gabbro	5.31E-04	5.19E-04	2.05	17.3	236	13
1205.96	Gabbro	2.69E-03	2.02E-03	2.66	22.3	152	21
1207.32	Gabbro	8.20E-03	2.76E-03	5.95	26.0	135	22
1220.47	Gabbro	4.51E-03	3.58E-03	2.52	20.4	118	13
1221.65	Gabbro	1.88E-03	1.92E-03	1.96	12.9	183	17
1222.95	Gabbro	4.22E-03	1.97E-03	4.29	50.8	135	24
1225.15	Gabbro	2.15E-03	4.68E-04	9.20	28.8	178	27
1238.50	Gabbro	3.24E-03	4.73E-04	13.69	31.4	160	20
1239.96	Diabase	9.03E-04	1.80E-03	1.00	58.6	125	17
1241.35	Gabbro	3.01E-03	8.11E-04	7.44	25.9	90	22
1242.87	Gabbro	9.40E-04	3.30E-04	5.70	31.7	295	23
1256.63	Gabbro	1.04E-03	2.95E-04	7.04	21.2	50	23
1258.09	Gabbro	1.37E-03	4.55E-04	6.03	18.9	200	21
1260.13	Gabbro	4.33E-04	4.23E-04	2.05	48.9	400	17
1272.75	Gabbro	2.91E-03	5.78E-04	10.06	20.1	221	23
1274.17	Gabbro	1.61E-03	4.03E-04	8.01	22.2	261	19
1275.45	Gabbro	1.33E-03	5.55E-04	4.81	25.0	281	23
1276.59	Gabbro	1.18E-03	2.76E-04	8.56	25.0	278	27
1290.07	Gabbro	7.96E-04	1.72E-04	9.25	26.6	258	24
1292.08	Gabbro	7.95E-04	2.71E-04	5.87	26.7	287	29
1295.09	Gabbro		2.68E-04	0.00		240	27
1307.75	Gabbro	6.59E-04	2.89E-03	0.46	34.9	180	23
1309.72	Gabbro	1.86E-03	8.32E-04	4.48	9.2	235	
1310.43	Pegmatite	3.15E-04	1.22E-04	5.16	22.8	280	21
1311.97	Gabbro	1.73E-03	4.26E-04	8.11	13.1	260	10
1325.15	Microgabbro	1.51E-03	3.04E-04	9.92	20.0	253	22
1326.79	Microgabbro	8.22E-04	9.93E-05	16.55	17.6	335	21
1328.19	Microgabbro	1.87E-03	4.93E-04	7.59	18.9	200	30
1329.64	Gabbro	2.43E-04	1.10E-04	4.40	10.7	357	12
1343.46	Gabbro	6.32E-04	3.51E-04	3.60	23.6	260	23
1344.76	Gabbro	1.29E-03	4.73E-04	5.44	13.7	236	16
1345.65	Layered Gabbro	9.44E-04	2.93E-04	6.43	8.9	225	9
1347.10	Very Coarse Gabbro	3.24E-04	1.15E-04	5.64	10.9	275	
1359.60	Gabbro	5.05E-04	2.04E-04	4.94	18.1	209	15
1360.97	Gabbro	3.22E-04	1.34E-04	4.81	13.5	248	10
1364.12	Gabbro	5.73E-04	2.89E-04	3.97	13.3	445	10
1368.65	Gabbro	2.46E-04	1.02E-04	4.80	9.4	98	12
1377.28	Layered Gabbro	1.04E-04	8.17E-05	2.54	19.1	264	25
1378.65	Layered Gabbro	3.80E-03	7.75E-04	9.81	14.8		23
1380.92	Layered Gabbro	2.28E-04	1.88E-04	2.43	15.7		14
1381.65	Layered Gabbro	3.94E-04	1.07E-04	7.32	5.0	330	11
1395.03	Gabbro	8.46E-04	1.80E-04	9.40	5.7	46	
1396.95	Gabbro	1.03E-02	1.82E-03	11.30	4.7		
1398.38	Gabbro	1.49E-05	2.86E-05	1.04	10.3	380	
1399.68	Gabbro	2.28E-03	6.97E-04	6.56	15.3	180	20
1412.58	Coarse Gabbro	1.25E-03	4.45E-04	5.61	22.8	194	28
1415.83	Coarse Gabbro	3.61E-03	6.33E-04	11.40	16.2	178	15

Depth (m)	Lithology	J_0 (emu/cc)	k (cgs)	Q	I_0	MDF (oe)	I_s
1416.78	Gabbro	4.37E-06	1.66E-05	0.53	16.1	315	
1430.25	Gabbro	8.67E-04	3.58E-04	4.84	19.1	245	21
1431.65	Gabbro	2.19E-03	9.67E-04	4.53	-15.1	146	-17
1433.67	Coarse Gabbro	1.53E-03	4.15E-04	7.35	24.3	173	20
1434.57	Coarse Gabbro	1.36E-03	5.02E-04	5.43	27.1	152	22
1447.50	Fine-grained Gabbro	2.05E-03	1.00E-03	4.11	18.7	198	17
1448.47	Fine-grained Gabbro	8.76E-04	1.15E-04	15.19	22.4	226	22
1450.22	Gabbro	3.17E-03	1.02E-03	6.24	18.8	176	20
1451.73	Gabbro	6.46E-04	2.47E-04	5.24	21.4	146	20
1465.46	Gabbro	4.88E-03	2.72E-03	3.59	20.4	150	10
1466.82	Gabbro	2.94E-03	1.19E-03	4.93	12.1	162	14
1468.15	Gabbro	1.50E-03	7.97E-04	3.76	16.4	194	16
1469.73	Diabase	6.41E-04	2.75E-04	4.66	27.9	267	23
1481.55	Gabbro	2.57E-04	1.07E-04	4.82	5.9	300	
1482.98	Gabbro	5.95E-04	2.04E-04	5.83	4.9	348	
1484.12	Gabbro	5.62E-04	5.95E-04	1.89	31.3	364	
1486.37	Gabbro	2.06E-04	8.65E-05	4.77	13.0	350	9
1498.56	Gabbro	2.64E-04	6.16E-05	8.58	2.3	400	
1500.98	Gabbro	1.68E-04	8.13E-05	4.13	-43.4	388	-43
1502.70	Gabbro	1.03E-04	6.38E-05	3.22	-66.2	300	-65
1515.72	Gabbro	2.62E-04	1.92E-04	2.73	-3.6	266	-9
1516.85	Gabbro	2.88E-04	1.10E-04	5.24	28.3	39	
1519.95	Gabbro		2.69E-04	0.00			20
1531.95	Coarse Gabbro	5.56E-04	2.42E-04	4.60	18.7	286	11
1534.68	Gabbro	1.55E-03	2.33E-04	13.32	18.5	400	20
1536.15	Gabbro	1.43E-03	5.30E-04	5.39	21.1	252	13
1549.08	Gabbro	4.38E-04	1.84E-04	4.75	26.0	262	25
1550.43	Gabbro	2.36E-04	1.39E-04	3.40	24.8	244	29
1551.75	Gabbro	3.04E-04	2.12E-04	2.87	18.6	267	18
1567.85	Gabbro	6.55E-04	3.10E-04	4.22	25.7	250	
1569.47	Gabbro	5.14E-04	2.93E-04	3.51	34.0	225	25
1583.70	Gabbro	1.31E-03	6.11E-04	4.29	20.2	204	20
1585.16	Gabbro	3.53E-04	2.50E-04	2.82	26.0	269	24
1586.73	Gabbro	1.18E-03	4.75E-04	4.96	1.7	264	15
1588.27	Gabbro	6.09E-04	3.66E-04	3.32	29.6	211	24
1600.90	Fine-grained Gabbro	7.98E-04	4.52E-04	3.53	20.9	274	16
1602.44	Fine-grained Gabbro	9.48E-04	5.55E-04	3.42	21.4	245	14
1603.55	Fine-grained Gabbro	1.69E-03	4.66E-04	7.25	11.5	300	11
1605.23	Fine-grained Gabbro	5.25E-04	2.91E-04	3.61	19.7	254	24
1617.89	Fine-grained Gabbro	9.24E-04	3.94E-04	4.69	21.0	282	16
1619.27	Layered Gabbro	3.08E-04	8.44E-05	7.30	13.7	475	
1620.75	Layered Gabbro	2.73E-04	1.93E-04	2.83	20.4	253	17
1622.03	Layered Gabbro	2.78E-04	7.12E-05	7.82	16.2	465	14
1635.62	Layered Gabbro	3.90E-04	2.02E-04	3.86	20.4	213	16
1638.58	Layered Gabbro	2.04E-04	1.53E-04	2.65	24.6	176	21
1640.04	Layered Gabbro	5.73E-04	2.76E-04	4.16	20.4	176	8
1652.68	Gabbro	7.07E-04	1.27E-04	11.09	14.2	385	12
1654.12	Gabbro	9.98E-04	3.85E-04	5.18	19.5	166	26
1655.33	Fine-grained Gabbro	2.93E-04	2.77E-04	2.11	24.6	194	18
1656.02	Medium-grain Gabbro	9.11E-04	2.36E-04	7.73	25.3	188	27
1669.64	Gabbro	4.77E-04	3.20E-04	2.98	17.0	214	22
	Gabbro	8.45E-04	6.41E-04	2.64	27.1		
1672.86	Gabbro	4.40E-04	2.28E-04	3.85	25.3	168	21
1673.98	Gabbro	6.13E-04	4.85E-04	2.53	40.7	300	22
1687.77	Gabbro	6.12E-04	4.85E-04	2.52	18.7	158	7
1688.77	Gabbro	4.82E-04	3.64E-04	2.65	23.0	180	21
1691.62	Gabbro	5.18E-04	4.10E-04	2.53	20.4	168	20
1692.43	Gabbro	6.05E-04	2.96E-04	4.09	31.1	143	7
1705.24	Gabbro	3.29E-04	1.61E-04	4.10	20.9		23
1705.53	Gabbro	5.49E-04	2.26E-04	4.86	15.9	201	13
1708.16	Gabbro	5.76E-04	3.19E-04	3.61	23.7	266	36
1709.23	Gabbro	6.76E-04	1.62E-04	8.34	13.6	190	15
1722.73	Gabbro	3.71E-04	1.31E-04	5.67	18.2	202	12
1723.88	Gabbro	1.86E-04	1.76E-04	2.11	21.3	185	17
1725.58	Gabbro	2.70E-04	3.99E-05	13.53	18.9	235	22
1727.36	Gabbro	5.03E-04	1.46E-04	6.88	24.7	197	21
1739.47	Gabbro	6.05E-04	6.31E-05	19.16	15.5	218	10
1740.72	Gabbro	6.58E-04	2.49E-04	5.28	28.9	655	4
1742.52	Gabbro	6.50E-04	3.14E-04	4.14	37.3	160	24
1744.79	Gabbro	4.55E-04	7.48E-05	12.16	7.9	730	

Depth (m)	Lithology	J_0 (emu/cc)	k (cgs)	Q	I_0	MDF (oe)	I_s
1755.66	Pyroxenite to Gabbro	3.97E-04	1.26E-04	6.29	17.2	251	
1757.52	Gabbro	9.35E-04	8.03E-04	2.33	18.0	134	18
1759.00	Gabbro	1.34E-03	6.44E-04	4.18	22.3	135	
1759.68	Pyroxenite/Melanogabbro	7.10E-04	2.82E-04	5.05	8.7	200	5
1772.93	Pyroxenite/Melanogabbro	3.59E-04	1.20E-04	6.00	23.4	217	18
1774.48	Pyroxenite/Melanogabbro	2.07E-03	9.78E-04	4.24	23.2	136	20
1775.77	Websterite/Pyroxenite	8.11E-04	4.41E-04	3.68	16.0	186	22
1777.52	Websterite/Pyroxenite	6.29E-04	4.80E-04	2.62	24.0	138	29
1790.76	Gabbro-Norite	7.64E-04	4.28E-04	3.57	24.4	130	20
1791.96	Websterite	3.38E-03	1.32E-03	5.10	25.5	118	17
1793.54	Websterite	6.73E-04	3.08E-04	4.37	22.2	200	18
1794.83	Websterite	1.77E-04	1.29E-04	2.75	21.2	202	13
1806.61	Websterite/Gabbro-Norite	3.83E-04	4.49E-04	1.71	15.2	237	8
1807.92	Websterite	8.18E-04	4.24E-04	3.86	22.3	149	15
1809.25	Gabbro	1.09E-04	2.87E-05	7.60	25.0		18
1810.41	Gabbro	1.78E-04	3.29E-05	10.81	15.7	600	15
1823.59	Websterite	2.39E-04	1.26E-04	3.79	14.4	220	8
1824.02	Websterite	6.57E-04	4.69E-04	2.80	25.9	160	13
1826.09	Websterite	2.28E-03	1.59E-03	2.86	38.5	85	8
1827.36	Olivine Websterite	4.05E-03	9.74E-04	8.32	4.8	158	-4
1836.22	Olivine Websterite	1.59E-04	1.40E-04	2.27	12.8	195	
1838.57	Olivine Websterite	1.30E-03	2.24E-03	1.16	30.4	111	16
1839.85	Olivine Websterite	4.78E-03	1.50E-03	6.37	47.1	75	19
1841.10	Olivine Websterite	8.40E-04	4.30E-04	3.90	31.0	120	16
1843.33	Coarse Websterite	2.01E-04	2.19E-04	1.83	20.6	181	17
1851.08	Websterite	2.80E-04	1.68E-04	3.33	25.2	249	24
1852.30	Coarse Gabbro	7.92E-04	3.98E-04	3.98	24.9	202	23
1853.75	Websterite	2.23E-03	1.06E-03	4.20	16.6	125	
1855.20	Websterite	3.25E-04	1.71E-04	3.79	13.4	240	9
1867.70	Olivine Websterite	1.76E-04	1.25E-04	2.81	29.6	354	23
1869.32	Olivine Websterite	4.38E-04	2.79E-04	3.14	29.9	193	14
1870.95	Coarse Websterite	3.67E-04	5.38E-04	1.36	28.7		8
1872.10	Websterite	5.88E-04	5.40E-04	2.18	30.3	158	13
1885.65	Coarse Websterite	8.82E-04	7.92E-04	2.23	18.0	155	8
1886.75	Olivine Websterite	1.71E-02	9.63E-03	3.55	57.2	100	30
1888.40	Olivine Websterite	5.28E-04	1.17E-04	9.00	11.0	169	15
1889.50	Olivine Websterite	5.71E-04	3.77E-04	3.03	27.3	165	16
1903.15	Coarse Olivine Websterite	3.88E-04	2.44E-04	3.18	13.3	318	5
1904.65	Websterite	4.37E-04	2.55E-04	3.42	22.5	262	17
1905.80	Websterite	3.77E-04	3.22E-04	2.34	22.6	208	17
1906.82	Olivine Websterite	2.95E-04	2.79E-04	2.11	17.6	249	13
1920.25	Websterite	5.70E-04	3.14E-04	3.63	24.0	192	14
1921.55	Websterite	4.04E-04	4.47E-05	18.09	17.2	237	13
1923.20	Websterite	7.36E-04	2.22E-04	6.63	26.6	173	20
1924.75	Websterite	9.35E-03	4.31E-03	4.34	36.6	124	18
1937.80	Websterite/Peridotite	1.92E-04	8.94E-05	4.30	38.9	275	39
1938.59	Websterite/Peridotite	1.36E-02	9.44E-03	2.88	30.8	98	21
1941.20	Olivine Websterite	9.68E-04	8.69E-04	2.23	19.1	181	
1953.95	Websterite	2.63E-04	1.47E-04	3.58	1.7	292	10
1955.20	Websterite	1.18E-03	6.98E-04	3.38	19.7	158	13
1956.70	Olivine Websterite	4.21E-04	2.48E-04	3.40	17.0	183	9
1958.00	Olivine Websterite	5.38E-04	3.52E-04	3.06	-44.2	216	-33
1968.10	Olivine Websterite	6.03E-04	2.87E-04	4.21	42.5	228	37
1969.75	Olivine Websterite	8.31E-04	5.10E-04	3.26	24.7	190	16
1971.30	Olivine Websterite	5.19E-03	2.25E-03	4.62	50.5	150	25
1980.70	Websterite	1.06E-04	1.26E-04	1.69	24.2		20
1982.10	Websterite	3.42E-04	2.26E-04	3.03	33.5	290	26
1984.00	Websterite	2.71E-04	2.59E-04	2.09	48.8	233	
1994.47	Websterite	2.08E-04	7.51E-05	5.54	22.2	390	21
1996.55	Websterite	1.71E-06	4.62E-05	0.07	33.5		35
1997.07	Websterite	9.01E-05	8.05E-05	2.24	25.6	320	19
2006.90	Websterite	3.61E-04	1.67E-04	4.32	25.9	295	22
2008.15	Websterite	2.20E-04	8.95E-05	4.92	34.2	370	32
2008.75	Websterite	7.54E-05			26.9		25
2019.18	Websterite	9.13E-04	5.69E-04	3.21	25.1	208	23
2020.50	Websterite	5.08E-04	1.34E-04	7.60	30.8	282	30
2021.95	Websterite	1.63E-03	6.65E-04	4.90	30.8	197	30
2032.00	Websterite	3.08E-04	9.06E-05	6.80	22.8	432	20
2033.50	Websterite	7.49E-04	1.70E-04	8.82	31.1	275	29
2034.75	Websterite	1.67E-03	6.52E-04	5.12	27.2	215	26

Depth (m)	Lithology	J_0 (emu/cc)	k (cgs)	Q	I_0	MDF (oe)	I_s
2044.75	Websterite	7.24E-04	4.17E-04	3.47	29.1	242	28
2046.10	Websterite	1.12E-04	1.57E-04	1.42	27.9	433	27
2047.60	Websterite	1.29E-03	5.00E-04	5.16	31.7	201	27
2058.10	Websterite	3.07E-04	1.58E-04	3.89	30.6	207	18
2059.50	Harzburgite	0.00166	1.83E-02	0.18	27.6	45	
2060.65	Websterite	6.26E-04	8.88E-04	1.41	28.3	260	25
2070.20	Websterite	3.45E-04	1.31E-04	5.28	17.7	323	22
2071.50	Websterite	8.99E-04	5.29E-04	3.40	20.4	200	17
2073.15	Websterite	7.48E-04	4.59E-04	3.26	27.7	232	23
2082.75	Websterite		3.40E-03	0.00			30
2084.35	Websterite	4.55E-04	1.29E-04	7.08	25.2	271	20
2085.63	Websterite	5.51E-04	6.32E-04	1.74	48.0	218	26
2096.80	Websterite	1.76E-03	1.44E-03	2.45	39.7	145	11
2098.20	Websterite	3.88E-04	2.40E-04	3.24	23.3	289	12
2107.80	Websterite	1.38E-03	3.72E-04	7.41	2.4	260	9
2109.30	Websterite	5.50E-04	1.82E-04	6.04	13.1	206	10
2110.80	Websterite	2.35E-03	6.00E-04	7.84	15.9	175	
2120.40	Websterite	1.20E-03	2.27E-04	10.59	6.0	228	
2121.50	Websterite	8.73E-04	2.85E-04	6.12	17.1	270	
2122.60	Websterite	1.77E-03	6.84E-04	5.17	16.1	237	
2132.95	Websterite/Gabbro-Norite	1.16E-04	4.26E-05	5.44	32.9	306	31
2134.40	Websterite/Gabbro-Norite	4.38E-04	9.16E-05	9.56	28.3	340	28
2136.00	Gabbro-Norite	4.89E-05	3.06E-05	3.19	28.3	453	28
2145.45	Websterite	2.51E-03	1.74E-03	2.89	1.9	157	
2147.40	Websterite	3.31E-04	8.77E-05	7.55	13.3	241	
2147.96	Websterite	1.86E-03	7.33E-05	50.75	28.2	27	28
2158.10	Websterite	1.57E-03	8.71E-04	3.61	37.2	155	32
2159.40	Websterite	4.27E-04	8.36E-05	10.21	24.1	248	22
2160.45	Websterite	6.24E-04	2.25E-04	5.54	24.0	232	14
2171.15	Websterite	1.79E-03	1.09E-03	3.28	21.6	158	14
2172.40	Websterite	1.26E-03	4.56E-04	5.52	17.6	219	13
2174.00	Websterite	2.32E-03	9.68E-04	4.80	22.6	214	13
2184.25	Websterite	1.67E-03	5.64E-04	5.92	37.5	193	
2185.50	Websterite	2.22E-03	9.10E-04	4.88	36.9	193	27
2187.10	Peridotite	9.42E-03	5.39E-03	3.50	44.4		20
2196.45	Websterite	6.63E-03	3.17E-03	4.18	47.2	182	25
2198.00	Websterite	1.87E-03	8.03E-04	4.66	32.5		23
2199.87	Websterite	1.30E-03	8.36E-04	3.11	20.4	184	25
2210.10	Websterite/Gabbronorite	1.18E-03	4.31E-04	5.47	21.6	210	20
2211.30	Websterite/Gabbronorite	1.22E-03	4.36E-04	5.59	25.0	220	17
2212.40	Websterite/Gabbronorite	8.14E-04	2.06E-04	7.90	23.7	220	22
2222.00	Gabbro-Norite	7.39E-04	1.21E-04	12.17	17.1	298	24
2222.90	Peridotite(Pyroxene)	7.66E-04	3.48E-04	4.40	33.2	232	2
2224.40	Peridotite(Pyroxene)	5.62E-03	9.80E-03	1.15	25.4	118	18
2234.10	Websterite	1.51E-03	5.34E-04	5.65	25.7	271	16
2237.30	Websterite	2.01E-03	3.07E-03	1.31	42.1	173	29
2246.75	Websterite	3.89E-04	7.96E-05	9.78	14.5	353	
2248.55	Websterite	9.86E-05	4.07E-05	4.84	10.5	400	10
2249.00	Websterite	2.55E-03	1.15E-03	4.45	22.5	203	26
2259.05	Websterite/Peridotite	1.23E-02	8.56E-03	2.87	-56.4	105	-30
2261.25	Peridotite	4.05E-03	2.61E-03	3.11	41.7	167	32
2263.10	Websterite/Peridotite	7.79E-04	2.63E-04	5.93	19.5	300	13

Zone B

As previously mentioned, this zone is made up primarily of diabase dikes with some altered gabbro screens. Susceptibility varies widely throughout this zone and has a mean value of 0.010 cgs (0.125 SI), the highest in the section. The J_o values are also quite scattered and have a mean of 3.1 A/m (0.0031 emu/cm^3). The average Q value through this narrow zone is only 0.7 and thus it has an in situ magnetization which is dominated by induced magnetization rather than remanent magnetization. MDF values are quite low at an average of 8.7 nT (87 oe) which suggests the unstable nature of the magnetization. Additionally, I_o values (see Table 1) reveal that a very large amount of scatter exists in the in situ directions. The I_s, however, has a mean value of 21° which agrees very well with the average I_s observed from CY-4 (20°). Finally, the magnetite grains observed within this section appear to be heavily recrystallized. The magnetite grains are very homogeneous (unlike magnetite grains observed in samples from the upper part of the section), and are commonly surrounded by sphene halos. Additionally, very few primary textures remain, although occasional relict ilmenite lamellae structures are observed to be replaced by sphene.

Zone C

The transition from sheeted dikes to gabbro occurs from 600 m to 1300 m in zone C with the largest drop in dike abundance (75 to 25%) taking place between 600 m and 800 m (Hall et al., 1988). A comparison of the magnetic properties of the two rock types can be made using the discrete sample data which is displayed in Figures 7 and 8. Diabase has a higher average k than gabbro (0.004 vs. 0.0012 cgs, or 0.050 vs. 0.015 SI), and a slightly lower J_o than gabbro (1.05 vs. 1.21 A/m, or 0.00105 vs. 0.00121 emu/cc). Because of this difference in magnetic properties between the two rock types, individual diabase dikes are clearly described in the susceptibility log by 'boxcar' shaped highs (see Figure 9). When examined on a fine scale, dike boundaries are also discernable in the magnetic anomaly log, but are much less obvious. Correlation with the core descriptions shows that individual dike boundaries are described very well by the susceptibility log and that a decay in dike population is indeed occuring through this zone. By using logging data to compare the susceptibility of dikes in zones A, B, and C it can be seen that zone A and C dikes have quite similar k values while zone B dikes have anomalously high k.

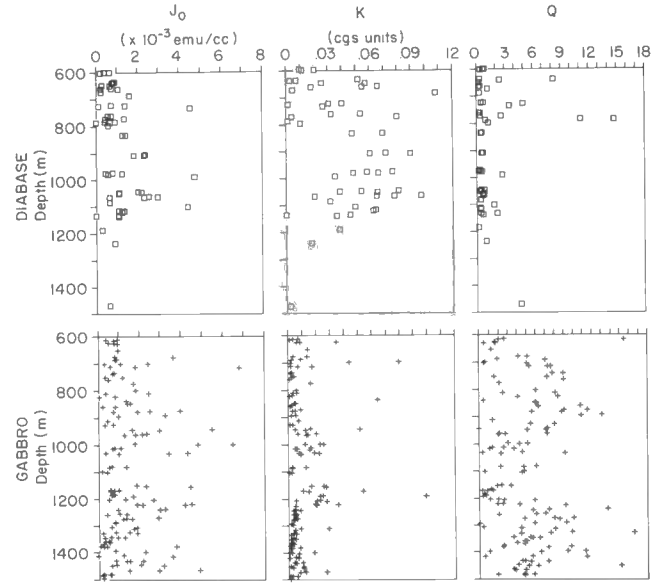

Figure 7: Magnetic properties of diabase and gabbro as measured on minicore samples are compared for magnetic zone C of CY-4. Susceptibility is $\times$ 10^{-1} cgs. Note that 1 Amp/m = 10^{-3} emu/cc and 1 cgs susceptibility unit = 4π(SI).

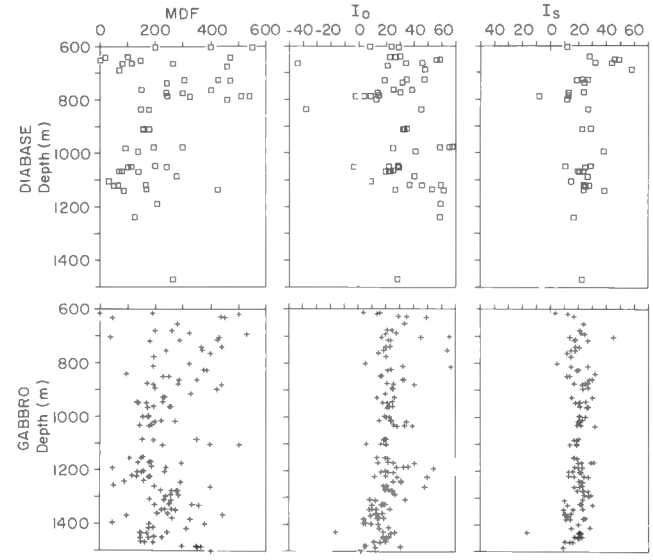

Figure 8: Mean demagnetizing field (MDF), initial inclination (I_o), and stable inclination as determined for diabase and gabbro minicore samples are plotted versus depth. MDF is in oersteds (10 oe = 1 nT) and inclination is in degrees.

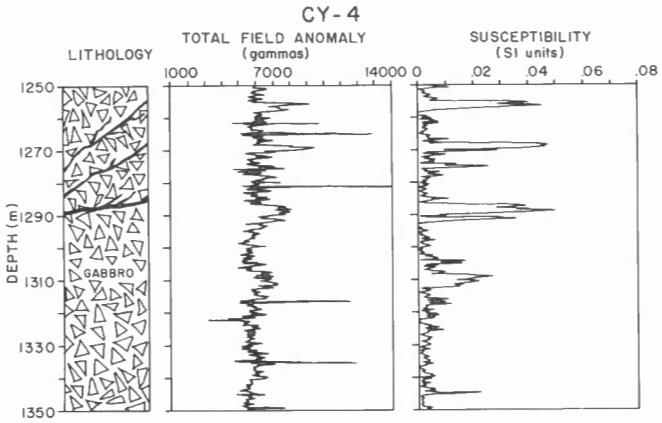

Figure 9: Magnetic logging data plotted versus depth for a small section of magnetic zone C where 1 gamma = 1 nT and 1 cgs susceptibility unit = 4π(SI). The wide peaks in the susceptibility log correspond to individual diabase dikes. Note that the dike signal is less easily discerned in the total field anomaly record.

Measurements of Q, MDF, I_s, and I_o give further insight into the contrasting nature of the magnetization of diabase and gabbro from zone C (Figures 7 and 8). The Q ratio is frequently used to determine whether in situ magnetization is dominated by remanent or induced magnetization. With the exception of a few very high Q values, diabase has a Q value which is close to, or less than one. Gabbro, on the other hand, has a widely varying Q which is almost always greater than one and thus the magnetic signal is dominated by remanent magnetization. Additionally, the MDF values of the two lithologies show that diabase typically has a much lower stability than gabbro. Finally, comparison of I_s to I_o of the two rock types shows that while gabbroic samples exhibit very little change between I_o and I_s, diabase has much more scatter in I_o directions. These data suggest that the magnetic carriers in the diabase are large, multi-domain grains which have acquired secondary (viscous or chemical) magnetic components (in this case usually at a steeper inclination). Gabbro, on the other hand, appears to be characterized magnetically by smaller, more stable grains. Opaque mineralogy studies agree with the above data as diabase typically bears very large (commonly 20 μm) oxidized titanomagnetite grains (now ilmenite plus magnetite) in high concentrations (5%) and gabbro typically carries much less than 1% magnetite, at sizes of approximately 1-5 μm.

Zone D

The gabbros between 1500 m and 1745 m are magnetically the most quiet and stable within the intrusive section. In agreement with the logging data, the mini-core measurements reveal the lowest values of J_o (0.6 A/m or 0.0006 emu/cc) and of k (0.0003 cgs or 0.0038 SI) of the intrusives. An average Q ratio of 5.1 and MDF of 25.8 nT (258 oe) indicate that this zone is dominated by a stable, albeit weak, magnetization. Examination of polished thin sections reveal that these gabbros are characterized by a very low content of magnetite and that the grains are small (commonly 4 μm) and in most cases included in large pyroxene grains.

A short, reversely magnetized zone can be seen in both the minicore measurements and the vertical magnetic anomaly log from 1500-1515 m (Figure 10) and is of interest because Troodos is generally believed to have formed during the Cretaceous Quiet Zone. This reversed zone suggests that at least some high temperature activity occurred during a period of reversed polarity following 83ma. The average inclination of this zone is only 15° and this agrees with a general shallowing trend that begins at 800 m.

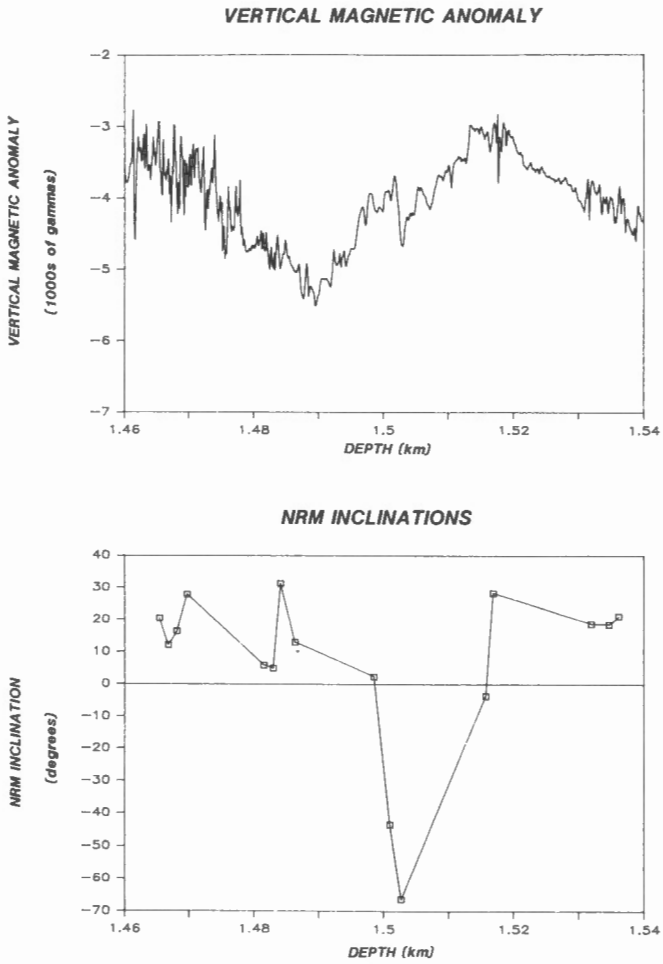

Figure 10: A short reversally magnetized zone within the gabbros is apparent from both the logging record (upper) and minicore measurements (lower).

Zone E

The websterite units in this zone interlayer with gabbro to the bottom of CY-4 and become increasingly serpentinized with depth in the section. While the gabbro units retain essentially the same magnetic properties as in zone D, the ultramafics have a higher average J_0 and k (1.5 A/m, and 0.0011 cgs or 0.0126 SI respectively). The mini-core data show many highly magnetized samples which appear in the more densely sampled logging data as extremely large, positive magnetic anomalies. These anomalies have the largest amplitude throughout the entire intrusive section and sometimes reach as much as 30,000 γ. Examination of polished thin sections from this zone reveals that the highly magnetized zones have been subjected to extensive serpentinization which has resulted in the production of large amounts of secondary magnetite. The MDF and Q ratios (21.1 nT or 211 oe and 4.8) indicate that this magnetization is fairly stable and, when in situ, is dominated by the remanent component. While it is possible that the observed alteration was due to ophiolite emplacement rather than crustal formation, the stable inclination has an average value of 18° which is only slightly lower than the average I_s within CY-4 and is thus consistent with the rest of the intrusive section.

CONCLUSION

Analysis of the five magnetic zones identified within CY-4 shows that they are strongly a function of both lithology and alteration. It therefore seems certain that detailed analyses of the conditions responsible for the differences in magnetic mineralogy and corresponding differences in magnetic properties will be very useful in studying crustal formation processes.

Magnetic logging correlates extremely well with both core descriptions and discrete sample magnetic measurements. The high resolution nature of the sampling can provide a detailed record of the magnetic structure of basic rocks. This indicates that this technique will be extremely useful in characterizing alteration and lithology within ODP drill holes where core recovery is commonly as low as 10 to 20%.

ACKNOWLEDGEMENTS

We would like to extend our thanks to J. and L. Hall for their hospitality during logging operations in Palekhori. The assistance of M. Salisbury and BPB Instruments Ltd., both during and after logging, is greatly appreciated. Finally, reviews by F. Vine and J. Hall were most helpful. This work was supported by NSF grants EAR 83-11776 and EAR 82-18096.

REFERENCES

Atwater, T.M. and Mudie, J.D.
1973: Detailed near-bottom geophysical study of the Gorda Rise; Journal of Geophysical Research, v. 78, p. 8665-8686.

Banerjee, S.K.
1980: Magnetism of the oceanic crust: evidence from ophiolite complexes; Journal of Geophysical Research, v. 85, p. 3557-3566.

Fox, P.J. and Opdyke, N.D.
1973: Geology of the oceanic crust: magnetic properties of oceanic rocks; Journal of Geophysical Research, v. 78, p. 5139-5154.

Hall, J.M., Fisher, B., Walls, C., Ward, T., Hall, L. and Johnson, H.P.
1988: Magnetic properties, oxide petrography, and alteration in the Cyprus Crustal Project Drill Hole CY-4 Section through the lower sheeted complex and upper plutonic complex of the Troodos, Cyprus, Ophiolite; (This volume)

Johnson, H.P.
1979: Magnetization of the oceanic crust; Reviews of Geophysics and Space Physics, v. 17, p. 215-226.

Johnson, H.P. and Pariso, J.E.
1985: Implications for a magnetic model of the ocean crust: new Troodos ophiolite data; EOS, American Geophysical Union, Transactions, v. 66, p. 1128.

Kent, D.V., Honnorez, B.M., Opdyke, N.D. and Fox, P.J.
1978: Magnetic properties of dredged oceanic gabbros and the source of marine magnetic anomalies; Geophysical Journal of the Royal Astronomical Society, v. 55, p. 513-537.

Klitgord, K.D., Huestis, S.P., Mudie, J.D. and Parker, R.L.
1975: An analysis of near-bottom magnetic anomalies, sea floor spreading and the magnetized layer; Geophysical Journal of the Royal Astronomical Society, v. 43, p. 387-424.

Levi, S. and Banerjee, S.K.
1977: The effects of alteration on the natural remanent magnetization of three ophiolite complexes: possible implications for the oceanic crust; Journal of Geomagnetism & Geoelectricity, v. 29, p. 421-439.

Macdonald, K.C.
1977: Near-bottom magnetic anomalies, asymmetric spreading, oblique spreading, and tectonics of the Mid-Atlantic ridge near lat. 37°N; Geological Society of America, Bulletin, v. 88, p. 541-555.

Salisbury, M. and Christensen, N.I.
1985: Velocity structure of the Troodos Ophiolite from borehole logs; EOS, American

Geophysical Union, Transactions, v. 66, p. 1122.

Swift, B.A. and Johnson, H.P.
1984: Magnetic properties of the Bay of Islands Ophiolite Suite and implications for the magnetization of oceanic crust; Journal of Geophysical Research, v. 89, no. B5, p. 3291-3308.

Talwani, J., Windisch, C.C. and Langseth, M.G.
1971: Reykjanes ridge crest: a detailed geophysical study; Journal of Geophysical Research, v. 76, p. 473-517.

Swift, B.A. and Johnson, H.P.
1984: Magnetic properties of the Bay of Islands Ophiolite Suite and implications for the magnetization of oceanic crust; Journal of Geophysical Research, v. 89, no. B5, p. 3291-3308.

Vine, F.J. and Moores, E.M.
1972: A model for the gross structure, petrology, and magnetic properties of oceanic crust; *in* Studies in Earth and Space Sciences, ed. R. Shagam, R.B. Hargraves, W.J. Morgan, F.B. Van Harten, C.A. Burk, H.D. Holland and L.C. Hollister; Geological Society of America, Memoir, v. 132, p. 195-205.

The Physical Properties of Diabases, Gabbros and Ultramafic Rocks from C.C.S.P. Drill Hole CY-4 at Palekhori, Cyprus

G.C. SMITH AND F.J. VINE

School of Environmental Sciences, University of East Anglia, Norwich, England, NR4 7TJ

Smith, G.C. and Vine, F.J., The physical properties of diabases, gabbros and ultramafic rocks from C.C.S.P. Drill Hole CY-4 at Palekhori, Cyprus; in *Cyprus Crustal Study Project: Initial Report, Hole CY-4, ed. I.L. Gibson, J. Malpas, P.T. Robinson and C. Xenophontos*; *Geological Survey of Canada, Paper 88-9, p. 295-314, 1989.*

Abstract

The physical properties bulk and grain density, porosity, compressional and shear wave velocity, electrical conductivity, intensity and inclination of the natural remanent magnetization and magnetic susceptibility have been measured. On the basis of these physical properties the CY-4 section is thought to provide an analogue of oceanic seismic layers 2C, 3A and 3B. Layer 2C which extends to 724 metres in CY-4, the midpoint of the transition from sheeted dykes to isotropic gabbro, is characterized by gradients in density, seismic velocities, porosity and electrical conductivity. Within layer 3A, the gabbros, there is little depth variation in physical properties. The 3A-3B boundary at a depth of 1750 metres is marked by a sharp increase in velocity and density from the gabbros above to the cumulate ultramafics below. Within layer 3B there is little variation in the physical properties with depth, except where there is an enhanced degree of serpentinization. This causes major changes in all the physical properties; a decrease in density and seismic velocities, an increase in Poisson's ratio, NRM intensity and susceptibility, and a decrease in electrical conductivity due to modification of the porosity. The inclinations of the remanent magnetization vectors in the ultramafics suggest that the serpentinization occurred on the seafloor rather than during the recent uplift of the ophiolite.

Résumé

Les propriétés physiques, densité moyenne et densité du solide, porosité, vitesse des ondes de compression et de cisaillement, conductivité électrique, intensité et inclinaison du magnétisme naturel rémanent, et enfin la susceptibilité magnétique ont été mesurées. D'après l'étude de ces propriétés, on croit que le trou de forage CY-4 fournit une analogie avec les couches séismiques océaniques 2C, 3A et 3B. La couche 2C s'étendant jusqu' à 724 m le long du forage, point central de la zone de transition entre les dykes groupés et les gabbro isotopiques, est caractérisée par des gradients de densité, de vélocité séismiques, de porosité et de conductivité électrique. Dans la zone 3A, les gabbros, il y a peu de variations des propriétés physiques avec la profondeur. Le contact entre 3A et 3B à la profondeur de 1750 m est marqué par une augmentation rapide de la densité et de la vitesse des ondes au passage des gabbros sus-jacents au cumulats ultramafiques sous-jacents. Dans la zone 3B, il y a peu de variations des propriétés physiques avec la profondeur sauf aux endroits où le degré de serpentinisation est plus élevé. La serpentinisation cause des changements majeurs à toutes les propriétés physiques: une décroissance de la densité et des vélocités séismiques, une augmentation du nombre de Poisson, de l'intensité MNR et de la susceptibilité magnétique, et enfin une diminution de la conductivité électrique dûe à la réduction de la porosité. Les inclinaisons des vecteurs du magnetisme rémanent suggèrent que la serpentinisation s'est produite sur le fond marin plutôt que durant le soulèvement récent de l'ophiolite.

INTRODUCTION

This paper summarizes and discusses measurements of the physical properties of samples from the Cyprus Crustal Study Project (C.C.S.P.) Drill Hole CY-4 into the Troodos ophiolite at Palekhori, Cyprus.

The drill hole extends 2263.44 m into the ophiolite from the lower part of the sheeted dyke complex through high-level ferrogabbros and leucocratic trondhjemites and diorites into isotropic gabbro overlying layered gabbros and websterites, terminating in olivine websterite and pyroxene-peridotite. Thus, by analogy, it might provide a reference section through part of oceanic seismic layer 2C (Houtz and Ewing, 1976), through layer 3A and into layer 3B (Sutton et al., 1971; Fox et al., 1973).

The properties measured were compressional (P) and shear (S) wave velocities (V_p and V_s), saturated bulk density (ρ_s) and grain density (ρ_g), porosity (ϕ), electrical conductivity (σ), intensity (J_{NRM}) and inclination (I_{NRM}) of the remanent magnetization, and magnetic susceptibility (χ). In addition the following parameters were derived from the above observations: Poisson's ratio (P.r.), Archie's exponent (m) and the Koenigsberger ratio (Q_n).

Laboratory data on the physical properties of rocks are essential to the interpretation of surface and downhole geophysical measurements. The Deep Sea Drilling Project (DSDP) has sampled layers 2A and 2B extensively but has only recently sampled layer 2C (Anderson et al., 1982). Physical property measurements for layer 3 samples have typically been made on rocks dredged from the sea-floor. Such samples tend to be more weathered than their equivalents at depth in the crust. Many are dredged from fracture zones and are therefore unrepresentative of 'normal' oceanic crust. Samples thought to be representative of seismic layer 3, have also been drilled at DSDP site 334 (Dunlop and Prevot, 1982) and recovered from the Mid-Cayman Rise by the DSRV *Alvin* (Karson and Fox, 1986). However, these rocks were sampled at the surface or at comparatively shallow depths in the crust (<120 m), have been tectonically emplaced, and exposed to sea-water circulating in the crust. It therefore seems unlikely that their physical properties will reflect those of in situ layer 3 rocks. Thus, the samples from CY-4 provide, for the first time, a continuous section at depth through part of a relatively unaltered and undeformed slice of oceanic lithosphere.

In this paper we discuss the physical properties of rocks from CY-4 according to lithology and depth in the section.

EXPERIMENTAL PROCEDURE

Samples were taken at approximately 5 metre intervals down the drillcore, providing 517 samples for physical property measurements. The measured samples were minicores of 25.4 mm diameter by 25.4 mm length to a depth of 480 m, and 22 mm diameter by 22 mm length below 480 m.

NRM intensities and inclinations were measured on a Digico Spinner Magnetometer. The measurement of intensity is accurate to better than $\pm 5\%$. The susceptibilities of the cores were measured on a commercial susceptibility bridge, also accurate to better than $\pm 5\%$.

A subset of 300 samples of known length and diameter was dried at 80°C under vacuum, weighed, saturated with seawater under vacuum and reweighed. Dry and saturated bulk densities, grain density and porosity were then calculated. Bulk densities are estimated to be accurate to ± 10 kg m^{-3}.

The grain or matrix density is calculated by subtracting the mass and volume of the pore fluid and recomputing the density. Accurate porosity results are difficult to obtain in low permeability, low porosity rocks. It is difficult to ensure that the rocks are completely dried before saturation and it is equally difficult to ensure that the rocks are fully saturated. We estimate that the measured porosities are accurate to within about 10% of the true porosity. Because the porosity is underestimated the calculated grain density will also be low. The maximum resulting error in the value of grain density will be no more than about 10 kg m^{-3}, based on an assumed error of 10% in the porosity for the most porous sample.

A further subset of 48 samples representing the range of textural and mineralogical variations, densities and porosities occurring throughout the core was selected for seismic velocity and electrical conductivity measurements. The compressional and shear wave velocities and electrical conductivities were determined at a range of pressures up to 0.2 GPa at 20°C with the pore space vented to the atmosphere, allowing water to drain from microcracks as the confining pressure was increased. Seismic velocities were measured by a pulse transmission technique (Birch, 1960). Conductivities were determined from the conductance of the sample at 1582 Hz measured on a Wayne-Kerr conductivity bridge.

The sample was clamped between two steel transducer holders, which act as electrodes for the conductivity measurements, and isolated from the confining pressure medium, in this case oil ('Plexol'), by a PTFE ('Teflon') sleeve.

P and S-wave velocities are estimated to be accurate to ± 0.02 km s^{-1} from a consideration of the errors incurred in measuring sample dimensions and, more critically, in 'picking' the onset of the P or S-wave. Electrical conductivities are estimated to be

accurate to ±5%.

RESULTS

The results of the physical property measurements are summarized in Table 1 for the six lithological classes identified in the drill hole: diabases, plagiogranites (trondhjemites and diorites), gabbros (including microgabbros and olivine gabbro), websterites, olivine websterites and pyroxene-peridotites. The lithological data are based on C.C.S.P. core descriptions (C.C.S.P. 1985), and visual inspection of the samples.

TABLE 1. Physical Properties of Rocks from C.C.S.P. Drill Hole CY-4

Property	n	Arith. Mean	s.e.	s.d.	Geom. Mean
		Diabase			
Comp. velocity (0.1 GPa)/km s^{-1}	16	6.50	0.09	0.37	
Shear velocity (0.1 GPa)/km s^{-1}	16	3.48	0.05	0.19	
Poisson's ratio	16	0.296	0.004	0.015	
Bulk density/kg m^{-3}	111	2,854	8	88	
Grain density/kg m^{-3}	111	2,882	7	75	
Porosity/% vol.	111	1.52	0.14	1.48	0.93
Elect. cond. (0.1 GPa)/mS m^{-1}	16	1.27	0.34	1.38	0.88
Archie's exp.	16	1.91	0.06	0.26	
NRM intensity/A m^{-1}	234	1.35	1.18	0.08	0.96
Inclination of NRM*/degrees	234	41.8	20.3	1.3	
Susceptibility/x10^{-3} S.I.Units	234	79.5	53.5	3.5	55.4
Koenigsberger ratio	234	0.87	1.72	0.11	0.48
		Plagiogranite			
Comp. velocity (0.1 GPa)/km s^{-1}	4	5.77	0.25	0.51	
Shear velocity (0.1 GPa)/km s^{-1}	4	3.35	0.12	0.24	
Poisson's ratio	4	0.243	0.023	0.046	
Bulk density/kg m^{-3}	9	2,741	29	88	
Grain density/kg m^{-3}	9	2,773	30	90	
Porosity/% vol.	9	1.79	0.40	1.21	1.40
Elect. cond. (0.1 GPa)/mS m^{-1}	4	2.11	1.30	2.59	1.00
Archie's exp.	4	2.03	0.07	0.15	
NRM intensity/A m^{-1}	15	1.41	0.50	1.93	0.50
Inclination of NRM/degrees	15	40.7	6.0	23.1	
Susceptibility/x10^{-3} S.I.Units	15	78.9	17.4	67.5	37.0
Koenigsberger ratio	15	0.66	0.26	1.00	0.38
		Gabbro			
Comp. velocity (0.1 GPa)/km s^{-1}	19	6.93	0.05	0.22	
Shear velocity (0.1 GPa)/km s^{-1}	17	3.68	0.04	0.18	
Poisson's ratio	17	0.303	0.004	0.018	
Bulk density/kg m^{-3}	106	2,981	9	97	
Grain density/kg m^{-3}	106	2,989	9	93	
Porosity/% vol.	106	0.424	0.057	0.583	0.290
Elect. cond. (0.1 GPa)/mS m^{-1}	19	0.408	0.089	0.389	0.327
Archie's exp.	19	1.61	0.04	0.16	
NRM intensity/A m^{-1}	175	1.53	0.12	1.60	1.00
Inclination of NRM/degrees	175	22.6	0.83	10.9	
Susceptibility/x10^{-3} S.I. Units	175	16.3	2.5	32.9	6.9
Koenigsberger ratio	175	4.55	0.20	2.67	3.50

Property	n	Arith. Mean	s.e.	s.d.	Geom. Mean
		Websterite			
Comp. velocity (0.1 GPa)/km s^{-1}	3	7.39	0.21	0.37	
Shear velocity (0.1 GPa)/km s^{-1}	3	4.00	0.15	0.27	
Poisson's ratio	3	0.293	0.009	0.015	
Bulk density/kg m^{-3}	15	3,112	34	131	
Grain density/kg m^{-3}	15	3,121	34	133	
Porosity/% vol.	15	0.443	0.072	0.280	0.371
Elect. cond. (0.1 GPa)/mS m^{-1}	4	0.143	0.021	0.043	0.138
Archie's exp.	4	1.71	0.08	0.16	
NRM intensity/A m^{-1}	20	0.86	0.18	0.82	0.62
Inclination of NRM/degrees	20	24.9	1.9	8.6	
Susceptibility/x10^{-3} S.I. Units	20	7.3	1.7	7.6	4.9
Koenigsberger ratio	20	4.03	0.45	2.03	3.53
		Olivine Websterite			
Comp. velocity (0.1 GPa)/km s^{-1}	5	7.26	0.11	0.24	
Shear velocity (0.1 GPa)/km s^{-1}	5	3.89	0.10	0.22	
Poisson's ratio	5	0.298	0.012	0.027	
Bulk density/kg m^{-3}	56	3,147	13	100	
Grain density/kg m^{-3}	56	3,158	13	99	
Porosity/% vol.	56	0.530	0.063	0.468	0.412
Elect. cond. (0.1 GPa)/mS m^{-1}	5	0.183	0.033	0.074	0.170
Archie's exp.	5	2.03	0.13	0.30	
NRM intensity/A m^{-1}	70	1.25	0.16	1.30	0.74
Inclination of NRM/degrees	70	26.4	1.2	10.2	
Susceptibility/x10^{-3} S.I. Units	70	10.2	1.5	12.6	5.6
Koenigsberger ratio	70	3.84	0.21	1.73	3.24
		Pyroxene-Peridotite			
Comp. velocity (0.1 GPa)/km s^{-1}	1	6.29			
Bulk density/kg m^{-3}	3	2,912	70	122	
Grain density/kg m^{-3}	3	2,921	71	123	
Porosity/% vol.	3	0.503	0.019	0.033	0.502
NRM intensity/A m^{-1}	3	7.95	2.03	5.52	7.46
Inclination of NRM/degrees	3	34.6	4.7	8.1	
Susceptibility/x10^{-3} S.I. Units	3	72.5	22.9	39.7	64.4
Koenigsberger ratio	3	3.31	0.48	0.84	3.25

n: number of samples, Arith. mean: arithmetic mean, s.e.: standard error of mean, s.d.: standard deviation of individual values, Geom. mean: geometric mean, *values given are for the modulus of the inclination

GEOLOGY

The alteration state of the diabase varies from fresh to highly altered. Alteration is typically 10-30% but locally may exceed 85%. The mafics are partly altered to chlorite and, to a lesser extent, to epidote and amphibole. The plagioclase may be saussuritized. The rock contains up to 10% disseminated magnetite.

Diorites and trondhjemites have typically over 50% plagioclase, with hornblende and clinopyroxene, or quartz respectively. The transition from the diabase sheeted complex to the gabbroic plutonic complex extends from 247 metres, the depth of the shallowest plutonic screen, to 1288 metres, the deepest dyke. The 'midpoint' of the transition, representing 50% dykes and 50% gabbro, occurs at 724 metres (Hall and Robinson, 1984).

The gabbros range in composition from

leucogabbro to melagabbro with an increase in the proportion of mafics down the section. The degree and nature of alteration also varies with depth. High-level gabbros are chloritized while in the lower-level gabbros pyroxenes have been altered to varying degrees to amphibole with minor serpentinite in fractures and veins. The lower cumulate gabbros have a sharp transition with the websterite which comprises clinopyroxene with minor orthopyroxene, olivine and plagioclase. The pyroxenes have been partly altered to chlorite and amphibole, olivine is partly serpentinized. Plagioclase is typically fresh where it is interstitial and is otherwise usually saussuritized.

The olivine websterite contains from 10-20% olivine, typically serpentinized. The pyroxene, mostly clinopyroxene, is uralitized to varying degrees. The pyroxene-peridotite contains up to 80% olivine. Locally there are thin layers of dunite. The olivine is heavily serpentinized.

Clearly the changes in mineralogy and alteration will be fundamental in the analysis of the variations in physical properties with depth and lithology. Of equal importance in a discussion of the variations in densities, seismic velocities and electrical conductivities, is a consideration of the degree and nature of porosity. Analysis of these properties without prior discussion of the variation in porosity would be premature.

DENSITY AND POROSITY

Figure 1 shows histograms of bulk and grain density and porosity for 300 samples by lithology.

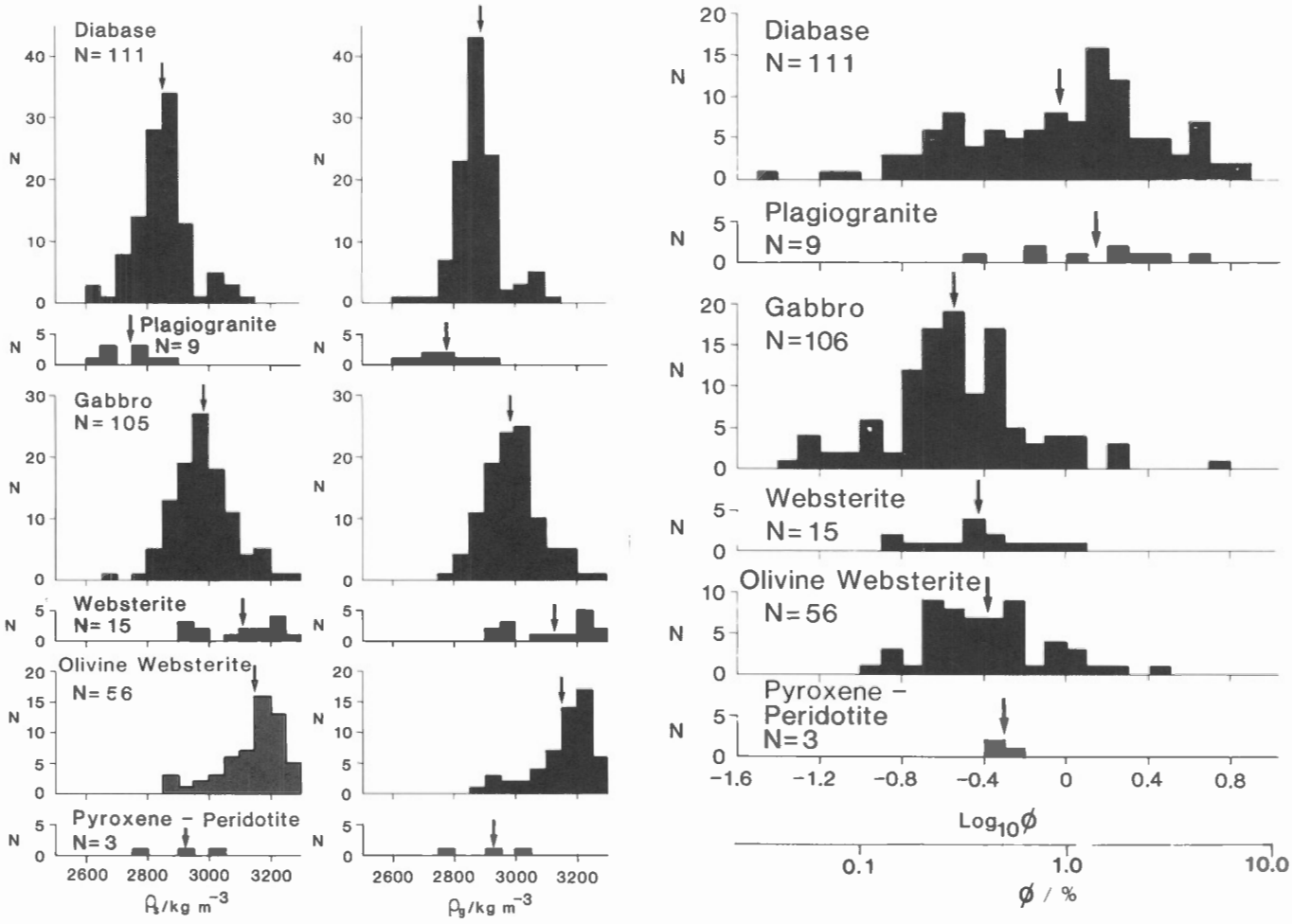

Figure 1: Histograms of saturated bulk density, grain density and $\log_{10}$ (percent porosity) for each major lithology. N is the number of samples. Mean values are arrowed (Geometric mean porosity).

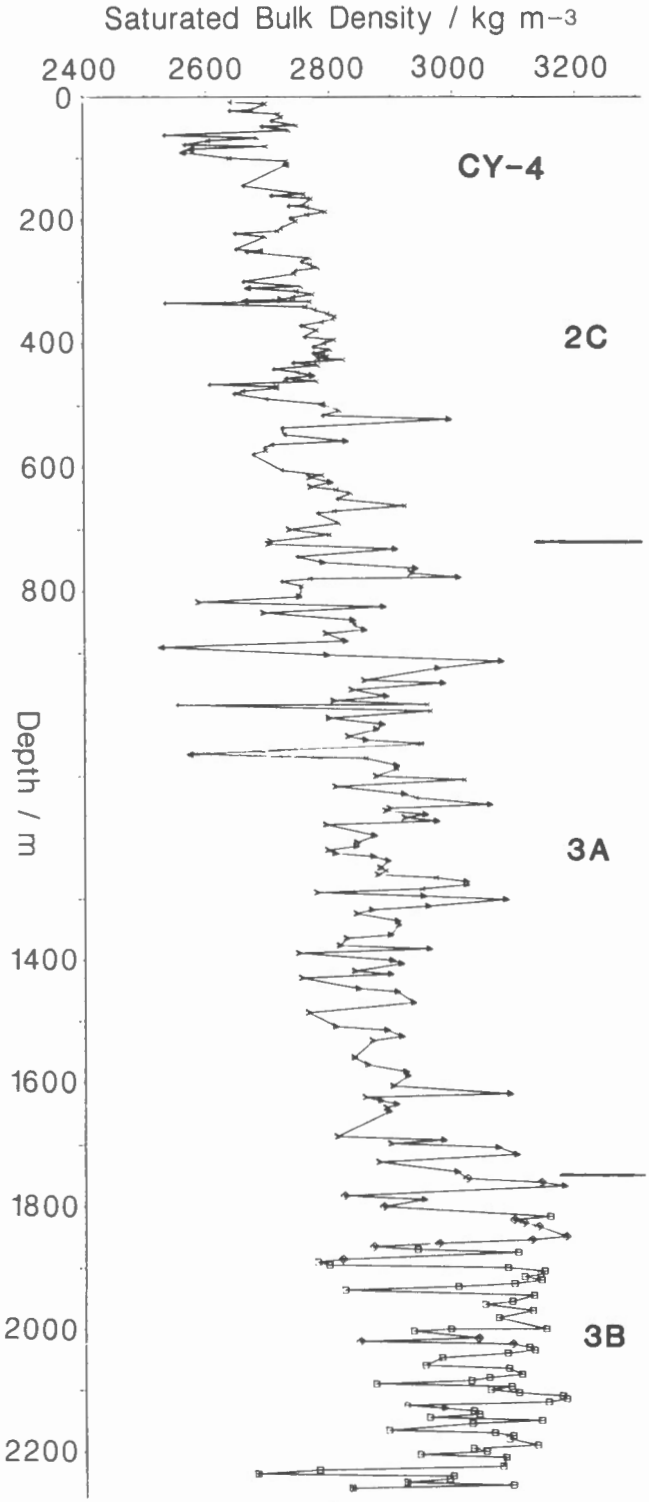

Figure 2a: Saturated bulk densities vs. depth for CY-4. Samples are coded according to lithology as follows:

× = Diabase
◁ = Plagiogranite
▷ = Gabbro
⊖ = Olivine Gabbro
◇ = Websterite
⊟ = Olivine Websterite
⊞ = Pyroxene-Peridotite

The bulk densities of 111 diabase samples range from 2,631 kg m^{-3} to 3,119 kg m^{-3} with a mean and standard deviation of individual values of 2,854 ± 88 kg m^{-3}. Part of the variation in bulk density is due to variations in porosity (from 0.08% to 6.79% with a geometric mean of 0.93%). The grain density ranges from 2,644 kg m^{-3} to 3,123 kg m^{-3} with a mean of 2,882 ± 75 kg m^{-3}. Over 80% of the grain densities are in the range, 2,800 to 2,950 kg m^{-3}. Low grain densities may reflect high proportions of plagioclase (ρ = 2,680 kg m^{-3}) and chloritization of pyroxenes. High grain densities correspond to melanocratic diabases, possibly with a high (up to 10%) proportion of disseminated magnetite. The density in the diabase increases with depth (Figure 2a) reflecting variations in mineralogy and a decrease in porosity with depth (Figure 2b).

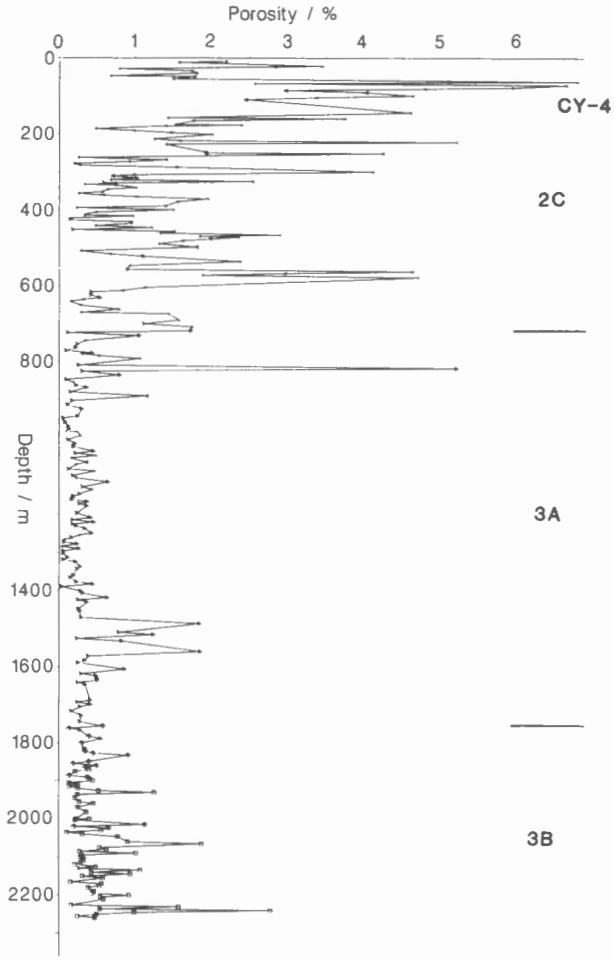

Figure 2b: Porosity vs. depth for CY-4. Symbols as for Figure 2a.

The mean bulk and grain densities of nine plagiogranites are 2,741 ± 129 kg m^{-3} and 2,773 ± 130 kg m^{-3} respectively. The low density of these samples is due to their dominant plagioclase and quartz (ρ = 2,650 kg m^{-3}) mineralogy. The porosities are similar to the diabase, averaging 1.40% (geometric mean).

The bulk densities of 106 gabbro samples range from 2,686 kg m^{-3} to 3,281 kg m^{-3} with a mean of 2,981 ± 97 kg m^{-3}. The grain densities range from 2,777 kg m^{-3} to 3,287 kg m^{-3} with a mean of 2,989 ± 93 kg m^{-3}. The wide range of densities results from the variable mineralogy of the gabbros since the porosity (geometric mean 0.29%) is very low. The data set includes microgabbros, greenschist and amphibolite facies metagabbros, leuco-, meso- and melagabbros and an olivine gabbro. Grain size is also very variable. A single sample of 22 mm length and diameter is inadequate to give a representative density for coarse grained and pegmatitic gabbros where the grain size may exceed the sample dimensions. This may explain, in part, the wide range of densities measured. Nevertheless, the mean values are, statistically, good estimates of the mean.

Websterites and olivine websterites are classified on the basis of the percentage of olivine being less than or greater than 10% respectively. The density of olivine is close to that of clino- and orthopyroxenes. Accordingly the mean bulk densities: 3,112 ± 131 kg m^{-3} and 3,147 ± 100 kg m^{-3}, and grain densities: 3,121 ± 133 kg m^{-3} and 3,158 ± 99 kg m^{-3} for 15 websterites and 56 olivine websterites respectively are very similar. Bulk densities for the two classes range from 2,878 kg m^{-3} to 3,283 kg m^{-3}. Grain densities range from 2,885 kg m^{-3} to 3,291 kg m^{-3}. The density distributions are asymmetrical with 85% of the bulk and grain densities greater than 3,000 kg m^{-3}. Lower values are due to serpentinization of olivine and alteration of pyroxenes to chlorite and amphibole. The geometric mean porosities for the websterites and olivine websterites are 0.37% and 0.41% respectively, significantly higher than the mean of 0.29% for the gabbro. These higher porosities may result from serpentinization (Macdonald and Fyfe, 1985).

The means of the bulk densities and grain densities of three pyroxene-peridotites are 2,913 ± 122 kg m^{-3} and 2,921 ± 123 kg m^{-3} respectively. The geometric mean porosity is 0.50%. If a linear relationship is assumed between the degree of serpentinization (%) and density from fresh peridotite (0%, ρ = 3,300-3,350 kg m^{-3}) and serpentinite (100%, ρ = 2,500-2550 kg m^{-3}) (Shelton, 1984) then the pyroxene-peridotite is 50% serpentinized. This figure compares favourably with estimates of the degree of serpentinization from the drillcore in hand specimen (C.C.S.P. 1985). A similar calculation suggests that the websterites and olivine websterites are on average about 20% serpentinized.

The porosity of the pyroxene-peridotite is greater than the websterite and olivine websterite, providing further evidence of the increase in porosity by serpentinization (see below).

COMPRESSIONAL AND SHEAR WAVE VELOCITIES

Compressional (P) and shear (S) wave velocities and Poisson's ratios are given in Table 2 at an 'effective' pressure (i.e. confining pressure minus pore fluid pressure) of 0.1 GPa which is representative of such pressures in the lower oceanic crust. There is a good correlation between the velocities and densities for the samples. Thus a large element of the variability in seismic velocities can be explained by variations in mineralogy.

P and S-wave velocities in the 16 diabase samples range from 5.92 km s^{-1} to 7.14 km s^{-1} and 3.14 km s^{-1} to 3.80 km s^{-1} respectively with mean values of 6.50 ± 0.37 km s^{-1} and 3.48 ± 0.19 km s^{-1}. The mean Poisson's ratio is 0.296 ± 0.015, between the Poisson's ratio of plagioclase and clinopyroxene. The more porous diabase samples tend to have slightly lower velocities. Diabase velocities increase down the drill hole with a P-wave velocity gradient of approximately 0.4 km s^{-1} which may reflect the decrease in porosity with depth (Figures 2b and 2c).

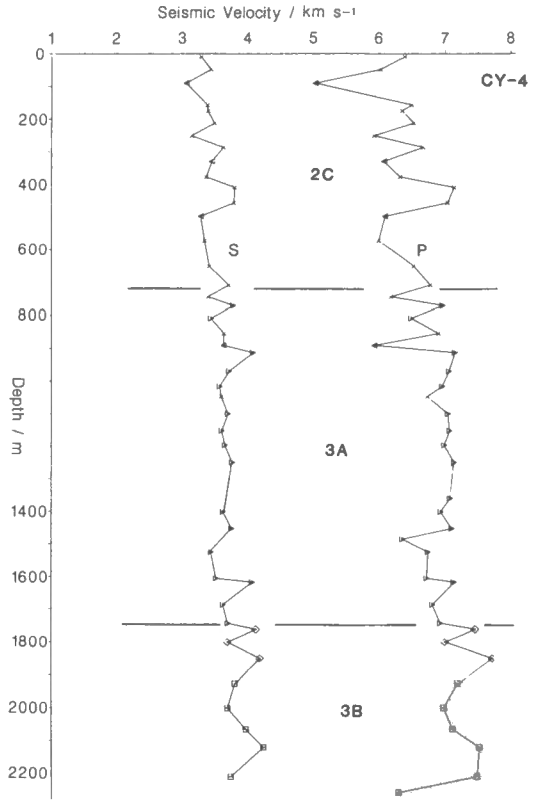

Figure 2c: Seismic velocities vs. depth for CY-4. Symbols as for Figure 2a.

TABLE 2. Seismic Velocities and Poisson's ratios at 0.1 GPa

n	Lithology	Depth (m)	d (kg m^{-3})	P (kms^{-1})	S (kms^{-1})	P.r.
CY-4-1	Diabase	10.05	2739	6.39	3.28	0.321
CY-4-15	Diabase	49.01	2790	6.02	3.43	0.260
CY-4-32	Trondhjemite	90.80	2663	5.02	3.06	0.205
CY-4-50	Diabase	157.87	2859	6.49	3.38	0.314
CY-4-55	Diabase	175.49	2858	6.34	3.39	0.300
CY-4-70	Diabase	212.85	2822	6.52	3.49	0.300
CY-4-90	Diabase	251.41	2766	5.92	3.14	0.304
CY-4-103	Diabase	286.94	2844	6.66	3.62	0.290
CY-4-119	Diorite	329.88	2763	6.07	3.45	0.261
CY-4-139	Diabase	377.45	2880	6.31	3.36	0.302
CY-4-152	Diabase	409.19	2903	7.14	3.80	0.303
CY-4-171	Diabase	455.86	2829	7.04	3.78	0.297
CY-4-188	Diorite	496.85	2888	6.08	3.28	0.295
CY-4-205	Diabase	571.50	2797	5.99	3.34	0.275
CY-4-220	Diabase	649.96	2912	6.52	3.41	0.312
CY-4-234	Diabase	707.86	2900	6.78	3.70	0.288
CY-4-242	Diabase	743.46	2846	6.18	3.39	0.284
CY-4-248	Mela-Gabbro	770.35	3033	6.96	3.77	0.292
CY-4-258	Altered-Gabbro	808.13	2851	6.49	3.44	0.304
CY-4-269	Diabase	854.08	2940	6.90	3.63	0.309
CY-4-275	Trondhjemite	890.03	2625	5.92	3.62	0.201
CY-4-279	Mela-Gabbro	912.42	3179	7.15	4.08	0.259
CY-4-290	Gabbro	968.87	2992	7.06	3.71	0.309
CY-4-296	Gabbro	1015.35	2986	6.96	3.57	0.321
CY-4-302	Diabase	1046.59	3049	6.73	3.59	0.301
CY-4-311	Leuco(?)Gabbro	1099.46	2975	7.04	3.70	0.309
CY-4-320	Gabbro	1151.38	2997	7.07	3.60	0.325
CY-4-328	Pegmatitic Gabbro	1195.78	2973	6.99	3.65	0.313
CY-4-337	Gabbro	1248.77	2982	7.14	3.76	0.308
CY-4-346	Gabbro	1300.88	3187	6.92	3.65	0.307
CY-4-355	Gabbro	1358.92	2999	7.08	—	—
CY-4-362	Gabbro	1400.18	3002	6.94	3.62	0.313
CY-4-371	Gabbro	1451.66	3010	7.11	3.75	0.307
CY-4-378	Gabbro	1485.14	2865	6.35	—	—
CY-4-384	Gabbro	1524.56	3017	6.74	3.44	0.324
CY-4-397	Gabbro	1605.35	3002	6.72	3.51	0.312
CY-4-399	Gabbro	1617.32	3192	7.14	4.06	0.260
CY-4-411	Mela(?)Gabbro	1686.16	2911	6.81	3.62	0.303
CY-4-421	Gabbro	1743.60	3106	6.93	3.69	0.302
CY-4-423	Websterite	1760.83	3243	7.46	4.12	0.281
CY-4-429	Websterite	1800.01	2986	7.00	3.69	0.308
CY-4-438	Websterite	1848.77	3282	7.72	4.18	0.293
CY-4-453	Olivine Websterite	1925.80	3198	7.19	3.80	0.306
CY-4-469	Olivine Websterite	1999.95	3094	6.98	3.69	0.307
CY-4-482	Olivine Websterite	2065.00	3189	7.12	3.97	0.275
CY-4-493	Olivine Websterite	2120.17	3253	7.52	4.23	0.268
CY-4-511	Olivine Websterite	2210.05	3184	7.49	3.74	0.334
CY-4-521	Pyroxene-Peridotite	2259.15	2933	6.29	—	—

n: sample number, d: saturated bulk density, P: P-wave velocity, S: S-wave velocity, P.r.: Poisson's ratio

The two diorites have comparable velocities and Poisson's ratios to the diabase. The two trondhjemites have anomalously low Poisson's ratios (0.205, 0.201) and P-wave velocities due to their high quartz content. The S-wave velocities are, however, comparable to those observed in the diabase. Because the diorite and trondhjemite are laterally discontinuous in the ophiolite section (and presumably in the oceanic section) the significance of the low velocities and Poisson's ratio will be limited.

Velocities in the gabbro range from 6.35 km s^{-1} to 7.15 km s^{-1} for P-waves and 3.44 km s^{-1} to 4.08 km s^{-1} for S-waves with mean values of 6.93 ± 0.22 km s^{-1} and 3.68 ± 0.18 km s^{-1} respectively. Poisson's ratios range from 0.295 to 0.325 with a mean of 0.303 ± 0.018. The range of P-wave velocities in the gabbro is comparable to that of the diabase. However, the range of values disguises the fact that the majority of velocities lie within a very narrow range. Fifteen of the nineteen P-wave velocities are between 6.8 km s^{-1} and 7.15 km s^{-1} while 11 of the 17 S-wave velocities are in the range 3.6 km s^{-1} to 3.8 km s^{-1}. The mean P and S-wave velocities are approximately 0.4 km s^{-1} and 0.2 km s^{-1} higher than mean velocities in the diabase. There is no apparent increase in velocity with depth in the gabbro.

The lowest velocities were observed in altered gabbros such as that from 808.13 m in which most of the pyroxene is altered to chlorite and amphibole, or from 1485.14 m where serpentine occurs in fractures. High velocities were measured in the more mafic samples such as that from 912.42 metres, a meta-melanogabbro with up to 90% of mafic minerals, or from 770.35 metres which contains over 60% of mafic minerals, mostly clinopyroxene. The melanogabbros have anomalously high S-wave velocities and correspondingly low Poisson's ratios as the Poisson's ratios of clinopyroxenes range from 0.21 to 0.27.

The mean velocities in the websterite and the olivine websterite are 7.39 ± 0.37 km s^{-1} and 7.26 ± 0.24 km s^{-1} for P-waves and 4.00 ± 0.27 km s^{-1} and 3.89 ± 0.22 km s^{-1} for S-waves for three websterite and five olivine websterite samples respectively. These velocities are approximately 0.4 km s^{-1} and 0.25 km s^{-1} higher than mean velocities in the gabbro. P and S-wave velocities range from 6.95 km s^{-1} to 7.72 km s^{-1} and 3.69 km s^{-1} to 4.23 km s^{-1} respectively. Poisson's ratios range from 0.268 to 0.334 with a mean of 0.296 ± 0.022. High Poisson's ratios of 0.306 to 0.334 were determined from partly serpentinized samples while the relatively fresh websterites and olivine websterites have lower Poisson's ratios of 0.268 to 0.293. There are negative correlations between S-wave velocity and Poisson's ratio, and between density and Poisson's ratio which suggest that the physical effects of serpentinization are a reduction in S-wave velocity over and above the reduction in the P-wave velocity, resulting in an increase in Poisson's ratio, and a reduction in density as described above.

The P-wave velocity in one sample of pyroxene-peridotite is 6.29 km s^{-1}. From estimates of the mineral composition of the lithologic unit from which this sample was taken we would expect a P-wave velocity of 8.17 km s^{-1} before serpentinization. P-wave velocities measured in oceanic serpentinites are as low as 4.10 km s^{-1} at 0.1 GPa (Christensen and Salisbury, 1975). Assuming a linear relationship between the degree of serpentinization and velocity, a P-wave velocity of 6.29 km s^{-1} indicates approximately 50% serpentinization, a similar value to that deduced from the density measurements and from a visual assessment of the extent of serpentinization.

The velocities throughout the section are systematically higher than were determined by logging of the drill hole (Salisbury, 1989). The discrepancy arises partly because the velocities quoted are at 0.1 GPa whereas 'effective' pressures in the drill hole will range from zero to 0.045 GPa at the base. In addition, part of the discrepancy may arise from the presence of macroscopic fractures and voids in situ which are not represented in the sample set. In particular, in the upper 500 metres of the section the velocity gradient deduced from logging may be as much as 1.0 km s^{-1}, significantly higher than that estimated from our laboratory measurements, suggesting that macroscopic fractures play an increasingly important role in lowering the in situ velocities towards the top of the drill hole.

On the basis of the laboratory seismic velocities, the section represented in CY-4 can be divided into three units which correlate with oceanic seismic layers 2C, 3A and 3B. The contacts between layers 2C and 3A, and 3A and 3B are drawn at 724 metres and 1750 metres respectively; at the midpoint of the gradual transition from the sheeted dykes to isotropic gabbro, and at the sharp transition from gabbro to cumulate ultramafics.

Within layer 2C, velocities (and densities) increase with depth with a decrease in porosity. P-wave velocities range from 6.0 to 7.0 km s^{-1}, compared with the typical layer 2C velocity (Houtz and Ewing, 1976) of 6.1 km s^{-1} determined from sonobuoy records.

Layer 3A velocities and densities determined from the Troodos gabbros are very uniform with little variation with depth. The mean velocity of 6.93 km s^{-1} is somewhat higher than the typical value of 6.7 km s^{-1} determined from oceanic refraction seismics. The in situ velocity may be substantially lower due to macroscopic fractures. The discrepancy between the in situ and laboratory values implies a macroscopic porosity of approximately 4% in addition to the laboratory small scale porosity of 0.4%.

The mean laboratory P-wave velocities for the CCSP diabase and gabbro samples (6.50 ± 0.37 and

6.93 ± 0.22 respectively) compare closely with mean values determined for a compilation of velocity measurements on 23 diabase and 54 gabbro samples from other ophiolite complexes (ie. from Papua New Guinea, (Kroenke et al., 1976), California, (Christensen, 1978), Samail, Oman, (Christensen and Smewing, 1981), and Bay of Islands, Newfoundland, (Salisbury and Christensen, 1978)) of 6.31 ± 0.41 and 7.01 ± 0.31 respectively.

A number of explanations have been proposed for the non-ubiquitous high velocity basal layer 3B of Sutton et al. (1971). It may be due to progressive serpentinization of ultramafic material thus giving an apparent thickening of the crust with age by depressing the seismic moho (Lewis and Snydsman, 1977). However, the serpentinization may occur to such an extent that a low velocity zone, rather than a high velocity basal layer, occurs at the base of the lower crust. Furthermore, the recent re-analysis of seismic data by McLain and Atallah (1986) suggests that serpentinization is not as important a process, and thickening of the crust not as substantial as was formerly thought. An alternative explanation draws largely upon evidence from ophiolites. Velocities measured on olivine gabbros from the Samail ophiolite (Christensen and Smewing, 1981) and the Bay of Islands ophiolite (Salisbury and Christensen, 1978) are comparable to layer 3B velocities determined from oceanic seismic studies. Ewing and Houtz (1979) equate the Bay of Islands pyroxene gabbro, olivine gabbro and troctolite with layer 3B. Karson et al. (1984) and Brocher et al. (1985) define a zone of interlayered mafic and ultramafic cumulates as the 'moho transition zone' which ranges from a sharp geological and seismic discontinuity to a 3 km thick transition zone between mafic and ultramafic lithologies, perhaps comparable to the super-moho cumulate sequence interpreted from reflection seismics in the western North Atlantic by Mutter et al. (1985).

The interpretation appropriate to the Troodos section draws on a combination of the above explanations. The 3A-3B boundary is geologically and seismically abrupt, reflecting the transition from mafic (gabbro) to ultramafic (predominantly websterite and olivine websterite) cumulates. The observed velocities in the ultramafics of V_p = 7.3 km s^{-1} and V_s = 3.9 km s^{-1} are intermediate between the mafic layer 3A velocities (V_p = 6.7 km s^{-1}, V_s = 3.7 km s^{-1}) and anhydrous peridotite (mantle) velocities (V_p = 8.1 km s^{-1}, V_s = 4.7 km s^{-1}) and fall clearly in the range of basal crustal layer velocities (V_p = 7.1 - 7.7 km s^{-1}). The observed velocities are lower than would be anticipated from fresh websterites and olivine websterites as they are slightly serpentinized (up to 20%). To the base of the recovered section the limited data suggest that much lower velocities and densities are associated with more highly serpentinized olivine-rich ultramafics, predominantly dunites and pyroxene-peridotites. The evidence from the Troodos thus suggests that layer 3B may consist of, or at least include, partially serpentinized cumulate ultramafics. Elsewhere, 3B velocities have been determined from serpentinized upper mantle and from olivine gabbros.

ELECTRICAL CONDUCTIVITY

Observed electrical conductivities, porosities and calculated values of Archie's exponent 'm' are given in Table 3. Conductivities are given at an 'effective' pressure of 0.1 GPa. The samples are saturated with seawater since it now seems clear that the oceanic crust is saturated with seawater to depths of several kilometres and most probably to the base of the crust (Drury, 1979). The electrical conductivity of laboratory samples depends upon a combination of conduction through pore-fluids, clay mineral conduction and mineral semi-conduction. Where pore-fluid conduction is dominant, the relationship between conductivity and porosity is given by Archie's Law (Archie, 1942) which states that:

$$\sigma = a\sigma_f\phi_v^{\,m}$$

where σ_f is the conductivity of the pore-fluid (here seawater; σ_f = 4.54 S m^{-1}), ϕ_v is the interconnected porosity expressed as a fraction of the rock's volume, and 'a' and 'm' are constants. 'a' is a dimensionless constant typically close to and often taken as one, and the exponent 'm' has been shown from analogue simulation of porosity using resistor arrays (Shankland and Waff, 1974) to be equal to one if the porosity is in the form of narrow ('low aspect-ratio') cracks, and two if in the form of rounded voids. However, previous measurements on fresh and mineralized lavas (Smith and Vine, 1987) have shown that in practice, if 'a' is assumed to be one, the value of 'm' may be as high as three where pore-fluid conduction is through randomly connected rounded vesicles. A good correlation between 'm' and porosity was noted. For the CY-4 samples, clay mineral conduction is typically of limited importance as the rocks are relatively fresh. At 20°C, mineral semi-conduction is negligible. Thus assuming an Archie relationship between electrical conductivity and porosity, 'm' can be calculated and may give an insight into the nature of the porosity.

The conductivities of the 16 diabase samples range from 0.301 mS m^{-1} to 5.70 mS m^{-1} with a geometric mean of 0.88 mS m^{-1}. The mean value of 'm' derived from Archie's law assuming 'a' = 1 and a pore-fluid conductivity of 4.54 S m^{-1} is 1.91 ± 0.26 suggesting that conduction in thin cracks and rounded voids are both significant. The diabase has minor vesicularity and it would appear that the vesicles are connected by a network of thin cracks.

TABLE 3. Electrical Conductivity at 0.1 GPa

Sample Number	Lithology	Depth	Electrical Conductivity (mSm^{-1})	Porosity (%)	Archie's Exponent 'm'
CY-4-1	Diabase	10.05	2.748	2.19	1.94
CY-4-15	Diabase	49.01	5.699	1.78	1.66
CY-4-32	Trondhjemite	90.80	5.784	4.02	2.08
CY-4-50	Diabase	157.87	0.681	1.42	2.07
CY-4-55	Diabase	175.49	1.120	1.52	1.99
CY-4-70	Diabase	212.85	1.310	1.24	1.86
CY-4-90	Diabase	251.41	2.473	4.25	2.38
CY-4-103	Diabase	286.94	0.870	1.54	2.05
CY-4-119	Diorite	329.88	0.380	0.72	1.90
CY-4-139	Diabase	377.45	0.414	1.54	2.23
CY-4-152	Diabase	409.19	0.732	0.37	1.56
CY-4-171	Diabase	455.86	0.689	1.51	2.10
CY-4-188	Diorite	496.85	2.062	1.80	1.92
CY-4-205	Diabase	571.50	1.110	1.87	2.09
CY-4-220	Diabase	649.96	0.301	0.28	1.63
CY-4-234	Diabase	707.86	1.078	1.74	2.06
CY-4-242	Diabase	743.46	0.490	0.34	1.61
CY-4-248	Mela-Gabbro	770.35	0.313	0.10	1.38
CY-4-258	Altered-Gabbro	808.13	0.511	0.26	1.53
CY-4-269	Diabase	854.08	0.242	0.19	1.57
CY-4-275	Trondhjemite	890.03	0.224	1.15	2.22
CY-4-279	Mela-Gabbro	912.42	0.320	0.11	1.41
CY-4-290	Gabbro	968.87	0.261	0.12	1.45
CY-4-296	Gabbro	1015.35	0.194	0.21	1.63
CY-4-302	Diabase	1046.59	0.435	0.49	1.74
CY-4-311	Leuco(?)Gabbro	1099.46	0.494	0.18	1.45
CY-4-320	Gabbro	1151.38	0.127	0.19	1.67
CY-4-328	Pegmatitic Gabbro	1195.78	0.199	0.24	1.66
CY-4-337	Gabbro	1248.77	0.286	0.43	1.77
CY-4-346	Gabbro	1300.88	0.250	0.06	1.31
CY-4-355	Gabbro	1358.92	0.270	0.19	1.55
CY-4-362	Gabbro	1400.18	0.398	0.29	1.60
CY-4-371	Gabbro	1451.66	0.268	0.27	1.65
CY-4-378	Gabbro	1485.14	1.875	1.84	1.95
CY-4-384	Gabbro	1524.56	0.234	0.24	1.63
CY-4-397	Gabbro	1605.35	0.836	0.86	1.81
CY-4-399	Gabbro	1617.32	0.338	0.29	1.63
CY-4-411	Mela(?)Gabbro	1686.16	0.402	0.41	1.70
CY-4-421	Gabbro	1743.60	0.178	0.27	1.72
CY-4-423	Websterite	1760.83	0.174	0.14	1.54
CY-4-429	Websterite	1800.01	0.185	0.30	1.74
CY-4-438	Websterite	1848.77	0.110	0.39	1.92
CY-4-445	Websterite	1885.50	0.102	0.14	1.63
CY-4-453	Olivine Websterite	1925.80	0.167	0.52	1.95
CY-4-469	Olivine Websterite	1999.95	0.175	0.40	1.84
CY-4-482	Olivine Websterite	2065.00	0.196	1.87	2.53
CY-4-493	Olivine Websterite	2120.17	0.084	0.21	1.77
CY-4-511	Olivine Websterite	2210.05	0.292	0.94	2.07

The conductivity of the four plagiogranite samples ranges from 0.224 to 5.78 mS m^{-1} with a geometric mean conductivity of 1.00 mS m^{-1}, comparable to the diabase. The Archie's exponent 'm' also has a similar mean value of 2.03. There is a good positive correlation between Archie's exponent and porosity for the diabase and plagiogranite suggesting, not surprisingly, that rounded voids constitute a higher proportion of the total porosity in the more porous samples. The conductivity of the diabase decreases down the section with a decrease in porosity (Figure 2d).

Conductivities in the gabbros range from 0.127 mS m^{-1} to 1.88 mS m^{-1} with a geometric mean of 19 samples of 0.327 mS m^{-1}, significantly lower than the diabase and plagiogranite. The low mean Archie's 'm' of 1.61 suggests that pore-fluid conduction is dominantly through narrow cracks. There is no apparent increase or decrease in the conductivity with depth.

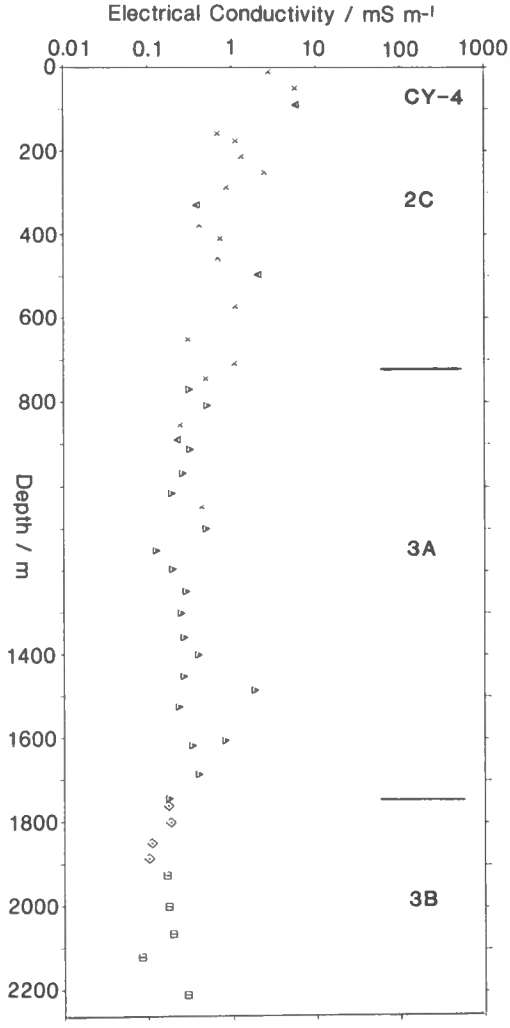

Figure 2d: Electrical conductivity vs. depth for CY-4. Symbols as for Figure 2a.

Although the porosity of the websterite and olivine websterite is greater than that of the gabbro, the conductivity is lower, ranging from 0.084 to 0.292 mS m^{-1} with a geometric mean for nine samples of 0.155 mS m^{-1}. As a result the mean value of 'm' of 1.89 is significantly higher than the gabbro and is comparable to that of the diabase. The porosity of the websterite and olivine websterite has been modified by alteration, most probably due to partial serpentinization along fractures. The volume porosity of several serpentinized peridotites was determined by Macdonald and Fyfe (1985) to be typically 2-3%. Under the scanning electron microscope stacks of platy lizardite were seen lying parallel to each other and perpendicular to the fracture walls. It is suggested that defects in the serpentine structure may be responsible for the significant porosity of the serpentinized peridotite. Similarly, it appears that serpentinization of the websterite and olivine websterite cause both an increase in porosity and an increase in the pore-aspect ratio by an increase in the fracture width and by the partial infilling of fractures with a relatively high aspect ratio framework of serpentine minerals. The measured conductivity is therefore lower than we would expect to measure from fresh rocks of similar porosity.

On the basis of the conductivity the section represented in CY-4 can be divided into three units which correlate with seismic layers 2C, 3A and 3B as defined above; the diabase and plagiogranite which have a relatively high conductivity and vesicular and crack porosity, the low porosity and conductivity gabbro with conduction predominantly through narrow cracks, and the cumulate ultramafics which are less conductive than the gabbro but of higher porosity with conduction through partly serpentinized fractures.

For all three units we note a good correlation between porosity and Archie's exponent. In particular, for the websterite and olivine websterite:

$$m = 1.61 + 0.504\,\phi$$

where ϕ is the percentage porosity. This relationship has a correlation coefficient of 0.97. It would be interesting to test the relationship over a wider range of degrees of serpentinization.

In situ conductivities will be greater than the values determined from these laboratory measurements due to additional conduction in macroscopic pores and fractures not represented in the laboratory sample set. Discrepancies between laboratory and, for example, logging data can give an indication of the extent of large scale fracturing in the crust.

MAGNETIC PROPERTIES

On the basis of the observed magnetic properties the section represented in CY-4 can be divided into three major units (III, IV and V) which correspond approximately to the diabase and plagiogranite; the gabbro, websterite and olivine websterite; and the pyroxene-peridotite. Units I, II and upper unit III are described by Smith and Vine (in prep.). The boundaries between these units are thought to be metamorphic in character and do not correlate with the layer boundaries defined from density, porosity, velocity and electrical conductivity measurements. Figure 3 shows histograms of the magnetic properties by lithology. NRM intensity, susceptibility and Koenigsberger ratio are log-normally distributed. It is usual practice therefore to give the geometric mean as a representative value of the sample set. However, in considering the potential of a unit as a source layer for marine anomalies it is the arithmetic mean which is applicable (Harrison, 1976). Therefore in Table 4 we have summarized both mean values of NRM, susceptibility and Koenigsberger ratio.

The magnetic properties of the diabase and the plagiogranite (unit III) are very similar. The NRM intensity is low (approximately 1 Am^{-1}) and the susceptibility very high so that the Koenigsberger ratio is less than one. Both the NRM intensity and susceptibility increase with depth in the section (Figures 2e and 2f) to a depth of approximately 600 metres. At 600 metres there is a sharp decrease in susceptibility and a small reduction in NRM intensity. There is a marked change in the values of Koenigsberger ratios from typically less than one in the dykes (and the few gabbros) above 600 m, to mostly greater than one in the gabbros (and in many of the dykes) below 600 m. This level is interpreted as the boundary between greenschist facies metamorphism above, and amphibolite facies metamorphism below.

The gabbro, websterite and olivine websterite (unit IV) have comparable NRM intensities to the diabase and plagiogranite, but much lower susceptibility giving a Koenigsberger ratio of typically greater than three. The NRM and susceptibility of the gabbro tend to decrease with depth. Values for the websterite and olivine websterite are more variable than for the gabbro.

The pyroxene-peridotite (unit V) is distinct from the gabbro and websterite unit above in having high NRM intensity and high susceptibility. However, as the values are an order of magnitude higher in each case the Koenigsberger ratios for the pyroxene-peridotites are directly comparable to those of the gabbros and websterites. The high intensities of magnetization in the pyroxene-peridotites have been noted previously (Vine et al. 1973). They are assumed to be due to an enhanced magnetite content in these rocks resulting from the higher degree of serpentinization than in the websterites above.

The NRM inclination data summarized in Table 1 and in Figures 2h and 3 are potentially relevant to a number of structural and lithological problems. Within the gabbros and ultramafics the inclination is remarkably consistent, averaging about +24°, but systematically lower than that of the primary (i.e. late Cretaceous) remanent magnetization vector deduced for the Troodos complex by Vine and Moores (1969) and Clube et al. (1985), i.e. 275°:+34°. Assuming that these inclinations are directed to the west, this could simply reflect an easterly tilt of the complex in this area, of approximately 10°, away from the centre of uplift to the west. (Clearly it would be more correct to use remanent magnetization data measured after 'cleaning' of the samples in making this comparison. However, other studies (eg. Moores and Vine, 1971; H.P. Johnson, pers. comm.) have shown that there is little or no change in the direction of the remanent magnetization of the gabbros and cumulate ultramafics with demagnetization.)

TABLE 4. Mean Values of Magnetic Properties

Lithology	N	J_{NRM}/A m^{-1}		$\chi/10^{-3}$ S.I.		Q_n	
		Arith. Mean	Geom. Mean	Arith. Mean	Geom. Mean	Arith. Mean	Geom. Mean
Diabase	234	1.35	0.96	79.5	53.5	0.87	0.48
Plagiogranite	15	1.41	0.50	78.5	37.0	0.66	0.38
Gabbro	175	1.53	1.00	16.3	6.9	4.55	3.50
Websterite	20	0.86	0.62	7.3	4.9	4.03	3.53
Olivine Websterite	70	1.25	0.74	10.2	5.6	3.84	3.24
Websterite + Olivine Websterite	90	1.16	0.71	9.6	5.4	3.88	3.30
Pyroxene-Peridotite	3	7.95	7.46	72.5	64.5	3.31	3.25

N: number of samples, Arith. mean: arithmetric mean, Geom. mean: geometric mean

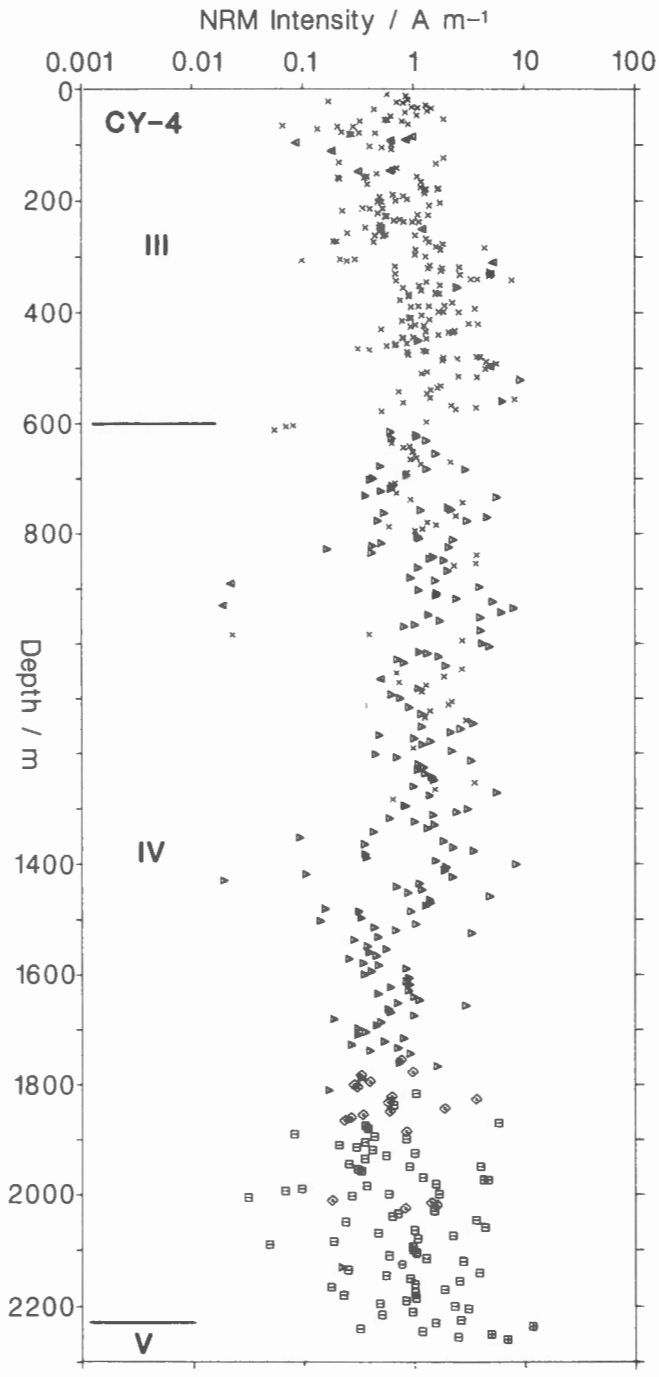

Figure 2e: NRM intensity vs. depth for CY-4. Symbols as for Figure 2a.

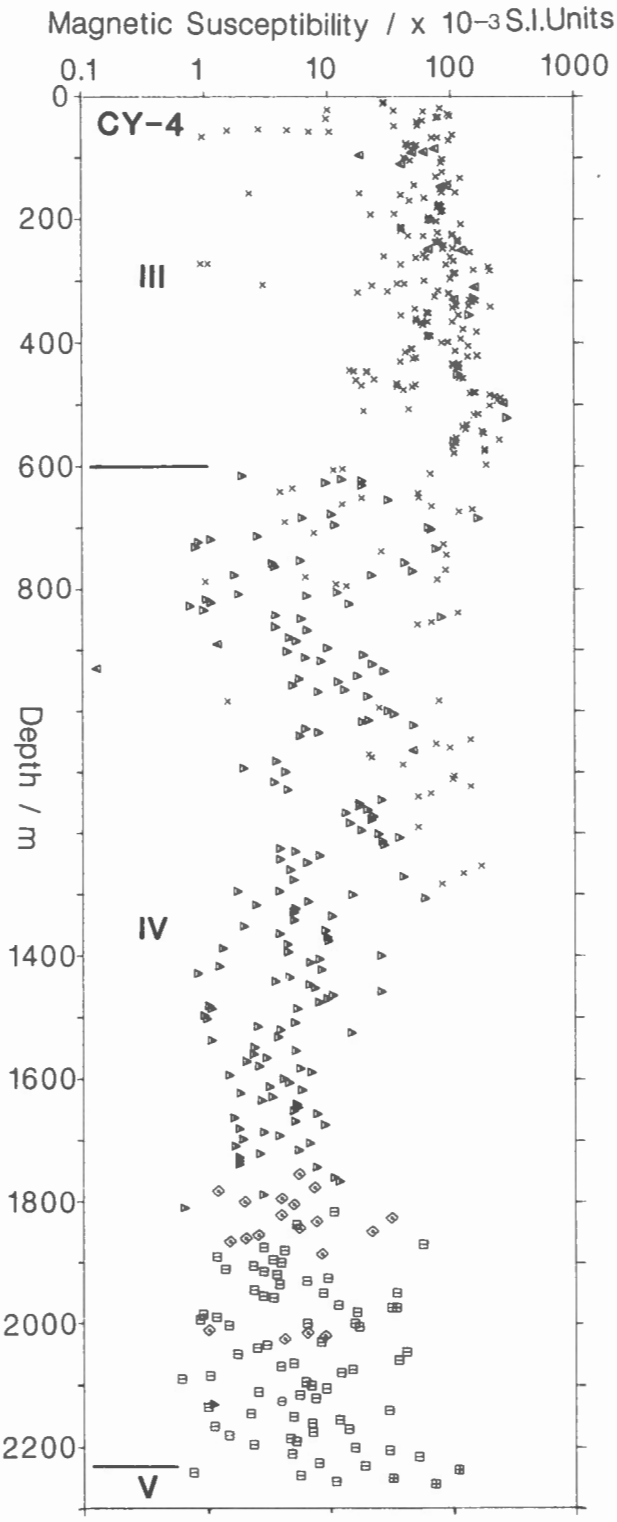

Figure 2f: Magnetic susceptibility vs. depth for CY-4. Symbols as for Figure 2a.

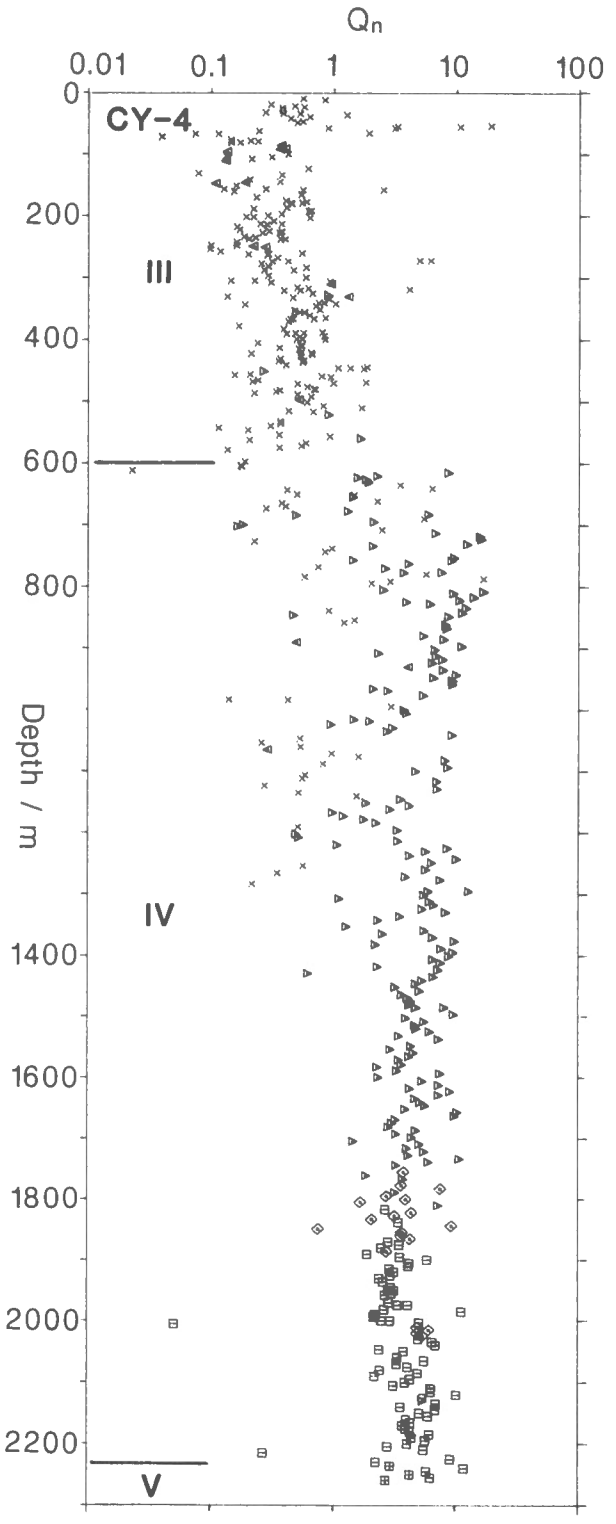

Figure 2g: Koenigsberger ratio vs. depth for CY-4. Symbols as for Figure 2a.

The fact that the NRM inclinations of the serpentinized ultramafics are very comparable to those of the gabbros, and so different to that of the present dipole field direction (+54°), strongly suggests that the serpentinization occurred in the Cretaceous and is a sea-floor process, rather than in the Late Tertiary, say, in association with the uplift of the complex. This lends support to the interpretation given above that the serpentinized ultramafics might be representative of all, or at least part, of oceanic layer 3B. In that the thermal regime at a ridge crest probably prohibits serpentinization in the immediate vicinity of the ridge axis, off-axis serpentinization is indicated. Thus, although some of this serpentinized material is very strongly magnetized, because the serpentinization occurs off axis and presumably at a sub-horizontal 'front', essentially controlled by a geotherm and the availability of water, it is very unlikely that it is a source region for the linear oceanic magnetic anomalies (Vine and Moores, 1972).

Within the sheeted diabases there is a large scatter of NRM inclinations with a mean inclination (+42°) intermediate between that of the gabbros and the present dipole field. Previous studies have shown that this scatter may be produced by secondary components of magnetization and/or structural rotations on listric faults (Moores and Vine, 1971; Allerton and Vine, 1987). Although such effects will clearly reduce the directional coherence and effective magnetization contrasts in the diabase layer the intensity of magnetization in the diabases, and in the gabbros, is such that they might well make a secondary but potentially important contribution to linear magnetic anomalies as discussed by Kidd (1977).

The NRM inclinations (Figures 2h and 3) are predominantly positive with the notable exception of a section within the olivine websterite. However, the negative inclinations determined in this section are not observed by other investigators and are therefore attributed to misorientation of the samples.

The distribution of rock-types in the section is shown schematically in Figure 2i.

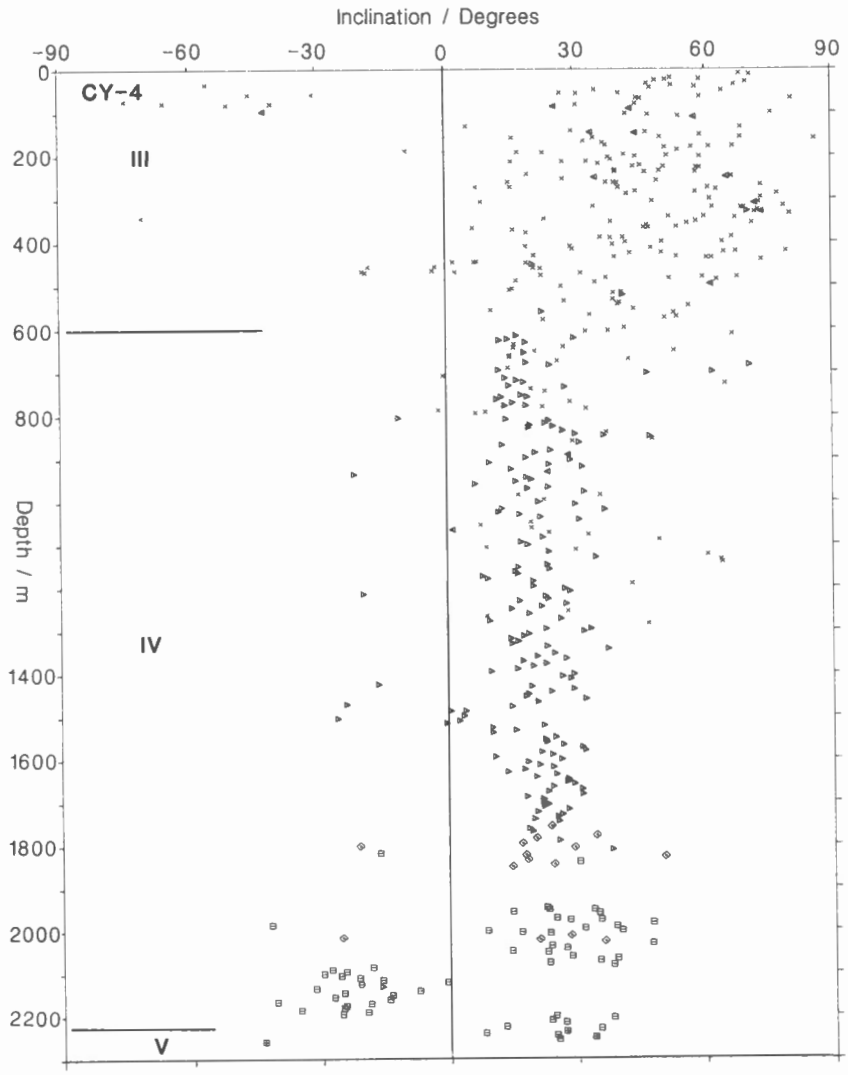

Figure 2h: NRM inclinations vs. depth for CY-4. Symbols as for Figure 2a.

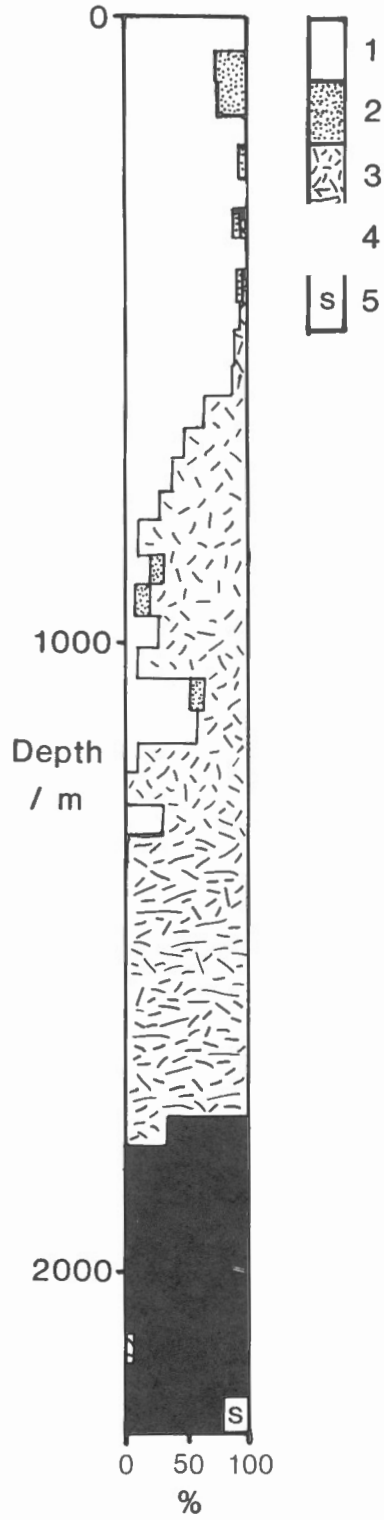

Figure 2i: Schematic geological section for CY-4 showing the variation in abundance of rock types over 50 m intervals. 1. Diabase; 2. Plagiogranite; 3. Gabbro; 4. Pyroxenite; 5. Highly serpentinized pyroxene-peridotite.

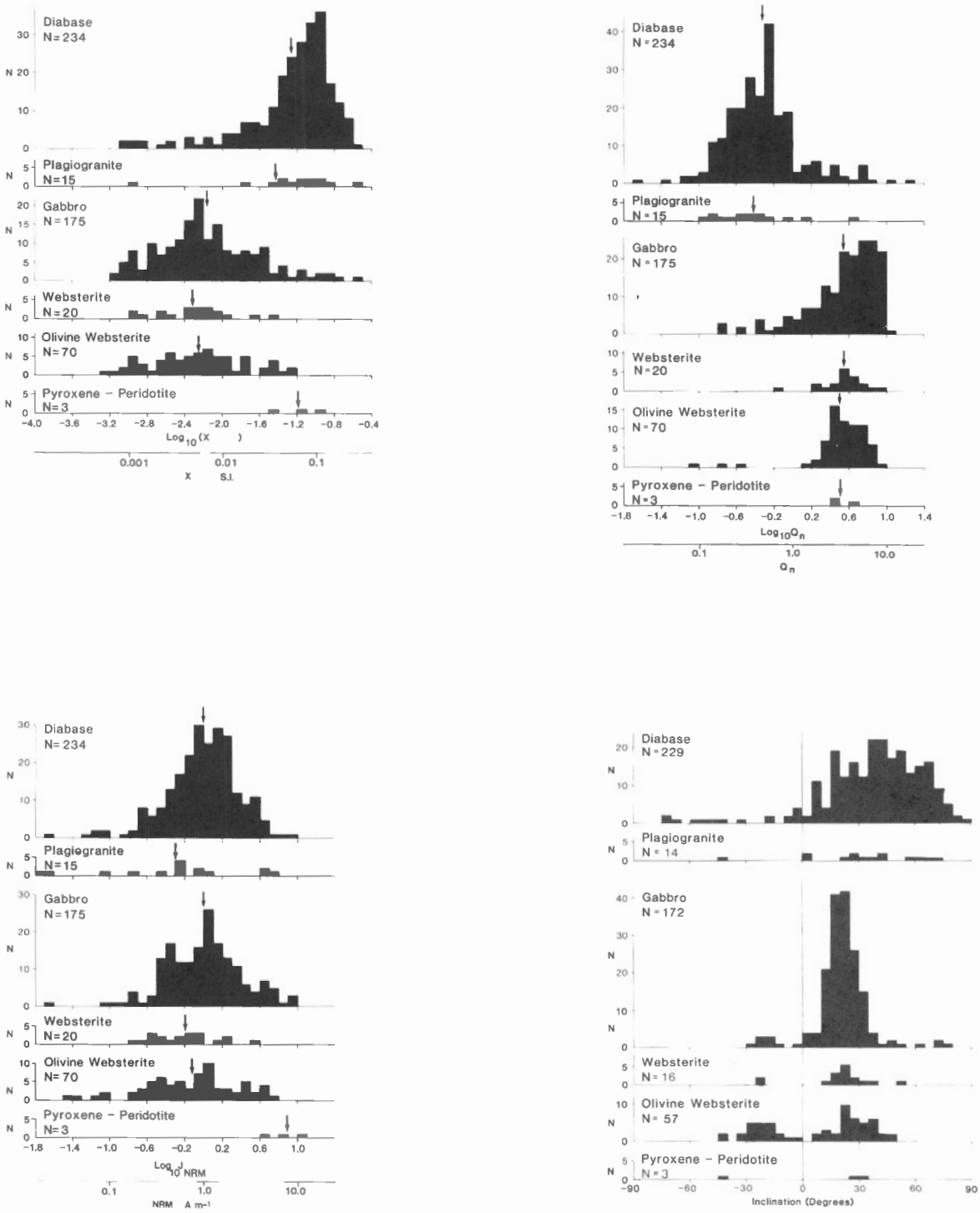

Figure 3: Histograms of $\log_{10}$ (NRM intensity), $\log_{10}$ (magnetic susceptibility), $\log_{10}$ (Koenigsberger ratio) and NRM inclination. N is the number of samples. Geometric mean values are arrowed.

SUMMARY

The laboratory measurements demonstrate that the section of the ophiolite represented in the CY-4 drillcore can be subdivided on the basis of physical properties into layers comparable to the oceanic seismic layers 2C, 3A and 3B.

Layer 2C, which extends to 724 metres, the midpoint of the transition from the sheeted dykes to isotropic gabbro, is characterized by gradients in the physical properties. Seismic velocities and densities increase with depth whereas porosity and electrical conductivity decrease. The NRM intensity and susceptibility both increase with depth down to 600 metres, the greenschist to amphibolite facies boundary. Within the gabbro, velocities, density, porosity and electrical conductivity show relatively little variation. Below 600 metres there is a gradual decrease in NRM intensity and susceptibility with depth. The layer 3A to 3B contact at 1750 metres corresponds to a sharp transition from gabbro to websterite reflected by a sharp increase in velocity and density. There is, however relatively little change in porosity, electrical conductivity or in magnetic properties at this boundary. The limited data available from the pyroxene-peridotites, websterites and olivine websterites suggest that profound changes in physical properties might occur within layer 3B as a result of serpentinization. The velocities and density are lowered and the Poisson's ratio increases as a result of serpentinization. There is evidence of an increase in porosity coupled with changes in the nature of the porosity itself resulting, paradoxically, in a decrease in conductivity. Furthermore the NRM intensity and susceptibility of the more highly serpentinized pyroxene-peridotite are anomalously high.

The features described above provide a qualitative model which compares well with observations in the oceans. A detailed quantitative comparison with measurements on drilled oceanic samples is beyond the scope of this paper. Suffice it to say that where legitimate comparisons can be made, the values determined in this study generally compare favourably with oceanic data although the magnetic susceptibility tends to be rather high (e.g. Dunlop and Prevot, 1982; Smith, 1985; Hyndman and Drury, 1976; Christensen and Salisbury, 1975, 1985; Hyndman 1979, Karson and Fox, 1986).

A remaining problem is that, in common with most ophiolites, the Cyprus section is anomalously thin compared to 'normal' oceanic crust. The 'oceanic layer' (layer 3A + 3B) is typically 5 km thick (Dunlop and Prevot, 1982) whereas layer 3 as we have defined it in CY-4 could well be less than 2 km thick. This may reflect the proximity of CY-4 to the Arakapas Fault Zone which is thought to be a fossil transform fault (Simonian and Gass, 1978). Thinning of the crust is commonly observed close to fracture zones (White et al., 1984). An alternative and tantalizing explanation is that had the drill hole extended several hundred metres further it might have broken through into a second magma chamber and therefore into a second plutonic sequence of isotropic and cumulate gabbro and ultramafics, as postulated by Moores and Vine (1971). Were the latter to be the case, cyclical variations in seismic velocities and density might be seen on a large scale, reflecting the alternating sequence of gabbro and ultramafics with major implications for seismic reflection experiments.

REFERENCES

Allerton, S. and Vine, F.J.
1987: Spreading structure of the Troodos ophiolite, Cyprus: some palaeomagnetic constraints; Geology, v. 15, p. 593-597.

Anderson, R.N., Honnorez, J., Becker, K., Adamson, A.C., Alt, J.C., Emmermann, R., Kempton, P.D., Kinoshita, H., Laverne, C., Mottl, M.J. and Newmark, R.L.
1982: DSDP Hole 504B, the first reference section over 1 km through Layer 2 of the oceanic crust; Nature, v. 300, p. 589-594.

Archie, G.E.
1942: The electrical resistivity log as an aid in determining some reservoir characteristics; American Institute of Mining, Metallurgical, and Petroleum Engineers, Transactions, Petroleum Division, v. 146, p. 54-67.

Birch, F.
1960: The velocity of compressional waves in rocks to 10 kilobars, Part 1; Journal of Geophysical Research, v. 65, no. 4, p. 1083-1102.

Brocher, T.M., Karson, J.A. and Collins, J.A.
1985: Seismic stratigraphy of the oceanic Moho based on ophiolite models; Geology, v. 13, p. 62-65.

C.C.S.P. (Cyprus Crustal Study Project)
1985: CY-4 Core Descriptions, Vol. 1-4.

Christensen, N.I.
1978: Ophiolites, seismic velocities and oceanic crustal structure; Tectonophysics, v. 47, p. 131-157.

Christensen, N.I. and Salisbury, M.H.
1975: Structure and constitution of the lower oceanic crust; Reviews of Geophysics and Space Physics, v. 13, no. 1, p. 57-86.
1985: Seismic velocities, densities and porosities of layer 2B and layer 2C basalts from hole 504B; *in* Initial Reports of the Deep Sea Drilling Project, Volume 83, ed. R.N. Anderson, J. Honnorez, K. Becker et al.; U.S. Government Printing Office, Washington, D.C., v. 83, p. 367-370.

Christensen, N.I. and Smewing, J.D.
1981: Geology and seismic structure of the northern section of the Oman Ophiolite; Journal of Geophysical Research, v. 86, no. B4, p. 2545-2555.

Clube, T.M.M., Creer, K.M. and Robertson, A.H.F.
1985: Palaeorotation of the Troodos microplate, Cyprus; Nature, v. 317, p. 522-525.

Drury, M.J.

1979: Electrical resistivity models of the oceanic crust based on laboratory measurements on basalts and gabbros; Geophysical Journal of the Royal astronomical Society, v. 56, p. 241-253.

Dunlop, D.J. and Prevot, M.
1982: Magnetic properties and opaque mineralogy of drilled submarine intrusive rocks; Geophysical Journal of the Royal astronomical Society, v. 69, p. 763-802.

Ewing, J. and Houtz, R.
1979: Acoustic stratigraphy and structure of the oceanic crust; *in* Deep Drilling Results in the Atlantic Ocean: Oceanic Crust, ed. M. Talwani, C. Harrison, and D. Hayes; AGU Monograph, Maurice Ewing Series, v. 2 , p. 1-14.

Fox, P.J., Schreiber, E. and Peterson, J.J.
1973: The geology of the oceanic crust: compressional wave velocities of oceanic rocks; Journal of Geophysical Research, v. 78, p. 5155-5172.

Hall, J.M. and Robinson, P.T.
1984: The transition from the sheeted complex to the intrusive complex in the Troodos ophiolite as recorded in Cyprus Crustal Study Project drill hole CY-4; Abstract, Geological Association of Canada, Joint Annual Meeting, London, Ontario, Canada.

Harrison, C.G.A.
1976: Magnetization of the oceanic crust; Geophysical Journal of the Royal astronomical Society, v. 47, p. 257-283.

Houtz, R. and Ewing, J.
1976: Upper crustal structure as a function of plate age; Journal of Geophysical Research, v. 81, no. 14, p. 2490-2498.

Hyndman, R.D.
1979: Poisson's ratio in the oceanic crust - a review; Tectonophysics, v. 59, p. 321-333.

Hyndman, R.D. and Drury, M.J.
1976: The physical properties of oceanic basement rocks from deep drilling on the Mid-Atlantic Ridge; Journal of Geophysical Research, v. 81, no. 23, p. 4042-4052.

Karson, J.A., Collins, J.A. and Casey, J.F.
1984: Geologic and seismic velocity structure of the crust/mantle transition in the Bay of Islands ophiolite complex; Journal of Geophysical Research, v. 89, p. 6126-6138.

Karson, J.A. and Fox, P.J.
1986: Geological and geophysical investigations of the Mid-Cayman spreading centre: seismic velocity measurements and implications for the constitution of layer 3; Geophysical Journal of the Royal Astronomical Society, v. 85, p. 389-411.

Kidd, R.G.W.
1977: The nature and shape of the sources of marine magnetic anomalies; Earth and Planetary Science Letters, v. 33, p. 310-320.

Kroenke, L.W., Manghnani, M.H., Fryer, C.S. and Ramananantoandro, R.
1976: Elastic properties of selected ophiolitic rocks from Papua New Guinea: nature and composition of oceanic lower crust and upper mantle; *in* The Geophysics of the Pacific Ocean Basin and it's Margin, ed. G.H. Sutton, M.H. Manghnani, and R. Moberly; AGU Monograph, no. 19, p. 407-421.

Lewis, B.T.R. and Snydsman, W.E.
1977: Evidence for a low velocity layer at the base of the oceanic crust; Nature, v. 266, p. 340-344.

Macdonald, A.H. and Fyfe, W.S.
1985: Rate of serpentinization in seafloor environments; Tectonophysics, v. 116, p. 123-135.

McLain, J.S. and Atallah, C.A.
1986: Thickening of the oceanic crust with age; Geology, v. 14, p. 574-576.

Moores, E.M. and Vine, F.J.
1971: The Troodos Massif, Cyprus, and other ophiolites as oceanic crust: evaluation and implications; *in* A Discussion on the Petrology of Igneous and Metamorphic Rocks from the Ocean Floor; Philosophical Transactions of the Royal Society of London, Series A, v. 268, p. 443-466.

Mutter, J.C. and North Atlantic Transect (NAT) Study Group
1985: Multichannel seismic images of the oceanic crust's internal structure: evidence for a magma chamber beneath the Mesozoic Mid-Atlantic Ridge; Geology, v. 13, p. 629-632.

Salisbury, M.H., Christensen, N.I., Vine, F.K., Smith, G.C. and Eleftheriou, S.
1989: Geophysical structure of the Troodos ophiolite from downhole logging; *in* Cyprus Crustal Study Project: Initial Report, Hole CY-4, ed. I.L. Gibson, J. Malpas, P.T. Robinson and C. Xenophontos; Geological Survey of Canada, Paper 88-9.

Salisbury, M.H. and Christensen, N.I.
1978: The seismic velocity structure of a traverse through the Bay of Islands ophiolite complex, Newfoundland: an exposure of oceanic crust and upper mantle; Journal of Geophysical Research, v. 83, no. B2, p. 805-817.

Shankland, T.J. and Waff, H.S.
1974: Conductivity in fluid-bearing rocks; Journal of Geophysical Research, v. 79, no. 2, p. 4863-4868.

Shelton, A.W.
1984: Geophysical studies on the northern Oman ophiolite; unpublished Ph.D. thesis, The Open University, Milton Keynes, U.K.

Simonian, K.O. and Gass, I.G.
1978: The Arakapas fault belt, Cyprus: a fossil transform fault; Geological Society of America Bulletin, v. 89, p. 1220-1230.

Smith, G.C. and Vine, F.J.
1987: Electrical conductivity of basalts from CCSP Drill Holes CY-2 and CY-2a at Agrokipia Mines,

Cyprus; *in* Cyprus Crustal Study Project, Initial Report: Holes CY-2 and 2a, ed. P.T. Robinson, I.L. Gibson and A. Panayiotou; Geological Survey of Canada, Paper 85-29, p. 339-346.

Smith, G.M.
1985: Source of marine magnetic anomalies: some results from DSDP Leg 83; Geology, v. 13, p. 162-165.

Sutton, G.H., Maynard, G.L. and Hussong, D.M.
1971: Widespread occurrence of a high-velocity basal layer in the Pacific crust found with repetitive sources and sonobuoys; *in* The Structure and Physical Properties of the Earth's Crust, Geophysical Monograph Series, Vol. 14, ed. J.G. Heacock; AGU, Washington, D.C., p. 193-209.

Vine, F.J. and Moores, E.M.
1969: Palaeomagnetic results of the Troodos igneous massif, Cyprus; EOS, American Geophysical Union Transactions, v. 50, p. 131.
1972: A model for the gross structure, petrology and magnetic properties of oceanic crust; *in* Studies in Earth and Space Sciences, ed. R. Shagam, R.B. Hargraves, W.J. Morgan, F.B. Van Harten, C.A. Burk, H.D. Holland and L.C. Hollister; Geological Society of America, Memoir, v. 132, p. 195-205.

Vine, F.J., Poster, C.K. and Gass, I.G.
1973: Aeromagnetic survey of the Troodos igneous massif, Cyprus; Nature, Physical Science, v. 244, no. 133, p. 34-38.

White, R.S., Detrick, R.S., Sinha, M.C. and Cormier, M.H.
1984: Anomalous seismic crustal structure of oceanic fracture zones; Geophysical Journal of the Royal Astronomical Society, v. 79, p. 779-798.

In Situ Stress Measurements and Natural Fracture Logging in Drill Hole CY-4, the Troodos Ophiolite, Cyprus

J. BAUMGARTNER[1], F. RUMMEL[1], B.C. HAIMSON[2] AND M.Y. LEE[2]

[1]Institute of Geophysics, Ruhr University Bochum, W. Germany
[2]Geological Engineering Program, University of Wisconsin-Madison, Madison, Wisconsin, 53706, USA

Baumgartner, J., Rummel, F., Haimson, B.C. and Lee, M.Y., In situ stress measurements and natural fracture logging in drillhole CY-4, the Troodos ophiolite, Cyprus; in *Cyprus Crustal Study Project: Initial Report, Hole CY-4, ed. I.L. Gibson, J. Malpas, P.T. Robinson and C. Xenophontos; Geological Survey of Canada, Paper 88-9, p. 315-330, 1989.*

Abstract

Hydraulic fracturing stress measurements were conducted in the upper open-hole segment of drillhole CY-4 (0-600 m). Based on the results of some twenty hydraulic fracture orientations two stress fields were discerned, one near the surface (50-200 m depth) and apparently strongly affected by local topographic relief, and another at 200-600 m. The latter stress field was calculated using two different data analysis methods. Based on conventional calculations the state of stress in the range of 200-600 m is given by $S_v = 0.28$ bar/m × depth (m), $S_h = 12 + 0.16$ bar/m × depth (m) at N22°W, $S_H = 7 + 0.25$ bar/m × depth (m) at N68°E (where S_v is the vertical stress, S_H is the major horizontal stress, and S_h is the minor horizontal stress). Using the P_s-technique, the state of stress in the 200-600 m zone is given by: $S_v = 0.28$ bar/m × depth (m), $S_h = 0.17$ bar/m × depth (m) at N11°W, $S_H = -6 + 0.28$ bar/m × depth (m) at N79°E. The two methods of interpretation yielded similar values for both magnitudes and direction of principal stresses. A borehole sonic televiewer (BHTV) was used to log natural fractures crossing the hole wall. The BHTV logging revealed a state of densely spaced natural fractures of varying inclinations and orientations, dominated by two steeply dipping sets. Also detected on the borehole wall were several segments of spalling (breakouts) which appear to be associated with zones of closely spaced natural fractures.

Résumé

Des mesures des contraintes de fractures hydrauliques ont été effectuées dans le segment ouvert supérieur du forage CY-4 (0-600 m). A partir des résultats vingt orientations préférentielles des fractures hydrauliques et deux champs de contraintes ont été définis; le premier près de la surface (50-200 m de profondeur) et apparemment fortement influencé par le relief topographique local et le deuxième à 200-600 m de profondeur. Ce dernier champ de contraintes a été calculé en utilisant deux méthodes d'analyse numérique différentes. Selon les calculs conventionnels de l'état des contraintes dans l'intervalle 200-600 m on obtient: $S_v = 0.28$ bar/m × profondeur (m) $S_h = 12 + 0.16$ bar/m × profondeur (m) à N22°W; $S_h = 7 + 0.25$ bar/m × profondeur (m) à N68°E (où S_v est la contrainte verticale, S_H la contrainte horizontale principale et S_h la contrainte horizontale mineure). En utilisant la technique de calcul–P_s, l'état des contraintes dans l'intervalle 200-600 m obtentu est: S_v= 0.28 bar/m × profondeur (m), $S_h = 0.17$ bar/m × profondeur (m) a Nll°W, $S_H = -6 + 0.28$ bar/m × profondeur (m) à N79°E. Les deux méthodes d'interprétation ont généré des valeurs comparables et pour les intensités et pour la direction des contraintes principales. Un moniteur sonique de sondage (MSS) a été utilisé pour repérer les fractures naturelles sur les parois du trou. L'enregistrement continu du MSS a montré un réseau dense de fractures naturelles d'inclinaison et d'orientation diverses où dominaient deux familles caractérisées par des forts pendages. De plus de nombreux intervalles à effritement (broyage) ont été détectés dans les portions du forages où les fractures naturelles sont les plus rapprochées.

INTRODUCTION

In situ measurements of the contemporary stress field in the upper earth's crust are necessary for constraining models of tectonic processes and plate motions, and for the understanding of crustal stability and seismicity (Haimson, 1978; Zoback and Zoback, 1980; Rummel et al., submitted for publication). The hydraulic fracturing technique (hydrofracturing) provides the opportunity to conduct in situ stress measurements in deep drill holes and to determine the variation of stresses with depth (Scheidegger, 1962; Kehle, 1964; Haimson, 1968; Von Schoenfeldt, 1970). In the specific tectonic situation of Cyprus, stress measurements may help understand the complex micro-plate system in the Eastern Mediterranean (McKenzie, 1972; Robertson and Woodcock, 1980; Shelton and Gass, 1980); however, no reliable stress data exist for this region.

During the summer of 1984, hydrofracturing stress measurements were conducted in drill hole CY-4, near the village of Palekhori as part of the Cyprus Crustal Study Project. This hole was drilled from an altitude of about 1000 m into the northeastern flank of the Cyprus Ophiolite Complex to a final depth of 2175 m. The stress measurements were limited to the upper 600 m because below this depth some 200 m of partly damaged casing remained stuck in the hole after the completion of drilling. For this reason all stress measurements performed were actually located above the sea level.

The in situ tests were carried out as a cooperative project between the University of Wisconsin (B. Haimson) and Ruhr University in Bochum (F. Rummel) using the Bochum wireline hydrofrac system. Test sections were selected by core inspection. In addition a borehole sonic televiewer (BHTV) logging was conducted by the University of Wisconsin to gain additional information on the distribution of natural fractures and to determine the existence of preferred fracture orientations. A series of laboratory tests on drill-core samples has also been performed to determine material properties such as fracture toughness, hydrofrac tensile strength, and permeability.

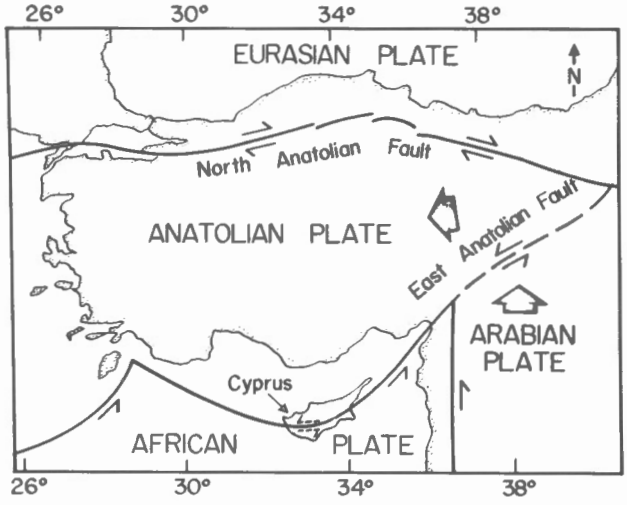

Figure 1: Tectonic condition in the Eastern Mediterranean region (from Turcotte and Schubert, 1982).

SITE DESCRIPTION

Cyprus is part of the complex Eastern Mediterranean micro-plate system, situated at the boundary between the African Plate and the Anatolian Plate; but its detailed plate tectonic condition is still not entirely understood. Some tectonic models expect a continuation of the Eastern Anatolian Fault in a loop through Cyprus towards the Cretean Arc near Rhodos (Lort, 1971; McKenzie, 1972) (Figure 1); however, no severe seismicity can be observed in Cyprus. Based mainly on palaeomagnetic data, several authors propose a rotation of the 'Cyprus Microplate' itself or a rotation of the whole Eastern Mediterranean region in the range of about 90° since the Campainian (85 Ma) (Moores and Vine, 1971; Shelton and Gass, 1980) (Figure 2).

The first deep in situ stress measurements in this tectonically complex region have been carried out in the CY-4 drill hole (34°54′06″N, 33°05′38″E; surface altitude: 1000 m above sea level) and are reported in this paper.

The drill core material down to 650 m consists mainly of medium to fine grained diabase (dykes) with a dense net of zeolite, calcite and epidote veins (see also: Horne and Robinson, 1984).

Figure 2: Rotation models: a) Cyprus only, b) regional rotation (from Shelton and Gass, 1980).

TECHNIQUES AND TESTING PROCEDURES

Fracture (Joint) Logging

Prior to hydrofracturing tests, the University of Wisconsin team used its slim borehole sonic televiewer (BHTV) to log the natural fractures (joints) crossing drill hole CY-4 between 50 and 620 m depth.

The BHTV is a downhole logging tool that can produce a continuous, oriented, acoustic image of the borehole wall (Zemanek et al., 1969). The major components of the BHTV are a piezoelectric transducer, a flux-gate magnetometer, and associated electronics. A motor inside the sonde rotates the transducer and the magnetometer three revolutions per second about the axis of the borehole. The transducer transmits and receives directed narrow acoustic pulses (at approximately 1.2 MHz) about 600 times per revolution. In an uncased hole the magnetometer senses the magnetic field of the earth and provides the orientation of the acoustic image with respect to magnetic north. As the tool is lifted on a wireline at a constant speed (typically 1.5-2 m/min) the emitted acoustic signal sweeps the borehole surface in the form of a densely spaced helix. The reflected acoustic pulse is conveyed as an electric signal to the surface panel via the wireline conductors. The amount of reflected energy depends on the surface properties of the borehole and is represented as the amplitude of the signal. If a discontinuity crosses the borehole wall the low reflectivity of the discontinuity results in a low amplitude of the reflected signal. The reflected acoustic signal is fed into a X-Y-Z CRT (Cathode Ray Tube) monitor for real-time display and to a video cassette recorder for permanent recording. Real-time recording is carried out by photographing the signal sweeping on the monitor. A resultant BHTV polaroid picture is obtained for each minute of BHTV travel showing the borehole wall folded out flat with azimuth as the X-axis, depth as the Y-axis, and intensity of the trace as the Z-axis. A bright trace represents good reflectivity, and a dark trace corresponds to low reflected amplitude such as when intercepting a discontinuity. A vertical fracture plane intersecting a vertical borehole is represented in the picture as two vertical dark lines 180° apart. Non-vertical fractures appear as dark sinusoidal signatures. The dip direction (90° to the strike) of non-vertical fractures is determined by the azimuth of the lower peak of the sinusoidal curve. The dip angle is calculated from the arctangent of the sinusoidal curve amplitude divided by the borehole radius. Horizontal fractures are represented by dark horizontal lines. Photographs of selected segments of CY-4 BHTV log are shown in Figure 3.

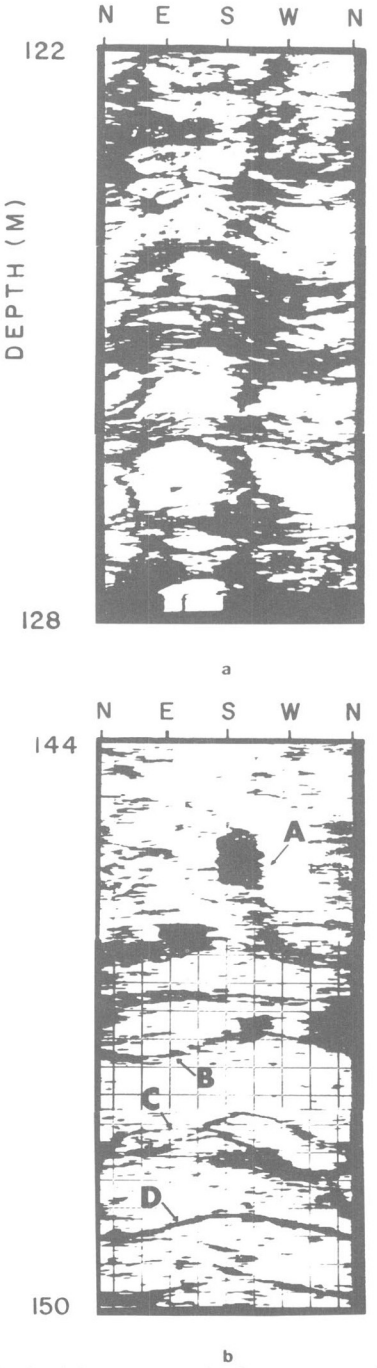

Figure 3: Typical borehole televiewer records in CY-4: (a) closely spaced fractures, strikes at N30°- 60°E and dipping 0-85° have created apparent borehole spalling (breakouts) along two vertical lines at N30°-60°E and at S30°- 60°W. (b) typical segment in which a variety of natural fractures are observed: (A) is a very steeply inclined fracture, striking at N45°E, and dipping 87° to the NW; fractures (B), (C), (D) are all steeply inclined (73°NE, 77°NW, 70°N, respectively) striking at widely different directions (N50°E, N32°E, N78°W, respectively).

Hydrofracturing

In 1973 a wireline-based hydraulic fracturing system was successfully developed at the Ruhr-University. This system is capable of measurements down to 1.5 km depth. Figure 4 shows a schematic view of the present system. Its main components are a straddle packer unit which is tripped into the borehole on a seven conductor logging cable, a heavy-duty aluminum tripod and a hydraulically driven winch and pumping system (maximum flow-rate 9 l/min, maximum pressure 500 bar) mounted on a trailer. All operations are controlled from inside a field truck which carries the main hydraulic switch board and the analog and digital data recording equipment. The packers and the injection interval are pressurized via a flexible high pressure hose, which is clamped to the borehole cable every 30 m. A precision push-pull valve mounted on top of the straddle packer assembly allows to switch from packer pressurization to injection into the hydrofrac interval, and the reverse, by simply releasing or pulling the borehole cable.

The straddle packer assembly consists of two 1 m long nylon reinforced rubber packers and a 70 cm injection adaptor. Injection and packer pressures are measured downhole by an integrated amplifier pressure transducer. Surface and downhole pressures, pumping rate, and total flow are recorded on a strip chart recorder, on an analog magnetic tape and are digitally stored on a hard disc. A detailed description of the hydrofrac system is given by Baumgartner (1987).

Hydrofracture orientations were determined by using an impression packer in conjunction with a magnetic-compass-single-shot tool. The impression packer consisted of a regular packer element around which was wrapped a soft synthetic rubber sheet which preserved an imprint of the drill hole wall when pressurized for more than 30 minutes. To avoid errors caused by magnetic field alteration, the initial tests were conducted using both a gyroscopic compass system (University of Wisconsin) and the magnetic compass device simultaneously. For these tests the magnetic single shot unit was attached to the bottom of the impression packer while the gyroscopic system was mounted on top of the packer.

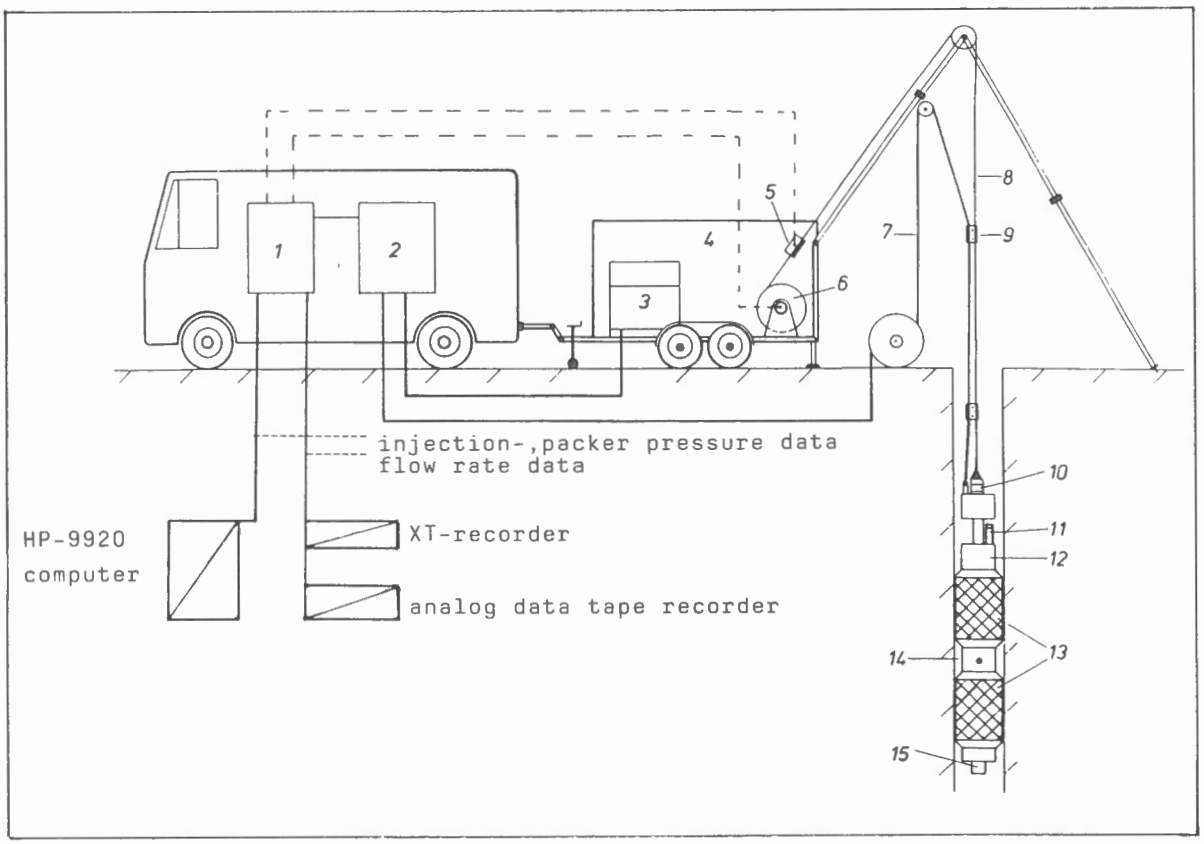

Figure 4: The wireline hydrofracturing system for stress measurements (1) data recording, (2) pressure and flow control, (3) pumping unit, (4) hydraulic winch, (5) depth measuring system, (6) cable drum, (7) high pressure hose, (8) seven conductor cable, (9) clamp to connect hose and cable, (10) cablehead including pressure transducer, (11) packer pressure release valve, (12) push-pull valve, (13) packer elements, (14) injection interval, (15) signal lead-through for additional components.

Generally, after inspection of both core and televiewer logs obviously unfractured drill hole sections were selected as test zones. After packers were set the testing procedure started with a permeability test. For this purpose the test interval was pressurized to a low pressure level (25-40 bar above the water column pressure) and the pump was then shut-off. The pressure drop within the closed system was observed for about 4-5 minutes. Rock permeability can be estimated from these tests by comparing the measured pressure decay with theoretically derived pressure decay curves (Heuser, 1982). In those test intervals proven intact by the permeability tests, the injection pressure was raised until a hydrofracture was initiated which was then propagated in several cycles at a maximum pumping rate of about 9 l/min. During each pumping cycle a volume of about 15-20 l was injected followed by pump shut-off. The pressure decrease was carefully recorded for the eventual identification of the shut-in pressure (P_s). Between injection cycles the whole system was completely vented.

For stress computation the pumping tests yielded the breakdown (critical) pressure, P_c, the hydrofracture reopening pressure, P_r, and the shut-in pressure, P_s, at which level the fracture was just barely open against the acting normal-stress component. In some cases slow pumping tests were used in order to obtain independent shut-in pressure data.

After completion of all the hydrofracturing tests, fracture orientations were obtained with the impression packer system described above. The fracture impression was documented by wrapping a transparent plastic sheet around the impression packer and then marking the fracture traces and the orientation line on it.

RESULTS

Fracture (Joint) Logging

The objective of the BHTV logging was to assess the fracture or joint regime in the hole and assist in selecting appropriate hydrofracturing test intervals. Attempts were made to correlate the fractures logged on the drill hole wall with those observed in the extracted core, and with the in situ stress results obtained from hydrofracturing.

The extracted core was carefully examined in order to identify the fractures shown on the BHTV pictures; however, it was nearly impossible to correlate them one-to-one. The difficulty was a result of the non-oriented nature of the cores, the large amount of mechanical breaks in the core, and the low resolution of BHTV records with respect to low angle fractures (dips under 30°). Although we could not match each fracture individually, we were able to correlate general trends such as zones of intense fracturing (e.g. 370-380 m) and segments of low fracture density (e.g. 260-280 m).

The borehole televiewer log is described in detail in Table 1. Generally drill hole CY-4 can be defined as moderately fractured with an overall density of about 1 fracture/meter. However, there are segments (such as at 50-118 m, 150-152 m, 370-380 m) where natural fractures are so closely spaced that it is impossible to count them. This intense fracturing has caused several apparent washouts, where the drill hole diameter has enlarged considerably in all directions, without preferential spalling. In addition to washout zones, several zones of preferential borehole spalling (breakouts) have also been detected (such as at 121-141 m, and 530-560 m), which seemed to be associated with the natural fracture system (Figure 3). The observed fractures do not seem to fall into the commonly experienced one or two sets. Their dip and strike of observed fractures vary considerably, sometimes within very short segments (see Figure 3). However, there appear to be two dominant general directions at N45°E ± 30° and N10°W ± 30°.

Hydrofracturing

All hydrofracture orientations are based on magnetic compass downhole surveying tool, and are listed in Table 2. A comparison between orientations independently determined by the gyroscopic system and the magnetic compass showed no significant deviations (see Table 3). As Table 2 shows, several fracture traces could be determined in most cases. Veins observed on the core material appeared also on the recorded impression. Although these can be considered as weakness planes within the rock material, they were not always hydraulically activated. In some tests a clear distinction between induced fractures and closed veins was not possible. These tests were not considered for stress computation and are marked with a star (*) in Table 2. The strike directions of all observed vertical and steeply inclined hydrofracture planes are shown in Figure 5. Down to 200 m depth these orientations scatter considerably. Below 200 m and down to 514 m the orientation tests yielded a preferred direction of about N66°E. Beyond 530 m no impressions were taken because after completion of the deepest injection test, it became difficult to pull the straddle packer tool through a zone of borehole spalling at 530-560 m, where loose rock particles dropped on the packer system. Hence the lowering of the orientation system below 530 m was considered too risky and was aborted.

A typical pressure-time record obtained during hydrofracturing tests is given in Figure 6a. An enlarged view of the third fracture reopening cycle of the same test is shown in Figure 6b. The

characteristic pressure values which are necessary for stress computations (P_c, P_s and P_r) were determined by analyzing enlarged plots of each pumping cycle. All measured P_c, P_r, and P_s values are summarized in Table 4. Breakdown pressures, P_c, of induced hydrofractures range between 74 to 204 bar; the shut-in pressure, P_s, shows an almost linear increase with depth from 21 bar at 74 m to 111 bar at 612 m; the P_r values are scattered with no clear trend.

A series of laboratory measurements was also conducted to determine some physical characteristics of the CY-4 diabase. These tests are discussed in the Appendix.

TABLE 1. State of Natural Fracture Regime in Drill Hole CY-4*

Depth (m)	Description
50 - 118	Intensely fractured zone with segments of borehole enlargement, possibly due to washout (66-70 m, 78-83 m, 92-98 m, 106-115 m).
118 - 121	Five separate fractures of widely varying strike directions, dipping 60°- 85°.
121 - 141	Densely fractured (4 fractures/m); dominant strike direction; N30°- 60°E. Visible borehole spalling (breakouts) at N30°- 60°E and S30°- 60°W apparently associated with the pre-existing natural fractures (see Figure 3).
141 - 183	Moderately fractured (2 fractures/m); widely varying strike directions and dipping mainly 45°- 80°. Two meter thick fracture zone at 160 m.
183 - 194	Two major vertical fractures, one at 187-189 m striking N80°E and the other at 193-194 m striking N45°E.
194 - 218	Low fracture density (1 fractures/m) of varying strike directions, dipping 45°- 85°.
218 - 260	Moderately fractured (1.5 fractures/m); varying strike directions and dips and with intermittant fracture zones (230-231 m, 236-237 m, 252-254 m). Open fracture at 242 m (about 30 cm wide) striking at N60°E and dipping 67°NW.
260 - 280	Low fracture density (1 fracture/m); varying strike directions and gently dipping.
280 - 370	Low to moderate fracture density (1.5 fractures/m); varying strike directions and dips. Open fractures at 281.5 m (about 15 cm wide) striking at N35°E and dipping 65°NW, and at 291.5 m (about 40 cm wide) striking at N25°W and dipping 60°W.
370 - 380	Badly damaged borehole wall, apparently associated with intense fracture density (see Figure 3).
380 - 386	Intensely fractured (5 fractures/m); striking at N30°- 40°E and dipping mainly 70°- 80°NW.
386 - 530	Low to moderate fracture density (1.5 fractures/m) at varying strike directions and dips.
530 - 620	Low to moderate fracture density (1.5 fractures/m); irregularly shaped vertical fracture (possible borehole spalling) striking N75°E at 530-560 m.

*Based on borehole televiewer logging

TABLE 2. Orientations of all Traces Observed on the Borehole Wall using an Impression Packer

Depth (m)		Strike (°)	Dip (°)		Strike (°)	Dip (°)
*53		85	76		102	53
		114	90			
74	>	46	90			
119	>	61	90		39	90
144	>	100	69		172	90
149	>	151	85		143	48
165	>	97	80	>	72	80
		81	90			
178	>	111	90		114	65
*184		96	90		166	73
200	>	23	53	>	91	90
214	>	45	60		67	90
239	>	75	90			
*275		33	68		71	90
		100	55		106	59
*276		37	54		35	61
		38	59			
349	>	72	90			
397	>	63	90			
399	>	41	55		179	68
		77	90			
421	>	55	90		8	33
		13	37			
439	>	67	90		98	49
		34	56			
474	>	66	90		110	56
484	>	62	85		73	90
501	>	81	90		52	67
		139	51			
514	>	77	90		47	76
*525		73	44			0
		86	90			

*Tests which were not considered for stress computation because a clear distinction between induced fractures and natural fractures was not possible, >: induced fractures used for P_s-method
All orientation are in terms of magnetic north.

TABLE 3. Comparison between Gyroscopic Instrument and Magnetic Compass Orientation Readings - Drill Hole CY-4

Depth (m)	Gyroscopic Instrument (°)	Magnetic Compass* (°)
74	134	137
144	70	74
149	40	44
239	57	56

*Corrected for magnetic north declination of 3°E of true north.
Readings are for orientation of reference line on impression packer.

TABLE 4. Pressure Data Obtained in Successful Hydraulic Fracturing Tests in the CY-4 Borehole

Depth (m)	P_c (bar)	P_r (bar)	P_s (bar)
74			21
144			33 - 31
149	74		31 - 29
165			30 - 29
178			32
200	137		51, 44 - 43
214	87	59	50 - 46
239	76	43	44 - 42
275	131		74 - 73
276			65 - 54
309			99 - 91
349	163	81	64 - 56
397	147	113	76 - 70
399			91
421	104	78	75
439	121	85	84 - 76
474	138	102	105- 84
484	128	83	96 - 86
486			82
514	120	85	88 - 87
525	204		138 - 130
577	111	67	101- 90
605			99 - 91
612	150	124	111 - 105

Note: P_r given is the mean of values in cycle 3 and 4 for each test (used in the conventional stress calculations). P_s given is the range of values obtained in all cycles for each test (used in the P_s method of stress calculation).

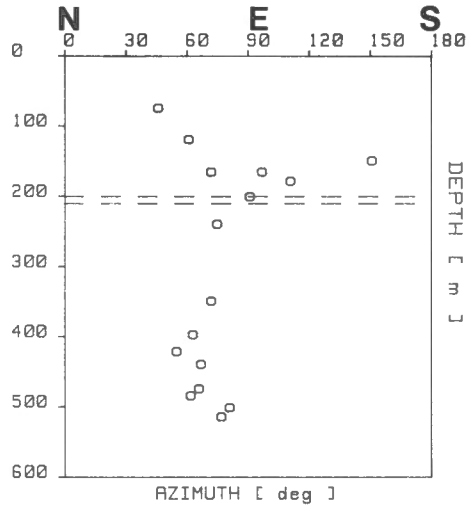

Figure 5: Directions of induced vertical and steeply inclined (dip >70°) hydrofractures.

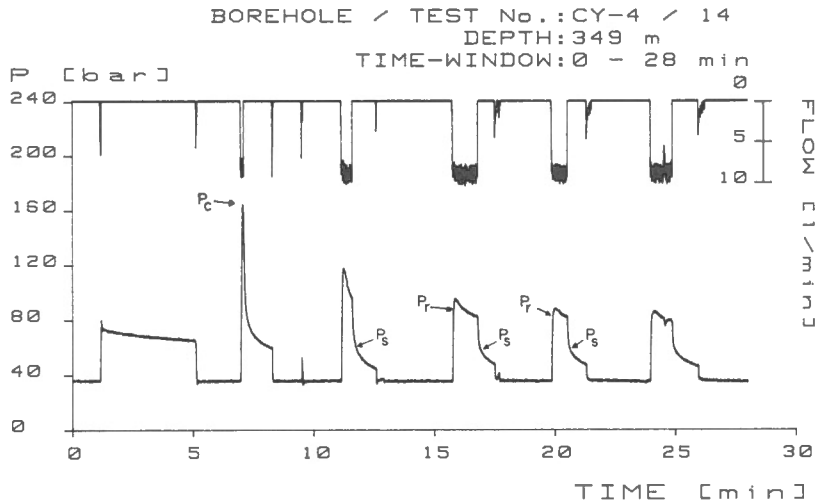

Figure 6a: Pressure-time and flowrate-time records obtained during hydrofracturing at 349 m depth in the CY-4 drill hole; showing P_c (breakdown pressure), P_r (hydrofracture reopening pressure) and P_s (shut-in pressure).

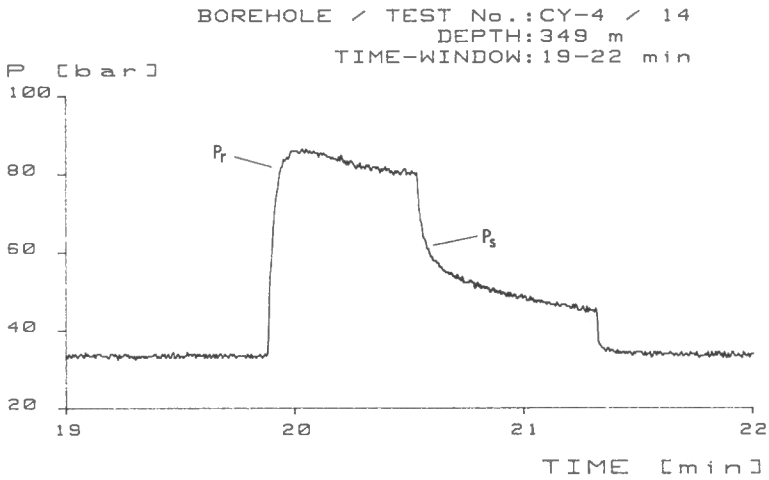

Figure 6b: Enlarged view of the third fracture reopening cycle of Figure 6a.

DATA INTERPRETATION

Conventional Method

Hydrofracturing data analysis was carried out using two independent methods. In tests below 200 m which resulted in vertical or subvertical hydrofractures, the conventional equations (Hubbert and Willis, 1957) were used to derive the two principal horizontal stresses:

$$P_c = 3\ P_s - S_H + T - P_o \qquad (1)$$

$$P_s = S_h \qquad (2)$$

where S_H and S_h are the maximum and the minimum horizontal stresses, respectively, P_o is the pore pressure at test depth and T is the hydrofracturing tensile strength. To avoid having to determine T, one of the more capricious rock parameters, Bredehoeft et al. (1976) suggested using the 'refrac' pressure, P_r, obtained in pressurization cycles subsequent to that which induced the hydrofracture. With the additional assumption that the hydrofracture closes completely between each cycle and allows no fluid permeation until a critical relationship similar to (1) is reached:

$$P_r = 3\ P_s - S_H - P_o \qquad (3)$$

One of the simplifying assumptions in equations (1) and (3) is that no borehole fluid penetrates into the surrounding rock during hydrofracturing and that the pore pressure throughout the rock remains at its background level, P_o. Haimson and Fairhurst (1967) showed that if rock is permeable to borehole fluid, relationship (3) becomes:

$$P_r - P_o = [3\ (S_h - P_o) - (S_H - P_o)]/K \qquad (4)$$

where $K = 2 - p(1 - 2v)/(1 - v)$, v is Poisson ratio, and p is the Biot poroelastic parameter. Later experimental work showed that for in situ stress levels not exceeding 250-300 bar the discrepancy in results between the two approaches represented by equations (3) and (4) is not significant (Haimson, 1978). The vertical stress component, S_v, was calculated based on the assumption that it is equal to the overburden weight ($S_v = rgZ$, where r is rock mass density, and g is the gravitational acceleration, and Z is the depth at the point of measurement). Table 5 summarizes the results of this analysis. The least horizontal stress component, S_h, in each test was based directly on the mean shut-in pressure in cycles 2-4. The shut-in pressure in each cycle was determined using a simple technique proposed by Gronseth and Kry (1983) which consists of determining the inflection point in the pressure-time curve following pump shut-off. The standard deviation from the mean P_s values given in Table 4 was never higher than ±10% of the calculated value. For the computation of S_H we used the mean P_r values in cycle 3 and 4. Each P_r value was determined as the point on the ascending portion of the pressure-time curve where the slope began to deviate from that recorded in the first cycle provided that the flow rate is kept the same as in the first cycle (see, for example, Zoback and Haimson, 1982). Again, the standard deviation of the mean P_r was always less than 10% of the calculated value. The direction of S_H based on the hydrofracture directions is very consistent at N68°E±6°.

TABLE 5. Conventional Hydrofracturing Data Analysis for CY-4

Depth (m)	P_c (bar)	P_r (bar)	P_s (bar)	P_o (bar)	S_v (bar)	S_h (bar)	S_H (bar)	S_H Direction
214	87	59	47	17	60	47	65	N67°E
239	76	43	43	19	67	43	67	N75°E
349	163	81	64	30	98	64	81	N72°E
397	147	113	76	35	111	76	80	N63°E
421	104	78	75	37	118	75	110	N55°E
439	121	85	84	39	123	84	128	N67°E
474	138	102	97	43	133	97	146	N66°E
484	128	83	93	44	135	93	152	N73°E
514	120	85	80	52	144	80	103	N77°E
577	111	67	91	53	161	91	153	*
612	150	124	111	56	171	111	153	*

*No impression tests were attempted.

Applying linear regression analysis to the results of the conventional data interpretation given in Table 5, the following stress profiles were obtained (correct only for the depth range of 200 m and 600 m):

$$S_v = 0.28\ (\pm 0.005)\ \text{bar/m x depth (m)}$$

$$S_h = 12 + 0.16\ (\pm 0.01)\ \text{bar/m x depth (m)}$$

$$S_H = 7 + 0.25\ (\pm 0.03)\ \text{bar/m x depth (m)}$$

$$S_H \text{ direction: N68°E} \pm 6° \qquad (5)$$

The values in parentheses are the estimated uncertainties for each of the principal stresses.

P_s-Method

A second stress computation method, called here the P_s-method, and introduced by Cornet and Valette (1984) and Baumgartner (1987), was also applied. The P_s-method is based on the measurement of the normal stress component acting across the induced hydrofractures. Field results from extensive hydrofrac test series at two different hot dry rock geothermal energy test locations (Le Mayet de Montagne, France and Falkenberg, W. Germany) showed that frac orientations may scatter due to material inhomogeneities, especially if low injection rates are used (Rummel and Alheid, 1979; Cornet, 1983). These experiences have led to a stress determination technique which is based on the measurement of the normal stress component acting across an arbitrarily oriented fracture plane (Cornet and Valette, 1984; Baumgartner, 1987). In addition to the conventional data interpretation this technique was applied here to include those hydrofrac tests in the stress computation which showed pre-existing weakness planes at the borehole wall. Thus, if the shut-in pressure, P_s, is used to measure the normal stress component acting across a hydrofracture plane, the problem consists of determining the stress field at a certain depth range from all the shut-in pressure data measured at the various depths and the corresponding fracture orientations (strike and dip) at the borehole wall. The assumption is made that the components of stress are linear functions of depth. If the linear dependence of the stress field with depth is:

$$S(Z) = A + BZ \qquad (6)$$

where S(Z) is the stress tensor at depth Z, A is the stress tensor at the surface (Z = 0), B is the increment of stress tensor per unit depth, then the normal stress component supported by the fracture plane and thereby the shut-in pressure, P_s, can be expressed as:

$$P_{s,i} = rgZ_i\cos^2 d_i + 0.5\sin^2 d_i[A_1+A_2+(B_1+B_2)Z_i - (A_1 - A_2)\cos 2(s_i - a) - (B_1 - B_2)Z_i\cos 2(s_i - (a+b))] \qquad (7)$$

where:

- $P_{s,i}$ is the normal stress acting on an ith fracture plane,
- s_i is the strike of an ith fracture plane + pi/2,
- d_i is the dip of an ith fracture plane,
- Z_i is the depth of a test interval with respect to the upper limit of the stress computation depth range,
- A_1 and A_2 are principal stresses at the upper boundary of the stress computation depth range
- B_1 and B_2 are eigen values of tensor B,
- a is the orientation of the principal stress A_1,
- b is the angle between the oriention of the eigen value of A and B,
- r is rock mass density.

The principal horizontal stress components S_H and S_h and the direction of S_H, a_o, are given by :

$$S_H = 0.5[A_1 + A_2 + (B_1 + B_2)Z + D] \qquad (8)$$

$$S_h = 0.5[A_1 + A_2 + (B_1 + B_2)Z - D] \qquad (9)$$

$$a_o = 0.5\arcsin[(B_1 - B_2)Z\sin 2b/D] + a \qquad (10)$$

where:

$$D = [(A_1 - A_2)^2 + (B_1 - B_2)^2Z^2 + 2(A_1 - A_2)(B_1 - B_2)Z\cos 2b]^{0.5} \qquad (11)$$

To determine the remaining six unknowns (A_1, A_2, B_1, B_2, a, b) a random sampling technique suggested by Baumgartner (1987) was used. The main steps of this procedure are as follows:

1. Definition of the sample ranges for all unknowns involved in equation (7) within the considered depth range.
2. Computation of theoretical P_s values for each test using randomly generated parameter sets within the defined sample ranges.
3. Computation of the parameter set with the least average error (AVE) while comparing theoretical and measured P_s values.
4. Storing the ten best models with least AVE.

Considering the orientations of the induced vertical fractures as an indicator of the stress field direction for the stress computation, the upper 600 m of the CY-4 borehole can be divided into two depth ranges: 0-200 m and 200-600 m (Figure 5).

Within each of these depth ranges the parameter b, which is used to describe a gradual rotation of the

stress regime with depth, is assumed to be zero. In this case equations (8), (9) and (10) become:

$$S_H = A_1 + B_1 Z_i \quad (12)$$

$$S_h = A_2 + B_2 Z_i \quad (13)$$

$$a_o = a \quad (14)$$

The consistent orientations of all vertical fractures obtained in the depth range below 200 m (Figure 5) as well as the linear increase of shut in pressure values with depth confirm this approach. After selecting reliable hydrofracture planes, the remaining data base for the 0-200 m depth range appears to be too small for the calculation of a possible gradual stress field rotation as the depth approaches 200-210 m. Above 200 m depth no preferred orientation of vertical fractures could be detected. Applying the P_s-method to seven hydrofrac tests between 75-200 m depth (see Table 2) results in the following horizontal principal stress ranges:

S_h = min: -15 + 0.255 bar/m x depth (m)
max: -3 + 0.22 bar/m x depth (m)

S_H = min: 5 + 0.2 bar/m x depth (m)
max: 12 + 0.205 bar/m x depth (m)

S_H direction: N26°W ± 3° (15)

In the depth range of 200-600 m the P_s-method was applied to 11 tests (see Table 2) and yielded the following stress profile (extrapolated to surface):

S_h = min: -2 + 0.17 bar/m x depth (m)
max: 3 + 0.17 bar/m x depth (m)

S_H = min: -3 + 0.22 bar/m x depth (m)
max: -16 + 0.32 bar/m x depth (m)

S_H direction: N79°E ± 4° (16)

As noted in equations (15) and (16) the P_s-method of random sampling yields ranges of stress profile values within which the correct magnitudes must lie. Further refinement using a scanning method reduces equations (16) to:

$$S_h = 0.17 \text{ bar/m x depth (m)}$$

$$S_H = -6 + 0.27 \text{ bar/m x depth (m)} \quad (17)$$

The scanning method produces no improvement in the 0-200 m range as given by equations (15).

DISCUSSION AND CONCLUSIONS

Equations (5) and (16) suggest that for the 200-600 m-depth considerable agreement exists between the principal stresses calculated by the conventional method and those obtained from the P_s-method (Figure 7). The mean directions of S_H agree within 11°. The direction of the maximum horizontal compression S_H above 200 m, as obtained by the P_s-method, is aligned with the longitudinal axis of the ophiolite complex (Figure 8). This direction may be interpreted, because of its limited depth, as affected by the local topographic relief around Palekhori (S_H is oriented roughly parallel to the 1000 m contour line). Between 200-600 m the measurements could still be influenced by topographic relief. However, N68°E-N79°E direction of maximum horizontal compression agrees well with the longitudinal axis of Cyprus and may be affected by the elevation of the entire island. The magnitudes of the horizontal stresses suggest a normal faulting stress regime ($S_h < S_H \leq S_v$) in a region where a compressional stress regime is expected, implying that within the depth range tested there may be little or no tectonic effects. A clear tectonic interpretation of the stress regime requires stress measurements within a depth range well below the island's topographic relief. In order to support theories of the actual tectonic processes in the Eastern Mediterranean region more stress measurements at different locations are necessary.

As shown in Table 1 the borehole televiewer log indicates a moderate to high fracture density and a marginally dominant northeastern directional preference. For such a condition of basically scattered fracture orientations and a general regime of $S_h < S_H \leq S_v$ we can estimate the critical S_h magnitudes for which normal or strike-slip faulting or a combination of both would be expected to occur on optimally oriented fracture planes. Using Brace and Kohlstedt's (1980) simple Coulomb frictional sliding model and Byerlee's (1978) experimental results for the coefficient of friction (0.6 to 1.0 independent of rock type) the expression for the critical minimum horizontal stress, $S_h$crit. is:

$$S_h\text{crit.} = (S_v - P_o)[(u^2 + 1)^{0.5} + u]^{-2} + P_o$$

For u = 1.0: $S_h$crit. = (0.18 x 0.17 + 0.1) x depth
= 0.13 bar/m x depth (m)
For u = 0.6: $S_h$crit. = (0.18 x 0.32 + 0.1) x depth
= 0.16 bar/m x depth (m) (18)

Comparing equations (18) to equations (5) and (17) we learn that the measured S_h is only slightly larger than the critical value based on the lower limit of the coefficient of friction (Figure 7). Thus, it appears that small perturbations in the magnitudes of S_h have the potential of inducing slip along existing discontinuities

of optimum orientation. Owing to the closeness of S_v magnitudes to those of S_H, normal, strike-slip or oblique slip faulting are possible.

The BHTV log of the natural fractures crossing the hole reveals two important characteristics:

(a) The direction of the generally dense fractures are scattered considerably, but show a preference for northeastern and north-northeastern orientations. The former is subparallel to S_H direction below 200 m. The existing of a fracture set subparallel to S_H has been established in many other locations (Haimson and Doe, 1983; Engelder, 1982).

(b) There are at least two breakout segments apparently related to the natural fractures crossing the drill hole resulted from the multiplicity of fractures crossing the borehole wall. This finding is quite rare. Except for Babcock (1978), all the borehole breakouts reported in the literature in the last 8 years have been thought to occur in intact rock and unaffected by pre-existing joints (see for example: Gough and Bell, 1982; Hickman et al., 1985). Our log shows that favorably oriented dense joints may play an important role in breakout development.

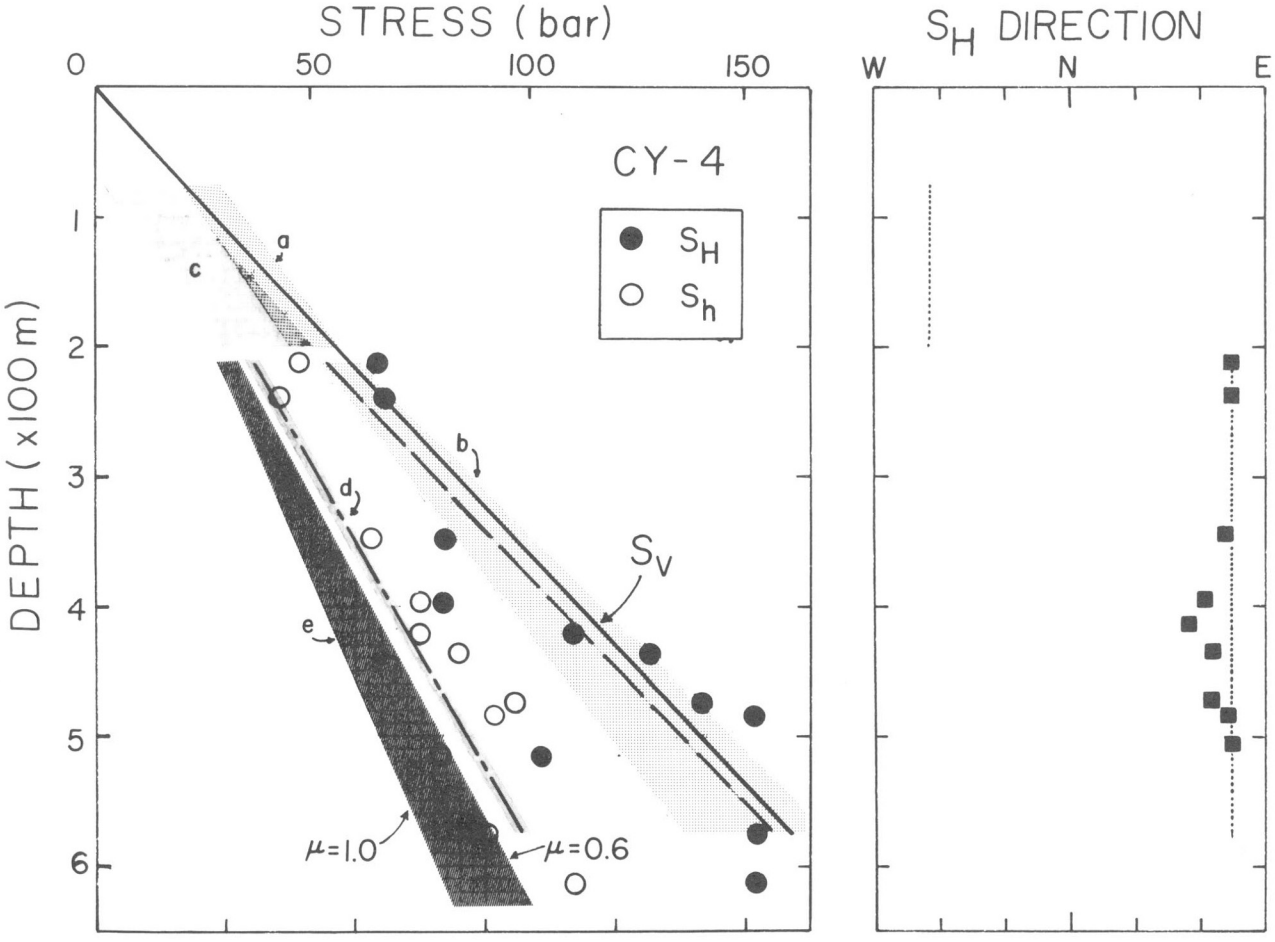

Figure 7: Magnitudes of the vertical stress (S_v), and the two horizontal principal stresses (S_H and S_h) and the direction of S_H in drill hole CY-4, Cyprus. Open and blocked circles are the magnitudes of S_h and S_H, respectively, as obtained by the conventional method of analysis. Shaded zones (a) and (b) represent the S_H range of values in the 75-210 m segment and 210-550 m segment, respectively, as obtained by the P_s-method of analysis. Shaded zones (c) and (d) represent the S_h range of values using the P_s-method. The dashed lines within (b) and (d) represent S_H and S_h, respectively, resulting from a scanning technique applied to the field data. Shaded zone (e) represents the range of calculated critical values of the least horizontal stress ($S_h$crit), i.e. the region in which the magnitude of S_h would be sufficiently low to bring about normal or strike-slip sliding (or a combination of the two) on favorably oriented fracture planes. Blocked squares give the direction of S_H for each test in which the conventional method was used. The dotted lines present the calculated S_H direction based on the P_s-method.

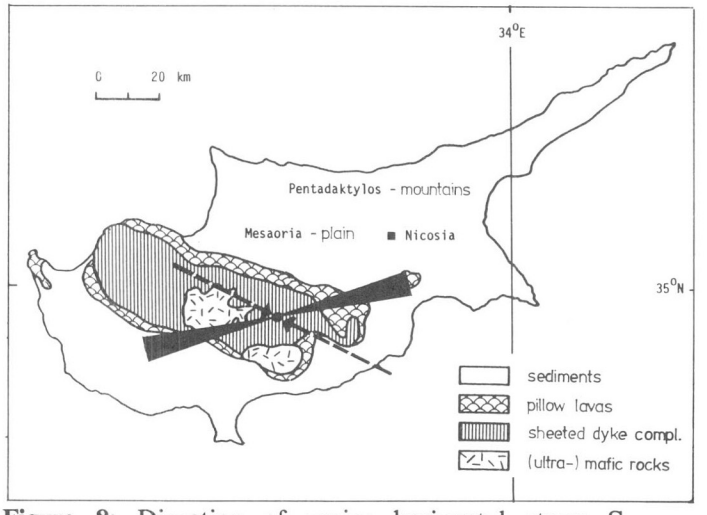

Figure 8: Direction of major horizontal stress S_H derived from hydraulic fracturing tests in the CY-4 drill hole. Dashed arrows represent the direction of S_H for the depth range above 200 m. Fat arrows characterize the direction of S_H for the depth range 210-650 m (geological map: Constantinou and Govett, 1973).

ACKNOWLEDGEMENTS

We are grateful to R. Busch, B. Kappernagel and Fl. Rummel who participated in the field work. The laboratory experiments were carried out by W. Muller and E. Rybacki. The authors would like to express their appreciation to the Geological Survey of Cyprus and in particular to Dr. Xenophontos for their organizational support. The work was supported by the Deutsche Forschungsgemeinschaft under contract number Ru 225/8 and by the U.S. National Science Foundation under grant number EAR-8212087.

REFERENCES

Babcock, E.A.
1978: Measurement of subsurface fractures from dipmeter log; American Association of Petroleum Geologists, Bulletin, v. 62, p. 1111-1126.

Baumgartner, J.
1987: Anwendung des Hydraulic-Fracturing-Verfahrens für Spannungsmessungen im geklüfteten Gebirge, dargestellt anhand von MeBergebnissen aus Tiefbohrungen in der Bundesrepublik Deutschland, Frankreich und Zypern; Berichte des Instituts für Geophysik der Ruhr-Universität Bochum, Reihe A, Nr. 21.

Brace, W.F. and Kohlstedt, D.L.
1980: Limits on lithospheric stress imposed by laboratory experiments; Journal of Geophysical Research, v. 85, p. 6248-6252.

Bredehoeft, J., Wolff, R., Keys, W. and Shuter, E.
1976: Hydraulic fracturing to determine the regional in-situ stress field, Piceance basin, Colorado; Geological Society of America Bulletin, v. 87, p. 250-258.

Byerlee, J.
1978: Friction of rocks; Pure and Applied Geophysics, v. 116, p. 615-626.

Constantinou, G. and Govett, G.J.S.
1973: Geology, geochemistry, and genesis of Cyprus sulfide deposits; Economic Geology, v. 68, no. 6, p. 843-858.

Cornet, F.H.
1983: Analysis of injection tests for in-situ stress determination; *in* Hydraulic Fracturing Stress Measurements, ed. M.L. Zoback and B.C. Haimson; National Academy Press, Washington, D.C., p. 149-158.

Cornet, F.H. and Valette, B.
1984: In situ stress determination from hydraulic injection test data; Journal of Geophysical Research, v. 89, no. B13, p. 11527-11537.

Engelder, T.
1982: Is there a genetic relationship between selected regional joints and contemporary stress within the lithosphere of North America; Tectonics, v. 3, p. 161-177.

Gough, D.I. and Bell, J.S.
1982: Stress orientation from borehole wall fractures with examples from Colorado, east Texas, and northern Canada; Canadian Journal of Earth Sciences, v. 19, p. 1358-1370.

Gronseth, J.M. and Kry, P.R.
1983: Instantaneous shut-in pressure and its relationship to the minimum in-situ stress; *in* Hydraulic Fracturing Stress Measurements, ed. M.L. Zoback and B.C. Haimson; National Academy Press, Washington, D.C., p. 28-43.

Haimson, B.C.
1968: Hydraulic fracturing in porous and nonporous rock and its potential for determining in situ stresses at great depth; Ph.D. thesis, University of Minnesota, Technical Report, no. 4-68, Missouri River Division, Corps of Engineers, Omaha, Nebraska.
1978: The hydrofracturing stress measuring method and recent field results; International Journal of Rock Mechanics and Mining Sciences, v. 15, p. 167-178.

Haimson, B.C. and Doe, T.W.
1983: State of stress, permeability, and fractures in the Precambrian granite of northern Illinois; Journal of Geophysical Research, v. 88, p. 7355-7371.

Haimson, B.C. and Fairhurst, C.
1967: Initiation and extension of hydraulic fracture

in rocks; Society of Petroleum Engineers Journal, v. 7, p. 310-318.
Heuser, U.
1982: Das Druckstoss-Test-Verfahren zur Bestimmung der Gebirgspermeabilitaet in Bohrungen, dargestellt am Beispiel von Permeabilitaetsmessungen im Eisenerzbergwerk Konrad/Salzgitter und in der IRDP-Forschungsbohrung in Ostisland, Diplomarbeit, Institut für Geophysik, Ruhr-Universität Bochum.
Hickman, S.J., Healy, J.H. and Zoback, M.D.
1985: In situ stress, natural fracture distribution, and borehole elongation in the Auburn geothermal well, Auburn, New York; Journal of Geophysical Research, v. 90, p. 5497-5512.
Horne, L. and Robinson, P.T.
1984: Cyprus Crustal Drilling Project, Hole CY-4 Core Descriptions, Volumes 1 and 2.
Hubbert, M.K. and Willis, D.G.
1957: Mechanics of hydraulic fracturing; American Institute of Mining, Metallurgical, and Petroleum Engineers (A.I.M.E.), Transactions, v. 210, p. 153-168.
Kehle, R.O.
1964: The determination of tectonic stresses through analysis of hydraulic well fracturing; Journal of Geophysical Research, v. 69, p. 259-273.
Lort, J.M.
1971: The tectonics of the Eastern Mediterranean: a geophysical review; Reviews of Geophysics and Space Physics, v. 9, no. 2, p. 189-216.
McKenzie, D.
1972: Active tectonics of the Mediterranean region; Geophysical Journal of the Royal Astronomical Society, v. 30, no. 2, p. 109-185.
Moores, E.M. and Vine, F.J.
1971: The Troodos Massif, Cyprus, and other ophiolites as oceanic crust: evaluation and implications; *in* A Discussion on the Petrology of Igneous and Metamorphic Rocks from the Ocean Floor; Philosophical Transactions of the Royal Society of London, Series A, v. 268, p. 443-466.
Robertson, A.H.F. and Woodcock, N.H.
1980: Tectonic setting of the Troodos massif in the east Mediterranean; *in* Ophiolites, Proceedings of the International Ophiolite Symposium, Cyprus, 1979, ed. A. Panayiotou; Cyprus Geological Survey Department, Ministry of Agriculture and Natural Resources, p. 36-49.
Rummel, F.
1987: Fracture mechanics approach to hydraulic fracturing stress measurements; *in* Fracture Mechanics of Rocks, ed. Atkinson; Academic Press, London, p. 217-239.
Rummel, F. and Alheid, H.J.
1979: Hydraulic fracturing stress measurements and tectonic stress pattern in central europe; Proceedings of the International Research Conference on Intra-Continental Earthquakes, Ohrid, Yugoslavia, p. 33-65.
Scheidegger, A.E.
1962: Stresses in the earth's crust as determined from hydraulic fracturing data; Geologie und Bauwesen, v. 27, p. 45-53.
Shelton, A.W. and Gass, I.G.
1980: Rotation of the Cyprus microplate; *in* Ophiolites, Proceedings of the International Ophiolite Symposium, Cyprus, 1979, ed. A. Panayiotou; Cyprus Geological Survey Department, Ministry of Agriculture and Natural Resources, p. 61-65.
Turcotte, D.L. and Schubert, G.
1982: Geodynamics, applications of continuum physics to geological problems; John Wiley and Sons, New York, p. 365-367.
Von Schoenfeldt, H.
1970: An experimental study of open-hole hydraulic fracturing as a stress measuring method with particular emphasis on field test; Ph.D. thesis, University of Minnesota, Technical Report, no. MRD-3-70, Missouri River Division, Corps of Engineers, Omaha, Nebraska.
Zemanek, J., Caldwell, R.L., Glenn, Jr., E.E., Holcomb, S.V., Norton, L.J. and Straus, A.J.D.
1969: The borehole televiewer - a new logging concept for fracture location and other types of borehole inspection; Journal of Petroleum Technology, p. 762-774.
Zoback, M.L. and Haimson, B.C.
1982: Status of the hydraulic fracturing method for in-situ stress measurements; *in* Issues in Rock Mechanics, Proceedings of the 23rd U.S. Symposium on Rock Mechanics, ed. R. Goodman and F. Heuze; Society of Mining Engineers of the American Institute of Mining Engineers (A.I.M.E.), New York, p. 143-156.
Zoback, M.L. and Zoback, M.D.
1980: State of stress in the conterminous United States; Journal of Geophysical Research, v. 85, p. 6113-6156.

APPENDIX

Laboratory hydraulic fracturing tests were conducted on 30 mm diameter specimens obtained from the core samples. Each specimen had a length of 40 mm and contained an axial injection drill hole of 2.5 mm in diameter. Confining pressures applied ranged up to 200 bar. The injection fluid used was a hydraulic oil with a viscosity of 30 cSt. All tests were

performed at a pressurization rate of 10 bar/sec which approximately corresponds to pressurization rates observed in situ. Fracture toughness was measured by three point bending tests on 30 mm diameter and 150 mm length specimens. A chevron notch with a tip angle of 90 was saw-cut in each sample. The complete testing procedure is described by Muller and Rummel (submitted for publication).

For laboratory testing, samples were taken from the extracted core (CY-4 depths: 186-187 m, 392-398 m) as well as from the outcropping rock around the CY-4 drill hole head. About 30% of all specimens tested appeared to be already prefractured or contained weakness planes like zeolite and calcite veins. Based on testing of intact rock, fracture toughness was determined to be:

$$K_{IC} = 3.0 \pm 0.3 \ MNm^{-3/2} \ (5 \text{ samples})$$

Laboratory hydrofrac tests under different confining pressures P_m resulted in two different P_c/P_m relations: one for the core and the other for the surface rock samples (Figure A.1):

a) $P_c = 370 (\pm 17) \text{ bar} + 1.6 (\pm 0.1) \times P_m$
(core material; 5 samples)

b) $P_c = 455 (\pm 15) \text{ bar} + 1.2 (\pm 0.1) \times P_m$
(surface rock; 7 samples)

Generally, laboratory hydraulic fracturing tensile strength was much higher than the in situ tensile strength. These results underline the apparent size effect on the tensile strength in the field (hole diameter of 96 mm) and the laboratory (diameter of 2.5 mm), and the importance of pre-existing weakness planes such as natural fissures or veins which are much more abundant in situ, where they may assist in the hydrofracture initiation. For both types of rock fracture gradients, k(a) = 1.6 and k(b) = 1.2, were less than the theoretical value k = 2 expected from the conventional stress analysis around a circular opening which assumes an impermeable uncracked material. Applying a fracture mechanics model of hydraulic fracturing (Rummel, 1987) to these data, an effective length of existing cracks of about 1 mm could be estimated. The laboratory tensile strength of those samples which were fractured along weakness planes scattered considerably and were roughly estimated at 180 ± 100 bar.

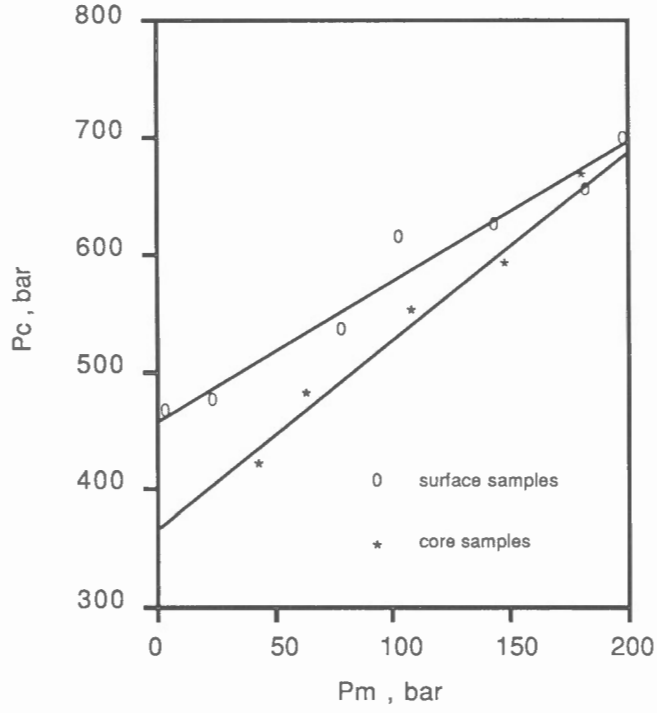

Figure A.1: Breakdown pressure, P_c, from hydrofracturing tests on mini core samples subjected to confining pressure, P_m; o: samples prepared from surface rock, *: samples prepared from core material.

A detailed list of the results of all laboratory tests is shown in Table A.1. In addition, a series of tests were conducted in the laboratory in which the rock permeability and porosity for all samples were found to be very nearly zero.

TABLE A.1. Laboratory Experimental Data

No.	Depth (m)	E (kbar)	V_p (km/sec)	K_{IC} (MNm)	r (g/ccm)	P_m (bar)	P_c (bar)
F1	surface		5.1		2.83	181	660
F2			5.1		2.83	1	462
F3			5.1		2.83	141	662
U1			5.1			102	620
U2			5.1			200	701
E0					2.83	78	535
E1		750	4.95	3.06	2.83	22	466
E2		670	4.95	2.55	2.83	38	(128)
E3			4.95		2.83	119	(249)
E4		730	4.95	3.43	2.83	59	(326)
A1	187	960	5.8	2.89	2.89	58	479
A2						12	(204)
A3						41	422
B1	392	980	5.75	3.06	2.91	108	553
B2						90	(444)
C1	397	720?	5.8		2.91	181	669
C2						150	595

E: Young's modulus, V_p: P-wave velocity, K_{IC}: fracture toughness, r: density, P_m: confining pressure during laboratory hydraulic fracturing tests, P_c: critical breakdown pressure (P_c values of those specimen which were fractured on visible weakness planes are in parentheses)

Geophysical Structure of The Troodos Ophiolite from Downhole Logging

M.H. SALISBURY[1], N.I. CHRISTENSEN[2], F.J. VINE[3], G.C. SMITH[3] AND S. ELEFTHERIOU[4]

[1]Centre for Marine Geology, Dalhousie University Halifax, Nova Scotia, Canada B3H 3J5
[2]Department of Earth and Atmospheric Sciences Purdue University, West Lafayette, IN., U.S.A. 47907
[3]School of Environmental Sciences University of East Anglia, Norwich United Kingdom NR4 7TJ
[4] Geological Survey Department, Nicosia, Cyprus

Salisbury, M.H., Christensen, N.I., Vine, F.J., Smith G.C., Eleftheriou, S., Geophysical structure of the Troodos ophiolite from downhole logging in *Cyprus Crustal Study Project: Initial Report, Hole CY-4, ed. I.L. Gibson, J. Malpas, P.T. Robinson and C. Xenophontos; Geological Survey of Canada, Paper 88-9, p. 331-349, 1989.*

Abstract

Velocity (Vp and Vs), density, porosity, natural gamma, resistivity, total magnetic field and magnetic susceptibility logs demonstrate that the Troodos ophiolite complex is geophysically similar to the oceanic crust. Insitu velocities (Vp) range from 3.2-3.5 km/s in the pillow basalts (Layer 2A) and then increase gradually through the pillow basalt/dike transition and the sheeted dikes (Layer 2B) to classic Layer 3 velocities (6.7-6.9 km/s) in the gabbros while Vs averages 2.1 km/s in the pillow basalts and rises to values of 3.2-3.5 km/s in the gabbros. In the pyroxenites, Vp increases only slightly (to 7.0 km/s) but Vs rises to 4.0 km/s. The porosity and natural gamma radiation decrease from averages of 20% and 30 API units, respectively, in the pillow basalts to negligible values in the gabbros, while the formation density and resistivity increase from 2.2 to 2.95 g/cm^3 and from 10 to 20K-50K ohm-m over the same interval, suggesting that seawater penetrates no deeper than the base of the dikes. Aside from Vs, the only property which changes at the gabbro/pyroxenite boundary is density, which increases abruptly to 3.1 g/cm^3 The magnetic susceptibility increases steadily from 0.5×10^{-3} S.I. units in the pillow basalts to 4×10^{-3} units at the 50% dike/50% gabbro transition, below which it decreases abruptly to 0.5×10^{-3} units. Since resistivity increases by an order of magnitude at the same depth and Vp increases rapidly from 5.75 to 6.4 km/s at this depth and then increases steadily to 6.8 km/s within the next few hundred meters, we interpret the dike/gabbro transition as the Layer 2/3 boundary of the oceanic crust.

Résumé

Les enregistrements continus, des vitesses séismiques Vp et Vs, densité, porosité, radioactivité naturelle, résistivité, champ magnétique total, susceptibilitè magnétique, constituent un ensemble géophysique similaire à celui de la croûte océanique. Les vitesses Vp mesurées in situ varient de 3.2 à 3.5 km/s dans les basaltes coussinées (Couche 2A) et augmentent progressivement vers la zone de transition de basaltes coussinés/dykes et le complexe filonien (Couche 2B) jusqu'à des vitesses caractéristiques de la Couche 3 (6.7-6.9 km/s) dans les gabbros. Parallèlement les vitesses moyennes Vs sont de l'ordre de 2.1 km/s dans les basaltes coussinés et croissent à 3.2-3.5 km/s dans les gabbros. Dans les pyroxénites les vitesses Vp augmentent légèrement à 7.0 km/s alors que les vitesses Vs s'accroissent à 4.0 km/s. La porosité et la radiation gamma naturelle décroissent respectivement depuis 20% et 30 unités API en moyenne dans les basaltes coussinés à des valeurs négligeables dans les gabbros. Dans le même intervalle, la densité et la résistivité augmentent respectivement de 2.2 à 2.95 g/cm^3 et de 10 à 20K-50K ohm-m, suggérant une pénétration maximale de l'eau de mer jusqu'à la base des dykes. En plus des vitesses Vs qui varient à l'interface gabbros/pyroxénites, la densité augmente brusquement à 3.1 g/cm^3. La susceptibilité magnétique croit continuellement de 0.5×10^{-3} unités S.I. dans les basaltes coussinés à 4×10^{-3} unités à la transition 50% dyke/50% gabbro. Sous cette zone la susceptibilité décroit brusquement à 0.5×10^{-3} unités. Puisque la résistivité augmente d'un ordre de grandeur à la même profondeur et que Vp s'accroit rapidement de 5.75 à 6.4 km/s et alors progressivement à 6.8 km/s à l'intérieur des quelques centaines de mètres suivants, nous interprétons la transition dykes-gabbros comme étant la limite des couches 2 et 3 de la croûte océanique.

INTRODUCTION

Since it was first proposed that the rock assemblages found in ophiolites represent fragments of oceanic crust tectonically emplaced on land, numerous investigations have been undertaken in these complexes to determine the validity of the hypothesis, or assuming it to be true, to determine the nature of oceanic crust. While hundreds of ophiolites have been identified and several dozen studied in detail (see Coleman, 1977, for review), the Troodos complex, which was first identified as an ophiolite in 1968 by Gass, remains one of the most extensively studied and convincing (e.g. Moores and Vine, 1971). While the exact provenance of the ophiolites remains uncertain - the presence of andesitic basalts and boninites in the Troodos extrusives suggests formation in a suprasubduction zone environment (Miyashiro, 1973; Robinson et al., 1983) - the presence of sheeted dikes, pillow basalts, massive sulphide deposits and fossilized smokers leaves no doubt that they formed in a submarine environment and represent, if not typical ocean crust, at least one of its variants. The recent discovery of dikes at a sub-basement depth of 500 m in two DSDP holes (418A and 504B; Leg 51-53 Shipboard Scientific Parties, 1980; Shipboard Scientific Party, 1985) and sheeted dikes at about 800 m in hole 504B lends further support to the hypothesis and suggests that in many key respects, ophiolites and ocean crust are indistinguishable.

Although the relative structural simplicity of the Troodos ophiolite has made it possible to determine the overall structure and stratigraphy of the complex, the discontinuous nature of the outcrops and the depth of weathering have made it difficult to determine important geochemical, magmatic and structural relationships with certainty. For example, it was unknown whether the extrusive and intrusive parts of any given vertical section were co-magmatic or whether the intrusives showed cryptic variation. Similarly, it was impossible to reconstruct a geophysical section through the complex based on hand samples because the physical properties of surface samples are strongly affected by alteration and because cracks, which strongly influence formation properties, are difficult to sample.

To address these questions and to determine the three-dimensional structure of the complex, the International Crustal Research Drilling Group (ICRDG) drilled an array of holes along a NE-SW transect across the northern flank of the ophiolite (Table 1; Figures 1 and 2). Since the complex is exposed in a broad anticline, with ultramafics and gabbros at the core, sheeted diabase dikes at higher levels and pillow basalts along the margins, the holes could be stacked to give a nearly complete cross-section through the crust (Figure 3).

TABLE 1: ICRDG Drillholes in the Troodos Ophiolite.

Hole	Coordinates	Penetration (m)	Logged Interval (m)	Crustal Level	Lithology	Depth[1] Range (m)
CY-1	35°02'54"N	485	-	Extrusives	Upper pillow basalts	0-300
	33°10'46"E				Lower pillow basalts	300-485
CY-2	35°02'43"N	226	-	Extrusives	Lower pillow basalts	0-226
	33°08'48"E				Hydrothermal stockwork	0-97
CY-2A	35°02'40"N	689	-	Extrusives	Lower pillow basalts	0-280
	33°08'55"E				Hydrothermal stockwork	154-297
					Basal group	280-689
CY-1A	35°02'10"N	701	-	Extrusives	Lower pillow basalts	0-200
	33°10'29"E				Basal group	200-701
CY-4	34°54'06"N	2263	0-2080	Plutonic	Lower sheeted dikes	0-675
	33°05'38"E				Massive gabbros	675-1330
					Cumulate gabbros	330-1740
					Cumulate ultramafics	1740-2263

(1) Based on petrology.

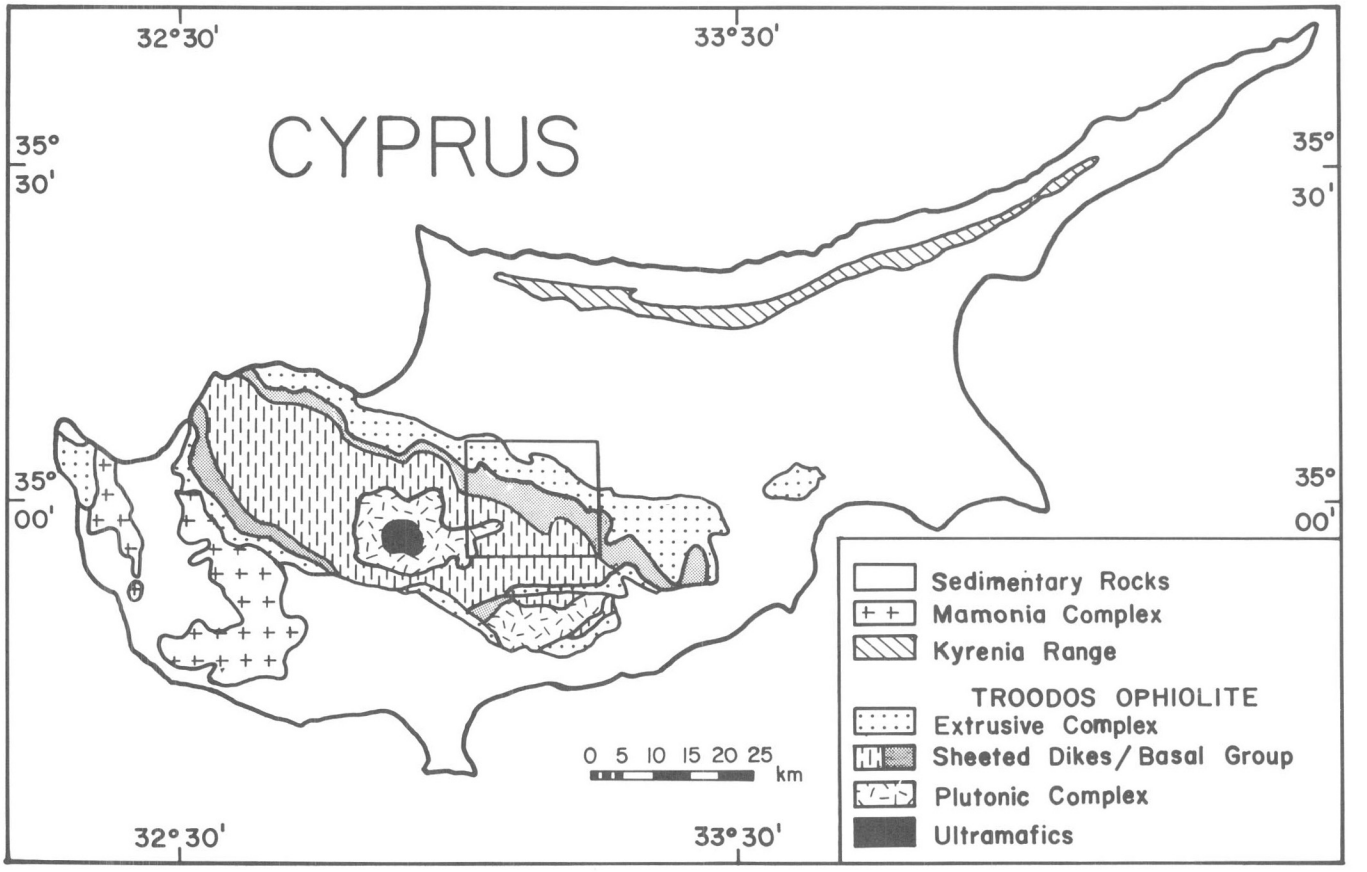

Figure 1: Geological map of Cyprus. Rectangle indicates area shown in Figure 2.

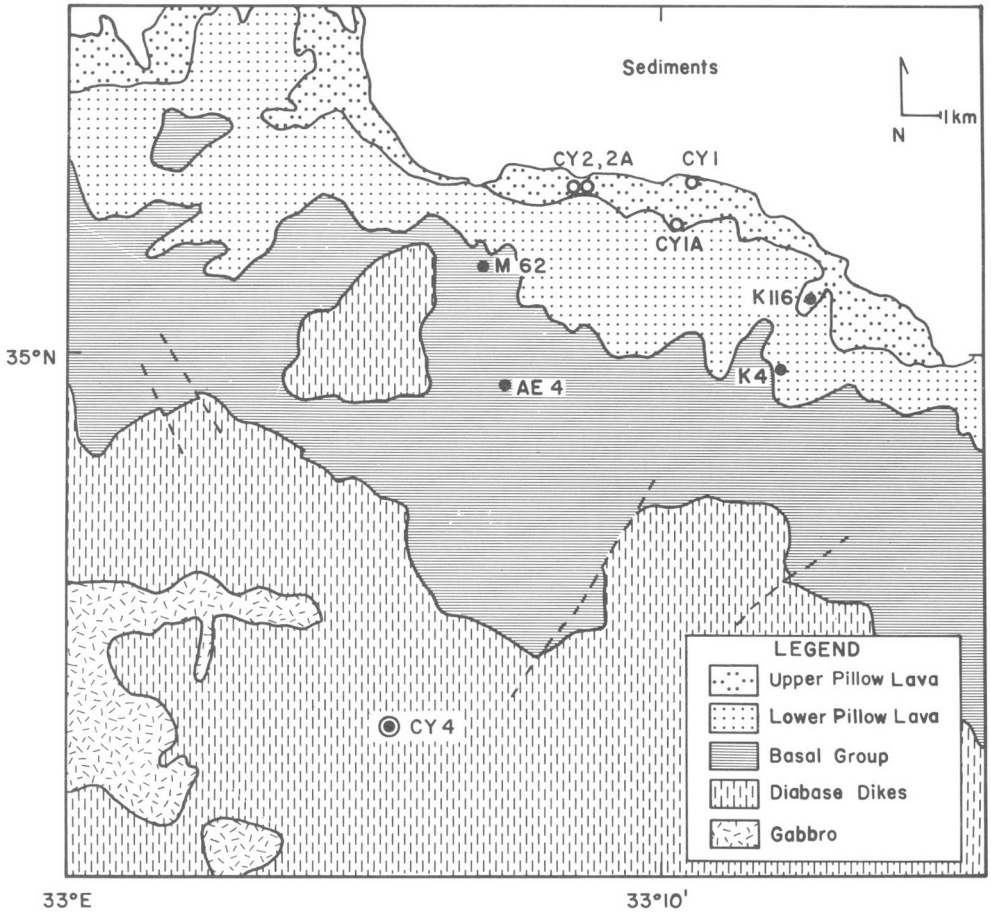

Figure 2: Holes drilled in Troodos ophiolite by the ICRDG (open circles), BRGM and Hellenic Mining. Logged holes indicated by filled circles.

From the inception of the project, it was recognized that the holes drilled through the Troodos ophiolite would provide an unparalled opportunity to determine the geophysical properties of oceanic crust by logging. Not only is the section virtually complete, but below the thin zone of surficial weathering described by field geologists, the alteration is submarine in origin (Gillis, 1986). Furthermore, the water table lies within a few metres of the surface, ensuring that conditions of water saturation are similar to those in the seafloor. Thus the present-day ophiolite only differs from its marine equivalents in terms of pore water salinity (salt water has been replaced by brackish water), effective confining pressure (the plutonic section has suffered a 0.5 to 1.0 kbar decompression due to uplift and erosion), temperature and crack density (new cracks were probably introduced during emplacement).

LOGGING OPERATIONS

To take advantage of this opportunity, a major downhole logging program was conducted in Cyprus during the summer of 1984 and again in the winter of 1985 using slimhole equipment supplied by BPB Instruments, Ltd. The logging suite (Table 2) consisted of eight separate tools selected to measure borehole temperature and diameter, natural gamma radiation, formation density and porosity, resistivity, compressional (Vp) and shear (Vs) wave velocity, magnetic field strength and magnetic susceptibility. The surface equipment consisted of a generator and a logging truck housing the power and control panels for each tool, recording equipment, a logging winch and calibration standards. The data from each tool was transmitted to the surface in analog form, then digitized and recorded for computer processing. Hard copies were made of the analog data for field interpretation.

TABLE 2: BPB Tools Used During Cyprus Logging Operations.

Tool	Measurement	Remarks
TT1	Temperature	Thermistor probe
DD3	Caliper Natural γ γ density	Single arm NaI/PMT sensor Borehole-compensated (2 channel)
NN1	Natural γ Neutron porosity	NaI/PMT sensor Borehole-compensated (2 channel)
RO1	Resistivity	3-electrode laterolog
MS1	V_p	Multichannel sonic (4 channel)
Shear wave	V_s	Clamped; full wave
Magnetometer	Field strength	3-axis flux gate
Susceptibility	Magnetic susceptibility	Induction tool

Tool Descriptions

Temperature (TT1).

The simplest tool deployed was a temperature probe consisting of a thermistor in a cage mounted at the base of a 1.5 m long x 3.8 cm (1-1/2") diameter pressure housing. The tool was rated to 100°C and could operate in either the absolute or temperature differential modes with sensitivities of 0.1 and 0.001°C, respectively.

Gamma density (DD3).

The γ density tool was a combination caliper/natural gamma density tool in a 3.5 m long x 4.8 cm (1-7/8") diameter housing. The caliper consisted of a single arm electromechanical device which was retracted while lowering, but could be extended out to 12" while logging, causing the tool to be excentralized and providing a continuous record of borehole diameter.

The natural γ tool employs an uncollimated NaI crystal coupled to a photo-multiplier tube to measure total natural γ radiation. The tool provides an indirect measure of the U, K and Th content of the formation within 6" of the borehole wall (the average penetration of gamma rays in basalt) but cannot be used to determine their relative abundances.

The γ density tool is a dual-spaced, borehole-compensated tool consisting of a collimated, Caesium 137 sidewall source at the base of the tool and two NaI gamma ray sensors spaced 15 and 40 cm, respectively, above the source. The tool uses Compton scattering of gamma rays to determine the electron density and thus, the bulk density, of the formation within a foot of the source. The tool design allows the formation density to be determined accurately in irregular, water-filled boreholes up to 8" in diameter and qualitatively in holes from 8 to 12" in diameter. Since high formation densities were anticipated, the tool was equipped with a high energy (150 mCi) source to increase the gamma ray count and thus, the density range of the tool.

Neutron porosity (NN1).

The neutron porosity tool was a combination neutron porosity/natural gamma tool in a 2.5 m long x 3.8 cm (1-1/2") diameter housing. The natural γ sensor was the same as that used in the density tool and was used for correlation between logs.

The neutron porosity tool, like the density tool, is a dual-spaced, borehole-compensated tool designed for use in irregular, water-filled boreholes up to 12" in diameter. Unlike the density tool, however, the neutron tool is neither clamped nor centralized. The tool consists of a 1 Ci, Am 241/Be uncollimated source at the base of the tool and two thermal neutron detectors located 25 and 45 cm, respectively, above the source. The porosity of the formation is measured by determining the ability of the formation to slow high energy neutrons. Since the energy loss is greatest for collisions between particles of equal mass, the number of low energy (thermal) neutrons reaching the detectors is related to the hydrogen content of the formation within one foot of the source. Since the hydrogen resides largely in water, the tool provides a measure of the water content or porosity of the formation. The tool works best in fresh water because Cl and B also moderate the neutron flux (although to a lesser degree).

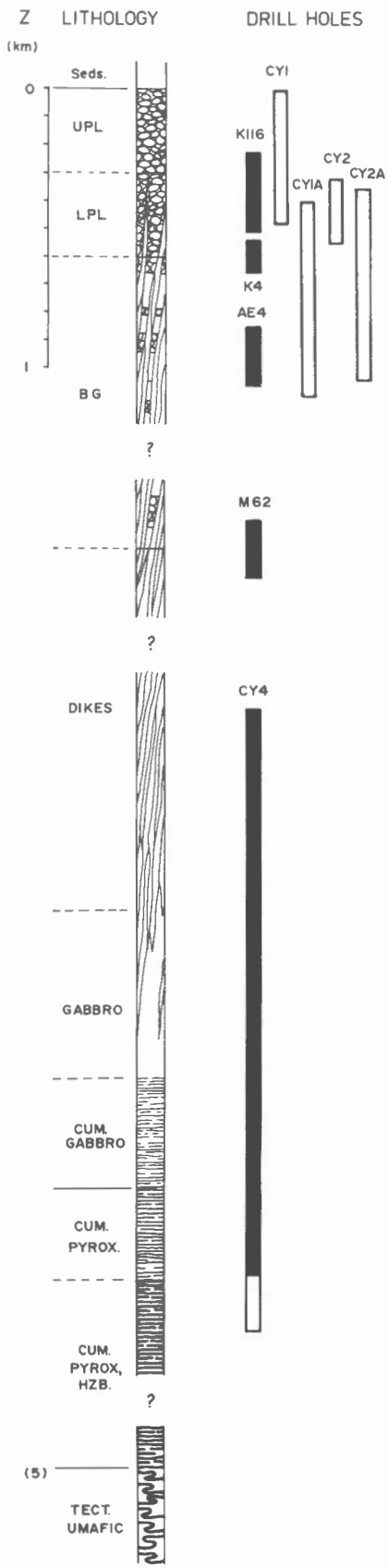

Resistivity (RO1).

The resistivity, or focussed electric sonde consists of a current electrode and two guard electrodes in a housing which measures 2.8 m long by 3.8 cm (1-1/2") in diameter. The tool measures formation resistivity as a function of depth by transmitting a constant current into the formation in the form of a thin, horizontal sheet and monitoring the voltage between an electrode located in the tool and a second electrode in a bridle 40 feet above the sonde. The tool can operate in fluid-filled holes up to 10" in diameter but works best in holes less than 8" in diameter. The depth of penetration depends on formation conditions, but often exceeds 1 m.

Compressional wave velocity (MS1).

Compressional wave velocities were measured using a multichannel sonic tool containing a ceramic transducer and four receivers spaced 60, 80, 100 and 120 cm, respectively, below the transmitter in a rigid housing measuring 3.4 m long by 6.5 cm (2-1/2") in diameter (including centralizers). Velocities were determined for different path lengths through the borehole wall by comparing the differences in first arrival times for different receiver pairs. The long (60 cm) path is felt to minimize the effects of rugosity and to provide the best average formation velocity while the short (20 cm) paths give fracture locations and the best bed resolution. The tool is designed to operate in water-filled boreholes up to 10" in diameter. Integrated travel times were computed from the velocity vs depth data after the completion of logging.

Shear wave velocity.

Shear wave velocities were determined using a prototype full wave sonic tool which was clamped against the borehole wall at selected depths, generally 10 m apart. The tool, which was 3 m long and 6.5 cm (2-1/2") in diameter has a rigid upper housing with an excentralizer at the top and an opposing retractable caliper arm at the lower end. The lower housing, which was flexible, contained a transducer at the base, a single receiver 50 cm above the transducer and two button standoffs on the side opposite the caliper arm, one near the transducer, the other near the receiver. When the tool was being lowered, the caliper was retracted but when positioned for a measurement, the caliper was extended, pressing the buttons against the borehole wall. Once the transducer was activated, P-waves were transmitted to the wall through the borehole fluid and S-waves were generated in the borehole wall by P to S conversion. Velocities of both S and P-waves were calculated from transit times measured on photographs of the waveforms.

Figure 3: Lithology vs. estimated depth in the Troodos ophiolite. Bars indicate positions of ICRGD and other drill holes: solid + logged; open + cored only. Abbreviations: UPL, LPL = upper and lower pillow lava; BG = basal group; CUM = cumulate; PYROX. = pyroxenite; BZB = harzburgite; TECT. = tectonite.

Magnetometer.

The total magnetic field was measured using a modified BPB verticality sonde (VO1). This normally consists of three orthogonal fluxgate magnetometers (one vertical, two horizontal) to measure tool azimuth and two inclinometers to measure tilt, in a 2.6 m long x 4.2 cm (1.7") diameter housing. In the present application, the physical configuration remained unchanged but the sensitivity of the fluxgate magnetometers was increased to 50γ so that the tool could function as a borehole magnetometer. Although the total field strength can be calculated as a function of depth from the 3-component fluxgate data, the declination cannot be determined because the tool was not gyro-stabilized. The tool was calibrated before and after each run by measuring the total field at the drillsite with both the borehole sonde and a proton precession magnetometer provided by the Cyprus Geological Survey. Since the borehole magnetometer data obtained in Cyprus is presented in detail elsewhere (Pariso and Johnson, this volume), it will not be discussed further in this paper.

Magnetic susceptibility.

The final tool was a Geoinstruments Ky magnetic susceptibility tool. The probe consisted of a solenoid sensing coil and associated electronics in a 2.5 m long x 5 cm (2") diameter housing. Since the tool only had a pressure rating of 150 bars (the strength of the fiberglass pressure case around the sensor), it could only be lowered to about 1600 m.

Downhole Operations

It was originally intended to log ICRDG holes CY-2, 2a and 4 upon the completion of drilling in CY-4 and then return to log CY-1 and 1a as drilling was completed in CY-1a. This would insure that the most important holes, CY-1a and 4, were logged immediately after drilling while the drill rig was still on site and before the holes had time to collapse. The strategy was successful as far as CY-4 was concerned, but hole CY-1a could not be logged because it tapped a high pressure aquifer and the remaining holes collapsed during or immediately after drilling. For this reason, a series of alternate holes (Table 3) drilled by Hellenic Mining and the Bureau de Recherches Geologiques et Minieres was logged in order to obtain data from sections equivalent to those drilled in holes CY-1, 1a, 2 and 2a (Figure 3).

As can be seen in Table 4, Table 5 and Figure 4, the logging operations themselves were very successful. Over 30.7 km of logs (280K data points) were obtained during the course of 43 separate lowerings in five holes. Nearly 3 km of section representing virtually every lithology in the complex except the ultramafic tectonites was logged, making this the most comprehensive suite of logs ever obtained in oceanic crust.

The deepest hole, CY-4, was logged in two stages: during the first, the interval from 862-2075 m was logged open-hole with all of the logging tools and the interval from 862 m to the surface was logged through the pipe (HQ) using the nuclear (ρ, γ, ϕ) and temperature tools. During the second stage, the interval from 0-640 m was re-logged open-hole with all of the logging tools after the pipe had been pulled. The interval from 640-862 m was never logged open-hole because of stuck pipe and the interval from 2075-2262 m was not logged because it was drilled after the completion of logging. The only difficulty encountered during the logging operations in CY-4 was the loss of the shear wave sonic tool on the last run in the lower part of the hole when the tool became stuck and the cable parted at 1997 m. The tool was successfully fished, however, and the logging run completed, leaving the hole open for further operations.

The logging operations in the alternate holes were completed almost without incident. The only difficulties encountered were an electronic failure in the magnetic susceptibility tool which prevented its use in holes K4, AE4 and M62 and the collapse of hole M62 before it could be logged with the caliper and nuclear tools.

As can be seen in Table 4 and Figure 5, the tools worked well and the hole conditions were optimal for almost all of the tools employed. The water table was close to the surface in all holes and borehole temperatures ranged from 18°C at the surface to a maximum of 45°C at the base of CY-4, or well within the operating limits of the tools. Although the shallow holes at the top of the section (K116, K4, AE4 and M62) were rugose, CY-4 was smooth-walled and all were in gauge (diam. <8") with few cavings. Only two problems were encountered: 1) The resistivity tool saturated intermittently in the lower levels of CY-4 because the formation resistivity exceeded the limits of the tool (80K ohm-m). This occurred because the formation fluid consists of relatively fresh water and the formation itself is tight. 2) The logs obtained between 640-862 m in CY-4 are only intermediate in quality because they were obtained through pipe.

DATA

The logging data obtained in holes K116, K4, AE4, M62 and CY-4 is presented in Figure 6. Only two corrections have been applied: 1) Natural gamma, porosity, density, velocity and resistivity data obtained above the water table and within ±1 m of the breakouts shown in Figure 5 have been deleted. 2) The nuclear logs obtained between 640-862 m in hole CY-4 have been corrected for the pipe by determining the average value for each parameter (natural gamma radiation, porosity, density) in the cased interval, the averages of the data 50 m above and below the casing and correcting the raw data by the differences (+1.5 API units, −7%, and −.14 g/cm^3, respectively).

TABLE 3: Supplementary Drillholes Examined by Logging

Hole[1]	Coordinates	Drilled by	Penetration (m)	Logged Interval (m)	Crustal Level	Lithology	Depth[2] Range (m)
K116	35°00'58"N 33°12'43"E	Hellenic Mining	300	283	Extrusives	Upper pillow basalts Lower pillow basalts	0-50 50-300
K4	34°59'58"N 33°12'15"E	BRGM[3]	116	110	Extrusives	Lower pillow basalts Basal group	0-70 70-116
AE	34°59'42"N 33°07'30"E	BRGM	216	212	Extrusives	Basal group	0-216
M62	35°01'23"N 33°07'05"E	BRGM	208	208	Extrusives Plutonic	Basal group Sheeted dikes	Gradational contact

(1) K = Klirou, AE = Ayios Epiphanious, M = Mitsero;
(2) Based on petrology; (3) BRGM = Bureau de Recherches Geologiques et Minieres.

Although most of the data may be taken at face value and compared directly with oceanic data, the porosity and resistivity data may not, the porosity data because the neutron porosity tool is not calibrated to work in mafic rocks, the resistivity data because the formation is saturated with fresh (actually slightly brackish) water rather than seawater. In consequence, both tools tend to read high.

An accurate porosity log can be calculated from the density log, however, if the grain density, ρ_g, is known as a function of depth, by using the relation:

$$\phi_D = \frac{\rho_g - \rho_{log}}{\rho_g - \rho_f}$$

where ϕ_D is the porosity determined from density, ρ_{log} is the density determined by logging and ρ_f the density of water (1.01 g/cm). In most logging operations, such a log is difficult to reconstruct because of poor recovery, but the ICRDG holes were continuously cored with extremely high recovery (99.9%) and grain densities were determined on core samples every 5 to 10 m (Figure 7). It was thus possible to calculate porosity logs for holes K116, K4, AE4 and CY-4 using the density logs shown in Figure 6 and the average and least squares grain density vs. depth solutions shown in Figure 7. These logs, together with the remaining logs from Figure 6 are presented in Figure 8 after smoothing with a 1000-point (100 m) running average in order to show average formation properties as a function of depth. The shear wave velocities have been smoothed with a 5-point (50 m) running average.

Finally, a synthetic resistivity log was calculated for insitu oceanographic conditions of water saturation and temperature from the calculated porosity log using Archie's Law:

$$R = \frac{R_f}{\phi_D^n}$$

where R is the formation resistivity, n = 2, ϕ_D is the calculated porosity from Equation 1 and R_f is the resistivity of the formation fluid (sea water) calculated from Arp's Law assuming a temperature of 60°C at the sediment/basement contact and a temperature gradient of 100°C/km as in hole 504B (Becker et al., 1985). The resulting log, also shown in Figure 8, was thus calculated on the assumption that the formation resistivity is controlled by porosity and does not take into account second order effects due to surface conduction and metallic minerals.

TABLE 4. Downhole operations summary (supplementary drillholes).

Hole	Run	Date	Logging Interval (m)	Water Table (m)	Logging Direction	Tool/Measurement	Remarks[1]
K116	1	7/2/84	0-283	10	Down	TT1 Temperature	24°C at base of hole
	2	7/2/84	6-283	10	Up	Magnetometer	Not centralized
	3	7/2/84	2-282	10	Up	DD3 Caliper	Rugose hole; ave.
						Natural γ	diameter = 5-3/4"
						γ density	
	4	7/2/84	10-283	10	Up	NN1 Neutron porosity	
						Natural γ	
	5	7/2/84	10-282	10	Up	RO1 Resistivity	
	6	7/2/84	10-282	10	Up	MS1 Vp	
	7	7/2/84	2-282	10	Up	Magnetic susceptibility	
	8	7/2/84	11-280	10	Up	Shear wave sonic	
K4	1	11/6/85	0-111	10	Down	TT1 Temperature	22°C at base of hole
	2	11/6/85	0-111	10	Up	Magnetometer	Not centralized
	3	11/6/85	10-111	10	Up	RO1 Resistivity	
	4	11/6/85	10-110	10	Up	MS1 Vp	Not centralized
	5	11/6/85	20-111	10	Up	Shear wave sonic	
	6	11/7/85	0-110	10	Up	DD3 Caliper	Rugose hole; ave.
						Natural γ	diameter = 5-1/2"
						γ density	
	7	11/7/85	2-111	10	Up	NN1 Neutron porosity	
						Natural γ	
AE4	1	11/9/85	0-213	14	Down	TT1 Temperature	22.5°C at base of hole
	2	11/9/85	17-213	14	Up	RO1 Resistivity	
	3	11/9/85	15-212	14	Up	MS1 Vp	
	4	11/9/85	0-212	14	Up	DD3 Caliper	Rugose hole; ave.
						Natural γ	diameter = 8"
						γ density	
	5	11/9/85	16-213	14	Up	NN1 Neutron porosity	
						Natural γ	
	6	11/9/85	0-213	14	Up	Magnetometer	
	7	11/9/85	20-210	14	Up	Shear wave sonc	
M62	1	11/5/85	1-208	0	Down	TT1 Temperature	22°C at base of hole
	2	11/5/85	1-192	0	Up	Magnetometer	Not centralized
	3	11/5/85	4-191	0	Up	RO1 Resistivity	R_f = 15 ohm/m at 19°C
	4	11/5/85	1-191	0	Up	MS1 Vp	
	5	11/5/85	4-189	0	Up	Shear wave sonic	Rugose hole; ave.
							diameter = 7-1/2"

(1) Data quality was good in all cases. Holes K116, K4, AE4 and M62 logged open-hole (no casing). Borehole fluid = groundwater.

TABLE 5. Downhole operations summary for CY-4.

Run	Date	Logging Interval (m)	Water Table (m)	Logging Direction	Tool/Measurement	Remarks[1]
1	6/26/84	0-862	80	Down	TT1 Temperature	Inside pipe
		862-2075	80		Temperature	45°C at base of hole
2	6/27/84	0-862	80	Up	DD3 Caliper	Inside pipe
		862-2075	80		Caliper	Smooth hole; diameter = 3-1/4"
		0-862	80		Natural γ	Data Fair. Through pipe
		862-2075	80		Natural γ	
		0-862	80		γ density	Data Fair. Through pipe
		862-2075	80		γ density	
3	6/27/84	864-2075	80	Up	MS1 Vp	Not centralized
4	6/27/84	80-862	80	Up	NN1 Neutron porosity	Through pipe
		862-2075	80		Neutron porosity	
		80-862	80		Natural γ	Data Fair. Through pipe
		862-2075	80		Natural γ	
5	6/28/84	864-2075	80	Up	RO1 Resistivity	R_f = 25 ohm/m at 19°C
6	6/28/–					
	6/29/84	864-2075	80	Up	Magnetometer	Not centralized
7	6/29/84	864-1580	80	Up	Magnetic susceptibility	Logged to pressure rating of tool
8	6/29/–					
	6/30/84	863-1997	45	Up	Shear wave sonic	Logged to bridge
9	7/13/84	0-640	45	Down	TT1 Temperature	23°C at base of logged interval
10	7/13/84	0-640	45	Up	DD3 Caliper	Smooth hole; diameter = 4-1/4"
					Natural γ	0-19 m through casing
					γ density	0-19 m through casing
11	7/13/84	46-639	45	Up	MS1 Vp	
12	7/13/84	0-640	45	Up	NN1 Neutron porosity	0-19 m through casing
					Natural γ	
13	7/13/84	20-640	45	Up	Magnetometer	Not centralized
14	7/13/84	46-640	45	Up	RO1 Resistivity	R_f = 20 ohm/m at 18°C
15	7/13/84	20-640	45	Up	Magnetic susceptibility	
16	7/13/84	50-630	45	Up	Shear wave sonic	

(1) Data quality is good accept where indicated. Runs 1-8: logged through casing plus HQ pipe from 0-19 m, through HQ pipe from 19-862 m, open-hole from 862-2075 m. Runs 9-16 logged through casing from 0-19 m, open-hole from 19-640 m. Borehole fluid - mixture of groundwater and Kutwell.

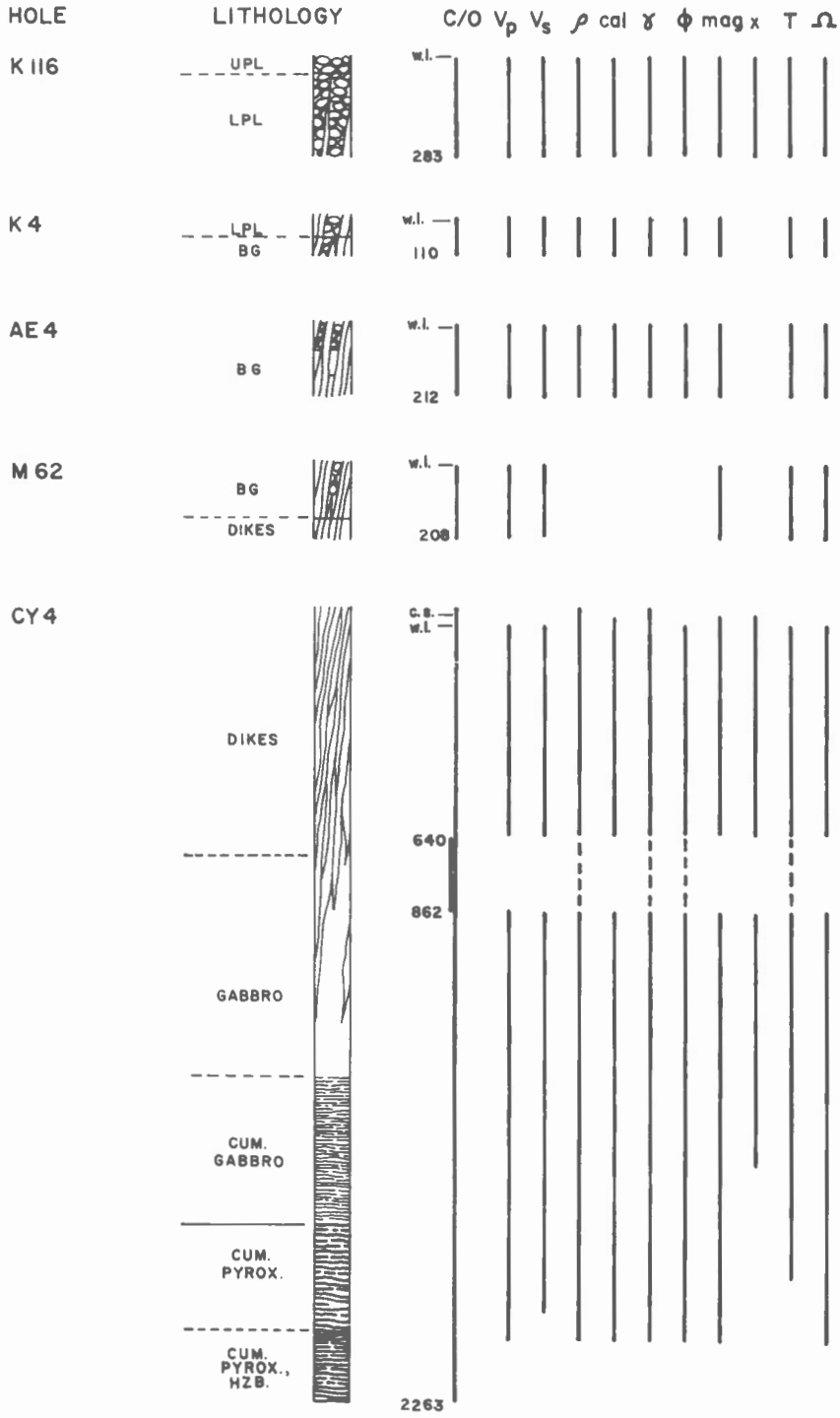

Figure 4: Log quality vs. depth in holes K116, K4, AE4, M62, and CY-4; solid line = good; dashed line = fair; Abbreviations: UPL = upper pillow lava; LPL = lower pillow lava; BG = basal group; CUM = cumulate; HXB = harzburg C/O = cased/open hole; Vp = compressional wave velocity; Vs = shear wave velocity; ρ = density; cal. = caliper; γ = natural gamma radiation; ϕ = neutron porosity; mag. = 3 axis magnetometer; x = magnetic susceptibility; T = temperature; ς = resistivity; w.l. = water level; c.s. = casing shoe. Depth in metres.

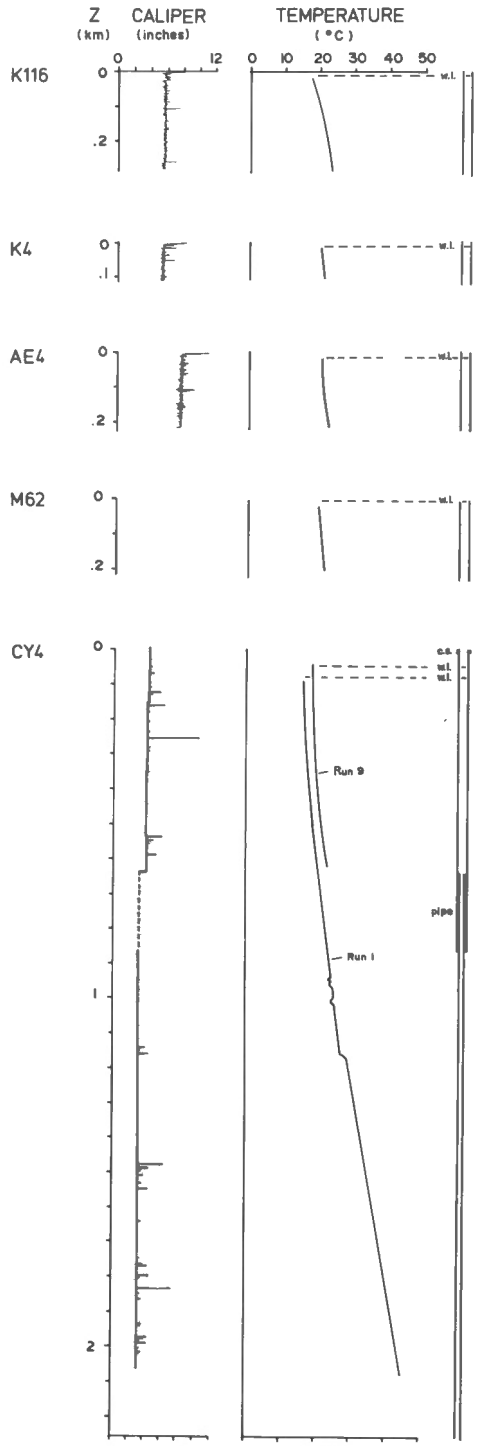

Figure 5: Hole conditions (borehole diameter, temperature) vs. depth in holes K116, K4, AE4, M62 and CY-4. Holes were logged openhole except for interval from 640-862 m in hole CY-4 which was logged through pipe. Abbreviations: w.l. = water level; c.s. = casing shoe

RESULTS

As can be seen in Figures 6 and 8, the geophysical formation properties of the Troodos ophiolite vary markedly with depth in response to changes in porosity and lithology:

Natural gamma radioactivity.

The natural gamma radioactivity of the complex is high and variable (10 to 50 API units about a mean of 30) in the pillow basalts, but decreases irregularly through the pillow basalt/dike transition zone to uniform values of 5-10 API units in the sheeted dikes and finally, to negligible values in the underlying plutonic section. The low natural gamma radioactivity of the plutonic section is typical of fresh rocks of the mafic-ultramafic rock series which normally contain only small amounts of K, U or Th. The higher radioactivity observed in the extrusives is similar to that observed in altered pillow basalts at sea (e.g. DSDP hole 418A; Salisbury et al., in press) where it is associated with K uptake in low temperature alteration products such as K-feldspar, palagonite and other clay minerals (Flower et al., 1980; Holmes, in press). The simultaneous disappearance of dikes and measurable high natural gamma radiation at a depth of 800-900 m in hole CY-4 suggests that sea water penetration in the oceanic crust is controlled by dikes.

Porosity.

As can be seen in Figures 6 and 8 respectively, the apparent and calculated porosities both decrease with depth from a maximum in the pillow basalts to a minimum in the gabbros and ultramafics. Specifically, the calculated porosity curve, which is considered an accurate estimate of the average formation porosity due to cracks, and microcracks, decreases from approximately 20% in the pillow basalts to 5-10% in the sheeted dikes and finally, to 2-4% in the gabbros and negligible values in the ultramafics. The values obtained in the pillow basalts are similar to those obtained at comparable levels in DSDP/ODP holes 418A and 504B (10-20%, and 10-15%, respectively; Becker et al., 1982; Salisbury et al., in press) where packer tests demonstrate that the extrusive section is highly permeable (Anderson and Zoback, 1982). The extremely low porosities measured at deeper levels in the Troodos ophiolite suggest that the intrusive section is tight.

The apparent porosity curve shown in Figure 6 displays the same trend of decreasing porosity with depth as the calculated porosity but invariably gives higher values. This is due to tool calibration problems and the fact that the neutron tool senses bound water as well as water associated with grain boundaries, cracks and interpillow voids. Thus the high apparent porosity in the pillow basalts is likely due to alteration and the slight increase in the ultramafics at the base of the section is probably due to partial serpentinization.

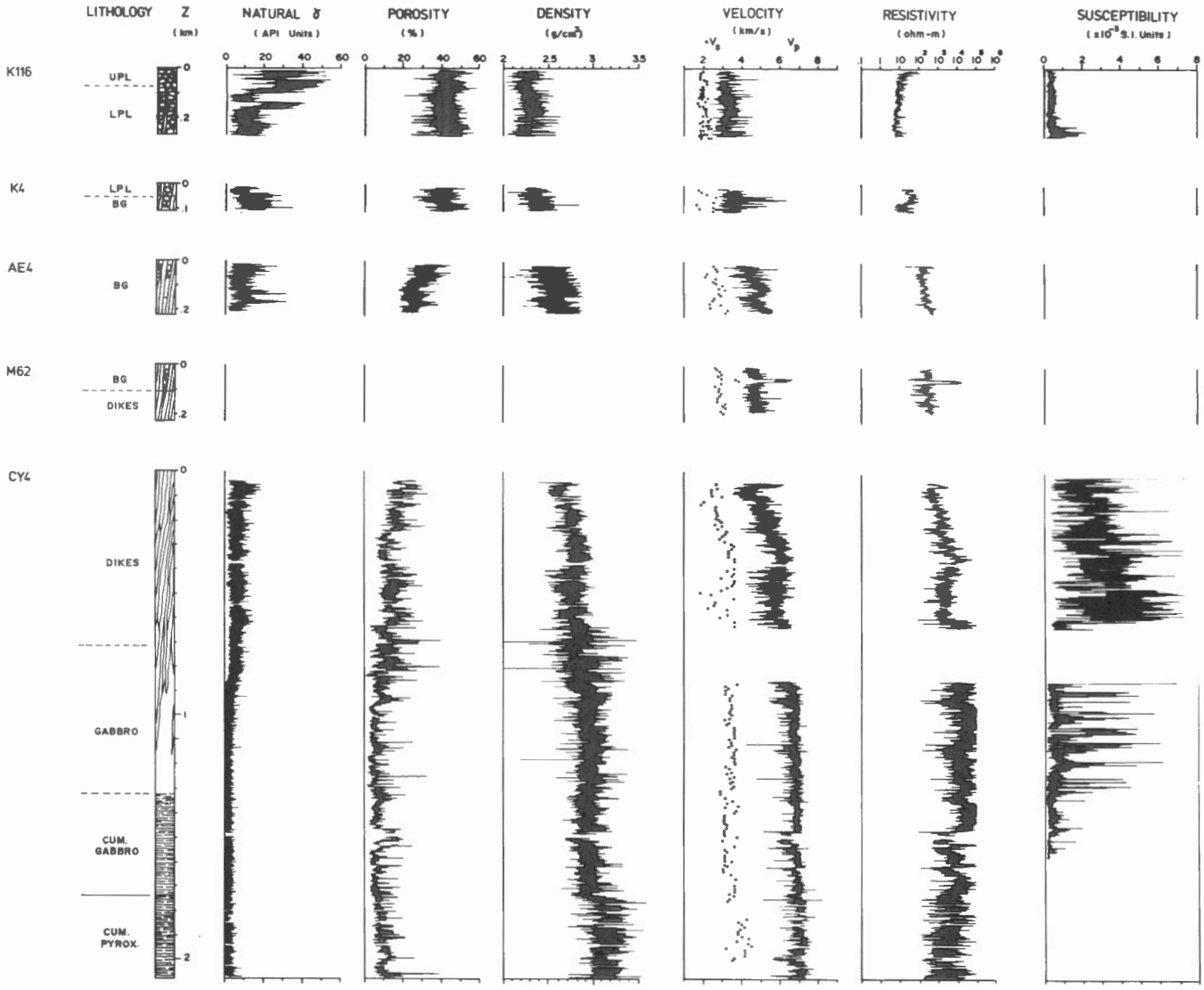

Figure 6: Natural gamma, apparent porosity, density, velocity (Vp and Vs), resistivity and susceptibility logging data from holes K116, K4, AE4, M62 and CY-4. Data from breakouts (see Figure 5) has been deleted and data from cased interval between 640-862 m has been corrected for pipe. Abbreviations as in Figure 4.

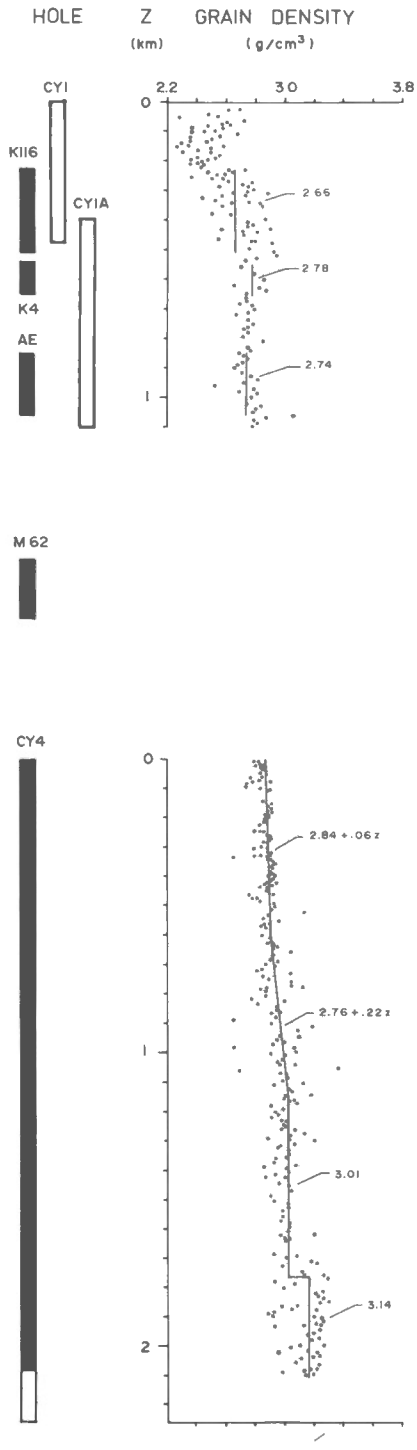

Figure 7: Laboratory grain density data for core samples from holes CY-1, CY-1a and CY-4. Curves represent averages and least squares solutions used to obtain corrected porostiy log.

Density.

As expected, the formation density increases with depth in response to increasing grain density and decreasing porosity. The average density ranges from 2.2-2.3 g/cm^3 in the altered pillow basalts at the top of the section, increases gradually through the pillow basalt/dike transition to values of 2.6-2.8 g/cm^3 in the dikes, increases again to values of 2.9-2.95 g/cm^3 in the gabbros and finally increases abruptly to 3.1 g/cm^3 at the gabbro/pyroxenite boundary. From Figure 8, it is clear that density is controlled largely by porosity since the density varies inversely with porosity. Nonetheless, the sharp increase in density at the top of the pyroxenites is clearly due to a change in composition since both the apparent and the calculated porosity show little change across the gabbro/pyroxenite boundary while the average grain density jumps by 0.13 g/cm^3 (Figure 7). It is also apparent from Figure 7 that the increase in formation density observed from the pillow basalts to the base of the gabbros is due in part to a gradual increase in grain density which we attribute, in turn, to decreasing alteration and glass content with depth.

Velocity.

Perhaps the most striking logs obtained in the Troodos ophiolite are the compressional and shear wave velocity logs. These show that Vp and Vs are low and fairly uniform in the pillow basalts (3.2-3.5 and 2.0-2.2 km/s, respectively), but increase irregularly through the pillow basalt/dike transition to values as high as 5.0 and 3.0 km/s, respectively, near the base of the transition zone (Basal Group). Within the sheeted dikes, velocities continue to increase irregularly with depth in response to increasing metamorphic grade (Christensen and Salisbury, this volume) and eventually, to the presence of gabbro screens. Near the base of the dikes, where the gabbro screens and dikes are about equally abundant (600 m in hole CY-4), Vp increases rapidly to 6.4 km/s and then more slowly through the remainder of the dike/gabbro transition to uniform values of 6.7-6.9 km/s in the gabbros, while Vs rises to 3.5 km/s in the transition and ranges between 3.2-3.5 km/s in the gabbros. In the deepest unit logged, the pyroxenites, Vp reaches values as high as 7.4 km/s but averages 7.0, while Vs averages 4.0 km/s. Since pyroxenites are often fast parallel to layering, however, and the logging tool only measures velocity in the vertical direction, the average compressional wave velocities reported here may be low.

As in the case of density, the velocity of the section is controlled largely by formation porosity and only secondarily by composition except in the gabbros and ultramafics where the porosity is negligible. Thus the formation velocities are generally lower than the measured velocities of rocks from equivalent depths (Smith and Vine, 1987; Christensen et al., 1987; Christensen and Salisbury, 1989).

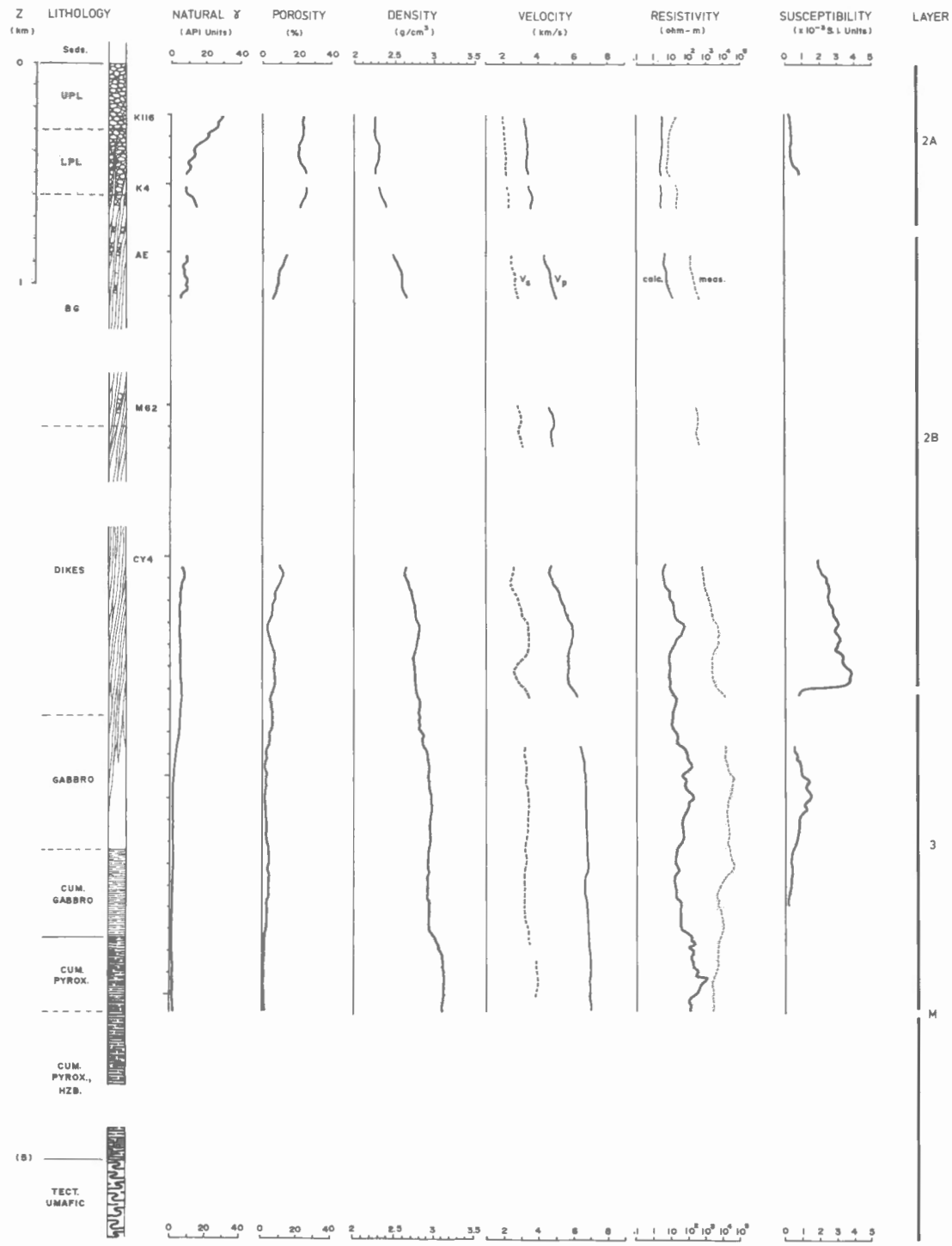

Figure 8: Average formation properties vs. depth and lithology in the Troodos ophiolite. Porosity log calculted for density log and measured grain densities; calculated resistivity log derived from calculated porosity log assuming cracks and pores are filled with seawater, T = 60°C at the sediment/basement contact and a geothermal gradient of 100°C/km as in DSDP hole 504B. Equivalent oceanic velocity layers are shown on right

Nonetheless, the velocity logs obtained in the Troodos ophiolite agree quite well with the limited suite of logs obtained to date in equivalent sections at sea. The compressional wave velocities obtained in DSDP/ODP hole 504B, for example, increase from approximately 3.5 km/s in the pillow basalts to 6.0 km/s in the sheeted dikes, while Vs increases from about 2.0 km/s to 3.2 km/s over the same interval (Newmark et al., 1985). Similarly, the compressional wave velocities logged in the only extensive interval of submarine gabbros drilled to date average 6.5-6.7 km/s (ODP hole 735; P.T. Robinson, personal communication) and would undoubtedly be higher at confining pressures equivalent to those logged in the Troodos Massif (the gabbros in hole 735 are exposed on the seafloor and are thus at a low effective confining pressure).

Resistivity.

As can be seen in Figures 6 and 8, the measured resistivity increases irregularly from a low of about 10 ohm-m in the pillow basalts to approximately 2000 ohm-m near the base of the dikes. At the dike/gabbro boundary defined above (50% dikes, 50% gabbro screens), the resistivity increases sharply by an order of magnitude and ranges between 20K-50K ohm-m in the massive gabbros before decreasing again in the cumulate gabbros and ultramafics to values as low as 3000 ohm-m. While the measured values shown in Figures 6 and 8 may be high compared to oceanic values since the formation fluid consists of brackish, rather than sea water, the trends would appear to be correct: resistivities are low in the pillow basalts due to high porosity and surface conduction in clays and other alteration products; the resistivity increases markedly with depth in response to decreasing porosity; near the bottom of the section, the resistivity decreases again due to mineral conduction in magnetite and to surface conduction in serpentine minerals.

The calculated resistivity is invariably lower than the measured resistivity since it takes into account the presence of sea water and assumes an oceanic geothermal gradient. While the two curves mimic each other throughout the dikes, the trend is less convincing in the pillow basalts at the top of the section and in the cumulate gabbros and ultramafics at the base. It is likely, however, that if mineral and surface conduction effects, were also taken into account, the calculated values would be lower in these intervals and the match would improve. Although resistivity logs have not been obtained in oceanic crust to the depths logged in Cyprus, where logs have been obtained in equivalent lithologies, the trends and values have been similar. For example, the resistivities increase with depth by more than an order of magnitude in the uppermost kilometer of hole 504B and range from 5-30 ohm-m in the pillow basalts to between 100-500 ohm-m in the sheeted dikes (Becker, 1985).

TABLE 6: Ocean Crust Layered Velocity Models.

Layer	Velocity Vp (km/s)	Thickness (km)
Raitt (1963)		
2	5.07 ± 0.63	1.71 ± 0.75
3	6.69 ± 0.26	4.86 ± 1.42
Mantle	8.13 ± 0.24	–
Peterson et al. (1974)		
1	1.7–2.0	0.5
2A	2.5–3.8	0.5–1.5
2B	4.0–6.0	0.5–1.5
3A	6.5–6.8	2.0–3.0
3B	7.0–7.8	2.0–5.0
Mantle	8.1	–
Houtz and Ewing (1976 Pacific case)		
2A	3.33 ± 0.10	0.74 ± 0.23
2B	5.23 ± 0.44	0.72 ± 0.26
2C	6.19 ± 0.16	1.83 ± 0.75(1)
3	6.92 ± 0.17	–(2)

(1) Cumulative thickness of Layers 2B and 2C.
(2) In general, the mantle and Layer 3 were not detected.

Magnetic Susceptibility.

The final, and perhaps most distinctive, log obtained in the Troodos ophiolite is the magnetic susceptibility log. As can be seen in Figures 6 and 8, the susceptibility is very low (less than 0.5×10^{-3} S.I. Units) in the pillow basalts but rises with increasing magnetite content through the sheeted dikes to an average of about 4×10^{-3} S.I. Units near the dike/gabbro transition at 600 m in hole CY-4. In the underlying gabbros, magnetite disappears and the susceptibility decreases abruptly to about 0.5×10^{-3} S.I. Units , with higher spikes marking individual dikes cutting the gabbro. Although not shown in these figures, the susceptibility values in the sheeted dikes display a bimodal distribution which suggests the presence of at least two generations of dikes.

CONCLUSIONS

It has been suggested that the ophiolites are fragments of oceanic crust which have been emplaced on land by tectonic processes and subsequently exposed by erosion. While attractive and accepted by most geologists, the hypothesis has been difficult to prove: Drilling in the ocean basins has failed to recover a complete section through the crust for comparison with the ophiolites. Dredging in oceanic transforms has recovered lithologies similar to those observed in ophiolites, but the crust is thin and sheared in the vicinity of transforms and was produced in an anomalous thermal environment (e.g., Mutter et al., 1984). Similarly, geophysical studies in the ophiolites have not been entirely successful in reconstructing the geophysical properties of the ophiolites for comparison with oceanic data: while recent refraction studies in the Troodos extrusives give velocities consistent with those of Layer 2 (Eleftheriou and Schoenharting, 1987), velocities characteristic of Layer 3 have not been detected deeper in the section (Khan et al., 1972). Similarly, laboratory studies of the velocities of samples from ophiolites tend to give maximum velocities, especially in the upper parts of the section, because they fail to take cracks into consideration (e.g. Salisbury and Christensen, 1978).

The insitu logging data obtained in the Troodos ophiolite, on the other hand, is in excellent agreement with logging data obtained in the upper levels of the oceanic crust and with the geophysical properties of the lower crust inferred from marine geophysical studies. From this fact, and the data presented in Figures 6 and 8, we conclude that:

1. In geophysical terms, the Troodos ophiolite is almost indistinguishable from oceanic crust. However, the Oceanic Layer (Layer 3) is thin, even though the total thickness of the crust falls within the range of thicknesses observed at sea (Table 5). This is consistent with formation near an oceanic fracture zone such as the Arakapas Fault.

2. From a comparison of velocity logs and petrology in the Troodos Massif, Layer 2A consists of pillow basalts, 2B consists of the pillow basalt to dike transition plus the underlying sheeted dikes, and Layer 3 consists of massive gabbros, cumulate gabbros and pyroxenites. If the section was restored to full pressure, the velocity of the sheeted dikes would almost certainly rise to those of Layer 2C as defined by Houtz and Ewing (1976) and the velocities of the pyroxenites would match those of Layer 3B or even the uppermost mantle, if measured in the horizontal direction. The harzburgites were not logged, but from laboratory studies of the velocities of samples from this interval (Christensen and Salisbury, this volume) it is clear they will display mantle velocities (7.8-8.1 km/s) since the formation porosity approaches zero.

3. The Layer 2/3 boundary marks the transition from sheeted dikes to massive gabbros and represents not only a velocity discontinuity, but a pronounced resistivity discontinuity (plus 10×) and a sharp magnetic susceptibility discontinuity (minus 5×).

4. Throughout the upper levels of the crust, most formation properties are controlled largely by porosity, which decreases dramatically with depth from a maximum of about 20% in the pillow basalts to negligible values at the base of the dike/gabbro transition. Thus the density, velocity and resistivity are all low and relatively uniform in the pillow basalts of Layer 2A but increase irregularly throughout Layer 2B in response to decreasing porosity.

5. Below the dike/gabbro transition, the formation properties are controlled by composition and approach rock properties. This implies that the lower oceanic crust is impermeable.

6. It follows that circulation involving sea water penetrates no deeper than the base of the dike/gabbro transition. This is confirmed by the absence of K-bearing clays at greater depths and demonstrates that except in anormalous regions such as fracture zones, rock-seawater interaction is limited to the upper levels of the crust.

ACKNOWLEDGEMENTS

We wish to thank Ken Lowe, Peter Mackowiak and Paul Stedman of B.P.B. Instruments for their assistance in obtaining the logs, Dr. Andreas Panayiotou and the Staff of the Geological Survey Department, Cyprus, for their excellent logistical support, Dr. James Hall and Lata Hall for their encouragement and considerable assistance in the field and the International Crustal Research Drilling Group for the opportunity to participate in the project. We also wish to thank Jane Barrett for typing the manuscript and Mel Best for serving as a reviewer. This work was supported under NSF grant EAR 82-18096, ONR contract N84K0207 and NSERC grant 0039133.

REFERENCES

Anderson, R.N. and Zoback, M.D.
1982: Permeability, under-pressures and convection in the oceanic crust near the Costa Rica Rift, eastern equatorial Pacific; Journal of Geophysical Research, v. 87, p. 2860-2868.

Becker, K.
1985: Large-scale electrical resistivity and bulk porosity of the oceanic crust, Deep Sea Drilling Project Hole 504B, Costa Rica Rift; *in* Initial Reports of the Deep Sea Drilling Project, R.N. Anderson, J. Honnorez, K. Becker, et al.; U.S. Government Printing Office, Washington, D.C., v. 83, p. 419-428.

Becker, K., Langseth, M.G., Von Herzen, R.P., Anderson, R.N. and Hobart, M.A.
1985: Deep crustal geothermal measurements, Hole 504B, Deep Sea Drilling Project, Legs 69, 70, 83 and 92; *in* Initial Reports of the Deep Sea Drilling Project, R.N. Anderson, J. Honnorez, K. Becker, et al.; U.S. Goverment Printing Office, Washington, D.C. v. 83 p. 405-418.

Becker, K., Von Herzen, R.P., Francis, T.J.G., Anderson, R.N., Honnorez, J., Adamson, A.C., Alt, J.C., Emmermann, R., Kempton, P.D., Kinoshita, H., Laverne, C., Mottl, M.J. and Newmark, R.L.
1982: In situ electrical resistivity and bulk porosity of the oceanic crust, Costa Rica Rift; Nature, v. 300, p. 594-598.

Christensen, N.I., Wepfer, W.W. and Salisbury, M.H.
1987: Seismic properties of samples from the volcanic section of the Troodos ophiolite, Hole CY-2a; *in* Cyprus Crustal Study Project Initial Report, Holes CY2-2a, ed. P.T. Robinson, I.L. Gibson and A. Panayiotou; Geological Survey of Canada, Paper 85-29, p. 307-316.

Christensen, N.I. and Salisbury, M.H.
1989: Velocity structure of the Troodos Massif, an arc-derived ophiolite; *in* Cyprus Crustal Study Project Initial Report, Hole CY-4, ed. I.L. Gibson, J. Malpas, P.T. Robinson and C. Xenophontos; Geological Survey of Canada, Paper 88-9.

Coleman, R.G.
1977: Ophiolites: Ancient Oceanic Lithosphere?; Springer-Verlag, Berlin; Heidelberg; New York.

Eleftheriou, S. and Schoenharting, G.
1987: A seismic survey at the Agrokipia mine, Cyprus: the velocity structure of a hydrothermally altered extrusive section of the Troodos ophiolite; *in* Cyprus Crustal Study Project Initial Report Holes CY2-2a, ed. P.T. Robinson, I.L. Gibson and A. Panayiotou; Geological Survey of Canada, Paper 85- 29, p. 317-326.

Flower, M., Ohnmacht, W., Robinson, P., Marriner, G. and Schminke, H.-U.
1980: Lithologic and chemical stratigraphy at Deep Sea Drilling Project Sites 417 and 418; *in* Initial Reports of the Deep Sea Drilling Project, Part 2, ed. T. Donnelly, J. Francheteau, W. Bryan, P. Robinson, M. Flower, M. Salisbury, et al.; U.S. Government Printing Office, Washington, D.C., v. 51, 52, 53, p. 939-956.

Gass, I.G.
1968: Is the Troodos Massif of Cyprus a fragment of Mesozoic ocean floor?; Nature, v. 220, p. 39-42.

Gillis, K.M.
1986: Multistage alteration of the extrusive sequence, Troodos ophiolite, Cyprus; unpublished Ph.D. Thesis, Dalhousie University, Halifax, Nova Scotia, Canada, 387 p.

Holmes, M.A.
In Press: Evidence for continuous and discontinuous alteration in DSDP Hole 418A basalts and its significance to natural gamma ray log readings; *in* Proceedings of the Ocean Drilling Program Initial Reports, ed. M.H. Salisbury, J.H. Scott, et al.; Part B, v. 102

Houtz, R. and Ewing, J.
1976: Upper crustal structure as a function of plate age; Journal of Geophysical Research, v. 81, p. 2490-2498.

Khan, M.A., Summers, C., Bamford, S.A.D., Chroston, P.N., Poster, C.K. and Vine, F.J.
1972: Reversed seismic refraction line on the Troodos Massif, Cyprus; Nature, v. 238, p. 134-136.

Miyashiro, A.
1973: The Troodos ophiolite complex was probably formed in an island arc; Earth and Planetary Science Letters, v. 19, no. 2, p. 218-224.

Moores, E.M. and Vine, F.J.
1971: Troodos Massif Cyprus, and other ophiolites as oceanic crust: evaluation and implications; *in* A discussion on the Petrology of Igneous and Metamorphic Rocks from the Ocean Floor; Philosophical Transactions of the Royal Society of London, Series A, v. 268, p. 443-466.

Mutter, J.C., Detrick, R.S. and NAT Study Group,
1984: Multichannel seismic evidence for anomalously thin crust at oceanic fracture zones; Geology, v. 12, p. 534-537.

Newmark, R.L., Anderson, R.N., Moos, D. and Zoback, M.D.
1985: Sonic and ultrasonic logging of Hole 504B and its implications for the structure, porosity and stress regime of the upper 1 km of the oceanic crust; *in* Initial Reports of the Deep Sea Drilling Project, R.N. Anderson, J. Honnorez, K. Becker, et al.; U.S. Government Printing Office, Washington, D.C., v. 83, p. 479-510.

Pariso, J. and Johnson, H.P.
1989: Magnetic properties of an analog of the lower oceanic crust: Magnetic logging and paleomagnetic measurements from drill hole CY-4 in the Troodos ophiolite; *in* Cyprus Crustal Study Project: Initial Report, Hole CY-4, ed. I.L.

Gibson, J. Malpas, P.T. Robinson and C. Xenophontos; Geological Surv of Canada, Paper 88-9.

Peterson, J.J., Fox, P.J. and Schreiber, E.,
1974: Newfoundland ophiolites and the geology of the oceanic layer; Nature, v. 247, p. 194-196.

Raitt, R.W.
1963: The crustal rocks; *in* The Sea, Ideas and Observations on Progress in the Study of the Seas, The Earth Beneath the Seas, ed. M.N. Hill; John Wiley and Sons New York, v. 3, p. 85-102.

Robinson, P.T., Melson, W., O'Hearn, T. and Schmincke, H.-U.
1983: Volcanic glass compositions of the Troodos ophiolite, Cyprus; Geology, v. 11, no. 7. p. 400-404.

Salisbury, M.H. and Christensen, N.I.
1978: The seismic velocity structure of a traverse through the Bay of Islands Ophiolite complex, Newfoundland: an exposure of oceanic crust and upper mantle; Journal of Geophysical Research, v. 83, no. B2 p. 805-817.

Salisbury, M.H., Scott, J.H., Auroux, C., Becker, K., Bosum, W., Gieskes, J., Holmes, M.A., Hoskins, H., Moos, D., Stephen, R. and Wilkens, R.
In Press: Old oceanic crust: Synthesis of logging, laboratory and seismic data from leg 102; *in* Proceedings of the Ocean Drilling Program Initial Reports, Part B., ed. M.H. Salisbury, J.H. Scott, et. al.; v. 102.

Shipboard Scientific Parties
1980: Site 418; *in* Initial Reports of the Deep Sea Drilling Project, Part 2., ed. T. Donnelly, J. Francheteau, W. Bryan, P. Robinson, M. Flower, M. Salisbury, et al.; U.S. Government Printing Office, Washington, D.C., v. 51, 52, 53, p. 351-626.

Shipboard Scientific Party
1985: Hole 504B, leg 83, *in* Initial Reports of the Deep Sea Drilling Project, R.N. Anderson, J. Honnorez, K. Becker, et al.; U.S. Government Printing Office, Washington, D.C., v. 83, p. 13-120.

Smith, G.C. and Vine, F.J.
1987: Seismic velocities in basalts from CCSP drill holes CY-2 and 2a at Agrokipia mines, Cyprus; *in* Cyprus Crustal Study Project Initial Report, Holes CY-2 and 2a, ed. P.T. Robinson, I.L. Gibson and A. Panayiotou; Geological Survey of Canada, Paper 85- 29, p. 295-306.

Velocity Structure of the Troodos Massif, an Arc-Derived Ophiolite

N.I. CHRISTENSEN[1] AND M.H. SALISBURY[2]

[1]Department of Earth & Atmospheric Sciences,
Purdue University, West Lafayette, IN., U.S.A. 47907
[2]Centre for Marine Geology, Dalhousie University,
Halifax, Nova Scotia, Canada B3H 3J5

Christensen, N.I. and Salisbury, M.H., Velocity structure of the Troodos Massif, an arc-derived ophiolite; in *Cyprus Crustal Study Project: Initial Report, Hole CY-4, ed. I.L. Gibson, J. Malpas, P.T. Robinson and C. Xenophontos; Geological Survey of Canada, Paper 88-9, p. 351-369, 1989.*

Abstract

The seismic velocity structure of a section of the Troodos Massif has been reconstructed in detail from values of compressional (Vp) and shear (Vs) wave velocities measured in the laboratory under elevated hydrostatic confining pressures for 74 samples obtained from drillhole CY-4 at Palekhori, Cyprus. The 2263 m thick section begins in sheeted dikes and continues through a gabbroic section into ultramafic rocks consisting of websterites, olivine websterites and minor lherzolites. The sheeted dike section shows strong velocity gradients with Vp increasing from 5.4 km/sec at the top to 6.8 km/sec at 630 m depth. Beneath the dike section, low velocity zones for both Vp and Vs originate from alteration of high level gabbros. Velocities from depths between 950 m and 1750 m agree well with oceanic Layer 3 velocities. The transition from gabbro to websterite and olivine websterite at 1750 m marks a sharp increase in velocity to Vs = 4.2 km/sec and Vp = 7.7 km/sec. These values fall within the range observed for the oceanic Mohorovicic discontinuity by refraction.

Résumé

La configuration des vitesses séismiques d'une section du massif de Troodos a été reconstituée en détail à partir des vitesses des ondes compîessives (Vp) et cisaillantes (Vs) mesurées en laboratoire sous des pressions hydrostatiques confinantes élevées. Les 74 échantillons étudiés proviennent du forage CY-4, à Palekhori, Chypre. La section, épaisse de 2263 m, débute dans le complexe filonien et traverse des roches gabbroïques à ultramafiques, ces dernières étant constituées de websterites, de websterites à olivine et de peu de lherzolites. La portion du complexe filonien montre un fort gradient de vitesse caractérisé par Vp croissant de 5.4 km/sec au sommet à 6.8 km/sec à 630 m de profondeur. Sous le complexe filonien des zones à faibles vitesses Vp et Vs sont observées sur les gabbros supérieurs métamorphisés. Les vitesses mesurées pour les profondeurs comprises entre 950 et 1750 m sont très comparables à celles mesurées dans la couche 3 de la croûte océanique. La zone de transition, depuis les gabbros jusqu'aux websterites et aux websterites à olivine à 1750 m, est marquée par des accroissements importants des vitesses Vs (4.2 km/sec) et Vp (7.7 km/sec). Ces vitesses se situent à l'intérieur de l'intervalle des valeurs mesurées par sismique-refraction pour la discontinuité Mohorovicic océanique.

INTRODUCTION

Beginning in the early 1970's, it became widely recognized that ophiolite complexes may represent on land exposures of oceanic crust and upper mantle (e.g., Coleman, 1971; Dewey and Bird, 1971; Moores and Vine, 1971). Although direct observations of the nature of the oceanic crust were limited to dredging and shallow drilling, the seismic structure of the oceanic crust was well known in many localities (Raitt, 1963; Shor et al., 1971). Thus, it was critical to examine the seismic properties of ophiolites and compare them with oceanic crustal structure determined by marine seismic investigations. Laboratory measurements of seismic velocities of major ophiolite lithologies (Peterson et al., 1973; Kroenke et al., 1976; Christensen, 1978) and rock suites from detailed traverses through complete or nearly complete ophiolite sections (Salisbury and Christensen, 1978; Christensen and Smewing, 1981; Christensen and Salisbury, 1982) demonstrated many similarities between ophiolite and oceanic crustal velocities. In addition, perhaps the most convincing evidence for ophiolite oceanic crustal models was the finding that seismic anisotropies of ophiolite ultramafic sections are similar to oceanic upper mantle anisotropies (e.g. Christensen and Salisbury, 1979; Christensen and Lundquist, 1982; Christensen, 1984).

Two major problems concerning the possibility of ophiolites as oceanic crustal analogs have persisted however. First, the thicknesses of crustal sections of many ophiolites, including the Troodos complex, appear thin compared with seismic measurements of oceanic crustal thickness (Christensen and Salisbury, 1975). Secondly, the chemistries of many ophiolites are calc-alkaline, suggesting that some may have originated in an island arc environment (e.g., Miyashiro, 1973). A probable origin at a spreading center located within an island arc for the Troodos ophiolite is supported by chemical studies of volcanic glass samples (Robinson et al., 1983).

In this paper, we investigate the detailed seismic and density structure of a major section of the Troodos ophiolite with the purpose of understanding the seismic structure of oceanic crust formed in an island arc environment. Seismic velocities at elevated pressures are presented along with densities for 74 samples from the sheeted dike section, the gabbroic section and the websterites and olivine websterites of drill hole CY-4 at Palekhori, Cyprus. Excellent depth control of the velocity and density profiles over the 2263 m thick section is made possible by the 99.9% core recovery. The high recovery also implies that the section is (relatively) free of open cracks and that laboratory measurements may be fairly representative of formation properties. Major velocity gradients and discontinuities in the Troodos ophiolite are found to have similarities with those in other ophiolites and some oceanic crustal seismic sections.

MEASUREMENT TECHNIQUES

Minicores approximately 2.45 cm in diameter and 3 to 6 cm in length were taken from the main drill core at approximately 20 to 40 m intervals. Each sample was selected as carefully as possible to be representative of the depth interval from which it was obtained. The samples were weighed dry, then saturated with water and reweighed. The bulk density of each sample was determined from its mass and dimensions and the porosity was calculated from its wet and dry weights. The mineralogy of each sample was determined from thin section analysis.

Compressional and shear wave velocities were measured using the pulse transmission technique described in detail by Birch (1960). All velocities were obtained at room temperature using water-saturated samples. Transducers with resonant frequencies of 1 MHz were used to generate and receive the compressional and shear waves. The samples were jacketed with copper foil and 100-mesh copper screens were placed between the cores and jackets to provide space for water to drain from microcracks as the confining pressure was increased. Thus, pore pressure was lower than confining pressure during the pressure cycles.

DATA AND DISCUSSION

Compressional and shear wave velocities, water saturated bulk densities (ρ) and porosities (ϕ) are given in Table 1. In addition to the velocities, velocity ratios (Vp/Vs), Poisson's ratios (σ), bulk moduli (K) and shear moduli (μ) are tabulated for various pressures. The elastic constants were calculated from the measured velocities and densities using the equations summarized by Birch (1961).

A stratigraphic section of the drill core along with measured densities and velocities from Table 1 are shown in Figure 1. Velocities at the top of the section were measured at a differential confining pressure of 90 MPa (0.9 kbar) while those shown at greater depths were at appropriate higher pressures. The lowermost velocities in Figure 1 are at confining pressures of 140 MPa (1.4 kbar). These pressures correspond to those extending from the lower portion of Oceanic Layer 2 to well into Layer 3. The velocity and density structures of the Troodos ophiolite shown in Figure 2 are based upon the relative abundances of each lithology as observed in the complete section of drill core. Also shown are envelopes defining the ranges of measured velocities and densities.

Based on the petrology of the drill hole and the velocity and density profiles of Figures 1 and 2, the ophiolite section sampled in hole CY-4 can be divided into four velocity zones. The uppermost consists of dike rocks. This zone is characterized by strong positive velocity gradients. Compressional wave velocities increase from approximately 5.4 km/sec at the top of the drill hole to 6.8 km/sec at a depth of 630 m and shear wave velocities

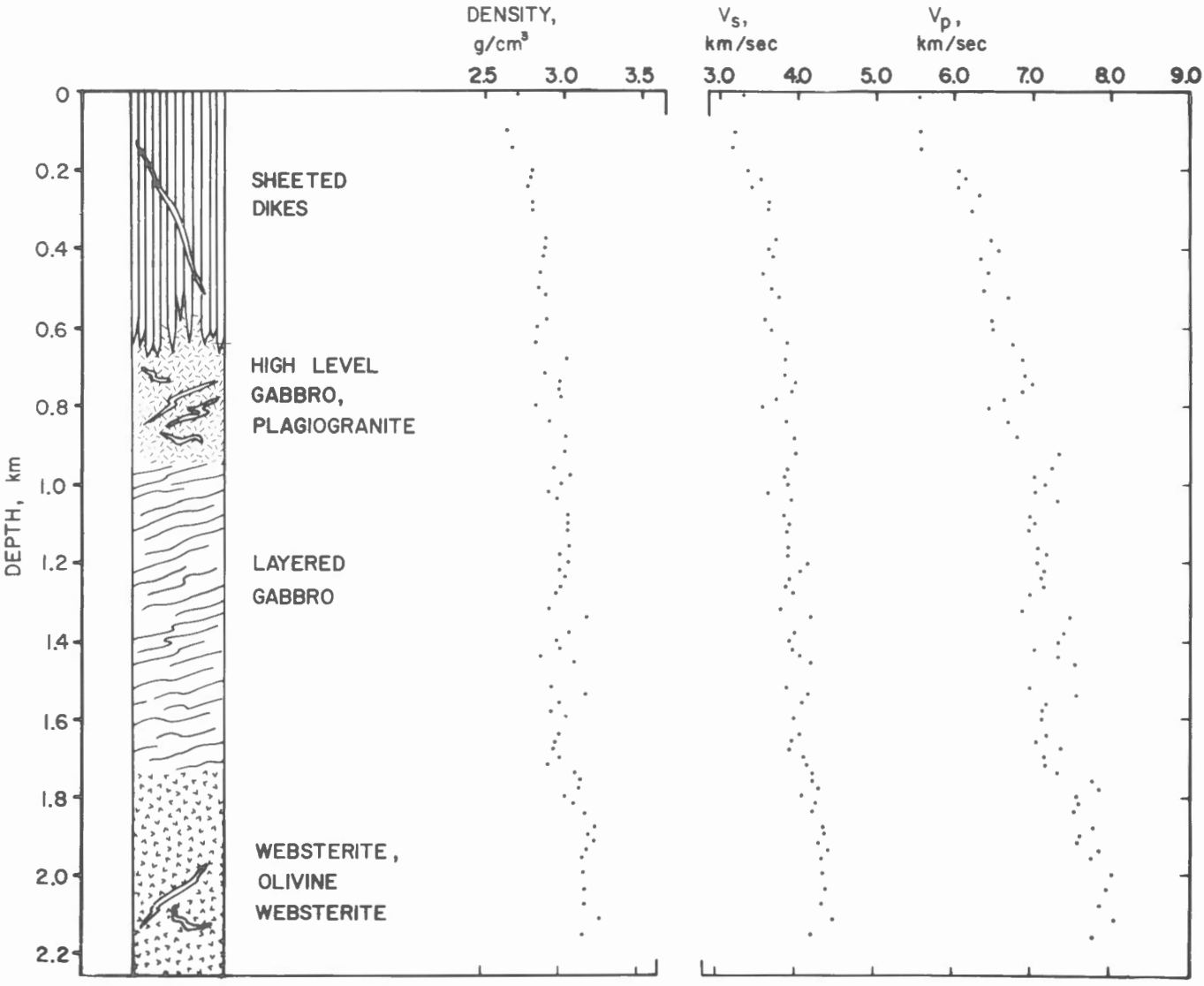

Figure 1: Density, compressional (Vp) and shear (Vs) wave velocities as a function of depth in hole CY-4.

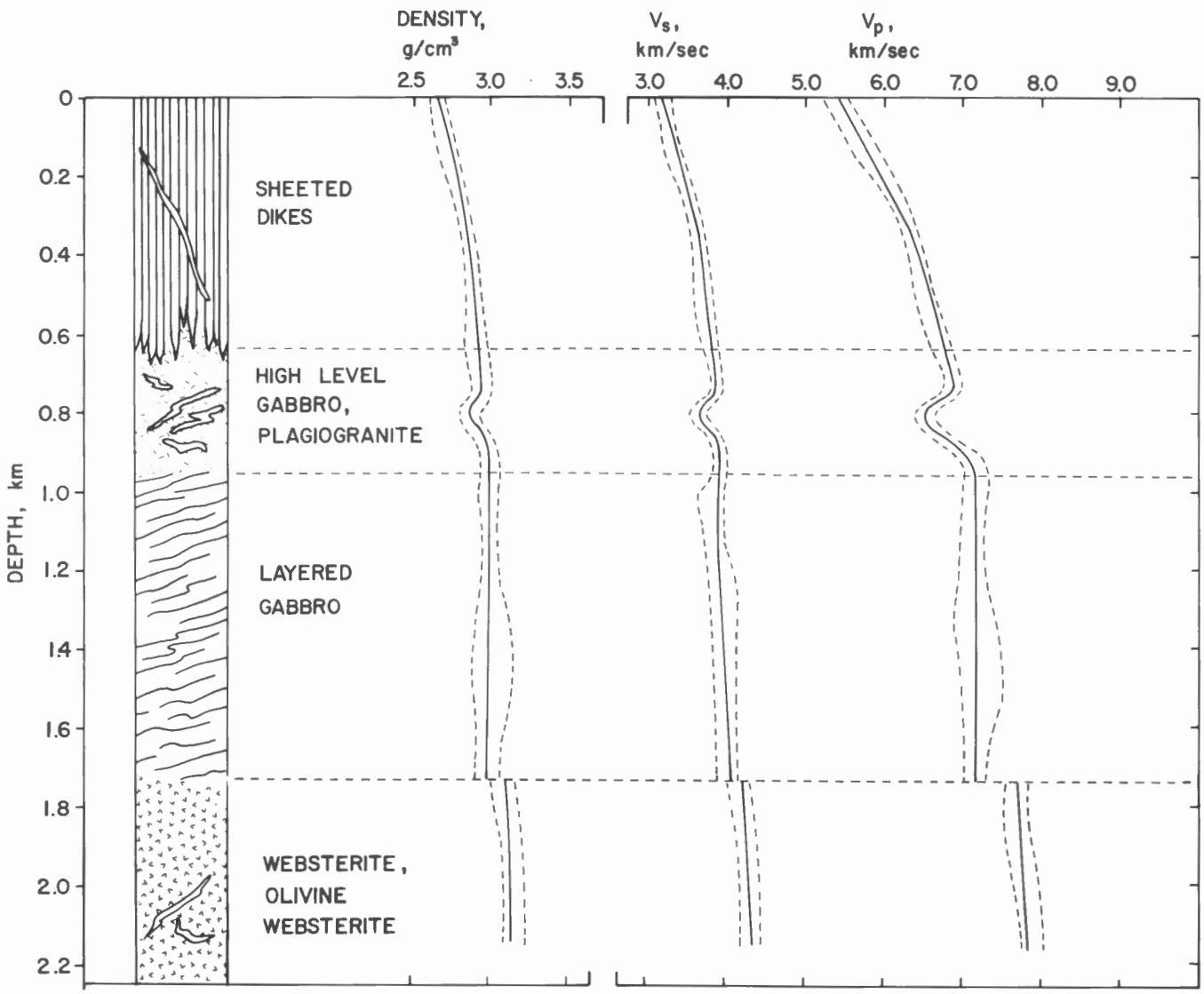

Figure 2: Envelopes of Compressional (Vp) and shear (Vs) wave velocity and density versus depth in hole CY-4. Solid lines represent best fit to the data.

TABLE 1: Compressional (Vp) and shear (Vs) wave velocities, Poisson's ratios σ, bulk moduli (K) and shear moduli μ versus pressure (P).

Sample	P (kb)	Vp (km/s)	Vs (km/s)	Vp/Vs	σ	K (Mb)	μ (Mb)
CY-4 61.75 m	0.2	5.45	3.19	1.71	0.24	0.44	0.27
Diabase	0.4	5.49	3.24	1.70	0.23	0.44	0.28
ρ = 2.70 g/cm^3	0.6	5.52	3.27	1.69	0.23	0.44	0.29
ϕ = 2.8%	0.8	5.54	3.29	1.68	0.23	0.44	0.29
	1.0	5.56	3.31	1.68	0.23	0.44	0.30
	2.0	5.64	3.34	1.69	0.23	0.46	0.30
	4.0	5.72	3.37	1.70	0.23	0.48	0.31
	6.0	5.77	3.38	1.70	0.24	0.49	0.31
CY-4 100.11 m	0.2	5.39	3.10	1.74	0.25	0.43	0.25
Diabase	0.4	5.46	3.14	1.74	0.25	0.44	0.26
ρ = 2.63 g/cm^3	0.6	5.51	3.17	1.74	0.25	0.45	0.26
ϕ = 3.2%	0.8	5.55	3.18	1.74	0.25	0.45	0.27
	1.0	5.57	3.20	1.74	0.25	0.46	0.27
	2.0	5.65	3.24	1.74	0.25	0.47	0.28
	4.0	5.69	3.26	1.74	0.25	0.48	0.28
	6.0	5.70	3.27	1.74	0.25	0.48	0.28
CY-4 140.81 m	0.2	5.30	3.03	1.75	0.26	0.42	0.24
Diabase	0.4	5.43	3.09	1.76	0.26	0.45	0.25
ρ = 2.66 g/cm^3	0.6	5.51	3.12	1.77	0.26	0.46	0.26
ϕ = 3.2%	0.8	5.56	3.14	1.77	0.27	0.47	0.26
	1.0	5.60	3.16	1.77	0.27	0.48	0.27
	2.0	5.68	3.21	1.77	0.27	0.49	0.27
	4.0	5.73	3.24	1.77	0.27	0.51	0.28
	6.0	5.76	3.26	1.77	0.26	0.51	0.29
CY-4 199.90 m	0.2	5.93	3.21	1.85	0.29	0.60	0.29
Diabase	0.4	5.98	3.27	1.83	0.29	0.61	0.30
ρ = 2.81 g/cm^3	0.6	6.02	3.31	1.82	0.28	0.61	0.31
ϕ = 1.5%	0.8	6.04	3.34	1.81	0.28	0.61	0.31
	1.0	6.06	3.36	1.81	0.28	0.61	0.32
	2.0	6.14	3.40	1.81	0.28	0.63	0.33
	4.0	6.22	3.43	1.81	0.28	0.65	0.33
	6.0	6.28	3.45	1.82	0.28	0.67	0.34
CY-4 219.28 m	0.2	6.00	3.44	1.74	0.26	0.56	0.33
Diabase	0.4	6.06	3.47	1.74	0.25	0.57	0.34
ρ = 2.79 g/cm^3	0.6	6.09	3.50	1.74	0.25	0.58	0.34
ϕ = 1.3%	0.8	6.11	3.51	1.74	0.25	0.58	0.34
	1.0	6.13	3.52	1.74	0.25	0.59	0.35
	2.0	6.19	3.56	1.74	0.25	0.60	0.35
	4.0	6.24	3.59	1.74	0.25	0.61	0.36
	6.0	6.26	3.60	1.74	0.25	0.62	0.36
CY-4 240.00 m	0.2	5.86	3.29	1.78	0.27	0.55	0.30
Diabase	0.4	5.93	3.34	1.78	0.27	0.56	0.31
ρ = 2.77 g/cm^3	0.6	5.98	3.37	1.77	0.27	0.57	0.32
ϕ = 1.2%	0.8	6.01	3.39	1.77	0.27	0.58	0.32
	1.0	6.04	3.41	1.77	0.27	0.58	0.32
	2.0	6.10	3.45	1.77	0.27	0.60	0.33
	4.0	6.16	3.48	1.77	0.27	0.61	0.34
	6.0	6.26	3.60	1.74	0.25	0.62	0.36

TABLE 1: (cont.)

Sample	P (kb)	Vp (km/s)	Vs (km/s)	Vp/Vs	σ	K (Mb)	μ (Mb)
CY-4 279.50 m	0.2	6.20	3.55	1.75	0.26	0.61	0.35
Diabase	0.4	6.26	3.59	1.74	0.26	0.62	0.36
ρ = 2.80 g/cm^3	0.6	6.29	3.61	1.74	0.26	0.62	0.36
ϕ = 0.4%	0.8	6.31	3.62	1.74	0.25	0.63	0.37
	1.0	6.33	3.63	1.74	0.25	0.63	0.37
	2.0	6.38	3.65	1.75	0.26	0.64	0.37
	4.0	6.43	3.67	1.75	0.26	0.66	0.38
	6.0	6.45	3.68	1.75	0.26	0.67	0.38
CY-4 299.57 m	0.2	6.09	3.54	1.72	0.24	0.57	0.35
Diabase	0.4	6.15	3.58	1.72	0.24	0.58	0.36
ρ = 2.80 g/cm^3	0.6	6.18	3.60	1.72	0.24	0.59	0.36
ϕ = 0.7%	0.8	6.20	3.61	1.72	0.24	0.59	0.37
	1.0	6.21	3.62	1.72	0.24	0.59	0.37
	2.0	6.27	3.65	1.72	0.24	0.60	0.37
	4.0	6.32	3.67	1.72	0.25	0.62	0.38
	6.0	6.35	3.68	1.73	0.25	0.63	0.38
CY-4 377.50 m	0.2	6.38	3.61	1.77	0.26	0.67	0.38
Diabase	0.4	6.42	3.66	1.76	0.26	0.67	0.39
ρ = 2.88 g/cm^3	0.6	6.45	3.68	1.75	0.26	0.68	0.39
ϕ = 0.3%	0.8	6.46	3.70	1.75	0.26	0.68	0.39
	1.0	6.47	3.71	1.75	0.26	0.68	0.40
	2.0	6.50	3.72	1.75	0.26	0.69	0.40
	4.0	6.55	3.73	1.75	0.26	0.70	0.40
	6.0	6.58	3.74	1.76	0.26	0.72	0.41
CY-4 399.11 m	0.2	6.47	3.51	1.85	0.29	0.73	0.35
Diabase	0.4	6.52	3.55	1.83	0.29	0.74	0.36
ρ = 2.88 g/cm^3	0.6	6.55	3.58	1.83	0.29	0.74	0.37
ϕ = 0.6%	0.8	6.57	3.60	1.82	0.28	0.74	0.37
	1.0	6.59	3.62	1.82	0.28	0.75	0.38
	2.0	6.65	3.66	1.82	0.28	0.76	0.39
	4.0	6.69	3.68	1.82	0.28	0.77	0.39
	6.0	6.71	3.68	1.82	0.28	0.78	0.39
CY-4 420.81 m	0.2	6.27	3.63	1.73	0.25	0.63	0.38
Diabase	0.4	6.30	3.65	1.73	0.25	0.63	0.38
ρ = 2.87 g/cm^3	0.6	6.32	3.67	1.72	0.25	0.63	0.39
ϕ = 0.6%	0.8	6.33	3.68	1.72	0.25	0.63	0.39
	1.0	6.33	3.68	1.72	0.24	0.63	0.39
	2.0	6.36	3.70	1.72	0.24	0.64	0.39
	4.0	6.40	3.72	1.72	0.25	0.65	0.40
	6.0	6.42	3.72	1.72	0.25	0.66	0.40
CY-4 459.60 m	0.2	6.31	3.49	1.81	0.28	0.67	0.35
Diabase	0.4	6.36	3.52	1.81	0.28	0.68	0.35
ρ = 2.85 g/cm^3	0.6	6.39	3.54	1.81	0.28	0.69	0.36
ϕ = 0.4	1.0	6.43	3.56	1.81	0.28	0.70	0.36
	2.0	6.48	3.58	1.81	0.28	0.71	0.37
	4.0	6.53	3.60	1.81	0.28	0.72	0.37
	6.0	6.56	3.61	1.82	0.28	0.73	0.37

TABLE 1: (cont.)

Sample	P (kb)	Vp (km/s)	Vs (km/s)	Vp/Vs	σ	K (Mb)	μ (Mb)
CY-4 497.13 m	0.2	6.27	3.64	1.72	0.25	0.62	0.38
Diabase	0.4	6.32	3.65	1.73	0.25	0.63	0.38
ρ = 2.84 g/cm^3	0.6	6.35	3.66	1.74	0.25	0.64	0.38
ϕ = 0.7%	0.8	6.37	3.67	1.74	0.25	0.65	0.38
	1.0	6.39	3.67	1.74	0.25	0.65	0.38
	2.0	6.42	3.69	1.74	0.25	0.66	0.39
	4.0	6.45	3.70	1.74	0.25	0.67	0.39
	6.0	6.46	3.70	1.74	0.26	0.67	0.39
CY-4 518.12 m	0.2	6.60	3.68	1.79	0.27	0.73	0.39
Diabase	0.4	6.64	3.71	1.79	0.27	0.74	0.40
ρ = 2.88 g/cm^3	0.6	6.68	3.73	1.79	0.27	0.75	0.40
ϕ = 0.4%	0.8	6.70	3.74	1.79	0.27	0.76	0.40
	1.0	6.71	3.75	1.79	0.27	0.76	0.41
	2.0	6.76	3.76	1.80	0.28	0.78	0.41
	4.0	6.79	3.76	1.80	0.28	0.79	0.41
	6.0	6.80	3.77	1.81	0.28	0.80	0.41
CY-4 579.32 m	0.2	6.35	3.49	1.82	0.28	0.70	0.35
Diabase	0.4	6.42	3.53	1.82	0.28	0.71	0.36
ρ = 2.89 g/cm^3	0.6	6.45	3.55	1.82	0.28	0.72	0.37
ϕ = 0.6%	0.8	6.48	3.57	1.82	0.28	0.72	0.37
	1.0	6.50	3.58	1.82	0.28	0.73	0.37
	2.0	6.57	3.62	1.82	0.28	0.75	0.38
	4.0	6.64	3.66	1.82	0.28	0.76	0.39
	6.0	6.68	3.68	1.81	0.28	0.77	0.40
CY-4 603.07 m	0.2	6.34	3.62	1.75	O.26	0.64	0.37
Diabase	0.4	6.41	3.65	1.76	O.26	0.66	0.38
ρ = 2.83 g/cm^3	0.6	6.45	3.66	1.76	O.26	0.67	0.38
ϕ = 0.6%	0.8	6.47	3.67	1.76	0.26	0.68	0.38
	1.0	6.49	3.68	1.76	0.26	0.68	0.38
	2.0	6.52	3.70	1.76	0.26	0.69	0.39
	4.0	6.54	3.71	1.76	0.26	0.70	0.39
	6.0	6.55	3.71	1.76	0.26	0.70	0.39
CY-4 640.30 m	0.2	6.58	3.76	1.75	0.26	0.69	0.40
Gabbro	0.4	6.65	3.80	1.75	0.26	0.71	0.41
ρ = 2.82 g/cm^3	0.6	6.69	3.83	1.75	0.26	0.71	0.41
ϕ = 0.0%	0.8	6.72	3.85	1.75	0.26	0.72	0.42
	1.0	6.74	3.86	1.75	0.26	0.72	0.42
	2.0	6.78	3.89	1.74	0.25	0.73	0.43
	4.0	6.81	3.90	1.75	0.26	0.74	0.43
	6.0	6.82	3.90	1.75	0.26	0.75	0.43
CY-4 680.10 m 0.2	0.2	6.68	3.72	1.80	0.28	0.80	0.42
Hornblende Gabbro	0.4	6.76	3.77	1.80	0.28	0.82	0.43
ρ = 3.04 g/cm^3	0.6	6.81	3.80	1.79	0.27	0.83	0.44
ϕ = 0.3%	0.8	6.85	3.82	1.79	0.27	0.83	0.44
	1.0	6.87	3.84	1.79	0.27	0.84	0.45
	2.0	6.93	3.92	1.77	0.26	0.84	0.47
	4.0	6.97	4.00	1.74	0.25	0.83	0.49
	6.0	6.99	4.04	1.73	0.25	0.83	0.50

TABLE 1: (cont.)

Sample	P (kb)	Vp (km/s)	Vs (km/s)	Vp/Vs	σ	K (Mb)	μ (Mb)
CY-4 720.18 m	0.2	6.77	3.79	1.79	0.27	0.77	0.41
Hornblende Gabbro	0.4	6.84	3.81	1.80	0.28	0.79	0.42
ρ = 2.88 g/cm^3	0.6	6.88	3.82	1.80	0.28	0.80	0.42
ϕ = 0.1%	0.8	6.90	3.83	1.80	0.28	0.81	0.42
	1.0	6.91	3.84	1.80	0.28	0.81	0.42
	2.0	6.94	3.86	1.80	0.28	0.82	0.43
	4.0	6.96	3.88	1.79	0.27	0.82	0.43
	6.0	6.97	3.89	1.79	0.27	0.82	0.44
CY-4 739.93 m	0.2	6.95	3.89	1.79	0.27	0.83	0.45
Hornblende Gabbro	0.4	6.98	3.93	1.77	0.27	0.83	0.46
ρ = 2.97 g/cm^3	0.6	6.99	3.95	1.77	0.26	0.83	0.46
ϕ = 0.2%	0.8	7.00	3.97	1.76	0.26	0.83	0.47
	1.0	7.01	3.97	1.76	0.26	0.83	0.47
	2.0	7.03	3.99	1.76	0.26	0.84	0.47
	4.0	7.05	4.01	1.76	0.26	0.84	0.48
	6.0	7.06	4.02	1.76	0.26	0.85	0.48
CY-4 759.90 m	0.2	6.79	3.86	1.76	0.26	0.78	0.44
Altered Hb. Gabbro	0.4	6.83	3.88	1.76	0.26	0.79	0.45
ρ = 2.97 g/cm^3	0.6	6.84	3.89	1.76	0.26	0.79	0.45
ϕ = 0.2%	0.8	6.85	3.90	1.76	0.26	0.79	0.45
	1.0	6.86	3.91	1.76	0.26	0.80	0.45
	2.0	6.89	3.93	1.75	0.26	0.80	0.46
	4.0	6.93	3.94	1.76	0.26	0.82	0.46
	6.0	6.95	3.95	1.76	0.26	0.82	0.47
CY-4 780.03 m	0.2	6.54	3.68	1.78	0.27	0.71	0.39
Altered Gabbro	0.4	6.58	3.70	1.78	0.27	0.72	0.39
ρ = 2.88 g/cm^3	0.6	6.60	3.71	1.78	0.27	0.73	0.40
ϕ = 0.1%	0.8	6.62	3.72	1.78	0.27	0.73	0.40
	1.0	6.63	3.73	1.78	0.27	0.73	0.40
	2.0	6.67	3.75	1.78	0.27	0.74	0.41
	4.0	6.70	3.79	1.77	0.26	0.75	0.42
	6.0	6.72	3.81	1.76	0.26	0.75	0.42
CY-4 800.05 m	0.2	6.34	3.44	1.84	0.29	0.69	0.34
Altered Gabbro	0.4	6.38	3.48	1.83	0.29	0.70	0.34
ρ = 2.83 g/cm^3	0.6	6.40	3.50	1.83	0.29	0.70	0.35
ϕ = 0.6%	0.8	6.42	3.52	1.83	0.29	0.70	0.35
	1.0	6.43	3.53	1.82	0.28	0.70	0.35
	2.0	6.48	3.57	1.82	0.28	0.71	0.36
	4.0	6.54	3.60	1.82	0.28	0.72	0.37
	6.0	6.57	3.62	1.82	0.28	0.73	0.37
CY-4 840.85 m	0.2	6.63	3.79	1.75	0.26	0.72	0.42
Gabbro	0.4	6.67	3.82	1.75	0.26	0.73	0.43
ρ = 2.92 g/cm^3	0.6	6.69	3.84	1.74	0.26	0.74	0.43
ϕ = 0.2%	0.8	6.71	3.85	1.74	0.25	0.74	0.43
	1.0	6.72	3.86	1.74	0.25	0.74	0.44
	2.0	6.76	3.89	1.74	0.25	0.75	0.44
	4.0	6.79	3.91	1.74	0.25	0.76	0.45
	6.0	6.81	3.92	1.74	0.25	0.76	0.45

TABLE 1: (cont.)

Sample	P (kb)	Vp (km/s)	Vs (km/s)	Vp/Vs	σ	K (Mb)	μ (Mb)
CY-4 880.12 m	0.2	6.63	3.88	1.71	0.24	0.72	0.45
Gabbro	0.4	6.69	3.91	1.71	0.24	0.74	0.46
ρ = 3.02 g/cm^3	0.6	6.73	3.92	1.72	0.24	0.75	0.47
ϕ = 0.2%	0.8	6.76	3.94	1.72	0.24	0.76	0.47
	1.0	6.78	3.95	1.72	0.24	0.76	0.47
	2.0	6.86	3.97	1.73	0.25	0.79	0.48
	4.0	6.94	3.99	1.74	0.25	0.82	0.48
	6.0	6.99	4.00	1.75	0.26	0.84	0.49
CY-4 919.96 m	0.2	7.25	3.94	1.84	0.29	0.96	0.47
Gabbro	0.4	7.29	3.95	1.85	0.29	0.97	0.47
ρ = 3.01 g/cm^3	0.6	7.32	3.96	1.85	0.29	0.98	0.47
ϕ = 0.1%	0.8	7.34	3.97	1.85	0.29	0.99	0.47
	1.0	7.35	3.98	1.85	0.29	0.99	0.48
	2.0	7.40	4.00	1.85	0.29	1.01	0.48
	4.0	7.45	4.02	1.85	0.29	1.03	0.49
	6.0	7.47	4.02	1.86	0.30	1.04	0.49
CY-4 960.78 m	0.2	7.00	3.78	1.85	0.29	0.88	0.42
Gabbro	0.4	7.12	3.83	1.86	0.30	0.92	0.43
ρ = 2.94 g/cm^3	0.6	7.18	3.85	1.86	0.30	0.94	0.44
ϕ = 0.1%	0.8	7.22	3.87	1.87	0.30	0.95	0.44
	1.0	7.24	3.87	1.87	0.30	0.95	0.44
	2.0	7.28	3.89	1.87	0.30	0.97	0.45
	4.0	7.31	3.91	1.87	0.30	0.98	0.45
	6.0	7.32	3.91	1.87	0.30	0.98	0.45
CY-4 980.03 m	0,2	6.91	3.80	1.82	0.28	0.87	0.44
Diabase	0.4	6.96	3.82	1.82	0.28	0.88	0.44
ρ = 3.05 g/cm^3	0.6	6.99	3.83	1.83	0.29	0.89	0.45
ϕ = 0.1%	0.8	7.02	3.84	1.83	0.29	0.90	0.45
	1.0	7.03	3.84	1.83	0.29	0.91	0.45
	2.0	7.08	3.86	1.84	0.29	0.92	0.45
	4.0	7.09	3.87	1.83	0.29	0.93	0.46
	6.0	7.09	3.87	1.83	0.29	0.93	0.46
CY-4 1000.06 m	0.2	7.09	3.86	1.84	0.29	0.91	0.44
Gabbro	0.4	7.13	3.87	1.84	0.29	0.92	0.45
ρ = 2.98 g/cm^3	0.6	7.14	3.88	1.84	0.29	0.92	0.45
ϕ = 0.0%	0.8	7.16	3.89	1.84	0.29	0.93	0.45
	1.0	7.16	3.89	1.84	0.29	0.93	0.45
	2.0	7.19	3.91	1.84	0.29	0.94	0.46
	4.0	7.22	3.92	1.84	0.29	0.95	0.46
	6.0	7.23	3.93	1.84	0.29	0.95	0.46
CY-4 1019.96 m	0.2	6.86	3.44	1.99	0.33	0.91	0.35
Gabbro	0.4	6.98	3.48	2.01	0.33	0.95	0.35
ρ = 2.91 g/cm^3	0.6	7.02	3.51	2.00	0.33	0.96	0.36
ϕ = 0.2	1.0	7.05	3.54	1.99	0.33	0.96	0.36
	2.0	7.07	3.57	1.98	0.33	0.96	0.37
	4.0	7.08	3.59	1.97	0.33	0.96	0.38
	6.0	7.09	3.60	1.97	0.33	0.97	0.38

TABLE 1: (cont.)

Sample	P (kb)	Vp (km/s)	Vs (km/s)	Vp/Vs	σ	K (Mb)	μ (Mb)
CY-4 1039.87 m	0.2	7.12	3.86	1.84	0.29	0.91	0.44
Gabbro	0.4	7.21	3.88	1.86	0.30	0.94	0.45
ρ = 2.96 g/cm^3	0.6	7.26	3.90	1.86	0.30	0.96	0.45
ϕ = 0.1	1.0	7.32	3.92	1.87	0.30	0.98	0.46
	2.0	7.36	3.95	1.87	0.30	0.99	0.46
	4.0	7.40	3.96	1.87	0.30	1.00	0.47
	6.0	7.41	3.97	1.87	0.30	1.01	0.47
CY-4 1079.85 m	0.2	6.85	3.80	1.80	0.28	0.84	0.44
Diabase	0.4	6.91	3.82	1.81	0.28	0.86	0.44
ρ = 3.03 g/cm^3	0.6	6.95	3.83	1.82	0.28	0.87	0.44
ϕ = 0.1%	0.8	6.97	3.84	1.82	0.28	0.88	0.45
	1.0	6.99	3.84	1.82	0.28	0.89	0.45
	2.0	7.03	3.85	1.82	0.29	0.90	0.45
	4.0	7.07	3.86	1.83	0.29	0.92	0.45
	6.0	7.09	3.86	1.83	0.29	0.93	0.46
CY-4 1100.00 m	0.2	6.85	3.84	1.78	0.27	0.83	0.45
Gabbro	0.4	6.92	3.87	1.79	0.27	0.85	0.45
ρ = 3.03 g/cm^3	0.6	6.96	3.88	1.79	0.27	0.86	0.46
ϕ = 0.2%	0.8	6.99	3.90	1.79	0.27	0.87	0.46
	1.0	7.01	3.90	1.80	0.28	0.87	0.46
	2.0	7.06	3.92	1.80	0.28	0.89	0.47
	4.0	7.09	3.94	1.80	0.28	0.90	0.47
	6.0	7.11	3.95	1.80	0.28	0.91	0.48
CY-4 1119.95 m	0.2	6.81	3.82	1.78	0.27	0.82	0.44
Diabase	0.4	6.87	3.84	1.79	0.27	0.84	0.45
ρ = 3.03 g/cm^3	0.6	6.91	3.86	1.79	0.27	0.85	0.45
ϕ = 0.1%	0.8	6.93	3.87	1.79	0.27	0.85	0.45
	1.0	6.95	3.87	1.79	0.27	0.86	0.45
	2.0	7.01	3.89	1.80	0.28	0.88	0.46
	4.0	7.07	3.90	1.81	0.28	0.90	0.46
	6.0	7.11	3.90	1.82	0.28	0.92	0.46
CY-4 1160.12 m	0.2	6.92	3.68	1.88	0.30	0.91	0.41
Gabbro	0.4	6.98	3.78	1.85	0.29	0.90	0.44
ρ = 3.04 g/cm^3	0.6	7.01	3.83	1.83	0.29	0.90	0.45
ϕ = 0.2%	0.8	7.04	3.87	1.82	0.28	0.90	0.46
	1.0	7.06	3.89	1.82	0.28	0.91	0.46
	2.0	7.13	3.92	1.82	0.28	0.92	0.47
	4.0	7.17	3.94	1.82	0.28	0.94	0.47
	6.0	7.18	3.95	1.82	0.28	0.94	0.48
CY-4 1180.00 m	0.2	7.03	3.70	1.90	0.31	0.93	0.41
Gabbro	0.4	7.09	3.78	1.87	0.30	0.93	0.43
ρ = 2.98 g/cm^3	0.6	7.13	3.82	1.86	0.30	0.93	0.44
ϕ = 0.2%	0.8	7.15	3.84	1.86	0.30	0.94	0.44
	1.0	7.17	3.86	1.86	0.30	0.94	0.44
	2.0	7.23	3.88	1.86	0.30	0.96	0.45
	4.0	7.27	3.89	1.87	0.30	0.98	0.45
	6.0	7.30	3.90	1.87	0.30	0.99	0.46

TABLE 1: (cont.)

Sample	P (kb)	Vp (km/s)	Vs (km/s)	Vp/Vs	σ	K (Mb)	μ (Mb)
CY-4 1200.00 m	0.2	6.88	4.04	1.70	0.24	0.78	0.50
Gabbro	0.4	6.95	4.08	1.71	0.24	0.80	0.51
ρ = 3.04 g/cm^3	0.6	7.00	4.10	1.71	0.24	0.81	0.51
ϕ = 0.1%	0.8	7.03	4.12	1.71	0.24	0.82	0.52
	1.0	7.05	4.13	1.71	0.24	0.82	0.52
	2.0	7.10	4.16	1.71	0.24	0.84	0.53
	4.0	7.15	4.17	1.72	0.24	0.86	0.53
	6.0	7.18	4.17	1.72	0.25	0.87	0.53
CY-4 1220.05 m	0.2	6.95	3.92	1.77	0.27	0.83	0.46
Gabbro	0.4	7.05	3.97	1.77	0.27	0.85	0.47
ρ = 2.97 g/cm^3	0.6	7.10	4.01	1.77	0.27	0.86	0.48
ϕ = 0.2%	0.8	7.13	4.03	1.77	0.27	0.87	0.48
	1.0	7.15	4.04	1.77	0.26	0.87	0.49
	2.0	7.20	4.08	1.77	0.26	0.88	0.50
	4.0	7.25	4.11	1.77	0.26	0.90	0.50
	6.0	7.27	4.12	1.77	0.26	0.91	0.51
CY-4 1240.02 m	0.2	6.91	3.86	1.79	0.27	0.84	0.45
Diabase	0.4	7.00	3.88	1.80	0.28	0.87	0.45
ρ = 3.02 g/cm^3	0.6	7.05	3.89	1.81	0.28	0.89	0.46
ϕ = 0.2%	0.8	7.08	3.90	1.82	0.28	0.90	0.46
	1.0	7.10	3.90	1.82	0.28	0.91	0.46
	2.0	7.14	3.92	1.82	0.28	0.92	0.46
	4.0	7.18	3.93	1.83	0.29	0.94	0.47
	6.0	7.19	3.93	1.83	0.29	0.95	0.47
CY-4 1260.00 m	0.2	6.91	3.69	1.87	0.30	0.89	0.41
Gabbro	0.4	7.01	3.77	1.86	0.30	0.90	0.43
ρ = 2.99 g/cm^3	0.6	7.07	3.82	1.85	0.29	0.91	0.44
ϕ = 0.2%	0.8	7.11	3.84	1.85	0.29	0.93	0.44
	1.0	7.15	3.86	1.85	0.29	0.93	0.44
	2.0	7.23	3.88	1.86	0.30	0.96	0.45
	4.0	7.31	3.90	1.88	0.30	1.00	0.46
	6.0	7.36	3.91	1.88	0.30	1.02	0.46
CY-4 1280.00 m	0.2	6.83	3.90	1.75	0.26	0.78	0.45
Gabbro	0.4	6.89	3.92	1.76	0.26	0.80	0.46
ρ = 2.96 g/cm^3	0.6	6.92	3.94	1.76	0.26	0.81	0.46
ϕ = 0.1%	0.8	6.95	3.95	1.76	0.26	0.82	0.46
	1.0	6.96	3.95	1.76	0.26	0.82	0.46
	2.0	7.02	3.96	1.77	0.26	0.84	0.47
	4.0	7.07	3.97	1.78	0.27	0.86	0.47
	6.0	7.10	3.97	1.79	0.27	0.88	0.47
CY-4 1320.00 m	0.2	6.70	3.72	1.80	0.28	0.77	0.40
Hornblende Gabbro	0.4	6.77	3.75	1.80	0.28	0.79	0.41
ρ = 2.91 g/cm^3	0.6	6.81	3.77	1.81	0.28	0.80	0.41
ϕ = 0.2%	0.8	6.84	3.78	1.81	0.28	0.80	0.42
	1.0	6.87	3.79	1.81	0.28	0.82	0.42
	2.0	6.94	3.81	1.82	0.28	0.84	0.42
	4.0	7.00	3.82	1.83	0.29	0.87	0.43
	6.0	7.03	3.82	1.84	0.29	0.88	0.43

TABLE 1: (cont.)

Sample	P (kb)	Vp (km/s)	Vs (km/s)	Vp/Vs	σ	K (Mb)	μ (Mb)
CY-4 1340.01 m	0.2	7.42	4.03	1.84	0.29	1.06	0.51
Gabbro	0.4	7.46	4.10	1.82	0.28	1.05	0.53
ρ = 3.16 g/cm^3	0.6	7.48	4.14	1.81	0.28	1.05	0.54
ϕ = 0.1%	0.8	7.49	4.17	1.80	0.28	1.05	0.55
	1.0	7.50	4.18	1.79	0.27	1.04	0.55
	2.0	7.53	4.21	1.79	0.27	1.05	0.56
	4.0	7.59	4.23	1.79	0.27	1.07	0.57
	6.0	7.62	4.24	1.80	0.28	1.09	0.57
CY-4 1380.23 m	0.2	7.21	3.84	1.88	0.30	0.98	0.45
Gabbro	0.4	7.29	3.90	1.87	0.30	1.00	0.46
ρ = 3.03 g/cm^3	0.6	7.33	3.93	1.86	0.30	1.00	0.47
ϕ = 0.2%	0.8	7.36	3.95	1.86	0.30	1.01	0.47
	1.0	7.38	3.97	1.86	0.30	1.01	0.48
	2.0	7.45	4.01	1.86	0.30	1.03	0.49
	4.0	7.59	4.23	1.79	0.27	1.07	0.57
	6.0	7.62	4.24	1.80	0.28	1.09	0.57
CY-4 1400.08 m	0.2	7.08	3.70	1.91	0.31	0.95	0.41
Gabbro	0.4	7.20	3.79	1.90	0.31	0.97	0.43
ρ = 2.97 g/cm^3	0.6	7.26	3.84	1.89	0.31	0.98	0.44
ϕ = 0.2%	0.8	7.30	3.87	1.89	0.30	0.99	0.45
	1.0	7.33	3.89	1.88	0.30	1.00	0.45
	2.0	7.38	3.92	1.88	0.30	1.02	0.46
	4.0	7.43	3.94	1.89	0.31	1.03	0.46
	6.0	7.45	3.94	1.89	0.31	1.04	0.47
CY-4 1420.08 m	0.2	6.80	3.79	1.80	0.28	0.79	0.42
Gabbro	0.4	6.90	3.86	1.79	0.27	0.80	0.43
ρ = 2.90 g/cm^3	0.6	6.95	3.90	1.78	0.27	0.81	0.44
ϕ = 0.2%	0.8	6.98	3.92	1.78	0.27	0.82	0.45
	1.0	7.00	3.93	1.78	0.27	0.83	0.45
	2.0	7.04	3.95	1.79	0.27	0.84	0.45
	4.0	7.08	3.96	1.79	0.27	0.85	0.46
	6.0	7.10	3.96	1.79	0.27	0.86	0.46
CY-4 1440.14 m	0.2	7.10	3.79	1.87	0.30	0.89	0.41
Gabbro	0.4	7.23	3.92	1.84	0.29	0.91	0.44
ρ = 2.86 g/cm^3	0.6	7.28	3.98	1.83	0.29	0.92	0.45
ϕ = 0.2%	0.8	7.32	4.00	1.83	0.29	0.92	0.46
	1.0	7.33	4.02	1.83	0.29	0.93	0.46
	2.0	7.38	4.04	1.83	0.29	0.94	0.47
	4.0	7.43	4.06	1.83	0.29	0.96	0.47
	6.0	7.45	4.07	1.83	0.29	0.97	0.48
CY-4 1459.68 m	0.2	7.28	4.09	1.78	0.27	0.95	0.52
Gabbro	0.4	7.39	4.12	1.79	0.27	0.99	0.52
ρ = 3.08 g/cm^3	0.6	7.46	4.14	1.80	0.28	1.01	0.53
ϕ = 0.2%	0.8	7.50	4.16	1.80	0.28	1.02	0.53
	1.0	7.53	4.17	1.81	0.28	1.03	0.54
	2.0	7.61	4.20	1.81	0.28	1.06	0.55
	4.0	7.69	4.24	1.82	0.28	1.09	0.56
	6.0	7.73	4.25	1.82	0.28	1.11	0.56

TABLE 1: (cont.)

Sample	P (kb)	Vp (km/s)	Vs (km/s)	Vp/Vs	σ	K (Mb)	μ (Mb)
CY-4 1520.12 m	0.2	6.79	3.71	1.83	0.29	0.81	0.40
Gabbro	0.4	6.87	3.79	1.81	0.28	0.82	0.42
ρ = 2.93 g/cm^3	0.6	6.91	3.83	1.80	0.28	0.83	0.43
ϕ = 0.2%	0.8	6.94	3.86	1.80	0.28	0.83	0.44
	1.0	6.96	3.87	1.80	0.28	0.83	0.44
	2.0	7.01	3.90	1.80	0.28	0.85	0.45
	4.0	7.05	3.92	1.80	0.28	0.86	0.45
	6.0	7.07	3.93	1.80	0.28	0.87	0.46
CY-4 1540.25 m	0.2	7.22	3.94	1.83	0.29	0.99	0.49
Gabbro	0.4	7.36	4.03	1.83	0.29	1.02	0.51
ρ = 3.15 g/cm^3	0.6	7.44	4.09	1.82	0.28	1.04	0.53
ϕ = 0.2%	0.8	7.49	4.12	1.82	0.28	1.05	0.53
	1.0	7.52	4.14	1.82	0.28	1.06	0.54
	2.0	7.59	4.17	1.82	0.28	1.08	0.55
	4.0	7.64	4.20	1.82	0.28	1.10	0.56
	6.0	7.68	4.21	1.82	0.29	1.12	0.56
CY-4 1559.39 m	0.2	6.88	3.71	1.85	0.29	0.86	0.41
Gabbro	0.4	7.04	3.91	1.80	0.28	0.87	0.46
ρ = 2.98 g/cm^3	0.6	7.12	4.00	1.78	0.27	0.87	0.48
ϕ = 0.3%	0.8	7.16	4.03	1.77	0.27	0.88	0.48
	1.0	7.18	4.05	1.77	0.27	0.89	0.49
	2.0	7.24	4.07	1.78	0.27	0.91	0.49
	4.0	7.30	4.08	1.79	0.27	0.93	0.50
	6.0	7.33	4.09	1.79	0.27	0.94	0.50
CY-4 1579.65 m	0.2	6.64	3.65	1.82	0.28	0.77	0.39
Gabbro	0.4	6.93	3.76	1.84	0.29	0.85	0.41
ρ = 2.93 g/cm^3	0.6	7.04	3.82	1.84	0.29	0.88	0.43
ϕ = 0.2%	0.8	7.09	3.86	1.84	0.29	0.89	0.44
	1.0	7.12	3.89	1.83	0.29	0.90	0.44
	2.0	7.18	3.93	1.83	0.29	0.91	0.45
	4.0	7.24	3.95	1.83	0.29	0.93	0.46
	6.0	7.27	3.96	1.84	0.29	0.94	0.46
CY-4 1600.54 m	0.2	6.82	3.72	1.84	0.29	0.85	0.42
Gabbro	0.4	6.98	3.84	1.82	0.28	0.88	0.45
ρ = 3.02 g/cm^3	0.6	7.05	3.91	1.80	0.28	0.89	0.46
ϕ = 0.2%	0.8	7.09	3.95	1.79	0.27	0.89	0.47
	1.0	7.11	3.97	1.79	0.27	0.89	0.48
	2.0	7.18	4.01	1.79	0.27	0.91	0.49
	4.0	7.24	4.03	1.80	0.28	0.94	0.49
	6.0	7.27	4.03	1.80	0.28	0.95	0.49
CY-4 1640.04 m	0.2	7.04	3.95	1.78	0.27	0.86	0.46
Gabbro	0.4	7.10	3.98	1.78	0.27	0.87	0.47
ρ = 2.98 g/cm^3	0.6	7.14	4.01	1.78	0.27	0.88	0.48
ϕ = 0.1%	0.8	7.16	4.02	1.78	0.27	0.89	0.48
	1.0	7.18	4.03	1.78	0.27	0.89	0.48
	2.0	7.23	4.05	1.78	0.27	0.90	0.49
	4.0	7.27	4.07	1.79	0.27	0.92	0.50
	6.0	7.29	4.08	1.79	0.27	0.93	0.50

TABLE 1: (cont.)

Sample	P (kb)	Vp (km/s)	Vs (km/s)	Vp/Vs	σ	K (Mb)	μ (Mb)
CY-4 1659.98 m	0.2	6.86	3.80	1.81	0.28	0.83	0.43
Gabbro	0.4	6.92	3.85	1.80	0.28	0.84	0.44
ρ = 2.96 g/cm^3	0.6	6.96	3.88	1.79	0.27	0.84	0.45
ϕ = 0.2%	0.8	6.98	3.90	1.79	0.27	0.84	0.45
	1.0	7.00	3.92	1.79	0.27	0.85	0.46
	2.0	7.06	3.99	1.77	0.27	0.85	0.47
	4.0	7.13	4.06	1.76	0.26	0.86	0.49
	6.0	7.17	4.10	1.75	0.26	0.87	0.50
CY-4 1680.06 m	0.2	7.15	3.82	1.87	0.30	0.93	0.43
Gabbro	0.4	7.24	3.85	1.88	0.30	0.96	0.44
ρ = 2.95 g/cm^3	0.6	7.29	3.87	1.88	0.30	0.98	0.44
ϕ = 0.1%	0.8	7.32	3.88	1.88	0.30	0.99	0.44
	1.0	7.33	3.90	1.88	0.30	0.99	0.45
	2.0	7.38	3.93	1.88	0.30	1.00	0.46
	4.0	7.42	3.97	1.87	0.30	1.01	0.47
	6.0	7.44	3.99	1.86	0.30	1.01	0.47
CY-4 1699.90 m	0.2	6.74	3.86	1.75	0.26	0.76	0.44
Gabbro	0.4	6.94	3.97	1.75	0.26	0.81	0.47
ρ = 2.98 g/cm^3	0.6	7.04	4.02	1.75	0.26	0.83	0.48
ϕ = 0.2%	0.8	7.09	4.05	1.75	0.26	0.85	0.49
	1.0	7.12	4.06	1.75	0.26	0.85	0.49
	2.0	7.16	4.09	1.75	0.26	0.87	0.50
	4.0	7.19	4.11	1.75	0.26	0.87	0.51
	6.0	7.21	4.12	1.75	0.26	0.88	0.51
CY-4 1720.12 m	0.2	6.74	3.95	1.71	0.24	0.72	0.46
Gabbro	0.4	6.98	4.03	1.73	0.25	0.79	0.47
ρ = 2.92 g/cm^3	0.6	7.07	4.07	1.74	0.25	0.82	0.48
ϕ = 0.2%	0.8	7.11	4.09	1.74	0.25	0.83	0.49
	1.0	7.13	4.10	1.74	0.25	0.83	0.49
	2.0	7.16	4.13	1.74	0.25	0.84	0.50
	4.0	7.19	4.15	1.73	0.25	0.84	0.51
	6.0	7.20	4.16	1.73	0.25	0.85	0.51
CY-4 1740.02 m	0.2	7.06	4.10	1.72	0.25	0.85	0.52
Gabbro	0.4	7.18	4.14	1.73	0.25	0.89	0.53
ρ = 3.09 g/cm^3	0.6	7.24	4.16	1.74	0.25	0.91	0.54
ϕ = 0.1%	0.8	7.28	4.18	1.74	0.25	0.92	0.54
	1.0	7.30	4.19	1.74	0.25	0.92	0.54
	2.0	7.36	4.23	1.74	0.25	0.94	0.55
	4.0	7.41	4.26	1.74	0.25	0.95	0.56
	6.0	7.43	4.27	1.74	0.25	0.96	0.57
CY-4 1759.86 m	0.2	7.60	4.15	1.83	0.29	1.08	0.54
Olivine Websterite	0.4	7.67	4.17	1.84	0.29	1.11	0.54
ρ = 3.11 g/cm^3	0.6	7.71	4.18	1.84	0.29	1.12	0.55
ϕ = 0.1%	0.8	7.73	4.19	1.85	0.29	1.13	0.55
	1.0	7.75	4.20	1.85	0.29	1.14	0.55
	2.0	7.80	4.20	1.86	0.30	1.16	0.55
	4.0	7.84	4.20	1.87	0.30	1.18	0.55
	6.0	7.86	4.20	1.87	0.30	1.20	0.55

TABLE 1: (cont.)

Sample	P (kb)	Vp (km/s)	Vs (km/s)	Vp/Vs	σ	K (Mb)	μ (Mb)
CY-4 1779.76 m	0.2	7.75	4.12	1.88	0.30	1.16	0.53
Websterite	0.4	7.79	4.18	1.87	0.30	1.17	0.54
ρ = 3.11 g/cm^3	0.6	7.81	4.21	1.86	0.30	1.16	0.55
ϕ = 0.2%	0.8	7.83	4.24	1.85	0.29	1.16	0.56
	1.0	7.85	4.26	1.84	0.29	1.16	0.56
	2.0	7.90	4.30	1.84	0.29	1.17	0.58
	4.0	7.96	4.32	1.84	0.29	1.20	0.58
	6.0	7.99	4.33	1.85	0.29	1.21	0.58
CY-4 1799.99 m	0.2	7.22	3.88	1.86	0.30	0.97	0.45
Websterite	0.4	7.41	3.95	1.88	0.30	1.03	0.47
ρ = 3.02 g/cm^3	0.6	7.49	4.00	1.87	0.30	1.05	0.48
ϕ = 0.2%	0.8	7.53	4.03	1.87	0.30	1.06	0.49
	1.0	7.55	4.04	1.87	0.30	1.06	0.49
	2.0	7.60	4.08	1.86	0.30	1.08	0.50
	4.0	7.65	4.09	1.87	0.30	1.10	0.51
	6.0	7.67	4.10	1.87	0.30	1.11	0.51
CY-4 1820.03 m	0.2	7.43	4.16	1.79	0.27	0.99	0.53
Websterite	0.4	7.50	4.23	1.77	0.27	0.99	0.55
ρ = 3.07 g/cm^3	0.6	7.53	4.27	1.76	0.26	0.99	0.56
ϕ = 0.2%	0.8	7.55	4.28	1.76	0.26	1.00	0.56
	1.0	7.56	4.29	1.76	0.26	1.00	0.57
	2.0	7.61	4.30	1.77	0.27	1.02	0.57
	4.0	7.68	4.31	1.78	0.27	1.05	0.57
	6.0	7.72	4.31	1.79	0.27	1.08	0.57
CY-4 1839.96 m	0.2	6.88	4.08	1.68	0.23	0.79	0.52
Olivine Websterite	0.4	7.21	4.12	1.75	0.26	0.92	0.53
ρ = 3.14 g/cm^3	0.6	7.36	4.15	1.78	0.27	0.98	0.54
ϕ = 0.2%	0.8	7.44	4.17	1.78	0.27	1.01	0.55
	1.0	7.48	4.18	1.79	0.27	1.02	0.55
	2.0	7.56	4.24	1.78	0.27	1.04	0.56
	4.0	7.62	4.29	1.78	0.27	1.06	0.58
	6.0	7.66	4.33	1.77	0.27	1.06	0.59
CY-4 1880.05 m	0.2	7.46	4.09	1.82	0.29	1.07	0.54
Olivine Websterite	0.4	7.62	4.19	1.82	0.28	1.11	0.57
ρ = 3.21 g/cm^3	0.6	7.68	4.25	1.81	0.28	1.12	0.58
ϕ = 0.1%	0.8	7.72	4.29	1.80	0.28	1.13	0.59
	1.0	7.74	4.31	1.80	0.28	1.13	0.60
	2.0	7.81	4.35	1.79	0.27	1.15	0.61
	4.0	7.87	4.38	1.80	0.28	1.17	0.62
	6.0	7.90	4.39	1.80	0.28	1.18	0.62
CY-4 1899.94 m	0.2	7.29	4.10	1.78	0.27	0.97	0.53
Plagioclase Websterite	0.4	7.41	4.23	1.75	0.26	0.99	0.57
ρ = 3.17 g/cm^3	0.6	7.49	4.29	1.75	0.26	1.00	0.58
ϕ = 0.1%	0.8	7.54	4.32	1.75	0.26	1.02	0.59
	1.0	7.57	4.33	1.75	0.26	1.03	0.60
	2.0	7.64	4.36	1.75	0.26	1.05	0.60
	4.0	7.67	4.37	1.75	0.26	1.06	0.61
	6.0	7.68	4.38	1.75	0.26	1.07	0.61

TABLE 1: (cont.)

Sample	P (kb)	Vp (km/s)	Vs (km/s)	Vp/Vs	σ	K (Mb)	μ (Mb)
CY-4 1919.98 m	0.2	7.32	4.11	1.78	0.27	0.99	0.54
Olivine Websterite	0.4	7.39	4.20	1.76	0.26	1.00	0.57
ρ = 3.21 g/cm^3	0.6	7.44	4.24	1.75	0.26	1.01	0.58
ϕ = 0.1%	0.8	7.48	4.26	1.76	0.26	1.02	0.58
	1.0	7.52	4.27	1.76	0.26	1.03	0.59
	2.0	7.62	4.30	1.77	0.27	1.07	0.60
	4.0	7.67	4.33	1.77	0.27	1.09	0.60
	6.0	7.67	4.34	1.77	0.26	1.09	0.61
CY-4 1939.88 m	0.2	7.49	4.17	1.80	0.28	1.04	0.55
Websterite	0.4	7.68	4.27	1.80	0.28	1.10	0.58
ρ = 3.16 g/cm^3	0.6	7.77	4.32	1.80	0.28	1.12	0.59
ϕ = 0.2%	0.8	7.80	4.36	1.79	0.27	1.13	0.60
	1.0	7.83	4.38	1.79	0.27	1.13	0.61
	2.0	7.87	4.43	1.78	0.27	1.14	0.62
	4.0	7.92	4.45	1.78	0.27	1.15	0.63
	6.0	7.94	4.47	1.78	0.27	1.16	0.63
CY-4 1960.08 m	0.2	7.55	4.20	1.80	0.28	1.05	0.55
Plagioclase Websterite	0.4	7.63	4.26	1.79	0.27	1.07	0.57
ρ = 3.13 g/cm^3	0.6	7.68	4.29	1.79	0.27	1.08	0.58
ϕ = 0.1%	0.8	7.71	4.30	1.79	0.27	1.09	0.58
	1.0	7.73	4.31	1.79	0.27	1.10	0.58
	2.0	7.77	4.33	1.80	0.28	1.11	0.59
	4.0	7.80	4.35	1.79	0.27	1.12	0.59
	6.0	7.81	4.36	1.79	0.27	1.13	0.60
CY-4 2000.00 m	0.2	7.78	4.19	1.86	0.30	1.17	0.55
Olivine Websterite	0.4	7.88	4.25	1.86	0.30	1.20	0.57
ρ = 3.14 g/cm^3	0.6	7.93	4.28	1.85	0.29	1.21	0.58
ϕ = 0.2%	0.8	7.97	4.30	1.85	0.29	1.22	0.58
	1.0	7.99	4.32	1.85	0.29	1.23	0.59
	2.0	8.06	4.37	1.84	0.29	1.24	0.60
	4.0	8.11	4.41	1.84	0.29	1.26	0.61
	6.0	8.14	4.44	1.83	0.29	1.26	0.62
CY-4 2039.81 m	0.2	7.71	4.30	1.80	0.28	1.10	0.58
Olivine Websterite	0.4	7.82	4.33	1.81	0.28	1.14	0.59
ρ = 3.15 g/cm^3	0.6	7.87	4.35	1.81	0.28	1.16	0.60
ϕ = 0.1%	0.8	7.91	4.36	1.81	0.28	1.17	0.60
	1.0	7.93	4.37	1.81	0.28	1.18	0.60
	2.0	7.98	4.40	1.82	0.28	1.20	0.61
	4.0	8.03	4.41	1.82	0.28	1.22	0.61
	6.0	8.06	4.42	1.82	0.29	1.23	0.62
CY-4 2079.89 m	0.2	7.61	4.12	1.85	0.29	1.11	0.53
Websterite	0.4	7.73	4.22	1.83	0.29	1.14	0.56
ρ = 3.14 g/cm^3	0.6	7.79	4.26	1.83	0.29	1.15	0.57
ϕ = 0.2%	0.8	7.82	4.28	1.83	0.29	1.16	0.58
	1.0	7.84	4.30	1.83	0.29	1.16	0.58
	2.0	7.89	4.33	1.82	0.28	1.17	0.59
	4.0	7.93	4.36	1.82	0.28	1.18	0.60
	6.0	7.95	4.38	1.81	0.28	1.19	0.61

TABLE 1: (cont.)

Sample	P (kb)	Vp (km/s)	Vs (km/s)	Vp/Vs	σ	K (Mb)	μ (Mb)
CY-4 2119.86 m	0.2	7.62	4.23	1.80	0.28	1.11	0.58
Olivine Websterite	0.4	7.82	4.32	1.81	0.28	1.18	0.61
ρ = 3.24 g/cm^3	0.6	7.92	4.38	1.81	0.28	1.20	0.62
ϕ = 0.1%	0.8	7.97	4.41	1.81	0.28	1.22	0.63
	1.0	8.00	4.43	1.81	0.28	1.23	0.64
	2.0	8.10	4.48	1.81	0.28	1.26	0.65
	4.0	8.20	4.53	1.81	0.28	1.30	0.67
	6.0	8.25	4.55	1.81	0.28	1.32	0.67
CY-4 2159.83 m	0.2	7.53	4.02	1.87	0.30	1.10	0.51
Olivine Websterite	0.4	7.59	4.08	1.86	0.30	1.11	0.52
ρ = 3.13 g/cm^3	0.6	7.62	4.12	1.85	0.29	1.11	0.53
ϕ = 0.2%	0.8	7.64	4.15	1.84	0.29	1.11	0.54
	1.0	7.66	4.17	1.84	0.29	1.11	0.55
	2.0	7.71	4.22	1.83	0.29	1.12	0.56
	4.0	7.75	4.25	1.82	0.29	1.13	0.57
	6.0	7.78	4.27	1.82	0.28	1.14	0.57

ρ = density; ϕ = porosity.

TABLE 2. Compressional Wave Velocities (Vp) and Anisotropies at 2 kb Confining Pressure

Rock	Vp (horiz.) km/sec	Vp (vert.) km/sec	Anisotropy
Gabbro, 1140m	6.84	7.12	4.0%
Websterite, 1893m	7.71	7.58	1.7%
Websterite, 1910m	7.78	7.60	2.3%

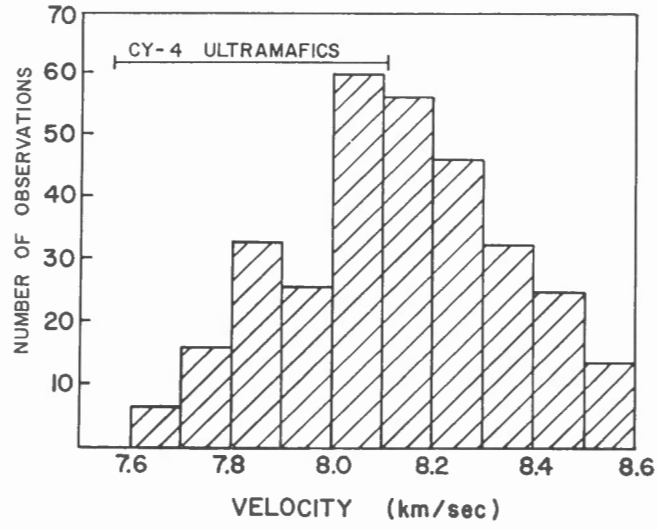

Figure 3: Comparison of CY-4 ultramafic rock velocities with histogram of Pacific upper mantle velocities (data from Christensen, 1982).

increase from 3.2 km/sec to 3.8 km/sec over the same interval. The gradients reflect both decreasing porosity and changes in secondary mineralogy caused by increasing metamorphic grade with increasing depth. Average porosities of dike rocks from the top of the drill hole are 3% whereas near the base of the sheeted dike section, porosities are generally less than 1% (Table 1). The uppermost dikes are primarily plagioclase-pyroxene rocks with less than 10% secondary minerals. With increasing depth, chlorite, laumontite, actinolite, epidote and hornblende become abundant in thin section. Note that compressional wave velocities for samples near the base of the sheeted dike section exceed the 6.69 km/sec average Layer 3 velocity of Raitt (1963).

The second interval of seismic interest extends from 630 m to 950 m. This zone consists of high level gabbro commonly containing amphibole. In addition, some dikes occur in the upper 100 m of this zone. With increasing depth, velocities first increase then decrease to 6.5 km/sec and 3.6 km/sec for Vp and Vs, respectively, at approximately 800 m. The velocity reversals originate from alteration of plagioclase and partial replacement of pyroxene by fibrous amphibole caused by deuteric alteration of the gabbro. Also within this region are dikes and sills of plagiogranite which have low velocities and densities (Christensen, 1977). No velocities were measured for the Troodos plagiogranite since only a small volume was encountered in the drill hole.

The third zone, extending from depths of 950 m to 1750 m, consists of relatively fresh pyroxene gabbros containing minor amphibole, olivine and serpentine. The gabbros within this region have remarkably uniform velocities with compressional and shear wave velocities averaging 7.2 km/sec and 4.0 km/sec, respectively. The velocities reported in Table 1 and shown in Figures 1 and 2 are for horizontal wave propagation. Petrographic examination of thin sections over this depth interval shows significant plagioclase orientation which produces some anisotropy. Plagioclase is oriented with (010) normals near vertical, which would produce fast compressional wave velocities for vertical wave propagation (Ryzhova, 1964). The velocity measurements presented in Table 2 for a gabbro sampled at 1140 m show that the resulting anisotropy is approximately 4%.

The lowest zone, extending from a core depth of 1750 m to the bottom of the hole, consists of ultramafic rocks. Lithologies are predominantly websterite and olivine websterite cut by diabase dikes. Although the rocks in this interval are quite fresh, serpentine is locally present. The 7.7 to 7.8 km/sec compressional wave velocities in this section are lower than many reported oceanic Pn velocities, but clearly fall within the range of observed upper mantle velocities (Figure 3). The sharp transition from gabbro to pyroxenite produces a major refractor for compressional waves. The shear wave velocity discontinuity, however, is not as abrupt (Figures 1 and 2). In addition, anisotropy in the ultramafic section is low (Table 2) compared to anisotropies observed in ultramafic rocks believed to have originated from the oceanic upper mantle (Christensen, 1984).

SUMMARY AND CONCLUSIONS

The velocity structure of the Troodos ophiolite as determined from laboratory studies is similar in many ways to that of normal oceanic crust. Rock velocities from the upper 700 m of the drill hole show strong positive gradients similar to those in oceanic crustal Layer 2. Near the base of the sheeted dikes an abrupt change of the velocity gradient could be interpreted as the boundary between Layers 2 and 3. Compressional wave velocities in the gabbroic section average approximately 7.0 km/sec, in reasonable agreement with logging data from the hole (6.7 ±0.3 km/s; Salisbury and Christensen, 1985) and with the many reported refraction velocities for Oceanic Layer 3. The major discontinuity at 1750 m depth, which separates overlying gabbros from ultramafic rocks, is similar to the oceanic Mohorovicic discontinuity, as defined by seismic studies. The petrologic Moho, which separates cumulate ultramafic rocks from underlying ultramafic tectonites, was not sampled by drilling and presumably lies deeper in the section.

There are, however, important differences between the structure of the CY-4 section and normal oceanic crust. These differences may be common in oceanic crust formed in an arc environment. Of major significance is the thickness of the gabbroic section commonly equated with Oceanic Layer 3. Average in situ Layer 3 thicknesses range between 4 and 5 km (Raitt, 1963; Christensen and Salisbury, 1975), whereas the apparent thickness of Layer 3 in drill hole CY-4 is only 1 km. The measured velocities in the underlying ultramafic section are clearly too high to be equated with Oceanic Layer 3, even if one assumes the presence of a high velocity basal Layer 3B as proposed by Sutton et al. (1971), but later questioned by Lewis and Snydsman (1977). Finally, the pyroxenite section from CY-4 does not show the strong azimuthal anisotropy commonly observed in the oceanic upper mantle. Since recovery textures become increasingly abundant toward the base of the hole, strongly anisotropic ultramafic tectonics may well exist deeper in the section.

ACKNOWLEDGMENTS

W. Wepfer, R. Rainy, C. Wilcox and C. Eddy assisted in the laboratory measurements. Financial support was provided by NSF Grant EAR 83-11776 and Office of Naval Research Contract N84K0207.

REFERENCES

Birch, F.
1960: The velocity of compressional waves in rocks to 10 kilobars, Part 1; Journal of Geophysical Research, v. 65, no. 4, p. 1083-1102.

Birch, F.
1961: The velocity of compressional waves in rocks to 10 kilobars, 2; Journal of Geophysical Research, v. 66, p. 2199-2224,

Christensen, N.I.
1977: The geophysical significance of oceanic plagio-granite; Earth and Planetary Science Letters, v. 36, p. 297-300.

Christensen, N.I.
1978: Ophiolites, seismic velocities and oceanic crustal structure; Tectonophysics, v. 47, p. 131-157.

Christensen, N.I.
1982: Seismic velocities; *in* Handbook of Physical Properties of Rocks, ed. R.S. Carmichael; CDC Press, Inc., Boca Raton, v. 11. p. 1-228.

Christensen, N.I.
1984: The magnitude, symmetry and origin of upper mantle anisotropy based on fabric analyses of ultramafic tectonites; Geophysics Journal of the Royal Astronomical Society, v. 76, p. 89-111.

Christensen, N.I. and Lundquist, S.M.
1982: Pyroxene orientation within the upper mantle; Geological Society of America, Bulletin, v. 93, p. 279-388.

Christensen, N.I. and Salisbury, M.H.
1975: Structure and constitution of the lower oceanic crust; Reviews of Geophysics and Space Physics, v. 13, no. 1, p. 57-86.

Christensen, N.I. and Salisbury, M.H.
1979: Seismic anisotropy in the oceanic upper mantle: evidence from the Bay of Islands ophiolite complex; Journal of Geophysical Research, v. 84, p. 4601-4610.

Christensen, N.I. and Salisbury, M.H.
1982: Lateral heterogeneity in the seismic structure of the oceanic crust; Geophysical Journal of the Royal Astronomical Society, v. 68, p. 675-688.

Christensen, N.I. and Smewing, J.D.
1981: Geology and seismic structure of the northern section of the Oman ophiolite; Journal of Geophysical Research, v. 86, no. B4, p. 2545-2555.

Coleman, R.G.
1971: Plate tectonic emplacement of upper mantle peridotites along continental edges; Journal of Geophysical Research, v. 76, p. 1212-1222.

Dewey, J.F. and Bird, J.M.
1971: Origin and emplacement of the ophiolite suite: Appalachian Ophiolites in Newfoundland; Journal of Geophysical Research, v. 76, p. 3179-3206.

Kroenke, L.W., Manghnani, M.H., Rai, C.S., Fryer, P. and Ramananantoandro, R.
1976: Elastic composition of oceanic lower crust and upper mantle; *in* The Geophysics of the Pacific Ocean Basin and its Margin, ed. G.H. Sutton, M.H. Manghnani and R. Moberly; Woollard Volume - Geophysical Monograph, American Geophysical Union, v. 19, p. 407-421.

Lewis, B.T.R. and Snydsman, W.E.
1977: Evidence for a low velocity layer at the base of the oceanic crust; Nature, v. 266, p. 340-345.

Miyashiro, A.
1973: The Troodos Ophiolitic complex was probably formed in an island arc; Earth and Planetary Science Letters, v. 19, no. 2, p. 218-224.

Moores, E.M. and F.J. Vine
1971: The Troodos Massif, Cyprus, and other ophiolites as oceanic crust: evaluation and implications; *in* A Discussion on the Petrology of Igneous and Metamorphic Rocks from the Ocean Floor; Philosophical Transactions of the Royal Society of London, Series A., v. 268, p. 443-466.

Peterson, J.J., Fox, P.J. and Schreiber, E.
1974: Newfoundland ophiolites and the geology of the oceanic layer; Nature, v. 247, p. 194-196.

Raitt, R.W.
1963: The crustal rocks; *in* The Sea, Ideas and Observations on Progress in the Study of the Seas, The Earth beneath the Sea, ed. M.N. Hill; John Wiley, New York, v. 3, p. 85-102.

Robinson, P.T., Melson, W.G., O'Hearn, T. and Schmincke, H.U.,
1983: Volcanic glass compositions of the Troodos Ophiolite, Cyprus; Geology, v. 11, p. 400-404.

Ryzhova, T.V.
1964: Elastic properties of plagioclase, Izvestia Geophysical Series, v. 7, p. 1049-1051.

Salisbury, M.H. and Christensen, N.I.
1978: The seismic velocity structure of a traverse through the Bay of Islands ophiolite complex, Newfoundland: an exposure of oceanic crust and upper mantle; Journal of Geophysical Research, v. 83, no. 2, p. 805-817.

Salisbury, M.H. and Christensen, N.I.
1985: Velocity structure of the Troodos ophiolite from borehole logs; American Geophysical Union, Transactions, v. 66, p.1122.

Shor, G.G., Jr., Menard, H.W. and Raitt, R.W.
1971: Structure of the Pacific basin; *in* The Sea, ed. A.E. Maxwell; John Wiley, New York, v. 4, p. 327.

Sutton, G.H., Maynard, G.L. and Hussong, D.M.
1971: Widespread occurrence of a high-velocity basal layer in the Pacific crust found with repetitive sources and sonobuoys; *in* The Structure and Physical Properties of the Earth's Crust, ed. J.G. Heacock; Geophysical Monograph Series, American Geophysical Union, Washington, D.C., v. 14, p. 193-209.

A Gravity Survey from Agrokipia to Papoutsa, Cyprus

S. KRAMVIS[1] AND K.L. VEROSUB[2]

[1]Cyprus Geological Survey, Nicosia, Cyprus
[2]Department of Geology, University of California,
Davis, California, 95616, U.S.A.

Kramvis, S. and Verosub, K.L., A gravity survey from Agrokipia to Papoutsa, Cyprus, in drill hole Cy-4, the Troodos ophiolite, Cyprus; in *Cyprus Crustal Study Project: Initial Report, Hole Cy-4, ed. I.L Gibson, J. Malpas, P.T. Robinson and C. Xenophontos; Geological Survey of Canada, Paper 88-9, p. 371-379, 1989.*

Abstract

We report the results of a gravity survey designed to provide a geophysical connection between holes CY-2a and CY-4 of the Cyprus Crustal Drilling Project. The survey consists of 93 stations on a 22.5 km line from Agrokipia to Papoutsa. The observed value of gravity at each station is determined from the datum in Nicosia previously used for an extensive gravity survey of the island. In the present survey, free air, simple Bouguer and complete Bouguer anomalies are reported for reduction densities of 2.50 and 2.67 gm/cc. For a reduction density of 2.50 gm/cc, the complete Bouguer anomaly reaches a maximum value of 195 mgal about one-third of the way from Agrokipia and Papoutsa with values of 185 and 178 at these two locations, respectively.

Résumé

Nous présentons les résultats d'une campagne de gravimétrie destinée à établir un pont géophysique entre les forages CY-2a et CY-4 du Projet d'étude de la croûte terrestre à Chypre. La campagne a permis le relevé de 93 sites distribués le long d'une ligne longue de 22.5 km entre Agrokipia et Papoutsa. La valeur gravitaire observée à chaque site est déterminée à partir de la référence à Nicosie et utilisée antérieurement lors d'une campagne de gravité exhaustive sur toute l'ile. Les résultats de la présente campagne comprennent les anomalies à l'air libre, de Bouguer simple et de Bouguer totale, calculées pour les densités de 2.50 et 2.76 gm/cc. Si on considère la densité 2.50 gm/cc, l'anomalie Bouguer totale atteint un maximum de 195 mgal à environ au tiers de la distance totale d'Agrokipia et Papoutsa, caractérisées par des anomalies de 185 et 178 mgal respectivement à ces deux extrémités.

INTRODUCTION

In order to provide a geophysical connection between holes CY-2a and CY-4, a gravity survey was conducted between the towns of Agrokipia and Papoutsa. This survey supplements an earlier gravity survey of Cyprus (Gass and Masson-Smith, 1963) and provides a detailed record of the variation in gravity between the two holes. In conjunction with the density profiles from the two holes, the survey can be used to model the subsurface structure in this area. This modelling will supplement ongoing field studies of the surficial geology.

DATA COLLECTION

The gravity survey is a 22.5 km line beginning at a point 0.5 km north of Agrokipia and ending near Papoutsa at a point 5.0 km west southwest of Palekhori (Figure 1). Over the first 15 km, the line runs almost due south, but at Aplik the direction changes to southwest. The elevation along the line increases from about 400 meters near Agrokipia to about 1400 meters at the end of the line. The primary rock units exposed at the surface along most of the line are the Sheeted Dyke Complex and extrusives of the Pillow Lava Series (Anonymous, 1979). The main exception is southwest of Palekhori where plagiogranites and gabbros of the Plutonic Complex are present.

The survey was conducted by one of us (S.K.) over a four-day period in the summer of 1981. Ninety-three stations were occupied at approximately equal intervals along the line. Station 36 was used as the primary base station, and a secondary base station was established at Station 68 using four separate ties to the primary base station. During the course of the survey one or the other of the two base stations was reoccupied about every two hours.

All of the measurements were made using a Worden gravimeter with a dial constant of 0.0967 mgals/div. The location of each station was determined in terms of Universal Transverse Mercator coordinates from 1:5000 topographic maps. The uncertainty of the locations in the horizontal plane is estimated to be 5 m. The actual elevation of the gravimeter at each station was determined by surveying. The vertical uncertainty is about 0.03 m.

DATA REDUCTION

The data were reduced using the computing facilities of the Geology Department of the University of California-Davis. Each station location was converted to its corresponding longitude and latitude. In order to make the results of this survey compatible with those of Gass and Masson-Smith (1963), the International Gravity Formula of 1930 was used for the calculation of the theoretical gravity values (Table 1). The dial readings were corrected for instrumental drift and for earth tides by first determining the time dependence of the repeat readings at the base stations and then reducing all of the station readings to a common time datum. The gravity difference between each station and Station 36 was then computed using the dial constant.

The observed value of gravity at each station in the present survey was tied to the primary datum of Gass and Masson-Smith (1963) in Nicosia via base stations 599 (Malounda) and ´625 (Mitsero) of that survey. Ideally these stations should have been tied to Station 36 of this survey, but due to logistical problems, the tie was made to Station 4, and the gravity difference between Stations 4 and 36 was used to obtain the observed value of gravity at Station 36. Three ties were made from Station 4 to the station at Malounda; two to that at Mitsero. The absolute values of gravity at Station 4 calculated from each of these stations differed by only 0.03 mgal. The absolute value of gravity for Station 36, determined from the gravity difference between it and Station 4 was 979802.62 mgal. Values of the observed gravity at the other stations in the survey were computed from this value (Table 1).

The value used for the gravity at the datum in Nicosia was 979850.10 mgal (Gass and Masson-Smith, 1963). According to Masson-Smith (written communication to C. Xenophontas, 1984), if the survey of Gass and Masson-Smith (1963) is to be consistent with the modern gravity system (IGSN71), the value for the datum in Nicosia should be revised to 979839.00 mgal, and the gravity differences from this datum should be reduced by 0.06%. For the stations at Malounda and Mitsero, these changes are .002 and .008 mgal, respectively. Because the results of the present survey are likely to be used in conjunction with those of Gass and Masson-Smith (1963), the original value for the datum in Nicosia has been retained. The revised datum would reduce all of the observed gravity values in Table 1 by 11.10 mgal.

The theoretical and observed values of gravity and the station elevations were used to compile the free air and simple and complete Bouguer anomalies (Table 2). The Bouguer reductions were determined for densities of both 2.50 gm/cc and 2.67 gm/cc. Terrain corrections were computed to a distance of 2.6 km, corresponding to Zone H of Hammer (1939). The terrain corrections, as a function of station number, are shown in Figure 2. The maximum terrain correction from Zone H was 0.6 mgals, and in most cases the contribution from this zone represented less than 10% of the total correction.

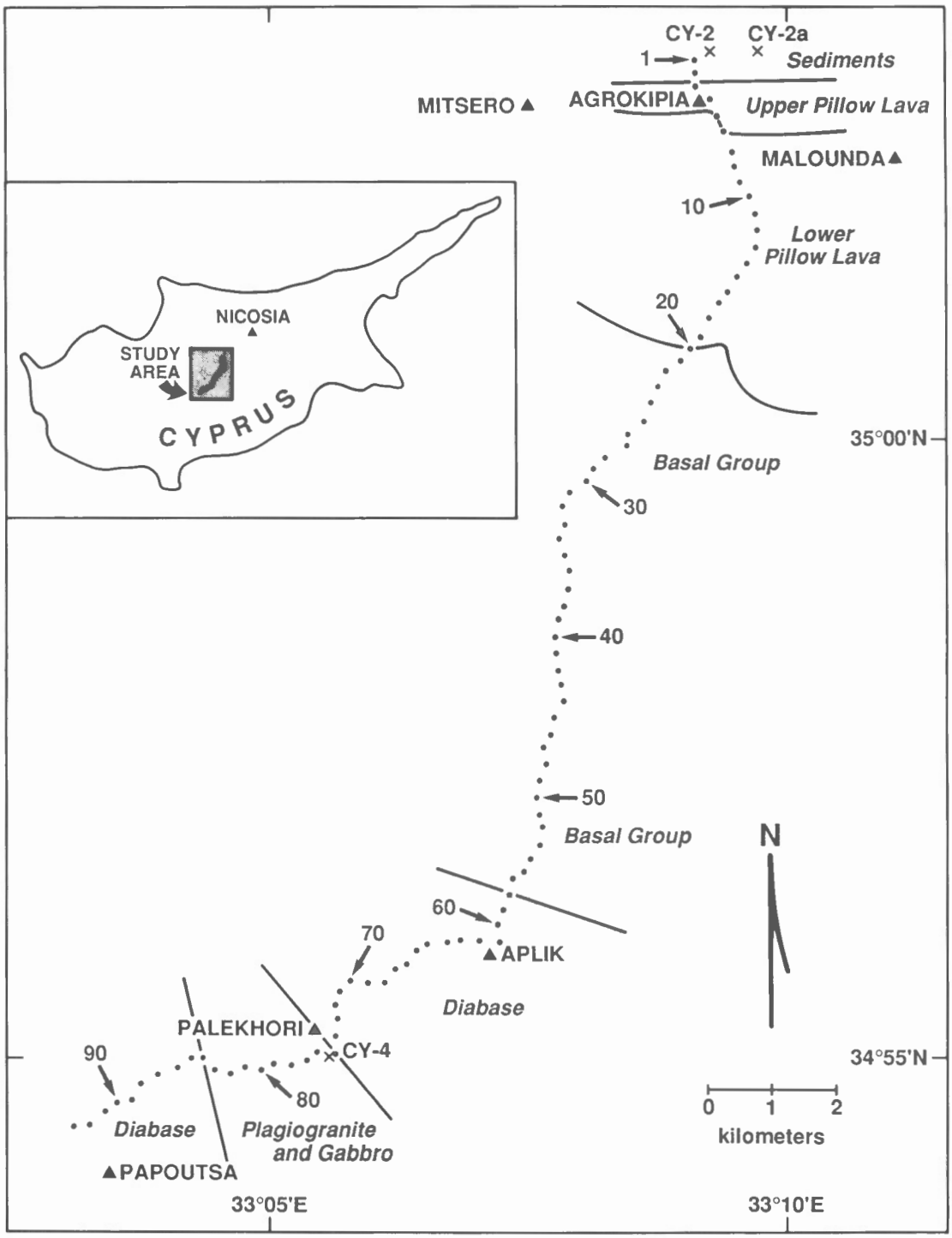

Figure 1: Map showing location of gravity stations (circles), towns and villages (triangles) and drill holes (crosses). The stations are numbered sequentially. The inset map shows the location of the gravity survey with respect to the island of Cyprus.

TABLE 1. Theoretical and Observed Gravity from Agrokipia to Papoutsa.

Station	Latitude North	Longitude east	elevation (ft.)	theoretical gravity	observed gravity
1	35°02'58"	33°09'03"	1468.4	979749.73	979839.72
2	35°02'52"	33°09'03"	1329.1	979749.59	979850.29
3	35°02'45"	33°09'04"	1268.0	979749.43	979855.56
4	35°02'39"	33°09'11"	1270.4	979749.29	979856.13
5	35°02'30"	33°09'15"	1272.2	979749.07	979856.28
6	35°02'24"	33°09'20"	1287.0	979748.93	979855.45
7	35°02'13"	33°09'23"	1295.1	979748.67	979855.17
8	35°02'06"	33°09'25"	1311.2	979748.51	979854.26
9	35°02'00"	33°09'29"	1333.1	979748.37	979852.97
10	35°01'54"	33°09'34"	1370.5	979748.23	979850.65
11	35°01'44"	33°09'38"	1402.7	979747.99	979848.52
12	35°01'37"	33°09'39"	1440.9	979747.83	979845.91
13	35°01'29"	33°09'38"	1435.3	979747.64	979846.24
14	35°01'21"	33°09'34"	1442.2	979747.45	979845.85
15	35°01'15"	33°09'27"	1452.8	979747.31	979845.61
16	35°01'08"	33°09'22"	1469.9	979747.14	979844.83
17	35°01'02"	33°09'18"	1489.5	979747.00	979843.90
18	35°00'57"	33°09'11"	1499.2	979746.89	979843.57
19	35°00'47"	33°09'06"	1506.8	979746.65	979843.37
20	35°00'41"	33°09'00"	1512.5	979746.51	979843.13
21	35°00'36"	33°08'53"	1517.3	979746.39	979842.98
22	35°00'32"	33°08'46"	1537.9	979746.30	979841.66
23	35°00'24"	33°08'41"	1565.4	979746.11	979839.39
24	35°00'16"	33°08'37"	1588.3	979745.92	979837.45
25	35°00'08"	33°08'32"	1589.0	979745.73	979837.58
26	35°00'02"	33°08'24"	1608.6	979745.59	979836.83
27	34°59'55"	33°08'20"	1623.0	979745.43	979836.44
28	34°59'49"	33°08'13"	1633.8	979745.29	979836.27
29	34°59'44"	33°08'06"	1647.2	979745.17	979835.30
30	34°59'37"	33°08'02"	1661.3	979745.00	979834.18
31	34°59'32"	33°07'52"	1678.9	979744.89	979832.63
32	34°59'24"	33°07'47"	1688.6	979744.70	979831.77
33	34°59'16"	33°07'50"	1711.1	979744.51	979830.02
34	34°59'09"	33°07'48"	1734.4	979744.34	979827.60
35	34°59'00"	33°07'51"	1745.7	979744.13	979826.72
36	34°58'54"	33°07'53"	1772.1	979743.99	979824.82
37	34°58'45"	33°07'52"	1803.9	979743.78	979823.00
38	34°58'37"	33°07'49"	1822.7	979743.59	979822.46
39	34°58'29"	33°07'45"	1840.6	979743.40	979820.92
40	34°58'23"	33°07'45"	1833.6	979743.26	979821.19
41	34°58'15"	33°07'46"	1840.1	979743.07	979820.05
42	34°58'06"	33°07'48"	1853.7	979742.86	979818.86
43	34°58'00"	33°07'48"	1877.5	979742.72	979816.98
44	34°58'50"	33°07'50"	1888.4	979743.90	979815.64

TABLE 1. (cont.)

Station	Latitude North	Longitude east	elevation (ft.)	theoretical gravity	observed gravity
45	34°58'43"	33°07'42"	1915.9	979743.73	979813.93
46	34°58'36"	33°07'41"	1976.8	979743.57	979809.31
47	34°58'28"	33°07'38"	1999.7	979743.38	979807.73
48	34°58'19"	33°07'40"	2016.7	979743.17	979805.11
49	34°58'13"	33°07'35"	2010.0	979743.03	979805.50
50	34°57'03"	33°07'34"	2001.0	979741.38	979805.19
51	34°56'58"	33°07'35"	2028.2	979741.26	979803.19
52	34°56'52"	33°07'38"	2030.8	979741.12	979801.96
53	34°56'44"	33°07'36"	2054.6	979740.93	979799.46
54	34°56'37"	33°07'30"	2086.2	979740.77	979797.09
55	34°56'31"	33°07'25"	2096.7	979740.63	979795.92
56	34°56'28"	33°07'20"	2130.7	979740.56	979794.30
57	34°56'19"	33°07'18"	2145.5	979740.35	979792.84
58	34°56'10"	33°07'13"	2200.6	979740.13	979789.07
59	34°56'03"	33°07'11"	2278.3	979739.97	979784.54
60	34°55'54"	33°07'11"	2333.9	979739.76	979780.97
61	34°55'55"	33°07'00"	2420.6	979739.78	979776.01
62	34°55'57"	33°06'49"	2510.6	979739.83	979770.82
63	34°55'55"	33°06'40"	2567.8	979739.78	979767.35
64	34°55'54"	33°06'30"	2625.2	979739.76	979764.37
65	34°55'50"	33°06'23"	2693.2	979739.66	979759.63
66	34°55'43"	33°06'18"	2738.8	979739.50	979756.34
67	34°55'41"	33°06'10"	2780.7	979739.45	979753.40
68	34°55'36"	33°06'05"	2837.4	979739.34	979749.12
69	34°55'34"	33°05'55"	2991.8	979739.29	979739.29
70	34°55'34"	33°05'46"	3008.4	979739.29	979739.04
71	34°55'31"	33°05'40"	2968.1	979739.22	979741.01
72	34°55'24"	33°05'36"	2934.0	979739.05	979742.15
73	34°55'18"	33°05'37"	2987.0	979738.91	979738.16
74	34°55'08"	33°05'35"	3029.0	979738.68	979734.72
75	34°55'00"	33°05'37"	3097.8	979738.49	979729.20
76	34°55'02"	33°05'26"	3096.3	979738.54	979729.57
77	34°54'57"	33°05'20"	3131.7	979738.42	979726.93
78	34°54'55"	33°05'10"	3168.3	979738.37	979725.16
79	34°54'55"	33°04'59"	3219.4	979738.37	979721.28
80	34°54'54"	33°04'52"	3279.3	979738.35	979717.07
81	34°54'54"	33°04'44"	3332.2	979738.35	979714.18
82	34°54'52"	33°04'34"	3383.0	979738.30	979711.01
83	34°54'54"	33°04'26"	3453.2	979738.35	979707.20
84	34°55'00"	33°04'20"	3476.7	979738.49	979707.08
85	34°55'00"	33°04'11"	3498.9	979738.49	979705.91
86	34°54'54"	33°04'05"	3518.8	979738.35	979703.40
87	33°54'52"	33°03'54"	3586.7	979738.30	979698.10
88	34°54'46"	33°03'44"	3775.8	979738.16	979685.39
89	34°54'39"	33°03'39"	3838.2	979738.00	979680.46
90	34°54'36"	33°03'29"	4008.4	979737.93	979669.04
91	34°54'32"	33°03'20"	4069.8	979737.83	979663.90
92	34°54'26"	33°03'12"	4121.0	979737.69	979659.99

TABLE 2. Calculated Bouger Anomaly from Agrokipia to Papoutsa.

Station	Free-air Anomaly	Simple Bouger Anomaly (2.5 gm/cc)	Complete Bouger Anomaly (2.5 gm/cc)	Simple Bouger Anomaly (2.67 gm/cc)	Complete Bouger Anomaly (2.67 gm/cc)
1	228.1	181.2	181.8	178.0	178.6
2	225.7	183.3	183.5	180.4	180.6
3	225.4	184.9	185.2	182.2	182.4
4	226.3	185.8	186.0	183.0	183.2
5	226.9	186.3	186.4	183.5	183.7
6	227.6	186.5	186.6	183.7	183.8
7	228.3	187.0	187.1	184.2	184.3
8	229.1	187.2	187.4	184.4	184.5
9	230.0	187.4	187.5	184.5	184.6
10	231.3	187.6	187.6	184.6	184.7
11	232.5	187.7	187.8	184.6	184.7
12	233.6	187.6	187.7	184.5	184.6
13	233.6	187.8	187.9	184.7	184.8
14	234.1	188.0	188.2	184.9	185.1
15	234.9	188.6	188.7	185.4	185.6
16	235.9	189.0	189.2	185.8	186.1
17	237.0	189.4	189.7	186.2	186.5
18	237.7	189.8	190.2	186.6	187.0
19	238.5	190.3	190.7	187.1	187.4
20	238.9	190.6	191.0	187.3	187.8
21	239.3	190.9	191.4	187.6	188.1
22	240.0	190.9	191.5	187.6	188.2
23	240.5	190.5	191.2	187.1	187.8
24	240.9	190.2	191.0	186.8	187.6
25	241.3	190.6	191.3	187.1	187.9
26	242.5	191.2	192.0	187.7	188.6
27	243.7	191.9	192.6	188.3	189.1
28	244.7	192.5	193.4	189.0	189.9
29	245.1	192.5	193.5	188.9	190.0
30	245.4	192.4	193.5	188.8	190.0
31	245.7	192.1	193.4	188.4	189.8
32	245.9	192.0	193.8	188.3	190.2
33	246.5	191.8	193.4	188.1	189.7
34	246.4	191.0	192.7	187.3	189.0
35	246.8	191.1	192.7	187.3	189.0
36	247.5	190.9	192.4	187.1	188.6
37	248.9	191.3	192.5	187.4	188.7
38	250.3	192.1	193.2	188.2	189.3
39	250.6	191.9	193.2	187.9	189.3
40	250.4	191.9	192.0	187.9	188.0
41	250.1	191.3	192.9	187.3	189.0
42	250.4	191.2	192.8	187.2	188.9
43	250.9	190.9	192.5	186.8	188.6
44	249.4	189.1	190.7	185.0	186.7

TABLE 2. (cont.)

Station	Free-air Anomaly	Simple Bouger Anomaly (2.5 gm/cc)	Complete Bouger Anomaly (2.5 gm/cc)	Simple Bouger Anomaly (2.67 gm/cc)	Complete Bouger Anomaly (2.67 gm/cc)
45	250.4	189.2	191.3	185.1	187.3
46	251.7	188.6	190.6	184.3	186.5
47	252.4	188.6	190.5	184.3	186.3
48	251.6	187.2	189.3	182.9	185.1
49	251.5	187.4	189.6	183.0	185.4
50	252.0	188.1	190.7	183.8	186.5
51	252.7	188.0	190.5	183.5	186.2
52	251.9	187.0	189.7	182.6	185.5
53	251.8	186.2	189.3	181.7	185.0
54	252.5	185.9	189.2	181.4	184.9
55	252.5	185.6	188.6	181.0	184.3
56	254.2	186.1	188.8	181.5	184.3
57	254.3	185.8	188.2	181.1	183.7
58	255.9	185.7	188.1	180.9	183.4
59	258.9	186.1	188.0	181.2	183.2
60	260.7	186.2	187.6	181.2	182.7
61	263.9	186.6	188.0	181.4	182.9
62	267.1	187.0	188.2	181.5	182.8
63	269.1	187.1	188.5	181.5	183.0
64	271.5	187.7	189.0	182.0	183.4
65	273.3	187.3	188.5	181.5	182.7
66	274.5	187.0	188.2	181.1	182.3
67	275.5	186.7	188.0	180.7	182.0
68	276.8	186.2	187.4	180.1	181.3
69	281.4	185.9	186.9	179.4	180.5
70	282.7	186.7	187.3	180.1	180.8
71	281.0	186.2	186.8	179.8	180.4
72	279.1	185.4	186.8	179.0	180.5
73	280.2	184.8	185.9	178.4	179.4
74	280.9	184.2	185.4	177.7	178.9
75	282.1	183.2	184.1	176.5	177.4
76	282.3	183.4	184.3	176.7	177.7
77	283.1	183.1	184.4	176.3	177.7
78	284.8	183.7	185.1	176.8	178.4
79	285.7	182.9	184.8	176.0	177.9
80	287.2	182.5	184.3	175.4	177.3
81	289.3	182.9	184.8	175.6	177.7
82	290.9	182.9	184.8	175.6	177.6
83	293.7	183.4	185.3	175.9	177.9
84	295.6	184.6	186.6	177.1	179.2
85	296.5	184.8	186.7	177.2	179.2
86	296.0	183.7	185.7	176.1	178.2
87	297.2	182.7	184.7	174.9	177.0
88	302.4	181.8	183.6	173.6	175.5
89	303.5	180.9	182.7	172.6	174.5
90	308.1	180.2	181.7	171.5	173.1
91	308.9	178.9	180.2	170.1	171.4
92	309.9	178.4	179.5	169.4	170.6
93	309.1	177.2	178.2	168.2	169.3

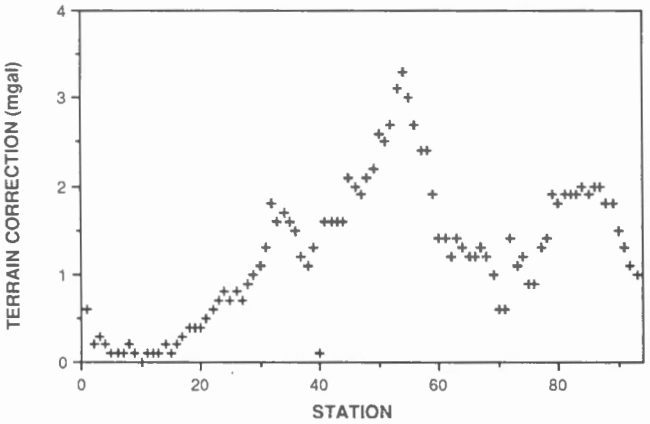

Figure 2: Terrain corrections to Hammer Zone H as a function of station number for a reduction density of 2.50 gm/cc.

DISCUSSION

Elevation, free-air anomaly, and complete Bouguer anomaly (for reduction densities of 2.50 gm/cc) are shown in Figure 3 as a function of station number. This lower density is consistent with the densities found in hole CY-2a (Smith and Vine, 1987). The free-air anomaly is large and positive and closely-correlated with the elevation, as is to be expected. The complete Bouguer anomaly is also large and positive because of the uncompensated mass of the ultramafic material in the Troodos complex. The complete Bouguer anomaly varies from 178 to 195 mgal. At station 3 in Agrokipia, it has a value of 185 mgal, and it increases relatively uniformly with a gradient of 1.3 mgal/km until station 28 where the maximum value of 195 mgal occurs. Between station 29 and station 84, the anomaly decreases with a gradient of –0.5 mgal/km, although there are systematic fluctuations of as much as 0.3 mgal. Beyond station 85 the anomaly falls even more rapidly as the gradient changes to –3.6 mgal/km. The lowest value of 178 mgal occurs at the end of the line.

In order to isolate the gravity variation due to the structure between the two holes from the regional gravity field of the entire ophiolite complex, it will be necessary to determine the regional anomaly and to subtract it from the observed profile. The rather complex nature of the regional anomaly (Gass and Masson-Smith, 1963) may preclude the use of a simple linear gradient and may require a more sophisticated approach such as a higher-order trend surface analysis.

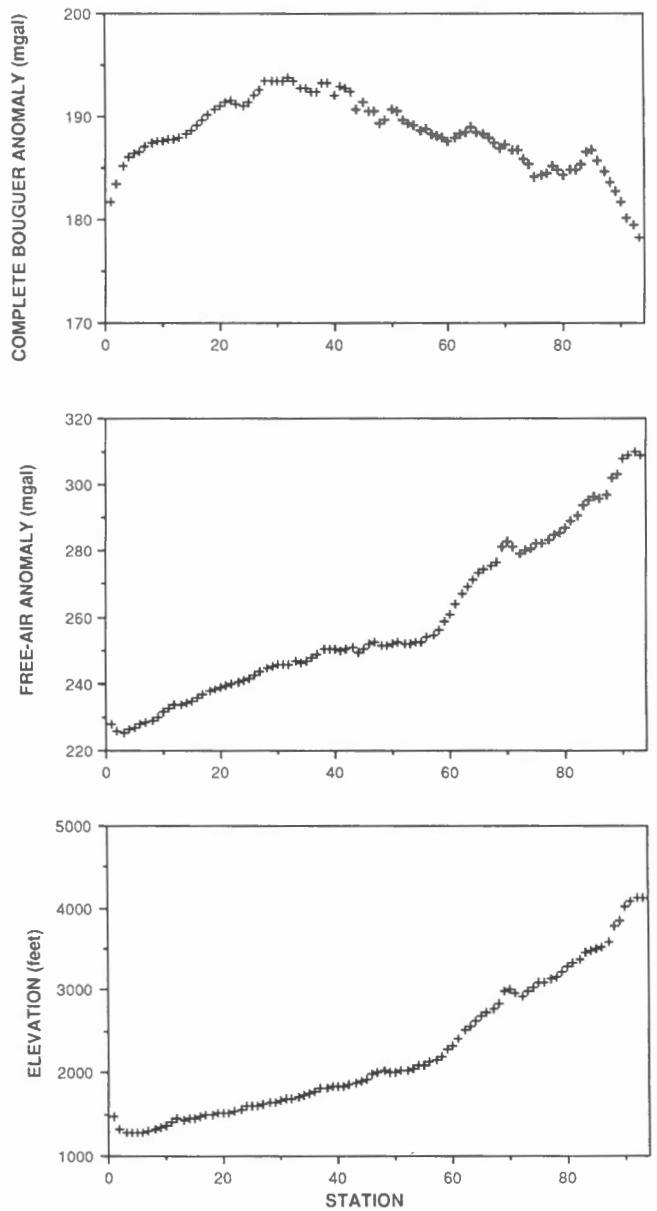

Figure 3: Elevation, free-air anomally, and complete Bouguer anomaly as a function of station number for a reduction density of 2.50 gm/cc.

ACKNOWLEDGMENTS

We thank C. Xenophontas, J. McClain and S. Hurst for their assistance, R. Harris for his calculation of the terrain corrections, and P. Waterstraat for his development of the computer programs used to analyze the data. E. Moores provided useful information about the geology of Cyprus and the Cyprus drilling program. This research was supported by National Science Foundation grant EAR-81-21189 to K.L.V.

REFERENCES

Anonymous.
1979: Geological map of Cyprus, scale 1:250,000; Geological Survey Department, Nicosia, Cyprus.

Gass, I.G., and D. Masson-Smith.
1963: The geology and gravity anomalies of the Troodos Massif, Cyprus; Philosophical Transactions of the Royal Society, London, Series A, v. 255, p. 417-467.

Hammer, S.
1939: Terrain corrections for gravimeter stations; Geophysics, v. 4, p. 184-194.

Smith, G.C., and F.J. Vine.
1987: Gravity and magnetic studies of the Agrokipia Sulphide Ore Bodies, Cyprus; *in* Cyprus Crustal Study Project Initial Report Holes CY-2 and 2a, ed. P.T. Robinson, I.L. Gibson, and A. Panayiotou; Geological Survey of Canada, Paper 85-29, p. 327-337.

Geology and Geophysics of Borehole CY-4 of the Cyprus Crustal Study Project: Summary

JOHN MALPAS[1], PAUL T. ROBINSON[2] AND MATTHEW SALISBURY[3]

[1]Department of Earth Sciences, Memorial University, St. John's, Newfoundland, Canada AlB 3X5
[2]Centre for Marine Geology, Dalhousie University, Halifax, Nova Scotia, Canada B3H 3J5
[3]Atlantic Geoscience Centre, Bedford Institute, Dartmouth, Nova Scotia, Canada B2Y 4A2

Robinson, P.T., Malpas, J. and Salisbury, M., Geology and Geophysics of Borehole CY-4 of the Cyprus Crustal Study Project: Summary; in *Cyprus Crustal Study Project: Initial Report, Hole CY-4, ed. I.L. Gibson, J. Malpas, P.T. Robinson and C. Xenophontos; Geological Survey of Canada, Paper 88-9, p. 381-393, 1989.*

Abstract

The CY-4 borehole provides a continuous sample (99% recovery) of a 2263 m-thick section through the sheeted dyke complex and plutonic sequence of the Troodos ophiolite. Five zones are recognized on the basis of lithology and phase chemistry: (1) 0-675 m. Sheeted diabase dykes. (2) 675-900 m. Fine- to medium-grained gabbro. (3) 900-1330 m. Fine- to medium-grained gabbro-norite and two-pyroxene diabase dykes. (4) 1330-1740 m. Medium- to coarse-grained gabbro-norite. (5) 1740-2263 m. Medium- to coarse-grained websterite and related rocks. Contacts between these zones are either gradational (Zone 2/3), intrusive (Zones 3/4) or faulted (Zones 4/5). Alteration throughout most of the plutonic section is limited to partial replacement of pyroxenes by actinolite; olivine is partially serpentinized but plagioclase remains essentially unaltered. There is a general trend towards more primitive primary mineral compositions with increasing depth with a sharp break at the intrusive contact between Zones 3 and 4. Results suggest that the gabbros and ultramafic rocks from Zones 4 and 5 crystallized in a relatively closed magma chamber. In contrast, the rocks of the upper zones appear to reflect crystallization in a magma chamber that was open to periodic replenishment. Laboratory measurements of magnetic and other physical properties and downhole logging of compressional and shear wave velocity, density, porosity, electrical resistivity, magnetic susceptibility and field strength, temperature and hole diameter, strongly suggest that the oceanic layer 2/3 boundary coincides with the sheeted dyke/gabbro transition.

Résumé

Le forage CY-4 procure un échantillon continu (recouvrement de 99%) d'une section de 2263 m d'épaisseur á travers un complexe de dyke effeuillé et une séquence plutonique de l'ophiolite de Troodos. Cinq zones sont identifiées, se basant sur la lithologie et la chimie des phases: (1) 0-675 m dykes à diabases. (2) 675-900 m gabbro, granulé fine et moyen. (3) 900-1330 m gabbro-norite et dykes à diabase deux-pyroxène. (4) 1330-1740 m gabbro-norite, granulé moyen et gros. (5) 1740-2263 m websterites et autres rocs similaires, granulés moyens et gros. Les contacts entre ces zones sont: graduels (Zone 2 à 3), intrusifs (Zone 3 à 4) ou en failles (Zone 4 à 5). Les transformations dans la majeure partie de la section plutonique se limitent á un remplacement partiel des pyroxènes par de l'actinolite; l'olivine est partiellement serpentinée mais le plagioclase demeure inaltéré. Les compositions minérales deviennent plus primitives à mesure que la profondeur augmente avec une discontinuité au contact intrusif entre les Zones 3 et 4. Les résultats suggèrent que les gabbros et rocs ultramafiques des Zones 4 et 5 se sont cristallisés dans une chambre magmatique relativement close. Par contre, les roches des zones supérieures semblent avoir été cristallisées dans une chambre magmatique fréquemment regénérée. Les analyses de laboratoire des propriétés magnétiques, physiques, les mesures de vitesse des ondes de chocs, la densité, porosité, résistance éléctrique, sensibilité magnétique et puissance du champ, la température et le diamètre du trou, tout suggère fortement que la limite de la couche océanique 2/3 coincide avec la transition dyke effeuillé/gabbro.

INTRODUCTION

Our inability to sample directly the deeper levels of in situ ocean crust has meant that nearly all information on the nature of oceanic Layer 3 has come from ophiolites. However, many years of study have resulted in conflicting models for the structure and petrology of ophiolitic plutonic suites and their relevance to in situ crust. Many models call for a heterogeneous cumulate section composed of numerous small plutons (Moores and Vine, 1971; Allen, 1975; Greenbaum, 1977) whereas others postulate formation from single, large, steady-state magma chambers (Greenbaum, 1972; Hopson and Pallister, 1980; Casey and Karson, 1981). Other unresolved questions include the nature and extent of alteration in the lower crust, the physical and magnetic properties of ophiolite gabbros and the relationship between plutonic and volcanic sequences in ophiolites.

The Cyprus Crustal Study Project, a combined field and drilling study of the Troodos ophiolite was undertaken by the International Crustal Research Drilling Group to determine the structure and petrology of that body and to compare it to in situ oceanic crust. Hole CY-4 is the deepest of five research holes drilled in Troodos, extending nearly 2.3 km into the lower parts of the ophiolite (Figure 1). The main objective of this hole was to sample the plutonic sequence and its transition into the sheeted dykes. By combining the drillhole data with information from surface geology it was hoped to produce a three dimensional model of the plutonic sequence. Other objectives included determination of the geochemical stratigraphy of the plutonic section, the nature and extent of alteration in these rocks and their physical and magnetic properties. A major program of downhole logging was carried out in order to compare the geophysical properties of the section with the core and with the properties of oceanic crust as determined by geophysical experiments performed at sea.

The borehole provides a continuous sample (99% recovery) of a 2263 m thick section through the sheeted dyke complex and plutonic sequence of the ophiolite. The hole sampled some 700 m of dyke section, 800 m of isotropic gabbros and associated differentiated rock types and approximately 760 m of layered gabbros, pyroxenite and peridotite. For financial reasons the drilling was halted before reaching the dunites thought to form the base of the cumulate sequence. Petrological evidence gained subsequently from the core suggests that dunite could occur at a depth of approximately 2550 m, approximately 300 m deeper than the bottom of CY-4.

The siting of hole CY-4 was controlled by both geological and logistical factors. Geologically, the hole was intended to sample the plutonic sequence beneath the lavas drilled in holes CY-1, 1a, 2 and 2a. It was hoped to sample the sheeted dyke-plutonic transition and to drill as deeply as possible into the cumulate section, perhaps to the petrological moho. Logistics on the other hand, required good access for vehicles, site stability and the availability of water. A site 1 km south of the village of Palekhori on the Palekhori-Agros road appeared to provide favorable conditions (Figure 2). In this area, mapping undertaken by the Cyprus Geological Survey Department indicated that the sheeted dyke complex was intruded by a high level plagiogranite body. Dykes of plagiogranite up to 3 m wide, containing xenoliths of diabase, cut the sheeted dykes in outcrops adjacent to the drill site. From our understanding of the ophiolite stratigraphy at the time of choosing the site, it was considered that the dykes would terminate some 70 to 100 m below ground level in a plagiogranitic stock. It was thought that the plagiogranite would then grade into diorites and gabbros representing a major portion of the plutonic complex. The subsequent drilling and a further consideration of the regional geology carried out in an associated field program, proved otherwise. It is now clear that swarms of diabase dykes cut the plutonic complex, including the plagiogranite, to considerable depths, forming part of the sheeted complex higher up and giving a relief of up to 500 m on the dyke-plutonic transition. This is a consequence of the construction of the ophiolite from multiple magma chambers, a feature that was not fully appreciated at the time of siting CY-4. Drilling apparently proceeded down such a dyke swarm so that the plutonic rocks were not encountered until some 700 m of core had been recovered. A second deep swarm of dykes was encountered between 1100 and 1200 m.

REGIONAL GEOLOGY

The area immediately adjacent to the drill site comprises approximately N-S trending, steeply-dipping diabase dykes locally intruded by plagiogranite. These are underlain by gabbroic rocks that crop out a few hundred metres to the west and south (Malpas and Brace, 1987). The gabbros and dykes show three distinct contact relationships: 1) dykes intrude the plutonic rocks; 2) dykes are intruded by the plutonic rocks; and 3) dykes arise directly from their plutonic equivalents. The first two relationships occur in approximately equal proportions and are far more common than the third. Near the contact between the dykes and the plutonic rocks, dykes are commonly separated by screens of plagiogranite or gabbro, but elsewhere dykes intrude other dykes. The gabbroic rocks form a number of plutons with complex intrusive relations. In addition to the dyke relationships described above, gabbro is commonly intruded by adjacent gabbro or plagiogranite with xenoliths of the older in the younger. Pyroxene and uralite gabbros are the most common and widespread varieties. The pyroxene gabbros are typically massive to poorly layered, mesocratic rocks consisting of augite, hypersthene, plagioclase and, close to transitions into diorite, quartz. The uralite gabbros, referred to by many workers as "high level gabbros", consist of zoned plagioclase, augite-salite, hypersthene, actinolitic hornblende, magnetite and quartz. Leucocratic, quartz-

bearing pegmatitic veins and pods with associated coarse-grained, acicular amphibole, are very common close to contacts with more differentiated rocks, and these segregations produce complex interfingering textures. The term "varitextured" is applied to this gabbro.

Plagiogranites intrude diabase and gabbros as veins, dykes and larger irregular bodies, and are considered to be the end products of fractional crystallization. The plagiogranites have clearly assimilated masses of hydrated diabase during intrusion into the sheeted complex, with ghost xenoliths in various stages of consumption visible around the marginal contacts. The widespread occurrence of secondary albite, chlorite, actinolite and quartz results from static hydrothermal metamorphism equivalent to greenschist facies. The most common rock type is hornblende trondhjemite which consists chiefly of plagioclase, quartz, and hornblende with minor ilmenite, sphene and diopside. Epidote is a common deuteric mineral.

Ultramafic cumulate rocks are only locally present in the area surrounding the drill hole. Where they do occur, the most common rock types are olivine norites and websterites, although rare wehrlites do occur. Ultramafic rocks occur either as layered sequences or smaller, isolated bands within the layered gabbros. The latter are generally less basic than the former. Poikilitic and allotriomorphic textures are common. Since contacts with gabbroic rocks are generally gradational where observed, the ultramafic cumulates are considered cogenetic with the more extensive gabbros and to have formed during the early stages of fractional crystallization.

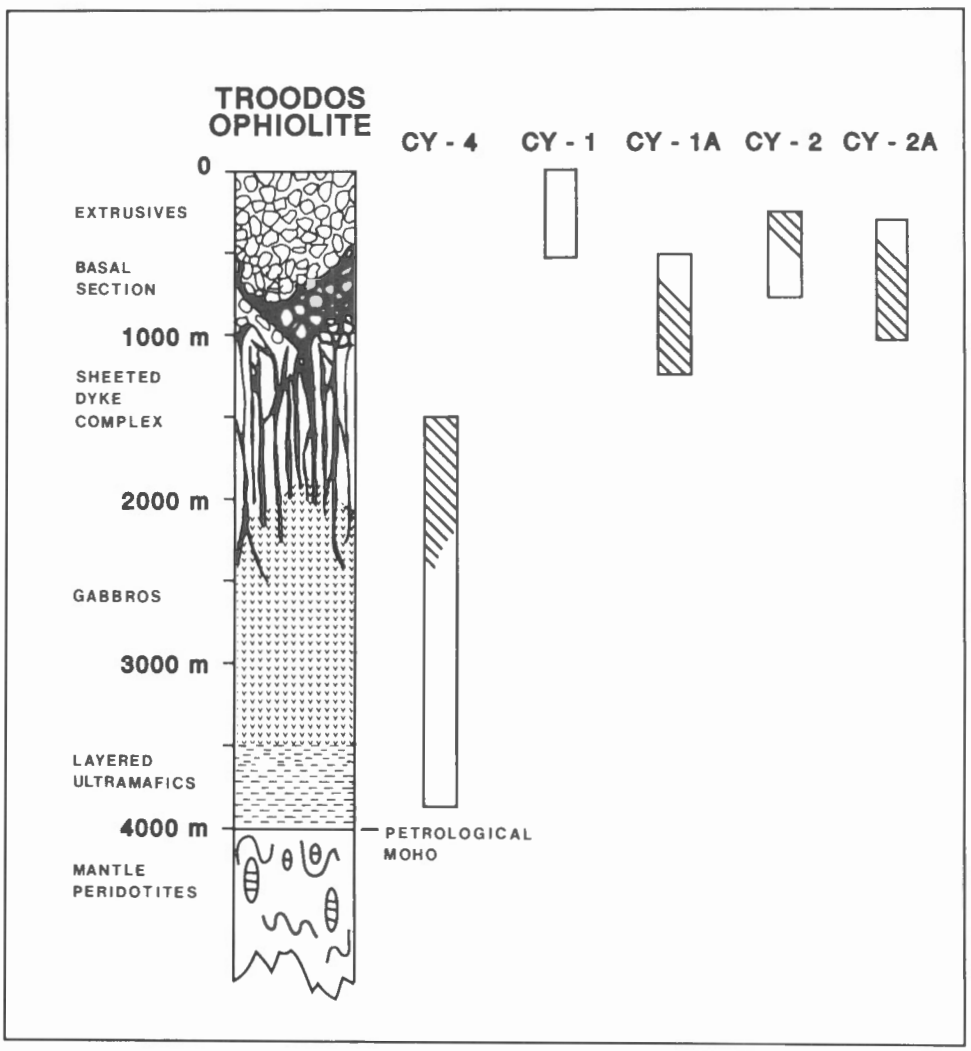

Figure 1: The 5 drillholes of the Cyprus Crustal Study Project and their relative stratigraphic positions.

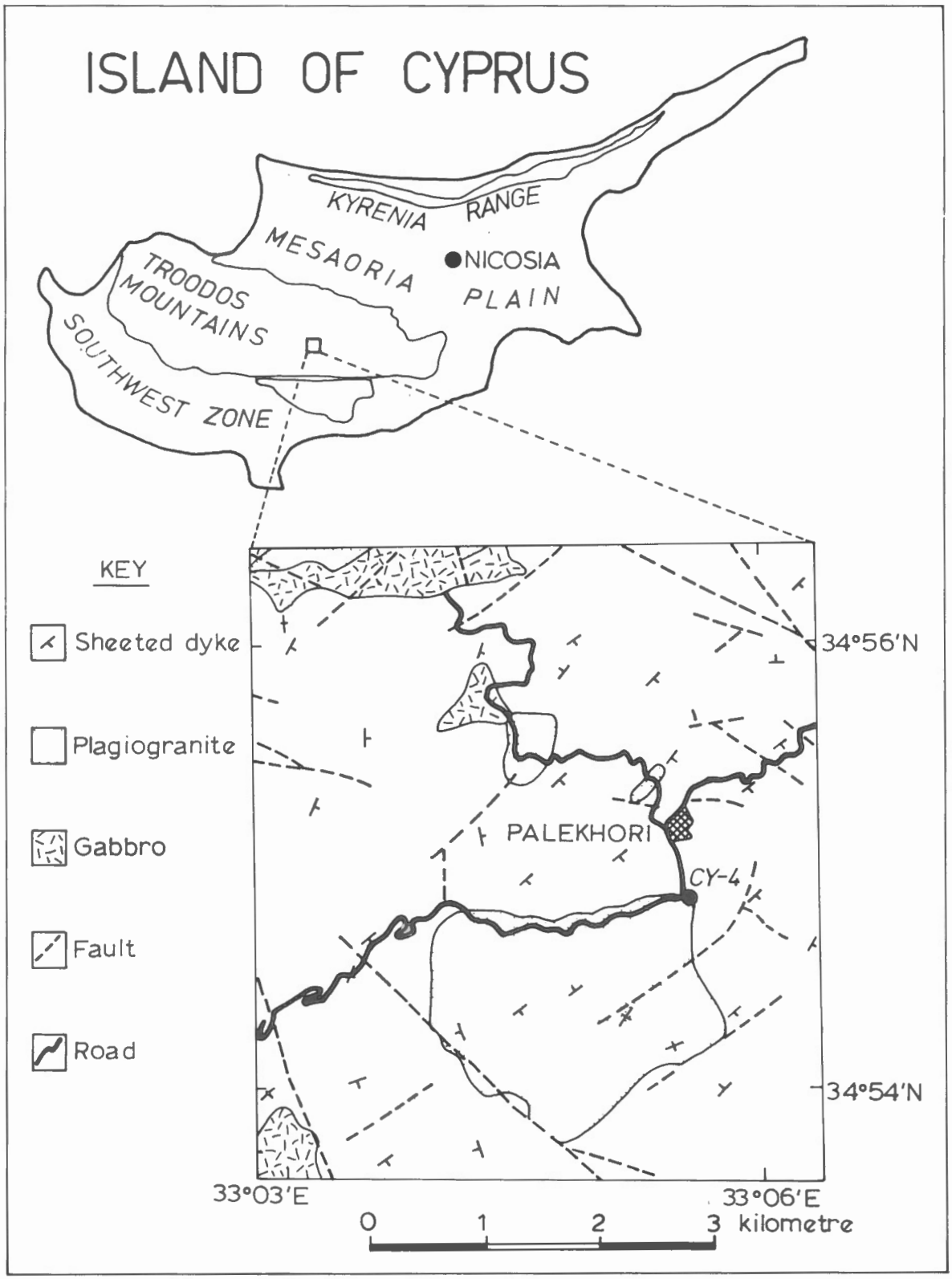

Figure 2: Site of CY-4 south of Palekhori Village.

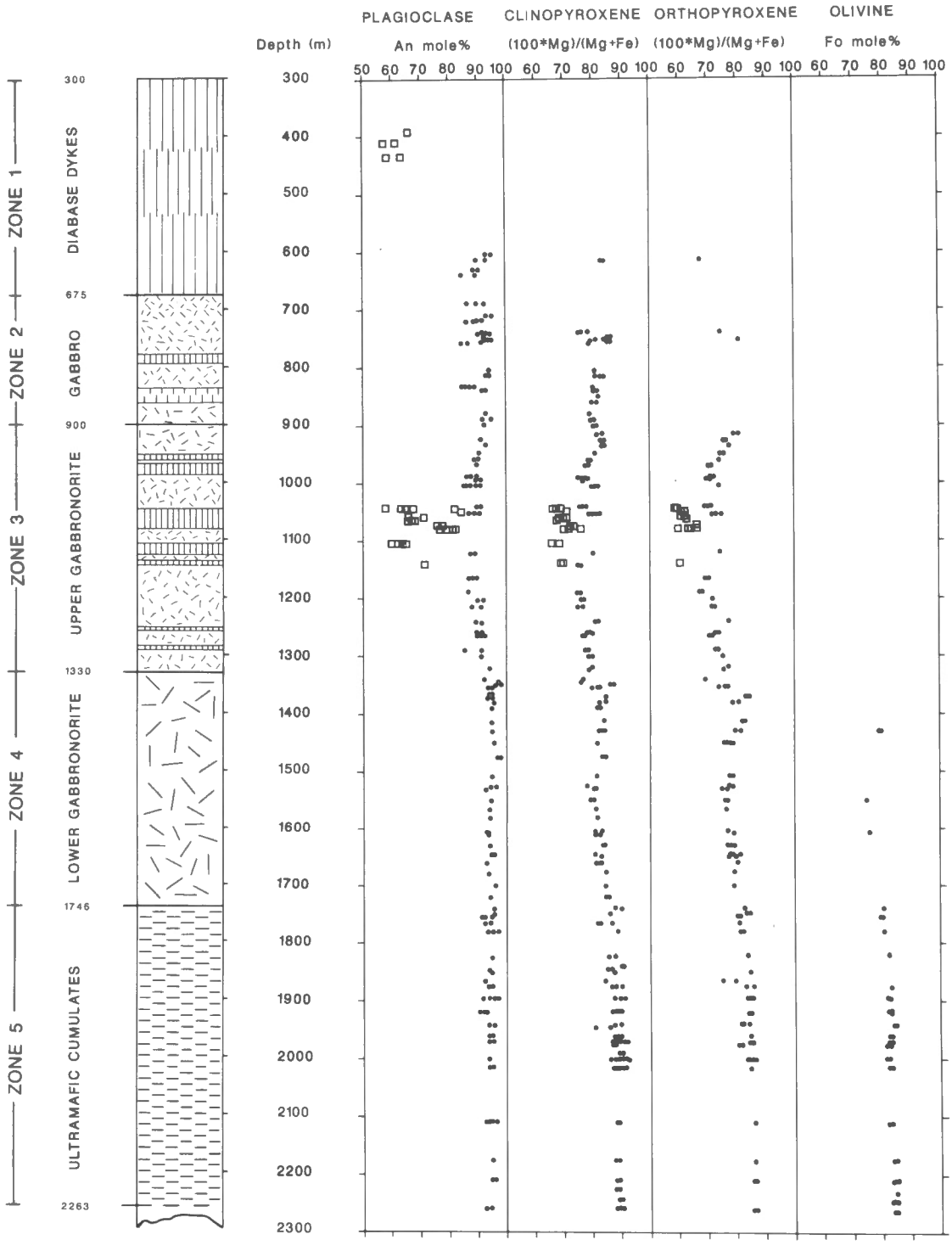

Figure 3: Lithologic zonal subdivisions of CY-4 core and related cryptic variation (□ = dyke analyses).

DRILLHOLE PETROLOGY

The section drilled in Hole CY-4 can be divided into five distinct zones on the basis of lithology and phase chemistry (Figure 3).

Zone 1 (0-675 m) Sheeted diabase dykes.
Zone 2 (675-900 m) Fine- to medium-grained gabbro.
Zone 3 (900-1330 m) Fine- to medium-grained gabbro-norite and two-pyroxene diabase dykes.
Zone 4 (1330-1740 m) Medium- to coarse-grained gabbro-norite.
Zone 5 (1740-2263 m) Medium- to coarse-grained websterite and related rocks.

Contacts between these zones are either gradational (Zone 2/3), faulted (Zones 4/5) or intrusive (Zones 3/4). The uppermost 675 m-thick section consists of pervasively altered, grey to greenish-grey, fine-grained, aphyric to marginally pyroxene-phyric, diabase dykes. These generally dip between 60 and 90 degrees and have vertical thicknesses in the core from 0.2 to 7 m. The percentage of gabbro screens increases downward and at approximately 675 m gabbro surpasses diabase as the dominant lithology. Pyroxenes in the diabases have invariably been totally replaced by uralite, beginning along crystal rims and proceeding into crystal cores. There is an abundance of secondary quartz and Fe-Ti oxides, the growth of which produces large variations in grain size.

Zones 2 and 3 represent an amphibole gabbro-norite sequence cut by a series of plagiogranitic dykes, diabase dykes and magnetite gabbros. Plagioclase is the dominant mineral and orthopyroxene a common matrix component, crystallizing before clinopyroxene. Magmatic hornblende is a late phase, often developed at the expense of both pyroxenes. Some rocks in these zones display a fine-scale planar lamination with well-developed adcumulus textures, but the majority are isotropic. Most contacts between rock types are gradational but others are defined by sharp changes in grain size. Dioritic and plagiogranitic rocks representing later differentiates of the magma characteristically intrude the gabbros as veins and dykes and are themselves cut in places by diabase dykes. Several swarms of pyroxene-phyric diabase dykes occur in zone 3 between 1100 and 1200 m. Some gabbros (e.g. between 1200 and 1220 m) are characterized by high modal percentages of magnetite, and magnetite is found as clots in coarse-grained amphibole gabbros in the area surrounding CY-4. The presence of amphibole and magnetite as magmatic phases in the gabbro suggests high water activity in the magma, which increases progressively with increasing percentages of crystallization. This water appears to have been derived in part from the assimilation of hydrated diabase as observed in the field studies.

The top of Zone 4 appears to be an intrusive boundary at which rocks lower in the drill core intrude those higher up. Rocks in the upper 2-3 m of Zone 4 are relatively fine grained, suggesting chilling at the contact. This zone is a well layered section comprising interlayered medium- to coarse-grained gabbro-norites, with lesser amounts of gabbro, olivine gabbro-norite and plagioclase-olivine websterite. The bottom of this zone is a sharp, inclined fault which marks the virtual disappearance of plagioclase as a cumulate phase. In contrast with the rocks lower down, olivine occurs in only small amounts in this zone and green hornblende occurs as a late deuteric phase. Layering occurs on a 1 to 10 m scale, and layers are generally homogeneous. However, grain size grading of some layers is observed, with more pegmatitic lithologies being common at the tops of the layers. Modal grading with concentrations of pyroxene and olivine at the base, grading into plagioclase-rich tops, occurs in some layers. Textures vary from adcumulate in the gabbro-norites to mesocumulate in the websterites.

Zone 5 is formed of well-layered websterite, clinopyroxenite, wehrlite, lherzolite and gabbro-norite sequences. Clinopyroxene is the dominant mineral phase and it is accompanied by abundant olivine below 2100 m. Layers are of variable thickness, from 5 cm to several metres. Contacts are usually marked by the appearance of one or more phases (phase contacts) and there is an associated grain size change. Although parallel lamination and modal lamination are well developed, parts of this section are affected by tectonic deformation which masks many original igneous features. Some olivine-rich layers are boudinaged and display porphyroclastic textures, with granulation and kink-banding of individual olivine crystals. Recovery textures (annealing) take the form of polygonal neoblasts of olivine and subgrain development in the pyroxenes. Such features are common in many of the ultrabasic rocks in the lower stratigraphic levels of the Troodos ophiolite and suggest that many cumulates found towards the base of the plutonic section may have undergone high temperature ductile deformation.

Throughout the drill core there is a general trend towards more primitive mineral compositions with increasing depth (Figure 3). Plagioclase shows a decrease in Ab mole per cent, clinopyroxene and orthopyroxene show a decrease in Fe/Mg ratios and olivine shows a decrease in Fa mole per cent. The dykes and gabbros in the upper part of the drill core have been altered, so original plagioclase compositions are sporadic and orthopyroxene compositions virtually unobtainable because of total replacement by amphibole.

Going upward in the core the solid solution series show essentially steady evolutions between 2263 m and 1330 m. There is an apparent reversal to slightly more Mg-rich compositions in the pyroxenes at 1550 m accompanied by a slight fall in the Ab content of plagioclases.

The intrusive contact at 1330 m is marked by both textural and mineralogical changes, particularly in the compositions of the clinopyroxenes (Malpas et al; Thy et al, this volume). The clinopyroxenes above the contact have significantly higher Ti contents, average TiO_2 = 0.35%, than those below in Zone 4, average TiO_2 = 0.18%.

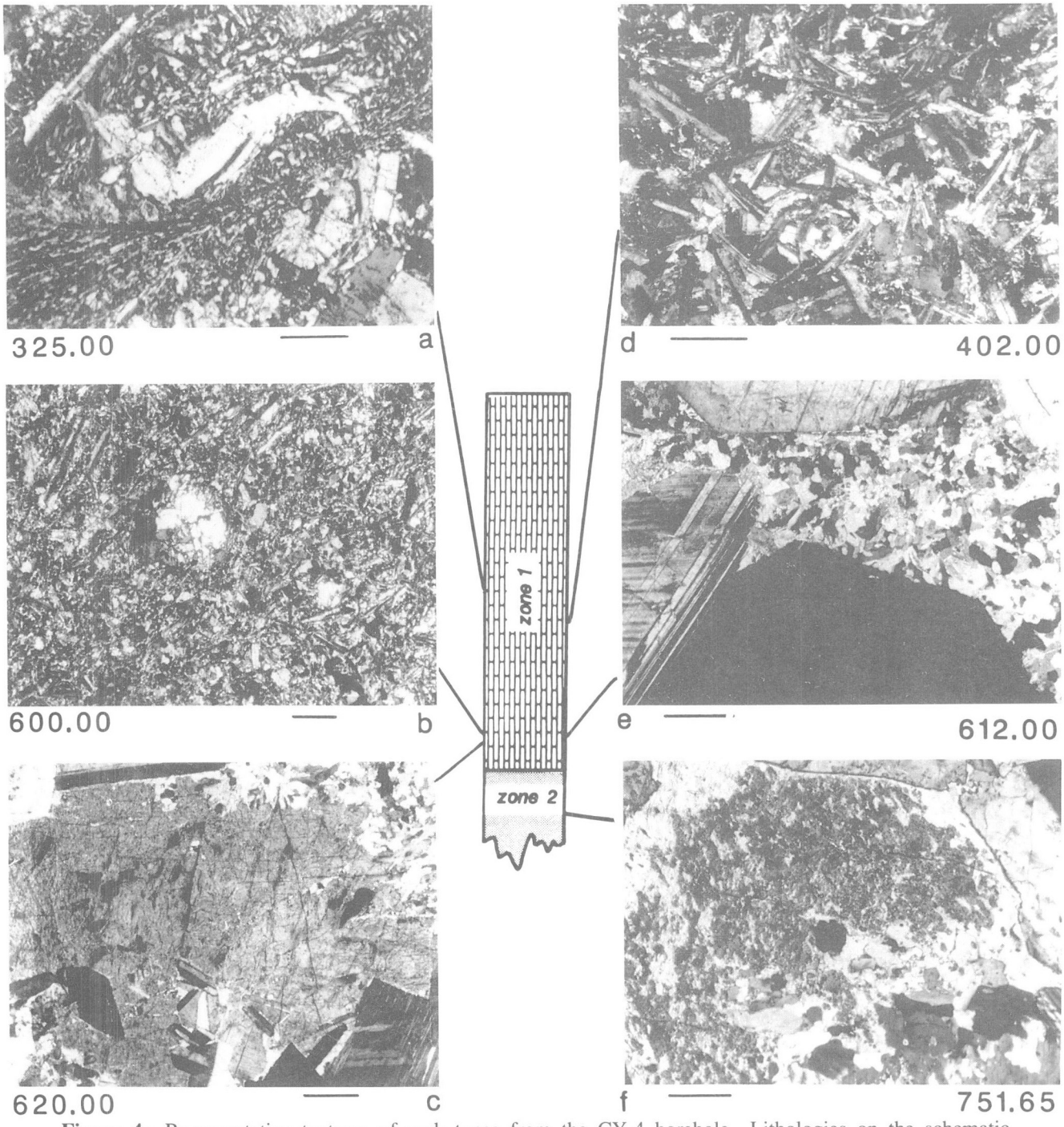

Figure 4: Representative textures of rock types from the CY-4 borehole. Lithologies on the schematic column are from Malpas, Brace and Dunsworth (this volume). Scale bars = 1 mm. (a) Diorite. X-nicols. The fan-type of texture is a result of micrographic intergrowth of quartz and plagioclase. (b) Diabase dyke rock. X-nicols. Fine-grained plagioclase-clinopyroxene phyric dyke. The clinopyroxene has been altered to amphibole. Minor (secondary?) quartz is also present. (c) Noritic gabbro. X-nicols. Relatively unaltered (approx. 7mm) oikocryst of orthopyroxene enclosing plagioclase. (d) Felsic dyke. X-nicols. Subophitic texture displayed in this dyke rock which has relatively large amounts of quartz and magnetite. (e) Noritic gabbro. X-nicols. Characteristic aggregate of small amphibole crystals infilling intersices between euhedral plagioclase crystals. (f) Gabbro. X-nicols. Large clinopyroxene crystal (dark areas) showing alteration to amphibole (light areas) especially around its margins.

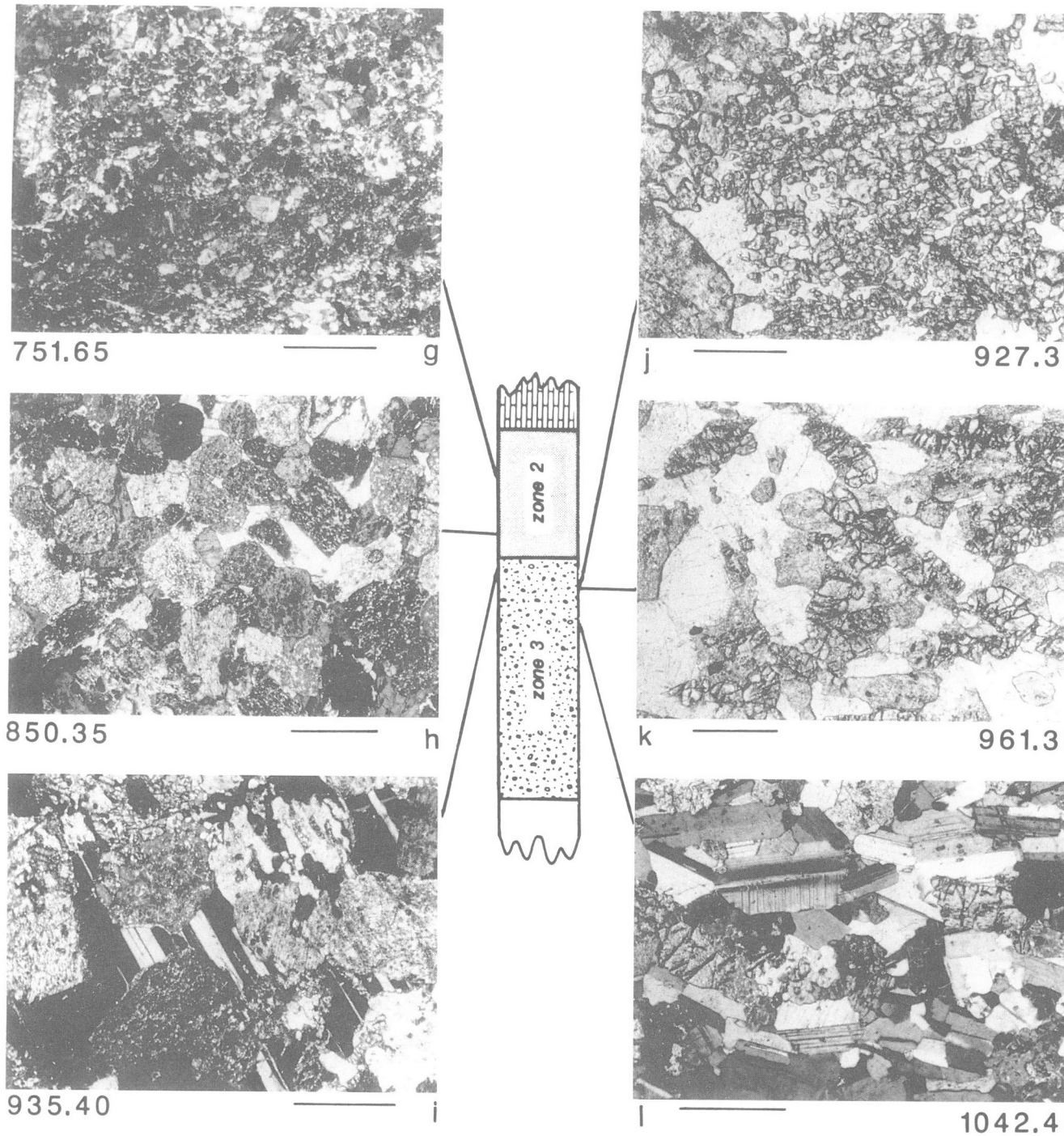

Figure 4 cont'd: (g) Sheared gabbronorite. X-nicols. Granulation of the mineralogy in this 5 cm-wide zone is a result of relatively low temperature subhorizontal shearing. (h) Clinopyroxenite. X-nicols. Cumulate crystals of clinopyroxene (Mg-rich augite) with minor intercumulate plagioclase. The clinopyroxene is partially altered to uralite. (i) Plagioclase websterite. X-nicols. Large plagioclase oikocryst (notice optical continuity) surrounding clinopyroxene in a rock from the top of Zone 3. (j) Plagioclase websterite. X-nicols. This granular nature is not uncommon in these rocks and might be a primary nucleation phenomenon. (k) Noritic gabbro. Plane light. Typical texture of these rocks with plagioclase (low relief), orthopyroxene (medium relief) and clinopyroxene (high relief). (l) Noritic gabbro. X-nicols. At this horizon there is a marked alignment of the plagioclase crystals as a result of magmatic flow.

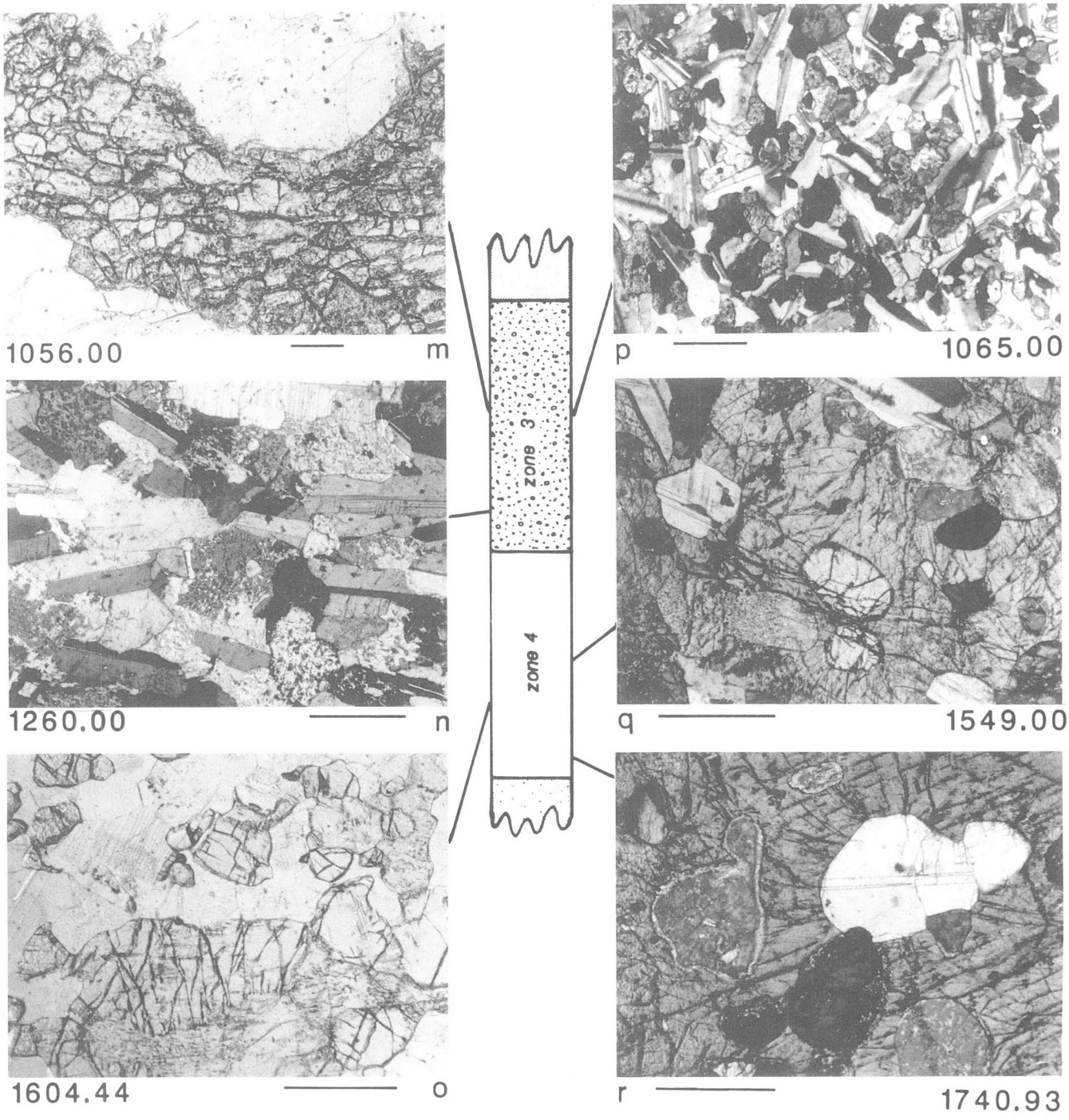

Figure 4 cont'd: m) Noritic gabbro. Plane light. Large orthopyroxene crystals are surrounded by clinopyroxene showing granulation and recrystallization as a result of high temperature shearing. (n) Coarse granular gabbroic dyke rock. X-nicols. Note the alignment of the plagioclase crystals as a result of primary magmatic flow. (o) Gabbronorite. Plane light. Note the contrasting habit, of granular and large prismatic orthopyroxene crystals. (p) Diabase dyke rock. X-nicols. Sub-ophitic to intersertal texture exhibited by this diabase that contains both ortho- and clinopyroxenes. (q) Olivine gabbronorite. X-nicols. Orthopyroxene poikilitically enclosing chadacrysts of olivine, plagioclase and clinopyroxene. (r) Olivine gabbronorite. X-nicols. Orthopyroxene poikilitically enclosing clinopyroxene, plagioclase and olivine.

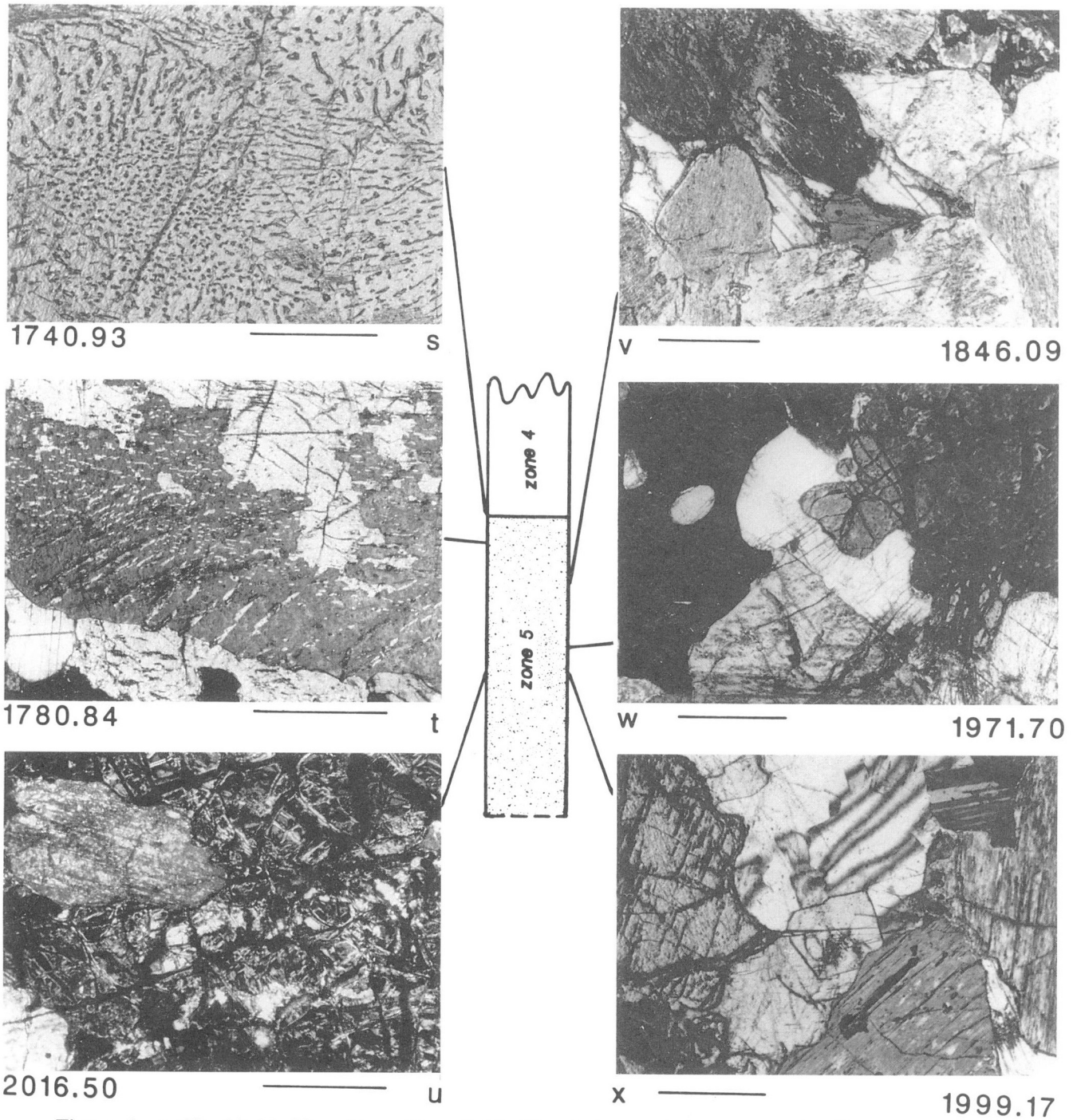

Figure 4 cont'd: (s) Noritic gabbro. Plane light. Vermicular exsolution textures in clinopyroxene. The exsolved mineral appears to be orthopyroxene. Note how the preferred orientations of the exsolution blebs indicate subgrain development. (t) Websterite. X-nicols. Deformed orthopyroxene exsolution lamellae in a magnesium-rich augite. (u) Wehrlite. X-nicols. Complete serpentinisation of both olivine and clinopyroxene. (v) Plagioclase clinopyroxenite. X-nicols. Euhedral cumulate clinopyroxene crystals surround intercumulate plagioclase. The clinopyroxene shows traces of fine-scale exsolution. (w) Olivine-plagioclase websterite. X-nicols. Rounded olivine chadacrysts in orthopyroxene oikocrysts to the left and intercumulus plagioclase in the centre of the photomicrograph (x) Gabbronorite. X-nicols. Note the undulose extinction resulting from kink-banding of the orthopyroxene crystal near the top margin of the photomicrograph.

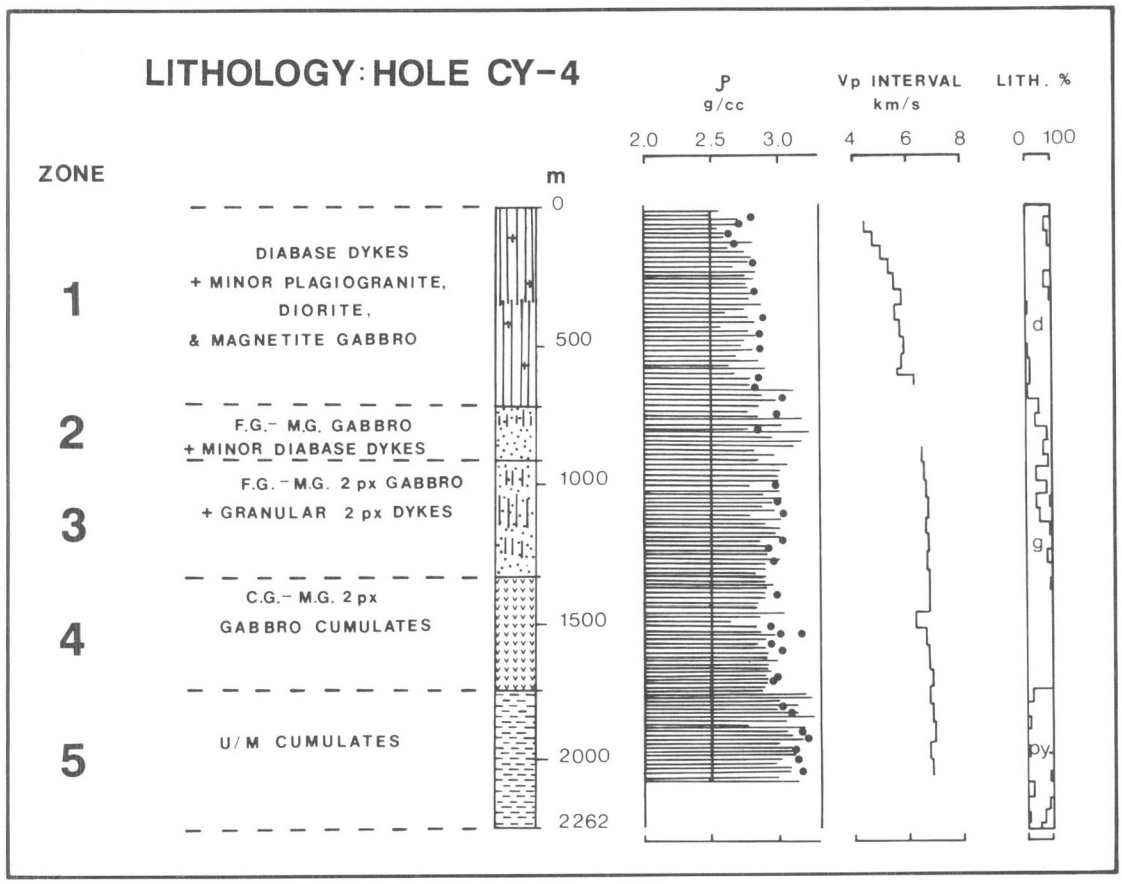

Figure 5: Variation in physical properties obtained by logging hole CY-4. Highlighted points in density log are laboratory measured densities of core samples. d = dykes, g = gabbros, py = pyroxenites in lithological column. f.g. = fine-grained, m.g. = medium-grained, c.g. = coarse-grained.

The upper gabbros in Zones 3 and 2 show complex cryptic variation representing at least two reversals in compositional trends. These transitions clearly occur over broad zones, between 1175 and 1075 m for the first and between 1000 and 900 m for the second.

Low temperature alteration throughout most of the plutonic section is limited to partial replacement of pyroxenes by actinolite. Plagioclase remains essentially unaltered. Olivine is partially serpentinized and veins of chrysotile occur in the deformed serpentinized lherzolites at the base of the section below 2000 m. Samples from the sheeted complex and gabbroic sequence show pervasive subsolidus hydrothermal oxygen isotope exchange with seawater. Whereas the sheeted dykes and high level gabbros show variable $\delta^{18}O$ depletion, deeper level gabbros are either depleted or enriched, relative to fresh oceanic basalts. The enrichments at depth are considered to be due in part to exchange at considerably lower temperatures with isotopically evolved seawater than has occurred with overlying rocks. Fluid inclusions from alteration minerals encountered in CY-4 result from two distinct hydrothermal fluids; evolved seawater with salinities of 0.7 to 8 wt % NaCl and a hypersaline brine resulting from the reaction of seawater with peridotite.

PHYSICAL AND MAGNETIC PROPERITES

In addition to providing a continuous petrologic section through the crust, a major objective of the drilling programme was to determine the geophysical properties of a major ophiolite by both laboratory measurements on core samples and by logging. Correlation of the laboratory with the logging results supported the validity of such measurements and, for the first time, the continuous seismic and magnetic structures of a major ophiolite can be compared with in situ oceanic crust in geophysical terms common to both. Both CY-4 and an array of shallower holes representing higher stratigraphic successions were logged using an extensive suite of slimhole tools developed by BPB Instruments, including sondes for measuring compressional and shear wave velocity, density, porosity, electrical resistivity, magnetic susceptibility and

field strength, temperature and hole diameter. With the exception of a brief interval from 640 m to 862 m which is cased, the entire section of CY-4 was successfully logged open-hole to 2080 m., the depth of the hole at the time of logging. In addition, borehole televiewer, hydrofracture and high resolution temperature studies were conducted at selected intervals in the hole. Since the water table was found to lie within a few metres of the surface, and the hole was saturated, only minor pressure and salinity corrections were necessary to restore the data to in situ oceanic conditions.

Analysis of palaeomagnetic results and magnetic logging show that there are five distinct magnetic zones within the local crustal rocks drilled at CY-4. These zones range from sheeted dike lithologies with high natural remanent magnetization and magnetic susceptibility to gabbros with low values.

Compressional (Vp) and shear (Vs) wave velocities measured in the laboratory under elevated hydrostatic confining pressures were used to construct a seismic velocity structure for the section represented by the CY-4 borehole. The dyke section shows strong velocity gradients with Vp ranging from 5.4 km/sec at the top to 6.8 km/sec at 630 m depth. Low velocity zones below this level result from alteration of high level gabbros, but otherwise velocities down to 1750 m agree well with oceanic layer three velocities. The transition from gabbro to ultramafic cumulates is marked by a sharp increase in Vp to 7.7 km/sec and Vs to 4.2 km/sec, values which fall within the range observed for the oceanic Moho by refraction. The compressional wave velocity increases steadily from 4.5 to 5.8 km/s in the sheeted dykes, then increases to 6.2 near the top of the dyke/gabbro transition at about 700 m and reaches values consistent with those of oceanic Layer 3 (6.7 ± 0.3 km/s) within the next few hundred metres, i.e. within the transition zone itself (Figure 5). Although the velocities obtained by logging continue to increase steadily with depth in the plutonic section, the gabbro/websterite transition is not marked by an increase in velocity, unlike that found in the laboratory synthesis. As can be seen in Figure 5 the density ranges between 2.7 and 2.8 g/cm^3 throughout the sheeted dykes and then increases markedly at the top of the dyke/gabbro transition to values of 2.8 and 2.9 and again at the top of the ultramafic rocks to well in excess of 3.0 g/cm^3.

CONCLUSIONS

The phase chemistry and textural layering of the gabbros and ultramafic rocks from Zones 4 and 5 of the CY-4 drill core suggest crystallization in a relatively closed magma chamber. Only one major period of magma rejuvenation is recorded. Such a system might be associated with a period of slow spreading at the ridge axis. In contrast, the upper zones appear to reflect crystallization in a magma chamber that was open to periodic replenishment and possibly associated with faster spreading rates. Both the intrusive nature of the Zone 3/4 boundary and field evidence from the surrounding areas suggest the construction of the ophiolite plutonic sequence by multiple magma chambers rather than by a single, long-lived, steady-state chamber beneath the ridge axis. Rocks from Zones 4 and 5 are considered to have crystallized from a later magma body than that which formed the plutonic rocks higher up. If the marked contrast in TiO_2 content of the pyroxenes above the Zone 3/4 boundary can be correlated with a parental magma that was more Ti-rich than that which produced the lower and younger part of the section, then it might be possible to make an association between the upper cumulates and the oldest part of the pillow lava sequence which is characterized by arc tholeiitic lavas. Likewise, the lower cumulates might correlate with the upper section of Troodos lavas which are essentially members of a depleted series. The chemistry of both the plutonic rocks, and more especially the lavas, support the hypothesis that the ophiolite was produced in a suprasubduction zone (SSZ) environment (Robinson et al., 1983). However, the processes which produced the Troodos ophiolite at a SSZ spreading axis resulted in a geophysical stratigraphy comparable to average oceanic crust. The density and seismic velocity data are particularly striking in that they strongly support the conclusion that the oceanic layer 2/3 boundary coincides with the sheeted dyke/gabbro transition.

ACKNOWLEDGEMENTS

Drilling operations at CY-4 were financed by the governments of Canada (NSERC), Cyprus (GSD), U.K. (NERC), U.S.A. (NSF), Denmark (SNF), the VW Foundation of West Germany and King Abdulazis University of Saudi Arabia. We thank the members of the Geological Survey Department of Cyprus, particularly Dr. George Constantinou, Andreas Panayiotou and Costas Xenophontos for their assistance with the project. Mr. Terry Brace of Memorial University assisted with production of microprobe data and with manuscript preparation.

REFERENCES

Allen, C.R.
1975: The petrology of a portion of the Troodos plutonic complex, Cyprus; unpublished Ph.D. thesis, University of Cambridge, p. 1-161.

Casey, J.F. and Karson, J.A.
1981: Magma chamber profiles from the Bay of Islands ophiolite complex; Nature, v. 292, p. 295-301.

Greenbaum, D.
1972: Magmatic processes at ocean ridges: evidence from the Troodos Massif, Cyprus; Nature, Physical Science, v. 238, no. 80, p. 18-21.

Greenbaum, D.

1977: The chromitiferous rocks of the Troodos ophiolite complex, Cyprus; Economic Geology, v. 72, p. 1175-1194.

Hopson, C.A. and Pallister, J.S.
1980: Semail ophiolite magma chamber: I, evidence from gabbro phase variation, internal structure and layering; *in* Ophiolites, Proceedings of the International Ophiolite Symposium, Cyprus, 1979, ed. A. Panayiotou; Cyprus Geological Survey Department, Ministry of Agriculture and Natural Resources, p. 402-404.

Malpas, J. and Brace, T.
1987: The geology for the Pano Amiandos-Palekhori area, Cyprus; 1:12500 map with marginal notes Cyprus Geological Survey Department.

Malpas, J., Brace, T. and Dunsworth, S.M.
1989: The regional geology and petrology of the CY-4 drillhole *in* Cyprus Crustal Study Project: Initial Report, Hole CY-4, ed. I.L Gibson, J. Malpas, P.T. Robinson and C. Xenophontos; Geological Survey of Canada, Paper 88-9.

Moores, E.M. and Vine, F.J.
1971: Troodos Massif, Cyprus and other ophiolites as oceanic crust: evaluation and implications; *in* A Discussion on the Petrology of Igneous and Metamorphic Rocks from the Ocean Floor; Philosophical Transactions of the Royal Society of London, v. 94, no 2, p. 443-466.

Thy, P., Schiffman, P. and Moores, E.M.
1988: Igneous Mineral Stratigraphy and Chemistry *in* Cyprus Crustal Study Project: Initial Report, Hole CY-4, ed. I.L. Gibson, J. Malpas, P.T. Robinson and C. Xenophontos; Geological Survey of Canada, Paper 88-9.